Technology in Practical Dermatology

Non-Invasive Imaging, Lasers and Ulcer Management

Michele Fimiani
Pietro Rubegni
Elisa Cinotti
Editors

MOREMEDIA

Springer

Technology in Practical Dermatology

Michele Fimiani
Pietro Rubegni • Elisa Cinotti
Editors

Technology in Practical Dermatology

Non-Invasive Imaging, Lasers and Ulcer Management

Springer

Editors
Michele Fimiani
Dermatology Unit, Department of
Medical, Surgical and Neuro-Sciences
University of Siena
Siena
Italy

Elisa Cinotti
Dermatology Unit, Department of
Medical, Surgical and Neuro-Sciences
University of Siena
Siena
Italy

Pietro Rubegni
Dermatology Unit, Department of
Medical, Surgical and Neuro-Sciences
University of Siena
Siena
Italy

ISBN 978-3-030-45350-3 ISBN 978-3-030-45351-0 (eBook)
https://doi.org/10.1007/978-3-030-45351-0

This Springer imprint is published by the registered company Springer Nature Switzerland AG
The registered company address is: Gewerbestrasse 11, 6330 Cham, Switzerland

Preface

The development of increasingly advanced technologies has contributed to substantial progress in the diagnosis, treatment, and research of many dermatologic diseases in the last decades. Sophisticated equipment such as laser and in vivo reflectance confocal microscopy, methodologies such as photodynamic therapy, and biological products such as acellular deepidermized dermis, stem cells, and in vitro expanded epidermis have progressively led to the identification and construction of a new and more effective approach to the management of dermatological patients suffering from complex diseases like epithelial and melanocytic tumors, pigmentation disorders, and loss of skin substance. This book aims to offer the medical reader and dermatologists, in particular, a consultation tool capable of presenting the huge amount of data that has been gradually accumulated in recent years clearly and synthetically.

Particular attention has been paid to the progress of technological innovations in the field of prevention, diagnostics, and treatment of some diseases such as chronic ulcers and epithelial tumors which are increasing in frequency and are becoming more severe due to the progressive increase in the average age of the population.

To make the consultation of the text easier and more effective, the various topics have been grouped by the affinity of their content into four main sections: Imaging techniques for skin diseases, Laser and light sources technologies in dermatology, Technological advances in wound management, and New tools for dermatologic diagnosis. The drafting of every single chapter, entrusted to experts with proven experience in the field, has been designed to provide the reader with a complete overview of the most significant progress made in recent years on specific issues, clearly highlighting the rational bases of use of many new technologies, their main indications, and their usefulness not only in the research field but, above all, in clinical practice.

Siena, Italy

Michele Fimiani
Pietro Rubegni
Elisa Cinotti

Contents

Part II Lasers and Light Sources Technologies in Dermatology

Part I

Imaging Techniques for the Evaluation of Skin Diseases

Elisa Cinotti

Dermoscopy: Fundamentals and Technology Advances

1

Linda Tognetti, Diletta Fiorani, Giulia Tonini, Lorenzo Zuliani, Gennaro Cataldo, Alberto Balistreri, Gabriele Cevenini, Elisa Cinotti, and Pietro Rubegni

1.1 Introduction

The term "*dermoscopy*" (or *dermatoscopy*) refers to the noninvasive examination of the skin using skin surface microscopy. Dermoscopy allows the rapid and magnified observation of structures in the epidermal and dermal layers otherwise not visible to the naked eye [1]. Therefore, it represents a valid tool for visualization of pigmented and non-pigmented lesions [2–5] and for the early detection of skin cancers [2, 6]. Indeed, when compared with naked eye examination, dermoscopy is believed to increase sensitivity in melanoma detection up to 25% depending on physicians experience and trainee [3, 7–10]. From the late 1960s, the diagnosis of skin tumors stimulated the progressive technologic improvement of dermoscopes and their diffusion in clinical setting and, in parallel, research besides dermoscopic imaging. Since 2000, the use of dermoscopy spread to several dermatological fields [11], including a growing variety of cutaneous conditions ranging from inflammatory [12, 13], autoimmune [14], granulomatous [15], and infectious diseases [12–14] to skin adnexa and oral/genital mucosae [16, 17]. Furthermore, dermoscopic examination was successfully applied in monitoring dermatological chronic conditions [18–20] and assessment of treatment efficacy, either topical [19–22] or system [23–25] or phototherapic treatments [19, 26].

Nowadays, other noninvasive diagnostic techniques (e.g., in vivo reflectance confocal microscopy and optical coherence tomography) have been developed for skin examination, allowing better resolution and higher specificity then dermoscopy [5, 8, 27, 28]. However, these devices are available in a minority of dermatologic centers because they are more expensive than dermoscopes, are less easy and rapid to use, and require a longer training in imaging interpretation [6, 9, 29, 30].

L. Tognetti (✉)
Dermatology Division, Department of Medical, Surgical and Neuro-Sciences, University of Siena, Siena, Italy

Department of Medical Biotechnologies, University of Siena, Siena, Italy

D. Fiorani · G. Tonini · G. Cataldo · E. Cinotti
P. Rubegni
Dermatology Division, Department of Medical, Surgical and Neuro-Sciences, University of Siena, Siena, Italy

L. Zuliani
Laboratory of Bioengineering and Informatics in Medicine, Department of Medical Biotechnologies, University of Siena, Siena, Italy
e-mail: lorenzo.zuliani@student.unisi.it

A. Balistreri · G. Cevenini
Department of Medical Biotechnologies, University of Siena, Siena, Italy
e-mail: alberto.balistreri@dbm.unisi.it; gabriele.cevenini@dbm.unisi.it

M. Fimiani et al. (eds.), *Technology in Practical Dermatology*,
https://doi.org/10.1007/978-3-030-45351-0_1

1.2 History of Dermoscopy

The term "*skin surface microscopy*" was coined in 1663 when Kolhaus first observed nail fold vessels with an optical microscope [31]. Ernst Abbe realized in 1878 that the application of oil, acting as an interface between the skin and the lens, could improve the image quality. Since then, various terms have been used to describe the process of dermoscopy, including "*incident light microscopy*" and "*epiluminescence light microscopy*," but the term "*dermoscopy*," which is the most accepted now, was first suggested by Friedman et al. in 1991 [32].

The first dermoscopic binocular was produced by Zeiss in the mid-twentieth century, and the term dermoscopy was coined by Saphier in 1920 [33]. Dermoscopic studies of pigmented skin lesions using different monocular epiluminescence tools began with Goldman in the 1940s based on the experiences on colposcopy for visualization of the cervical region [34–36]. Then, the production of the first portable dermoscope dates back to 1958 [36].

In 1971, the routine use of specific oil-immersion fluid was recognized to improve quality and resolution of structure visualization under the dermoscopic lens [37]. Then in the late 1980s, technical improvement allowed the realization of large dedicated dermoscopic devices. Since the early 1990s, hand-held devices started to be developed for clinical use, all contact dermoscopy (also called "traditional") devices. The first polarized dermoscope was created in 2001 (3Gen DermLite), starting the series of polarized contact/non-contact dermoscopes. In the last few years, hybrid devices polarized/non-polarized have been created [38, 39].

1.3 Hand-Held Dermoscope: Contact, Polarized, Hybrid

Hand-held dermoscope (i.e., an ergonomic device which can be easily managed with one/two hands) was developed in order to allow a routine use in clinical practice, ensuring a rapid and easy examination of the lesion in any body area [36].

Generally, a dermoscope is characterized by a spherical, achromatic high-quality lens combined with a bright halogen beam that allows a magnification ranging from 10× to 20×. The transilluminating lightening system uses an incident halogen light source that is directed with a 30–45° angle [16, 17, 29]. Under normal conditions, most of the light that is delivered on the skin surface will be reflected;: this is caused by the different refractive of the stratum corneum, which is higher than that of the air [19] (Fig. 1.1).

1.3.1 Contact Dermoscopy

In contact dermoscopy, a fluid (mineral oil or alcohol) is placed on the lesion to be examined before the application of dermoscopic lens. Fluid interface eliminates surface light reflection and renders the stratum corneum transparent [1], allowing visualization of epidermis, dermo–epidermal junction, and the superficial dermis, and it also suggests the location and distribution of melanin. Different dermoscopy fluids and application techniques can be used: Gewirtzman et al. [40] have tried to determine the best techniques for the application of immersion fluid and to discover which immersion fluid creates less air inclusions. It is better to apply an alcoholic fluid that creates less air inclusion if compared with mineral oil fluid, with an eyedropper directly into the skin [40].

With regard to the quality of dermoscopic image, structures are equally clear with alcohols and liquid paraffin, while ultrasound gel and water create blurred images [40].

These systems have many advantages: achievement of well-focused images, visualization of superficial dermal vessels [30], and identification of hyperkeratotic lesions such as seborrheic keratosis, peppering, lighter colors, and blue-white areas [28, 41]. The two main limitations are represented by compression of superficial capillaries if high pressure is applied on the lesion and the need of the dermoscopic lens to be cleaned/sterilized after examination, especially in case of infectious lesions such as warts or molluscum contagiosum [42].

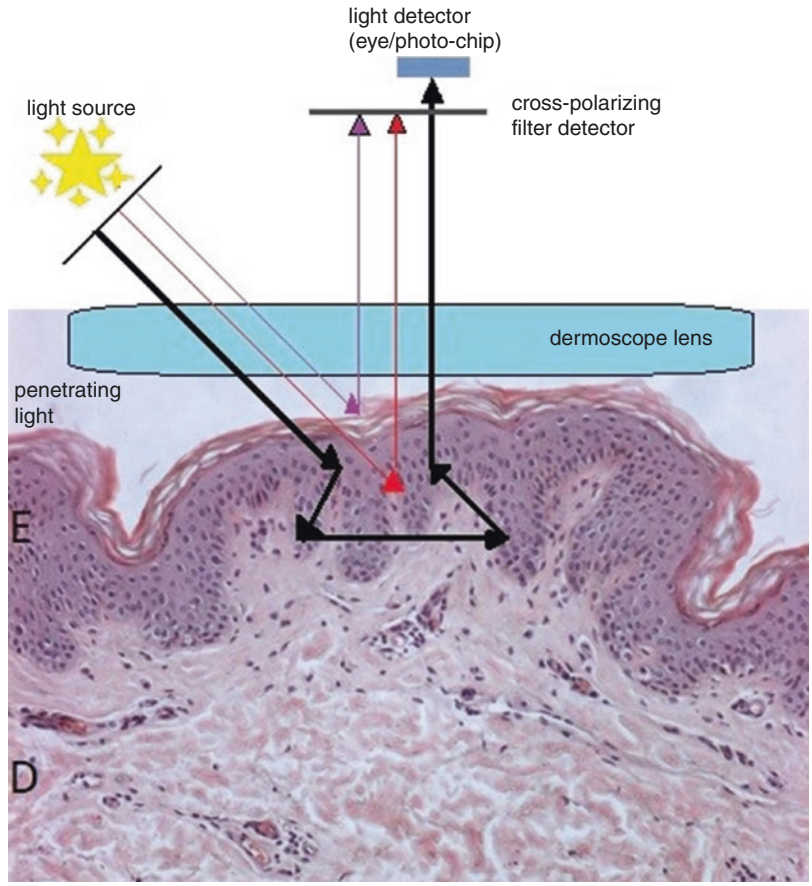

Fig. 1.1 Schematic representation of light reflection through the two main components of the dermoscope (i.e., dermoscopic lens, filter detector, light detector) on the skin surface at common sites (E = epidermis, D = reticular dermis)

1.3.2 Polarized Dermoscopy

Polarized dermoscopy allows the visualization of skin structures without the necessity of a liquid interface apposition (*contact polarized dermoscopy*) or without direct skin contact (*non-contact polarized dermoscopy*). This technique relies on the principle of reflection of surface-light illumination coupled with a cross-polarized viewer (i.e., two polarizers with orthogonal axes) [43]. On the one hand, contact polarized dermoscopy partially reduces the physiological skin surface reflection, allowing the visualization of skin structures ("depolarization" phenomenon) without using an immersion fluid (Fig. 1.1). On the other hand, non-contact dermoscopy is very useful for a quicker examination of patients with multiple nevi, and ensure the visualization of brilliant fibrotic structures (i.e., shiny white streaks, white scar-like areas, blue-gray color, pink/red areas). Given the absence of compression on vascular structures, superficial vessel pattern can be visualized without "ischemic artifacts" caused by the compression of the skin by a glass contact plate. Furthermore, polarized dermoscopy is recommended in the evaluation of hair shaft disorders and nail plate surface [44].

1.3.3 Hybrid Dermoscopy

We know today that the capabilities of non-polarized dermoscopy and polarized dermoscopy are not equivalent, but complementary. Indeed, images obtained by polarized light dermoscopes are essentially different from those obtained by a traditional contact dermoscope. To overcome these "problems" and facilitate rapid examination in clinical activity, some "hybrid" hand-held dermoscope have been developed. These devices

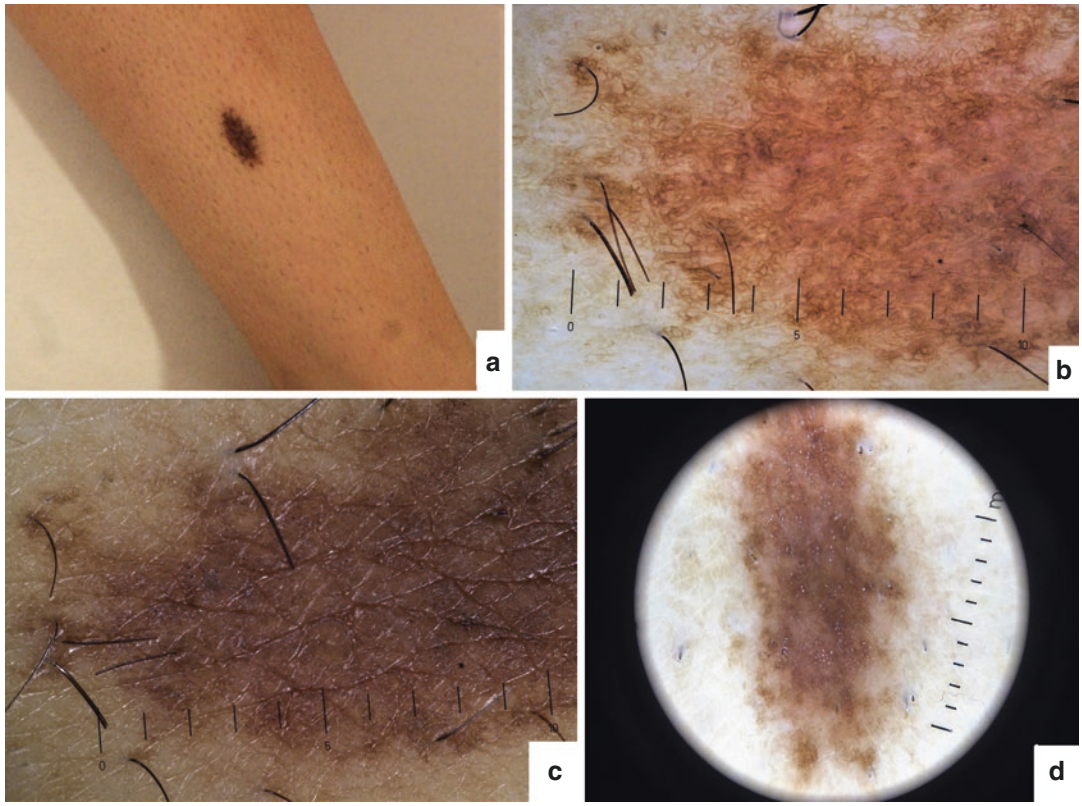

Fig. 1.2 Clinical picture of a congenital melanocytic nevus of the leg of an 18-year-old female (**a**): contact oil dermoscopy 20× [*Heine delta 20 T*] (**b**), low polarization contact dermoscopy 2LED [*Heine delta 20 T*] (**c**), and high polarization contact dermoscopy 4LED [*Dermlite 200 HR*] (**d**)

(e.g., DermLite DL200 Hybrid and Delta 20T Heine) allow the visualization in both contact and non-contact modalities, having the possibility to manually switch between non-polarized and polarized illumination. The illuminating source is represented by a composition of both non-polarized and polarized LEDs: 21 LEDs (15 polarized, 6 non-polarized) in DL200 Hybrid; 4 high quality LEDs (2 polarized, 2 non-polarized) in Delta 20T (Fig. 1.2).

1.4 Portable Hand-Held Dermoscope/Camera Systems

The main limitation of hand-held dermoscope was the impossibility to obtain and store dermoscopic images. Thus, in recent decades, two kinds of solution for portable dermoscope-camera systems have been adopted. One was the creation of digital photocameras with the possibility to attach a polarized optic filter (e.g., DermLite photosystem) with 17–18× magnification (Fig. 1.3a). Second, the creation of specific adapters able to connect some models of hand-held dermoscope (e.g., Heine Delta 20) with digital camera (e.g., Canon/Nikon) or a smartphone (e.g., iPhone) [45]. These combined system allow to use the dermoscope both as an independent unit and as a camera sub-unit, according to clinical practice needs, either in polarized and non-polarized mode (Fig. 1.3b). The dermatologist has the possibility of placing the lens on the desired lesional point and shoot the camera directly over the viewing area of the dermoscope, which is reproduced on the camera display. One disadvantage is that both hands are required to

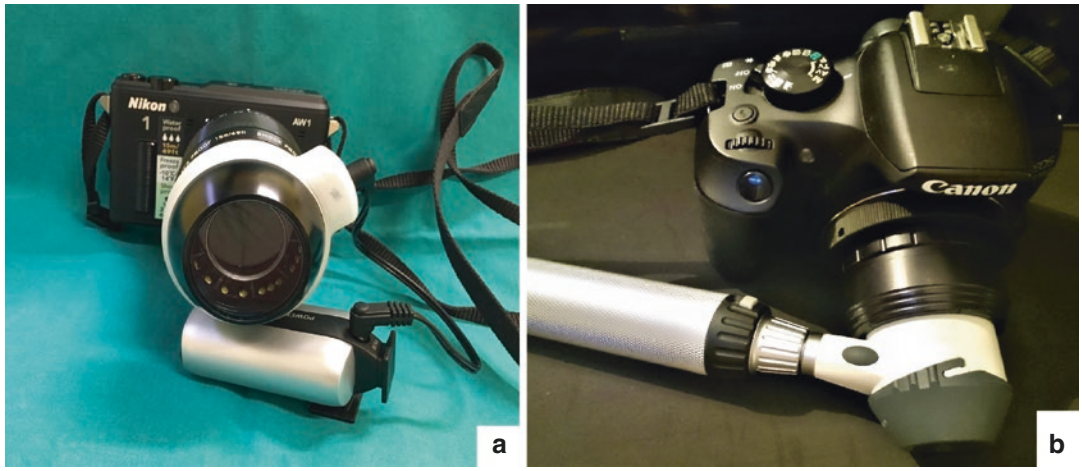

Fig. 1.3 Examples of portable dermoscope-camera systems: a digital photocamera combined with special polarized lens [*DermLite photo-system*] (**a**); hand-held dermoscope connected with a reflex mirrorless camera [*Canon-Heine Delta20*] (**b**). Courtesy of DermLite®, San Juan Capistrano, California (USA)

produce a good-quality image. It should be taken into account that there are considerable differences in the quality of images depending on both the device and the camera used, especially if the image has to be cropped or magnified. Moreover, each camera-system need to be pre-calibrated according to the technical specifics of both the camera and the hand-held dermoscope (shooting mode/ISO/opening time/light/color, etc.).

1.5 Video-Dermoscopy and High-Resolution Dermoscopy

A video-dermoscope is a system that includes a hand-held dermoscopic probe connected to a viewing monitor and a dedicated computer usually with a USB connection. The possibility to evaluate the image in a monitor allows to observe high-quality and high-magnification images. Also, the image displayed on the monitor can be "shared" in real-time with the patient, if needed, for counseling purposes. These instruments consist of a high-resolution color video camera which is incorporated into the final part of a probe [46, 47]. They offer both polarized and non-polarized light and a real-time zooming up to 1000 times magnification, although image quality is not superior if compared with hand-held devices [48]. The presence of a dedicated software for videodermoscopy facilitates a rapid storage, organization, and comparison of different dermoscopic and clinical images [46]. Videodermoscopes are generally easy to use and require only some technical skills, they allow an easy storage and retrieval of images for follow-up examination and, when connected to telematic networks, they offer the possibility for teledermoscopy consultation [49].

Today, a large number of videodermoscopes is available, of different costs according to the quality of the lens, lighting system, and specific software features (e.g., whole body mapping systems and advanced serial image capturing dermoscopy systems). High-quality videodermoscopes are still limited to research centers (Fig. 1.4a–c).

Videodermoscopy is also of potential interest for the evaluation of skin color and xerosis. However, the majority of videodermoscopes offer a variable quality of the images, and this depends on several factors such as the lighting of the room; this is the reason why they are not at all useful for quantitative studies. In recent years technical improvements have led to the creation of an ultra-high definition videomicroscope—C-Cube® (Pixience, Toulouse, France)—which allows to obtain images that are independent from external

Fig. 1.4 Different models of video dermoscopes, using different probe camera and software: Horus HS600 (Adamo SrL, Italy) (**a**), FotoFinder (Fotofinder Systems GmbH Bad Birnbach, Germany) (**b**), VISIOMED D200EVO (Canfield, Canfield Imaging Systems, Fairfield, NJ, USA) (**c**), hand-held super-high definition videodermoscope (C-CUBE Pixience, Toulouse, France) (**d**), and camera probe able to achieve 400× magnifications (FotoFinder Systems) (**e**). (Courtesy of: Adamo SrL, Fotofinder, Canfield, Pixience)

lightening and are reproducible. This device has three main peculiarities: a 10 MPx CMOS sensor that allows to obtained an UHD image of a field of view of 1.6 mm × 1.2 mm at 50× magnification; a specific lighting principle that is able to achieve homogeneous lighting without any glare; a real-time color calibration procedure that corrects the live and acquired images from a RGB sensor to an sRGB color space and then to a CIELab color space, obtaining reproducible images among different C-Cube probes as well as reliable color measurements [37]. The main advantage of this portable videodermoscope is the possibility to collectively detect and measure several different parameters, such as erythema, yellowness, color homogeneity, and xerosis, that were previously described with colorimeter or corneometer [37] (Fig. 1.4d).

Technical progress in digital imaging has stimulated the improvement of dermoscopic images, especially digital magnification and quality resolution. For example, with Fotofinder Medicam 1000 (Fotofinder System, Bad Birnbach, Germany), pigmented lesion can be observed at up to 400 times the original magnification [50] (Fig. 1.4e). However, further studies are required in order to clearly define if morphologic structures observed with this super-high-magnification videodermoscope can add more information in the evaluation of skin lesions compared to traditional videodermoscopes [50].

1.6 Evolution of Dermoscopic "Language"

After many years, we can definitely say that "dermoscopy," the science that studies the appearance of skin under the dermoscopic lens, has its own language. Indeed, since its birth, the dermoscopic "vocabulary" has progressively expanded and modified according to several authors' proposal. Traditionally, the first effort made to provide a standardized descriptive approach to pigmented skin lesions dates back to 1987, when the concept of "pattern analysis" was first introduced [38]. Then in 1989, the first Consensus Conference on Skin Surface microscopy was held in Hamburg [51]. In the same year, Soyer et al. described for the first time the correlation between dermoscopic features and histopathologic structures [52]. Over the 1990s, several groups developed different diagnostic methods for a better analysis of dermoscopic images [53–57]. To summarize, we can assess that, when observing a lesion under the dermoscopic lens, the dermatologist/physician has to simultaneously consider the dermoscopic pattern, lesion-specific features, color, and symmetry (Fig. 1.5). The correct interpretation of these dermoscopic elements allow to achieve the correct diagnosis with dermoscopic examination.

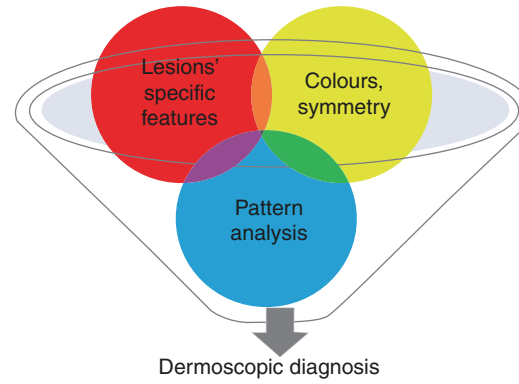

Fig. 1.5 Schematic representation of dermoscopic examination approach to pigmented skin lesion

1.6.1 Pattern Analysis

A "dermoscopic pattern" is intended as a specific combination and disposition of characteristic colors/shape/pigment within a skin area, which could be observed in different lesions and patients that exhibit the same morphology. In particular, pattern analysis relies on pattern recognition and pattern comparison. First, the novice has to recognize one among nine characteristic patterns: *reticular, globular, homogeneous, multicomponent, cobblestone, parallel, starburst, lacuna, and unspecific*. In Table 1.1, they are listed along with their definitions.

Furthermore, the same type of lesions usually show different patterns according to the body area, the age, and the skin phototype of the patient Table 1.2.

Table 1.1 Definition of the main general dermoscopic pattern, along with their clinical significance

Dermoscopic pattern	Definition	Clinical significance
Reticular	Pigment network	Typical pigment networks: acquired melanocytic nevi, solar lentigo Fine peripheral network: dermatofibroma Atypical pigment network: dysplastic nevi/melanoma
Globular	Numerous, variously sized, round to oval structures with various shades of brown and gray-black coloration	E.g., acquired melanocytic nevi in young people
Homogenous	A diffuse area of color in the absence of a pigment network or other distinctive local features	Melanocytic lesions, blue nevi, seborrhoeic keratoses, etc.
Multicomponent	Combination of patterns such as globular, reticular, and homogenous	The combination of ≥3 patterns within a lesion, with asymmetrical e features, is suggestive of dysplastic nevus/melanoma
Cobblestone	Large, closely aggregated, more or less angulated globules disposed to create a "cobblestone"	Dermal nevi composed by large dermal nests of melanoctyes
Parallel	Pigment arranged in parallel lines	Parallel ridge/furrow: acral lesions Parallel-like fingerprint: solar lentigo
Starburst	Radial arrangement of pigmented streaks	Spitzoid lesions (nevus of Reed, atypical Spitz tumors, spitzoid melanoma)
Lacuna	Round/oval, variously sized structures with smooth borders, reddish, blue-purplish or black	Angioma, angiokeratoma, vascular lesions
Unspecific	Featureless lesions that cannot be classified by any of the other previous patterns	Suggestive for malignancy

Table 1.2 Definitions of metaphoric terms according to the third consensus conference of the International Dermoscopy Society in 2016

Term	Definition
Pigment network	
Pigment network	Grid-like pattern consisting of interconnecting pigmented lines surrounding hypopigmented holes
Typical pigment network	Network with minimal variability in the color, thickness, and spacing of the lines; symmetrically distributed
Delicate network	Light brown, thin network lines
Atypical pigment network	Network with increased variability in the color, thickness, and spacing of the lines of the network; asymmetrically distributed; gray color
Broadened network	Widening of the network lines
Negative network	Serpiginous interconnecting broadened hypopigmented lines that surround elongated and curvilinear globules
Shiny white structures	
Shiny white streaks	Short discrete white lines oriented parallel and orthogonal (perpendicular) to each other seen only under polarized dermoscopy
Shiny white blotches and strands	Bright white structures in the form of circles, oval structures (shiny white clods), large structureless areas, or longer and less well-defined lines than shiny white steaks oriented parallel or distributed haphazardly; seen only under polarized dermoscopy
Rosettes	Four bright white dots or clods arranged together as a square (or a four-leaf clover)
Globules	
Regular	Globules with minimal variability in their color, size, and shape
Cobblestones	Polygonal globules symmetrically distributed throughout the lesion
Rim of brown globules	Globules distributed at the periphery of the lesion
Irregular	Globules with variability in color, size, shape, or spacing and distributed in an asymmetric fashion

Table 1.2 (continued)

Term	Definition
Dots	
Regular	Dots distributed all over the lesion or clustered at the center of the lesion, or located on the network lines (also called target network)
Irregular	Any distribution of dots other than dots as described for regular dots
Streaks	
Radial streaming	Radial linear extensions at the lesion edge
Pseudopods	Bulbous and often kinked projections seen at the lesion edge, often directly associated with a network
Branched streaks	Broadened or widened network with broken lines and incomplete connections
Patterns	
Starburst pattern	This pattern consists of peripheral globules, pseudopods, or streaks (or a combination of them), located around the entire perimeter of the lesion
Homogeneous pattern	A pattern lacking any definable pigment structures, structureless pattern
Cerebriform pattern	Thick curved lines created by gyri and keratin-filled sulci; these gyri and sulci coalesce forming a brain-like appearance
Fingerprint pattern	Light brown thin curved lines that do not interconnect to form a network; these tend to be linear to curvilinear; they correspond to small and thin gyri
Rainbow pattern	Circumscribed structureless areas displaying colors of the whole spectrum of visible light
Strawberry pattern	Reddish pseudonetwork (erythema and wavy fine vessels) around hair follicle openings that are accentuated with a white halo appearance
Blotch	Dark structureless areas
Regular	One blotch within the center of the lesion and surrounded by network
Irregular	More than one blotch or a blotch that is located off the center
Regression structures	
Peppering/granularity	Consists of fine dots with a blue-gray color
Scarlike depigmentation	Area of white that is whiter than surrounding normal-appearing skin (true scarring); it should not be confused with hypopigmentation or depigmentation caused by simple loss of melanin; shiny white structures and blood vessels are not seen in areas of regression
Blue whitish veil	An irregular shaped blotch of blue hue with an overlying whitish ground-glass haze
Angulated lines (polygons, zig-zag pattern)	Gray-brown lines that are connected at an angle or coalescing to form polygons
Central white patch	Central white structureless area
Leaflike areas	Brown to gray/blue discrete linear or bulbous structures coalescing at a common off-center base creating structures that resemble a leaflike pattern
Spoke wheel area	Well-circumscribed radial projections, usually light brown but sometimes blue or gray in color meeting at a central darker clod that has a dark brown, black, or blue color
Blue gray ovoid nest	Well-circumscribed ovoid structures with confluent or near confluent blue-gray pigmentation
Milia-like cyst (cloudy or starry)	White to yellowish round opalescent structures corresponding to intraepidermal cysts; when they are small and bright they are called starry; when they are larger and less bright they are called cloudy
Comedo-like opening	Round to oval keratin-filled clefts
Crypts	Keratin-filled invaginations that are larger than comedo-like openings
Moth-eaten border	Border with concave or sharp punched-out invaginations
Milky-red areas	Milky-white appearance or pinkish structureless areas (strawberry ice cream–like) with no specific distinguishable vessels
Facial skin	
Annular granular pattern	Dots and structureless areas arranged around follicle openings (and involving adnexal opening)
Rhomboids	Gray-brown angulated lines forming a polygonal shape around adnexal openings
Pseudonetwork	A structureless pigment area interrupted by nonpigmented adnexal openings
Asymmetric pigmented follicular openings	Pigment associated with adnexal opening that does not uniformly surround the entire opening or curved (or crescent-shaped) pigment lines partially surrounding adnexal openings

(continued)

Table 1.2 (continued)

Term	Definition
Acral skin	
Parallel furrow pattern	Volar pigmentation forming parallel, thin, solid or dotted lines on the furrows (sulci superficiales or invaginations in dermatoglyphics); the lines are occasionally doubled, each line along a furrow
Parallel ridge pattern	Volar pigmentation forming parallel, diffuse, and irregular lines along the ridges or cristae superficiales (raised portion of the dermatoglyphics)
Lattice-like pattern	Volar pigmentation forming thin parallel lines on the furrows or sulci superficiales and crossing perpendicular on the ridges
Fibrillar pattern	Linear pigmented filamentous lines of similar length with one end at the furrows and oriented at a certain angle to the furrows, crossing the ridges

Modified from ref. [70]

1.6.1.1 Age

In lesions on the same body area, for example, the trunk, we usually observe a pattern evolution of nevi through the years: globular pattern <16 years, reticular pattern in 30–50 years, homogenous pattern >50 years. A lesion showing globular pattern/peripheral globules is suggestive for activity, and over the age of 40 years should be regarded with suspect and selected for strict follow-up.

1.6.1.2 Skin Type

Furthermore, in a given body area, we can detect different patterns in nevi according to the skin phototype: in patients with skin type I, the pattern is more commonly that of a homogenous center with a peripheral reticular pattern; in skin type III patients, the pattern is more commonly that of a uniform reticular pattern.

1.6.2 Lesion-Specific Features: The Analytic Approach

In general, two main strategies were developed to approach dermoscopic images, the "analytic" and the "heuristic" approach [58]. The analytic approach was essentially based on the assessment of peculiar/predefined features inside the skin lesion [58, 59]. The diagnostic conclusion is obtained scoring the individual features and following the calculation proposed by one of the algorithms. Several algorithms aimed to help novices in achieving the correct dermoscopic diagnoses that have been proposed in the last decades: in general, they were developed based on a calculation checklist and individual scoring assigned to pre-selected dermoscopic features [60].

1.6.3 Color and Symmetry: The Heuristic Approach

When evaluating a pigmented skin lesion, the novice is required to assess the color/s and symmetry/asymmetry of the dermoscopic image.

1.6.3.1 Color

In case of pigmented lesions, the color observed under the dermoscopic lens mainly depends on the depth of melanin/melanocytic nest localization, resulting from the reflection through the light overlying dermal/epidermal layer (Fig. 1.6). Hence, recognizing a specific color helps the novice to determine the level of melanin in the skin. The schematic classification for melanocytic skin lesions on common sites (see below) can be summarized as follow (Fig. 1.6):

- *Black color—superficial epidermis*
- *Brown color—epidermal–dermal junction*
- *Gray color—papillary dermis*
- *Blue color—reticular dermis*

Non-melanocytic skin lesions display a great variety of colors, including brown (e.g., pigmented actinic keratosis), black (e.g., melanoacanthoma, congealed blood), blue (e.g., foreign body/radiation therapy tattoo), gray (e.g., seborrheic keratoses, lichenoid keratoses), white

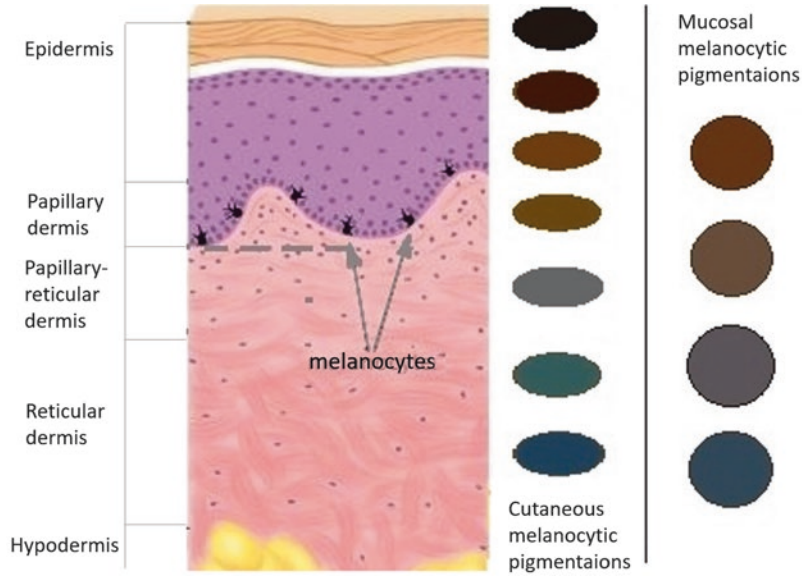

Fig. 1.6 Perception of melanin localized at different epidermal/dermal levels due to the optical interference of keratin/cellular layer. From left to right: histological section; color range generated by melanin localized at common body site; color range generated by melanin localized at mucous membranes. *Black* = stratum corneum; *dark brown* = epidermis; *brown* = basal layer of the epidermis; *light brown* = epidermal–dermal junction; *light gray* = papillary dermis; *gray* = papillary dermis and *blue* = reticular dermis

(e.g., keratinized/milia cysts/scarring lesions/dermatofibroma/melanoma regression [61]), yellow (e.g., xanthomatous lesions, drug pigmentations [62, 63]), orange (e.g., granulomatous lesions, sebaceous hyperplasia), red (e.g., vascular lesions [64]), and pink (e.g., increased inflammation, psoriasis, and melanoma). In general, we can observe one to three combinations of defined color in benign lesions, while the presence of multiple inhomogeneous colors variously mixed is suggestive for malignancy. The exception of hypo/amelanotic melanoma or featureless melanoma should always be kept in mind: in these cases, few or no pigmentation is visible, and only the vascular pattern and the strict follow-up can allow to diagnose these lesions [17, 29, 30].

1.6.3.2 Symmetry

Together with the pattern analysis, the recognition of lesion-specific features, and color, the degree of symmetry of a lesion should be evaluated. In general, greater degrees of symmetry are more likely to be benign, whereas malignant lesions are more frequently highly asymmetrical. The degree of symmetry/asymmetry is quite subjective, accordingly it must be considered in combination with all other dermoscopic and non-dermoscopic features to help formulate a diagnosis. The ABCD rule of dermoscopy includes this evaluation (i.e., "A", asymmetry) suggesting "to define the presence of asymmetry of contour, colours and structures in 0/1/2 perpendicular axes" [57].

In general, the pigment network of an acquired melanocytic nevus is defined "symmetric"—and thus, typical—if it displays a regularly meshed, narrowly spaced network, usually thinning out at the periphery (e.g., "gently fading borders"), light to dark brown in color, distributed more or less regularly throughout the lesion. Streaks and globules must be symmetrically distributed at the periphery to suggest benignity. An asymmetric—atypical—pigmented network is irregularly meshed, often thickened, it is composed of pigment lines irregularly distributed throughout the lesion, usually ending abruptly at the periphery (e.g., "clear-cut borders"), and it is characterized by one or multiple colors (black, brown, or gray colors or a combination of these). The presence of irregularly sized dots/globules, especially if

situated near the periphery, may contribute to the asymmetry.

For what concerns the "visual-global heuristic approach," it is focused on the recognition and description of general characteristics of the lesion, such as heterogeneity in color, architectural disorders, symmetry, and border sharpness (e.g., CASH algorithm) [61] or on the individuations of the entity of chaos of structures inside the lesions and/or of specific clues suggestive for diagnosis (e.g., CHAOS and CLUES) [65].

1.6.4 Analytic vs. Heuristic Approach

Mixed approaches relies on the individuation of both elements [66, 67]. Thus, the more the physician increases his experience in dermoscopy, the more he is able to rapidly recognize the overall pattern of the given lesion, thus moving from the analytic to the heuristic approach. Indeed, both approaches required a long and specific dermoscopic trainee in order to be able to correctly interpret dermoscopy images. In addition, no one between analytic and heuristic seems to be more efficient than the other for teaching dermoscopy to novices [68]. In particular, the algorithm derived from the analytic approach required high levels of dermoscopic skills and resulted often poorly clear and feasible for the novices in dermoscopy [69].

1.6.5 Dermoscopy Consensus in the Years 2000–2018

The dermoscopic vocabulary evolved through the decades, as real language do: a huge number of terms and definition were variously used, often similar, sometimes evolving into new ones. In general, the *descriptive* dermoscopic terms were progressively "coded" into *metaphoric* terms, hence one referring to specific aspect/biological structure of the lesions [3, 7, 8, 70]. As an example, the descriptive terminology "*Lines, white, perpendicularly*" corresponds to the "*Shiny white streaks* (former synonyms: *chrysalis/chrysalids/crystalline structures*)" metaphoric term, the descriptive term "*Structureless zone, white*" corresponds to the metaphoric "*Scarlike depigmentation*" term, while the "*Structureless zone, pink*" is the descriptive term for "*Milky-red areas*" metaphoric term.

To overcome the "confusion" in dermoscopic terminology, in 2003 the Consensus Net Meeting on dermoscopy was held in order to well define the dermoscopic structures and to validate a two-step procedure for the evaluation of pigmented lesions [3, 7, 8]. Subsequently, evolving dermoscopic terminology has led to initiate new consensus in order to establish a dictionary of standardized terms. Furthermore, a third new algorithmic morphologic method based on pattern analysis was proposed by Kittler in 2007, based on the individuation of five simple geometric elements (lines, pseudopods, circles, clods, and dots) that variously combined and constitute all patterns observable by dermoscopy [70]. Several dermoscopic dictionaries are available online nowadays, but www.dermoscopedia.org still represents the referring "e-learning manual" of dermoscopy, supported by the International Society of Dermoscopy (IDS). This web platform is continuously enriched by the contributions of about 150 dermatologists all over the world and currently coordinated by R Braun, A Lallas, A Marghoob, and K Hoffmeyer. In 2016, the results of the third consensus conference of IDS were published [70]. In that was reported the "glossary" of descriptive-metaphoric terminology, along with the "biological" significance of each structure [70]. As an example, the metaphoric term "*pigment network*" was established to code the descriptive terminology "*Lines, reticular*," suggesting melanoma. "*Lines, reticular and thick*" was coded as "*broadened network,*" "*Lines, reticular and thin*" was coded as "*delicate network,*" with biological significance of a melanocytic nevus. "*Lines, reticular and thick or reticular lines that vary in color*" corresponds to the "*Atypical pigment network,*" with the biological significance of melanoma. The description "Lines, reticular, hypopigmented, around brown clods" corresponds to the metaphoric term "Negative pigment network (synonyms: *inverse network/reticular depigmentation*)," that is found in Spitz nevi (regular) or in spitzoid melanoma (irregular).

1.7 Dermoscopy at Special Body Sites

We said that the dermoscopic appearance of a pigmented lesion varies depending on the body site. Indeed, the body surface can be divided into two macro-areas for dermoscopic examination [69]. A third macro-area of dermoscopy application is the observation of adnexa, namely hair and nails. Thus, we can distinguish three fields of examination of our dermoscope according to anatomical classification, as follows:

1. *Common sites*: Trunk, scalp, neck, arms, forearms, back of the hands, bottom, thighs, legs, and back of the feet
2. *Special sites*: Face, nipple and areola, palms, soles, oral/genital/anal mucosa (i.e., *mucoscopy*), conjunctiva, and sclera
3. *Adnexa*: Hairs (i.e., *trichoscopy*) and nails (i.e., *onichoscopy*)

We should remind that the aforementioned dermoscopic classifications and considerations are globally valid for lesions localized on common body sites. On the other hand, lesions at special body site show peculiar features and a very different dermoscopic appearance, thus they are separately discussed here below [71–79].

1.7.1 Palmoplantar Skin

Pigmented skin lesions developing on glabrous skin of palms and soles display peculiar clinical shapes and thus dermoscopic features different from all other body sites. This results from the specific anatomy of the skin and the geometry of melanin disposition in these locations, as illustrated in Fig. 1.7 [79]. Taken together, findings from physical, optical, histopathological, and electron microscopy studies [79–81] together revealed that benign melanocytic nests are dis-

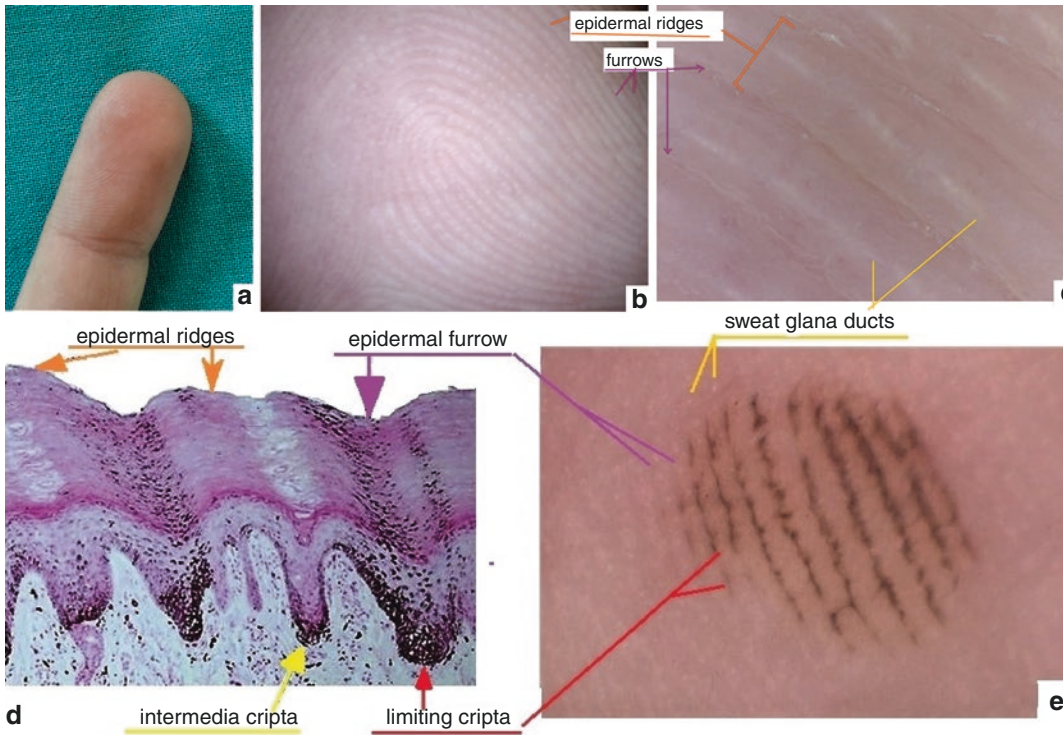

Fig. 1.7 Alternation of epidermal ridges and furrows that characterize palmar skin, clinical (**a**) and dermoscopic appearance under low (**b**) and high magnification (**c**) polarized dermoscopy (*HorusHS600*). Histological section of a plantar nevus (HE staining, 20×) (**d**) shows both the pigment distribution in cripta limitans and, in a lesser extent, in cripta intermedia, and their alignment with surface ridge/furrows; polarized dermoscopy (17×) of a typical parallel furrow pattern of a plantar nevus (**e**)

tributed in *crista limitans* and, in a lesser extent, in *cripta intermedia*, generate an optical reflection of melanin on the stratum corneum (Fig. 1.7c), resulting in brown parallel lines. Cripta limitans are anatomically alienated with the surface furrows (Fig. 1.7a,b), thus generating the dermoscopic "parallel furrow" pattern (Fig. 1.7d), which is the most frequently detected in plantar/palmar nevi. Then, several other dermoscopic patterns and/or their variants can be encountered on palmoplantar skin, here enlisted:

- *Parallel furrow pattern*
- *Fibrillar*
- *Lattice-like*
- *Homogeneous*
- *Globular*
- *Globulo-streak-like*
- *Reticular*
- *Non-typical*

We must remind that the dermoscopic appearance of acral lesions is largely influenced by the different degree of pressure at different foot point, generating a horizontal shift of the melanin column in the stratum corneum [82]. Nevertheless, it should be kept in mind that a physiological benign evolution can be observed, especially in plantar nevi: homogeneous to fibrillar pattern transformation, probably due to repetitive microtraumatism; fibrillar/homogenous to parallel furrow pattern, probably resulting from a combination of age-related changes and pressure-induced changes [80, 81].

Melanocytic pigmentation on the ridge is suggestive for malignant proliferation, thus the "parallel ridge pattern" is considered a hallmark of acral melanoma, with high specificity at all ages [78, 83]. In addition, considering the global approach to the lesion, two other elements can suggest the diagnosis of acral melanoma, namely irregular diffuse pigmentation (i.e., asymmetry of colors, irregular blotches) and the bizarre pattern (i.e., asymmetry of structures).

On the other hand, there is a series of benign conditions showing "false-positive" parallel ridge pattern, such as drug-induced pigmentation (e.g., 5-fluorouracile and capecitabine) [62], exogenous stain pigmentation (e.g., paraphenylenediamine), post-traumatic hemosiderin accumulation under the stratum corneum [77], vascular pigmentations, exogenous parasites pigmentations, and Peutz-Jeghers syndrome. Finally, there are benign congenital acral nevi that can display parallel furrow pattern lifelong [84], while acral melanoma can sometime simulate a double parallel furrow pattern [85]. A thorough monitoring should always be adopted in these patients; in addition, the "furrow ink test" could be of help recognizing the pattern in doubtful cases [85].

1.7.2 Facial Skin

Pigmented lesions of the face are generally grouped into flat, palpable, and nodular.

1.7.2.1 Pigmented Flat Lesions

Facial skin is characterized by flattened rete ridge and presence of regularly spaced follicular infundibula sebaceous glands and acrosyringia. Pigment network is formed by the pigmentation of the elongated rete ridges of the epidermis with melanocytes in the basal layer of the epidermis or melanin in basal keratinocytes. Dense pigment rings (the grid) are due to projections of rete pegs or ridges. The paler "holes" are due to projections of dermal papillae. Since the dermo–epidermal junction is flat on the face and rete ridges are quite not present, flat pigmented lesions of the face display a widened meshed pigmented network (pseudonetwork or homogeneous pattern) resulting from the combination of larger "holes" corresponding to adnexa and a homogeneous pigmentation around. The diagnosis of flat pigmented lesions on the face may be challenging because of the morphologic overlap of biologically different lesions, such as benign nevi, lentigo, pigmented actinic keratoses, lichenoid keratosis, and early lentigo maligna [86]. In general, observing the presence of gray color in a flat facial lesion under dermoscopy should induce to suspect malignancy until

diversely demonstrated (i.e., lichenoid keratoses). The presence of scale, white circles, and a sharply demarcated border are clues to the dermoscopic diagnosis of pigmented actinic keratoses. In the early differential diagnosis lentigo maligna from pigmented actinic keratosis, dermoscopy alone still demonstrates poor sensitivity, and the histopathology remains to date the gold standard [87].

1.7.2.2 Palpable and Nodular Lesions

Dermoscopic clues for benign (e.g., seborrheic keratoses, dermatofibroma, Spitz nevus, xanthogranuloma and Leishmaniasis) and malignant (keratoacanthoma, squamous cell carcinoma, basal cell carcinoma, and Merkel cell carcinoma) palpable to nodular neoformations of the face are basically the same as in other body sites and are listed in Table 1.3.

Table 1.3 Overview of dermoscopic structures, named either in the descriptive and metaphoric terminology, and their clinical significance, according to the third consensus conference of the International Dermoscopy Society in 2016

Descriptive term	Metaphotric term	Clinical significance
Lines		
Lines, reticular	Pigment network	Melanocytic lesions dermatofibroma, solar lentigo
Lines, reticular, and thick	Broadened network	Melanoma
Lines, reticular, and thin	Delicate network	Melanocytic nevi
Lines, reticular, and thick or reticular lines that vary in color	Atypical pigment network	Melanoma
Lines, reticular, hypopigmented, around brown clods	Negative pigment network (former synonyms: inverse network and reticular depigmentation)	Melanoma, Spitz nevus
Lines, white, perpendicularly	Shiny white streaks (former synonyms: chrysalis, chrysalids and crystalline structures)	Melanoma, BCC, Spitz nevus, dermatofibroma
Lines, branched	Branched streaks	Melanocytic lesion
Lines, radial (always at periphery)	Streaks	Reed nevus, melanoma, recurrent nevus
Lines, radial, and segmental	Radial streaming	Melanoma, recurrent nevi
Lines, radial, connected to a common base	Leaflike areas (sometimes variously shaped large clods have also been termed leaflike areas)	BCC
Lines, radial, converging to a central dot or clod	Spoke wheel area (sometimes a clod within a clod has also been termed spoke-wheel area/concentric structure)	BCC
Lines, curved, and thick	Cerebriform pattern (former synonyms: brainlike appearance) to describe the pattern and fissures and ridges (former synonyms gyri and sulci and fat fingers) to describe the structural components of the pattern	SK
Lines, brown, curved, parallel, thin	Fingerprinting	Solar lentigo
Lines, curved, and thick, in combination with clods	Crypts	SK
Lines, parallel, short, crossing ridges (volar skin)	Fibrillar pattern	Acral nevi
Lines, parallel, thick, on the ridges (volar skin)	Parallel ridge pattern	Acral melanoma
Lines, parallel, thick, in the furrows, and crossing the ridges (volar skin)	Latticelike pattern	Acral nevi

(continued)

Table 1.3 (continued)

Descriptive term	Metaphotric term	Clinical significance
Lines		
Lines, parallel, thin, in the furrows (volar skin)	Parallel furrows pattern	Acral nevi
Lines, angulated, or polygonal (facial skin)	Rhomboids/zig-zag pattern	Lentigo maligna
Lines, angulated, or polygonal (nonfacial skin)	Angulated lines/polygons	Lentiginous melanomas (nonfacial, nonacral)

Pseudopods		
Radial, circumferential pseudopods, or lines	Starburst pattern	Reed nevus

Clods		
Clods, small, round, or oval	Globules	Various diagnoses
Clods, brown, circumferential	Rim of brown globules	Growing nevi
Clods, brown, yellow, or orange (rarely black)	Comedo-like openings	SK
Clods, brown or blue, concentric (clod within a clod)	Concentric globules	BCC
Clods, brown or skin colored, large and polygonal	Cobblestone pattern	Dermal nevi
Clods, blue, large, clustered	Blue-gray ovoid nests	BCC
Clods, blue, small	Blue globules	BCC
Clod within a clod (concentric clods)	Variant of spoke wheel area	BCC
Clods, white, shiny	Shiny white blotches and strands	BCC
Clods, pink, and small	Milky-red globules	Melanoma
Clods, red, or purple	Red lacunes	Hemangioma

Dots		
Dots, any color	Granularity or granules	Various diagnoses
Dots, gray	Peppering	Melanoma, LPLK
Dots, gray and circles, gray	Annular-granular pattern	Lentigo maligna
Dots or clods, white, clustered or disseminated	Milia-like cysts, cloudy or starry	SK
Dots, white, four, arranged in a square	Rosettes	Various diagnoses but mainly AK, SCC, actinic-damaged skin
Dots, peripheral, arranged in lines	Linear dots	Pigmented Bowen's disease
Dots, brown, central (in the center of hypo-pigmented spaces between reticular lines)	Targetoid dots	Congenital nevi

Circles		
Circles, white		SCC
Circles, concentric	Circle within a circle	Lentigo maligna
Circles, incomplete	Asymmetric pigmented follicular openings	Lentigo maligna

Structureless		
Structureless zone, brown or black	Blotch	If central: hypermelanotic Clark (dysplastic) nevus; if eccentric: melanoma
Structureless zone, blue	Blue-whitish veil	Melanoma
Structureless zone, pink	Milky-red areas	Melanoma
Structureless zone, white	Scarlike depigmentation	Melanoma
Structureless zone, white, central	Central white patch	Dermatofibroma
Structureless zone, polychromatic	Rainbow pattern	Various diagnoses
Structureless, red, interrupted by follicular openings	Strawberry pattern	AK
Structureless, brown (tan), eccentric		Melanoma
Structureless, any color	Homogenous pattern	Various diagnoses
Structureless, brown, interrupted by follicular openings (facial skin)	Pseudonetwork	Facial pigmented lesions

Table 1.3 (continued)

Other			
Sharply demarcated, scalloped border		Moth-eaten border	Solar lentigo
Vessel morphology			
Dots		Tiny pinpoint vessels	Flat melanocytic lesions, inflammatory diseases, Bowen's disease
Clods	Red-purple lacunes	More or less sharply demarcated, roundish, or oval areas with a reddish, red-bluish, maroon, or dark red to black coloration, separated from each other by intervening stroma, without vessels inside the lacunae	Hemangioma
Linear		Linear, mildly curved vessels, considered irregular when different sizes, shapes, and curves with a haphazard, or random distribution are presented and considered regular when short and fine (thin) linear vessels prevail	Various diagnoses
Coiled	Glomerular	Tightly coiled vessels resembling the glomerular apparatus of the kidney	Bowen's disease
Looped	Hairpin	Two parallel linear vessels forming a half-looped or hairpin-like structure	SK, viral warts
Serpentine	Linear irregular	Linear vessels with multiple bends	Flat BCC, melanoma
Helical	Corkscrew	Twisted looped vessels with bends twisted along a central axis	Melanoma, metastasis
Curved	Comma	Linear, curved, short vessels	Dermal nevi
Monomorphous		One type of vessel dominates	Various diagnoses
Polymorphous		Multiple types of vessels are present	May indicate malignancy in appropriate context, for example in flat melanocytic lesions
Vessel arrangement			
Radial	Crown vessels	Radial, serpentine, or arborizing vessels at the periphery of the lesion that radiate toward the center but do not cross the midline of the lesion	Sebaceous hyperplasia
Serpiginous	String of pearls	Coiled or dotted vessels arranged in lines	Clear cell acanthoma
Branched	Arborizing vessels	Bright red, sharply in focus, large or thick-diameter vessels dividing into smaller vessels	BCC
Clustered		Coiled or glomerular vessels arranged in groups	Bowen's disease
Centered dots	Targetoid vessels	Red dots (vessels) in the center of hypopigmented space between reticular lines	Congenital melanocytic nevus

Modified from ref. [70]
BCC basal cell carcinoma, *SK* seborrheic keratosis, *LPLK* lichen planus-like keratosis, *AK* actinic keratosis, *SCC* squamous cell carcinoma

1.7.3 Nipple and Areola

Nipple and areola can be considered as special sites as well, as lesion on these areas show site-specific appearance that significantly differs from that of pigmented skin lesions at common body sites [72]. Nevi on areola/nipple are quite common and often display "peculiar" features, such as hormone-induced hyperpigmentation, inflammation due to micro-traumatism, particular/less regular vascular pattern (i.e., nipple and areola skin shows an erythematous background and focused linear vessels even in normal conditions). It is not infrequent to see these lesions

biopsied in the suspicion of melanoma, which is actually rare on this site. Another malignant tumor affecting this area is Paget's disease, which can mimic both eczema and inflammatory diseases. Dermoscopy is thus particularly useful at this site, where a wide spectrum of conditions from benign tumors to inflammatory diseases cannot be differentiated on clinical ground only. Careful comparative dermoscopy examination can hence reduce the need for a surgical excision in order to have a histological diagnosis is frequent, sparing possible functional and esthetic sequelae in this sensitive site [72, 88].

1.7.4 Oral and Anogenital Mucosa

Oral semi-mucosae and mucosa include a series of special body sites, such as the lips, the palate, the tongue, and the gingiva. Anogenital semimucosae and mucosae include anal semimucosa, perineum; major labia, minor labia, external vagina, and gland. All these areas are characterized by a thinner epidermis, the absence of the stratum corneum, and the presence of an overlying physiological mucus, producing different optical effects under dermoscopy (also defined as "mucoscopy") [75, 89]. Generally, pigmented lesions in these areas show homogenous pattern, unfocused pigment network and less clear-cut border, compared with other common sites. Moreover, colors of benign pigmentation belong to a narrow range of nuances from brownish-gray to gray. In particular, the gray homogenous color of benign mucosal melanosis, in absence of other asymmetric structures of multicomponent coloration, is likely to be related to the presence of melanin-laden inflammatory cells in the papillary dermis [74]. In general, the combination of structureless zones with blue/gray/white color in mucosal lesions is the most significant dermoscopic sign of malignancy [90]. Other peculiarities of tumors at mucosal sites are yellowish fibrinous superficial material instead of erosion, absence of keratinization, papillomatous surface (especially the tongue), and evidence of Wickham reticulum in lichen planus lesions. Non-pigmented tumoral lesions can be more difficult to identify because they can mimic inflammatory and infectious diseases; in these cases, the presence of specific vascular pattern/in-focus vessels and/or regression signs should be researched.

1.7.5 Conjunctiva/Sclera

Conjunctival lesions include a large and varied spectrum of conditions, ranging from inflammatory lesions to benign or malignant epithelial/vascular/melanocytic/lymphoid tumors. Though extremely useful to spare surgical biopsy for histopathological confirmation, dermoscopic examination in this area requires particular equipment. The ophthalmologic examination is currently performed through the slit lamp, a binocular microscope equipped with an optical system that only provides clinical images of the anterior segment of the eye at high magnifications. A way to realize high-quality dermoscopic examination is using a digital camera combined with a videodermoscope (or a hand-held camera photosystem) at 20× magnification, covering the tip of the dermoscope with a sterile transparent film to be changed for each patient. A topical anesthetic ointment (e.g., oxybuprocaine hydrochloride/tetracaine hydrochloride 1%) must be applied in the inferior conjunctival fornix of the eye and an appropriate transparent ophthalmic gel should be delivered over the sclera/conjunctiva region to be examined [71, 91].

Compared with nevi, melanomas of the conjunctiva are reported to have a more intense pigmented network, irregular dots confluent in a structureless pattern and a higher prevalence of gray color, probably determined by the melanocytic invasion of the superficial stromal portion. Indeed, conjunctival melanoma is by definition not limited to the epithelium (i.e., a proliferation of melanocytes that invade the stroma) differently from cutaneous melanoma. Primary acquired melanoses often show regularly distributed light brown dots, and small cysts are frequently observed in congenital/acquired nevi. Squamous cell carcinomas display peculiar hairpin and glomerular vessels.

1.8 Dermoscopy of the Nails and Hairs

1.8.1 Onichoscopy

Dermoscopy of the nails (i.e., onichoscopy) includes the examination of the nail plate, the proximal nail fold, the hyponychium, and the distal edge of the nail plate. A complete dermoscopic examination should include both contact oil immersion dermoscopy and polarized contact dermoscopy, to ensure optimal observation of the nail structures and avoid keratin-induced reflection. Onichoscopy is today essential to differentiate acral melanoma from acquired nevi of the nail plate in case of longitudinal melanonychia. Signs of malignancy described to date include width of the pigmented band (≥2/3 of the nail plate), gray and/or black color, irregularly pigmented lines, Hutchinson (i.e., pigmentation extending to the proximal nail fold) and micro-Hutchinson signs, a nail dystrophy, and granular pigmentation [92]. Furthermore, onichoscopy is useful to recognize and differentiate a wide range of infective (e.g., tinea unguium), inflammatory (e.g., lichen planus and psoriasis), autoimmune (e.g., alopecia areata), paraneoplastic and drug-induced (e.g., anti-proliferative agents) conditions affecting the nail apparatus, and/or monitor their response to therapy [44, 93].

1.8.2 Trichoscopy

Introduced in 2006, the term trichoscopy collectively refers to the examination of the hairs and scalp surface [94]. Low magnification (17–20×) hand-held dermoscopy can support the physician in the diagnosis of scarring and non-scarring alopecia of the scalp and scalp pigmented neoformation (e.g., nevus sebaceous [95]). Moreover, defined trichoscopic patterns have been described to differentiate infectious (e.g., pediculosis and tinea capitis) [96] and/or inflammatory (e.g., alopecia areata) [14], or post-traumatic lesions [97], especially in pediatric population. The effectiveness of therapies for alopecia areata/alopecia androgenetica/telogen effluvium, etc. can be easily carried out by means of hand-held dermoscopy [98].

High-magnification videodermoscopy (40–100×) and super high magnification videodermoscopy (400×) allow to analyze the structure and size of growing hair shafts directly on the scalp, avoiding the necessity of pulling of multiple hairs differently from light microscopy method [99]. The spectrum of genetic disorders variously affecting the hair growth and hair shafts is large, and early trichoscopic examination can help dermatologists and pediatricians to early diagnose of otherwise unrecognized de novo syndromic conditions [98, 99].

References

1. Tanaka M. Dermoscopy. J Dermatol. 2006; 33:513–7.
2. Argenziano G, Soyer HP. Dermoscopy of pigmented skin lesions – a valuable tool for early diagnosis of melanoma. Lancet Oncol. 2001;2:443–9.
3. Argenziano G, et al. Dermoscopy of pigmented skin lesions: results of a consensus meeting via the Internet. J Am Acad Dermatol. 2003;48:679–93.
4. Pehamberger H, Binder M, Steiner A, Wolff K. In vivo epiluminescence microscopy: improvement of early diagnosis of melanoma. J Invest Dermatol. 1993;100:356S–62S.
5. Sinz C, et al. Accuracy of dermatoscopy for the diagnosis of nonpigmented cancers of the skin. J Am Acad Dermatol. 2017;77:1100–9.
6. Babino G, et al. Dermoscopy of melanoma and non-melanoma skin cancer. G Ital Dermatol Venereol. 2015;150:507–19.
7. Weber P, Tschandl P, Sinz C, Kittler H. Dermatoscopy of neoplastic skin lesions: recent advances, updates, and revisions. Curr Treat Options in Oncol. 2018;19:56.
8. Kittler H, Pehamberger H, Wolff K, Binder M. Diagnostic accuracy of dermoscopy. Lancet Oncol. 2002;3:159–65.
9. Vestergaard ME, Macaskill P, Holt PE, Menzies SW. Dermoscopy compared with naked eye examination for the diagnosis of primary melanoma: a meta-analysis of studies performed in a clinical setting. Br J Dermatol. 2008;159:669–76.
10. Mayer J. Systematic review of the diagnostic accuracy of dermatoscopy in detecting malignant melanoma. Med J Aust. 1997;167:206–10.
11. Russo T, Piccolo V, Lallas A, Argenziano G. Recent advances in dermoscopy. F1000Res. 2016;5.
12. Tognetti L, et al. Ecthyma contagiosum (Orf): reflectance confocal microscopy and histopathological cor-

relates. Skin Res Technol. 2019;25(2):234–7. https://doi.org/10.1111/srt.12618.
13. Tognetti L, Sbano P, Fimiani M, Rubegni P. Dermoscopy of Biett's sign and differential diagnosis with annular maculo-papular rashes with scaling. Indian J Dermatol Venereol Leprol. 2017;83:270–3.
14. Tognetti L, Cinotti E, Perrot J-L, Campoli M, Rubegni P. Syphilitic alopecia: uncommon trichoscopic findings. Dermatol Pract Concept. 2017;7:55–9.
15. Tognetti L, et al. New findings in non-invasive imaging of cutaneous endometriosis: dermoscopy, high-frequency ultrasound and reflectance confocal microscopy. Skin Res Technol. 2018;24:309–12.
16. Micali G, Lacarrubba F, Massimino D, Schwartz RA. Dermatoscopy: alternative uses in daily clinical practice. J Am Acad Dermatol. 2011;64:1135–46.
17. Micali G, Verzì AE, Lacarrubba F. Alternative uses of dermoscopy in daily clinical practice: an update. J Am Acad Dermatol. 2018;79:1117–1132.e1.
18. Jha AK, Sonthalia S, Lallas A. Dermoscopy as an evolving tool to assess vitiligo activity. J Am Acad Dermatol. 2018;78:1017–9.
19. Errichetti E, Stinco G. Clinical and dermoscopic response predictors in psoriatic patients undergoing narrowband ultraviolet B phototherapy: results from a prospective study. Int J Dermatol. 2018;57:681–6.
20. Manfredini M, et al. In vivo monitoring of topical therapy for acne with reflectance confocal microscopy. Skin Res Technol. 2017;23:36–40.
21. Lacarrubba F, Nasca MR, Verzì AE, Micali G. A novel topical agent in the treatment of seborrheic keratoses: a proof of concept study by clinical and dermoscopic evaluation. Dermatol Ther. 2017;30.
22. Benati E, et al. Dermoscopy and reflectance confocal microscopy for monitoring the treatment of actinic cheilitis with ingenol mebutate gel: Report of three cases. Dermatol Ther. 2018;31:e12613.
23. Micali G, et al. Clinical, ultrasound, and videodermatoscopy monitoring of psoriatic patients following biological treatment. Skin Res Technol. 2016;22:341–8.
24. Ribero S, et al. Confocal microscopy and dermoscopy for the monitoring of BRAF inhibitor therapy of melanoma skin metastases. Br J Dermatol. 2017;176:1101–2.
25. Dermoscopic follow-up of therapeutic response in mantle cell lymphoma with secondary involvement of the scalp. – PubMed – NCBI. https://www.ncbi.nlm.nih.gov/pubmed/30520227. Accessed 20 Dec 2018.
26. Borgia F, Giuffrida R, Lentini M, Palazzo R, CANNAVò SP. Follicular mucinosis with diffuse scalp alopecia treated with narrow-band UVB phototherapy: the role of trichoscopy in monitoring therapeutic outcomes. G Ital Dermatol Venereol. 2016;151:212–5.
27. Xiong Y-Q, et al. Comparison of dermoscopy and reflectance confocal microscopy for the diagnosis of malignant skin tumours: a meta-analysis. J Cancer Res Clin Oncol. 2017;143:1627–35.
28. Wang SQ, et al. Differences in dermoscopic images from nonpolarized dermoscope and polarized dermoscope influence the diagnostic accuracy and confidence level: a pilot study. Dermatol Surg. 2008;34:1389–95.
29. Campos-do-Carmo G, Ramos-e-Silva M.Dermoscopy: basic concepts. Int J Dermatol. 2008;47:712–9.
30. Dermoscopy. http://www.dermoscopy.org/. Accessed 16 Dec 2018.
31. Stolz W, Braun-Falco O, Bilek P, et al., editors. Color atlas of dermatoscopy. Oxford, UK: Blackwell Science Inc; 1994. p. 3.
32. Friedman RJ, Rigel DS, Silverman MK, Kopf AW, Vossaert KA. Malignant melanoma in the 1990s: the continued importance of early detection and the role of physician examination and self-examination of the skin. CA Cancer J Clin. 1991;41:201–26.
33. Saphir J. Die Dermatoskopie. I. Mitteilung. Arch Dermatol Syph. 1920;128:1–19.
34. Goldman L, Younker W. Studies in microscopy of the surface of the skin; preliminary report of technics. J Invest Dermatol. 1947;9:11–6.
35. Goldman L. Some investigative studies of pigmented nevi with cutaneous microscopy. J Invest Dermatol. 1951;16:407–27.
36. Goldman L. A simple portable skin microscope for surface microscopy. AMA Arch Derm. 1958;78:246–7.
37. Cinotti E, et al. Season and anatomic site effect on skin color and xerosis quantified using an ultra-high definition videodermoscope. IEEE. 2016; https://doi.org/10.1109/MeMeA.2016.7533791.
38. Pehamberger H, Steiner A, Wolff K. In vivo epiluminescence microscopy of pigmented skin lesions. I. Pattern analysis of pigmented skin lesions. J Am Acad Dermatol. 1987;17:571–83.
39. Steiner A, Pehamberger H, Wolff K. In vivo epiluminescence microscopy of pigmented skin lesions. II. Diagnosis of small pigmented skin lesions and early detection of malignant melanoma. J Am Acad Dermatol. 1987;17:584–91.
40. Gewirtzman AJ, Saurat J-H, Braun RP. An evaluation of dermoscopy fluids and application techniques. Br J Dermatol. 2003;149:59–63.
41. Benvenuto-Andrade C, et al. Differences between polarized light dermoscopy and immersion contact dermoscopy for the evaluation of skin lesions. Arch Dermatol. 2007;143:329–38.
42. Introduction to Dermoscopy | DermNet New Zealand. https://www.dermnetnz.org/cme/dermoscopy-course/introduction-to-dermoscopy/. Accessed 16 Dec 2018.
43. Pan Y, et al. Polarized and nonpolarized dermoscopy: the explanation for the observed differences. Arch Dermatol. 2008;144:828–9.
44. Alessandrini A, Starace M, Piraccini BM. Dermoscopy in the evaluation of nail disorders. Skin Appendage Disord. 2017;3:70–82.
45. Ingraffea AA. Innovative use of a polarized magnifier and a smart phone: a microscope in your pocket. Dermatol Surg. 2013;39:796.

46. Fleming MG. Digital dermoscopy. Dermatol Clin. 2001;19:359–367, ix.
47. Kardynal A, Olszewska M. Modern non-invasive diagnostic techniques in the detection of early cutaneous melanoma. J Dermatol Case Rep. 2014;8:1–8.
48. Micali G, Lacarrubba F. Dermatoscopy: instrumental update. Dermatol Clin. 2018;36:345–8.
49. Bleicher B, Levine A, Markowitz O. Going digital with dermoscopy. Cutis. 2018;102:102–5.
50. Dusi D, Rossi R, Simonacci M, Ferrara G. Image gallery: the new age of dermoscopy: optical super-high magnification. Br J Dermatol. 2018;178:e330.
51. Bahmer FA, et al. Terminology in surface microscopy. Consensus meeting of the Committee on Analytical Morphology of the Arbeitsgemeinschaft Dermatologische Forschung, Hamburg, Federal Republic of Germany, Nov. 17, 1989. J Am Acad Dermatol. 1990;23:1159–62.
52. Soyer HP, Smolle J, Hödl S, Pachernegg H, Kerl H. Surface microscopy. A new approach to the diagnosis of cutaneous pigmented tumors. Am J Dermatopathol. 1989;11:1–10.
53. Argenziano G, et al. Epiluminescence microscopy for the diagnosis of doubtful melanocytic skin lesions. Comparison of the ABCD rule of dermatoscopy and a new 7-point checklist based on pattern analysis. Arch Dermatol. 1998;134:1563–70.
54. Dal Pozzo V, Benelli C, Roscetti E. The seven features for melanoma: a new dermoscopic algorithm for the diagnosis of malignant melanoma. Eur J Dermatol. 1999;9:303–8.
55. Kenet RO, et al. Clinical diagnosis of pigmented lesions using digital epiluminescence microscopy. Grading protocol and atlas. Arch Dermatol. 1993;129:157–74.
56. Menzies SW, Ingvar C, McCarthy WH. A sensitivity and specificity analysis of the surface microscopy features of invasive melanoma. Melanoma Res. 1996;6:55–62.
57. Nachbar F, et al. The ABCD rule of dermatoscopy. High prospective value in the diagnosis of doubtful melanocytic skin lesions. J Am Acad Dermatol. 1994;30:551–9.
58. Scope A, Benvenuto-Andrade C, Agero ALC, Marghoob AA. Nonmelanocytic lesions defying the two-step dermoscopy algorithm. Dermatol Surg. 2006;32:1398–406.
59. Marghoob AA, Braun R. Proposal for a revised 2-step algorithm for the classification of lesions of the skin using dermoscopy. Arch Dermatol. 2010;146:426–8.
60. Carrera C, et al. Validity and reliability of dermoscopic criteria used to differentiate nevi from melanoma: a web-based international dermoscopy society study. JAMA Dermatol. 2016;152:798–806.
61. Rubegni P, et al. A risk scoring system for the differentiation between melanoma with regression and regressing nevi. J Dermatol Sci. 2016;83:138–44.
62. Tognetti L, Fimiani M, Rubegni P. Benign dermoscopic parallel ridge pattern in plantar hyperpigmentation due to capecitabine. Dermatol Pract Concept. 2015;5:79–81.
63. Tognetti L, Garosi G, Rongioletti F, Fimiani M, Rubegni P. Livedo racemosa and hemolytic uremic syndrome induced by gemcitabine. Int J Dermatol. 2016;55:e555–6.
64. Tognetti L, et al. Benign and malignant collision tumors of melanocytic skin lesions with hemangioma: dermoscopic and reflectance confocal microscopy features. Skin Res Technol. 2018;24:313–7.
65. Rosendahl C, Cameron A, McColl I, Wilkinson D. Dermatoscopy in routine practice – 'chaos and clues'. Aust Fam Physician. 2012;41:482–7.
66. Soyer HP, et al. Three-point checklist of dermoscopy. A new screening method for early detection of melanoma. Dermatology. 2004;208:27–31.
67. Argenziano G, et al. Seven-point checklist of dermoscopy revisited. Br J Dermatol. 2011;164:785–90.
68. Tschandl P, Kittler H, Schmid K, Zalaudek I, Argenziano G. Teaching dermatoscopy of pigmented skin tumours to novices: comparison of analytic vs. heuristic approach. J Eur Acad Dermatol Venereol. 2015;29:1198–204.
69. Tognetti L, et al. An integrated clinical-dermoscopic risk scoring system for the differentiation between early melanoma and atypical nevi: the iDScore. J Eur Acad Dermatol Venereol. 2018;32:2162–70.
70. Kittler H, et al. Standardization of terminology in dermoscopy/dermatoscopy: results of the third consensus conference of the International Society of Dermoscopy. J Am Acad Dermatol. 2016;74:1093–106.
71. Cinotti E, et al. Dermoscopy for the diagnosis of conjunctival lesions. Dermatol Clin. 2018;36:439–49.
72. Cinotti E, et al. Nipple and areola lesions: dermoscopy and reflectance confocal microscopy features. J Am Acad Dermatol. 2018;81:610–3.
73. Cinotti E, Perrot J-L, Labeille B, Cambazard F. A dermoscopic clue for scurvy. J Am Acad Dermatol. 2015;72:S37–8.
74. Cinotti E, et al. In vivo confocal microscopic substrate of grey colour in melanosis. J Eur Acad Dermatol Venereol. 2015;29:2458–62.
75. Cinotti E, et al. Dermoscopic and reflectance confocal microscopy features of two cases of vulvar basal cell carcinoma. Dermatol Pract Concept. 2018;8:68–71.
76. Feci L, Fimiani M, Rubegni P. Parallel-ridge pattern on dermatoscopy: observation in a case of purpura traumatica pedis. Dermatol Pract Concept. 2015;5:27–9.
77. Rubegni P, Feci L, Fimiani M. Talon Noir: utility of dermoscopy for differential diagnosis with respect to other acral skin growths. G Ital Dermatol Venereol. 2012;147:133–4.
78. Rubegni P, et al. Dermoscopy and digital dermoscopy analysis of palmoplantar 'equivocal' pigmented skin lesions in Caucasians. Dermatology. 2012;225:248–55.
79. Balois T, Chatelain C, Ben Amar M. Patterns in melanocytic lesions: impact of the geometry on growth and transport inside the epidermis. J R Soc Interface. 2014;11:20140339.

80. Saida T, Koga H, Goto Y, Uhara H. Characteristic distribution of melanin columns in the cornified layer of acquired acral nevus: an important clue for histopathologic differentiation from early acral melanoma. Am J Dermatopathol. 2011;33:468–73.
81. Nagashima Y, Tsuchida T. Correspondence between dermoscopic features and epidermal structures revealed by scanning electron microscope. J Dermatol. 2011;38:35–40.
82. Ozdemir F, Karaarslan IK, Akalin T. Variations in the dermoscopic features of acquired acral melanocytic nevi. Arch Dermatol. 2007;143:1378–84.
83. Lallas A, et al. The BRAAFF checklist: a new dermoscopic algorithm for diagnosing acral melanoma. Br J Dermatol. 2015;173:1041–9.
84. Roldán-Marín R, et al. Atypical dermoscopic presentation of an acral congenital melanocytic nevus in an adult: parallel ridge pattern and its histologic correlation. Dermatol Pract Concept. 2015;5:23–6.
85. Braun RP, Thomas L, Kolm I, French LE, Marghoob AA. The furrow ink test: a clue for the dermoscopic diagnosis of acral melanoma vs nevus. Arch Dermatol. 2008;144:1618–20.
86. Tschandl P, Rosendahl C, Kittler H. Dermatoscopy of flat pigmented facial lesions. J Eur Acad Dermatol Venereol. 2015;29:120–7.
87. Costa-Silva M, et al. Dermatoscopy of flat pigmented facial lesions-evolution of lentigo maligna diagnostic criteria. Dermatol Pract Concept. 2018;8:198–203.
88. Kolm I, et al. Diagnostic pitfall: pigmented lesion of the nipple – correlation between dermoscopy, reflectance confocal microscopy and histopathology. Dermatology. 2011;222:1–4.
89. Jha AK, Zeeshan MD, Jha Amar AK. Mucoscopy in lingual varicosities. Dermatol Pract Concept. 2018;8:54–5.
90. Blum A, et al. Dermoscopy of pigmented lesions of the mucosa and the mucocutaneous junction: results of a multicenter study by the International Dermoscopy Society (IDS). Arch Dermatol. 2011;147:1181–7.
91. Cinotti E, et al. Handheld reflectance confocal microscopy for the diagnosis of conjunctival tumors. Am J Ophthalmol. 2015;159:324–333.e1.
92. Benati E, et al. Clinical and dermoscopic clues to differentiate pigmented nail bands: an International Dermoscopy Society study. J Eur Acad Dermatol Venereol. 2017;31:732–6.
93. Piraccini BM, Bruni F, Starace M. Dermoscopy of non-skin cancer nail disorders. Dermatol Ther. 2012;25:594–602.
94. Pirmez R, Tosti A. Trichoscopy tips. Dermatol Clin. 2018;36:413–20.
95. Ankad BS, Beergouder SL, Domble V. Trichoscopy: the best auxiliary tool in the evaluation of nevus sebaceous. Int J Trichology. 2016;8:5–10.
96. Elghblawi E. Tinea capitis in children and trichoscopic criteria. Int J Trichology. 2017;9:47–9.
97. Cutrone M, Grimalt R. The dermoscopic 'pluck out sign' for beard trichotillomania. Skin Appendage Disord. 2018;4:15–7.
98. Verzì AE, Lacarrubba F, Micali G. Use of low-cost videomicroscopy versus standard videodermatoscopy in trichoscopy: a controlled, blinded noninferiority trial. Skin Appendage Disord. 2016;1:172–4.
99. Rudnicka L, Olszewska M, Waśkiel A, Rakowska A. Trichoscopy in hair shaft disorders. Dermatol Clin. 2018;36:421–30.

2 Dermoscopy for Benign Melanocytic Skin Tumors

Giulia Tonini, Andrea Andreassi, and Elisa Cinotti

Although histopathology at the present stage remains the "gold" standard in the diagnosis of melanocytic proliferations, the introduction of dermoscopy opened a new morphologic dimension and allowed clinicians to observe colors and structures within nevi not visible to the unaided eye, to more precisely predict the histopathology diagnosis and therefore to improve on their clinical diagnostic accuracy [1]. Melanocytic nevi (MN) are heterogeneous benign melanocytic proliferations, most frequently located in the skin. Their development is a multifactorial process under genetic and environmental influences [2]. Acquired melanocytic nevi (AMN) are the most common group of nevi. They can occur on any cutaneous site and usually measure less than 6 mm [3]. Three main clinical categories of AMN, which relate to their dermoscopic and histopathological growth pattern, have been described: junctional nevi (JN), dermal nevi (DN), and compound nevi (CN) [2].

2.1 Junctional Nevi

JN are light to dark brown macules with uniform color distribution, but typically darker in the center [2, 4]. JN are usually non-palpable and are not restricted to sun-exposed anatomical areas, although their development has been associated with sun exposure [1, 5]. They usually arise during childhood and tend to be smaller than DN or CN [4].

On dermoscopy, a uniform reticular pattern of a light to dark brown color typically dominates with the occasional inclusion of small dots and globules [4]. Reticular pattern consists of a network of brownish interconnected lines over a background of a tan diffuse pigmentation (Fig. 2.1a) [1]. Individuals with skin phototype I typically exhibit nevi with a light brown reticular pattern (which is however sometimes less evident or visible) and a central hypopigmentation, whereas individuals with a skin phototype IV mostly show nevi with a dark brown reticular pattern and a central hyperpigmentation (so-called black or hypermelanotic nevi) [1, 4].

Reticular pattern is predominantly found in adults and is commonly observed in AMN on the upper and mid back [2]. It has frequently been correlated with JN histology, which is characterized by nests of melanocytes at the tips of regularly elongated, notedly pigmented rete ridges [1].

2.2 Dermal Nevi

DN are skin-colored or light brown papules that are either soft dome-shaped or pedunculated. Their surfaces can be smooth or mamillated.

G. Tonini (✉) · A. Andreassi · E. Cinotti
Department of Medical, Surgical and Neurological Science, Dermatology Section, University of Siena, S. Maria alle Scotte Hospital, Siena, Italy

M. Fimiani et al. (eds.), *Technology in Practical Dermatology*,
https://doi.org/10.1007/978-3-030-45351-0_2

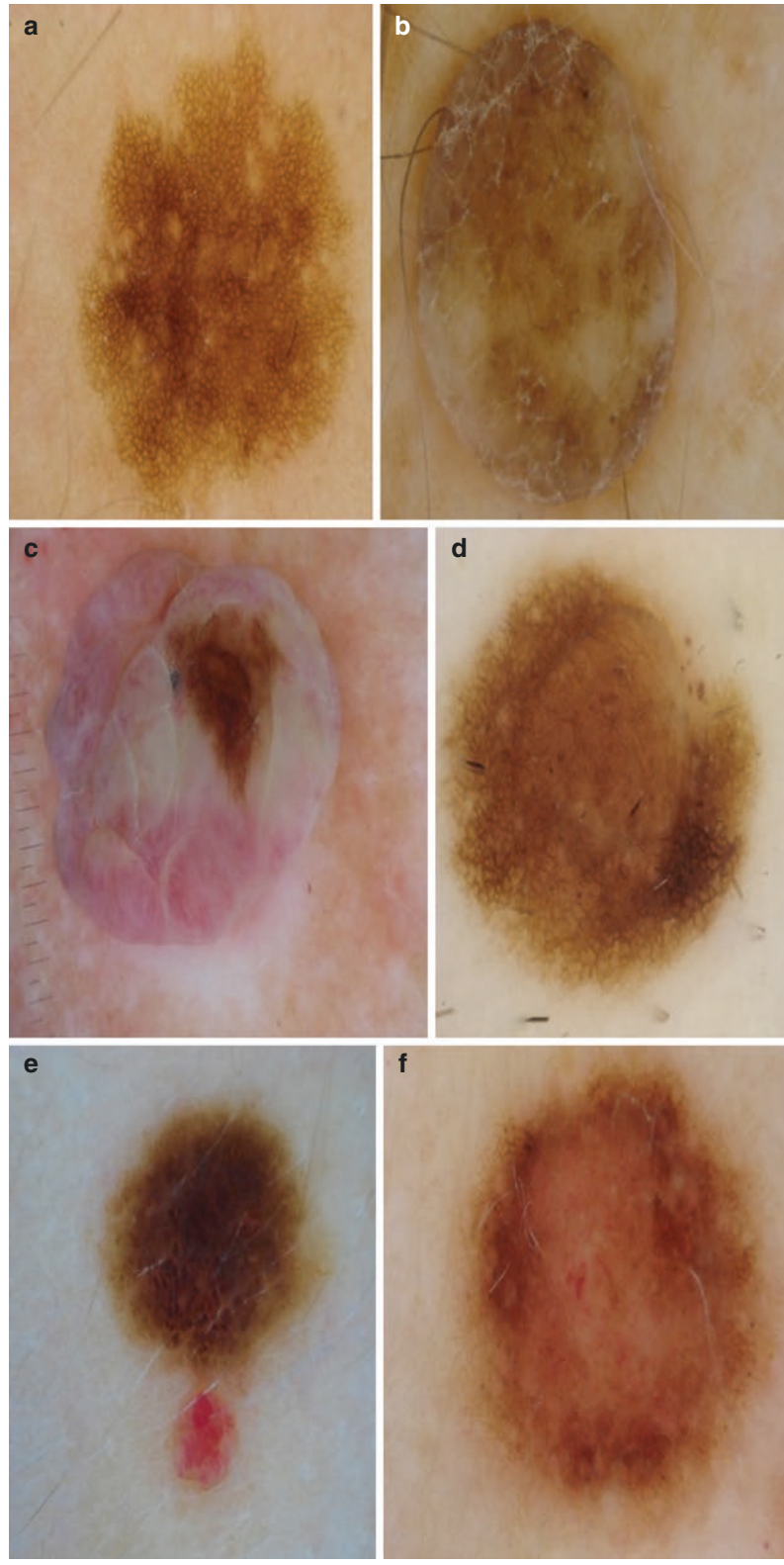

Fig. 2.1 Dermoscopy of junctional, dermal, and compound nevi. (**a**) Reticular pattern in a junctional nevus. (**b**) Light brown dermal nevus with terminal hair. (**c**) Eccentric light brown pigmentation in homogeneous pattern in a pink dermal nevus. (**d**) Raised papular compound nevus with peripheral pigmented network. (**e**) Compound nevus with homogeneous and globular pattern. (**f**) Compound nevus with peripheral reticular pattern and linear and comma vessels in the hypopigmented center of the lesion

DN are often associated with terminal hairs or even telangiectatic vessels (Fig. 2.1b), which may help to distinguish them from other types of common nevi or nodular basal cell carcinomas. In larger lesions, pseudohorn cysts (accumulations of keratin within epidermal invaginations) can be observed [2, 4]. Another unique characteristic of intradermal nevi is the presence of a "wobble" sign, which is defined as the mobility of a lesion when the dermoscopic head compresses the nevus and its ability to be manipulated in a gentle rocking motion. The wobble sign can be particularly useful in helping to differentiate an intradermal nevus from a basal cell carcinoma [6].

On dermoscopy, intradermal nevi typically lack a pigment network; if pigment is present, it is usually light brown and found in a homogenous pattern (structureless pigmentation in the absence of pigment network or other distinctive local features) (Fig. 2.1c) or occasionally in globular (numerous, variously sized, round to oval structures with various shades of brown and gray-black) or cobblestone pattern (large, closely aggregated, somehow angulated globule-like structures resembling a cobblestone) [1, 4]. In hypopigmented or non-pigmented nevi, vascular features may be the most prominent dermoscopic features. Comma vessels are the most commonly found, with hairpin vessels and dotted vessels also found occasionally [4].

Homogenous patterns are frequently seen in DN, often with many comma vessels. Arborizing vessels are less frequently observed. The out-focus of these vessels helps to distinguish them from those seen in basal cell carcinoma. DN can also show comedo-like openings and milia-like cysts [2].

The globular pattern is more frequent in childhood and is commonly found in AMN arisen on the upper trunk. The presence of peripheral globules has been shown to correlate to growing nevi. Cobblestone pattern nevi have been associated with the presence of terminal hairs, comedo-like openings, and/or milia-like cysts. Like the globular pattern, it is commonly found in AMN arisen on the upper trunk, and it is also common in congenital nevi. The cobblestone pattern is not associated with any particular age [2].

DN histopathology is characterized by variable large nests of melanocytes in the dermis [1].

Variants of intradermal nevi include *Unna nevi* and *Miescher nevi* [4].

Unna nevi are found on the trunk and extremities, and they can exhibit a variety of dermoscopic patterns. The homogenous pattern is the most common, followed by the globular and reticular ones. *Unna nevi* exhibiting the globular pattern may present with a cerebriform feature. Large light or dark brown globules of uniform size and distribution are seen, along with exophytic papillary structures sometimes separated by comedo-like openings. Comma vessels are most commonly observed, while dotted and polymorphous vessels are occasionally found [4, 7].

Miescher nevi are located on the face, and they typically show a pseudonetwork pattern arranged around facial follicular openings. Comedo-like openings and milia-like cysts may also be visible [4, 8].

2.3 Compound Nevi

CN are slightly elevated, pigmented papules with either a smooth or a papillomatous surface (Fig. 2.1d). With age, these nevi may become more elevated and change color. Their color is often homogenous and can range from tan to dark brown. Acquired CN are often difficult to differentiate from smaller congenital nevi, as they may also demonstrate terminal hairs [2, 4].

On dermoscopy, CN typically show a globular pattern with uniform-sized globules distributed throughout the lesion (Fig. 2.1e). A cobblestone pattern may be seen if the globules are large and closely aggregated. A reticular pattern is usually found at the periphery (Fig. 2.1f). Regularly distributed areas of hypopigmentation can also be present. Vascular features are difficult to appreciate under dermoscopy, but when they are visible, linear irregular vessels or comma vessels may be detected (Fig. 2.1f) [1, 4].

Variants of CN count the solid pink, eclipse, cockade, and halo nevi.

Solid pink nevi are typically seen in fair-skinned individuals with skin phototypes I and II. They are characterized by the absence of a prominent pigment network or by dotted or polymorphous vessels [4, 9].

Eclipse nevi are tan macules with a brown peripheral rim with overall starburst appearance. Clinically, the brown rim may appear asymmetric and irregular when it is discontinuous. The size of eclipse nevi ranges from 4 mm to greater than 10 mm. They may be located on the trunk in adults as an individual's signature nevi and on the scalp in children. Dermoscopically, the peripheral rim demonstrates an organized pigment network, that is absent in the central area [4, 10].

Cockade nevi are pink to darkly pigmented, targetoid, often papular lesions that appear morphologically similar to eclipse nevi except that they include a central area of pigmentation. They are typically 4–10 millimeters in size and are most commonly found on the trunk and on the scalp of children and adolescents [4, 11]. The target-like shape arises from a centrally pigmented zone being surrounded by an intermediate non-pigmented area that is then bordered by a pigmented rim [4]. On dermoscopy, cockade nevi show an organized pigment network in both the central and peripheral pigmented areas, while the non-pigmented intermediate zone is pigment-free [4]. Histologically, the central nevus is junctional or compound, whereas the non-pigmented zone is free from nevus cells, and the peripheral halo is composed of junctional melanocytic nests [11, 12].

Halo nevi (Sutton nevi) are pigmented melanocytic nevi surrounded by a ring of depigmentation. They are most frequently seen in children or young adults (approximately 15 years of age) [11]. Although most commonly found on the back, they may be present at any anatomic site and may even be arranged in a cluster [4]. Halo nevi typically undergo four different stages of evolution, which may overlap: the pigmented portion of the nevus (stage I) may change to become pink colored (stage II) and may eventually disappear, leaving only a circular area of depigmentation (stage III), which may undergo gradual repigmentation (stage IV) taking months to years until completion [4]. On dermoscopy, halo nevi typically show a globular or homogenous pigment pattern with blue pepper-like granules and additionally white scar-like regions [11]. As halo nevi evolve and the central melanocytic area becomes pink, the only dermoscopic feature that may be evident in the previously pigmented lesion may be dotted vessels and some telangiectasias in the surrounding depigmented halo [13]. In histopathology, a dermal lichenoid infiltrate composed of lymphocytes and melanophages is observed [11, 12]. An isolated melanocytic lesion with a halo component, asymmetric, and with unknown evolution in an adult needs histopathologic examination to exclude a melanoma, due to the existence of a rare phenomenon called halo melanoma [13].

2.4 Congenital Melanocytic Nevi

Congenital melanocytic nevi (CMN) are characteristically present at birth or appear shortly thereafter. They may not become visible until months to years after birth, due to inherent delays in the development of pigment. With time, CMN can enlarge, become darker, develop terminal hairs, or form new nodules [4]. About size, CMN may be classified into different categories: small (<1.5 cm); medium (M1: 1.5–10 cm, M2: 10–20 cm); large (L1: 20–30 cm, L2: 30–40 cm); and giant (G1: 40–60 cm, G2: >60 cm) [14]. CMN are typically brown to black macules or patches with either a smooth or gravelly texture and with irregular borders [4]. CMN most frequently occur on the trunk, followed by the extremities and head and neck [2]. Histopathological features of CMN include nevus cells in the deep reticular dermis and in the subcutis, nevus cells in and around adnexal structures (hair follicles and eccrine glands), and horizontal, dermal infiltrations of nevus cells between collagen bundles [15].

On dermoscopy, CMN show different pigment patterns: reticular, globular, cobblestone,

or homogenous [2]. The globular pattern is more commonly found in children under the age of 12 years and tends to present on the head, neck, and trunk. Instead, the reticular pattern is more commonly found in patients more than 12 years of age and is more frequently observed on the extremities [4]. Dermoscopic features, such as target network or globules, presence of terminal hairs, target vessels, and hypopigmentation of the skin furrows and around hair follicle openings, may help to distinguish CMN from AMN [2, 16].

2.5 Blue Nevi

Blue nevi (BN) are dermal proliferation of spindle melanocytes that generally arise during childhood or adolescence. Different variants of BN include common, cellular, sclerosing/desmoplastic, epithelioid combined, amelanotic, and deep penetrating [17]. BN are most common in younger patients and women. Although the majority of BN present as solitary lesions, cases of agminated blue nevi have been described (Fig. 2.2a,b) [18]. The characteristic gray-blue color seen in BN is

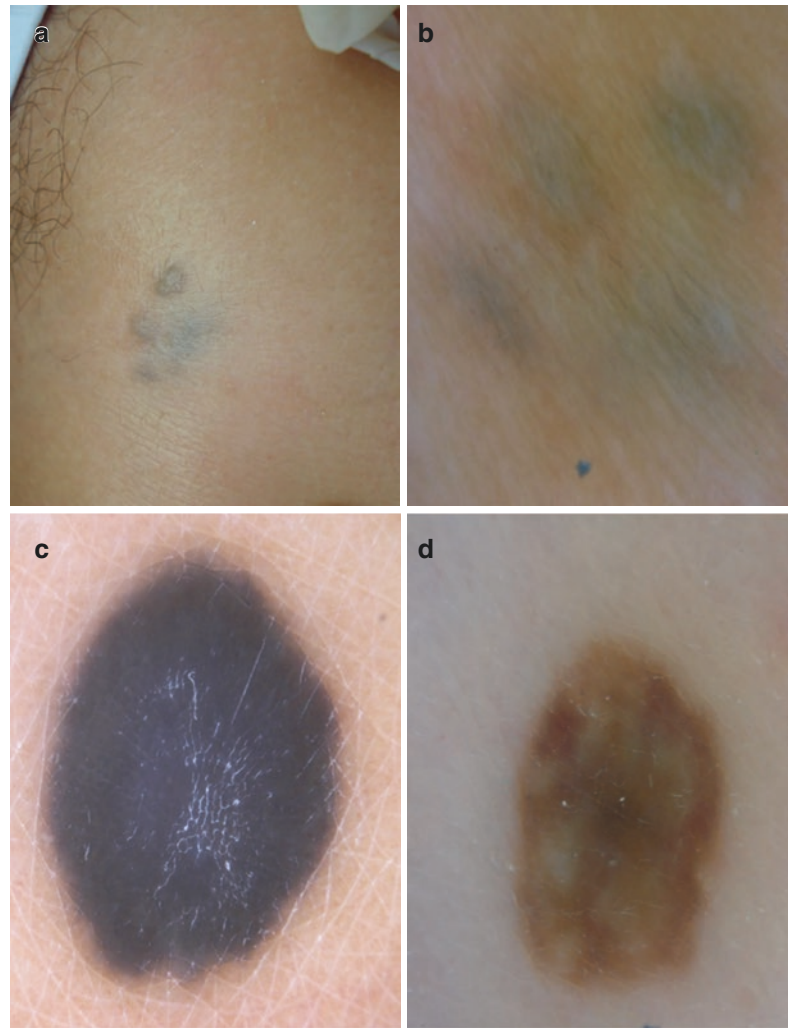

Fig. 2.2 Blue nevi. (**a**) Clinic and (**b**) dermoscopy of agminated blue nevus. (**c**) Dermoscopy of common blue nevus shows homogeneous and steel blue pigmentation. (**d**) Desmoplastic blue nevus shows regression features and polychromatic pattern with white, brown, and blue colors

due to the Tyndall effect, resulting from light scattering by dermal melanin [2].

Common BN usually present as macules or dome-shaped papules less than 10 mm in size. They most commonly arise on the scalp, neck, dorsum of hand or foot, and sacrum. Common BN can also be found on extra-cutaneous sites, in particular the uterus or cervix [19].

Cellular BN tend to present as black to gray-blue nodules or plaques measuring 1–3 cm. They are usually located on the sacrum or buttocks, but they can also arise on the head or feet [2].

Sclerosing or desmoplastic BN appear as blue papules or nodules with no anatomic predilection [2].

Epithelioid BN are usually located on the extremities and trunk and are more common in younger patients [20]. This type of BN is frequently associated with Carney complex/LAMB syndrome. Some lesions with features of epithelioid BN are referred to as pigmented epithelioid melanocytoma, which encompasses lesions ranging from benign epithelioid BN to borderline atypical epithelioid BN-like tumors [20].

Dermoscopically, BN are generally characterized by homogeneous, steel blue pigmentation resulting from melanocytes in the reticular dermis and absence of pigment network (Fig. 2.2c). The presence of this feature without any other findings is suggestive of BN with high specificity (99%) [21]. The main differential diagnosis is melanoma metastasis, and therefore, the clinical history and evolution are fundamental for a correct diagnosis. Other dermoscopic features, such as dots or globules, peripheral streaks, and network-like patterns, have been observed in 50% of lesions [21]. Whitish, scar-like areas corresponding to dermal fibrosis can also be present [22]. Different variants of BN can show peculiar dermoscopic features. The common type usually appears with a truly blue tone (Fig. 2.2c). The amelanotic type appears to have a whitish hue overlying the blue pigmentation. Combined BN show a focal brownish-blue color under dermoscopy due to the combination of a blue nevus with another melanocytic lesion [17]. Deep penetrating blue nevi tend to be polychromatic [17] with rapid morphologic changes [23]. Desmoplastic BN show regression features and polychromatic pattern with white and blue areas (Fig. 2.2d). Thirteen percent of BN demonstrate vessels (polymorphic, dotted, and comma) [24] [2]. Some differences in the morphology of BN can be observed depending on the use of polarized or non-polarized dermoscopy. Under non-polarized light, the blue pigmentation can appear darker and more heterogeneous, and local features (i.e., dots and globules) can become clearer. Under polarized light, BN can appear brownish or polychromatic [25].

Histopathologically, BN are dermal proliferations of pigmented spindle-shaped melanocytes, which can be located into the reticular dermis and involve adnexal structures. Most BN demonstrate stromal fibrosis, which is exaggerated in sclerosing BN, and pigmented melanophages. A junctional component is generally absent, with the exception of combined BN [2].

2.6 Spitz Nevi

Spitz nevi (SN) are congenital or acquired nevi, and they usually occur in children or young adults, appearing in individuals under the age of 20 years in a half to two thirds of cases [2, 11]. They arise as single, pink to red or skin-colored, dome-shaped papule usually measuring less than 1 cm [2]. SN are usually smooth, but can be verrucous [26]. Flat and polypoid variants are also described. SN are usually soft, but can be firm with a dermatofibroma-like texture [2]. Multiple lesions have been reported and can follow trauma, i.e. prior excision or radiation therapy [27]. In children, they usually appear on the face or head, while in young adults, they usually arise on the lower extremities, in particular in women [28].

Pigmented spindle cell nevi, or Reed nevi, are a variant of SN. They usually appear as dark brown to black papules with a smaller diameter than SN. They most frequently occur on the extremities, especially the lower legs of 30–40 years old women [2].

Dermoscopically, Spitz nevi are classified in three main patterns: "starburst pattern" (51%), a pattern of regularly distributed dotted vessels (19%) and globular pattern with reticular depigmentation (17%) [29].

Several infrequent dermoscopic patterns have also been reported in Spitz nevi and suggested to correspond to peculiar histopathological variants such as angiomatoid or desmoplastic Spitz nevus (Fig. 2.3a) [29].

The "starburst pattern," consisting of a central area of homogeneous black-blue pigmentation and symmetrically distributed peripheral streaks or pseudopods in a radial arrangement, typifies Reed nevus (Fig. 2.3b), while the globular pattern with reticular depigmentation (white lines surrounding globules) is associated with pigmented SN (Fig. 2.3c) [29]. Several additional patterns are also associated with pigmented Spitz nevus, including homogeneous, reticular, and multicomponent pattern [30].

Changes from globular (Fig. 2.3d) to starburst to homogenous patterns have been observed in evolving lesions, and they represent different stages of growth: during the phase of growth, they present with peripheral regular streaks, finger-like and globule-like pigmentation in a radiating pattern (starburst) which disappear after a few months, resulting in a homogeneous dermoscopic pattern with structureless brown/black pigmentation and finally spontaneous involution (Fig. 2.3e) [2, 11]. Pigmented SN can also be associated with blue-white veils, negative pigment networks, and polarizing shiny white structures [2]. The homogeneous and reticular patterns have been suggested to represent later evolution phases of the starburst pattern [29]. The reticular pattern can be regular and well defined or atypical due to broadened and thickened network lines [31]. A superficial black network has been observed in approximately 10% of lesions [32]. The prominent black lines seen in this kind of network are due to an abundance of melanin in the stratum corneum [31].

Non-pigmented Spitz nevi frequently display a pattern of dotted vessels in a regular distribution associated with reticular depigmentation or negative pigment network, consisting of white lines surrounding vessels (Fig. 2.3f) [29]. Regularly distributed dotted vessels represent the dermoscopic hallmark of non-pigmented Spitz nevus, and reticular depigmentation represents a frequent additional feature. In raised and nodular Spitz nevi, the vessels might project as larger red globules, coiled vessels, or even hairpin or corkscrew vessels with symmetry all over the lesion [29].

Histopathologically, SN are typically composed of vertically arranged nests or fascicles of large spindle and/or epithelioid cells. SN with spindle cells are usually junctional and are more frequently found on the lower limbs. SN with epithelioid cells tend to be intradermal and usually arise on the head [33].

2.7 Meyerson's Nevi (Eczematous Nevi)

Meyerson's phenomenon is defined as an eczematous halo around one or more nevi [34]. Clinical features consist of the appearance of erythematous halos with overlying scales sometimes accentuated at the peripheries of the erythematous zones. Eczematous nevi show a predilection for young healthy adults [12]. Most patients complain slight pruritus [35, 36]. Eczematous lesions become desquamative and clear spontaneously or resolve under topical corticosteroid therapy, while the nevus persists unchanged [12].

Dermoscopy is often challenging: even if Meyerson's phenomenon does not modify dermoscopic characteristics of involved nevi, patterns are often blurred by a yellowish overlying superficial serocrusts [11, 37].

Histopathological examination shows a nevus, generally compounded with associated parakeratosis, acanthosis, and sometimes epidermal spongiosis. Upper dermis has a perivascular lymphocytic infiltrate and sometimes with eosinophils [12].

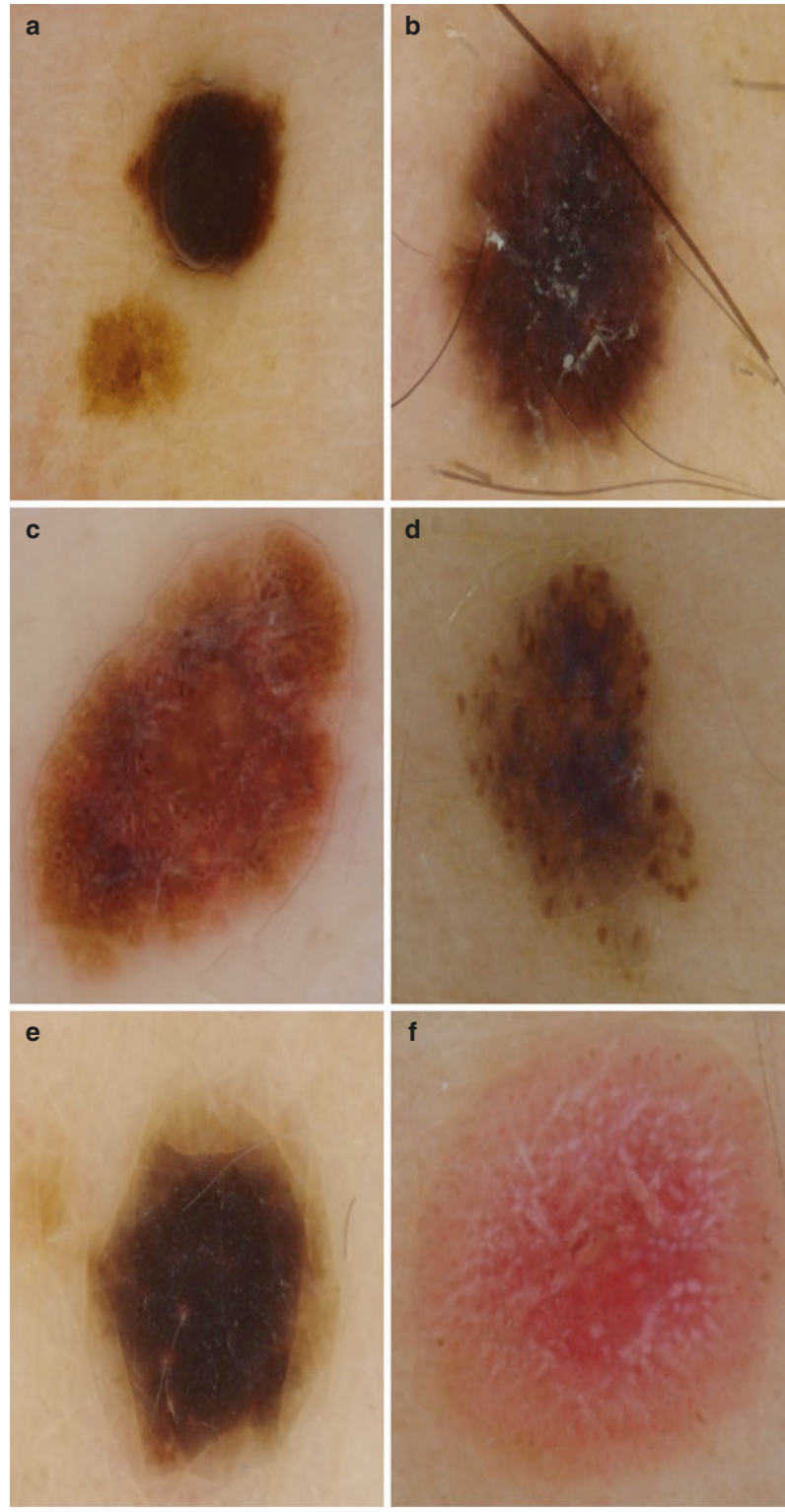

Fig. 2.3 Dermoscopy of Spitz–Reed nevi. (**a**) Dermoscopy of desmosplastic Spitz nevus with homogeneous pattern. (**b**) Reed nevus with "starburst pattern," consisting of a central area of homogeneous black-blue pigmentation and symmetrically distributed radial streaks at the periphery of the lesion. (**c**) Pigmented Spitz nevus shows globular pattern with reticular depigmentation. (**d**) Globular pattern in a Reed nevus. (**e**) Reed nevus shows homogeneous dermoscopic pattern with structureless brown/black pigmentation. (**f**) Non-pigmented Spitz nevus displays a pattern of dotted vessels in a regular distribution associated with reticular depigmentation

2.8 Desmoplastic Nevi

Desmoplastic nevi (DN) are a rarely reported, poorly characterized, benign melanocytic proliferation [38, 39]. They are usually small (up to 1 cm in diameter), flesh-colored, erythematous, or slightly pigmented papules or nodules often occurring on the extremities of young adults (mean age, 30 years), with a slight female predominance [39].

Dermoscopically, DN exhibit a tiny light brown network on a pinkish erythematous background [38]. DN are usually symmetric in color and structure, and they do not show any melanoma-specific criteria. DN share features with dermatofibroma, such as location on the extremities and size (ranging from few millimeters to 1 or 2 cm). Clinically, both lesions appear as firm papules or nodules that may sometimes cause clinical symptoms such as pain or itch. However, clinical dimpling sign [40] and the dermoscopic central white patch surrounded by a delicate pigment network [41] are quite specific features of dermatofibroma that are not detected in DN [12].

Histopathologically, DN show spindle-shaped or epithelioid melanocytes within a fibrotic stroma [38, 41].

2.9 Balloon Cell Nevi

Balloon cell nevi usually present as asymptomatic brown papules or polypoid lesions on the head/neck, trunk and extremities during the first three decades of life. They have typical histopathological features: typical large, vesicular, clear melanocytes called balloon cells. Balloon cells are melanocytes with pale-staining and vacuolated cytoplasms with a deficit in melanosome formation [12]. They are commonly seen in young adolescents with multiple nevi [11]. The most common site of the lesion appears to be the head and neck areas, followed by the trunk and extremities [42]. Dermoscopically, numerous aggregated white to yellow globular/clod structures correlate with the balloon cells found in histopathology [43–45].

2.10 Sclerosing Nevi with Pseudomelanomatous Features

Sclerosing nevi with pseudomelanomatous features or "nevi with regression-like fibrosis" (NRLF) are a recently classified entity which simulates regressing melanoma. They are induced by minor or unnoticed trauma on pre-existing nevi [46, 47]. NRLF is typically found on the convex area of the back of young to middle-aged men, i.e., the scapular area, probably due to the chronic trauma that frequently occurs in this body area or due to the effect of some concurrent "deep" inflammatory dermatosis (e.g., acne).

Dermoscopically, NRLF presents as atypical pigmented lesions showing overall features of regression, which is invariably extensive (between 10% and 50%) and polychromatic (coexisting white and blue areas), without melanoma-specific criteria [11, 12]. There are some criteria that rise the index of suspicion regarding NRLF: young or middle-aged patients; involvement of convex area of the back; regression with symmetric central distribution; blue or polychromatic regression; limited regression (<50% in the convex area of the back; <10% elsewhere) [12].

Histopathologically, a typical trizonal pattern can be observed: (I) atypical junctional proliferation and pagetoid spreading; (II) atypical melanocytic nests within dermal sclerosis; and (III) residual nevus tissue (often with congenital-like features) surrounding and within the cicatricial tissue [12]. In contrast with regressing melanoma, NRLF does not show cytological atypia, dermal mitosis, necrosis, tumoral melanosis, and nodules of atypical melanocytes [46, 47].

2.11 Targetoid Hemosiderotic Nevi

Targetoid hemosiderotic nevus (THN) is characterized by the sudden development of an asymptomatic ecchymotic, violaceous halo causing a target-like phenomenon around a long-lasting central elevated or exophytic nevus (globular nevi) [48]. It most frequently occurs on the upper

thorax of children and adolescents [48, 49]. Mechanical irritation, even not apparent, by clothing, shaving, or scratching is most common causes of injury. Tenderness and itching are common symptoms. It has been proposed that the rarity of THN is due to its spontaneous and rapid regression [48]. The main differential diagnosis is with targetoid hemosiderotic hemangioma (THH) that appears as a single, small, annular target-like lesion on the trunk or an extremity of young adults. THN is composed of a brown to violaceous central papule surrounded by a thin, pale area and a peripheral ecchymotic ring that enlarged and subsequently disappears, while the central papule persists. Other differential diagnoses are melanoma, traumatized angiokeratoma, hemosiderotic dermatofibroma, and cockade nevus [50, 51].

Dermoscopically, THN presents the typical features of globular melanocytic nevus with vascular hemorrhagic (red to purple or black) changes overlapped on the nevus and particularly around it: irregular sized and shaped, jet-black areas, and often comma-shaped vessels can be seen. The targetoid halo demonstrates a pale, ill-defined inner area surrounded by a homogeneous reddish zone with jagged margins [48, 49]. During the evolution, the central nevus persists and the ecchymotic halo ultimately disappears, without tendency to recur. Dermoscopy is of great help to differentiate blood (THH) from melanin pigmentation (THN) [12].

On histopathological examination, fibrin deposits, extravasates of erythrocytes and an increased number of ectatic blood vessels with hobnail endothelial cells are detected, amalgamated with nevus cells. Peripheral halo is characterized by extensive hemorrhage and hemosiderin deposits together with irregular, thin-walled, slit-shaped vascular channels that dissect between collagen bundles of the papillary dermis. A mild eosinophilic inflammatory infiltrate is also observed. After the eczema disappears, only scant hemosiderin deposits, fibrosis, and few collapsed vascular lumina in the papillary and mid-reticular dermis are seen [12].

References

1. Zalaudek I, Manzo M, Savarese I, Docimo G, Ferrara G, Argenziano G. The morphologic universe of melanocytic nevi. Semin Cutan Med Surg. 2009;28(3):149–56.
2. Rogers T, Marino ML, Raciti P, Jain M, Busam KJ, Marchetti MA, et al. Biologically distinct subsets of nevi. G Ital Dermatol E Venereol Organo Uff Soc Ital Dermatol E Sifilogr. 2016 Aug;151(4):365–84.
3. Oliveria SA, Yagerman SE, Jaimes N, Goodwin AI, Dusza SW, Halpern AC, et al. Clinical and dermoscopic characteristics of new naevi in adults: results from a cohort study. Br J Dermatol. 2013 Oct;169(4):848–53.
4. Kim JK, Nelson KC. Dermoscopic features of common nevi: a review. G Ital Dermatol Venereol. 2012;147:141–8.
5. Brodell R, Sims DM, Zaim MT. Natural history of melanocytic nevi. Am Fam Physician. 1988 Nov;38(5):93–101.
6. Braun RP, Krischer J, Saurat JH. The "wobble sign" in epiluminescence microscopy as a novel clue to the differential diagnosis of pigmented skin lesions. Arch Dermatol. 2000 Jul;136(7):940–2.
7. Niederkorn A, Ahlgrimm-Siess V, Fink-Puches R, Wolf IH, Richtig E, Lackner HK, et al. Frequency, clinical and dermoscopic features of benign papillomatous melanocytic naevi (Unna type). Br J Dermatol. 2009 Sep;161(3):510–4.
8. Rao BK, Wang SQ, Murphy FP. Typical dermoscopic patterns of benign melanocytic nevi. Dermatol Clin. 2001 Apr;19(2):269–84.
9. Johr RH. Pink lesions. Clin Dermatol. 2002 Jun;20(3):289–96.
10. Schaffer JV, Glusac EJ, Bolognia JL. The eclipse naevus: tan centre with stellate brown rim. Br J Dermatol. 2001 Dec;145(6):1023–6.
11. Woltsche N, Schmid-Zalaudek K, Deinlein T, Rammel K, Hofmann-Wellenhof R, Zalaudek I. Abundance of the benign melanocytic universe: dermoscopic-histopathological correlation in nevi. J Dermatol. 2017 May;44(5):499–506.
12. Larre Borges A, Zalaudek I, Longo C, Dufrechou L, Argenziano G, Lallas A, et al. Melanocytic nevi with special features: clinical-dermoscopic and reflectance confocal microscopic-findings. J Eur Acad Dermatol Venereol. 2014 Jul;28(7):833–45.
13. Kolm I, Di Stefani A, Hofmann-Wellenhof R, Fink-Puches R, Wolf IH, Richtig E, et al. Dermoscopy patterns of halo nevi. Arch Dermatol. 2006 Dec;142(12):1627–32.
14. Krengel S, Scope A, Dusza SW, Vonthein R, Marghoob AA. New recommendations for the categorization of cutaneous features of congenital melanocytic nevi. J Am Acad Dermatol. 2013 Mar;68(3):441–51.

15. Cribier BJ, Santinelli F, Grosshans E. Lack of clinical-pathological correlation in the diagnosis of congenital naevi. Br J Dermatol. 1999 Dec;141(6):1004–9.
16. Seidenari S, Pellacani G, Martella A, Giusti F, Argenziano G, Buccini P, et al. Instrument-, age- and site-dependent variations of dermoscopic patterns of congenital melanocytic naevi: a multicentre study. Br J Dermatol. 2006 Jul;155(1):56–61.
17. Ferrara G, Soyer HP, Malvehy J, Piccolo D, Puig S, Sopena J, et al. The many faces of blue nevus: a clinicopathologic study. J Cutan Pathol. 2007 Jul;34(7):543–51.
18. Pizzichetta MA. Clinical and dermoscopic features of agminated blue nevus. Arch Dermatol. 2007 Sep 1;143(9):1209.
19. Ishida M, Kagotani A, Yoshida K, Iwai M, Okabe H. Endometrioid adenocarcinoma concurrent with a blue nevus of the endometrium and uterine cervix: a case report. Oncol Lett. 2013 Nov;6(5):1219–21.
20. Zembowicz A, Carney JA, Mihm MC. Pigmented epithelioid melanocytoma: a low-grade melanocytic tumor with metastatic potential indistinguishable from animal-type melanoma and epithelioid blue nevus. Am J Surg Pathol. 2004 Jan;28(1):31–40.
21. Di Cesare A, Sera F, Gulia A, Coletti G, Micantonio T, Fargnoli MC, et al. The spectrum of dermatoscopic patterns in blue nevi. J Am Acad Dermatol. 2012 Aug;67(2):199–205.
22. Ma C, Chambers CJ, Kiuru M, Marsee DK, Silverstein M. Amelanotic blue nevus. JAAD Case Rep. 2017 Mar;3(2):93–4.
23. Guadagni M, Nazzari G. Clinical and dermoscopic features of an evolving deep-penetrating nevus. Arch Dermatol. 2005;141:1490.
24. Zembowicz A, Phadke PA. Blue nevi and variants: an update. Arch Pathol Lab Med. 2011 Mar;135(3):327–36.
25. Argenziano G, Soyer HP, Chimenti S, Talamini R, Corona R, Sera F, et al. Dermoscopy of pigmented skin lesions: results of a consensus meeting via the Internet. J Am Acad Dermatol. 2003 May;48(5):679–93.
26. Moscarella E, Al Jalbout S, Piana S, Argenziano G, Lallas A, Longo C, et al. The stars within the melanocytic garden: unusual variants of Spitz naevi. Br J Dermatol. 2015 Apr;172(4):1045–51.
27. Levy RM, Ming ME, Shapiro M, Tucker M, Guerry D, Cirillo-Hyland VA, et al. Eruptive disseminated Spitz nevi. J Am Acad Dermatol. 2007 Sep;57(3):519–23.
28. Saroufim M, Novy M, Taraif S, Habib RH, Loya A, Rauscher B, et al. BRAF mutational epidemiology in dysplastic nevi: does different solar UV radiation exposure matter? J Eur Acad Dermatol Venereol. 2014 May;28(5):615–25.
29. Lallas A, Apalla Z, Ioannides D, Lazaridou E, Kyrgidis A, Broganelli P, et al. Update on dermoscopy of Spitz/Reed naevi and management guidelines by the International Dermoscopy Society. Br J Dermatol. 2017 Sep;177(3):645–55.
30. Peris K, Ferrari A, Argenziano G, Soyer HP, Chimenti S. Dermoscopic classification of Spitz/Reed nevi. Clin Dermatol. 2002 Jun;20(3):259–62.
31. Kerner M, Jaimes N, Scope A, Marghoob AA. Spitz nevi. Dermatol Clin. 2013 Apr;31(2):327–35.
32. Argenziano G, Soyer HP, Ferrara G, Piccolo D, Hofmann-Wellenhof R, Peris K, et al. Superficial black network: an additional dermoscopic clue for the diagnosis of pigmented spindle and/or epithelioid cell nevus. Dermatology. 2001;203(4):333–5.
33. Requena C, Requena L, Kutzner H, Yus ES. Spitz nevus: a clinicopathological study of 349 cases. Am J Dermatopathol. 2009 Apr;31(2):107–16.
34. Meyerson LB. A peculiar papulosquamous eruption involving pigmented nevi. Arch Dermatol. 1971 May;103(5):510–2.
35. Schepis C, Siragusa M. The Meyerson phenomenon in a teenager. Dermatol Online J. 2008 Feb 28;14(2):28.
36. Elenitsas R, Halpern AC. Eczematous halo reaction in atypical nevi. J Am Acad Dermatol. 1996 Feb;34(2 Pt 2):357–61.
37. Longo C, Segura S, Cesinaro A, Bassoli S, Seidenari S, Pellacani G. An atypical Meyerson's naevus: a dermoscopic, confocal microscopic and immunohistochemical description of one case. J Eur Acad Dermatol Venereol. 2007 Mar;21(3):414–6.
38. Ferrara G, Brasiello M, Annese P, Francione S, Giorgio CM, Moscarella E, et al. Desmoplastic nevus: clinicopathologic keynotes. Am J Dermatopathol. 2009 Oct;31(7):718–22.
39. Mackie RM, Doherty VR. The desmoplastic melanocytic naevus: a distinct histological entity. Histopathology. 1992 Mar;20(3):207–11.
40. Meffert JJ, Peake MF, Wilde JL. "Dimpling" is not unique to dermatofibromas. Dermatology. 1997;195(4):384–6.
41. Poulalhon N, Dalle S, Thomas L. Diagnostic dermoscopique des dermatofibromes. Ann Dermatol Vénéréologie. 2008 Dec;135(12):886–7.
42. Martinez-Casimiro L, Sánchez Carazo J-L, Alegre V. Balloon cell naevus. J Eur Acad Dermatol Venereol. 2009 Feb;23(2):236–7.
43. Oliveira A, Zalaudek I. Balloon cell naevus: new perspectives using high-definition optical coherence tomography with dermoscopic and reflectance confocal microscopic correlation. J Eur Acad Dermatol Venereol. 2016 Sep;30(9):1624–5.
44. Jaimes N, Braun RP, Stolz W, Busam KJ, Marghoob AA. White globules correlate with balloon cell nevi nests. J Am Acad Dermatol. 2011 Oct;65(4):e119–20.
45. Cinotti E, Perrot JL, Labeille B, Douchet C, Thuret G, Cambazard F. Yellow globules in balloon cell naevus: yellow globules in balloon cell naevus. Australas J Dermatol. 2013 Nov;54(4):268–70.
46. Fabrizi G, Pennacchia I, Pagliarello C, Massi G. Sclerosing nevus with pseudomelanomatous features. J Cutan Pathol. 2008 Nov;35(11):995–1002.
47. Ferrara G, Amantea A, Argenziano G, Broganelli P, Cesinaro AM, Donati P, Pellacani G, Zalaudek I, Tomasini C. Sclerosing nevus with pseudomelanoma-

tous features and regressing melanoma with nevoid features. J Cutan Pathol. 2009 Aug;36(8):913–5.
48. Patrizi A, Giacomini F, Savoia F, Misciali C, Neri I. Targetoid hemosiderotic naevus. J Eur Acad Dermatol Venereol. 2009 Apr;23(4):493–4.
49. Tomasini C, Broganelli P, Pippione M. Targetoid hemosiderotic nevus. Dermatology. 2005;210(3):200–5.
50. Kovács S, Megahed M. Targetoider hämosiderotischer Nävus: Ein Melanomsimulator. Hautarzt. 2007 Nov;58(11):931–2.
51. Scalvenzi M, Balato A, De Natale F, Francia MG, Mignogna C, De Rosa G. Hemosiderotic dermatofibroma: report of one case. Dermatology. 2007;214(1):82–4.

Dermoscopy for Melanoma

3

Alessandro Di Stefani and Luigi Cornacchia

3.1 Introduction

Melanoma has one of the fastest rising incidence rates of any cancer. It accounts for a small percentage of skin cancer cases but is responsible for the majority of skin cancer deaths. Although history and visual inspection of a suspicious lesion are usually the primary in a series of 'tests' to diagnose skin cancer, dermoscopy has become an essential tool to assist diagnosis by dermatologists [1]. It is well known that diagnosis of melanoma at an early stage is a critical factor in reducing morbidity and mortality rates. The accuracy of the clinical diagnosis of cutaneous melanoma with the unaided eye is only about 60%. Published data reveal that the use of dermoscopy improves the diagnostic sensitivity for melanoma by up to 35% compared to clinical examination alone, particularly in experienced practitioners. For the revolution determined by dermoscopy in the dermatologic semiology, the dermatoscope can be nowadays considered as the dermatologists' stethoscope [2–5].

A. Di Stefani (✉) · L. Cornacchia
Fondazione Policlinico Universitario A. Gemelli IRCCS, Rome, Italy

Institute of Dermatology, Catholic University of the Sacred Heart, Rome, Italy

3.2 Non-glabrous Skin Melanoma

The two-step dermoscopy algorithm represents the basis for dermoscopic evaluation of skin lesions. It was introduced by the panel of the Consensus Internet Meeting on Dermoscopy in 2003 and has successively undergone several modifications [6, 7] and was developed to serve as general guidelines, should be tailored with an open mind to the lesion at hand [8]. In the first step, the observer has to decide whether a lesion is melanocytic or nonmelanocytic, while in the second step the observer focuses on differentiating melanoma from benign melanocytic lesions using several diagnostic algorithms, such as pattern analysis, ABCD rule of dermoscopy, Menzies method, 7-point checklist and CASH algorithm [9–12]. Other algorithms, such as the three-point checklist of dermoscopy, have been created with the purpose of allowing nonexperts to improve their diagnostic accuracy for the management of pigmented skin lesions, and particularly for the early detection of melanoma [13]. According to the latest meta-analysis on the use of dermoscopy, there is no clear evidence that accuracy is improved by the use of any named or published algorithm to assist diagnosis [14].

In this chapter, we will focus instead on pattern analysis method, through the description of the dermoscopic patterns and the specific dermoscopic structures of melanoma, which are best

M. Fimiani et al. (eds.), *Technology in Practical Dermatology*,
https://doi.org/10.1007/978-3-030-45351-0_3

suited for educational purposes, so that the reader can develop his own personal method of use of dermoscopy [1, 15]. In evaluating a melanocytic lesion using the pattern analysis method, it should be determined whether or not the lesion shows one of the global patterns and then the dermatologist proceeds to analyse the local features. The melanoma-specific structures are, by convention, termed atypical/irregular. Different terminologies exist to define morphologic structures in dermoscopy, and many efforts have been made to standardize and make these terms more homogeneous and descriptive [16]. The terminology used herein is the traditional metaphoric one. The most frequent melanoma subtype in non-glabrous skin is the superficial spreading, and it is characterized by the following global patterns: the multicomponent pattern, the nonspecific pattern and the atypical pattern. The multicomponent pattern is a combination of three or more patterns (e.g., reticular, globular, and homogeneous), asymmetrically distributed in the lesion (Fig. 3.1). The nonspecific pattern lacks any recognizable global pattern of pigmentation. A deviation from the benign patterns also defines an atypical pattern. The classic reticular pattern presents a diffuse pigment network composed of lines that have minimal variation in their colour and thickness. The holes of the network also appear homogeneous in size, and the network tends to fade towards the periphery. Other benign subtypes of the reticular pattern include the reticular patchy pattern, the peripheral reticular pattern with central hypo/hyperpigmentation, peripheral reticular pattern with central globule or peripheral globules with central network. The homogeneous pattern is characterized by a diffuse homogeneous structureless pattern in a stable and non-changing lesion; it is characteristic of the blue nevi. The globular pattern presents globules of similar shape, size and colour which are distributed throughout the lesion; globules may be large and angulated, creating a cobblestone pattern. A symmetrical combination of benign patterns also configures a benign pattern, as in the case of the two-component pattern, that presents a combination of two patterns with one half of the lesion manifesting one pattern and the other half another pattern [17, 18]. Lesions displaying a deviation from the benign patterns, a multicomponent or nonspecific pattern, are further examined for the melanoma-specific structures: atypical network, regression structures, blue-whitish veil, peripheral streaks, negative network, off-centred blotches, atypical dots and/or globules, atypical vascular structures, shiny white lines, brown peripheral structureless areas [19]. Atypical network is characterized by increased variability in the width of the network lines, their colour and distribution; it may end abruptly at the periphery [20]. Regression structures, including granularity (also known as peppering) and scar-like areas, are characterized by the presence of blue and white areas within the same lesion, usually overlying macular areas. Irregular regression structures tend to be asymmetrically located and to involve more than 50% of the lesion [21]. Blue-whitish veil overlying raised areas is characterized by a confluent blue pigmentation with an overlying white "ground glass" haze, which tends to be asymmetrically located or diffuse in the nodular part of the lesion. Peripheral streaks (pseudopods and radial streaming) are radial projections located at the periphery of the lesion, extending from the tumour towards the surrounding normal skin. The presence of irregularly, asymmetric, and focally distributed streaks are highly suggestive of melanoma. Pseudopods

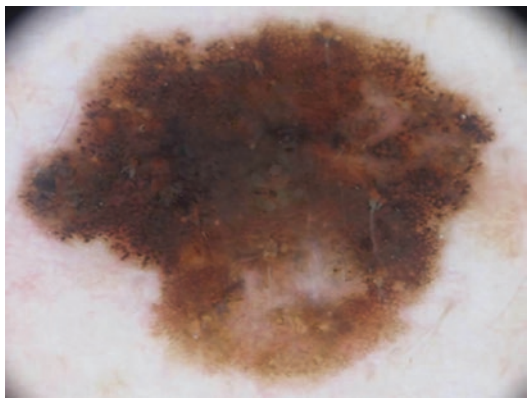

Fig. 3.1 Superficial spreading melanoma in non-glabrous skin. Dermoscopy reveals a multicomponent pattern with the presence of atypical pigment network, irregular black dots and globules and regression structures as granularity and white scarlike area

are finger-like projections with small knobs at their tips, whereas radial streaming indicates the same structures without the knobs [22]. Negative network is characterized by a relatively light areas making up the cords of the network and darker areas filling the holes; it has also been defined as reticular depigmentation [23]. Off-centred blotches are black, brown and/or grey structureless areas with irregular shape and asymmetrical distribution within the lesion [24]. Atypical dots and/or globules are black, brown, round to oval variously sized structures, irregularly distributed within the lesion. Atypical vascular structures, linear-irregular, dotted and polymorphous/atypical vessels were the most frequent vascular structures in melanoma, whereas milky red globules/areas were the most predictive ones [25]. Shiny white lines (also known as crystalline structures and chrysalis) are thick, short, bright whitish linear structures, sometimes distributed in a roughly orthogonal fashion [26, 27]. Brown peripheral structureless areas may represent a suspicious feature, in particular when located at the periphery of the lesion [28] (Fig. 3.1).

3.3 Melanoma on Facial Skin

The most common subtype of melanoma presenting on the face is lentigo maligna (LM), which shows a different set of dermoscopic structures. Stratum corneum of facial skin is thinner than that of the trunk and limbs, while pilosebaceous units and sweat glands are densely present. The thin epidermis allows blood vessels or melanophages to be observed more easily; in addition, a conventional pigment network is rarely found on adult facial skin because the rete ridges are flat or absent, and consequently there is no presence of the pigmented network. Instead, a pseudonetwork with a broad mesh and holes is created by the numerous pigment-free terminal and vellus hair follicles, as well as the openings of sweat glands. This pseudonetwork is location dependent and therefore present in both melanocytic lesions and nonmelanocytic lesions, such as solar lentigo or seborrheic keratoses, on the face.

Stolz and colleagues have identified a progression model for LM, comprising four steps of invasion of the hair follicles, by dermoscopic examination [29]. Initially, one finds hyperpigmented, asymmetric, follicular openings, representing the uneven descent of malignant melanoma cells into individual hair follicles. With further progression, this initially thin underlining becomes thicker and irregular, creating signet-ring-shaped structures. Then short, fine streaks, dots, and globules appear around the follicles, producing the annular-granular pattern. In this early phase, the pigmented structures are mainly caused by melanin in macrophages, not by melanoma cells, although later both may be responsible for the colour changes. Furthermore, pigmented, rhomboidal structures (lozenge-shaped) are created in the perifollicular area while progressing. As the hyperpigmentation coalesces, it may become homogeneous and blue-grey. Initially, follicular openings are respected, but eventually they are obliterated (Fig. 3.2). In advanced LM melanoma, white scarlike areas may be present as well as milky-red areas and other features associated with a vertical growth phase like in the superficial spreading melanoma [29].

Pralong and colleagues described other four dermoscopic features in LM: darkening at dermoscopic examination (the observation on der-

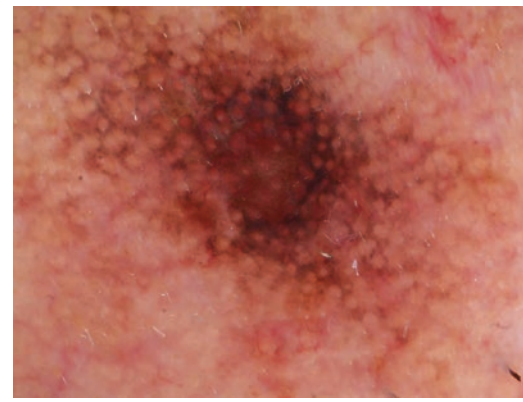

Fig. 3.2 Lentigo maligna melanoma of the face. Dermoscopic image showing atypical pseudo-network characterized by hyperpigmented and asymmetric follicular openings, annular-granular pattern with initial rhomboids structures and focal obliterated follicle

moscopic images of the presence of a colour, invisible to the naked eye, and darker than all clinically observable shades of brown or grey); target-like pattern (the presence of a dark dot, that is not a hair, in the centre of the dark circle of a hyperpigmented hair follicle); red rhomboidal structure (a lozenge-shaped vascular pattern occurring in the area separating the hair follicles from the others); increased density of the vascular network, defined as a vascular network of higher density within the lesion than in peripheral skin [30]. Cognetta and colleagues described an additional dermoscopic structure for LM consisting of fine concentric pigmented rings encircling each other, named concentric isobar pattern and also known as circle within a circle [31]. Slutsky and colleagues described another criteria for LM, the polygonal structures (zig-zag lines), brown to bluish grey dots and lines arranged in an angulated linear fashion [32]. Peris and colleagues recently reported that in some cases of facial LM, the combination of light-to-dark irregular brown dots and globules, associated with brown background pigmentation, may represent the predominant dermoscopic clue for the diagnosis [33]. Another simple approach for diagnosing malignant lesions on the face was based on the evaluation of grey colour as the only clue for malignancy. Although very easy to apply in practice, and promising in terms of sensitivity for melanoma (85.1%), its specificity was rather low (39.7%) [34]. Some algorithms have been proposed to help in the differential diagnosis, in particular between facial LM and pigmented actinic keratosis that can show several of the above mentioned dermoscopic features [35].

3.4 Acral Melanoma

Acral melanoma (AM) includes those melanomas located on volar surfaces of the palms and soles. The most frequent subtype on volar skin is the acral lentiginous type. The particular anatomy of this region constituted by the parallel arrangement of dermatoglyph in ridges and furrows leads to a peculiar disposition of the pigment. On acral skin, it is usual to distinguish benign pigmented patterns and malignant pigmented patterns [36, 37]. The three benign patterns are the parallel furrow pattern with its variants, the lattice-like pattern, and the fibrillar pattern. The presence of one or more of the three benign patterns within a pigmented multicomponent acral lesion is not sufficient to rule out melanoma.

The two malignant patterns are the parallel ridge pattern and irregular diffuse pigmentation (Fig. 3.3) [37]. The parallel ridge pattern is characterized by the presence of the pigment on the dermatoglyph's ridges; the ridges are distinguished from the furrows not only by their elevation but also by their anatomic properties, namely they appear larger than the furrows and with the sweat-gland openings located in the centre. If this is not enough to make an accurate distinction between ridges and furrows, one can use the ink test (if ink is deposited on the acral skin, after gentle cleaning of the ink, its remnant stays in the furrows) [36]. Irregular diffuse pigmentation is characterized by the presence of multiple structureless areas of pigmentation of different shades of brown, grey, or black, generally arranged asymmetrically and irrespective of the dermatoglyph architecture. The presence of irregular diffuse pigmentation and parallel ridge pattern, even in a small portion of a lesion, has to be considered sufficient to suspect the diagnosis of melanoma (Fig. 3.3).

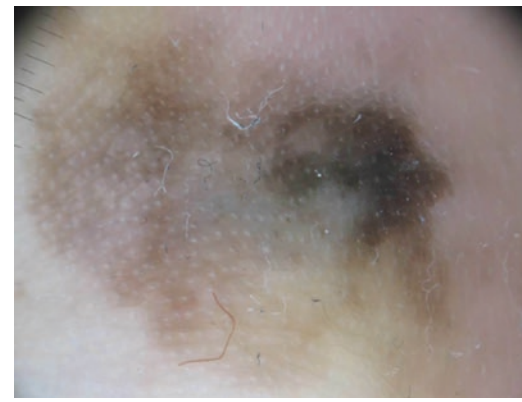

Fig. 3.3 Acral lentiginous melanoma. Dermoscopy displays a parallel ridge pattern and an irregular diffuse grey-black pigmentation in a structureless area at the periphery

Advanced melanoma of the palms and soles may also show dermoscopic features characteristic of melanoma of non-glabrous skin, including irregular dots/globules, irregular streaks, blue-white veil, regression structures and polymorphous vessels [37, 38]. Some algorithms (three-step algorithm and BRAAFF checklist) for improve the diagnostic accuracy of melanoma on the palms and soles have been proposed [39, 40].

3.5 Nail Melanoma

Pigmented nail-unit melanoma is initially characterized by the presence of a brown/black background of the pigmentation and by a pigmented longitudinal band (melanonychia) with its lines characterized by irregular thickness, spacing, parallelism and colour. Sometimes melanoma presents with a very dark background that does not allow visualization of longitudinal lines [41]. The periungual spread of pigment is called the Hutchinson sign. It can involve the proximal and lateral nail folds and also the hyponychial skin, and it is considered a clue to the diagnosis of subungual melanoma. Occasionally an only-dermoscopically visible periungual pigmentation (also known as the micro-Hutchinson sign) is seen on the proximal nail-fold skin [42]. When the Hutchinson sign involves the hyponychium, dermoscopy reveals the parallel ridge pattern as in acral lentiginous melanoma [43]. Other clues significantly associated with nail melanoma are a width of the pigmented band higher than 2/3 of the nail plate, grey and black colour and a granular pigmentation, defined as fine light to dark brown granularity [44]. In more advanced pigmented melanoma, dermoscopic features also include scar-like depigmentation, prominent periungual pigmentation with a parallel ridge pattern, blue-black structureless areas, blood spots, atypical vasculature areas, erosion of the nail plate, or ulceration of the nail bed [45]. Amelanotic nail-unit melanoma presents as a subungual nodule that may ulcerate. This lesion is characterized by an atypical pattern of the vessels (linear and irregular and/or multiple-pattern vessels and/or presence of milky red areas). Nail plate changes are also common [38].

3.6 Nodular Melanoma

Nodular melanoma is a rapidly growing neoplasm that accounts for 10%–30% of all melanomas, frequently not diagnosed until progressing to an advanced stage. This variant often lacks the "classic" melanoma-specific criteria; nevertheless, there are some clues that can help in a correct diagnosis [46]. Argenziano and colleagues introduced the "blue-back rule," suggesting that the simultaneous presence of blue and black pigmented areas involving at least 10% of the lesion surface each were significantly associated with pigmented nodular melanoma [47] (Fig. 3.4).

Zalaudek and colleagues suggested that "atypical" vascular structures, including polymorphic vessels, milky red areas and homogeneous red areas, are also significantly associated with the thickness of nodular melanoma [46–48]. Sometimes also crystalline structures and other criteria visible with polarized light der-

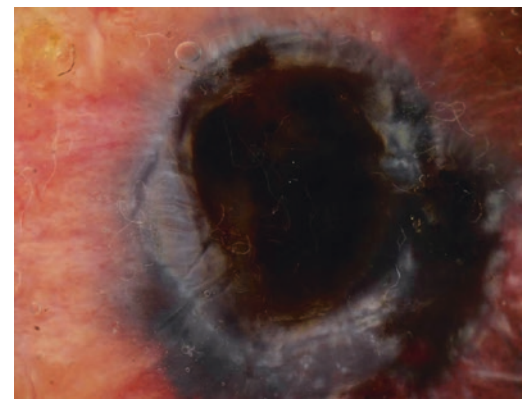

Fig. 3.4 Nodular melanoma. Dermoscopic examinations revealing the simultaneous presence of blue and black pigmented areas involving almost the entire lesion surface; polymorphic vessels can be observed at the periphery

moscopy may be useful for the diagnosis, when associated with features suggesting melanocytic nature [26].

3.7 Amelanotic and Hypomelanotic Melanoma

Amelanotic and hypomelanotic melanoma are relatively rare, accounting for less than 2% of all melanomas. Their clinical recognition is particularly difficult, since they might mimic several benign hypopigmented skin lesions, often resulting in a significant delay in diagnosis [1]. Amelanotic melanoma might develop as a reddish to pinkish macule, papule, plaque or nodule that rapidly changes in size, shape and colour. Hypopigmented melanoma displays small foci of pigmentation, more frequently located at the periphery of the lesion. Since the vast majority of melanoma-associated dermoscopic structures are pigmented, amelanotic melanoma is usually dermoscopically "featureless" and thus difficult to recognize. The most useful dermoscopic criteria are a milky red colour and an atypical vascular pattern, consisting of either linear irregular vessels or dotted plus linear vascular structures [46, 49] (Fig. 3.5).

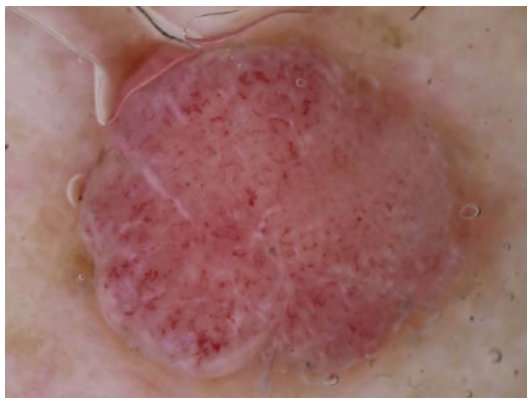

Fig. 3.5 Amelanotic melanoma. Dermoscopy shows an atypical vascular pattern, consisting of polymorphic either linear irregular or dotted or glomerular vessels as the only dermoscopic clues

3.8 Follow-up or Excision?

The primary purpose of examining a skin lesion with a dermatoscope is to determine whether the lesion should be excised or not [1]. This decision should be based upon the combination of clinical and dermoscopic examination of the lesion in question as well as surrounding lesions and patient history (new growing lesion, personal and family history of melanoma and other skin cancers). In patients with multiple nevi, it is useful to identify the "signature nevus" pattern (the predominant type of nevus) as well as lesions that deviate from the predominant pattern ("ugly duckling" lesions), both clinically and dermoscopically [50, 51]. After a complete clinical and dermoscopic examination, if the lesion is considered to be benign, the patient can be reassured, educated on the importance of self-skin examination, and instructed to return if changes are detected. If the lesion is considered a melanoma, it must undergo excision and histological confirmation. If the lesion is considered suspicious, there are two options: perform an excision or short-term monitoring, which consists of comparing digital dermoscopic images of the same lesion taken approximately 3–4 months apart, performed in specialized centres by experienced clinicians and only for moderately atypical lesions, which are not elevated on the skin surface, with no melanoma-specific features or history of changes and in patients with good compliance. The detection of changes in dermoscopic criteria in a dermoscopic follow-up examination should suggest the surgical excision of the lesion [52]. Enlarging lesions in adults, especially if showing a peripheral rim of brown globules, should be surgically excised [53, 54]. Nodular, palpable lesions showing atypical features should never be submitted to a dermoscopic follow-up, since the differential diagnosis is nodular melanoma. In such cases, surgical excision is mandatory [17, 55–59].

References

1. Massone C, Di Stefani A, Soyer HP. Dermoscopy for skin cancer detection. Curr Opin Oncol. 2005;17(2):147–53.

2. Tripp MK, Watson M, Balk SJ, Swetter SM, Gershenwald JE. State of the science on prevention and screening to reduce melanoma incidence and mortality: the time is now. CA Cancer J Clin. 2016;66(6):460–80.
3. Soyer HP, Argenziano G, Talamini R, Chimenti S. Is dermoscopy useful for the diagnosis of melanoma? Arch Dermatol. 2001;137(10):1361–3.
4. Argenziano G, Soyer HP. Dermoscopy of pigmented skin lesions—a valuable tool for early diagnosis of melanoma. Lancet Oncol. 2001;2(7):443–9.
5. Lallas A, Argenziano G. Dermatoscope-the dermatologist's stethoscope. Indian J Dermatol Venereol Leprol. 2014;80(6):493–4.
6. Argenziano G, Soyer HP, Chimenti S, Talamini R, Corona R, Sera F, et al. Dermoscopy of pigmented skin lesions: results of a consensus meeting via the internet. J Am Acad Dermatol. 2003;48(5):679–93.
7. Marghoob AA, Braun R. Proposal for a revised 2-step algorithm for the classification of lesions of the skin using dermoscopy. Arch Dermatol. 2010;146(4):426–8.
8. Scope A, Benvenuto-Andrade C, Agero ALC, Marghoob AA. Nonmelanocytic lesions defying the two-step dermoscopy algorithm. Dermatol Surg. 2006;32(11):1398–406.
9. Nachbar F, Stolz W, Merkle T, Cognetta AB, Vogt T, Landthaler M, et al. The ABCD rule of dermatoscopy. J Am Acad Dermatol. 1994;30(4):551–9.
10. Pehamberger H, Steiner A, Wolff K. In vivo epiluminescence microscopy of pigmented skin lesions. I. Pattern analysis of pigmented skin lesions. J Am Acad Dermatol. 1987;17(4):571–83.
11. Argenziano G, Fabbrocini G, Carli P, De Giorgi V, Sammarco E, Delfino M. Epiluminescence microscopy for the diagnosis of doubtful melanocytic skin lesions. Comparison of the ABCD rule of dermatoscopy and a new 7-point checklist based on pattern analysis. Arch Dermatol. 1998;134(12):1563–70.
12. Henning JS, Dusza SW, Wang SQ, Marghoob AA, Rabinovitz HS, Polsky D, et al. The CASH (color, architecture, symmetry, and homogeneity) algorithm for dermoscopy. J Am Acad Dermatol. 2007;56(1):45–52.
13. Soyer HP, Argenziano G, Zalaudek I, Corona R, Sera F, Talamini R, et al. Three-point checklist of dermoscopy: a new screening method for early detection of melanoma. Dermatology. 2004;208(1):27–31.
14. Dinnes J, Deeks JJ, Chuchu N, Ferrante di Ruffano L, Matin RN, Thomson DR, et al. Dermoscopy, with and without visual inspection, for diagnosing melanoma in adults. Cochrane Database Syst Rev. 2018;12:CD011902.
15. Carli P, Quercioli E, Sestini S, Stante M, Ricci L, Brunasso G, et al. Pattern analysis, not simplified algorithms, is the most reliable method for teaching dermoscopy for melanoma diagnosis to residents in dermatology. Br J Dermatol. 2003;148(5):981–4.
16. Kittler H, Marghoob AA, Argenziano G, Carrera C, Curiel-Lewandrowski C, Hofmann-Wellenhof R, et al. Standardization of terminology in dermoscopy/dermatoscopy: results of the third consensus conference of the International Society of Dermoscopy. J Am Acad Dermatol. 2016;74(6):1093–106.
17. Marghoob AA, Jaimes N. Dermoscopic evaluation of skin lesions. In: Tsao H, ed. UpToDate Corona R: UpToDate Inc. https://www.uptodate.com. Accessed 14 Feb 2019.
18. Jaimes N, Marghoob AA. The morphologic universe of melanoma. Dermatol Clin. 2013;31(4):599–613.
19. Menzies SW, Ingvar C, McCarthy WH. A sensitivity and specificity analysis of the surface microscopy features of invasive melanoma. Melanoma Res. 1996;6(1):55–62.
20. Salopek TG, Kopf AW, Stefanato CM, Vossaert K, Silverman M, Yadav S. Differentiation of atypical moles (dysplastic nevi) from early melanomas by dermoscopy. Dermatol Clin. 2001;19(2):337–45.
21. Zalaudek I, Argenziano G, Ferrara G, Soyer HP, Corona R, Sera F, et al. Clinically equivocal melanocytic skin lesions with features of regression: a dermoscopic-pathological study. Br J Dermatol. 2004;150(1):64–71.
22. Pizzichetta MA, Stanganelli I, Bono R, Soyer HP, Magi S, Canzonieri V, et al. Dermoscopic features of difficult melanoma. Dermatol Surg. 2007;33(1):91–9.
23. Pizzichetta MA, Talamini R, Marghoob AA, Soyer HP, Argenziano G, Bono R, et al. Negative pigment network: an additional dermoscopic feature for the diagnosis of melanoma. J Am Acad Dermatol. 2013;68(4):552–9.
24. Sadayasu A, Tanaka M, Maumi Y, Ikeda E, Sawada M, Ishizaki S, et al. Abrupt intralesional color change on dermoscopy as a new indicator of early superficial spreading melanoma in a Japanese woman. Case Rep Dermatol. 2015;7:123–8.
25. Argenziano G, Zalaudek I, Corona R, Sera F, Cicale L, Petrillo G, et al. Vascular structures in skin tumors: a dermoscopy study. Arch Dermatol. 2004;140(12):1485–9.
26. Di Stefani A, Campbell TM, Malvehy J, Massone C, Soyer HP, Hofmann-Wellenhof R. Shiny white streaks: an additional dermoscopic finding in melanomas viewed using contact polarised dermoscopy. Australas J Dermatol. 2010;51(4):295–8.
27. Benvenuto-Andrade C, Dusza SW, Agero ALC, Scope A, Rajadhyaksha M, Halpern AC, et al. Differences between polarized light dermoscopy and immersion contact dermoscopy for the evaluation of skin lesions. Arch Dermatol. 2007;143(3):329–38.
28. Annessi G, Bono R, Sampogna F, Faraggiana T, Abeni D. Sensitivity, specificity, and diagnostic accuracy of three dermoscopic algorithmic methods in the diagnosis of doubtful melanocytic lesions. The importance of light brown structureless areas in differentiating atypical melanocytic nevi from thin melanomas. J Am Acad Dermatol. 2007;56(5):759–67.

29. Stolz W, Schiffner R, Burgdorf WHC. Dermatoscopy for facial pigmented skin lesions. Clin Dermatol. 2002;20(3):276–8.
30. Pralong P, Bathelier E, Dalle S, Poulalhon N, Debarbieux S, Thomas L. Dermoscopy of lentigo maligna melanoma: report of 125 cases. Br J Dermatol. 2012;167(2):280–7.
31. Cognetta AB, Stolz W, Katz B, Tullos J, Gossain S. Dermatoscopy of lentigo maligna. Dermatol Clin. 2001;19(2):307–18.
32. Slutsky JB, Marghoob AA. The zig-zag pattern of Lentigo Maligna. Arch Dermatol. 2010;146(12):1444.
33. Peris K, Maiorino A, Di Stefani A, Longo C, Piana S, Argenziano G. Brown globules in lentigo maligna: a useful dermoscopic clue. J Am Acad Dermatol. 2016;75(2):429–30.
34. Tiodorovic-Zivkovic D, Zalaudek I, Lallas A, Stratigos A, Piana S, Argenziano G. The importance of gray color as a dermoscopic clue in facial pigmented lesion evaluation: a case report. Dermatol Pract Concept. 2013;3(4):37–9.
35. Micantonio T, Neri L, Longo C, Grassi S, Di Stefani A, Antonini A, et al. A new dermoscopic algorithm for the differential diagnosis of facial lentigo maligna and pigmented actinic keratosis. Eur J Dermatol. 2018;28(2):162–8.
36. Braun RP, Thomas L, Kolm I, French LE, Marghoob AA. The furrow ink test: a clue for the dermoscopic diagnosis of acral melanoma vs nevus. Arch Dermatol. 2008;144(12):1618–20.
37. Saida T, Oguchi S, Miyazaki A. Dermoscopy for acral pigmented skin lesions. Clin Dermatol. 2002;20(3):279–85.
38. Thomas L, Phan A, Pralong P, Poulalhon N, Debarbieux S, Dalle S. Special locations dermoscopy: facial, acral, and nail. Dermatol Clin. 2013;31(4):615–24.
39. Koga H, Saida T. Revised 3-step dermoscopic algorithm for the management of acral melanocytic lesions. Arch Dermatol. 2011;147(6):741–3.
40. Lallas A, Kyrgidis A, Koga H, Moscarella E, Tschandl P, Apalla Z, et al. The BRAAFF checklist: a new dermoscopic algorithm for diagnosing acral melanoma. Br J Dermatol. 2015;173(4):1041–9.
41. Di Chiacchio N, de Farias DC, Piraccini BM, Hirata SH, Richert B, Zaiac M, et al. Consensus on melanonychia nail plate dermoscopy. An Bras Dermatol. 2013;88(2):309–13.
42. Baran R, Kechijian P. Hutchinson's sign: a reappraisal. J Am Acad Dermatol. 1996;34(1):87–90.
43. Kawabata Y, Ohara K, Hino H, Tamaki K. Two kinds of Hutchinson's sign, benign and malignant. J Am Acad Dermatol. 2001;44(2):305–7.
44. Benati E, Ribero S, Longo C, Piana S, Puig S, Carrera C, et al. Clinical and dermoscopic clues to differentiate pigmented nail bands: an International Dermoscopy Society study. J Eur Acad Dermatol Venereol. 2017;31(4):732–6.
45. Ronger S, Touzet S, Ligeron C, Balme B, Viallard AM, Barrut D, et al. Dermoscopic examination of nail pigmentation. Arch Dermatol. 2002;138(10):1327–33.
46. Russo T, Piccolo V, Lallas A, Argenziano G. Recent advances in dermoscopy. F1000Res. 2016;5. https://doi.org/10.12688/f1000research.7597.1
47. Argenziano G, Longo C, Cameron A, Cavicchini S, Gourhant JY, Lallas A, et al. Blue-black rule: A simple dermoscopic clue to recognize pigmented nodular melanoma. Br J Dermatol. 2011;165(6):1251–5.
48. Zalaudek I, Kreusch J, Giacomel J, Ferrara G, Catricala C, Argenziano G. How to diagnose nonpigmented skin tumors: a review of vascular structures seen with dermoscopy: part I. Melanocytic skin tumors. J Am Acad Dermatol. 2010;63(3):361–6.
49. Pizzichetta MA, Talamini R, Stanganelli I, Puddu P, Bono R, Argenziano G, et al. Amelanotic/hypomelanotic melanoma: clinical and dermoscopic features. Br J Dermatol. 2004;150(6):1117–24.
50. Suh KY, Bolognia JL. Signature nevi. J Am Acad Dermatol. 2009;60(3):508–14.
51. Gaudy-Marqueste C, Wazaefi Y, Bruneu Y, Triller R, Thomas L, Pellacani G, et al. Ugly duckling sign as a major factor of efficiency in melanoma detection. JAMA Dermatol. 2017;153(4):279–84.
52. Kittler H, Pehamberger H, Wolff K, Binder M. Follow-up of melanocytic skin lesions with digital epiluminescence microscopy: patterns of modifications observed in early melanoma, atypical nevi, and common nevi. J Am Acad Dermatol. 2000;43(3):467–76.
53. Kittler H, Seltenheim M, Dawid M, Pehamberger H, Wolff K, Binder M. Frequency and characteristics of enlarging common melanocytic nevi. Arch Dermatol. 2000;136(3):316–20.
54. Rhodes AR. Common acquired nevomelanocytic nevi and the fourth dimension. Arch Dermatol. 2000;136(3):400–5.
55. Menzies SW, Gutenev A, Avramidis M, Batrac A, McCarthy WH. Short-term digital surface microscopic monitoring of atypical or changing melanocytic lesions. Arch Dermatol. 2001;137(12):1583–9.
56. Argenziano G, Mordente I, Ferrara G, Sgambato A, Annese P, Zalaudek I. Dermoscopic monitoring of melanocytic skin lesions: clinical outcome and patient compliance vary according to follow-up protocols. Br J Dermatol. 2008;159(2):331–6.
57. Kittler H, Binder M. Risks and benefits of sequential imaging of melanocytic skin lesions in patients with multiple atypical nevi. Arch Dermatol. 2001;137(12):1590–5.
58. Chimenti S, Argenziano G, Di Stefani A, Andreassi L, Carli P, De Giorgi V, et al. Guidelines in dermoscopy | Linee guida in dermoscopia. G Ital Dermatol Venereol. 2005;140(4):329–47.
59. Bowling J, Argenziano G, Azenha A, Bandic J, Bergman R, Blum A, et al. Dermoscopy key points: recommendations from the International Dermoscopy Society. Dermatology. 2006;214(1):3–5.

4 Dermoscopy for Non-melanocytic Benign Skin Tumors

Arianna Rizzo, Niccolò Nami, and Elisa Cinotti

4.1 Epithelial Tumors

4.1.1 Seborrheic Keratosis

Clinical Features

Early seborrheic keratoses are light brown macules with sharply demarcated borders. As the lesions progress, they transform into brownish papules with a verrucous surface. Diagnosis of seborrheic keratoses is mainly clinical, but in some cases differentiating them from malignant melanoma is difficult [1].

Dermoscopy Features

- *Milia-like cysts* are small, white or yellow cystic structures resembling milia which shine brightly and correspond to intraepidermal cysts that are filled with keratin (Fig. 4.1a) [2, 3]. They are better visible under non-polarized dermoscopy.
- *Comedo-like openings* are round, brown or black structures that correspond to keratin-filled invaginations (Fig. 4.1a) [2–4].
- *Fissures* are irregular linear depressions filled with keratin that give a brain-like o cerebriform appearance to the lesion. This pattern has also been named fissures and ridges or "gyri and sulci" (Fig. 4.1b, c) [2, 3].
- *Fingerprint-like structures* are thin, brown, parallel lines looking like fingerprints (Fig. 4.1b) [2, 3]. Although they can be seen in some flat seborrheic keratosis, they are predominant features of solar lentigo [5].
- *Moth-eaten border* is a sharply demarcated and irregularly concave border that gives a moth-eaten aspect to the lesion (Fig. 4.1b). This feature is typically seen in some flat seborrheic keratosis on the face [2, 3, 6].
- *Hairpin blood vessels* are elongated vessels folded in a loop that resembles a hairpin. They are mainly distributed in the periphery of the lesions (Fig. 4.1d). In most of the cases, they are grouped together and surrounded by a hypopigmented halo, which gives them a "grape-like" appearance [2–4, 7].
- *Network-like structures* can be observed in pigmented seborrheic keratoses. This "reticulation" is larger than those seen in a typical network of nevi and does not correspond to melanin pigment in keratinocytes or in melanocytes along the dermal–epidermal junction but appears to be due to keratin-filled structures [2, 3].
- *Sharp demarcation*: An abrupt interruption of the edge of the lesion is often present [3].

A. Rizzo (✉) · N. Nami · E. Cinotti
Department of Medical, Surgical and Neurological Science, Dermatology Section, University of Siena, S. Maria alle Scotte Hospital, Siena, Italy

M. Fimiani et al. (eds.), *Technology in Practical Dermatology*,
https://doi.org/10.1007/978-3-030-45351-0_4

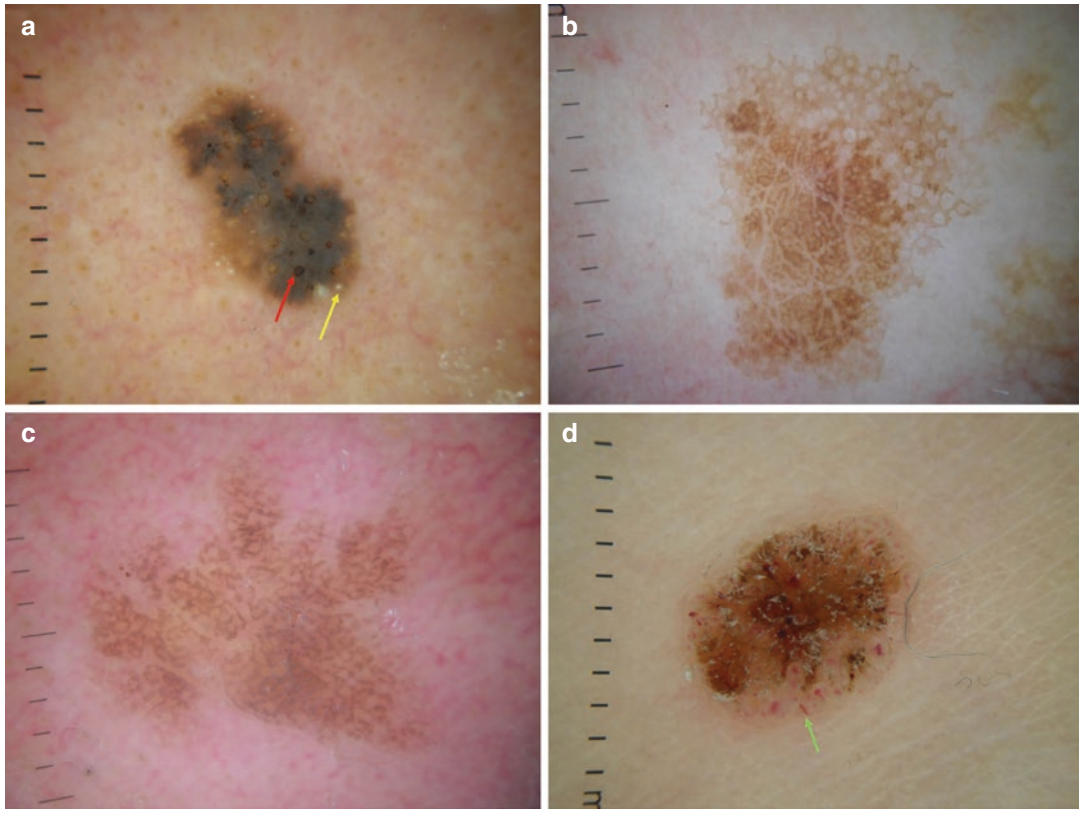

Fig. 4.1 Seborrheic keratoses can assume various dermoscopic features. (**a**) Typical comedo-like openings (red arrow) and milia-like cysts (yellow arrow) inside a dark brown lesion with sharply demarcated borders. (**b**) Fingerprint-like structures and a cerebriform pattern in the center of the lesion and at the periphery moth-eaten borders which can also be observed in solar lentigo. (**c**) Another example of a regular succession of fissures and ridges that give to the lesion a cerebriform pattern. (**d**) Hairpin vessels (green arrow) at periphery which are very common on traumatized seborrheic keratosis

4.1.2 Solar Lentigo

Clinical Features

Solar lentigines are pigmented benign lesions due to increased accumulation of melanin in keratinocytes [4]. They represent initial seborrheic keratoses, and for this reason, they share some features with them [8]. They may be oval, round or irregular in shape and can vary from a few millimeters to a few centimeters in diameter (Fig. 4.2a). Most lesions have a uniform light brown color. However, there is a variant of solar lentigo that has a jet-black color named ink spot lentigo [3]. A differential diagnosis between solar lentigo and lentigo maligna, especially if located on the face, can be a challenge [8].

Dermoscopy Features

- *Moth-eaten border* is a shared feature with seborrheic keratosis (Fig. 4.2b) [3].
- *A faint pigment network* corresponds to an elongation of the rete ridges and to an increase in melanin in the keratinocytes of the basal layer of the epidermis [4, 6].
- *Fingerprint-like structures* can be found in seborrheic keratosis, but they are predominantly found in solar lentigo [4, 5, 8].
- *Structureless areas* are homogenous brown areas without distinct dermoscopic structures [3].
- *Pseudonetwork* is usually found in pigmented lesions of the face because of a scarce or

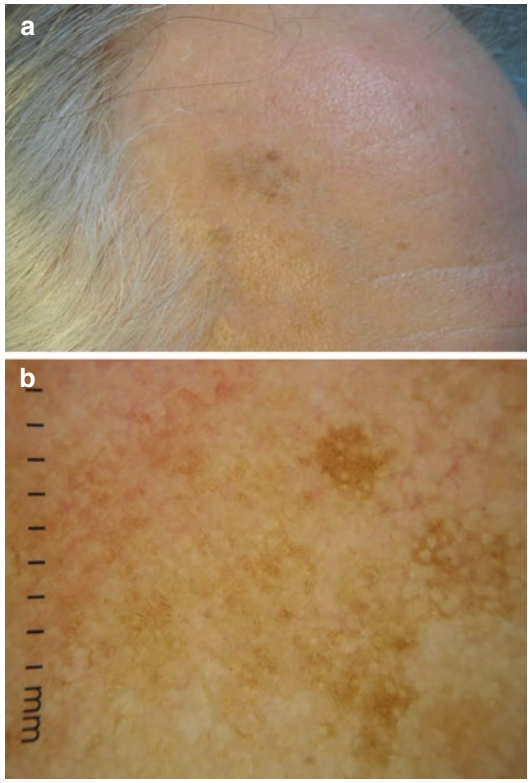

Fig. 4.2 Solar lentigo of the face: Clinical (**a**) and dermoscopic (**b**) aspect. Dermoscopy (**b**) shows uniform light brown structureless areas that form and a pseudo-network interrupted by white holes; concave borders give at the periphery a moth-eaten aspect to the lesion

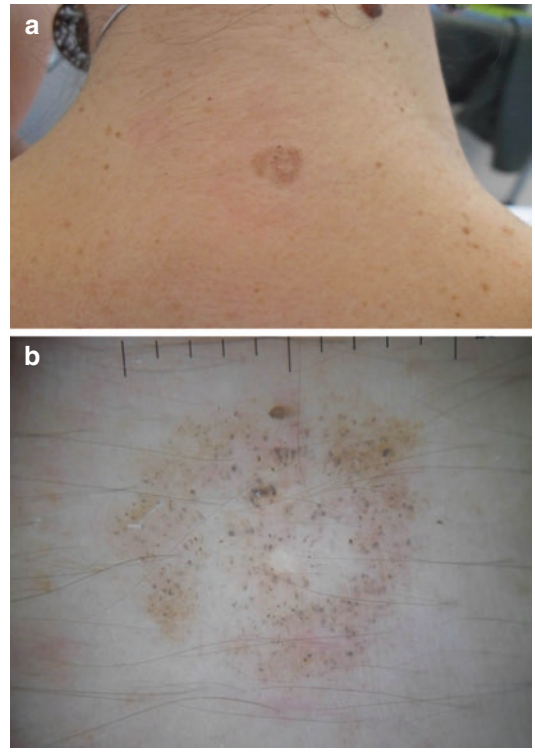

Fig. 4.3 Lichen planus like keratosis: Clinical (**a**) and dermoscopic (**b**) images. Regressing stage with blue-gray fine dots diffuse regularly on the lesion and residual light brown pseudonetwork at the periphery

absent presence of rete ridges in this area. It is due to a diffuse basal pigmentation of the epidermis interrupted by follicular and adnexal openings of the face (Fig. 4.2). The brown lines correspond to the pigment and the white holes to the openings of the adnexal structures [3, 8].

4.1.3 Lichen Planus-like Keratosis

Clinical Features

Lichen planus-like keratosis (LPLK) usually presents as a small single lesion, pink to gray-blue, which is mainly localized on the trunk, head or neck (Fig. 4.3a) [9]. It is the result of an inflammatory process to eliminate an epidermal lesion like a solar lentigo or a seborrheic keratosis that generally resolves spontaneously in a variable time [10]. Typically, there are two phases: inflammation followed by regression [11].

Dermoscopy Features

Dermoscopy features change with lesion progression [10]. In the initial phase, a light brown pseudonetwork and pinkish area are predominant. In the late regressing stage, regularly distributed annular granular structures and blue-gray fine dots are visible. In the late stage, a lichenoid keratosis might show irregular dots or globules (Fig. 4.3b), irregular streaks or rhomboid structures and simulate lentigo maligna. In these cases, a biopsy is necessary [9, 10].

- *Light brown pseudonetwork* is due to residual solar lentigo or seborrheic keratosis [10].
- *Pinkish area* is a homogeneous area on the background corresponding to capillary

dilatation during the inflammatory lichenoid reaction [10].

- *Blue-gray fine dots/annular granular structures* correspond to melanophages and can be localized or diffuse on the lesion. The localized granular pattern has the characteristic "salt-and-pepper" appearance (Fig. 4.3b) [9, 10].

4.1.4 Clear Cell Acanthoma

Clinical Features

It presents as a solitary pink papule mainly localized on the lower extremities (Fig. 4.4a) [12]. The differential diagnosis should include pyogenic granuloma, dermatofibroma, basal cell carcinoma, Bowen disease, amelanotic melanoma and even psoriasis [12, 13].

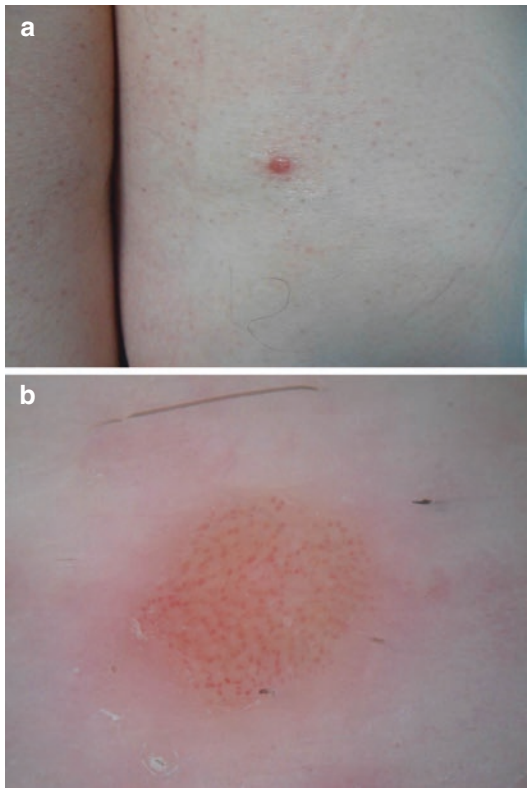

Fig. 4.4 Clear cell acanthoma: clinical (**a**) and dermoscopic (**b**) images. Dermoscopy examination shows red dotted vessels arranged in linear pattern forming a string of pearls

Dermoscopy Features

Clear cell acanthoma shows dermoscopically a stereotypical and specific vascular pattern [14].

- *String of pearls pattern* is characterized by dotted or glomerular vessels arranged in linear or serpiginous patterns that resembles a string of pearls (Fig. 4.4b). Multiple linear formations combine to form a reticular model that can cover the entire lesion or only a part of it. Dotted or glomerular vessels can be a feature of other lesions like psoriasis, Bowen's disease, dysplastic nevi, Spitz nevi, or melanomas. However, in these conditions, vessels are not organized in this distinct vascular pattern [7, 13].
- *Pink background*: The background upon which the vessels are set is typically pale pink [12].

4.2 Vascular Tumors

4.2.1 "Cherry" Angioma

Clinical Features

"Cherry" angiomas are very common benign skin tumors due to an abnormal proliferation of blood vessels [15]. They are more frequent with advancing age and are mainly distributed on the trunk.

Clinically, hemangioma appears as a small cherry red to violaceous macule, papule, or polypoid papule (Fig. 4.5a). In some cases, a partial thrombosis of the angioma appears clinically as a focal change of color, including black. This may clinically mimic melanoma [3, 11, 15].

Dermoscopic Features

- *Lacunae* are the common dermoscopic feature in vascular lesions. They are round or oval, red to violaceus and well-demarcated structures (Fig. 4.5b) [3, 15].

4.2.2 Angiokeratoma

Clinical Features

Angiokeratomas are benign vascular lesions that consist of dilated vessels associated with overly-

ing hyperkeratosis [16]. Clinically, they are red to black papules or nodules with a keratotic surface (Fig. 4.6a).

Dermoscopic Features

Angiokeratomas are often mistaken for other tumors like melanoma or pigmented basal cell carcinomas. Dermoscopy examination has improved the diagnosis of these lesions [15, 17].

- *Lacunae* in angiokeratoma can be red or dark. The dark lacunae are the most frequent dermoscopic finding and have high specificity. The dark color corresponds to vascular spaces that are partially or completely thrombosed (Fig. 4.6b) [15, 16].
- *Whitish veil* is a whitish structureless area due to hyperkeratosis and acanthosis overlying the vascular spaces [15, 16].
- *Hemorrhagic crusts* are visible if the lesion is traumatized and/or thrombosed [15, 16].

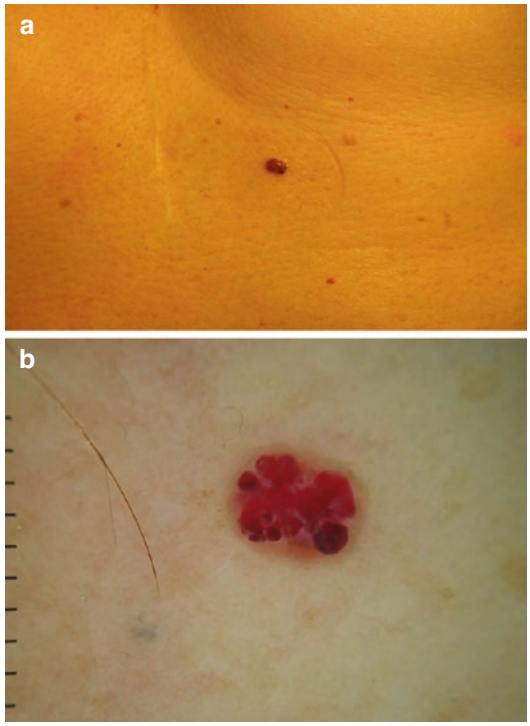

Fig. 4.5 Cherry angioma: Clinical (**a**) and dermoscopic (**b**) images. On dermoscopy, it is possible to observe red to violaceus, well-demarcated multiple lacunae

4.2.3 Pyogenic Granuloma

Clinical Features

Pyogenic granuloma is a common, benign, acquired, vascular lesion of the skin and mucous membranes that represent a reactive hyperproliferative vascular response to a variety of external stimuli [18].

It usually presents as a solitary, rapidly growing, papule or polyp that bleeds easily after minor trauma (Fig. 4.7a). In most cases, patient history, clinical appearance, and dermoscopic patterns allow to make the correct diagnosis. However, in some cases, the differential diagnosis with amelanotic melanoma and other tumors can be difficult, and surgical removal and histopathological study should be considered mandatory in adulthood [18, 19].

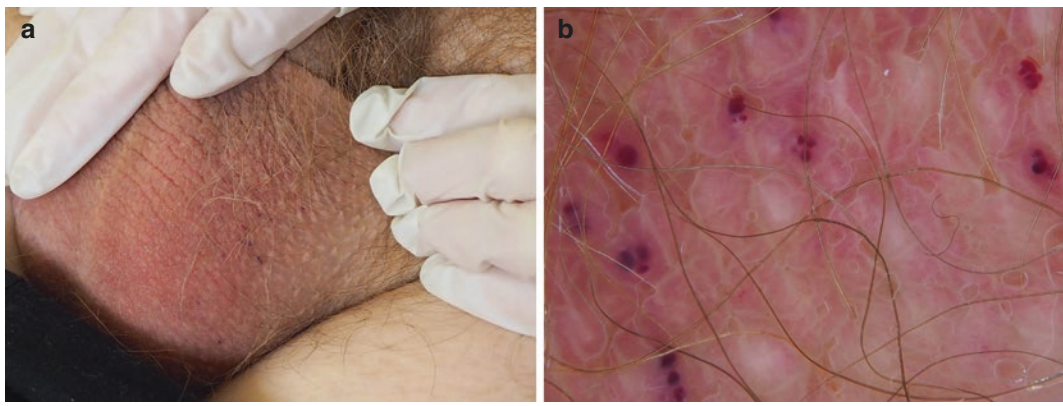

Fig. 4.6 Angiokeratoma: Clinical (**a**) and dermoscopic (**b**) images. Dermoscopy (**b**) shows dark lacunae

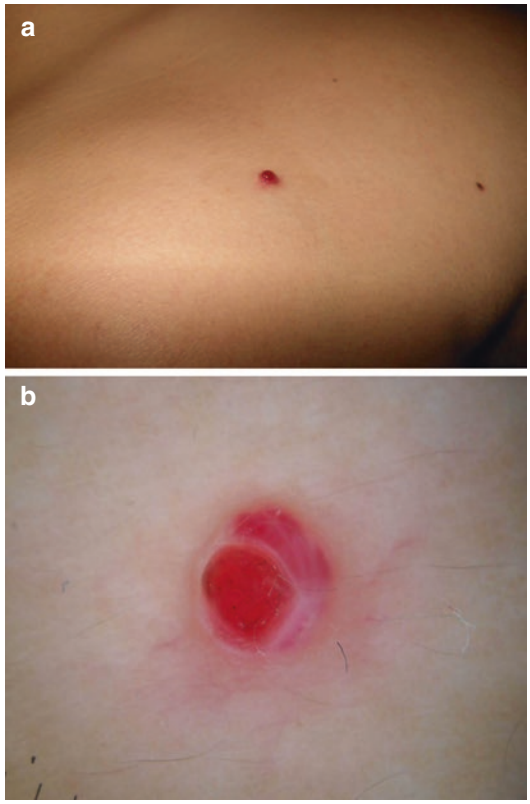

Fig. 4.7 Pyogenic granuloma: Clinical (**a**) and dermoscopic (**b**) images. Dermoscopy (**b**) shows typical red-whitish homogeneous areas, white rail lines that intersect the lesions and a peripheral white collarette

Dermoscopic Features

- *Red-whitish homogeneous area* is a red-whitish structureless area (Fig. 4.7b) that histopathologically corresponding a proliferation of capillary-sized vessels set in a myxoid stroma or separated by fibrous connective tissue septa [19]. It is the most common dermoscopic structure seen in pyogenic granulomas although is a nonspecific because it is commonly found in other tumors, especially amelanotic melanomas.
- *White collarette* is a ring-shaped whitish border at the periphery of the lesion (Fig. 4.7b) and corresponds to an epidermal collarette formed by elongated rete ridges or sweat ducts. It is the most specific structure for pyogenic granulomas [19].
- *White rail lines* are white lines similar to double rail that intersect the lesion (Fig. 4.7b) and correspond histologically to the fibrous septa that surround the small vessels [18, 19].
- *Vascular structures* usually are irregular linear vessels that are also the most common vascular structures observed in melanomas [19].

4.3 Connective Tissue Tumors

4.3.1 Dermatofibroma

Clinical Features

Dermatofibromas are common benign fibrosing cutaneous tumors characterized by an increased number of fibrocytes in the dermis. Clinically they appear as single papules with a smooth surface with a color variable from light brown to dark brown, purple, or yellow (Fig. 4.8a).

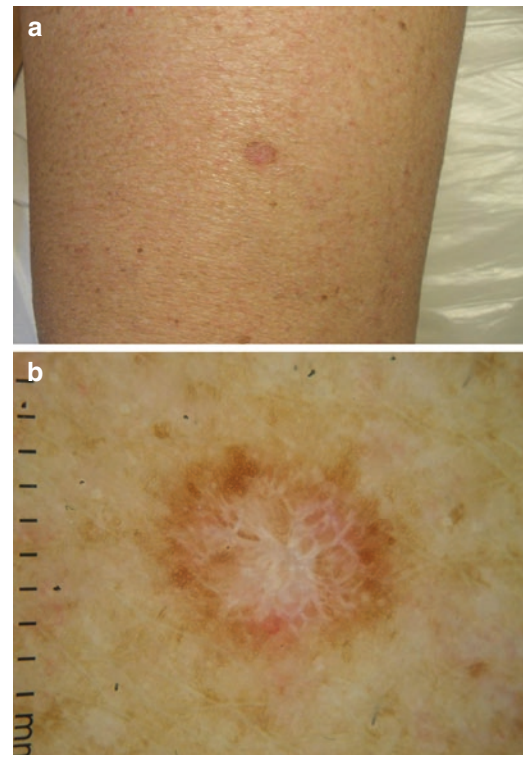

Fig. 4.8 Dermatofibroma: Clinical (**a**) and dermoscopic (**b**) images. On dermoscopy (**b**) it is well recognizable as a white scar-like area at the center of the lesion and a peripheral light brown network

They most frequently affects young adults and have a predilection for the lower extremities [20]. On palpation, lesions are firm and produce the "dimple sign" with the lateral compression [3, 21].

Dermoscopy Features

The most common pattern is pigment network and central white patch that is usually is easy to recognize. However, this tumor has a wide range of presentations, and in some cases, the differentiation from melanoma and other tumors may be difficult [20–22].

- *Central white patch* is a white scar-like area localized in the center of the lesion corresponding to the fibrotic area of the tumor (Fig. 4.8b) [3]. Vascular structures can be present in this area [21]. Mostly in large lesions, it is possible to see a central white network (white shiny streaks) [20].
- *Peripheral pigment network* is usually light brown and delicate and gradually fades at the periphery of the lesion (Fig. 4.8b). The pigment network results from the accumulation of melanin into basal keratinocytes. In some cases, the progressive accumulation of melanin can give a homogenous brown area [3, 20]. Although the presence of a pigment network is a major dermoscopic criterion for melanocytic lesions, dermatofibroma defies this rule. Dermatofibromas with prominent or atypical pigment network may be difficult to differentiate from melanoma and biopsy is mandatory [20, 22].

4.3.2 Lymphangioma

Clinical Features

Lymphangiomas are localized proliferations of lymphatic vessels which present as clusters of translucent vesicles, resembling frog spawn, containing serum, and serohematic fluid. The color changes from pink to purple reflecting hemorrhage into the lymphatic spaces [11, 23, 24]. The main differential diagnoses are with lymphangiectasis, hemangioma, angiokeratoma, molluscum contagiosum [23].

Dermoscopic Features

- *Yellow Lacunae* are roundish areas corresponding to the lymphatic vessels that contain clear fluid without blood. They are typically surrounded by pale septa [23, 24].
- *Reddish to bluish lacunae* can be present sue to the inclusion of blood in the lymphatic vessels. This presentation makes the differential diagnosis with hemangioma difficult [25]. In some of these lacunae, it is possible to see an additional dermoscopic clue "feature similar to the hypopyon." This pattern is due to the accumulated blood in the lowest part of the lacuna resulting in an appearance similar to the so-called hypopyon of the eye [23, 26].

4.4 Adnexal Tumors

4.4.1 Sebaceous Hyperplasia

Clinical Features

Sebaceous hyperplasia is a benign proliferation of the sebaceous glands that clinically appears as a small yellow or white papule with a central umbilication (Fig. 4.9a) [27]. It is more common with increasing age and is mainly localized on the face [27]. If large they may mimic skin cancers, particularly nodular basal cell carcinomas [27, 28].

Dermoscopy Features

- *Yellow/white globules*: White or yellow ovoid aggregated areas resembling a cumulus cloud (Fig. 4.9b). This feature is called cumulus sign and corresponds to the accumulation of sebum produced by hyperplastic sebaceous glands [28].
- *Crown vessels*: Scarcely branched vessels at the periphery of the lesion that may extend toward the center but which do not cross it (Fig. 4.9b) [7, 29].
- *Central umbilication* is also called "Bonbon toffee sign" (Fig. 4.9a).

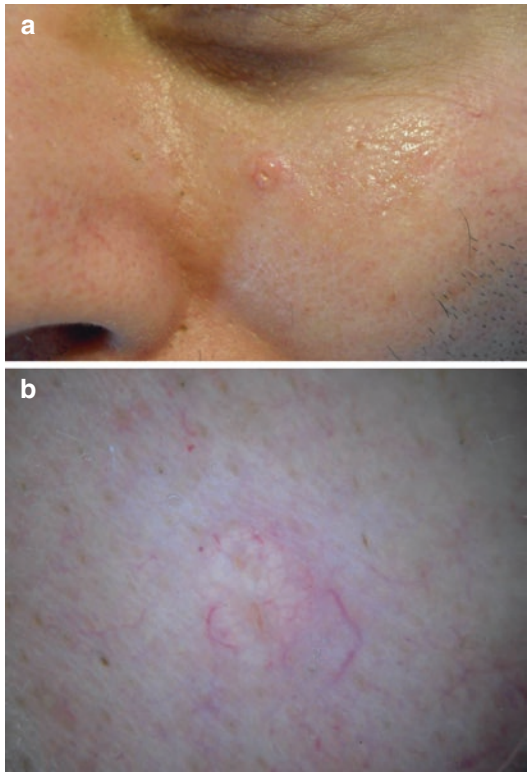

Fig. 4.9 Sebaceous hyperplasia: Clinical (**a**) and dermoscopic (**b**) images. On dermoscopy (**b**) sebaceous hyperplasia shows a central umbilication, aggregated yellow globules (cumulus sign) and crown vessels at the periphery which do not cross the center

4.4.2 Eccrine Poroma

Clinical Features

Eccrine poroma is a rare benign adnexal tumor that originates from the terminal ductal portion of the sweat glands. It usually appears as non-pigmented nodule or papule even if a pigmented variant exists. It is typically located on palms and soles which are the sites with higher concentration of eccrine sweat glands [30]. Because of its morphologic variability, it is usually difficult to recognize and is often confused with other skin tumors. For these reasons, eccrine poroma can be considered as "great imitator," and the diagnosis remains histopathological [31]. However, some dermoscopic features that may be useful in differentiating the eccrine poroma from other skin tumors have been described [32].

Dermoscopy Features

- *Vessels* are mainly glomerular and hairpin shaped, followed by linear irregular vessels [32].
- *Halo* is a white-to-pink halo surrounding the vessels. It is the most frequently dermoscopic feature found [32].
- *Structureless areas*: Multiple round to oval, pink to white structureless areas are often observed [32].

References

1. Salerni G, Alonso C, Gorosito M, Fernández-Bussy R. Seborrheic keratosis-like melanoma. J Am Acad Dermatol. 2015;72(1 Suppl):S53–5.
2. Braun RP, et al. Dermoscopy of pigmented seborrheic keratosis: a morphological study. Arch Dermatol. 2002;138(12):1556–60.
3. Malvehy J, Braun RP, Puig S, Marghoob AA, Kopf AW. Handbook of dermoscopy. Oxon, UK: CRC Press; 2006.
4. Elgart GW. Seborrheic keratoses, solar lentigines, and lichenoid keratoses. Dermatoscopic features and correlation to histology and clinical signs. Dermatol Clin. 2001;19(2):347–57.
5. Schiffner R, et al. Improvement of early recognition of lentigo maligna using dermatoscopy. J Am Acad Dermatol. 2000;42(1 Pt 1):25–32.
6. Kelly CAPJ. An atlas of surface microscopy of pigmented skin lesions: dermoscopy, 2nd edn. Australas J Dermatol. 2003;44(4):303–4.
7. Zalaudek I, Kreusch J, Giacomel J, Ferrara G, Catricalà C, Argenziano G. How to diagnose nonpigmented skin tumors: a review of vascular structures seen with dermoscopy: part II. Nonmelanocytic skin tumors. J Am Acad Dermatol. 2010;63(3):377–86; quiz 387–388.
8. Sahin MT, Oztürkcan S, Ermertcan AT, Güneş AT. A comparison of dermoscopic features among lentigo senilis/initial seborrheic keratosis, seborrheic keratosis, lentigo maligna and lentigo maligna melanoma on the face. J Dermatol. 2004;31(11):884–9.
9. Raptoulis G, Spencer R, Einstein B, Oliviero M, Braun R, Rabinovitz H. Lichen planus-like keratosis of the face: a simulator of melanoma in situ. Dermatol Surg. 2007;33(7):854–6.
10. Watanabe S, Sawada M, Dekio I, Ishizaki S, Fujibayashi M, Tanaka M. Chronology of lichen planus-like keratosis features by dermoscopy: a summary of 17 cases. Dermatol Pract Concept. 2016;6(2):29–35.
11. Bowling J. Diagnostic dermoscopy: the illustrated guide. Oxford, UK: Wiley-Blackwell; 2011.

12. Cunha DG, Kassuga-Roisman LEBP, Silveira LKCB, de Macedo FC. Dermoscopic features of clear cell acanthoma. An Bras Dermatol. 2018;93(3):449–50.
13. Zalaudek I, Hofmann-Wellenhof R, Argenziano G. Dermoscopy of clear-cell acanthoma differs from dermoscopy of psoriasis. Dermatology. 2003;207(4):428; author reply 429.
14. Tiodorovic-Zivkovic D, Lallas A, Longo C, Moscarella E, Zalaudek I, Argenziano G. Dermoscopy of clear cell acanthoma. J Am Acad Dermatol. 2015;72(1 Suppl):S47–9.
15. Grazzini M, et al. Dermoscopy, confocal laser microscopy, and hi-tech evaluation of vascular skin lesions: diagnostic and therapeutic perspectives. Dermatol Ther. 2012;25(4):297–303.
16. Zaballos P, et al. Dermoscopy of solitary angiokeratomas: a morphological study. Arch Dermatol. 2007;143(3):318–25.
17. Kim JH, Kim MR, Lee S-H, Lee SE, Lee SH. Dermoscopy: a useful tool for the diagnosis of angiokeratoma. Ann Dermatol. 2012;24(4):468–71.
18. Zaballos P, Llambrich A, Cuellar F, Puig S, Malvehy J. Dermoscopic findings in pyogenic granuloma. Br J Dermatol. 2006;154(6):1108–11.
19. Zaballos P, et al. Dermoscopy of pyogenic granuloma: a morphological study: dermoscopy of pyogenic granuloma. Br J Dermatol. 2010;163(6):1229–37.
20. Zaballos P, Puig S, Llambrich A, Malvehy J. Dermoscopy of dermatofibromas: a prospective morphological study of 412 cases. Arch Dermatol. 2008;144(1):75–83.
21. Ferrari A, et al. Typical and atypical dermoscopic presentations of dermatofibroma. J Eur Acad Dermatol Venereol. 2013;27(11):1375–80.
22. AlJasser MI, Martinka M, Kalia S. Dermatofibroma mimicking melanoma dermoscopically. Clin Exp Dermatol. 2014;39(1):69–70.
23. Massa AF, Menezes N, Baptista A, Moreira AI, Ferreira EO. Cutaneous lymphangioma circumscriptum—dermoscopic features. An Bras Dermatol. 2015;90(2):262–4.
24. Jha AK, Lallas A, Sonthalia S. Dermoscopy of cutaneous lymphangioma circumscriptum. Dermatol Pract Concept. 2017;7(2):37–8.
25. Arpaia N, Cassano N, Vena GA. Dermoscopic features of cutaneous lymphangioma circumscriptum. Dermatol Surg. 2006;32(6):852–4.
26. Gencoglan G, Inanir I, Ermertcan AT. Hypopyon-like features: new dermoscopic criteria in the differential diagnosis of cutaneous lymphangioma circumscriptum and haemangiomas? J Eur Acad Dermatol Venereol. 2012;26(8):1023–5.
27. Oztas P, Polat M, Oztas M, Alli N, Ustun H. Bonbon toffee sign: a new dermatoscopic feature for sebaceous hyperplasia. J Eur Acad Dermatol Venereol. 2008;22(10):1200–2.
28. Bryden AM, Dawe RS, Fleming C. Dermatoscopic features of benign sebaceous proliferation. Clin Exp Dermatol. 2004;29(6):676–7.
29. Zaballos P, Ara M, Puig S, Malvehy J. Dermoscopy of sebaceous hyperplasia. Arch Dermatol. 2005;141(6):808.
30. Bombonato C, Piana S, Moscarella E, Lallas A, Argenziano G, Longo C. Pigmented eccrine poroma: dermoscopic and confocal features. Dermatol Pract Concept. 2016;6(3):59–62.
31. Lallas A, et al. Eccrine poroma: the great dermoscopic imitator. J Eur Acad Dermatol Venereol. 2016;30(10):e61–3.
32. Ferrari A, et al. Eccrine poroma: a clinical-dermoscopic study of seven cases. Acta Derm Venereol. 2009;89(2):160–4.

Dermoscopy for Non-melanocytic Malignant Skin Tumors

5

Gaetano Licata and Elvira Moscarella

5.1 Dermoscopic Criteria of BCC

Basal cell carcinoma is the most common skin cancer affecting middle-aged and fair-skinned individuals. Sun exposure is one of the main BCC risk factors, other risk factors include PUVA therapy, radiation therapy, immunosuppressive medications, and chronic arsenic toxicity. Genetic involvement has been demonstrated in patients with familial basal cell nevus syndrome (Gorlin syndrome).

There are different clinicopathologic types, namely nodular, micronodular, superficial, morpheaform, fibroepithelial, and basosquamous. Each subtype can be clinically pigmented or not pigmented. According to the degree of pigmentation, some BCCs can mimic melanoma or other pigmented skin lesions [1].

The use of dermoscopy has improved BCC detection and is also useful in the management of BCC because it can help discriminating superficial BCCs from other non-superficial subtypes, thus helping the treatment decision.

Dermoscopic pattern of BCC depends on a combination of several factors which are associated with the patient (gender, age, pigmentary trait) and others related with histopathologic subtype and anatomic site. Dermoscopy structures can be divided into three different groups: vascular structures, structures related to pigment, and nonvascular non-pigmented structures [2].

5.1.1 Vascular Structures

5.1.1.1 Arborizing Vessels (Branched Vessels)

These consist of stem vessels of large caliber, usually longer than 1 mm, with multiple branching capillaries in a tree-like pattern. The vessels are shiny red and sharp in focus due to their position just beneath the epidermidis. Histopathologically, the arborizing vessels are wide vessels, and they represent the supportive neovasculature of the dermal basal cell tumor islands. This dermoscopic feature is mainly associated mainly with nodular BCC [3, 4].

5.1.1.2 Short Fine Telangiectasias (Serpentine Vessels)

They are superficial short, fine vessels less than 1 mm long with a small diameter without clear-cut tree-like ramifications. It is common to see these structures in white to red background. They are located in the papillary dermis [3, 4].

G. Licata · E. Moscarella (✉)
Dermatology Unit, University of Campania, Luigi Vanvitelli, Naples, Italy

M. Fimiani et al. (eds.), *Technology in Practical Dermatology*,
https://doi.org/10.1007/978-3-030-45351-0_5

5.1.2 Structures Related to Pigment

5.1.2.1 Blue-Gray Ovoid Nests (Blue, Gray Clods)

These structures are made of well-defined oval-shaped large melanin nests. Histopathologically, the presence of an ovoid nest corresponds to a tumor island with pigment aggregates located in the dermis. It is easy to find these structures in a nodular BCC. Blue-gray globules are similar to blue-gray ovoid nests, but the difference is the size, indeed the blue-gray globules are smaller than the ovoid nests.

5.1.2.2 Multiple Blue-Gray Globules

Blue-gray globules are well-circumscribed oval/round structures, larger than dots but smaller than ovoid nests. The color of these structures depends on their location in the dermis, usually they are located in papillary dermis and/or reticular dermis, sometimes they are blue or gray, but they can also be brown or pink. These structures correspond to tumor islands located in the dermis and can be seen in all BCC subtypes.

5.1.2.3 In-Focus Dots

These structures are formed by a small, well-defined gray dot which appears in focus at dermoscopic examination. Histopathologically, these dots corresponds to melanophages and free pigment along the dermo–epidermal junction.

5.1.2.4 Spoke Wheel Areas (Radial Lines that Converge at a Central Dot or Clod)

These are a radial projections converging at central darker point. Usually these projections are brown/tan, but it is possible to find other colors like blue or gray. In dermoscopy, it is rare to find these structures, but they are specific for BCC especially for the superficial subtype. On microscopy, they correspond to tumor nests connected to the epidermis.

5.1.2.5 Maple Leaf-like Areas (Peripheral Radial Lines with a Common Base)

These areas are defined as linear extensions connected to a common base area, generating a leaf-like pattern. They are usually brown or gray in color. This dermoscopic feature is quite specific for superficial BCC. Sometimes these extensions can be mistaken with the steaks seen in melanoma. In histopathology, this dermoscopic feature corresponds to multifocal tumor nests containing pigment connected to each other by lobular extensions. These structures are localized in the epidermidis.

5.1.2.6 Concentric Structures

They represent the "predecessor" of the spoke wheel areas. On dermoscopy, they appear like irregular globular structures with different colors (blue, gray, brown, black) and a darker central area.

5.1.3 Non-Vascular Non-Pigmented Structures

5.1.3.1 Ulceration

Ulceration is characterized by the loss of epidermis and a portion of the dermis; these shallow erosions may be covered with coagulated blood or serous crust. On dermoscopy, these areas appear as structureless areas of red to black color. It is common to find these structures in nodular tumors.

5.1.3.2 Multiple Small Erosions

These structures are smaller in size than ulcerations and usually covered with a yellowish crust with maximum diameter less than 1 mm. Histopathologically, it is possible to see a complete or partial absence of epidermis, and generally they are associated with superficial BCC.

5.1.3.3 Shiny White-Red Structureless Areas

Appear as areas of white to red color sometimes translucent or opaque. This dermoscopic feature corresponds to fibrosis in the dermis associated with tumor stroma.

5.1.3.4 Chrysalis or White Streaks (White Lines)

It is possible to see these structures only with polarized dermoscopy and consist in short and thick white lines corresponding to dermal fibrosis.

5.2 Basosquamous Carcinoma

This tumor shows basaloid and squamoid differentiation, resulting in a more aggressive tumor compared to BCC. Indeed local invasion is common, and there is a possibility of distant metastasis. On dermoscopy, it is possible to see unfocused arborizing vessels, short fine telangiectasia, ulceration, blue-gray globules, keratin masses with blood crusts, and white structureless areas. Histopathologically, it is common to find features related to both BCC and SCC [5] (Fig. 5.1).

5.3 Squamous Cell Carcinoma

Squamous cell carcinoma is the second most common skin cancer after basal cell carcinoma, with an increasing incidence in the last decades. This tumor typically occurs in elderly, fair-skinned individuals. It usually arises on sun-exposed areas of the skin, common sites are the face, scalp, neck, forearms, dorsal hands, and lower lips.

The most frequent presentation of SCC in situ is an erythematous scaly patch or elevated plaque. Invasive SCC is often an indurated firm, skin colored or pink to red nodule whose growth can progress rapidly. Other presentations include plaque like papilomatous or exophytic morphology [6]. About 2% of SCCs are fatal, while the majority have a good prognosis.

SCC can cause relevant morbidity because its recurrence rate after surgery is high. The risk of recurrence depends on many factors like patient's immune efficiency, tumor size, location, perineural involvement, and the grade of histopathological differentiation. Poor differentiation is a risk

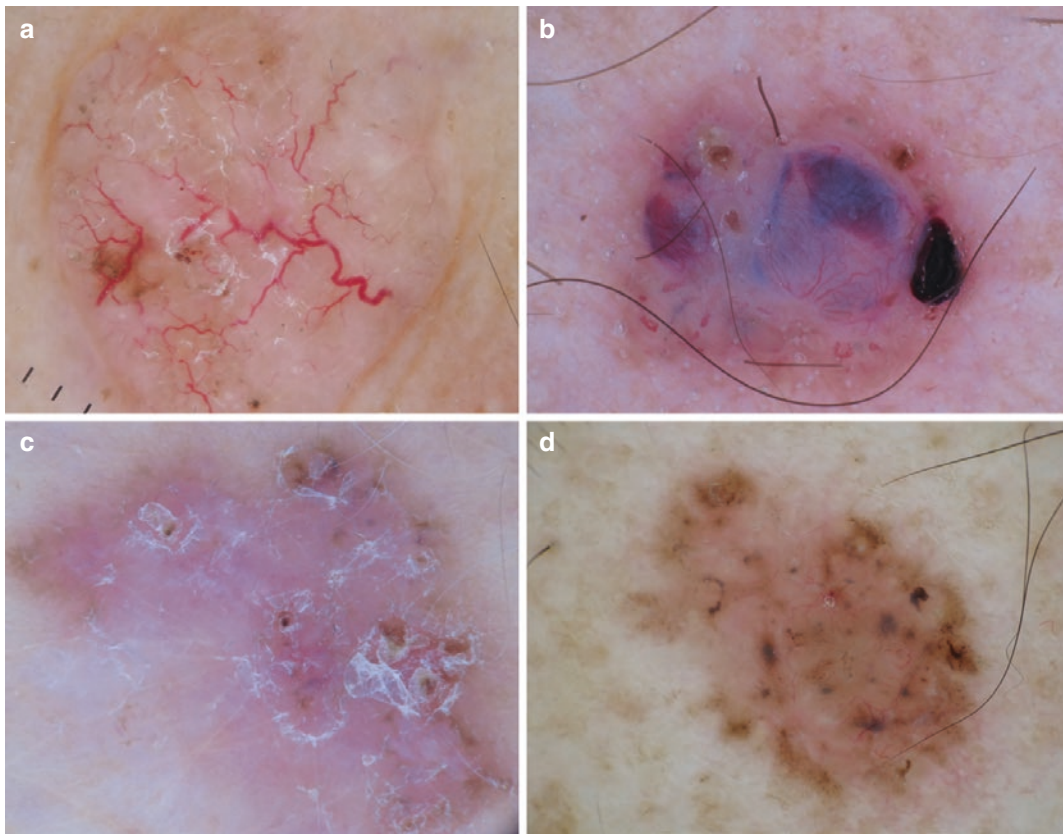

Fig. 5.1 Dermoscopy of basal cell carcinoma. (**a**) Nodular non-pigmented BCC, arborizing vessels well in focus. (**b**) Nodular pigmented BCC with arborizing vessels and multiple blue globules. (**c**) Superficial non-pigmented BCC, white-pink background, and multiple small erosions. (**d**) Superficial pigmented BCC, white structureless central area, multiple gray-brown dots, and concentric structures

Table 5.1 Dermoscopic features of SCC

Criterion	Definition
Erythema	Structureless pale-red background
Pink structureless areas	Structureless pink areas in the absence of any recognizable structure
Rosettes	Four aggregated white, small dots in correspondence to follicular opening in square criteria. These structures look like four-leaf clover
White structureless areas	White structureless areas in the absence of any structure not corresponding to scales/keratin, they may cover large areas of the tumor
White circles/ targetoid hair follicle	Round structures composed of yellow to brown structureless center and white outer rim, this pattern corresponds to keratotic plugs within follicular openings
Erosion/ ulceration	Small to large red to brown structureless areas
Scales	White or yellow areas on the tumor's surface
Keratin mass	White or yellow keratin mass located at the center of the lesion, without any recognizable structure
Dotted vessels	Tiny red dots distributed next to each other
Glomerular vessels	Variation on theme of dotted vessels but distributed in cluster, they have convoluted morphology
Polymorphic vessels	Presence of vessels with different morphology and dimension

factor for recurrence, in contrast, well-differentiated SCCs have a better prognosis.

The most common dermoscopic criteria of SCC are summarized in Table 5.1 [7].

5.3.1 Bowen's Disease (BD)

Is an intraepithelial carcinoma or in situ squamous cell carcinoma most frequent in women and occurs on the lower extremities. The risk of progression of BD to invasive SCC varies between 3% and 20%. There are two different forms: pigmented and non-pigmented (Fig. 5.2).

5.3.2 Non-pigmented BD

The clinical appearance of classical non-pigmented BD is an erythematous, well-demarcated plaque with a scaly surface that may be eroded or ulcerated. The growth of this tumor is slow. On dermoscopy, BD is characterized by two types of vascular patterns: small *dotted vessels* and *glomerular vessels*. The glomerular vessels represent a variation on the theme of dotted vessels, they are a tortuous capillaries larger than dotted vessels and are often distributed in cluster mimicking the glomerular apparatus of the

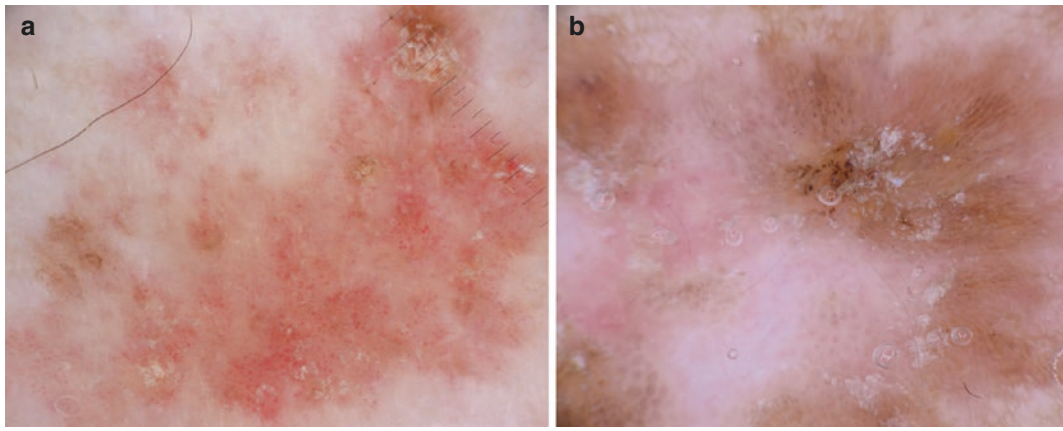

Fig. 5.2 Dermoscopy of Bowen's disease. (**a**) Non-pigmented BD, with structureless white area and multiple clustered dotted/glomerular vessels. (**b**) Pigmented BD, with structureless white area and multiple brown dots in a line at the periphery of the lesion

kidney. Histopathologically, this dermoscopic criterion corresponds to dilated capillaries in the dermal papillae and papillary dermis. Additional dermoscopic feature is the presence of white to yellow surface scales corresponding to hyperkeratosis [8].

5.3.3 Pigmented BD

Pigmented Bowen's disease is an uncommon variant and is more common in darker skin phenotypes. The clinical differential diagnosis includes a melanocytic lesion, pigmented basal cell carcinoma, solar lentigo, seborrheic keratosis, and pigmented actinic keratosis. On dermoscopy, it is possible to find small brown or gray dots which are regularly packed in a patchy distribution, brown structureless areas, and hypopigmented (white to pink) structureless areas. Rarely it is possible to see pigment network and streaks [9].

5.3.4 Keratoacanthoma (KA)

KA is a well-differentiated variant of squamous cell carcinoma. Clinically, it is characterized by an initial rapid growth followed by spontaneous involution over 4–6 months. KA appears as a concentric circle of central crater, surrounded by a whitish area and adjacent peripheral vessels. Dermoscopy of KA shares some features with SCC, but there are several dermoscopic criteria that may help to distinguish KA from SCC. The most important dermoscopic feature is the presence of white circles also called targetoid hair follicles. These are round structures composed of yellow to brown structureless center and white outer rim. The follicle may have a targetoid appearance with central keratotic plug surrounded by the white halo [10]. Histophologically, they reveal acanthosis and hypergranulosis of the infundibular epidermidis. Another dermoscopic feature is the keratin mass located at the center of the tumor. This appears as an amorphous structureless white to yellow area that is surrounded by elongated telangiectasias which appear as linear irregular vessels (serpentine vessels) with a large caliber and few branches. In addition to these criteria, it is common to find hairpin and dotted vessel, this gives to KA a polymorphous patter. Thus, the typical dermoscopic pattern of KA consists of peripherally distributed elongated vessels and centrally located keratin masses.

5.3.5 Invasive Squamous Cell Carcinoma

Invasive squamous cell carcinoma appears clinically as a papulonodular, plaque-like, ulcerated papilomatous or exophytic lesion. The dermoscopic pattern is closely related to the grade of histopathological differentiation. Well-differentiated and moderately differentiated SCCs display signs of keratinization as a central distribution of scales/keratin, white structureless areas, yellow keratotic follicular plug surrounded by a white rim (white circle), and areas of ulceration. At the periphery, it is common to see hairpin vessels and linear irregular vessels (serpentine). In contrast, poorly differentiated SCCs are clinically typified by a flat appearance, on dermoscopy they reveal a predominant red color and the lack of signs of keratinization [11]. They are characterized by polymorphous vascular pattern with hairpin vessels, glomerular and dotted vessels, linear irregular vessels over a reddish background. In conclusion, the presence of vessels in more than 50% of the lesion and bleeding are markers of poor differentiation, while scales, keratin, and white circles are indicative of well- or moderately differentiated tumors [12, 13] (Fig. 5.3).

5.3.6 Pigmented Squamous Cell Carcinoma

Pigmented SCC is an uncommon variant. This tumor can present dermoscopic features typical of melanocytic lesion such homogeneous blue pigmentation, radial streaks, blue-gray globules. In these cases, the differential diagnosis with melanocytic lesions can be difficult [14].

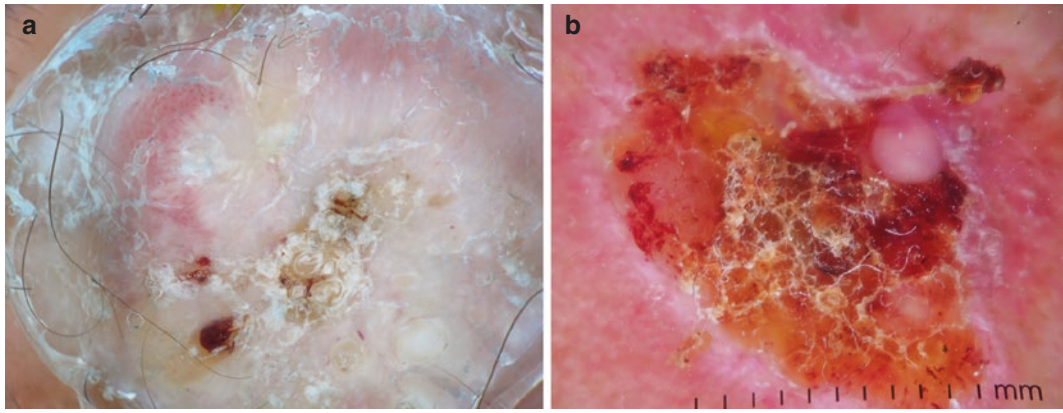

Fig. 5.3 Dermoscopy of invasive SCC. (**a**) Well-differentiated SCC, with the prevalence of white color, white circles surrounding follicular structures. (**b**) Poorly differentiated SCC with red background and serous crust

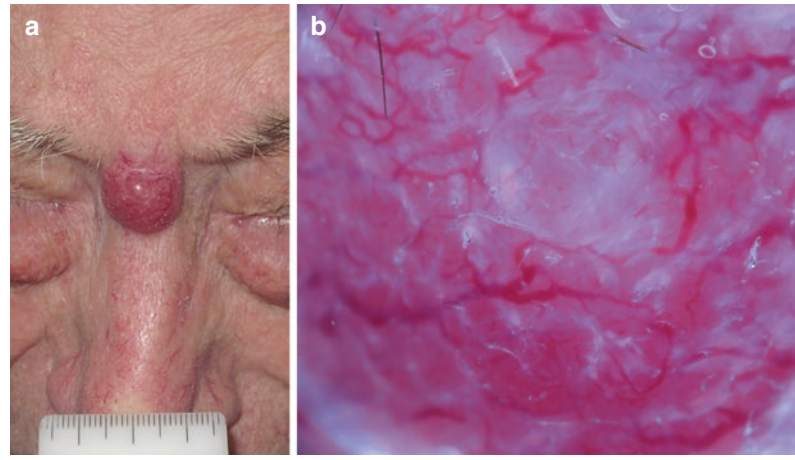

Fig. 5.4 Merkel cell carcinoma arising on the glabella of an 85-year-old man. Clinical (**a**) and dermoscopic (**b**) appearance with milky red background and large diameter vessels

5.3.7 Merkel Cell Carcinoma (MCC)

Merkel cell carcinoma is a neuroendocrine carcinoma of the skin, associated with high risk of locoregional recurrence, metastasis, and mortality [15]. MCC is extremely rare, but its incidence has tripled in recent years. The outcome of this tumor is very poor because of its aggressive behavior and propensity for early metastasis in regional lymph nodes [16]. There are several risk factors for the development of MCC, like UV exposure, male sex, immunosuppression, hematological neoplasm, and older age [17]. Indeed, most MCCs are found on sun-exposed skin of white people older than 50 years [18]. MCC presents as an asymptomatic, rapidly growing red or pink nodule that develops over the course of weeks to months. It occurs mainly on the face, neck, extremities followed by trunk and buttocks. The differential diagnosis includes amelanotic melanoma, basal cell carcinoma, porocarcinoma, cutaneous lymphoma, angiosarcoma, atypical fibroxanthoma, and skin metastasis from internal malignancy.

5.3.8 Dermoscopic Criteria of MCC

On dermoscopy, this tumor shows overlapping features with other skin cancer [19]. There are two most important dermoscopic features, milky red background and polymorphous vascular pattern (Fig. 5.4).

5.3.9 Milky Red Background

Milky red background represents a red or pink region that corresponds to an area with increased vascularity. These milky-red areas are commonly associated with other vascular structures like linear irregular vessels, arborizing vessels, and dotted and glomerular vessels. This combination of features is an indication to excision because it is very commonly found in amelanotic melanoma and in other malignancies.

5.3.10 Polymorphous Vascular Pattern

MCC shows different types of vessels like arborizing vessels, dotted and glomerular vessels, and irregular vessels. Arborizing vessels consist of a large stem vessel with fine irregular branches. This dermoscopic feature is generally associated with basal cell carcinoma; in BCC, these vessels are located superficially and consequently are in focus. In contrast the arborizing vessels present in MCC are located deeper and consequently are out of focus. MCC exhibits other vascular features such as dotted and glomerular vessels common in squamous cell carcinoma, and linear irregular vessels present in SCC and in melanoma. The simultaneous presence of more than one morphological type of vessel is also suggestive for malignant tumor, so it is important to perform a biopsy [20].

References

1. Altamura D, Menzies SW, Argenziano G, et al. Dermatoscopy of basal cell carcinoma: morphologic variability of global and local features and accuracy of diagnosis. J Am Acad Dermatol. 2010;62:67–75.
2. Wozniak-Rito A, Zalaudek I, Rudnicka L. Dermoscopy of basal cell carcinoma. Clin Exp Dermatol. 2018;43:241–7.
3. Lallas A, Apalla Z, Agenziano G, et al. The dermatoscopic universe of basal cell carcinoma. Dermatol Pract Concept. 2014;4:11–24.
4. Lallas A, Apalla Z, Ioannides D, et al. Dermoscopy in the diagnosis and management of basal cell carcinoma. Future Oncol. 2015;11(22):2975–84.
5. Garcia C, Poletti E, Crowson AN. Basosquamous carcinoma. J Am Acad Dermatol. 2009;60:137–43.
6. Warzawik-Hendzel O, Olzewska M, Maj M. Non-invasive diagnostic techniques in the diagnosis of squamous cell carcinoma. J Dermatol Case Rep. 2015;4:89–97.
7. Lallas A, Pyne J, Kygidis A, et al. The clinical and dermoscopic features of invasive cutaneous squamous cell carcinoma depend on histopathological grade of differentiation. Br J Dermatol. 2015;172:1308–15.
8. Zalaudek I, Argenziano G, Leinweber B, et al. Dermoscopy of Bowen's disease. Br J Dermatol. 2004;150:1112–6.
9. Zhou LL, Mistry N. Pigmented Bowen disease. CMAJ. 2017;189(47):E1462.
10. Kwiek B, Schwartz R. Keratoacanthoma: an update and review. J Am Acad Dermatol. 2016;74:1220–33.
11. Rosendahl C, Cameron C, Argenziano G, et al. Dermoscopy of squamous cell carcinoma and keratoacanthoma. Arch Dermatol. 2012;148(12):1386–92.
12. Zalaudek I, Argenziano G. Dermoscopy of actinic keratosis, intraepidermal carcinoma and squamous cell carcinoma. Curr Probl Dermatol. 2015;46:70–6.
13. Manfredini M, Longo C, Ferrari B, et al. Dermoscopic and reflectance confocal microscopy features of cutaneous squamous cell carcinoma. J Eur Acad Dermatol Venereol. 2017;31:1828–33.
14. de Giorgi V, Alfaioli B, Papi F, et al. Dermoscopy in pigmented squamous cell carcinoma. J Cutan Med Surg. 2009;13(6):326–9.
15. Sadeghinia A, Ghanadan A, Ehsani A, et al. Can dermoscopy open a new way to diagnosing Merkel cell carcinoma? Int J Dermatol. 2019;58:e52–77.
16. Dalle S, Parmentier L, Moscarella E, et al. Dermoscopy of Merkel cell carcinoma. Dermatology. 2012;224:140–4.
17. Jalilian C, Chamberlain M, Haskett M, et al. Clinical and dermoscopic characteristic of Merkel cell carcinoma. Br J Dermatol. 2013;169:294–7.
18. Scalvenzi M, Palmisano F, Ilardi G, et al. Clinical, dermoscopic and histological features of a Merkel cell carcinoma of the hand. J Dermatol Case Rep. 2013;7(1):15–7.
19. Harting M, Ludgate M, Fullen D, et al. Dermatoscopic vascular patterns in cutaneous Merkel cell carcinoma. J Am Acad Dermatol. 2012;66:923–7.
20. Lallas A, Moscarella E, Argenziano G, et al. Dermoscopy of un common skin tumors. Australas J Dermatol. 2014;55:53–62.

6 Dermoscopy for Inflammatory Diseases

Francesco Lacarrubba, Anna Elisa Verzì, and Giuseppe Micali

6.1 Introduction

Dermoscopy, a noninvasive technique widely used in dermatology for the evaluation of skin tumors, may also be useful for the diagnosis and treatment monitoring of several inflammatory cutaneous disorders [1–5]. In some cases it may be diagnostic, in others it may help to narrow down the spectrum of possible diagnoses, thus reducing the need for biopsy.

In the evaluation of inflammatory lesions, different features should be considered, including background color, vascular pattern, color and distribution of the scales, follicular structures, and other variable findings depending on the disorder considered. The handheld dermoscope, which allows 10× magnification, is suitable for the evaluation of inflammatory disorders, and polarized light that allows a better visualization of vascular structures and scales is preferable. In some cases, the use of higher magnification (up to 100×), achieved through the use of a videodermatoscope, is necessary, mainly because it is able to provide a better evaluation of the vascular pattern [6].

In this chapter, the dermoscopy features of the main inflammatory diseases in which dermoscopy may aid in clinical practice are reported and discussed.

6.2 Darier's Disease

The main dermoscopic feature of Darier's disease consists of polygonal, star-like or roundish/oval-shaped yellowish/brownish structures surrounded by a whitish halo (Fig. 6.1). These structures are generally superimposed on a pinkish, homogeneous, structureless background, and dotted/linear vessels may also be observed [7, 8]. Histopathologically, the star-like structures correspond to hyperparakeratotic areas of different shape and size surrounded by an acanthotic epidermis. The same aspect may also be seen in other disorders sharing similar microscopic features, such as the Darier-like subtype of Grover's disease, Dowling–Degos disease and acantholytic dyskeratotic acanthoma [9–12].

6.3 Discoid Lupus Erythematosus

Active lesions of discoid lupus erythematosus display at dermoscopy a diffuse, homogeneous background erythema, whitish scaling, irregularly distributed dotted and\or linear vessels and follicular yellowish plugs with a perifollicular whitish halo (Fig. 6.2). The latter structures are histopatho-

F. Lacarrubba (✉) · A. E. Verzì · G. Micali
Dermatology Clinic, University of Catania, Catania, Italy

M. Fimiani et al. (eds.), *Technology in Practical Dermatology*,
https://doi.org/10.1007/978-3-030-45351-0_6

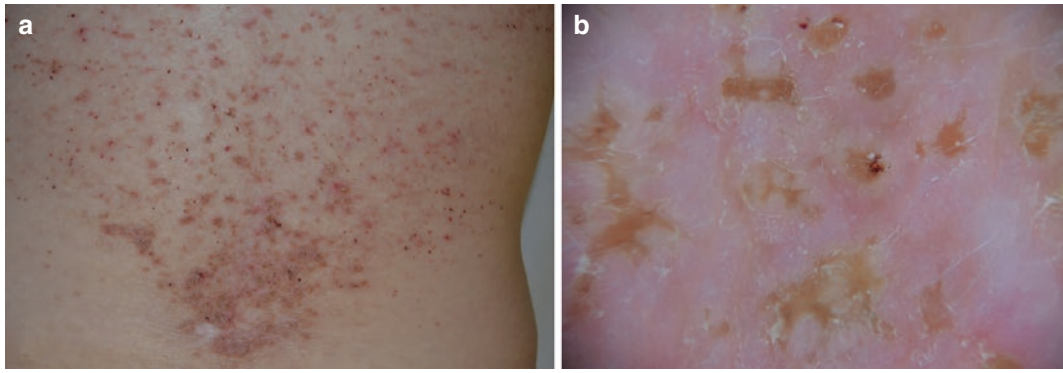

Fig. 6.1 Darier's disease. (**a**) Clinical aspect of the back. (**b**) Dermoscopy showing polygonal, yellowish/brownish structures surrounded by a whitish halo, superimposed on a pinkish, homogeneous background

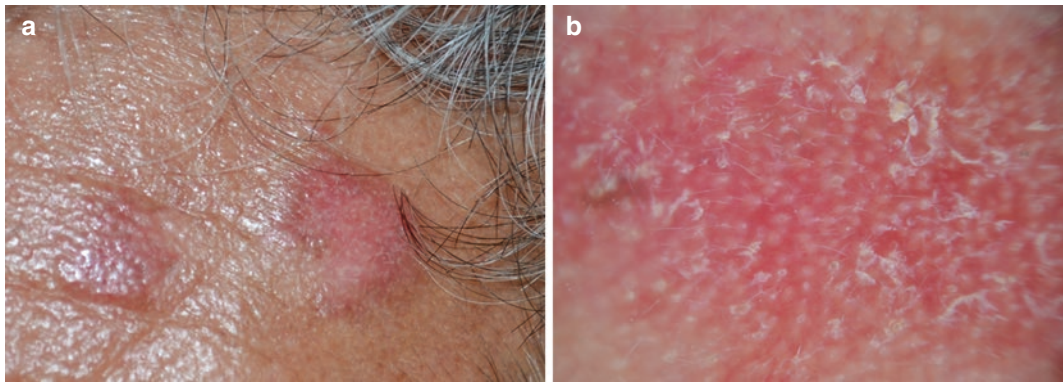

Fig. 6.2 Discoid lupus erythematosus. (**a**) Clinical aspect of two lesions of the forehead. (**b**) Dermoscopy showing diffuse, homogeneous background erythema, whitish scaling, and follicular yellowish plugs with a perifollicular whitish halo

logically related to follicular hyperkeratosis and perifollicular fibrosis [4, 13, 14]. Later, in scarring lesions, whitish structureless areas reflecting the diffuse dermal fibrosis, telangiectatic vessels, and pigmentary changes (hyperpigmentation) are observed. Hyperpigmentation correlates with the presence of melanophages located in the upper dermis that can be observed in all types of interface dermatitis as an expression of the basal layer damage with diffusion of melanin in the upper dermis [3]. Dermoscopy is particularly useful for the differential diagnosis with other erythematous-desquamative patchy lesions such as that of psoriasis.

6.4 Eczematous Dermatitis

In acute eczematous lesions, dermoscopy shows an erythematous background and yellowish scales with a patchy distribution due to the presence of spongiosis and serum exudation within the stratum corneum (Fig. 6.3) [15–18]. Moreover, irregularly distributed vessels with prominent dotted morphology may be generally observed. This pattern has low specificity as it may be observed, besides the different varieties of eczema, in acantholytic disorders and other superinfected dermatoses.

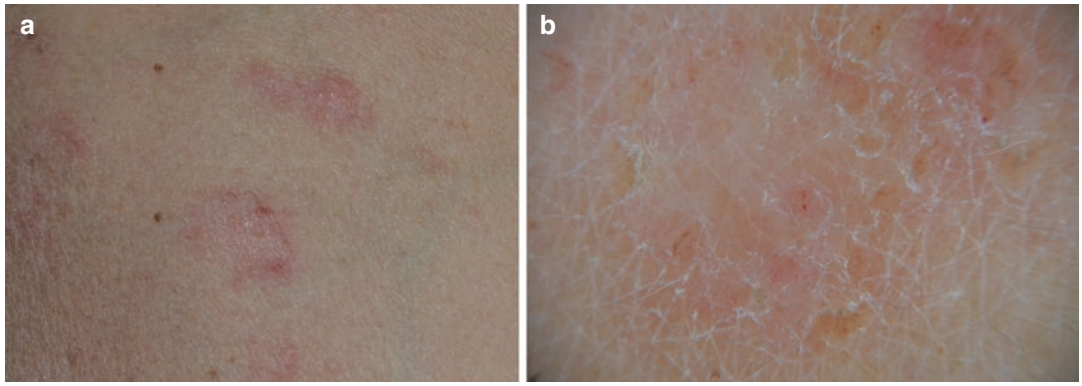

Fig. 6.3 Eczematous dermatitis. (**a**) Clinical aspect of multiple patches of the shoulder. (**b**) Dermoscopy showing yellowish scales and dotted vessels with an irregular distribution

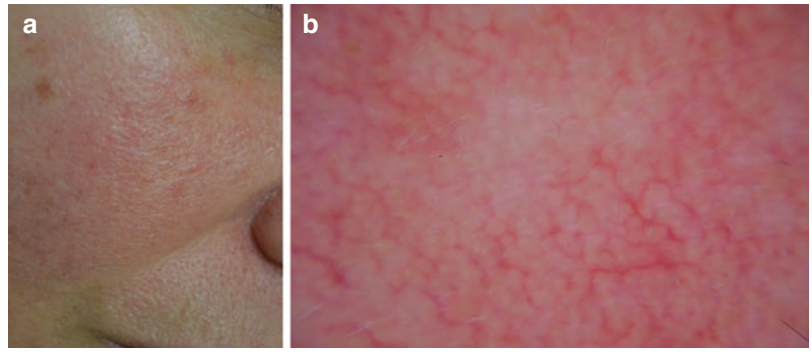

Fig. 6.4 Erythemato-telangiectatic rosacea. (**a**) Clinical aspect of the cheek. (**b**) Dermoscopy showing reddish background and prominent, linear vessels often arranged in a polygonal network

6.5 Erythemato-Telangiectatic Rosacea

Dermoscopy highlights the typical vascular alterations of erythemato-telangiectatic rosacea [19–21]. It is able to distinguish between the reddish background (background erythema) and the characteristic presence of prominent, linear vessels often arranged in a polygonal network, corresponding to the dilatation of the vessels of the sub-papillary plexus (telangiectasia) [22, 23]. The coexistence of both the components is frequently observed (Fig. 6.4). Higher magnifications allow to measure vessel caliber. Dermoscopy is particularly useful for the differential diagnosis with seborrheic dermatitis, which shows the same features of eczematous lesions. Dermoscopy may be also useful for treatment planning: based on dermoscopy findings, it may be possible to identify the most appropriate therapeutic strategy according to the ratio of the vascular components.

6.6 Granulomatous Diseases

Granulomatous skin diseases such as sarcoidosis, granuloma foreign body reaction, lupus vulgaris, and cutaneous leishmaniasis share similar dermoscopic features, consisting of the presence of orange-yellowish globular-like or structureless areas, histopathologically related to the granulomatous inflammatory infiltrate, and linear vessels (Fig. 6.5) [24–28].

6.7 Lichen Planus

Dermoscopy of lichen planus shows the typical presence of pearly, whitish lines, clinically corresponding to the "Wickham's striae," over a pinkish to light red background (Fig. 6.6) [29–31]. These lines, that in palmo-plantar lesions display a yellowish color, may have a different

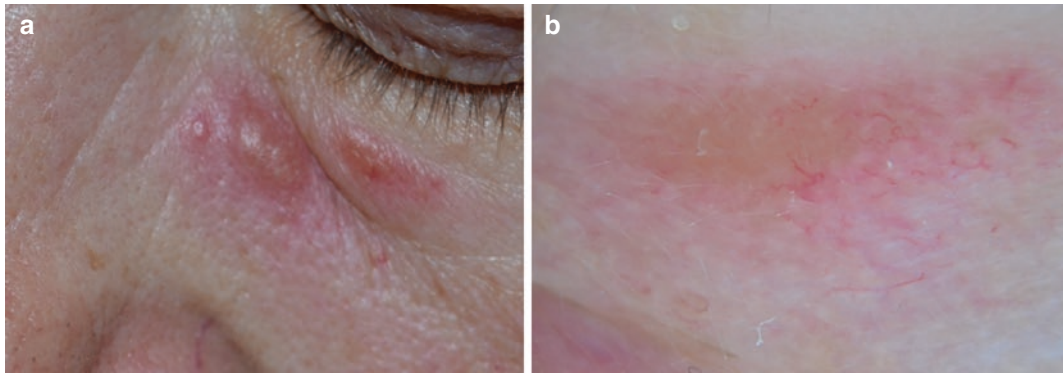

Fig. 6.5 Sarcoidosis. (**a**) Clinical aspect of facial lesions. (**b**) Dermoscopy showing orange-yellowish structureless areas and linear vessels

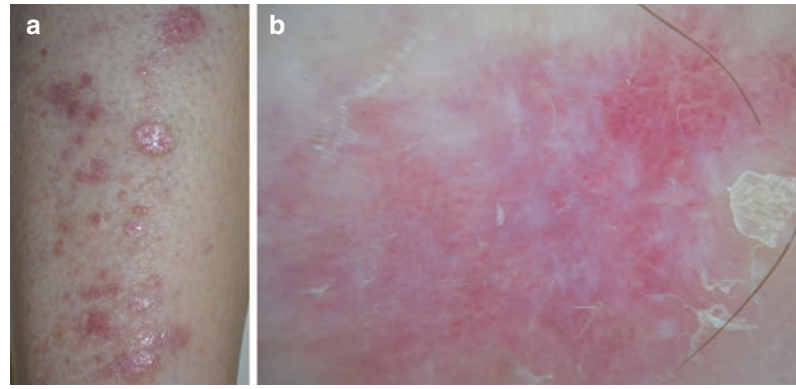

Fig. 6.6 Lichen planus. (**a**) Clinical aspect of multiple papules of the leg. (**b**) Dermoscopy showing pearly, whitish lines ("Wickham's striae") over a pinkish to light red background

configuration: reticular, arboriform, annular, globular, or homogeneous. They histopathologically correspond to areas of wedge-shaped hypergranulosis. Moreover, prominent linear vessels may be observed at the periphery of the whitish lines with a characteristic radial distribution [1, 3].

In pigmented lichen planus, dermoscopy reveals grayish to brown dots, due to the presence of melanophages, over a brownish background.

6.8 Lichen Sclerosus

In anogenital lichen sclerosus, dermoscopy shows patchy whitish areas [32–36], histopathologically corresponding to epidermal atrophy and dermal fibrosis, and linear and/or dotted vessels (Fig. 6.7). Purpuric dots/globules due to hemorrhages and erosions can sometimes be observed. Extragenital lichen sclerosus displays the presence of whitish, homogenous bright areas associated with follicular yellow circles (comedo-like openings) (Fig. 6.8) [37–40], the latter corresponding to follicular keratotic plugs. Dermoscopy may be useful for the differential diagnosis with morphea, which shows whitish clouds (or white beams), histologically corresponding to dermal sclerosis, crossed by linear irregular vessels; structureless or reticular brownish areas may also be observed [33].

6.9 Pigmented Purpuric Dermatoses

The different forms of pigmented purpuric dermatoses (Schamberg's disease, Majocchi's disease, Gougerot–Blum syndrome, lichen aureus, and eczematid-like purpura of Doucas and Kapetanakis) show at dermoscopy the presence of irregular, roundish, reddish dots, globules, and

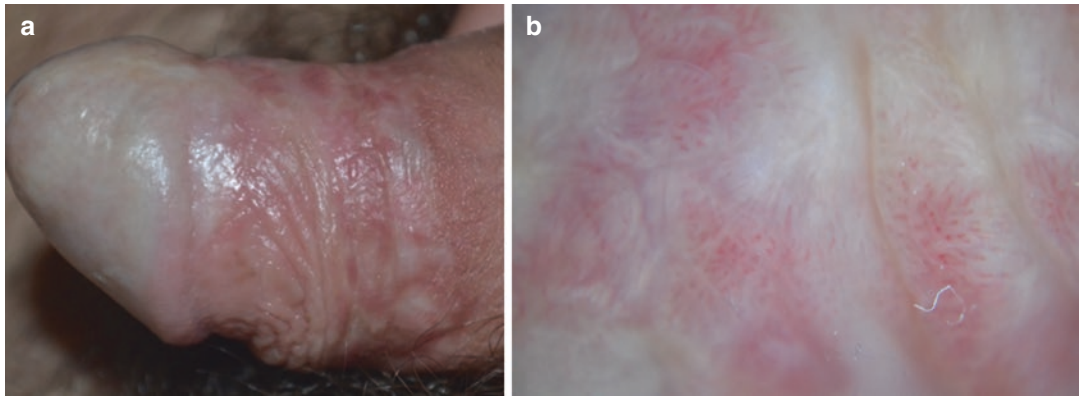

Fig. 6.7 Genital lichen sclerosus. (**a**) Clinical aspect. (**b**) Dermoscopy showing patchy whitish areas and linear and dotted vessels

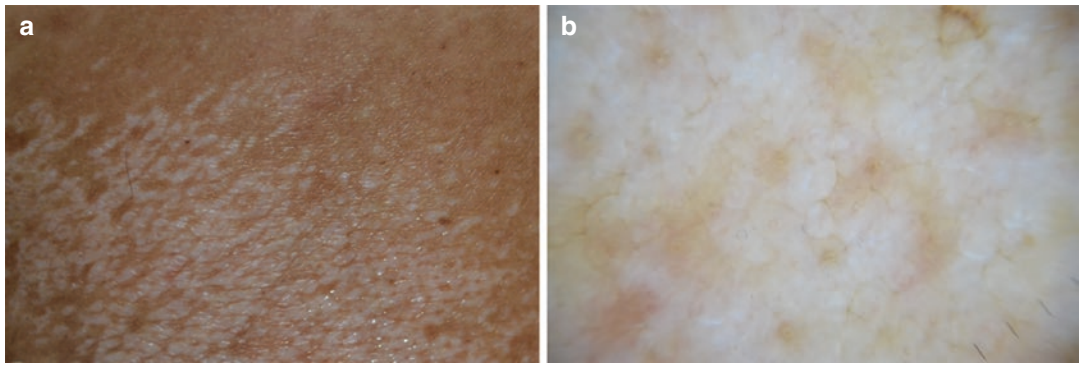

Fig. 6.8 Extragenital lichen sclerosus. (**a**) Clinical aspect of a plaque of the trunk. (**b**) Dermoscopy showing whitish, homogenous bright areas associated with follicular yellow circles (comedo-like openings)

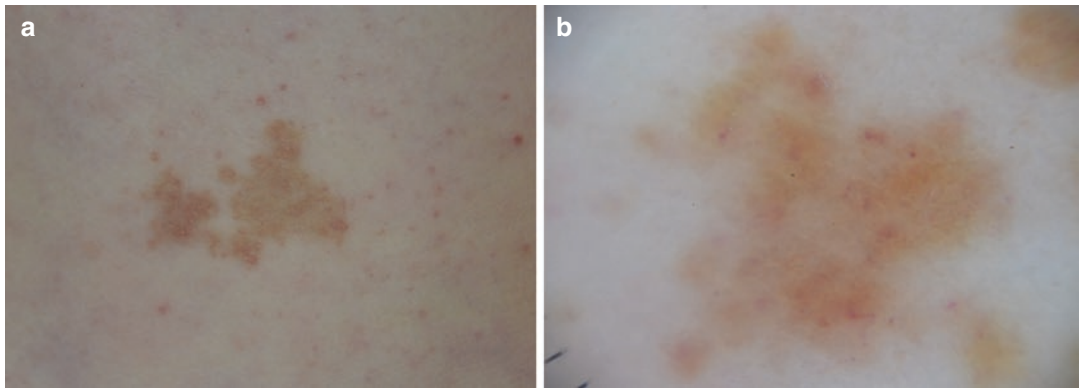

Fig. 6.9 Lichen aureus. (**a**) Clinical aspect of a patch of the leg. (**b**) Dermoscopy showing irregular, roundish reddish dots and globules over a red-coppery diffuse homogeneous background pigmentation

patches over a red-brownish or red-coppery diffuse homogeneous background pigmentation (Fig. 6.9) [41]. This pattern histopathologically corresponds to hemosiderin deposition within the papillary dermis due to erythrocytes extravasations and may sometimes be observed in other conditions, such as urticarial vasculitis and pigmented lichen planus [41, 42].

6.10 Pityriasis Lichenoides

The papules of pityriasis lichenoides chronica shows at dermoscopy the peculiar presence of orange-yellowish structureless areas that histopathologically correspond to hemosiderin degradation from erythrocyte extravasation [43]. Moreover, irregularly distributed, linear or dotted vessels are generally present (Fig. 6.10). In pityriasis lichenoides et varioliformis acuta (PLEVA), papular and crusted lesions show a central whitish patch or amorphous brownish structure, respectively, surrounded by dotted and/or linear vessels [44].

6.11 Pityriasis Rosea

The roundish patches of pityriasis rosea show at dermoscopy a pinkish homogeneous background, irregular or patchy dotted vessels, and whitish scales with a typical peripheral distribution (Fig. 6.11) [4, 16, 45]. Dermoscopy may allow the differential diagnosis with some clinically similar disorders, such as guttate psoriasis and pityriasis lichenoides chronica, but cannot exclude other lesions such as tinea corporis or erythema annulare centrifugum.

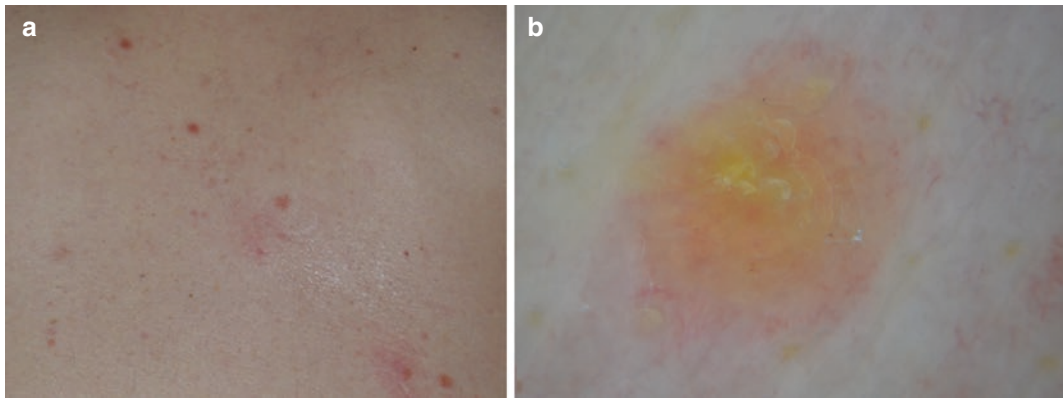

Fig. 6.10 Pityriasis lichenoides chronica. (**a**) Clinical aspect of multiple papules of the trunk. (**b**) Dermoscopy showing orange-yellowish structureless areas and irregularly distributed, linear and dotted vessels

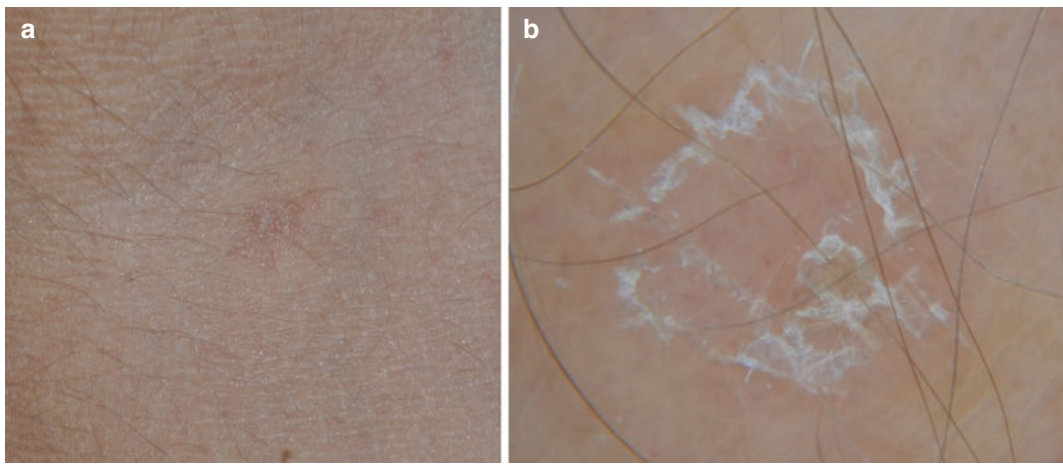

Fig. 6.11 Pityriasis rosea. (**a**) Clinical aspect of a small lesion of the trunk. (**b**) Dermoscopy showing whitish scales with a typical peripheral distribution and irregular dotted vessels

6.12 Porokeratosis

Dermoscopy of porokeratosis shows a central, homogeneous, whitish or brownish area delimited by a typical, double-marginated, white peripheral rim (Fig. 6.12) [1, 46–49]. This peripheral border, histopathologically corresponding to the cornoid lamella, has been described as "white track." Dotted or linear vessels may also be observed.

6.13 Psoriasis

In plaque psoriasis, dermoscopy shows a peculiar pattern, consisting of diffuse white scales and regularly distributed dotted vessels (or "red dots") over a light red background (Fig. 6.13) [3, 29, 30, 50]. At high magnifications (≥100×), the dotted vessels appear as dilated and twisted capillaries, with a "bushy" aspect. Each "bush" measures about 70–90 μm in diameter (vs. 15–25 μm of the normal capillary loops of healthy skin). The dotted vessels correlate with the microvascular modifications of psoriasis represented by ectatic and convoluted capillaries within elongated dermal papillae [51, 52]. Dermoscopy demonstrated to be a useful diagnostic tool in the different clinical localization of plaque psoriasis [15, 53–56]. When the whitish scales that correspond at histopathology of the typical hyperkeratosis of psoriasis are prominent, as in scalp or palmo-plantar psoriasis, the correct visualization of the dotted vessels may be hampered; in these cases, removal of the scales with keratolytic agents is suggested. Conversely, the vascular pattern is more evident in inverse psoriasis and psoriatic balanitis or vulvitis, in which generally the scales are minimal or absent. Higher magnifica-

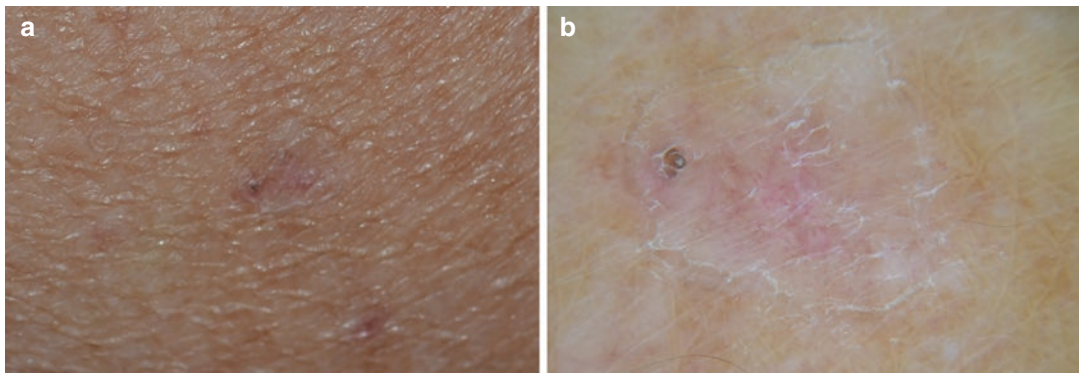

Fig. 6.12 Porokeratosis. (**a**) Clinical aspect of a lesion of the trunk. (**b**) Dermoscopy showing a whitish area delimited by a double-marginated, white peripheral rim ("white track")

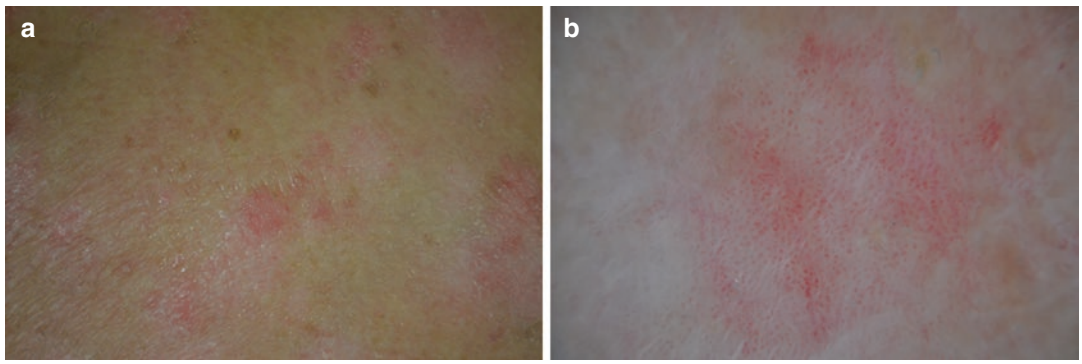

Fig. 6.13 Psoriasis. (**a**) Clinical aspect of plaques of the trunk. (**b**) Dermoscopy showing regularly distributed dotted vessels over a light red background

tion may be also indicated for therapeutic monitoring, helping to get a better visualization of the diameter reduction of the caoillary "bushes" during topical or systemic treatments [57–61].

6.14 Urticaria Pigmentosa

Macules and papules that characterize urticaria pigmentosa show at dermoscopy a combination of light-brown blots and pigment network [62–65] (Fig. 6.14) that is likely related to hyperpigmentation of basal keratinocytes induced by the mast cell growth factor that stimulates melanocyte proliferation and melanogenesis. In some cases, thin reticular telangiectasias on a mild erythematous background can be appreciated.

6.15 Zoon's Mucositis

The main dermoscopic aspect of Zoon's balanitis is represented by the presence of red to orange, structureless, homogeneous areas, corresponding to hemosiderin deposition, associated with fairly focused curved vessels with different morphology, including serpentine, convoluted, "chalice-shaped" and spermatozoa-like vessels (Fig. 6.15) [36, 66, 67]. The same aspects may be observed in Zoon's vulvitis [68].

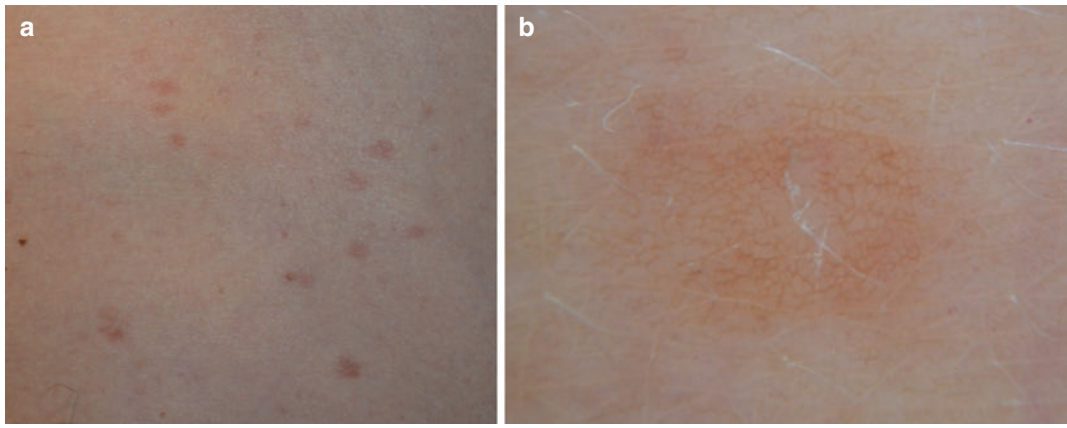

Fig. 6.14 Urticaria pigmentosa. (**a**) Clinical aspect of multiple papules of the trunk. (**b**) Dermoscopy showing a fine pigment network

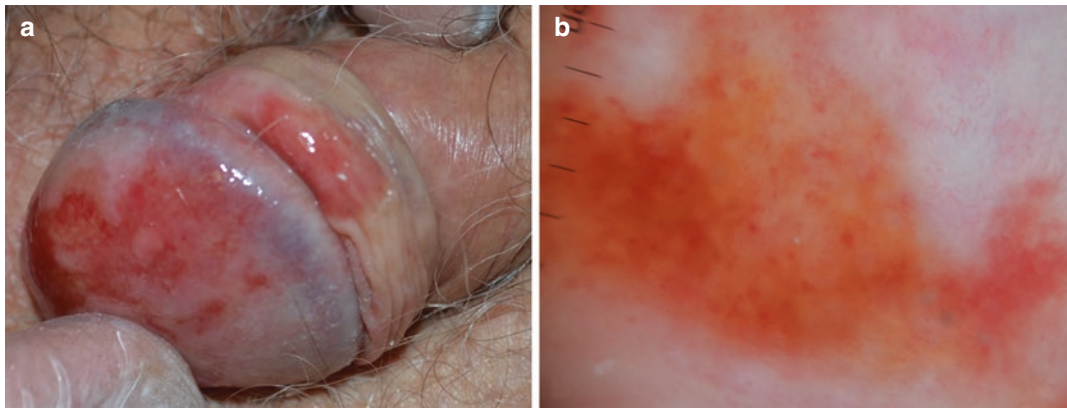

Fig. 6.15 Zoon's balanitis. (**a**) Clinical aspect. (**b**) Dermoscopy showing orange, structureless, homogeneous areas, and fairly focused curved vessels with different morphology

References

1. Micali G, Lacarrubba F, Massimino D, Schwartz RA. Dermatoscopy: alternative uses in daily clinical practice. J Am Acad Dermatol. 2011;64(6):1135–46.
2. Lallas A, Zalaudek I, Argenziano G, Longo C, Moscarella E, Di Lernia V, et al. Dermoscopy in general dermatology. Dermatol Clin. 2013;31:679–94.
3. Lacarrubba F, Verzì AE, Dinotta F, Scavo S, Micali G. Dermatoscopy in inflammatory and infectious skin disorders. G Ital Dermatol Venereol. 2015;150(5):521–31.
4. Micali G, Verzì AE, Lacarrubba F. Alternative uses of dermoscopy in daily clinical practice: an update. J Am Acad Dermatol. 2018;79(6):1117–32.e1.
5. Lacarrubba F, D'Amico V, Nasca MR, Dinotta F, Micali G. Use of dermatoscopy and videodermatoscopy in therapeutic follow up: a review. Int J Dermatol. 2010;49:866–73.
6. Micali G, Lacarrubba F. Dermatoscopy: instrumental update. Dermatol Clin. 2018;36(4):345–8.
7. Lacarrubba F, Verzì AE, Errichetti E, Stinco G, Micali G. Darier's disease: dermoscopy, confocal microscopy and histological correlations. J Am Acad Dermatol. 2015;73(3):e97–9.
8. Errichetti E, Stinco G, Lacarrubba F, Micali G. Dermoscopy of Darier's disease. J Eur Acad Dermatol Venereol. 2016;30(8):1392–4.
9. Errichetti E, De Francesco V, Pegolo E, Stinco G. Dermoscopy of Grover's disease: variability according to histological subtype. J Dermatol. 2016;43(8):937–9.
10. Lacarrubba F, Boscaglia S, Nasca MR, et al. Grover's disease: dermoscopy, reflectance confocal microscopy and histopathological correlation. Dermatol Pract Concept. 2017;7(3):51–4.
11. Sadayasu A, Maumi Y, Hayashi Y, Dekio I, Ishizaki S, Fujibayashi M, Tanaka M. Dermoscopic features of a case of transient acantholytic dermatosis. Australas J Dermatol. 2017;58(1):50–2.
12. Giacomel J, Zalaudek I, Argenziano G. Dermatoscopy of Grover's disease and solitary acantholytic dyskeratoma shows a brown, star-like pattern. Australas J Dermatol. 2012;53:315–6.
13. Lallas A, Apalla Z, Lefaki I, Sotiriou E, Lazaridou E, Ioannides D, et al. Dermoscopy of discoid lupus erythematosus. Br J Dermatol. 2013;168(2):284–8.
14. Inui S, Itami S, Murakami M, Nishimoto N. Dermoscopy of discoid lupus erythematosus: report of two cases. J Dermatol. 2014;41(8):756–7.
15. Lacarrubba F, Musumeci ML, Ferraro S, Stinco G, Verzì AE, Micali G. A three-cohort comparison with videodermatoscopic evidence of the distinct homogeneous bushy capillary microvascular pattern in psoriasis vs atopic dermatitis and contact dermatitis. J Eur Acad Dermatol Venereol. 2016;30(4):701–3.
16. Lallas A, Kyrgidis A, Tzellos TG, Apalla Z, Karakyriou E, Karatolias A, et al. Accuracy of dermoscopic criteria for the diagnosis of psoriasis, dermatitis, lichen planus and pityriasis rosea. Br J Dermatol. 2012;166:1198–205.
17. Errichetti E, Stinco G. Dermoscopy in differential diagnosis of palmar psoriasis and chronic hand eczema. J Dermatol. 2016;43(4):423–5.
18. Suh KS, Park JB, Yang MH, Choi SY, Hwangbo H, Jang MS. Diagnostic usefulness of dermoscopy in differentiating lichen aureus from nummular eczema. J Dermatol. 2017;44(5):533–7.
19. Lallas A, Argenziano G, Apalla Z, Gourhant JY, Zaballos P, Di Lernia V, Moscarella E, Longo C, Zalaudek I. Dermoscopic patterns of common facial inflammatory skin diseases. J Eur Acad Dermatol Venereol. 2014;28:609–14.
20. Lallas A, Argenziano G, Longo C, Moscarella E, Apalla Z, Koteli C, Zalaudek I. Polygonal vessels of rosacea are highlighted by dermoscopy. Int J Dermatol. 2014;53:e325–7.
21. Rosina P, Zamperetti MR, Giovannini A, Chieregato C, Girolomoni G. Videocapillaroscopic alterations in erythematotelangiectatic rosacea. J Am Acad Dermatol. 2006;54:100–4.
22. Micali G, Gerber PA, Lacarrubba F, Schäfer G. Improving treatment of erythematotelangiectatic rosacea with laser and/or topical therapy through enhanced discrimination of its clinical features. J Clin Aesthet Dermatol. 2016;9(7):30–9.
23. Micali G, Dall'Oglio F, Verzì AE, Luppino I, Bhatt K, Lacarrubba F. Treatment of erythemato-telangiectatic rosacea with brimonidine alone or combined with vascular laser based on preliminary instrumental evaluation of the vascular component. Lasers Med Sci. 2018;33(6):1397–400.
24. Balestri R, La Placa M, Bardazzi F, Rech G. Dermoscopic subpatterns of granulomatous skin diseases. J Am Acad Dermatol. 2013;69(5):e217–8.
25. Bombonato C, Argenziano G, Lallas A, Moscarella E, Ragazzi M, Longo C. Orange color: a dermoscopic clue for the diagnosis of granulomatous skin diseases. J Am Acad Dermatol. 2015;72:S60–3.
26. Lallas A, Zaballos P, Zalaudek I, Apalla Z, Gourhant JY, Longo C, et al. Dermoscopic patterns of granuloma annulare and necrobiosis lipoidica. Clin Exp Dermatol. 2013;38(4):425–7.
27. Pellicano R, Caldarola G, Filabozzi P, Zalaudek I. Dermoscopy of necrobiosis lipoidica and granuloma annulare. Dermatology. 2013;226(4):319–23.
28. Ramadan S, Hossam D, Saleh MA. Dermoscopy could be useful in differentiating sarcoidosis from necrobiotic granulomas even after treatment with systemic steroids. Dermatol Pract Concept. 2016;6(3):17–22.
29. Vázquez-López F, Manjón-Haces JA, Maldonado-Seral C, Raya-Aguado C, Pérez-Oliva N, Marghoob AA. Dermoscopic features of plaque psoriasis and lichen planus: new observations. Dermatology. 2003;207:151–6.
30. Zalaudek I, Argenziano G. Dermoscopy subpatterns of inflammatory skin disorders. Arch Dermatol. 2006;142:808.

31. Vázquez-López F, Maldonado-Seral C, López-Escobar M, Pérez-Oliva N. Dermoscopy of pigmented lichen planus lesions. Clin Exp Dermatol. 2003;28:554–64.
32. Lacarrubba F, Dinotta F, Nasca MR, Fabbrocini G, Micali G. Localized vascular lesions of the glans in patients with lichen sclerosus diagnosed by dermatoscopy. G Ital Dermatol Venereol. 2012;147:510–1.
33. Shim WH, Jwa SW, Song M, Kim HS, Ko HC, Kim MB, Kim BS. Diagnostic usefulness of dermatoscopy in differentiating lichen sclerous et atrophicus from morphea. J Am Acad Dermatol. 2012;66:690–1.
34. Larre Borges A, Tiodorovic-Zivkovic D, Lallas A, Moscarella E, Gurgitano S, et al. Clinical, dermoscopic and histopathologic features of genital and extragenital lichen sclerosus. J Eur Acad Dermatol Venereol. 2013;27:1433–9.
35. Borghi A, Corazza M, Minghetti S, Bianchini E, Virgili A. Dermoscopic features of vulvar lichen sclerosus in the setting of a prospective cohort of patients: new observations. Dermatology. 2016;232(1):71–7.
36. Lacarrubba F, Verzì AE, Ardigò M, Micali G. Handheld reflectance confocal microscopy, dermatoscopy and histopathological correlation of common inflammatory balanitis. Skin Res Technol. 2018;24(3):499–503.
37. Garrido-Ríos AA, Alvarez-Garrido H, Sanz-Muñoz C, Aragoneses-Fraile H, Manchado-López P, Miranda-Romero A. Dermoscopy of extragenital lichen sclerosus. Arch Dermatol. 2009;145:1468.
38. Horcajada-Reales C, Campos-Domínguez M, Conde-Montero E, Parra-Blanco V, Suárez-Fernández R. Comedo-like openings in dermoscopy: an essential diagnostic clue for lichen sclerosus, even in children. J Am Acad Dermatol. 2015;72:S4–5.
39. Lacarrubba F, Pellacani G, Verzì AE, Pippione M, Micali G. Extragenital lichen sclerosus: clinical, dermoscopic, confocal microscopy and histologic correlations. J Am Acad Dermatol. 2015;72:S50–2.
40. Lacarrubba F, Ardigò M, Di Stefani A, Verzì AE, Micali G. Dermatoscopy and reflectance confocal microscopy correlations in nonmelanocytic disorders. Dermatol Clin. 2018;36(4):487–501.
41. Zaballos P, Puig S, Malvehy J. Dermoscopy of pigmented purpuric dermatoses (lichen aureus): a useful tool for clinical diagnosis. Arch Dermatol. 2004;140:1290–1.
42. Vázquez-López F, Fueyo A, Sánchez-Martín J, Pérez-Oliva N. Dermoscopy for the screening of common urticaria and urticaria vasculitis. Arch Dermatol. 2008;144:568.
43. Errichetti E, Lacarrubba F, Micali G, Piccirillo A, Stinco G. Differentiation of pityriasis lichenoides chronica from guttate psoriasis by dermoscopy. Clin Exp Dermatol. 2015;40(7):804–6.
44. Lacarrubba F, Micali G. Dermoscopy of pityriasis lichenoides et varioliformis acuta. Arch Dermatol. 2010;146:1322.
45. Thomas M, Yadav T, Khopkar U. The role of dermoscopy using a triple light source in the diagnosis of pityriasis rosea: an observational pilot study. Int J Dermatol. 2017;56(7):e147–8.
46. Delfino M, Argenziano G, Nino M. Dermoscopy for the diagnosis of porokeratosis. J Eur Acad Dermatol Venereol. 2004;18:194–5.
47. Panasiti V, Rossi M, Curzio M, Bruni F, Calvieri S. Disseminated superficial actinic porokeratosis diagnosed by dermoscopy. Int J Dermatol. 2008;47:308–10.
48. Zaballos P, Puig S, Malvehy J. Dermoscopy of disseminated superficial actinic porokeratosis. Arch Dermatol. 2004;140:1410.
49. Jha AK, Sonthalia S, Lallas A. Dermoscopy of porokeratosis of mibelli. Indian Dermatol Online J. 2017;8(4):304–5.
50. Kim GW, Jung HJ, Ko HC, Kim MB, Lee WJ, Lee SJ, Kim DW, Kim BS. Dermoscopy can be useful in differentiating scalp psoriasis from seborrhoeic dermatitis. Br J Dermatol. 2011;164:652–6.
51. Micali G, Lacarrubba F, Musumeci ML, Massimino D, Nasca MR. Cutaneous vascular patterns in psoriasis. Int J Dermatol. 2010;49:249–56.
52. Lacarrubba F, Pellacani G, Gurgone S, Verzì AE, Micali G. Advances in non-invasive techniques as aids to the diagnosis and monitoring of therapeutic response in plaque psoriasis: a review. Int J Dermatol. 2015;54:626–34.
53. Micali G, Nardone B, Scuderi A, Lacarrubba F. Videodermatoscopy enhances the diagnostic capability of palmar and/or plantar psoriasis. Am J Clin Dermatol. 2008;9:119–22.
54. Lacarrubba F, Nasca MR, Micali G. Videodermatoscopy enhances diagnostic capability in psoriatic balanitis. J Am Acad Dermatol. 2009;61:1084–6.
55. Musumeci ML, Lacarrubba F, Catalfo P, Scilletta B, Micali G. Videodermatoscopy evaluation of the distinct vascular pattern of psoriasis improves diagnostic capability for inverse psoriasis. G Ital Dermatol Venereol. 2017;152(1):88–90.
56. Rosina P, Zamperetti MR, Giovannini A, Girolomoni G. Videocapillaroscopy in the differential diagnosis between psoriasis and seborrheic dermatitis of the scalp. Dermatology. 2007;214:21–4.
57. Rosina P, Giovannini A, Gisondi P, Girolomoni G. Microcirculatory modifications of psoriatic lesions during topical therapy. Skin Res Technol. 2009;15:135–8.
58. Stinco G, Lautieri S, Piccirillo F, Valent F, Patrone P. Response of cutaneous microcirculation to treatment with mometasone furoate in patients with psoriasis. Clin Exp Dermatol. 2009;34:915–9.
59. Musumeci ML, Lacarrubba F, Fusto CM, Micali G. Combined clinical, capillaroscopic and ultrasound evaluation during treatment of plaque psoriasis with oral cyclosporine. Int J Immunopathol Pharmacol. 2013;26:1027–33.
60. Stinco G, Buligan C, Maione V, Valent F, Patrone P. Videocapillaroscopic findings in the microcirculation of the psoriatic plaque during etanercept therapy. Clin Exp Dermatol. 2013;38:633–7.

61. Micali G, Lacarrubba F, Santagati C, Egan CG, Nasca MR, Musumeci ML. Clinical, ultrasound, and videodermatoscopy monitoring of psoriatic patients following biological treatment. Skin Res Technol. 2016;22(3):341–8.
62. Akay BN, Kittler H, Sanli H, Harmankaya K, Anadolu R. Dermatoscopic findings of cutaneous mastocytosis. Dermatology. 2009;218:226–30.
63. Vano-Galvan S, Alvarez-Twose I, De las Heras E, Morgado JM, Matito A, Sánchez-Muñoz L, et al. Dermoscopic features of skin lesions in patients with mastocytosis. Arch Dermatol. 2011;147:932–40.
64. Miller MD, Nery NS, Gripp AC, Maceira JP, Nascimento GM. Dermatoscopic findings of urticaria pigmentosa. An Bras Dermatol. 2013;88(6):986–8.
65. Micali G, Verzì AE, Quattrocchi E, Ng CY, Lacarrubba F. Dermatoscopy of common lesions in pediatric dermatology. Dermatol Clin. 2018;36(4):463–72.
66. Corazza M, Virgili A, Minghetti S, Toni G, Borghi A. Dermoscopy in plasma cell balanitis: its usefulness in diagnosis and follow-up. J Eur Acad Dermatol Venereol. 2016;30(1):182–4.
67. Errichetti E, Lacarrubba F, Micali G, Stinco G. Dermoscopy of Zoon's plasma cell balanitis. J Eur Acad Dermatol Venereol. 2016;30(12):e209–10.
68. Corazza M, Toni G, Virgili A, Borghi A. Plasma cell vulvitis: further confirmation of the diagnostic utility of dermoscopy. Int J Dermatol. 2018;57(12):e164–5.

Dermoscopy for Infectious Diseases

7

Sean Ekinde and Elisa Cinotti

7.1 Introduction

Dermoscopy is a noninvasive, in vivo technique traditionally used to improve diagnostic accuracy of the pigmented skin lesions. It allows physicians to examine the morphology of skin lesions, helping to identify subtle clinical clues, confirming naked-eye clinical diagnoses, and monitoring treatment progress. In the past years, the applications of dermoscopy expanded the dermoscopic features of several infectious skin diseases, including those of viral, fungal and parasitic origin have been described, assisting the clinical diagnosis of these conditions and reducing the need of semi-invasive or invasive procedures, such as skin scrapings and/or biopsies. The use of newer-generation polarized dermatoscopes may be particularly useful for examining infectious skin diseases because they avoid direct contact with the skin, minimizing the risk of cross-infection between patients. This chapter summarizes essential dermoscopic features of the most commonly known skin infections and infestations.

S. Ekinde (✉) · E. Cinotti
Department of Medical, Surgical and Neurological Science, Dermatology Section, University of Siena, S. Maria alle Scotte Hospital, Siena, Italy

7.2 Parasitic Disorders

7.2.1 Scabies

The host-specific mite *Sarcoptes scabiei* var. *hominis* is the parasite known to cause scabies disease. Scabies can be transmitted into two different ways: directly by close contact or indirectly due to fomites. Moreover, this kind of disease is found more often in crowded environments such as schools, nursing homes, prisons, and refugee camps [1]. The clinical suspicion of scabies arises in case of intense pruritus, accentuated at nighttime, and typically located on wrists, axillae, waist, umbilicus, ankles, buttocks, genitalia, areolae, and nipples. Although the pathognomonic sign is the burrow which can be of about 3–10 mm long with a wavy, thread-like, grayish-whitish feature (Fig. 7.1a), it may be hard to detect at clinical observation because of the intense scratching that lead to other lesions such as small erythematous papule and excoriations, often with signs of secondary bacterial infection. These clinical manifestations may mimic other conditions, including insect bites, folliculitis, viral exanthema, and papular urticaria [2]. A positive clinical history for similar symptoms in household members or close personal contacts may help in the differential diagnosis. The definitive diagnosis of scabies is made by the microscopic visualization of mites, eggs, or feces from skin scraping samples. The diagnostic accuracy

M. Fimiani et al. (eds.), *Technology in Practical Dermatology*,
https://doi.org/10.1007/978-3-030-45351-0_7

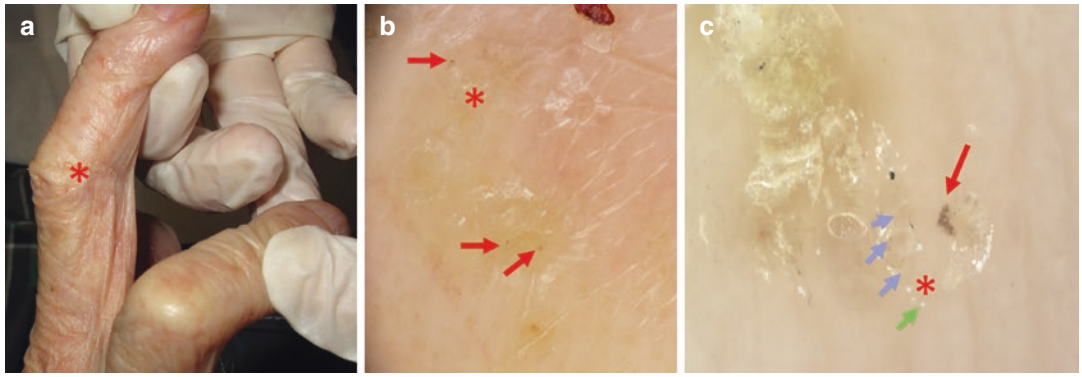

Fig. 7.1 Scabies: clinical (**a**) and dermoscopic (**b**, 20×; **c**, 70×) images. Kite sign or wing jet sign (**b**, **c**): small dark triangular structures (red arrows) located at the end of wavy lines corresponding to the burrows (red asterisks). Eggs (**c**, blue arrow) and droppings (**c**, green arrow) are visible at high-magnification dermoscopy

of dermoscopy has been reported to be at least equal to traditional ex vivo optical microscopic examination, while requiring less time, cost, and experience [3, 4]. Indeed, it allows a rapid, non-traumatic, in vivo examination of the entire skin surface reducing the false-negative results caused by the limited examinable area which can be scraped for the microscopic test. Scabies is characterized by a specific dermoscopic pattern consisting a triangular brown structure ("delta wing jet sign" or "kite sign") corresponding to the fore portion of the mite usually found at the end of a curvy and wavy line corresponding to the burrow similar to a "kite leaving a contrail" (Fig. 7.1b) [5, 6]. Moreover, other diagnostic features include a burrow filled with eggs, which appears as a "string of pearls" [7]. Dermoscopy is also particularly useful to screen asymptomatic contacts and for post-therapeutic follow-up, ruling out the persistence of viable mites [4, 8, 9]. However, in pretreated patients, it is not possible to establish if mites are dead or not, and they can also be confused with excoriations and/or splinter hemorrhages that may frequently occur because of repeated scratching [3, 8, 10, 11]. High magnification videodermoscopy is particularly useful when the burrow behind the parasite is absent and a parasite might be misinterpreted as a crust at conventional 10–20× dermoscopy. Using high magnification dermoscopy, it is possible to clearly identify the brown cephalic portion of the parasite followed by its ovoid body often visible with two brownish parallel bands (Fig. 7.1c) [10, 11]. Moreover, high-magnification dermoscopy allows detecting mite eggs and droppings easily (Fig. 7.1c). Dermoscopy is also well tolerated by the pediatric population because it is not painful and does not require blades for skin scraping [12]. On pigmented skin, the "kite sign" is hardly discernible [3, 13].

7.2.2 Pediculosis

Dermoscopy has demonstrated to be useful for assisting the clinical diagnosis and therapeutic monitoring of pediculosis capitis and phthiriasis pubis by revealing the lice or the nits fixed to the hair shaft [14].

7.2.3 Pediculosis of the Scalp

Pediculosis capitis is widespread in all geographical areas and usually cause small epidemics in school-aged children and in members of the same household. Girls seem to be more frequently affected, probably because of long hair and the habit of sharing brushes and hair accessories [1].

The main clinical symptom is an intense scalp pruritus associated with excoriations and secondary bacterial infection, primarily on the occipital and retroauricular region. This clinical presentation may mimic other conditions such as

tinea capitis, atopic dermatitis, and seborrheic dermatitis. This infestation is caused by *Pediculus humanus* var. *capitis*, a flattened louse, 2–3 mm long, wingless and with three pair of legs. The female louse secretes chitinous material to fix her eggs (nits) to the hair shafts close to the scalp. Active pediculosis infestation can be confirmed by identifying the nits on the scalp's surface [15]. The identification of empty or dead nits after the therapy is crucial to monitor the treatment response. Dermoscopy can help the clinician to identify the nits and to distinguish between empty nits and nits containing nymphs. The latter appear brown, ovoid, firmly attached to the hair shafts, whereas empty nits appear translucent and typically show a plane and fissured free ending, and they may persist after the healing [16–18]. Dead nits have a focal brown area (collapsed nymph) and a translucent area (air pocket) [19, 20]. The dermoscopical examination can also help to distinguish clinical findings that resemble nits (pseudonits), such as scales of seborrheic dermatitis [19], hair casts [20], white piedra [21, 22], or trichorrhexis nodosa. Pseudonits are not firmly attached to the hair shaft and appear dermoscopically as amorphous, whitish structures [23]. Polarized non-contact dermoscopy is recommended because it minimizes the risk of infestation transmission to other patients [24].

7.2.4 Phthiriasis

Phthiriasis pubis, officially classified as a sexually transmitted disease because of the direct contact transmission and the typical infestation of the pubic hair, can also be found in other areas such as scalp, eyebrows, eyelashes (phthiriasis palpebrarum) and can occasionally be seen in children. The infestation is caused by *Pthirus pubis*, a roundish louse, 1–2 mm long. The main clinical symptom is pruritus, sometimes associated with excoriations and gray-blue macules (maculae ceruleae) on the thighs or trunk. Dermoscopy easily helps to diagnose both phthiriasis pubis and phthiriasis palpebrarum by identifying the louse firmly attached to the pubic hairs [25–27]. It can also help to distinguish full and empty nits from pseudonits like in pediculosis capitis [28].

7.2.5 Tungiasis

Tungiasis is a skin infestation caused by the wingless flea *Tunga penetrans* (1 mm long), endemic in Caribbean islands, Central and South America, Pakistan, Africa, and India. The typical lesion of tungiasis is caused by the burrowing female flea that requires a warm-blooded animal for the egg maturation. Because of the limited jumping ability of the flea, the lesions are usually localized on the feet, in particular on the periungual area of the toes and on the soles. The first sign after the puncture is a small black dot with erythema which evolves into a pearl-like whitish papule and then a larger black nodule surrounded by a white halo. In consideration of its low incidence outside endemic areas, its clinical features may be confused with other conditions such as plantar warts, tick bite reactions, or squamous cell carcinoma. Dermoscopy has been reported to be a viable diagnostic tool to help the clinician in the differential diagnosis, in particular in non-endemic areas [29–35]. Dermoscopy of tungiasis shows a brown or flesh-colored nodule with a brown ring at the center, which surrounds a blackish pore (posterior opening of the parasite) [29, 35]. The eggs appear like gray-blue blotches or white ovals organized in chain-like structures [30, 35]. Shaving the superficial part of the lesion may reveal clusters of eggs contained in the jelly sac abdomen of the parasite [30]. Ex vivo examination may also be helpful for diagnosis confirmation after the extraction of the flea from the lesion [34].

7.2.6 Cutaneous Leishmaniasis

Leishmaniases are a group of chronic parasitic diseases caused by various species of the protozoan Leishmania, an obligate intracellular parasite of mononuclear phagocytes. Leishmania is transmitted by inoculation of the parasite in its promastigote form by infected female sandflies

(Phlebotomus and Lutzomyia) [36]. There are many clinical subtypes of Leishmania (cutaneous, mucocutaneous, visceral), and the clinical manifestations correlate with the host immune response and with the species of Leishmania involved. The disease is diffused worldwide, endemic in South America, parts of Africa and Asia, and in the Mediterranean region. Cutaneous manifestation usually begins with a small erythematous papule in the site of inoculation (usually in exposed body areas such as face, legs, ankles, hands, and forearms). During several weeks, the starting lesion slowly enlarges into an infiltrated nodule or plaque with central ulceration. In most cases, acute cutaneous leishmaniosis resolves spontaneously in several months, but a minority may become chronic and develop satellite lesion with a sporotrichoid spread pattern. The differential diagnosis of cutaneous leishmaniasis includes basal cell carcinoma, mycobacterial infections, and subcutaneous mycoses; skin biopsies are needed to demonstrate the presence of the parasite in dermal macrophages (amastigote form) and confirm the clinical suspect. Dermoscopy shows many different patterns that seem to have a correlation with the clinical evolution and may help the clinician to enhance the clinical diagnosis [37–40]. In the papular lesion, the most common findings are yellow tear-like structures (keratin plugs), diffuse erythema and vessels of various shape (dots, glomerular-like, commas, hairpin, arborizing). In the nodular chronic lesion, the predominant pattern consists of white starburst-like pattern associated with ulceration, scales, and peripheral vascular structures. Other dermoscopic findings are yellow-salmon colored areas, milia-like cysts, and a perilesional hypopigmented area [37, 39, 40].

7.2.7 Cutaneous Larva Migrans

Cutaneous larva migrans (creeping eruption) is caused by the epidermic infestation of hookworms that usually infect domestic animals (cats and dogs). The hookworms penetrate and migrate through the epidermis causing intense localized pruritus and a linear or serpiginous erythematous eruption that corresponds to the larva progression (1–2 cm per day) (Fig. 7.2a). The infestation remains localized in the epidermis because the parasite lacks collagenase, necessary to pass through the basement membrane. The lesions are most frequently localized on the extremities or buttocks. The infection is acquired by contact with animal feces especially by walking barefoot on contaminated ground. The main species of hookworms correlated with creeping eruptions are *Ancylostoma braziliense* and *A. caninum*. Cutaneous larva migrans has a worldwide distribution but occurs most frequently in warmer climates. The typical cutaneous eruptions associated

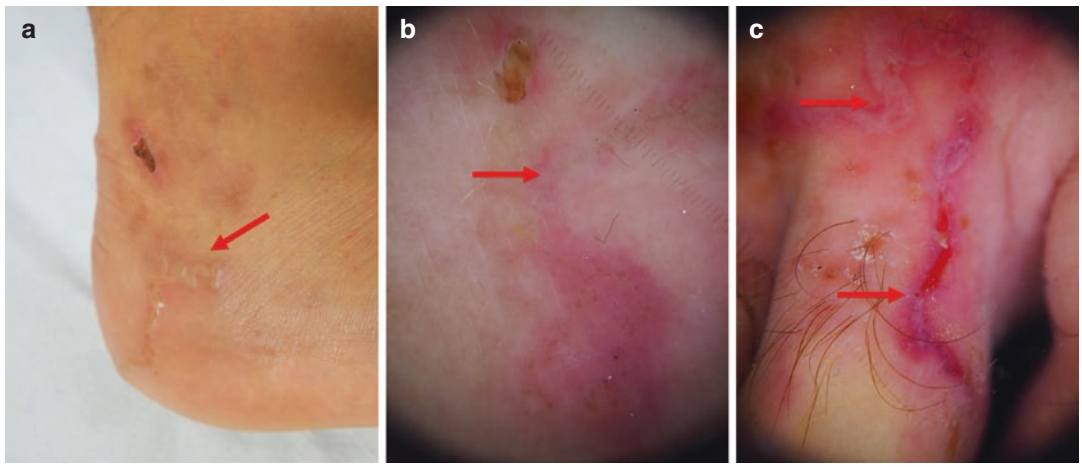

Fig. 7.2 Cutaneous larva migrans: clinical (**a**) and dermoscopic (**b**, **c**, 20×) images. Creeping eruptions: serpiginous erythematous tracts that corresponds to the larva progression (red arrows)

with the clinical history are the basis for the diagnosis. Dermoscopy may help to better observe the serpiginous tract formed by the larva (Fig. 7.2b), and it has been claimed that it can also identify the larva by revealing a translucent brownish structureless area on the serpiginous tract [6, 41–43]. However, in our experience, it seems not to be feasible to differentiate the larva from the excoriations and vesicles that are on the serpiginous tract.

7.2.8 Tick Bites

Dermoscopy can be used to locate the tick (Fig. 7.3a) and to help the clinician to perform a complete removal. The tick's body and anterior legs can be seen protruding from the surface of the skin; they appear as a brown/gray translucent shield with brown/black streaks (Fig. 7.3b). After the tick's removal, residual body parts appear like brown to black to gray areas of pigmentation [44, 45].

7.3 Viral Disorders

7.3.1 Cutaneous and Anogenital Warts

Human papillomaviruses (HPVs) are a large group of DNA viruses responsible of asymptomatic infections of the epithelia of skin and mucosa, some genotypes are correlated with benign proliferation (warts and papillomas) or skin cancers [46, 47]. Cutaneous HPV infection occurs most commonly via direct skin to skin contact (intimate contact for anogenital infection) and less frequently through contaminated objects. Warts classification is based on anatomic location, histology, and clinical morphologic criteria. *Common warts* (verrucae vulgaris) are exophytic, hyperkeratotic papules with rough top (Fig. 7.4a), localized mainly on hands and fingers, other body parts like face and neck may also be involved, especially by pedunculated and filiform warts. *Palmar and plantar warts* appear as hyperkeratotic, tick, endophytic papules with a central depression, localized on palms and soles and usually painful. Plantar warts may coalesce into larger lesions (mosaic warts or myrmecia). *Flat warts* (verrucae planae) are flat-topped papules, skin colored or brown/pink pigmented, with smooth surface, usually located on arms, face, and dorsal hands with a linear distribution pattern. *Anogenital warts* (condylomata acuminata) may appear as exophytic pedunculated papillomas with smooth surface or sessile papules, skin-colored, whitish (when macerated), or brown. They usually involve the external genitalia, perineum, inguinal folds, pubis, or perianal areas. Warts diagnosis is generally clinical, even though dermoscopy can be useful to distinguish from other cutaneous lesions such as tylosis or amelanotic melanoma [48, 49]. The dermoscopy pat-

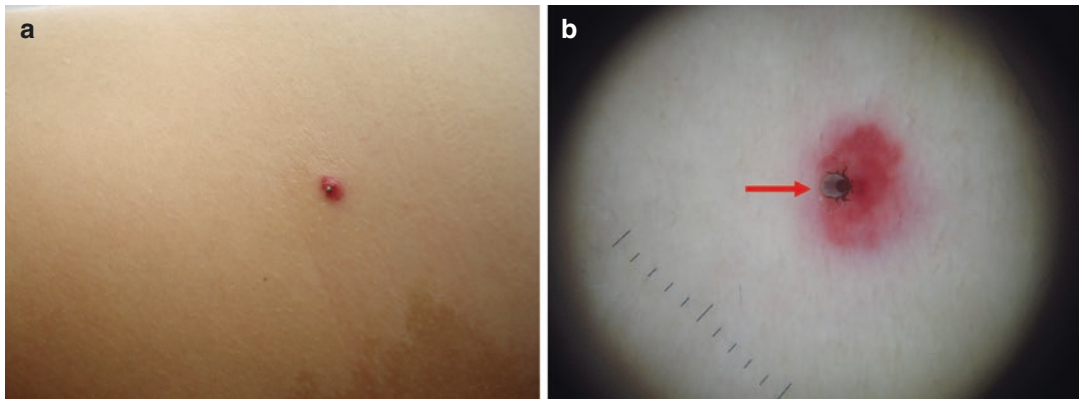

Fig. 7.3 Tick bite: clinical (**a**) and dermoscopic (**b**, 20×) images. Dermoscopy shows a tick's body with anterior legs protruding from the surface of the skin (red arrow)

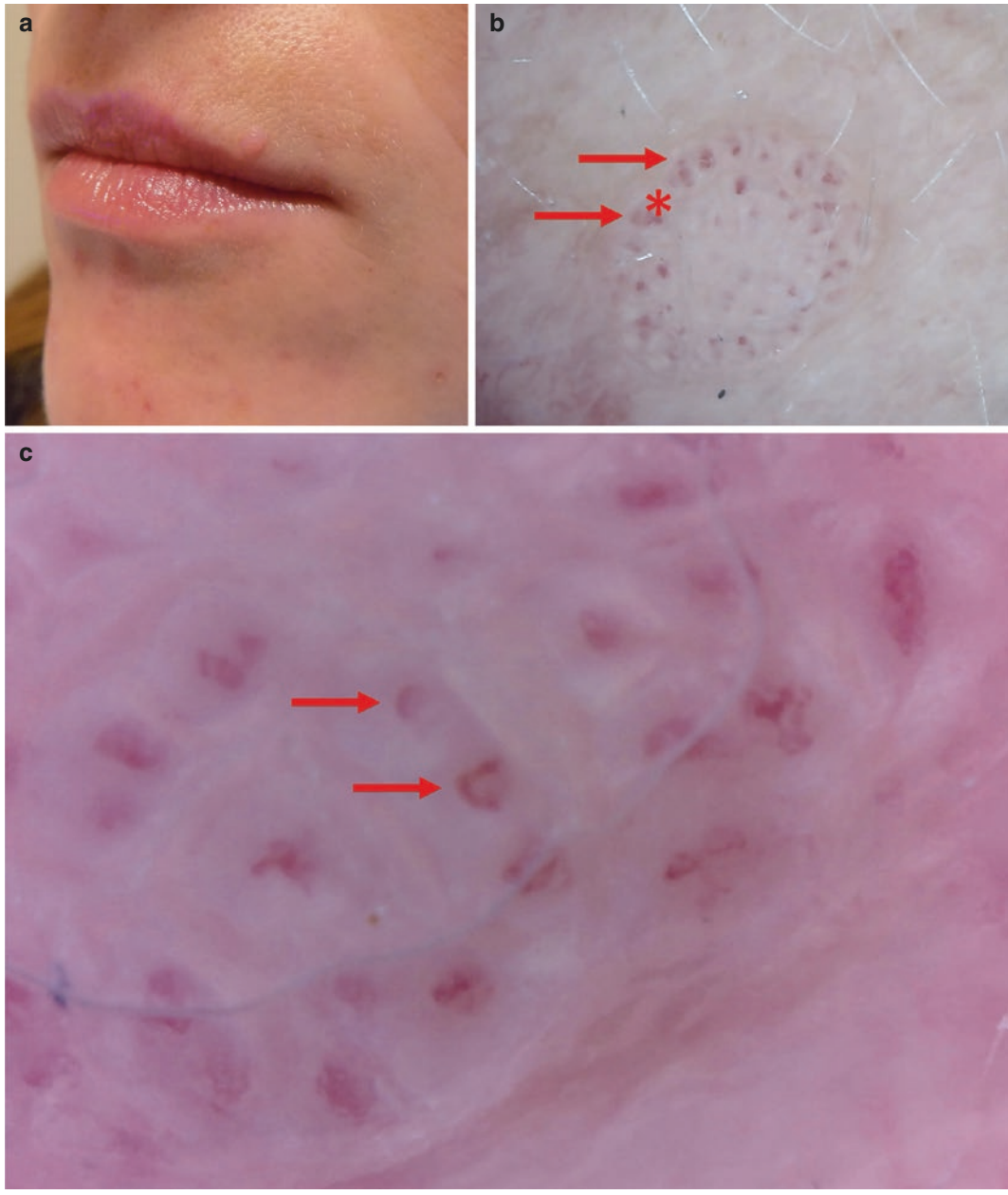

Fig. 7.4 Common wart: clinical (**a**) and dermoscopic (**b**, 20×; **c**, 150×) images. Dermoscopy shows dilated dermal capillaries visible as red dots (**b**, red arrows) or glomerular vessels (**c**, red arrows) depending on the magnification, and surrounded by a whitish halo (red asterisk)

tern of *common warts* displays multiple papillae, densely packed, with hemorrhagic red dots or lops in the center of each one and a whitish halo in the periphery (Fig. 7.4b,c). Signs of hemorrhages may be additional finding appearing as black dots or streak with an irregular distribution [6, 50, 51]. Exophytic lesions appear as multiple digitiform projections with a central dilated vessel and whitish periphery [6, 51–54]. Dermoscopy of *palmoplantar warts* reveals multiple signs of

hemorrhages as black dots and streaks with an irregular distribution on a yellowish papilliform surface associated with the disruption of dermatoglyphics, useful pattern to discriminate warts from tylomas [48]. Dermoscopy of *flat warts* reveals red dots (dilated dermal capillaries) with a regular distribution on a light-brown or yellow background [55, 56]. *Anogenital warts* reveal different dermoscopic patterns comparing early and advanced stages. Early and clinically flat lesions display a mosaic pattern (whitish network with regularly distributed dotted vessel) while advanced and raised papillomatous warts show a finger-like or knob-like pattern [57]. Dermoscopy may be useful to differentiate HPV-related lesions from other anogenital growths such as vestibular papillae, molluscum contagiosum, or pearly penile papules [56, 58, 59]. Recent studies show that dermoscopy may also help the clinician to monitor the treatment progress [48].

7.3.2 Molluscum Contagiosum

Molluscum contagiosum (MC) is a cutaneous, highly contagious, viral infection caused by a DNA poxvirus. The disease is common and self-limited in children, and it also occurs in sexually active adults and immunocompromised patients. The transmission occurs by skin-to-skin contact or, less frequently, by fomites. The diagnosis is often clinical based because of the classic characteristics of the lesions (umbilicated, dome-shaped, pearly, or skin-colored papules) without a typical localization on the body surface (Fig. 7.5a). Dermoscopy can be useful to differentiate MC from other disorders such as milia, acne lesions, warts, or Spitz nevi [60–64]. The stereotypic dermoscopic pattern of MC lesions is characterized by a central pore (umbilication) associated with polylobular, yellowish/white, amorphous structures, surrounded by branched or linear vessels (red corona) (Fig. 7.5b). This pattern correlates histopathologically with the hyperplastic squamous epithelium with dilated dermal vessels and large keratinocytes with cytoplasmic inclusions (Henderson-Paterson bodies) [60, 61].

7.4 Fungal Disorders

7.4.1 Tinea Capitis

Tinea capitis is a common dermatophyte infection of the scalp hair occurring predominantly in prepubescent children, often associated with poor hygiene or direct contact with pets. Many species of dermatophyte can invade the hair shaft and cause tinea capitis. Despite the clinical presentation is quite variable, the main three types of shaft invasion partially correlate with the clinical presentation and with the fungi genera. In the ectothrix form (Microsporum species), the hair is invaded by hyphae outside the shaft, then the infection spreads inside and down into follicles and penetrates the cortex. Clinically this type of infection causes scaly and inflamed area with hair loss (hair shaft breaks 2–3 mm above the scalp level). In the endothrix form (Trichophyton species), hyphae spread only inside the hair shaft causing negative results under Wood's light, differently from Microsporum species that emit fluoresce with

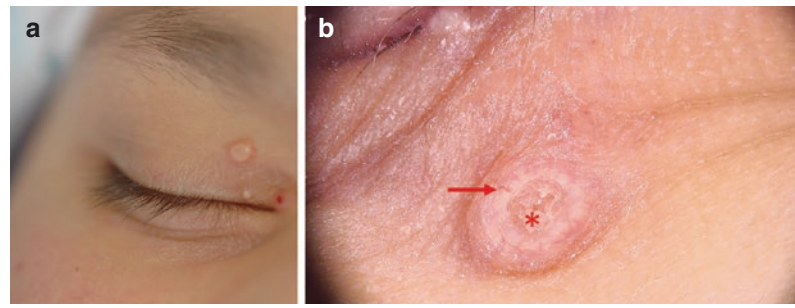

Fig. 7.5 Molluscum contagiosum: clinical (**a**) and dermoscopic (**b**, 20×) images. Dermoscopy shows a central pore filled with whitish amorphous material (red asterisk) and surrounded by radial linear vessels (red arrow)

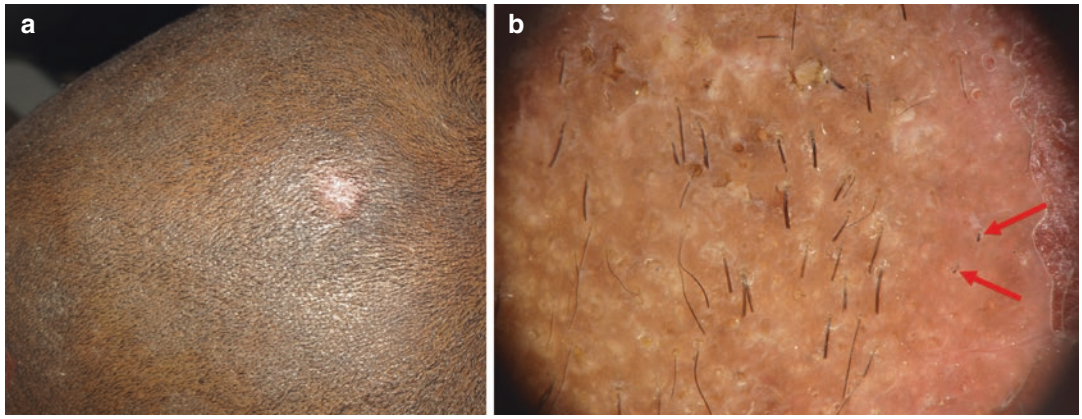

Fig. 7.6 Tinea capitis: clinical (**a**) and dermoscopic (**b**, 20×) images. Dermoscopy shows broken hair (red arrows) on a scaly and inflamed background with hair loss

wood lamp. Clinically the hairs break at scalp level leaving hair stubs within the follicles (Fig. 7.6a). In the favic infection (*T. schoenleinii*), hyphae form large clusters at scalp level where they penetrate the follicle from the base of hairs. Although hairs result less damaged compared to the other types of tinea capitis and they may keep growing, this last form can cause cicatricial alopecia if not treated. The diagnosis of tinea capitis relies on direct microscope observation of the hyphae from skin scraping samples and mycological cultures that allow identifying the type of dermatophyte. Recently many studies point out the importance of dermoscopy in the evaluation of hair diseases and in the early clinical diagnosis of tinea capitis. There are many dermoscopic findings that correlate with tinea capitis such as diffuse scaling, broken hairs, bent hairs, black dots, tufted folliculitis, zig-zag hairs, interrupted hairs (Morse or barcode-like) (Fig. 7.6b) [65–77]. Comma-hairs (C-shaped, thickened, and sharp ended) are more specifically correlated with *T. tonsurans* and *M. canis* (along with dystrophic and elbow-shaped hairs). Corkscrew-shaped hairs (short hairs with multiple twists) are typical of dark-skinned patients infected by *T. violaceum* and *T. soudanense*[75]. Trichoscopy may be useful to differentiate tinea capitis from other forms of alopecia such as alopecia areata and trichotillomania and to steer the clinical on the right dermatophyte subtype.

7.4.2 Tinea Nigra

Tinea nigra is a cutaneous superficial fungal infection caused by *Hortaea werneckii* (*Cladosporium werneckii* or *Exophiala werneckii*) [15]. This fungus provides single, irregular brown to black macule without associated symptoms that usually developed on the stratum corneum of palm and soles mimicking melanocytic lesions [78]. Dermoscopy can be useful to enhance the clinical diagnosis and prevent biopsies. Tinea nigra is characterized by fine pigmented spicules corresponding to hyphae in the stratum corneum that do not follow the dermatoglyphic furrows and ridges [6, 79, 80]. This pattern is useful to distinguish tinea nigra from melanocytic lesions which are characterized by a pigment distribution along furrow and ridges. There are only a few cases in literature about *Hortaea werneckii* having a parallel dermoscopic pattern [81–85].

7.5 Bacterial Disorders

Dermoscopy is usually not essential to diagnose bacterial skin disorders, and no specific dermoscopic patterns have been generally accepted as characteristics of these conditions. However, such examination could be of significant help for atypical bacterial skin infections

in order to exclude other skin diseases or in case of peculiar clinical aspects such as syphilitic alopecia (SA).

7.5.1 Syphilitic Alopecia

SA is a non-scarring hair loss, uncommon manifestation of secondary syphilis. The "moth-eaten" form is the most frequent subtype of SA followed by the diffuse form that mimic telogen effluvium and the mixed form, with the characteristics of both the previous subtypes. SA may clinically resemble many other hair disorders such as trichotillomania, alopecia areata, lichen planus pilaris, or tinea capitis; in addition, the affected patients may not show other clinical signs of secondary syphilis leading clinicians to delay the diagnoses. Despite trichoscopic descriptions of the various forms of SA are based on very few cases, in the absence of other syphilis manifestations, dermoscopy can be a useful tool to help the clinicians in the differential diagnosis.

The moth-eaten form is a patchy alopecia with alopecic areas of about 1–3 mm. Dermoscopy of the patches shows black dots at the periphery and yellow dots in the center, hypopigmentation of hair shafts with vellus hairs and empty follicles in a background of dilated capillaries with small blood extravasation [86, 87]. Diffuse SA involves the whole scalp, and trichoscopic observation does not show significant alterations [87]. Trichoscopy of mixed SA displays the same characteristics of the moth-eaten form plus some additional features such as focal follicular hyperkeratosis, diffuse scaling, and single- or double-bending tapering hairs at the periphery of the alopecic areas [88].

References

1. Verzì AE, Lacarrubba F, Dinotta F, Micali G. Dermatoscopy of Parasitic and Infectious Disorders. Dermatol Clin. 2018;36:349–58.
2. Chosidow O. Scabies. N Engl J Med. 2006;354:1718–27.
3. Dupuy A, Dehen L, Bourrat E, et al. Accuracy of standard dermoscopy for diagnosing scabies. J Am Acad Dermatol. 2007;56:53–62.
4. Park JH, Kim CW, Kim SS. The Diagnostic Accuracy of Dermoscopy for Scabies. Ann Dermatol. 2012;24:194.
5. Argenziano G, Fabbrocini G, Delfino M. Epiluminescence microscopy. A new approach to in vivo detection of Sarcoptes scabiei. Arch Dermatol. 1997;133:751–3.
6. Zalaudek I, Giacomel J, Cabo H, et al. Entodermoscopy: A New Tool for Diagnosing Skin Infections and Infestations. Dermatology. 2008;216:14–23.
7. Rubegni P, Mandato F, Risulo M, Fimiani M. Non-invasive diagnosis of nodular scabies: The string of pearls sign: The string of pearls. Australas J Dermatol. 2011;52:79.
8. Lacarrubba F, D'Amico V, Nasca MR, et al. Use of dermatoscopy and videodermatoscopy in therapeutic follow-up: a review: Dermatoscopy and therapeutic monitoring. Int J Dermatol. 2010;49:866–73.
9. Hamm H, Beiteke U, Höger PH, et al. Treatment of scabies with 5% permethrin cream: results of a German multicenter study. J Dtsch Dermatol Ges. 2006;4:407–13.
10. Cinotti E, Labeille B, Cambazard F, et al. Videodermoscopy compared to reflectance confocal microscopy for the diagnosis of scabies. J Eur Acad Dermatol Venereol. 2016;30:1573–7.
11. Cinotti E, Perrot J-L, Labeille B, Cambazard F. Diagnostic de la gale par épimicroscopie à fort grossissement : l'aspect « en deltaplane » de Sarcoptes scabiei. Ann Dermatol Vénéréologie. 2013;140:722–3.
12. Lacarrubba F, Musumeci ML, Caltabiano R, et al. High-magnification videodermatoscopy: a new noninvasive diagnostic tool for scabies in children. Pediatr Dermatol. 2001;18:439–41.
13. Walter B, Heukelbach J, Fengler G, et al. Comparison of dermoscopy, skin scraping, and the adhesive tape test for the diagnosis of scabies in a resource-poor setting. Arch Dermatol. 2011;147:468.
14. Devore CD, Schutze GE. AAP, Council on school health, committee on infectious dises. Head lice. Pediatrics. 2015;135(5):e1355–e1365. Pediatrics. 2015;136:781–2.
15. Paller A, Mancini AJ, Hurwitz S. Hurwitz clinical pediatric dermatology: a textbook of skin disorders of childhood and adolescence. New York: Elsevier/Saunders; 2011. http://www.clinicalkey.com/dura/browse/bookChapter/3-s2.0-C20090462809. Accessed 2 Nov 2018.
16. Martins LG, Bernardes Filho F, Quaresma MV, et al. Dermoscopy applied to pediculosis corporis diagnosis. An Bras Dermatol. 2014;89:513–4.
17. Nikam VV, Mehta HH. A nonrandomized study of trichoscopy patterns using nonpolarized (contact) and polarized (noncontact) dermatoscopy in hair and shaft disorders. Int J Trichology. 2014;6:54–62.
18. Di Stefani A, Hofmann-Wellenhof R, Zalaudek I. Dermoscopy for diagnosis and treatment monitoring of pediculosis capitis. J Am Acad Dermatol. 2006;54:909–11.
19. Zalaudek I, Argenziano G. Dermoscopy of Nits and Pseudonits. N Engl J Med. 2012;367:1741.

20. Doche I, Vincenzi C, Tosti A. Casts and pseudocasts. J Am Acad Dermatol. 2016;75:e147–8.
21. Zhuang K, Ran X, Dai Y, et al. An Unusual Case of White Piedra Due to Trichosporon inkin Mimicking Trichobacteriosis. Mycopathologia. 2016;181:909–14.
22. Miteva M, Tosti A. Dermatoscopy of hair shaft disorders. J Am Acad Dermatol. 2013;68:473–81.
23. Lallas A, Zalaudek I, Argenziano G, et al. Dermoscopy in General Dermatology. Dermatol Clin. 2013;31:679–94.
24. Bakos RM, Bakos L. Dermoscopy for diagnosis of pediculosis capitis. J Am Acad Dermatol. 2007;57:727–8.
25. DeFazio JL, Spencer P. Dermoscopy of Phthiriasis. N Engl J Med. 2010;362:e33.
26. Lacarrubba F, Micali G. The Not-so-naked Eye: Phthiriasis Palpebrarum. Am J Med. 2013;126:960–1.
27. Chuh A, Lee A, Wong W, et al. Diagnosis of Pediculosis pubis: a novel application of digital epiluminescence dermatoscopy. J Eur Acad Dermatol Venereol. 2007;21:837–8.
28. Micali G, Lacarrubba F. Phthiriasis Palpebrarum in a Child. N Engl J Med. 2015;373:e35.
29. Bauer J, Forschner A, Garbe C, Röcken M. Dermoscopy of Tungiasis. Arch Dermatol. 2004;140:761–3.
30. Cabrera R, Daza F. Tungiasis: eggs seen with dermoscopy: Correspondence. Br J Dermatol. 2007;158:635–6.
31. Cataldo K, Alvarez S, Abarzua A. Dermoscopy in tungiasis. Indian J Dermatol Venereol Leprol. 2014;80:371.
32. Criado PR, Landman G, dos Reis VMS, Belda JW. Tungiasis under dermoscopy: in vivo and ex vivo examination of the cutaneous infestation due to Tunga penetrans. An Bras Dermatol. 2013;88:649–51.
33. Bakos RM, Bakos L. 'Whitish chains': a remarkable in vivo dermoscopic finding of tungiasis. Br J Dermatol. 2008;159:991–2.
34. Dunn R, Asher R, Bowling J. Dermoscopy: Ex vivo visualization of fleas head and bag of eggs confirms the diagnosis of Tungiasis: Dermoscopy benefits early diagnosis. Australas J Dermatol. 2012;53:120–2.
35. Di Stefani A, Rudolph CM, Hofmann-Wellenhof R, Müllegger RR. Comments and opinions. Arch Dermatol. 2005;141:1045–6.
36. Torres-Guerrero E, Quintanilla-Cedillo MR, Ruiz-Esmenjaud J, Arenas R. Leishmaniasis: a review. F1000Research. 2017;6:750.
37. Ayhan E, Ucmak D, Baykara SN, et al. Clinical and dermoscopic evaluation of cutaneous leishmaniasis. Int J Dermatol. 2015;54:193–201.
38. Llambrich A, Zaballos P, Terrasa F, et al. Dermoscopy of cutaneous leishmaniasis. Br J Dermatol. 2009;160:756–61.
39. Taheri AR, Pishgooei N, Maleki M, et al. Dermoscopic features of cutaneous leishmaniasis. Int J Dermatol. 2013;52:1361–6.
40. Yücel A, Günaşti S, Denli Y, Uzun S. Cutaneous leishmaniasis: new dermoscopic findings. Int J Dermatol. 2013;52:831–7.
41. AlJasser MI, Lui H, Zeng H, Zhou Y. Dermoscopy and near-infrared fluorescence imaging of cutaneous larva migrans: letter to the editor. Photodermatol Photoimmunol Photomed. 2013;29:337–8.
42. Elsner E, Thewes M, Worret WI. Cutaneous larva migrans detected by epiluminescent microscopy. Acta Derm Venereol. 1997;77:487–8.
43. Veraldi S, Schianchi R, Carrera C. Epiluminescence microscopy in cutaneous larva migrans. Acta Derm Venereol. 2000;80:233.
44. Matsuda M, Oiso N, Yano Y, Kawada A. Dermoscopy for Tick Bite: Reconfirmation of the Usefulness for the Initial Diagnosis. Case Rep Dermatol. 2011;3:94–7.
45. Oiso N, Kawara S, Yano Y, Kawada A. Diagnostic effectiveness of dermoscopy for tick bite. J Eur Acad Dermatol Venereol. 2010;24:231.
46. Forcier M, Musacchio N. An overview of human papillomavirus infection for the dermatologist: disease, diagnosis, management, and prevention: Overview of HPV for the dermatologist. Dermatol Ther. 2010;23:458–76.
47. Al Aboud AM, Nigam PK. Wart (Plantar, Verruca Vulgaris, Verrucae). In: StatPearls. Treasure Island (FL): StatPearls Publishing; 2018. http://www.ncbi.nlm.nih.gov/books/NBK431047/. Accessed 4 Nov 2018.
48. Bae JM, Kang H, Kim HO, Park YM. Differential diagnosis of plantar wart from corn, callus and healed wart with the aid of dermoscopy. Br J Dermatol. 2009;160:220–2.
49. Dalmau J, Abellaneda C, Puig S, et al. Acral Melanoma Simulating Warts: Dermoscopic Clues to Prevent Missing a Melanoma. Dermatol Surg. 2006;32:1072–8.
50. Tanioka M, Nakagawa Y, Maruta N, Nakanishi G. Pigmented wart due to human papilloma virus type 60 showing parallel ridge pattern in dermoscopy. Eur J Dermatol. 2009;19:643–4.
51. Yoong C, Di Stefani A, Hofmann-Wellenhof R, et al. Unusual clinical and dermoscopic presentation of a wart. Australas J Dermatol. 2009;50:228–9.
52. Micali G, Lacarrubba F. Possible applications of videodermatoscopy beyond pigmented lesions. Int J Dermatol. 2003;42:430–3.
53. Micali G, Lacarrubba F. Augmented diagnostic capability using videodermatoscopy on selected infectious and non-infectious penile growths: using VD on selected infectious and non-infectious penile growths. Int J Dermatol. 2011;50:1501–5.
54. Lacarrubba F, Verzì AE, Dinotta F, et al. Dermatoscopy in inflammatory and infectious skin disorders. G Ital Dermatol E Venereol Organo Uff Soc Ital Dermatol E Sifilogr. 2015;150:521–31.
55. Vázquez-López F, Kreusch J, Marghoob AA. Dermoscopic semiology: further insights into vascular features by screening a large spectrum of nontumoral skin lesions. Br J Dermatol. 2004;150:226–31.

56. Micali G, Lacarrubba F, Massimino D, Schwartz RA. Dermatoscopy: Alternative uses in daily clinical practice. J Am Acad Dermatol. 2011;64:1135–46.
57. Dong H, Shu D, Campbell TM, et al. Dermatoscopy of genital warts. J Am Acad Dermatol. 2011;64:859–64.
58. Watanabe T, Yoshida Y, Yamamoto O. Differential diagnosis of pearly penile papules and penile condyloma acuminatum by dermoscopy. Eur J Dermatol. 2010;20:414–5.
59. Kim S-H, Seo S-H, Ko H-C, et al. The use of dermatoscopy to differentiate vestibular papillae, a normal variant of the female external genitalia, from condyloma acuminata. J Am Acad Dermatol. 2009;60:353–5.
60. Zaballos P, Ara M, Puig S, Malvehy J. Dermoscopy of molluscum contagiosum: a useful tool for clinical diagnosis in adulthood. J Eur Acad Dermatol Venereol. 2006;20:482–3.
61. Morales A, Puig S, Malvehy J, Zaballos P. Dermoscopy of Molluscum Contagiosum. Arch Dermatol. 2005;141.
62. Lacarrubba F, Verzì AE, Ardigò M, Micali G. Handheld reflectance confocal microscopy for the diagnosis of molluscum contagiosum: Histopathology and dermoscopy correlation. Australas J Dermatol. 2017;58:e123–5.
63. Ianhez M, Cestari S da CP, Enokihara MY, Seize MB de PM. Dermoscopic patterns of molluscum contagiosum: a study of 211 lesions confirmed by histopathology. An Bras Dermatol. 2011;86:74–9.
64. Alfaro-Castellón P, Mejía-Rodríguez SA, Valencia-Herrera A, et al. Dermoscopy Distinction of Eruptive Vellus Hair Cysts with Molluscum Contagiosum and Acne Lesions. Pediatr Dermatol. 2012;29:772–3.
65. Amer M, Helmy A, Amer A. Trichoscopy as a useful method to differentiate tinea capitis from alopecia areata in children at Zagazig University Hospitals. Int J Dermatol. 2017;56:116–20.
66. Bourezane Y, Bourezane Y. Analysis of trichoscopic signs observed in 24 patients presenting tinea capitis: Hypotheses based on physiopathology and proposed new classification. Ann Dermatol Vénéréologie. 2017;144:490–6.
67. Brasileiro A, Campos S, Cabete J, et al. Trichoscopy as an additional tool for the differential diagnosis of tinea capitis: a prospective clinical study. Br J Dermatol. 2016;175:208–9.
68. Ekiz Ö, Şen BB, Rifaioğlu EN, Balta I. Trichoscopy in paediatric patients with tinea capitis: a useful method to differentiate from alopecia areata. J Eur Acad Dermatol Venereol. 2014;28:1255–8.
69. Elghblawi E. Idiosyncratic findings in trichoscopy of tinea capitis: comma, zigzag hairs, corkscrew, and Morse code-like hair. Int J Trichology. 2016;8:180.
70. Hernández-Bel P, Malvehy J, Crocker A, et al. Un nuevo marcador dermatoscópico de tinea capitis: «pelos en coma». Actas Dermosifiliogr. 2012;103:836–7.
71. Hughes R, Chiaverini C, Bahadoran P, Lacour J-P. Corkscrew hair: a new dermoscopic sign for diagnosis of tinea capitis in black children. Arch Dermatol. 2011;147:355.
72. Mapelli ETM, Gualandri L, Cerri A, Menni S. Comma hairs in tinea capitis: a useful dermatoscopic sign for diagnosis of tinea capitis. Pediatr Dermatol. 2012;29:223–4.
73. Neri I, Starace M, Patrizi A, Balestri R. Corkscrew hair: a trichoscopy marker of tinea capitis in an adult white patient. JAMA Dermatol. 2013;149:990.
74. Pinheiro AMC, Lobato LA, Varella TCN. Dermoscopy findings in tinea capitis: case report and literature review. An Bras Dermatol. 2012;87:313–4.
75. Schechtman RC, Silva NDV, Quaresma MV, et al. Dermatoscopic findings as a complementary tool in the differential diagnosis of the etiological agent of tinea capitis. An Bras Dermatol. 2015;90:13–5.
76. Slowinska M, Rudnicka L, Schwartz RA, et al. Comma hairs: a dermatoscopic marker for tinea capitis. J Am Acad Dermatol. 2008;59:S77–9.
77. Wang H-H, Lin Y-T. Bar code–like hair: dermoscopic marker of tinea capitis and tinea of the eyebrow. J Am Acad Dermatol. 2015;72:S41–2.
78. Babel DE, Pelachyk JM, Hurley JP. Tinea nigra masquerading as acral lentiginous melanoma. J Dermatol Surg Oncol. 1986;12:502–4.
79. Gupta G, Burden AD, Shankland GS, et al. Tinea nigra secondary to Exophiala werneckii responding to itraconazole. Br J Dermatol. 1997;137:483–4.
80. Smith SB, Beals SL, Elston DM, Meffert JJ. Dermoscopy in the diagnosis of tinea nigra plantaris. Cutis. 2001;68:377–80.
81. Noguchi H, Hiruma M, Inoue Y, et al. Tinea nigra showing a parallel ridge pattern on dermoscopy. J Dermatol. 2015;42:518–20.
82. Nazzaro G, Ponziani A, Cavicchini S. Tinea nigra: a diagnostic pitfall. J Am Acad Dermatol. 2016;75:e219–20.
83. Lacarrubba F, Dall'Oglio F, Dinotta F, Micali G. Exogenous pigmentation of the sole mimicking in situ acral melanoma on dermoscopy. J Dermatol Case Rep. 2012;6:100–1.
84. Criado PR, Delgado L, Pereira GA. Dermoscopy revealing a case of Tinea Nigra. An Bras Dermatol. 2013;88:128–9.
85. Rossetto AL, Corrêa PR, Cruz RCB, et al. A case of Tinea nigra associated to a bite from a European rabbit (Oryctolagus cuniculus, Leporidae): the role of dermoscopy in diagnosis. An Bras Dermatol. 2014;89:165–6.
86. Ye Y, Zhang X, Zhao Y, et al. The clinical and trichoscopic features of syphilitic alopecia. J Dermatol Case Rep. 2014;8:78–80.
87. Piraccini BM, Broccoli A, Starace M, et al. Hair and scalp manifestations in secondary syphilis: epidemiology, clinical features and trichoscopy. Dermatology. 2015;231:171–6.
88. Tognetti L, Cinotti E, Perrot J-L, et al. Syphilitic alopecia: uncommon trichoscopic findings. Dermatol Pract Concept. 2017;7:55–9.

Digital Dermoscopy Analysis

8

Linda Tognetti, Marco Burroni, Ivana Guidi, Filomena Russo, Martina Vispi, Gennaro Cataldo, Alberto Balistreri, Gabriele Cevenini, and Pietro Rubegni

8.1 Computer-Assisted Diagnosis (CAD): Basics and Introduction

Early detection of skin cancer is always important for clinicians in order to provide the best prognosis and less invasive treatment: The most effective management for malignant melanoma remains the early recognition and surgical excision of thin lesions [1, 2]. To date, in daily practice, the majority of dermatologists identify suspect pigmented lesions by visual examination and then perform dermoscopy on selected lesions. However, both the methods are highly dependent on specific training, and diagnostic accuracy can vary greatly among individuals with varied experiences [3, 4]. Moreover, dermoscopy requires formal training as well as skill in image interpretation through the so-called pattern analysis is highly dependent on subjective interpretation, thus results are scarcely reproducible, with low inter-observer agreement, especially on difficult lesions [5]. To overcome some problems, several scoring systems and algorithms such as the ABCD rule, the 7-point checklist, chaos and clues, the iDScore, have been proposed to improve the diagnostic performance of less experienced clinicians: these "simplificated" algorithms provided a more standardized approach to melanocytic skin lesions even if in two of the most detailed multicenter studies reveal still mean to low intraobserver agreement and a lower accuracy respect to the pattern analysis [4, 6, 7].

In the last two decades, many studies have been proposed using computerized objective measurements obtained without any clinician interactions. In an attempt to increase the accuracy, we added some objective variables defining a new integrated method in order to provide good to high accuracy and reproducibility in selected case studies to be evaluated on a larger scale [1–4, 6–9]. However, a gray zone of diagnostic uncertainty rests for clinically and dermoscopically difficult skin lesions, which relies on the intrinsic subjectivity of dermoscopic pattern analysis [7, 9]. It is important to clarify the difference between subjective and objective assessments: a subjective assessment concerns with the clinician's judgment of some aspect on the base of his perception, e.g., visually estimating the kind of shape of a specific feature or evaluating a presence or absence of color-related feature inside a lesion [5–7, 9]. An objective assessment,

L. Tognetti (✉) · I. Guidi · F. Russo · M. Vispi
P. Rubegni
Dermatology Unit, Department of Medical, Surgical and Neuro-Sciences, University of Siena, Siena, Italy

M. Burroni
Italimaging Startup, Siena, Italy
e-mail: marco.burroni1@tin.it

G. Cataldo · A. Balistreri · G. Cevenini
Bioengineering & Biomedical Data Science Lab, Department of Medical Biotechnologies, University of Siena, Siena, Italy
e-mail: alberto.balistreri@dbm.unisi.it; gabriele.cevenini@dbm.unisi.it

M. Fimiani et al. (eds.), *Technology in Practical Dermatology*,
https://doi.org/10.1007/978-3-030-45351-0_8

instead, can be the age of the patient, objective by itself, or a computerized measurement of a feature, e.g., the maximum diameter of a lesion, thus resulting independent by the observer [3, 4]. With the development of computer-aided image analysis technologies, physicians may obtain an objective "second opinion" from *computer-aided diagnosis* (CAD) software to refine their diagnoses [5, 10–28]. In general, CAD systems are intended to assist doctors in the interpretation of medical images and rely on the use of image-derived objective variables to formulate the correct diagnosis [10–15]. Beside dermatology, CAD has been widely used in several medical specialties requiring accurate lesion detection and image interpretation, such as radiology (e.g., breast lesion detection in mammography [11], lung nodule detection on chest radiographs or CT scans [12], polyp detection in CT colonography [13], nuclear medicine [14], and histopathology [15]. CAD usually expresses also objective evaluations indicating through measurement the motivations of eventual alarms.

8.2 Digital Dermoscopy Analysis (DDA) and CAD

In the dermatology field in the last years, one of the most effective example of CAD system is based on the generically named "Digital Dermoscopy Analysis" (DDA). In particular, DDA system relies on an objective image analysis, as it takes into account only observer-independent image evaluations. Briefly, a DDA objective system should consist of (1) the acquisition of standardized digital dermoscopic images; (2) mathematical objective evaluation of the morphological aspects of the images; (3) image and parameter storage for the follow-up and further examinations. The acquisition of images can be obtained through digital cameras or video-probes connected to the PC. Dermatoscopic probes are generally composed of high-definition color cameras equipped with optics using the cross-polarization or the immersion technology and then connected to a PC through digital interfaces. The color calibration of the video probes plays a paramount role in the image quality process, and it is preferably to adopt a fine RGB color tuning. The CAD consists of employing proper classification methods based on the processing of the objective values in order to achieve a diagnostic aid. Usually Artificial Neural Networks and Similarity algorithms are used by CAD systems based on a proper solid thesaurus of peculiar lesions [18, 19, 22, 24]. Further advantages are offered by real-time evaluations and pre-selection aid [25, 28].

8.3 DDA Siena Experience: The DB-Mips® Software

In early 1990, an image processing software (DB-Mips® Dell'Eva-Burroni, Biomips Engineering) was developed for the daily storage and image analysis of pigmented skin lesions with the aim to help clinicians in the rationalization and objective evaluation of features through the diffusing pattern analysis in epiluminescence. Scientific cooperation with the Department of Dermatology of the University of Siena and some colleagues from other Universities and IRCCS permitted to statistically and clinically evaluate the software variables through proper scientific studies [16–18] toward a new dermatological approach in the pigmented lesions understanding. Its peculiar innovations were independence from the subjectivity of the clinician, automatic and "in vivo" measure and classification, acquisition of high-quality dermoscopic images, comparison with the archived previous images. The original 1991 device consisted of a PC connected to a 3CCD camera mounted on an operating microscope, providing 6× to 40× magnifications at 1 megapixels of resolution with 16 millions of colors. The software identified the examining lesions and was able to evaluate 36 parameters processed by an artificial neural network trained on a subset of peculiar lesions [17]. After some preliminary accuracy tests, a further set of patterns have been added tending to objectively describe the kind of color patterns inside the lesions and named Burroni's Islands. The islands of colors refer to the kind and homogeneity of the color clusters inside the lesion and range from

macro patterns [19]. Accuracy evaluations have been performed in order to verify the usefulness of the islands of colors in the differential diagnosis of pigmentary lesions [20].

Some years later, we defined our first approach toward a new quantitative semiology based exclusively over three groups of objective variables, thus resulting not depending on the observer's subjectivity [16]. Briefly, the geometric variables are *area, perimeter, maximum and minimum diameters, radius, variance of the symmetry of the contour, circularity, irregularities of the edges,* and *ellipsoidalness*. The chromatic variables are *average values of blue, green and red inside the lesion, quartiles and deciles of red, green, and blue inside the lesion, green and blue of the healthy skin around the lesion, average gradient of the skin lesion, variation of the boundary gradient, homogeneity of the borders* and *border breaks*, *medium contrast, and entropy of the area inside the lesion*. The islands of color variables are *peripheral dark regions, dark area, dark region imbalance, total imbalance, green area, light red area, dominant green region imbalance, blue-gray area, gray-blue regions, transition area, imbalance of the transition region, background area, background region imbalance, red, green and blue multicomponent, and number of red, green, and blue percentiles within the lesion*. Stepwise discriminant analyses have been applied in several studies to the whole set of variables in order to verify and test their reliability and contribute to better standardize the diagnostic process in the differentiation of pigmented skin lesions [25].

One of the most underestimated advantages of a validated objective-based pattern analysis software is related not only to the aided diagnosis but mainly on the possibility to perform observer's independent statistical analyses in order to differentiate the main features belonging to different categories of lesions. During the last 25 years, we performed several statistical analysis in order to increase the features understanding the differentiating melanoma from dysplastic moles, Spitz moles from melanoma and generally define objective subsets for many other kind of pigmented skin lesions [24–30]. Today we know that if we want to optimize a generic DDA methodology, it is important both to screen the lesions to be submitted to the automated analysis and to use reliable statistical classification methods [28–30].

A recent software named DDAVL-HD® (*Italimaging Startup, Siena, Italy*) evaluates the 49 DB-Mips variables oriented to the aided diagnosis into the early melanoma detection to be used, at the same, both in the daily practice and the advanced objective evaluations into the differential diagnosis of pigmented skin lesions [25], their follow-up [27, 28], and their objective definitions [21]. The DDAVL-HD® provides the in vivo variable detection of the lesion prior to image acquisition and its real-time aided diagnosis (Fig. 8.1b), the possibility to connect with a small ergonomic videodermatoscope probe or with a dermatoscope, the total body photography management, a patient's smart database (Fig. 8.1a). Proper calibrations in order to obtain standardized visual colors and tests to verify low

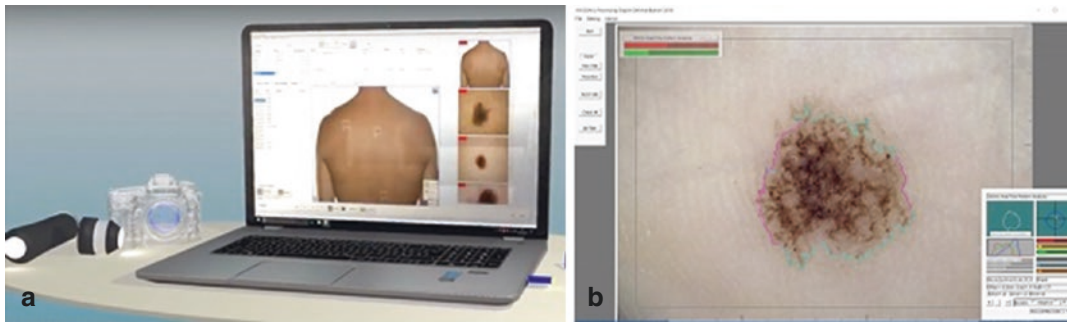

Fig. 8.1 DDAVL-HD system® (**a**) with a detail of the *real-time* lesion analysis and diagnostic aid (**b**)

objective value variations between different probes have been performed by the authors and deposited as the so-called technical dossier.

8.4 DDA Focused on Early Melanoma and Dysplastic Nevi

We carried out several studies to establish the gain in diagnostic accuracy when using the DB-Mips® (Dell'Eva-Burroni) variables in differentiating early melanomas from atypical nevi [22–24], or evaluating MM thickness [26] and for MM follow-up [27]. In a series of 147 clinically and dermoscopically atypical melanocytic skin lesions excised in the suspect of malignancy (90 nevi and 57 early MM), the DB-Mips® system demonstrated, despite the restricted range of lesions and the difficulty target, a sensitivity of 88% and a specificity of 81% [25]. Actually, is not infrequent to have discrepancies in histologic reports from different observer pathologists on atypical moles and in situ MM [3, 7]. In the retrospective study to evaluate cutaneous melanoma thickness by DDA, 141 melanoma images were evaluated for 49 DDA parameters: the group of melanomas thicker than 1 mm had a larger area, more clear-cut and indented borders (skin-lesion gradient and variance of contour symmetry), a greater presence of blue and a greater randomness in the disposition of pattern components than thinner melanomas (less than 1 mm). Four variables (area, skin-lesion gradient, skin green average, variance of border interruptions) were then selected by stepwise multivariate logistic regression analysis to determine whether their extrapolation could predict melanoma thickness, with a resultant accuracy of 86.5% [26]. The DB-Mips® system was thus able to add clear advantages in preoperative assessment of early MM, such as better organization of surgical/diagnostic priorities based on distinction of lesions at high and low risk of progression; excision with sufficient surgical margins at the first operation, avoiding a second more radical operations; excision and sentinel lymph node biopsy (if needed) in a single operation, saving time and costs. The impact on the quality and effectiveness of atypical pigmented skin lesion follow-up was also assessed, demonstrating clear advantages in terms of feasibility, accuracy, and reproducibility between different operators [26–28].

8.5 DDA and Spitz Nevus/ Atypical Spitz Tumors

Spitzoid melanocytic lesions are usually classified as Spitz nevi (SN), atypical Spitz tumors (ASTs), and spitzoid melanomas (SM) [29, 30]. Due to their peculiar morphology, SN are still considered one of the highest simulator of MM, then DDA accuracy in discriminating them from early MM is slightly lower than non-spitzoid atypical nevi: clinical examination, patients age, and body site evaluations rest fundamental in these cases [3, 4]. Furthermore, when considering AST, the differential diagnosis is even more challenging because this entity of uncertain malignancy potential shares histologic features of both SN and SM, and its exact clinicopathologic definition is a matter of ongoing debate among dermatopathologists [29, 30]. Thus, we aimed to test if DDA was able to provide significant help in noninvasive differential diagnosis of these entities [30]. A total of 41 lesions with spitzoid features excised in the suspect of malignancy (21 AST and 19 SN) and analyzed with DB-Mips® system with were retrospectively collected. In monovariate analysis, AST resulted to be significantly larger in area than SN; three variables related to multicomponent pattern (*Red HOM*, *Green HOM*, and *Blue HOM*) were significant; the greater concentration of pigment clusters at the periphery of the lesion and sharp interruption of the border showed statistically significant differences between SN and AST. On the contrary, in multivariate analysis, the results were disappointing, showing an accuracy of only 65.5%. Based on that case study, we concluded that, although certain morphological characteristics are more typical of SN than AST and vice versa, it is not possible to clearly separate these

two entities. This is because AST should be considered within a spectrum ranging from benign to clear-cut malignant lesions, rather than a separate entity [30].

8.6 DDA and Regressing Nevi/MM with Regression

Regression features including white scar-like areas, pepper-like granules, shiny white streaks, which correspond to dermal scarring, pigment incontinence and presence of melanophages were historically considered suggestive for malignancy [31–36]. However, we should note that, although regression is observed in about 10–15% of melanomas (i.e., melanoma with regression (MwR)), variable degree of spontaneous/post-inflammatory regression can occur in about 6–10% of nevi, so-called regressing nevi (rN) [31, 32]. Some authors have recently highlighted the difficulty to delineate clear-cut histopathological features to distinguish benign regression of rN from malignant regression of MwR [35, 36]. In this context, we aimed to investigate whether DDA could be able to improve diagnostic accuracy in differentiating rN from MwR [33]. In a series of 202 melanocytic skin lesions exhibiting dermoscopic features of regression, consecutively excised in the suspected of malignancy (i.e., 112 rN and 90 MwR), 12 out of 48 tested variables were significantly associated with malignancy on monovariate analysis: *Area, Shape, Maximum diameter, Gradient, Entropy Peripheral Dark, Green HOM, Blue HOM, Red HOM, Shape, Entropy Grad Peaks, Grad Sigma*. Of note, the multivariate analysis selected *Green HOM* (i.e., difference of shape and number of green structures inside the lesion) and *Grad Sigma* (i.e., width of border indentation). Stepwise discriminant analysis showed a very reliable model: AUC = 0.84 (IC 95%: 0.76–0–92), SE = 76% and SP = 92%. Thus, in a preselected group of dermoscopic images with regression, DDA can help the physician in orienting the correct diagnosis. According to our experience, nR are more common on the upper trunk (i.e., inflammatory/micro-trauma-induced regression) and in children and young adults (spontaneous regression) [33]. Taking together into account the age and body location of the patient and this DDA algorithm data, we can spare unnecessary surgical excision in clinical practice [33, 34].

8.7 DDA and Palmoplantar Lesions

The diagnosis of palmoplantar melanoma is often delayed and misdiagnosis is common. Acral melanoma is a distinctive subtype of melanoma, with different prevalence according to the race [37, 38]: it is reported to constitute 60–75% of all cutaneous melanomas in blacks, 43–49% in Asians, and 5–7% in whites; however, absolute incidences of acral melanoma seem to be almost the same in all races. Although the proportion of acral melanoma is low in Caucasians, pigmented skin lesions of the hands and feet are very common in this population. Many factors seem to contribute to the delay in diagnosis: advanced age of patients, difficulty in exploring plantar sites, and unusual presentation, not infrequently without pigmentation. However, pigmented lesions in acral sites do not show the classical pigment network pattern and/or other classical dermoscopic features typical of other skin areas. Thus, acral nevi are a source of confusion that challenges physicians and in the differentiation between atypical acral nevi (aN) and acral melanoma (aMM) [37–39]. Despite the undoubtful usefulness of dermoscopy in increasing diagnostic accuracy of acral pigmented lesions, diagnosis is nevertheless subjective and affected by low inter-observer agreement, especially for lesions located on pressure areas of the plants that show multiple dermoscopic patterns. To overcome these problems, dermoscopic algorithms were developed [37]. Our contribution on this topic was a multicenter study aimed to test on the DDA ability to improve the diagnostic accuracy acral pigmentations and to differentiate aN from aMM and to further design a simple scoring model [39]. A series of 445 images (25 aMM and

Univariate logistic regression analysis		
Variables	**SDP Wald**	***p***
age	210,713	0
max diameter	195,021	0
Area	111,265	0
Dmin	105,241	0
AN	99,857	0
BWN	98,019	0
SWS	93,588	0
IPB	64,494	0
IS	54,217	0
PA	51,09	0
BMVgt30	46,666	0
site_exposure	45,168	0
WSA	40,417	0
Perim	39,274	0
BGP	37,587	0
BWVlt30	30,573	0
site_exposure B	28,122	0
IDG	23,064	0
AVP	21,175	0
BGG	13,494	0
HA	13,133	0
site_exposure C	12,511	0
site_exposure A	9,788	0,002
sex	0,911	0,34
Circ	0,642	0,423
Symvar	0,63	0,427
Shape	0,011	0,916

a

Multivariate logistic regression analysis		
Variables	**SDP Wald**	***p***
age	122,981	,000
Max diameter	50,114	,000
site_exposure	47,517	,000
AN	45,712	,000
Rhom	35,585	,000
BGP	26,735	,000
Umbal	23,819	,000
IDG	22,520	,000
Dratio	21,936	,000
IPB	11,731	,001
WSA	11,177	,001
SWS	9,309	,002
IS	8,134	,004
BWV	7,600	,006

b

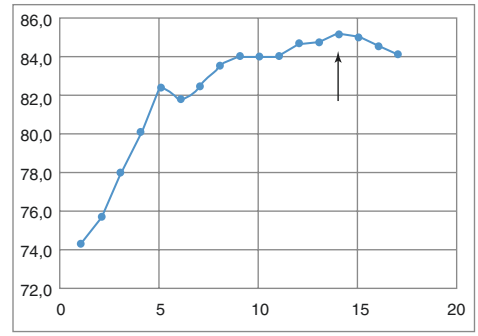

c

Fig. 8.2 Statistical analysis of the i-DDA study 2018 based on the integration between 49 DDAVL parameters (*ITALICS*), 12 dermoscopic variables (CAPITAL) and five clinical-anamnestic variables: univariate analysis (**a**), multivariate stepwise analysis (**b**), and corresponding stepwise selection curve (leave-one-out technique) (**c**). [SDP = Wald statistical discriminant power]

420 aN) were analyzed with the DBMips: 416 patients were Caucasian [259 females (58.2%); mean age 29.3 years; 186 males (41.8%); mean age 25.7 years], ranging in age from 18 to 82 years. Statistically significant subset of DDA parameters selected by the scoring model, able of optimally distinguishing benign from malignant, included *area, peripheral dark regions, total imbalance of colors, entropy, dark area, red* and *blue component*. For each lesion, the total score, *S*, was obtained by considering the seven DDA parameters selected, comparing their values with the corresponding cut-offs and adding the contributions of the associated risk scores to S when the cut-off conditions were met (Fig. 8.2). The model showed high accuracy (AUC = 0.983). Setting a score threshold $T = 4$ and removing lesions having a score S > T avoided false negatives, giving a sensitivity of 100% and a specificity of 83.1% (71 false positives). Of note, when all seven parameters were used in a multivariate mode to evaluate the percentage of correct classification between aMM and aN, setting sensitivity at 100% to avoid false negatives (false-negative ratio = 0), a minimum specificity of about 80% was estimated, meaning that only one fifth (false-positive ratio) of benign lesions were indicated for removal [39].

8.8 Real-Time Artificial Intelligence and Pre-selection Aid in the Daily Routine (già detto sopra)

One of the first approaches to increase the support given by the aided diagnosis came from the real-time analysis feature of the DB-Mips® grabbing module. Also it is quite common that observing patients having many suspicious lesions, it is quite intuitive how the real-time aid, i.e., provided while a dermatoscopic probe is scanning the patient's moles, can help much more than the static analysis over a grabbed frame. In the second decade of 1990, some independent clinicians used the DB-Mips® in order to verify the software's accuracy reporting 100% in sensitivity with 92% of specificity when used in the daily routine [40].

Between 2002 and 2010, two multicenter studies have been performed in order to verify the DB-Mips® integrated artificial intelligence used among images obtained by different cameras reporting always similar results in terms of accuracy in the daily routine grabbed lesions [24, 27]. These studies were performed over a daily routine study population to test the reliability of the DB-Mips integrated classifier, but also canonical statistical analysis has been adopted as a further proof of reliability: sensitivity higher than 90% and specificity higher than 78% were reported, showing very similar trends even when performed using different kinds of cameras and clinicians experience under different studies. In the first study we tested the integrated DB-Mips classifier over patient's lesions during a 4-year daily routine image storaging. All the excised lesions have been diagnosed by histology leading to 391 melanomas (among which 51 situ melanoma and 103 < 0.75 mm Breslow thickness) and 449 melanocytic nevi. Depending on the center's population, the sensitivity of the DB-Mips varied between 93% and 98% while the specificity was between 78% and 79% [24]. In the second subsequent study, 1308 patients and 3544 pigmented lesions were evaluated in three centers: a total of 466 pigmented lesions were surgically removed and classified by histopathology. Among those, 52 melanomas and 299 dysplastic nevi have been identified. Depending on each single center, the sensitivity of the DB-Mips varied between 90% and 95% while the specificity between 79% and 93%. It is important to underline the fact that using some CAD systems such as DB-Mips and DDAVL-HD® durting lesion examination allows to have the aided suggestion in real time on the monitor as a live *warning* [28]. This can also help in the pre-selection of suspicious lesions to be saved and compared in a second time [27].

8.9 Integration of Clinical-Personal Objective Variables into DDA: The i-DDA 2015 Study

In recent years, we explored the new field of research: the integration of clinical–personal data into dermoscopy (DS) based on classic dermoscopic pattern analysis, named "iDS" [3, 4]. Then, we tested the impact of adding few iDS variables in the DDA system. These newly developed systems were named integrated "i-DS-DDA" and were dedicated to dermatologists mainly concerned with equivocal "difficult" pigmented skin lesions [39].

A series of 856 dermoscopic images of clinically atypical pigmented skin lesions excised in the suspect of malignancy (i.e., 584 nevi and 272 MM) were analyzed by the DDAVL-HD® software: the software evaluated 48 objective parameters to be studied as possible discriminant variables, grouped into four categories (geometries, colors, textures, and islands of color). We also collected three objective clinical-anamnestic parameters (age, sex, body site) and three dermoscopic data such as the presence/absence of three dermoscopic patterns (i.e., blue-white veil, regression, and vascular structure polymorphism) according to experts' evaluation. The choice of these three dermoscopic parameters was made on the basis of the consideration that they strongly correlate with melanoma. The three clinical-anamnestic objective variables and the three der-

Table 8.1 Stepwise logistic regression model designed on the i-DDA 2015 over an integrated database of 48 DDA variables (*ITALICS*), 3 three dermoscopic patterns (CAPITAL), and three personal variables: multivariate analysis

Step	48 DDA variables	i-DDA variables
1	*Red multicomponent*	*Red multicomponent*
2	*Imbalance*	REGRESSION STRUCTURES
3	*Perimeter*	Age
4	*Green multicomponent*	*Green multicomponent*
5	*Minimum diameter*	*Shape*
6	*Border interruptions*	*Border interruptions*
7	*Mean skin-lesion gradient*	*Entropy*
8	–	*Minimum diameter*
9	–	*Imbalance*

Reproduced with permission from [41]

moscopic subjective variables were integrated in the statistical analysis to the DDAVL-HD® variables, for each image/case: all variables were dichotomized according to positive (melanoma) or negative (nevi) outcome. Univariate analysis of the integrate database showed that patient age was greater for melanomas (age range: 40–50 years) than for atypical nevi (age range: 30–40 years); all three dermoscopic variables were indicative of melanoma ($p < 0.05$); among the personal data, only "age" proved to be statistically significant. Multivariate analysis chooses "regression structures" and "age" as the second and third most important significant parameters in the i-DDA method (Table 8.1). The i-DDA model showed 100% sensitivity, 40.8% specificity, 89.2% accuracy (AUC = 0.89); the DDA model showed 84.4% of accuracy (AUC = 0.84) and poor specificity of 13.4% [39]. We thus demonstrated that the inclusion of objective parameters increased significantly the accuracy of the DDA in melanoma detection among borderline-excised pigmented skin lesions [39].

8.10 Evolution of DDA Software

In our experience, we think that these new technologies can be used both in the daily practice and in evaluating borderline lesions [24, 25, 42, 43]. The real-time aid also provided by the DDAVL-HD® (Burroni-Dell'Eva, Italimaging Startup), using the DB-Mips® variables, is optimal as a first computerized support when used on groups of lesions that are to undergo the traditional DDA inspection for an in-depth analysis. The DDAVL-HD® evaluates in a "real-time" mode the aforementioned variables, so that the clinicians can interpret them through the software diagrams, having also the aid response. The DDAVL-HD® database stores each lesion's objective values along with patient's anamnestic data so that the computer not only deal with digital images measurements but also with other clinical and anamnestic data of the patient as an exhaustive database (it is well known that sometimes differentiation between a Reed/Spitz nevus and melanoma is based more on age of onset than on fine clinical-dermoscopic parameters) [3, 4].

8.11 Integration of Clinical–Personal and Dermoscopical Variables into DDA: The i-DDA 2018 Study

Introduction. Between 2016 and 2017, we retrospectively analyzed a case study of 450 dermoscopic images of clinically and dermoscopically "difficult" melanocytic skin lesions: all were consecutively excised in the suspect of malignancy. Histopathological analysis was performed based on 2/3 pathologists' agreement, resulting in 300 nevi and 150 early melanomas. To ensure the homogeneity of the dermoscopic image database, palmar and plantar lesions were excluded, due to their peculiar "special-site dermoscopic pattern"; all images were acquired with polarized light at standardized enlargement (17×). Since they represent clinical simulator of early melanomas in clinical practice, Spitz and Reed nevi were included too [4]. Dermoscopic subjective evaluations (i-DDA) were performed by five different experts in dermoscopy blinded to histopathological diagnosis. Fleiss' κ was calculated to measure concordance level between experts in the description of dermoscopic parameters for each MSL. The power of the studied variables in dis-

criminating malignant from benign lesions was also investigated through F-statistics. According to monovariate analysis, the variables "age" and "maximum diameter" supplied the highest discriminant power (F = 253 and 227, respectively); atypical network, blue white veil, and white shiny streaks were the most significant dermoscopic patterns suggestive of malignancy (F = 110, 104 and 99.5, respectively). Shiny white streaks were the only dermoscopic parameter to obtain satisfactory concordance value. The problems of low concordance between experts [4], due to subjective assessments, are also reported on other multicenter studies [6, 7]. In term of accuracy in that case study, the specific statistical weight of clinical and personal objective data (i.e., "patient's age" and "lesion diameter") surpassed those of atypical dermoscopic features [4].

These findings suggested to add the objective parameters provided by the DDAVL-HD® software. Moreover, we aimed to compare the performance of a) the dermoscopic pattern analysis alone (DS); b) an integrated dermoscopy system, based on the 12 dermoscopic patterns and clinical–personal data that resulted significant in the previous study: i-DS [3]; c) a new "i-DS-DDA" method.

Materials and methods. We performed an image quality selection of 435 images (104 MM and 301 nevi, 1 image/lesion) out of the database of 450 [3]. We then collected for each patient/lesion four clinical (maximum diameter, lesion body site, UV-related site exposure classification), two personal (age, gender) as reported in Table 8.2. According to 2/3 expert dermoscopists' agreement, we assessed the presence/absence of 12 dermoscopic pattern in each lesion, including shiny white streaks (SWS), irregular dots and globules (IDG), blue-white veil (BWV), blue-gray globules (BGG), hypopigmented areas (HA), irregular streaks (IS), atypical network (AN), white scar-like areas (WSA), pigmented areas (PA), blue-white veil >30 (BWV > 30), atypical vascular pattern (AVP), and blue-gray peppering (BGP). Finally, all 435 images were elaborated by DDAVL-HD® software: this analysis generated the extraction of 49 DDAVL-HD® variables, grouped into eight geometric variables, 14 color variables, two structural variables, 25 Burroni's island. The final integrated database was composed of 435 images associated with 66 variables: five objective clinical-anamnestic data (age, sex, body site, diameter, UV-exposure classification),

Table 8.2 Descriptive statistics of the case study analyzed in the i-DDA 2018 study

Clinical-anamnestic variables	Nevi (n = 301)	MM (n = 134)
	Lesion number (%)/range; average value	
Sex		
M	143 (47%)	66 (49%)
F	158 (52%)	68 (51%)
Age (years)	1–87; 38.1	23–89; 53.6
0–10	0	0
11–20	35 (11.6%)	0
21–30	66 (22%)	9 (3%)
31–40	83 (27.5%)	19 (6.3%)
41–50	58 (19.2%)	36 (12%)
51–60	34 (11.3%)	20 (6.6%)
61–70	13 (4.3%)	28 (9.3%)
71–80	11 (3.6%)	16 (5.3%)
>80	4 (1.3%)	6 (2%)
Maximum diameter (mm)	2–16; 7	1–19; 9.51
<5	43 (14.2%)	2 (1.5%)
5–7	151 (50%)	41 (30.5%)
8–9	68 (22.5%)	37 (27.6%)
>10	39 (13%)	54 (40%)
Lesion body site, UV-exposure classification		
A. Upper extremities (*chronically photoexposed*)	24 (8%)	19 (14%)
• Head	2 (1.5%)	0
• Neck	0	1 (0.7%)
• Arms/hands	22 (7%)	18 (13.4%)
B. Lower extremities (*frequently photoexposed*)	46 (15.2%)	37 (27.6%)
• Thigh	0	0
• Leg	44 (14.6%)	35 (26%)
• Ankle/back of the feet	2 (1.5%)	2 (1.5%)
C. Upper trunk (*seldom photoexposed*)	161 (53.4%)	57 (42.2%)
• Shoulders	0	2 (1.5%)
• Chest	41 (13.6%)	12 (9%)
• Upper back	120 (40%)	43 (32%)
D. Lower trunk (*rarely photoexposed*)	70 (22.2%)	21 (15.7%)
• Abdomen	38 (12.6%)	13 (9.7%)
• Bottom	11 (3.65%)	3 (2.2%)
• Side	20 (6.6%)	5 (3.7%)

12 dermoscopic parameters, and 49 DDAVL-HD® parameters. Thus, a total of 28.710 variables were dicothomized for benign/malignant according to histological evaluation, in order to perform monovariate and multivariate stepwise analysis.

Results. Univariate analysis demonstrated that age of the patient and diameter of PSL represents the most significantly variables associated with melanoma, with a statistical discriminant power of 210 and 195, respectively, followed by two DDAVL-HD® variables, namely *area* and *Dmin* (Fig. 8.2a). Another important consideration emerging from the univariate analysis of the study is that all of the 12 dermoscopic variables are significantly associated with early melanoma detection, the most important being atypical network, blue-white veil, and shiny white structures. The multivariate stepwise analysis selected a series of 17 variables (age, maximum diameter, UV-exposure site, atypical network, *RedHOM*, *chronically photoexposed areas*, frequently *photoexposed areas*, blue-gray peppering, *UMBAL*, irregular dots and globules, *DRATIO*, irregular pigmented blotches, white scar-like areas, irregular streaks, blue-white veil) (Fig. 8.2b). The stepwise selection based on the leave-one-out technique stopped at step 17 as illustrated in Fig. 8.2c (arrow at step 14, higher value of AUC). The performances of the three methods are represented in discriminating atypical nevi from early MM and are illustrated by corresponding ROC curves are in Fig. 8.3: DS (a), clinical–personal variables (b), i-DS (c), and i-DS-DDA (d). The highest accuracy was obtained by the system i-DS-DDA that reached an AUC of 0.921, SE = 100%, SP = 58% (best accuracy: SE = 90%, SP = 74%) (d), followed by selected clinical–personal variables "age," "maximum diameter," and UV-related classification of body—i.e., site exposure—(AUC = 0.833) the system and the i-DS system (AUC = 0,881) (b). Then, the dermoscopy performance, although based on selected significant dermoscopic variables and evaluation of experts dermoscopists, was quite accurate but with unacceptable accuracy in this difficult subset of lesions (AUC = 0.79) (a).

Discussion. In line with the observations of other authors [31], incorporating patient age as metadata determined a sharp improvement in correct diagnostic rate for early melanomas (MM in situ, MM < 1 mm thick) and benign melanocytic lesions [3, 4, 34, 41].

However, many studies, based on subjective methods, have been reported showing how the assessments of the visual features of the examining lesions depend on the knowledge degree of the clinicians and consequently low concordance values also between expert dermatologists are widely reported [4, 6, 7]. Reproducible and diagnostic significant objective variables imply a better standardization in terms of the final result of the dermatoscopic analysis. Some equivocal subjective assessments leading to low concordance among dermatologists should be better investigated in this field of noninvasive technologies.

In term of accuracy, from this study, we can assert that selected objective patient's related information (age, lesions site and gender) along with validated objective robust variables [16, 19] and a weighty and robust contribution [3, 4, 21, 24, 34, 41].

8.12 Future Perspective in the Aided Diagnosis

Our approach based on an "*objective semiology*," applied upon the several studies here reported, has multiple advantages to provide a reliable diagnostic method and to indicate to the clinicians which parameters are statistically significant for the final result. In our opinion, this is actually the real meaning of "aided diagnosis": not merely reaching a final diagnosis/results "no-reason explained," but mainly helping experts in a deeper knowledge of the skin lesions visual features. This is particularly applied to the delicate field of histopathological diagnosis of "difficult" skin tumors, where a simple dicotomic "benign/malignant" cut-off is often difficult to achieve, and we should rather reason in terms of malignancy degree.

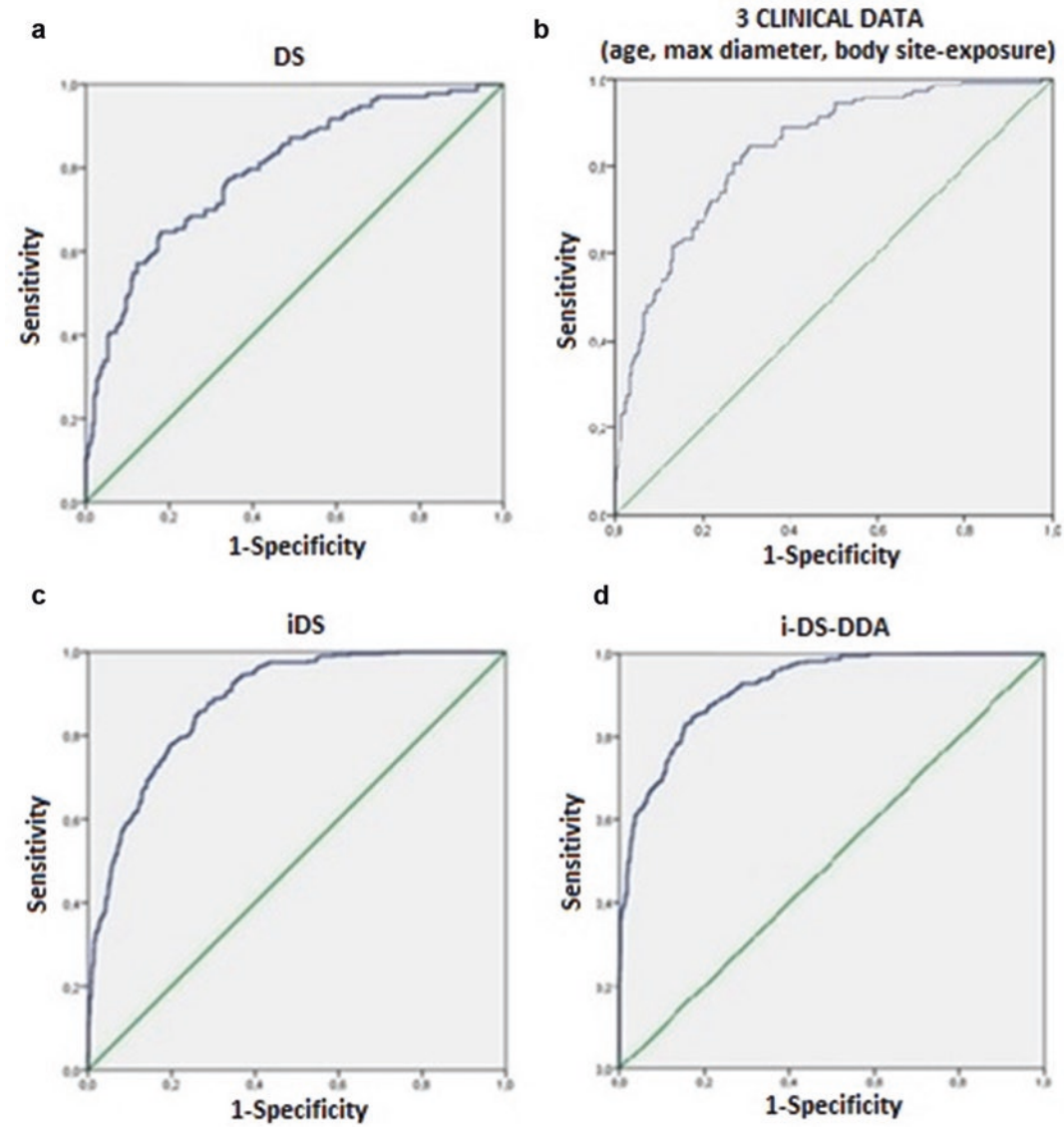

Fig. 8.3 Comparison between the performances of the dermoscopy (**a**), three clinical–personal selected variables (**b**), integrated-DS (**c**), and i-DS-DDA (**d**) in discriminating atypical nevi from early MM in the 2018 study: DS AUC = 0.79 [IC 95% = 0.769–0.822](**a**); clinical–personal variable AUC = 0.833 [IC 95% = 0.81–0.857] (**b**); i-DS AUC = 0.881 [IC 95% = 0.863–0.899](**c**); i-DS-DDA AUC = 0.921 [IC 95% = 0.906–0.935] (**d**)

References

1. Moffatt CRM, Green AC, Whiteman DC. Diagnostic accuracy in skin cancer clinics: the Australian experience. Int J Dermatol. 2006;45(6):656–60.
2. Youl PH, Raasch BA, Janda M, Aitken JF. The effect of an educational programme to improve the skills of general practitioners in diagnosing melanocytic/pigmented lesions. Clin Exp Dermatol. 2007;32(4):365–70.
3. Tognetti L, Cevenini G, Moscarella E, et al. An integrated clinical and dermoscopic risk scoring system (iDScore) for the differentiation between early melanoma and atypical nevi. J Eur Acad Dermatol Venereol. 2018;32:2162–70.
4. Tognetti L, Cinotti E, Moscarella E, et al. Impact of clinical and personal data in the dermoscopic differ-

entiation between early melanoma and atypical nevi. Dermatol Pract Concept. 2018;8(4):324–7.
5. Stanganelli I, Burroni M, Rafanelli S, Bucchi L. Intraobserver agreement in interpretation of digital epiluminescence microscopy. J Am Acad Dermatol. 1995;33:584–9.
6. Argenziano G, Soyer HP, Chimenti S, et al. Dermoscopy of pigmented skin lesions: results of a consensus meeting via the Internet. J Am Acad Dermatol. 2003;48(5):679–93.
7. Carrera C, Marchetti MA, Dusza S, et al. Validity and reliability of dermoscopic criteria used to differentiate nevi from melanoma: a web-based international dermoscopy society study. JAMA Dermatol. 2016;152(7):798–806.
8. Rubegni P, Tognetti L, Argenziano G, et al. A risk scoring system for the differentiation between melanoma with regression and regressing nevi. J Dermatol Sci. 2016;83(2):138–44.
9. Annessi G, Bono R, Sampogna F, et al. Sensitivity, specificity, and diagnostic accuracy of three dermoscopic algorithmic methods in the diagnosis of doubtful melanocytic lesions. J Am Acad Dermatol. 2007 May;56(5):759–67.
10. Doi K. Current status and future potential of computer-aided diagnosis in medical imaging. Br J Radiol. 2005;78(1):s3–s19.
11. Fenton JJ, Taplin SH, Carney PA, et al. Influence of computer-aided detection on performance of screening mammography. N Engl J Med. 2007;356(14):1399–409.
12. Kim J-S, Kim J-H, Cho G, Bae KT. Automated detection of pulmonary nodules on CT images: effect of section thickness and reconstruction interval—initial results. Radiology. 2005;236(1):295–9.
13. Li J, Van Uitert R, Yao J, Petrick N, Franaszek M, Huang A, et al. Wavelet method for CT colonography computer-aided polyp detection: false positive reduction for CTC CAD. Med Phys. 2008;35(8):3527–38.
14. Shiraishi J, Li Q, Appelbaum D, Pu Y, Doi K. Development of a computer-aided diagnostic scheme for detection of interval changes in successive whole-body bone scans: CAD for detection of bone scan interval changes. Med Phys. 2006;34(1):25–36.
15. Sertel O, Kong J, Shimada H, Catalyurek UV, Saltz JH, Gurcan MN. Computer-aided prognosis of neuroblastoma on whole-slide images: classification of stromal development. Pattern Recogn. 2009;42(6):1093–103.
16. Andreassi L, Perotti R, Rubegni P, Burroni M, Cevenini G, Biagioli M, Taddeucci P, Dell'Eva G, Barbini P. Digital dermoscopy analysis for the differentiation of atypical nevi and early melanoma—a new quantitative semiology. Arch Dermatol. 1999;135(12):1459–65.
17. Perotti R, Biagioli M, Burroni M, et al. Image analysis of pigmented lesions: clinico-histopathological correlation. Am J Dermatolopathol. 1994;16:103–4.
18. Andreassi L, Perotti R, Burroni M. Computerized image analysis of pigmented lesions. Chonic Dermatol. 1995;1:11–24.
19. Burroni M. Understanding digital melanoma: Islands of colors. Melanoma Res. 1997;11(1):S22.
20. Bauer P, Cristofolini P, Boi S, et al. Digital epiluminescence microscopy: usefulness in the differential diagnosis of cutaneous pigmentary lesions. A statistical comparison between visual and computer inspection. Melanoma Res. 2000;10(4):345–9.
21. Andreassi L, Perotti R, Rubegni P, Burroni M, et al. Digital dermoscopy analysis for the differentiation of atypical nevi and early melanoma: a new quantitative semiology. Arch Dermatol. 1999;135:1459–65.
22. Rubegni P, Cevenini G, Burroni M, et al. Automated diagnosis of pigmented skin lesions. Int J Cancer. 2002;101(6):576–80.
23. Rubegni P, Burroni M, Andreassi L, Fimiani M. The role of dermoscopy and digital dermoscopy analysis in the diagnosis of pigmented skin lesions. Arch Dermatol. 2005;141:1444–6.
24. Rubegni P, Burroni M, Cevenini G, et al. Digital dermoscopy analysis and artificial neural network for the differentiation of clinically atypical pigmented skin lesions: a retrospective study. J Invest Dermatol. 2002;119:471–4.
25. Burroni M, Corona R, Dell'Eva G, et al. Melanoma computer-aided diagnosis: reliability and feasibility study. Clin Canc Res. 2004;10:1881–6.
26. Rubegni P, Cevenini G, Sbano P, et al. Evaluation of cutaneous melanoma thickness by digital dermoscopy analysis: a retrospective study. Melanoma Res. 2010;20(3):212–7.
27. Rubegni P, Cevenini G, Burroni M, et al. Objective follow-up of atypical melanocytic skin lesions: a retrospective study. Arch Dermatol Res. 2010;302:551–60.
28. Burroni M, Wollina U, Torricelli R, et al. Impact of digital dermoscopy analysis on the decision to follow up or to excise a pigmented skin lesion: a multicentre study. Skin Res Technol. 2011;17(4):451–60.
29. Rubegni P, Ferrari A, Cevenini G, et al. Differentiation between pigmented Spitz naevus and melanoma by digital dermoscopy and stepwise logistic discriminant analysis. Melanoma Res. 2001;11(1):37–44.
30. Rubegni P, Tognetti L, Pellegrino M, et al. Spitz nevus versus atypical Spitz tumor: objective morphological differentiation by digital dermoscopy analysis. 2016 IEEE International Symposium on Medical Measurements and Applications (MeMeA), University of Sannio, Benevento, Italy; 15 May 2016 through 18 May 2016, pp. 529–533.
31. Lallas A, Apalla Z, Moscarella E, et al. Extensive regression in pigmented skin lesions: a dangerous feature. Dermatol Pract Concept. 2012;2(2):202–8.
32. Pattanaprichakul P, Shea CR, Reed JA, Prieto VG. Halo nevus versus melanoma with regression. Pathology of Challenging Melanocytic Neoplasms; Shea, Reed, Prieto eds. Springer; New York. Chapter 7, p. 55–61, August 2015.
33. Tognetti L, Burroni M, Nami N, et al. Digital dermoscopy analysis for differential diagnosis of regressing nevi and melanoma with regression. 11th IEEE International Symposium on Medical Measurements

and Applications, MeMeA 2016; University of Sannio Benevento; Italy; 15 May 2016 through 18 May 2016, p. 80–85.
34. Rubegni P, Tognetti L, Argenziano G, Nami N, Brancaccio G, Cinotti E, Miracco C, Fimiani M, Cevenini G. A risk scoring system for the differentiation between melanoma with regression and regressing nevi. J Dermatol Sci. 2016;83(2):138–44.
35. Fabrizi G, Pennacchia I, Pagliarello C, Massi G. Sclerosing nevus with pseudomelanomatous features. J Cutan Pathol. 2008;35:995–1002.
36. Ferrara G, Amantea A, Argenziano G, et al. Sclerosing nevus with pseudomelanomatous features and regressing melanoma with nevoid features. J Cutan Pathol. 2009;36:913–5.
37. Saida T, Miyazaki A, Oguchi S, et al. Significance of dermoscopic patterns in detecting malignant melanoma on acral volar skin: results of a multicenter study in Japan. Arch Dermatol. 2004;140:1233–8.
38. Palicka GA, Rhodes AR. Acral melanocytic nevi: prevalence and distribution of gross morphologic features in white and black adults. Arch Dermatol. 2010;146:1085–94.
39. Rubegni P, Cevenini G, Nami N, Argenziano G, Saida T, Burroni M, et al. Dermoscopy and digital dermoscopy analysis of palmoplantar equivocal pigmented skin lesions in caucasians. Dermatology. 2012;225:248–55.
40. Seidenari S, Pellacani G, Giannetti A, et al. Melanoma Res. Digital videomicroscopy and image analysis with automatic classification for detection of thin melanomas. 1999;9(2):163–71.
41. Rubegni P, Feci L, Nami N, et al. Computer-assisted melanoma diagnosis: a new integrated system. Melanoma Res. 2015;25(6):537–42.
42. Janda M, Soyer HP. Skin cancer detection by one click—are we any closer? Med J Aust. 2013;199(11):739.
43. Liu Z, Sun J, Smith M, Smith L, Warr R. Incorporating clinical metadata with digital image features for automated identification of cutaneous melanoma. Br J Dermatol. 2013;169(5):1034–40.

9 Optical Super-High Magnification Dermoscopy

Gerardo Ferrara, Daniele Dusi, Marco Sigona, Marco Simonacci, and Renato Rossi

Recent technical progress in digital imaging has given us the opportunity to refine techniques used in dermoscopy. By means of the capillaroscopy objective of FotofinderMedicam 1000 (Fotofinder System, Bad Birnbach, Germany), a pigmented lesion can be observed at up to 400 times the original magnification [1]. Such an optical super-high-magnification dermoscopy (OSHMD) can allow visualize even single-pigmented cells within the epidermis and the superficial dermis, in a strikingly similar fashion as reflectance confocal microscopy (RCM). In the real-time mode, even the flow of single erythrocytes within the capillary bed can be nicely observed. In order to give an idea about the power of resolution of this technique, Fig. 9.1 shows a scabies mite with its eggs and embryos.

G. Ferrara
Anatomic Pathology Unit, Macerata General Hospital, AV3-ASUR Marche, Macerata, Italy
e-mail: gerardo.ferrara@libero.it

D. Dusi · M. Sigona · M. Simonacci
Dermatology Unit, Macerata General Hospital, AV3-ASUR Marche, Macerata, Italy
e-mail: danieledusi@libero.it; marco.sigona@sanita.marche.it; marcosimonacci@libero.it

R. Rossi (✉)
Skin Center Senigallia, Senigallia, Italy
e-mail: rossirenat@libero.it

Since this technique enables even visualization of single cells, a more careful evaluation of some "local" dermoscopic features of pigmented skin tumors is possible, thereby giving additional parameters for clinically difficult-to-diagnose tumors.

The following "local" dermoscopic features of skin tumors can be more carefully investigated and redefined based on OSHMD.

Pigment network—At the dermoepidermal junction, melanocytes aggregate into brown rings composed of small brown round/polygonal "small circles" (each one corresponding to a single melanocyte) surrounding the dermal papillae; within the latter, small blood capillary loops are seen. This arrangement is strikingly similar to the "edged papilla" arrangement as seen in reflectance confocal microscopy [2]. Dermal papillae may be variously sized and shaped; importantly, however, in nevi they are "on focus," with sharp outlines of the polygonal pebbles, whereas in melanoma they are "blurred" and with variously merging shades of brown; such a "local" finding is hardly appreciated with conventional dermoscopy. In addition, the pigment network of melanoma is associated with capillary loops which are not centered to the papilla, but are irregularly distributed throughout the pigmented area (Fig. 9.2).

Dots—As for conventional dermoscopy, they appear as discrete roundish collections of pigment [3]. Different from conventional dermos-

M. Fimiani et al. (eds.), *Technology in Practical Dermatology*,
https://doi.org/10.1007/978-3-030-45351-0_9

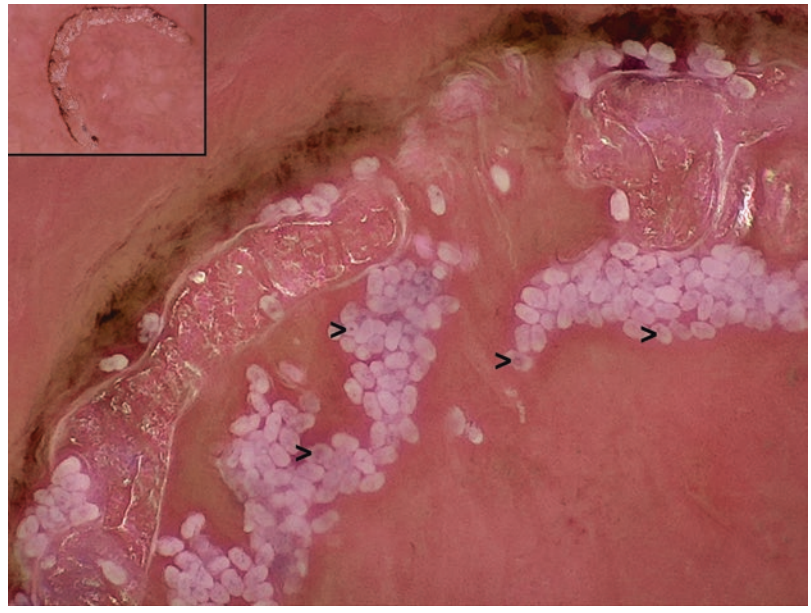

Fig. 9.1 Scabies on OSHM. A curvilinear borrow (inset) with the convex outline demarcated by hemorrhagic crusts and the concave outline filled with white oval-polygonal white lentil-like structures corresponding to the eggs of the mite; the arrowheads indicate the embryos within the eggs. Note the head of the mite (inset)

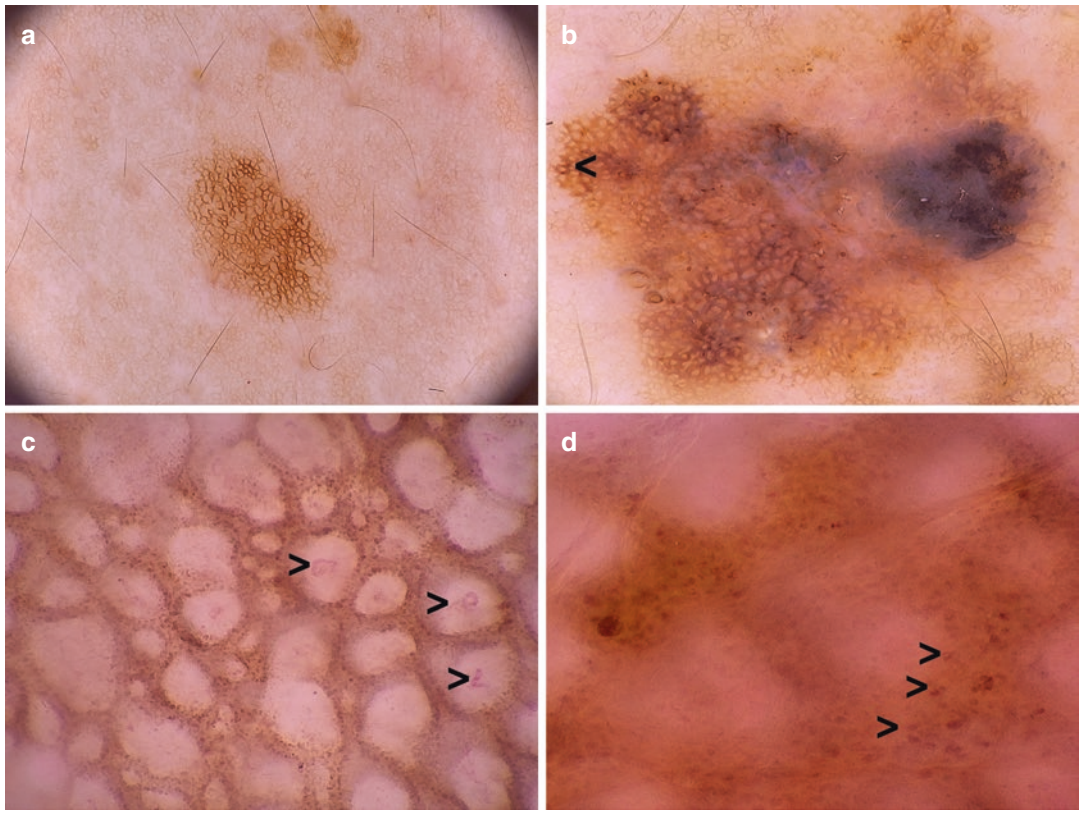

Fig. 9.2 A side-by-side comparison between the pigment network in a nevus (**a**, **c**) and in a melanoma (**b**, **d**). The dermoscopic diagnosis is obvious in both the cases. With OSHMD, the pigment network of a nevus appears as on-focus brown rings composed of small brown round/polygonal circles surrounding dermal papillae; within the latter, small blood capillary loops with blood vessels are seen (arrowheads). In melanoma, the pigment network (in the area indicated by the arrowhead in Fig. 9.2a) is out of focus, with untidy capillary loops (arrowheads)

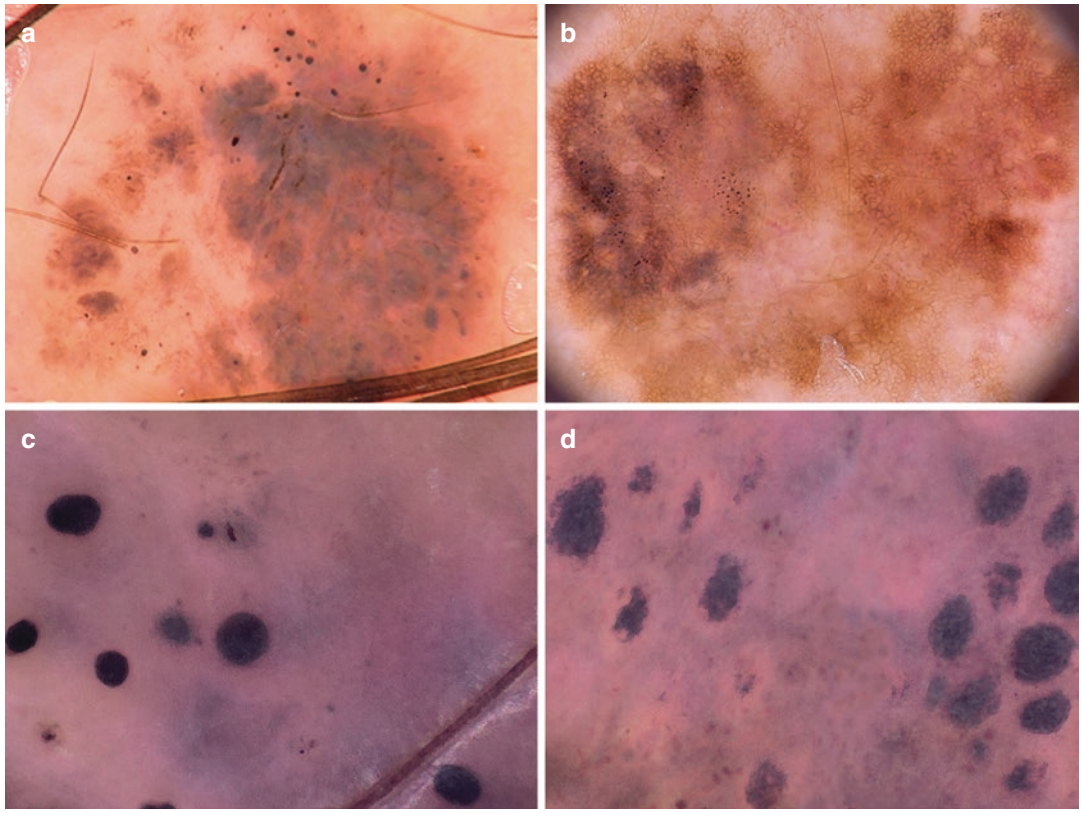

Fig. 9.3 A side-by-side comparison between dots of basal cell carcinoma (**a**, **c**) and dots of melanoma (**b**, **d**). On conventional dermoscopy (**a**, **b**), black dots look the same; with OSHMD, in basal cell carcinoma, they show round contours ("blueberry pattern"; **c**), whereas in melanocytic tumors, they show jagged outlines ("blackberry" pattern; **d**)

copy, OSHMD discloses dots whose morphology is better appreciated and can make the difference. In melanocytic tumors, dots are polychromatic and with jagged outlines ("blackberry" pattern); instead in basal cell carcinoma, they are homogeneously black and perfectly round ("blueberry" pattern) (Fig. 9.3). In melanoma, the presence of dots of different size outside the pigment lines may be a clue to pagetoid spread (Fig. 9.4).

Globules—On OSHMD, these appear as small circles aggregated into uniform polycyclic, sharply outlined papillary structures. Defined as such, they are diagnostic of dermal nevi (Fig. 9.5). As for conventional dermoscopy [3], the histopathological counterpart of papillary structures is given by roundish nests of dermal melanocytes underlying a papillated epidermis (Fig. 9.6).

White scar-like areas—As a rule, these dermoscopic structures warrant surgical excision, although they can be seen both in nevi and in melanoma [4, 5]. White, mostly structureless, scar-like areas, as seen on conventional dermoscopy, are not structureless on OSHMD, inasmuch as they are characterized by faint remnants of pigment network. In nevi, such a pigment network still discloses an "edged papilla-like" arrangement (Fig. 9.7); instead, in melanoma, at least focally, these remnants of pigment are

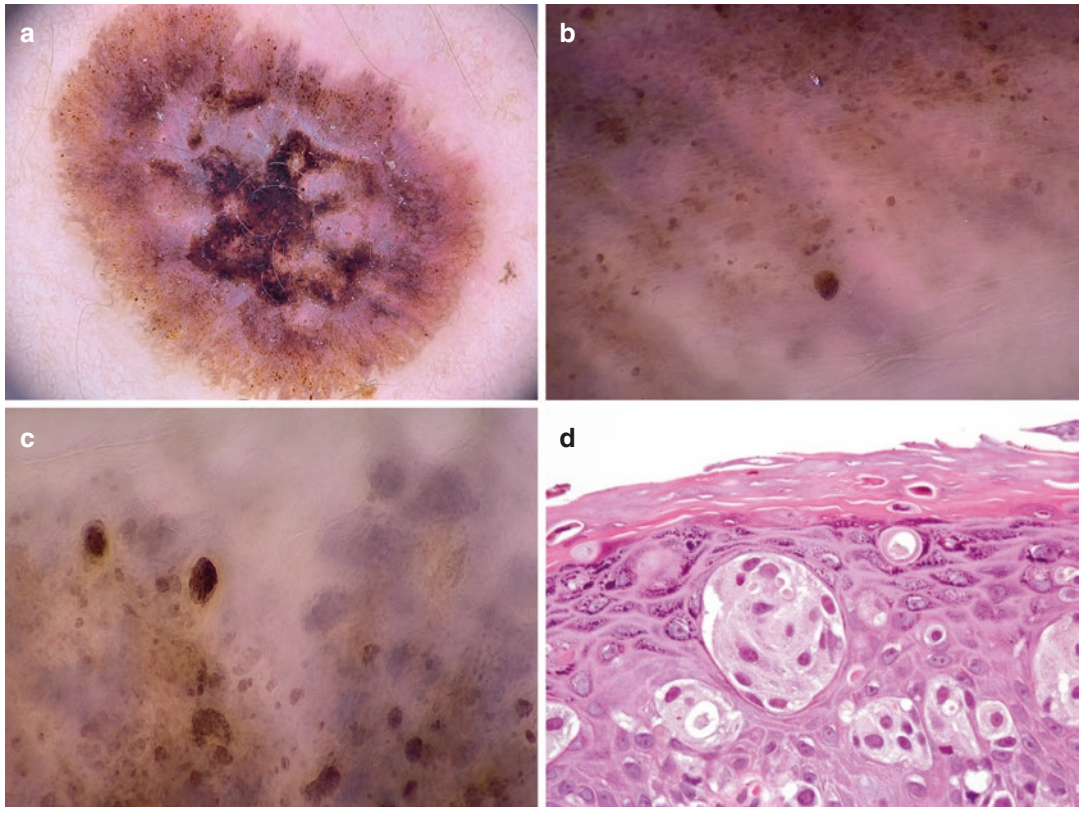

Fig. 9.4 A melanoma with 'spitzoid' dermoscopic feaures (**a**) characterized by variously sized dots (**b**, **c**), the latter corresponding to single melanocytes and small aggregates of melanocytes within the upper layers of the epidermis (**d**)

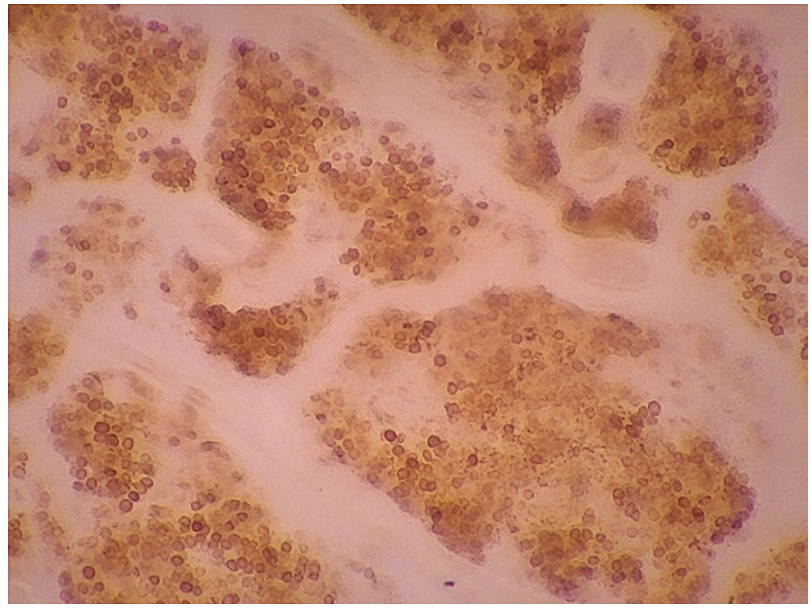

Fig. 9.5 Classical OSHMD picture of a dermal nevus, composed of uniform circles aggregated into papillary structures

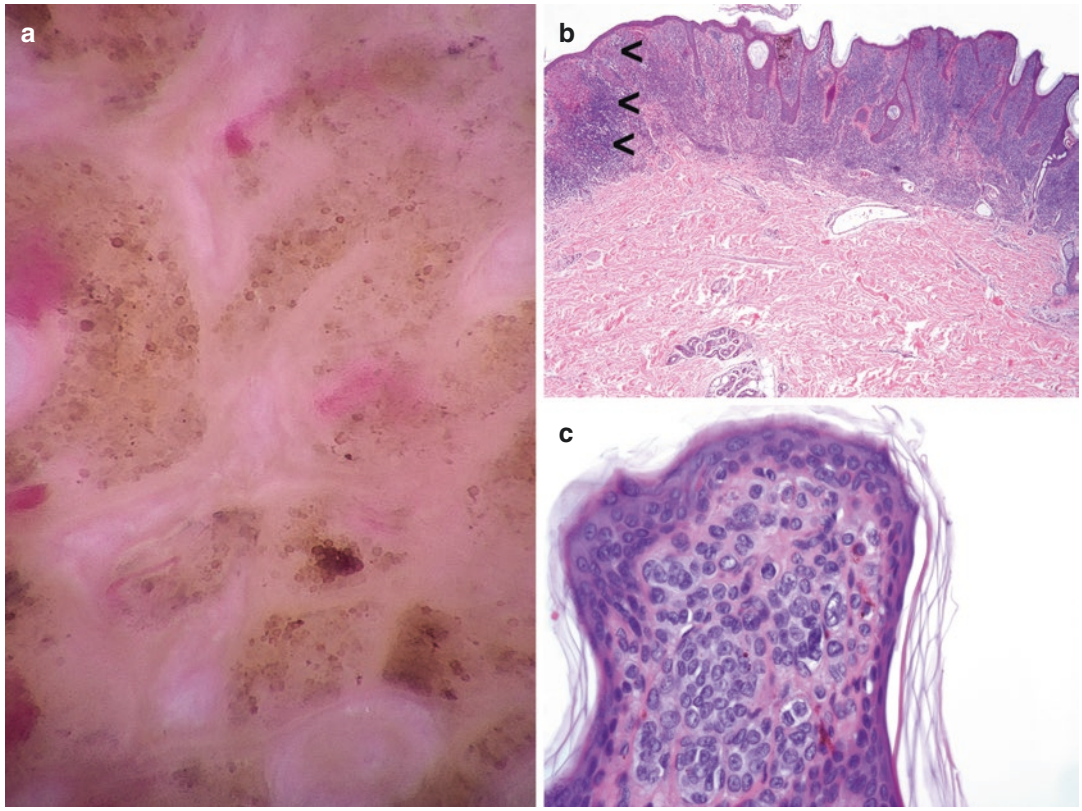

Fig. 9.6 OSHMD of a dermal nevus featuring papillary structures made up of aggregates of uniform circles of round/polygonal cells (**a**). The lesion was removed because it was associated with a melanoma (**b**, arrowheads); its benign component was characterized by a papillated epidermal hyperplasia with dermal roundish aggregates of monomorphic melanocytes (**c**). The dermal aggregates of melanocytes are the histopathological counterpart of the aggregates of circles seen in Fig. 9.6a

more densely and irregularly arranged and show angular contours. We have termed such structures "angled nests" and have found them to be 100% melanoma-specific (Ferrara G. et al; submitted). Histopathologically, "angled nests" correspond to irregular in size, spaced, and shaped nests of melanocytes within an irregularly hyperplastic epidermis; quite characteristically, the epidermis is untidily compressed by untidily arranged subepidermal collagen bundles (Fig. 9.8).

Site-specific structures—Conventional dermoscopic features of lentigo maligna (gray dots, pseudonetwork, rhomboidal structures, pigmented follicles, annular-granular structures) [6] are better defined on OSHMD, with a sharper definition of different colors. In lentigo maligna, the grayish color seen on conventional dermoscopy [6] splits into different colors ranging from black to blue; instead in epithelial tumors (seborrheic keratosis, lichen planus-like keratosis, pigmented actinic keratosis), the prevailing color is brown (Fig. 9.9).

In keratinocytic tumors, OSHMD allows a better visualization of the "strawberry pattern" of actinic keratosis; likewise the disappearance of

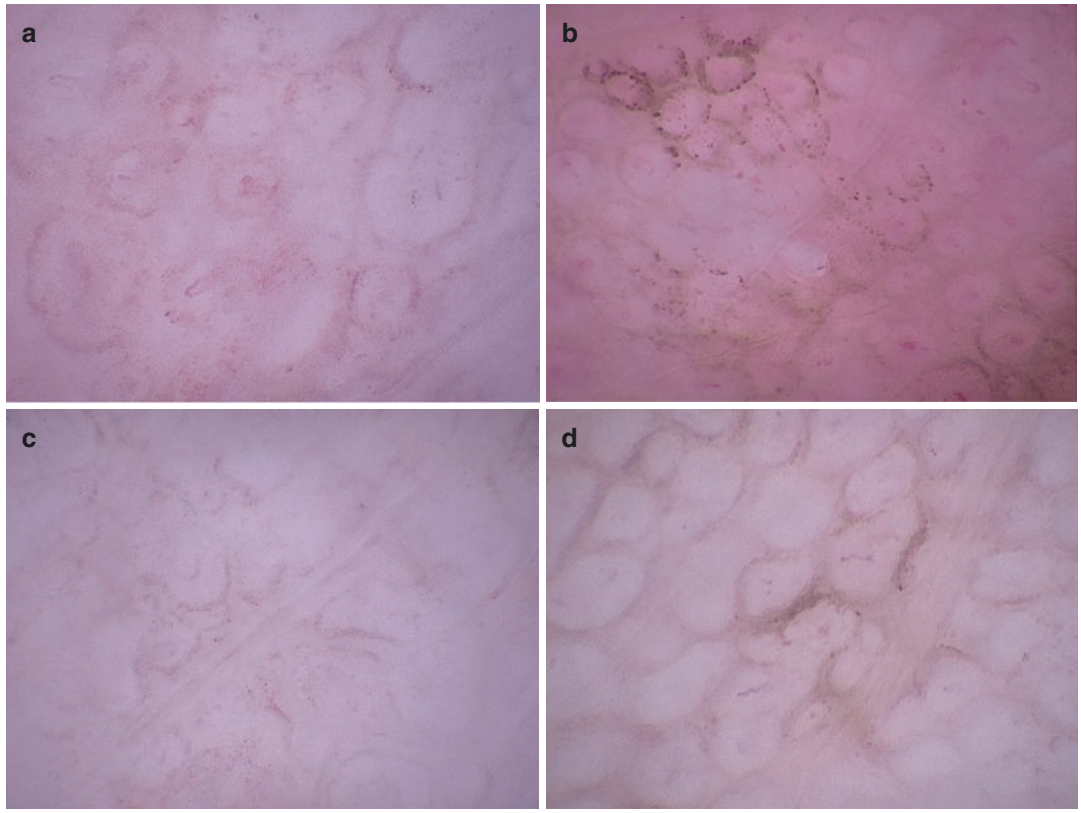

Fig. 9.7 (**a**–**d**) Four examples of scar-like regressive areas of a Clark nevus. The remnants of pigment are relatively homogeneous and arranged in an "edged papilla-like" fashion

the follicles in early invasive squamous cell carcinoma [7] can be probably detected in an earlier phase than with conventional dermoscopy (Fig. 9.10).

Vascular structures—In regressing melanoma with relative preservation of epidermal hyperplasia, conventional dermoscopy shows areas of reticular depigmentation which, on OSHMD, discloses peculiar "targetoid" structures. Such structures are typified by a diffuse brownish pigmentation surrounding a white area centered by a large capillary loop of the dermal papilla ("target capillary") (Fig. 9.11). On histopathology, such "targetoid" structures correspond to newly formed superficial vessels embedded by fibrosis and surmounted by a proliferation of melanocytes mainly arranged in single units at the junction; in such a context, the epidermis typically shows a relatively preserved retiform epidermal hyperplasia, which, in conjunction with dermal fibrosis, is responsible for the reticular depigmentation as seen on conventional dermoscopy [8].

In conclusion, OSHMD is a promising tool for the management of clinically ambiguous skin tumors. The impact of such a new technique in routine practice is being evaluated by ad hoc ongoing studies.

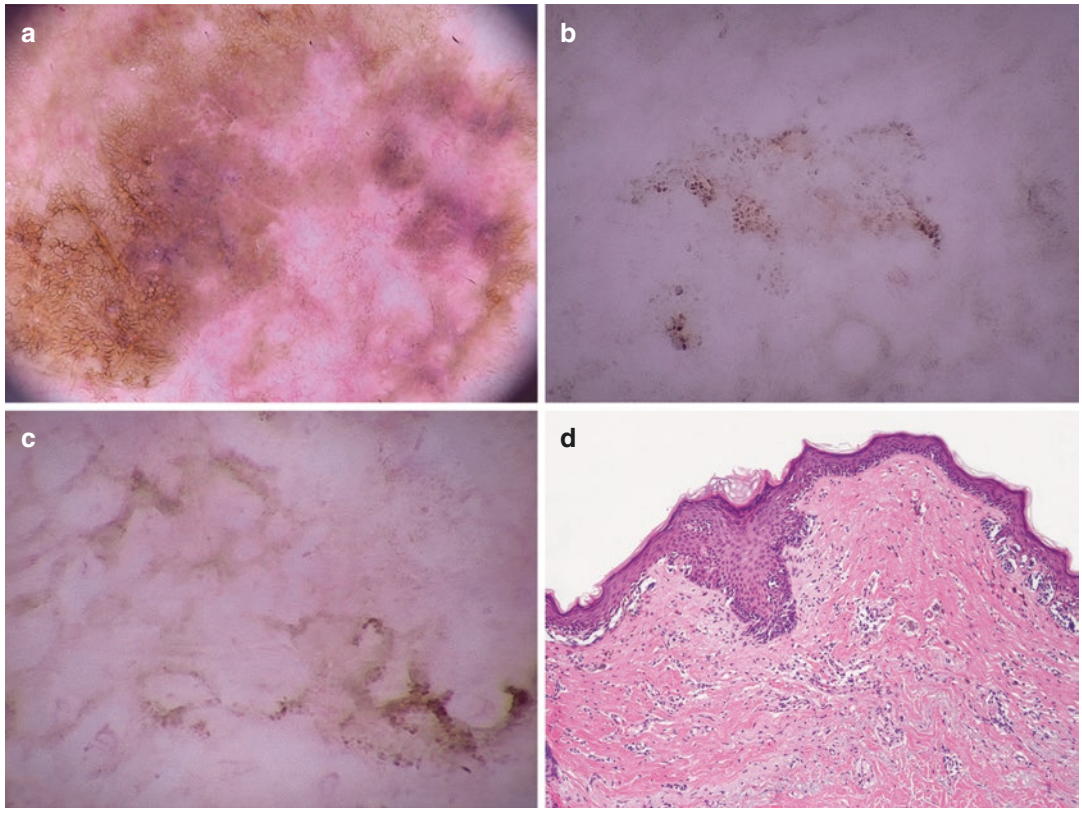

Fig. 9.8 A melanoma with regression. Dermoscopy featuring a disrupted pigment network with multiple white scar-like areas (**a**); prominent "angled" nests on OSHMD with very thick and irregular pigment lines (**b**, **c**); the histopathological picture characterized by irregular epidermal hyperplasia, irregular basilar proliferation of single and nested melanocytes, irregular collagen bundles in the dermis (**d**)

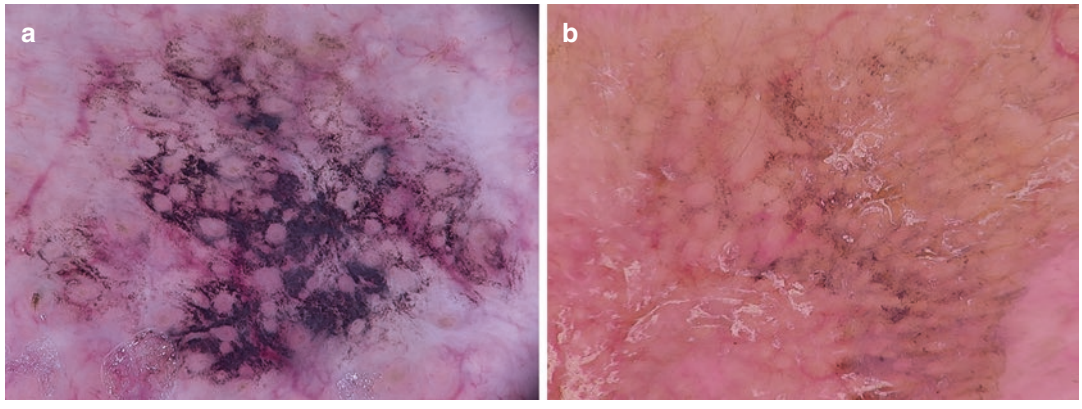

Fig. 9.9 A side-by-side comparison between lentigo maligna and pigmented actinic keratosis. On conventional dermoscopy (**a**, **b**), both are characterized by a grayish pigmentation. With OSHMD, lentigo maligna appears with different shades of color, ranging from black to blue (**c**), reflecting the different depth of pigment; instead in pigmented actinic keratosis, the brown color is strikingly prevailing (**d**) because of the prevailing pigmentation of basilar keratinocytes

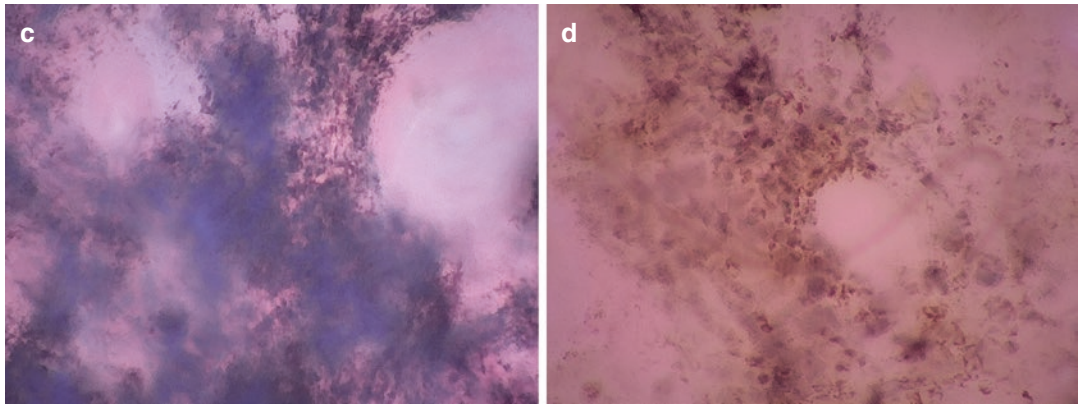

Fig. 9.9 (continued)

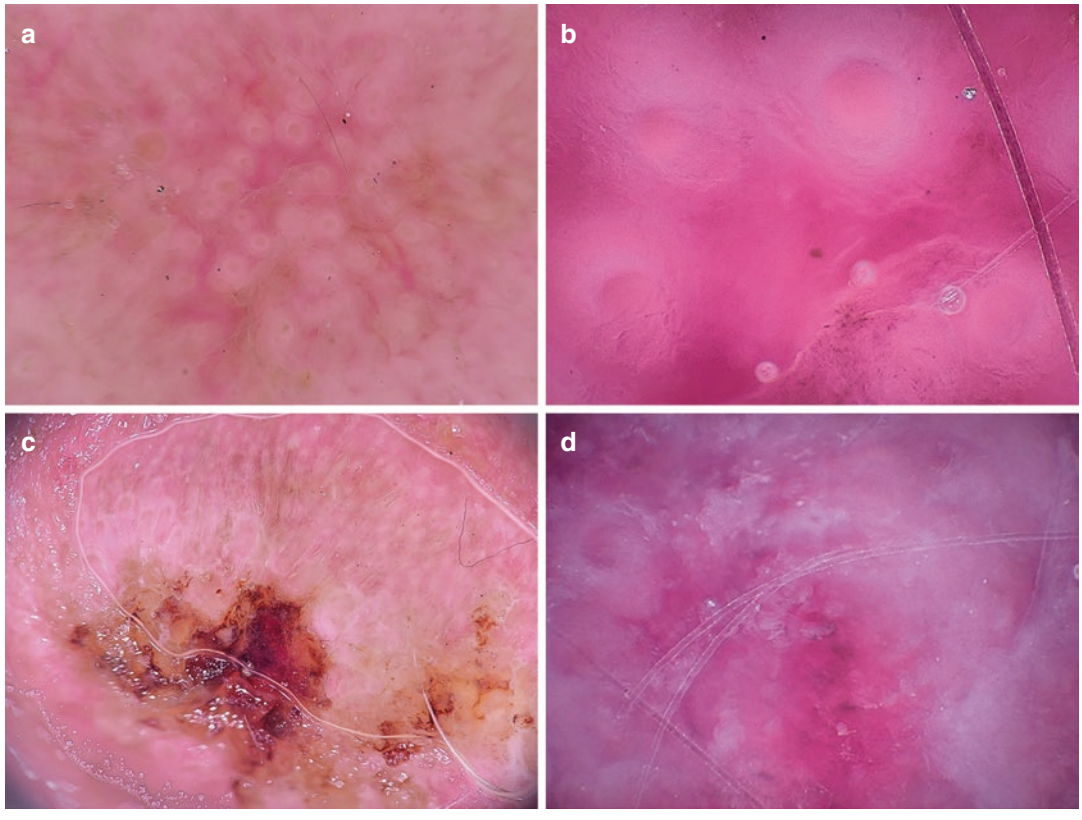

Fig. 9.10 Dermoscopic features of a pigmented actinic keratosis, with the strawberry pattern as seen on conventional dermoscopy (**a**), which corresponds to a diffuse interfollicular erythema with horny plugs on OSHMD (**b**). In comparison, on OSHMD, ulcerated squamous cell carcinoma (**c**) discloses an obliteration of the hair follicles at the borders of the ulcer (**d**)

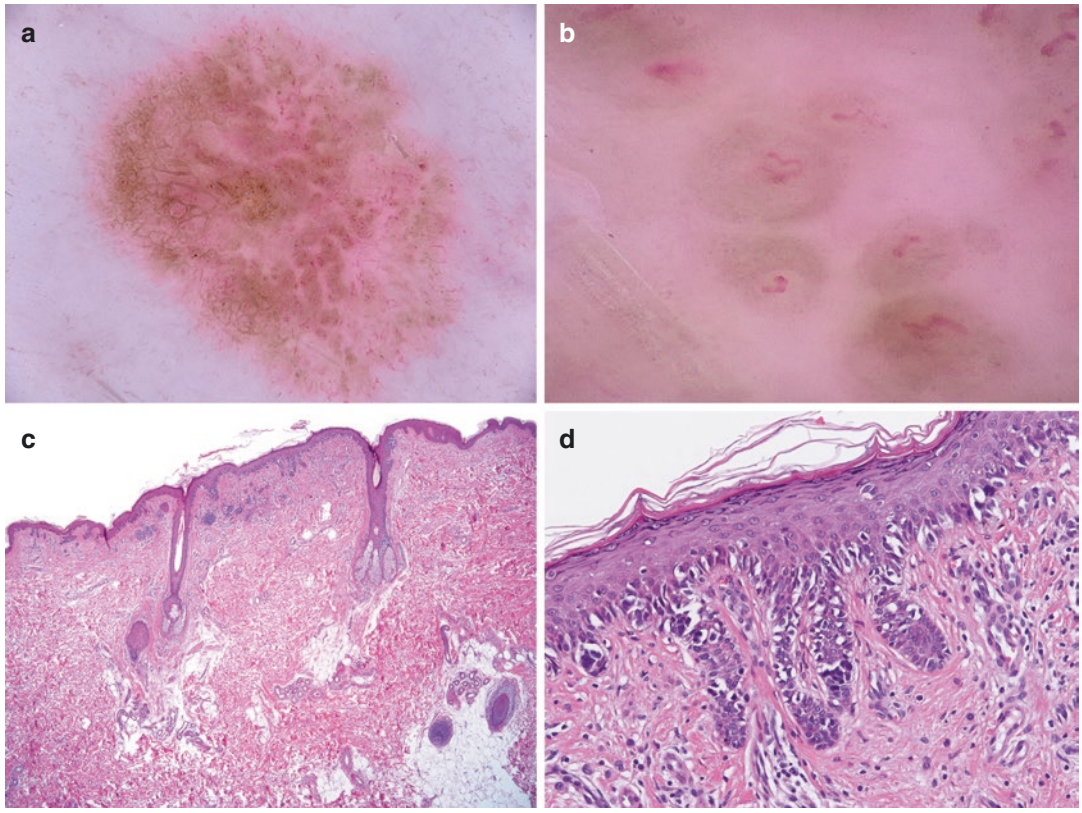

Fig. 9.11 Regressing melanoma. Conventional dermoscopy characterized by reticular depigmentation (**a**); on OSHMD, huge capillary loops surrounded by a hypopigmented halo, the latter surrounded by a brownish hue (targetoid appearance; **b**). On histopathology, a melanocytic tumor with focal regression (**c**) characterized by newly formed superficial vessels embedded by fibrosis and surmounted by a proliferation of melanocytes mainly arranged in single units at the junction with relatively preserved retiform epidermal hyperplasia (**d**)

References

1. Dusi D, Rossi R, Simonacci M, Ferrara G. Image gallery: the new age of dermoscopy: optical super-high magnification. Br J Dermatol. 2018;178:e330.
2. Pellacani G, Cesinaro AM, Longo C, Grana C, Seidenari S. Microscopic in vivo description of cellular architecture of dermoscopic pigment network in nevi and melanomas. Arch Dermatol. 2005;141:147–54.
3. Argenziano G, Soyer HP, Chimenti S, Talamini R, Corona R, Sera F, Binder M, Cerroni L, De Rosa G, Ferrara G, Hofmann-Wellenhof R, Landthaler M, Menzies SW, Pehamberger H, Piccolo D, Rabinovitz HS, Schiffner R, Staibano S, Stolz W, Bartenjev I, Blum A, Braun R, Cabo H, Carli P, De Giorgi V, Fleming MG, Grichnik JM, Grin CM, Halpern AC, Johr R, Katz B, Kenet RO, Kittler H, Kreusch J, Malvehy J, Mazzocchetti G, Oliviero M, Ozdemir F, Peris K, Perotti R, Perusquia A, Pizzichetta MA, Puig S, Rao B, Rubegni P, Saida T, Scalvenzi M, Seidenari S, Stanganelli I, Tanaka M, Westerhoff K, Wolf IH, Braun-Falco O, Kerl H, Nishikawa T, Wolff K, Kopf AW. Dermoscopy of pigmented skin lesions: results of a consensus meeting via the Internet. J Am Acad Dermatol. 2003;48:679–93.
4. Yélamos O, Braun RP, Liopyris K, Wolner ZJ, Kerl K, Gerami P, Marghoob AA. Dermoscopy/dermatoscopy and dermatopathology correlates of cutaneous neoplasms. J Am Acad Dermatol 2018; Oct 12. [Epub ahead of print].
5. Zalaudek I, Argenziano G, Ferrara G, Soyer HP, Corona R, Sera F, Cerroni L, Carbone A, Chiominto A, Cicale L, De Rosa G, Ferrari A, Hofmann-Wellenhoff R, Malvenhy J, Peris K, Pizzichetta MA, Puig S, Scalvenzi M, Staibano S, Ruocco V. Clinically equivocal melanocytic skin lesions withy features of

regression: a dermoscopic-pathological study. Br J Dermatol. 2004;150:64–71.
6. Tschandl P, Gambardella A, Boespflug A, Deinlein T, de Giorgi V, Kittler H, Lallas A, Malvehy J, Moscarella E, Puig S, Scalvenzi M, Thomas L, Zalaudek I, Alfano R, Argenziano G. Seven non-melanoma features to rule out facial melanoma. Acta Dem Venereol. 2017;97:1219–24.
7. Ulrich M, Zalaudek I, Welzel J. Shining into the white: the spectrum of epithelial tumors from actinic keratosis to squamous cell carcinoma. Dermatol Clin. 2016;34:459–67.
8. Botella-Estrada R, Requena C, Traves V, Nagore E, Guillen C. Chrysalis and negative pigment network in Spitz nevi. Am J Dermatoapthol. 2012;34:188–91.

Fluorescence Videodermoscopy

10

Elisa Cinotti, Alessio Adamo, and Paolo Broganelli

The panorama of videodermatoscopy or videodermoscopy is expanding, and fluorescence can be used to obtain additional information that can be integrated with current diagnostic technology [1]. Fluorescence is a process whereby a molecule absorbs radiation at a wavelength and emits it at a higher wavelength. The peak of absorption of a wavelength is characteristic of specific molecules and can be visualized by a radiative (photon emission) or non-radiative (total absorption) phenomenon. Fluorescence of the skin can be caused either by endogenous substances that cause autofluorescence of the tissue (i.e., self-fluorescence without any specific additives on or inside the skin) or by fluorescent dyes or markers introduced into the organism from outside, which, when they accumulate in definite structures of the tissue, for example in tumors, make it capable of secondary fluorescence [2]. Under the action of ultraviolet (UV) radiation or blue light, all tissues possess the capability for autofluorescence in one degree or another. There are many endogenous fluorophores in the upper skin (proteins and pigments such as flavins, collagen, elastin, melanin, and hemoglobin), each with its specific absorption spectrum. However, the overlap of the spectral bands of these fluorophores in combination with light scattering and the absorption of radiation in the tissue make the autofluorescence spectra of biological tissue wide and weakly structured especially if the field of view (FOV) is wide. Therefore, fluorescence markers have been studied to identify specific target like tumors (e.g., aluminolevulinic acid used for photodynamic therapy to induce the production of the endogenous chromophore protoporphyrin IX). The differences of fluorescence in the normal and in pathologic skin can manifest themselves both in the spectral properties and in the observed morphological pattern. Accordingly, the apparatus for fluorescence diagnosis is either spectral or imaging.

Many prototypes of videodermoscopes that exploit autofluorescence are under study. For example, Forschner et al. [3] studied the different fluorescence spectra of melanin in cutaneous melanoma (peaked at 640 nm) and melanocytic nevi (peaked at 590 nm) and created a computer algorithm with a defined set of parameters that allowed to interpret melanin fluorescence in the area imaged by videodermoscopy. Under normal conditions, melanin fluorescence is surpassed by the autofluorescence of the remaining endogenous fluorophores in the cells. In order to obtain

E. Cinotti (✉)
Department of Medical, Surgical and Neurological Science, Dermatology Section, University of Siena, S. Maria alle Scotte Hospital, Siena, Italy

A. Adamo
Adamo S.r.l., Trapani, Italy
e-mail: a.adamo@adamosrl.com

P. Broganelli
Department of Medical Sciences, Dermatologic Clinic, University of Turin, Turin, Italy

M. Fimiani et al. (eds.), *Technology in Practical Dermatology*,
https://doi.org/10.1007/978-3-030-45351-0_10

a more selective fluorescence, melanin was excited via stepwise two-photon absorption with nanosecond laser pulses at 800 nm. Although the resulting melanin fluorescence was detected in a wide range of approximately 385–785 nm, their device had a sensitivity of 89.1% and a specificity of 44.8% for melanoma on 476 equivocal pigmented lesions.

One of the few autofluorescence videodermoscopes that provides skin images and that is available on the market is fluorescence advanced videodermatoscopy (FAV).

10.1 Fluorescence Advanced Videodermatoscopy

Fluorescence advanced videodermatoscopy (FAV) is a new imaging noninvasive technique that couples videodermoscopy with the information derived from the autofluorescence of some skin molecules such as hemoglobin and melanin [4]. FAV is an optical electronic system that uses a handheld Horus probe (Adamo S.r.l., Trapani, Italy) with a monochromatic light-emitting source with a wavelength of 405 nm (±5 nm) and a fixed angle of incidence [4].

The probe uses a monochromatic 640 × 480 pixel charge-coupled device (CCD) sensor with high spectral sensitivity for λ = 380–830 nm, with a high frame-rate of 120 frames/s managed by a dedicated firmware. The optical system consists of several coupled lenses that allow primary magnification of about 12× mounted on a mechanical support with screw coupling and a relative axial sliding of 500 μm/360°. In this way, it is possible to obtain an excellent control with axial variations of about 7 μm. The depth of field obtained is about 30–50 μm and allows a pseudo-3D view of the structure under examination. The optical resolution obtained is approximately 1 μm. The FAV method is based on the absorption level of some endogenous chromophores at specific wavelengths. This absorption translates visually into a level of gray tending to black for those chromophores that absorb the totality of the irradiated light. Fluorescence, not selectively filtered, is visually represented by gray levels tending to white (black no fluorescence, white highest fluorescence). The different refractive index of the stratum corneum determines a scattering phenomenon that is eliminated using glycerol which also allows a better permeability of light radiation.

The examination is carried out in vivo and the optical device is directly applied on the skin. By manually regulating the focus on the optical device, it is possible to scan different depths of the skin. The field of view is 340 μm and the optical penetration depth (OPD) is around 200–400 μm, reaching the dermis. Subcutaneous structures are poorly viewed in the UV region, and this is because this radiation does not penetrate the skin very far. FAV allows for a fast and dynamic examination of superficial skin structures with a resolution on a cellular level and can directly visualize pathogens in selected skin infections, skin microcirculation, and pigmented tumors. The instrument is coupled with a videodermoscope (Horus System HS600) with high-definition probe, double-diode polychromatic lighting with and without cross-polarization selectable automatically, and 30× (field of view—FOV 7.4 mm) and 150× (FOV 1.7 mm) magnifications that can be useful to compare images.

Healthy skin: In healthy skin, it is possible to observe the structures endowed with endogenous chromophores (melanin and hemoglobin) up to the superficial dermis with great precision. It is also possible to observe the stratum corneum (Fig. 10.1a) without interface fluid, exploiting the reflection of keratin [4]. The underlying layers are seen with the aid of an interface liquid. Keratinocytes have bright cytoplasm and dark nuclei (Fig. 10.1b). By manually adjusting the focus depth, it is possible to go deeper and observe the dermal papillae (Fig. 10.1b and c), projecting into the overlying epidermis. They are characterized by a circular design and by a greater brightness on the periphery, due to the vertical addition of the chromophores (melanin) that are present in the basal layer of the epidermis. There is an excellent correlation between horizontal histology and in vivo fluorescence microscopy (Fig. 10.1d). Proceeding toward the deeper structures, it is possible to observe the red blood cells moving inside the capillaries of the dermal papillae (Fig. 10.1c); the walls of the vessels are not distinguished, but the hemoglobin allows to mark

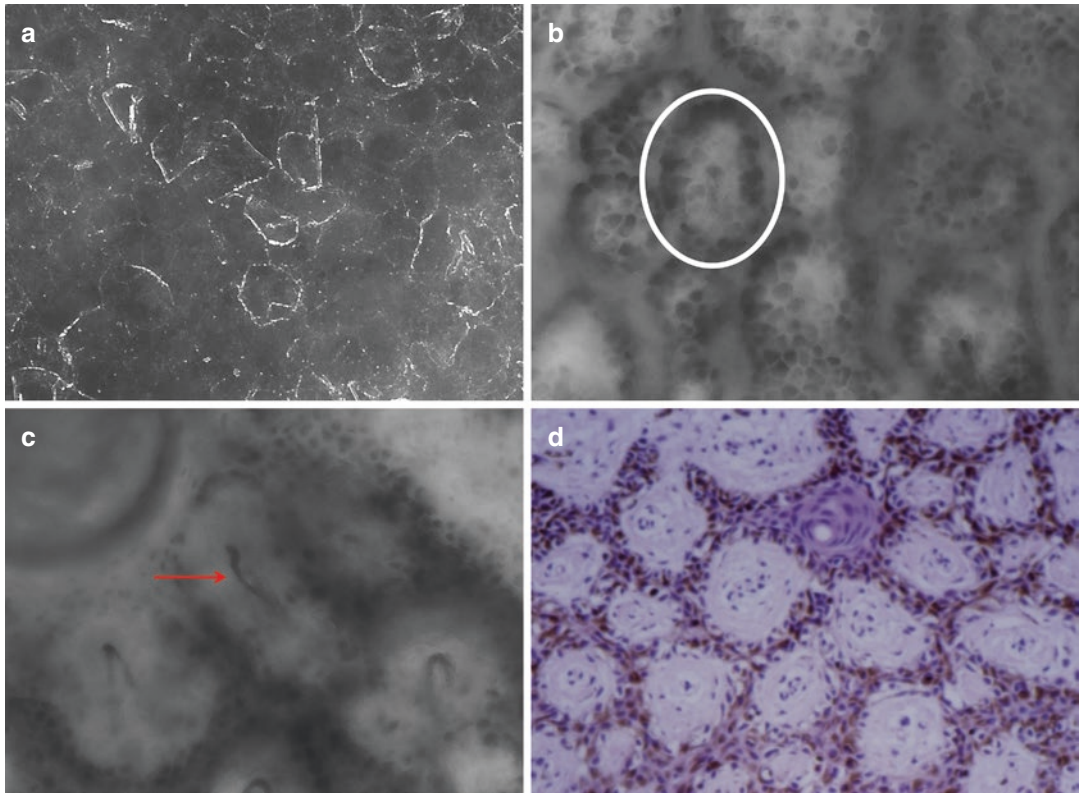

Fig. 10.1 In vivo fluorescence-advanced videodermatoscopy (FAV, **a**–**c**) of healthy skin and correlation with histology (**d**). FAV without interface liquid shows the stratum corneum (**a**), whereas FAV with interface liquid shows deeper layers (**b** and **c**). Dermal papillae hilltops project in the overlying epidermis covered by round cells with light cytoplasm (**b**, the white circle highlights a single papilla) and correlate with horizontal histology (**d**, 400×, hematoxylin and eosin stain). Red arrow indicates the capillary loops in the dermal papillae (**c**)

the red blood cells perfectly. In the periungual site, red blood cells are more visible due to the superficial capillaries. Follicular structures are clearly observed; the hair follicle (Fig. 10.2) appears as a dark circular structure, often filled with keratin and sebaceous material. Around the hair follicles, basal keratinocytes densely disposed circumferentially can be observed.

Superficial skin mycosis: It is possible to see dermatophytes as elongated thin structures (Fig. 10.3). Interface fluid should be used to eliminate images of scaling corneocytes at the skin surface because their contours can mimic fungal hyphae. Hyphae are usually bright, but they can be dark in tinea nigra due to their pigmentation.

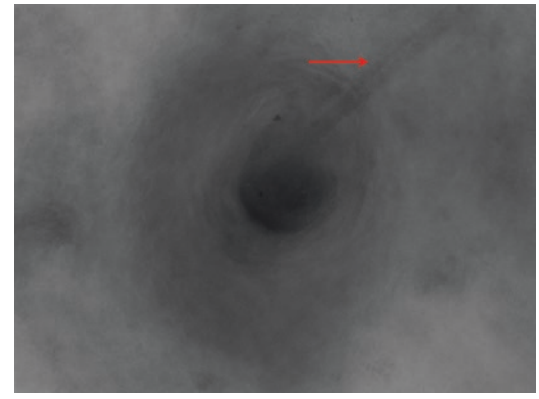

Fig. 10.2 In vivo fluorescence-advanced videodermatoscopy (FAV) image of a hair follicle with a hair shaft (red arrow)

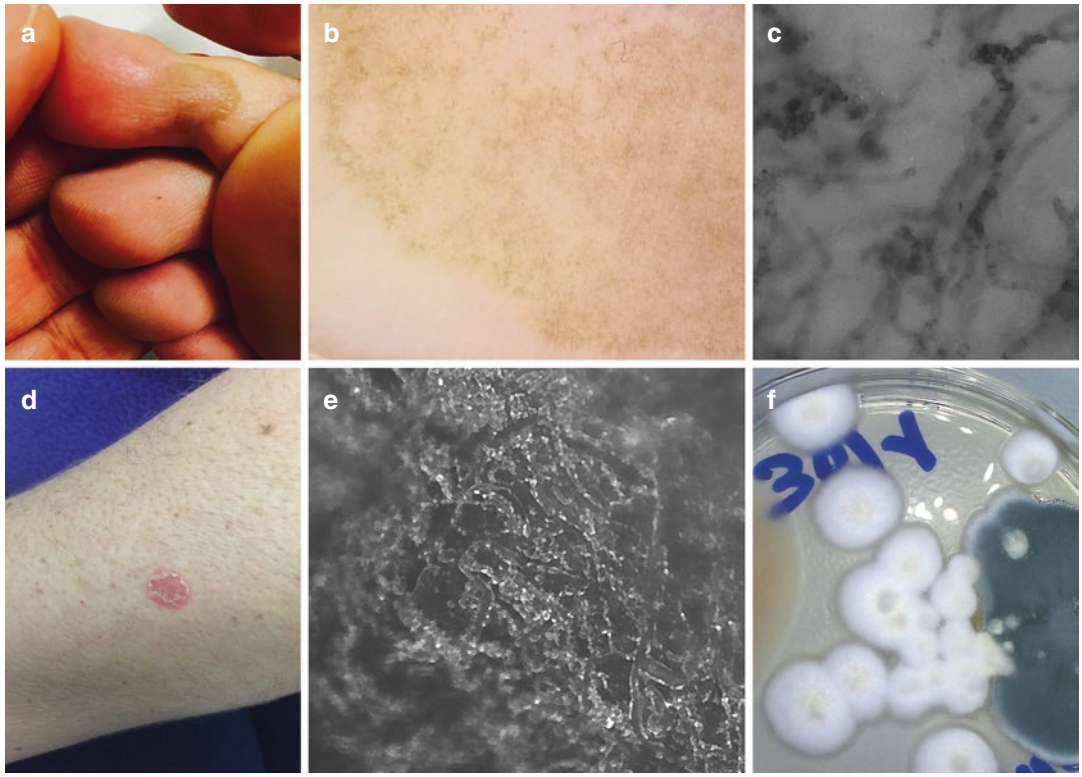

Fig. 10.3 Clinical, dermoscopic, fluorescence-advanced videodermatoscopy (FAV) and microscopic examination of dermatophytosis. Clinical (**a**), dermoscopic (**b**), and FAV (**c**) presentation of a plantar tinea nigra; dermoscopy (**b**) shows uniform brown spicules with a reticular-like pattern, and FAV (**c**) shows the hyphae of *Phaeoannellomyces werneckii*. Clinical (**d**) and FAV (**e**) presentation of a tinea corporis and correlation with the (**f**) fungal culture obtained by scraping the skin lesion; fungal hyphae appear as bright structures under FAV (**e**)

Parasitoses: Main skin parasites can be observed under FAV [4]. The tails of *Demodex folliculorum* mite are visible as bright roundish or elongated structures in the context of the hair follicle (Fig. 10.4). By modulating the penetration depth, it is possible to evaluate the distribution of the mites in the hair follicle; their heads upside down in the deeper part of the follicle and the elongated cone-shaped bodies and tails protruding from the follicle's ostium.

Sarcoptes scabiei hominis can be observed in the different phases of its development, as well as its droppings and eggs (Fig. 10.5). Adult mites appear as ovoid bodies with four pairs of short leg. Their eggs can be identified as ovoid structures with a darker thin wall. *Larva migrans* can be seen in its tunnel as an oval structure with a highly bright edge.

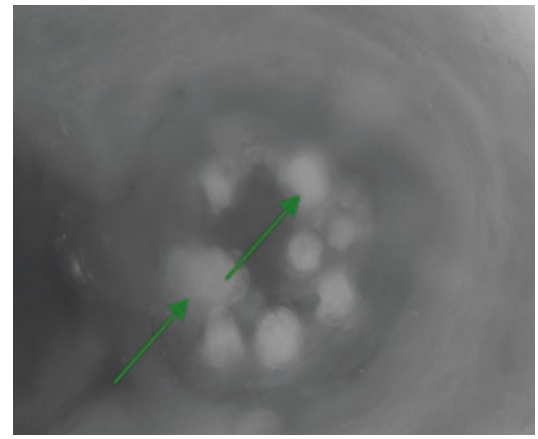

Fig. 10.4 Fluorescence-advanced videodermatoscopy images of *Demodex* mites occupying a hair follicle: green arrows in the figure indicate the mites observed from above which protrude from the follicle ostium

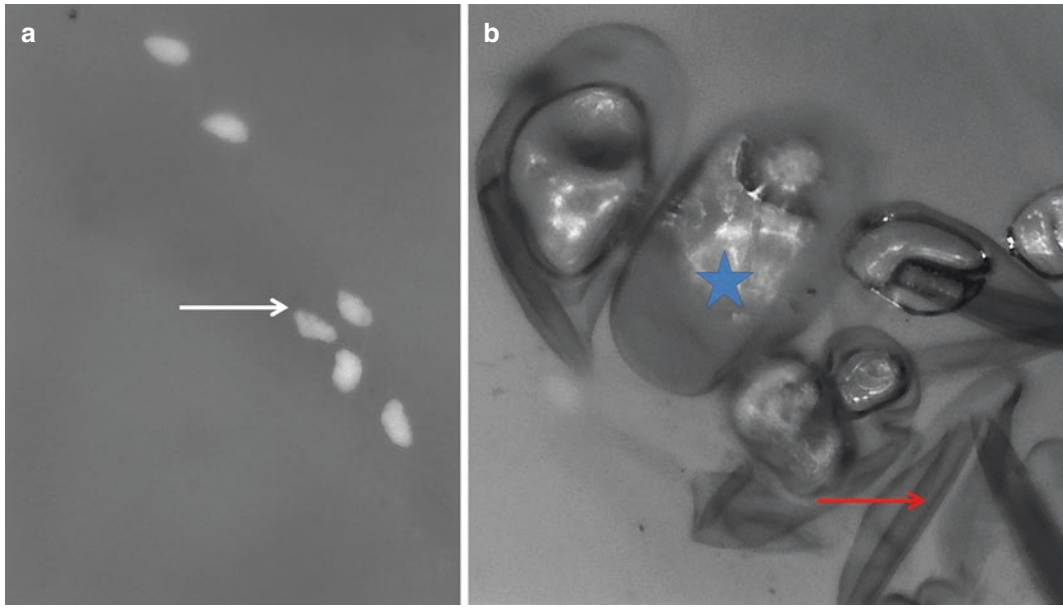

Fig. 10.5 Fluorescence-advanced videodermatoscopy images of scabies. Mite's droppings (**a**), mite's eggs ((**b**) blue star, ovoid structures with a thin black outline), and envelopes of the hatched eggs (red arrow) along the burrow are visible

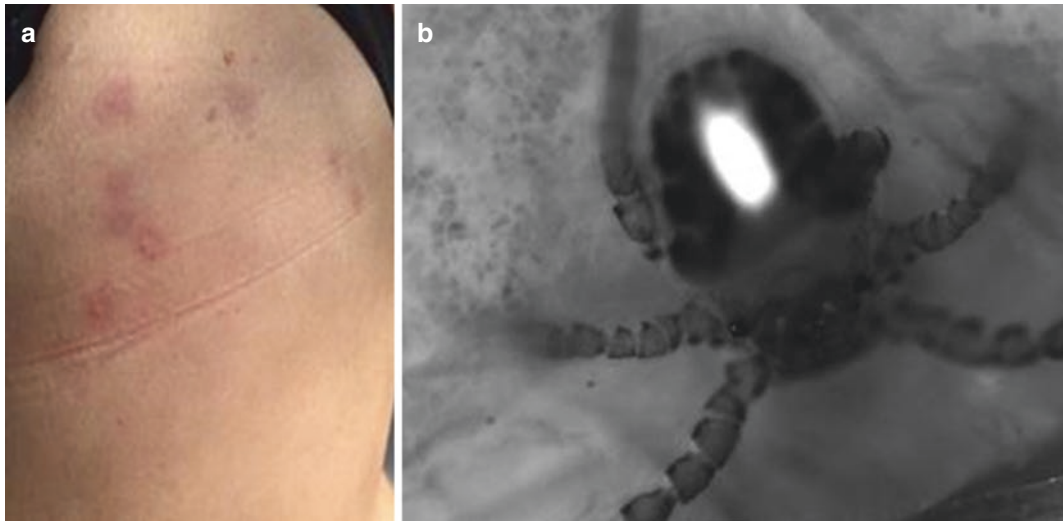

Fig. 10.6 Clinical (**a**) image of an entomodermatitis caused by *Trombicula autumnalis* and fluorescence-advanced videodermatoscopy (FAV, **b**) image of the insect. FAV shows the parasite in its larval form (three pairs of legs)

FAV also allows to identify insects moving on the skin surface. For example, *Trombicula autumnalis* does not excavate tunnels in the skin but attaches to the glabrous skin (Fig. 10.6) and feeds for a period of 2–10 days. At the end of the meal, it leaves the skin and returns to the ground where it develops in nymphs (four pairs of legs) in 5–6 weeks. In the autumn period, it is responsible for the trombiculosis affecting numerous mammals including humans.

Skin tumors: FAV can help to identify the increased vascularization of malignant skin tumors such as basal cell carcinoma (Fig. 10.7), squamous cell carcinoma (SCC), and melanoma.

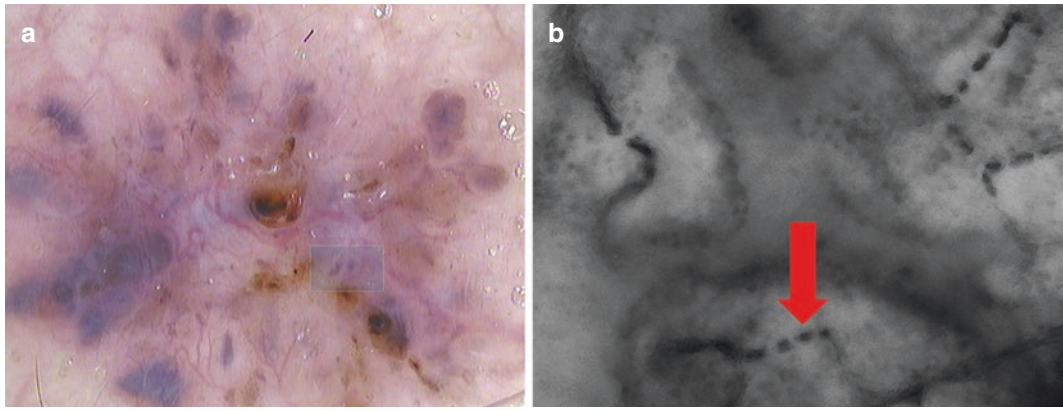

Fig. 10.7 Dermoscopic (**a**, 30×) and fluorescence-advanced videodermatoscopy (FAV, **b**) images of a basal cell carcinoma. Capillaries visible in dermoscopy (**a**, white rectangle) are better seen under FAV as elongated dark structures formed by single red blood cells (**b**, red arrow)

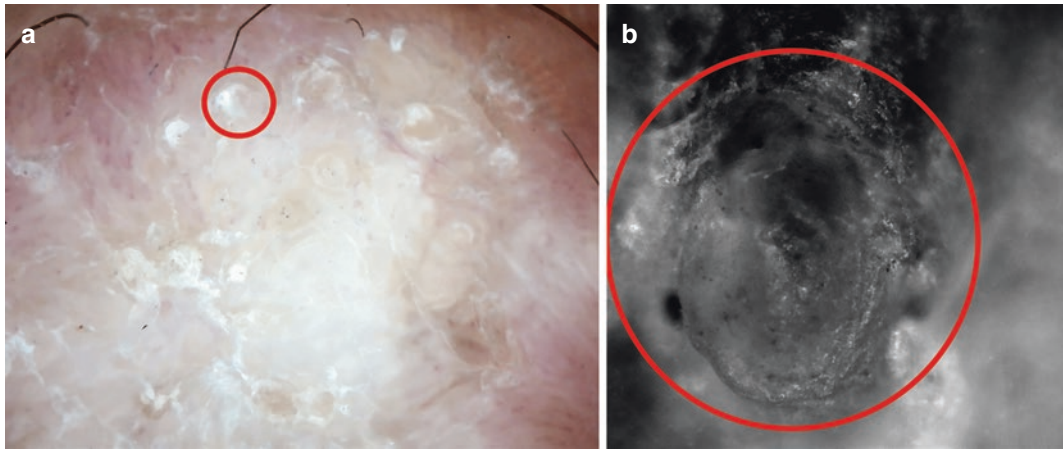

Fig. 10.8 Dermoscopic (**a**, 30×) and fluorescence-advanced videodermatoscopy (FAV, **b**) images of a squamous cell carcinoma. White circles (red circles) visible in dermoscopy (**a**) are better seen under FAV (**b**) as keratotic concentric structures

In benign vascular tumors, such as capillary angiomas, the red blood cells have a slow flow and accumulate in dilated tortuous spaces, separated by bright lines corresponding to the collagen bundles. In keratinizing tumors such as SCC, FAV highlights the keratotic component (Fig. 10.8). Malignant melanocytes can be observed as roundish dark cells heterogeneous in pigmentation, shape, and size (Figs. 10.9 and 10.10). Since the provided images correspond to a small FOV, the videodermoscope coupled with FAV can be used to target the areas of interest (Fig. 10.11) The main limitation of FAV for the diagnosis of skin tumors is that only pigmented cells are visible, and therefore, single cells of SCC and basal cell carcinoma are not visible when not pigmented, and it is possible that malignant melanocytes are only partially seen.

Other applications: FAV could be useful for the diagnosis and follow-up of many skin diseases. Since the vascularization is well visible, all inflammatory diseases should be explored in future studies (Fig. 10.12). Moreover, FAV can be used to enhance videocapillaroscopy.

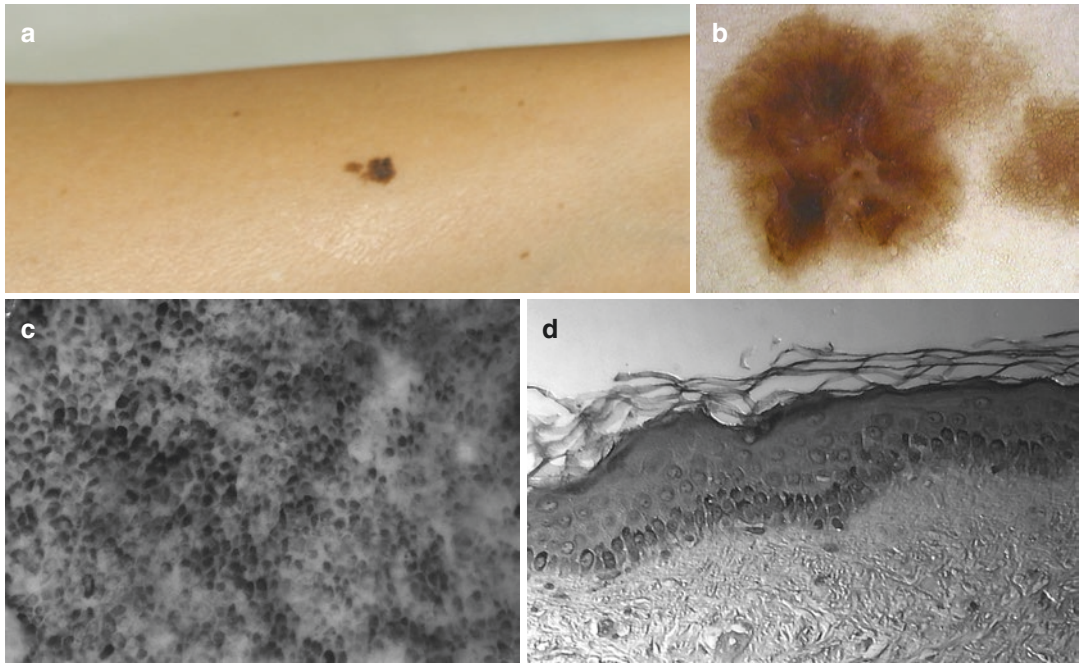

Fig. 10.9 Clinical (**a**), dermoscopic (**b**), fluorescence-advanced videodermatoscopy (FAV, **c**), and histological (**d**) images of a melanoma in situ. Malignant melanocytes can be observed as roundish dark cells heterogeneous in pigmentation, slighlty irregular in shape and size in both examinations. Histology is showed in grayscale to better observe the correlation with FAV

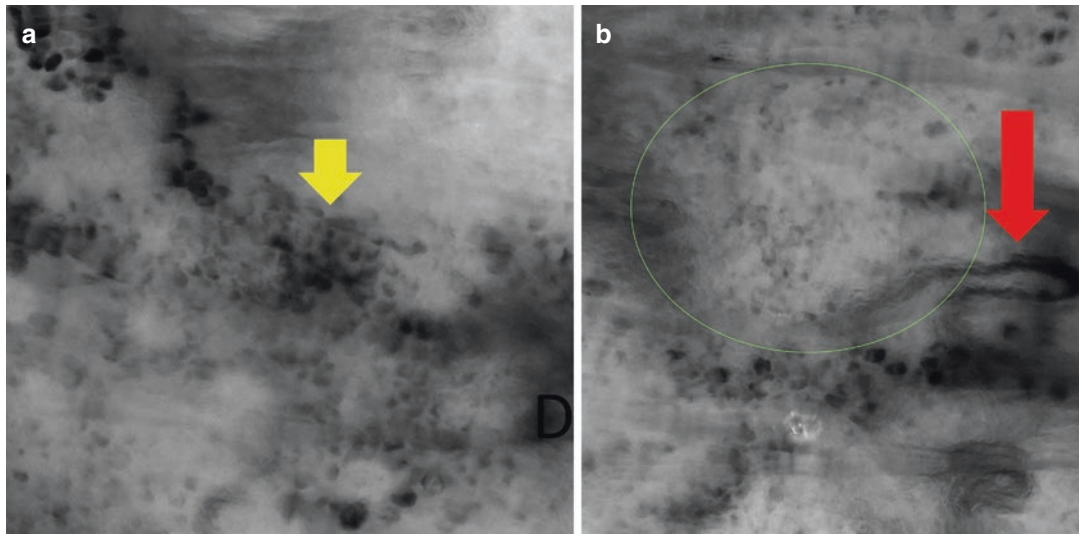

Fig. 10.10 Fluorescence-advanced videodermatoscopy (FAV) of a superficial spreading melanoma (**a**–**d**). Malignant melanocytes can be observed as roundish dark cells that could be more (yellow arrow) or less (green circle) pigmented. Green circle indicates areas of regression up to a total disappearance of melanocytes (blue star). Neovascularization is marked by a red arrow

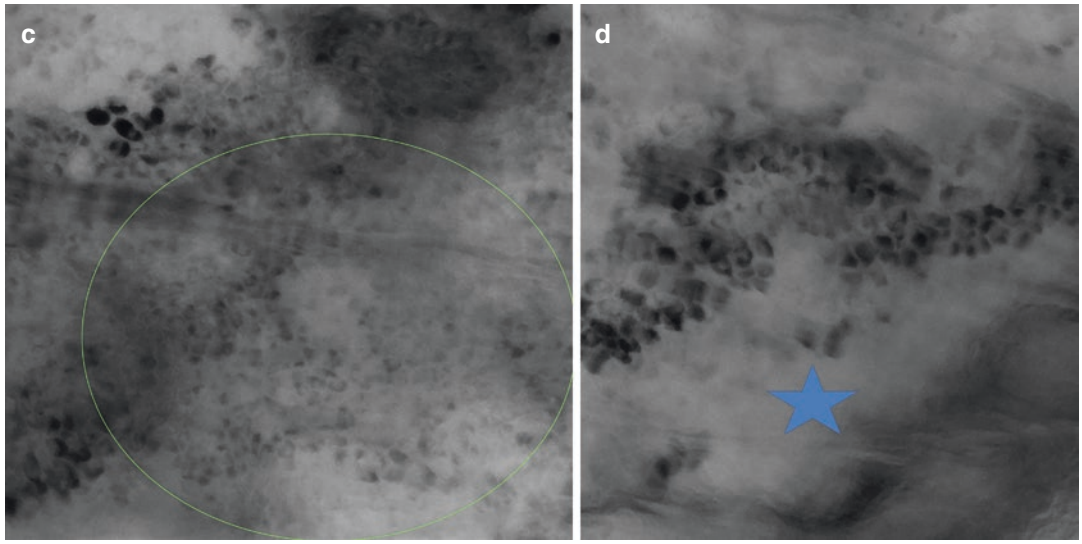

Fig. 10.10 (continued)

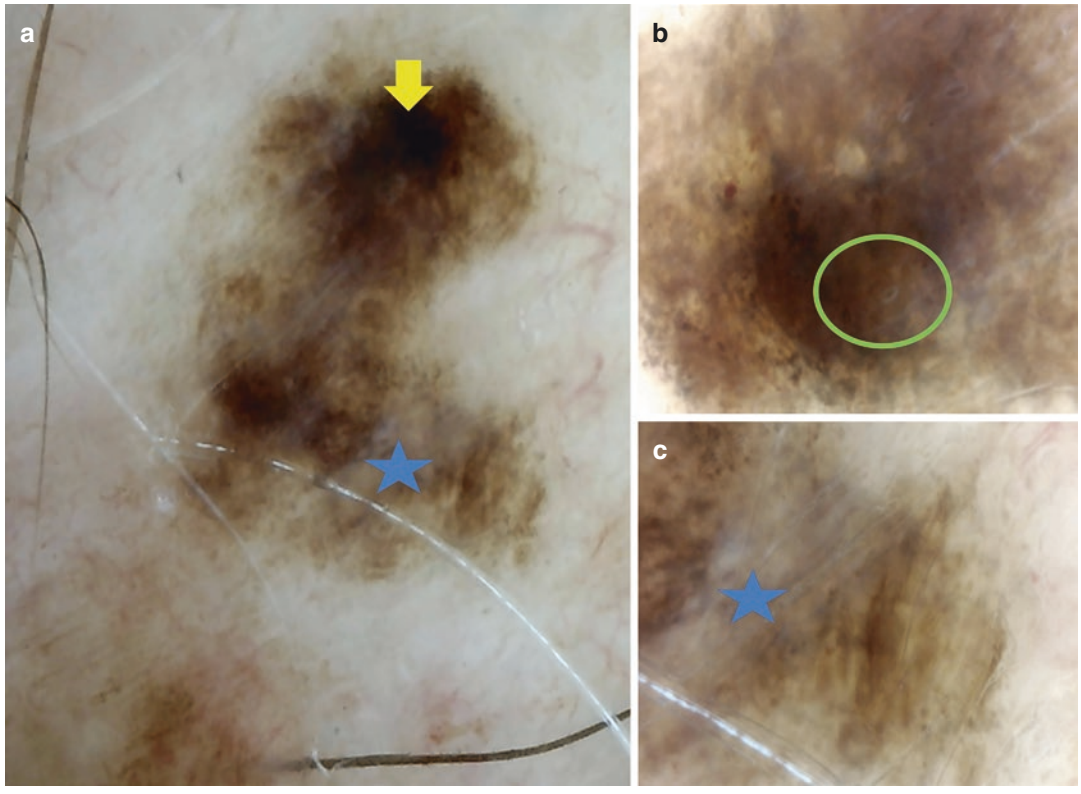

Fig. 10.11 Dermoscopy at 30× (**a**) and 150× (**b**, **c**) magnifications of the previous melanoma shows dark blotches (yellow arrow), less-pigmented areas (green circle), and areas of regression (blue star)

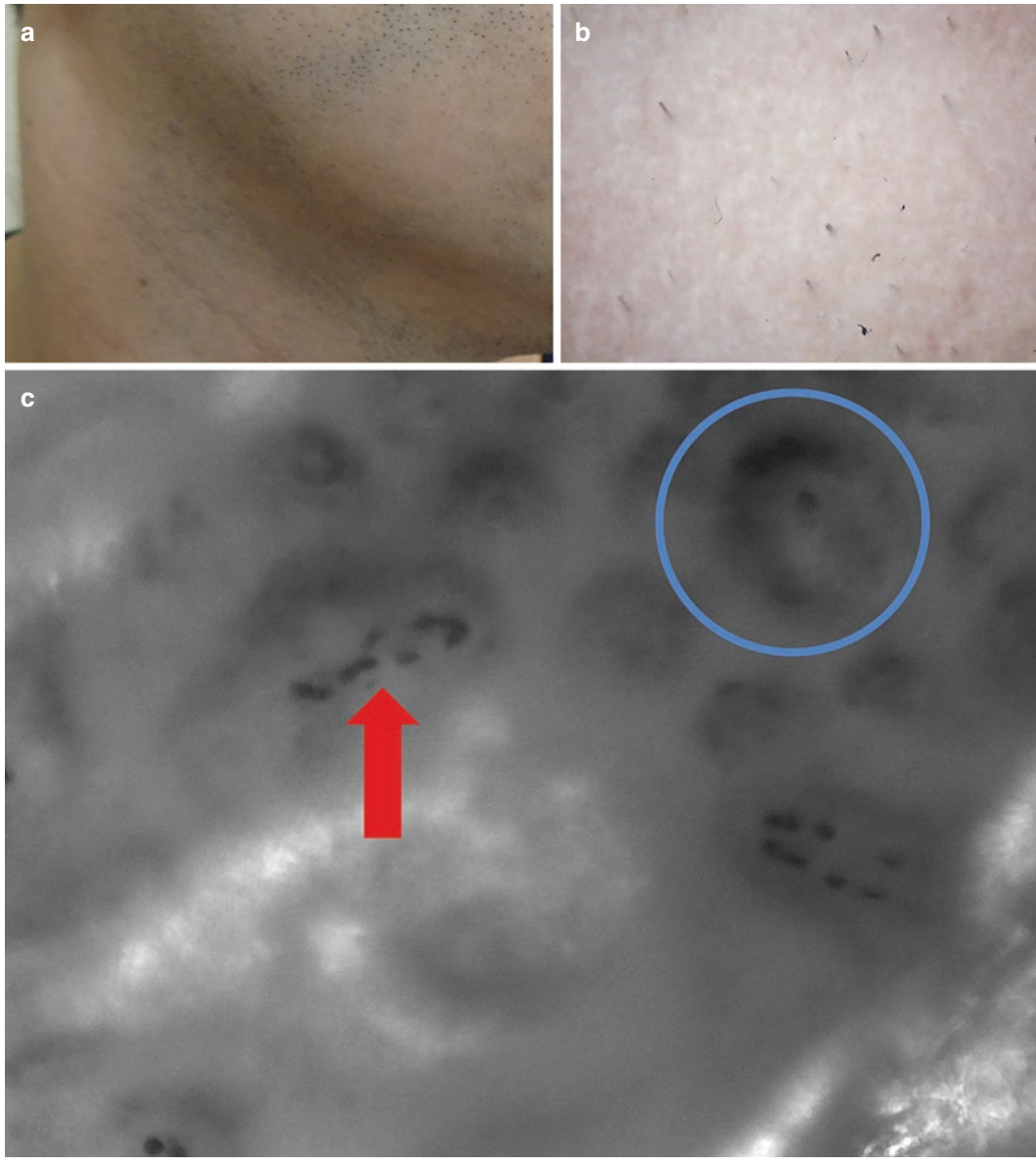

Fig. 10.12 Clinical (**a**), dermoscopy at 30× (**b**), and fluorescence-advanced videodermatoscopy (FAV, **c**) of alopecia areata of the beard. FAV shows hairpin capillaries (red arrow) inside the dermal papillae (blue circle)

References

1. Cinotti E, Rubegni P. Dermoscopy is looking for a technical evolution to improve its diagnostic potential. Br J Dermatol. 2018;179(2):255–6.
2. Spigulis J. Multispectral, fluorescent and photoplethysmographic imaging for remote skin assessment. Sensors. 2017:17(5).
3. Forschner A, Keim U, Hofmann M, Spänkuch I, Lomberg D, Weide B, Tampouri I, Eigentler T, Fink C, Garbe C, Haenssle HA. Diagnostic accuracy of dermatofluoroscopy in cutaneous melanoma detection: results of a prospective multicentre clinical study in 476 pigmented lesions. Br J Dermatol. 2018;179(2):478–85.
4. Sanlorenzo M, et al. Fluorescence-advanced videodermatoscopy: a new method for in vivo skin evaluation. Br J Dermatol. 2017;177(5):e209–10.

11 Total Body Photography and Sequential Digital Dermoscopy for Melanoma Diagnosis

Maria Antonietta Pizzichetta
and Ignazio Stanganelli

11.1 Introduction

Dermoscopy is a noninvasive technique that increases the accuracy and improves the sensitivity and specificity of a melanoma diagnosis compared to clinical diagnosis by the naked eye [1]. Several dermoscopic features have been identified, and algorithms have been developed to distinguish melanocytic from non-melanocytic proliferations on the basis of structural, chromatic, and vascular patterns. However, this method has low sensitivity for some early melanomas, called "featureless melanomas," which lack the specific surface characteristics on which a diagnosis can be made [2, 3]. In addition, this method is not able to differentiate between some melanomas and atypical nevi. Moreover, dermoscopic criteria have not been standardized, and some have poor to fair interobserver agreement [4].

M. A. Pizzichetta (✉)
Dermatologic Clinic, University of Trieste, Trieste, Italy

Department of Medical Oncology, Centro di Riferimento Oncologico di Aviano (CRO) IRCCS, Aviano, Italy
e-mail: pizzichetta@cro.it

I. Stanganelli
Skin Cancer Unit, IRCCS Istituto Scientifico Romagnolo per la Cura e lo Studio dei Tumori, Meldola, Italy

Department of Dermatology, University of Parma, Parma, Italy

The diagnosis of melanoma requires an examination of the entire skin surface and clinical information such as age, skin type, personal or family history of melanoma, number of lesions, time of onset, and changes of the lesions [3]. The changes in a lesion, documented over time by medical history or dermoscopy, provide important information for the identification of early and featureless melanomas [5, 6]. Two main techniques for melanoma monitoring are total body photography and sequential digital dermoscopy of individual lesions [6, 7]. This chapter discusses these two methods plus their combination and integration with reflectance confocal microscopy.

11.2 Total Body Photography

In total body photography (TBP), a patient's whole skin surface is clinically photographed. At the first examination, 12–24 baseline photographs are taken to allow comparison at subsequent examinations over the years, to detect new lesions and changes in preexisting lesions (Fig. 11.1). Therefore, TBP allows the identification of both de novo melanomas and melanomas arising in association with a nevus, presenting as a change in a preexisting lesion. TBP has been reported to help in the early diagnosis of non-melanoma skin cancers and of new, subtly changing melanomas that did not have classic

M. Fimiani et al. (eds.), *Technology in Practical Dermatology*,
https://doi.org/10.1007/978-3-030-45351-0_11

Fig. 11.1 Long-term monitoring with total body photography. *Left*, baseline image shows multiple atypical nevi on the back of a young woman, and one melanoma (red circle) that was subsequently excised. *Right*, after 8 years, total body photography revealed new lesions, changes in preexisting lesions, and a de novo melanoma (red circle) arising on normal skin

"ABCD" features [8]. TBP also helped in the early detection of melanomas in a single-center cohort of high-risk patients with many nevi, including atypical ones, and a personal or family history of melanoma [9]. In these patients, the incidence of new and changed nevi reduced with increasing age, but the number of melanomas increased [9]. Furthermore, TBP has been reported to increase the sensitivity and specificity of melanoma detection, resulting in a 3.8-fold reduction in excisions of benign melanocytic lesions [10].

11.3 Sequential Digital Dermoscopy

With sequential digital dermoscopy (SDD), dermoscopic images of an individual melanocytic lesion are taken periodically over a period of time and saved electronically, to facilitate the evaluation of changes. SDD is useful for monitoring flat (i.e., not palpable), atypical melanocytic lesions that lack the clinical or dermoscopic features of melanoma at baseline but may undergo subtle changes in dimension, color, or structure over time. SDD is also useful for examining difficult-to-diagnose melanomas that look like atypical nevi at baseline, and it helps avoid unnecessary excisions [11, 12]. While benign nevi tend not to change over time, melanoma do change, and this permits their identification with SDD. This method should be avoided, however, in cases of atypical papular or nodular lesions, because with a delayed assessment it is impossible to exclude the diagnosis of a fast-growing nodular melanoma [13]. SDD is usually performed following one of two schedules: short-term and long-term monitoring.

Short-term monitoring of skin lesions, with an interval of 3 months, is used when there are a few stable, atypical lesions or unstable, mildly atypical lesions without evidence of melanoma. Any changes during short-term monitoring lead to

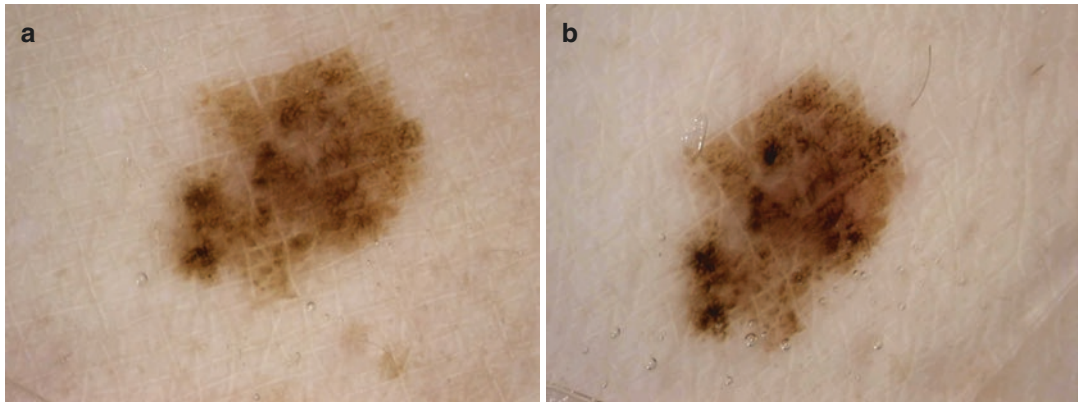

Fig. 11.2 Short-term dermoscopic monitoring of an atypical melanocytic lesion with multifocal hypo- and hyperpigmentation found on the leg of a female patient. (**a**) Baseline image. (**b**) At 3 months, dermoscopy revealed changes in color and structure, and the appearance of brown and black dots distributed irregularly. The histologic diagnosis was melanoma in situ

surgical excision and histological examination (Fig. 11.2). Short-term monitoring has been shown to be useful in diagnosing featureless melanomas, and in one observational trial, it was able to detect 34% of 53 melanomas [14]. The sensitivity and specificity for a melanoma diagnosis using SDD in another study were 94% and 84%, respectively [15]. When lentigo maligna is in the differential diagnosis, monitoring should be done again after an additional 3-month interval (for a total of 6 months).

Short-term monitoring may also be used as the first stage of long-term monitoring. In persons with multiple atypical nevi at high risk of melanoma, long-term monitoring permits the surveillance of more lesions after an interval of 6–12 months [11]. The exact follow-up schedule for each patient depends on the number of nevi, the degree of clinical atypia, and the existence (or not) of a personal or family history of melanoma. A high specificity (95–96%) for the diagnosis of melanoma was found in one study that used long-term monitoring over 4 years [14, 16].

Changes during long-term monitoring that lead to excision include asymmetrical modifications in color or structure, focal changes in color or structure, and the appearance of melanoma-specific features such as blue-white veil, atypical or negative pigment network, atypical vascular patterns, irregular dots and globules, streaks, irregular blotches, peripheral pigmented structureless areas, and regression (Fig. 11.3) [17, 18]. In one multicenter study of 92 melanomas that were followed by SDD for at least 1 year, the proportion of lesions that were negative for all diagnostic criteria for melanoma decreased from 62% at 1.5 months to 45% at 4.5 months and 35% at 8 months [18]. However, subtle changes visible only on side-by-side comparisons of dermoscopic images were mainly structural (focal increase of pigment network irregularity and regression).

According to two studies of persons at high risk for melanoma, SDD with short- and long-term monitoring was able to detect 18 of the 53 melanomas [14] or 39% [19] of all melanomas. In a retrospective analysis of routine dermatologic practice, the changes observed with SDD allowed the diagnosis of 12 of 99 melanomas [20]. In addition, SDD has been shown to reduce the ratio of benign moles excised for each melanoma diagnosed [19, 21], thereby reducing the number needed to treat.

According to a meta-analysis [11], in high-risk patients with multiple nevi, SDD examination of melanocytic lesions allowed the diagnosis of a higher number of in situ and microinvasive melanomas and required fewer unnecessary excisions than that expected during clinical–dermoscopic follow-up alone. However, this meta-analysis found low agreement among different studies regarding inclusion criteria (clini-

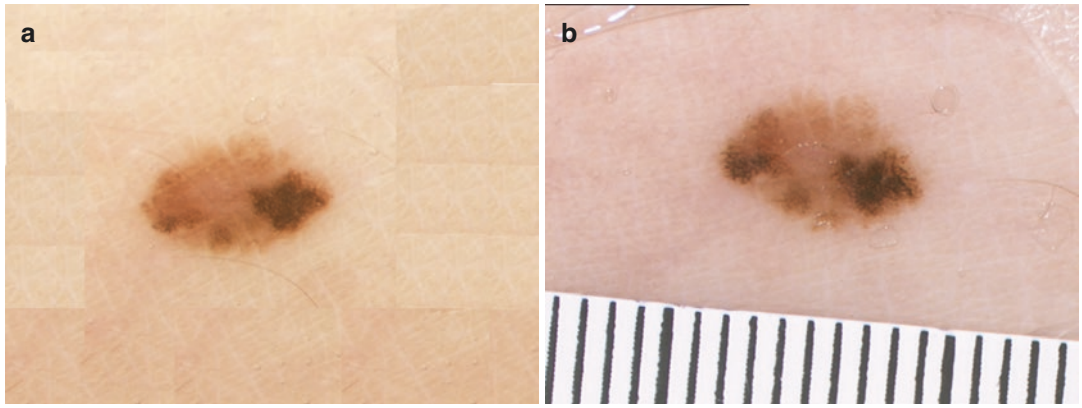

Fig. 11.3 Long-term dermoscopic monitoring of an atypical melanocytic lesion with eccentric hyperpigmentation. (**a**) At baseline, the lesion has eccentric hyperpigmentation, with some parts darker than others. (**b**) At 24 months, dermoscopy showed that the lesion had enlarged, the eccentric hyperpigmentation had expanded, and there were irregular blotches and color and structural changes in the pigment network. The histological diagnosis was melanocytic nevus associated with melanoma in situ

cal features, and clinical and dermoscopic criteria), dermoscopic evaluation methods, diagnostic parameters, and patient risk factors [11].

11.4 Choosing between TBP and SDD

TBP and SDD should be used in different situations. TBP is indicated for very high-risk people who have many nevi and multiple dysplastic nevi. Moreover, TBP is supportive for patients doing self-examinations, because it helps them distinguish between changing and stable lesions [22]. SDD is best for monitoring flat lesions lacking clinical or dermoscopic features of melanoma. SDD has many advantages, but it also has an equal number of disadvantages (Box 11.1). In particular, numerous instruments are available for SDD, but no formal technological assessment has been made nor has a set of minimal requirements been established [23, 24].

Using TBP and SDD together provides optimal surveillance in high-risk cases. One study reported that melanomas diagnosed by TBP and SDD were thinner than those found by clinical and dermoscopic evaluation alone [7]. Another study reported that these strategies together were less expensive and more effective than standard diagnoses [25]. Finally, the combined use of these techniques allowed the early detection of melanomas with few excisions of benign lesions in a high-risk cohort [25].

11.5 Confocal Microscopy

With reflectance confocal microscopy (RCM), dermatologists can perform a noninvasive, optical digital biopsy. RCM reveals the cytologic and architectural morphology of the superficial layers of skin tissue, at nearly the histopathological level. It increases the diagnostic confidence and reduces unnecessary excisions [26]. In the examination of flat lesions, melanoma can be suspected when RCM shows an irregular epidermis with widespread or localized bright, roundish, or dendritic cells, a disarranged dermal–epidermal junction with non-edge papillae and atypical bright cells; homogeneous dense or sparse nests associated with punctate or plump bright cells in the superficial dermis may also be detected. On the contrary, the detection of a ringed pattern and edged papillae are typical of junctional or compound nevi. In addition, the presence of a meshwork pattern or clod pattern throughout the lesion, without atypical cytologic or structural features, is indicative of melanocytic nevi [27, 28].

The combination of digital dermoscopy with RCM is useful for equivocal lesions and lesions

that change during SDD. RCM is especially useful for examining slow-growing melanomas with subtle chromatic and structural changes, with no change or minimal (≤2 mm) change in size [18, 29]. A recent report suggested that the number needed to treat (i.e., number of excised lesions needed to find one melanoma) can be reduced by 50% by combining RCM with SDD [29].

11.6 Conclusions

The combination of clinical and instrumental diagnostic methods is crucial for a correct diagnosis of suspicious melanocytic lesions, especially in high-risk persons with multiple melanocytic nevi. SDD alone or combined with TBP is recommended for the monitoring and management of flat atypical melanocytic nevi that are difficult to differentiate from melanoma. Short- and long-term monitoring procedures are recommended on the basis of meta-analyses and longitudinal studies. RCM can add information about cytological and architectural features to help distinguish melanocytic nevi and melanoma. New technologies such as three-dimensional total body mapping and computerized mole tracking using artificial intelligence are the promises of the future.

Box 11.1 Advantages and limitations of skin surveillance using digital dermoscopy

Advantages

1. Identification of dermoscopic parameters in featureless melanomas and detection of melanomas at an early stage
2. Identification of small-diameter melanomas
3. Evaluation of atypical chromatic and structural changes
4. High sensitivity in melanoma detection
5. Low number of unneeded biopsies
6. Good patient compliance with short-term monitoring
7. Beneficial approach in high-risk patients
8. Better patient performance in skin self-examinations
9. Simple communication between patient and clinician
10. Combination with total body photography
11. Combination with confocal laser microscopy

Limitations

1. Time consuming (30–60 min per examination).
2. Low patient compliance with long-term monitoring.
3. Variability in the scheduling of appointments for long-term monitoring.
4. Inhomogeneous patient risks.
5. Different qualitative and quantitative criteria for selecting lesions (subjective parameters).
6. Numerous instruments are commercially available, but standardized technical requirements are lacking.
7. Dermoscopy results vary depending on the operator's technique and the computer hardware and software used to visualize the images.
8. Slow-growing melanomas can undergo subtle and inconspicuous changes over time, requiring multiple follow-up examinations.
9. Risk not removing a suspicious lesion at the first examination.
10. High level of clinical expertise required.
11. High cost, low benefit for low-risk patients.

Acknowledgments Valerie Matarese provided scientific editing.

References

1. Vestergaard ME, Macaskill P, Holt PE, et al. Dermoscopy compared with naked eye examination for the diagnosis of primary melanoma: a meta-analysis of studies performed in a clinical setting. Br J Dermatol. 2008;159(3):669–76.
2. Menzies SW, Ingvar C, Crotty KA, McCarthy WH. Frequency and morphologic characteristics of

invasive melanomas lacking specific surface microscopic features. Arch Dermatol. 1996;132:1178–82.
3. Pizzichetta MA, Stanganelli I, Bono R, et al. Dermoscopic features of difficult melanoma. Dermatol Surg. 2007;33:91–9.
4. Carrera C, Marchetti MA, Dusza SW, et al. Validity and reliability of dermoscopic criteria used to differentiate nevi from melanoma: a web-based international Dermoscopy Society Study. JAMA Dermatol. 2016;152(7):798–806.
5. Skvara H, Teban L, Fiebiger M, et al. Limitations of dermoscopy in the recognition of melanoma. Arch Dermatol. 2005;141:155–60.
6. Malvehy J, Puig S. Follow-up of melanocytic skin lesions with digital total-body photography and digital dermoscopy: a two-step method. Clin Dermatol. 2002;20:297–304.
7. Salerni G, Carrera C, Lovatto L, et al. Benefit of total body photography and digital dermatoscopy ("two-step method of digital follow-up") in the early diagnosis of melanoma in patients at high risk for melanoma. J Am Acad Dermatol. 2012;67(1):e17–27.
8. Feit NE, Dusza SW, Marghoob AA. Melanomas detected with the aid of total cutaneous photography. Br J Dermatol. 2004;150:706–14.
9. Banky JP, Kelly JW, English DR, et al. Incidence of new and changed nevi and melanomas detected using baseline images and dermoscopy in patients at high risk for melanoma. Arch Dermatol. 2005;141:998–1006.
10. Truong A, Strazzulla L, March J, et al. Reduction in nevus biopsies in patients monitored by total body photography. J Am Acad Dermatol. 2016;75:135–43.
11. Salerni G, Terán T, Puig S, et al. Meta-analysis of digital dermoscopy follow-up of melanocytic skin lesions: a study on behalf of the International Dermoscopy Society. J Eur Acad Dermatol Venereol. 2013;27(7):805–14.
12. Argenziano G, Mordente I, Ferrara G, et al. Dermoscopic monitoring of melanocytic skin lesions: clinical outcome and patient compliance vary according to follow-up protocols. Br J Dermatol. 2008;159:331–6.
13. Bowling J, Argenziano G, Azenha A, et al. Dermoscopy key points: recommendations from the International Dermoscopy Society. Dermatology. 2007;214:3–5.
14. Haenssle HA, Krueger U, Vente C, et al. Results from an observational trial: digital epiluminescence microscopy follow-up of atypical nevi increases the sensitivity and the chance of success of conventional dermoscopy in detecting melanoma. J Invest Dermatol. 2006;126(5):980–5.
15. Altamura D, Avramidis M, Menzies SW. Assessment of the optimal interval for and sensitivity of short-term sequential digital dermoscopy monitoring for the diagnosis of melanoma. Arch Dermatol. 2008;144(4):502–6.
16. Robinson JK, Nickoloff BJ. Digital epiluminescence microscopy monitoring of high-risk patients. Arch Dermatol. 2004;140(1):49–56.
17. Kittler H, Guitera P, Riedl E, et al. Identification of clinically featureless incipient melanoma using sequential dermoscopy imaging. Arch Dermatol. 2006;142:1113–9.
18. Terushkin V, Dusza SW, Scope A, et al. Changes observed in slow-growing melanomas during long-term dermoscopic monitoring. Br J Dermatol. 2012;166(6):1213–20.
19. Moloney FJ, Guitera P, Coates E, et al. Detection of primary melanoma in individuals at extreme high risk: a prospective 5-year follow-up study. JAMA Dermatol. 2014;150(8):819–27.
20. Salerni G, Teran R, Alonso C, et al. The role of dermoscopy and digital dermoscopy follow-up in the clinical diagnosis of melanoma: clinical and dermoscopic features of 99 consecutive primary melanomas. Dermatol Pract Concept. 2014;4(4):39–46.
21. Tromme I, Sacrè L, Hammouch F, et al. Availability of digital dermoscopy in daily practice dramatically reduces the number of excised melanocytic lesions: results from an observational study. Br J Dermatol. 2012;167:778–86.
22. Secker LJ, Bergaman W, Kukutsch NA. Total body photography as an aid to skin self-examination: a patient's perspective. Acta Derm Venereol. 2016;96(2):186–90.
23. Pagliarello C, Stanganelli I, Fabrizi G, Feliciani C, Di Nuzzo S. Digital dermoscopy monitoring: is it time to define a quality standard? Acta Derm Venereol. 2017;97(7):864–5.
24. Finnane A, Curiel-Lewandrowski C, Wimberley G, et al. International Society of Digital Imaging of the Skin (ISDIS) for the International Skin Imaging Collaboration (ISIC). Proposed technical guidelines for the acquisition of clinical images of skin-related conditions. JAMA Dermatol. 2017;153(5):453–7.
25. Watts CG, Cust AE, Menzies SW, et al. Cost-effectiveness of skin surveillance through a specialized clinic for patients at high risk of melanoma. J Clin Oncol. 2017;35(1):63–71.
26. Pellacani G, Witkowski A, Cesinaro AM, et al. Cost-benefit of reflectance confocal microscopy in the diagnostic performance of melanoma. J Eur Acad Dermatol Venereol. 2016;30(3):413–9.
27. Farnetani F, Scope A, Braun RP, et al. Skin cancer diagnosis with reflectance confocal microscopy: reproducibility of feature recognition and accuracy of diagnosis. JAMA Dermatol. 2015;151(10):1075–80.
28. Pellacani G, De Pace B, Reggiani C, et al. Distinct melanoma types based on reflectance confocal microscopy. Exp Dermatol. 2014;23(6):414–8.
29. Stanganelli I, Longo C, Mazzoni L, et al. Integration of reflectance confocal microscopy in sequential dermoscopy follow-up improves melanoma detection accuracy. Br J Dermatol. 2015;172:65–371.

12 History and Fundamentals of Reflectance Confocal Microscopy

Belén Encabo, Gonzalo Segurado, and Salvador González

12.1 Reflectance Confocal Microscopy: From the Past to the Present

A long time has passed since the first reflectance confocal microscopy (RCM) device was developed in 1955 by Marvin Minsky. The aim of this microscope was to study in vivo the brain tissue without the need of a surgical biopsy to avoid the inconveniences associated with this procedure [1]. A decade later, Petran, Hadravsky and colleagues developed another reflectance microscopy system, using a mercury lamp as light source, which was applied to animals [2]. In 1995, RCM was used for the first time in human skin and the first microscopic skin features were described by Rajadhyaksha and colleagues, initially focusing on melanocytic lesions [3]. The light sources used in these first human-applied devices were lasers of different wavelengths (400–800 nm). In the late 1990s, the Vivascope 1000® (Fig. 12.1a) was the first RCM system commercialized by Lucid Inc. (Rochester, NY, USA) [4]. It used a diode laser with a wavelength of 830 nm, the same as nowadays RCM devices, with an illumination up to 20 mW, physical parameters which do not cause tissue damage, and an imaging area of 1.5 × 1.5 mm with single images of 128 μm × 260 μm [5, 6]. In the year 2000, the Vivascope 1500® was commercialized

Fig. 12.1 Vivascope 1000

B. Encabo (✉)
Skin Cancer Unit, Grupo de Dermatología PJ, Madrid, Spain

G. Segurado
Skin Cancer Unit, Grupo de Dermatología PJ, Madrid, Spain

Dermatology Department, Hospital Ramón y Cajal, Madrid, Spain

S. González
Skin Cancer Unit, Grupo de Dermatología PJ, Madrid, Spain

Medicine and Medical Specialties Department, Alcalá University, Madrid, Spain

M. Fimiani et al. (eds.), *Technology in Practical Dermatology*,
https://doi.org/10.1007/978-3-030-45351-0_12

(Fig. 12.1b). It used the same wavelength as previous Vivascope system (830 nm), 30× magnification and a medium power of 110–240 V. Significant advantages with respect to Vivascope 1000® were the reduction of the size, the increase in the dimensions of the imaging area, with basic images of 500 μm × 500 μm and the ability to create mosaics up to 8 × 8 mm.

Both Vivascope 1000® and 1500®, also called Wide-Probe Confocal Device, are large devices, with one articulated arm, that hampers its use in certain difficult-to-access areas, such as ears, periorbital area and skin folds. For this reason, the Vivascope 3000® (Fig. 12.1c), also called the Hand-Held reflectance confocal microscope, was later developed. It has the main advantage of reaching difficult areas, but is not recommended for melanocytic lesions, such as atypical nevi or to discard melanoma. It captures single basic images of 1000 × 1000 μm, as well as stacks, from the superficial to the deeper layers of the skin, but it is not able to make mosaics, so it does not provide information about the global architecture of the lesion.

The previously explained devices are designed for in vivo assessment, but there has also been developed an ex vivo microscope, called VivaScope 2500®, which is a reflectance and fluorescence device. It is being used mainly for imaging excised tissue as a useful tool in Mohs surgery.

The images provided by Vivascope 1500® and 3000® systems are in a grey scale, making interpretation difficult for non-experienced dermatologists and dermatopathologists, more used to interpreting histological samples in different colours. Additionally, although reflectance contrast can enhance architectural skin features and intracellular components, such as the nucleus or the cytoplasm, it has the limitation that is not able to distinguish organelles and other microstructural cellular components [7, 8]. For this reason, Vivascope 2500® uses several fluorescent dyes for imaging excised tissue, and only a few dyes have been approved for human use (e.g., methylene blue). Acridine orange is a dye which is characterized by bounding to nucleic acid. It is used in excised tissue to enhance the cellular nucleus that appears bright in the obtained images. These dyes may be nonspecific, or they can target a specific cell structure [9].

12.2 Physical and Optical Principles

RCM is able to visualize very thin sections of skin with a near to histology resolution without physical sectioning. This aspect has the great advantage that it can be used as many times as the physician needs without any injury to the patient. As well, it can provide a microscopic diagnosis at patient's bedside, so it is a very efficient technique. Another advantage of real-time RCM when compared to histology is that the physician who performs the clinical and dermoscopical examination also does the microscopical one, so he has more information to make a correct correlation and orientate the diagnosis.

RCM is based on the detection of reflectance differences in the cellular components of skin tissue, which is illuminated in a focal point by the laser source.

The main parts of the confocal microscope are the light source, which is a laser with a wavelength of 830 nm, the condenser and the objective lens (30× water immersion). (Fig. 12.2) [10]. This enables a lateral resolution of 0.1–1 μm and a section thickness of 1–5 μm (Table 12.1). The optical sectioning depends on the pinhole size. With larger pinholes, there will be a loss of optical sectioning with a subsequent reduction in contrast. But closing the pinhole will result in an artefact called speckle noise. This is an interference pattern which has a salt-and-pepper-like appearance. So, difficulty lies in finding the appropriate pinhole size that has an adequate optical sectioning reducing as much as possible the speckle noise [7, 11].

The different refractivity index of the components of skin allows to differentiate them when illuminated. Melanin is the substance with the highest refractivity index ($n = 1.72$), followed by keratin ($n = 1.51$) and collagen ($n = 1.43$) [3, 12]. On the one hand, the more refractive a structure is, the brighter and white-coloured it will be

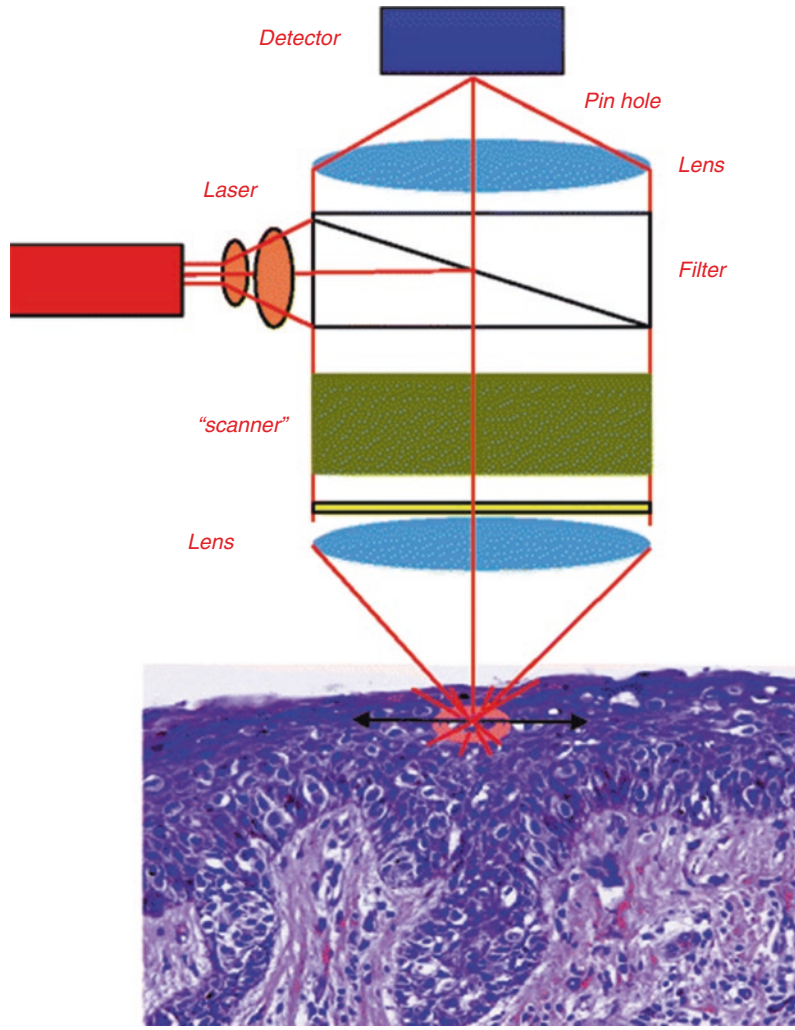

Fig. 12.2 Schematic illustration of a reflectance confocal microscope (reproduced with permission from Springer "Reflectance Confocal Microscopy for Skin Diseases" (eds. Rainer Hofmann-Wellenhof, Giovanni Pellacani, Joseph Malvehy, Hans Peter Soyer). Vivascope 1500)

Table 12.1 Confocal parameters

Wavelength (λ)	830 nm
Maximum imaging depth	150–250 μm at λ = 830 nm
Section thickness	1–5 μm Noninvasive, optical
Lateral resolution	0.1–1 μm
Immersion media	Water or oil
Magnification	40–100×
Field of view	0.5 mm
Contrast mechanism	Endogenous reflective microstructures
Contrast agents/ stains	Melanin Keratin Collagen

Reproduced by permission of Taylor and Francis, a division of Informa plc., ©2008 from *Reflectance Confocal Microscopy of Cutaneous Tumors* by S. González et al.

represented in the image. On the other hand, skin components with lower refractivity, such as water (n = 1.33) or air, are displayed as dark grey or black. Another natural contrast source is the different organelle diameter [7]. The reflected light passes through a pinhole and is collected by a detector, producing a pixel. The point source of the light, the small scanned skin area and the pinhole in front of the detector are in optically conjugated focal planes. This is why this system is named confocal [13].

The resolution of the obtained images is based on one side on the scattering properties of the skin tissue, which is relatively high compared to other human tissues, and on the other side on the wavelength of the light source [14]. It has been demon-

strated that shorter wavelengths scatter more readily than longer ones. So, to reach deeper skin layers, we need longer wavelengths, decreasing resolution. On in vivo RCM, the wavelength of 830 nm allows to visualize with adequate resolution up to a depth of 200–250 μm, which corresponds to the superficial reticular dermis.

12.3 Practical Aspects for Obtaining a High-Quality Image

As it has previously been explained, there are two different devices, Wide-Probe and Hand-Held confocal devices for in vivo RCM. This section will be divided into two different parts, to show how to obtain adequate images with both of them, but several recommendations shared by Wide-Probe and Hand-Held Confocal devices will be given first.

- ***Preparing the patient***

Several aspects need to be considered before taking images: Firstly, cleaning the skin surface of the lesion and the adjacent area with an antiseptic solution like chlorhexidine, to remove materials such as make-up which can be a potential artefact-maker. Another important consideration is that if the lesion is in a hairy area, such as the scalp or extremities, hair must be removed first, since as previously explained, the hair follicles may artefact the examination.

12.3.1 Obtaining Images with Wide-Probe Confocal Device (Fig. 12.3)

- ***Mosaicking = obtaining vivablocks***

Traditional RCM mosaic (or block) is composed of basic images of 500 × 500 μm in an horizontal field of view (x, y), and this allows to examine a lesion up to 8 × 8 mm, which corresponds to 256 basic images [15]. When the patient is correctly prepared, the next step is to put a drop of oil and an adhesive cover slide in contact with the lesion area, followed by taking a dermoscopic picture. Above this slide, a water-

Fig. 12.3 Imaging preparation: Images 1–6 illustrate the most important steps to image acquisition with the VivaScope® 1500 (reproduced with permission from Springer "Reflectance Confocal Microscopy for Skin Diseases" (eds. Rainer Hofmann-Wellenhof, Giovanni Pellacani, Joseph Malvehy, Hans Peter Soyer). Vivascope 3000)

based gel must be poured prior to adapting the microscope head (Fig. 12.3) [16]. This water-based gel (i.e., ultrasound gel) has a similar refractive index to the stratum corneum (n = 1.34), allowing visualization of underlying skin layers.

In order to perform a complete microscopic examination, at least four mosaics must be taken: one of the stratum corneum, one of the spinous layer, one of the dermo–epidermal junction and one of the dermis (Fig. 12.4).

12.3.2 Obtaining Images with Hand-Held Confocal Device

- ***Video-mosaicking***

This device allows dynamic evaluation, so it does not require an adhesive slide, as the dermatologist handles the microscope head enabling whole lesion scanning. It is necessary to pour a drop of oil also in the microscopic head plastic cover. The main inconvenience of this device is that

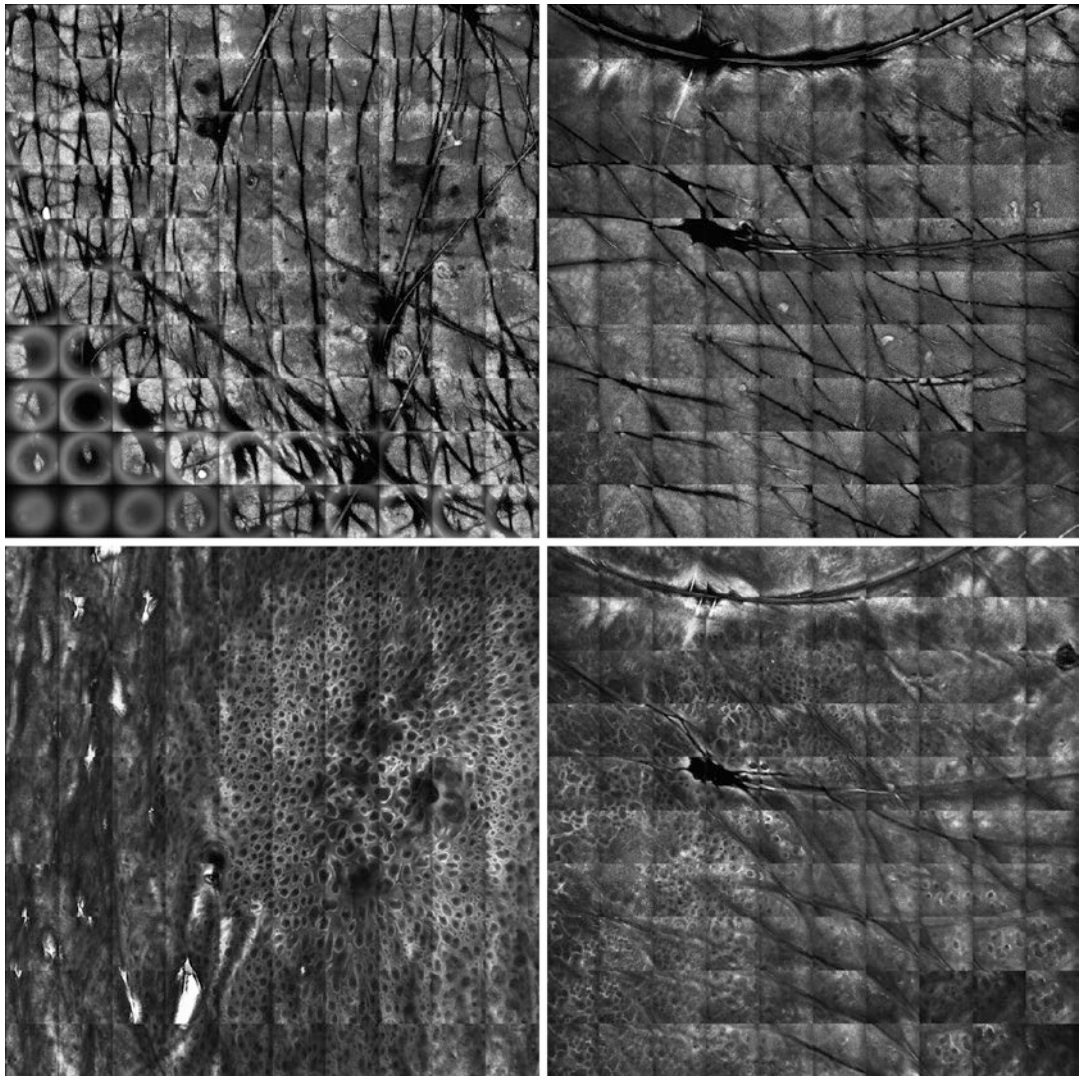

Fig. 12.4 4 layers

it does not allow to obtain mosaics or blocks, so information about the global structure of the lesion is lacking. This is an important limitation when examining melanocytic and pigmented lesions.

This RCM system is based on the capture of basic images of 500 μm × 500 μm, but apart from taking static images it also provides in vivo important information about dynamic events, such as vascularization of the tumour or inflammatory diseases.

- ***Z-stacking***

This mode is common for both the systems. It comprises the examination from the surface to deeper layers (up to 250 μm) of a specific area. It is called Z-stack because it explores the lesion in the "*z*-axis" (Fig. 12.5). This mode complements the mosaics and the basic images to have an adequate complete evaluation.

Fig. 12.5 Vivastack

12.4 Conclusions: Summary and Future in RCM Technique

RCM is a relatively novel diagnostic technique based on the visualization of skin at cellular resolution through different refractive index of skin structures. It consists of a diode laser of 830 nm, harmless for the patient, so it can be used as many times as needed at patient's bedside. This allows its use for patient follow-up of several treatments, as well as for the assessment of skin lesions through telemedicine [17, 18].

There are different RCM devices: Vivascope 1500® and Vivascope 3000® for in vivo examination and Vivascope 2500® for ex vivo evaluation. All of them share the same physical principles which have been described in this chapter, but they have different indications and applications, based on their design and particularities, as it has been explained.

RCM in vivo had a notable evolution, from the first Vivascope 1000® which needed a whole room for it, to nowadays Vivascope 1500® or 3000® that are much more portable and manageable. Nevertheless, new lines of investigation are focused on making this technique more accessible and affordable for general dermatologists, through the design of smaller and cheaper devices [19].

The limited penetration depth is being also under investigation. For this purpose, a combined device based on reflectance confocal microscopy and optical coherence tomography probe (OCT) has been developed [20]. This combined system has the advantage of presenting the near-to-histology resolution of the RCM and the visualization of the lesion in depth through the OCT.

Therefore, it can be concluded that RCM has proved to be a very useful tool for the diagnosis of skin tumours but also for inflammatory lesions. It is considered a useful imaging technique to complement the clinical and dermoscopical examination, as it significantly increases the diagnostic accuracy and confidence of the dermatologist [21]. Although relevant changes have been incorporated to this technique in the last years, it is always under investigation to reduce its limitations and to make it more accessible to general dermatologists.

References

1. Minsky M. Memoir on inventing the confocal scanning microscope. Scanning. 1988;10(4):128–38.
2. Egger MD, Petran M. New reflected-light microscope for viewing unstained brain and ganglion cells. Science. 1967;157(3786):305–7.
3. Rajadhyaksha M, Grossman M, Esterowitz D, Webb RH, Anderson RR. In vivo confocal scanning laser microscopy of human skin: Melanin provides strong contrast. J Invest Dermatol. 1995;104(6):946–52.
4. Larson B, Rajadhyaksha M, Abeytunge S. Fundamentals of reflectance confocal microscopy. In: González S, editor. Reflectance confocal microscopy of cutaneous tumors. 2nd ed. CRC Press; 2017. p. 2–10.
5. Rajadhyaksha M, González S, Zavislan JM, Anderson RR, Webb RH. In vivo confocal scanning laser microscopy of human skin II: Advances in instrumentation and comparison with histology. J Invest Dermatol. 1999;113(3):293–303.
6. Sauermann K, Clemann S, Jaspers S, et al. Age related changes of human skin investigated with histometric measurements by confocal laser scanning microscopy in vivo. Skin Res Technol. 2002;8:52–6.
7. Rajadhyaksha M, Gonzalez S, Zavislan JM. Detectability of contrast agents for confocal reflectance imaging of skin and microcirculation. J Biomed Opt. 2004;9(2):323–31.
8. Tannous Z, Torres A, González S. In vivo real-time confocal reflectance microscopy: a noninvasive guide for Mohs micrographic surgery facilitated by aluminum chloride, an excellent contrast enhancer. Dermatologic Surg. 2003;29(8):839–46.
9. Karen JK, Gareau DS, Dusza SW, Tudisco M, Rajadhyaksha M, Nehal KS. Detection of basal cell carcinomas in Mohs excisions with fluorescence confocal mosaicing microscopy. Br J Dermatol. 2009;160(6):1242–50.
10. Kolm I, Braun RP. How reflectance confocal microscopy works. In: Hofmann-Wellenhof R, Pellacani G, Malvehy J, Peter Soyer H, editors. Reflectance confocal microscopy for skin diseases: Springer-Verlag; 2012. p. 8.
11. Glazowski C. Optimal detection pinhole for lowering speckle noise while maintaining adequate optical sectioning in confocal reflectance microscopes. J Biomed Opt. 2012;17(8):085001.
12. Vitkin IA, Woolsey J, Wilson BC, Anderson RR. Optical and thermal characterization of natural (Sepia officinalis) Melanin. Photochem Photobiol. 1994;59(4):455–62.
13. Gareau DS, Patel YG, Rajadhyaksha M. Basic principles of reflectance confocal microscopy. In: González S, Gill M, Halpern AC, editors. Reflectance confocal miscroscopy of cutaneous tumors. An atlas with clinical, dermoscopic and histological correlations. London: Informa Healthcare; 2008. p. 1–7.

14. Jonasson H, Fredriksson I, Bergstrand S, Östgren CJ, Larsson M, Strömberg T. In vivo characterization of light scattering properties of human skin in the 475- to 850-nm wavelength range in a Swedish cohort. J Biomed Opt. 2018;23(12):1–6.
15. Wurm EMT, Kolm I, Ahlgrimm-Siess V. A hands-on guide to confocal imaging. In: Hofmann-Wellenhof R, Pellacani G, Malvehy J, Soyer HP, editors. Reflectance confocal microscopy for skin diseases. Berlin: Springer; 2012. p. 11–23.
16. Wurm EMT, Kolm I, Ahlgrimm-Siess V. A hands-on guide to confocal imaging. In: Hofmann-Wellenhof R, Pellacani G, Malvehy J, Soyer HP, editors. Reflectance confocal microscopy for skin diseases. Berlin: Springer; 2012. p. 12.
17. Witkowski AM, Łudzik J, Arginelli F, Bassoli S, Benati E, Casari A, et al. Improving diagnostic sensitivity of combined dermoscopy and reflectance confocal microscopy imaging through double reader concordance evaluation in telemedicine settings: a retrospective study of 1000 equivocal cases. PLoS One. 2017;12(11):e0187748.
18. Łudzik J, Witkowski AM, Roterman-Konieczna I, Bassoli S, Farnetani F, Pellacani G. Improving diagnostic accuracy of dermoscopically equivocal pink cutaneous lesions with reflectance confocal microscopy in telemedicine settings: double reader concordance evaluation of 316 cases. PLoS One. 2016;11(9):e0162495.
19. Freeman EE, Semeere A, Osman H, Peterson G, Rajadhyaksha M, González S, et al. Smartphone confocal microscopy for imaging cellular structures in human skin in vivo. Biomed Opt Express. 2018;9(4):1906–15.
20. Sahu A, Yélamos O, Iftimia N, Cordova M, Alessi-Fox C, Gill M, et al. Evaluation of a combined reflectance confocal microscopy-optical coherence tomography device for detection and depth assessment of basal cell carcinoma. JAMA Dermatol. 2018;154(10):1175–83.
21. Edwards SJ, Osei-Assibey G, Patalay R, Wakefield V, Karner C. Diagnostic accuracy of reflectance confocal microscopy using VivaScope for detecting and monitoring skin lesions: a systematic review. Clin Exp Dermatol. 2017;42(3):266–75.

13 In Vivo Reflectance Confocal Microscopy for Benign Melanocytic Skin Tumors

Marco Campoli, Jean Luc Perrot, and Elisa Cinotti

Histopathology is considered the "gold" standard for the diagnosis and classification of melanocytic nevi. However, the widespread use of in vivo diagnostic noninvasive technologies such as dermoscopy and reflectance confocal microscopy (RCM) has improved our knowledge about the melanocytic lesions. Dermoscopy has allowed for a greater clinical diagnostic accuracy of nevi and may also help for their classification. RCM is a novel emerging morphologic technique that allows for noninvasive imaging of the epidermis, the dermo–epidermal junction (DEJ), and the upper dermis at near-histologic resolution [1]. The clinical application of RCM seems to be very promising for the evaluation of melanocytic lesions, owing to the high contrast provided by hyper-reflective melanin and melanosomes [2]. For more than 15 years, RCM features that are useful for the distinction between melanocytic nevi and melanomas (MMs) have been identified and have been correlated with histopathologic features [3–5].

M. Campoli (✉) · E. Cinotti
Department of Medical, Surgical and Neurological Science, Dermatology Section, University of Siena, Siena, Italy

J. L. Perrot
Department of Dermatology, University Hospital of St-Etienne, Saint-Etienne, France
e-mail: j.luc.perrot@chu-st-etienne.fr

13.1 Correlations of Dermoscopic Features with In Vivo Confocal Microscopy and Histopathology

Dermoscopy is the most used noninvasive imaging technique for the clinical diagnosis of melanocytic skin lesions [6–8]. This technique is based on the magnification and identification of some specific structures within the examined lesion. Although some dermoscopic features correspond to histologic findings, a direct and exact correlation is difficult to determine. RCM produces images that are closer to histopathology and is particularly useful for noninvasive differential diagnosis of nevi and MM [3, 9, 10]. Correlations among some dermoscopic features found in nevi such as pigment network, globules, streaks, and blue structures and RCM and histologic aspects have recently been shown [4, 11–13].

13.1.1 Common Nevi

13.1.1.1 Pigment Network

Benign junctional melanocytic nevi (Fig. 13.1a) usually present a typical pigment network under dermoscopy (Fig. 13.1b) and reveal on RCM a ringed pattern (Fig. 13.1c) or a meshwork pattern at the DEJ. Ringed pattern corresponds to well-defined (edged) papillae rimmed by bright

M. Fimiani et al. (eds.), *Technology in Practical Dermatology*,
https://doi.org/10.1007/978-3-030-45351-0_13

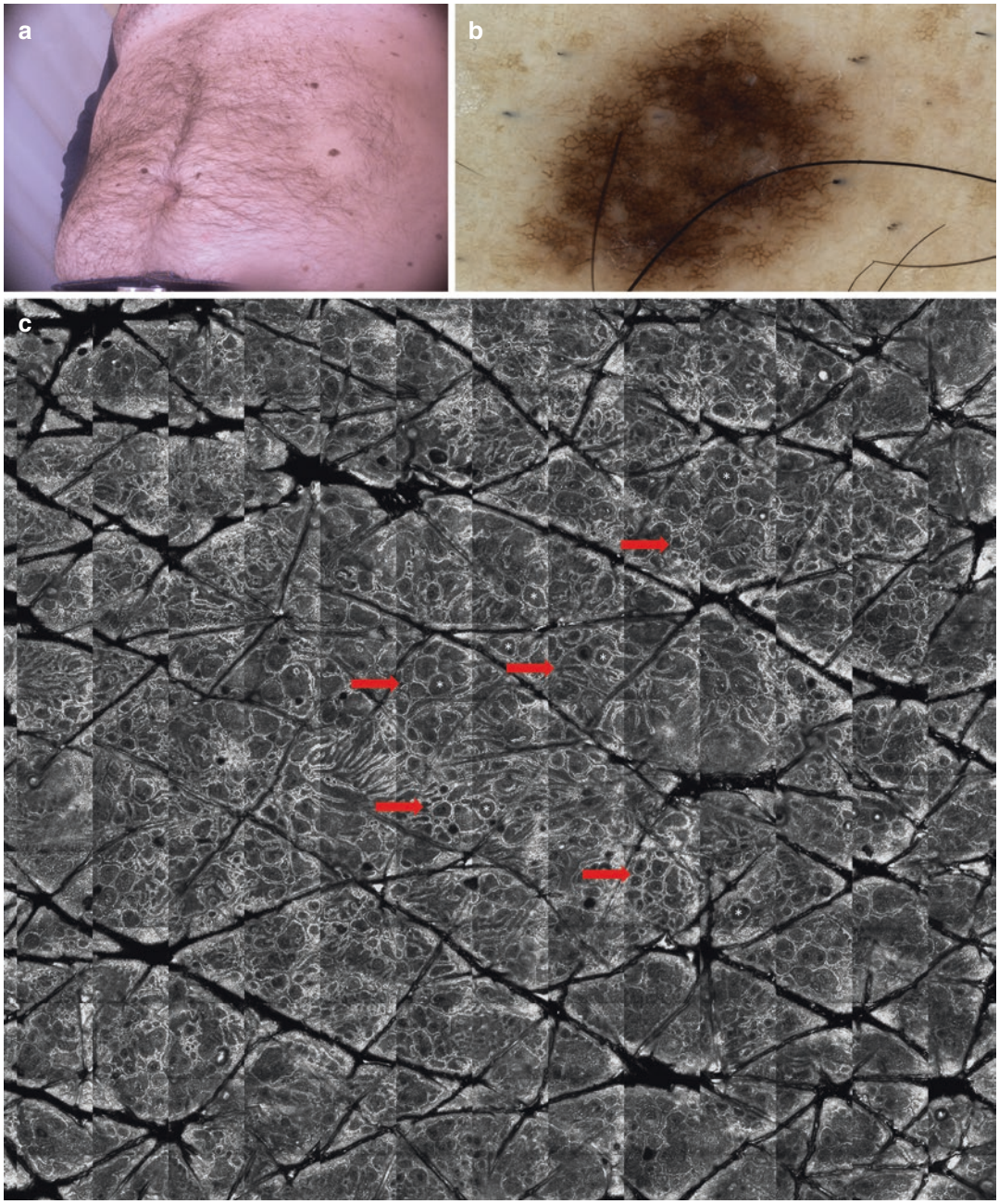

Fig. 13.1 Junctional nevus: clinical (**a**), dermoscopic (**b**), and reflectance confocal microscopy (RCM, **c**) images. Dermoscopy shows a reticular pattern. RCM shows the presence of a ringed pattern at the dermo–epidermal junction (red arrow; dermal papillae are indicated by white asterisk). (Photographer: Marco Campoli, University Hospital of Siena)

polygonal and roundish cells (keratinocytes and melanocytes, respectively) surrounding roundish to oval dark areas (dermal papillae) [14]. On the other hand, meshwork pattern is characterized by junctional thickenings (i.e., widening of the interpapillary rete ridges). Nevi with the ringed pattern

on RCM mostly have a lentiginous pattern on histopathology, with predominance of single junctional melanocytes and pigmented basal keratinocytes along elongated rete ridges, with only sporadic small junctional nests. Nevi with RCM meshwork pattern show on histopathology junctional melanocytic nests that are larger than those seen in junctional nevi with a ringed pattern. These junctional nests are located at the tips and sides of the rete ridges, and they predominate over single junctional melanocytes [14].

Benign melanocytic nevi less frequently present an atypical pigment network at dermoscopy, corresponding to irregular in shape and size dermal papillae separated by thick irregular interpapillary spaces with nests of hyper-reflective melanocytes at RCM [14].

13.1.1.2 Pigment globules

Dermal (Fig. 13.2a) and compound (Fig. 13.3a) melanocytic nevi usually present regular homogeneous globules at dermoscopy. Less common in nevi are globules irregular in size, shape, pigmentation, and/or distribution [14]. When globules are large, the pattern is called cobblestone.

Globular dermoscopic pattern (Figs. 13.2b and 13.3b) can reveal at RCM a meshwork pattern composed of numerous junctional clusters that appear to bulge into the dermal papillae and/or to dense nests (Figs. 13.2c and 13.3c) within the papillary dermis [14]. An exact correspondence in shape is observed between globules on dermoscopy and the dense melanocytic clusters on RCM, appearing as compact aggregates with a sharp margin of large roundish cells similar in morphologic features and reflectivity [14].

Nevi with a cobblestone dermoscopic pattern reveal on RCM large bright roundish cell clusters that fill the dermal papillae. This type of distribution is called "clod pattern" in RCM [14]. The polygonal shape of the dermal nests on RCM corresponds to the angulated, polygonal shape of the cobblestone globules on dermoscopy. These RCM findings correlate on histopathology with large nests of melanocytes in an enlarged papilla [14]. Cobblestone pattern is usually seen in dermal nevi that have no connection to the basal cell layer of the epidermis. In these nevi, some large, roundish nucleated cells loosely aggregated can be sometimes visible in the upper portion of the nests. In depth, clusters are more compact and homogeneous, and they lose evident cell contours due to resolution loss of RCM.

13.1.1.3 Pigment Dots

In nevi, brown and black dots on dermoscopy correspond at RCM to reflecting spots (melanin clumps) within the epidermis and less frequently to single melanocytes aggregated in small clusters, with reflective cytoplasm and dark nucleus in a pagetoid spread. On the other hand, bluish and gray dots correspond to small aggregates of plump bright cells within the dermal papillae on RCM and to melanophages located in the upper part of the dermal papilla on histologic examination [14].

13.1.1.4 Peripheral Structures

Benign melanocytic lesions and especially Reed nevus (Fig. 13.4a) may also present radial streaks (Fig. 13.4b), peripheral globules, and pseudopods on dermoscopy. At RCM, radial streaming consists of lines of interpapillary thickening of the DEJ projected toward the periphery, separated by narrow elongated darker areas corresponding to dermal papillae [14]. On histopathology, elongated and parallel oriented epidermal cristae are observable at the periphery of the lesion. Peripheral globules are similar to other globules, corresponding to melanocytic nests at the DEJ on RCM and histopathology [14]. On RCM, pseudopods appear as dense nests located immediately below the epidermal basal layer and characterized by sharp borders only in the outside front and connected at the lesion core by a sheet of loosely aggregated cells, giving rise to a comet star–like appearance [14]. On histopathology, pseudopods correspond to a well-defined nest, located at the tip of enlarged and parallel oriented rete ridges.

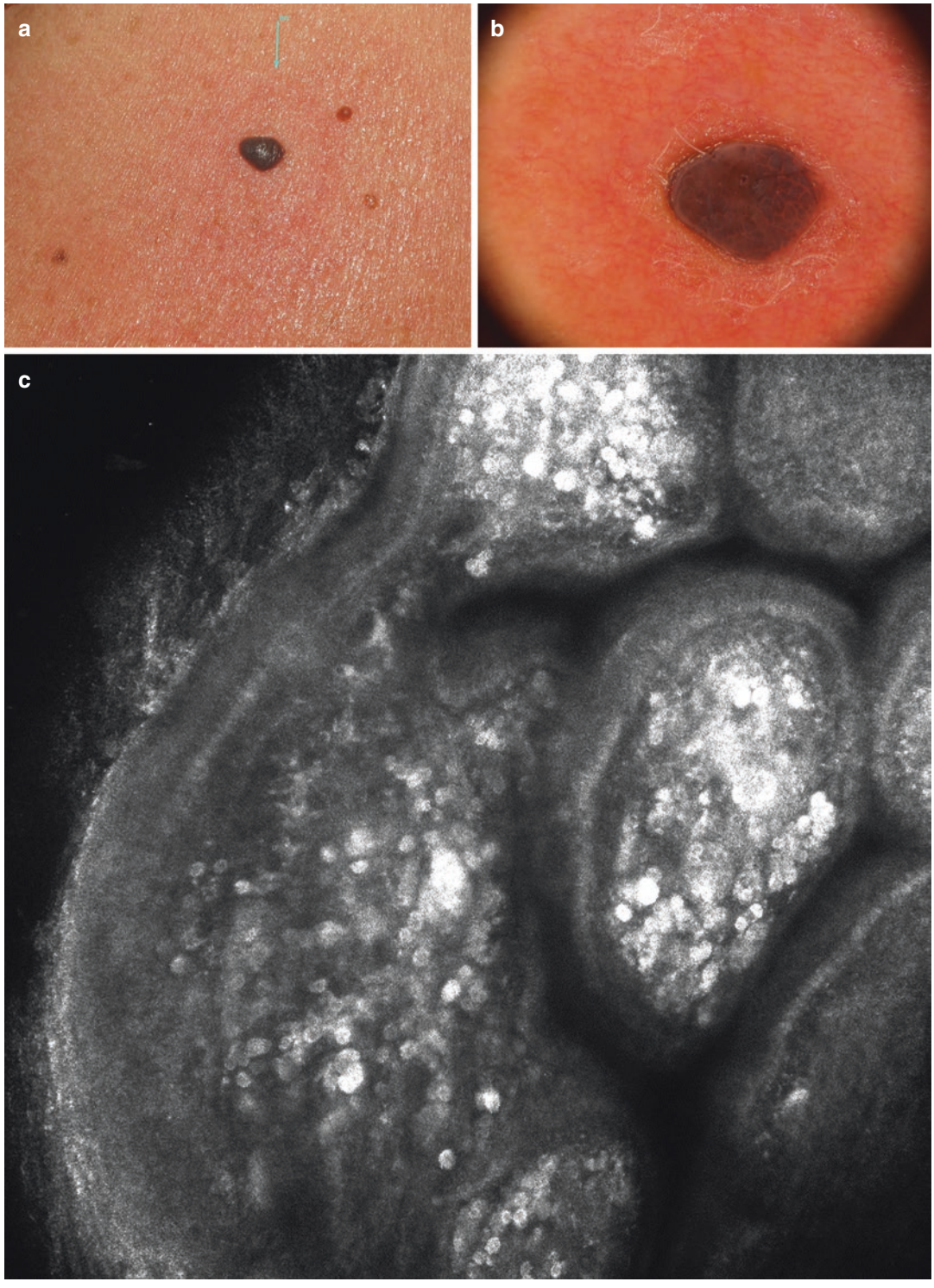

Fig. 13.2 Dermal nevus: clinical (**a**), dermoscopic (**b**), and reflectance confocal microscopy (RCM, **c**) images. Dermoscopy shows a globular and homogeneous pattern. RCM reveals a clod pattern in the upper dermis. (Photographer: Cinotti Elisa, University Hospital of Siena)

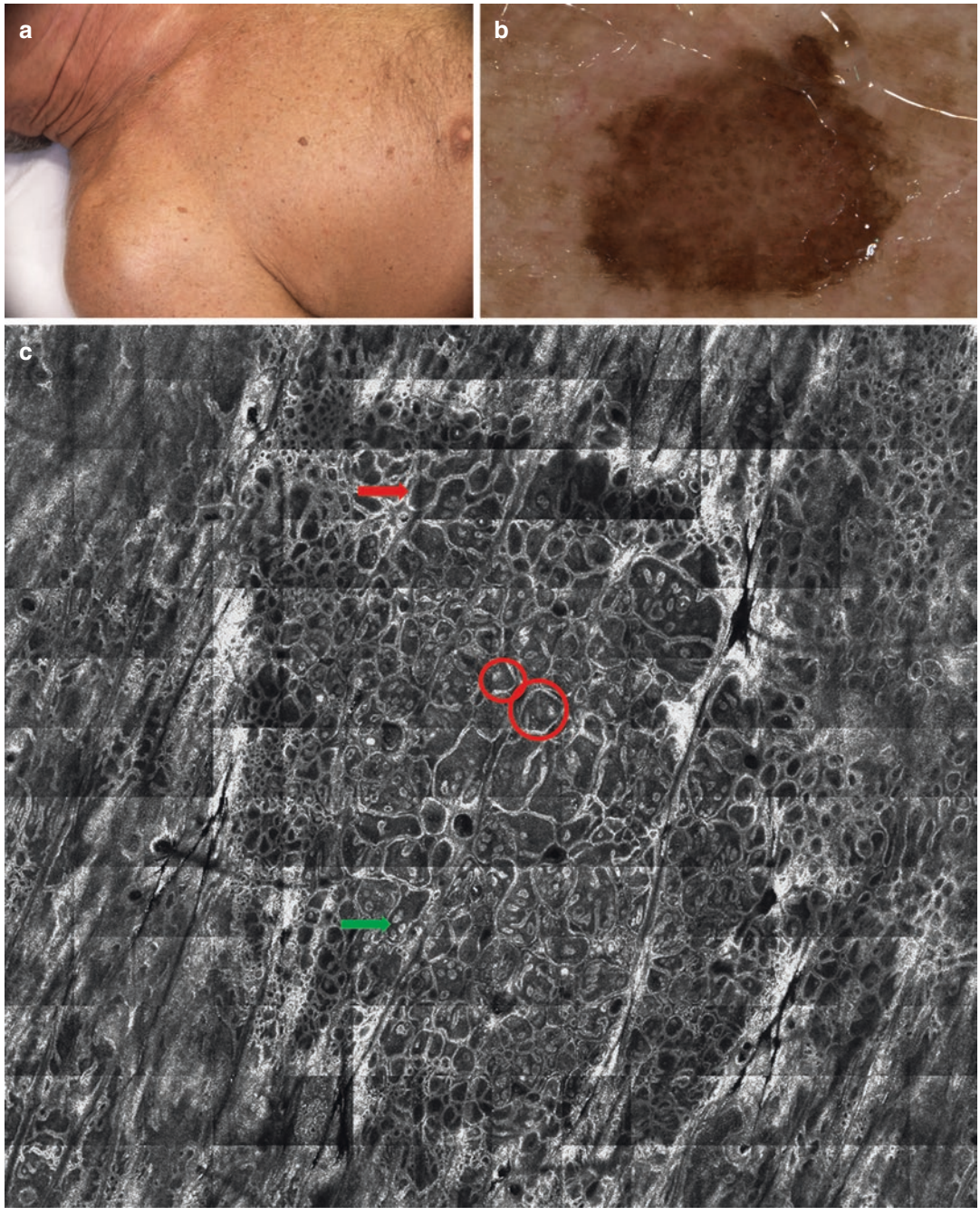

Fig. 13.3 Compound nevus: clinical (**a**), dermoscopic (**b**), and reflectance confocal microscopy (RCM, **c**) images. Dermoscopy shows a globular pattern in the center and a reticular pattern at the periphery. RCM reveals a junctional component characterized by a ringed pattern (ring pattern red arrow and bulbous projections inside the papillae green arrow) with edged papillae fulfilled by dermal nests showing different degrees of reflectance (red circle). (Photographer: Cinotti Elisa, University Hospital of Siena)

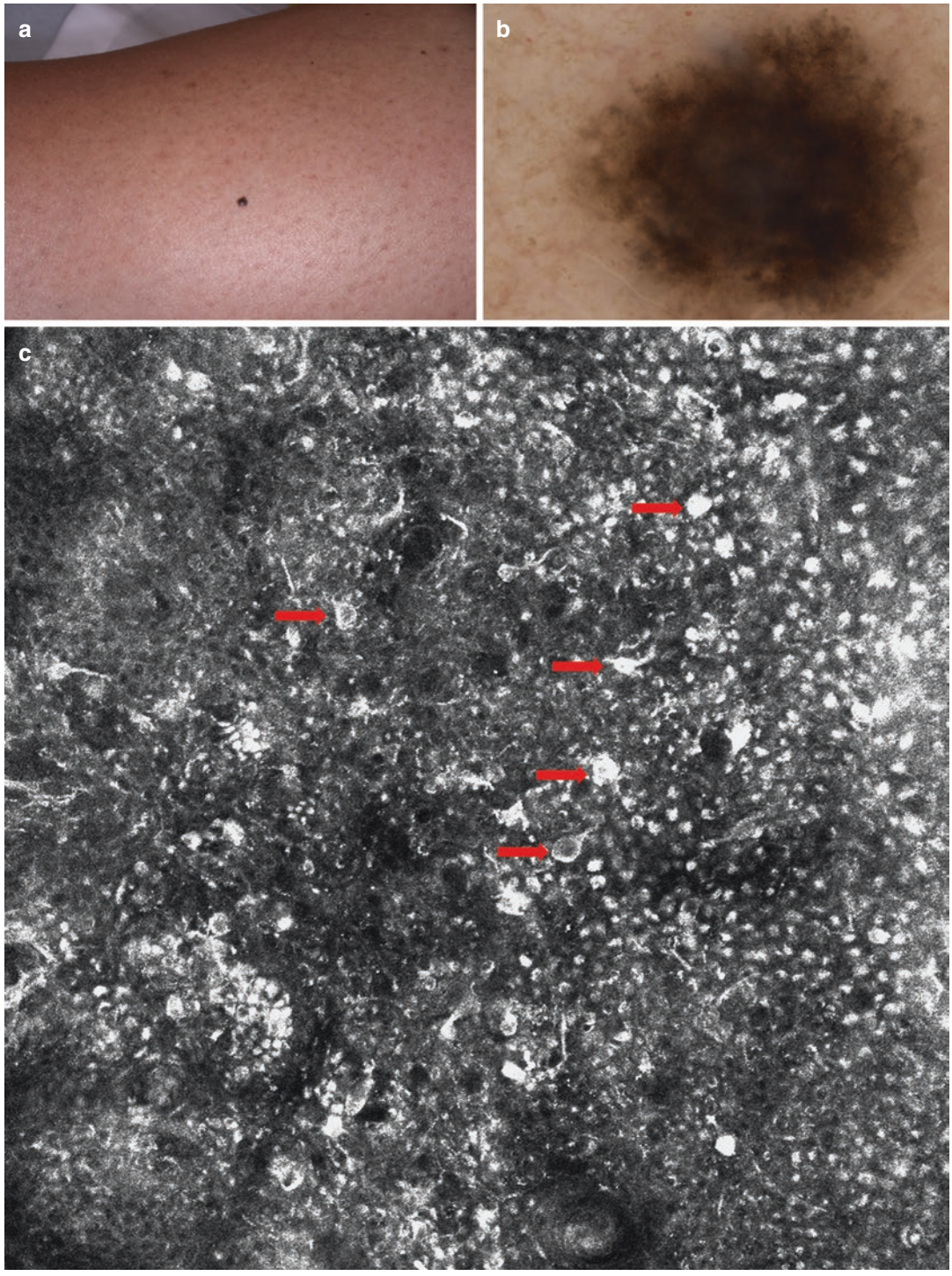

Fig. 13.4 Reed nevus: clinical (**a**), dermoscopic (**b**), and reflectance confocal microscopy (RCM, **c**) images. Dermoscopy shows a homogeneous central pattern and radial streaks. RCM reveals at the level of the suprabasal epidermis numerous large atypical cells, predominantly spindled and roundish in shape (red arrow). (Photographer: Cinotti Elisa, University Hospital of Siena)

13.1.1.5 Diffuse Pigmentation

Diffuse light brown pigmentation in benign nevi usually corresponds on RCM to a ringed pattern at the DEJ with small, weakly reflecting, dense, and regular nests. Histologic analysis reveals little pigmentation in the epidermal layers [14]. Diffuse dark pigmentation and pigment blotches visible at dermoscopy show high reflective epidermis (owing to the abundant content of melanin within the keratinocytes) and/or a bright cobblestone pattern on RCM [14].

13.1.2 Special Nevi

13.1.2.1 Blue Nevus

The loss of image resolution at increasing depth commonly invalidates correct evaluation of deep nevi such as blue nevi under RCM. Therefore, only a part of blue nevi can be imaged by RCM. In these cases, the most relevant findings are in the dermis, where RCM discloses hyper-refractive dendritic cells arranged in nests and surrounded by bright collagen fibers. Also, plump bright cells with ill-defined cell borders and intensely reflecting grainy cytoplasm, scattered throughout the dermal stroma and between collagen bundles, could be observed, as well as the classic sheet aspect of dermal melanocyte distribution [15]. The regular honeycomb pattern of epidermal keratinocytes is usually preserved with regular edged papillae at the DEJ. Epidermis might be slightly acanthotic.

13.1.2.2 Spitz Nevus

Spitz and Reed (pigmented Spitz) nevi (Fig. 13.4a) are characterized by epithelioid and/or spindle cell melanocytes, sometimes leading to diagnostic confusion with MM. Lack of characteristic features in some Spitz nevi, diagnostic difficulties in the non-pigmented variety or the presence of MMs mimicking these nevi, lead to surgical excision in many cases.

On RCM, junctional nests, sharp border cutoffs, and plump bright cells are characteristics of Spitz nevi. Few (or sometimes numerous) large atypical cells, predominantly spindled, and/or roundish/polygonal in shape can be observed in the epidermis (Fig. 13.4c) and the DEJ [16]. Junctional and dermal nests are usually seen as regular dense nests, sometimes in combination with inhomogeneous and sparse cell nests. Spitz nevi are frequently characterized by sharp borders, constituted by a rim of dense clusters at the periphery of the lesions or by a clearly outlined contour between the skin and the lesion. Large plump bright melanophages are present in the majority of Spitz nevi, although they are also frequently observed in MMs and other nevi [16]. The main limitation of RCM for the differential diagnosis between Spitz nevus and MM is the impossibility to identify deep mitoses that are in favor of MM[16].

13.1.2.3 Dysplastic Nevus

Dysplastic nevi were thought to be precursors of MM during a stepwise process. However, this concept is controversial, and precise correlation between clinical and histopathologic features is not clear. Histopathologically, dysplastic nevi are characterized by some features that overlap with both common nevi and MM and, consequently, at RCM, dysplastic nevi show intermediate features between non-dysplastic nevi and MM. Concerning the general architecture, moderately and severely dysplastic nevi usually show asymmetry. In the epidermis, dysplastic nevi may present large nucleated roundish cells in a pagetoid spread, with an ascending trend from mildly to severely dysplastic nevi. At the DEJ, a large proportion of dysplastic nevi show a so-called ringed meshwork pattern, where a central meshwork pattern is surrounded by a ringed pattern at the DEJ [17]. Papillae are clearly detectable in almost all cases, with some cases showing poorly outlined contours (non-edged papillae). A nonspecific pattern of the DEJ, usually with a limited extent, could be observed. Most cases show junctional nests that are irregular in size and shape and have short interconnections, corresponding to the bridging in histopathology. Atypical junctional cells are frequently observed in dysplastic nevi, mostly roundish. The concentration of the atypical cells in the center of the lesion may help the differential diagnosis with MM that has atypical cells in the center and the periphery. Within the papillary

dermis, coarse collagen fibers and plump bright cells and/or bright particles (corresponding to inflammatory cells) are often visible [17].

13.1.2.4 Acral Nevus

Palms and soles are rarely studied by RCM because of the increased thickness of the epidermis that hampers the visualization of deeper layers. However, skin thickness varies depending on age, sex, and different acral sites. In many cases, it is possible to reach the DEJ and identify regular melanocytic nests at the DEJ and in the superficial dermis. In acral nevi, the epidermis is usually spared from pagetoid spread, but in some cases pagetoid cells (dendritic and/or roundish) can be found. These cells are usually far from acrosyringia different from acral MM. Small dendritic hyper-reflective cells can also be frequently observed in the epidermis of acral nevi and correspond to Langerhans cells [18].

13.1.2.5 Combined Nevus

Combined melanocytic nevi are defined as the histopathological presence of two different types of melanocytic proliferations within the same nevus. The most stereotypical appearance of a combined nevus is that of a central structureless blue papule (blue nevus) surrounded by a brownish area (common nevus). Because of the presence of two nevus cell populations, color variegations or more than one structure, depending on the nevus types, are often present. The most classic type (blue nevus associated with common compound or dermal nevus) is characterized by a delicate peripheral reticular pattern and/or globular pattern and a central structureless blue pigmentation. Combined nevi lacking a blue nevus component might reveal less specific features under dermoscopy. RCM can detect the combination of two nevus cell types [19]. Moreover, in case of a differential diagnosis with MM, RCM can reveal the presence or absence of specific MM features. One limit in the RCM evaluation can be the case of a deep dermal or blue nevus not detectable, because of the limits in depth penetration of RCM [19].

13.1.2.6 Recurrent Nevi

Recurrent nevi (RN) are benign melanocytic nevi that regrow after incomplete surgical excision or trauma. Clinically, they present as a scar with variegated hyperpigmentation. Differential diagnosis of RN includes recurrent MM and melanotic pigmentation (post-inflammatory reactive pigmentation) within a scar. Benign recurrences are confined to the scar, usually arising in the center of the scar. On the contrary, recurrent MM tends to diffuse outside the scar. RCM features of RN and their differential diagnosis with MM have been recently described. RN do not exhibit prominent pagetoid or lateral spread of melanocytes nor atypical nests at the DEJ. Although some cases showed atypical cells in the junctional component, these cells were few in number and cytologically monomorphous [19].

13.1.2.7 Sclerosing Nevi with Pseudomelanomatous Features

Sclerosing nevus with pseudomelanomatous features is a recently described entity which can clinically and histopathologically simulate regressing MM. It is also called "nevus with regression-like fibrosis" (NRLF). NRLF can be differentiated from regressing MM on histopathology by lacking specific MM features. NRLF are pigmented atypical lesion showing overall features of regression on dermoscopy, which is invariably extensive (between 10 and 50%) and polychromatic (coexisting white and blue areas), in the absence of MM-specific criteria. There are some criteria that raise the index of suspicion of NRLF: young/middle-aged patients, lesions located in the convex area of the back, symmetric-central distribution of regression and limited regression (<50% in the convex area of the back; <10% elsewhere). RCM shows the presence of ill-defined lesion, with junctional thickening and numerous melanophages at the DEJ. In RCM, the presence of cellular atypia and focal pagetoid spread did not always allow an accurate differential diagnosis with regressive MM, reflecting the difficulties often encountered also in histopathology [19].

13.1.2.8 Sutton Nevus

Halo nevus (HN), also termed Sutton's nevus, is a benign melanocytic nevus surrounded by an achromic rim. It most commonly involves compound nevi. Both congenital and acquired nevi can be concerned. Histopathologically, a heavy, lichenoid lymphocytic infiltrate within the dermis is noticed, with nevus cells arranged in nests or singly among the inflammatory cells. The whitish halo shows an absence of melanin and melanocytes in the basal layer. On dermoscopy, the central nevus component typically shows a globular and/or homogeneous pattern, which is surrounded by a variable rim of a white regression-like depigmentation. The central nevus component may also display a reticular pattern. RCM features of halo nevi have been recently described only in few small case series. Features that can be found in this nevus include pagetoid cells, non-edged dermal papilla and junctional thickening and nucleated cells and plump bright cells in the dermal papillae. Therefore, RCM examination in HN can show atypical features that overlap with those observed in MM [19, 20].

13.1.2.9 Meyerson's Nevus (Eczematous Nevus)

Meyerson's phenomenon is characterized by the development of an eczematous halo around one or more pigmented nevi. RCM imaging of Meyerson's nevi allows the visualization of spongiotic vesicles, as round to ovoidal dark spaces with bright particles inside (corresponding to inflammatory cells), visible in the superficial layers of the epidermis around a typical melanocytic nevus [21, 22].

13.1.2.10 Nevus of Ota

The Nevus of Ota (NO) is a bluish or grayish hyperpigmentation caused by an accumulation of dermal melanocytes that typically extend to the innervated parts of the ophthalmic and maxillary divisions of the trigeminal nerve, involving the facial skin, the uvea, the iris, and the sclera. In RCM examination, melanocytes of NO are highly reflective large and monomorphous dendritic cells diffused among the collagen fibers [23]. These cells are seen elongated either with only two visible dendrites (spindle shape) or with multiple visible dendrites. In some areas, they form small clusters within the diffuse proliferation. In contrast to melanocytes typically seen in cutaneous melanocytic nevi, the melanocytes of NO often show well visible hypo-reflective nuclei [23].

References

1. González S, Gilaberte-Calzada Y, González-Rodríguez A, Torres A, Mihm MC. In vivo reflectance-mode confocal scanning laser microscopy in dermatology. Adv Dermatol. 2004;20:371–87.
2. Rajadhyaksha M, Grossman M, Esterowitz D, Webb RH, Anderson RR. In vivo confocal scanning laser microscopy of human skin: melanin provides strong contrast. J Invest Dermatol. 1995;104:946–52.
3. Langley RG, et al. Confocal scanning laser microscopy of benign and malignant melanocytic skin lesions in vivo. J Am Acad Dermatol. 2001;45:365–76.
4. Pellacani G, Cesinaro AM, Longo C, Grana C, Seidenari S. Microscopic in vivo description of cellular architecture of dermoscopic pigment network in nevi and melanomas. Arch Dermatol. 2005;141:147–54.
5. Gerger A, et al. Diagnostic applicability of in vivo confocal laser scanning microscopy in melanocytic skin tumors. J Invest Dermatol. 2005;124:493–8.
6. Pehamberger H, Steiner A, Wolff K. In vivo epiluminescence microscopy of pigmented skin lesions. I. Pattern analysis of pigmented skin lesions. J Am Acad Dermatol. 1987;17:571–83.
7. Kenet RO, et al. Clinical diagnosis of pigmented lesions using digital epiluminescence microscopy. Grading protocol and atlas. Arch Dermatol. 1993;129:157–74.
8. Argenziano G, et al. Dermoscopy of pigmented skin lesions: results of a consensus meeting via the Internet. J Am Acad Dermatol. 2003;48:679–93.
9. Pellacani G, Cesinaro AM, Seidenari S. Reflectance-mode confocal microscopy of pigmented skin lesions—improvement in melanoma diagnostic specificity. J Am Acad Dermatol. 2005;53:979–85.
10. Pellacani G, et al. The impact of in vivo reflectance confocal microscopy for the diagnostic accuracy of melanoma and equivocal melanocytic lesions. J Invest Dermatol. 2007;127:2759–65.
11. Pellacani G, Cesinaro AM, Seidenari S. In vivo assessment of melanocytic nests in nevi and melanomas by reflectance confocal microscopy. Mod Pathol. 2005;18:469–74.

12. Scope A, et al. Correlation of dermoscopic structures of melanocytic lesions to reflectance confocal microscopy. Arch Dermatol. 2007;143:176–85.
13. Scope A, et al. Correlation of dermoscopy with in vivo reflectance confocal microscopy of streaks in melanocytic lesions. Arch Dermatol. 2007;143:727–34.
14. Pellacani G, et al. In vivo confocal microscopic and histopathologic correlations of dermoscopic features in 202 melanocytic lesions. Arch Dermatol. 2008;144:1597–608.
15. Puig S, et al. Reflectance confocal microscopy of blue nevus. Eur J Dermatol. 2012;22:552–3.
16. Pellacani G, et al. Spitz nevi: In vivo confocal microscopic features, dermatoscopic aspects, histopathologic correlates, and diagnostic significance. J Am Acad Dermatol. 2009;60:236–47.
17. Pellacani G, et al. In vivo confocal microscopy for detection and grading of dysplastic nevi: A pilot study. J Am Acad Dermatol. 2012;66:e109–21.
18. Cinotti E, et al. Reflectance confocal microscopy features of acral lentiginous melanoma: a comparative study with acral nevi. J Eur Acad Dermatol Venereol. 2016;30:1125–8.
19. Larre Borges A, et al. Melanocytic nevi with special features: clinical-dermoscopic and reflectance confocal microscopic-findings. J Eur Acad Dermatol Venereol. 2014;28:833–45.
20. Schwartz RJ, Vera K, Navarrete N, Lobos P. In vivo reflectance confocal microscopy of halo nevus. J Cutan Med Surg. 2013;17:33–8.
21. Longo C, et al. An atypical Meyerson's naevus: a dermoscopic, confocal microscopic and immunohistochemical description of one case. J Eur Acad Dermatol Venereol. 2007;21:414–6.
22. Ardigò M, Longo C, Cristaudo A, Berardesca E, Pellacani G. Evaluation of allergic vesicular reaction to patch test using in vivo confocal microscopy. Skin Res Technol. 2012;18:61–3.
23. Grechenig C, et al. Examination of the melanocytes of the Nevus of Ota with in vivo reflectance confocal microscopy: 15 cases. J Eur Acad Dermatol Venereol. 2018;32:e241–2.

14 In Vivo Reflectance Confocal Microscopy for Melanoma

Marco Campoli, Jean Luc Perrot, and Elisa Cinotti

In the recent years, we are observing an increase in the incidence of melanoma worldwide. Although increased awareness of melanoma has led to more efficient screening and improved understanding of melanoma tumorigenesis has guided the development of new therapeutic options, melanoma still carries significant morbidity and mortality. As many other cancers, early diagnosis and prompt surgical excision are essential. Early detection necessarily implied the development of new noninvasive diagnostic techniques. Reflectance confocal microscopy (RCM) allows dynamic imaging of the skin at cellular resolution in real time, performing optical biopsies [1–3]. Microscopic tissue elements reflect light with different refractive indices. RCM is particularly useful for imaging melanocytic lesions, such as nevi or melanoma [4, 5], because melanin has the highest refractive index of all tissue elements (n = 1.7) and acts as a naturally occurring "endogenous" contrast [4]. Several studies have demonstrated that RCM evaluation has the potential to increase sensitivity (improves melanoma detection) [6, 7] and specificity (reduces excisions of benign lesions) for melanoma [8–11].

M. Campoli (✉) · E. Cinotti
Department of Medical, Surgical and Neurological Science, Dermatology Section, University of Siena, S. Maria alle Scotte Hospital, Siena, Italy

J. L. Perrot
Department of Dermatology, University Hospital of St-Etienne, Saint-Etienne, France
e-mail: j.luc.perrot@chu-st-etienne.fr

14.1 RCM Features According to Melanoma Subtype

The term cutaneous melanoma includes a heterogeneous subset of malignant melanocytic proliferations that differ significantly in their epidemiology, morphology, growth dynamics, and clinical behavior. Four major histological subtypes of melanoma have been described: superficial spreading melanoma (SSM), nodular melanoma (NM), lentigo maligna melanoma (LMM), and acral lentiginous melanoma (ALM). Less common melanoma subtypes include nevoid melanoma, desmoplastic melanoma, clear cell sarcoma, and solitary dermal melanoma.

14.1.1 Superficial Spreading Melanoma

SSM is the most common melanoma subtype (50–80% of all melanoma diagnoses) (Figs. 14.1, 14.2). The name is derived from a prolonged radial (lateral) growth phase before invasive (vertical) growth starts. Although it can develop in any anatomic location, it most likely occurs on sun-exposed areas such as the back in men and the lower limbs in women. Few melanomas can

M. Fimiani et al. (eds.), *Technology in Practical Dermatology*,
https://doi.org/10.1007/978-3-030-45351-0_14

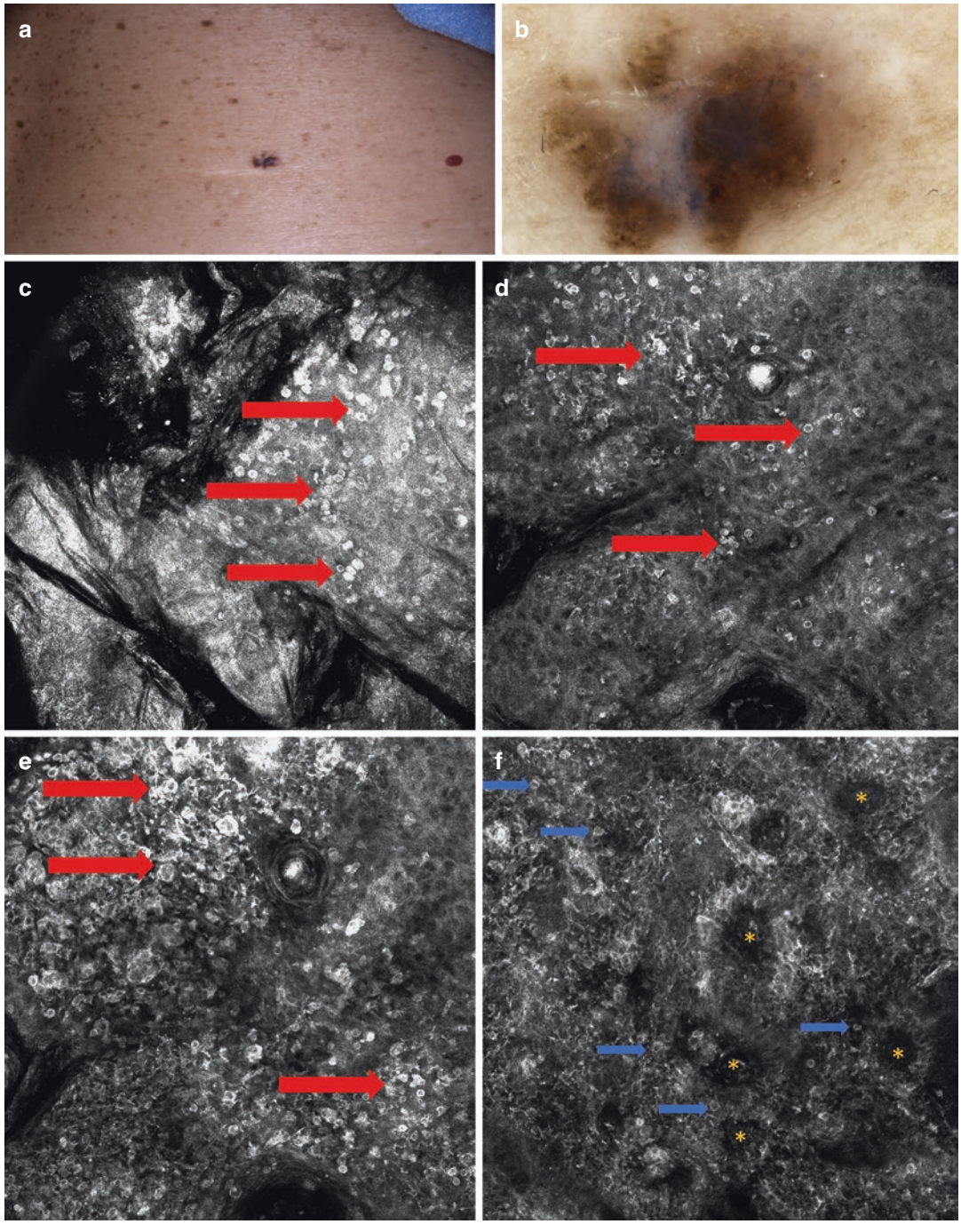

Fig. 14.1 Superficial spreading melanoma: clinical (**a**), dermoscopic (**b**), and reflectance confocal microscopy (RCM, **c**–**f**) images. RCM shows pagetoid cells (**c**, **d**, **e**, *red arrows*) in the stratum corneum (**a**), granulosum (**b**), and spinosum (**c**) of the epidermis and atypical cells (**f**, *blue arrows*) with non-edged papillae (**f**, *yellow asterisks*) at the dermo–epidermal junction that appears disarranged (**f**). (Photographer: Marco Campoli, University of Siena)

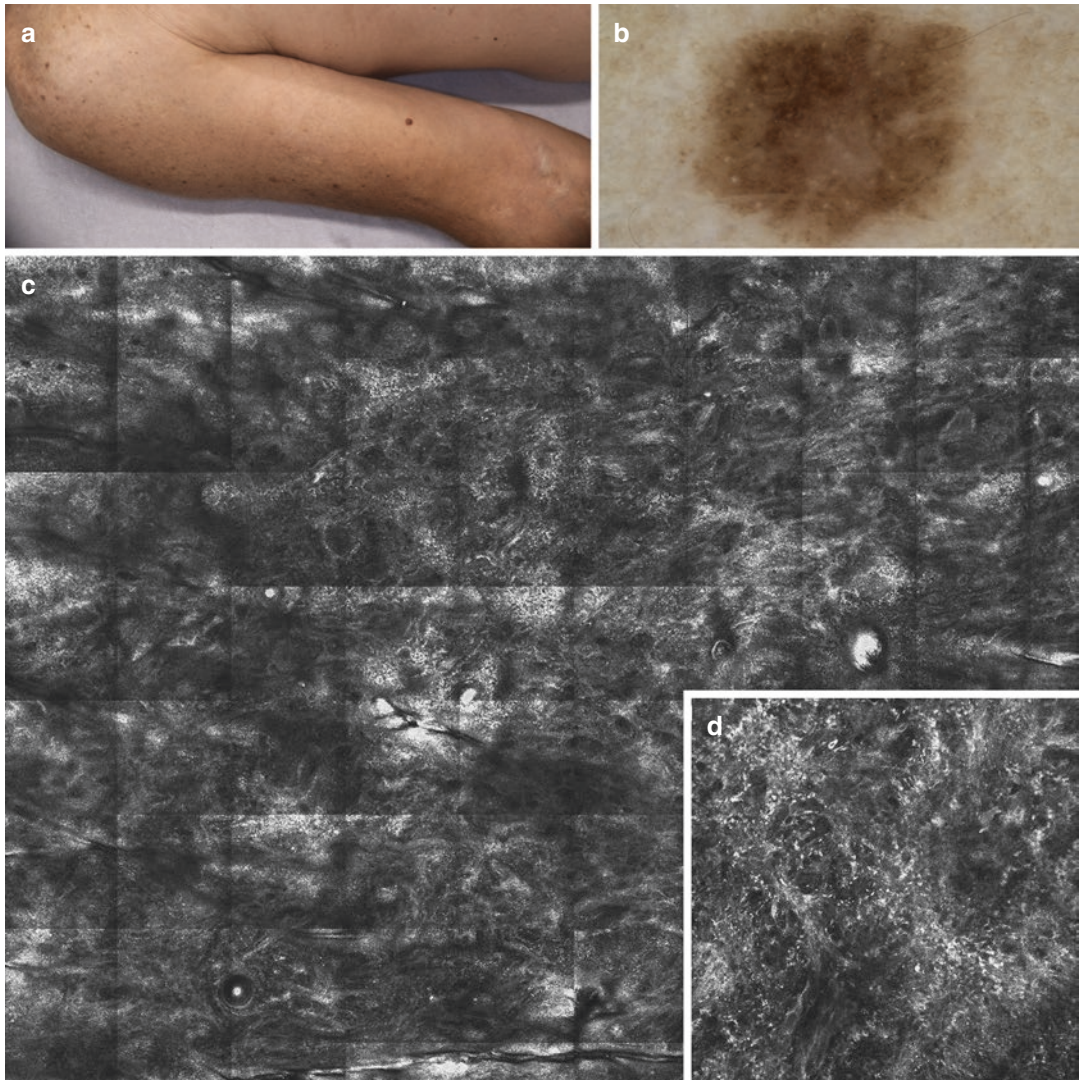

Fig. 14.2 Superficial spreading melanoma: clinical (**a**), dermoscopic (**b**), and reflectance confocal microscopy (RCM, **c** and **d**) images. RCM shows a disarranged dermal epidermal junction (**c**) due to the proliferation of bright atypical cells (**d**, detail of figure **c**). (Photographer: Marco Campoli, University of Siena)

arise from a precursor nevus and mostly occur de novo. SSM is characterized histologically by pagetoid spread and nests of the epithelioid melanocytes at the dermo–epidermal junction (DEJ). Poor circumscription with variable epidermal thickening is also common. Cytologically, melanocytes may have one or more large nuclei with an abundant cytoplasm that is often amphophilic, eosinophilic, or finely pigmented with melanin granules.

RCM criteria vary according to the examined skin layer (Table 14.1) [12]. Pagetoid spread is well visible in the epidermis (Fig. 14.1c–e). Notably, pagetoid cells appear as large hyperreflective nucleated cells in SSM. These melanocytes are mostly rounded with variably short and thick dendrites. Additionally, dendritic melanocytes could be detected, although this melanoma subtype is mainly characterized by the presence of roundish atypical melanocytes [13]. By definition, pagetoid cells under RCM have a large size (they are larger than the surrounding keratinocytes) and are scattered within the suprabasal epidermal layers without any cell connection with

Table 14.1 Reflectance confocal microscopy features of superficial spreading melanoma

Layer	Features	Description
Suprabasal epidermis	Pagetoid cells (roundish, dendritic or spindled)	Hyper-reflective (bright), large, nucleated cells (larger than the surrounding keratinocytes), typically round but may be pleomorphic
	Atypical honeycomb or atypical cobblestone pattern	Partial (poorly visible) or complete (nonvisible) loss of the normal honeycomb or cobblestone pattern caused by pagetoid spread of malignant melanocytes
DEJ	Disarranged DEJ	Irregular clod, irregular meshwork, and/or irregular ringed pattern up to complete destruction of the DEJ architecture
	Proliferation of atypical cells in single units or nests	Large cells with large nuclei and irregular size and shape
	Non-edged dermal papillae	Dermal papillae are not visible or not demarcated by a normal rim of small hyper-reflective and monomorphous keratinocytes but rather by large hyper-reflective atypical melanocytes
Upper dermis	Atypical nests	Nests composed of large and nucleated round or pleomorphic cells
	Hyper-reflective cells distributed in sheet-like structures with consequent loss of normal DEJ architecture	Hyper-reflective cells distributed in the same plane and loss of dermal papillae

the neighboring keratinocytes, giving the impression of floating cells. In situ melanomas present few or localized pagetoid cells compared with invasive tumors in which a florid pagetoid infiltration could be detected in the entire melanoma and at all epidermal layers, even in the stratum corneum [13]. The presence of atypical melanocytes can subvert the typical epidermal architecture, leading to the loss of the normal honeycomb or cobblestone pattern. Under RCM, three main tumor architectures can be detected at the DEJ: irregular ringed, irregular meshwork, and irregular clod, as well as variable combinations of all of them [13]. Furthermore, many tumors might not display any of those but rather a nonspecific pattern: dermal papillae are not clearly visible or not well demarcated by a normal rim of bright cell but rather by large reflective cells corresponding to malignant melanocytes (loss of the normal-edged dermal papillae, Figs. 14.1f and 14.2c, d). In more advanced cases, the DEJ is totally disarranged by the melanocytic proliferation. Distinct nest types can be observed according to the growth phase of the tumor: dense nests are found in early phase, whereas dense and sparse and sheet-like structures are typical of the dermal invasion [13].

14.1.2 Nodular Melanoma

NM has a fast growth rate and is associated with a higher rate of death [14]. Amelanotic or hypomelanotic presentation of NM is particularly challenging [15] and can be mistaken for benign tumors. At RCM (Table 14.2), NM reveals a thinned epidermis (epidermal consumption) with the typical epidermal architecture still recognizable and few pagetoid cells [16]. The DEJ is completely disrupted, and the dermal compartment is filled with a solid proliferation of melanocytes with variable shape and size arranged as single cells or clustered. The so-called sheet-like structures that represent a proliferation of dyscohesive atypical melanocytes with prominent nuclei are frequent in NM. Remarkably, melanocytic nests with cerebriform appearance (cerebriform nests) are specific of NM and melanoma skin metastasis. Those nests show up as dark hyporeflective clusters of melanocytes that are outlined by brighter collagen fibers. Enlarged and tortuous vessels can also be frequently found. Tumor clusters are commonly found in proximity to these newly formed vessels [12].

Table 14.2 Reflectance confocal microscopy features of nodular melanoma

Layer	Features	Description
Suprabasal epidermis	Few or no pagetoid cells	Pure NM have fewer pagetoid cells than SSM
	Thin epidermis with normal epidermal architecture	Preserved honeycomb or cobblestone pattern (differing from SSM that exhibit distortion of the normal epidermal pattern)
DEJ	No visible dermal papillae	Substituted by a proliferation of atypical melanocytes often arranged in sheets
Upper dermis	Cerebriform nests	Aggregation of small compact cells with cerebriform appearance
	Enlarged vessels	

14.1.3 Lentigo Maligna and Lentigo Maligna Melanoma

Lentigo maligna (LM) presents as a slowly progressive pigmented macule on sun-exposed areas, most commonly on the face (Figs. 14.3a and 14.4a) and neck, and LMM is its invasive counterpart. Its clinical diagnosis is often challenging because it shows overlapping features with benign lesions. As it is often large and located on esthetic and functional areas, noninvasive imaging techniques such as dermoscopy and RCM are of great interest for its diagnosis. Dermoscopy has improved the diagnosis of LM/LMM, but they remain a challenge owing to overlapping features with solar lentigo, pigmented actinic keratosis, and lichenoid keratosis (Figs. 14.3b and 14.4b) [17, 18]. Histopathology could also be of difficult interpretation due to atypical melanocytic proliferation on sun-damaged skin [19]. RCM has proved to be helpful to enhance diagnosis of LM/LMM. Features of LM/LMM using RCM are well described [20–25] (Table 14.3). The earliest histopathological finding in LM is the proliferation of atypical melanocytes at the DEJ [26] that correlate with large hyper-reflective polymorphic cells under RCM (Figs. 14.3c and 14.4c, d). Numerous large pagetoid cells and consequent epidermal disarray are subsequently found. In LM/LMM, atypical melanocytes are more often dendritic than roundish and are typically located around and inside hair follicles (Figs. 14.3c and 14.4c, d). In some cases, only numerous hyper-reflective dendrites are visible, and not cell bodies and these hyper-reflective long dendrites form "medusa head-like structures" (Fig. 14.3c) around hair follicles. Advanced cases show large nucleated cells organized in nests in the upper dermis [12].

14.1.4 Acral Lentiginous Melanoma

The clinical and histological diagnosis of ALM may be very difficult, especially in the early phase of growth. Palms and soles are rarely studied by RCM because of the increased thickness of the epidermis that hampers the visualization of deeper layers. However, RCM can also be useful in acral site because early ALM is characterized by a lentiginous spread [27], and the epidermal thickness of acral areas is variable.

Pagetoid cells are the predominant clue for suspecting ALM by RCM [28]. The pagetoid spread of melanocytes also determines a disarrangement of the normal honeycomb pattern of the epidermis. Noteworthy in case of a thick stratum corneum, a skin scraping could allow to identify pagetoid cells in the epidermis that are at first not visible. It should be noticed that a proliferation of solitary arranged melanocytes can also be detected within the epidermis of melanocytic acral nevus with intra-epidermal ascent (MANIACs) [29]. However, pagetoid cells in these cases are monomorphous [28].

A characteristic feature of ALMs is the infiltration of sweat duct structures by atypical bright cells that correspond to a melanocytic extension along adnexal structures in histology. Nevi show more rarely a melanocytic proliferation around sweet duct structures and in these cases, melanocytes are mainly organized in nests [28, 30]. Another peculiar feature of ALM is the higher presence of granular dust-like hyper-reflective particles in the epidermis compared to

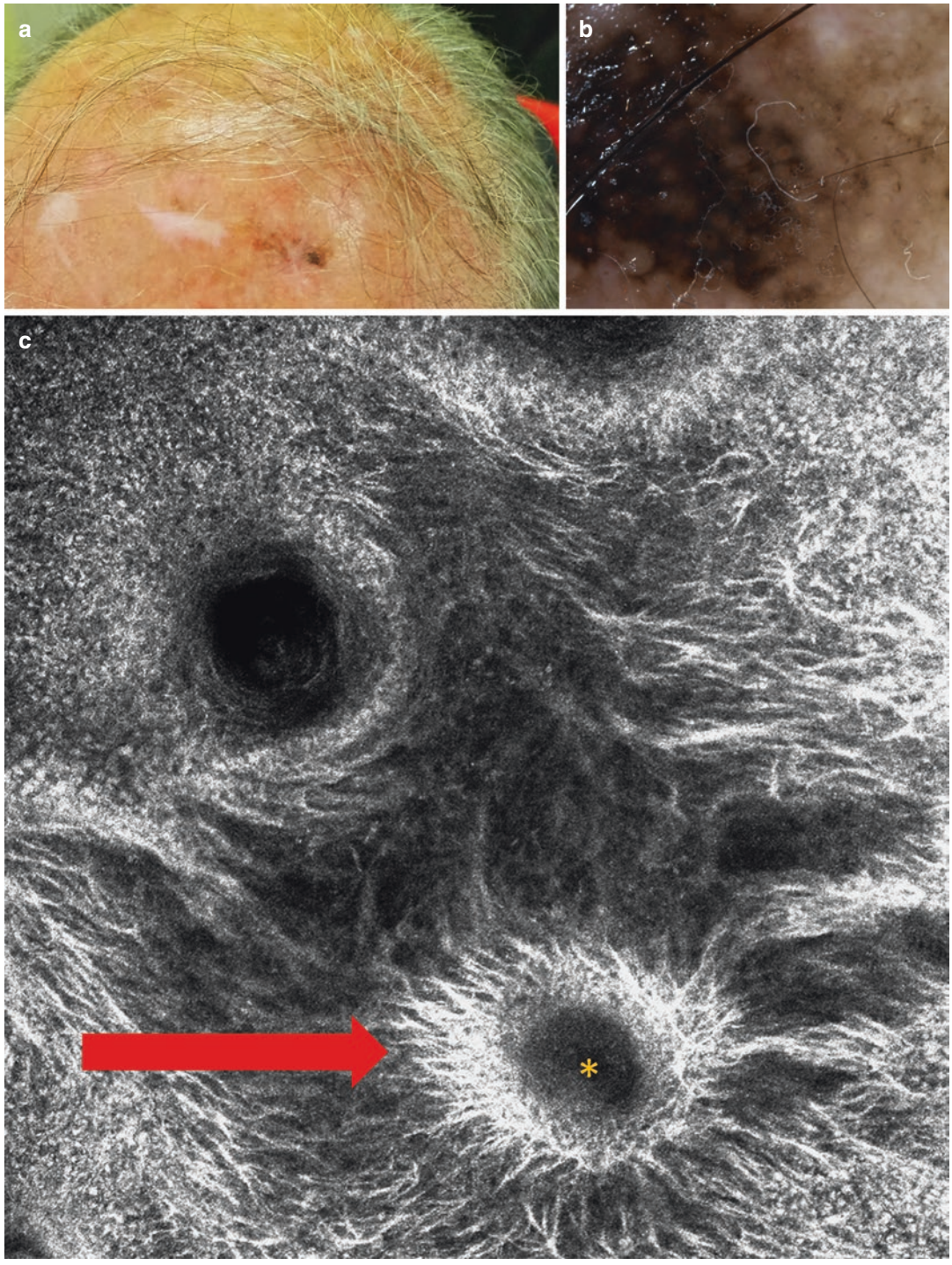

Fig. 14.3 Lentigo maligna: clinical (**a**), dermoscopic (**b**), and reflectance confocal microscopy (RCM, **c**) images. RCM shows a proliferation of atypical dendritic melanocytes in the epidermis (*red arrow*) that mainly infiltrate hair follicles (*yellow asterisk*) with the so-called medusa head-like structures. (Photographer: Elisa Cinotti, University of Siena)

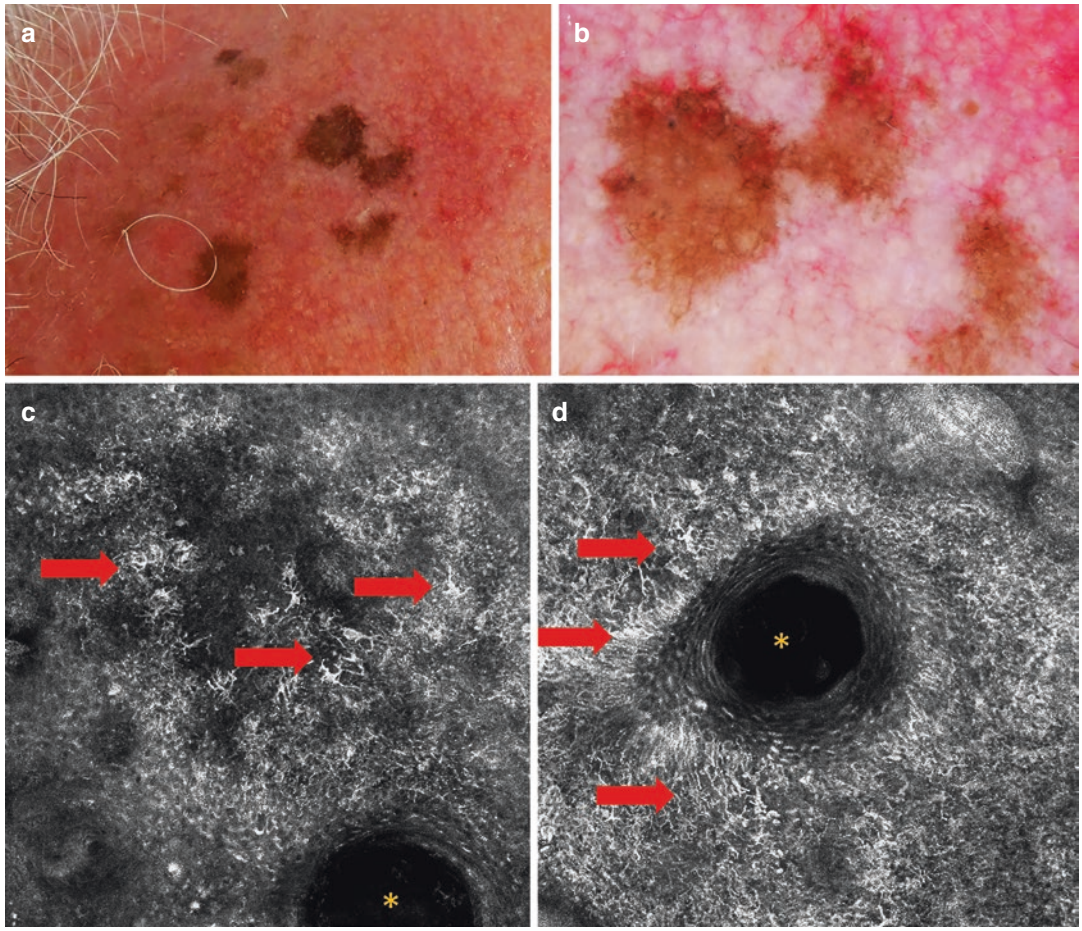

Fig. 14.4 Lentigo maligna: clinical (**a**), dermoscopic (**b**), and reflectance confocal microscopy (RCM, **c**) images. RCM shows a proliferation of atypical melanocytes in the epidermis (*red arrow*) that have a tropism for hair follicles (yellow asterisk). (Photographer: Elisa Cinotti, University of Siena)

Table 14.3 Reflectance confocal microscopy features of lentigo maligna/lentigo maligna melanoma

Layer	Features	Description
Suprabasal epidermis	Large dendritic and/or roundish hyper-reflective pagetoid cells	
	Epidermal disarray	No recognizable honeycomb or cobblestone pattern
DEJ	Non-edged papillae	Loss of normal rim of bright keratinocytes around the dermal papillae due to atypical cell proliferation
	Follicular localization of atypical cells	Large dendritic and/or roundish cells around and inside hair follicles
	Medusa head-like structures	Elongated bundles, composed of dendritic atypical cells, extending from the hair follicles
Upper dermis	Isolated large nucleated cells in the dermal papillae	
	Dermal nests	Aggregation of atypical melanocytes

nevi, possibly corresponding to free pigment. Free pigment is randomly distributed in ALMs and tends to be arranged in columns in the furrows in nevi [30].

In all ALMs with a visible dermis, sheets and/or nests of large atypical cells are usually seen, whereas these features are never found in nevi [28]. However, ALM diagnosis cannot be excluded in the absence of RCM signs because early ALM can present only subtle atypia such as slight proliferation of atypical melanocytes at the DEJ that may not be identified under RCM [28].

14.1.5 Desmoplastic Melanoma

Desmoplastic melanoma is a rare melanoma subtype that most commonly occurs on chronically sun-exposed areas of elderly patients. Misdiagnosis is common as it is often amelanotic and may mimic a scar or benign cutaneous tumor, such as dermatofibroma [31]. This melanoma is characterized by bundles of spindle-shaped melanocytes admixed with dense collagen and patchy lymphoid infiltrate in the dermis. These cells have a fibroblast-like appearance but hyperchromatic and bizarre nuclei are visible. The junctional component is minimal.

RCM features that may suggest the diagnosis of desmoplastic melanoma in the upper dermis are spindle melanocytes (elongated hyper-reflective large and often nucleated cells) and inflammation (presence of small hyper-reflective roundish cells).

14.1.6 Amelanotic Melanoma

The diagnosis of amelanotic melanoma is clinically challenging (Fig. 14.5a). Confusions with benign skin lesions or nonmelanoma skin cancer are potential pitfalls. Dermoscopic evaluation is useful to detect subtle signs of amelanotic melanoma, such as the presence of dotted vessels, linear irregular vessels, and milky red areas (Fig. 14.5b) [32, 33]. Amelanotic lesions are a major indication for RCM, as even small amounts of melanin can be seen with RCM [20]. RCM findings in amelanotic melanoma are similar to pigmented melanoma and include the proliferation of polymorphic large cells in the epidermis, DEJ (Fig. 14.5c, d) and dermis, loss of normal honeycomb pattern in the suprabasal epidermis, and DEJ disarray with irregular dermal papillae [34]. Pagetoid cells may appear dendritic or roundish. Unlike the hyper-reflective atypical cells of pigmented melanomas, melanocytes of amelanotic or hypomelanotic melanomas are hypo-reflective because of the lack of melanin and may appear as dark holes in the epidermis [35].

14.1.7 RCM Diagnostic Algorithms for Melanoma Diagnosis

Five main scoring systems and algorithms have been developed for the diagnosis of melanoma using RCM [1, 20, 36–41].

- The Modena algorithm: Pellacani et al. identified six RCM criteria that independently correlate with the diagnosis of melanoma and may be used to differentiate melanomas from nevi [42, 43]. The scoring algorithm is composed of two major criteria (two points each) and four minor criteria (one point each). A score greater than or equal to 3 is strongly associated with the diagnosis of melanoma (97.3% sensitivity and 72.3% specificity).
  The major criteria (+2 points per feature) are:
  - Non-edged dermal papillae
  - Atypical cells at the DEJ

  The minor criteria (+1 point per feature) are:
  - Roundish pagetoid cells
  - Pagetoid cells widespread throughout the lesion
  - Cerebriform clusters in the papillary dermis
  - Isolated nucleated cells within dermal papilla
- The Barcelona algorithm: Segura et al. [37] developed a two-step method for differentiating melanocytic from nonmelanocytic lesions and melanoma from nevi using RCM.

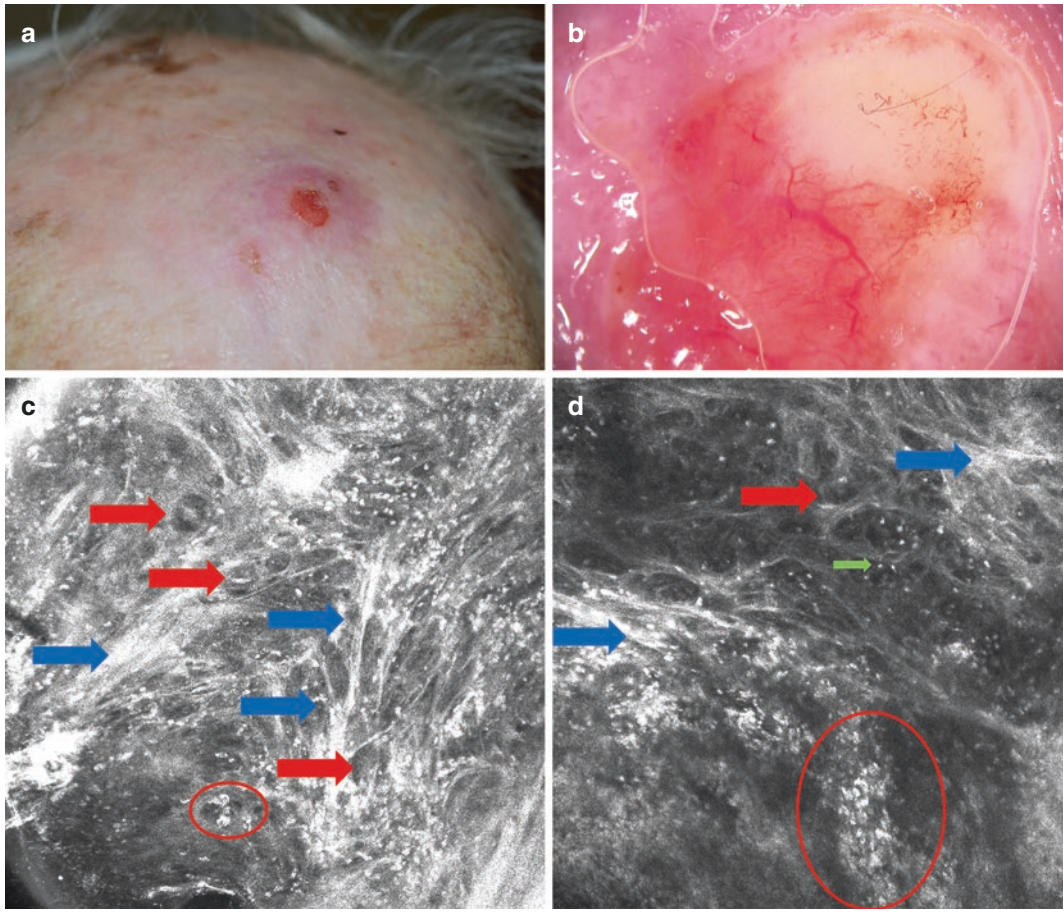

Fig. 14.5 Amelanotic nodular melanoma: clinical (**a**), dermoscopic (**b**), and reflectance confocal microscopy (RCM, **c**, **d**) images. RCM shows in the dermis nests of hypo-reflecting (*red arrows*) and hyper-reflective (*red circle*) atypical cells surrounded by collagen fibers (*blue arrows*) and isolated small hyper-reflective cells corresponding to inflammatory cells (*green arrow*). (Photographer: Elisa Cinotti, University of Siena)

The two steps are:

- Step 1: to determine if the lesion is melanocytic or nonmelanocytic. A melanocytic lesion is suspected based on the presence of at least one of four RCM features. Features of a melanocytic lesion include cobblestone pattern, pagetoid spread, meshwork appearance at DEJ and presence of dermal clusters of cells or dermal nests.
- Step 2: to determine if the lesion is a nevus or a melanoma using a scoring system. Benign features (absence of basal cell atypia and edged papillae) are given a score of −1, while malignant features (roundish pagetoid cells and atypical dermal nucleated cells) a score of +1. Lesions with a score greater than or equal to −1 have a sensitivity and specificity, respectively, of 86.1 and 95.3%, for melanoma. However, with this threshold there were five false-negative results in their study, including four in situ and one SSM, indicating the possible limitation of the algorithm in thin melanoma. A score greater than or equal to −2 had an increased sensitivity of 100% but specificity reduced to 57%. The authors calculated that, despite a lower specificity, half of biopsies could be avoided, without missing a melanoma.

- Guitera et al. [36] described a two-step method to diagnose melanoma and basal cell carcinoma (BCC). Independently significant RCM features were identified to establish the following criteria in a two-step algorithm. The first step is to determine if the lesion is a BCC by the analysis of positive and negative features.
- The second step is to determine if the lesion is a melanoma using the Modena algorithm.
- Borsari et al. [41] recently proposed a diagnostic score for melanoma in situ (MIS) combining dermoscopic and RCM features. Dermoscopic finding of atypical pigment network and regression gives 1 point each. On RCM, the observation of pagetoid cells gives 1 point and cytologic atypia 1 point if it is focal and 1 points if it is widespread. The presence of dense nests and melanophages was found to be protective of MIS and given −1 point each.
- Guitera et al. [20] developed the LM score to assist in differentiating LM from equivocal pigmented macules of the face. Six features that independently correlate with the diagnosis of LM were identified. The score consists of two major and four minor criteria. With a score more than or equal to 2 points, a sensitivity and specificity of 85 and 76%, respectively (odds ratio: 18.6; 95% CI: 9.3–37.1), were achieved for LM diagnosis. The major criteria are: non-edged dermal papillae (+2) and large round pagetoid cells (+2). The minor criteria are: nucleated cells in the dermal papillae (+1), atypical cells at the DEJ (+1), adnexal spread of atypical cells (+1), and broadened honeycomb pattern (−1).

14.1.8 Clinical Application of RCM for LM/LMM

Among all melanoma subtypes, RCM is most applicable to the management of LM and LMM due to the radial growth of this neoplasia and the limited depth penetration of RCM. Moreover, noninvasive diagnosis and identification of surgical margins are particularly important for LM/LMM because this melanoma is mainly located on esthetic and functional areas such as the face, and it may have subclinical extension.

14.1.9 Guide for Biopsies

LM/LMM often has a large surface, and a single biopsy could miss the area with the typical histological features. RCM may be used to assist in targeting the area for incisional biopsy to the most suspicious area for a correct diagnosis and for assessing the level of invasion [44].

14.1.10 Preoperative Mapping

LM/LMM has the highest risk of residual disease and highest recurrence rate of all melanoma subtypes after surgical excision [45]. RCM may allow the identification of subclinical cancer invasion [25, 46]. Presurgical mapping of the suspicious area helps surgeons planning the surgery and the eventual reconstruction. It has been used successfully intraoperatively to achieve negative surgical margins in a case of standard excision [47] and also in combination with the staged excision spaghetti technique [48, 49]. Margin delineation of LM and LMM with the handheld RCM (HRCM) could be limited by the lack of precise orientation during imaging and the small field of view in the absence of mosaics. Video mosaicking of HRCM images is a novel technique developed to overcome this limitation [50].

14.1.11 Monitoring of Nonsurgical Therapies

RCM can be used to assess response to treatment of LM/LMM and allow detection of treatment failure with better diagnostic accuracy than dermoscopy, especially after nonsurgical treatments (e.g., radiation therapy or topical imiquimod) [51, 52]. An advantage of RCM is that it enables the clinician to follow difficult cases with serial noninvasive “virtual biopsies” of the skin.

References

1. Pellacani G, Cesinaro AM, Seidenari S. Reflectance-mode confocal microscopy of pigmented skin lesions–improvement in melanoma diagnostic specificity. J Am Acad Dermatol. 2005;53:979–85.
2. Rajadhyaksha M, González S, Zavislan JM, Rox Anderson R, Webb RH. In vivo confocal scanning laser microscopy of human skin II: advances in instrumentation and comparison with Histology11The authors have declared conflict of interest. J Investig Dermatol. 1999;113:293–303.
3. Longo C, et al. Is confocal microscopy a valuable tool in diagnosing nodular lesions? A study of 140 cases. Br J Dermatol. 2013;169:58–67.
4. Rajadhyaksha M, Grossman M, Esterowitz D, Webb RH, Anderson RR. In vivo confocal scanning laser microscopy of human skin: melanin provides strong contrast. J Invest Dermatol. 1995;104:946–52.
5. Yamashita T, Kuwahara T, González S, Takahashi M. Non-invasive visualization of melanin and melanocytes by reflectance-mode confocal microscopy. J Investig Dermatol. 2005;124:235–40.
6. Stanganelli I, et al. Integration of reflectance confocal microscopy in sequential dermoscopy follow-up improves melanoma detection accuracy. Br J Dermatol. 2015;172:365–71.
7. Ferrari B, et al. Dermoscopic difficult lesions: an objective evaluation of reflectance confocal microscopy impact for accurate diagnosis. J Eur Acad Dermatol Venereol. 2015;29:1135–40.
8. Alarcon I, et al. Impact of *in vivo* reflectance confocal microscopy on the number needed to treat melanoma in doubtful lesions. Br J Dermatol. 2014;170:802–8.
9. Pellacani G, Pepe P, Casari A, Longo C. Reflectance confocal microscopy as a second-level examination in skin oncology improves diagnostic accuracy and saves unnecessary excisions: a longitudinal prospective study. Br J Dermatol. 2014;171:1044–51.
10. Guitera P, et al. In vivo reflectance confocal microscopy enhances secondary evaluation of melanocytic lesions. J Investig Dermatol. 2009;129:131–8.
11. Pellacani G, et al. Cost-benefit of reflectance confocal microscopy in the diagnostic performance of melanoma. J Eur Acad Dermatol Venereol. 2016;30:413–9.
12. Waddell A, Star P, Guitera P. Advances in the use of reflectance confocal microscopy in melanoma. Melanoma Management. 2018;5:MMT04.
13. Longo C, Pellacani G. Melanomas. Dermatol Clin. 2016;34:411–9.
14. Cicchiello M, Lin MJ, Pan Y, McLean C, Kelly JW. An assessment of clinical pathways and missed opportunities for the diagnosis of nodular melanoma versus superficial spreading melanoma: pathways for diagnosis of NM versus SSM. Australas J Dermatol. 2016;57:97–101.
15. Moloney FJ, Menzies SW. Key points in the dermoscopic diagnosis of hypomelanotic melanoma and nodular melanoma: Dermoscopy of amelanotic and nodular melanoma. J Dermatol. 2011;38:10–5.
16. Segura S, et al. In vivo microscopic features of nodular melanomas: dermoscopy, confocal microscopy, and Histopathologic correlates. Arch Dermatol. 2008;144(10):1311–20.
17. Lallas A, et al. Diagnosis and management of facial pigmented macules. Clin Dermatol. 2014;32:94–100.
18. Cinotti E, et al. Dermoscopy vs. reflectance confocal microscopy for the diagnosis of lentigo maligna. J Eur Acad Dermatol Venereol. 2018;32:1284–91.
19. Star P, Guitera P. Lentigo Maligna, macules of the face, and lesions on sun-damaged skin. Dermatol Clin. 2016;34:421–9.
20. Guitera P, et al. The impact of in vivo reflectance confocal microscopy on the diagnostic accuracy of Lentigo Maligna and equivocal pigmented and non-pigmented macules of the face. J Investig Dermatol. 2010;130:2080–91.
21. Langley RGB, Burton E, Walsh N, Propperova I, Murray SJ. In vivo confocal scanning laser microscopy of benign lentigines: comparison to conventional histology and in vivo characteristics of lentigo maligna. J Am Acad Dermatol. 2006;55:88–97.
22. Ahlgrimm-Siess V, et al. Reflectance confocal microscopy of facial lentigo maligna and lentigo maligna melanoma: a preliminary study. Br J Dermatol. 2009;161:1307–16.
23. Tannous ZS, Mihm MC, Flotte TJ, González S. In vivo examination of lentigo maligna and malignant melanoma in situ, lentigo maligna type by near-infrared reflectance confocal microscopy: comparison of in vivo confocal images with histologic sections. J Am Acad Dermatol. 2002;46:260–3.
24. Guitera P, et al. Surveillance for treatment failure of lentigo maligna with dermoscopy and *in vivo* confocal microscopy: new descriptors. Br J Dermatol. 2014;170:1305–12.
25. Guitera P, et al. Improving management and patient Care in Lentigo Maligna by mapping with in vivo confocal microscopy. JAMA Dermatol. 2013;149:692.
26. Reed JA, Shea CR. Lentigo maligna: melanoma in situ on chronically sun-damaged skin. Arch Pathol Lab Med. 2011;135:838–41.
27. Phan A, et al. Acral lentiginous melanoma: histopathological prognostic features of 121 cases. Br J Dermatol. 2007;157:311–8.
28. Cinotti E, et al. Reflectance confocal microscopy features of acral lentiginous melanoma: a comparative study with acral nevi. J Eur Acad Dermatol Venereol. 2016;30:1125–8.
29. LeBoit PE. A diagnosis for maniacs. Am J Dermatopathol. 2000;22:556–8.
30. Saida T, Koga H, Goto Y, Uhara H. Characteristic distribution of melanin columns in the cornified layer of acquired acral nevus: an important clue for histopathologic differentiation from early acral melanoma. Am J Dermatopathol. 2011;33:468–73.
31. Chen LL, Jaimes N, Barker CA, Busam KJ, Marghoob AA. Desmoplastic melanoma: a review. J Am Acad Dermatol. 2013;68:825–33.

32. Pizzichetta MA, et al. Amelanotic/hypomelanotic melanoma: clinical and dermoscopic features. Br J Dermatol. 2004;150:1117–24.
33. Menzies SW, et al. Dermoscopic evaluation of Amelanotic and Hypomelanotic melanoma. Arch Dermatol. 2008;144(9):1120–7.
34. Gill M, González S. Enlightening the Pink Dermatologic Clinics. 2016;34:443–58.
35. Losi A, et al. Hyporeflective pagetoid cells: a new clue for amelanotic melanoma diagnosis by reflectance confocal microscopy. Br J Dermatol. 2014;171:48–54.
36. Guitera P, et al. In vivo confocal microscopy for diagnosis of melanoma and basal cell carcinoma using a two-step method: analysis of 710 consecutive clinically equivocal cases. J Investig Dermatol. 2012;132:2386–94.
37. Segura S, Puig S, Carrera C, Palou J, Malvehy J. Development of a two-step method for the diagnosis of melanoma by reflectance confocal microscopy. J Am Acad Dermatol. 2009;61:216–29.
38. Langley RGB, et al. The diagnostic accuracy of in vivo confocal scanning laser microscopy compared to Dermoscopy of benign and malignant melanocytic lesions: a prospective study. Dermatology. 2007;215:365–72.
39. Gerger A, et al. Diagnostic image analysis of malignant melanoma in *in vivo* confocal laser-scanning microscopy: a preliminary study. Skin Res Technol. 2008;14:359–63.
40. Gerger A, et al. Sensitivity and specificity of confocal laser-scanning microscopy for in vivo diagnosis of malignant skin tumors. Cancer. 2006;107:193–200.
41. Borsari S, et al. *In vivo* dermoscopic and confocal microscopy multistep algorithm to detect *in situ* melanomas. Br J Dermatol. 2018;179:163–72.
42. Pellacani G, et al. The impact of in vivo reflectance confocal microscopy for the diagnostic accuracy of melanoma and equivocal melanocytic lesions. J Invest Dermatol. 2007;127:2759–65.
43. Pellacani G, Cesinaro AM, Seidenari S. Reflectance-mode confocal microscopy for the in vivo characterization of pagetoid melanocytosis in melanomas and nevi. J Invest Dermatol. 2005;125:532–7.
44. Hibler BP, et al. Handheld reflectance confocal microscopy to aid in the management of complex facial lentigo maligna. Cutis. 2017;99:346–52.
45. Bolshinsky V, et al. Frequency of residual melanoma in wide local excision (WLE) specimens after complete excisional biopsy. J Am Acad Dermatol. 2016;74:102–7.
46. Chen C-SJ, Elias M, Busam K, Rajadhyaksha M, Marghoob AA. Multimodal in vivo optical imaging, including confocal microscopy, facilitates presurgical margin mapping for clinically complex lentigo maligna melanoma. Br J Dermatol. 2005;153:1031–6.
47. Hibler BP, Cordova M, Wong RJ, Rossi AM. Intraoperative real-time reflectance confocal microscopy for guiding surgical margins of lentigo maligna melanoma. Dermatol Surg. 2015;41:980–3.
48. Champin J, et al. In vivo reflectance confocal microscopy to optimize the spaghetti technique for defining surgical margins of Lentigo Maligna. Dermatol Surg. 2014;40:247–56.
49. Couty E, et al. In vivo reflectance confocal microscopy combined with the 'spaghetti technique' for the identification of surgical margins of lentigo maligna: experience in 70 patients. J Eur Acad Dermatol Venereol. 2018;32:e366–8.
50. Kose K, et al. Video-mosaicing of reflectance confocal images for examination of extended areas of skin *in vivo*. Br J Dermatol. 2014;171:1239–41.
51. Nadiminti H, Scope A, Marghoob AA, Busam K, Nehal KS. Use of reflectance confocal microscopy to monitor response of Lentigo Maligna to nonsurgical treatment. Dermatol Surg. 2010;36:177–84.
52. Alarcon I, et al. In vivo reflectance confocal microscopy to monitor the response of lentigo maligna to imiquimod. J Am Acad Dermatol. 2014;71:49–55.

15 In Vivo Reflectance Confocal Microscopy for Nonmelanocytic Benign Skin Tumors

Francesca Farnetani, Silvana Ciardo, and Giovanni Pellacani

Benign nonmelanocytic lesions including lichen planus-like keratosis (LPLK), solar lentigo (SL), and seborrheic keratosis (SK), and dermatofibroma (DF) usually present as large pigmented macules mostly occurring on the face and sun-exposed areas. Despite their variable clinical presentation and dermoscopic aspects, the diagnosis can be challenging because they share many clinical and dermoscopic features with other skin tumors [1]. RCM can assist in differential diagnosis of these lesions especially in the presence of ambiguous dermoscopy criteria [2, 3]. RCM criteria for classic SL, SK, LPLK, and DF were defined with a perfect histopathological agreement [4].

Avoidable biopsies and excisions of benign lesions such as SL, LPLK, LM, and LMM may be misdiagnosed as benign SL, and biopsy may not be performed, missing the possibility for early diagnosis [5].

In the current chapter, we will describe only the benign epithelial tumors, because the RCM parameters for such lesions are already established with a perfect histological agreement.

Instead for adnexal tumors the main parameters have been identified, but the agreement is not yet established also for the reasons that such lesions are located deep in dermis where the power of resolution of RCM decreased [6, 7].

15.1 Solar Lentigo

SL shows on dermoscopy sharply demarcated lesion borders (moth-eaten borders), a regular pigment network, finger printing, or a so-called pseudonetwork [8].

The main RCM features of SL observable in the superficial layer are a regular honeycomb pattern without the presence of cytologic atypia.

Dermo–epidermal junction reveals densely packed edged papillae, polycyclic papillary contour, bright branching tubular structures and bulbous projections (cord-like rete ridges). In addition, multiple plump-bright cells, suggestive of aggregates of melanophages, are often found due to partial regression. Confocal criteria suggestive of a melanoma are never seen [9, 10].

The most difficoult pattern in solar lentigo by RCM is observed at dermo–epidermal junction with the presence of increase in density of dermal-papillae surrounded by a bright monomorphic layer of cells, as these papillae can assume irregular geometric shape with a rim of bright monomorphic and cytologically benign-appearing cells (Fig. 15.1) [11].

F. Farnetani (✉) · S. Ciardo · G. Pellacani
Department of Dermatology, University of Modena and Reggio Emilia, Modena, Italy

M. Fimiani et al. (eds.), *Technology in Practical Dermatology*,
https://doi.org/10.1007/978-3-030-45351-0_15

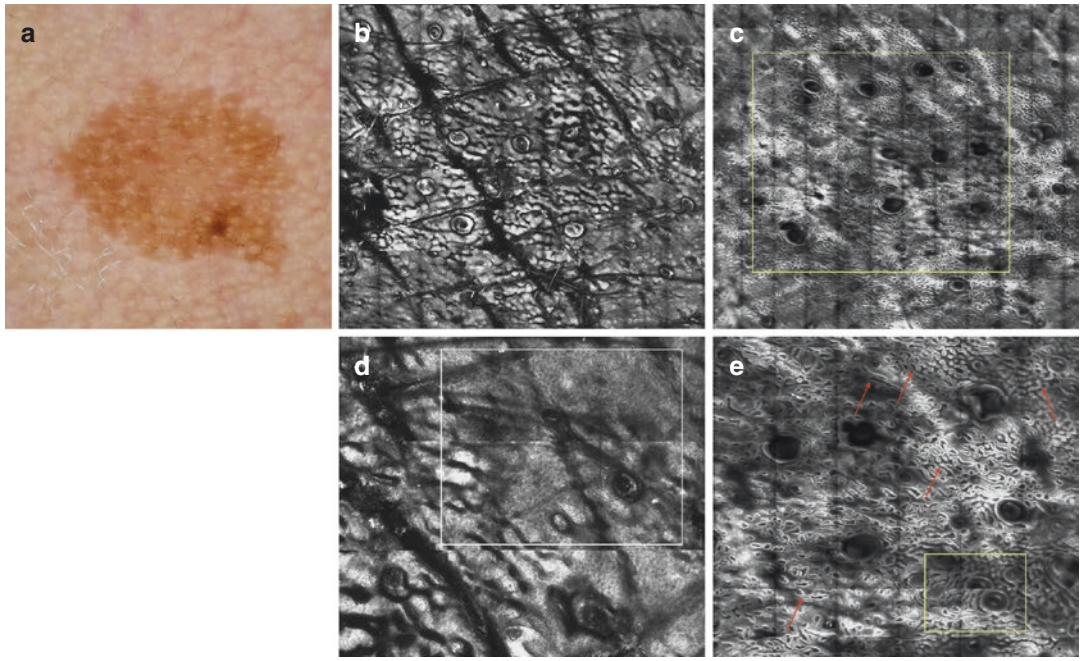

Fig. 15.1 (**a**) Solar lentigo. (**c**) RCM mosaic (6 × 6 mm) at the DEJ. Edged dermal papillae and cord-like rete ridges (*yellow rectangles*). (**b**, **d**) Typical honeycomb pattern (*white rectangles*). (**e**) At the magnification, it is possible to clearly delineate polycyclic papillary. Bright, branching tubular structures with bulbous projections (*yellow rectangles and red arrows*)

Lentigines exhibit an absence of atypical melanocytes, whereas the melanoma shows atypical, bright polymorphous atypical cells [11].

15.2 Seborrheic Keratosis

Seborrheic keratosis can present with different dermoscopic pattern, the most common dermoscopic features of SK are: sharp demarcation, ridge and cryptae, cerebriform pattern, milia-like cysts, comedo-like opening, yellowish keratin and hairpin vessels, the presence of blue black pigmentation, atypical vessels is not infrequent and therefore does not rule out melanoma [12, 13].

Different characteristics in confocal laser microscopy have been described, and the main important criteria included regular honeycombed pattern or cobblestone in epidermal layers, epidermal projection filed with keratin in epidermis, cord-like rete ridges with edged papillae at dermo–epidermal junction and the presence of abundant plump bright cells in the dermis, most of these features are detected with high sensitivity (Fig. 15.2) [14].

In a study by Siess et al., the most frequent RCM parameters for the diagnosis of SK were highlighted: epidermal projections (96%), keratin filled invaginations (80%), corneal pseudocysts (42%), melanophages (47%), and dilated vessels (47%). Pigmented SK that displayed the presence of hyperpigmented basal layer keratinocytes deserves a special mention, and the presence of these pigmented polygonal basal cells along with hyperplastic epidermis and no cytological atypia were suggestive of probable diagnosis of pigmented SK [14–16] (Fig.15.3).

Most of these features are also important parameters to make a correct diagnosis in case of SK that simulates other lesions at dermoscopy and in particular melanoma [17].

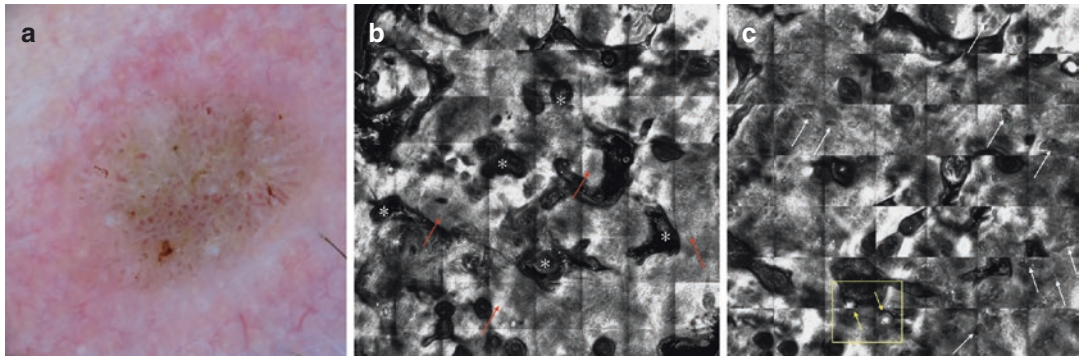

Fig. 15.2 (**a**) SK (seborrheic keratosis). (**b**) Epidermal projections with a typical honeycomb pattern (*red arrows*) and keratin-filled invaginations (*white asterisk*). (**c**) Vessels (*white arrows*) and bright reflecting horn cysts (*yellow rectangle and arrows*)

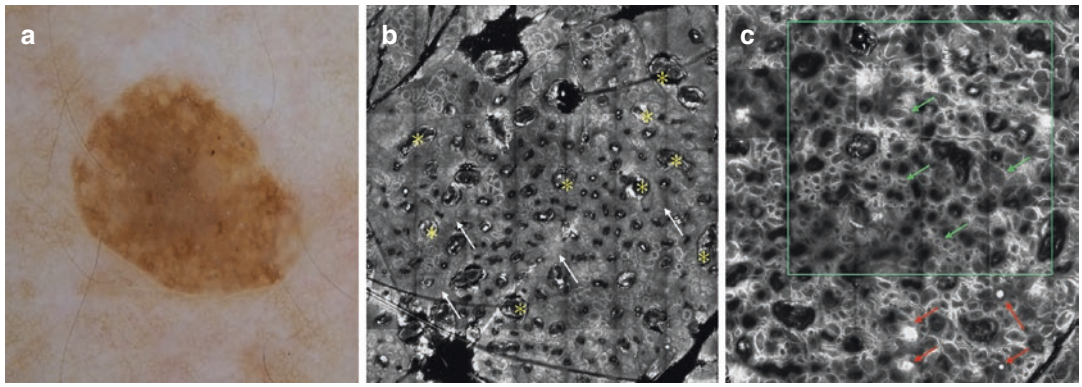

Fig. 15.3 (**a**) SK (seborrheic keratosis). (**b**) Epidermal projections with a typical honeycomb pattern (*white arrows*) and keratin-filled invaginations correlating to comedo-like openings in dermoscopy (*yellow asterisk*). (**c**) Cord-like rete ridges with bulbous projections (*green rectangle and arrows*) and bright reflecting horn cysts of variable size correlating to milia-like cysts in dermoscopy (*red arrows*)

15.3 Lichen Planus-Like Keratosis

LPLK appears like a solitary macule with subtle scaling of the lesions surface; with dermoscopy the main criteria are a diffuse annular–granular structure, with coarse gray blue granules, and dermoscopy structure of SL or SB may be additionally detected.

A the main RCM pattern are a regular epidermal architecture and eventually presence of corneal cysts and\or dark holes corresponding to comedo-like openings on dermoscopy and to keratin-filled invagination on histopathology [18].

At DEJ, according with regressive stage, RCM can include both disruption of dermal–epidermal junction or similar to SL or SK, elongated cords. In the dermis, the main criteria observed are bright nucleated cells that can be or like bright spots or like not nucleated plum bright cells [19].

When marked inflammation is present, the infiltrate is composed of bright stellate spots, and non-aggregate plum bright cells alternately increased density of plum bright cells forming aggregates that often fills the dermal papillae (Fig. 15.4).

To summarize the main RCM criteria for the diagnosis of LPLK are typical honeycomb pattern of the epidermis, elongated cords at DEJ and numerous bright spots or bright cells in the superficial dermis.

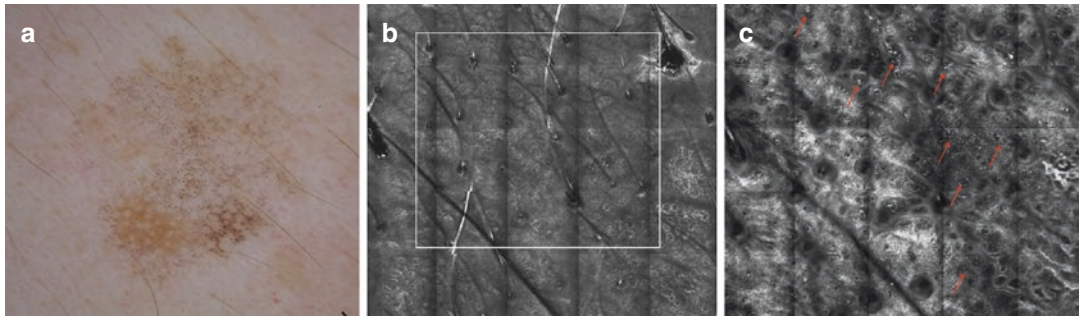

Fig. 15.4 (**a**) LPLK (liken planus-like keratosis). (**b**) Regular epidermal architecture (*white rectangles*). (**c**) Focal aggregates of melanophages correlating to *gray* granules in dermoscopy (*red arrows*)

15.4 Dermatofibroma

The most common clinical presentation of DF is a firm nodule with a color ranging from pink-red or flesh to brown, lateral pressure leads to the appearance of a depression on its surface (button-holing sign).

On dermoscopy it typically presents a central white scar-like patch consisting of a structureless area corresponding to the fibrotic area of the lesion with a symmetric peripheral pigment network.

At RCM the main criteria are typical cobblestone or honeycombed patterns at epidermis [20, 21]. At the dermo–epidermal junction, dermal papillae are seen like ring pattern, and the central white scar-like area observed on dermoscopy is seen on RCM as wider and more spaced dermal papillae [22].

References

1. Cohen LM. Lentigo maligna and lentigo maligna melanoma. J Am Acad Dermatol. 1995;33:923–36; quiz 37–40.
2. Bugatti L, Filosa G. Dermoscopy of lichen planus-like keratosis: a model of inflammatory regression. J Eur Acad Dermatol Venereol. 2007;21:1392–7.
3. de Giorgi V, Massi D, Salvini C, Sestini S, Carli P. Features of regression in dermoscopic diagnosis: a confounding factor? Two clinical, dermoscopic-pathologic case studies. Dermatol Surg. 2006;32:282–6.
4. Langley RG, Burton E, Walsh N, Propperova I, Murray SJ. In vivo confocal scanning laser microscopy of benign lentigines: comparison to conventional histology and *in vivo* characteristics of lentigo maligna. J Am Acad Dermatol. 2006;55:88–97.
5. Rajadhyaksha M, Grossman M, Esterowitz D, Webb RH, Anderson RR. In vivo confocal scanning laser microscopy of human skin: melanin provides strong contrast. J Invest Dermatol. 1995;104:946–52.
6. Propperova I, Langley RG. Reflectance-mode confocal microscopy for the diagnosis of sebaceous hyperplasia *in vivo*. Arch Dermatol. 2007;143(1):134.
7. Fraga-Braghiroli NA, Stephens A, Grossman D, Rabinovitz H, Castro RP, Scope A. Use of handheld reflectance confocal microscopy for *in vivo* diagnosis of solitary facial papules: a case series. J Eur Acad Dermatol Venereol. 2014;28(7):933–42.
8. Elgart GW. Seborrheic keratoses, solar lentigines, and lichenoid keratoses. Dermatoscopic features and correlation to histology and clinical signs. Dermatol Clin. 2001;19(2):347–57.
9. González S, Gill M, Halpern AC. Reflectance confocal microscopy of cutaneous tumors. An atlas with clinical, dermoscopic and histological correlations. London: Informa healthcare; 2008.
10. Langley RGB, Burton E, Walsh N, et al. In vivo confocal scanning laser microscopy of benign lentigines: comparison to conventional histology and in vivo characteristics of lentigo maligna. J Am Acad Dermatol. 2006;55:88–97.
11. de Carvalho N, Farnetani F, Ciardo S, Ruini C, Witkowski AM, Longo C, Argenziano G, Pellacani G. Reflectance confocal microscopy correlates of dermoscopic patterns of facial lesions help to discriminate lentigo maligna from pigmented nonmelanocytic macules. Br J Dermatol. 2015 Jul;173(1):128–33.
12. Braun RP, Rabinovitz HS, Krischer J. Dermoscopy of pigmented seborrheic keratosis: a morphological study. Arch Dermatol. 2002;138(12):1556–60.
13. Kopf AW, Rabinovitz H, Marghoob A, Braun RP, Wang S, Oliviero M, Polsky D. "Fat fingers": a clue in the dermoscopic diagnosis of seborrheic keratoses. J Am Acad Dermatol. 2006;55(6):1089–91.
14. Ahlgrimm-Siess V, Cao T, Oliviero M, et al. Seborrheic keratosis: reflectance confocal microscopy

features and correlation with dermoscopy. J Am Acad Dermatol. 2013;69(1):120–6.
15. Longo C, Zalaudek I, Moscarella E, et al. Clonal seborrheic keratosis: Dermoscopic and confocal microscopy characterization. J Eur Acad Dermatol Venereol. 2014;28(10):1397–400.
16. Busam KJ, Charles C, Lee G, Halpern AC. Morphologic fea- tures of melanocytes, pigmented keratinocytes and melano- phages by in vivo confocal scanning laser microscopy. Mod Pathol. 2001;14(9):862–8.
17. Pezzini C, Mandel VD, Persechino F, Ciardo S, Kaleci S, Chester J, De Carvalho N, Persechino S, Pellacani G, Farnetani F. Seborrheic keratoses mimicking melanoma unveiled by in vivo reflectance confocal microscope. Skin Res Technol. 2018 May;24(2):285–93.
18. Laur WE, Posey RE, Waller JD. Lichen planus-like keratosis. A clinic histopathologic correlation. A clinicohistopathologic correlation. J Am Acad Dermatol. 1981;4(3):329–33.
19. Bassoli S, Rabinovitz HS, Pellacani G, et al. Reflectance confocal microscopy criteria of lichen planus-like keratosis. J Eur Acad Dermatol Venereol. 2012;26:578–90.
20. Sánchez V, González S. Dermatofibroma. In: González S, editor. Reflectance confocal microscopy in dermatology: fundamentals and clinical applications. Madrid: Grupo aula médica; 2012. p. 113–4.
21. Moscarella E, Zalaudek I, Ferrara G, Catricalà C, Argenziano G. Potpourri of nonmelanocytic skin lesions. In: Hofmann-Wellenhoff R, Pellacani G, Malvehy J, Soyer HP, editors. Reflectance confocal microscopy for skin diseases. Berlin: Springer; 2012. p. 336–8.
22. Scope A, Ardigo M, Marghoob AA. Correlation of dermoscopic globule-like structures of dermatofibroma using reflectance confocal microscopy. Dermatology. 2008;216:81–2.

16 In Vivo Reflectance Confocal Microscopy for Non-Melanocytic Malignant Skin Tumours

Diletta Fiorani and Elisa Cinotti

16.1 Introduction

Non-melanoma skin cancer (NMSC) is the most common human malignancy in the Caucasian population with rapid increasing incidence rates [1]. Basal cell carcinoma (BCC) is four times more frequent than squamous cell carcinoma (SCC), although this ratio is inverted in immunosuppressed patients [2]. Naked-eye examination is the first screening used by clinicians for the diagnosis of NMSC, but sometimes it is not possible to distinguish a benign lesion from a malignant one. Skin biopsy for histological examination is the gold standard; however, it is painful and not suitable in patients with multiple suspicious lesions [3]. In recent years, novel non-invasive diagnostic techniques have been developed, such as dermoscopy, optical coherence tomography and reflectance confocal microscopy (RCM) [3, 4]. RCM is an imaging technique that allows in vivo real-time examination of the epidermis and superficial dermis at quasi-histologic resolution. RCM analysis contributes to ameliorate diagnostic accuracy of NMSC, sparing time for the patient and costs for the public health system [5]. Numerous studies have identified the main RCM features of skin tumours, demonstrating the good correlation of these features with certain dermoscopic patterns and histologic findings [6–9].

BCC is particularly suitable to be observed with RCM and RCM criteria, and algorithms for the diagnosis of BCC are well defined [10–12] even in clinically equivocal lesions [13]. On the contrary, keratinizing tumours such as actinic keratosis (AK) and SCC are often difficult to diagnose with RCM because the scaling surface can obscure the underlying structures, and less studies have described RCM features of AK and SCC [14]. RCM also enables to monitor the treatment of NMSC [15–17].

16.2 Basal Cell Carcinoma

Basal cell carcinoma is the most frequent tumour, and epidemiological data indicate that the overall incidence is increasing worldwide significantly by about 3–10% per year with an average lifetime risk for Caucasian to develop BCC of 30% [18, 19].

Constitutional and environmental factors are implicated in the development of BCC such as sun exposure, immunosuppression and exposure to ionizing radiation, arsenic, coal tar derivatives and oral psoralen [20].

Four major distinctive clinical-pathologic subtypes have been described: nodular, superficial, sclerodermiform and fibroepithelial (also referred as fibroepithelioma of Pinkus). Different subtypes

D. Fiorani (✉) · E. Cinotti
Dermatology Unit, Department of Medical, Surgical and Neurological Science, University of Siena, S. Maria alle Scotte Hospital, Siena, Italy

M. Fimiani et al. (eds.), *Technology in Practical Dermatology*,
https://doi.org/10.1007/978-3-030-45351-0_16

of BCC can be pigmented and can simulate melanoma [21].

Although many BCCs are clinically evident, sometimes diagnosis of BCC can be difficult, especially in those cases that do not show clear dermoscopic features. RCM increases diagnostic accuracy for BCC [22]. Although both RCM probes (Vivascope® 1500 and 3000, Caliber Imaging and Diagnostics, Rochester, NY, USA; distributed in Europe by MAVIG GmbH, Munich, Germany) demonstrated high positive predictive value, Vivascope® 1500 showed higher negative predictive value probably because its larger field of view permits a more detailed examination [23, 24].

In 2002 Gonzalez et al. described confocal features of BCC for the first time [25].

In particular, they identified the following criteria:

- Hyper-reflective islands of tumour cells often well-defined from the surrounding dermis by cleft-like spaces corresponding to mucinous stroma (Fig. 16.1) [6]

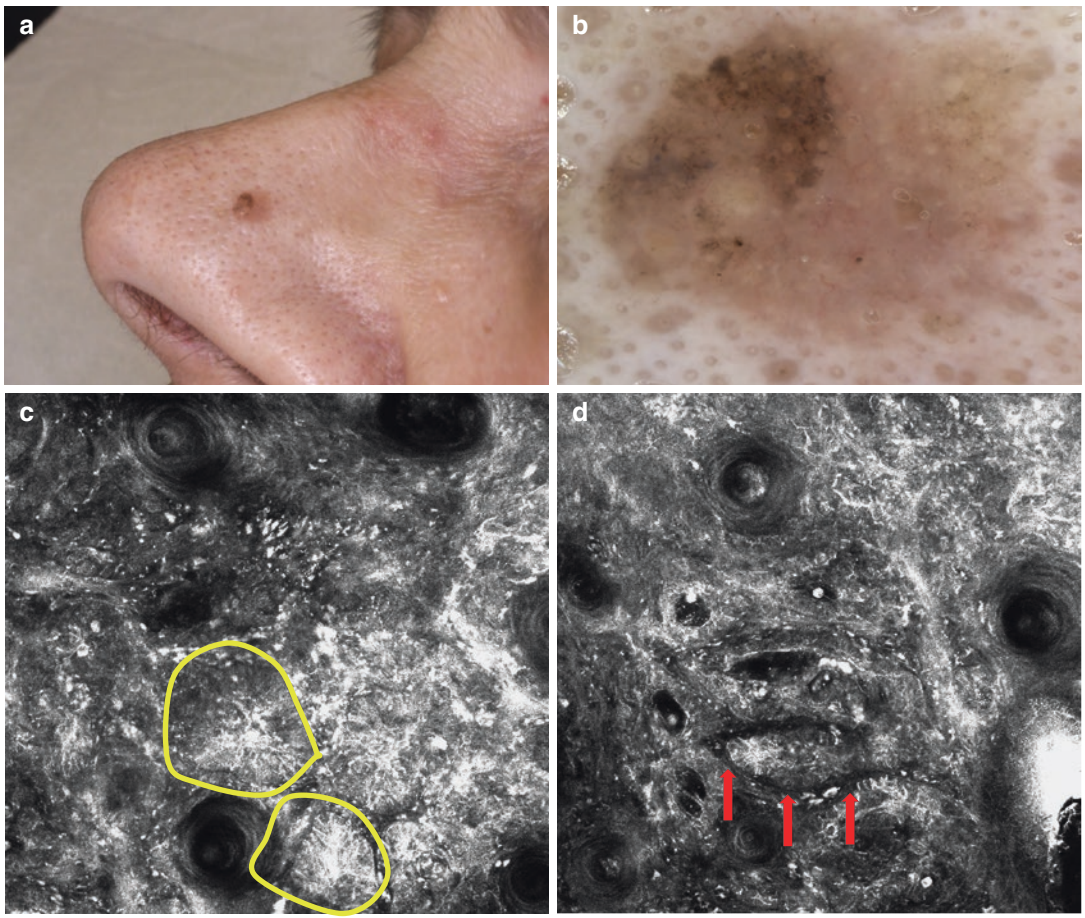

Fig. 16.1 Pigmented nodular basal cell carcinoma: clinical (**a**), dermoscopic (**b**) and reflectance confocal microscopy (**c**, **d**) aspect. Clinical image (**a**) shows a pigmented and translucent papule. Dermoscopy (**b**) shows *brown*, *black* and *grey dots* and globules, areas of *brown* and *pinkish* structureless pigmentation and fine linear vessels. Reflectance confocal microscopy shows tumour islands (**c**, *yellow circle*) with tightly packed, hyper-refractive cells with peripheral palisading of nuclei and tumour islands clearly surrounded by hypo-reflective clefts (**d**, *red arrows*). (Photographer: Elisa Cinotti, University of Siena)

- Abundant dilated blood vessels, also seen as in focus vessels in dermoscopy [26]
- Inflammatory infiltrate inside BCC islands: small bright cells corresponding to lymphocytes and neutrophils
- Keratinocyte atypia with pleomorphism, architectural disarray and parakeratotic nuclei in the stratum corneum
- Focally elongated keratinocytes with nuclei assuming a polarized appearance (*streaming*) (Fig. 16.2) [22]

More recently, additional features have been described:

- Hyper-reflective (bright) tumour islands can be oval, elongated or polycyclic cord-like structures (Fig. 16.1) [10]. Tumour islands are better visible in pigmented BCC and are composed of tightly packed, weakly to moderately reflective cells with peripheral palisading of nuclei (Fig. 16.1) [21]; pigmented islands represent nests of pigmented basaloid tumour cells on histopathology and blue-grey ovoid nests and leaf-like structures on dermoscopy [12, 27].
- Bright dendritic cells, corresponding to melanocytes and Langerhans cells, can be present inside tumour islands [12, 21, 28].
- Dark silhouette [29, 30] consisting of tumour islands that appear as footprint-like shadow in a context of bright compact collagen and are mainly found in non-pigmented BCC.
- Epidermal shadow defined as large featureless area with blurred border altering the normal architecture of epidermis and corresponding to the horizontal clefting [6].

Longo et al. [31] defined the RCM criteria of different BCC subtypes:

- Superficial BCC reveals cord-like structures connected to epidermis and polarization of nuclei in the epidermis.
- Dark silhouettes are hallmarks of infiltrative non-pigmented BCC.
- Nodular and micronodular BCC show large tumour islands with peripheral palisading and fibrotic septa; nodular BCC present more frequently peritumoural clefting, bright tumour islands and larger calibre vessels compared with superficial and infiltrative subtypes [31, 32].

Another rare variant of BCC is represented by *Fibroepithelioma of Pinkus* that usually presents as a skin-coloured papulo-nodule that can mimic intradermal nevus (Fig. 16.3) [33, 34]. Few studies have described RCM characteristics of this BCC variant: a fenestrated pattern consisting of tumour islands (often with a cord-like appearance) with palisading cells at the periphery, which surround hypo-reflective 'holes' corresponding to the fibrous stroma (Fig. 16.3) [34, 35].

Lastly, RCM represents a useful procedure to improve the identification of proper lateral margins for surgical excision in BCC with clinically and dermoscopically ill-defined margins [36, 37].

16.3 Actinic Keratosis

Actinic keratosis have historically been defined precancerous lesions because atypical keratinocytes are confined to the epidermis, although a minority think they are malignant in the same sense of Bowen disease (SCC in situ) or intraepithelial melanoma [38, 39]. They typically present on sun-damaged skin of the head, neck, trunk and extremities as rough erythematous papules covered by white to yellow scale. Advanced lesions are thicker with more visible hyperkeratosis and erythema. Clinical subtypes include the classic variant described above, hyperkeratotic, pigmented, lichenoid, atrophic, bowenoid and actinic cheilitis.

It is well known that actinic keratosis can progress to SCC, underscoring the need to identify and treat patients at risk [40]. Modern imaging techniques such as dermoscopy, RCM and high-definition optical coherence tomography may have potential to identify subclinical lesions, monitor the evolution of actinic field damage, and evaluate treatment response [41, 42].

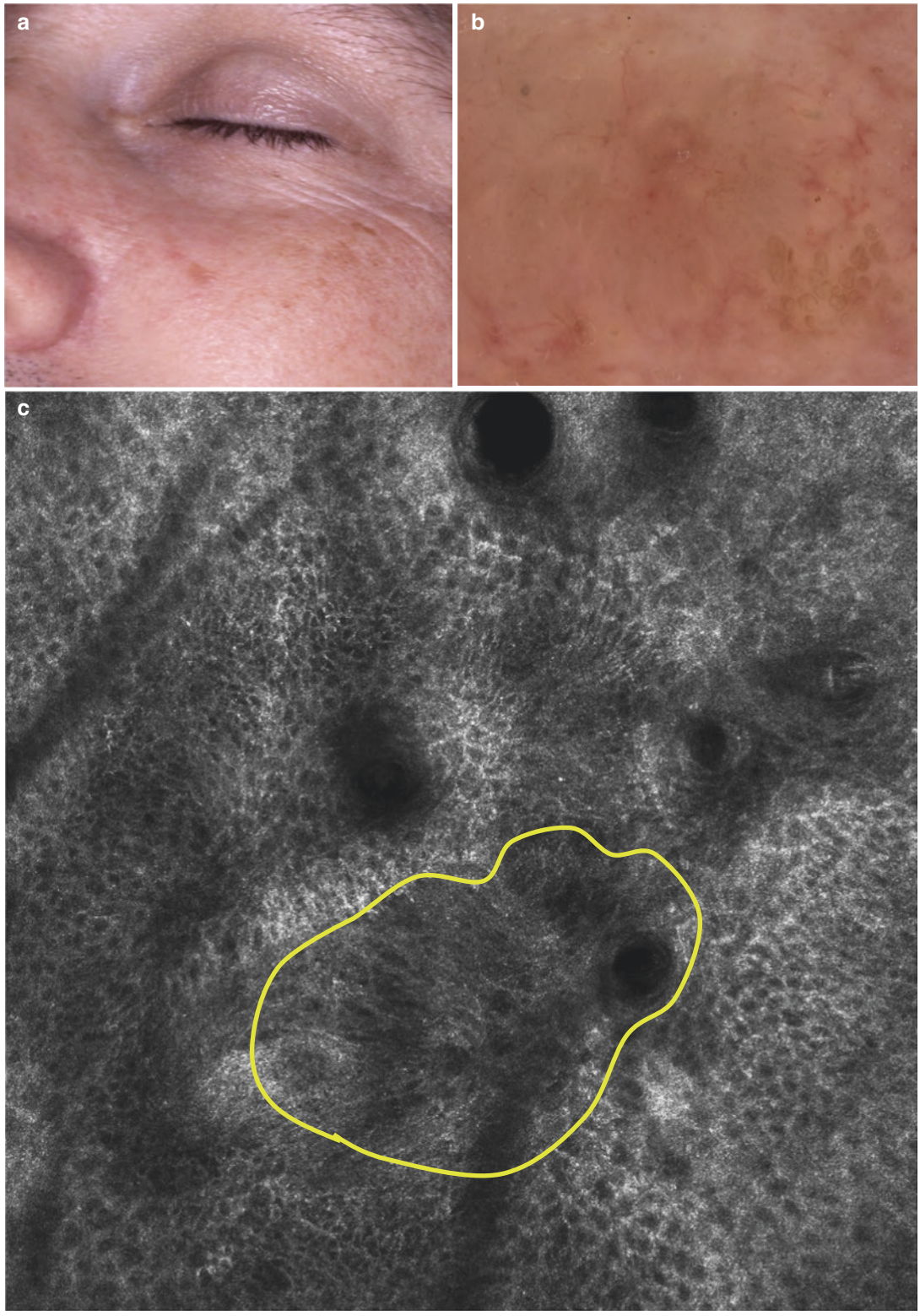

Fig. 16.2 Superficial basal cell carcinoma: clinical (**a**), dermoscopic (**b**) and reflectance confocal microscopy (**c**) aspect. Reflectance confocal microscopy shows focally elongated keratinocytes with the same parallel orientation (*yellow circle*). (Photographer: Elisa Cinotti, University of Siena)

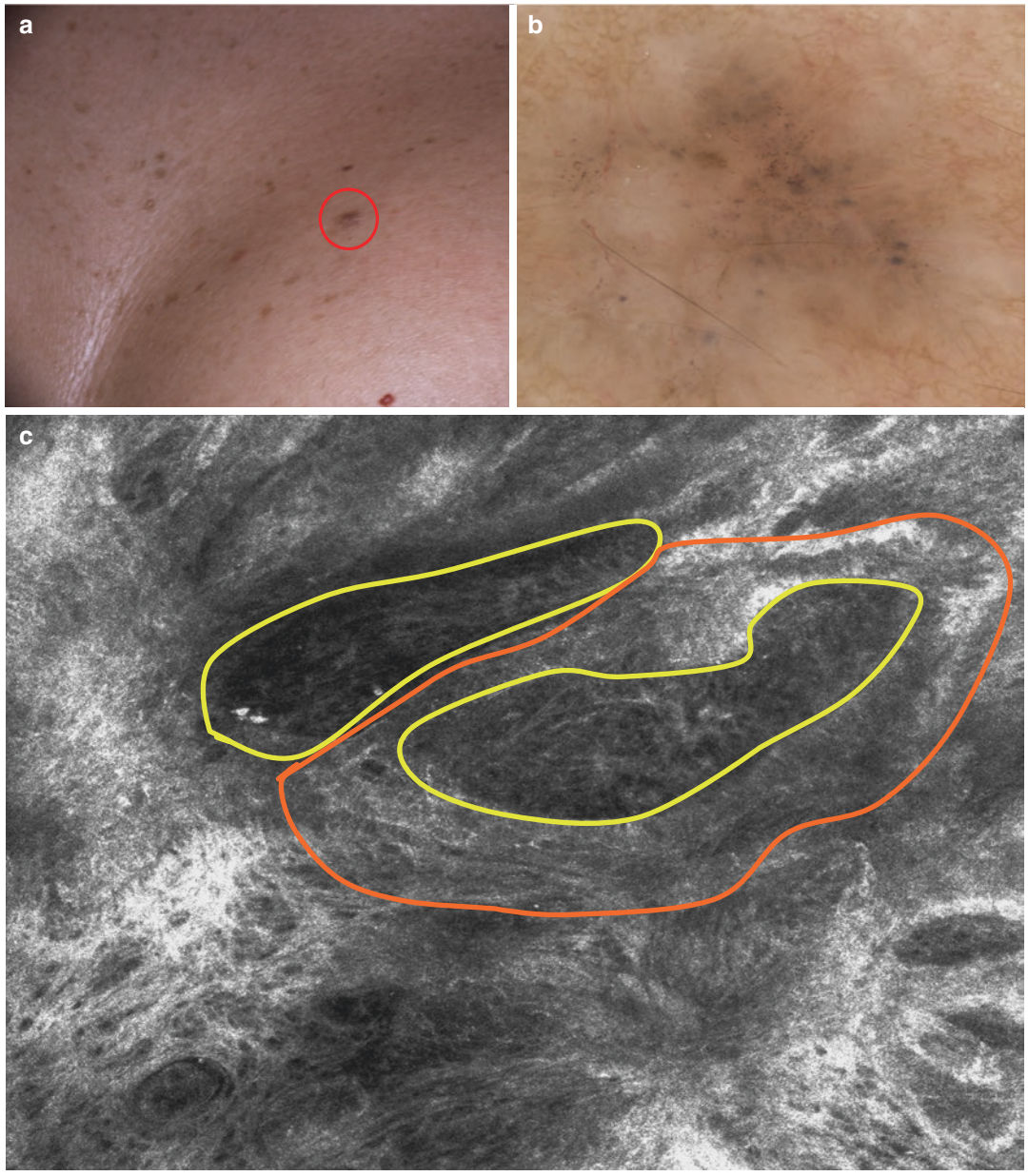

Fig. 16.3 Fibroepithelioma of Pinkus: clinical (**a**), dermoscopic (**b**) and reflectance confocal microscopy (**c**) aspect. Reflectance confocal microscopy shows a fenestrated pattern consisting of tumour islands with a cord-like appearance (*orange*) and palisading cells at the periphery, which surround hypo-refractive areas (*yellow*) corresponding to the fibrous stroma). (Photographer: Elisa Cinotti, University of Siena)

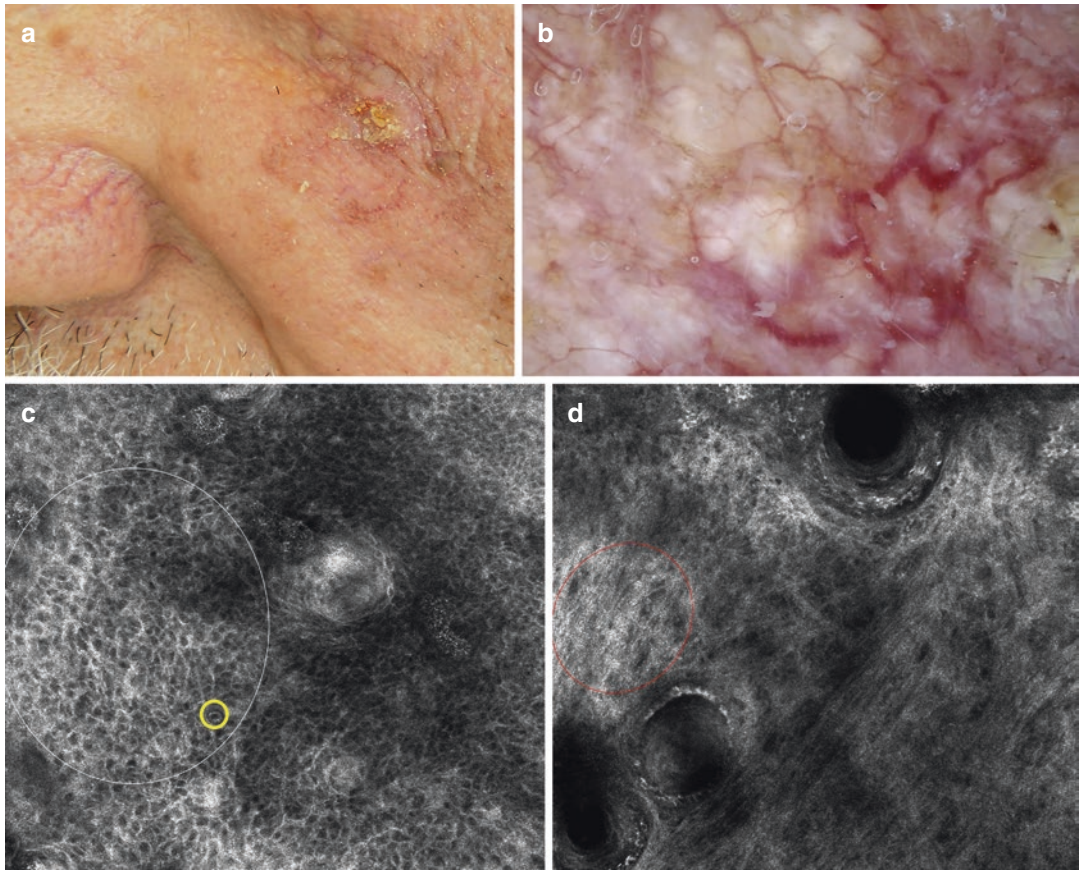

Fig. 16.4 Actinic keratosis: clinical (**a**), dermoscopic (**b**) and reflectance confocal microscopy (**c**, **d**) images. Reflectance confocal microscopy shows atypical honeycombed pattern of the epidermis (**c**) characterized by polygonal keratinocytes of different size and shape with a bright irregular contour (*white circle*) and dyskeratosis (*yellow circle*) and solar elastosis in the superficial dermis (**d**, *red circle*) with moderately refractive lace-like material adjacent to collagen bundles. (Photographer: Elisa Cinotti, University of Siena)

Several RCM features of AKs have been described:

- Hyperkeratotic centre of the lesion with detached keratinocytes that can make difficult the visualization of deeper layers [14, 43]
- Parakeratosis in the stratum corneum: keratinocytes with a hypo-reflective central nucleus [30, 44]
- Atypical honeycombed pattern of the epidermis with polygonal keratinocytes of different size and shape and bright irregular contour (Fig. 16.4) [14, 43, 45]
- Solar elastosis in the dermal layers with moderately reflective lace-like material adjacent to collagen bundle in the superficial dermis (Fig. 16.4);
- Inflammatory infiltrate characterized by lymphocytes in epidermal layers and superficial dermis
- Dilated blood vessels with erythrocytes [46]

Ulrich et al. showed that RCM features of AKs correlated well with routine histological examination [45]. Recently Pellacani et al. [47] have evaluated the correlation between keratinocyte atypia observed upon RCM and histopathology in order to develop a more objective atypia grading scale for RCM quantification:

- In grade 1 AK focal isolated areas of atypical honeycombed pattern are observed at the level of stratum spinosum.
- Grade 2 AK presents multiple and more diffuse areas of keratinocyte atypia involving stratum spinosum and granulosum.
- Grade 3 AKs shows marked atypical honeycombed pattern.

Different clinical subtypes of AK have been described with RCM.

Pigmented AK remains a frequent diagnostic challenge for clinicians because it often shows overlapping clinical and dermoscopic features with lentigo maligna/lentigo maligna melanoma [48–50]. A score has been developed in order to facilitate the diagnosis of pigmented macules of the face [51, 52]. RCM features of this difficult to diagnose lesion have been defined and are as follows:

- Presence of epidermal alterations such as atypical keratinocytes, parakeratosis, scaling
- Increased epidermal thickness
- Bright, small, dermal papillae with enlarged interpapillary spaces
- Intraepidermal and interfollicular dendritic cells referable to Langerhans cells without folliculotropism
- Absence of features suggestive of melanocytic lesions (nesting, meshwork pattern or atypical cells infiltrating the derma–epidermal junction (DEJ) and hair follicle) [53, 54]

Moreover, *hyperkeratotic AKs* represent one of the most important differential diagnoses for SCC. However, the presence of thick scale limits the visualization of deeper layers. It can be useful to apply keratolytic agents or to practice gentle superficial curettage before the evaluation [14].

On the contrary, *actinic cheilitis* can be better visualized under RCM because lips present a thinner stratum corneum. However, marked inflammation represents a potential diagnostic pitfall [55].

16.4 Squamous Cell Carcinoma

SCC is a common skin tumour derived from epidermal keratinocytes.

Bowen's disease is a form of SCC in situ that appear as an erythematous scaly patch or slightly elevated plaque that arise on sun-exposed skin of elderly people (Fig. 16.5). Histologically it is characterized by proliferation of atypical, pleomorphic keratinocytes involving the whole epidermis.

Ulrich et al. [56] have evaluated ten cases of Bowen's disease and found the following criteria:

- Superficial epidermal disruption with single detached and nucleated keratinocytes corresponding to parakeratosis (Fig. 16.5).
- Atypical honeycomb pattern at granular-spinous layer with great variations in cell and nuclear morphology involving the whole thickness of the epidermis (Fig. 16.5); two types of targetoid cells can be appreciated in the context of atypical honeycombed pattern: large cells with a hyperreflective centre surrounded by a dark halo and large cells with a dark centre and a bright rim and a surrounding dark halo. These cells correspond to dyskeratotic cells at different stages.
- Neutrophils within the stratum corneum.
- S-shaped blood vessels in the centre of dermal papillae (Fig. 16.5).

The RCM criteria for the diagnosis of *SCC* have been identified in 2009 by Rishpon et al. [14]:

- Scale and crust on stratum corneum appearing as bright reflective areas
- Parakeratosis of stratum corneum corresponding to polygonal nucleated cells
- Atypical honeycomb and/or a disarranged pattern of the stratum spinosum and granulosum of the epidermis
- Round nucleated cells in the spinosum-granular layer corresponding to dyskeratotic cells
- Round blood vessels in the superficial dermis

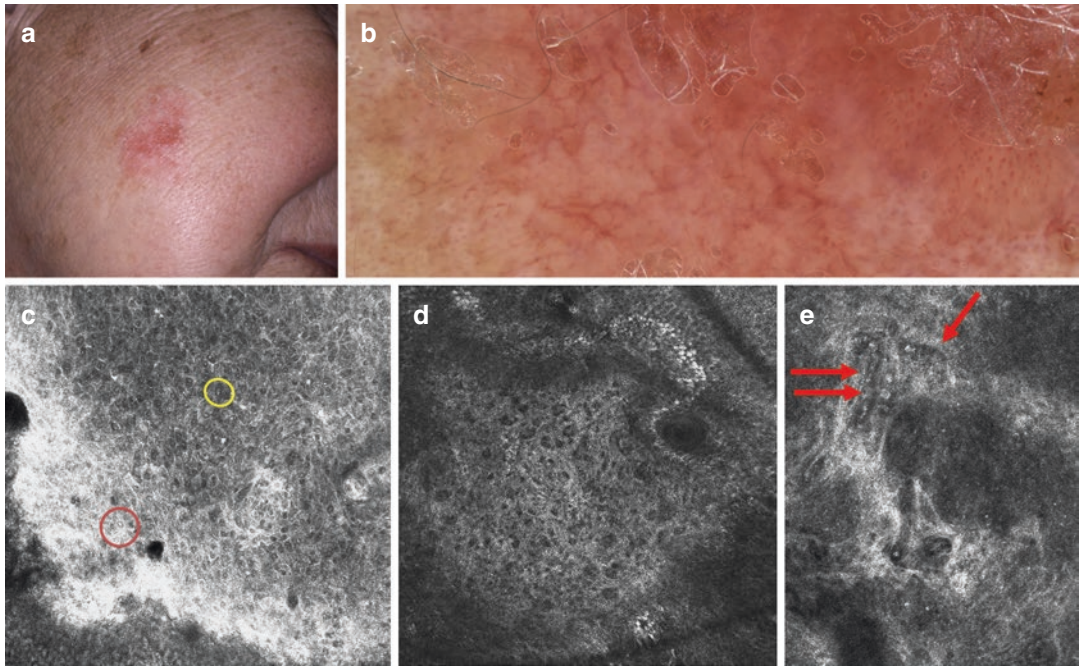

Fig. 16.5 Bowen's disease: clinical (**a**), dermoscopic (**b**) and reflectance confocal microscopy (**c**, **d**, and **e**) images. Reflectance confocal microscopy shows parakeratosis (**c**, *yellow circle*), atypical honeycomb pattern of the epidermis (**c**, **d**), targetoid keratinocytes (**c**, *red circle*, large cells with hyper-refractive centre surrounded by a *dark halo*), S-shaped vessels in the superficial dermis (**e**, *red arrows*). (Photographer: Elisa Cinotti, University of Siena)

Pigmented SCC represents a diagnostic challenge, and it is difficult to diagnose by clinical and dermoscopic examinations. RCM is useful in the differential diagnosis of melanoma [57].

Pigmented SCC is characterized by the absence of:

- Roundish or polymorphic pagetoid cells
- Non-edged papillae at DEJ or loss of the DEJ architecture
- Irregular nests of melanocytes at the DEJ or superficial dermis

It is possible to observe:

- Scale/parakeratosis
- Irregular honeycomb pattern characterized by thickened and broadened keratinocyte outlines with pleomorphic cells
- Large, round, nucleated cells at the spiny granular layer
- Spindle-shaped cells with dendritic branches infiltrating the epidermis
- Edged papillae
- Small bright spots corresponding to inflammatory cells
- Dilated looping blood vessels within dermal papillae

Notably, the presence of dendritic cells infiltrating the epidermis may erroneously lead the RCM reader to the diagnosis of melanoma [58]. However, in pigmented SCC, this dendritic cell infiltration principally involves stratum spinosum and granulosum; on the contrary, in melanoma, the infiltration of bright cells is almost always denser at the DEJ than the epidermal layers [57].

Manfredini et al. [59] have tried to evaluate if specific dermoscopic and RCM criteria can predict the diagnosis of invasive SCC vs. in situ SCC.

RCM features of invasive SCC are:

- Erosion/ulceration
- Architectural disarrangement
- Marked pleomorphism in bright and size of keratinocytes
- Speckled nucleated cells (roundish, polygonal, with a speckled appearance and a dark nucleus) in the dermis
- Atypical bright keratinizing tumour nests
- Irregularly dilated vessels

By contrast, in situ SCC shows a rich hyperkeratotic component, bottom-hole vessels inside dermal papillae and a slight architectural disarrangement.

References

1. Ridky TW. Nonmelanoma skin cancer. J Am Acad Dermatol. 2007;57:484–501.
2. Lomas A, Leonardi-Bee J, Bath-Hextall F. A systematic review of worldwide incidence of nonmelanoma skin cancer. Br J Dermatol. 2012;166:1069–80.
3. Malvehy J, Pellacani G. Dermoscopy, confocal microscopy and other non-invasive tools for the diagnosis of non-melanoma skin cancers and other skin conditions. Acta Derm Venereol. 2017;(Suppl 218):22–30.
4. Giavedoni P, Puig S, Carrera C. Non invasive imaging for nonmelanoma skin cancer. Semin Cutan Med Surg. 2016;35:31–41.
5. Ferrari B, et al. Non-melanoma skin cancer of the head and neck: the aid of reflectance confocal microscopy for the accurate diagnosis and management. G Ital Dermatol E Venereol. 2017;152:169–77.
6. Ulrich M, et al. Peritumoural clefting in basal cell carcinoma: correlation of in vivo reflectance confocal microscopy and routine histology. J Cutan Pathol. 2011;38:190–5.
7. Casari A, et al. Pigmented nodular basal cell carcinomas in differential diagnosis with nodular melanomas: confocal microscopy as a reliable tool for in vivo histologic diagnosis. J Skin Cancer. 2011;2011:406859.
8. Langley RGB, Burton E, Walsh N, Propperova I, Murray SJ. In vivo confocal scanning laser microscopy of benign lentigines: comparison to conventional histology and in vivo characteristics of lentigo maligna. J Am Acad Dermatol. 2006;55:88–97.
9. Shahriari N, Grant-Kels JM, Rabinovitz H, Oliviero M, Scope A. In vivo reflectance confocal microscopy image interpretation for the dermatopathologist. J Cutan Pathol. 2018;45:187–97.
10. Guitera P, et al. In vivo confocal microscopy for diagnosis of melanoma and basal cell carcinoma using a two-step method: analysis of 710 consecutive clinically equivocal cases. J Invest Dermatol. 2012;132:2386–94.
11. Cinotti E, et al. Sensitivity of handheld reflectance confocal microscopy for the diagnosis of basal cell carcinoma: a series of 344 histologically proven lesions. J Am Acad Dermatol. 2015;73:319–20.
12. Agero ALC, et al. Reflectance confocal microscopy of pigmented basal cell carcinoma. J Am Acad Dermatol. 2006;54:638–43.
13. Ruini C, et al. The invisible basal cell carcinoma: how reflectance confocal microscopy improves the diagnostic accuracy of clinically unclear facial macules and papules. Lasers Med Sci. 2016;31:1727–32.
14. Rishpon A, et al. Reflectance confocal microscopy criteria for squamous cell carcinomas and actinic keratoses. Arch Dermatol. 2009;145:766–72.
15. Ulrich M, Lange-Asschenfeldt S, Gonzalez S. The use of reflectance confocal microscopy for monitoring response to therapy of skin malignancies. Dermatol Pract Concept. 2012;2:202a10.
16. Venturini M, Sala R, Gonzàlez S, Calzavara-Pinton PG. Reflectance confocal microscopy allows in vivo real-time noninvasive assessment of the outcome of methyl aminolaevulinate photodynamic therapy of basal cell carcinoma. Br J Dermatol. 2013;168:99–105.
17. Couzan C, et al. Reflectance confocal microscopy identification of subclinical basal cell carcinomas during and after vismodegib treatment. J Eur Acad Dermatol Venereol. 2018;32:763–7.
18. Lear JT, Smith AG. Basal cell carcinoma. Postgrad Med J. 1997;73:538–42.
19. Roewert-Huber J, Lange-Asschenfeldt B, Stockfleth E, Kerl H. Epidemiology and aetiology of basal cell carcinoma. Br J Dermatol. 2007;157(Suppl 2):47–51.
20. Rubin AI, Chen EH, Ratner D. Basal-cell carcinoma. N Engl J Med. 2005;353:2262–9.
21. Scope A, Mecca PS, Marghoob AA. skINsight lessons in reflectance confocal microscopy: rapid diagnosis of pigmented basal cell carcinoma. Arch Dermatol. 2009;145:106–7.
22. Nori S, et al. Sensitivity and specificity of reflectance-mode confocal microscopy for in vivo diagnosis of basal cell carcinoma: a multicenter study. J Am Acad Dermatol. 2004;51:923–30.
23. Castro RP, et al. Accuracy of in vivo confocal microscopy for diagnosis of basal cell carcinoma: a comparative study between handheld and wide-probe confocal imaging. J Eur Acad Dermatol Venereol. 2015;29:1164–9.
24. Que SKT, Grant-Kels JM, Rabinovitz HS, Oliviero M, Scope A. Application of handheld confocal microscopy for skin Cancer diagnosis: advantages and limitations compared with the wide-probe confocal. Dermatol Clin. 2016;34:469–75.

25. González S, Tannous Z. Real-time, in vivo confocal reflectance microscopy of basal cell carcinoma. J Am Acad Dermatol. 2002;47:869–74.
26. Zalaudek I, et al. How to diagnose nonpigmented skin tumours: a review of vascular structures seen with dermoscopy: part II. Nonmelanocytic skin tumours. J Am Acad Dermatol. 2010;63:377–86; quiz 387–388.
27. Segura S, Puig S, Carrera C, Palou J, Malvehy J. Development of a two-step method for the diagnosis of melanoma by reflectance confocal microscopy. J Am Acad Dermatol. 2009;61:216–29.
28. Segura S, Puig S, Carrera C, Palou J, Malvehy J. Dendritic cells in pigmented basal cell carcinoma: a relevant finding by reflectance-mode confocal microscopy. Arch Dermatol. 2007;143:883–6.
29. Braga JCT, et al. The significance of reflectance confocal microscopy in the assessment of solitary pink skin lesions. J Am Acad Dermatol. 2009;61:230–41.
30. Guida S, et al. Update on the use of confocal microscopy in melanoma and non-melanoma skin cancer. G Ital Dermatol E Venereol. 2015;150:547–63.
31. Longo C, et al. Classifying distinct basal cell carcinoma subtype by means of dermatoscopy and reflectance confocal microscopy. J Am Acad Dermatol. 2014;71:716–724.e1.
32. Peppelman M, et al. In vivo diagnosis of basal cell carcinoma subtype by reflectance confocal microscopy. Dermatol Basel Switz. 2013;227:255–62.
33. Reggiani C, et al. Fibroepithelioma of Pinkus: case reports and review of the literature. Dermatol Basel Switz. 2013;226:207–11.
34. Perrot JL, et al. Contribution of reflectance confocal microscopy to the diagnosis of fibroepithelioma of Pinkus. Ann Dermatol Venereol. 2014;141:643–5.
35. Longo C, et al. In vivo confocal microscopic pattern of fibroepithelioma of pinkus. Arch Dermatol. 2012;148:556.
36. Venturini M, et al. A new approach for presurgical margin assessment by reflectance confocal microscopy of basal cell carcinoma. Br J Dermatol. 2016;174:380–5.
37. Gualdi G, Venturini M, Zanca A, Calzavara-Pinton PG, Pellacani G. Pre-surgical basal cell carcinoma margin definition: the SMART approach. J Eur Acad Dermatol Venereol. 2016;30:474–6.
38. Ackerman AB, Mones JM. Solar (actinic) keratosis is squamous cell carcinoma. Br J Dermatol. 2006;155:9–22.
39. Basset-Seguin N. The real face of actinic keratosis: field of cancerisation and squamous cell carcinoma. Eur J Dermatol. 2012;22(Suppl 1):5–9.
40. Lebwohl M. Actinic keratosis: epidemiology and progression to squamous cell carcinoma. Br J Dermatol. 2003;149(Suppl 66):31–3.
41. Ulrich M, et al. Reflectance confocal microscopy for noninvasive monitoring of therapy and detection of subclinical actinic keratoses. Dermatol Basel Switz. 2010;220:15–24.
42. Salasche SJ. Epidemiology of actinic keratoses and squamous cell carcinoma. J Am Acad Dermatol. 2000;42:4–7.
43. Ulrich M, Zalaudek I, Welzel J. Shining into the white: the Spectrum of epithelial tumours from actinic keratosis to squamous cell carcinoma. Dermatol Clin. 2016;34:459–67.
44. Actinic Keratosis and Non-Invasive Diagnostic Techniques: Biomedicines. 2018;6:8.
45. Ulrich M, et al. Clinical applicability of in vivo reflectance confocal microscopy for the diagnosis of actinic keratoses. Dermatol Surg. 2008;34:610–9.
46. Aghassi D, Anderson RR, González S. Confocal laser microscopic imaging of actinic keratoses in vivo: a preliminary report. J Am Acad Dermatol. 2000;43:42–8.
47. Pellacani G, et al. Grading keratinocyte atypia in actinic keratosis: a correlation of reflectance confocal microscopy and histopathology. J Eur Acad Dermatol Venereol. 2015;29:2216–21.
48. Zalaudek I, et al. Pitfalls in the clinical and dermoscopic diagnosis of pigmented actinic keratosis. J Am Acad Dermatol. 2005;53:1071–4.
49. Pock L, Drlík L, Hercogová J. Dermatoscopy of pigmented actinic keratosis—a striking similarity to lentigo maligna. Int J Dermatol. 2007;46:414–6.
50. Cinotti E, et al. Dermoscopy vs. reflectance confocal microscopy for the diagnosis of lentigo maligna. J Eur Acad Dermatol Venereol. 2018;32:1284–91.
51. Guitera P, et al. The impact of in vivo reflectance confocal microscopy on the diagnostic accuracy of lentigo maligna and equivocal pigmented and nonpigmented macules of the face. J Invest Dermatol. 2010;130:2080–91.
52. de Carvalho N, et al. Reflectance confocal microscopy correlates of dermoscopic patterns of facial lesions help to discriminate lentigo maligna from pigmented nonmelanocytic macules. Br J Dermatol. 2015;173:128–33.
53. Moscarella E, et al. Dermoscopy and reflectance confocal microscopy of pigmented actinic keratoses: a morphological study. J Eur Acad Dermatol Venereol. 2015;29:307–14.
54. Wurm EMT, et al. Confocal features of equivocal facial lesions on severely sun-damaged skin: four case studies with dermatoscopic, confocal, and histopathologic correlation. J Am Acad Dermatol. 2012;66:463–73.
55. Ulrich M, et al. Non-invasive diagnosis and monitoring of actinic cheilitis with reflectance confocal microscopy. J Eur Acad Dermatol Venereol. 2011;25:276–84.

56. Ulrich M, et al. Evaluation of Bowen disease by in vivo reflectance confocal microscopy. Br J Dermatol. 2012;166:451–3.
57. Shahriari N, Grant-Kels JM, Rabinovitz HS, Oliviero M, Scope A. Reflectance confocal microscopy criteria of pigmented squamous cell carcinoma in situ. Am J Dermatopathol. 2018;40:173–9.
58. Debarbieux S, et al. Reflectance confocal microscopy of pigmented Bowen's disease: misleading dendritic cells. Skin Res Technol. 2017;23:126–8.
59. Manfredini M, et al. Dermoscopic and reflectance confocal microscopy features of cutaneous squamous cell carcinoma. J Eur Acad Dermatol Venereol. 2017;31:1828–33.

17 In Vivo Reflectance Confocal Microscopy for Inflammatory Diseases

Marco Ardigo, Chiara Franceschini, and Flavia Persechino

Abbreviations

ACD	Allergic contact dermatitis
DEJ	Dermo–epidermal junction
DLE	Discoid lupus erythematosus
ICD	Irritant contact dermatitis
LP	Lichen planus
PP	Plaque psoriasis
RCM	Reflectance confocal microscopy
SD	Seborrheic dermatitis

17.1 Reflectance Confocal Microscopy: The Device

Commercially available reflectance confocal microscopy (RCM, Vivascope 1500® and Vivascope 3000®—the handheld version, Caliber-Mavig Technologies, Henrietta, New York, USA) for in vivo skin imaging operates with a diode Class 3A Laser (European version), at a wavelength of 830 nm, with power less than 35 mW at tissue level. The system includes a 30 × 0.9 NA water-immersion objective lens. Real-time RCM operates by detecting back-scattered photons from the illuminated living tissue. The contrast in confocal images is provided by reflectance index differences between cellular structures, subcellular structures, and their surroundings. Melanin and keratin have a high reflectance index and to a lesser extent white blood cells, chromatin, and dermal fibers. RCM provides cellular details that are similar to those of histopathology detectable at lower magnification. The measured lateral resolution has been shown to be around 0.5 μm and the measured axial resolution around 3.5 μm. Immersion oil or water has to be applied on the skin lesion in order to have a refractive index close to that of the stratum corneum. The immersion lens requires to be used with water/water-gels placed between the window and objective lens with a refractive index close to that of the epidermis. The handheld RCM, thanks to its ergonomic and the optic structure, does not need to be connected, as the standard confocal microscope, by an adhesive window to the skin, but can be moved free on the skin surface enabling to access "difficult" body sites with curved anatomic structures (nose, hear) that are inaccessible to the standard version of RCM. Moreover, the intrinsic horizontal, in vivo RCM approach to the tissue supports the evaluation of the skin layer by layer from the top of the stratum corneum to the upper dermis at the depth of around 250 μm. In specific, in order to obtain

M. Ardigo (✉) · C. Franceschini · F. Persechino
Clinical Dermatology, San Gallicano Institute IRCCS, Rome, Italy
e-mail: marco.ardigo@ifo.gov.it

M. Fimiani et al. (eds.), *Technology in Practical Dermatology*,
https://doi.org/10.1007/978-3-030-45351-0_17

informative features about all the skin layers detecting the specific changes descriptive for the different inflammatory entities, the correct RCM acquisition method is generally made by four mosaics (moving from 1 × 1 mm to 8 × 8 mm) taken respectively at the level of the stratum corneum, the spinosum, the dermo–epidermal junction (DEJ), and the upper dermis. One or more stacks (vertical sectioning of the skin) moving from the stratum corneum to the deep limit of imaging has been required in order to evaluate specific single microscopic criterion related to the thickness of the different skin layers. Moreover, during real-time imaging, video registrations can be acquired for analysis and record of dynamic processes such as blood flow in dermal vessels. Typically, leukocytes can be seen rolling through the vessel lumen (Fig. 17.1).

17.2 Reflectance Confocal Microscopy: From Skin Cancer to Inflammatory Diseases

RCM is a noninvasive tool for microscopic evaluation of the skin that is prevalently used for skin tumor diagnosis and clinical decision management with prevalent application on melanocytic lesions [1]. RCM provides a sort of "virtual" skin biopsies offering detailed microscopic changes of the different skin layers with an en-face approach to the tissue providing cellular-level resolution close to conventional histopathology. Recently, prospective studies demonstrated that the systematic use of RCM, generally applied as a second-level examination in skin melanocytic and non-melanocytic tumors, improves diagnostic

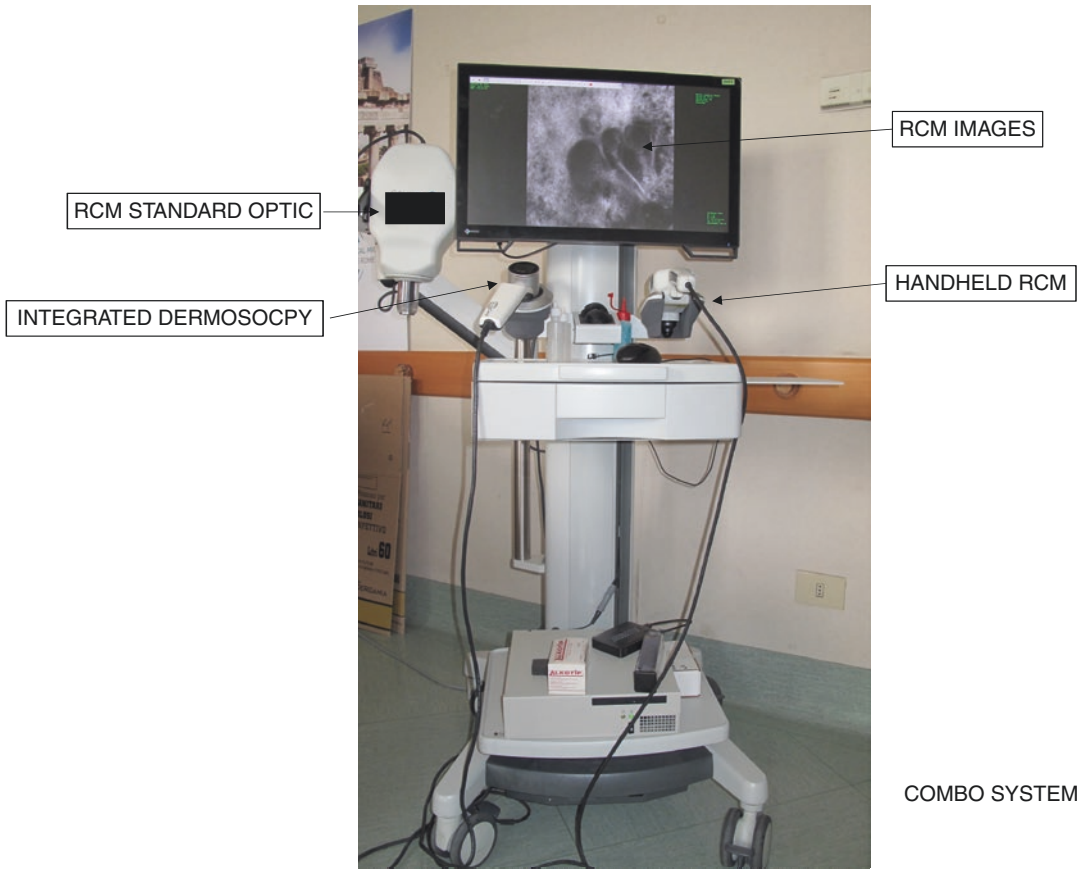

Fig. 17.1 Commercially available confocal microscope and its components

accuracy [2]. Data collected disclosed the potential of RCM as an alternative noninvasive, real-time diagnostic method for a prehistologic diagnosis to be used for a better patient management. Higher sensitivity and specificity values in comparison to the standard methods as dermoscopy have been demonstrated for RCM, and in particular, some confocal criteria for melanocytic and non-melanocytic lesions have been identified. For these reasons, in the last years, RCM became a widespread method used for the reduction of unnecessary biopsies for histopathologic examination [3, 4]. If in the field of dermato-oncology RCM has been proved to provide information related to the nature of the skin lesions and its malignant potential, in inflammatory skin diseases RCM is still under study and has been prevalently tested for the clinical microscopic correlation providing in real-time microscopic features for clinical diagnosis confirmation. More in detail, during the last 10 years, RCM has been used for the evaluation of several inflammatory skin conditions such as psoriasis, contact dermatitis, seborrheic dermatitis, lichen planus, and contact dermatitis showing the possibility of the identification of specific confocal features supporting the clinical diagnostic suspect useful for patient management, treatment definition, and clinical follow-up [3]. Data related to confocal microscopy of single inflammatory skin diseases and focus on confocal–histology correlation, therapeutic follow-up, and only rarely on differential diagnosis have been published to date in the literature till now. Larger comparative studies demonstrating the effective diagnostic and differential diagnosis value of RCM in these fields are still needed, but preliminary multicenter studies have been already performed on a significant number of cases. In this chapter, a detailed description of the RCM features related to the most common inflammatory skin disease, useful for the differentiation between the three main inflammatory diseases groups: psoriasiform, spongiotic, and interface dermatitis are described.

17.3 Clinical Applications in Inflammatory Skin Diseases

Similarly, to stand histology approach, application of RCM on inflammatory diseases based on the description of the histologic pattern and collection of RCM images showing microscopic feature involving the stratum corneum, epidermis, and superficial dermis have been described. In literature, using a defined pattern analysis method, RCM has been applied to inflamed skin by the examiner in order to collect features defining the three main categories of inflammatory diseases: psoriasiform dermatitis, interface dermatitis, and spongiotic dermatitis. Starting from the common classification of inflammatory skin diseases, psoriasiform dermatitis refers to the inflammatory skin processes characterized clinically by scales and erythema and microscopically showing an epidermal pattern characterized by thickening of the stratum corneum and of the epidermis associated with a pattern of the epidermis defined as papillomatosis characterized by the elongation of the rete ridge. The prototypic diseases of this group are plaque psoriasis (PP) and seborrheic dermatitis (SD) that are characterized by a similar clinical presentation and similar microscopic changes that differs in distribution and amount of the single features. Differently, the group of interface dermatitis includes those skin inflammatory dermatoses characterized by an inflammatory process that involves prevalently the dermo–epidermal junction (DEJ), with damage of basal cell keratinocytes due to the inflammatory process with necrosis of keratinocytes, associated with vacuolar changes of the DEJ or lichenoid (band like) distribution of the inflammatory process in the upper dermis just below the basal layer of the epidermis. In this group of conditions, the prototypic and most common diseases are represented by lichen planus (LP) and discoid lupus erythematosus (DLE). The latter group is represented by the spongiotic dermatitis that are characterized by the presence of inter- or

intracellular edema and infiltration of the epidermis due to inflammatory cells and perivascular inflammation at the level of the upper dermis. The commonly diagnosed interface dermatitis are irritant contact dermatitis (ICD) and allergic contact dermatitis (ACD). In the clinical practice, in most of the cases, the use of RCM lets the clinician/confocalist to consider the skin lesion as one of previous mentioned groups thanks to the identification of the major RCM descriptors of patterns of descriptors specific for one of the inflammatory diseases suspected. Later, in order to better define the differential diagnosis between inflammatory diseases belonging to the same group, the collection of additional criteria involving the different skin layers can better orient the diagnosis (Fig. 17.2). The sensitivity and specificity of the method increased proportionally with the number of RCM features composing the pattern of the clinically suspected skin disease detectable in the lesion.

17.4 Description of the RCM Features of the Main Groups of Inflammatory Skin Diseases and the Distinctive Patterns Useful for Differential Diagnosis

17.4.1 Spongiotic Dermatitis

The main descriptor for spongiotic dermatitis on optical histology is the detection of intraepidermal spongiosis associated with the presence of inflammatory cells into the epidermis diffused or

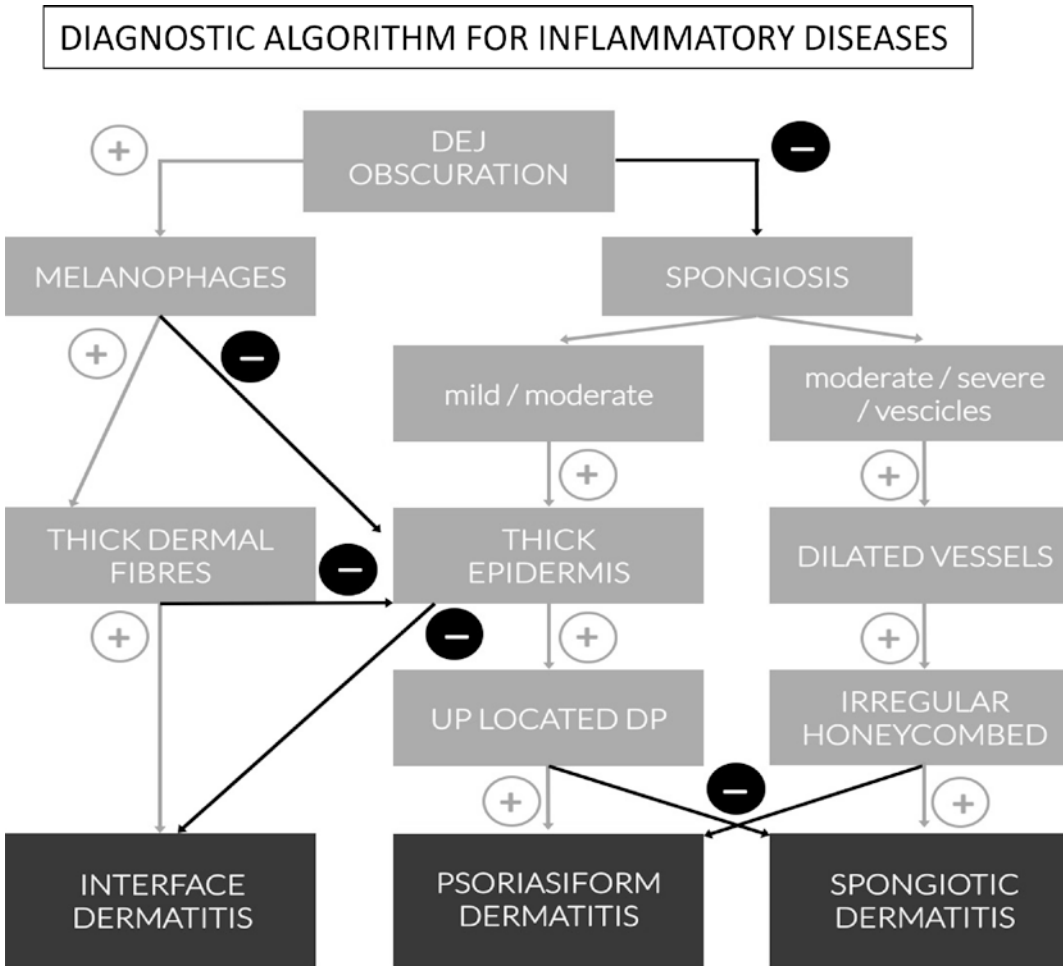

Fig. 17.2 Algorithm for the diagnosis of inflammatory skin conditions using RCM in inflammatory skin diseases

in clusters forming intra-epidermal vesicles. Several inflammatory processes can show mild to moderate spongiosis, but the prevalence of this feature is a characteristic of spongiotic dermatitis. In this case, the semi-quantitative estimation of the severity of the spongiosis (moderate to severe till the massive spongiosis) has to be more considered as more indicative for an acute spongiotic dermatitis. Moreover, absence of interface changes as well as signs referring to papillomatosis, typically detected respectively in interface dermatitis and psoriasiform dermatitis, helps to confirm the clinical suspect of spongiotic dermatitis. In the case of spongiotic dermatitis, on RCM, spongiosis is detectable as dark areas at the level of the epidermis in comparison with the surrounding epithelium, with broadband intercellular spaces and associated with round to oval bright cellular structures between keratinocytes spaces corresponding to inflammatory cells. When spongiosis is massive, as in the case of intra-epidermal vesicle, this aspect is detected on RCM as well-demarcated dark spaces between granular and spinous keratinocytes, filled by "floating" inflammatory cells. Hyper-refractile cellular structures corresponding to necrotic keratinocytes can also be visualized inside the vesicles floating in the dark area of the vesicle [5]. Moreover, in spongiotic dermatitis, RCM can reveal disrupted corneum layer and detached corneocytes. Individual corneocytes may appear as detached and highly refractile polygonal cellular structures corresponding clinically to subtle desquamation that reflects the loss cohesiveness between corneocytes generally in response to contact irritants agents. Differentiation between ICD and ACD is generally difficult on the basis of clinical presentation. This differentiation can be done with RCM through the analysis of the changes involving the stratum corneum during time. In detail ICD reaction shows a pronounced superficial disruption of the stratum corneum after exposure to contact irritants (<24 h); this is generally absent in ACD. In the dermal compartment, dilated vessels and dermal inflammation can be visualized representing a secondary confocal feature in both ICD and ACD [6, 7]. ICD and ACD differ in their kinetic evolution: ICDs have typically a more rapid onset and shows a faster recovery compared to ACDs. Moreover, it has also been demonstrated that RCM allows the detection of subclinical reaction to in lab application of antigens when clinical features are absent or subtle, thereby verifying clinical readings of patch test (Fig. 17.3).

17.4.2 Psoriasiform Dermatitis

The most common psoriasiform inflammatory skin disorders are PP and SD. In literature, most of the papers have been focused on the description of the confocal features of those conditions, on the use of RCM in the therapeutic follow-up and in the descriprion of the impact of a drug on the specific confocal microscopic changes characterizing the inflammatory disease. PP is a chronic inflammatory skin disease characterized on histopathology by acanthosis, hyperkeratosis, papillomatosis, an increased vascularization, and variable infiltration of lymphocytes and polymorphonucleated cells into the skin tissue. RCM has been demonstrated to be able to provide imaging of the whole stratum corneum and epidermis with the possibility of upper dermis evaluation through the DP window. For that reason, RCM lets the evaluation of all the skin compartments involved by the pathological process with valuable histopathology correlates and good reproducibility between observer and high grade of correspondence. Moreover, thanks to the possibility of detailed microscopic changes follow-up, recent studies on PP and other inflammatory skin diseases confirmed the usefulness of RCM for in vivo evaluation of therapeutic follow-up and disease progression in PP. RCM descriptors of psoriasiform dermatitis are characterized by the presence of thickened epidermis (>60–80 μm), to be considered according to the different skin sites involved by the lesion and the skin type of the patient, as the main confocal feature. Moreover, considering the superficial layers, thickening of the stratum corneum can be detected (>20–40 μm). Hyperkeratosis can be seen in association of RCM with the presence of high refractive round to polygonal structures inside the stratum corneum corresponding to parakeratosis.

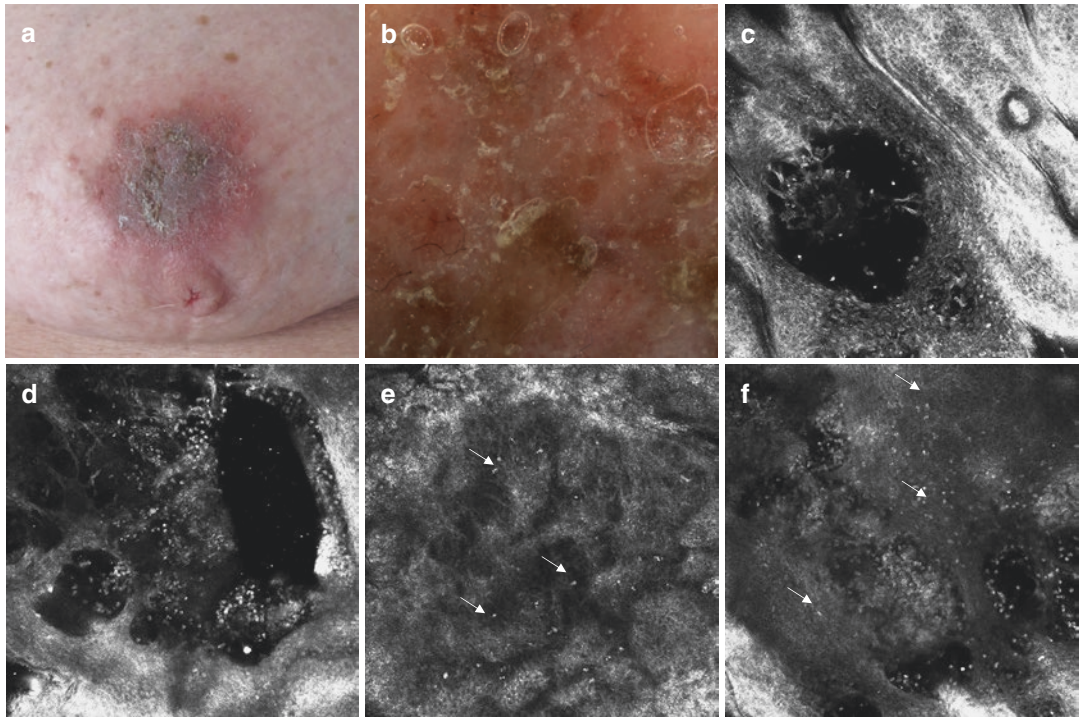

Fig. 17.3 Example of spongiotic dermatitis. Eczema of the nipple (**a**), dermoscopy (**b**), RCM (**c**–**f**), showing spongiotic vesicle (**c**, **d**), disruption of the stratum corneum with inflammatory cells (*arrows*) (**e**), spongiosis with inflammatory cells (*arrows*) (**f**)

Detection and measurement of thickening of stratum corneum and epidermis can be evaluated on RCM using the stack software analysis; in particular, the number of single frames needed to move from the first cellulated layer of the epidermis to the DEJ can calculate epidermal acanthosis. Differently, hyperkeratosis can be measured counting stack images needed to move from the top of the stratum corneum and progressing deeper in 3–5 μm step to the first cellulated epidermal layer [8] (Fig. 17.4). Moreover, considering the secondary RCM descriptors for PP useful for the definition of a confocal pattern, up located, enlarged dermal papillae with thin interpapillary epidermal spaces are commonly detected as signs of elongation of the rete ridges (papillomatosis). Differently, in SD papillomatosis is also detectable, but is generally more irregular. Moreover, different amount of spongiosis can be seen in SD in comparison to PP. This feature can be used as support for the differential diagnosis between PP and SD. In PP, at the level of the upper dermis, prominent dark canalicular structures filling the dermal papillae are detectable in a vertical orientation. Differently dilated vessels, but horizontally oriented and mainly located around adnexal structures, are commonly detected SD and can also be used for differential diagnosis. Finally, detection of *Demodex folliculorum* located in the ostium of the sebaceous glands has been reported exclusively for SD on RCM. This is consistent with the hyper-seborrhea characterizing SD that sustains *Demodex folliculorum* in opposition to the high keratinocyte turnover of PP that contrast their proliferation [9].

17.4.3 Interface Dermatitis

The term interface dermatitis refers to skin inflammatory processes in which inflammatory cells involve the DEJ causing focal or diffuse involve-

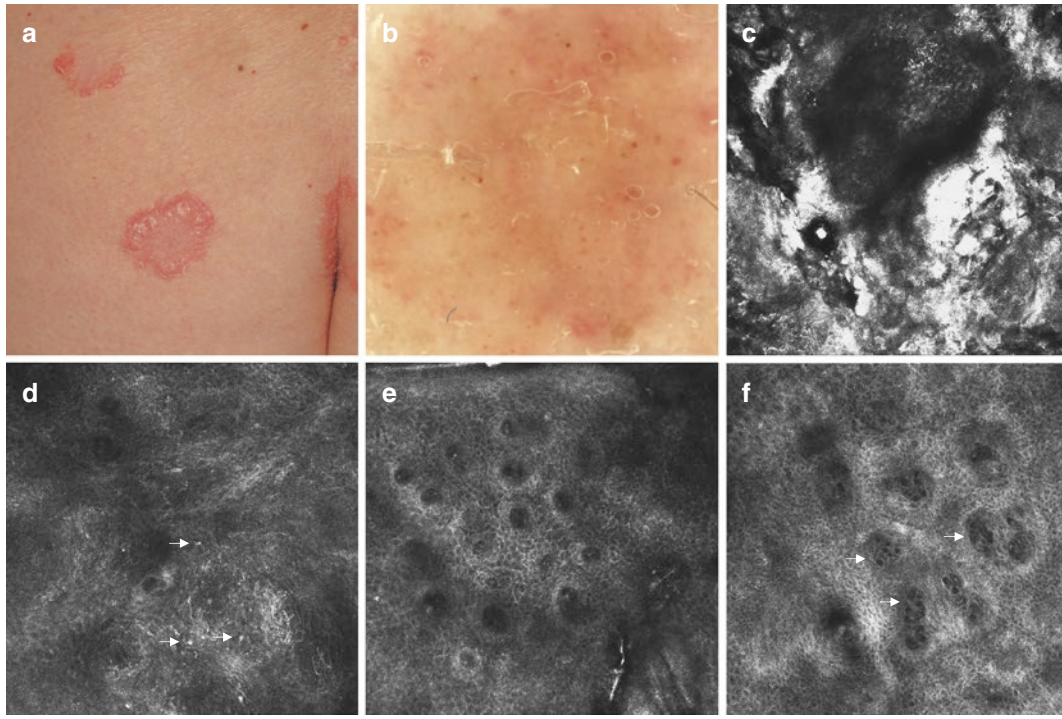

Fig. 17.4 Example of psoriasiform dermatitis. Plaque psoriasis on the back (**a**), dermoscopy (**b**), RCM (**c**–**f**), showing hyperkeratosis (**c**), mild spongiosis with inflammatory cells (*arrows*) (**d**), papillomatosis (**e**), dilated vertically oriented vessels (*arrows*) (**f**)

ment of the keratinocytes of the basal layer of the epidermis with obscuration of the DEJ and necrosis. DLE and LP are the prototypes and the most common diseases of this group of inflammatory conditions. On standard histology, DLE is characterized by the presence of an interface involvement detectable as focal vacuolar changes at the basal membrane of the epidermis; LP typically shows a band-like (lichenoid) infiltrate at the level of the upper dermis with erosion of the basal layer [10]. RCM have been used for the evaluation of interface dermatitis demonstrating the possibility to detect the major signs of DEJ involvement. In detail, on RCM, both histologic features of lichenoid and vacuolar inflammatory changes can be visualized as the presence of multiple refractive cells obscuring the papillary rims that are respectively uniformly distributed along the lesion in LP and more focally distributed in DLE. In detail, in interface dermatitis, the papillary rims are obscured by the presence of the inflammatory cells with obliteration of the ring-like structures around dermal papillae that appeared as not still detectable and not surrounded by the bright rims usually seen in normal skin. The interface involvement is generally associated with the presence of polygonal, plump bright cellular elements, usually without a visible nucleus, located in the upper dermis corresponding to melanophages. As secondary RCM features characterizing interface dermatitis, inflammatory cells can also be detected at the level of the epidermis as well as in the upper dermis around vessels and especially around adnexal structures in DLE. Generally, a prevalence of melanophages can be seen in late stage lesions [11]. When the lesion involves the scalp, adnexal structure infiltration represents the main expression of the interface change, and in lichen plano-pilaris, it can be the prevalent location of the inflammatory cell infiltration. Detection of a more prominent thickening of the dermal fibers as sign of scar evolution of the late stage of the process is more distinctive and characteristic for DLE (Fig. 17.5).

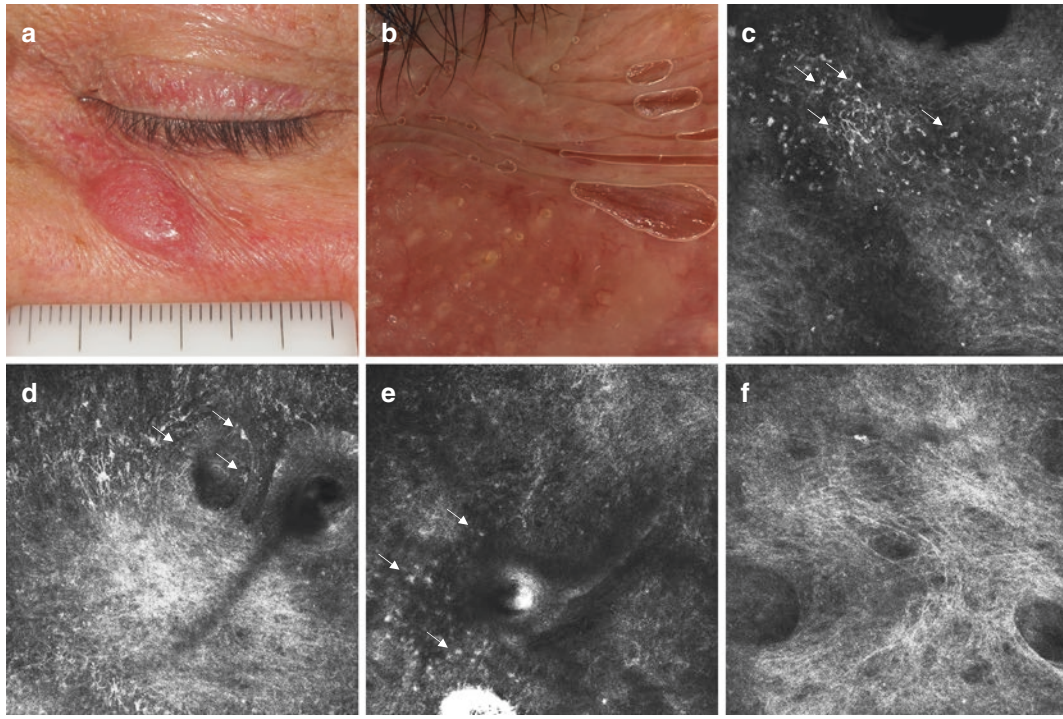

Fig. 17.5 Example of interface dermatitis. Discoid lupus erythematosus (**a**), dermoscopy (**b**), RCM (**c**–**f**), showing inflammatory cells infiltration of the epidermis (*arrows*) (**c**), inflammatory cells infiltrating the adnexal structures (*arrows*) (**d**), DEJ obscuration due to the presence of inflammatory cells and melanophages (*arrows*) (**e**), thickening of the dermal fibers as sign of dermal scar (**f**)

17.4.4 Therapeutic Follow-Up and Biopsy Site Selection

Once descriptive parameters for specific entity are defined. The progressive normalization of the aspects can be used for the therapeutic response assessment. Several examples are reported in literature such as psoriasis and scalp alopecia. Not only the recovery of normal tissue but also the lack of response to drug has been reported in literature with description of the changes due to the direct ecctc of the active on the microscopic pattern of the disease [12–18]. Inflammatory skin diseases are characterized by different phase of the lesion with an acute phase, a longstanding phase, and a post-inflammatory phase. A typical example is represented by LP that has an acute phase in which it is possible to detect all the changes characterizing the condition and a late stage in which only dermal melanophages are detectable. In order to reduce the number of useful skin biopsy provided to the pathologist, selectin of the site of the biopsy can be performed using RCM.

17.5 Limits

RCM application on inflammatory skin can be difficult in relation to different anatomical sites, specific characteristic of the lesion itself, or the intrinsic nature of the inflammatory condition. Palm and sole are characterized physiologically by the presence of hyperkeratosis and acanthosis epidermis that limit the penetration of the light and determinate a high backscattering of the light with severe limits in confocal imaging. All the hyperkeratotic processes have to be preventively treated with keratolytic ointment before confocal examination in order to reduce the backscattering of light letting the light penetrate into the tissue. Similarly, in ulcerated tissue (due to erosions or

scratches) fibrin, coagulated blood and keratin aggregates can limit significantly the examination. In that case, only peri-ulcer tissue can be examined with confocal microscopy with limited data collection. When granulomatous diseases (granuloma anularis, lupus vulgaris, sarcoidosis) or deep inflammatory processes (lupus tumidus, deep fungal infections) are suspected, those conditions cannot be evaluated using confocal microscopy because of the limit of penetration to the upper dermis during the examination.

References

1. Langley RG, Rajadhyaksha M, Dwyer PJ, Sober AJ, Flotte Thomas J. Anderson Rox R confocal scanning laser microscopy for benign and malignant melanocytic lesions in vivo. J Am Acad Dermatol. 2001;45:365–76.
2. Guida S, Longo C, Casari A, Ciardo S, Manfredini M, Reggiani C, et al. Update on the use of confocal microscopy in melanoma and non-melanoma skin cancer. G Ital Dermatol Venereol. 2015;150(5):547–63.
3. González S. Confocal reflectance microscopy in dermatology: promise and reality of non invasive diagnosis and monitoring. Actas Dermosifiliogr. 2009;100(Suppl. 2):59–69.
4. Farnetani F, Scope A, Braun RP, Gonzalez S, Guitera P, Malvehy J, et al. Skin cancer diagnosis with reflectance confocal microscopy: reproducibility of feature recognition and accuracy of diagnosis. JAMA Dermatol. 2015;151(10):1075–80.
5. Gonzalez S, Gonzalez E, White WM, Rajadhyaksha M, Anderson RR. Allergic contact dermatitis: correlation of in vivo confocal imaging to routine histology. J Am Acad Dermatol. 1999;40:708–13.
6. Astner S, Gonzalez S, Gonzalez E. Non invasive evaluation of allergic and irritant contact dermatitis by in vivo reflectance confocal microscopy. Dermatitis. 2006;17:182–91.
7. Windells K, Burnett N, Rius-Diaz F, Gonzalez E, Mihm MC, Gonzalez S. Reflectance confocal microscopy may differentiate acute allergic and irritant contact dermatitis in vivo. J Am Acad Dermatol. 2004;50:220–8.
8. Ardigo M, Cota C, Berardesca E, González S. Concordance between in vivo reflectance confocal microscopy and histology in the evaluation of plaque psoriasis. J Eur Acad Dermatol Venereol. 2009;23:660–7.
9. Agozzino M, Berardesca E, Donadio C, Franceschini C, de Felice CM, Cavallotti C, et al. Reflectance confocal microscopy features of seborrheic dermatitis for plaque psoriasis differentiation. Dermatology. 2014;229:215–21.
10. Moscarella E, González S, Agozzino M, Sánchez-Mateos JL, Panetta C, Contaldo M, et al. Pilot study on reflectance confocal microscopy imaging of lichen planus: a real-time, non-invasive aid for clinical diagnosis. J Eur Acad Dermatol Venereol. 2012;26:1258–65.
11. Ardigo M, Maliszewski I, Cota C, Scope A, Sacerdoti G, Gonzalez S, et al. Preliminary evaluation of in vivo reflectance confocal microscopy features of discoid lupus erythematosus. Br J Dermatol. 2007;156:1196–203.
12. Białek-Galas K, Wielowieyska-Szybińska D, Dyduch G, Wojas-Pelc A. The use of reflectance confocal microscopy in selected inflammatory skin diseases. Pol J Pathol. 2015;66(2):103–8. Review
13. Ardigo M, Agozzino M, Longo C, Conti A, Di Lernia V, Berardesca E, et al. Psoriasis plaque test with confocal microscopy: evaluation of different microscopic response pathways in NSAID and steroid treated lesions. Skin Res Technol. 2013;19:417–23.
14. Ardigò M, Agozzino M, Longo C, Lallas A, Di Lernia V, Fabiano A, et al. Reflectance confocal microscopy for plaque psoriasis therapeutic follow up during an anti-TNF-α monoclonal antibody: an observational multicentre study. J Eur Acad Dermatol Venereol. 2015;24:2363–8. [Epub Ahead Of Print]
15. Wolberink EA, van Erp PE, de Boer-van Huizen RT, van de Kerkhof PC, Gerritsen MJ. Reflectance confocal microscopy: an effective tool for monitoring ultraviolet B phototherapy in psoriasis. Br J Dermatol. 2012;167:396–403.
16. Başaran YK, Gürel MS, Erdemir AT, Turan E, Yurt N, Bağci IS. Evaluation of the response to treatment of psoriasis vulgaris with reflectance confocal microscopy. Skin Res Technol. 2015;21(1):18–24.
17. Agozzino M, Donadio C, Franceschini C, Ardigò M. Therapeutic follow-up of lichen Planopilaris using in vivo reflectance confocal microscopy: a case report. Skin Res Technol. 2015;21(3):380–3.
18. Hoogedoorn L, Peppelman M, van de Kerkhof PC, van Erp PE, Gerritsen MJ. The value of in vivo reflectance confocal microscopy in the diagnosis and monitoring of inflammatory and infectious skin diseases: a systematic review. Br J Dermatol. 2015;172(5):1222–48.

18 In Vivo Reflectance Confocal Microscopy for Infectious Diseases

Luca Provvidenziale, J. L. Perrot, and Elisa Cinotti

18.1 Introduction

Reflectance confocal microscopy (RCM) is a high-resolution noninvasive imaging technique, which optically sections the living tissue at various depths, to image horizontal layers of the skin and appendages with resolution at a cellular level and without alteration of the tissue surface. The use of RCM in dermatology was first described roughly 30 years ago [1, 2] and was initially focused on the diagnosis of skin cancers, but a rising number of other indications have been later described among which the diagnosis and management of infectious dermatological disorders. RCM has a lateral resolution of 1.25 μm and an axial resolution of 5 μm [1, 2]. This means that structures with bigger size than 1.25 μm could theoretically be studied. Most skin parasites are well visible under RCM because they are large and sometimes also visible to naked eye. Fungi responsible for superficial mycoses of the skin are generally visible under RCM. Virus could not be identified because they are too small. However, viral cytopathic effects can be observed in vivo on keratinocytes [3–5]. Among bacteria only *Treponema pallidum* has been identified [6].

L. Provvidenziale (✉) · E. Cinotti
Department of Medical, Surgical and Neurological Science, Dermatology Section, University of Siena, S. Maria alle Scotte Hospital, Siena, Italy

J. L. Perrot
Department of Dermatology, University Hospital of Saint Etienne, Saint-Etienne, France
e-mail: j.luc.perrot@chu-st-etienne.fr

18.2 Reflectance Confocal Microscopy for Parasitosis

Sarcoptes scabiei [7–14] (Fig. 18.1), *Demodex folliculorum* [7, 8, 15–18], *Pyemotes ventricosus* [19], *Cimex lectularius* [20], *Dermanyssus gallinae*, and Ixodes [21] (Fig. 18.2) have been identified using RCM.

The optical microscopic examination of a specimen obtained from skin scraping is the reference technique to recognize parasites, eggs, and/or droppings in case of scabies. However, this technique is time consuming and can give false-negative results [22]. Currently, this method is frequently replaced by dermoscopy, which shows the "delta-wing jet" sign that consists in the cephalic portion of *S. scabiei* and its furrow [9] (Fig. 18.1b). Nevertheless, this sign is sometimes hard to detect, and some locations such as inter-digital spaces, one of the most affected sites, are impossible to be explored by the dermoscope due to the excessive tip size [10]. The identification of *S. scabiei* by RCM was first reported in 2005 [9], and the introduction of the handheld camera allowed the use of this technique for the diagnosis of scabies in clinical routine [10, 11]. Under RCM, *S. scabiei* presents with an

M. Fimiani et al. (eds.), *Technology in Practical Dermatology*,
https://doi.org/10.1007/978-3-030-45351-0_18

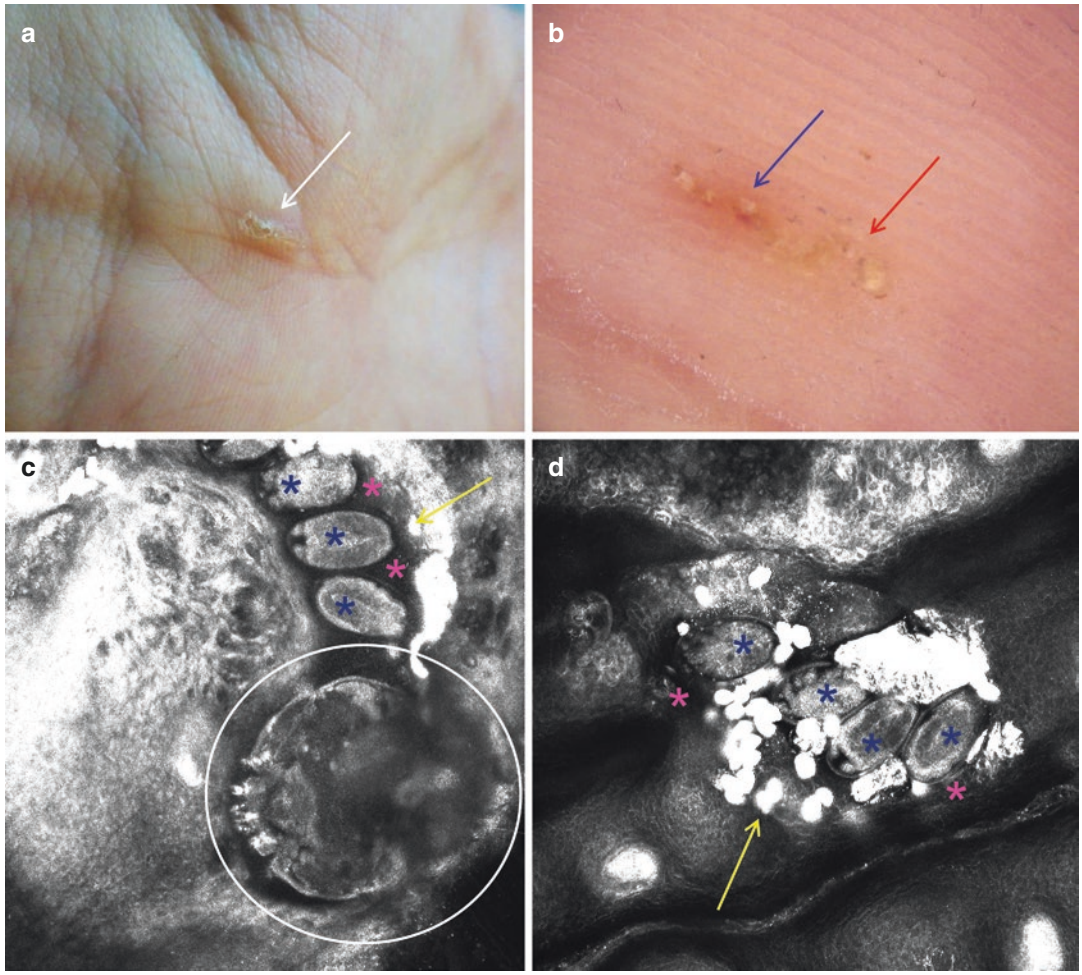

Fig. 18.1 Clinical (**a**), dermoscopical (**b**), and reflectance confocal microscopy (**c**, **d**) aspect of a case of scabies. Cutaneous burrow (**a**, *white arrow*). Dermoscopy shows the "delta wing sign," a triangular brown structure corresponding to the fore portion of the *Sarcoptes scabiei* (**b**, *red arrow*) usually found at the end of a burrow (*blue arrow*). Reflectance confocal microscopy shows *Sarcoptes scabiei* as an inhomogeneously refractive ovoid body (**c**, *white circle*) with hypo-refractive eggs (**c**, **d**, *blue asterisk*) and hyper-reflective droppings (**c**, **d**, *yellow arrow*). (Photographer: Elisa Cinotti, University Hospital of Santa Maria alle Scotte, Siena)

inhomogeneously refractive ovoid body and short legs [11, 14] (Fig. 18.2c). Adult females are 400 × 300 μm in size, while males are just over half this size [11, 14].

Eggs are hypo-refractive, 200 × 100 μm, and have ovoid structures with a hyper-refractive thin wall [11, 14] (Fig. 18.1c, d). Furthermore, although the morphology of different developmental stages of *S. scabiei* is similar, examination by RCM allows to distinguish adults from larvae based on their size (larvae are smaller than adults) and number of pairs of legs (four pairs of legs for adults and three pairs of legs for larvae) [11]. Droppings are easily identified as they are superficial hyper-reflective roundish bodies of around 15 μm in diameter that can be a useful marker of a nearby presence of an adult parasite [14] (Fig. 18.1c, d).

Unlike dermoscopy, RCM can be used for the follow-up after treatment, due to its non-invasive real-time examination that allows to distinguish living mites from the dead ones as all the vital functions of the parasites are visible, from intestinal peristalsis to defecation [10, 12, 23].

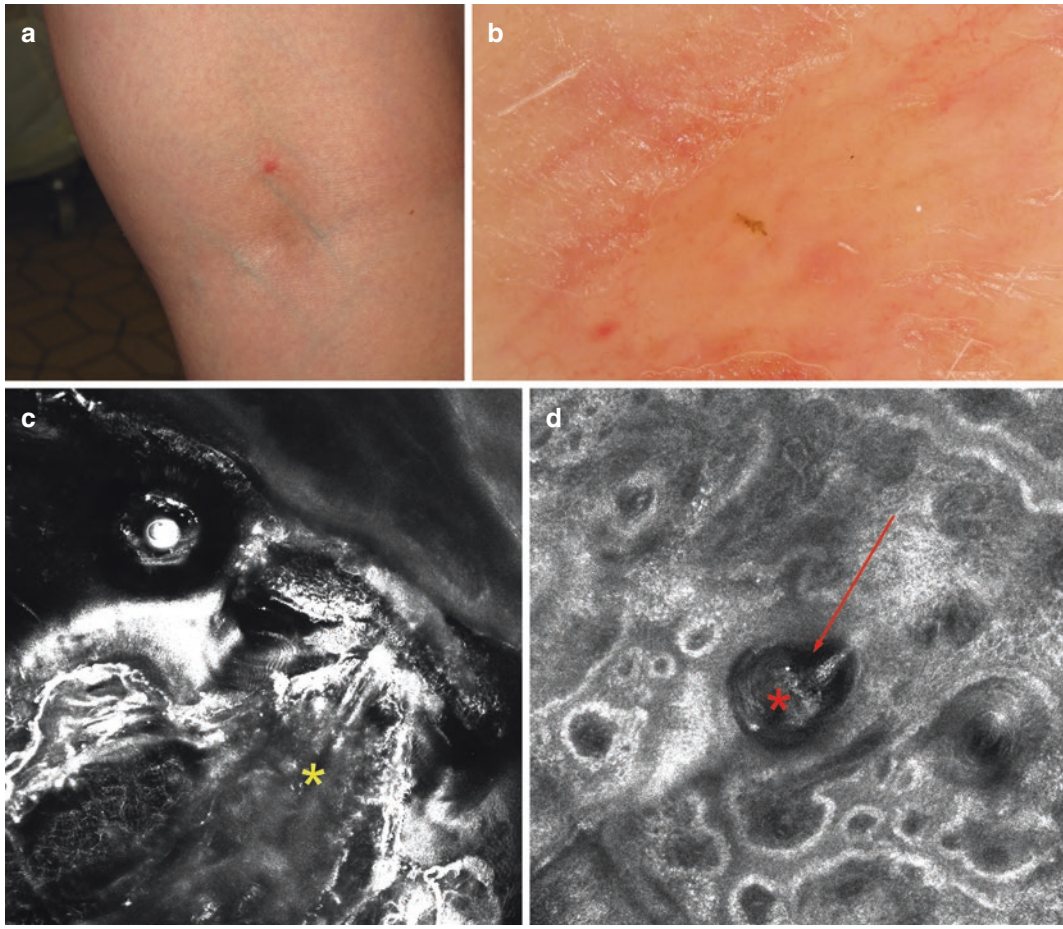

Fig. 18.2 Remnant of a tick identified by clinical (**a**) and dermoscopical (**b**) examination is confirmed by reflectance confocal microscopy (**c**, **d**) that can identify different segments of the parasite such as the rostrum (**c**, *yellow arrow*) or a part of the body (**d**, *red asterisk*) inside a skin hole (*red arrow*). (Photographer: Elisa Cinotti, University Hospital of Santa Maria alle Scotte, Siena)

Moreover, dead parasites can be identified not just because they do not move but also because they have a hyper-reflecting appearance, with blurred edges and homogenization of internal structures [11]. A recent study that compared the diagnostic accuracy of the sequence videodermoscopy followed by RCM and RCM followed by videodermoscopy for the diagnosis of scabies in 148 patients found that if the two devices are available, it is better to perform videodermoscopy first, that is, more sensitive, and then RCM to confirm the diagnosis [24]. Videodermoscopy offers a larger field of view, whereas RCM has the capacity of being able to clearly differentiate living from dead parasites in case of posttreatment follow-up. The parasitological confirmation of scabies is crucial for patients, environmental hygiene, and prevention measures. RCM is also suitable for pathophysiological studies, being able to reveal the exact localization of parasites, their eggs and droppings in the epidermis, and their activity over time. It even allows to count them [14].

Demodex mites are involved to play a pathogenic role when they are present in excessive number and are implicated in several skin conditions such as rosacea, demodecidosis, and pityriasis folliculorum [7, 15, 16, 18, 25, 26]. Until

now, the gold-standard diagnostic test to detect Demodex mites and confirm the diagnosis of related dermatitis has been the standardized superficial skin biopsy (SSSB) technique, which utilizes cyanoacrylate glue on a glass slide to extract the content of facial hair follicles. Nevertheless, this technique may cause discomfort to the patient. RCM can identify all the mites directly on the skin, inside the follicle, reaching mites that are hidden inside the elongated and hyper-keratotic follicles and that would not be counted on SSSB [16, 27].

Demodex folliculorum is easy to be recognized by RCM, lying upside down within the follicular infundibulum and appearing as a small (5 μm in diameter) round body with a hyper-reflective contour, corresponding to the horizontal section of the parasite, or as a lengthy cone-shaped structure when it met a little sideways [7, 8, 15] (Fig. 18.3). Multiple parasites are usually assembled within the same hair follicle. *Demodex brevis* has not been identified by the reflectance confocal microscope dedicated to dermatology [26]. However, Randon et al. [28] have detected *D. brevis* with the help of the ophthalmologic reflectance confocal microscope: the parasite was seen at the very bottom of the follicle or inside the meibomian glands meatus.

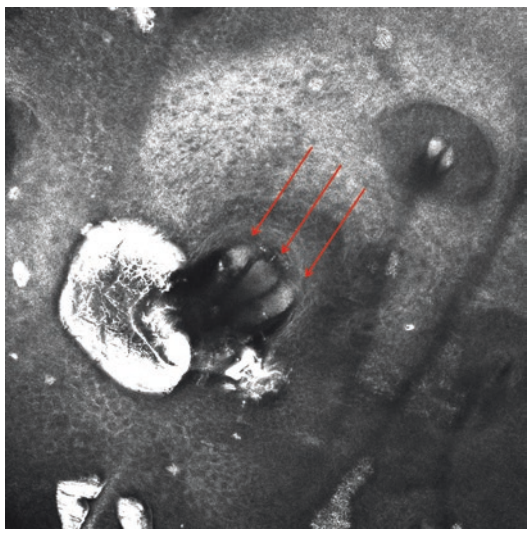

Fig. 18.3 Under reflectance confocal microscopy, *Demodex folliculorum* appears as a small round body with a hyper-reflective contour (*red arrow*), corresponding to the horizontal section of the parasite. Multiple parasites are grouped within the same hair follicle. (Photographer: Elisa Cinotti, University Hospital of Santa Maria alle Scotte, Siena)

RCM has also been used to identify *Pyemotes ventricosus*, an ectoparasite of arthropod larvae invading furniture [19]. This parasite is responsible for a pruritic erythematous rash with maculopapules with a central microvesicle sometimes associated with lymphangitis. RCM showed an ovoid body of intermediate reflectance with morphological features suggestive of *P. ventricosus* inside a cutaneous microvesicle of an infested patient [19]. However, the quality of the published image does not allow confirming that the RCM image corresponds to this parasite.

Cutaneous leishmaniasis has also been observed under RCM [29, 30]: a dermal inflammatory infiltrate with multinucleated cells was visible. RCM could also study the anatomical details of some parasites that are visible to the naked eye, such as ticks and lice. Besides, RCM can be used to differentiate either the hypostome [21] or other tick body parts on the skin from a simple hemorrhagic crust or a traumatized hyperpigmented skin lesion. Using RCM, we can also identify the skin hole caused by the sting of an insect by allowing to quickly differentiate insect bites from other inflammatory dermatoses [31].

18.3 Reflectance Confocal Microscopy and Superficial Mycosis

Conventional techniques to confirm the clinical diagnosis of superficial mycosis are direct light microscopic examination and fungal culture. The first can give false-negative results in case of low fungal load or sampling error, whereas the latter is time consuming. In vivo RMC has been recently used for the diagnosis of dermatophytosis with the convenience of (1) being noninvasive, (2) requiring no skin sample for ex vivo analysis, (3) being performed on the spot without any previous preparation, and (4) evaluating the whole lesion surface and not just the scales removed for a conventional ex vivo analysis.

Moreover, RCM can allow to confirm the diagnosis of dermatophytosis during the dermatological consultation and to initiate an appropriate treatment without waiting for the conventional mycological examination [32–36]. Dermatophytes under RCM in the skin, the nail plate, and hairs appear as thin, high-reflective, and longitudinal structures with a serpentine shape [32, 37, 38] (Fig. 18.4).

The identification of fungi requires experience because fungi can be misdiagnosed for cell membranes of keratinocytes and inversely. However, a better diagnostic accuracy of in vivo RCM than conventional microscopic examination has been found in a prospective trial on 50 toes suspicious of onychomycosis (sensitivity 79 vs. 74% and specificity 81 vs. 76%) [39] and in a trial on 55 patients affected by tinea corporis (sensitivity 89.1 vs. 80.0%) [40].

Recent studies confirmed the high specificity of RCM [33, 41] but underlined a lower sensitivity for both onychomycosis (52.9% of sensitivity in a series of 58 patients) [33] and skin dermatophytosis (64% of sensitivity in 22 patients with tinea manus and pedis; 83% of sensitivity in 23 cases of tinea cruris) [41].

Our group recently demonstrated the possibility of RCM use to identify not only filaments but also conidia, which corresponds to roundish hyper-reflective bright structures [38]. The RCM aspect of yeasts in onychomycosis has been reported only by Arrese et al. [42], while few cases of nail infestation by molds have been included in the series of Pharaon et al. [33], but no specific features are reported. In our experience, it is possible to identify Candida's pseudofilaments and/or conidia on oral mucosa (Fig. 18.5) and nails.

18.4 Reflectance Confocal Microscopy and Cutaneous Bacterial Infections

Treponema pallidum has been described by RCM in cutaneous lesions of secondary syphilis [6, 43] as bright particles intermingled with keratinocytes. However, it is challenging to differentiate these particles from the hyper-reflective cell membranes of keratinocytes.

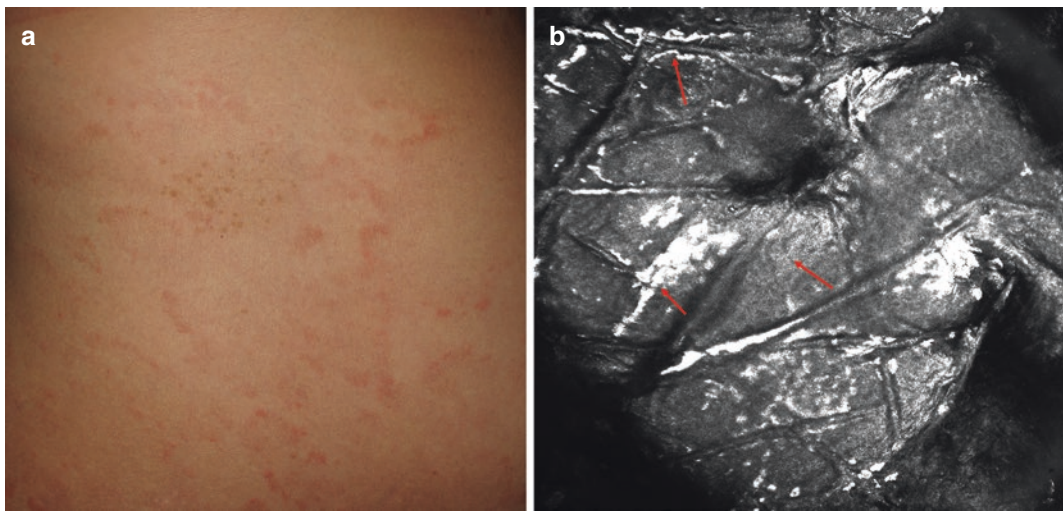

Fig. 18.4 Dermatophytosis. Clinical aspect (**a**): erythematous scaling annular plaques. Dermatophytes are easily identified under reflectance confocal microscopy (**b**) as thin, high-reflective, and longitudinal structures with a linear shape (*red arrow*). (Photographer: Elisa Cinotti, University Hospital of Santa Maria Alle Scotte, Siena)

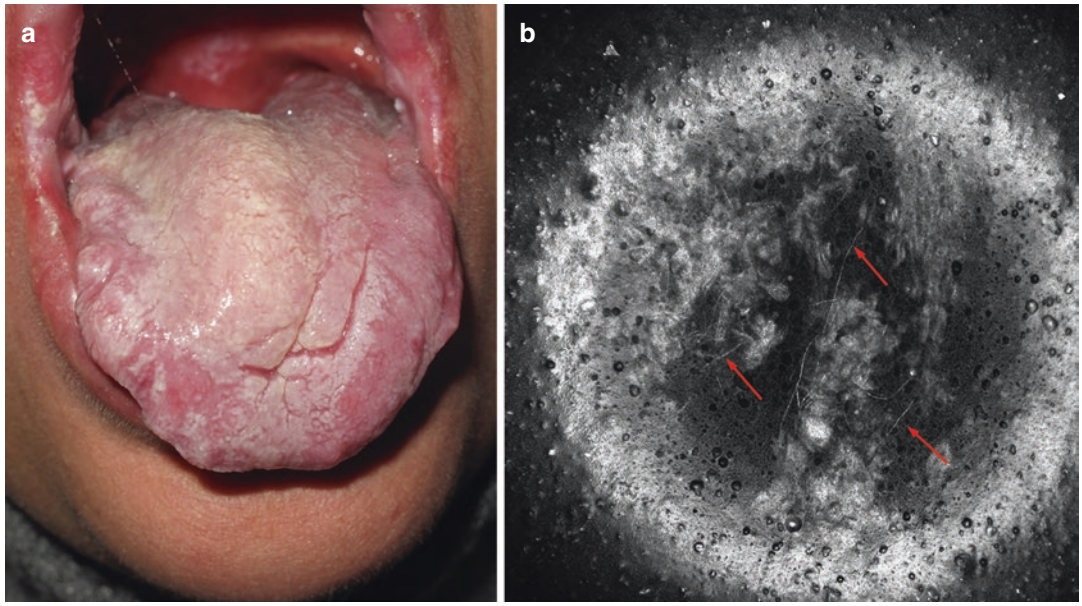

Fig. 18.5 Clinical (**a**) and reflectance confocal microscopy (RCM, **b**) aspect of an oral mucosa Candida infection. RCM shows pseudofilaments (*red arrow*). (Photographer: Elisa Cinotti, University Hospital of Santa Maria Alle Scotte, Siena)

18.5 Reflectance Confocal Microscopy and Viral Infections

RCM has been used to identify the cytopathic effects of *Herpes simplex* and *Varicella-zoster* virus [3, 4] (Fig. 18.6) *Molluscipoxvirus* [5] (Fig. 18.7) and *Parapoxvirus* [44] in the skin. In the first two infections, RCM reveals the presence of intra-epidermal cavities with acantholytic cells admixed with pleomorphic large keratinocytes and multinucleated giant cells corresponding to herpes virus-infected keratinocytes (Fig. 18.6a, b). In case of *Molluscipoxvirus* infection, RCM reveals a round, well-circumscribed lesion with central round cystic areas filled with brightly refractive material consisting in the characteristic eosinophilic inclusion bodies (molluscum bodies) of the histopathological examination [5] (Fig. 18.7b). The cutaneous lesions induced by these viruses are most often clinically typical, and they do not require any complementary investigation. Few cases are atypical, mostly in the case of a preexisting skin disease such as Darier's disease and atopic dermatitis, or in immunocompromised patients, where the diagnosis requires investigations such as Tzanck cytodiagnosis, direct fluorescence assay, viral cultures, PCR, or histopathological examination. Compared with standard techniques, RCM has the benefits of being noninvasive and rapid and able to image the entire affected cutaneous surface. Moreover, it can be useful for a noninvasive diagnosis in an early pre-vesicular stage. Physiological studies can also be performed, for example, to investigate the viral effects on a same location over time. In our experience, RCM could also be useful to identify intraepidermal vesicles and few ballooned cells in clinically atypical cases of hand, foot, and mouth disease due to coxsackievirus infection, but it was not possible to detect the cytopathic effect of human papillomavirus in common warts with the characteristics of large vacuolated cells. We suppose that this aspect could be related to the marked hyperkeratosis and acanthosis that reduce the resolution of

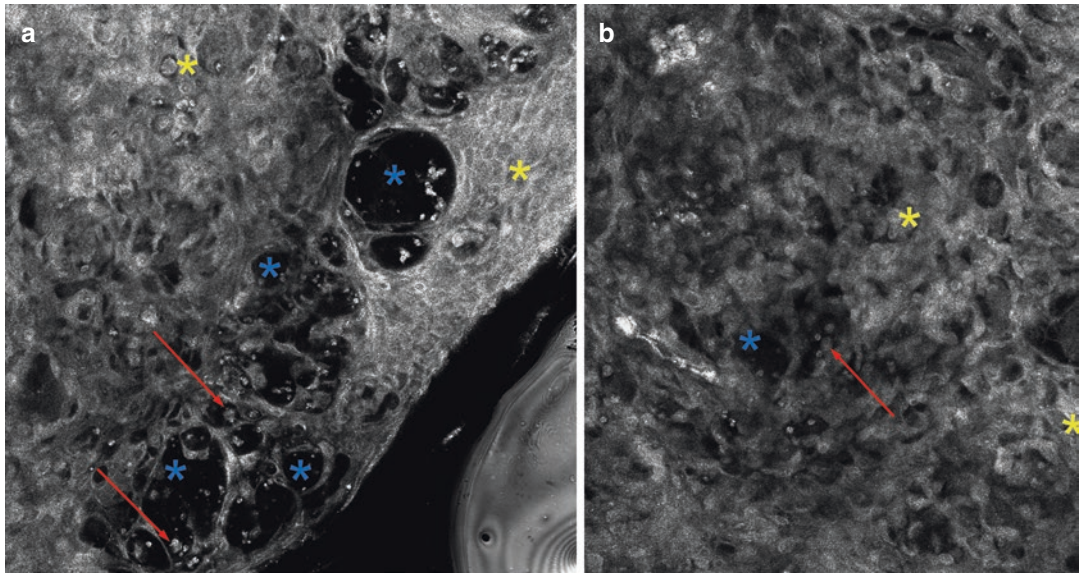

Fig. 18.6 Reflectance confocal microscopy of herpes zoster (**a**, **b**): presence of pleomorphic large keratinocytes (*yellow asterisk*), intra-epidermal cavities (*blue asterisk*) with large acantholytic cells (*red arrow*). (Photographer: Elisa Cinotti, University Hospital of Santa Maria Alle Scotte, Siena)

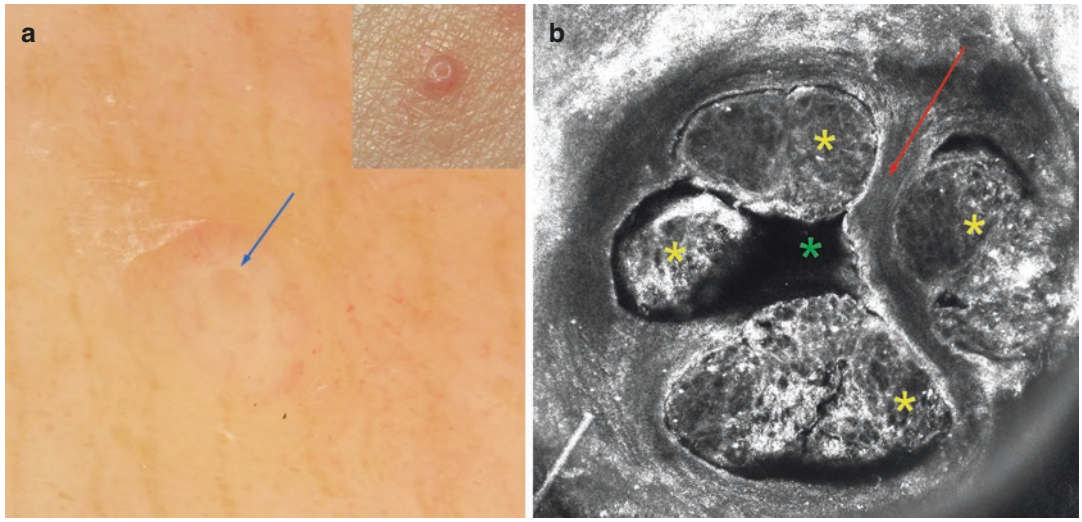

Fig. 18.7 Molluscum contagiosum: clinical (inset), dermoscopic (**a**), and reflectance confocal microscopy (**b**) aspect. A central pit is visible under dermoscopy (**a**, *blue arrow*). Reflectance confocal microscopy (**b**) shows a round, well-circumscribed lesion with a central crater (*green asterisk*), large lobules (*yellow asterisk*) separated by fine septa (*red arrow*) and filled with roundish bodies. (Photographer: Elisa Cinotti, University Hospital of Siena)

RCM images in the underlying epidermal layers. However, papillomatosis of the filiform variants can be observed. *Parapoxvirus* (orf virus that causes contagious ecthyma) has also been described by RCM as numerous hyper-reflective roundish corps corresponding to viral inclusions in the keratinocytes of a pseudoepitheliomatous hyperplastic epidermis [44].

18.6 Reflectance Confocal Microscopy for the Diagnosis of Virus-Induced Neoplasia and Neuropathy

RCM could be used for an early diagnosis of vaginal intraepithelial neoplasia with cytopathic effect induced by *Human papillomavirus* [31]. RCM has also been used for quantitative assessment of distal sensory polyneuropathy associated with human immunodeficiency virus due to measuring the density per mm^2 of the Meissner corpuscles at the volar side of the hand and foot [45].

Contagion risk associated with RCM examination in case of a suspected infection or infestation, a disposable transparent film (for example, Visulin, Paul Hartmann AG, Germany) should be applied on the tip of the RCM camera [46]. If this film is not used, a decontamination of the tip of the camera should be performed with a disposable virucidal, fungicidal, and bactericidal cleansing wipe (for example, Sani-Cloth Active, PDI, UK, or Alkotip, Servoprax, Germany). This wipe has no proved activity against parasites, but the mechanical cleaning action, repeatedly performed on the smooth surface of the tip, allows their elimination.

18.7 Conclusions

In conclusion, in vivo RCM can be used to reveal the cutaneous parasites (mainly *Sarcoptes scabiei, Demodex folliculorum*, and *Ixodes*) and fungi (mainly dermatophytes) and to identify the cytopathic effects associated with virus in real time, within a few minutes, without causing discomfort to the patient and without requiring any further equipment or laboratory devices. As RCM examination is rapid and performed by the dermatologist himself, it can be at once followed by the prescription of the treatment during a routine consultation. The cost of the machine is a limiting factor. However, for the dermatological centers where such a machine for the detection of skin tumors is already present, infestations and infections are additional possible diagnostic applications. Being noninvasive, RCM is also suitable for follow-up after therapy and for the study of physiology and pathogenesis with repeated examinations over time.

References

1. Piérard GE. In vivo confocal microscopy: a new paradigm in dermatology. Dermatol Basel Switz. 1993;186(1):4–5.
2. Corcuff P, Bertrand C, Leveque JL. Morphometry of human epidermis in vivo by real-time confocal microscopy. Arch Dermatol Res. 1993;285(8):475–81.
3. Goldgeier M, Alessi C, Muhlbauer JE. Immediate noninvasive diagnosis of herpesvirus by confocal scanning laser microscopy. J Am Acad Dermatol. 2002;46(5):783–5.
4. Abraham LS, Costa MC, Agozzino M, Amorosi B, Cota C, Ardigo M. In vivo reflectance confocal microscopy for varicella prompt diagnosis and treatment in a severely immunosuppressed patient. Skin Res Technol. 2012;18(3):386–8.
5. Scope A, Benvenuto-Andrade C, Gill M, Ardigo M, Gonzalez S, Marghoob AA. Reflectance confocal microscopy of molluscum contagiosum. Arch Dermatol. 2008;144(1):134.
6. Leclercq A, et al. Apport de la microscopie confocale par réflectance dans le diagnostic de syphilides ano-vulvaires, premier cas relaté. Ann Dermatol Vénéréologie. 2016;143(11):687–90.
7. Longo C, Pellacani G, Ricci C, De Pace B, Argenziano G, Zalaudek I. In vivo detection of Demodex folliculorum by means of confocal microscopy. Br J Dermatol. 2012;166(3):690–2.
8. Slutsky JB, Rabinovitz H, Grichnik JM, Marghoob AA. Reflectance confocal microscopic features of dermatophytes, scabies, and demodex. Arch Dermatol. 2011;147(8):1008.
9. Longo C, Bassoli S, Monari P, Seidenari S, Pellacani G. Reflectance-mode confocal microscopy for the in vivo detection of Sarcoptes scabiei. Arch Dermatol. 2005;141(10):1336.
10. Cinotti E, Perrot J-L, Labeille B, Cambazard F. On the feasibility of confocal microscopy for the diagnosis of scabies. Ann Dermatol Venereol. 2013;140(3):215–6.
11. Perrot J-L, et al. Rapid diagnosis of scabies by manual confocal reflectance microscopy. Ann Dermatol Venereol. 2012;139(6–7):502–5.
12. Levi A, Mumcuoglu KY, Ingber A, Enk CD. Assessment of Sarcoptes scabiei viability in vivo by reflectance confocal microscopy. Lasers Med Sci. 2011;26(3):291–2.
13. Turan E, Erdemir AT, Gurel MS, Yurt N. A new diagnostic technique for tinea incognito: in vivo reflectance confocal microscopy. Report of five cases. Skin Res Technol. 2013;19(1):e103–7.
14. Cinotti E, et al. Reflectance confocal microscopy for quantification of Sarcoptes scabiei in Norwegian scabies. J Eur Acad Dermatol Venereol. 2013;27(2):e176–8.

15. Sattler EC, Maier T, Hoffmann VS, Hegyi J, Ruzicka T, Berking C. Noninvasive in vivo detection and quantification of Demodex mites by confocal laser scanning microscopy. Br J Dermatol. 2012;167(5):1042–7.
16. Veasey J, Framil V, Ribeiro A, Lellis R. Reflectance confocal microscopy use in one case of Pityriasis folliculorum: a Demodex folliculorum analysis and comparison to other diagnostic methods. Int J Dermatol. 2014;53(4):e254–7.
17. Yuan C, et al. Comparison of reflectance confocal microscopy and standardized skin surface biopsy for three different lesions in a pityriasis folliculorum patient. Br J Dermatol. 2015;172(5):1440–2.
18. Turgut Erdemir A, et al. Reflectance confocal microscopy vs. standardized skin surface biopsy for measuring the density of Demodex mites. Skin Res Technol Off. 2014;20(4):435–9.
19. Del Giudice P, et al. Pyemotes ventricosus dermatitis, southeastern France. Emerg Infect Dis. 2008;14(11):1759–61.
20. Cinotti E, Espinasse M, Labeille B, Cambazard F, Perrot JL. Dermoscopy, confocal microscopy and optical coherence tomography for the diagnosis of bedbug infestation. J Eur Acad Dermatol Venereol. 2017;31(4):e203–4.
21. Erdoğan S, Dorittke P, Kardorff B. Identification of a foreign body--tick (Ixodes)--with confocal laser scan microscopy (CLSM) in comparison to histology in a mouse model. J Dtsch Dermatol. 2012;10(4):277–8.
22. Dupuy A, et al. Accuracy of standard dermoscopy for diagnosing scabies. J Am Acad Dermatol. 2007;56(1):53–62.
23. Levi A, Mumcuoglu KY, Ingber A, Enk CD. Detection of living Sarcoptes scabiei larvae by reflectance mode confocal microscopy in the skin of a patient with crusted scabies. J Biomed Opt. 2012;17(6):060503.
24. Cinotti E, et al. Videodermoscopy compared to reflectance confocal microscopy for the diagnosis of scabies. J Eur Acad Dermatol Venereol. 2016;30(9):1573–7.
25. Lacey N, Forton FMN, Powell FC. Demodex quantification methods: limitations of confocal laser scanning microscopy. Br J Dermatol. 2013;169(1):212–3.
26. Cinotti E, Fiorani D, Labeille B, Cambazard F, Rubegni P, Perrot JL. Demodex induced Blepharitis diagnosed by in vivo confocal microscopy. J Dermatol Pigm Res. 2017;1(1):1–3.
27. Sattler EC, Maier T, Hoffmann VS, Ruzicka T, Berking C. Noninvasive in vivo detection and quantification of Demodex mites by confocal laser scanning microscopy: reply from the authors. Br J Dermatol. 2013;169(1):213–5.
28. Randon M, et al. *In vivo* confocal microscopy as a novel and reliable tool for the diagnosis of *Demodex* eyelid infestation. Br J Ophthalmol. 2015;99(3):336–41.
29. Alarcon I, Carrera C, Puig S, Malvehy J. In vivo confocal microscopy features of cutaneous leishmaniasis. Dermatol Basel Switz. 2014;228(2):121–4.
30. Buljan M, Zalaudek I, Massone C, Hofmann-Wellenhof R, Fink-Puches R, Arzberger E. Dermoscopy and reflectance confocal microscopy in cutaneous leishmaniasis on the face: Dermoscopy and RCM of skin leishmaniasis. Australas J Dermatol. 2016;57(4):316–8.
31. Cinotti E, Perrot JL, Labeille B, Cambazard F. Reflectance confocal microscopy for cutaneous infections and infestations. J Eur Acad Dermatol Venereol. 2016;30(5):754–63.
32. Cinotti E, et al. Tinea corporis diagnosed by reflectance confocal microscopy. Ann Dermatol Venereol. 2014;141(2):150–2.
33. Pharaon M, et al. Diagnosis and treatment monitoring of toenail onychomycosis by reflectance confocal microscopy: prospective cohort study in 58 patients. J Am Acad Dermatol. 2014;71(1):56–61.
34. Piérard GE, et al. Microscopic diagnosis of onychomycoses. Ann Dermatol Venereol. 1994;121(1):25–9.
35. Hongcharu W, Dwyer P, Gonzalez S, Anderson RR. Confirmation of onychomycosis by in vivo confocal microscopy. J Am Acad Dermatol. 2000;42(2 Pt 1):214–6.
36. Markus R, Huzaira M, Anderson RR, González S. A better potassium hydroxide preparation? In vivo diagnosis of tinea with confocal microscopy. Arch Dermatol. 2001;137(8):1076–8.
37. Cinotti E, Fouilloux B, Perrot JL, Labeille B, Douchet C, Cambazard F. Confocal microscopy for healthy and pathological nail. J Eur Acad Dermatol Venereol. 2014;28(7):853–8.
38. Cinotti E, Perrot JL, Labeille B, Raberin H, Flori P, Cambazard F. Hair dermatophytosis diagnosed by reflectance confocal microscopy: six cases. J Eur Acad Dermatol Venereol. 2015;29(11):2257–9.
39. Rothmund G, et al. Confocal laser scanning microscopy as a new valuable tool in the diagnosis of onychomycosis—comparison of six diagnostic methods. Mycoses. 2013;56(1):47–55.
40. Liansheng Z, Xin J, Cheng Q, Zhiping W, Yanqun L. Diagnostic applicability of confocal laser scanning microscopy in tinea corporis. Int J Dermatol. 2013;52(10):1281–2.
41. Hui D, Xue-cheng S, Ai-e X. Evaluation of reflectance confocal microscopy in dermatophytosis. Mycoses. 2013;56(2):130–3.
42. Arrese J-E, Quatresooz P, Piérard-Franchimont C, Piérard G-E. Nail histomycology. Protean aspects of a human fungal bed. Ann Dermatol Venereol. 2003;130(12 Pt 2):1254–9.
43. Venturini M, Sala R, Semenza D, Santoro A, Facchetti F, Calzavara-Pinton P. Reflectance confocal microscopy for the in vivo detection of Treponema pallidum in skin lesions of secondary syphilis. J Am Acad Dermatol. 2009;60(4):639–42.
44. Tognetti L, et al. Ecthyma contagiosum (Orf): Reflectance confocal microscopy and histopathological correlates. Skin Res. Technol. 2019;25(2):234–37.
45. Almodovar JL, Schifitto G, McDermott MP, Ferguson M, Herrmann DN. HIV neuropathy: an in vivo confocal microscopic study. J Neurovirol. 2012;18(6):503–10.
46. Cinotti E, et al. How transparent film applied on dermatologic imaging devices in order to prevent infections affects image quality? Skin Res. Technol. 2019;25(2):229–33.

19 In Vivo Reflectance Confocal Microscopy for Mucous Membranes

Elisa Cinotti, Diletta Fiorani, and Jean Luc Perrot

Recently, reflectance confocal microscopy (RCM) devices dedicated to the skin have been applied to perform "virtual biopsies" of the oral, genital, and ocular mucosa, sensitive areas where noninvasive imaging techniques are of high interest in order to avoid surgical biopsies and excisions that could have functional and esthetic consequences for the patient [1, 2]. Mucosa is different from skin because its epithelium is not keratinized; therefore, no stratum granulosum and corneum are present.

For this reason, mucosa is particularly suitable for RCM examination: its thin or absent cornified layer and its thin epithelium allow a deeper penetration of the laser than in the skin with the consequent possibility of exploring deeper tissue levels. Moreover, different from the skin, there are no hair follicles and the epithelium–lamina propria junction is often flattened. RCM is particularly helpful for the differential diagnosis between melanosis, the most common benign lesion of the mucosa histopathologically characterized by hyperpigmented keratinocytes, and melanoma, two entities that can have overlapping clinical and dermoscopic features [3–7]. RCM may also be helpful to identify the area to be biopsied in case of large or multifocal lesions and may be regarded as a complementary technique for noninvasive assessment of treatment efficacy [8].

E. Cinotti · D. Fiorani (✉)
Department of Medical, Surgical and Neurological Science, Dermatology Section, University of Siena, S. Maria alle Scotte Hospital, Siena, Italy

J. L. Perrot
Department of Dermatology, University Hospital of St-Etienne, Saint-Etienne, France
e-mail: j.luc.perrot@chu-st-etienne.fr

19.1 Normal Ocular Surface

RCM can be very useful not only in dermatology but also in ophthalmology since it allows an in vivo examination of the human cornea at the cellular level. Cornea is particularly suited to be explored by RCM because of its transparency. First RCM images of the human cornea had been taken in 1985 by Lemp and associates [9], and since then clinical applications of in vivo RCM expanded thanks to its total safety and noninvasiveness. Two in vivo reflectance confocal microscopes are available in ophthalmology: the confocal four-slit scanning confocal microscope (Nidek, Gamagori, Japan) and the laser scanning confocal microscope Heidelberg Retina Tomograph equipped with the Rockstock Cornea Module (Heidelberg Engineering GmbH, Heidelberg, Germany). However, these two devices cannot be used for the examination of the whole eye surface owing to the absence of handling.

Hand-held RCM dedicated to skin (Vivascope 3000, Caliber, New York, distributed in Europe by MAVIG GmbH, Munchen, Germany) allows a better examination of the eye surface. It is very

M. Fimiani et al. (eds.), *Technology in Practical Dermatology*,
https://doi.org/10.1007/978-3-030-45351-0_19

manageable and permits to explore not only the cornea and the bulbar conjunctiva, but also the ciliar margin, the lacrimal punctum, the internal and external canthi, and both the surfaces of the eyelids comprising Meibomian glands [1, 2, 10–12]. It is fundamental that patients avoid movement to spare excessive pressure of the camera against the ocular surface. Before the examination, a topical anesthesia should be administered (e.g., oxybuprocaine hydrochloride 1.6 mg/0.4 mL and tetracaine hydrochloride 1%) and applied in the lower conjunctival sac of the eye. A transparent ophthalmic gel (e.g., Gel larme Thea, Thea, Clermont-Ferrand, France) should be applied on the ocular region to be examined instead of using the oil normally employed for skin examination.

The aspect of the conjunctiva is similar to the skin under RCM. It shows a stratified squamous epithelium formed by polygonal medium-sized cells with hyper-reflective borders, hyporeflective cytoplasm, and medium reflective round nucleus that is similar to the honeycombed pattern of the normal skin. The epithelial–stromal junction appears flat. The stroma (lamina propria) shows vessels and collagen fibers that are thinner than those of skin dermis [13]. Differently from the skin, conjunctival epithelium is not keratinized [3, 13].

19.2 Conjunctival Tumors

The highest refractivity observed by RCM is shown by melanin, contained in melanosomes, melanocytes, melanophages, and pigmented keratinocytes, followed by structures containing keratin [14]. Therefore, RCM represents a useful diagnostic tool for helping the clinical diagnosis of pigmented and keratinizing conjunctival tumors that is often challenging [15–18].

Nevi are the most common pigmented conjunctival tumors and are characterized by the presence of junctional and/or stromal nests of monomorphic medium-sized roundish hyperreflective cells with the absence of pagetoid cells, atypical cells at the epithelium–stromal junction and altered architecture of the epithelial layers [19, 20]. More than 50% of conjunctival nevi contain micro-cysts partly filled with monomorphous material and are called conjunctival epithelial cystic nevus [21].

Pigmented acquired melanosis (PAM) represents 20% of conjunctival pigmented tumors [22]. It usually affects middle-aged people and is usually unilateral. Typical features in RCM are hyper-reflective cells confined to the basal layer of epithelium and small intraepithelial dendritic cells (<20 μm) [23, 24]. In PAM with atypia (the counterpart of melanoma in situ in ophthalmology), it is possible to observe large dendritic cells (>20 μm) throughout the epithelium [19].

Melanoma is characterized by the presence of large dendritic or roundish cells (pagetoid spread) in the epithelium that appears disarranged and by atypical cells at the epithelial–stromal junction and in the stroma [19, 25].

Also basal cell carcinoma, squamous cell carcinoma, and lymphoma of eyelid margin and conjunctiva have been described under RCM with criteria similar to the cutaneous counterparts [19]. However dilated vessels, that in normal skin can be suggestive of malignancy, are less specific in conjunctiva; moreover inflammatory cells could be easily found and are confounders [2].

Differently from the skin, in conjunctival lesions, it is possible to identify in a more accurate way the localization of tumor cells in the vertical axis because ocular surface is convex, and consequently vertical sections can be acquired with RCM [1]. Moreover, RCM is extremely helpful for the follow-up of patients with ocular melanoma in order to identify a disease recurrence in an early phase [11, 26].

19.3 Healthy Oral Mucosa

Four layers can be distinguished in oral mucosa, and each of them can present different features according to the location (lining mucosa, masticatory mucosa, and specialized mucosa) [27, 28].

In *lining mucosa* (lip, cheek and ventral tongue), we can observe the following characteristics:

- The spinous layer: It is constituted by large cells delimited by thin, bright borders with a roundish bright structure in the center (the nucleolus) surrounded by a darker halo that has been interpreted as the nucleus. A grainy dark to grayish cytoplasm can be observed [27]. Passing from the superficial layer to deeper layers, the nucleus and the borders are less visible.
- The epithelium–lamina propria interface: Keratinocytes acquire ellipsoidal more elongated shape with a cytoplasm that becomes darker. Only bright borders are visible, neither nucleoli nor grainy grayish cytoplasm is observed. This pattern corresponds to the so-called *frosted glass-like structure*, with polygonal cells of different dimensions connected by thin bright outline [27, 29]. It is different from the honeycombed pattern of the normal skin because in this last case hexagonal and more regular borders can be appreciated.
- The lamina propria: It contains horizontally oriented vessels with small bright cells (erythrocytes) inside them. When visible, papillae of the lamina propria have a round to oval shape and are surrounded by keratinocytes [27, 29, 30].
- The submucosa is clearly visible only in the lining mucosa where horizontally oriented vessels can be seen.

In *masticatory gingival mucosa*, the superficial layer is bright, and no individual cells and organelles are identifiable [27]. Individual keratinocytes with a bright contour and a grainy cytoplasm become recognizable at deeper layers of the stratum spinosum where also papillae can be already observed because of the high epithelium–lamina propria interdigitations. The gingival submucosa cannot be clearly imaged owing to the keratinization.

In *specialized mucosa* (dorsal tongue and tongue margins) superficial layer shows filiform and fungiform papillae. Filiform papillae are elongated and flexible and are characterized by a stromal central axis and peripheral epithelium. Fungiform papillae appear as islands of tissue separated by a dark cleft from the stroma [31]. Taste buds can be visualized if RCM is pressed on the tongue, and they show large fusiform cells with a hyper-reflective nucleolus surrounded by a dark halo corresponding to the nucleus [32].

At the lamina propria, the connective tissue papillae increased their diameter preserving a constant density; keratinocytes maintained their bright cellular contours. Submucosa could not be visualized because of the thickness of the epithelium.

19.4 Oral Tumors

RCM represents an adjunct tool for the diagnosis of pigmented lesions of the oral mucosa in which tissue preservation is fundamental.

Melanosis (or melanotic macule) versus melanoma. Melanosis is the most frequent lesion of the oral mucosa and is due to increase in melanin in the basal layer of the epithelium with a consequent hyperpigmentation of basal keratinocytes, a normal or slightly higher number of melanocytes, and a possible increased number of melanophages. Although oral melanoma is a rare malignancy, its differential diagnosis with melanosis is of paramount importance due to its poor prognosis [33].

At RCM examination, melanosis shows a regular epidermal architecture with a regular honeycombed pattern. On the contrary, a disarranged honeycombed pattern is observed in melanoma [34]. Melanoma shows hyper-reflective pagetoid cells in the epithelium that are usually different in shape (roundish or dendritic) and size [5, 35]. A little percentage of melanosis shows pagetoid cells too, but in these cases, they usually have a dendritic shape, and they are usually located around papillae in the basal layer of the epithelium, without involving superficial layers of epithelium, and only in a little percentage of cases, they are located in the interpapillary spaces [2, 5]. These cells mainly correspond to Langerhans cells and in a minor extent to activated melanocytes and can have the same RCM aspect of malignant melanocytes of melanoma. At the epithelium–lamina propria junction, regularly distributed roundish (ringed pattern) or elongated (draped pattern) or polycyclic papillae rimmed by monomorphous hyper-reflective cells are observed in melanosis [36] (Fig. 20.1).

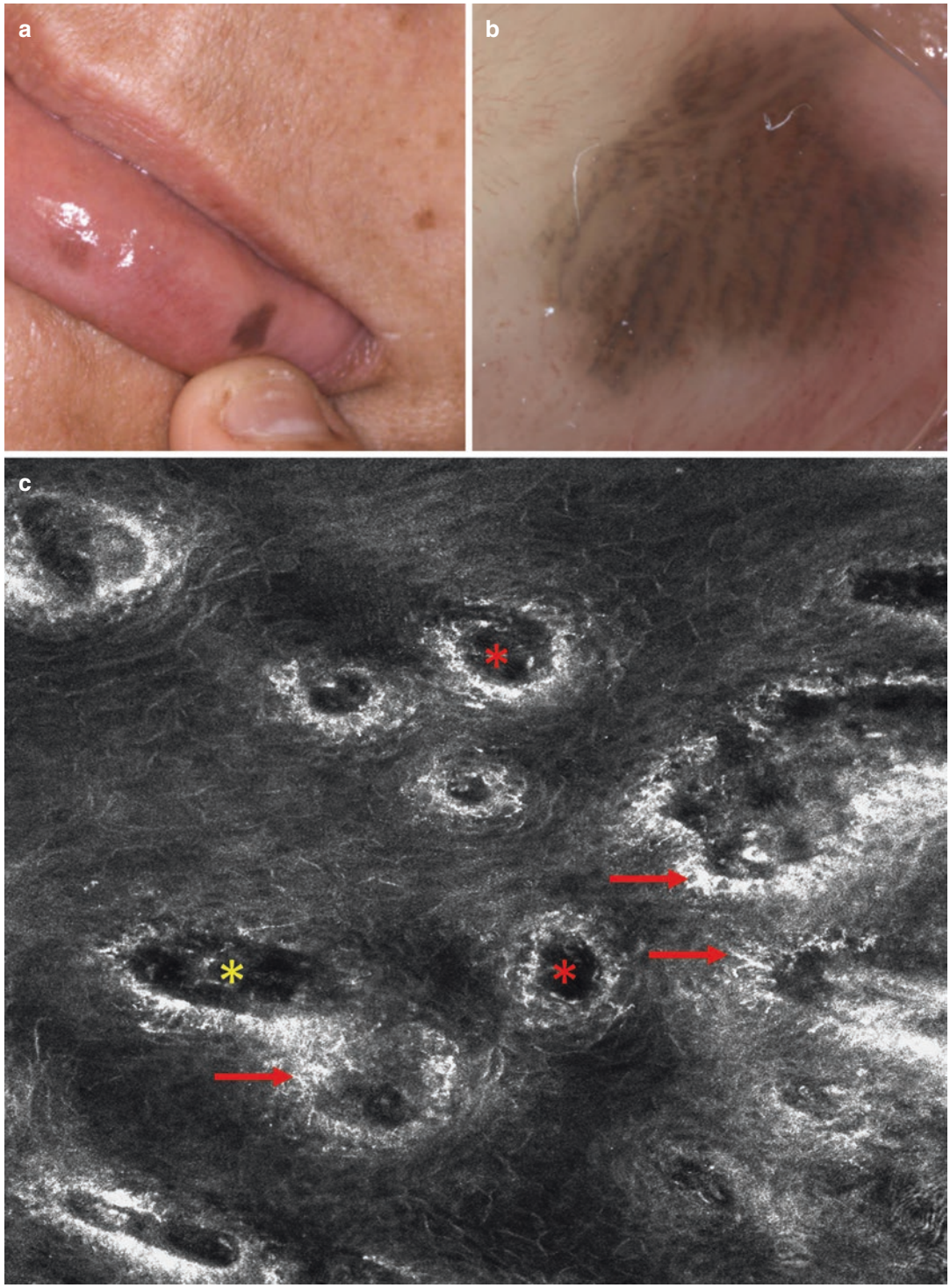

Fig. 20.1 Labial melanosis: clinical (**a**), dermoscopic (**b**), and reflectance confocal microscopy (**c**) images. Reflectance confocal microscopy (**c**) shows roundish (*red asterisk*) and elongated (*yellow asterisk*) papillae surrounded by pigmented keratinocytes. Numerous dendritic cells with short and thin dendrites can also be observed around the papillae (*red arrow*)

Melanoma shows non-evenly distributed papillae in an atypical ring or draped pattern or in a nonspecific pattern. Atypical roundish or dendritic cells around non-edged irregular papillae are specific features of melanoma especially when they are abundant. These atypical cells can also be observed in the interpapillary spaces [5].

19.5 Healthy Genital Mucosa

The epithelium of genital mucosa shows a honeycombed pattern similar to the oral mucosa with characteristic clearly visible nucleoli (Fig. 20.2). At the epithelium–chorion junction, edge papillae are less visible than in the skin because of the flattening of the junction. However, when papillae are visible, they are grouped in small clusters, and they can be round (ring pattern), elongated (draped pattern), or polycyclic, and they are rimmed by monomorphous hyper-reflective cells [7]. In many areas, interpapillary spaces are large because of the presence of large rete-ridges. Some isolated hyper-reflective dendritic cells can be observed around the papillae [7]. Dendritic or roundish cells are usually not visible in the superficial layers of the normal epithelium [2].

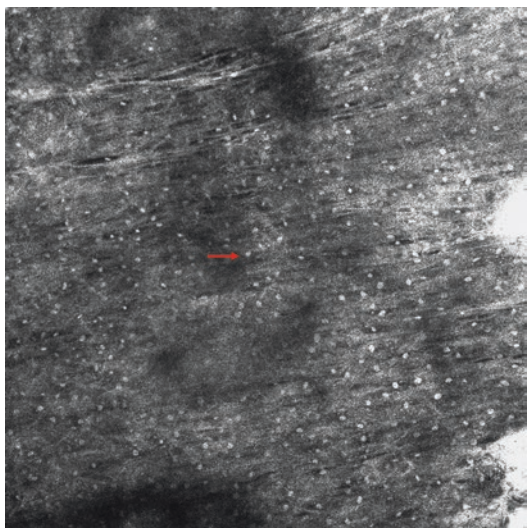

Fig. 20.2 Epithelium of genital mucosa: reflectance confocal microscopy shows the characteristic clearly visible nucleoli of the keratinocytes (*red arrow*)

The lamina propria is characterized by hyper-reflecting bundles of collagen fibers as in the dermal layer of the skin. Capillaries are better seen than in the skin due to the lack of stratum corneum. They could be horizontal or vertical. When papillae are present, capillaries are vertical, and their horizontal sections can be appreciated inside the papillae as dark roundish areas. In some cases, especially on the glans, capillaries can be vermicular. Small hyper-reflecting cells corresponding to blood cells moving inside blood vessels can be easily observed.

19.6 Genital Tumors

Melanosis of genitalia may show clinical features that overlap with melanoma such as asymmetry, variegated pigmentation from light to dark brown, irregular borders, multifocality, and large size. Under RCM, genital melanosis has the same aspect as oral melanosis with papillae that are rimmed by monomorphous hyper-reflective cells that correspond to hyperpigmented keratinocytes of the basal layer of the epithelium (Fig. 20.3). At the epithelium–chorion junction papillae can be round or polycyclic (ring pattern) or elongated (draped pattern). Sometimes it is possible to find rare dendritic bright cells (corresponding to Langerhans cells and few melanocytes) around the papillae [5, 7].

Melanoma of the genital area shows typical features of cutaneous melanoma: a disarranged pattern of the epithelium (Fig. 20.4), presence of pagetoid melanocytes (Fig. 20.4), loss of the normal chorion papillae architecture (Fig. 20.4) and abundant atypical cells in sheet-like structures in the chorion in case of invasive tumors [1, 5]. When located in the epithelium–chorion junction, neoplastic melanocytes appear as large hyper-reflective cells that destroy the architecture of the papillae that are not rimmed anymore.

In genital melanoma in situ, visible neoplastic melanocytes at RCM can be few both in the epithelium and at the epithelium–chorion junction, and the diagnosis can be challenging. On the contrary, in case of invasive melanoma, neoplastic

Fig. 20.3 Vulvar melanosis: clinical (**a**), dermoscopic (**b**), and reflectance confocal image (**c**). Reflectance confocal microscopy shows a ring pattern characterized by edged papillae (*red asterisk*) surrounded by hyperrefractive keratinocytes

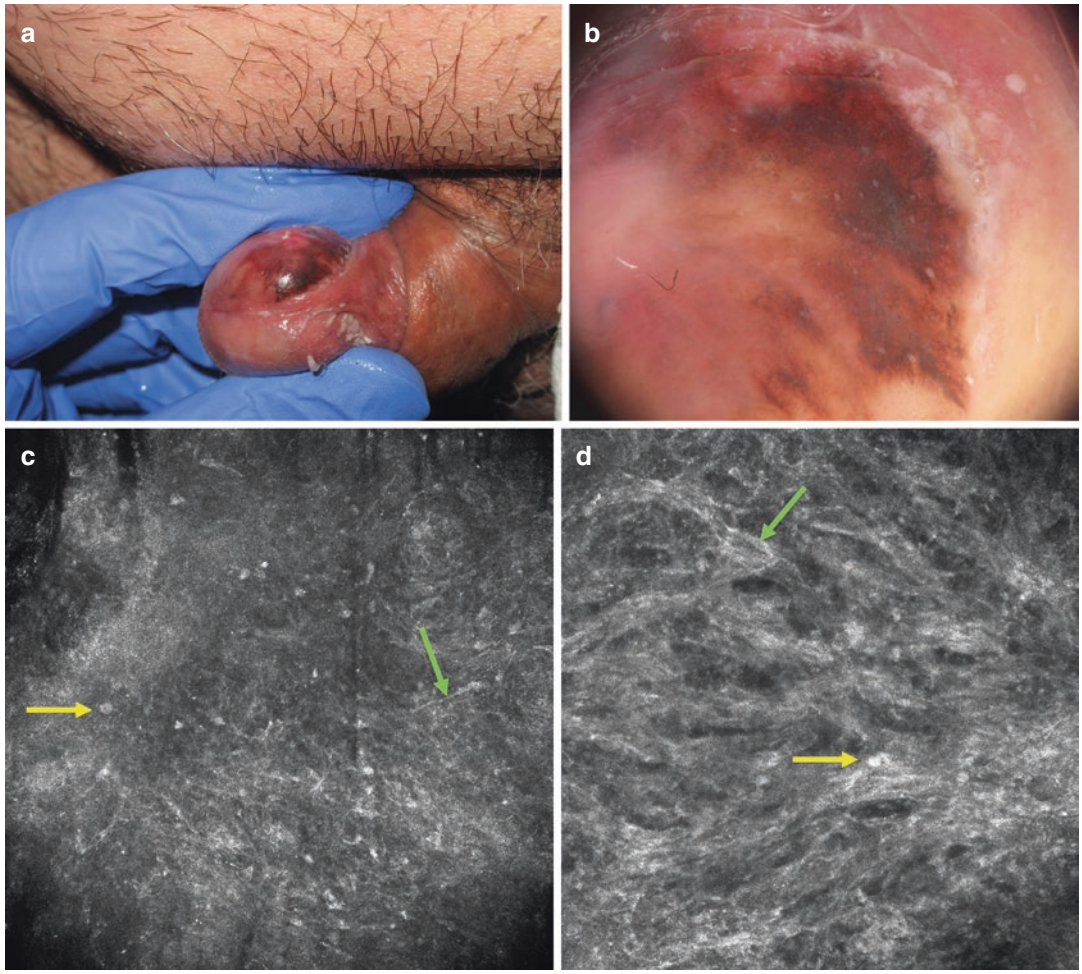

Fig. 20.4 Melanoma of the genital area: clinical (**a**), dermoscopic (**b**), and reflectance confocal microscopy (**c**, **d**) images. Reflectance confocal microscopy shows a disarranged pattern of the epithelium (**c**) with pagetoid roundish (**c**, *yellow arrow*) and dendritic (**c**, *green arrow*) melanocytes and a proliferation of atypical roundish (**d**, *yellow arrow*) and dendritic (**d**, *green arrow*) melanocytes at the epithelium–chorion junction that destroy the normal chorion papillae architecture (**d**)

melanocytes are usually numerous in the epithelium and form sheet-like structures (atypical melanocytic proliferation in single units) that obscure papillae.

Genital melanosis and melanoma are often multifocal, and RCM allows exploring the entire lesions, helping the clinician to identify the most significant area to be biopsied.

Genital *nevi* show the same characteristics observed in the skin (Fig. 20.5). One exception is represented by genital atypical nevus [37], a benign lesion that can mimic melanoma clinically and histologically. It is characterized by large discohesive junctional nests, possible mild cytological atypia, pagetoid spread, and inflammation that make difficult the differential diagnosis with melanoma [38]. Despite its atypical histologic features, there is no evidence of malignant transformation [39, 40]. RCM examination of atypical genital nevus shows round large roundish hyper-reflective melanocytes and large confluent dyshesive nests. A lichenoid infil-

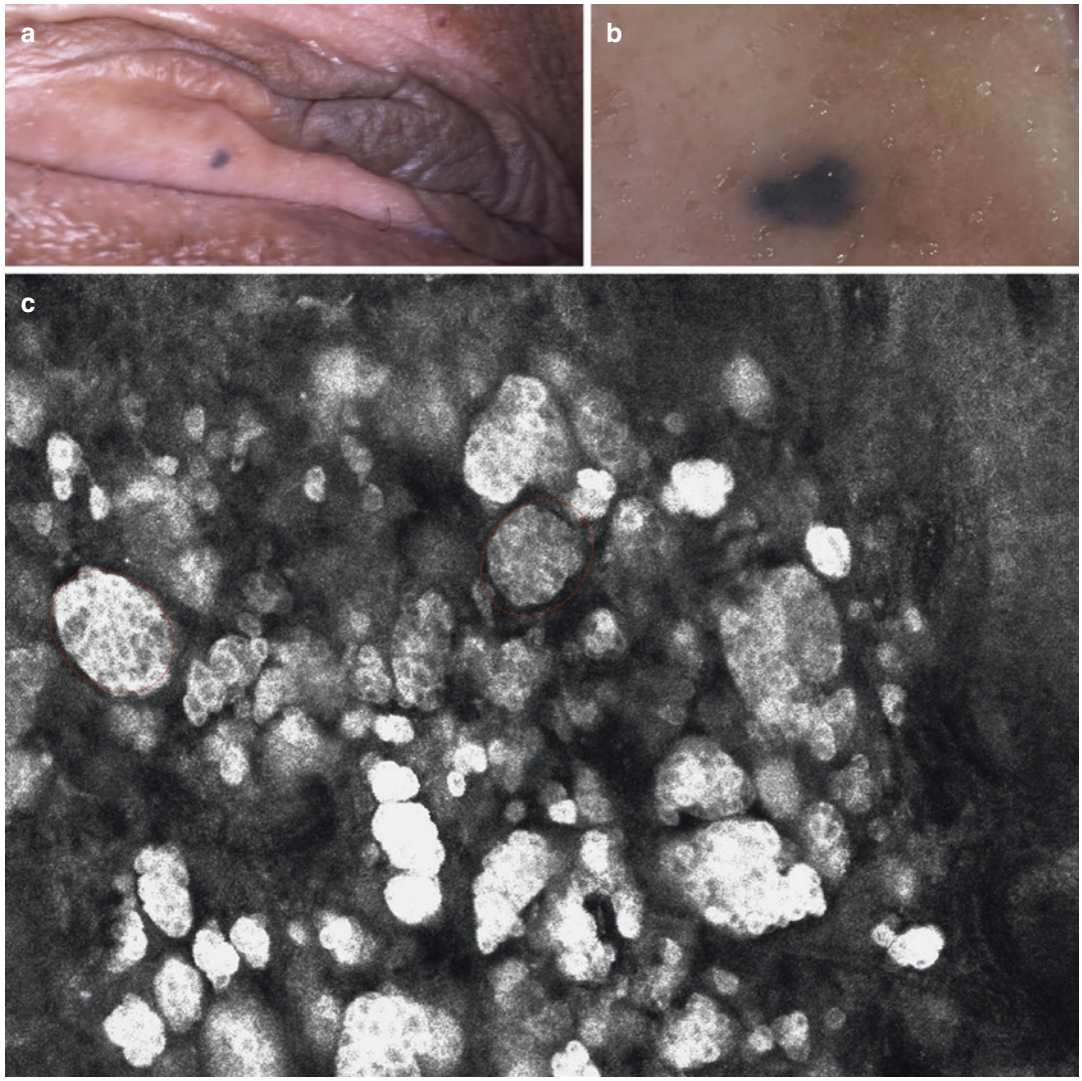

Fig. 20.5 Intradermal vulvar nevus: clinical (**a**), dermoscopic (**b**), and reflectance confocal microscopy (**c**). Dermoscopy (**b**) shows homogeneous *blue* pattern. Reflectance confocal microscopy (**c**) shows dense nests of monomorphous melanocytes (*red circles*)

trate at the junction can also be observed [37, 41]. Since atypical genital nevus cannot be easily distinguished from melanoma, it is reasonable to biopsy all cases presenting atypical RCM features.

References

1. Cinotti E, Labeille B, Cambazard F, Perrot J-L. Confocal microscopy for special sites and special uses. Dermatol Clin. 2016;34:477–85.
2. Cinotti E, et al. Reflectance confocal microscopy for mucosal diseases. G Ital Dermatol Venereol. 2015;150:585–93.
3. Theillac C, et al. Evaluation of large clinically atypical vulvar pigmentation with RCM: atypical melanosis or early melanoma? J Eur Aca Dermatol Venereol. 2018; https://doi.org/10.1111/jdv.15141.
4. Cinotti E, et al. In vivo confocal microscopic substrate of grey colour in melanosis. J. Eur. Acad. Dermatol. Venereol. 2015;29:2458–62.
5. Debarbieux S, et al. Reflectance confocal microscopy of mucosal pigmented macules: a review of 56 cases including 10 macular melanomas. Br J Dermatol. 2014;170:1276–84.

6. Cinotti E, et al. Anal melanosis diagnosed by reflectance confocal microscopy. Australas J Dermatol. 2014;55:286–8.
7. Cinotti E, Perrot JL, Labeille B, Adegbidi H, Cambazard F. Reflectance confocal microscopy for the diagnosis of vulvar melanoma and melanosis: preliminary results. Dermatol Surg. 2012;38:1962–7.
8. Cinotti E, et al. Laser photodynamic treatment for in situ squamous cell carcinoma of the glans monitored by reflectance confocal microscopy. Australas J Dermatol. 2014;55:72–4.
9. Minsky M. Memoir on inventing the confocal scanning microscope. Scanning. 1988;10:128–38.
10. Cinotti E, et al. In vivo confocal microscopy for eyelids and ocular surface: a new horizon for dermatologists. G Ital Dermatol Venereol. 2015;150:127–9.
11. Cinotti E, et al. The role of in vivo confocal microscopy in the diagnosis of eyelid margin tumors: 47 cases. J Am Acad Dermatol. 2014;71:912–918.e2.
12. Cinotti E, et al. Optical diagnosis of a metabolic disease: cystinosis. J Biomed Opt. 2013;18:46013.
13. Messmer EM, Mackert MJ, Zapp DM, Kampik A. In vivo confocal microscopy of normal conjunctiva and conjunctivitis. Cornea. 2006;25:781–8.
14. Rajadhyaksha M, Grossman M, Esterowitz D, Webb RH, Anderson RR. In vivo confocal scanning laser microscopy of human skin: melanin provides strong contrast. J Invest Dermatol. 1995;104:946–52.
15. Maschi C, Caujolle J-P, Liolios I, Costet C. Benign conjunctival tumors. J Fr Ophtalmol. 2013;36:796–802.
16. Falke K, Zhivov A, Zimpfer A, Stachs O, Guthoff RF. Diagnosis of conjunctival neoplastic lesions by confocal in-vivo microscopy. Klin Monatsbl Augenheilkd. 2012;229:724–7.
17. Folberg R, Jakobiec FA, Bernardino VB, Iwamoto T. Benign conjunctival melanocytic lesions. Clinicopathologic features. Ophthalmology. 1989;96:436–61.
18. Ranty M-L, Quintyn J-C, Uro-Coste E, Delisle M-B. Ocular conjunctival pathology. A ten-year retrospective study in Toulouse-Rangueil university hospital and literature review. Ann Pathol. 2012;32:170–6.
19. Cinotti E, et al. Handheld reflectance confocal microscopy for the diagnosis of conjunctival tumors. Am J Ophthalmol. 2015;159:324–333.e1.
20. Guitera P, et al. In vivo confocal microscopy for diagnosis of melanoma and basal cell carcinoma using a two-step method: analysis of 710 consecutive clinically equivocal cases. J Invest Dermatol. 2012;132:2386–94.
21. Kaspi M, et al. The role of reflectance confocal microscopy and optical coherence tomography in the diagnosis of epithelial-cystic conjunctival nevus. Ann Dermatol Venereol. 2016;143:653–6.
22. Kaspi M, et al. Contribution of reflectance confocal microscopy in the diagnosis of conjunctival primary acquired melanosis without atypia. Ann Dermatol Venereol. 2018;145:141–3.
23. Langley RGB, Burton E, Walsh N, Propperova I, Murray SJ. In vivo confocal scanning laser microscopy of benign lentigines: comparison to conventional histology and in vivo characteristics of lentigo maligna. J Am Acad Dermatol. 2006;55:88–97.
24. Messmer EM, Mackert MJ, Zapp DM, Kampik A. In vivo confocal microscopy of pigmented conjunctival tumors. Graefes Arch Clin Exp Ophthalmol. 2006;244:1437–45.
25. Cinotti E, Haouas M, Grivet D, Perrot JL. In vivo and ex vivo confocal microscopy for the Management of a Melanoma of the eyelid margin. Dermatol Surg. 2015;41:1437–40.
26. Cinotti E, et al. Handheld in vivo reflectance confocal microscopy for the diagnosis of eyelid margin and Conjunctival Tumors. JAMA Ophthalmol. 2017;135:845–51.
27. Contaldo M, et al. In vivo characterization of healthy oral mucosa by reflectance confocal microscopy: a translational research for optical biopsy. Ultrastruct Pathol. 2013;37:151–8.
28. García-Hernández A, Roldán-Marín R, Iglesias-Garcia P, Malvehy J. In vivo noninvasive imaging of healthy lower lip mucosa: a correlation study between high-definition optical coherence tomography, reflectance confocal microscopy, and histology. Dermatol Res Pract. 2013;2013:205256.
29. Jabbour JM, et al. Reflectance confocal endomicroscope with optical axial scanning for in vivo imaging of the oral mucosa. Biomed Opt Express. 2014;5:3781–91.
30. White WM, Rajadhyaksha M, González S, Fabian RL, Anderson RR. Noninvasive imaging of human oral mucosa in vivo by confocal reflectance microscopy. Laryngoscope. 1999;109:1709–17.
31. Cinotti E, Labeille B, Cambazard F, Perrot JL. Dermoscopy and reflectance confocal microscopy examination of pigmented fungiform papillae of the tongue. Ann Dermatol Venereol. 2017;144:323–5.
32. Just T, Zeisner C, Stave J, Pau HW. Confocal laser-scanning microscopy to analyse the epithelium of the tongue. Laryngorhinootologie. 2004;83:108–12.
33. Sortino-Rachou AM, de Camargo Cancela M, Voti L, Curado MP. Primary oral melanoma: population-based incidence. Oral Oncol. 2009;45:254–8.
34. Pellacani G, et al. The impact of in vivo reflectance confocal microscopy for the diagnostic accuracy of melanoma and equivocal melanocytic lesions. J Invest Dermatol. 2007;127:2759–65.
35. Maher NG, Solinas A, Scolyer RA, Guitera P. In vivo reflectance confocal microscopy for evaluating melanoma of the lip and its differential diagnoses. Oral Surg Oral Med Oral Pathol Oral Radiol. 2017;123:84–94.
36. Uribe P, Collgros H, Scolyer RA, Menzies SW, Guitera P. In vivo reflectance confocal microscopy for the diagnosis of melanoma and Melanotic macules of the lip. JAMA Dermatol. 2017;153:882–91.
37. Cinotti E, et al. Reflectance confocal microscopy for the diagnosis of vulvar naevi: six cases. J Eur Acad Dermatol Venereol. 2016;30:30–5.

38. Brenn T. Atypical genital nevus. Arch Pathol Lab Med. 2011;135:317–20.
39. Quddus MR, Rashid LB, Sung CJ, Robinson-Bostom L, Lawrence WD. Atypical melanocytic nevi of genital type: a distinctive pigmented lesion of the genital tract often confused with malignant melanoma. Dermatol Online J. 2010;16:9.
40. Clark WH, Hood AF, Tucker MA, Jampel RM. Atypical melanocytic nevi of the genital type with a discussion of reciprocal parenchymal-stromal interactions in the biology of neoplasia. Hum Pathol. 1998;29:S1–24.
41. Agozzino M, et al. Noninvasive assessment of benign pigmented genital lesions using reflectance confocal microscopy. Br J Dermatol. 2015;173:1312–5.

Ex Vivo Confocal Microscopy

20

Caterina Longo

20.1 Introduction

While the vast majority of basal cell carcinomas (BCCs) can be effectively managed on the basis of clinical examination, in some instances further imaging are needed for optimal management. In particular the need of imaging for BCC can be readily summarized by the following points: (1) diagnosing with high diagnostic accuracy a given BCC; (2) subtyping a BCC into superficial versus non-superficial forms; (3) defining tumor margins in Mohs setting.

In the field of novel diagnostic imaging tools, confocal microscopy has been claimed in the last decades as the new revolutionary pivotal instrument for skin cancer diagnosis.

Basically, confocal microscopes can work with two different modalities: in reflectance mode and in fluorescence mode. The confocal microscope in reflectance mode (RCM) is used in vivo at patient's bedside for the diagnosis of BCC and further histologic subtyping.

Instead, the confocal microscope used in fluorescence mode (FCM) is a tool that can be applied in ex vivo setting on freshly excised specimens during Mohs surgery. FCM uses agents several fluorophores as fluorescent among which acridine orange is one of the most commonly used in Mohs setting for epithelial cancer [1, 2].

Micrographic Mohs surgery is a precise and complete excision of a skin cancer that is guided by the examination of margins with frozen histopathology during surgery. It has been developed several years ago, and it is still applied in clinical dermatologic setting especially for some cancers such as BCC and squamous cell carcinoma (SCC).

However, this technique has some drawbacks: the preparation of histopathology, however, is labor intensive and time consuming, and multiple serial excisions are often necessary to achieve cancer-free margins, with frozen tissue preparation requiring 20–45 min for each excision, and furthermore there are cost-related issues.

FCM has been introduced in clinical setting in the last decades as a revolutionary tool capable to offer a quasi-histologic view of a given skin tumor in few minutes.

20.2 Standard Operating Procedure of FCM

Ex vivo fluorescence confocal microscopy (FCM) is used on freshly excised tumors in the operating room. Different fluorophores such as Fluorescein, Nile blue, Patent blue, Methylene blue, and acridine orange can be used at different

C. Longo (✉)
Dermatology Unit, University of Modena and Reggio Emilia, Arcispedale Santa Maria Nuova-IRCCS, Reggio Emilia, Italy

Azienda Unità Sanitaria Locale – IRCCS di Reggio Emilia, Centro Oncologico ad Alta Tecnologia Diagnostica-Dermatologia, Reggio Emilia, Italy

M. Fimiani et al. (eds.), *Technology in Practical Dermatology*,
https://doi.org/10.1007/978-3-030-45351-0_20

wavelength. However, acridine orange is one of the commonly used for its capability to provide an excellent contrast. Confocal mosaics are acquired using an ex vivo fluorescence confocal microscope (Vivascope®2500, Mavig, Munich, Germany). The laser illumination wavelength is 488 nm. The depth is manually adjusted to image the surface. Imaging is with a 30×, 0.9 numerical aperture water immersion lens which provides optical sectioning of ~1.5 microns and resolution of ~0.4 microns at the 488 nm wavelength. Acridine orange (0.6 milliMolar, 10–20 s) is used as the contrast agent.

Briefly, each margin of a given tumor is stained separately in a 0.6 mM solution of acridine orange dye for 10–20 s and subsequently sandwiched between two glass slides, keeping the "tissue orientation." The slides were then fixed with silicon glue and positioned onto the platform of the inverted microscope. FCM provides an excellent correlation on high-resolution gray scale bitmap images with conventional frozen sections. Furthermore, it holds the great advantage of fat tissue preservation and other structures that might be otherwise affected by tissue processing in Mohs surgery. After FCM imaging, the tissue can be routinely processed for conventional or frozen pathology.

20.3 Ex Vivo Applications of FCM

20.3.1 Basal Cell Carcinoma

Specific FCM BCC criteria have been described and correlated with the conventional histopathologic findings [3–18]. Basically, FCM criteria include the presence of: (1) *Fluorescence*. Fluorescence corresponds to nucleated cells stained with acridine orange. Area of higher fluorescence consistently showed nuclear morphology compared with a darker appearing background of dermis; fluorescence is typically seen as forming structures/aggregates (i.e., tumor islands); (2) *Tumor demarcation*. Outline of tumor profile; (3) *Nuclear crowding*. Nuclear crowding was determined when the nuclear density was higher than that of the surrounding epidermis and adnexal structures; (4) *Peripheral palisading*. Palisading is described by the tendency of basal cells to be arranged in a parallel-polarized way along the periphery of the BCC tumor. This is seen mainly in nodular subtypes of BCCs; (5) *Clefting*. Hypofluorescent dark-appearing space surrounding basaloid islands; it partially outlines the islands in micronodular and infiltrative subtypes of BCCs, whereas it is more evident in superficial and nodular tumors; (6) *Nuclear pleomorphism*. Nuclear pleomorphism is a deviation from the normal round or oval shapes of nuclei present in normal keratinocytes; (7) *Increased nucleus : cytoplasm ratio*. BCC nests are seen as crowded roundish masses of elongated heterogeneous nuclei with poor or absent cytoplasm; (8) *Stroma*. Tumoral stroma is the modified dermis surrounding the BCC nests appearing as dark background with fluorescent dots and filaments corresponding to fibroblasts, collagen fibers, and inflammatory infiltrate (Figs. 20.1, 20.2).

Furthermore, distinct BCC subtypes reveal specific morphologic aspects. In fact, superficial BCCs show a proliferation of atypical basaloid cells that form an axis parallel to the epidermal surface, are extensions from the dermal–epidermal junction, and demonstrate slit-like retraction of the palisaded basal cells from the subjacent stroma (cleft-like spaces). Nodular BCCs are typified by small to large nodules with peripheral palisading and clefting, whereas the micronodular subtype reveals monotonous small rounded and sharply demarcated islands with roughly the

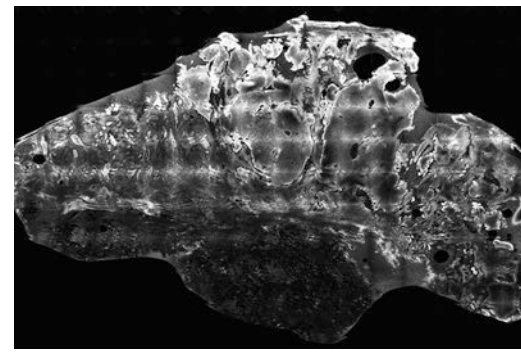

Fig. 20.1 FCM imaging of a BCC. On the whole architecture, it is possible to observe fluorescent basaloid tumoral islands

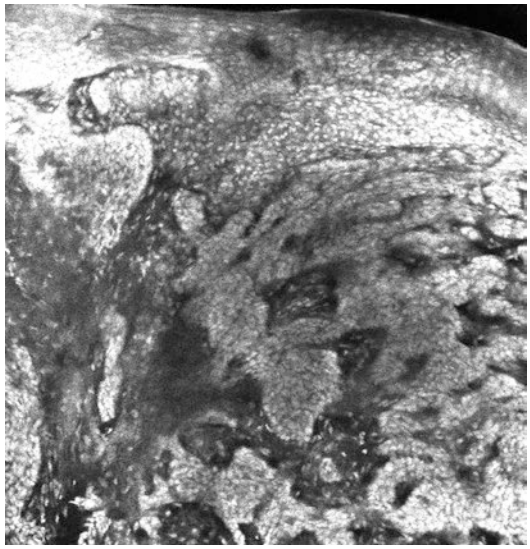

Fig. 20.2 High-resolution FCM imaging of a BCC. Highly fluorescent tumor islands are seen in the dermis with infiltrative pattern of growth

same shape and contour. Infiltrative BCCs are the most challenging tumors to be identified. Typically, they appear as columns and cords of basaloid cells one to two cells thick with sharp angulation, enmeshed in a densely collagenized stroma. To further complicate the matter, palisading and clefting are rarely identifiable.

Although it is a relatively new imaging tool applied in clinical practice, several studies have been conducted to assess the value of FCM for BCC margin assessment. A study conducted by Bennassar et al. on 80 BCCs using these FCM criteria demonstrated an overall sensitivity and specificity of detecting residual BCC of 88 and 99%, respectively [14]. An additional advantage of FCM is the reduction of the time invested in Mohs surgery setting when compared to the conventional processing of frozen sections, accounting for almost two thirds [15]. Reading and interpreting FCM images are not easy in all cases since several diagnostic pitfalls may occur [16]. In particular, it could be challenging to distinguish tiny and angulated cords and strands of fluorescent cells typically found in infiltrative BCCs from the surrounding stroma. Another possible challenging situation is due to the presence of several sebaceous glands that might resemble BCC islands at first glance [16]. Recently, Longo et al. demonstrated a high diagnostic accuracy of FCM demonstrated on a large data set of 753 specimens that FCM is a valid imaging tool to assess BCC margins in Mohs surgery with high diagnostic accuracy when compared to frozen sections. When evaluating the performance of FCM as compared to frozen sections 79.8% sensitivity, 95.8% specificity, 80.5% positive predicting, and 95.7% negative predicting values were found (area under the curve: 0.88, 95% CI 0.84–0.92; $P < 0.001$) [18].

20.3.2 Squamous Cell Carcinoma

Few preliminary reports describe the feasibility of FCM for SCC diagnosis and margin assessment. Longo et al. [19] defined the FCM criteria to grade SCC tumors. This pilot study demonstrated that the presence of well-defined tumor silhouette, numerous keratin pearls, keratin formation, and scarce nuclear pleomorphism on FCM images were correlated with the diagnosis of well-differentiated SCC. Conversely, an ill-defined tumor silhouette, paucity, or absence of keratin pearls as well as marked nuclear pleomorphism was observed in poorly differentiated tumors. SCCs that were moderately differentiated revealed an intermediate pattern of growth with the presence of keratin formation [19].

20.4 Other Tumors

FCM has been used to assess the margins during Mohs surgery of eccrine syringomatous carcinoma [20]. On FCM, the tumor appears highly fluorescent. Epidermis is spared of any neoplastic proliferation while neoplastic cords of monomorphous fluorescent cells can be seen in the dermis. Those structures are similar to eccrine gland tubular structure [20].

20.5 Conclusions

The use of FCM in ex vivo Mohs setting holds the promise to change radically the current approach new device permits to have a digital

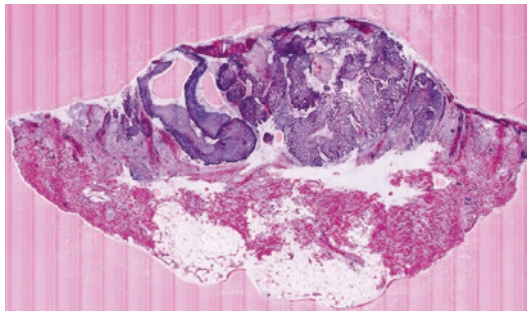

Fig. 20.3 FCM imaging of a BCC obtained with digital staining. Purple basaloid aggregates showing peripheral palisading and clefting

staining (Fig. 20.3) that resemble the H&E-stained sections of conventional histopathology. This could be a further step for the use of FCM in pathology laboratories and general surgery that are more familiar with histology rather than FCM or other imaging devices.

Future development of technology and understanding of the training process will definitely implement the use of confocal microscopy in clinical setting.

Conflict of Interest The author has no conflict of interest to disclose

References

1. Rajadhyaksha M, Menaker G, Flotte T, Dwyer PJ, González S. Confocal examination of nonmelanoma cancers in thick skin excisions to potentially guide Mohs micrographic surgery without frozen histopathology. J Invest Dermatol. 2001;117:1137–43.
2. Chung VQ, Dwyer PJ, Nehal KS, Rajadhyaksha M, Menaker GM, Charles C, Jiang SB. Use of ex vivo confocal scanning laser microscopy during Mohs surgery for nonmelanoma skin cancers. Dermatol Surg. 2004;30:1470–8.
3. Gareau DS, Li Y, Huang B, Eastman Z, Nehal KS, Rajadhyaksha M. J confocal mosaicing microscopy in Mohs skin excisions: feasibility of rapid surgical pathology. J Biomed Opt. 2008;13(5):054001.
4. Gareau DS, Karen JK, Dusza SW, Tudisco M, Nehal KS, Rajadhyaksha M. Sensitivity and specificity for detecting basal cell carcinomas in Mohs excisions with confocal fluorescence mosaicing microscopy. J Biomed Opt. 2009;14(3):034012.
5. Karen JK, Gareau DS, Dusza SW, Tudisco M, Rajadhyaksha M, Nehal KS. Detection of basal cell carcinomas in Mohs excisions with fluorescence confocal mosaicing microscopy. Br J Dermatol. 2009;160(6):1242–50.
6. Bennàssar A, Vilalta A, Carrera C, Puig S, Malvehy J. Rapid diagnosis of two facial papules using ex vivo fluorescence confocal microscopy: toward a rapid bedside pathology. Dermatol Surg. 2012;38(9):1548–51.
7. Abeytunge S, Li Y, Larson B, Toledo-Crow R, Rajadhyaksha M. Rapid confocal imaging of large areas of excised tissue with strip mosaicing. J Biomed Opt. 2011;16(5):050504.
8. Abeytunge S, Li Y, Larson B, Peterson G, Seltzer E, Toledo-Crow R, Rajadhyaksha M. Confocal microscopy with strip mosaicing for rapid imaging over large areas of excised tissue. J Biomed Opt. 2013;18(6):61227.
9. Larson B, Abeytunge S, Seltzer E, Rajadhyaksha M, Nehal K. Detection of skin cancer margins in Mohs excisions with high-speed strip mosaicing confocal microscopy: a feasibility study. Br J Dermatol. 2013;169:922–6.
10. Gareau DS. Feasibility of digitally stained multimodal confocal mosaics to simulate histopathology. J Biomed Opt. 2009;14(3):034050.
11. Gareau DS, Jeon HS, Nehal KS, Rajadhyaksha M. Rapid screening of cancer margins in tissue with multimodal microscopy. J Surg Res. 2012;178:533–8.
12. Gareau D, Bar A, Snaveley N, et al. Tri-modal confocal mosaics detect residual invasive squamous cell carcinoma in Mohs surgical excisions. J Biomed Opt. 2012;17(6):066018.
13. Longo C, Ragazzi M, Castagnetti F, Gardini S, et al. Inserting ex vivo fluorescence confocal microscopy perioperatively in Mohs micrographic surgery expedites bedside assessment of excision margins in recurrent basal cell carcinoma. Dermatology. 2013;227(1):89–92.
14. Bennàssar A, Carrera C, Puig S, Vilalta A, Malvehy J. Fast evaluation of 69 basal cell carcinomas with ex vivo fluorescence confocal microscopy: criteria description, Histopathological correlation, and Interobserver agreement. JAMA Dermatol. 2013;149(7):839–47.
15. Bennàssar A, Vilata A, Puig S, Malvehy J. Ex vivo fluorescence confocal microscopy for fast evaluation of tumour margins during Mohs surgery. Br J Dermatol. 2014;170(2):360–5.
16. Longo C, Rajadhyaksha M, Ragazzi M, Nehal K, Gardini S, Moscarella E, Lallas A, Zalaudek I, Piana S, Argenziano G, Pellacani G. Evaluating ex vivo fluorescence confocal microscopy images of basal cell carcinomas in Mohs excised tissue. Br J Dermatol. 2014 Sep;171(3):561–70.
17. Xiong YD, Ma S, Li X, Zhong X, Duan C, Chen Q. A meta-analysis of reflectance confocal microscopy for the diagnosis of malignant skin tumours. J Eur Acad Dermatol Venereol. 2016 Aug;30(8):1295–302.
18. Longo C, Pampena R, Bombonato C, Gardini S, Piana S, Mirra M, Raucci M, Kyrgidis A, Pellacani G, Ragazzi M. Diagnostic accuracy of ex vivo fluores-

cence confocal microscopy in Mohs surgery of basal cell carcinomas: a prospective study on 753 margins. Br J Dermatol. 2018;180:1473–80.
19. Longo C, Ragazzi M, Gardini S, Piana S, Moscarella E, Lallas A, Raucci M, Argenziano G, Pellacani G. Ex vivo fluorescence confocal microscopy in conjunction with Mohs micrographic surgery for cutaneous squamous cell carcinoma. J Am Acad Dermatol. 2015 Aug;73(2):321–2.
20. Longo C, Ragazzi M, Gardini S, Moscarella E. Argenziano G ex vivo fluorescence confocal microscopy of Eccrine Syringomatous carcinoma: a report of 2 cases. JAMA Dermatol. 2015;151(9):1034–6.

Ultrasound

21

Linda Tognetti, Flavio Giulio Liso, Gianluca Nazzaro, Luca Provvidenziale, Enresto De Piano, Andrea Carraro, and Jean Luc Perrot

21.1 Ultrasound for Skin Imaging

Ultrasound (US) imaging is an essential instrument for most medical specialties for its versatility, painless, lack of risk, noninvasiveness. In the field of dermatology, machines that work with high and variable-frequency probes can view changes within superficial structures of the skin. Furthermore, blood flow can be estimated with color Doppler use. These tools combined with clinical examination can support diagnosis and management in a wide range of skin disorders, such as skin cancer, benign process, some inflammatory, and infectious cutaneous diseases [1, 2]. Reflection of the ultrasonic waves from the tissues with different acoustic properties is the basis for ultrasound imaging of the skin. Ultrasonic waves are generated by a probe maintained in direct contact with the patient's skin with the interposition of a gel (which eliminates the air interposed between probe and patient's skin, allowing ultrasound to penetrate the anatomical segment examined); the same probe is able to collect the signal of return, which is appropriately processed by a computer and presented on a monitor for the transduction of sound waves into visual images. Two-dimensional US, B-mode scanning, the method of choice in dermatology, translates the reflected waves into "brightness" values on a gray scale and provides an ecotomographic image of the echoes coming from the structures under examination. For dermatologic applications, US frequencies range from 7.5 to 100 MHz [2]. The most suitable frequency is chosen considering that higher frequencies have greater resolving power of the image, but less depth of penetration into the subject. High frequency from 50 to 100 MHz probes can analyze only the epidermal layer, high frequency 20 MHz probes can reach about 10 mm (epidermis and dermis), medium frequency (MFUS) probes from 10 to 7.5 MHz can reach 4–5 cm of depth with visualization of subcutis and lymphnodes [1]. High-resolution US (HFUS) 20–100 MHz, sacrificing the depth of tissue penetration for more detailed superficial pictures, is now recommended for US

L. Tognetti (✉)
Dermatology Unit, Department of Medical, Surgical and Neuro-Sciences, University of Siena, Siena, Italy

Department of Medical Biotechnologies, University of Siena, Siena, Italy

F. G. Liso · L. Provvidenziale · E. De Piano
A. Carraro
Dermatology Unit, Department of Medical, Surgical and Neuro-Sciences, University of Siena, Siena, Italy

G. Nazzaro
Department of Pathophysiology and Transplantation, Università degli Studi di Milano, I.R.C.C.S. Foundation, Cà Granda Ospedale Maggiore Policlinico, Milan, Italy

J. L. Perrot
Dermatology Unit, University Hospital of St-Etienne, Saint Etienne, France
e-mail: j.luc.perrot@chu-st-etienne.fr

M. Fimiani et al. (eds.), *Technology in Practical Dermatology*,
https://doi.org/10.1007/978-3-030-45351-0_21

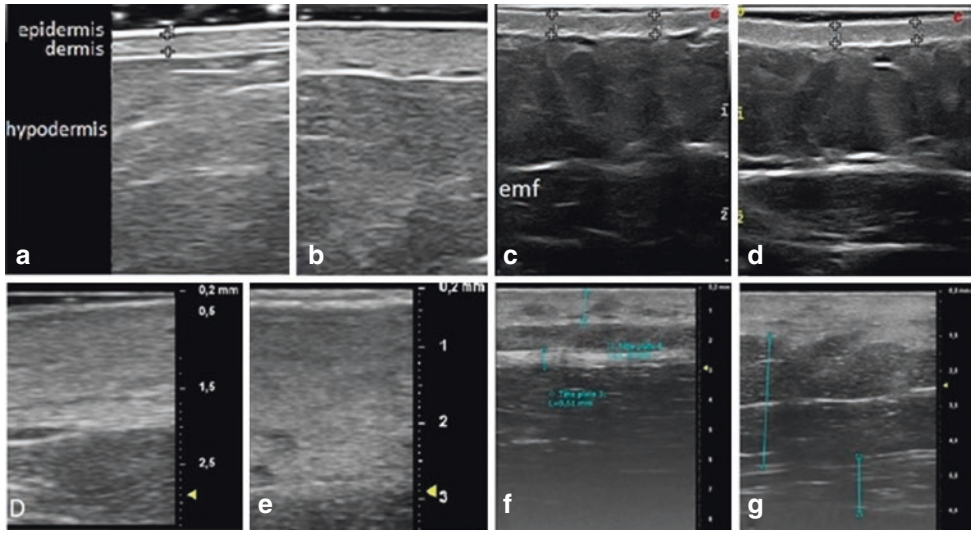

Fig. 21.1 HFUS 20 MHz: healthy skin (40 years, F, thigh) (**a**) and contralateral localized scleroderma patch, increased dermal thickness, and hyperechogenicity (**b**); healthy skin and subcutaneous tissue (33 years, M, thigh) (**c**); contralateral EF lesion late stage, sclerotic external muscularis fascia (emf) generating double hyperechoic bands (railway track sign). HFUS 70 MHz: healthy skin (60 years, F, breast) (**d**); contralateral post-radiotherapy sclerodermic patch with 3 mm dermal thickness (**e**); healthy skin (50 years, M, forearm) and contralateral EF lesion, early sclerotic phase, with increased thickness of inflamed dermal layer and of external muscularis fascia generating multiple echos (**f**); binary track signs (**g**)

application in dermatology. The healthy skin is divided into three layers: epidermis—highly echogenic band, dermis—heterogeneous signals, and the subcutaneous tissue—an anechoic or low echogenicity layer mixed with hyperechoic fibrous septa; superficial fascia also has reflection [2] (Fig. 21.1).

21.2 US in General and Geriatric Dermatology

HFUS associated with the clinical examination provides useful details about size, relationship with other anatomical structures, and vascularization. Information such as skin thickness and density measurement can allow an objective assessment of skin neoformations/foreign bodies (Fig. 21.2), including [3]:

- *Epidermal cyst*: cavity surrounded by epithelium of epidermal derivation and filled with keratin. Clinically it is an elevated or embedded node, located in the dermis or subcutis, of pasty consistency, often connected to the skin

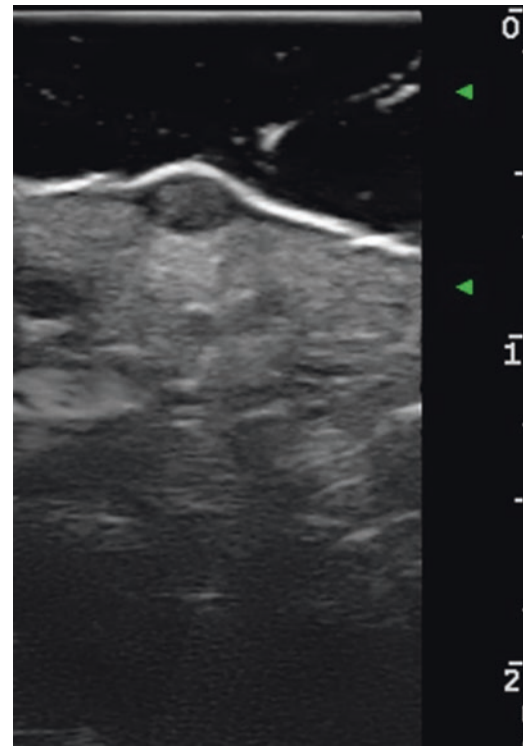

Fig. 21.2 Polarized dermoscopy (20×) of a linear foreign body (**a**) and corresponding HFUS 70 MHz (**b**): linear hypoechoic area localized in the deep papillary dermis and upper reticular dermis, generating a posterior echo

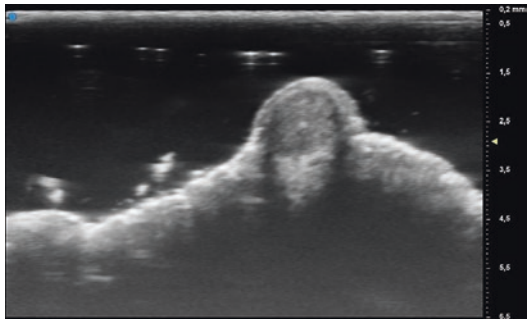

Fig. 21.3 HFUS 70 MHz evaluation of a nipple epidermal cyst in a 45-year-old male: double hyperechoic signal generated by a hyperkeratotic epidermal layer covering an homogenously hyperechoic mass localized at dermal–epidermal junction and associated posterior echo

surface by a small orifice. HFUS shows a well-defined, round-shaped hypoechoic structure located in the dermis and hypodermis with a posterior acoustic reinforcement artifact (Fig. 21.3) [1]. Color Doppler US can show increased vascularity in the periphery of the cyst as a sign of inflammation.

- *Pilomatrixoma*/calcifying epithelioma of Malherbe: derives from hair follicle matrix. On HFUS, it has a target appearance with hyperechoic center corresponding to calcification and a hypoechoic rim [4].
- *Dermatofibroma*: benign proliferation of connective tissue whose origin is a reaction to trauma or insect bites or directly neoplastic. Clinically is a raised lesion of hard consistency and red brownish color. HFUS shows an ill-defined dermo-hypodermic lesion, of hypoechoic heterogeneous appearance. Often there is distortion of the regional hair follicles. Power Doppler sometimes shows slightly increased vascularity within the lesion [1].
- *Lipoma*: of adipose origin, with over or under fascia localization. Clinically it is a node of round shape, often lobulated, soft-elastic consistency, easily compressible, covered by normal skin. HFUS demonstrates oval shape, moderately hyperechoic/echogenicity identical to subcutaneous tissue lesion with no perfusion in Doppler mode [3].
- *Hemangioma*: composed of endothelial proliferations, it is the most frequent soft tissue tumor of infancy. Clinically, it presents two phases: a fast growth after birth and for the first 1–2 years and a slow regression period that usually lasts for 4–5 years. In the proliferative phase, it shows a heterogeneous US pattern with prominent hypoechoic areas corresponding to the most proliferative zones and hyperechoic areas that represent an initial involution fibrotic part [1].
- *Seborrheic keratoses*: of epidermal origin, superficial, and well-delimited papule with a finely granular, greasy, and hyperkeratotic surface. HFUS shows the epidermal "entry echo" and under a hypoechoic, heterogeneous lesion that compresses the underlying dermis.

21.3 US for Skin Tumors

HFUS provides valuable information about the tumor characteristics such as size (lateral extension and depth), shape, consistency, and vascularity before invasive skin biopsy or surgery is planned. HFUS is also able to detect local recurrence during postoperative follow-up or monitor skin metastases during chemotherapy [5]. In general, malignant neoplasms appear as hypoechoic to mixed echogenic focal lesions [1, 5]. The Doppler examination is fundamental for the identification of vascular component and consequent discrimination between benign and malignant tumors, more intensely vascularized (Fig. 21.4) [6, 7].

A series of skin tumors with peculiar echographic aspects have been described [1, 6, 7], including:

- *Basal cell carcinoma* (BCC): tends to show as well-defined, oval-shaped, hypoechoic lesions that often present hyperechoic spots. Increased low flow vascularity is commonly detected within or surrounding the tumor. The pigmented and nodular lesions show a thickened, hyperechoic entry echo with posterior acoustic shadowing. Two US artifacts have been reported: the "angles at the bottom" (produced by significant inflammation due to dilated vessels and giant cells which can produce a

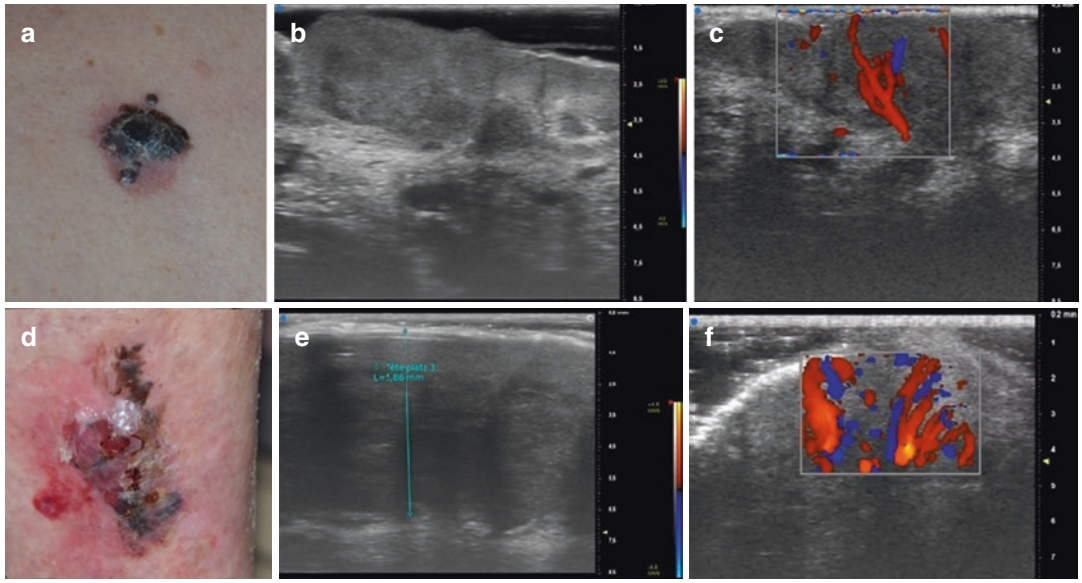

Fig. 21.4 Clinical appearance of a nodular melanoma on the back of a 76-year-old male (**a**); HFUS 70 MHz shows alteration and disruption of the epidermal layer architecture, underlying hyperechoic dishomogeneous dermal layer due to the dense tumor infiltrate and multiple hypoechoic roundish areas corresponding to tumor nests; in the reticular dermis, hyperechogenic homogenous bundles are visible, corresponding to tumor-reactive fibrotic stroma (**b**). Color Doppler examination reveals an abnormally increased arterial vascular flow (**c**). Pigmented basal cell carcinoma in a 86-year-old female on the leg (**d**): HFUS 70 MHz performed over the central nodular portion of the lesion shows thickened hypoechoic areas with sparse roundish nests (on the right) filled with large globular cells (**e**); arterial vascular flow is increased and abnormal on color Doppler examination (**f**)

hypoechoic angled band at the bottom of the lesion) and the "blurry tumor" (caused by extensive hyperplasia of sebaceous glands which generate blurriness or almost isoechogenicity of the lesion with the surrounding tissue) [6–8].

- *Squamous cell carcinoma* (SCC): according to the frequency employed, SCC may appear as well-defined or irregular hypoechoic lesions with/without focal hyperechoic spots. Also, tumor hypervascularity with low-flow vessels may be detected.
- *Melanomas*: tend to show defined, fusiform hypoechoic lesions characterized by prominent vascularity, with/without focal hyperechoic spots associated. HFUS can discriminate between melanomas that measure < or >1 mm (depth), which is important for deciding on the performance of a sentinel node procedure. Also, HFUS allows us to detect satellite, in-transit, or nodal metastases. The vascular density in melanoma has been correlated with the metastatic potential, and neovascularization has been reported as a prognostic factor for metastasis equivalent to the Breslow index [9].
- *Lymph nodes involvement*: Though in normal conditions lymph nodes cannot be distinguished from the neighboring tissues, when inflammation/metastatic process occurs, their acoustic impedance increase: a "reactive" lymph node is generally oval in shape, with hypoechogenic periphery and hyperechogenic centers, and is <3 mm in size. Conversely a tumoral lymph node has a diameter of over 1 cm, is hypoechogenic, spherical, or irregular in shape. HFUS should be performed for the preoperative and postoperative assessment of peripheral lymph nodes; thus, it also has prognostic value in some cases. Doppler examination is crucial for the detection of small hypoechogenic metastases <3 mm located in the marginal hypoechogenic area of a reactive lymph node [10].

21.4 US in Dermosurgery

Imaging technologies are now commonly used in the planning of surgical reconstructions, especially for perforator flaps. MFUS (10–15 MHz) represents the most used in the evaluation of superficial vessels, with the adjustment of the pulse repetition frequency for velocities of 5–45 cm/s [11]. Color Doppler ultrasonography allows to identify the perforator close to the defect and therefore to plan a flap with the smallest arc of transposition and a lower risk of complications [12]. In facial reconstructions, the rich superficial vascularization often allows to identify perforating vessels without the aid of ultrasound probes. Doppler is however often used for the common paramedian line forehead flaps, as well as in the planning of the supratrochlear artery axial propeller flaps, which, differently from the previous ones, allows the execution of the intervention in a single operative stage using the same artery (supratrochlear artery) [13, 14]. The lateral nasal artery branches from the facial artery at the nasolabial sulcus level, identified by Doppler, allow the creation of flaps for the reconstruction of defects of the ala nasi [14].

21.5 US for Infective Dermatoses

MFUS is widely used for the differential diagnosis among abscesses, cellulitis, and hematomas. It has high accuracy (96%) and is easy to find in all emergency medicine departments [15]. The cobblestone appearance is a common finding in cellulitis and is seen as hypoechoic strands in the subcutaneous tissue caused by the swelling. Of converse, abscesses usually appear as spherical or elliptical hypoechoic masses surrounded by edema (Fig. 21.5a). Abscessual or necrotic areas of the leg can develop within large long-standing hematomas which are defined by hypoechoic areas surrounded by hyperechoic strands due to vascular and fibrotic components (Fig. 21.5b). US is also useful to differentiate abscess of the extremities from liquefied gouty tophi [16]. Furthermore, large skin parasites can be detected by HFUS (Fig. 21.6).

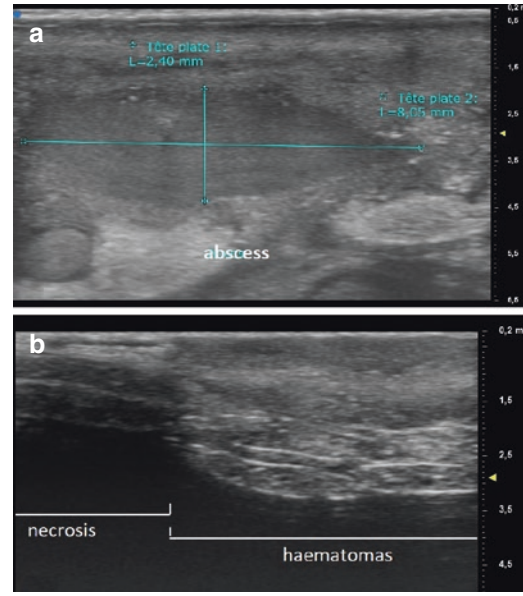

Fig. 21.5 HFUS 70 MHz: definition of a necrotic area developed within a large long-standing hematoma (62 years, F, leg) (**a**) and of an abscess developed within an area of cellulitis (53 years, F, thigh) (**b**)

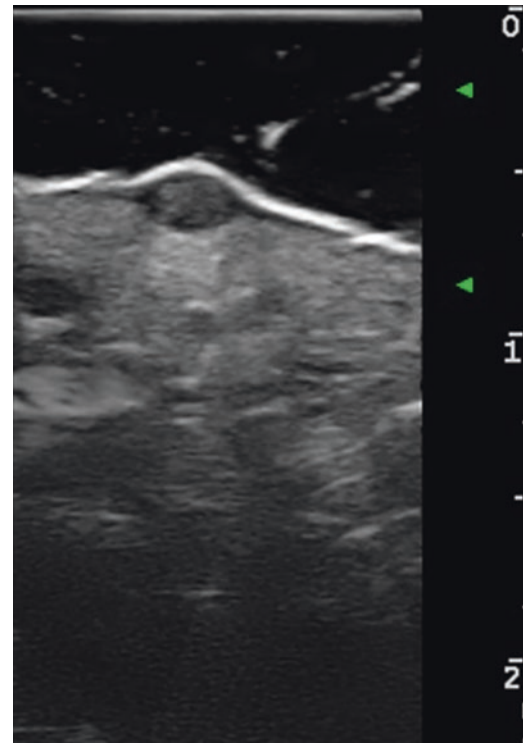

Fig. 21.6 HFUS 20 MHz of a palpable burrow of the heal of a 31-years old male: homogeneoulsy hyperechoic cylindrical mass generating a posterior echo, supporting the diagnosis of Larva migrans parasitosis

21.6 US for Hidradenitis Suppurativa and Autoinflammatory Diseases

The diagnosis of hidradenitis suppurativa (HS), a chronic recurrent inflammatory disease characterized by painful nodules, abscesses, and sinus tracts in the apocrine gland-bearing areas, is based on the association of clinical and sonographic features [17]. Indeed, US demonstrated to be more sensitive than clinical palpation for diagnosing HS lesions [18]. Moreover, the response to therapy may be evaluated with Power Doppler as vascularization is the earliest parameter reducing with therapy [19]. US criteria include widening of the hair follicles; thickening or abnormal echogenicity of the dermis; dermal pseudocystic nodules; fluid collections; and fistulous tracts (Fig. 21.7). A three-stage scoring system, named Sonographic Score in Hidradenitis Suppurativa (SOS-HS), was proposed: stage I for patients showing the previous reported dermal changes affecting a single body segment with single fluid collection and without fistulous tract; II for patients with two to four fluid collections or a single fistulous tract; and III for patients with more than four fluid collections or two or more fistulous tracts or the involvement of at least three body segments.

Psoriasis presents thickening of the epidermis (55% on average) in the affected skin, while inflammatory diseases such as contact dermatitis have increased thickness of dermis with heterogeneous texture and collection of hypoechoic edema [20]. A possible application is also monitoring the entity of a tattoo reaction (i.e., allergic contact dermatitis) and the effect of laser therapy removal (Fig. 21.8).

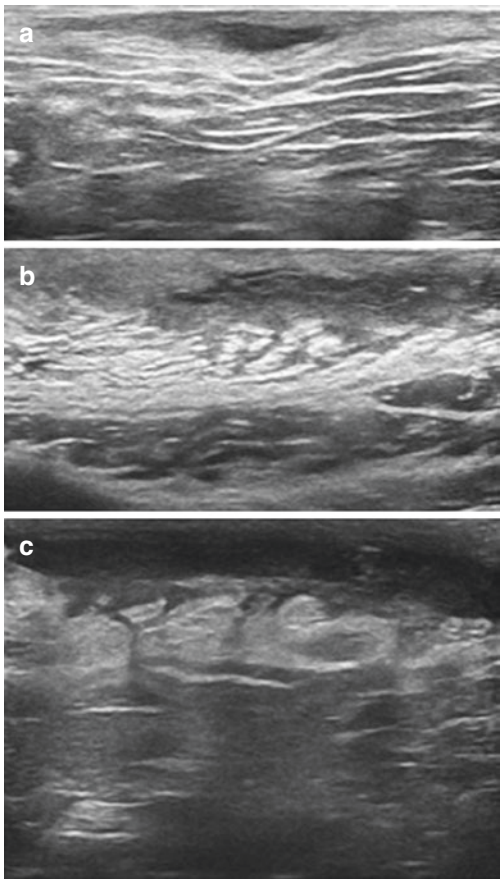

Fig. 21.7 HFUS 20 MHz of a pseudo-cystic nodule (**a**), fluid collection (**b**) and fistulous tract (**c**)

21.7 US for Scleroderma, Scleroderma-Like Diseases, Fat Necrosis, and Rare Conditions

Ultrasonography in scleroderma, localized (i.e., morphea), and deep (i.e., eosinophilic fasciitis-EF) or systemic (i.e., systemic sclerosis), and in scleroderma-like disease (chronic sclerosing graft-versus-host disease, pretibial myxoedema of Graves, scleredema adultorum, scleromyxedema, nephrogenic fibrosing dermopathy, lichen sclerosus lipodermatosclerosis) is used both to confirm the diagnostic clinical suspect and to monitor response to therapy. Various probes have been used, from MFUS 15–20 MHz to HFUS 50–70 MHz [21, 22]. US findings of a sclerodermic lesion may vary according to the disease subtype and phase. In general, hypoechogenicity due to edema is observed in the inflammatory phase, hyperechogenicity in the sclerotic phase due to collagen deposition and increased thickness of dermal layer, while a thinned epidermal layer and normal echogenicity of dermal layer in the atrophic phase. In the post-inflammatory EF phase, thickened hyperechogenic external muscularis fascia is detectable with MFUS and HFUS (Fig. 21.1). MFUS is also useful in various

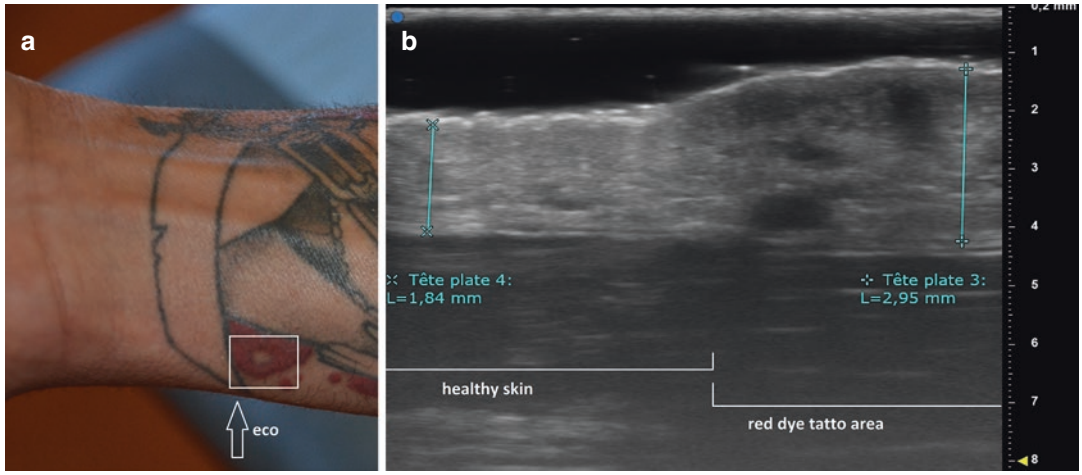

Fig. 21.8 Chronic allergic reaction to red dye in a bilocolour tattoo (*red-black*) of the arm of a 25 years-old mal, strictly limited to the skin areas stained with red pigment (**a**). HFUS 70 MHz reveal the transition between the normal skin (*left*) and the chronic allergic dermatitis areas (*right*) showing a spongiotic appearance with increased dermal thickness and hypoechoic holes corresponding to vesicles

conditions (i.e., post-trauma or medical interventions) where we need to identify an area of necrosis/sclerosis/granulomatous reaction to external body/inflammation within the dermis and adipose tissue [23]. Finally, HFUS can be used to identify ectopic endometrial tissue in patients with cutaneous endometriosis, with different IS features according to the activity phase [24].

References

1. Wortsman A. Ultrasound in dermatology: why, how, and when? Semin Ultrasound CT MRI. 2013;34(3):177–95.
2. Polańska A, et al. Current applications of high-frequency ultrasonography in dermatology. Adv Dermatol Allergol. 2017;34(6):535–42.
3. Ulrich J, et al. Sonographic diagnostics in dermatology. J Dtsch Dermatol Ges. 2014;12:1083–99.
4. Mandava A, Ravuri P, Konathan R. High-resolution ultrasound imaging of cutaneous lesions. Indian J Radiol Imaging. 2013;23(3):269.
5. Bhatt KD, Tambe SA, Jerajani HR, Dhurat RS. Utility of high-frequency ultrasonography in the diagnosis of benign and malignant skin tumors. Indian J Dermatol Venereol Leprol. 2017;83(2):162–82.
6. Wortsman X. Common applications of dermatologic sonography. J Ultrasound Med Off J Am Inst Ultrasound Med. 2012;31(1):97–111.
7. Crisan M, Crisan D, Sannino G, et al. Ultrasonographic staging of cutaneous malignant tumors: an ultrasonographic depth index. Arch Dermatol Res. 2013;305(4):305–13.
8. Bobadilla F, Wortsman X, Muñoz C, et al. Pre-surgical high resolution ultrasound of facial basal cell carcinoma: correlation with histology. Cancer Imaging. 2008;8:163–72.
9. Wortsman X. Sonography of the primary cutaneous melanoma: a review. Radiol Res Pract. 2012:1–6.
10. Lassau N, et al. Prognostic value of angiogenesis evaluated with high-frequency and colour Doppler sonography for preoperative assessment of primary cutaneous melanomas: correlation with recurrence after a 5 year follow-up period. Cancer Imaging. 2006;6:24–9.
11. Saba L, et al. Non-invasive vascular imaging in perforator flap surgery. Acta Radiol. 2013;54(1):89–98.
12. Ibrahim RM, et al. Color Doppler ultrasonography targeted reconstruction using Pedicled perforator flaps—a systematic review and meta-analysis. Eur J Plast Surg. 2018;41(5):495–504.
13. Stigall LE, et al. The Paramidline forehead flap: a clinical and microanatomic study. Dermatol Surg. 2016;42(6):764–71.
14. Karsidag S, et al. Single-stage Ala Nasi reconstruction: lateral nasal artery perforator flap. J Craniofac Surg. 2010;21(6):1887–9.
15. Cammarota T, Pinto F, Magliaro A, Sarno A. Current uses of diagnostic high-frequency US in dermatology. Eur J Radiol. 1998;27(2):S215–23.
16. Tognetti L, Cinotti E, Fiorani D, Rubegni P, Perrot JL. Non invasive diagnosis of liquefied gouty tophus: reflectance confocal microscopy as an alternative to polarizing light microscopy analysis. Skin Res Technol. 2018;25(2):240–1.
17. Wortsman X, Moreno C, Soto R, Arellano J, Pezo C, Wortsman J. Ultrasound in-depth characterization and staging of hidradenitis suppurativa. Dermatol Surg. 2013;39:1835–42.

18. Nazzaro G, Passoni E, Muratori S, et al. Comparison of clinical and sonographic scores in hidradenitis suppurativa and proposal of a novel ultrasound scoring system. G Ital Dermatol Venereol. 2018 Oct 4.
19. Caposiena Caro RD, Solivetti FM, Bianchi L. Power Doppler ultrasound assessment of vascularization in hidradenitis suppurativa lesions. J Eur Acad Dermatol Venereol. 2017; epub.
20. Raju BI, et al. Quantitative ultrasonic methods for characterization of skin lesions in vivo. Ultrasound Med Biol. 2003;29(6):825–38.
21. Knobler R, Moinzadeh P, Hunzelmann N, et al. European dermatology forum S1 guideline on the diagnosis and treatment of sclerosing diseases of the skin, part 1: localized scleroderma, systemic sclerosis and overlap syndromes. J Eur Acad Dermatol Venereol. 2017;31:1401–24.
22. Tognetti L, Cinotti E, Perrot JL, Neri G, Pianigiani E, Fimiani M, Rubegni P. Preliminary experience of the use of high-resolution skin ultrasound for the evaluation of extrathyroidal manifestations of Graves' disease and response to UVA-1 phototherapy. Photodermatol Photoimmunol Photomed. 2019;35(2):129–31.
23. Tognetti L, Cinotti E, Tonini G, Habougit C, Cambazard F, Rubegni P, Perrot JL. New findings in non-invasive imaging of cutaneous endometriosis: Dermoscopy, high-frequency ultrasound and reflectance confocal microscopy. Skin Res Technol. 2018;24(2):309–12.
24. Tognetti L, Filippou G, Bertrando S, Picerno V, Buonocore G, Frediani B, Fimiani M, Rubegni P. Subcutaneous fat necrosis in a newborn after brief therapeutic hypothermia: ultrasonographic examination. Pediatr Dermatol. 2015;32(3):427–9.

Optical Coherence Tomography

22

Victor Desmond Mandel and Giovanni Pellacani

22.1 Introduction

Optical coherence tomography (OCT) was first used in skin imaging in 1997 [1], and since then, it has undergone considerable development of its technology as well as its clinical applications. It is a non-invasive imaging technology, which enables real-time, high-resolution, non-invasive, cross-sectional, and en-face imaging by detecting reflected light from the tissue.

In dermatology, OCT is able to visualize the stratum corneum, epidermis, dermal–epidermal junction (DEJ), upper dermis, skin appendages, sweat ducts, and blood vessels. It can be used for the investigation of many skin disorders such as tumours and inflammatory diseases, for the monitoring of wound healing processes, for the quantification of skin changes and for the evaluation of treatment effects.

22.1.1 Instrument

OCT is an in vivo imaging technique, based on the interference (Michelson interferometry) of infrared light in living tissue, which allows the assessment of the skin at high-resolution and with no discernible effect on the tissue [1]. It relies on the small intensity variations of backscattered light from different tissue cellular microstructures to reveal the tissue morphology. Conventional OCT systems provide images in monochrome and can achieve a penetration depth of up to 2 mm with a resolution of 3–15 μm.

Recently, speckle variance OCT has been introduced and made commercially available, permitting the detection of blood flow in real-time. The technology has been termed dynamic OCT (D-OCT), and, in addition to the images of traditional OCT scans, it allows the study of vessels in transversal and en-face/horizontal sections [2, 3]. D-OCT creates images of the skin microangiography in superficial and deep dermal components (up to a depth of 0.5 mm). Vascular pattern is assessed in en-face images, and two types of parameters can be evaluated: the global analysis of pattern architecture (D-parameters) and the description of specific shapes of vessels (S-parameters) [4].

The D-parameters include the depth, the density, the diameter, the direction and the distribution of the vessels on the scan.

The S-parameters focus on the analysis of the single vessel, and six different shapes can be

Electronic supplementary material The online version of this chapter (https://doi.org/10.1007/978-3-030-45351-0_22) contains supplementary material, which is available to authorized users.

V. D. Mandel (✉) · G. Pellacani
Dermatology Unit, Surgical, Medical and Dental Department of Morphological Sciences related to Transplant, Oncology and Regenerative Medicine, University of Modena and Reggio Emilia, Modena, Italy
e-mail: giovanni.pellacani@unimore.it

M. Fimiani et al. (eds.), *Technology in Practical Dermatology*,
https://doi.org/10.1007/978-3-030-45351-0_22

observed on D-OCT: dots (small red points), blobs (larger round to oval red globules), coiled (spiral-like or convoluted lines/circles), linear (fine lines), curved (comma-like lines) and serpiginous vessels. Furthermore, the dots, blobs and coiled vessel could be described as mottled in case they are distributed in limited but sharply demarcated areas, while the linear vessels can be defined as a mesh when they are interconnected generating a reticular structure. Finally, the linear, curved and serpiginous vessels can present branching defined as vessels forking from the main structure and sub-classified as arborizing (with progressively thinner branching) or bulging (dilated, aneurismatic-like areas).

In cross-sectional images, two vessel patterns can be observed: spikes (needle-shaped narrow peaks of vessels vertically directed towards the surface) and columns (brighter rectangular-shaped structures with an upper horizontal sharply demarcated border) [4].

22.2 Indications

The application of OCT in diagnosing skin disorders is mainly focused on changes in the epidermis, in the DEJ, and in the upper dermis due to the limitations of the penetration depth. The knowledge of the appearance of healthy skin is essential in order to be able to understand changes in diseased skin.

22.2.1 Normal Skin and Healthy Nails

The appearance of normal skin in OCT images varies according to regional differences. The degree of vascularity and the presence of hair follicles, sebaceous glands and eccrine glands also varied with the site of imaging [5]. Nevertheless, the epidermis and the DEJ can always be reliably recognized, but there is a great diversity in epidermal thickness across the body, especially when comparing the palm and sole to other areas. Hair follicles and sebaceous glands are more visible on the face and forearms, while eccrine ducts are more easily visualized in the palms and soles.

In the cross-sectional OCT images, the structures of healthy skin are easily recognizable because different layers have diverse optical properties (Fig. 22.1). The stratum corneum is seen as a narrow hyperreflective band followed by the epidermis, which is slightly less signal intense and appears as a heterogeneous granular textured band of varying thickness. The DEJ and the papillary dermis are again more signal intense, while the reticular dermis offers a less intense signal. The DEJ is seen as a marked change in contrast between the epidermis and the papillary dermis.

Differences in thicknesses of layers and in scattering, caused by different structures and components within the tissue, can be used to quantify acanthosis, atrophy or oedema [6].

D-OCT allows visualization of the vascular networks in the normal skin, and, due to the varying thickness of the epidermis at different body locations, the vessels in the D-OCT images come into view at different depths beneath the skin surface [2]. In the en-face view of normal facial skin (Fig. 22.1 and video), the diameters of the individual vessels appear larger, and the network is cruder compared to the vessels of normal skin located on the arm or the leg. However, independently of body location, the vascular networks appear well-organized, and the individual vessels can usually be easily outlined in the en-face D-OCT images. Instead, dermal papillary loops can be recognized in the cross-sectional view as small dots distributed in close proximity to the DEJ.

The nail unit can also be investigated by OCT, and the healthy nail plate appears as a layered structure containing a varying number of horizontal homogeneous bands of varying intensity and thickness (Figs. 22.2 and 22.3) [7]. The first change in OCT image intensity after the entrance signal corresponds to the border between nail plate and nail bed. Under the cuticle, a black shadow is generally seen due to the hyperreflective quality of a hyperkeratosis, while the lunula appears as a strongly reflective white band that fades away in the matrix. The skin overlying the proximal nail fold meets the nail plate at a shallow angle.

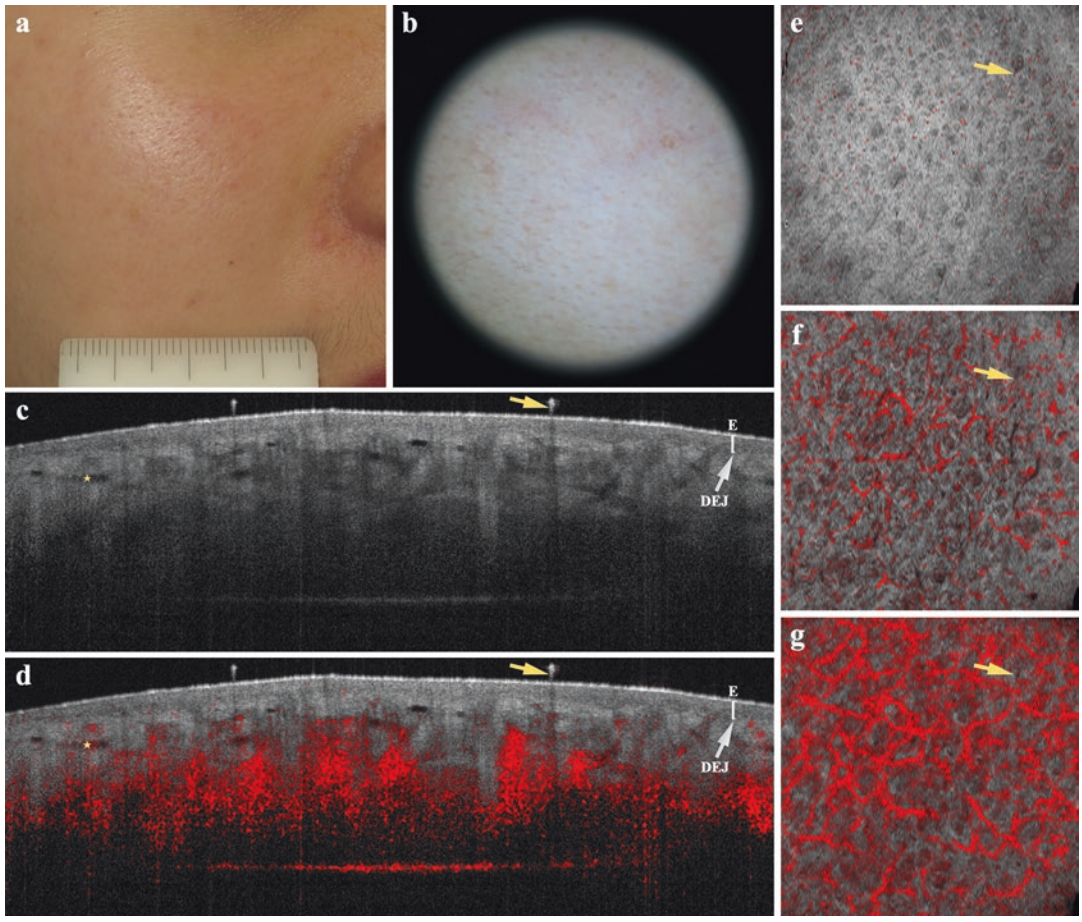

Fig. 22.1 Illustration of the clinical (**a**), dermoscopic (**b**), structural (**c**, **d**) and microvascular (**e**–**g**) features of the normal facial skin. Structural, cross-sectional views (VivoSight®; image size: 6 mm × 6 mm) display the stratum corneum (narrow hyperreflective band), the epidermis (heterogeneous darker granular textured band), the dermal–epidermal junction (DEJ) (change in contrast between the epidermis and the papillary dermis), the dermis (the papillary dermis is again more signal intense, while the reticular dermis offers a less intense signal) (**c**) and a normal vascularization with the dermal papillary loops (**d**). Also vessels in the papillary dermis (*yellow asterisks*) and hair follicles, with the hair shaft protruding above the epidermal surface (*yellow arrows*) are visible. Microvascular en-face D-OCT images [VivoSight®; size: 6 mm × 6 mm; skin depth 150 μm (**e**), 300 μm (**f**) and 500 μm (**g**)] show well-defined larger individual vessels and a well-organized vascular network

On D-OCT imaging, healthy nails contain thin blood vessels with an organized reticular pattern that is visualized with the en-face view (Figs. 22.2, 22.3 and videos) [2]. In the cross-sectional D-OCT images, the vessels are less striking and usually appear as thin vertical red streaks that tend not to extend very superficially. No defined vascular architecture is seen distal to the cuticle under the nail plate and the overall dynamic signal is reduced.

22.2.2 Basal Cell Carcinoma (BCC)

The main features of BCC are a palisading cellular border around the periphery of the tumour lobules with decreased reflectance, hyporeflective ovoid structures corresponding to the tumour islands, disruption of the DEJ and dark, round, hyporeflective structures in the dermis correlating with dermal cysts in histopathology [8]. Hyporeflective ovoid structures protruding from

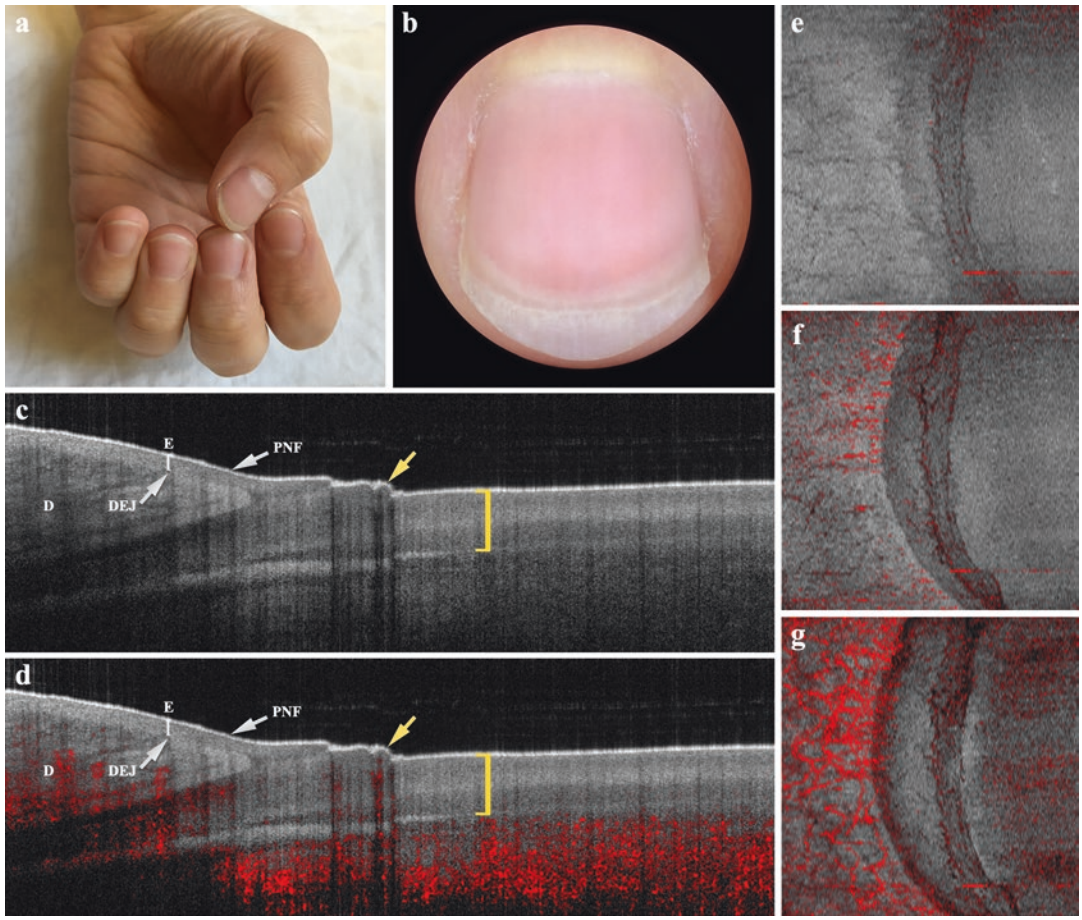

Fig. 22.2 Illustration of the clinical (**a**), dermoscopic (**b**), structural (**c**, **d**) and microvascular (**e–g**) features of the proximal part of the healthy nail. Structural, cross-sectional views (VivoSight®; image size: 6 mm × 6 mm) display a smooth nail surface with the skin overlying the proximal nail fold that meets the nail plate at a shallow angle (*yellow arrows*), a layered nail plate characterized by horizontal homogeneous bands (*yellow brackets*), a linear regular nail bed (**c**), thin vertical red streaks not protruding very superficially, no defined vascular architecture distal to the cuticle under the nail plate and a reduced overall dynamic signal (**d**). Microvascular en-face D-OCT images [VivoSight®; size: 6 mm × 6 mm; skin depth 150 μm (**e**), 300 μm (**f**) and 500 μm (**g**)] show thin blood vessels with an organized reticular pattern

the epidermis are generally observed in the superficial BCC (sBCC), while sharply demarcated hyporeflective ovoid structures located within the dermis are usually detected in the nodular subtype (nBCC) (Fig. 22.4) [9]. The presence of dark peripheral border at the margin of hyporeflective ovoid structures is negatively correlated with the infiltrative BCC (iBCC) [9]. Typically, BCC is accompanied by enlarged blood vessels. A recent D-OCT study on BCC found significant associations with the tumour subtypes for some type of vessels [9]. Branching/arborizing vessels are correlated to a lower risk of observing sBCC, while the vascular lines are commonly observed. Serpiginous vessels, branching/arborizing vessels and vessels creating a circumscribed figure are all associated with a higher risk of the subtype being nBCC (Fig. 22.4 and video). The risk of iBCC, when observing highly present vascular lines (≥10 linear vessels), is significantly reduced.

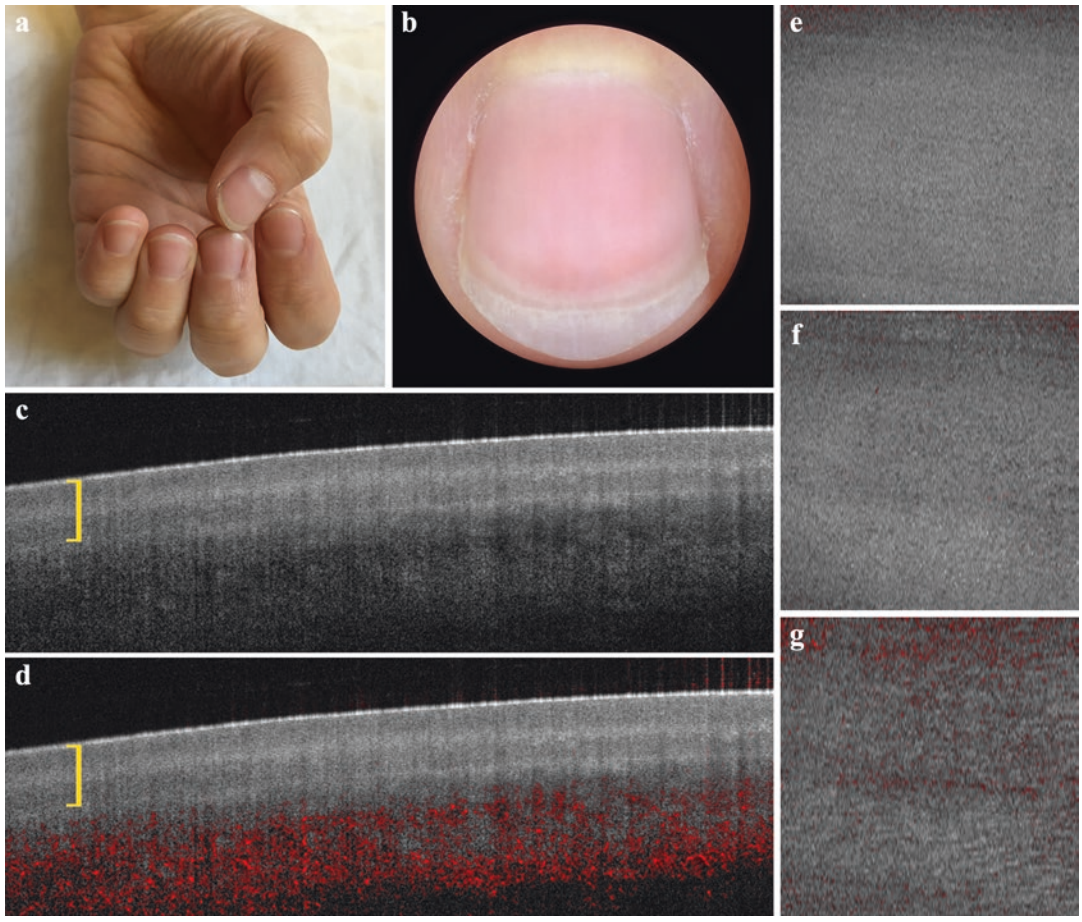

Fig. 22.3 Illustration of the clinical (**a**), dermoscopic (**b**), structural (**c**, **d**) and microvascular (**e**–**g**) features of the distal part of the healthy nail. Structural, cross-sectional views (VivoSight®; image size: 6 mm × 6 mm) display a layered nail plate characterized by horizontal homogeneous bands (*yellow brackets*), a linear regular nail bed (**c**), no defined vascular architecture under the nail plate and a reduced overall dynamic signal (**d**). Microvascular en-face D-OCT images [VivoSight®; size: 6 mm × 6 mm; skin depth 150 µm (**e**), 300 µm (**f**) and 500 µm (**g**)] show a smooth nail surface

22.2.3 Actinic Keratoses (AKs) and Squamous Cell Carcinoma (SCC)

AKs are characterized by a thickening and a stronger scattering of the stratum corneum due to parakeratosis, a thickened epidermis and a clear visibility of the DEJ (Fig. 22.5) [2]. Stratum corneum disruption may be ranging from severe forms of compact hyperkeratotic scales with bright reflection to hyporeflective scales. On D-OCT imaging, AKs show a red pseudonetwork, which resembles the network of normal skin, but the vessels tend to form a larger calibre and a slightly irregular, broader network (Fig. 22.5 and video) [10]. Moreover, vascular curves are predominantly present in AKs.

The features of Bowen's disease (BD)/SCC in situ are similar to AKs, but they often tend to be less hyperkeratotic and show a marked thickening of the epidermis (Fig. 22.6) [2]. By using D-OCT in BD/SCC in situ, the most prevalent types of vessels are the dots and blobs (Fig. 22.6 and video) [10]. The dotted vessels seen in these

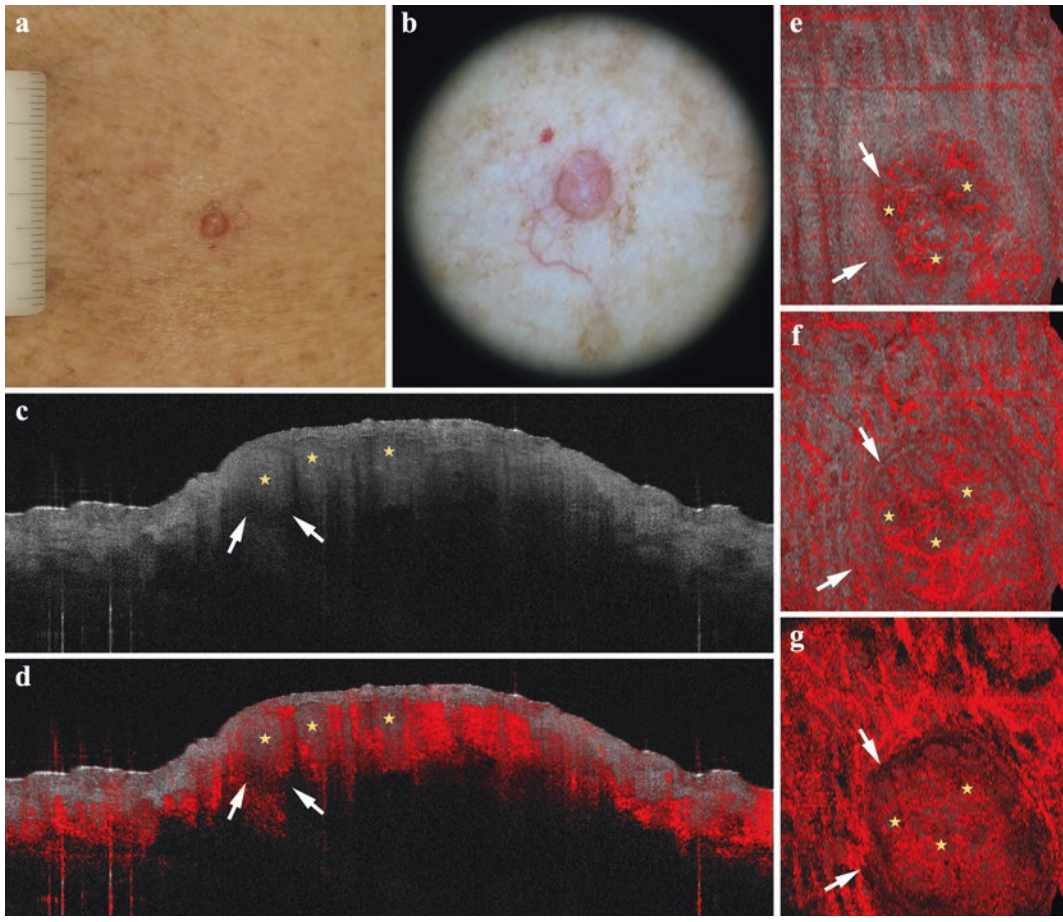

Fig. 22.4 Illustration of the clinical (**a**), dermoscopic (**b**), structural (**c**, **d**) and microvascular (**e**–**g**) features of the nodular basal cell carcinoma. Structural, cross-sectional views (VivoSight®; image size: 6 mm × 6 mm) display hyporeflective ovoid structures (*yellow asterisks*) with dark peripheral borders at its margins (*white arrows*) (**c**) and an increased vascularization (**d**), especially around the tumour islands. Microvascular en-face D-OCT images [VivoSight®; size: 6 mm × 6 mm; skin depth 150 μm (**e**), 300 μm (**f**) and 500 μm (**g**)] show the presence of the serpiginous vessels, the branching/arborizing vessels and vessels creating a circumscribed figure

lesions are larger than the capillaries observed in normal skin or psoriasis, independently of their body site location. Moreover, in contrast to AKs, the vessels in (BD)/SCC in situ are not arranged in a network.

Criteria for invasive SCC include the loss of the typical layering (as visible in AKs/BD/SCC in situ), loss of the dark line normally representing the DEJ due to the infiltration of tumour cells into the dermis and round or ovoid structures in the dermis of varying reflectivity (Fig. 22.7) [2].

Hyperkeratotic scales produce a signal shadow that can impair the visualization of deeper structures, impede the clear visualization of the DEJ and disguise the tumour below. Therefore, the presence of severe hyperkeratosis in AKs, BD and SCC represents a problem in OCT examination. In all these cases, before doing the examination, it is better to apply for few weeks a topical product helpful in reducing the thickness of the lesion. On D-OCT imaging, invasive SCC shows a diversified and chaotic pattern of irregularly shaped and arranged vessels of different calibre (Fig. 22.7 and video) [10].

Angiogenesis evolves during tumour development starting in early AKs with vascular

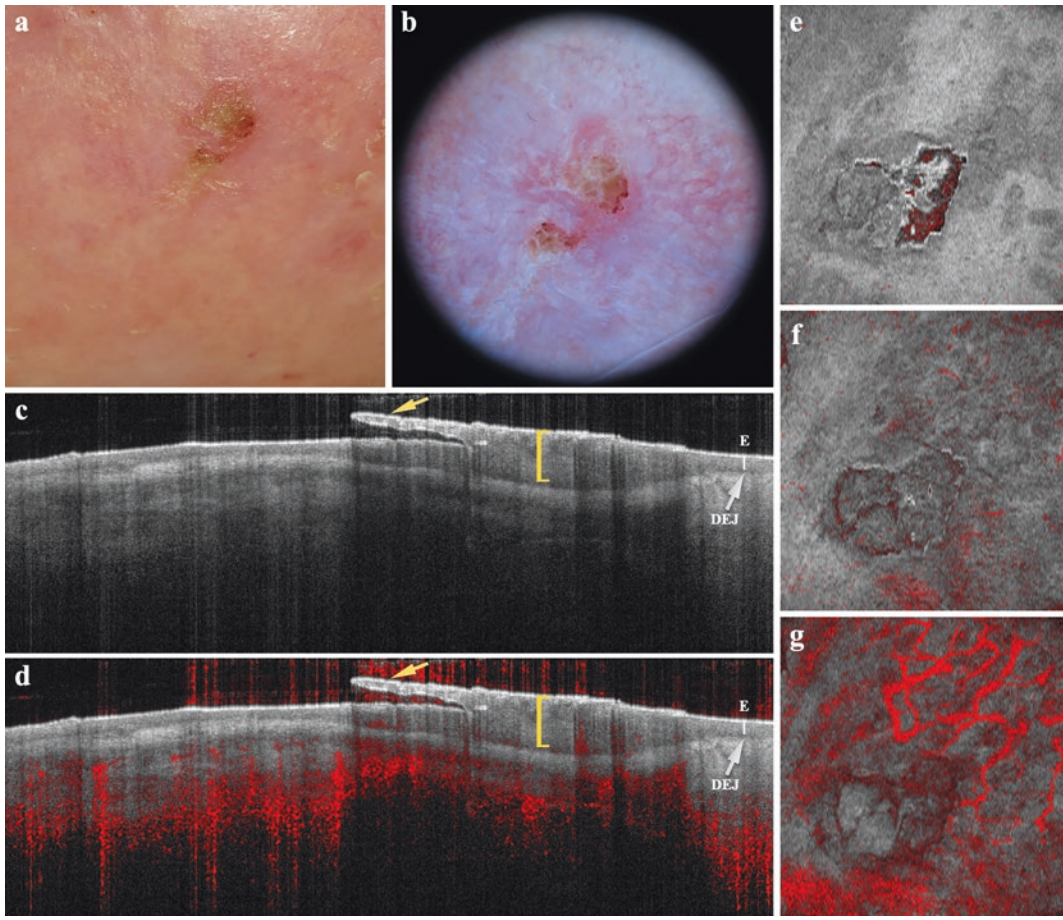

Fig. 22.5 Illustration of the clinical (**a**), dermoscopic (**b**), structural (**c**, **d**) and microvascular (**e**–**g**) features of the actinic keratosis. Structural, cross-sectional views (VivoSight®; image size: 6 mm × 6 mm) display a thickening and a stronger scattering of the stratum corneum (hyperkeratosis) (*yellow arrows*), a thickened epidermis (acanthosis) (*yellow brackets*), a clear visibility of the dermal–epidermal junction (DEJ) (**c**) and a slightly increased vascularization (**d**). Microvascular en-face D-OCT images [VivoSight®; size: 6 mm × 6 mm; skin depth 150 μm (**e**), 300 μm (**f**) and 500 μm (**g**)] show a red pseudonetwork resembling that of normal skin, but the vessels appear slightly more enlarged and less well-organized, and vascular curves

features similar to the surrounding normal skin, then dotted and/or blob vessels and finally progressing to a polymorphous pattern in invasive SCC lesions [10].

22.2.4 Nevi and Melanoma

Nevi and melanoma show an irregular scattering in OCT, due to the presence of melanin within pigmented lesions [11].

Nevi are characterized by a homogenous epidermis with a relatively strong signal, a clear demarcation of DEJ, hyperreflective dense clusters of melanocytes in the DEJ zone and/or papillary dermis, a finger-shaped elongation of rete ridges, a dark round to oval cavities in the dermis corresponding to dilated blood vessels, and bright horizontal linear structures in the reticular dermis [12]. In compound nevi, the overlying epidermis may be flat, show some acanthosis or have a seborrheic keratosis-like appearance, even with horn cysts.

Strongly pigmented nevi show a significant reduction of reflectivity underneath the epidermal layer, and this is probably a result of scatter caused by melanin.

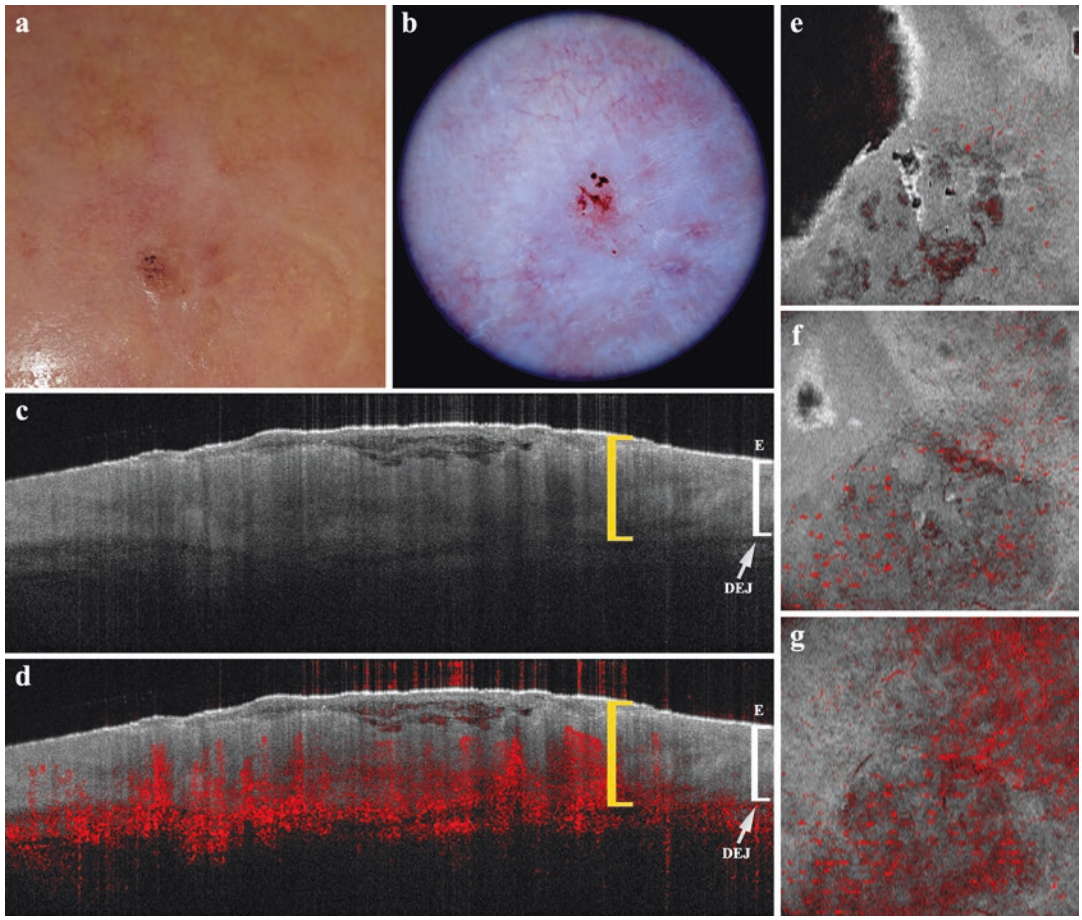

Fig. 22.6 Illustration of the clinical (**a**), dermoscopic (**b**), structural (**c**, **d**) and microvascular (**e**–**g**) features of the squamous cell carcinoma in situ. Structural, cross-sectional views (VivoSight®; image size: 6 mm × 6 mm) display a similar aspect than actinic keratosis, but it often appears less hyperkeratotic and with a marked thickening of the epidermis (acanthosis) (*yellow brackets*) (**c**, **d**). Microvascular en-face D-OCT images [VivoSight®; size: 6 mm × 6 mm; skin depth 150 μm (**e**), 300 μm (**f**) and 500 μm (b)] show the presence of the dots and blob vessels

In differentiating melanomas from nevi, normal skin architecture is less frequent, the DEJ is not detectable due to the infiltrative tumour growth, and a finger-shaped elongation of the rete ridges is rare. Moreover, malignant melanoma shows the presence of more or less large vertical icicle-shaped structures that partly reached the reticular dermis with their peak aspect and on histology correspond to dense infiltrates consisting of tumour cells and lymphocytes [12].

In thin melanomas, OCT can be used to measure the thickness of the lesions and to detect their lower border, which appears as the scattering within the tumours that differs from the surrounding collagen fibres [11].

Melanocytic lesions are characterized by a variable vascular pattern according to their nature [2].

On D-OCT imaging, junctional nevi or nevi with a minimal dermal involvement displaying regularly distributed dotted structures immediately below the epidermis (Fig. 22.8 and video). This vascular pattern is usually comparable with the surrounding normal skin or it is occasionally more pronounced. A thin reticular architecture can be identified only in the deep

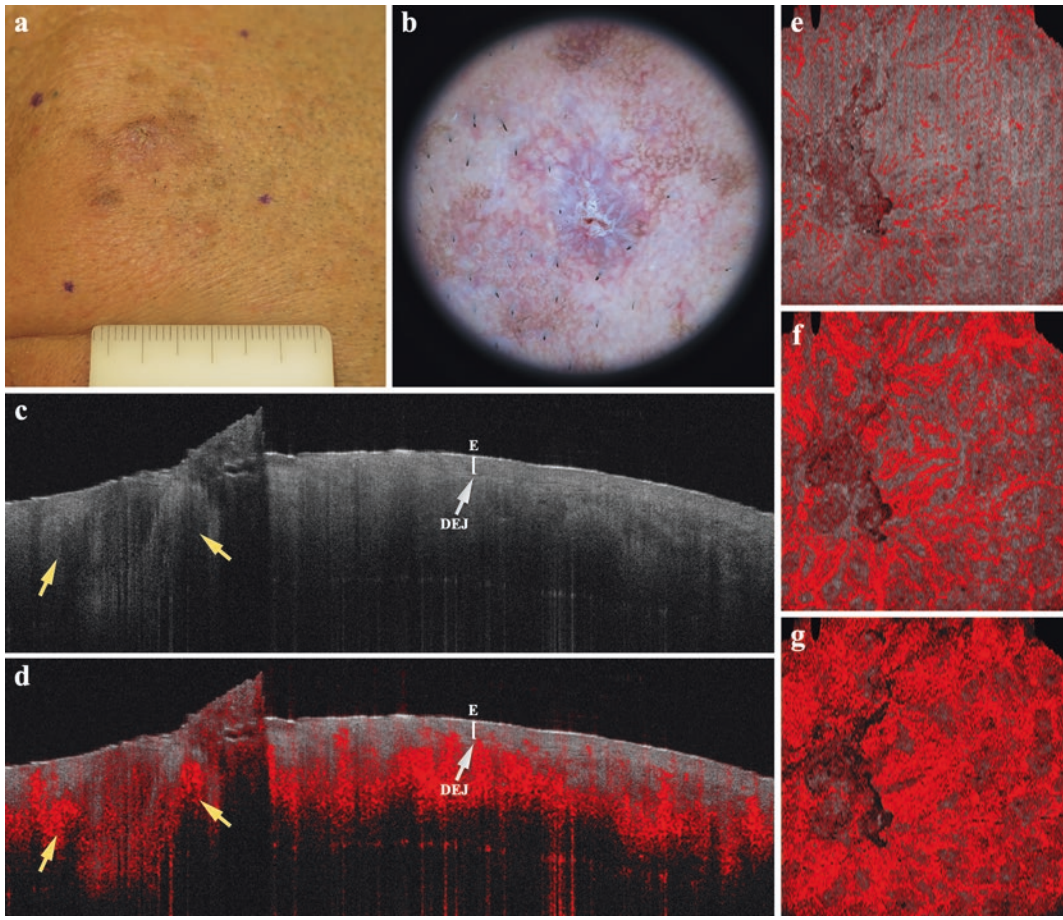

Fig. 22.7 Illustration of the clinical (**a**), dermoscopic (**b**), structural (**c**, **d**) and microvascular (**e**–**g**) features of the invasive squamous cell carcinoma. Structural, cross-sectional views (VivoSight®; image size: 6 mm × 6 mm) display the loss of the dark line normally representing the dermal–epidermal junction (DEJ) due to the infiltration of tumour cells into the dermis, the presence of round or ovoid structures in the dermis of varying reflectivity (*yellow arrows*) (**c**) and an increased vascularization (**d**). Microvascular en-face D-OCT images [VivoSight®; size: 6 mm × 6 mm; skin depth 150 μm (**e**), 300 μm (**f**) and 500 μm (**g**)] show a diversified and chaotic pattern of irregularly shaped and arranged vessels of different calibre

dermal component. Instead, nevi with a conspicuous dermal component show larger dotted vessels with an arcuate aspect, starting from the bottom of the lesion and directed towards the surface (Fig. 22.9 and video). The length of these vessels is related to the depth of the melanocytic lesion, and they are regularly distributed throughout the nevus.

In melanoma, the peripheral area is composed of typical capillaries derived from pre-existing vessels, whereas the vessels of the central portion of the lesion are in part generated by tumour cells during the process of vasculogenic mimicry [13]. On D-OCT imaging, with the increasing Breslow stage and tumour thickness, dotted vessels becoming more irregularly distributed and other vascular morphologies can be detected [14]. Curved vessels usually occur in melanomas with Breslow thickness >1.00 mm (Fig. 22.10 and video), while coiled and serpiginous vessels are commonly detected in those >2.00 mm. Finally, thicker melanomas show branching vessels, which are predominantly sub-classified as bulging structures visible in deeper layers and may correspond to aneurismatic vessels generated by a rapid and chaotic growth pattern.

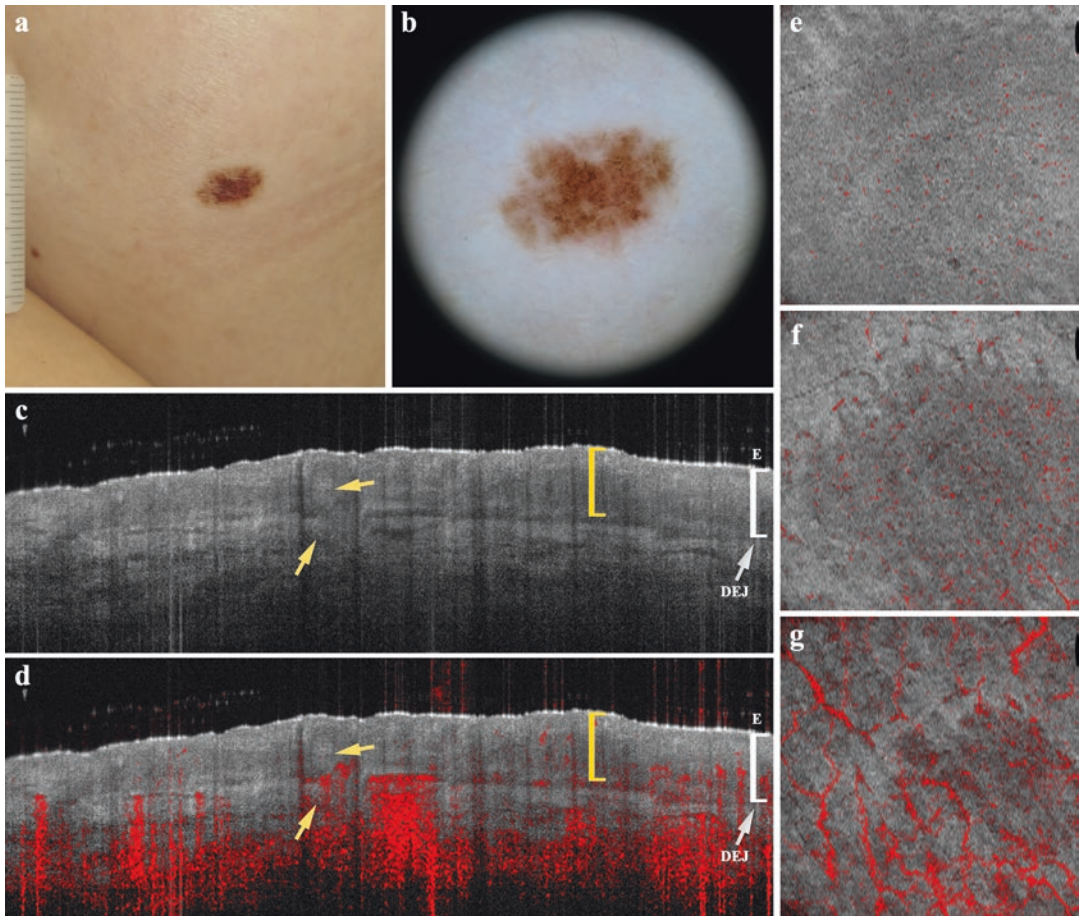

Fig. 22.8 Illustration of the clinical (**a**), dermoscopic (**b**), structural (**c**, **d**) and microvascular (**e**–**g**) features of the compound nevus. Structural, cross-sectional views (VivoSight®; image size: 6 mm × 6 mm) display a thickened epidermis (acanthosis) (*yellow brackets*), a clear demarcation of the dermal–epidermal junction (DEJ), hyperreflective dense clusters of melanocytes in the DEJ zone and papillary dermis (*yellow arrows*), a finger-shaped elongation of rete ridges, dilated blood vessels in the dermis, bright horizontal linear structures in the reticular dermis (**c**) and a slightly increased vascularization characterized by the presence of thin regular columns (**d**). Microvascular en-face D-OCT images [VivoSight®; size: 6 mm × 6 mm; skin depth 150 μm (**e**), 300 μm (**f**) and 500 μm (**g**)] show a regular distribution of dotted vessels and the occurrence of a thin reticular architecture in the deep dermal component of the nevus

In cross-sectional images, the presence of thin regular columns is commonly observed in nevi, while the vessels are organized in large irregularly distributed vertical columns in melanoma [15].

Differently from the keratinizing tumours and BCC, melanomas have more heterogeneous vascular patterns, a higher variability in thinner lesions and progressive changes of the vascular pattern according to the depth [14]. Since vascular progression is theoretically linked with tumour aggressiveness, the evaluation of vascular morphology in melanomas may prove a biomarker to estimate the invasiveness in vivo.

22.2.5 Psoriasis

Psoriasis is characterized by thickened and bright stratum corneum corresponding to parakeratosis, by acanthosis with severely elongated rete ridges in a regular pattern and by an increase number of

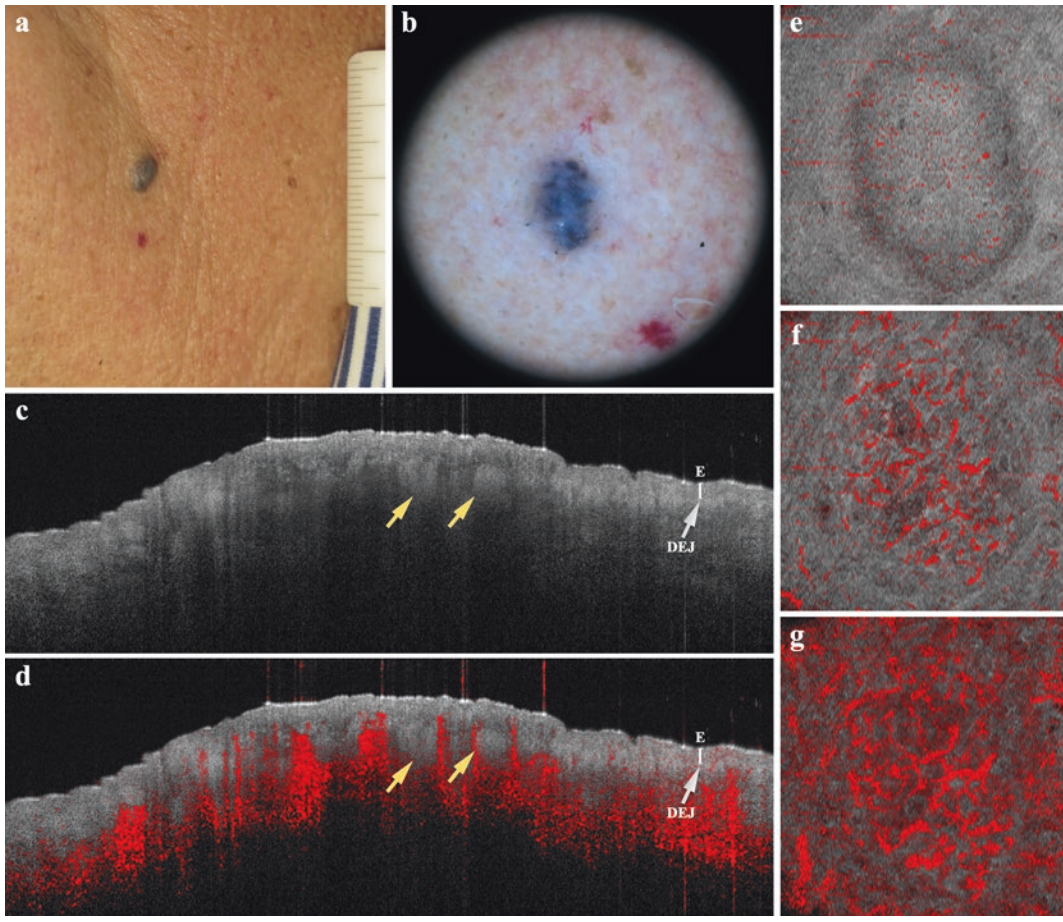

Fig. 22.9 Illustration of the clinical (**a**), dermoscopic (**b**), structural (**c**, **d**) and microvascular (**e**–**g**) features of the blue nevus. Structural, cross-sectional views (VivoSight®; image size: 6 mm × 6 mm) display a clear demarcation of the dermal–epidermal junction (DEJ), hyperreflective dense clusters of melanocytes in the dermis (*yellow arrows*), a finger-shaped elongation of rete ridges (**c**) and a slightly increased vascularization characterized by the presence of thin regular columns (**d**). This nevus shows a significant reduction of reflectivity underneath the epidermal layer, which is probably due to the scatter caused by melanin. Microvascular en-face D-OCT images [VivoSight®; size: 6 mm × 6 mm; skin depth 150 µm (**e**), 300 µm (**f**) and 500 µm (**g**)] show the occurrence of larger dotted vessels with an arcuate aspect, starting from the bottom of the lesion and directed towards the surface

dilated blood vessels in the upper dermis (Fig. 22.11) [2, 11]. Inflammatory infiltration and oedema in the dermis lead to a lower scattering.

D-OCT shows dotted vessels regularly distributed in en-face images and spikes of small vessel loops in the papillary dermis in cross-sectional examination (Fig. 22.11 and video) [2].

The response to treatment can be evaluated by measuring the epidermal thickness, the signal attenuation coefficient, the diameter and the density of the dermal vessels [11].

22.2.6 Bullous Diseases

OCT images may match histopathology regarding the level and the architecture of the blisters in bullous diseases such as bullous pemphigoid (BP) and pemphigus.

OCT allows the precise definition of the bullae location in patients affected by BP (Fig. 22.12) and pemphigus (Fig. 22.13) [16]. BP presents with subepidermal blisters that appear as dark, ovoid to round, areas covered by epidermis of full

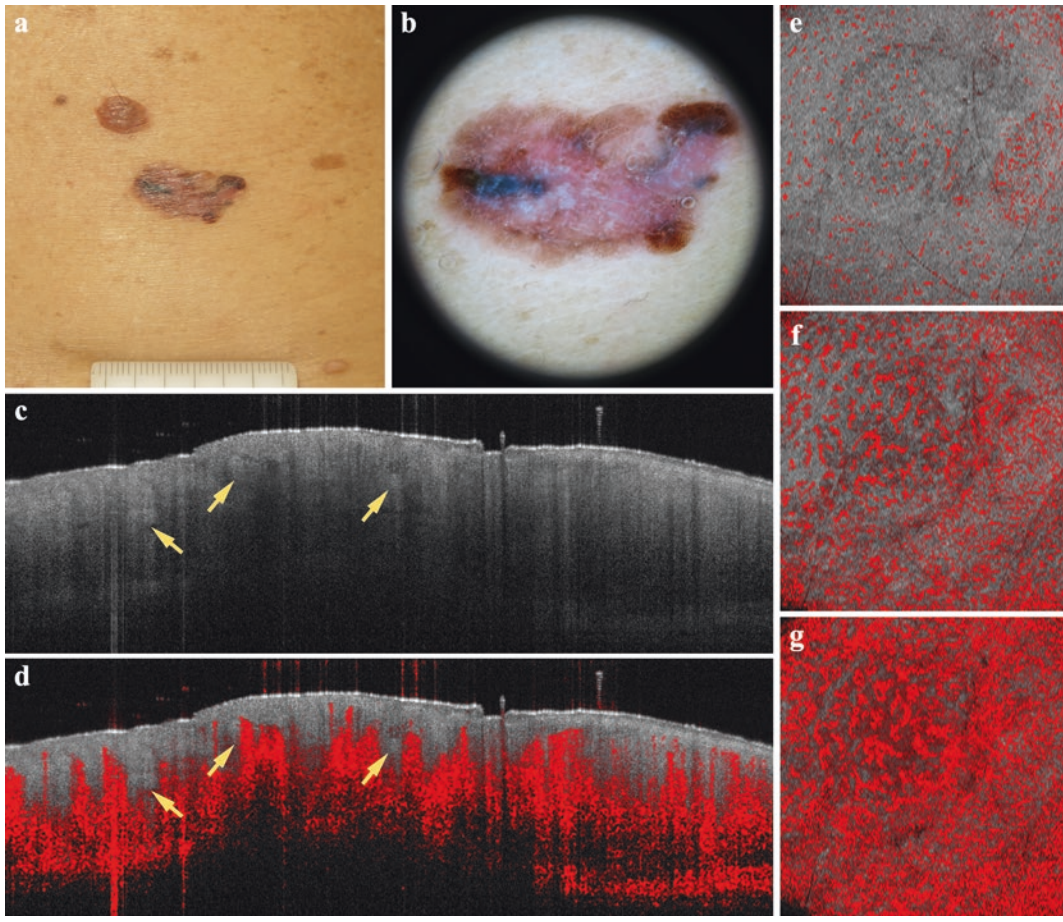

Fig. 22.10 Illustration of the clinical (**a**), dermoscopic (**b**), structural (**c**, **d**) and microvascular (**e**–**g**) features of the melanoma (Breslow 1.44 mm). Structural, cross-sectional views (VivoSight®; image size: 6 mm × 6 mm) display the loss of the normal skin architecture with the dermal–epidermal junction (DEJ) not detectable, the presence of large vertical icicle-shaped structures that partly reached the reticular dermis with their peak aspect (*yellow arrows*) (**c**) and an increased vascularization with the vessels organized in large irregularly distributed vertical columns (**d**). Microvascular en-face D-OCT images [VivoSight®; size: 6 mm × 6 mm; skin depth 150 μm (**e**), 300 μm (**f**) and 500 μm (**g**)] show an irregular distribution of dotted and curved vessels. Some vessels also present an evident dilatation of their calibre, with bulging branches

thickness and localized at the dermal–epidermal junction. Instead, pemphigus is characterized by the presence of dark, ovoid to round, areas within the epidermal layer corresponding to the intra-epidermal blisters.

Linear, thin dark structures in the upper dermis correspond to the dilated blood vessels and are usually detected in BP and pemphigus. Inflammatory cells inside the blisters, which appear as grey pinpoint structures, are more frequently detected in BP than in pemphigus. Grey homogeneous material inside the blisters corresponding to fibrin deposition can be commonly found in BP, but not in pemphigus. Moreover, OCT enables the identification of subclinical bullae on the clinically healthy skin of patients with BP (Fig. 22.12) and pemphigus (Fig. 22.13) [16].

Currently, there are no studies regarding the application of D-OCT in bullous diseases.

Therefore, OCT offers useful information for a rapid non-invasive diagnosis of bullous disease, identification of biopsy site and treatment monitoring, especially in the cases of subclinical lesions [15]. However, OCT cannot replace histopathologic and immunologic examinations that are still required for diagnosis confirmation.

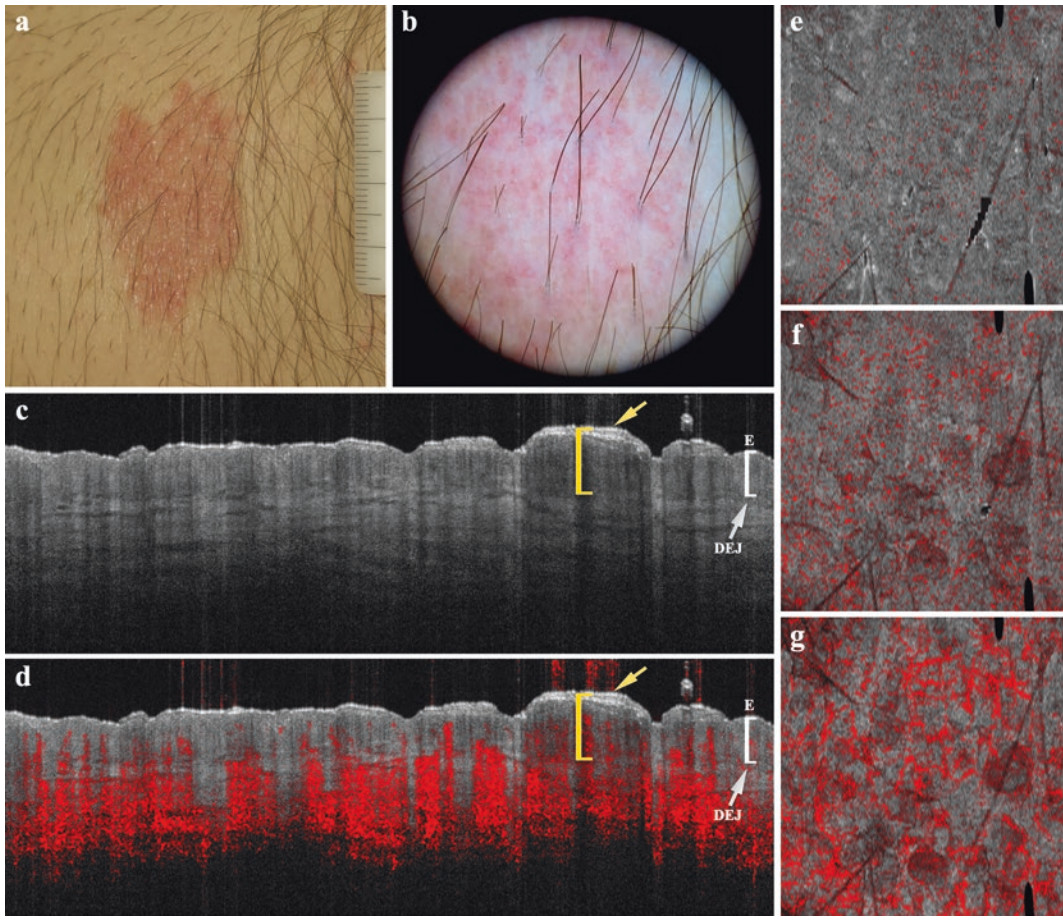

Fig. 22.11 Illustration of the clinical (**a**), dermoscopic (**b**), structural (**c**, **d**) and microvascular (**e**–**g**) features of the psoriasis. Structural, cross-sectional views (VivoSight®; image size: 6 mm × 6 mm) display a thickened and bright stratum corneum (parakeratosis) (*yellow arrows*), a thickened epidermis (acanthosis) (*yellow brackets*) with severely elongated rete ridges in a regular pattern, dilated blood vessels in the upper dermis (**c**) and an increased vascularization with spikes of small vessel loops in the papillary dermis (**d**). Microvascular en-face D-OCT images [VivoSight®; size: 6 mm × 6 mm; skin depth 150 µm (**e**), 300 µm (**f**) and 500 µm (**g**)] show a regular distribution of dotted vessels and presence of loops of dilated capillaries in the upper stratum papillare

22.2.7 Wounds

OCT allows a non-invasive and reliable observation of morphological changes during the three different phases (inflammatory, proliferative and remodelling) of wound healing [17]. Monitoring of this process is indispensable for the therapeutic effectiveness and improved care of chronic wounds (Fig. 22.14), which are generally characterized by a prolonged or excessive inflammatory phase, persistent infections, and the inability of dermal or epidermal cells to respond to reparative stimuli.

The inflammatory phase is characterized by the damage to the epidermis, the dermal-epidermal junction that is no longer visible and the presence of an almost transparent fluid on the surface of the wound edge. Therefore, a deeper insight into the dermis is provided, revealing fewer visible vessels than healthy skin.

In the proliferation phase, the epithelialization from the edge of the wound occurs, a new and less intense signal above the dermis is displayed with a DEJ, there is an increased amount of vessels in reticular dermis, and the collagen appears brighter.

In the remodelling phase, epidermal epithelialization is completed with a continuous epidermal layer. The reticular dermis has large and distinct vessels, bright and hyperreflective

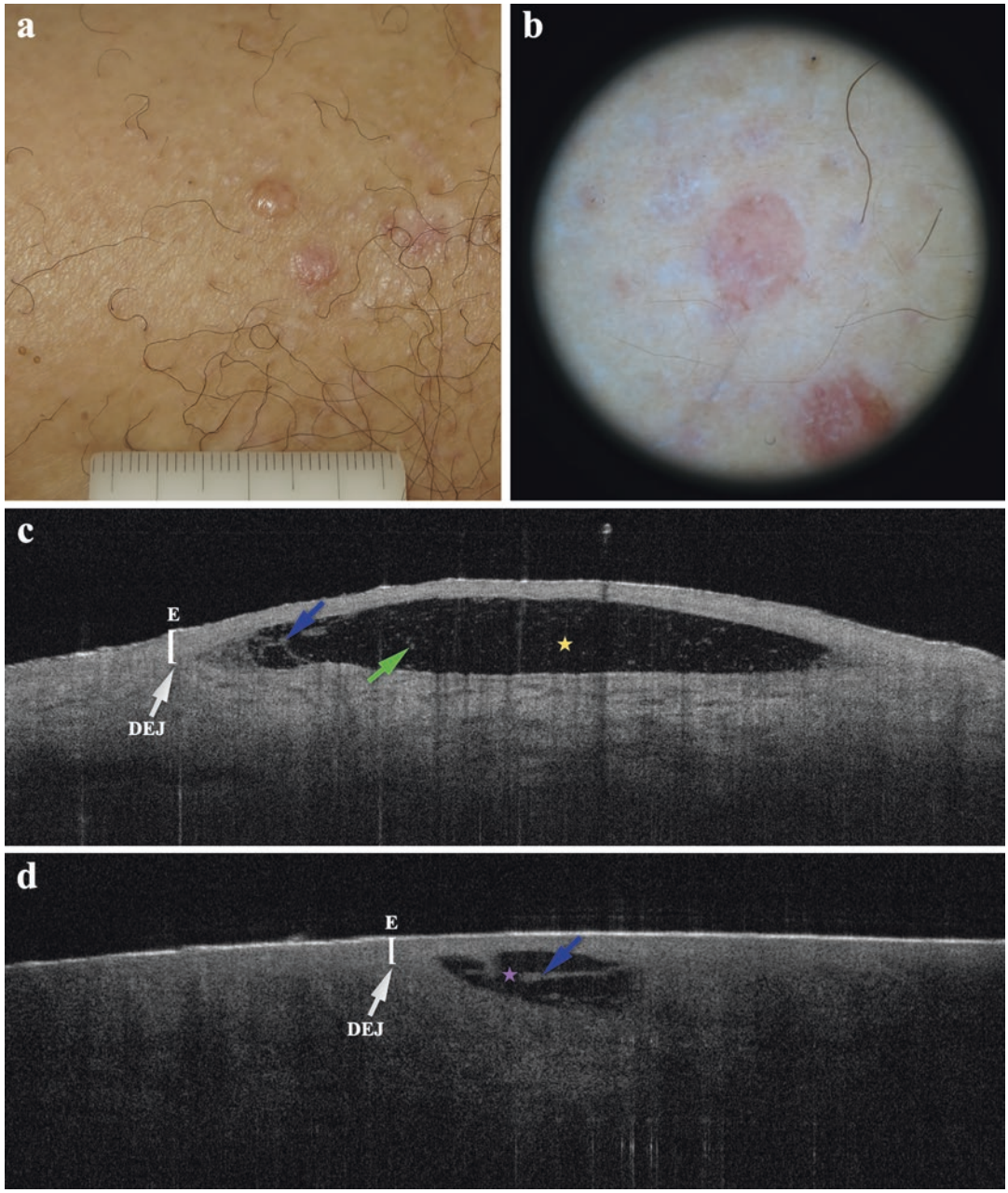

Fig. 22.12 Illustration of the clinical (**a**), dermoscopic (**b**) and structural (**c**, **d**) features of the bullous pemphigoid. Structural, cross-sectional views (VivoSight®; image size: 6 mm × 6 mm) display the presence of subepidermal bulla (*yellow asterisk*) at the level of the dermal–epidermal junction (DEJ), with some inflammatory cells (*green arrow*) and fibrin deposition (*blue arrow*) inside the blister, dilated blood vessels in the upper dermis (**c**) and subclinical cleft (*purple asterisk*) on the clinically healthy skin (at 2 cm from the lesion) with fibrin deposition (*blue arrow*) inside it (**d**)

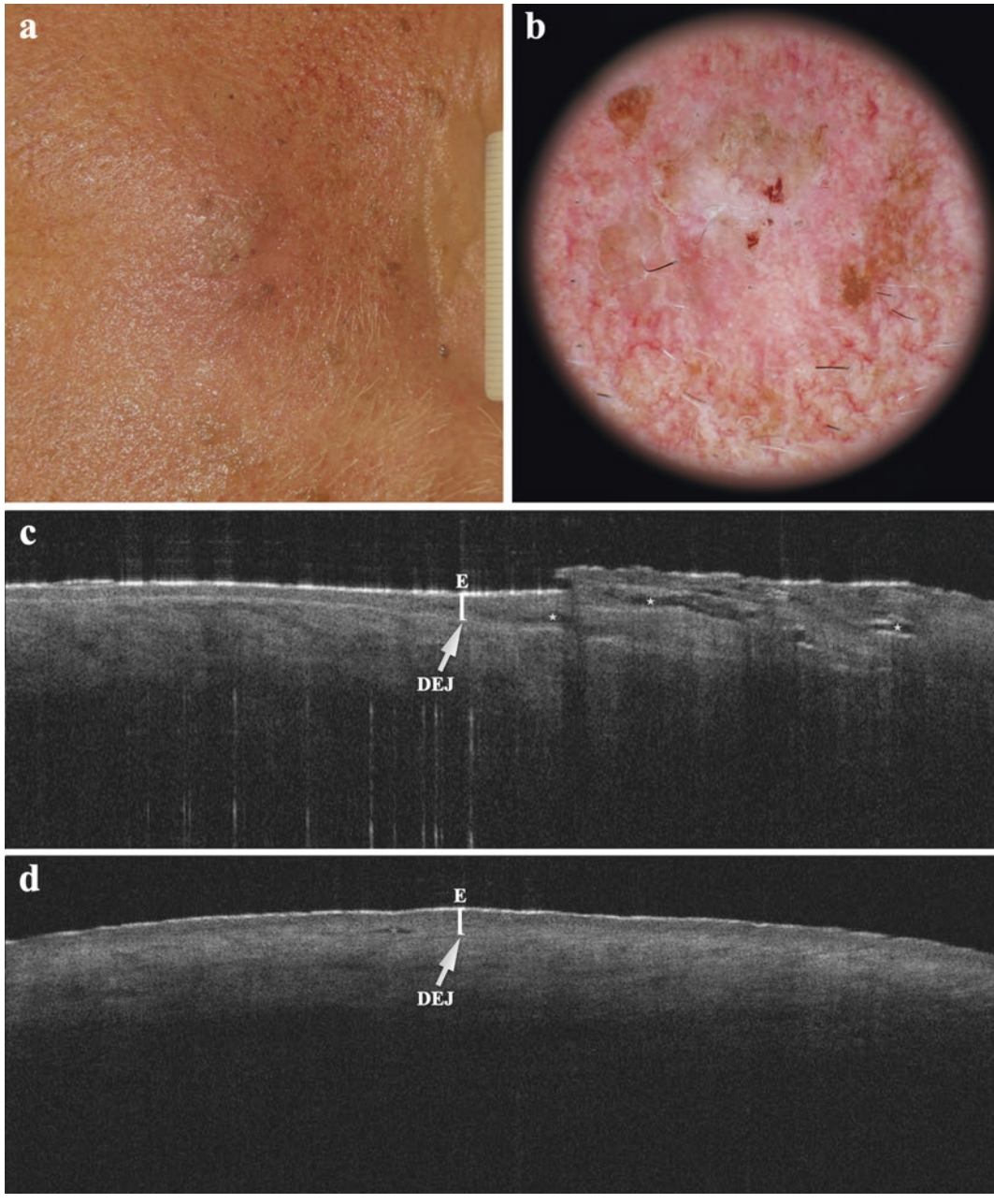

Fig. 22.13 Illustration of the clinical (**a**), dermoscopic (**b**) and structural (**c**, **d**) features of the pemphigus. Structural, cross-sectional views (VivoSight®; image size: 6 mm × 6 mm) display the presence of intra-epidermal bulla (*yellow asterisks*) at the level of the dermal–epidermal junction (DEJ), dilated blood vessels in the upper dermis (**c**) and subclinical cleft (*purple asterisk*) on the clinically healthy skin (at 2 cm from the lesion) (**d**)

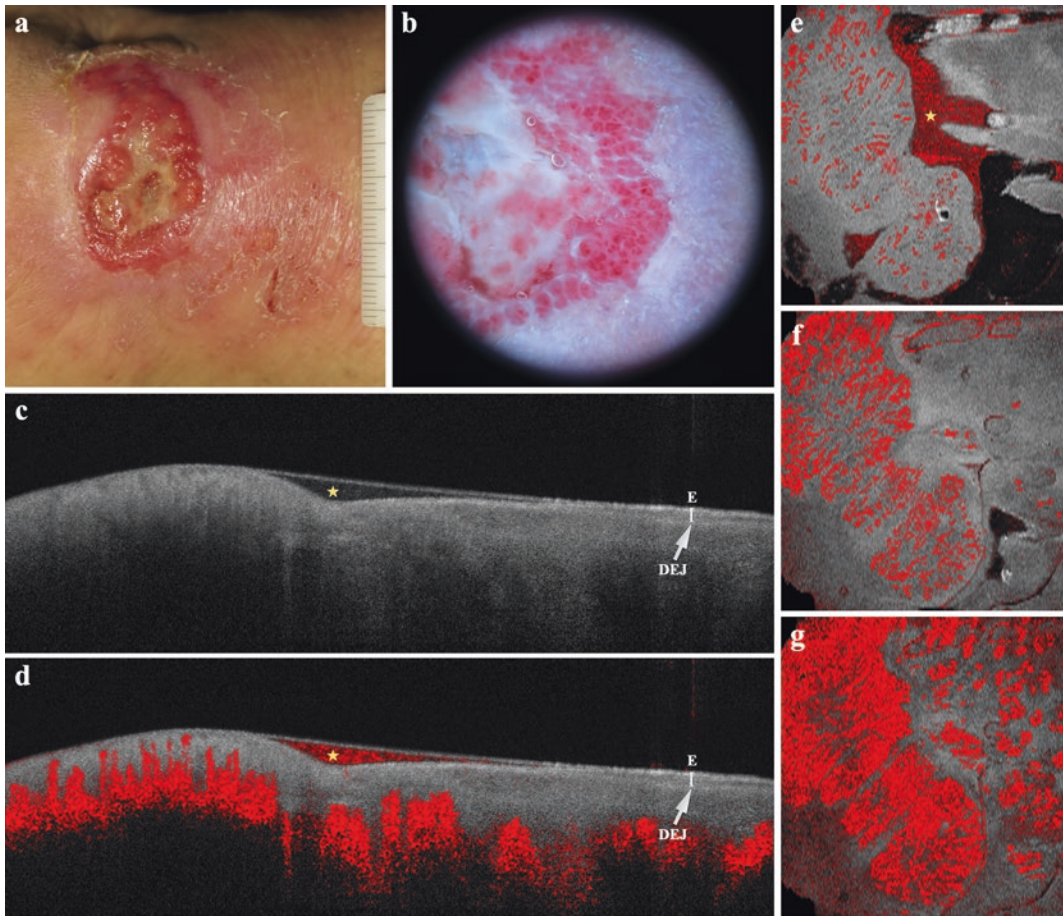

Fig. 22.14 Illustration of the clinical (**a**), dermoscopic (**b**), structural (**c**, **d**) and microvascular (**e**–**g**) features of the chronic wound. Structural, cross-sectional views (VivoSight®; image size: 6 mm × 6 mm) display the damage to the epidermis with the loss of the less intense signal above the dermis, the dermal–epidermal junction (DEJ) no longer visible and an almost transparent fluid (*yellow asterisks*) on the surface of the wound edge (inflammatory phase), but also the epithelialization from the edge of the wound with the reappearance of the DEJ, the dermal regeneration and the formation of granulation tissue (proliferative phase) (**c**) and an increased amount of vessels in reticular dermis (**d**). Differentiation between papillary and reticular dermis is lost (**c**, **d**). Microvascular en-face D-OCT images [VivoSight®; size: 6 mm × 6 mm; skin depth 150 μm (**e**), 300 μm (**f**) and 500 μm (**g**)] show capillaries in the wound bed that develop a glomerulus-like configuration with convoluted vessels

collagen with orientated dense fibres and no appendages. In comparison with healthy skin, the OCT image appears hyperreflective throughout.

On D-OCT imaging, the capillaries in the wound bed develop a glomerulus-like configuration with convoluted vessels (Fig. 22.14 and video) [2].

OCT can also be useful for the differential diagnosis of chronic wounds and the assessment of burns [2]. In acute burn wounds, the determination of the burn depth is very important because it defines the choice of the therapeutic regime.

For all these reasons, OCT is suited for wound assessment and can represent an alternative for punch biopsies in studies of wound healing [16]. However, in case of suspect malignant degeneration of chronic wounds into cancer or suspicious malignancies that present as chronic wounds, this instrument cannot replace histology, which still represents the gold standard for the determination of pathological modifications.

22.2.8 Hair

Among the three conventional racial human subgroups (Afro-ethnic, Asian and Caucasian), hair is most similar in terms of the chemical composition (proteins and amino acids constituting keratin), but it differs for fibre shape and mechanical properties [18]. Afro-ethnic hair has an elliptical shape and presents a high level of irregularity in the diameter along the hair shaft. Asian and Caucasian hairs have a circular and cylindrical shape, respectively. Generally, Asian presents a greater diameter than Afro-ethnic and Caucasian hair. OCT can be used to determine the structural and morphological features of hair [18].

OCT may be a useful tool for the diagnosis of cicatricial alopecia such as the frontal fibrosing alopecia (FFA), and it can assist in monitoring disease activity in a non-invasive manner.

OCT study on FFA found that epidermal thickness is increased in the inflammatory hairline (0.13 mm) and decreased in the alopecic band (0.08 mm) compared to controls (0.10 mm) [19]. This finding can be explained by the presence of inflammatory infiltrate and oedema in the areas of disease activity, and atrophy in zones of scarring.

On clinically inflammatory and cicatricial hairline, OCT shows partial or complete loss of follicular openings with an irregular distribution (Fig. 22.15). Collagen appears as concentric hyperreflective inter-follicular "onion-shaped" bundles around follicular remnants, and its distribution in the inflammatory hairline is irregular.

On D-OCT imaging, vascular flow in cicatricial skin is decreased compared to inflammatory regions and controls (up to 0.20 mm), but the relationship reverses compared to normal at deeper depths (Fig. 22.15 and video). Inflammatory tissue shows significantly increased vascular flow throughout.

Therefore, distinct features of FFA can be recognized during different disease states with OCT.

22.2.9 Nail Diseases

Nail diseases such as onychomycosis and psoriasis are often very troublesome to the patient and may present a diagnostic challenge to the dermatologist.

OCT offers a quick and non-invasive view of the patient's nail in real-time, resulting a valuable tool for the evaluation of underlying nail disease.

The standard diagnosis for onychomycosis involves clinical suspicion and at least one positive laboratory test. However, all evaluations of the laboratory diagnostic methods (KOH preparation, fungal culture, PCR and histopathology with PAS staining) presuppose the correct sampling of the material in order to avoid false-negative results and contamination. Therefore, the correct prior disinfection, the knowledge on the best area of the nail for sampling and a sufficient amount of material obtained are essential.

On OCT imaging, the nail with distal subungual onychomycosis not complicated by dermatophytoma shows a loss of organization and the presence of multiple, hyperreflective, poorly defined, wisplike streaks within the nail plate and parallel to the nail surface [20]. These high scattering elongated structures, surrounded by inhomogeneous low scattering areas, correspond to accumulations of fungal hyphae. Instead, the dermatophytoma nail presents a demarcated homogenous accumulation, representing the fungal mass, localized in a deep to a disorganized, rough-contoured, inhomogeneous nail plate (Fig. 22.16) [20].

On D-OCT imaging, healthy nails display a clear distinction between the vascular nail bed and avascular nail plate, while the nail with dermatophytoma exhibits an avascular mass immediately above the vascular nail bed (Fig. 22.16 and video).

Then, nails with distal subungual onychomycosis and dermatophytoma show peculiar OCT findings that can help the physician to make quick diagnosis.

On OCT imaging, psoriatic nails appear thicker than healthy nails and present a wavy, layered nail plates (Figs. 22.17 and 22.18) [21]. The nail surface is rough and irregular with superficial fissuring. Moreover, the skin overlying the proximal nail fold is ragged and indurated and meets the nail plate at a steep angle in comparison to the shallow angle of the healthy nails.

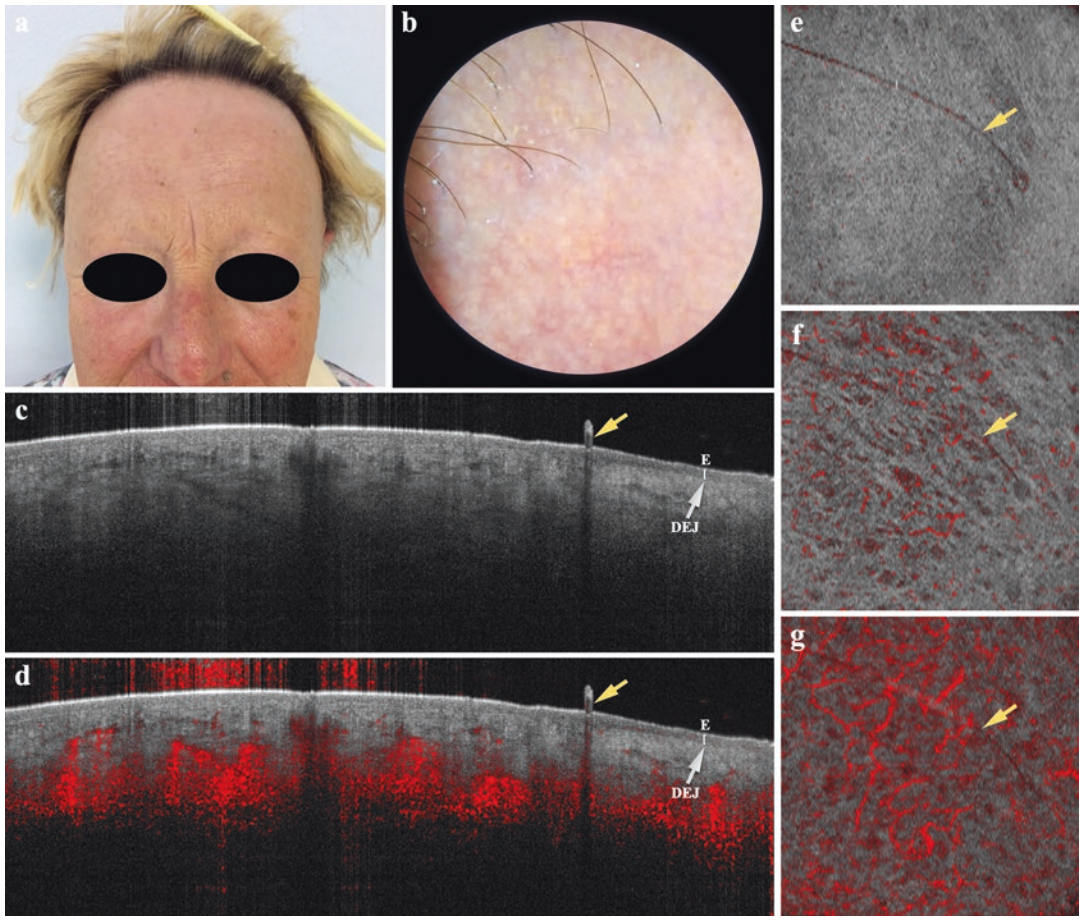

Fig. 22.15 Illustration of the clinical (**a**), dermoscopic (**b**), structural (**c**, **d**) and microvascular (**e**–**g**) features of the frontal fibrosing alopecia. Structural, cross-sectional views (VivoSight®; image size: 6 mm × 6 mm) display a decreased epidermal thickness in the alopecic band, an almost complete loss of follicular openings, the concentric hyperreflective inter-follicular "onion-shaped" bundles around follicular remnants, the presence of "lonely hair" (*yellow arrows*) (**c**) and a slightly increased vascularization in reticular dermis compared to the normal hairline (**d**). Microvascular en-face D-OCT images [VivoSight®; size: 6 mm × 6 mm; skin depth 150 μm (**e**), 300 μm (**f**) and 500 μm (**g**)] show that the vascular flow of the cicatricial tissue is decreased below the skin surface (up to 0.20 mm), but it is increased at deeper depths

White streaks are commonly observed within the nail plate, predominantly in the mid-layer of the distal part of the nail, and correlate clinically as leukonychia. Pitting appears as a focal dark irregularity with underlying shadowing in cross-sectional image and as a black-ringed shapes in en-face view.

Within the nail bed, in the areas of onycholysis, it is possible to appreciate abnormalities consisting of subungual ridges alongside highly reflective white wispy sheets and dense white specks. Predominant black empty areas surrounding highly reflective tufts, which resemble cotton balls or cloud-like structures, are also contained in the deep nail bed.

Using the en-face D-OCT views standardized at 0.60 mm in depth, the psoriatic nails display dilated blood vessels with a haphazard architecture (Figs. 22.17, 22.18 and videos) compared to healthy nails that contain thin vessels with an

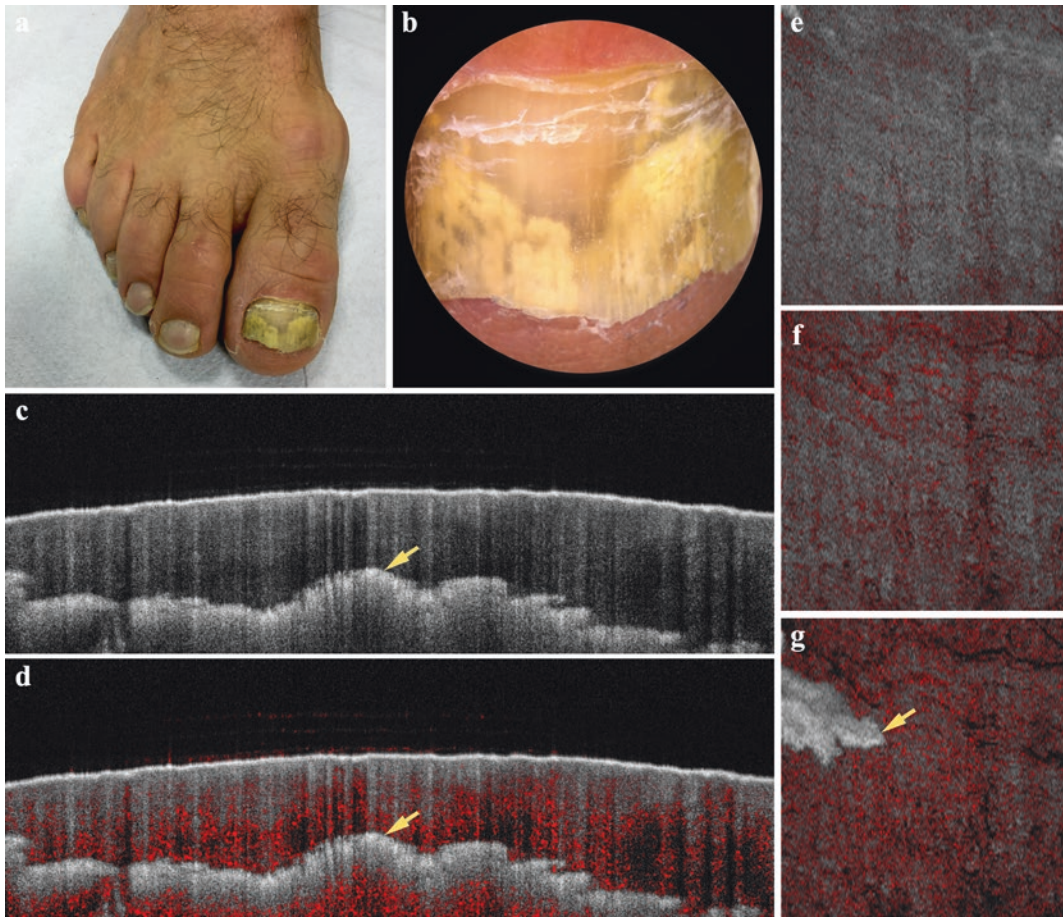

Fig. 22.16 Illustration of the clinical (**a**), dermoscopic (**b**), structural (**c**, **d**) and microvascular (**e**–**g**) features of the dermatophytoma. Structural, cross-sectional views (VivoSight®; image size: 6 mm × 6 mm) display a sharply demarcated avascular mass (*yellow asterisks*) lying within an inhomogeneous nail plate without distinct parallel bands and immediately above the vascular nail bed (**c**, **d**). Microvascular en-face D-OCT images [VivoSight®; size: 6 mm × 6 mm; skin depth 150 μm (**e**), 300 μm (**f**) and 500 μm (**g**)] show an avascular mass (*yellow asterisk*) localized in a deep to a disorganized, rough-contoured, inhomogeneous nail plate

organized reticular pattern [21]. On the cross-sectional D-OCT view, psoriatic nails show a dense arrangement of blood vessels protruding superficially, while the healthy nails are characterized by thin and less-striking blood vessels, not extending as superficially. Despite the increased thickness of the psoriatic nails, an increased dynamic signal can be diffusely seen under the proximal nail plate.

Therefore, OCT can identify structural and vascular features specific to nail psoriasis and may be useful for diagnosis as well as treatment monitoring of this disease.

22.2.10 Quantification of Skin Changes and Therapy Monitoring

Several studies of UV radiation therapy, steroid atrophy, wound healing or nail hydration over time demonstrate that OCT is a valuable tool for monitoring of therapeutical effects and quantification of skin changes [11]. Moreover, OCT permits to control the therapeutic efficacy of nonsurgical treatment options such as imiquimod or photodynamic therapy, and it can help to avoid repetitive biopsies, keeping a non-invasive approach.

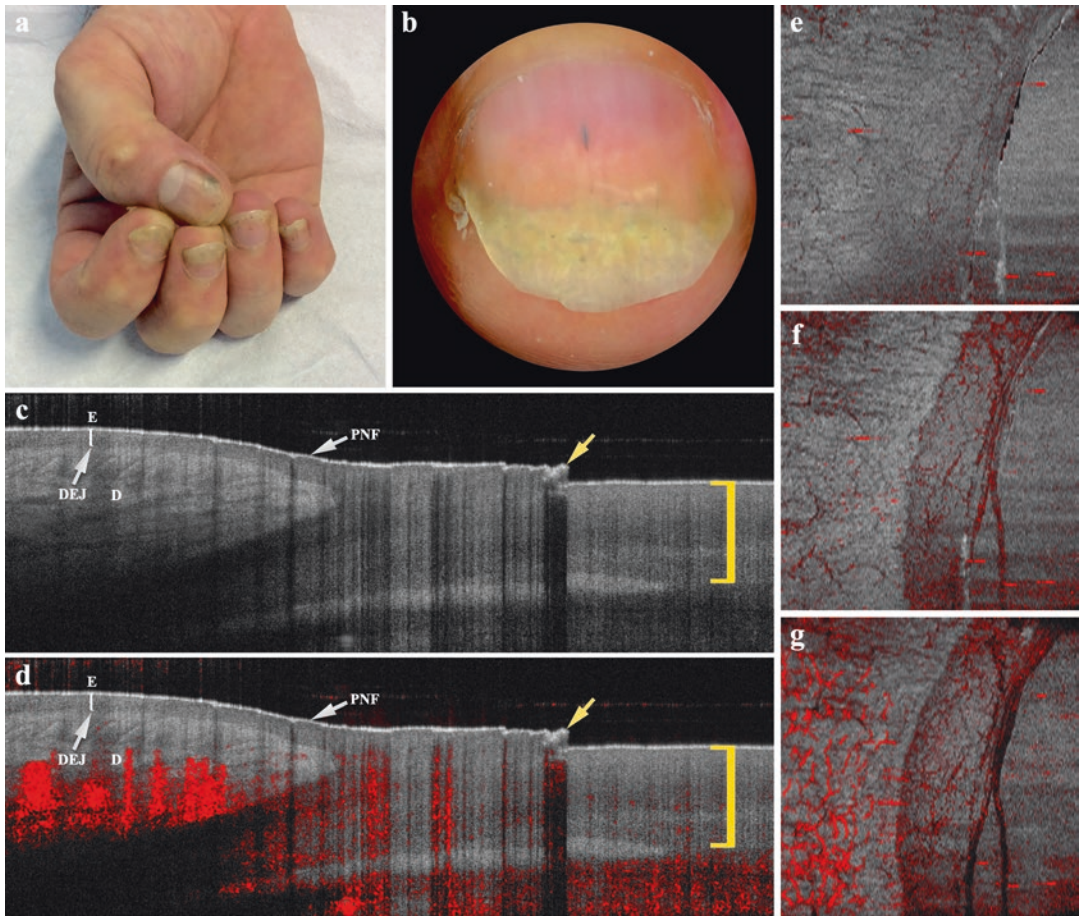

Fig. 22.17 Illustration of the clinical (**a**), dermoscopic (**b**), structural (**c**, **d**) and microvascular (**e**–**g**) features of the proximal part of the psoriatic nail. Structural, cross-sectional views (VivoSight®; image size: 6 mm × 6 mm) display a thickened nail (*yellow brackets*) with the skin overlying the proximal nail fold that meets the nail plate at a steep angle (*yellow arrows*), a wavy and layered nail plate (**c**), a dense arrangement of blood vessels protruding superficially and an increased dynamic signal diffusely visible under the proximal nail plate (**d**). Microvascular en-face D-OCT images [VivoSight®; size: 6 mm × 6 mm; skin depth 150 μm (**e**), 300 μm (**f**) and 500 μm (**g**)] show dilated blood vessels with a haphazard architecture and the presence of ragged and indurated skin overlying the proximal nail fold

22.3 Conclusion

OCT has been studied in a variety of dermatological disorders, but the majority of the studies have investigated non-melanoma skin cancers, especially BCC and its mimickers. Therefore, the diagnostic accuracy and criteria are better described in this area and the prime indications for OCT are the non-melanoma skin cancers. This technique enables a fast detection of the tumour and can allow an estimation of infiltrative growth. When using nonsurgical treatment options, OCT is useful in order to avoid repetitive biopsies and to control the therapeutic efficacy. Additionally, it can be performed for diagnosis and monitoring of melanocytic lesions, inflammatory diseases, wounds, hair, and nail disorders.

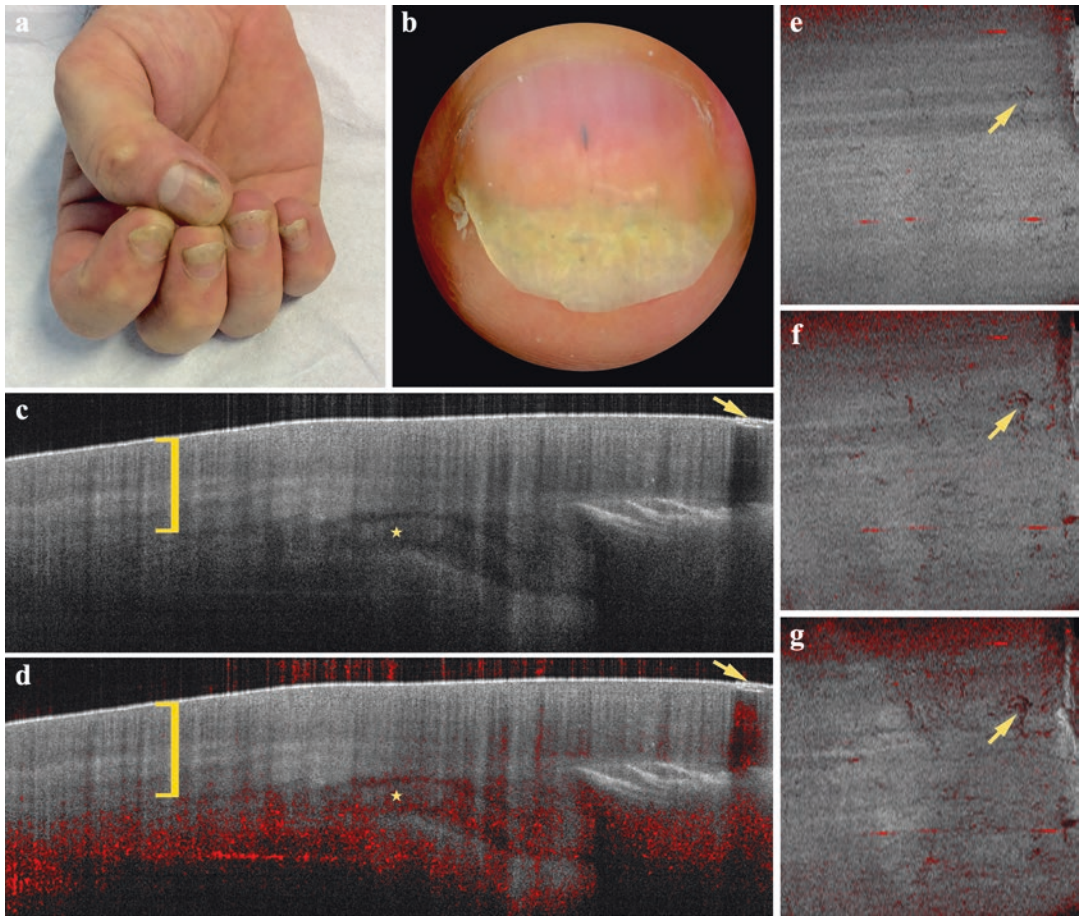

Fig. 22.18 Illustration of the clinical (**a**), dermoscopic (**b**), structural (**c**, **d**) and microvascular (**e**–**g**) features of the distal part of the psoriatic nail. Structural, cross-sectional views (VivoSight®; image size: 6 mm × 6 mm) display a thickened nail (*yellow brackets*), a wavy and layered nail plate, pitting (*yellow arrows*), salmon patch (*yellow asterisks*), onycholysis, subungual ridges alongside highly reflective white wispy sheets within the nail bed, predominant black empty areas surrounding highly reflective tufts (**c**) and an increased vascularization in the nail bed (**d**). Microvascular en-face D-OCT images [VivoSight®; size: 6 mm × 6 mm; skin depth 150 μm (**e**), 300 μm (**f**) and 500 μm (**g**)] show a rough and irregular nail surface with superficial fissuring and pitting (*yellow asterisks*)

Information on the vasculature of skin diseases adds more information and improve the diagnostic value of OCT technology. D-OCT permits to study the in vivo characterization of blood vessels and lymphatic vessels. Therefore, it is applicable in a variety of skin diseases, and it may potentially help to identify high-risk tumours.

In conclusion, OCT and D-OCT offer images with a good balance between a sufficient depth and a high axial and lateral resolution. This technique provides the opportunity to evaluate dynamic changes in the skin over time and without interfering with the tissue, and it may not only help in a better understanding of skin pathology, but also in the development of new treatments.

References

1. Welzel J, Lankenau E, Birngruber R, Engelhardt R. Optical coherence tomography of the human skin. J Am Acad Dermatol. 1997;37(6):958–63.
2. Ulrich M, Themstrup L, de Carvalho N, Manfredi M, Grana C, Ciardo S, Kästle R, Holmes J, Whitehead R, Jemec GB, Pellacani G, Welzel J. Dynamic optical coherence tomography in dermatology. Dermatology. 2016;232(3):298–311.
3. Themstrup L, Welzel J, Ciardo S, Kaestle R, Ulrich M, Holmes J, Whitehead R, Sattler EC, Kindermann N, Pellacani G, Jemec GB. Validation of dynamic optical coherence tomography for non-invasive, in vivo microcirculation imaging of the skin. Microvasc Res. 2016;107:97–105.
4. Ulrich M, Themstrup L, de Carvalho N, Ciardo S, Holmes J, Whitehead R, Welzel J, Jemec GBE, Pellacani G. Dynamic optical coherence tomography of skin blood vessels—proposed terminology and practical guidelines. J Eur Acad Dermatol Venereol. 2018;32(1):152–5.
5. O'Leary S, Fotouhi A, Turk D, Sriranga P, Rajabi-Estarabadi A, Nouri K, Daveluy S, Mehregan D, Nasiriavanaki M. OCT image atlas of healthy skin on sun-exposed areas. Skin Res Technol. 2018;24(4):570–86.
6. Welzel J, Reinhardt C, Lankenau E, Winter C, Wolff HH. Changes in function and morphology of normal human skin: evaluation using optical coherence tomography. Br J Dermatol. 2004;150(2): 220–5.
7. Mogensen M, Thomsen JB, Skovgaard LT, Jemec GB. Nail thickness measurements using optical coherence tomography and 20-MHz ultrasonography. Br J Dermatol. 2007;157(5):894–900.
8. Wahrlich C, Alawi SA, Batz S, Fluhr JW, Lademann J, Ulrich M. Assessment of a scoring system for basal cell carcinoma with multi-beam optical coherence tomography. J Eur Acad Dermatol Venereol. 2015;29(8):1562–9.
9. Themstrup L, De Carvalho N, Nielsen SM, Olsen J, Ciardo S, Schuh S, Nørnberg BM, Welzel J, Ulrich M, Pellacani G, Jemec GBE. In vivo differentiation of common basal cell carcinoma subtypes by microvascular and structural imaging using dynamic optical coherence tomography. Exp Dermatol. 2018;27(2):156–65.
10. Themstrup L, Pellacani G, Welzel J, Holmes J, Jemec GBE, Ulrich M. In vivo microvascular imaging of cutaneous actinic keratosis, Bowen's disease and squamous cell carcinoma using dynamic optical coherence tomography. J Eur Acad Dermatol Venereol. 2017;31(10):1655–62.
11. Sattler E, Kästle R, Welzel J. Optical coherence tomography in dermatology. J Biomed Opt. 2013;18(6):061224.
12. Gambichler T, Regeniter P, Bechara FG, Orlikov A, Vasa R, Moussa G, Stücker M, Altmeyer P, Hoffmann K. J Am Acad Dermatol. 2007;57(4):629–37.
13. Zidlik V, Brychtova S, Uvirova M, Ziak D, Dvorackova J. The changes of angiogenesis and immune cell infiltration in the intra- and peritumoral melanoma microenvironment. Int J Mol Sci. 2015;16(4):7876–89.
14. De Carvalho N, Welzel J, Schuh S, Themstrup L, Ulrich M, Jemec GBE, Holmes J, Kaleci S, Chester J, Bigi L, Ciardo S, Pellacani G. The vascular morphology of melanoma is related to Breslow index: an in vivo study with dynamic optical coherence tomography. Exp Dermatol. 2018;27(11):1280–6.
15. De Carvalho N, Ciardo S, Cesinaro AM, Jemec G, Ulrich M, Welzel J, Holmes J, Pellacani G. In vivo micro-angiography by means of speckle-variance optical coherence tomography (SV-OCT) is able to detect microscopic vascular changes in naevus to melanoma transition. J Eur Acad Dermatol Venereol. 2016;30(10):e67–8.
16. Mandel VD, Cinotti E, Benati E, Labeille B, Ciardo S, Vaschieri C, Cambazard F, Perrot JL, Pellacani G. Reflectance confocal microscopy and optical coherence tomography for the diagnosis of bullous pemphigoid and pemphigus and surrounding subclinical lesions. J Eur Acad Dermatol Venereol. 2018;32(9):1562–9.
17. Kuck M, Strese H, Alawi SA, Meinke MC, Fluhr JW, Burbach GJ, Krah M, Sterry W, Lademann J. Evaluation of optical coherence tomography as a non-invasive diagnostic tool in cutaneous wound healing. Skin Res Technol. 2014;20(1):1–7.
18. Martinez-Velasco MA, Perper M, Maddy AJ, Cervantes J, Eber AE, Verne SH, Vazquez-Herrera NE, Nouri K, Tosti A. In vitro determination of Mexican mestizo hair shaft diameter using optical coherence tomography. Skin Res Technol. 2018;24(2):274–7.
19. Vazquez-Herrera NE, Eber AE, Martinez-Velasco MA, Perper M, Cervantes J, Verne SH, Magno RJ, Nouri K, Tosti A. Optical coherence tomography for the investigation of frontal fibrosing alopecia. J Eur Acad Dermatol Venereol. 2018;32(2):318–22.
20. Verne SH, Chen L, Shah V, Nouri K, Tosti A. Optical coherence tomography features of Dermatophytoma. JAMA Dermatol. 2018;154(2):225–7.
21. Aldahan AS, Chen LL, Fertig RM, Holmes J, Shah VV, Mlacker S, Hsu VM, Nouri K, Tosti A. Vascular features of nail psoriasis using dynamic optical coherence tomography. Skin Appendage Disord. 2017;2(3–4):102–8.

High-Definition Optical Coherence Tomography

23

Mariano Suppa, Makiko Miyamoto, Véronique Del Marmol, and Marc Boone

23.1 Introduction

Optical coherence tomography (OCT) is a non-invasive imaging technique based on low-coherence interferometry. It uses near-infrared light to capture two-dimensional (2D) and three-dimensional (3D) images of scattering media, such as biological tissue, with variable micrometric resolution.

OCT was first introduced as a tool in ophthalmology in 1991, as the transparency of the ocular tissue represents an ideal condition for its employment [1]. OCT has subsequently been used in several medical fields including cardiology [2, 3], gastroenterology [4, 5], vascular surgery [6], dentistry [7], as well as dermatology [8, 9].

The biggest limitation of conventional OCT is represented by its limited lateral and axial resolution, which makes the visualization of individual cells impossible. In this scenario, a significant improvement has been achieved with the introduction of high-definition OCT (HD-OCT) (*Skintell*®, Agfa Healthcare Mortsel, Belgium and Munich, Germany), a device that features a high resolution of 3 μm in all three dimensions—thus allowing the visualization of individual cells—as well as an extremely quick generation of 3D images [10].

23.2 Technical Characteristics of HD-OCT

Like conventional OCT, HD-OCT is an interferometer able to carry out optical imaging deeply within highly scattering media—such as the skin—with micrometric resolution in both transversal and axial directions [11]. HD-OCT uses a two-dimensional, infrared-sensitive (1000–1700 nm) imaging array for light detection rather than a single pin diode, thus enabling the focal plane to be continuously moved throughout the sample (focus tracking). The device is able (1) to synchronize the movements of the focal plane and the reference mirror and (2) to take into account the refractive index of the sample. This results in a high *lateral resolution* of 3 μm at all depths of the sample. Moreover, the use of a broadband thermal light source combined with a special filter allows an equally high (3 μm) *axial resolution*. HD-OCT is able to capture a *slice* (cross-sectional, vertical) image and an *en-face* (horizontal) image in real time, as well as a 3D *volume* in only 35 s. The field of view is 1.8 × 1.5 mm. The tissue penetration goes up to a depth of 570 μm. Therefore, a HD-OCT 3D volume measures 15,400 million μm^3 (=1500 μm × 1800 μm × 570 μm) or approximately 57 million

M. Suppa (✉) · M. Miyamoto · V. Del Marmol
M. Boone
Department of Dermatology, Université Libre de Bruxelles, Hôpital Erasme, Brussels, Belgium
e-mail: dr.boone@scarlet.be

M. Fimiani et al. (eds.), *Technology in Practical Dermatology*,
https://doi.org/10.1007/978-3-030-45351-0_23

voxels (1 voxel = 27 μm^3). The system works in direct contact with the skin, using an optical matching gel comparable to the common ultrasound gel. The total light power at the tissue is <3.5 mW (harmless) [11].

23.3 Normal Skin

The HD-OCT features of the normal skin have been reported for the first time by Boone et al. in 2012 [11]. HD-OCT allows the 3D visualization of the different layers of the skin by providing images on both vertical and horizontal planes, the orientation of which are comparable to histopathology and confocal microscopy, respectively.

Different cutaneous structures vary in terms of their refraction index: this accounts for the contrast seen in a common HD-OCT image. In particular, melanin and keratin represent strong sources of contrast and appear bright on the images. The vertical images allow the examination of the global architecture of the skin (Fig. 23.1a). The dermal–epidermal junction (DEJ) appears as a dark homogeneous band that separates the epidermis from the underlying papillary dermis. Its weaker refraction index (which explains its darkness) is due to the retention of water by the glycosaminoglycans that are part of it. On the horizontal plane, the DEJ is characterized by the juxtaposition of annular structures corresponding to the dermal papillae surrounded by the basal keratinocytes, similarly to what is commonly observed in confocal microscopy (Fig. 23.1b). The dermal papillae can be more or less outlined depending on the melanin content of the basal keratinocytes and therefore on the skin's phototype. The epidermal thickness can be evaluated on the vertical images, whereas the global architecture of the epidermis is better seen on the horizontal plane. In the normal skin, the stratum *granulosum* and the stratum *spinosum*

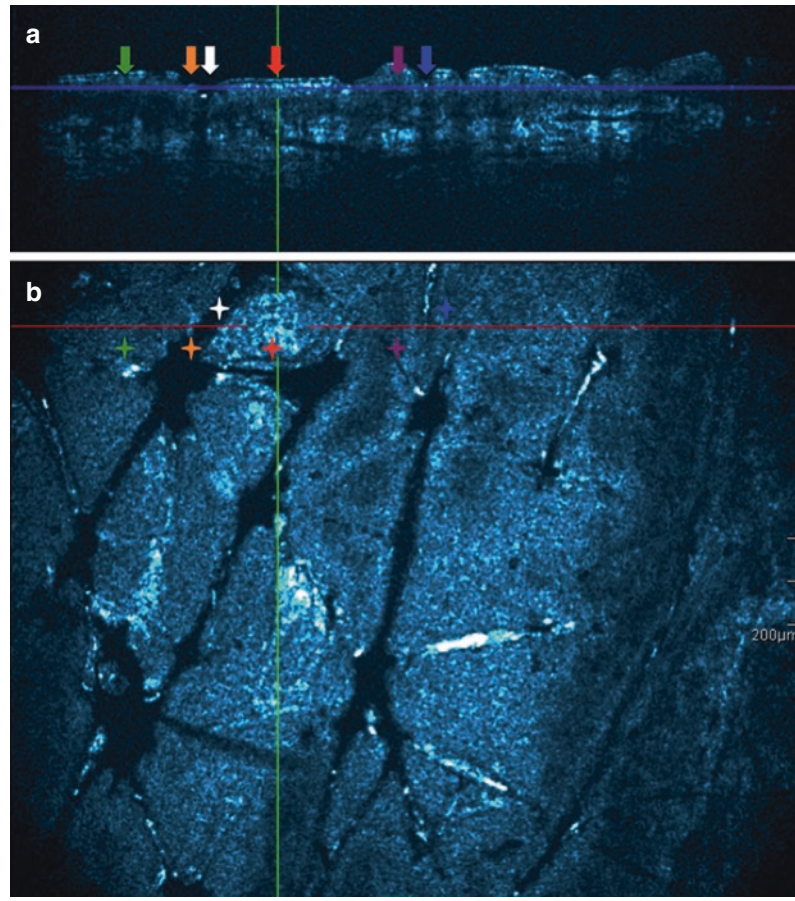

Fig. 23.1 HD-OCT *slice* (vertical plane, **a**) and *en face* (horizontal plane, **b**) mode. Normal skin. Several structures can be appreciated: skin fold (*white arrow and star*), stratum corneum (*orange arrow and star*), stratum granulosum (*red arrow and star*), stratum spinosum (*green arrow and star*), basal layer/dermal papilla (*purple arrow and star*) and hair follicle/shaft (*blue arrow and star*)

are characterized by a regular honeycomb pattern characterized by well-delimited cells, which are homogeneous in shape, size and reflectivity. The papillary dermis is characterized by a non-cellular network made by collagen fibres. The latter can be more or less dense/reflecting according to the degree of solar elastosis. Blood vessels are visible in the dermis as dark, circular/tubular structures. The reticular dermis consists of a reticulated network of fibres and small blood vessels in which cells are not easily discernible [11].

23.4 Non-melanoma Skin Cancer

Several studies found a good correlation between HD-OCT and histopathological images in different areas of dermatology. The possibility of examining the skin in the vertical plane has led to a particular interest for HD-OCT in non-melanoma skin cancer. Indeed, the diagnosis of both basal cell carcinoma (BCC) and squamous cell carcinoma (SCC) is mainly based on features that are better seen in the vertical rather than horizontal plane: for BCC, the subtype discrimination depends on the location of the basaloid tumour islands within the dermis; for SCC, the discrimination between actinic keratosis (AK) and invasive SCC depends on the integrity of the DEJ and the level of epidermal invasion.

23.4.1 Basal Cell Carcinoma

HD-OCT characteristics of BCC mainly include: (1) lobular structures within the dermis, corresponding to basaloid tumour islands (Fig. 23.2); (2) streaming effect of the tumour nests on the stromal fibres that consequently appear stretched (Fig. 23.3); (3) dilated blood vessels juxtaposed to the tumour islands (Fig. 23.3); and (4) variable degree of actinic

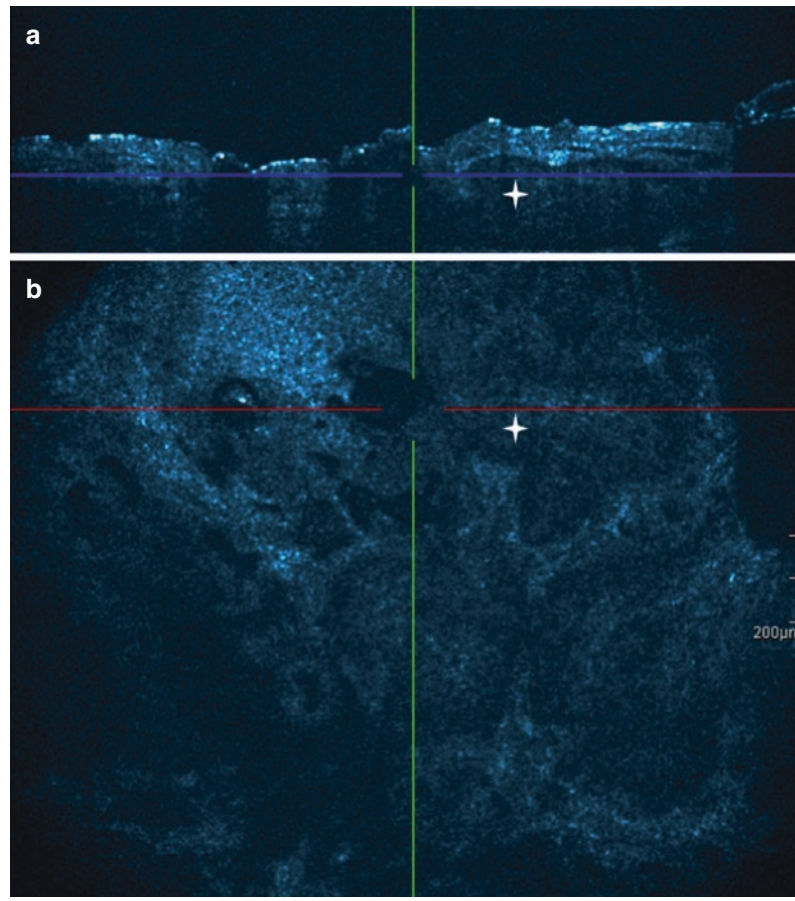

Fig. 23.2 HD-OCT *slice* (vertical plane, **a**) and *en face* (horizontal plane, **b**) mode. Nodular basal cell carcinoma. Presence of lobular structures corresponding to basaloid tumour islands (*white stars*) within the dermis

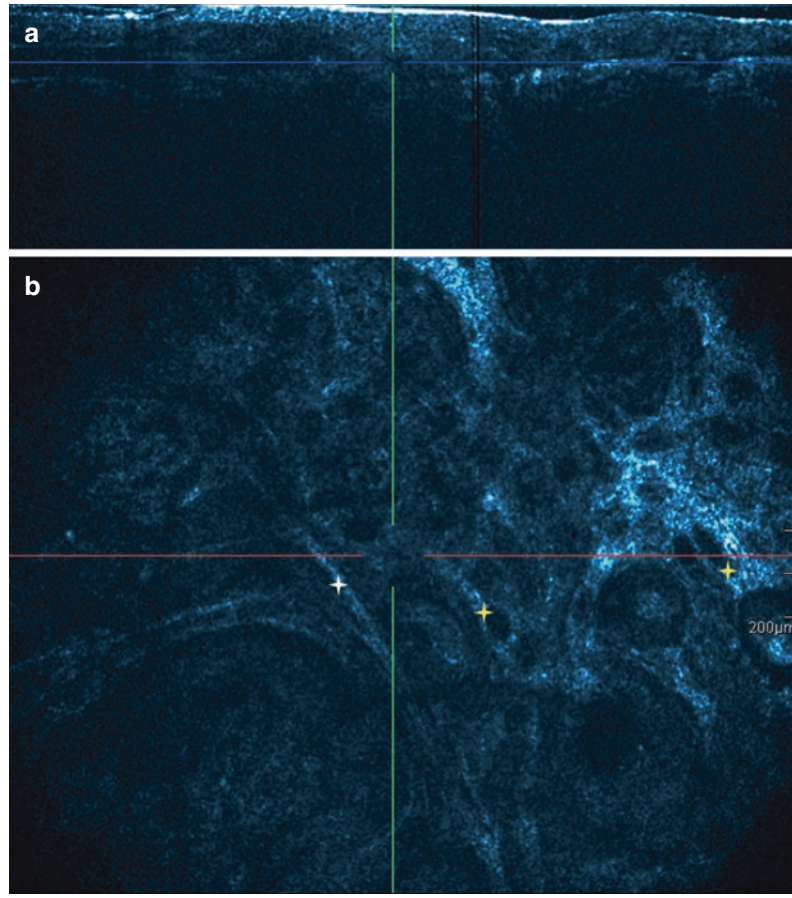

Fig. 23.3 HD-OCT *slice* (vertical plane, **a**) and *en face* (horizontal plane, **b**) mode. Nodular basal cell carcinoma. Streaming effect of the tumour nests on the stromal fibres that consequently appear stretched (*white star*). Dilated blood vessels juxtaposed to the tumour islands (*yellow star*)

damage of the epidermis (Fig. 23.4) [12, 13]. The typical morphology of the lobular structures seen in both HD-OCT modes is effective in differentiating BCC from clinical imitators such as AK, compound/intradermal naevi, amelanotic melanoma, sebaceous hyperplasia and small haemangioma [14]. Moreover, the location of the roof of BCC lobules, the vascular pattern of the papillary plexus, and the stretching effect on the stroma allow discriminating between BCC subtypes, thus directly influencing the therapeutic choice [14]. Finally, HD-OCT appears to be valuable in the non-invasive follow-up/monitoring of the medical treatment of BCC [15]. A pilot study of HD-OCT during micrographic surgery for BCC showed the possibility to reduce the excision margins and achieve the complete removal of the lesion at the same time [16].

23.4.2 Actinic Keratosis/Squamous Cell Carcinoma

It has been shown that HD-OCT facilitates the in vivo diagnosis of AK as well as its differentiation from invasive SCC [17, 18]. Contrary to normal skin, both AK and SCC present the following characteristics on HD-OCT examination: (1) a disarranged epidermal architecture, including alternating hyperkeratosis/parakeratosis (Fig. 23.5a) and—for SCC especially—alternating hypertrophy/atrophy (Fig. 23.5b) and acantholysis (Fig. 23.5c); (2) an alteration of the honeycomb pattern of the epidermis (the epidermal keratinocytes become irregular in size, shape and reflectivity), which is mildly atypical in AK and severely atypical in SCC (Fig. 23.6a, b); and (3) an adnexal involvement (disappearance of the typical *cockade* image of

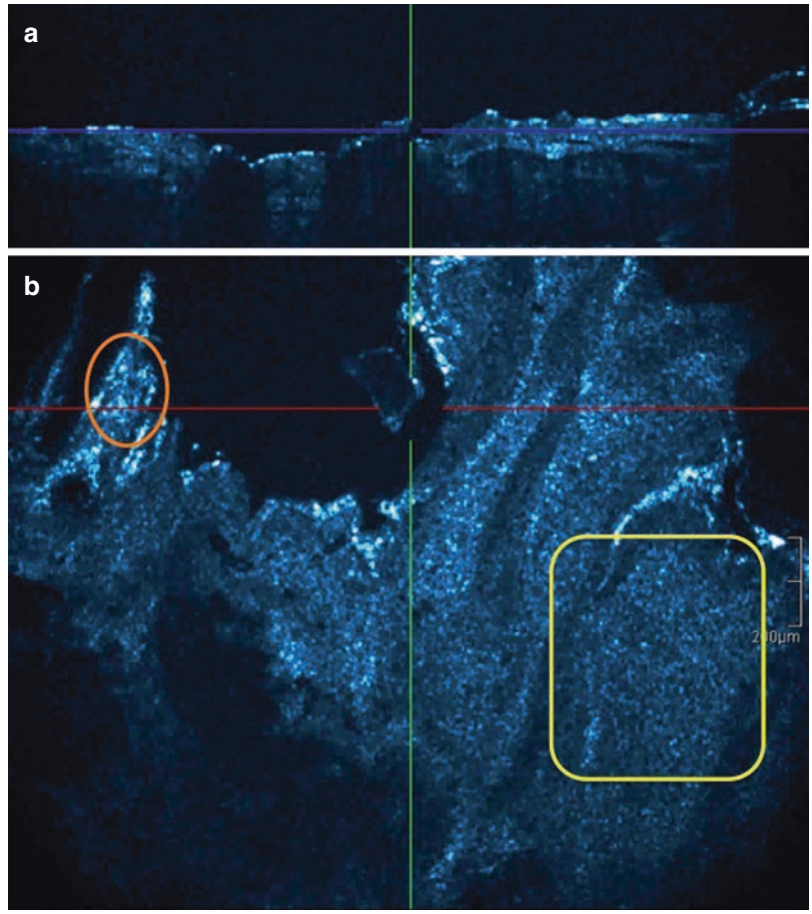

Fig. 23.4 HD-OCT *slice* (vertical plane, **a**) and *en face* (horizontal plane, **b**) mode. Nodular basal cell carcinoma. Actinic damage of the epidermis: parakeratosis (presence of nuclei within the stratum corneum, orange circle) and atypical honeycomb pattern (cellular pleomorphism, *yellow square*)

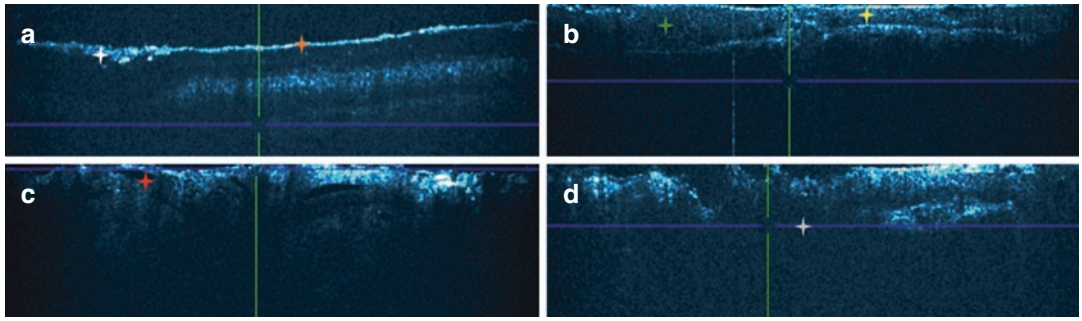

Fig. 23.5 HD-OCT *slice* mode (vertical plane). Disarranged epidermal architecture in actinic keratosis/squamous cell carcinoma: alternating hyperkeratosis (*white star*) and parakeratosis (orange star) (**a**); alternating hypertrophy (*green star*) and atrophy (*yellow star*) (**b**); and acantholysis (*red star*) (**c**). Disrupted dermal–epidermal junction in a squamous cell carcinoma (*grey star*) (**d**)

the hair follicle), which is present in about half of the AKs and virtually in the totality of SCCs (Fig. 23.6c, d). SCC can be differentiated from AK because of the presence of a disrupted DEJ (Fig. 23.5d) and of rounded projections of the epidermis into the dermis (budding and periadnexal collars) [17]. A good correlation between the above-mentioned HD-OCT features and histopathological findings has been demonstrated [19].

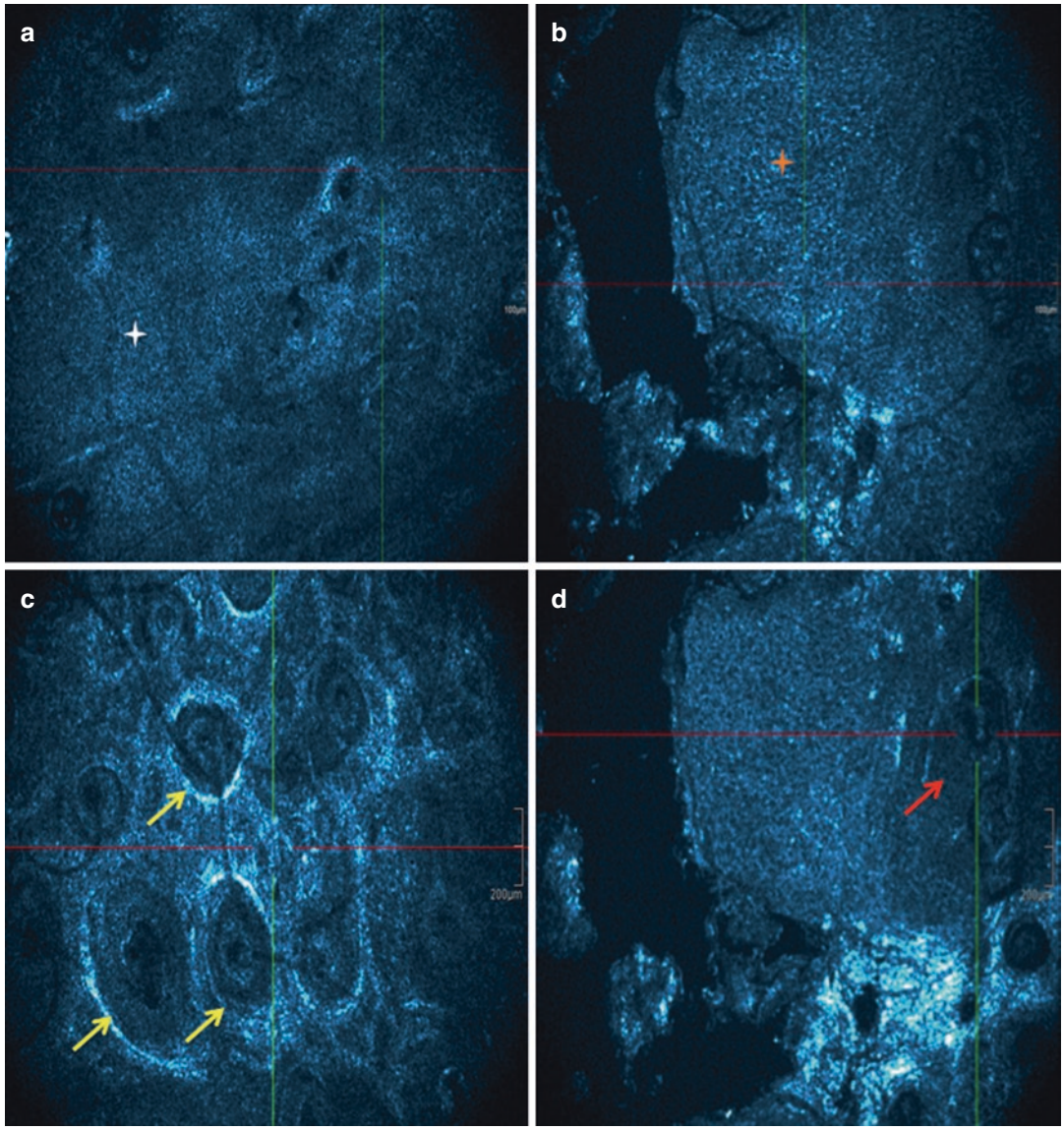

Fig. 23.6 HD-OCT *en face* mode (horizontal plane). Honeycomb pattern: typical in normal skin (the epidermal keratinocytes are regular in size, shape and reflectivity, *white star*, **a**) and atypical in an actinic keratosis (the epidermal keratinocytes are irregular in size, shape and reflectivity, *orange star*, **b**). Adnexal involvement in actinic keratosis can be absent (the typical *cockade* morphology of the hair follicle is visible, *yellow arrows*, **c**) or present (the typical *cockade* morphology of the hair follicle is lost, *red arrow*, **d**)

23.5 Other Applications in Dermatology

23.5.1 Melanocytic Lesions

The identification of architectural patterns and cytological features of pigmented cells is possible by using HD-OCT. Therefore, this technique is able to offer additional 3D information to that coming from confocal microscopy. However, because of the lower lateral resolution (3 vs. 1 µm), HD-OCT remains inferior to confocal microscopy with regard to the differential diagnosis of benign and malignant melanocytic lesions [20–23].

23.5.2 Inflammatory Diseases

HD-OCT was shown to be useful in detecting different patterns of inflammatory diseases such as spongiotic, psoriasiform, interface and ballooning dermatitis [24]. Indeed, both HD-OCT imaging modes provide morphological features that are very similar to those detected by confocal microscopy and histopathology and, therefore, appear to be a promising method for non-invasive diagnosis, evaluation and management of common inflammatory skin diseases.

23.5.3 Contact Dermatitis

It has been demonstrated that HD-OCT provides an important help in differentiating allergic from irritant contact dermatitis, a differential diagnosis of great importance because of the different management that the two entities require [25]. In particular, the increased epidermal thickness observed in irritant but not in allergic dermatitis represented a significant finding in that regard.

23.5.4 Autoimmune Diseases

The additional value of HD-OCT in the diagnosis and management of morphea has been reported [26]. The most useful HD-OCT feature in this scenario is represented by the hyporefractivity of the dermis, which correlates with the thickening/hyalinization of the collagen and the decrease in adnexal structures, blood vessels and inflammatory infiltrate observed in histopathology.

23.5.5 Granulomatous Reactions

Sub-epidermal pigment and granulomatous changes after permanent make-up treatments can be visualized on HD-OCT examination and correlate well with the histopathological findings. Moreover, treatment-induced regression of the lesions can also be documented [27].

23.5.6 Zoonoses

HD-OCT allows the fast and non-invasive in vivo recognition of demodex folliculorum mites and is therefore useful in the diagnosis and treatment/monitoring of demodex-related skin diseases [28].

23.5.7 Skin Graft Evaluation

Boone et al. demonstrated that HD-OCT permits the real-time 3D visualization of the impact of selected agents on human skin allografts and is therefore important in the evaluation of the quality of dermal matrices [29].

23.5.8 Skin Ageing

Age-related changes in the morphology/organization of the dermal matrix fibres, in the dermal microvasculature and in the brightness/compaction of the different skin layers can be observed by means of HD-OCT [30].

23.5.9 Optical Properties of Skin Conditions

The assessment of in vivo optical properties of tissue by HD-OCT is able to enhance the diagnostic accuracy for several cutaneous diseases, and our group has performed several studies in this regard. As compared to the in vivo HD-OCT analysis of morphology alone, this approach was shown to improve the discrimination of BCC subtypes [31], the discrimination of AK from SCC as well as AK sub-differentiation [32], and the differential diagnosis between melanoma and benign melanocytic lesions [33].

23.6 Conclusions

In conclusion, HD-OCT is a non-invasive skin imaging technique able to provide the 3D visualization of the skin. It is able to increase the diag-

nostic accuracy for skin cancer, and it is of particular value for '*vertical*' diagnoses such as the discrimination of BCC subtypes as well as the differentiation of AK from invasive SCC. While dermoscopy should stay as the first-line examination for the diagnosis/management of skin cancer and other cutaneous conditions, HD-OCT and confocal microscopy should be regarded as second-line tools that should be available in specialized centres.

References

1. Huang D, Swanson EA, Lin CP, Schuman JS, Stinson WG, Chang W, et al. Optical coherence tomography. Science. 1991;254(5035):1178–81.
2. Nadkarni SK, Pierce MC, Park BH, de Boer JF, Whittaker P, Bouma BE, et al. Measurement of collagen and smooth muscle cell content in atherosclerotic plaques using polarization-sensitive optical coherence tomography. J Am Coll Cardiol. 2007;49(13):1474–81.
3. Fujimoto JG, Brezinski ME, Tearney GJ, Boppart SA, Bouma B, Hee MR, et al. Optical biopsy and imaging using optical coherence tomography. Nat Med. 1995;1(9):970–2.
4. Bouma BE, Tearney GJ, Compton CC, Nishioka NS. High-resolution imaging of the human esophagus and stomach in vivo using optical coherence tomography. Gastrointest Endosc. 2000;51(4 Pt 1):467–74.
5. Vakoc BJ, Shishko M, Yun SH, Oh WY, Suter MJ, Desjardins AE, et al. Comprehensive esophageal microscopy by using optical frequency-domain imaging (with video). Gastrointest Endosc. 2007;65(6):898–905.
6. Patel NA, Li X, Stamper DL, Fujimoto JG, Brezinski ME. Guidance of aortic ablation using optical coherence tomography. Int J Cardiovasc Imaging. 2003;19(2):171–8.
7. Fried D, Xie J, Shafi S, Featherstone JD, Breunig TM, Le C. Imaging caries lesions and lesion progression with polarization sensitive optical coherence tomography. J Biomed Opt. 2002;7(4):618–27.
8. Welzel J, Lankenau E, Birngruber R, Engelhardt R. Optical coherence tomography of the human skin. J Am Acad Dermatol. 1997;37(6):958–63.
9. Bechara FG, Gambichler T, Stucker M, Orlikov A, Rotterdam S, Altmeyer P, et al. Histomorphologic correlation with routine histology and optical coherence tomography. Skin Res Technol. 2004;10(3):169–73.
10. Marneffe A, Suppa M, Miyamoto M, Del Marmol V, Boone M. High-definition optical coherence tomography: presentation of the technique and applications in dermatology. Ann Dermatol Venereol. 2015;142(6–7):452–5.
11. Boone M, Jemec GB, Del Marmol V. High-definition optical coherence tomography enables visualization of individual cells in healthy skin: comparison to reflectance confocal microscopy. Exp Dermatol. 2012;21(10):740–4.
12. Boone MA, Norrenberg S, Jemec GB, Del Marmol V. Imaging of basal cell carcinoma by high-definition optical coherence tomography: histomorphological correlation. A pilot study. Br J Dermatol. 2012;167(4):856–64.
13. Boone M, Suppa M, Miyamoto M, Marneffe A, Jemec GB, Pellacani G, et al. Three-dimensional high-definition optical coherence tomography image acquisition procedure for basal cell carcinoma. Br J Dermatol. 2015;172(4):1153–4.
14. Boone MA, Suppa M, Pellacani G, Marneffe A, Miyamoto M, Alarcon I, et al. High-definition optical coherence tomography algorithm for discrimination of basal cell carcinoma from clinical BCC imitators and differentiation between common subtypes. J Eur Acad Dermatol Venereol. 2015;29(9):1771–80.
15. Maier T, Kulichova D, Ruzicka T, Berking C. Noninvasive monitoring of basal cell carcinomas treated with systemic hedgehog inhibitors: pseudocysts as a sign of tumor regression. J Am Acad Dermatol. 2014;71(4):725–30.
16. Maier T, Kulichova D, Ruzicka T, Kunte C, Berking C. Ex vivo high-definition optical coherence tomography of basal cell carcinoma compared to frozen-section histology in micrographic surgery: a pilot study. J Eur Acad Dermatol Venereol. 2014;28(1):80–5.
17. Boone MA, Marneffe A, Suppa M, Miyamoto M, Alarcon I, Hofmann-Wellenhof R, et al. High-definition optical coherence tomography algorithm for the discrimination of actinic keratosis from normal skin and from squamous cell carcinoma. J Eur Acad Dermatol Venereol. 2015;29(8):1606–15.
18. Marneffe A, Suppa M, Miyamoto M, Del Marmol V, Boone M. Validation of a diagnostic algorithm for the discrimination of actinic keratosis from normal skin and squamous cell carcinoma by means of high-definition optical coherence tomography. Exp Dermatol. 2016;25(9):684–7.
19. Boone MA, Norrenberg S, Jemec GB, Del Marmol V. Imaging actinic keratosis by high-definition optical coherence tomography. Histomorphologic correlation: a pilot study. Exp Dermatol. 2013;22(2):93–7.
20. Boone MA, Norrenberg S, Jemec GB, Del Marmol V. High-definition optical coherence tomography imaging of melanocytic lesions: a pilot study. Arch Dermatol Res. 2014;306(1):11–26.
21. Picard A, Tsilika K, Long-Mira E, Hofman P, Passeron T, Lacour JP, et al. Use of high-definition optical coherent tomography (HD-OCT) for imaging of melanoma. Br J Dermatol. 2013;169(4):950–2.
22. Gambichler T, Plura I, Schmid-Wendtner M, Valavanis K, Kulichova D, Stucker M, et al. High-definition optical coherence tomography of melanocytic skin lesions. J Biophotonics. 2015;8(8):681–6.

23. Gambichler T, Schmid-Wendtner MH, Plura I, Kampilafkos P, Stucker M, Berking C, et al. A multicentre pilot study investigating high-definition optical coherence tomography in the differentiation of cutaneous melanoma and melanocytic naevi. J Eur Acad Dermatol Venereol. 2015;29(3):537–41.
24. Boone M, Norrenberg S, Jemec G, Del Marmol V. High-definition optical coherence tomography: adapted algorithmic method for pattern analysis of inflammatory skin diseases: a pilot study. Arch Dermatol Res. 2013;305(4):283–97.
25. Boone MA, Jemec GB, Del Marmol V. Differentiating allergic and irritant contact dermatitis by high-definition optical coherence tomography: a pilot study. Arch Dermatol Res. 2015;307(1):11–22.
26. Su P, Cao T, Tang MB, Tey HL. In vivo high-definition optical coherence tomography: a bedside diagnostic aid for morphea. JAMA Dermatol. 2015;151(2):234–5.
27. Maier T, Flaig MJ, Ruzicka T, Berking C, Pavicic T. High-definition optical coherence tomography and reflectance confocal microscopy in the in vivo visualization of a reaction to permanent make-up. J Eur Acad Dermatol Venereol. 2015;29(3):602–6.
28. Maier T, Sattler E, Braun-Falco M, Ruzicka T, Berking C. High-definition optical coherence tomography for the in vivo detection of demodex mites. Dermatology. 2012;225(3):271–6.
29. Boone M, Draye JP, Verween G, Pirnay JP, Verbeken G, De Vos D, et al. Real-time three-dimensional imaging of epidermal splitting and removal by high-definition optical coherence tomography. Exp Dermatol. 2014;23(10):725–30.
30. Boone MA, Suppa M, Marneffe A, Miyamoto M, Jemec GB, Del Marmol V. High-definition optical coherence tomography intrinsic skin ageing assessment in women: a pilot study. Arch Dermatol Res. 2015;307(8):705–20.
31. Boone M, Suppa M, Miyamoto M, Marneffe A, Jemec G, Del Marmol V. In vivo assessment of optical properties of basal cell carcinoma and differentiation of BCC subtypes by high-definition optical coherence tomography. Biomed Opt Express. 2016;7(6):2269–84.
32. Boone MA, Suppa M, Marneffe A, Miyamoto M, Jemec GB, Del Marmol V. A new algorithm for the discrimination of actinic keratosis from normal skin and squamous cell carcinoma based on in vivo analysis of optical properties by high-definition optical coherence tomography. J Eur Acad Dermatol Venereol. 2016;30(10):1714–25.
33. Boone MA, Suppa M, Dhaenens F, Miyamoto M, Marneffe A, Jemec GB, et al. In vivo assessment of optical properties of melanocytic skin lesions and differentiation of melanoma from non-malignant lesions by high-definition optical coherence tomography. Arch Dermatol Res. 2016;308(1):7–20.

3D Imaging

24

Irene Campana, Giulia Tonini, Jean Luc Perrot, and Elisa Cinotti

24.1 Introduction

Many noninvasive imaging techniques have been developed over the years to supply an objective evaluation of healthy and diseased human skin [1–4], but the design of technologies able to precisely measure the surface and volume of the skin remains a continuous challenge [5]. In order to follow up skin changes over time, or before and after intervention, the dermatologist traditionally has had only his eyes, his memory, and at best a two-dimensional (2D) digital camera. Images can be used to check response to treatment, to document the localization of excised lesions, and to control disease progression. Whereas 2D photography surmounts the limit of memory recall, the problem of perspectively projecting a 3D object onto a 2D plane makes precise quantitative measurements from single 2D views impossible [5]. Three-dimensional (3D) imaging, on the other hand, provides an accurate and objective assessment of geometric and volumetric changes of the skin and can be better used for outcome simulation, treatment follow-up, and help in medico-legal questions [6–8].

Since the rise of computed tomography (CT) [9] in 1967 and magnetic resonance imaging (MRI) [10] in 1971, the term "three-dimensional (3D) imaging" has been related to techniques that can process true internal 3D data by catching volumetric pixels (or voxels) of the measured target. As opposed to CT and MRI, an imaging process measuring and analyzing surfaces (x, y, and z coordinates) in a 3D space is called "3D surface imaging" [11]. Since the 1940s, 3D surface imaging technologies have analyzed the complexities of an object with stereophotogrammetry [12, 13], image-subtraction techniques [14], Moiré topography [15] (e.g., Saito et al. [16] in 2008 used this method to identify the characteristics of cheek sagging by analyzing skin displacement along the *x, y*, and *z* axes in 3D images), liquid crystal scanning [17], light luminance scanning [18], laser scanning [19], structured light [20], stereolithography [21], and video systems [22–25]. These systems offer 3D analysis successfully [17, 23–25], but most have not been employed in clinical routine due to time-consuming processes, poor image quality, and unpredictable costs. In the last decade, progresses in optical systems including structured light [26] and stereophotogrammetry [27] have produced 3D surface imaging with less time consumption, generating precise 3D surface images, handling vast data

I. Campana (✉) · G. Tonini · E. Cinotti
Department of Medical, Surgical and Neurological Science, Dermatology Section, University of Siena, Siena, Italy

J. L. Perrot
Department of Dermatology, University Hospital of St-Etienne, Saint-Etienne, France
e-mail: j.luc.perrot@chu-st-etienne.fr

M. Fimiani et al. (eds.), *Technology in Practical Dermatology*,
https://doi.org/10.1007/978-3-030-45351-0_24

formats efficiently, and being more accessible to patient protocols [26, 28].

Structured light technology (e.g., Axis Three) evaluates the 3D surface of an object by the deformation of a projected pattern. The simplest set-up consists of one projector, which projects a pattern (stripes, grid, dots, etc.) onto the object's surface, and a calibrated camera which catches an image of the object overlaid by the pattern from a viewing direction different from the projector to see the deformation of the projected pattern. Knowing the design and geometry of a projected pattern and perception of the deformation by the 3D surface of the object, it is possible to estimate the 3D surface of the object and produce a 3D surface image [26]. The benefits are that it can be applied on surfaces without any color textures (e.g., ceramic and steel) and that is relatively unaffected by specular reflection [29]. However, both strip projections and video cameras need to be checked by a computer, which can make the system bulky to operate or move. Another disadvantage is that image texture is acquired independently from the surface which can result in a potential shift between geometry and color texture [29]. Because these tools require a time sequence of images to be recorded, any skin movement while recording further affects the accuracy of such systems [5].

Stereophotogrammetry (e.g., 3dMD, Canfield, and Di3D) instead makes use of multiple simultaneous views and image correlation to rebuild 3D surfaces [30]. The fundamental principle is similar to the human visual perception. "Stereovision" systems are attractive as they allow direct visualization of the subject in 3D with stereo glasses. Whereas image acquisition occurs within 1/200 s, the main disadvantages are that these instruments require textured surfaces to operate and may be sensitive to specular reflection. "Auto-calibration" can be employed when only stereovision is of interest, but it is obligatory to rely upon absolute calibration in order to obtain useful geometric measurements [31].

There are three kinds of stereophotogrammetry: active, passive, and hybrid. Active stereophotogrammetry is based on structured light. It sends out a light pattern onto the surface of an object and uses two (or more) cameras to capture the deformation of the pattern by the objects' surface from different viewpoints. A 3D surface image is created by a process called triangulation, calculating the 3D coordinates of each 2D point (pixel) visible in both camera views, with no additional lighting [28]. By contrast, "passive stereophotogrammetry" gives life to 3D surface images based only on the images taken by two (or more) cameras without the projection of a pattern. Due to the missing projected pattern, finding correspondences between views and images is more difficult and ambiguous. It is of paramount importance to select high-quality cameras, to catch surface details and sufficient texture information of the objects of interest including natural patterns, such as pores, freckles, scars, and rhytides. The lighting conditions must be carefully checked, since a strong directional ambient light may cause glare, decreasing the surface details [28]. Lastly, "hybrid stereophotogrammetry" merges both active and passive, to gain higher accuracy and quality in 3D surface imaging [32].

24.2 3D Surface-Imaging Systems for the Face and Small Body Parts Based on Stereovision

Most 3D cameras that are available for dermatology on the market have been designed for the face and small body parts and are based on stereovision with absolute calibration to be utilized for accurate 3D reconstruction and quantification of skin structures [5] (e.g., LifeViz™, QuantifiCare, Valbonne, France; 3dMD™Inc., Atlanta, GA, USA; Di3D™Ltd, Glasgow, Scotland; Vectra H1®, H2® and XT 3D-SI®, Canfield Imaging Systems, Fairfield, NJ, USA). Two-dimensional images acquired from three different perspectives are automatically merged in a 3D image. One of the major advantages of the passive stereovision system is its facility of use. Image acquisition can be performed in a practical and rapid way which is of great advantage in clinical routine as well as in clinical studies.

Reproducible pictures are usually possible to obtain without repositioning systems, thanks to a dual beam pointer. When the two convergent beams overlap, the doctor is at the right distance to take the pictures. The cameras are matched with software for image management, 3D surface reconstruction/visualization, and 3D surface analysis (measurement of volume, depth, and perimeter). The scanned image can be usually seen in two or three dimensions, changing the viewing angle and adjusting the magnification for close examination of the areas of interest.

Skvara H et al. [5] used LifeVizto to monitor 13 BCCs treated with a topical hedgehog inhibitor (LDE225) versus 14 BCCs treated with a vehicle during 4 weeks. This stereovision system was used to measure 3D surface, 3D volume, and lesion height that resulted sensitively reduced after 29 days of treatment with LDE225. Unpublished findings have shown that this technology is also ideally adapted for the in vivo investigation of the treatment success after filler application into fine wrinkles, wound management, as well as treatment of acne scars and keloids [5].

3dMD is currently one of the most widely used digital stereophotogrammetry technology [33]. It exploits hybrid stereophotogrammetry (active and passive), with the software algorithms using both projected random patterns and texture of the skin (pore, freckles, etc.) to produce a 3D surface image (Fig. 24.1) [34–37]. System calibration takes up to several minutes depending on the hardware set-up [32]. 3dMD offers six different hardware products, each adapted for a specific application: 3dMD face, 3dMD head, 3dMD torso, 3dMD body, 3dMD trio, and 3dMD dynamic 4D systems (which capture up to 10 min of sequential 3D surface images of 60 frames per second, showing the movement of a 3D surface over time) [32]. 3dMD face system consists of two modular units, each of which contains one full color and two black-and-white machine vision cameras, and an industrial-grade flash system synchronized in a single capture [38]. All cameras are positioned at a fixed distance and angle to ensure overlapping fields of view [28], and they simultaneously capture all images in 1.5 ms, limiting the risk of motion artifacts, with another 30 s of processing to automatically generate the final 3D model [33]. System calibration takes about 2 min. The 3dMD Vultus software can be used to visualize 3D volumes and simulate soft-tissue outcomes (surgical and nonsurgical) by making a fusion between 3D surface image and CT and CBCT (cone beam CT) and employing a biomechanical mass-spring model [39].

DI3D employs standard digital still cameras and normal photographic flash illumination to

Fig. 24.1 Images of a face (upper line) and a skin tumor (lower line) taken with LifeVizTM 3 camera (QuantifiCare, Valbonne, France). Visualization software allows to rotate the body changing the viewing angle in order to observe the skin from different perspectives

catch in 1 ms simultaneously one or more stereo pairs of images of a subject. Each stereo pair of images is elaborated using Dimensional Imaging's proprietary passive stereophotogrammetry software to produce automatically a dense range map image. The range map images and original high-resolution color images are then fused to create a highly defined 3D surface image. Unlike other methods of 3D scanning, DI3D does not need any pattern projection or laser scanning onto the scene [40]. In fact, it exploits passive stereophotogrammetry. System calibration takes about 5 min. The standard system is the DI3D FCS-100 [32] that is planned specifically to capture high-definition 3D surface images of the human face. It utilizes four cameras to produce 3D facial surface images with highly detailed surface texture maps. Dimensional Imaging's passive stereophotogrammetry software quickly processes captured stereo pairs of images into complete seamless 3D models [40]. Ultimately DI3D view is a 3D analysis, simulation, and measurement software which can merge the resulting 3D surface image with CT/CBCT [32]. It permits even the highest-resolution DI3D 3D surface images to be viewed at full definition, so that every detail is clearly displayed. Several high-resolution DI3D 3D surface images can be opened and seen simultaneously in multiple views, remarkably improving efficiency and communication [40]. Besides in 2010 Di3D launched a 4D system, which captures 3D video sequences of dynamically changing surfaces [32].

The Vectra H1 system consists of a single handheld Canon camera body fitted with a special lens and a range-finding apparatus to allow for 3D capture. Because the Vectra H1 system comprises a single camera, each individual capture is limited in surface coverage. Thus, three sequential captures are necessary to obtain the facial surface from ear to ear. Through the capture process, patients must be seated and directed to keep a neutral facial expression. For the first capture, the camera need to be positioned 45° to the patient's right and approximately 30 cm below the patient's face (at chest level), such that the camera is tilted slightly upwards. This position ensures that the underside of the chin and nose are adequately captured. The Vectra H1 system guides the user with visual prompts to ensure that the camera is at the correct distance from the facial target, with two projected green dots functioning as a guide. When the dots converge on the facial surface, the camera distance is correct. For the first capture, the patient is positioned properly when the converged green dot is located on the right cheek, at the level of the right nasal ala horizontally and the outer corner of the right eye vertically. The second capture is a frontal shot taken at face level, with the green dot positioning guide located on the participant's philtrum. The third capture repeats the process for the first capture but positioned to the patient's left side. For each capture, the participant remains immobile, and the camera user is required to move to the necessary position. According to the manufacturer, the speed of each capture is 2 ms. The minimum time between captures is approximately 5 s, so that the entire capture process takes about 20–30 s to be completed [33].

The first validation study of Vectra H1 was produced by Camison L et al. [33]: the authors compared 3D facial images of 26 adult participants captured with the Vectra H1 system and with the previously validated 3dMD face system showing that the first images were highly comparable to the second ones. The results of this study suggest that the Vectra H1 camera system is accurate and reliable enough for most clinical and research applications and that 3D facial surfaces collected from Vectra H1 and 3dMD can be compared and/or combined in most circumstances. Gibelli D et al. confirmed the results of Camison L et al. [41]. The authors compared Vectra H1 portable stereophotogrammetric device with static Vectra M3 devices showing that the first one proved reliable for assessing linear measurements, angles, and surface areas; conversely, the influence of involuntary facial movements on volumes and distances was more important compared with the static device. Peculiar fields of application of Vectra H1 are objective burn scar measurements [42], intraoperative evaluation of body surface improvement in plastic surgery [43], and analysis of the surface change in response to targeted facial fat grafting [44]. The device has also been used as tool for 3D photo-

graphic documentation in a trial for the evaluation of antiaging efficacy of melatonin-based day and night creams [45] and in forensic pathology representing relatively low-cost solutions for three-dimensional surface postmortem body documentation [46].

Vectra H2 is a portable lightweight 3D imaging device ideal not only for facial esthetics, but even for breast and body ones. The camera provides two unique sets of ranging lights, one for face and one for body, to ensure optimal capture distance and resolution. The device provides a quantitative approach to soft tissue change assessment that characterizes the degree of stretch, compression, lift, and volumization.

Vectra XT 3D-SI can capture 3D face, breast, and body ultra-high-resolution color images. Thanks to a capture time of 3.5 ms, it is immune to subject movement. In 2018 O'Connell RL et al. validated the use of this device for measuring breast volume and symmetry showing that the device is able to measure the volume of a simple breast-shaped object with an average accuracy of about 2.2% underestimation of the true volume and with satisfactory repeatability and reproducibility [47].

24.3 3D Reconstruction from 2D Image Analysis

There are programs that produces 3D surface images from three 2D digital pictures (one frontal and two profiles) taken with a consumer camera, physical distance measurements of the patient's anatomy, and a set of landmarks. Crisalix™ (Crisalix, Switzerland) was the first web-based 3D simulator for plastic surgery and esthetic procedures. Being a web-based application, it provides worldwide access allowing for online discussions between physicians and simplifies upgrades and maintenance since doctors have only to login and use the application. Crisalix does not disclose how fast the 3D surface image is generated or the duration of the entire process, but considering the image acquisition time, it can be 10–15 min. A simulator for biomechanical simulations of breast implants and skin elasticity and a simulator for surgical and nonsurgical facial procedures are available [32]. The latter creates a patient-specific virtual 3D face on which physicians can directly show the intended procedural changes to the patient with the 3D planning tools (filling, skin clearing or rejuvenation, and rhinoplasty) in different points of view.

The study of Oliveira-Santos in 2013 [48] has showed that physicians are able to reconstruct faces of patients in less than an average of 5 min with a 3D web system similar to Crisalix, which allows the application to be used within standard consultation time. The most time-consuming parts of the procedure are the manual definition of the body landmarks and correction of the body contours (averaging around 2 and 3 min, respectively).

Three-dimensional reconstruction was developed with the aim to facilitate communication between physicians and patients. Patient understanding about the esthetic procedure, and consequently satisfaction with the consultation, is expected to grow up with the use of 3D virtual face representation and procedure planning [48].

24.4 3D Cameras for Close-up Images of Small Body Areas

3D cameras have also been developed to obtain close-up images of small areas allowing finer, detailed observations of the skin (e.g., LifeViz® Micro, QuantifiCare, Valbonne, France, which has a field of view of 50 × 70 mm).

Three-dimensional cameras able to obtain close-up images can be used for example to objectively assess acne scars during treatment, especially in clinical research [49]. Two-dimensional scar imaging has inbuilt limitations for the evaluation of scars as a result of variability with environmental factors such as lighting, shadows, and camera positioning. Furthermore, many of the current full-face digital camera devices lack sufficient resolution to reliably detect and quantify scar volumes.

It is important to find a reliable, repeatable, and standardized methodology for analyzing 3D images. Some studies reported that 3D imaging measurements of scar volume decreased after pulsed laser treatment but did not describe the methodology for the computation of volume [50]. The study of Petit et al. identified a normalized parameter (*Valley void volume*, volume of scars mm^2) for the observation of atrophic scars by the 3D camera [49]. These parameters were related to clinical severity, repeatable, statistically correlated with clinical observations of scars in the range of 2–4 mm, and little influenced by positive volume (due to papules/pustules or other primary acne lesions) [49].

Some 3D cameras besides allow multispectral analysis of epidermis and dermis pigmentation [51]. Antera 3D® (MIRAVEX Dublin, Ireland) illuminates the skin with light-emitting diodes (LEDs) of different wavelengths from different directions and takes advantage of reflectance mapping of seven different light wavelengths spanning the whole visible spectrum. It measures a small area of 56 × 56 mm and can project any part of the body. The images obtained are not dependent on lighting conditions—achieved by a combination of polarized filters and proprietary technology—which guarantees reproducible conditions and accuracy of the results [52]. Thanks to the multispectral sources and the three-dimensional mapping of the skin surface, the measurement of melanin and hemoglobin is accurate. Moreover, it is possible to determine the size, extension, and distribution of capillaries, to give a quantitative measure of skin roughness and texture and to measure width, length, and depth of fine lines, wrinkles, and grooves. Antera 3D also has a "spot-on-automatic image" function that assures the coincidence between the selected areas in different images, compensating for the differences due to the different positioning of the patient during the acquisition of the images. Antera 3D® is more sensitive in the detection of rhytides compared with VISIA® system [52]. Otherwise there is an acceptable correlation between the two instruments in measuring skin color [52].

24.5 Other Cameras for the Whole Face Surface

Although VISIA® system (Canfield Imaging Systems, Fairfield, NJ, USA) does not provide 3D images, it is a standardized photography system that allows an analysis of the whole face with information that approximates to 3D imaging. It is one of the most widely used imaging analysis device in the dermatology research, esthetic practices, and skin care industry, providing a guide for the selection of skin care products and treatment options.

It consists of a facial imaging chamber (Fig. 24.2) which is connected to a computer for a quantitative analysis [52, 53].

VISIA® has three kinds of light sources: standard incandescent light, UV light, and polarized light (Table 24.1). The standard flash light is suitable to identify spot, wrinkle, texture, and pore (Fig. 24.3). Spots are recognized by their color and contrast from the surrounding skin,

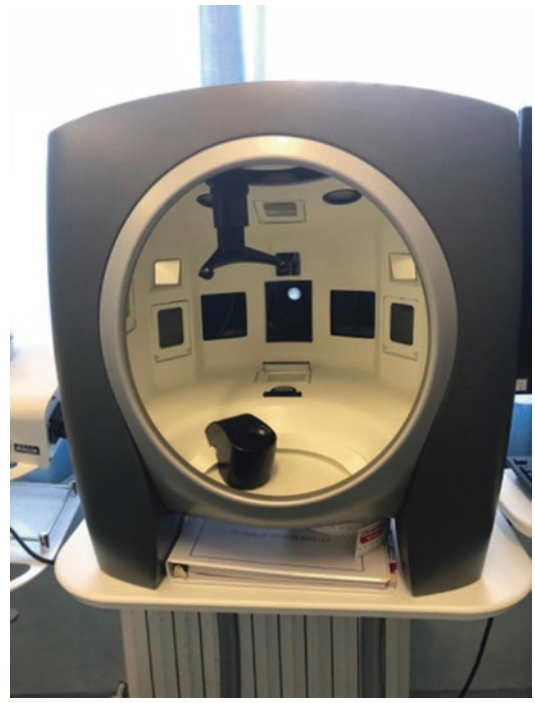

Fig. 24.2 VISIA® system (Canfield Imaging Systems, Fairfield, NJ, USA)

including freckles, acne scars, and vascular lesions. Wrinkles are identified by their long narrow shape. Besides there can be variation in the measurement of wrinkles based on facial expression. The images derived from standard lighting can also focus on the texture of the skin, reporting elevations and depressions on the skin surface. Finally, pore size is identified by identifying very small spots.

Table 24.1 Different skin features observed by VISIA

Type of flashlighting	Skin characteristic analyzed
Standard	Spots, rhytides, texture, pore size
Ultraviolet	Ultraviolet spots, porphyrin
Cross-polarized	Brown spots, red areas

The ultraviolet flash light instead is used to highlight the ultraviolet spot and porphyrin (Fig. 24.3). The ultraviolet lighting takes advantage of the selective absorption of ultraviolet light by epidermal melanin in comparison to deeper melanin, thereby stressing solar len-

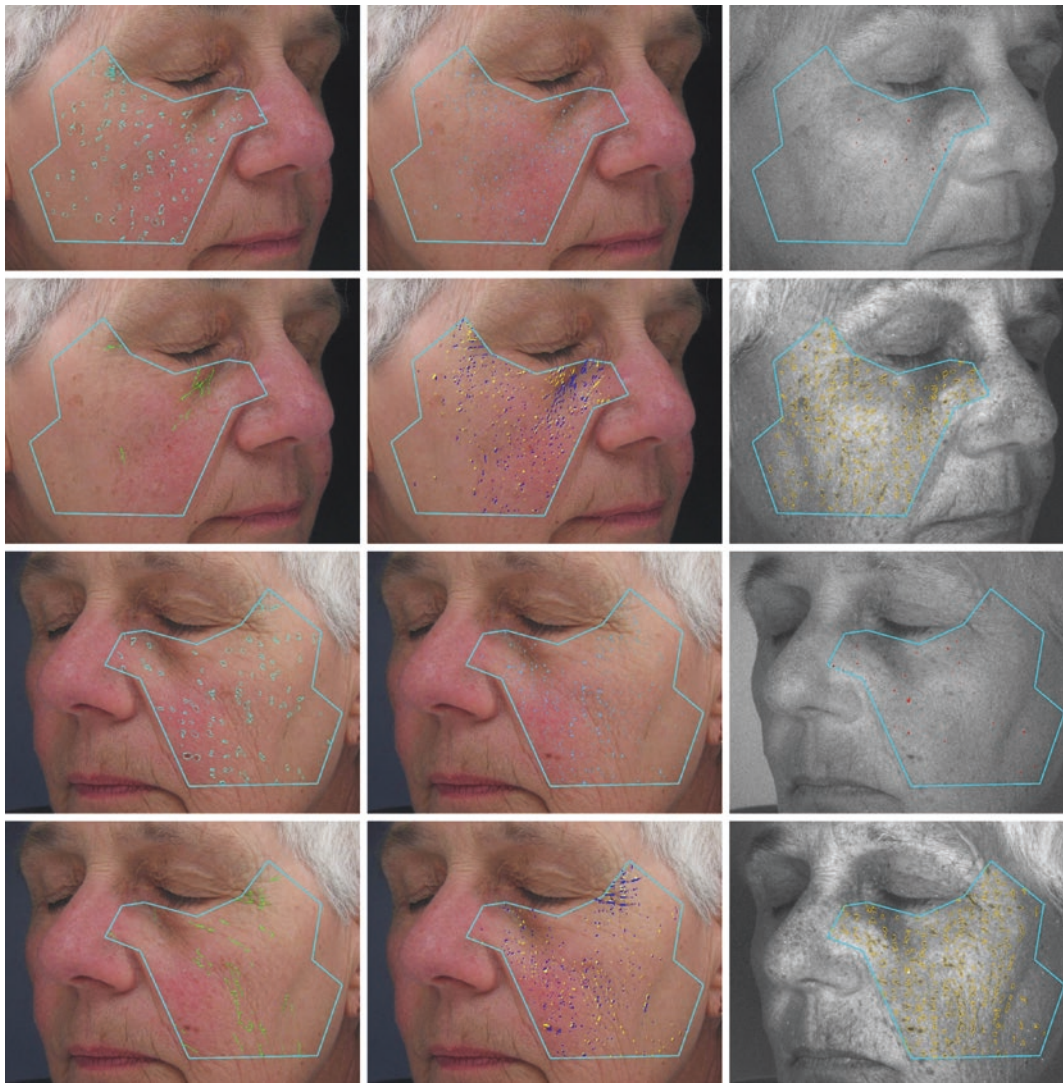

Fig. 24.3 Face images acquired with VISIA® system with standard incandescent light (left and central column) and UV light (right column). Starting from the first image, spots, pores, porphyrins (UV light), wrinkles, texture, and UV spots (UV light) are visible on the right (images 1–6) and left (images 7–12) sides of the face

tigines. Porphyrin becomes fluorescent when exposed to ultraviolet light. Porphyrins are produced by bacteria, specifically *Propionibacterium acnes*, in the skin. Porphyrin bioburden in follicles and sebaceous glands may be linked to acne or suggest a propensity for breakouts [53].

Orthogonal, cross-polarized flashlight is helpful for viewing the brown spot and red area by Canfield's patented RBX™ [53]. This system targets the main chromophores affecting the remitted light (i.e., skin color): melanin and hemoglobin. Thanks to the cross-polarized lighting, VISIA RBX system is capable to detect deeper deposition of melanin than is detected using the ultraviolet images. From the brown component image, a secondary hyperpigmented spot detection image can be created. The hemoglobin helps to measure the amount of redness in the skin, including background erythema, telangiectasia, and vascular lesions. From the red component image, a secondary, vascular feature can be employed which delineates remarkable blood vessels [54].

Insofar that primary color signatures red and brown are related to hemoglobin and melanin components, respectively, and this color space is called Red/Brown/X (RBX). The skin image caught by the digital camera comprises Red (R), Green (G), and Blue (B) channels and is presented in a RGB space. RBX transforms this RGB image into the RBX color-space where the *Red* and *Brown* channels stand for hemoglobin and melanin distributions, respectively. For accurate imaging of melanin and hemoglobin, it is essential that the re-emitted light from the skin lack specular reflections. The skin image is captured under polarized illumination with a pair of orthogonally polarized filters located over the flash and on the camera lens, respectively. Cross-polarization removes specular reflections from the skin surface, improving visibility of re-emitted light from the epidermis and dermis where melanin and hemoglobin reside. *Red/Brown* images can be further elaborated to calculate severity scores correlated with the degree of pigmentation and with vascularization. The severity scores can be employed for controlling the progress after treatment for hyperpigmentation and vascularization. The follow-up images are essentially more demonstrable than those captured with conventional photographic technique [55]. VISIA can also measure changes in eyelash length, for example, with the use of bimatoprost [53].

The Reveal® Imager (Canfield) clearly shows clients what is between them and the beautiful appearance they desire and provides a printed report with treatment recommendations. Its main features are:

- *Loupe-tool* targets a selected area of the image for maximum impact. It is possible to zoom within, expand, or shrink the loupe using a mouse or touchscreen.
- *Reproducible facial photography* ensures repeatable images between time-points with built-in positioning aids and standardized lighting.
- *Multi-mode illumination* through standard white light and cross-polarized flash photography to record surface and sub-surface skin condition.
- *Aging simulation* simulates the aging process to show clients older or younger by 5–7 years for spots, wrinkles, or both.
- *3D Viewer* visualizes the skin's surface in three dimensions from any angle, rendered in natural skin tone, color relief, or gray scale.
- *Eyelash analysis* evaluates the results of lash improvement treatments with numerical assessments and graphic visualizations [56].

24.6 3D Total Body Photography

In order to monitor different skin diseases and in particular pigmented tumors, dermatologists have traditionally been dependent on visual evaluation, clinical memory recall, and, if available, a 2D digital camera. However, the manipulation of a 3D surface like human skin into a 2D photograph can prejudice the accuracy of the image and is time consuming. It needs multiple separate images of the patient to be caught in a variety of anatomical positions which can then overlap or

conversely fail to include nevi if they are not captured from the specific anatomical angle of the single camera.

Total body photography has recently viewed an evolution from 2D imaging to a 3D representation of the patient. A 3D imaging system combining total body photography and sequential digital dermoscopic imaging (SDDI) of individual skin lesions enables all existing melanocytic lesions on a patient to be monitored from a macroscopic perspective in combination with the dermoscopy morphology. Since 2015, a prototype 3D total body photography (TBP) imaging system (Vectra WB360, Canfield Scientific Inc, Parsippany, NJ, USA) made up of 46 cameras has been utilized in clinical trials for the follow-up of high-risk individuals at the Princess Alexandra Hospital, Brisbane, Australia. In 2017, the commercial system was launched, with improved imaging capacities through 92 cameras pared within 46 pods, each pod aimed at designated portions of the body from different angles. The cameras catch the images simultaneously, and then the software automatically combines all the 2D photographs to build a digital 3D avatar of the patient. Both standard non-polarized lighting and cross-polarized lighting are used, and all necessary lighting is provided within the system. The patient has to hold only one anatomical position, and the image acquisition happens within 3 ms. The 3D representation makes the 360-degree rotation possible to view all body angles, including curved surfaces which are particularly compromised with 2D imaging. Although the 3D image represents a relatively high-resolution macroscopic image, additional digital dermoscopy, which captures an image so close to what is seen through a handheld dermoscope, is often required for an exhaustive evaluation. The dermoscopic images are connected to the corresponding lesion marked on the 3D avatar thanks to DermaGraphix software. This permits accurate documentation of the exact anatomical position of all lesions, with the aim to assess their evolution. Because modification in a lesion is the most sensitive way to detect skin cancer early, this approach may allow for closer monitoring of suspicious lesions with more accurate assessments of change over time, minimizing unnecessary biopsies, and capturing malignant evolution at an earlier stage [57]. TBP and SDDI may be established at various remote sites and managed by nurses, clinical assistants, and junior doctors, who can then send images to teledermatologists.

The 3D imaging approach offers several advantages over the standard 2D imaging techniques for clinicians and patients:

(1) First and foremost, the time needed to image the patient is significantly shorter, requiring only one near-instantaneous image capture rather than the repositioning and series of photographs of the two-dimensional approach. This means less time for the patient to be exposed and only one pose necessary, determining an overall more comfortable experience. In fact the time the patient is nude or semi-nude is reduced by 10–20 min compared to 2D photography body mapping systems, reducing patient anxiety.
(2) Only one 3D image is required to create a body map, instead of 16 or more 2D images, eliminating the need for a skilled photographer taking 10–20 min to capture the images.
(3) Easy and immediate mapping, measuring, and tracking of pigmented lesions and distributed skin conditions such as psoriasis throughout the entire body. This provides additional information to assist the clinician when assessing the patient's condition. This data is also useful for medical studies associated with skin conditions;
(4) The images in the 3D TBP are included into one comprehensive digital model, eliminating the overlap between adjacent images that happens with 2D TBP. This helps to give consistency in the appearance of the size of lesions, whereas with the 2D imaging, if an image is taken at an angle, it may appear larger than its actual size.
(5) 3D imaging can recreate the surface texture and allows a lesion to be viewed from all angles. The digital model can be moved and rotated as wanted to gain a better visualization of a particular lesion. This is useful for looking moles on curved body surfaces [57, 58].

Unfortunately, these techniques have a lot of limits:

(1) 2–8% of melanomas are hypopigmented, and their detection on a 3D total body photography imaging system may be less reliable than with pigmented lesions.
(2) The large physical size of the unit and the important expense and complexities around its management and storage.
(3) Incapability of monitoring lesions in the genital, acral, and scalp body sites and within body folds. These locations need to be independently assessed and documented with separate photography.

Therefore, 3D TBP is still living its infancy, requiring ongoing research and validation before it will have a significant impact on standard dermatological care [57].

References

1. Rajadhyaksha M, Grossman M, Esterowitz D, Webb RH, Anderson RR. In vivo confocal scanning laser microscopy of human skin: melanin provides strong contrast. J Invest Dermatol. 1995;104:946–52.
2. Jasaitiene D, et al. Principles of high-frequency ultrasonography for investigation of skin pathology. J Eur Acad Dermatol Venereol JEADV. 2011;25:375–82.
3. Cal K, Stefanowska J, Zakowiecki D. Current tools for skin imaging and analysis. Int J Dermatol. 2009;48:1283–9.
4. Breunig HG, Studier H, König K. Multiphoton excitation characteristics of cellular fluorophores of human skin in vivo. Opt Express. 2010;18:7857–71.
5. Skvara H, et al. Quantification of skin lesions with a 3D stereovision camera system: validation and clinical applications. Skin Res Technol. 2013;19:e182–90.
6. Ort R, et al. The reliability of a three-dimensional photo system- (3dMDface-) based evaluation of the face in cleft lip infants. Plast Surg Int. 2012;2012:1–8.
7. Guillard G, Lagarde J. Skin lesions segmentation and quantification from 3D body's models. Skin Res Technol Off J Int Soc Bioeng Skin ISBS Int Soc Digit Imaging Skin ISDIS Int Soc Skin Imaging ISSI. 2005;11:123–31.
8. Zhou Y, Smith M, Smith L, Warr R. Using 3D differential forms to characterize a pigmented lesion in vivo. Skin Res Technol. 2010;16:77–84.
9. Richmond C. Sir Godfrey Hounsfield. BMJ. 2004;329:687.
10. Damadian R. Tumor detection by nuclear magnetic resonance. Science. 1971;171:1151–3.
11. Geng J. Structured-light 3D surface imaging: a tutorial. Adv Opt Phot. 2011;3:128e60.
12. Thalmaan D. Die Stereogrammetrie: ein diagnostisches Hilfsmittel in der Kieferorthopaedie [Stereophotogrammetry: a diagnostic device in orthodontology]. Zurich: University Zurich, Switzerland; 1944.
13. Burke PH, Beard FH. Stereophotogrammetry of the face. A preliminary investigation into the accuracy of a simplified system evolved for contour mapping by photography. Am J Orthod. 1967;53:769e82.
14. Neely JG, Cheung JY, Wood M, Byers J, Rogerson A. Computerized quantitative dynamic analysis of facial motion in the paralyzed and synkinetic face. Am J Otol. 1992;13:97–107.
15. Takasaki H. Moire topography. Appl Opt. 1970;9:1467–72.
16. Saito N, Nishijima T, Fujimura T, Moriwaki S, Takema Y. Development of a new evaluation method for cheek sagging using a Moire 3D analysis system. Skin Res Technol. 2008;14:287–92.
17. Inokuchi I, Sato K, Ozaki Y. Range-imaging system for 3-D range imaging. Paper presented at: 7th ICPR Proceeding; Montreal, Canada. 1984. p.806.
18. Meier-Gallati V, Scriba H, Fisch U. Objective scaling of facial nerve function based on area analysis (OSCAR). Otolaryngol Head Neck Surg. 1998;118:545e50.
19. Bush K, Antonyshyn O. Three-dimensional facial anthropometry using a laser surface scanner: validation of the technique. Plast Reconstr Surg. 1996;98:226e35.
20. Geng ZJ. Rainbow three-dimensional camera: new concept of high-speed three-dimensional vision systems. Opt Eng. 1996;35:376–83.
21. Moss JP, Grindrod SR, Linney AD, Arridge SR, James D. A computer system for the interactive planning and prediction of maxillofacial surgery. Am J Orthod Dentofac Orthop. 1988;94:469–75.
22. Bajaj-Luthra A, Mueller T, Johnson P Quantitative analysis of facial motion components: anatomic and nonanatomic motion in normal persons and in patients with complete facial paralysis. Plast Reconstr Surg.1997;99:1894–1902. discussion 903e4.
23. Ferrario VF, Sforza C, Poggio CE, Tartaglia G. Distance from symmetry: a three-dimensional evaluation of facial asymmetry. J Oral Maxillofac Surg. 1994;52:1126–32.
24. Trotman C, Gross M, Moffatt K. Reliability of a threedimensional method for measuring facial animation: a case report. Angle Orthod. 1996;66:195–8.
25. Frey M, Giovanoli P, Gerber H, Slameczka M, Stu¨ssi E. Threedimensional video analysis of facial movements: a new method to assess the quantity and quality of the smile. Plast Reconstr Surg. 1999;104:2032–9.
26. Olesen OV, Paulsen RR, Hojgaar L, Roed B, Larsen R. Motion tracking in narrow spaces: a structured

light approach. Med Image Comput Comput Assist Interv. 2010;13:253–60.
27. Edge JD, Hilton A, Jackson P. Model-based synthesis of visual speech movements from 3D video. EURASIP J Audio Speech Music Process. 2009;2009:12.
28. Lane C, Harrell W Jr. Completing the 3-dimensional picture. Am J Orthod Dentofac Orthop. 2008;133:612–20.
29. Tian GY, Lu RS, Gledhill D. Surface measurement using active vision and light scattering. Opt Laser Eng. 2007;45:131–9.
30. Li W, Li YF. Single-camera panoramic stereo imaging system with a fisheye lens and a convex mirror. Opt Express. 2011;19:5855–67.
31. Wei GQ, Dema S. Implicit and explicit camera calibration—theory and experiments. IEEE Trans Pattern Anal Mach Intell. 1994;16:469–80.
32. Tzou C-HJ, et al. Comparison of three-dimensional surface-imaging systems. J Plast Reconstr Aesthet Surg. 2014;67:489–97.
33. Camison L, et al. Validation of the Vectra H1 portable three-dimensional photogrammetry system for facial imaging. Int J Oral Maxillofac Surg. 2018;47:403–10.
34. Aldridge K, Boyadjiev SA, Capone GT, DeLeon VB, Richtsmeier JT. Precision and error of three-dimensional phenotypic measures acquired from 3dMD photogrammetric images. Am J Med Genet Part A. 2005;138A:247–53.
35. Weinberg SM, Naidoo S, Govier DP, Martin RA, Kane AA, Marazita ML. Anthropomet- ric precision and accuracy of digital threedimensional photogrammetry: comparing the Genex and 3dMD imaging systems to one another and to direct anthropometry. J Craniofac Surg. 2006;17:477–83.
36. Wong JY, Oh AK, Ohta E, Hunt AT, Rogers GF, Mulliken JB, Deutsch CK. Validity and reliability of craniofacial anthropometric measurement of 3D digital photogrammetric images. Cleft Palate Craniofac J. 2008;45:232–9.
37. Heike CL, Cunningham ML, Hing AV, Stuhaug E, Starr JR. Picture perfect? Reliability of craniofacial anthropometry using threedimensional digital stereophotogrammetry. Plast Reconstr Surg. 2009;124:1261–72.
38. https://www.aniwaa.com/product/3d-scanners/3dmd-3dmdface-system/.
39. Schendel SA, Montgomery K. A web-based, integrated simulation system for craniofacial surgical planning. Plast Reconstr Surg. 2009;123:1099–106.
40. http://www.dirdim.com/pdfs/DDI_Dimensional_Imaging_DI3D.pdf.
41. Gibelli D, Pucciarelli V, Cappella A, Dolci C, Sforza C. Are portable stereo photogrammetric devices reliable in facial imaging? A validation study of VECTRA H1 device. J Oral Maxillofac Surg. 2018;76:1772–84.
42. Lee KC, Dretzke J, Grover L, Logan A, Moiemen N. A systematic review of objective burn scar measurements. Burns Trauma. 2016;4:14.
43. Mitsuno D, Ueda K, Itamiya T, Nuri T, Otsuki Y. Intraoperative evaluation of body surface improvement by an augmented reality system that a clinician can modify: Plast. Reconstr Surg Glob Open. 2017;5:e1432.
44. Schreiber JE, et al. The boomerang lift: A three-step compartment-based approach to the youthful cheek. Plast Reconstr Surg. 2018;141:910–3.
45. Milani M, Sparavigna A. Antiaging efficacy of melatonin-based day and night creams: a randomized, split-face, assessor-blinded proof-of-concept trial. Clin Cosmet Investig Dermatol. 2018;11:51–7.
46. Urbanová P, Hejna P, Jurda M. Testing photogrammetry-based techniques for three-dimensional surface documentation in forensic pathology. Forensic Sci Int. 2015;250:77–86.
47. O'Connell RL, et al. Validation of the Vectra XT three-dimensional imaging system for measuring breast volume and symmetry following oncological reconstruction. Breast Cancer Res Treat. 2018;171:391–8.
48. Oliveira-Santos T, et al. 3D face reconstruction from 2D pictures: First results of a web-based computer aided system for aesthetic procedures. Ann Biomed Eng. 2013;41:952–66.
49. Petit L, et al. Validation of 3D skin imaging for objective repeatable quantification of severity of atrophic acne scarring. Skin Res Technol. 2018;24:542–50.
50. Brauer JA, et al. Use of a picosecond pulse duration laser with specialized optic for treatment of facial acne scarring. JAMA Dermatol. 2015;151:278.
51. http://www.cmconsulenze.it/antera_3d_analisi_cutanea.php.
52. Linming F, et al. Comparison of two skin imaging analysis instruments: The VISIA ® from Canfield vs the ANTERA 3D ® CS from Miravex. Skin Res Technol. 2018;24:3–8.
53. Goldsberry A, Hanke CW, Hanke KE. VISIA system: a possible tool in the cosmetic practice. J Drugs Dermatol JDD. 2014;13(11):1312–4.
54. Cygler K. VISIA complexion analysis med spa. Recorded Nov 5, 2013. http://www1.gotomeeting.com/register/783169248. Accessed 16 May 2014
55. Demirli R, Otto P, Viswanathan R, Patwardhan S, Larkey J RBX® technology overview. 1701–13. http://www.canfieldsci.com/FileLibrary/RBX%20tech%20overview-LoRz1.pdf.
56. https://www.canfieldsci.com/imaging-systems/reveal-imager/.
57. Rayner JE, et al. Clinical perspective of 3D total body photography for early detection and screening of melanoma. Front Med. 2018;5.
58. Hibler B, Qi Q, Rossi A. Current state of imaging in dermatology. Semin Cutan Med Surg. 2016;35:2–8.

Raman Spectroscopy

25

Elisa Cinotti, Luca Provvidenziale, and Jean Luc Perrot

25.1 Introduction

In the field of skin research, Raman spectroscopy (RS) is an upcoming analytical technique capable of analyzing the chemical composition of materials by measuring vibrational modes of biomolecules which derives from an inelastic light scattering process. With RS, a laser photon is scattered by a sample molecule and loses or gains energy during the process. RS is commonly visualized by the wave number shift from incident to scattered photons against the scattering intensity. The patterns of wavelength shifts after irradiation of a sample with laser light are a sole characteristic for a specific chemical structure, otherwise said "molecular fingerprint" [1]. In fact, the amount of energy lost is seen as a change in energy of the irradiating photon: this energy loss is characteristic for a unique and particular bond in the molecule [2].

RS, as a diagnostic tool, has the advantage of being nondestructive, requires no sample preparation [3], and is less influenced by strong water signals than Fourier transform infrared spectroscopy [4, 5] entailing larger measuring depths. It is particularly sensitive with the possibility of analyzing small volumes, and confocal RS has a spatial resolution below 1 micron [1]. Biological samples can be examined in their physiological environment [6] which facilitates in vivo applications on skin. Raman spectra can also be used to generate images of the skin. Hence, in contrast to other noninvasive optical methods for skin imaging such as optical coherence tomography, reflectance confocal microscopy (RCM), or multiphoton tomography, RS is molecular specific [7]. Besides, the combination of RS and RCM on a handheld camera that works in vivo unlocked new opportunities [1, 8] as the information on chemical composition and on distribution of components are added to the horizontal topographic spatiality, and these data can be obtained directly on the patient.

Due to these advantages, RS bears great potential for diverse skin applications. Besides it allows, among the others, the study of skin physiology such as measuring the hydration of the stratum corneum [9–11] or acquiring penetration depth profiles of topically applied substances to the skin [12, 13]. RS is considerably interesting for skin cancer diagnosis, and it can be used for intra-operative tumor margin assessment [14].

E. Cinotti · L. Provvidenziale (✉)
Department of Medical, Surgical and Neurological Science, Dermatology Section, University of Siena, Siena, Italy

J. L. Perrot
Department of Dermatology, University Hospital of St-Etienne, Saint-Etienne, France
e-mail: j.luc.perrot@chu-st-etienne.fr

M. Fimiani et al. (eds.), *Technology in Practical Dermatology*,
https://doi.org/10.1007/978-3-030-45351-0_25

25.2 Main Ex vivo Skin Applications

The studies illustrated in this section show some of the versatility and the multiple ex vivo applications of RS for the evaluation of the skin. First ex vivo investigations of human skin by RS started in the early 1990s by analyzing the physiology in comparison to vibrational spectroscopy. Barry et al. [15] assigned the respective Raman spectra to the corresponding dermal component using cadaver skin and demonstrated the efficacy of RS for the study of excised skin biopsies (SB). Their studies went on studying a mummy of about 5000 years, found frozen in the South Tyrol [16]. The composition and structures of lipids in the mummy's skin under RS turned out to be even unaltered.

The acquisition of Raman data in z-direction series consents to investigate the penetration behavior of the substances. This profile can evaluate the effectiveness of topical drug delivering in different skin layers. Tfayly et al. [17] tracked the penetration of metronidazole through excised skin ex vivo. A study of Ashtikar et al. [18] presented a relatively simple method to obtain z-Raman profiles of human stratum corneum using RS on intact full-thickness SB of untreated skin and diffusion patterns for deuterated water and beta-carotene. Also Anigbogu et al. [19] described the mechanism of skin absorption of dimethyl sulfoxide. They reported a change in the tertiary protein structure of keratin at the level of the stratum corneum and an increase in lipid fluidity.

A new application concerns the exact identification of foreign bodies in the skin such as soft tissue fillers (Fig. 25.1) and tattoo pigments [20–22] and the recognition of endogenous substances accumulated during storage diseases such as cystine (Fig. 25.2) [23].

25.3 Main In vivo Skin Applications

In addition to the RS ex vivo applications, numerous authors have been reported about clinical potential of Raman on in vivo skin research. Aside from studies about the physiological state

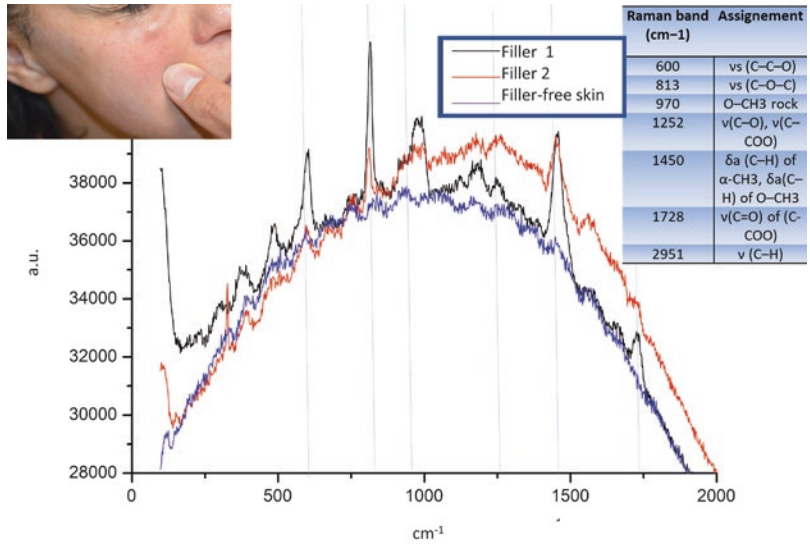

Fig. 25.1 Ex vivo Raman spectra of microspheres of fillers show a series of peaks at 600, 813, 970, 1252, 1450, and 1728 cm^{-1} characteristic of polymethylmethacrylate (PMMA); *y*-axis: intensity in arbitrary units (a.u.); peak at 2951 cm^{-1} is not shown in the present spectrum, and a luminescence signal is also present in the graph; *x*-axis: wavenumber (cm^{-1}). Inset on the left shows the clinical aspect of the subcutaneous nodules that has been biopsied in order to identify the injected filler by Raman spectroscopy and inset on the right shows the Raman peaks of PMMA

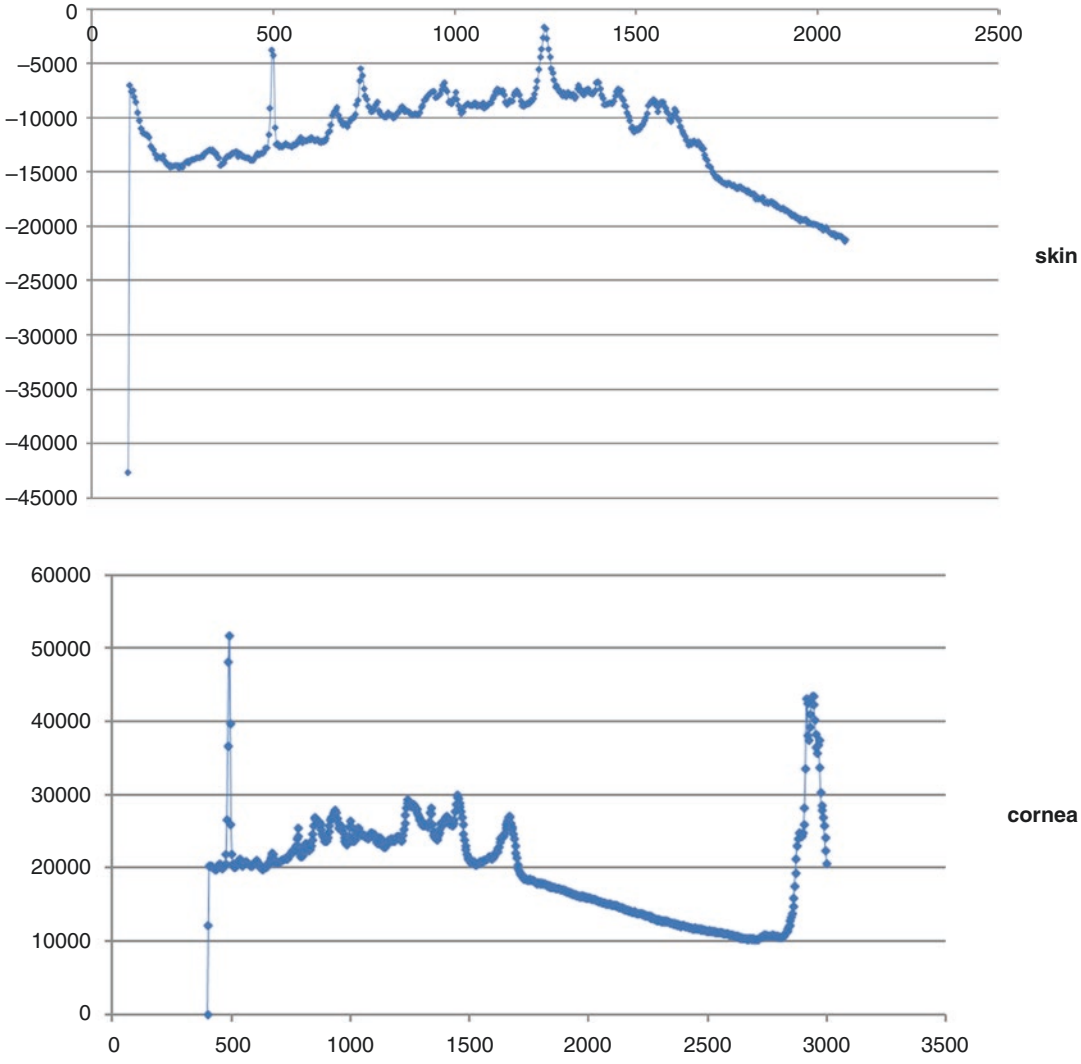

Fig. 25.2 Ex vivo Raman spectra of the forearm skin and cornea of a patient suffering from cystinosis (intensity in arbitrary unit in the axis of ordinates and Raman shift in cm^{-1} in the axis abscissas). The specific signature of cystine is clearly identified in both tissues thanks to the band at 499 cm^{-1}

and evaluations of topical substances penetration, RS also leads to the potential for diagnosis in vivo and the follow-up of therapeutic effects.

The high specificity of RS bearded out the high heterogeneity of skin, and an extreme variety of applications of RS to study its physiological properties have been tested. Huang et al. [24] verified that there is no spectral difference between the synthesized eumelanin and the one examined in vivo. Discriminate between age-related skin damage and photodamage was the subject of the analysis by Gonzales et al [25]. Tfayli et al. [26], by principle RS analysis, described changes in the lipid composition of the skin related to aging. Lately, Barba et al. [27] evaluated the different capability of two-solvent systems on inducing changes in the lipids of the stratum corneum.

By using RS, Vyumvuhore et al. [28] discriminated parameters between xerotic and normal skins, such as the lack of organization and conformation of lipids in this skin, an increase in the

trans-epidermal water loss (TEWL) and a low hydration rate in xerotic skin. Over time, other investigations on the state of skin hydration state took place. Egawa conducted numerous studies on skin hydration, describing the different amount of water present in the skin according to the season, area of the body, age [29], and depending on the exposure of the skin to water [30]. To verify the effectiveness of various emollient creams in dermatology, Chrit et al. described the level of skin hydration after application of moisture enhancements [31]. Nowadays the measure of skin hydration with RS has become an established and standardized procedure. Its reliability, reproducibility, and its noninvasive nature have made this measurement one of the most popular applications of RS.

Pharmaceutical investigations such as drug penetration kinetics within the different skin layers were conducted by numerous groups of study. Topically applied substances can be checked in depth by confocal RS, considering penetration behavior in vivo. An example for topical delivery by a skin formulation is the application of sunscreens. The latter is supposed to stay in the superficial layer to perform their functions. Recently, Tippavajhala et al. [32] tested commercial sunscreens on healthy human volunteers with RS, to find out that the penetration was restricted to stratum corneum.

Broding et al. [33] were able to demonstrate the ability of RS to detect the percutaneous penetration of several potentially dangerous substances into the skin. 2-Butoxyethanol, toluene, and pyrene were applied in pure form, diluted in water, or in ethanol on the skin of three healthy volunteers. In addition to the spectral results, they observed a marked difference in penetration timing when the substance was dissolved in water instead of ethanol.

A study conducted by Mélot et al. [34] compared the propriety of several penetration enhancers to facilitate retinol delivery through the skin. All enhancers considerably increased the penetration deepness of the active principle. Mohammed et al. [35] evaluated the penetration of various niacinamide formulations by high-performance liquid chromatography in vitro compared with results obtained by RS in vivo.

Psoriasis has been characterized by Egawa et al. [36] exploring involved and uninvolved areas of skin. RS and optical coherence tomography found lower water contents and a thicker stratum corneum in the psoriatic areas. After treatment, all the monitored skin structures, even natural moisturizing factor and ceramides, normalized. Alda et al. [37] studied changes of the skin components of patients suffering from nickel allergy. RS could plainly differentiate between healthy and affected skin areas.

O'Regan et al. [38] differentiated three filaggrin genotypes causing atopic dermatitis under RS considering the RS signatures of the natural moisturizing factor present in the corneum layer.

Monitoring the level of urea is useful in patients with renal disease and to control the benefits of dialytic therapy. Wascotte et al. [39] found that a source of urea in the skin, unrelated to the concentration circulating in the blood, can be demonstrated by RS in the flux extracted by iontophoresis across the skin.

Schallreuter et al. [40] observed that Dead Sea water is able to break up hydrogen peroxide (H_2O_2). The result of their study, assessed using RS to follow the decompose of H_2O_2 in the skin affected by vitiligo, showed a significantly quick start of repigmentation after a combination of 21 days of climatotherapy at the Dead Sea in combination with a pseudo catalase cream.

Until now, distinguishable divergence in the spectroscopic patterns of healthy and diseased skin have been found. This implicates the potential for global characterization and classification of spectral analysis by RS in vivo. Despite being promising, larger data sets are required to establish accurate diagnostic power, define cost-effectiveness criterions, and extend the applicability to the detection of serial parameters.

25.4 Skin Cancer Diagnosis

With modern Raman microscopic devices, it is already possible to successfully identify skin cancers in SB and in a real-time in vivo setting. There is no Raman spectrum specific of a skin cancer type, and different studies used different

statistical analysis in order to differentiate skin lesions. Gniadecka et al. [41] compared with RS several SB of melanoma, pigmented nevi, and normal skin reporting 85% of sensitivity and 99% of specificity for melanoma. Nijssen et al. [42, 43] were able to discriminate basal cell carcinoma (BCC) from the surrounding skin. RS was compared to histological staining methods. The analysis succeeded in differentiating between dermis and BCC, but it was hard to find differences between epidermis and BCC. Afterwards, evaluating a wide panel of SB, Lieber et al. [44] were able to discern between the different types of malignant skin cancers (BCC, squamous cell carcinoma, melanoma) and normal skin with a high diagnostic accuracy. Larraona-Puy et al. [45] found the same diagnostic accuracy of RS and expert histopathologists for the differentiation of BCC from hair follicles.

Lately, Lui et al. [46] evaluated the use of RS in the in vivo setting. In total 518 benign and malignant skin lesions from 453 patients were evaluated with RS including melanomas, BCCs, squamous cell carcinomas, actinic keratoses, atypical nevi, melanocytic nevi, blue nevi, and seborrheic keratoses. They reached an area under the receiver operating characteristic curve (ROC AUC) of 0.879 for differentiating malignant and premalignant lesions from benign skin lesions in vivo. The same group [47] also found a ROC AUC of 0.894 when analyzing additional 127 cases.

Philipsen et al. [48] investigated how skin pigmentation influenced Raman spectra and skin tumor diagnostics in vivo. They demonstrated that RS is useable for melanoma and BCC discrimination in vivo and that pigmentation of the skin or lesion does not influence the diagnosis.

The prospects are promising, and in the near future, RS could be used as a complement of the current diagnostic methods for automatic in vivo skin cancer diagnosis. However, further improvements in cost-effectiveness, in establishing algorithms, and in standardizing instruments are necessary.

25.5 Conclusions

Gradually, RS has obtained increasing interest for the investigation of physiological and pathological states of the skin. In the last few years, many investigations focused on the very high potential of RS in skin research. RS demonstrates the potential to become a standard tool at the service of pharmacology and cosmetology for the assessment of novel drugs and cosmetics. Particularly for depth features of substance penetration, both ex vivo and in vivo, RS has established its value. For the in vivo investigations, the high pattern variability still means a major challenge for researchers and statistical-standardized data analysis. Another enforcement with very hopeful perspective is diagnosis and characterization of skin diseases. With RS it is already possible to detect skin cancer ex vivo and in vivo. Nevertheless, the use of the equipment and the analysis of spectral elements requires training and experience. Subsequent simplification and standardization in measurement systems and analysis are needed to release all the potential of RS. Thus, there will be available in the everyday practice economically disposable and increasingly functional devices that will lead RS to become a standard analytical technique.

References

1. Franzen L, Windbergs M. Applications of Raman spectroscopy in skin research-From skin physiology and diagnosis up to risk assessment and dermal drug delivery. Adv Drug Deliv Rev. 2015;89:91–104.
2. Zhao J, Zeng H, Kalia S, Lui H. Using Raman spectroscopy to detect and diagnose skin cancer in vivo. Dermatol Clin. 2017;35(4):495–504.
3. Gniadecka M, Wulf HC, Nielsen OF, Christensen DH, Hercogova J. Distinctive molecular abnormalities in benign and malignant skin lesions: studies by Raman spectroscopy. Photochem Photobiol. 1997;66(4):418–23.
4. Krafft C, Codrich D, Pelizzo G, Sergo V. Raman mapping and FTIR imaging of lung tissue: congenital cystic adenomatoid malformation. Analyst. 2008;133(3):361–71.
5. Byrne HJ, et al. Spectropathology for the next generation: quo vadis? Analyst. 2015;140(7):2066–73.

6. Verrier S, Zoladek A, Notingher I. Raman microspectroscopy as a non-invasive cell viability test. Methods Mol Biol Clifton NJ. 2011;740:179–89.
7. Alawi SA, et al. Optical coherence tomography for presurgical margin assessment of non-melanoma skin cancer—a practical approach. Exp Dermatol. 2013;22(8):547–51.
8. Patil CA, Arrasmith CL, Mackanos MA, Dickensheets DL, Mahadevan-Jansen A. A handheld laser scanning confocal reflectance imaging-confocal Raman microspectroscopy system. Biomed Opt Express. 2012;3(3):488–502.
9. Caspers PJ, Lucassen GW, Wolthuis R, Bruining HA, Puppels GJ. In vitro and in vivo Raman spectroscopy of human skin. Biospectroscopy. 1998;4(5): S31–9.
10. Caspers PJ, Lucassen GW, Puppels GJ. Combined in vivo confocal Raman spectroscopy and confocal microscopy of human skin. Biophys J. 2003;85(1):572–80.
11. Schleusener J, et al. In vivo study for the discrimination of cancerous and normal skin using fibre probe-based Raman spectroscopy. Exp Dermatol. 2015;24(10):767–72.
12. Lademann J, et al. In vivo methods for the analysis of the penetration of topically applied substances in and through the skin barrier. Int J Cosmet Sci. 2012;34(6):551–9.
13. Franzen L, Selzer D, Fluhr JW, Schaefer UF, Windbergs M. Towards drug quantification in human skin with confocal Raman microscopy. Eur J Pharm Biopharm Off J Arbeitsgemeinschaft Pharm Verfahrenstechnik EV. 2013;84(2):437–44.
14. Haka AS, et al. In vivo margin assessment during partial mastectomy breast surgery using raman spectroscopy. Cancer Res. 2006;66(6):3317–22.
15. Barry BW, Edwards HGM, Williams AC. Fourier-transform Raman and infrared vibrational study of human skin—assignment of spectral bands. J Raman Spectrosc. 1992;23:641–5.
16. Williams AC, Edwards HG, Barry BW. The "Iceman": molecular structure of 5200-year-old skin characterised by Raman spectroscopy and electron microscopy. Biochim Biophys Acta. 1995;1246(1):98–105.
17. Tfayli A, Piot O, Manfait M. Confocal Raman microspectroscopy on excised human skin: uncertainties in depth profiling and mathematical correction applied to dermatological drug permeation. J Biophotonics. 2008;1(2):140–53.
18. Ashtikar M, Matthäus C, Schmitt M, Krafft C, Fahr A, Popp J. Non-invasive depth profile imaging of the stratum corneum using confocal Raman microscopy: first insights into the method. Eur J Pharm Sci Off J Eur Fed Pharm Sci. 2013;50(5):601–8.
19. Lawson EE, Anigbogu AN, Williams AC, Barry BW, Edwards HG. Thermally induced molecular disorder in human stratum corneum lipids compared with a model phospholipid system; FT-Raman spectroscopy. Spectrochim Acta A Mol Biomol Spectrosc. 1998;54A(3):543–58.
20. Cinotti E, et al. Identification of a soft tissue filler by ex vivo confocal microscopy and Raman spectroscopy in a case of adverse reaction to the filler. Skin Res Technol Off J Int Soc Bioeng Skin ISBS Int Soc Digit Imaging Skin ISDIS Int Soc Skin Imaging ISSI. 2015;21(1):114–8.
21. Cinotti E, Labeille B, Boukenter A, Ouerdane Y, Cambazard F, Perrot JL. Characterization of coal tattoos by Raman spectroscopy. Skin Res Technol Off J Int Soc Bioeng Skin ISBS Int Soc Digit Imaging Skin ISDIS Int Soc Skin Imaging ISSI. 2015;21(4):511–2.
22. Cinotti E, Labeille B, Perrot JL, Boukenter A, Ouerdane Y, Cambazard F. Characterization of cutaneous foreign bodies by Raman spectroscopy. Skin Res Technol Off J Int Soc Bioeng Skin ISBS Int Soc Digit Imaging Skin ISDIS Int Soc Skin Imaging ISSI. 2013;19(4):508–9.
23. Cinotti E, et al. Optical diagnosis of a metabolic disease: cystinosis. J Biomed Opt. 2013;18(4):046013.
24. Huang Z, Lui H, Chen XK, Alajlan A, McLean DI, Zeng H. Raman spectroscopy of in vivo cutaneous melanin. J Biomed Opt. 2004;9(6):1198–205.
25. González FJ, et al. Noninvasive estimation of chronological and photoinduced skin damage using Raman spectroscopy and principal component analysis. Skin Res Technol Off J Int Soc Bioeng Skin ISBS Int Soc Digit Imaging Skin ISDIS Int Soc Skin Imaging ISSI. 2012;18(4):442–6.
26. Tfayli A, Guillard E, Manfait M, Baillet-Guffroy A. Raman spectroscopy: feasibility of in vivo survey of stratum corneum lipids, effect of natural aging. Eur J Dermatol EJD. 2012;22(1):36–41.
27. Barba C, Alonso C, Martí M, Manich A, Coderch L. Skin barrier modification with organic solvents. Biochim Biophys Acta. 2016;1858(8):1935–43.
28. Vyumvuhore R, et al. Lipid organization in xerosis: the key of the problem? Int J Cosmet Sci. 2018;40:549–54.
29. Egawa M, Tagami H. Comparison of the depth profiles of water and water-binding substances in the stratum corneum determined in vivo by Raman spectroscopy between the cheek and volar forearm skin: effects of age, seasonal changes and artificial forced hydration. Br J Dermatol. 2008;158(2):251–60.
30. Egawa M, Kajikawa T. Changes in the depth profile of water in the stratum corneum treated with water. Skin Res Technol Off J Int Soc Bioeng Skin ISBS Int Soc Digit Imaging Skin ISDIS Int Soc Skin Imaging ISSI. 2009;15(2):242–9.
31. Chrit L, et al. In vitro and in vivo confocal Raman study of human skin hydration: assessment of a new moisturizing agent, pMPC. Biopolymers. 2007;85(4):359–69.
32. Tippavajhala VK, de Oliveira Mendes T, Martin AA. In vivo human skin penetration study of sunscreens by confocal Raman spectroscopy. AAPS PharmSciTech. 2018;19(2):753–60.
33. Broding HC, van der Pol A, de Sterke J, Monsé C, Fartasch M, Brüning T. In vivo monitoring of epidermal absorption of hazardous substances by confocal

Raman micro-spectroscopy. J Dtsch Dermatol Ges J Ger Soc Dermatol JDDG. 2011;9(8):618–27.
34. Mélot M, Pudney PDA, Williamson A-M, Caspers PJ, Van Der Pol A, Puppels GJ. Studying the effectiveness of penetration enhancers to deliver retinol through the stratum cornum by in vivo confocal Raman spectroscopy. J Control Release Off J Control Release Soc. 2009;138(1):32–9.
35. Mohammed D, Crowther JM, Matts PJ, Hadgraft J, Lane ME. Influence of niacinamide containing formulations on the molecular and biophysical properties of the stratum corneum. Int J Pharm. 2013;441(1–2):192–201.
36. Egawa M, et al. In vivo characterization of the structure and components of lesional psoriatic skin from the observation with Raman spectroscopy and optical coherence tomography: a pilot study. J Dermatol Sci. 2010;57(1):66–9.
37. Alda J, Castillo-Martinez C, Valdes-Rodriguez R, Hernández-Blanco D, Moncada B, González FJ. Use of Raman spectroscopy in the analysis of nickel allergy. J Biomed Opt. 2013;18(6):061206.
38. O'Regan GM, et al. Raman profiles of the stratum corneum define 3 filaggrin genotype-determined atopic dermatitis endophenotypes. J Allergy Clin Immunol. 2010;126(3):574–580.e1.
39. Wascotte V, Caspers P, de Sterke J, Jadoul M, Guy RH, Préat V. Assessment of the "skin reservoir" of urea by confocal Raman microspectroscopy and reverse iontophoresis in vivo. Pharm Res. 2007;24(10):1897–901.
40. Schallreuter KU, Moore J, Behrens-Williams S, Panske A, Harari M. Rapid initiation of repigmentation in vitiligo with Dead Sea climatotherapy in combination with pseudocatalase (PC-KUS). Int J Dermatol. 2002;41(8):482–7.
41. Gniadecka M, et al. Melanoma diagnosis by Raman spectroscopy and neural networks: structure alterations in proteins and lipids in intact cancer tissue. J Invest Dermatol. 2004;122(2):443–9.
42. Nijssen A, et al. Discriminating basal cell carcinoma from perilesional skin using high wave-number Raman spectroscopy. J Biomed Opt. 2007;12(3):034004.
43. Nijssen A, et al. Discriminating basal cell carcinoma from its surrounding tissue by Raman spectroscopy. J Invest Dermatol. 2002;119(1):64–9.
44. Lieber CA, Majumder SK, Billheimer D, Ellis DL, Mahadevan-Jansen A. Raman microspectroscopy for skin cancer detection in vitro. J Biomed Opt. 2008;13(2):024013.
45. Larraona-Puy M, et al. Development of Raman microspectroscopy for automated detection and imaging of basal cell carcinoma. J Biomed Opt. 2009;14(5):054031.
46. Lui H, Zhao J, McLean D, Zeng H. Real-time Raman spectroscopy for in vivo skin cancer diagnosis. Cancer Res. 2012;72(10):2491–500.
47. Zhao J, Lui H, Kalia S, Zeng H. Real-time Raman spectroscopy for automatic in vivo skin cancer detection: an independent validation. Anal Bioanal Chem. 2015;407(27):8373–9.
48. Philipsen PA, Knudsen L, Gniadecka M, Ravnbak MH, Wulf HC. Diagnosis of malignant melanoma and basal cell carcinoma by in vivo NIR-FT Raman spectroscopy is independent of skin pigmentation. Photochem Photobiol Sci Off J Eur Photochem Assoc Eur Soc Photobiol. 2013;12(5):770–6.

26 Multispectral and Hyperspectral Imaging for Skin Acquisition and Analysis

Lou Gevaux, Jean Luc Perrot, and Mathieu Hébert

26.1 Introduction

Multispectral and hyperspectral imaging are methods for measuring the spectral reflectance of surfaces, which have shown high potential for skin analysis. They provide noninvasive, in vivo, pixel-by-pixel measurements. The spectral reflectance is the radiometric quantity describing how much incident light is reflected by an object according to the wavelength of the light [1]. This quantity can be used to simulate color under any illuminant (such as natural sunlight, indoor lighting), to reveal information usually invisible to the naked eye, and to estimate the optical properties of a material, making it suited to numerous applications in various fields including heritage, art, agronomy, biology, and medicine [2–6]. Originally developed for observing Earth from space, spectral modalities of imaging have become more and more prevalent in the last decade, thanks to the progress in sensor performances and computational power. The development of applications that can be used for skin acquisition and analysis is still in its infancy today, but it is foreseeable that new optical tools for noninvasive diagnosis will be available in the future.

Skin, considered here as an optical component, can be described as a heterogeneous translucent material that absorbs and scatters light [7] (skin also contains elements that reemit light by fluorescence, but this property is not discussed in this chapter). Incident light on skin, apart from the portion of flux that is specularly reflected at the interface with air, undergoes multiple subsurface scattering events resulting from inhomogeneity in biological structures, as well as absorption by chromophores such as melanin and hemoglobin. The light that has not been absorbed and that has been backscattered toward the surface can exit the material and be captured by the eye or by a camera. Given that the optical properties of each skin component are wavelength-dependent, the received signal carries a "spectral signature" related to the skin that has been traversed. As such, appearance and measured spectral reflectance both contain information pertaining to skin structure and composition. Measuring the spectral reflectance of skin and analyzing its spectral signature can therefore be used as a method for investigating the condition of a person's skin, without the need for sample excision. A number of studies have explored the potential medical applications of spectral imaging, including for burn analysis [8], melanoma detection [9], erythema grading [10], characterization of vascular structures [11], and chromophore map estimation [12, 13].

L. Gevaux (✉) · M. Hébert
Univ Lyon, UJM-Saint-Etienne, CNRS, Institut d Optique Graduate School, Saint-Etienne, France
e-mail: Lou.gevaux@univ-st-etienne.fr; mathieu.hebert@univ-st-etienne.fr

J. L. Perrot
Department of Dermatology, University Hospital of Saint Etienne, Saint-Etienne, France
e-mail: j.luc.perrot@chu-st-etienne.fr

M. Fimiani et al. (eds.), *Technology in Practical Dermatology*,
https://doi.org/10.1007/978-3-030-45351-0_26

In this chapter, we outline various spectral imaging techniques. The potential for spectral imaging to reveal or enhance relevant details for skin investigation is then discussed and illustrated with examples on both normal and pathological skin. Finally, methods for analysis using spectral images are presented, before drawing conclusions.

26.2 Spectral Imaging Techniques

Spectral imaging extends conventional RGB color imaging by replacing the three channels corresponding to three large wavebands (red, green, blue) with a considerably higher number of wavebands [14]. Multispectral imaging and hyperspectral imaging are based on a similar principle and differ only in the number of channels acquired. While multispectral imaging typically measures 4–15 wavebands, hyperspectral imaging comprises up to hundreds of narrow wavebands of similar bandwidth covering contiguously the visible spectrum, as well as the ultraviolet (UV) and infrared (IR) domains. Spectral imaging can also be compared to spectroscopy, whereas spectroscopy measures the average spectral reflectance of a given area, spectral imaging provides a value for each pixel of the camera's field, therefore a spectrum in many small areas on the observed surface, making it especially suitable for the observation of heterogeneous surfaces. Spectral image data are often called "hypercubes" since they are three dimensional: two dimensions corresponding to the spatial domain, one dimension corresponding to the spectral domain.

Many near-field spectral imaging systems have been developed using various technologies and physical principles, with different specificities in terms of spatial resolution, spectral resolution, surface shape constraints and acquisition time. The capacity to distinguish details on a spectral image is dependent on both the spectral and spatial resolutions. A good spectral resolution allows discrimination between very subtle variations in the spectral reflectance which can indicate variations in the material composition. A good spatial resolution makes it possible to see very fine details. With the exception of snapshot cameras [15], which acquire the spectral image instantaneously (providing multispectral data only), the acquisition of a "hypercube" requires a temporal scan. Two methods, illustrated in Fig. 26.1, are commonly used [6, 14]. The first method is the staring approach, also called the wavelength scanning approach, which records the full spatial information for each spectral band

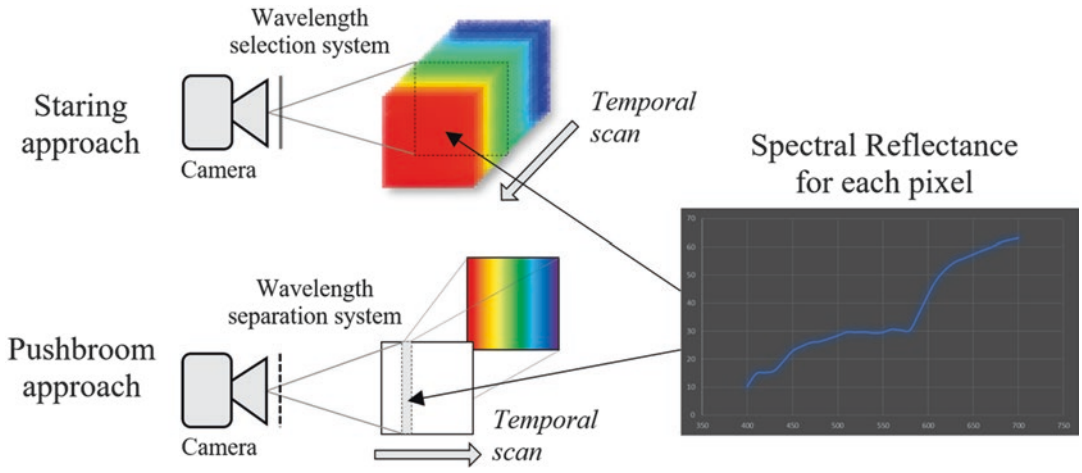

Fig. 26.1 Concepts of the staring and pushbroom approaches for hyperspectral imaging

and requires a temporal scan of the spectral dimension. This method relies on a wavelength selection system, such as a filtering wheel, a tunable filter, or a set of monochromatic LEDs to light the set-up. The second method, the pushbroom approach or line scanning approach, consists of acquiring the spectral information for a single line of an image. The complete image is then retrieved by performing a temporal scan of the second spatial dimension. This second method uses a wavelength separating system such as a diffraction grating or a prism.

The spectral reflectance information is obtained after a calibration step using a perfectly diffusing white sample. Experimentally, the spectral reflectance is generally not measured directly: the spectral reflectance is defined as the ratio of reflected flux to incident flux, and it is difficult to precisely measure the incident flux. Spectral reflectance factor is often measured rather than reflectance. The reflectance factor is obtained by dividing the spectral radiance measured from the object with the spectral radiance measured from a reference surface (a perfectly white diffuser) that is illuminated and viewed in the same way as the object. When the measured surface is uniformly diffusing (i.e., Lambertian), which is approximatively the case for skin if we ignore the gloss reflection, spectral reflectance factor and spectral reflectance are equal to each other [1]. However, when measuring parts of the body that are not flat, the calibration method does not account for the illumination variations that can occur. In shadows, the measured reflectance varies proportionally to the local irradiance of the surface.

Although spectral imaging is an active field of research with innovative solutions regularly presented, many of the existing spectral imaging systems are not entirely suited to acquisitions on living organs. In vivo skin applications require good spatial resolution in order to distinguish small elements, good spectral resolution to enable physics-based analysis, and short acquisition time to reduce the risk of the subject moving during the acquisition. As high-resolution spectral imaging most often uses a temporal scan, this latter requirement is especially challenging.

26.3 Spectral Images of Normal and Pathological Skin

The images presented in this section have been obtained using the SpectraCam® and SpectraFace® hyperspectral cameras [12, 13] developed by Newtone Technologies, France. For both the cameras, acquisition time is approximatively 2 s, and spectral resolution is 31 wavelengths, sampled every 10 nm in the visible spectrum between 400 nm and 700 nm. The specular reflection on the stratum corneum, usually related to the visual sensation of gloss, is discarded using polarization filters in a cross-polarization configuration [13]. The SpectraCam® camera acquires images from areas of 5 × 4 cm, while the SpectraFace® can acquire a full face. The images taken with these cameras have shown their capacity to reveal relevant skin properties. Images of pathological skin have also been acquired to illustrate the potential contribution of spectral imaging as a tool for diagnosis.

The spectral images can be visualized either wavelength by wavelength, or as a color image obtained by converting the spectrum in each pixel into RGB color values (or color coordinates in another color space) by considering one illuminant, i.e., one spectral power distribution for the light source (Fig. 26.2d). Figure 26.2a, b, and c show the same hyperspectral image displayed at three different wavelengths, each of them highlighting a specific skin characteristic, such as skin translucency (which increases with wavelength), or melanin and hemoglobin light absorption properties.

The images of Fig. 26.2 are displayed as gray levels as follows. Light gray levels correspond to areas of skin that reflects a lot of the incident light toward the camera, and dark gray levels correspond to areas of skin that absorb a lot of light. They can be analyzed in conjunction with the graph displayed in Fig. 26.3, showing the absorption properties of the main skin chromophores according to the wavelength of light [16–18]. On this graph, the plotted quantity is the spectral absorption coefficient μ_a (in $cm^{-1}.g^{-1}.L$), defined as the probability for one photon

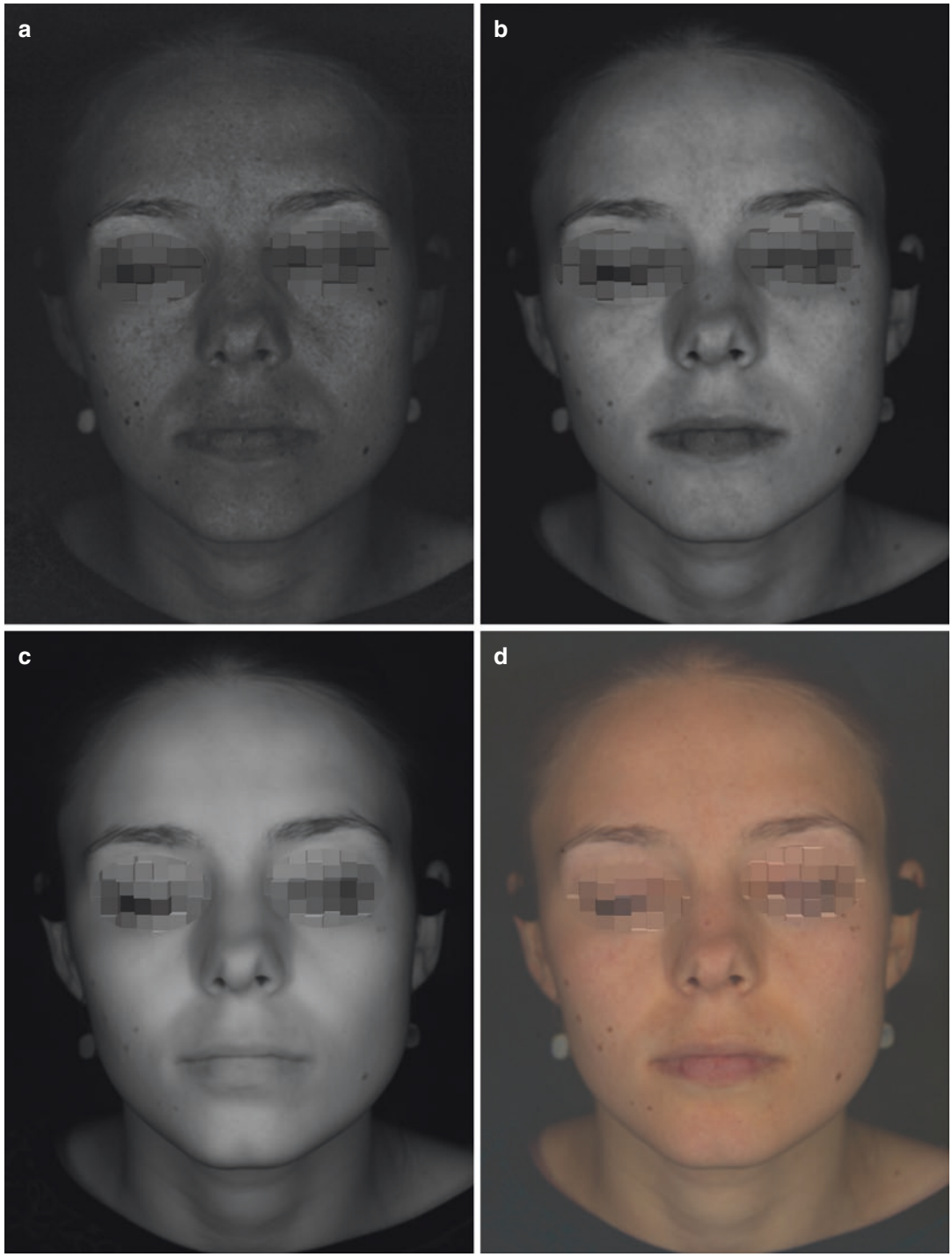

Fig. 26.2 Example of a hyperspectral image: Image at 420 nm (**a**), at 590 nm (**b**), at 700 nm (**c**), color image after D65 illuminant RGB conversion (**d**)

of light to be scattered when traveling through 1 cm of a material containing 1 g of chromophore per liter.

At low wavelengths (Fig. 26.2a), which are often called the blue wavelengths, melanin stains are especially visible, as melanin mainly absorbs UV and blue light. Skin is also strongly scattering at these wavelengths, which means that blue light cannot travel very deep into the skin before exiting (skin is strongly opaque in this spectral domain). The consequence of this property on the hyperspectral image is that skin superficial structure and fine lines are clearly visible.

Blood vessels appear (Fig. 26.2b) with a good contrast between 530 nm and 600 nm (green and orange colors), due to a peak in the absorption properties of hemoglobin in this part of the visible spectrum. At these wavelengths, it can also be noticed in Fig. 26.3 that the absorption of oxyhemoglobin and deoxyhemoglobin differs, a property used in pulse oximetry to calculate the oxygen saturation level.

Beyond 650 nm (red color and infrared radiations) (Fig. 26.2c), skin is less scattering and therefore more translucent, which allows light to travel deeper. Consequently, skin appears more uniform at higher wavelengths, as the details on its surface are blurred by multiple scattering. Finally, skin chromophores are also almost transparent (i.e., their absorption coefficient is close to zero) for red light: lips and skin have the similar gray levels at 700 nm.

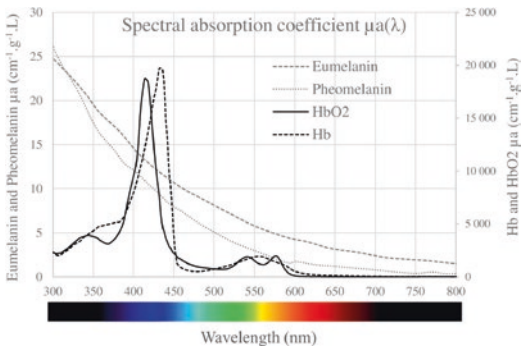

Fig. 26.3 Spectral absorption coefficient μ_a (λ) for eumelanin, pheomelanin, oxygenated hemoglobin (HbO2), and deoxygenated hemoglobin (Hb) [16–18]

Various effects that can be observed on pathological skin are illustrated by two examples in Fig. 26.4.

Figure 26.4.a shows the presence of angiomas and lentigos, whose appearance varies according to two distinct patterns when looking at different wavelengths. These distinct patterns may constitute a classification criteria. On the image at 440 nm, both angiomas and lentigos appear as dark spots, as a consequence of light absorption by both melanin and hemoglobin at this wavelength. At higher wavelengths, the blood contained in angiomas, visible with a high contrast at 520 nm and 580 nm, suddenly "disappears" from the image between 620 nm and 700 nm, as it is transparent in this spectral range (its absorption coefficient is almost zero beyond 600 nm, as shown in Fig. 26.3). The visual variation, of lentigos is different: their visibility gradually fades as the wavelength increases.

The second example (Fig. 26.4b), showing a hemangioma and a scar, demonstrates how spectral imaging can reveal information about how deep blood vessels are in skin. At 440 nm, a few blood vessels can be distinguished, but since skin is very scattering at this wavelength, light cannot propagate very deep in the tissue, and we can deduce that these blood vessels are very close to the surface. As the wavelength increases (see, for example, at 520 nm and 580 nm), skin becomes more and more translucent, and we can see more and more vessels. For each spectral image, the newly visible vessels are located a bit deeper in skin than the one visible at the previous wavelength. At 620 nm and 700 nm, blood is transparent; therefore, blood vessels are no longer visible and skin appears very homogeneous. The scar color does not visibly vary according to the wavelength, as scar tissue does not contain melanin or blood vessels.

26.4 Spectral Image Analysis

In this section, we consider a typical application of spectral image analysis: the calculation of chromophore maps [12, 13]. Skin analysis from

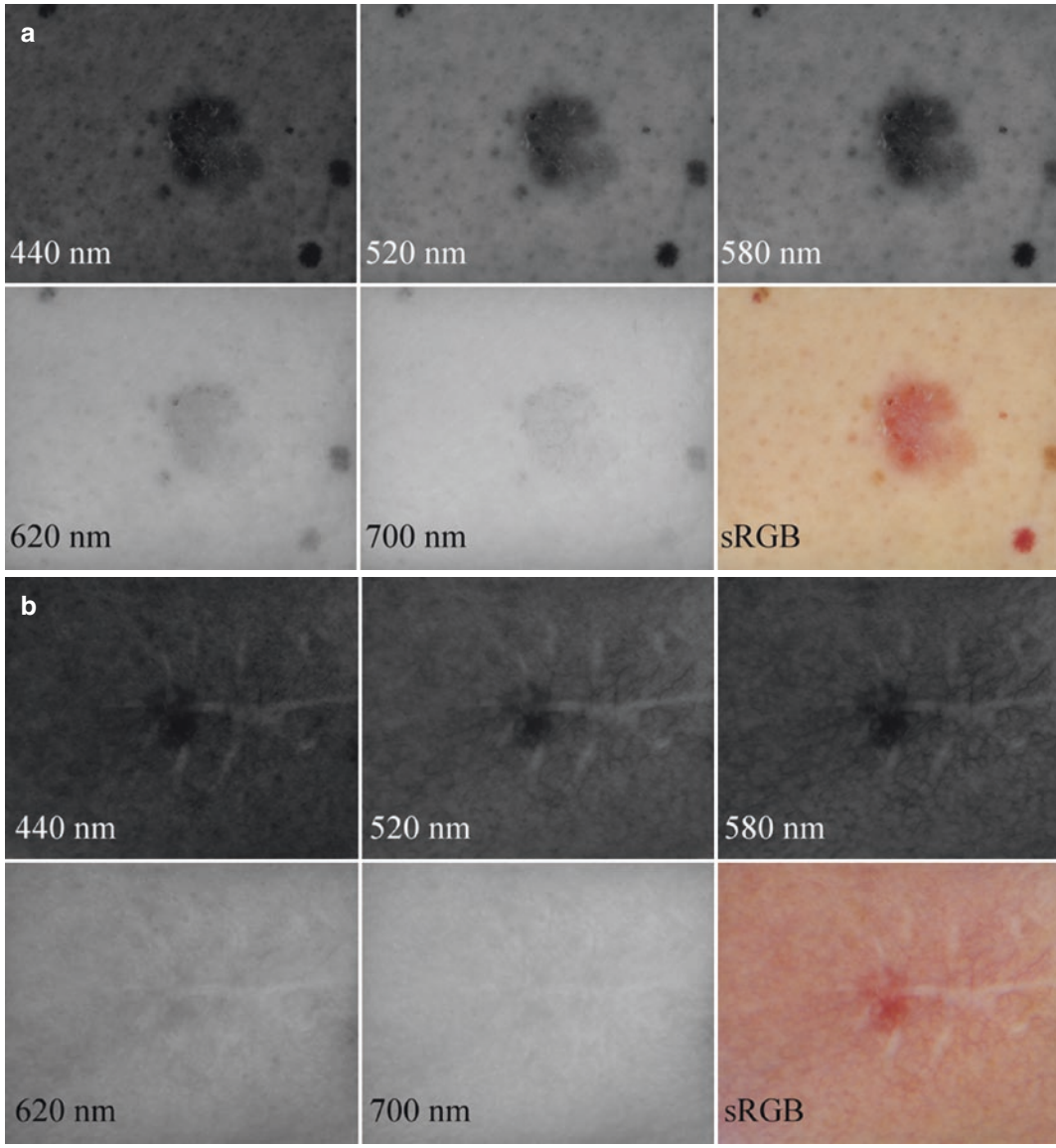

Fig. 26.4 Spectral images of a 5 × 4 cm area of skin at various wavelengths and color representation (sRGB) for angiomas and lentigos (**a**), and for a hemangioma and a scar (**b**)

hyperspectral data can be described as an inverse problem: from experimental measurements, the causes of a phenomena are sought. In the case of chromophore map calculations, this inverse problem is rather complex, as it must take into account a number of parameters (melanin concentration, oxygen rate, blood content, and so on). The solution that we have selected describes the direct problem by using a skin model and a light radiative model and uses an optimization algorithm to estimate the skin parameters. This method can be described as a "physics-based" approach, since it relies on a physical model of light–skin interactions.

According to this approach, skin is modeled as a two-layer material. The upper layer represents the epidermis and contains melanin. The bottom layer, assumed to be semi-infinite, represents the dermis and contains hemoglobin in its oxygenated and deoxygenated forms. Regarding

the interactions between light and translucent materials, the radiative transfer theory [19] is a powerful formalism which models absorption and multiple scattering phenomena. However, this method is computationally consuming. A simplified model is often preferred. One such model is the two-flux theory [20–22], especially adapted to multilayer media. This method considers the propagation of two diffuse light fluxes in opposite directions (forwards and backwards) and their mutual exchanges. The method allows for the calculation of spectral reflectance of the layered material given the optical properties (absorption and scattering) of each layer. Finally, the Beer–Lambert–Bouguer law [23] gives the relationship between the absorption properties of each layer, the chromophore concentrations and the individual absorption properties of each chromophore.

The direct model described above yields the skin spectral reflectance when the skin chromophore composition is known. Inversely, the skin chromophore concentration can be estimated from the measured spectral reflectance by a process of optimization. This consists of finding, for each pixel, the parameters that minimize the distance between the measured spectrum and the spectrum predicted by the model. The optimization parameters concern only the absorption properties of skin chromophores, the scattering properties are assumed to be constant on the face. Typical values from the literature are used [16–18].

Figure 26.5 illustrates results obtained from applying this analysis method on a full-face hyperspectral image. Figure 26.5a, b, and c show maps that respectively represent blood volume content, oxygen rate, and melanin concentration, computed from the concentrations of oxyhemoglobin, deoxyhemoglobin, and melanin provided by the optimization process.

This method yields good results when applied to normal skin. However, for pathological skin, the results are far more uncertain, since the optical model does not account for specific structures or chromophores that can be found in pathological tissues. Hence, the study of pathological skin using a physics-based approach would require a more complex model of skin.

Databases and artificial intelligence can therefore help, for example, through utilizing an artificial neuron network to solve complex, nonlinear problems. Such an approach is based on learning a set of data for which both the cause and the measured phenomena are known. This approach is for example used in the MelaFind™ system [24], which is especially designed to facilitate melanoma identification. A multispectral image composed of 10 channels in the visible and near infrared domains is acquired, then compared to a database of over 9000 lesions that were imaged and biopsied with histopathology results. The comparison, performed using pattern recognition, allows for a scoring, providing a general recommendation for or against biopsy.

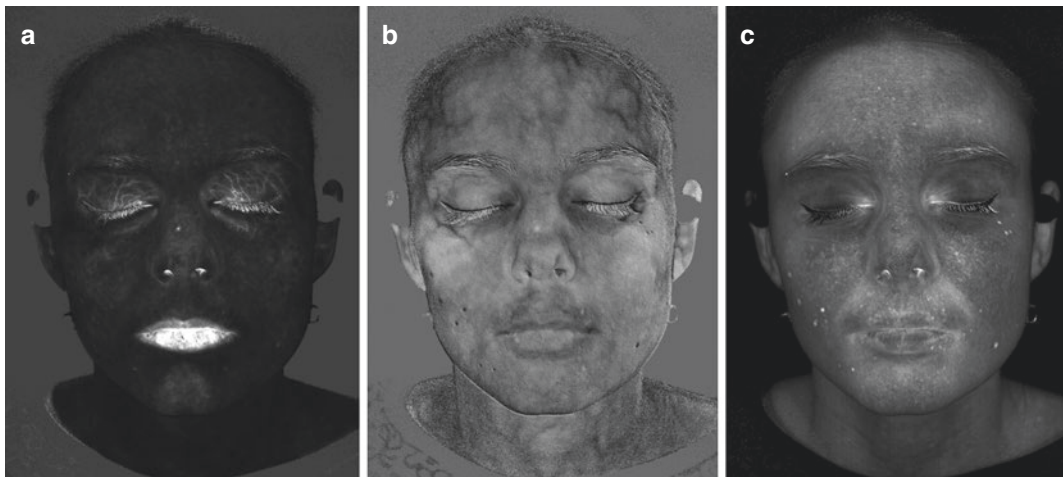

Fig. 26.5 Maps of blood volume content (**a**), oxygen rate (**b**), and melanin concentration (**c**)

Finally, for many applications, the aim of spectral image analysis is not to precisely retrieve the complete optical properties, but to identify the presence or the absence of a specific optical signature in the measured signal. With this goal in mind, high resolution spectral imaging and physics-based analysis methods can be used in preliminary research in order to design cheaper and faster analysis methods.

26.5 Conclusion

Multispectral and hyperspectral imaging have already shown their potential for skin study and are active fields of research in optics for biomedical applications. The development of further optical devices for skin study can also be expected, as they can perform in vivo, noninvasive, and fast acquisitions. Their emergence can be credited to the improvement of both measurement systems and computer calculation power, which allow for the solving of increasingly complex problems. The ability to acquire images with a high spatial resolution is particularly beneficial for applications in dermatology, as the observed objects might contain very small details. A good spectral resolution, such as the one characterizing hyperspectral imaging, is also advantageous for skin study as it provides optical information which can be related to material characteristics using a physical model used in inverse approach. However, high spectral resolution systems remain complex and expensive devices, which are often fragile and can impose acquisition constraints and thus limit their use outside of a research context. In parallel to the development of high-resolution acquisition cameras, current research is trending toward using artificial intelligence and big data to compensate for the shortcomings of acquisition systems. Another tendency has been to design simpler and cheaper systems for large consumer applications, based on the acquisition of few well-chosen wavebands, in order to exhibit very specific properties.

References

1. Hébert M, Hersch RD, Emmel P. Fundamentals of optics and radiometry for color reproduction. In: Kriss M, editor. Handbook of digital imaging. Chichester, UK: John Wiley & Sons, Ltd; 2014. p. 1–57.
2. Liang H. Advances in multispectral and hyperspectral imaging for archaeology and art conservation. Applied Physics A. 2012;106(2):309–23.
3. Cucci C, Delaney JK, Picollo M. Reflectance hyperspectral imaging for investigation of works of art: Old master paintings and illuminated manuscripts. Acc Chem Res. 2016;49(10):2070–9.
4. Lorente D, et al. Recent advances and applications of hyperspectral imaging for fruit and vegetable quality assessment. Food Bioprocess Tech. 2012;5(4):1121–42.
5. Manley M. Near-infrared spectroscopy and hyperspectral imaging: non-destructive analysis of biological materials. Chem Soc Rev. 2014;43(24):8200–14.
6. Lu G, Fei B. Medical hyperspectral imaging: a review. J Biomed Opt. 2014;19(1):010901.
7. Igarashi T, Nishino K, Nayar SK. The appearance of human skin: a survey. Foun Trends® Comput Graph Vis. 2007;3(1):1–95.
8. Calin MA, et al. Characterization of burns using hyperspectral imaging technique—A preliminary study. Burns. 2015;41(1):118–24.
9. Tomatis S, et al. Automated melanoma detection with a novel multispectral imaging system: results of a prospective study. Phys Med Biol. 2005;50(8):1675–87.
10. Madooei A, et al. Hyperspectral image processing for detection and grading of skin erythema. Presented at SPIE Medical Imaging, 24 February 2017, Orlando, Florida, United States; 2017.
11. Randeberg LL, Larsen ELP, Svaasand LO. Characterization of vascular structures and skin bruises using hyperspectral imaging, image analysis and diffusion theory. J Biophotonics. 2009;3(1–2):53–65.
12. Seroul P, et al. Model-based skin pigment cartography by high-resolution hyperspectral imaging. J Imaging Sci Technol. 2016;60(6):60404–1.
13. Gevaux L, et al. Three-dimensional hyperspectral imaging: a new method for human face acquisition. Electron Imaging. 2018;2018(8):152-1–152-10.
14. Garini Y, Young IT, McNamara G. Spectral imaging: principles and applications. Cytometry A. 2006;69A(8):735–47.
15. Hagen N, Kudenov MW. Review of snapshot spectral imaging technologies. Opt Eng. 2013;52(9):090901.
16. Jacques SL. Optical properties of biological tissues: a review. Phys Med Biol. 2013;58(11):R37–61.
17. Jacques SL. https://omlc.org/spectra/melanin/

18. Prahl S. https://omlc.org/spectra/hemoglobin/.
19. Magnain C, Elias M, Frigerio J-M. Skin color modeling using the radiative transfer equation solved by the auxiliary function method. J Opt Soc Am A. 2007;24(8):2196.
20. Kubelka P, Munk F. An article on optics of paint layers. Z. Tech. Phys. 1931;16:593–609.
21. Kubelka P. New contributions to the optics of intensely light-scattering materials part II: Nonhomogeneous layers∗. J Opt Soc Am. 1954;44(4):330.
22. Hébert M, Emmel P. Two-flux and multiflux matrix models for colored surfaces. In: Kriss M, editor. Handbook of digital imaging. Chichester, UK: John Wiley & Sons, Ltd; 2015. p. 1–45.
23. Wyszecki G, Stiles WS. Color science: concepts and methods, quantitative data and formulae. 2nd ed. New York: Wiley; 1982.
24. Kupetsky EA, Ferris LK. The diagnostic evaluation of MelaFind multi-spectral objective computer vision system. Expert Opin Med Diagn. 2013;7(4):405–11.

27 Electrical Impedance in Dermatology

Josep Malvehy, Alicia Barreiro-Capurro, and Susana Puig

27.1 Introduction

Electrical impedance (EI) is the measure of the opposition that a circuit presents to an alternating electrical current when a voltage is applied with various frequencies [1, 2]. When this current is applied to a biological material or tissue, electrical impedance reflects the clinical status of the tissue under study. In general, impedance at low electrical frequencies is related mainly to the molecular properties of the extracellular component, whereas the capacitive properties of the cell membranes and the intra- and extracellular component of the tissue are reflected by electrical impedance at both high and low frequencies.

In previous investigations, it was measured and estimated the electrical properties for a large number of tissue types, in conjunction with a broad range of electrical impedance applications [1]. Electrical impedance has been used in a wide range of clinical applications, ranging from differentiation of different cancer types [3–5], tomography in lung and cardiac disorders, myography of neuromuscular disorders and body composition [6, 7].

In initial studies from 1998 to 2005, different authors reported that there are statistically significant electrical impedance differences between healthy reference skin, basal cell carcinoma (BCC) and squamous cell carcinoma (SCC) [3–5]. In these preliminary studies [8–11], it was demonstrated that it is possible to use the differences in electrical impedance between melanocytic benign lesions and BCC to classify the two categories with accuracy. In 2004, Dua R and co-workers [9] and Åberg P and co-workers [10] demonstrated that EI measured with non-invasive method on the skin can be used to differentiate BCCs, actinic keratosis, SCC and benign melanocytic nevi. The same authors showed that with a lower accuracy at that time it is possible to rule out melanoma.

In 2003, Åberg P and co-workers [11] proposed a microinvasive electrode composed with extremely small pins that penetrate into the stratum corneum with the intention to reduce the electrical impedance of the stratum corneum, and, consequently, be less influenced by possibly irrelevant biological variations than electrical impedance measured with a non-invasive flat electrode. The same group reported in 2005 in a pilot study including a limited number of 16 melanomas that the accuracy of these new electrodes was higher than the regular non-invasive flat electrode [12].

J. Malvehy (✉) · S. Puig
Dermatology Department, Hospital Clinic of Barcelona, IDIBAPS, University of Barcelona, Barcelona, Spain

CIBER de Enfermedades Raras, Barcelona, Spain
e-mail: jmalvehy@clinic.cat

A. Barreiro-Capurro
Dermatology Department, Hospital Clinic of Barcelona, IDIBAPS, University of Barcelona, Barcelona, Spain
e-mail: barreiro@clinic.cat

M. Fimiani et al. (eds.), *Technology in Practical Dermatology*,
https://doi.org/10.1007/978-3-030-45351-0_27

27.1.1 Principle of Electrical Impedance Spectroscopy (EIS) in the Skin

Electrical impedance is a measure of the skin's opposition to the flow of alternating electric currents of various frequencies [1]. The electrical impedance of skin lesions reflects the clinical status of the tissue under study. Normal and pathologic tissue differ with regard to cell size, shape, orientation, compactness, structure of cell membranes and molecular composition. These properties of the skin tissue affect its capability to store and conduct electricity and they are reflected in the EI measurement (Fig. 27.1). Finally, a skin tumour that would be diagnosed by clinical, dermoscopic or histological examination can also be classified by analyses of the impedance spectrum.

In general, impedance at high frequencies is related both to the reactance of the cell membranes and to the resistive properties of the extra- and intracellular components, whereas impedance at low electrical frequencies is related mainly to the resistive properties of the extracellular component of the lesion (Fig. 27.1). Therefore, a given outcome of an EIS measurement is both magnitude and phase shift at each frequency included in the spectrum.

27.1.2 Electrical Impedance Measurements

27.1.2.1 Electrical Impedance Spectrometer

Different electrical impedance spectrometers have been used in previous studies with almost equivalent modes of operation, but only Nevisense has been approved for the clinical use in dermatology. The most recent version of this device will be described in this chapter. The Nevisense technology for EIS is a patented technology developed over 20 years at the Karolinska Institute in Stockholm [14] and is distributed by SciBase. It is based on substantial research and has achieved positive results in the largest clinical study of its type conducted within the detection of malignant melanoma. Nevisense is CE marked in Europe, has TGA approval in Australia, and now also has a FDA clearance in the United States.

In contrast to previous versions of Nevisense, there is no longer a need for a separate reference measurement for each lesion to be tested. Healthy skin features previously taken from the reference measurement can now be extracted from the lesion. Eliminating the reference means that there are fewer steps to perform which makes it easier to integrate the test into clinical practice.

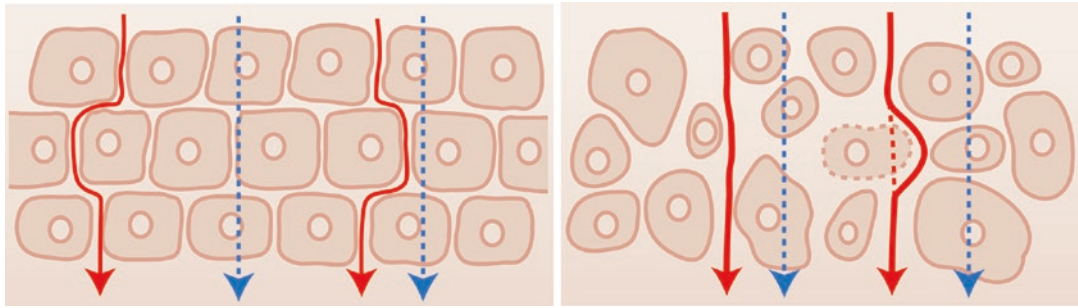

Fig. 27.1 Schematic representation of current pathways of low and high frequencies. Yellow lines represent low frequency currents that primarily reflect the extracellular environment. High frequencies represented in red lines reflect both the intra- and extracellular environment. The EIS is different in healthy tissue (upper schematic) compared to abnormal tissue with disorganized cellularity (inferior schematic) (Reproduced with permission from [13]). "Courtesy of SciBase GmbH", 2020, All rights reserved)

The device holds a database for storing and sharing of patient data and examination. Utilizing Artificial Intelligence (AI) for improved user feedback is integrated in the software to guide the operator and increase efficiency in clinical practice.

The EIS system consists of a control unit, a measurement probe and a disposable microinvasive electrode as shown in Fig. 27.2.

The **control unit** processes examination data and presents the results of the EIS measurement on the display. The **display** is equipped with a touch screen for user interaction. The **probe unit**, connected to the control unit through a cable, is used to initiate the electrical impedance measurements. The system measures electrical impedance at 35 set frequencies, logarithmically distributed from 1.0 kHz to 2.5 MHz. An EIS measurement includes both magnitude and phase shift at each frequency in the spectrum (Fig. 27.3). A complete electrical impedance measurement takes less than 10 s. The applied voltage and resulting current are limited to 150 mV and 75 μA, respectively, which is imperceptible to the patient. This results in a maximum of power and energy that can be delivered to the skin tissue of 11.25 μW and 113 μJ, respectively. EIS is a measure of the overall resistance within the tissue at alternating currents of various frequencies.

Fig. 27.2 EIS system consists of a control unit, a measurement probe and a disposable microinvasive electrode (Courtesy of SciBase GmBH, 2019)

Microinvasive Electrode

Before every examination, a disposable electrode is attached to the probe. The electrode is for single-patient use and after every examination and a maximum of 20 lesion measurements, the operator removes the electrode and disposes of it. The electrode has five bars with 45 microscopic pins on each bar. The electrode surface and microinvasive pins are coated with a thin gold layer. Each pin is pyramid shaped and is approximately 150 μm high with a 170 mm triangular base. The electrical signals pass between the bars and measure the impedance in the lesion as illustrated in Fig. 27.3 covering a measurement area of 5 mm × 5 mm. The pins are designed to penetrate approximately 10–20 μm in depth into the stratum corneum, thus not producing any harm in

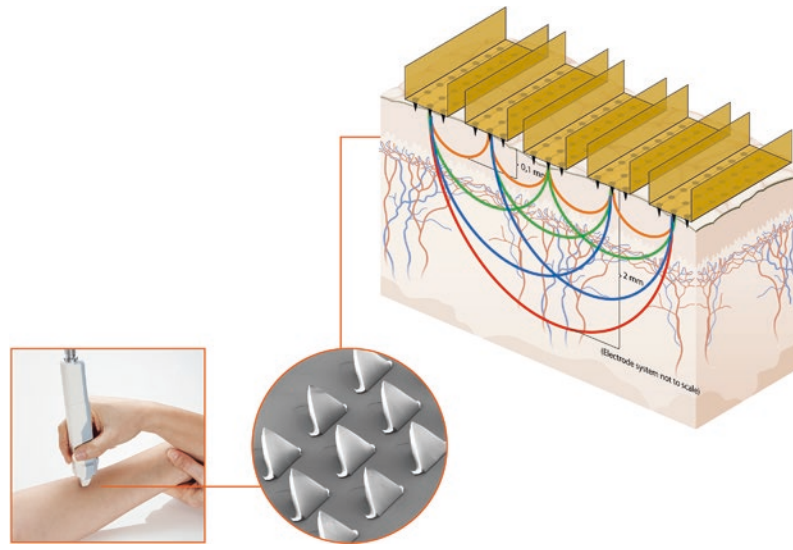

Fig. 27.3 The EI is measured by applying an unnoticeable alternating potential between the bars on the tip of the probe. In order to cover the lesion in width and depth, the measurement is performed in 10 permutations covering shallow measurements between neighbouring electrode bars as well as deeper measurements between more distant electrode bars at four different depths (Courtesy of SciBase GmBH, 2019)

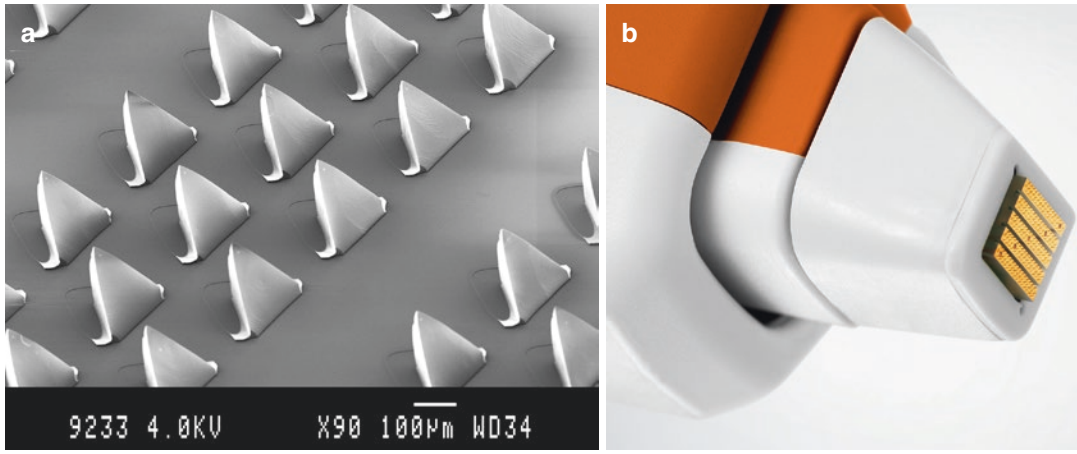

Fig. 27.4 Electrode used for EIS. Image of the probe with the electrode (**a**) and electron micrograph of the micro-pins on the surface of the electrode system (**b**). The pins are 150 µm long with a 170 µm triangular base (Courtesy of SciBase GmBH, 2019)

the epidermis component (Fig. 27.4a and b). The pins are 150 µm long with a 170 µm (triangular base). Since the pins neither reach the blood vessels nor the sensory nerves in the dermis, the probe is classified as microinvasive and measurements with the electrodes are painless.

EIS is measured by applying an alternating potential between the bars of the electrode. To cover the lesion in both area and depth, the measurement is performed in 10 permutations covering both shallow measurements between neighbouring electrode bars as well as deeper measurements between more distant electrode bars at four different depths [13].

The system can also be equipped with a flat concentric electrode that is not yet used in standard clinical practice, but is used in research.

27.1.2.2 General Examination Procedure

Electrical impedance measurements are performed after entering patient data into the control unit via the touch screen. In previous versions of the system, the operator had to perform at least 2 measurements, one on typical healthy skin (reference) located nearby to the lesion and one or more on the lesion. Recently, the method has been modified and the reference measurement is no longer required.

Prior to measurements, the lesion surface is moistened with physiological saline solution (0.9% salt concentration) for a minimum of 30 s. Thereafter the excess fluid is wiped off with a dry compress. The electrode is placed against the lesion and a measurement is initiated. The outcome of the measurement is curves illustrating phase shift (degrees) and magnitude (in kOhms) at multiple depths and permutations (Fig. 27.5). The lesion measurement takes about 10 s to perform but more than one measurement may be needed to cover the entire lesion.

The results of the measurements are analysed and displayed on the Nevisense screen. The Nevisense classifier provides an EIS score output from 0 to 10 reflecting the degree of atypia identified by the method. This can be used together with clinical information and the results of other examinations such as dermoscopy or confocal microscopy (Figs. 27.6, 27.7, 27.8 and 27.9).

27.1.2.3 Clinical Studies of EIS in Dermatology

Electrical impedance is a fast, non-invasive and painless safe tool with a relatively low cost and has been used in measuring skin or stratum corneum hydration [15–24].

EIS has also been applied to distinguish allergic and irritant contact dermatitis by evaluating

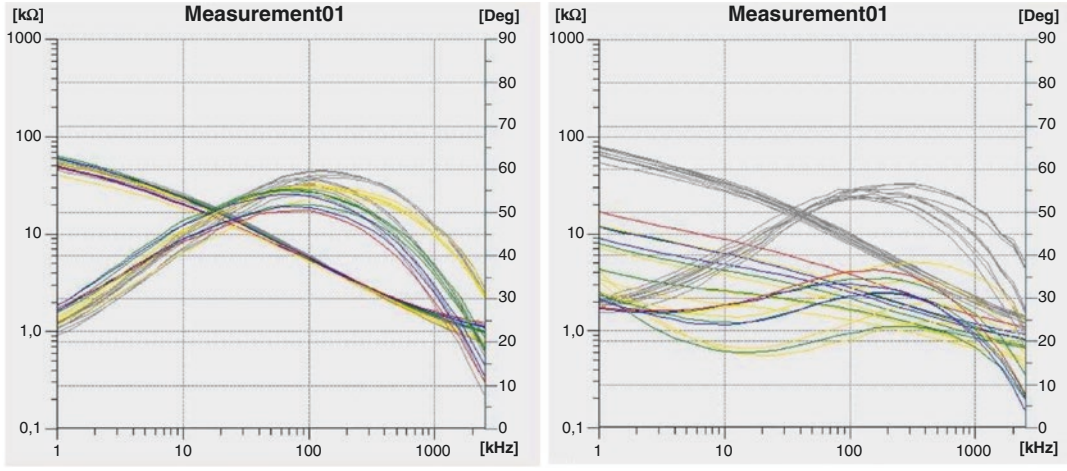

Fig. 27.5 Graphic representation of the measurement of the EIS in a melanoma (Reproduced with permission from [13])

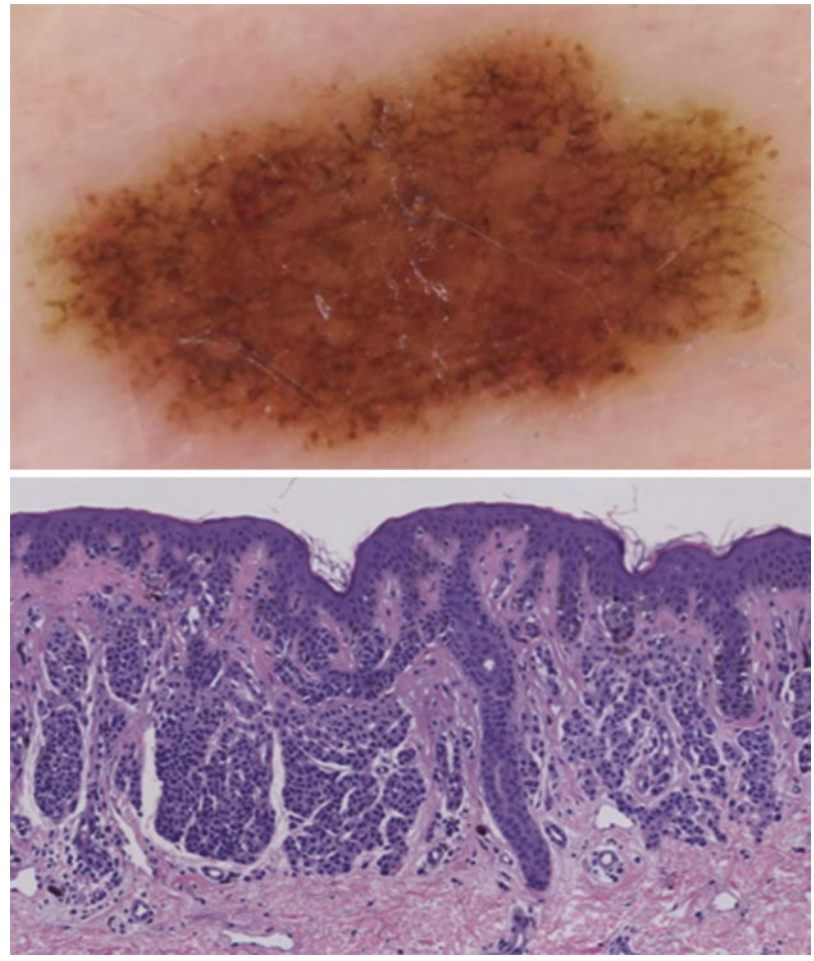

Fig. 27.6 Dermoscopy and histopathology of atypical melanocytic nevi with an EIS score of 2

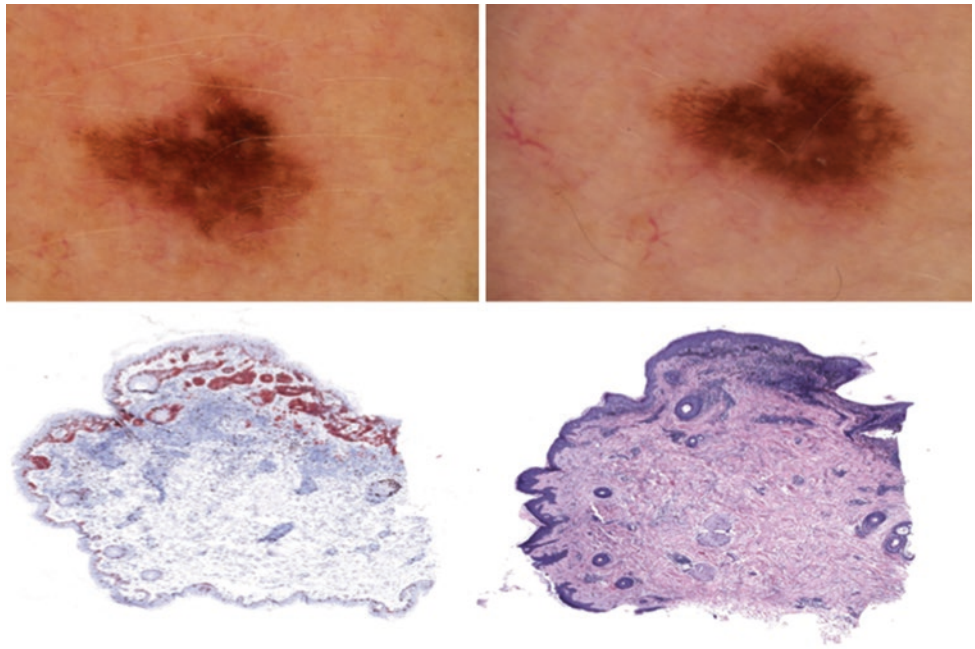

Fig. 27.7 Digital follow-up of a patient with *CDKN2A* mutation. Dermoscopy shows enlargement and atypical pigment network. Histopathology reveals an in situ melanoma. EIS score 4

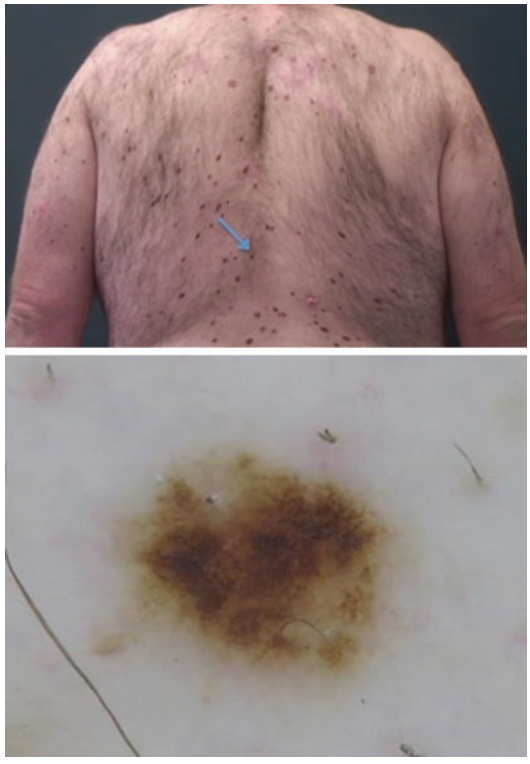

Fig. 27.8 42-year-old man with atypical mole syndrome. A new melanocytic lesion on the back with EIS score 1. The pathology reports a benign nevi

the degree of irritation in human skin [25–27]. In addition, the electrical impedance values have been assessed to discriminate skin tumours, such as basal cell carcinoma, melanoma or dysplastic nevi [4, 9, 28–32].

In this section, we will review the main studies in dermatology.

Studies in Non-tumour Diseases

In 1992, Ollmar and co-workers [33] reported on healthy volunteers subjected to irritation by sodium lauryl sulphate at different concentrations and measured with electrical impedance. Good agreement between concentration and an irritation index calculated from electrical impedance parameters was found over the whole concentration range for most test persons. These results suggested that EI could be used as an objective tool to record irritation, and the authors suggested that electrical impedance might be a more sensitive method than the commonly used visual readings. Other consequent studies explored EIS in contact dermatitis [33–36]. Nyren M and co-workers found that through the application of the impedance technique, it could be possible to characterize objectively and quantify the wheal reaction. The

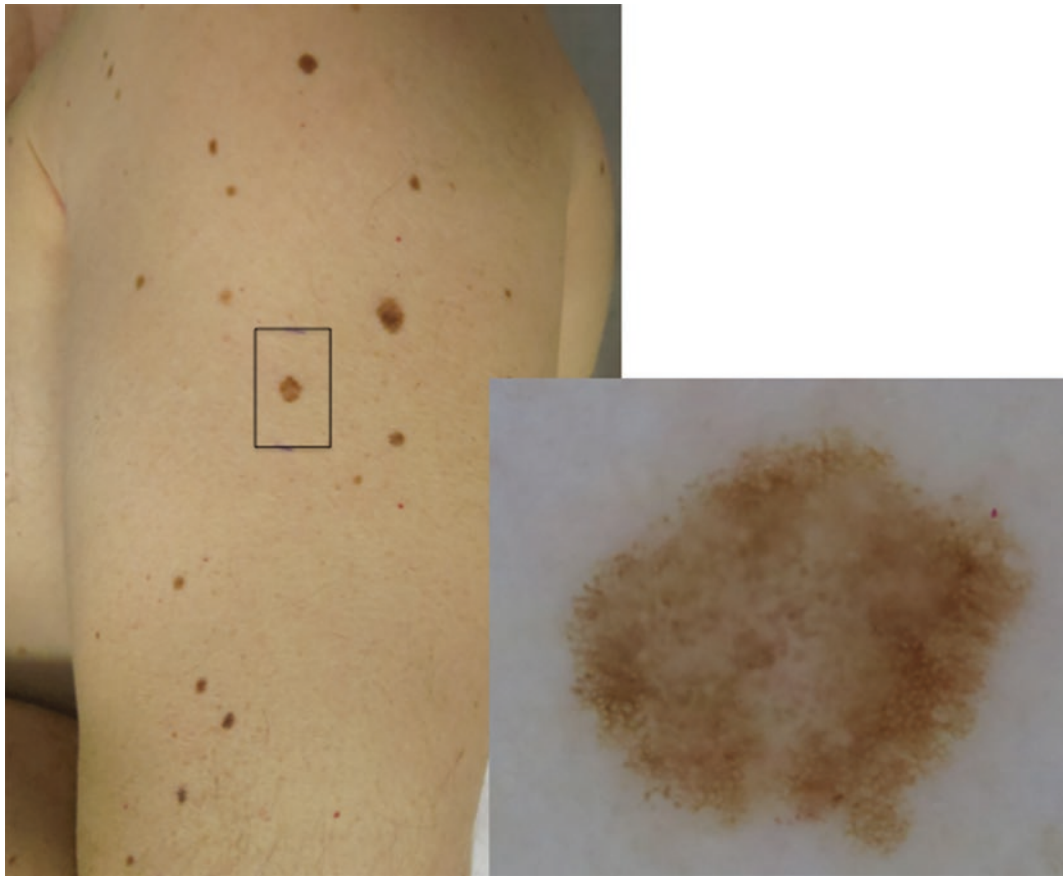

Fig. 27.9 A SSMM Breslow 0.16 mm. EIS score 6

results of this study also suggested that cutaneous reactions of completely different causes, such as allergic skin reactions of the late and immediate type, and irritant contact reactions, might be distinguished by the EIS [37].

The same group compared EIS in irritant contact dermatitis and nickel-induced allergic dermatitis. At the magnitude of skin reactions induced in this study, unlike the irritant reactions, no significant increases in transepidermal water loss occurred in the allergic contact reactions. It was speculated that allergic contact reactions did not significantly affect the epidermis because the inflammatory process is located deeper in the dermis than an irritant reaction. The authors concluded that EIS is suitable for distinguishing between contact reactions of allergic and irritant nature [27]

In studies in the oral mucosa, the differences in electrical impedance between various anatomical locations were mapped and the ability of the impedance technique to detect mild reactions in the buccal mucosa including those induced by the irritant sodium lauryl sulphate has been explored. [38–40]

In a study for the evaluation of the effects of topical clobetasol propionate in normal skin, Emtestam L and co-workers reported in 10 healthy volunteers, treated with clobetasol propionate on the forearm covered by a dressing overnight, that the dermal blanching can be evaluated with a skin impedance spectrometer [41].

EIS was observed to be dependent on the lipid content of the stratum corneum as studied by lipid extraction [42]. The same group evaluated the EIS properties of clinically normal atopic skin with that of non-atopic skin. The results showed that EIS was a useful method for detection of changes in the lipid content of the stratum corneum by discriminating healthy looking

atopic skin from healthy control skin, and to detect changes in reactivity between the two groups [43].

Hung CY and co-workers evaluated EIS for the differentiation between clavus and verruca in 57 lesions from hands and feet [44].

27.1.2.4 Clinical Studies of EIS in Skin Cancer

In a first study in 1998, Emtestam L and co-workers evaluated EIS in 11 patients with a total of 12 nodular BCC, diagnosed clinically and histologically [32]. The non-invasive measurements were performed by transepidermal water loss (TEWL) and electrical impedance. For reference, normal looking contralateral or ipsilateral skin was used.

The EI measurements of BCCs showed statistically significant changes of the impedance indices compared to non-affected skin. Compared to controls, the mean TEWL of BCC was increased, but this finding was not statistically significant.

A preclinical study was conducted by Glickman YA and co-workers on nude mice injected subcutaneously with a human melanoma strain. Impedance measurements were recorded every week to correlate electrical changes with tumour growth and histological findings. A clinical study was also performed on 178 human suspicious skin lesions including melanoma and BCCs before excision. The impedance measurements were correlated to the histopathological results. The authors concluded that electrical impedance measurements reflect morphological changes related to the growth of a cancerous skin lesion in the animal model [28].

In an investigation published at the same year, Aberg P and co-workers assessed benign pigmented cellular nevus, BCC, dermatofibroma, dysplastic nevus, and seborrheic keratoses using in vivo EIS [4]. After the impedance measurements, the lesions were histopathologically diagnosed. The authors reported significant differences between the lesions and their controls for all the lesions except for dermatofibroma. Similar preliminary results in skin tumours using EIS were described by Dua R [9] and Beetner [30].

In 2011, Aberg P, Birgersson U and co-workers from the Karolinska institute reported the results of a prospective multicentre study at 12 clinics around Europe, to investigate the accuracy of electrical impedance spectra to distinguish between malignant melanoma and benign skin lesions using an automated classification algorithm [45]. An algorithm for automatic detection of melanoma was trained using 285 histologically analysed lesions. Another data cohort of 210 blinded lesions (148 various benign lesions and 62 malignant melanomas where 38 being from Breslow thickness ≤ 1 mm) from 183 patients was thereafter used to estimate the accuracy of the technique that showed sensitivity to malignant melanoma of 95% (59/62) and specificity of 49% (72/148). The authors concluded that, although the accuracy of the device was clinically promising, the overall performance, and the sensitivity to thin malignant melanomas, must be improved and thoroughly validated.

In 2013, Mohr P and co-workers [46] conducted a larger prospective study with the aim of the study to develop a classification algorithm to distinguish between melanoma and benign lesions of the skin with a sensitivity of at least 98% and specificity approximately 20 percent higher than the diagnostic accuracy of dermatologists. In a multicentre, prospective, non-randomized clinical trial from 19 centres around Europe, a total of 1300 lesions were collected and excised for subsequent independent evaluation by a panel of three expert dermatopathologists. From the data, two classification algorithms were developed and verified. For the first classification algorithm, approximately 40% of the data were used for calibration and 60% for testing. In this study, the observed sensitivity for melanoma was 98.1% (101/103), non-melanoma skin cancer 100% (25/25) and dysplastic nevus with severe atypia 84.2% (32/38). The overall observed specificity was 23.6% (66/280). For the second classification algorithm, approximately 55% of the data were used for calibration. The observed sensitivity for melanoma was 99.4% (161/162), for non-melanoma skin cancer was 98.0% (49/50) and dysplastic nevus with severe atypia was 93.8% (60/64). The overall observed specificity was 24.5% (116/474). The authors concluded for this results that EIS had the potential to be an adjunct diagnostic tool to help clinicians differ-

entiate between benign and malignant (melanocytic and non-melanocytic) skin lesions.

Finally, in the largest prospective study reported in melanoma diagnosis, Malvehy J and co-workers [47] assessed the effectiveness and safety of EIS using the Nevisense system in the distinction of benign lesions of the skin from melanoma. This multicentre, prospective, and blinded clinical study was conducted at five American and 17 European investigational sites. All eligible skin lesions in the study were examined with the EIS-based Nevisense system, photographed, removed by excisional biopsy and subjected to histopathological evaluation. In accordance with standard clinical practice, eligible and evaluable lesions were excised and subjected to the investigational site's histopathology evaluation and managed accordingly. A further histopathological evaluation was completed by a panel of three experienced histopathologists who evaluated each lesion independently and were blinded from the investigational site's original histopathology diagnosis. In the case of agreement among the experts, the diagnosis was considered as the study's histopathological gold standard (HGS). If there was significant disagreement among the pathology reviewers on whether the lesion represented a malignancy, the respective slides were submitted to two additional experts whose diagnosis was then chosen as the HGS if they reached agreement.

A postprocedure clinical follow-up was conducted at 7 + 3 days from the initial measurement. A total of 1951 patients with 2416 lesions were enrolled into the study; 1943 lesions were eligible and evaluable for the primary efficacy end point, including 265 melanomas—112 in situ and 153 invasive melanomas with a median Breslow thickness of 0.57 mm [48 basal cell carcinomas (BCCs) and seven squamous cell carcinomas (SCCs)].

The exclusion criteria for patients were: men or women of any ethnic group aged < 18 years; patient not willing or able to read, understand and sign the study-specific informed consent form. Exclusion criteria for lesions were: metastases or recurrent lesions; lesions < 2 mm or > 20 mm in diameter; lesions located on acral skin, e.g. sole or palm; lesions located on areas of scars, crusts, psoriasis, eczema or similar skin conditions; lesions on hair-covered areas, e.g. scalp, beards, moustaches or whiskers; lesions located on genitalia; lesions located in an area that has been previously biopsied or subjected to any kind of surgical intervention or trauma; lesions located on mucosal surfaces; lesion with foreign matter, e.g. tattoo or splinter; lesion and/or reference located on acute sunburn; skin surface not measurable, e.g. lesion on a stalk; skin surface not accessible, e.g. inside ears, under nails; skin not intact (measurement area), e.g. bleeding or with clinical noticeable ulceration.

The dichotomous outcome of the Nevisense system was compared with the HGS. Of the 1943 eligible and evaluable lesions, 265 (13.2%) were cutaneous melanoma, 55 (28%) were non-melanoma skin cancer (NMSC), including basal cell carcinomas (BCCs) and squamous cell carcinomas (SCCs), of which Nevisense correctly identified 256 melanomas and all 55 NMSCs, yielding an observed sensitivity of 96.6% and 100.0%, respectively. A total of 157 naevi with severe dysplasia were included, of which Nevisense gave a positive reading for malignancy in 132 cases. Seven out of eight actinic keratoses gave a positive reading. One Merkel cell carcinoma was included, which was correctly identified as malignant. Out of the remaining 1457 lesions, 501 were diagnosed as negative, yielding an observed specificity of 34.4%. No significant difference in the presented sensitivity and specificity was encountered, when the possible dependency in outcome between the lesions of the same patient was accounted for through a generalized linear mixed model. The positive predictive value (PPV) of Nevisense was 21.1% and the negative predictive value (NPV) was 98.2%. The Nevisense score was compared with lesion severity and a clear step function is evident for the score outcome with increasing lesion severity.

The latest version of the system is called Nevisense 3.0 also resulted in improved accuracy [14]. When tested on the dataset from the Malvehy study, the sensitivity increased slightly to 97.0% and specificity increased to 37.5%. In addition, the Negative Predictive Value (NPV) increased from 98% to 99%. Validation of the accuracy of the latest version of Nevisense was

performed on the dataset from the Malvehy study as with the previous version of Nevisense. The dataset from this study was not used in the development process of the latest Nevisense version but was used only for validation once the updated version was finalized.

EIS has also been explored in **high-risk patients for melanoma** under short-term follow-up by the group of, in Sydney, L. Rocha and co-workers [48]. These authors evaluated the effect of adding an EIS measurement at baseline to suspicious melanocytic lesions undergoing routine short-term sequential digital dermoscopy imaging (SDDI) at the dermatology department. Patients presented with suspicious melanocytic lesions with no clear feature of melanoma on dermoscopy that were eligible for short-term follow-up with digital dermoscopy, were explored by EIS at the first visit following dermoscopic photography. In this study, when the EIS score was ≥ 7 the lesion was excised immediately owing to the high risk of melanoma. Lesions with a score < 7 were monitored with standard SDDI over a 3-month period. From a total of 160 lesions analysed, 128 of 154 benign lesions received an EIS score of 0–6, giving a specificity of the EIS method for the diagnosis of melanoma of 83.1% [95% confidence interval (CI) 76.3–88.7]. Five of the six melanomas found in this study had an EIS score ≥ 7, with sensitivity for melanoma diagnosis of 83.3% (95% CI 35_9–99_6). When EIS was 0–6 lesions were subsequently followed up and one additional melanoma was detected (EIS = 6) giving a sensitivity for the diagnosis of melanoma overall of 100% (95% CI 54.1–100; six of six malignant melanomas excised) and a specificity of 69.5% (95% CI 61.5–76.6; 107 of 154 benign lesions not excised). The authors concluded that the inclusion of EIS in their selection of equivocal suspicious lesions for short-term follow-up was reduced by 46.9% (n = 75/160; 95% CI 39.0–54.9) if the lesions had EIS score ≤ 3. They proposed an algorithm in this situation (Fig. 27.10).

In a recent study, Svoboda RM and co-workers analysed the impact of Nevisense in the clinical management of pigmented skin lesions [49]. In this study, 164 dermatology trainees completed an online survey presenting clinical images of 45 pigmented lesions (28 benign, 17 melanoma). For each image, respondents were asked if they would recommend biopsy on the basis of morphologic assessment alone, and then asked again once presented with the corresponding EIS score (along with positive and negative predictive values). The proportion of clinical decisions for which the addition of EIS score altered the decision to biopsy was calculated.

In addition, the sensitivity, specificity and proportion of missed melanomas and benign biopsies were determined for morphologic assessment alone and for morphologic assessment plus EIS score. In this study, EIS score led to a change in the decision to biopsy in 25% of cases and improved diagnostic accuracy, resulting in fewer biopsies of benign lesions and more biopsies of melanomas, without significantly changing the total number of biopsies. The authors stated that a limitation of this study was that additional clinical data, such as patient history, risk factors and dermoscopic images, were not available to participants. In addition, as this study only included trainees, the results might not extrapolate to more experienced clinicians. However, EIS had a meaningful impact on the decision to biopsy pigmented lesions with atypical features.

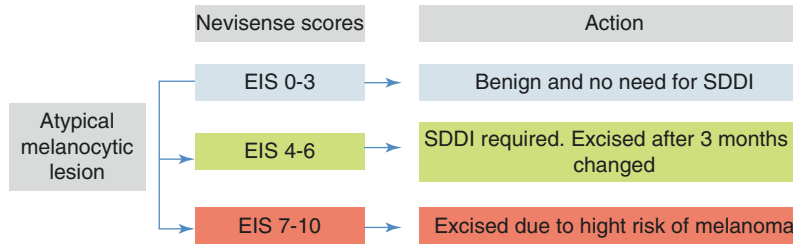

Fig. 27.10 Integration of EIS and dermoscopy imaging (SDDI) follow-up in the decision tree for the management of atypical lesions proposed by Rocha et al. [48]

27.2 Conclusions

According to the evidence from different studies in melanocytic equivocal lesions, EIS when combined with morphologic assessment and dermoscopy improves accuracy and could significantly change the overall biopsy rate. This may assist the clinician in the management of patients and facilitate an early diagnosis of melanoma [50]. More research is ongoing for the integration of Nevisense in the diagnostic armamentarium in dermatology in combination with the clinical information, stratification according to risk for melanoma and other non-invasive techniques such as dermoscopy, digital monitoring and reflectance confocal microscopy. Finally, improvements in the technology may increase the usability and clinical benefit of EIS in skin cancer detection including melanoma and non-melanoma skin cancer and in the investigation of inflammatory skin diseases.

References

1. Grimnes S, Martinsen Ø. Bioimpedance and bioelectricity basics. London (UK): Academic Press; 2000.
2. Ollmar S, Nicander I. Within and beyond the skin barrier. In: Fluhr JW, Elsner P, Berardesca E, Maibach HI, editors. Bioengineering of the skin—Water and the stratum corneum. 2nd ed. Boca Raton: CRC Press; 2005. p. 335–50.
3. Emtestam L, Nicander I, Stenström M, Ollmar S. Electrical impedance of nodular basal cell carcinoma: a pilot study. Dermatology. 1998;197:313–6.
4. Åberg P, Nicander I, Holmgren U, Geladi P, Ollmar S. Assessment of skin lesions and skin cancer using simple electrical impedance indices. Skin Res Technol. 2003;9:257–61.
5. Beetner DG, Kapoor S, Manjunath S, Zhou X, Stoecker W. Differentiation among basal cell carcinoma, benign lesions, and normal skin using electrical impedance. IEEE Trans Biomed Eng. 2003;50:1020–5.
6. Lobo B, Hermosa C, Abella A, Gordo F. Electrical impedance tomography. Ann Transl Med. 2018 Jan;6(2):26.
7. Sanchez B, Rutkove SB. Electrical impedance myography and its applications in neuromuscular disorders. Neurotherapeutics. 2017 Jan;14(1):107–18.
8. Åberg P, Nicander I, Holmgren U, Hansson J, Ollmar S. Bioimpedance as a potential diagnostic decision tool for skin neoplasms. In Proc. EMBEC'02, Vienna, vol. 3, p. 80–81, Dec. 2002.
9. Dua R, Beetner DG, Stoecker WV, Wunsch DC. Detection of basal cell carcinoma using electrical impedance and neural networks. IEEE Trans Biomed Eng. 2004;51(1):66–71.
10. Åberg P, Nicander I, Hansson J, Geladi P, Holmgren U, Ollmar S. Skin cancer identification using multi-frequency electrical impedance—a potential screening tool. IEEE Trans Biomed Eng. 2004;51(12):2097–102.
11. Åberg P, Nicander I, Ollmar S. Minimally invasive electrical impedance spectroscopy of skin exemplified by skin cancer assessments. In Proc. IEEE EMBS'03, Cancun (MX), p. 3211–3214, Sep. 2003.
12. Åberg P, Geladi P, Nicander I, Hansson J, Holmgren U, Ollmar S. Noninvasive and microinvasive electrical impedance spectra of skin cancer—a comparison between two techniques. Skin Res Technol. 2005;11:281–6.
13. Birgersson U. Electrical impedance of human skin and Tissue alterations: mathematical modeling and measurements. Thesis 2012. Department of clinical science, intervention and technology, Karolinska institutet, Stockholm, Sweden, Open Access publication.
14. https://scibase.com/the-nevisense.
15. Johnsen GK, Martinsen OG, Grimnes S. Estimation of *in vivo* water content of the stratum corneum from electrical measurements. Open Biomed Eng J. 2009;3:8–12.
16. Martinsen OG, Grimnes S, Sveen O. Dielectric properties of some keratinised tissues. Part 1: Stratum corneum and nail in situ. Med Biol Eng Comput. 1997;35:172–6.
17. Yamamoto T, Yamamoto Y. Electrical properties of the epidermal stratum corneum. Med Biol Eng. 1976;14:151–8.
18. Nicander I, Norlen L, Brockstedt U, Rozell BL, Forslind B, et al. Electrical impedance and other physical parameters as related to lipid content of human stratum corneum. Skin Res Technol. 1998;4:213–21.
19. Grimnes S. Skin impedance and electro-osmosis in the human epidermis. Med Biol Eng Comput. 1983;21:739–49.
20. Martinsen OG, Grimnes S. Facts and myths about electrical measurement of stratum corneum hydration state. Dermatology. 2001;202:87–9.
21. Sethson B, Han S, Ollmar S, Nicander I, Jonsson G, et al. Multivariate analysis of skin impedance data in long-term type 1 diabetic patients. Chemometr Intell Lab Syst. 1998;44:381–94.
22. Birgersson U, Birgersson E, Aberg P, Nicander I, Ollmar S. Non-invasive bioimpedance of intact skin: mathematical modeling and experiments. Physiol Meas. 2011;32:1–18.
23. Curdy C, Naik A, Kalia YN, Alberti I, Guy RH. Non-invasive assessment of the effect of formulation excipients on stratum corneum barrier function *in vivo*. Int J Pharm. 2004;271:251–6.

24. Nicander I, Nyren M, Emtestam L, Ollmar S. Baseline electrical impedance measurements at various skin sites——related to age and sex. Skin Res Technol. 1997;3:252–8.
25. Ollmar S, Nyren M, Nicander I, Emtestam L. Electrical impedance compared with other non-invasive bioengineering techniques and visual scoring for detection of irritation in human skin. Br J Dermatol. 1994;130:29–36.
26. Nicander I, Ollmar S, Eek A, Lundh Rozell B, Emtestam L. Correlation of impedance response patterns to histological findings in irritant skin reactions induced by various surfactants. Br J Dermatol. 1996;134:221–8.
27. Nyren M, Kuzmina N, Emtestam L. Electrical impedance as a potential tool to distinguish between allergic and irritant contact dermatitis. J Am Acad Dermatol. 2003;48:394–400.
28. Glickman YA, Filo O, David M, Yayon A, Topaz M, Zamir B, Ginzburg A, Rozenman D, Kenan G. Electrical impedance scanning: a new approach to skin cancer diagnosis. Skin Res Technol. 2003 Aug;9(3):262–8.
29. Kuzmina N, Talme T, Lapins J, Emtestam L. Non-invasive preoperative assessment of basal cell carcinoma of nodular and superficial types. Skin Res Technol. 2005;11:196–200.
30. Beetner DG, Kapoor S, Manjunath S, Zhou X, Stoecker WV. Differentiation among basal cell carcinoma, benign lesions, and normal skin using electric impedance. IEEE Trans Biomed Eng. 2003;50: 1020–5.
31. Nicander I, Hansson J, Geladi P, Holmgren U, et al. Skin cancer identification using multifrequency electrical impedance-a potential screening tool. IEEE Trans Biomed Eng. 2004;51:2097–102.
32. Emtestam L, Nicander I, Stenstrom M, Ollmar S. Electrical impedance of nodular basal cell carcinoma: a pilot study. Dermatology. 1998;197:313–6.
33. Ollmar S, Emtestam L. Electrical impedance applied to non-invasive detection of irritation in skin. Contact Dermatitis. 1992;27(1):37–42.
34. Emtestam L, Ollmar S. Electrical impedance index in human skin: measurements after occlusion, in 5 anatomical regions and in mild irritant contact dermatitis. Contact Dermatitis. 1993 Feb;28(2):104–8.
35. Ollmar S, Nyrén M, Nicander I, Emtestam L. Electrical impedance compared with other non-invasive bioengineering techniques and visual scoring for detection of irritation in human skin. Br J Dermatol. 1994 Jan;130(1):29–36.
36. Nicander I, Ollmar S, Rozell BL, Eek A, Emtestam L. Electrical impedance measured to five skin depths in mild irritant dermatitis induced by sodium lauryl sulphate. Br J Dermatol. 1995;132(5): 718–24.
37. Nyrén M, Ollmar S, Nicander I, Emtestam L. An electrical impedance technique for assessment of wheals. Allergy. 1996;51(12):923–6.
38. Nicander I, Rundquist L, Ollmar S. Electric impedance measurements at six different anatomic locations of macroscopically normal human oral mucosa. Acta Odontol Scand. 1997;55(2):88–93.
39. Nicander I, Rozell BL, Rundquist L, Ollmar S. Electrical impedance. A method to evaluate subtle changes of the human oral mucosa. Eur J Oral Sci. 1997;105(6):576–82.
40. Ollmar S. Quantification of skin and mucosal reactions by electrical impedance. Med Biol Eng Comput. 1996;34(Supplement 1, Part 2):145–6.
41. Emtestam L, Kuzmina N, Talme T. Evaluation of the effects of topical clobetasol propionate by visual score, electrical impedance and laser Doppler flowmetry. Skin Res Technol. 2007;13(1):73–8.
42. Norlen L, Nicander I, Lundh Rozell B, Ollmar S, Forslind B. Inter- and intra-individual differences in human stratum corneum lipid content related to physical parameters of skin barrier function in vivo. J Invest Dermatol. 1999;112(1):72–7.
43. Nicander I, Ollmar S. Clinically normal atopic skin vs. non-atopic skin as seen through electrical impedance. Skin Res Technol. 2004;10(3):178–83.
44. Hung CY, Sun PL, Chiang SJ, Jaw FS. In vitro differential diagnosis of clavus and verruca by a predictive model generated from electrical impedance. PLoS One. 2014;9(4):e93647.
45. Aberg P, Birgersson U, Elsner P, Mohr P, Ollmar S. Electrical impedance spectroscopy and the diagnostic accuracy for malignant melanoma. Exp Dermatol. 2011;20(8):648–52.
46. Mohr P, Birgersson U, Berking C, Henderson C, Trefzer U, Kemeny L, Sunderkötter C, Dirschka T, Motley R, Frohm-Nilsson M, Reinhold U, Loquai C, Braun R, Nyberg F, Paoli J. Electrical impedance spectroscopy as a potential adjunct diagnostic tool for cutaneous melanoma. Skin Res Technol. 2013;19(2):75–83.
47. Malvehy J, Hauschild A, Curiel-Lewandrowski C, et al. Clinical performance of the Nevisense system in cutaneous melanoma detection: an international, multicentre, prospective and blinded clinical trial on efficacy and safety. Br J Dermatol. 2014;171(5):1099–107.
48. Rocha L, Menzies SW, Lo S, Avramidis M, Khoury R, Jackett L, Guitera P. Analysis of an electrical impedance spectroscopy system in short-term digital dermoscopy imaging of melanocytic lesions. Br J Dermatol. 2017;177(5):1432–8.
49. Svoboda RM, Prado G, Mirsky RS, Rigel DS. Assedssment of clinician accuracy for diagnosing melanoma on basis of electrical impedance spectroscopy score plus morphology versus lesion morphology alone. J Am Acad Dermatol. 2018; https://doi.org/10.1016/j.jaad.2018.08.048.
50. Braun RP, Mangana J, Goldinger S, French L, Dummer R, Marghoob AA. Electrical impedance spectroscopy in skin cancer diagnosis. Dermatol Clin. 2017;35(4):489–93.

Part II

Lasers and Light Sources Technologies in Dermatology

Marco Dal Canton

28 Laser Light and Light–tissue Interaction

Orazio Svelto

28.1 Introduction

As perhaps it is well known, the word LASER is an acronym from *Light Amplification by Stimulated Emission of Radiation*. Thus lasers are essentially based on the phenomenon of stimulated emission, predicted by A. Einstein more than 100 years ago [1], wherein the emission of a given element (atom or molecule) of the active medium is stimulated by light emitted by some other element of the same medium. The light from the second element is then emitted along the same direction as that of the first element. Overall light is thus emitted in only one preferential direction, i.e., orthogonal to the two mirrors which comprise the active element and recycle the laser light. Furthermore, since light is made up of (electromagnetic) waves, the emissions of all elements add up in phase among them. In contrast to this situation, light arising from lamps or incandescent materials (including sun and stars) is based on the phenomenon of spontaneous emission. In this case, the emission of a given element occurs independently from that of all other elements and thus may occur in every direction and with a random phase.

We will not attempt in this work discussing the operating principles of a laser nor the principal types of lasers being used; we will neither present, at any length, a description of the properties of the output beam. For all these topics, we refer to the available literature [2, 3]. We limit ourselves stating that laser light is coherent, i.e., conceptually different from the incoherent light emitted by a lamp. In fact, laser light is monochromatic, i.e., corresponding to a given color or better to a well-defined wavelength, and directional. This last property means the beam tends to propagate without appreciable spreading and can thus be focused to a small spot, e.g., into the core of an optical fiber. The coherence properties of a laser beam, together with the possibility of generating high powers, high intensities, high fluences as well as the possibility of a large variability of the emitted wavelength and very large variability of the pulse duration, have allowed laser use in several fields of science and technology, notably in biomedicine In this last case, laser use has proved to be particularly advantageous when, using the peculiar properties of a laser beam mentioned above, one succeeds interacting with the tissue to be destroyed, or modified, in a *selective way*, i.e., saving to a large degree the functionality of the organs or of the tissue around the target one. Historically, ophthalmology has been the first field where the great potential of laser beams to spare very delicate organs such as eye has been achieved. More recently, laser use has been introduced in a somewhat massive way in dermatology, notably in aesthetic dermatology.

O. Svelto (✉)
Physics Department, Politecnico di Milano, Milan, Italy
e-mail: orazio.svelto@polimi.it

M. Fimiani et al. (eds.), *Technology in Practical Dermatology*,
https://doi.org/10.1007/978-3-030-45351-0_28

Here again, in fact, it is important to act in a selective way so as to spare or to even improve the physical appearance of our skin.

28.2 Laser Operating Regimes

The main laser operating regimes, of interest to our purposes, can be summarized as follows.

Continuous wave, or cw, operation. In this case, the active material is continuously excited by the so-called pumping process (which may be optical, e.g., by a suitable lamp or by another laser, or electrical, i.e., by a suitable electrical discharge into the active medium, which may be a gas or a semiconductor) and, if given threshold conditions are satisfied, the laser starts oscillating upon emitting radiation with constant power. Depending upon laser type and given application, output power may range from mW to a few tens of W, for medical applications, while it can reach values of a few tens of kW for industrial applications (and some MW for military applications). In dermatology, cw lasers are mostly used for surgery, with the CO_2 laser, oscillating at the wavelength of 10.6 μm, being the most used one.

Free-running. In this regime, the excitation is pulsed and the laser is free, by any constraint, to follow the time behavior of the pumping process. Thus, the duration of the output pulse is about the same as that of the pumping process and it may range from a few hundredth microseconds (μs) to about 100 millisecond (ms) for solid-state lasers (ruby, neodymium, alexandrite, holmium, erbium) and from about 0.5 to 10–20 ms for organic-dye lasers (e.g., rhodamine 6G, oscillating in the yellow and often referred to as a Pulsed Dye Laser, PDL). In a pulsed CO_2 laser, e.g., used for ablative skin rejuvenation, pulse duration usually ranges from microseconds (μs), for the so-called ultrapulse mode, to ms for the so-called superpulse mode of operation [4]. Pulsed duration may go down to about 100 nanosecond (ns) for excimer lasers (mostly used, in biomedicine, for correction of corneal visual defects). Since emission time in this regime is relatively longer than those considered later on, this regime in dermatology is also, arguably, named as long-pulse regime or long-pulse laser. Pulsed excitation in the free-running regime can then be periodically repeated with time and this case is usually referred to as repetitive free-running. In a single-pulse regime or when pulses are spaced by a sufficiently long time, the most important parameter for tissue–radiation interaction is the fluence of the laser beam, i.e., the energy of the laser pulse per unit target area (usually measured in J/cm^2). In the repetitive free-running regime and when time separation between two consecutive pulses is appreciably smaller than the so-called thermal relaxation time of the interested tissue (to be considered later on), the effect of a repetitive free-running laser tends to become equal to that of a corresponding cw laser (i.e., with the same power and wavelength). For this reason, one usually refers to this case as that of a pseudo-continuous regime.

Q-switching. In this case, laser action is first impeded, in a suitable way and for some appropriate time. Under this condition, excitation arising from the pumping process accumulates excitation energy (more precisely population inversion) in the active medium until it reaches very high values. At this point, laser action is suddenly allowed and, due to the high laser gain arising from the large amount of the excitation energy being stored, the stored energy is released in an intense and short pulse. Pulse duration will depend upon the amount of energy being stored and on the length of laser cavity and usually ranges from a few to a few tens of nanoseconds (typically 5–50 ns). The word Q-switching arises from the fact that the so-called cavity Q-factor (related to cavity losses) is suddenly switched from a low value (corresponding to high cavity losses, which impede laser action) to a high value (corresponding to very low cavity losses, where laser action takes place). In dermatology, this regime is also named, very arguably, as quality-switching. Q-switched laser pulses can then be repeated in time and, in such a case, one talks about repetitive Q-switching. For dermatological applications, repetition rate is always quite low (up to about 10 Hz) so that the overall effect on the tissue is simply due to the cumulative effect of each pulse.

Mode-locking. In this case, laser is constrained to emit a train of pulses, each of short duration (from a few hundredth of picosecond, the thousandth of a nanosecond, to a few tens of femtosecond, the thousandth of a picosecond) and spaced by a time which depends upon cavity length and which is typically equal to a few nanoseconds. The entire mode-locking train can last theoretically for an infinite time for a cw laser (cw mode-locking) or be equal to the pulse duration for either free-running or Q-switching operation. This last case is often referred to as simultaneous Q-switching and mode-locking operation. It appears to be extensively used in dermatology notably for tattoo removal, and this kind of laser is usually referred to, in short, as a picosecond laser.

It is worthwhile mentioning at this point that, if a so-called second-harmonic crystal is inserted within a laser cavity, this crystal converts the original laser light to light at a wavelength which is half the original one. Thus, if the active medium is Nd:YAG, the emitted wavelength will not be that characteristic of this medium, namely 1064 nm, but half of this value, i.e., 532 nm. Since the most used second-harmonic crystal is Potassium Titanil Phosphate ($KTiOPO_4$ or, in short, KTP) this kind of laser, in biomedicine, is often referred to as KTP laser. Of course, since Nd:YAG laser can be made to operate in the three operating regimes discussed above (i.e., free-running, Q-switching, and mode-locking)[1], also the corresponding KTP laser can operate in the same regimes (with pulse duration slightly shorter than the corresponding values of the Nd:YAG laser).

28.3 Fundamentals of Laser–tissue Interaction

We will now proceed discussing a few fundamental ideas about light–tissue interaction. Before proceeding, it is however important to point out that, given the uncertain and somewhat variable physical parameters involved and the complexity of the biological reactions of the tissue, limitation will be made to a very coarse description of the phenomena occurring. Therefore, our purpose is just to give a general idea of what is happening or, perhaps, of what is to be expected in a given situation rather than to reach precise and quantitative conclusions.

Under the previous limitation, we begin observing that when light is incident on human skin a fraction of this light is reflected (about 5% for normal incidence). The remaining fraction (about 95%) penetrates into the tissue and is absorbed. For linear absorption processes, absorption is usually described by the absorption coefficient, μ_a. It is often measured in cm^{-1} and its inverse gives the tissue depth, in centimeter, at which laser intensity is reduced to about 36.8% of that entering the tissue.

Skin absorption in the wavelength range from the UV spectral region (200 nm) to about 10 μm in the middle infrared is shown in Fig. 28.1. One can see from this figure that, for an oxygenated skin, the main molecules responsible for absorption are water, oxyhemoglobin, and melanin. In the same figure, the wavelengths of the most common lasers used in dermatology are also shown. It should be noted that on the vertical axis (in logarithmic units) the so-called molar attenuation (or extinction) coefficient is shown. It is the absorption coefficient corresponding to the standard density of 1 mole/liter of the given molecule. To convert these numbers into the actual values of tissue absorption coefficient, one should know the values of the (average) density of the molecule under consideration into such heterogeneous medium as the skin. These values are, in fact, subject to great variations from one skin type to another (particularly for the amount of melanin) and, for the same person, even from time to time (particularly for the average blood content). This, together with the different measurement techniques, may possibly explain the large variation of tissue absorption coefficients reported by various researchers [5]. Furthermore, proper account should be taken of tissue scattering, which arises from local refractive-index

[1] Nd:YAG laser can also operate cw and, accordingly, one can also have a cw-operating KTP laser. This regime, however, is not used in dermatology (although it is used in other specialties of medicine such as, e.g., urology).

changes of filamentous proteins (such as keratins and collagen) and other microscopic structures (such as melanosomes). In the following, data considered will refer to a "Caucasian" skin type.

Given all previous considerations, the molar extinction coefficient, as originally adopted by Anderson and Parrish in their classical work on the optics of human skin [6], is thus the only quantity that can be shown without incurring into a somewhat arbitrary representation. As we shall see later on, however, the representation of Fig. 28.1, i.e., in terms of molar extinction coefficient, is nonetheless useful to understand the role of the various molecules involved (i.e., oxyhemoglobin, deoxyhemoglobin, melanin, and water) and to perform some quantitative comparison when the same molecule is playing the only dominant role.

We first consider tissue absorption at the CO_2 laser wavelength (10.6 μm), where absorption is essentially due to water (see Fig. 28.1). At this wavelength, assuming an equivalent volume fraction $f_{\upsilon,\text{water}} \cong 70\%$ for water contained into the skin and taking into account published values of water at this wavelength (see Fig. 11 of ref. [7]), we can get a penetration depth of about 20 μm. One can also see from Fig. 28.1 that the strongest peak for water absorption occurs at 2.94 μm, which just happens to coincide with the emission wavelength of the Er:YAG laser. Again from the same figure of ref. [7] and again for a 70% water content in the skin, we now get a penetration depth of only 1 μm. Upon proceeding in a completely similar way, we get a depth of about 2 mm at the Er:glass laser wavelength (1.54 μm), where absorption is still mainly due to water (see also Fig. 28.1).

From the red to the near infrared region of the electromagnetic spectrum (more precisely from 650 nm to 1400 nm) absorption is mostly due to melanin, contained in melanosomes (see also Fig. 15 of ref. [7]). From this quoted figure, using realistic values of equivalent volume fraction of cutaneous melanosomes within skin tissue ($f_{\upsilon,\text{melanosome}} = 3 \div 5\%$, [7]), one can get a rough estimate

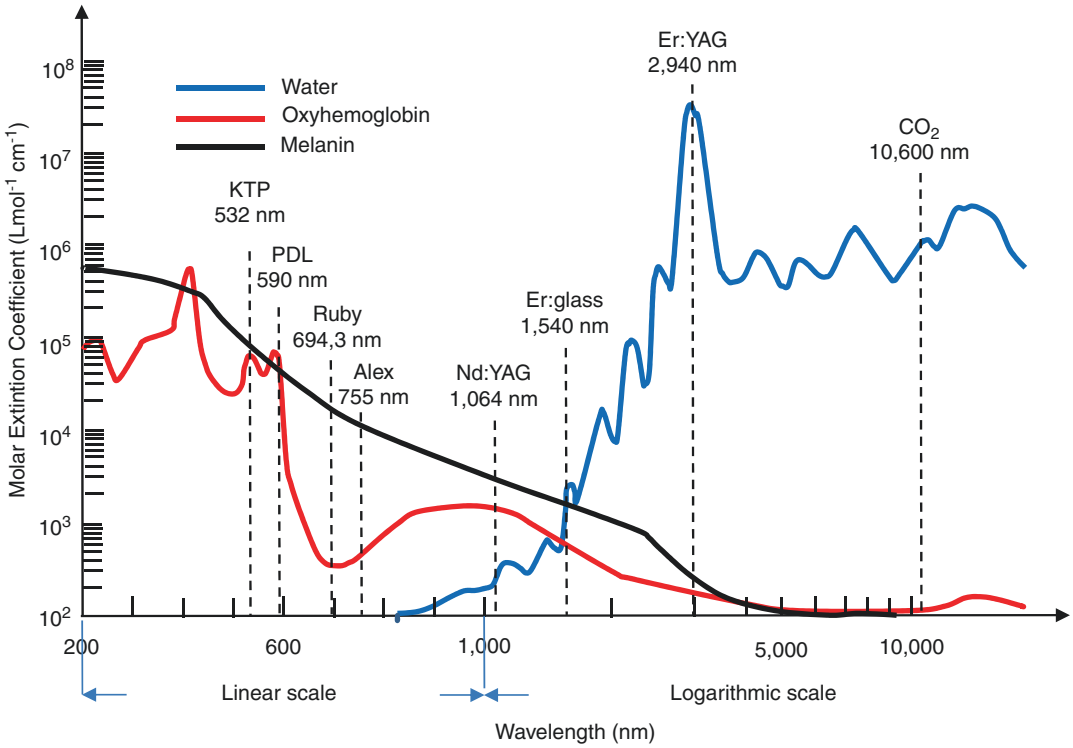

Fig. 28.1 Absorption of skin tissue (reproduced with permission from reference [4])

of the penetration depths at the various laser wavelengths. One then obtains penetration depths of 3 ÷ 4 mm, 1.2 ÷ 2 mm and 0.9 ÷ 1.5 mm, at the wavelengths of Nd:YAG (1064 nm), Alexandrite (760 nm, central wavelength), and Ruby (694.3 nm) lasers, respectively.

At the wavelength of 577 nm, possible emission wavelength of a pulsed dye laser and corresponding to one of the two absorption peaks of oxyhemoglobin (Fig. 28.1), absorption seems to be due to both melanin and oxyhemoglobin (see also Fig. 15 of ref. [7]). Again from this figure, using realistic estimates of both the average volume fractions for dermal blood ($f_{v,\,blood} \cong 0.2\%$) [4, 7] and for cutaneous melanosomes within skin tissue ($f_{v,\,melanosome} = 3 \div 5\%$, [7]), we get a rough estimate of a penetration depth of 0.5 ÷ 1 mm. Under the same values of the equivalent volume fraction, we can estimate a penetration depth of 0.3 ÷ 0.6 mm at the 532 nm wavelength of the KTP laser (about corresponding to the second peak of oxyhemoglobin, see again Fig. 28.1). Penetration depth is now somewhat smaller than that at 577 nm due to the increased absorption of melanin with decreasing wavelength (see Fig. 28.1).

As a conclusion to this discussion, we report in Table 28.1 the penetration depths of all cases considered above. It should be stressed again, however, that the quoted values in the 500 ÷ 1000 nm range are just rough estimates. Actual values may be substantially different on account of the different equivalent volume fractions of both dermal blood and melanin from person to person and, for the same person, from time to time.

So far, only linear absorption has been considered. Given the high peak intensities often involved in laser–tissue interaction, nonlinear absorption should also be taken into account. Amongst the various nonlinear phenomena that may occur (e.g., two-photon absorption), the so-called Laser Induced Optical Breakdown (LIOB) appears to be particularly relevant in dermatology. This phenomenon occurs when the pulse intensity is high enough to strip electrons from the exposed material, generating a high-density plasma (i.e., a vaporized ensemble of electrons and parent ions). Once formed, the plasma absorbs the remaining part of the laser pulse, which rapidly heats and expands the plasma to form a cavitation bubble. The phenomenon is currently used in ophthalmology, for e.g., the so-called LASIK procedure of cornea reshaping, to produce a corneal flap by an intense femtosecond laser. It has also been recently proposed for performing a novel type of fractional laser for skin resurfacing [8]. Except for these cases, LIOB is to be avoided for all other laser treatments considered in this book for at least two main reasons: (1) For a non-focused laser beam, LIOB would stop the remaining part of the laser beam from entering the skin, thus preventing its therapeutical effect. (2) The strong UV emission of the plasma may be potentially dangerous for the skin. It should be noted that with the most intense laser sources so far available in dermatology (e.g., 5 J/cm^2 with 450 ps pulse duration, as for a picosecond Nd:YAG laser) a laser intensity on the skin of about 10 GW/cm^2 can readily be

Table 28.1 Skin penetration depths of most common lasers used in dermatology

Laser type	Wavelength	Penetration depth	Comments
CO_2	10.6 μm	20 μm	Strong water absorption
Er:YAG	2.94 μm	1 μm	Strongest water absorption
Er:glass	1.54 μm	2 mm	Moderate water absorption
Nd:YAG	1,064 μm	3 ÷ 4 mm	Mostly due to melanin with a small contribution by oxyhemoglobin.
Alexandrite	760 nm	1.2 ÷ 2 mm	Essentially due to melanin.
Ruby	694.3 nm	0.9 ÷ 1.5 mm	Essentially due to melanin
Pulsed dye laser	577 nm	0.5 ÷ 1 mm	Approximately equal contributions by oxyhemoglobin and melanin
KTP	532 nm	0.3 ÷ 0.6 mm	Approximately equal contributions by oxyhemoglobin and melanin. Compared to 577 nm wavelength, absorption is somewhat stronger, at this wavelength, due to increased melanin absorption.

calculated. This value falls in the lower range of the considered intensities for this phenomenon to occur on the skin [9, 10].

28.4 Laser-Selective Photothermolysis

Let us now go back to the linear absorption phenomena considered in previous section and discuss their effect on the tissue. Following absorption, the absorbed energy in a given target of the tissue is mostly transformed into internal energy of the molecules making the tissue, i.e., it is transformed into heath. This energy is then transformed into kinetic energy of the molecules involved, which means that the temperature of the target containing the molecules is increased. However, while temperature rises, a fraction of the heath tends to diffuse away from the volume under consideration. This phenomenon follows well-defined laws of heath diffusion and, accordingly, one can roughly define a thermal relaxation time, τ_r, as, e.g., the time it takes for half of the absorbed energy to diffuse away from the target where it was produced.

Now, to maximize the effect of laser–tissue interaction in the given volume while sparing the surrounding tissue, we may require that the time duration of the laser pulse, τ_p, be substantially smaller than the thermal relaxation time considered above. In this case, in fact, energy absorbed is mostly used to increase the temperature of the target tissue, i.e., to produce a therapeutical effect. This constitutes the basis of the concept of selective photothermolysis, proposed many years ago by Anderson and Parrish in a seminal paper [11]. More precisely, selective photothermolysis requires the following three basic conditions: (1) The laser wavelength is chosen to be preferentially absorbed by the chromophore of the target tissue. (2) Pulse duration must be shorter than the thermal relaxation time of the target. (3) Laser fluence should be high enough to cause thermal injury to the desired skin structure. Concerning these three conditions, we may observe that too short pulses below the thermal relaxation time may lead to vaporization or shock wave formation in the given target leading to damage of the surrounding structure. Likewise, too high laser fluence, beyond that causing thermal injury to the target, may cause again a substantial damage of the surrounding skin.

To be more specific, we recall that, according to heath diffusion theory, thermal relaxation time is approximately given by

$$\tau_r \cong \left(d^2 / 27k\right) \tag{28.1}$$

for a spherical target of diameter d, where k is the thermal diffusivity of the target. Relaxation time is, however, given by

$$\tau_r \cong \left(d^2 / 16k\right) \tag{28.2}$$

for a long cylindrical target again of diameter d. For a comparison we may note that, for the same values of target diameter and thermal diffusivity, relaxation time of a sphere is about (27/16), i.e., 1.7 times shorter than that of a cylinder. This is because thermal diffusion may occur along the three radial directions of the sphere while, for a cylinder, diffusion may occur only along its two radial directions.

As a first example, we will consider the case of blood vessels with either 100 μm or 1 mm diameter and assume that thermal diffusivity for both the vessel and surrounding tissue is equal to that of water ($k \cong 1.3 \times 10^{-3}$ cm^2 s^{-1}) [11]. From Eq. (28.2), as appropriate for a cylindrically shaped target, we then get $\tau_r \cong 5$ ms and $\tau_r \cong 500$ ms, for the two cases considered. Required laser pulse duration can thus range from about one millisecond to about hundred milliseconds, in the two cases respectively. As a second example we consider the case of tattoo removal, where tattoo particles may range from a few tens of nm to a few μm (for the aggregate particles). Assuming all particles being of spherical shape, we should use now Eq. (28.1) with k representing the thermal diffusivity of the particle. For particle made of graphite, Ho and coworkers, in their extensive computer simulation study [12], calculate a value of $\tau_r \cong 10$ ps for a particle diameter of 50 nm. It then follows from Eq. (28.1) that, for a particle diameter of 1 μm, i.e., 20 times larger, predicted thermal relaxation time would be 400 times larger, i.e., 4 ns.

Thus, for the range of tattoo particles considered here, laser pulse duration ranging from a few picoseconds to about one nanosecond should be required.

28.4.1 Treatment of Vascular Lesions

Vascular lesions, e.g., facial telangiectasia or port-wine stains (PWSs), were the first cases where the basic concept of laser-selective photothermolysis was applied. To this purpose, the yellow light of a Pulsed Dye Laser (PDL) was used since its range of possible emission wavelengths corresponds to the yellow absorption peak of oxyhemoglobin (see Fig. 28.1) [13]. The wavelength used in early PDLs, 577 nm, was indeed selected to match this yellow peak. It was later established that the 585 nm wavelength resulted in more effective treatment of PWSs [14]. For deeper lying and larger vessels (up to perhaps 1 mm in depth and 1 mm in width) such as those of legs, PDL emitting at the still longer wavelength of 595 nm was, later on, introduced [15, 16]. The rationale for this choice comes from the fact that, to maximize interaction with a given vessel, one must take into account not only the vessel absorption but also the transmission of the skin tissue overlying the vessel itself. As vessels lying deeper in the tissue are considered, the optimum wavelength may then be moved to somewhat longer values than the peak value because, as discussed in Sect. 28.3 of this work, the absorption of both melanin and of oxyhemoglobin present in the overlying structure is reduced upon moving to longer wavelengths (see also Fig. 28.1). In other words, in order to produce a therapeutical effect, laser light not only needs to be reasonably absorbed by the target but also needs to reach the target itself. For the same reason, leg veins of still larger diameter (1.5–3 mm) and lying deeper in the tissue seem to be best treated by a free-running Nd:YAG laser [17]. In fact, as discussed in Sect. 28.3, penetration depth at the corresponding wavelength (1064 nm) is limited by melanin absorption (and scattering processes) and may be as high as 3–4 mm. On the other hand, the 1064 nm wavelength besides being well transmitted by the skin is also well absorbed by oxygenated blood, since oxyhemoglobin shows a secondary and broad absorption band centered around 950 nm (see Fig. 28.1).[2]

Pulse duration for the early PDLs covered the range of 0.5 ÷ 1.5 ms. According to considerations developed in Sect. 28.4, this range can be considered to be somewhat optimal for vessel diameters from 50 to 100 μm. As explained earlier, however, for vein diameters of 1 mm or larger, pulse duration must then be raised to a few tens to several tens of millisecond. This appears to be the case, either for 595 nm PDL or for free-running Nd:YAG, for therapy of leg veins (where pulse durations ranging from 20 to 100 ms have been reported) [17].

Once laser energy is selectively absorbed by the given vein, laser fluence needs to be chosen so as to raise the blood temperature above 70°C (temperature at which blood coagulation occurs). Vessel damage is then believed to occur either by thrombosis secondary to this vessel coagulation or by vessel contraction secondary to collagen shrinkage.

28.4.2 Tattoo Removal

Tattoo removal represents the second case where the concepts of selective photothermolysis have successfully been applied. Tattoo inks in general usage contain, in fact, nanoparticles. Their average sizes range from less than 100 nm for black pigments (generally made of carbon) to about 120 nm for blue, 180 for green, 170 nm for yellow, and 145 for red pigments [18]. When injected intra-dermally, perhaps to a 1 to 2 mm depth, pigments form aggregates within resident dermal cells with diameter ranging from 0.5 to 40 μm [19]. For these larger granules, according to the estimates of the thermal relaxation time discussed

[2]Absorption coefficient of a fully oxygenated blood vessel, at 1064 nm wavelength, can be estimated from Fig. 10 of ref [8] to be $\mu_a \cong 5\ cm^{-1}$. This means that, for a 2 mm diameter vein, approximately 63% of the radiation incident on the vein will be absorbed by the blood.

above, nanosecond pulses are just needed to fulfill the second requirement of selective photothermolysis (namely that pulse duration be equal to or somewhat smaller than thermal relaxation time). Thus Q-switched lasers with pulse duration ranging from a few to a few tens of nanoseconds are typically used. It should be observed however that these granules become smaller in tattoos that have already been treated by a Q-switched laser [19]. For these smaller granules as well as for the original nanoparticles which are still present within the tissue, lasers with shorter pulse duration down to the picosecond range are expected to be even more efficient [12].

To fulfill the first requirement of selective photothermolysis discussed above, we must also require that the selected laser wavelength be preferentially absorbed by the given pigment. Now, it is a well-known law of colorimetry that a pigment of a given color preferentially absorbs the so-called complementary color. Thus red light (such as that of a ruby laser, at 694.3 nm) or the deep-red light of alexandrite laser (at 755 nm) is preferentially absorbed by green pigments. Conversely, green light (such as that of the so-called KTP laser at 532 nm) is preferentially absorbed by red pigments. Black pigments, on the other hand, mean that absorption occurs somewhat uniformly throughout all visible range. It has been proved, however, that black pigments used for tattoos respond even better in the near infrared, i.e., at the 1064 nm wavelength of a Nd:YAG laser, presumably due to the larger penetration depth of the tissue at this wavelength. Penetration depths at all these laser wavelengths have, in fact, been discussed in Sect. 28.3 of this work (see Table 28.1). One can then see that these depths are always substantially longer (for Nd:YAG, Alexandrite, and Ruby lasers) or comparable (for KTP laser) than presumable depths where tattoo particles are residing within the skin. It should be noted, at this point, that a yellow pigment is expected to preferentially absorb blue light. Thus blue emitting (Q-switched) lasers would be required to treat this pigment. Blue laser light (e.g., at 400 nm), however, would be strongly absorbed by the tissue (due to a strong absorption peak of oxyhemoglobin at this wavelength, see Fig. 28.1). Thus, such a laser beam would hardly be able to reach the required depth and thus likely result into substantial damage of the overlying tissue.

If laser light penetrates well into the tissue, if pulse duration is of the order of the thermal relaxation time of the tattoo particle and if the laser fluence is sufficiently high (generally in the range of a few J/cm^2), a fast and high rise of the particle temperature, during laser pulse, occurs. This temperature increase then results in a stress wave (i.e., a pressure or acoustic wave) which propagates from the outside surface of the particle toward its center. When the tensile or compressive component of this wave exceeds the corresponding strength limits of the particle, fracture occurs and the original particle breaks downs into smaller fragments [12]. Most of these fragments are, then, removed by scavenger cells to the local lymph nodes while some of them are picked up again by resident macrophage cells [20]. Thus the main mechanism for tattoo removal is considered to arise from a photoacoustic (or photomechanical) effect [12].

According to the previous considerations, nanosecond-pulse Q-switched lasers of Nd:YAG, Alexandrite, Ruby, and the nanosecond KTP laser are now commonly used for tattoo removal. Emission wavelength, range of pulse duration and repetition rate and typical range of laser fluence on the tissue are shown in Table 28.2. After a given treatment, smaller fragments as well as untreated small particles remain into the tissue. Therefore, several (up to 6–10) treatments are required to break down these particles of smaller size. Time between two successive treatments must allow skin to a complete recovery (typically 4–6 weeks).

Despite this considerable success of nanosecond Q-switched laser to effectively treat tattoo during last 20 years or more, total tattoo clearance remains a difficult task to be achieved. The problem arises from the difficulty of the patient adherence with the prolonged treatment timetable and the difficulty in fragmenting the smallest ink granules, with thermal relaxation time much smaller than 10 ns [21]. Furthermore, a few colors, such as blue and green and, particularly,

yellow, appear to be only partially addressable by Q-switched lasers. The more so, in a comparative and seminal paper published more than 20 years ago, black tattoos were shown to be more effectively cleared by a Q-switched and mode-locked Nd:YAG laser, with 35 ps pulses, than by a Nd:YAG Q-switched laser giving 10 ns pulses. The difficulties encountered in tattoo removal with Q-switched lasers and this earlier study have spurred the development of a new class of commercial lasers, simultaneously operating in the Q-switching and mode-locking operation, to generate pulses in the picoseond domain. These so-called picosecond lasers have been developed with the specific goal of abbreviating the overall duration of treatment and clearing tattoos which had previously resisted to treatment with a nanosecond laser. Table 28.3 summarizes a few parameters of picosecond lasers so far developed.

A comparison between performances of picosecond to nanosecond lasers for tattoo removal seems at this point to be appropriate [22]. To this purpose we note that the first comparative study between a picosecond and a nanosecond Nd:YAG laser has to be found in the already mentioned paper by Ross et al. [23]. Although the paper clearly indicated the superiority of the picosecond laser for the cases considered (black tattoos), duration of the corresponding pulses was 35 ps, i.e., one order of magnitude shorter than those presently available by picosecond lasers. A second and more recent paper compares a nanosecond-domain laser to two picosecond-domain lasers in a randomized study on 49 patients [24]. The study uses a split tattoo design, where one half of a tattoo was treated with one of the two picosecond-domain lasers and the other with a Q-switched, nanosecond-domain laser. Although picosecond lasers were shown to be more effective than the nanosecond counterpart, the nanosecond laser appears, however, to significantly underpowered compared to most nanosecond devices currently on the market. Lastly, Pinto et al., in a randomized and controlled single-blind clinical trial and in a split design approach, compared a modern picosecond to a modern nanosecond Nd:YAG for black tattoo removal [25]. They conclude that there was no difference between the two treatments. Unfortunately, however, therapy was limited to two treatments only, at a 6-week interval. Thus the logical possi-

Table 28.2 Nanosecond lasers most commonly used for tattoo removal and corresponding colors of the pigments which can be addressed

Laser type	Emission wavelength (nm)	Pulse duration (ns)	Pulse repetition rate (Hz)	Laser fluence (J/cm^2)	Color of pigment
Nd:YAG	1,064	5–20	1–10	5–6	Black
Alexandrite	755	50–100	1–15	5–6	Black
					Blue
					Green
Ruby	694.3	30–40	0.5	4–6	Green
					Black
					Blue
KTP	532	5–20	1–10	2–4	Red
					Purple
					Orange

Table 28.3 Picosecond lasers most commonly used for tattoo removal. The colors of the pigments to be addressed are obviously the same as for the corresponding nanosecond case

Laser type	Emission wavelength (nm)	Pulse duration (ps)	Pulse repetition rate (Hz)	Laser fluence (J/cm^2)
Nd:YAG	1,064	450	1–10	5–6
Ti:sapphire	785	300	1–10	3
Alexandrite	755	750–900	5	2.5
KTP	532	370	1–10	2–4

bility of superior performance of the picosecond lasers to treat smaller and smaller particles arising from repeated treatments, thus reducing the number of treatments, was not really tested. Concerning difficult to clear colored pigments, it should be noted that, although blue and green pigments have recently been very successfully removed by a picosecond alexandrite laser [26], the same kind of laser, operating in the nanosecond regime, is known to be optimal for removing blue and green pigments [27, 28]. The most striking case, however, appears to be the effective clearance, in a few treatments, of yellow-ink tattoos by a picosecond KTP laser [29, 30]. Notoriously, the yellow ink is a very difficult pigment to be cleared out by KTP nanosecond lasers, presumably because green light is little absorbed by yellow pigments. It then follows that, in this case, the resulting maximum tensile stress accumulated within the yellow pigments may be insufficient to produce particle fracture. Upon going from nanosecond to picosecond lasers, pulse duration is reduced by more than one order of magnitude (compare Table 28.2 with Table 28.3). The expected maximum tensile strength within the particle is then expected to increase by appreciably more than one order of magnitude (see Fig. 8 of Ref. [12]) thus, perhaps, reaching the fracture limit of the pigment (see also ref. [29]). It should be noted, however, that yellow tattoos seldom occur in treated patients [31].

As a conclusion of this discussion we may say that, although picosecond-domain lasers appear to be a logical solution for reducing the number of treatments as well as for clearing tattoos which had previously resisted to nanosecond-laser treatments, further controlled and comparative studies, made on a statistically significant number of patients, are needed to assess these quite interesting possibilities.

28.5 Conclusions

We believe that a thorough knowledge of the content of this chapter may be of help to the dermatologist to realize the type of laser that is useful for a given application as well as to more deeply understand the clinical results being obtained.

References

1. Einstein A. On the quantum theory of radiation. Z. Phys. 1917;18:121–3.
2. Svelto O. Principles of Lasers. Fifth ed. New York: Springer; 2010.
3. Siegman AE. Lasers. Mill Valley CA: University Science Books; 1986.
4. Omi T, Numano K. The role of the CO_2 laser and fractional CO_2 laser in dermatology. Laser Therapy: J Laser Surg Phototherapy Photobioactivation. 2014;23(1): 49–60. 10.5978/islsm.14-RE-01; Online ISSN: 1884-7269, Print ISSN: 0898-5901.
5. For a review see: Lister T, Wright PA, Chappell PH. Optical properties of human skin, in light-tissue interaction using computational methods. Lasers Med. Sci. 2017;32:1909–1918.
6. Anderson RR, Parrish JA. The optics of human skin. J Invest Dermatol. 1981;77:13–9.
7. Jacques S. Optical properties of biological tissues: a Review. Phys Med Biol. 2013;58:37–61.
8. Habbema L, Verhagen R, Van Hal R, Liu Y, Varghese B. Minimally invasive non-thermal laser technology using laser-induced optical breakdown for skin rejuvation. J Biophotonics. 2012;5:194–9.
9. Kennedy PK. A first model for computation of laser-induced breakdown thresholds in ocular and acqueous media: Part I – Theory. IEEE J Quantum Electron. 1995;31:2241–9.
10. Kennedy PK, Boppart SA, Hammer DX, Rockwell BA, Noojin GD, Roach WP. A first model for computation of laser-induced breakdown thresholds in ocular and acqueous media: Part II – Comparison to experiments. IEEE J Quantum Electron. 1995;31:2250–7.
11. Anderson RR, Parrish JA. Selective photothermolysis: precise microsurgery by selective absorption of pulsed radiation. Science. 1983;220:524–7.
12. Ho DM, London R, Zimmerman GB, Young DA. Laser-tattoo removal: A study of the mechanism and the optimal treatment strategy via computer simulations. Lasers Surg Med. 2002;30:389–97.
13. Goldman MP, Bennet RG. Treatment of telangiectasia: A review. J Am Acad Dermatol. 1987;17:167–82.
14. Tan OT, Murray S, Urban AK. Action spectrum of vascular specific injury using pulsed radiation. J Invest Dermatol. 1989;92:868–71.
15. Kienle A, Hibst R. Optimal parameters for laser treatment of leg telangectasia. Lasers Surg Med. 1997;20:346–53.
16. Hsia J, Lowery JA, Zellickson B. Treatment of leg telangectasia using long-pulse dye laser at 595 nm. Lasers Surg Med. 1997;20:1–5.
17. Kunishige JH, Glodberg LH, Friedman PM. Laser therapy for leg veins. Clin Dermatol. 2007;25:454–61.
18. Høgsberg T, Loeschner K, Löft D, Serup J. Tattoo inks in general usage contain nanoparticles. Brit Jour Derm. 2011;165:1210–8.
19. Taylor CR, Anderson RR, Gange RW, Michaud NA, Flotte TJ. Light and electron microscopy analysis of tattoo treated by Q-switched ruby laser. J Invest Dermatol. 1991;97:131–6.

20. Kilmer SL. Laser treatment of tattoos. Dematol Clin. 1997;15:409–17.
21. Jow T, Brrown A, Goldberg DJ. Patient compliance as a major determinant of laser tattoo removal success rate: a 10-year retrospective study. J Cosmet Laser Ther. 2010;12:166–9.
22. Bernstein EF, Bhawalkar J, Schomacker KT. A novel titanium sapphire picosecond-domain laser safely and efectively removes purple, blue and green tattoo inks. Lasers Surg Med. 2018;50:704–10.
23. Ross V, Naseef G, Lin C, Kelly M, Michaud N, Flotte T, Raythen J, Anderson RR. Comparison of responses of tattoos to picosecond and nanosecond Q-switched neodymium: YAG lasers. Arch Dermatol. 1998;134:167–71.
24. Lorgeou A, Perillat Y, Gral N, Lagrange S, Lacour JP, Passeron T. Comparison of two picosecond lasers to a nanosecond laser for treating tattoos: a prospective randomized study on 49 patients. J Eur Acad Dermatol Veneorol. 2017;32:265–70.
25. Pinto F, Groβe-Büning S, Karsai S, et al. Neodymium-doped yttrium aluminium garnet (Nd:YAG) 1064-nm picosecond laser vs Nd:YAG 1064-nm nanosecond laser in tattoo removal: a randomized controlled single-blind clinical trial. Br J Dematol. 2017;176:457–64.
26. Brauer JA, Reddy KK, Anolik R, et al. Successful and rapid treatment of blue and green tattoo pigment with a novel picosecond laser. Arch Dermatol. 2012;148:820–3.
27. Fitzpatrick RE, Goldman MP. Tattoo removal using the alexandrite laser. Arch Dermatol. 1994;130:1508–14.
28. Leuenberger ML, Mulas MW, Hata TR, Goldman MP, Fitzpatrik RE, Grevelink JM. Comparison of the Q-switched alexandrite, Nd:YAG and ruby lasers in treating blue-black tattoos. Dematol Surg. 1999;25:10–4.
29. Bernstein EF, Schomaker KT, Basilavecchio LD, Plugis JM, Bhawalkar JD. A novel dual-wavelength, Nd:YAG, Picosecond-domain laser safely and effectively removes multicolor tattoos. Lasers Surg Med. 2015;47:542–8.
30. Alabdulrazzaq H, Braur JA, Bae YS, Geronemus RG. Clearance of yellow tattoo ink with a novel 532-nm picosecond laser. Lasers Surg Med. 2015;47:285–8.
31. Bencini PL, Cazzaniga S, Tourlaki A, Galimberti MG. Removal of tattoos by Q-switched laser: variable influencing outcome and sequelae in a large cohort of treated patients. Arch Dermatol. 2012;148:1364–9.

Laser and Light Sources: Safety and Organization Issues

29

Marco Dal Canton

29.1 Introduction

Light Amplification by Stimulated Electron Radiation (LASER) is a known acronym denoting a technology which converts electrical energy in a monochromatic, coherent and collimated light in the range of visible or invisible light spectrum (for medical purposes, usually between 308 nm and 10,600 nm)

In a laser, the collimated light is delivered through an articulated arm equipped with a mirror system or through optical fibers, focusing potentially very high energies in a very small area, within picosecond to millisecond pulse width ranges.

When activating a medical laser, high energies are delivered on specific targets for therapeutic purposes, nonetheless with potentially dangerous consequences if the laser beam unintentionally impacts directly, is reflected or is diffused against unwanted objects.

High energy polychromatic light sources (PCLs), commonly defined *Intense Pulsed Lights* (IPLs, an originally proprietary acronym), differ from lasers since they generate a pulsed, intense polychromatic, non-focused, non-collimated, diffuse light extending from the shorter blue visible wavelengths to the near IR, usually in the 400–1200 nm range. The pulsed light is generated by a gas-filled flashlamp pumped with a charge of high voltage electrical energy stored in a capacitor [1]: the intense light is passed through cutoff filters stopping the shorter wavelengths interfering with melanins and those in the harmful UV range, and a recent IPL model is equipped also with an IR cutoff filter. The light is delivered through a handpiece, usually encasing the flashlamp, which is equipped with a crystal prism: this must be placed in close contact to the skin and optically coupled with the treatment area, with the auxiliary help of optical grade contact gel. When activating an IPL pulse, the patient, the operator, and the operative area are exposed to potential hazards if not properly protected from the intense light diffused through the crystal applicator.

Medical Light Emitting Diodes (LEDs) are optoelectronic devices producing polychromatic light in a narrow spectrum, almost monochromatic, with a peak wavelength which usually identifies the LED source, depending upon the emitting semiconductor. High energy LEDs for medical purposes are used principally for photodynamic therapy, photobiomodulation and biophotonic therapy, deliver relatively high and diffuse light energy and, based on the available evidences, are considered generally safe [2].

M. Dal Canton (✉)
Societa Italiana di Dermatologia Chirurgica ed Oncologica (SIDCO), Siena, Italy

Private practice, Qderm, Belluno, Italy
e-mail: mdc@qderm.it

M. Fimiani et al. (eds.), *Technology in Practical Dermatology*,
https://doi.org/10.1007/978-3-030-45351-0_29

Most side effects of low level light therapy (LLLT) [1] used alone (i.e., not associated to external factors as in PDT or biophotonic therapy) are related to the intense light glare and to potential corneal overheating, particularly by IR LED sources. For these reasons, it is worthwhile to use also during LED therapy an appropriate protection of the operator and patient's eye.

This chapter is aiming to focus on some basic safety rules when using a medical laser or PCL. Actually the eye of the patient, of the operator, and all assisting persons is the main concern in the protection expedients in the laser safety guidelines and safety regulations, and an insufficient training on these safety issues poses a potentially serious safety problem.

This multifaceted matter is related to specific international and national standards that can differ in each country.

Whatever herein synthetically described could not necessarily comprehensively correspond and adapt to any operative setting.

Therefore it is important for the reader to refer to the manufacturer instruction manuals and to the international standards and national guidelines and all locally applicable relevant regulations.

29.2 Operating with a Medical Laser Light Source

Owning and operating with high energy light sources for medical purposes, as lasers, polychromatic intense pulsed light devices (IPL) and LEDs, is today widespread in healthcare inpatient and outpatient offices since such medical devices are suitable to treat several different skin conditions.

In the new millennium, we are assisting to a combination of singularities in patient information and expectations on technology, including medical lasers and light sources and, in general, on hi-tech energy-based devices, which a physician is invited to take into consideration:

- an increasing interest and spreading information on energy-based technologies in patient communities, seeking for offers of effective but low risk and low or no-downtime procedures
- an extensive, mainly web and social media based commercial pressure on the general public and on the medical market, with frequently unscrupulous advertisement claiming for occasionally pretentious results related to sometimes questionable scientific evidences and technologies
- the spreading spa-culture of wellness, implicating a blurring boundary between the perception of the differences between medical and purely aesthetic professional competences and the related intrinsic quality of technologies
- an expanding offer by manufacturers in the ambiguous market of wellness, competing on performances and reduced production and distribution costs
- a competitive market on (mainly aesthetic) procedures, fighting to offer the better technology at the lowest possible costs, albeit claiming first class results

The temptation for a physician to purchase a low-cost device to enter a very competitive market should be tempered by a simple but essential consideration: quality in high technology has always a not negligible native cost.

Quality engineering, manufacturing, and assembling reliable components to produce a trustworthy laser or IPL implicates incontestable basic costs for the manufacturer, not taking into consideration the cost of a consistent clinical research, official clearance procedures, and conformity certification for original indications of new or existing technologies, and, last but not least, the quality of post-market assistance.

When purchasing any hi-tech instrument or a medical device, one should always balance the costs/benefits ratio, bearing in mind that our reputation is based upon the quality of the results we will be able to offer our patients, independent by our tools.

The intrinsic quality of the device we are interested in should be unquestionable, therefore it must be carefully evaluated before making a usually significant investment.

Relying on a reputable company, on a trustworthy and documented technology referring to

the available relevant scientific literature; to get acquainted with a trusted local distributor; talking thoroughly with colleagues already experienced with that specific company and technology; and obtaining references on the pre-emptive and on-demand assistance services provided after market, all these should be the fundamental principles conditioning our final purchase decision.

29.3 Accommodating and Operating with a Laser Or High Energy Light Source

The implementation of a medical laser or a high energy light source for medical purposes implies room systems integrations, professional training on technology, organization and on safety issues indispensable for the patient, the operator, the assistants and any other attending individual and for environment inside and surrounding the designed operative area.

The importance of safety when operating with a laser or polychromatic light high energy device should never be underestimated since this implicates documented objective risks of significant health injury, particularly for the eye.

There are for this reason international standards and norms on safety requirements applicable not only to the device, but also to the operative setting and the professional individuals eligible to use it.

These international technical regulations usually can be slightly dissimilar on each continent and differently fulfilled in distinct countries. Hence the reader is invited to analyze the relevant specific regulations in own country and local area.

29.4 Classification of Lasers

There are two main classification systems of lasers, one based on the international standard IEC 60825-1 (IEC: International Electrotechnical Commission, a global organization for the preparation and publication of International Standards for all electrical, electronic, and related technologies) and another, the ANSI (American National Standards Institute) Z136.1, based on the US FDA laser regulations. The two hazard classifications are mostly converging and only slightly differing in some parts.

Hazard levels of lasers are categorized by IEC 60825 based upon wavelength and energy output into classes, according to their capability to produce injury in exposed individuals, from class 1 (no hazard) to class 4 (severe hazard for eyes and skin) (Table 29.1).

The US-ANSI classification assigns lasers to one of 4 hazard classes (1, 2, 3a, 3b and 4), established on the potential for biological damage, calculated based on exposure time, wavelength, and output power for CW or PW lasers and on total energy per pulse for pulsed lasers.

Medical lasers are mostly included in class 4 on IEC and ANSI classification, the higher class of hazard for inadvertent eye or skin exposure.

The manufacturer must certify the classification and CE compliance (in the EU market) of a laser/PCL/LED providing an official conformity certificate and must apply to the case of the device specific warning labels. An acceptance test must be performed after the placement of the medical device in the office and the outcome of the test must be signed by the technician.

The compliance of the laser to all prescribed technical and safety requirements is understandably obligatory in the clearance phase, nevertheless during the whole operative life of the device, a lifelong maintenance of the compliance to the required standards must be periodically certified as a base to renew the validity of the original conformity certificate.

The conformity certificate of a medical device and the evidence of its regular maintenance are essential documents which must be readily available in case of an inspection of the office by local authorities.

The classification of a laser is based on the concept of accessible emission limits (AEL) defined for each laser class.

Each medical laser product shall comply with all of the applicable requirements for laser products of its class. In addition, any Class 3B or

Table 29.1 IEC 60825 classification of lasers

1	• safe under all conditions of normal use	
1M	• safe for all conditions of use except when passed through magnifying optics (for example, magnifying glasses, microscopes)	• avoid use with optical instruments
2	• safe for accidental exposure (< 0.25 s). • avoid pointing at the face and staring at the laser beam.	• the blink reflex will limit the exposure to no more than 0.25 s • limited to visible (400–700 nm) 1 mW continuous wave, or more if pulse width < 0.25 s or if the light is not spatially coherent.
2M	• safe eye exposure < 0.25 s, except when passed through magnifying optics (for example, magnifying glasses, microscopes)	• avoid use with optical instruments
3R	• safe if handled carefully • avoid pointing at the face and staring at the laser beam	• the MPE can be exceeded, with a limited risk of injury • visible continuous lasers limited to 5 mW • other wavelengths and pulsed lasers have other restrictions
3B	• hazardous if the eye is exposed directly • diffuse reflections are not harmful	• continuous lasers from 315 nm to far-IR limited to 0.5 W • pulsed lasers between 400 and 700 nm, limited to 30 mJ • other limits apply to other wavelengths and to ultrashort pulsed lasers • must be equipped with a key switch and a connection to an emergency master disconnect interlock or to a room door safety interlock. • designate a superintending laser safety officer (LSO) • delimit and regulate the access to the laser work area • warning signs outside the room • use only by qualified operators • protective wavelength specific eyewear (PPE) is required where *direct* viewing laser beam • specific training for operators and maintenance personnel
4	• dangerous as a result of *direct* and *diffuse* beam viewing • potentially permanent eye injury • can burn the skin • may ignite combustible materials (fire risk)	• all lasers with output power greater than class 3B • same precautions of 3B lasers • personal protection equipment (PPE)—wavelength (specific protective eyewear and fire resisting garments) is obligatory for *direct* beam and *diffuse* light protection • specific training for operators and maintenance personnel

Class 4 medical laser product shall comply with IEC 60601-1 regarding the requirements for electrical medical devices [3].

29.4.1 Training

Class 4 medical laser systems can represent a hazard to the operator and to other individuals over a considerable distance, from either the direct beam or also from its specular and diffuse reflections.

Because of this hazard potential, the IEC 60825 prescribes that only persons who have received a formal training to an appropriate level should be placed in control of such systems. The training, which may be given by the manufacturer or by the supplier of the system, the designated Laser Safety Officer (LSO), or by an approved external organization, should include (not limited to):

1. *familiarization with system operating procedures*
2. *the proper use of hazard control procedures, warning signs, etc.*
3. *the need for personal protection*
4. *accident reporting procedures*
5. *effects of the laser upon the eye and the skin*

Each laser, IPL, or LED platform should be accompanied by an identifiable instruction manual, in EU provided in the national language, containing indications on the pre-emptive and on-demand maintenance.

29.4.2 The Class 4 Medical Lasers: Operative Setting

Class 4 laser system must incorporate an emergency stop button and a removable key-operated master control: the laser radiation must not be accessible when the key is removed.

The laser-controlled area (LCA), within a dedicated room or space, should have minimal dimensions greater than the *nominal ocular hazard distance* (NOHD) or *nominal hazard zone* (NHZ), the distance at which the beam irradiance or radiant exposure equals the appropriate corneal *maximum permissible exposure* (MPE): in practice, the NOHD is the distance over which the beam does not determine any damage to the eye (Fig. 29.1)

The LCA should be clearly identifiable from the outside, labelled with specific warning signs and symbols (featured as indicated in the technical standards and local regulations—Fig. 29.2): a room or emergency general interlock should interrupt the laser beam in the case of an inadvertent unauthorized access to the LCA when the laser is activated to deliver light energy above the MPE (Fig. 29.3). Furthermore, in most cases an illuminated warning sign (as an intermittent red light) outside the area should be interfaced with the master controller and automatically activated or even manually switched before the activation of the laser beam, while in some countries an illuminated warning device must be installed also inside the LCA to be easily viewable to individuals within.

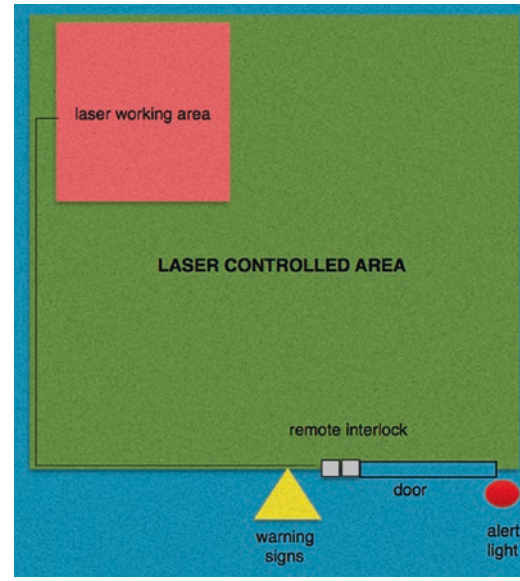

Fig. 29.1 Laser-controlled area

Fig. 29.2 Laser warning signs to be positioned outside the laser-controlled area (IEC 60825-1 for EU zone and ANSI Z136.1 in the USA)

Attendance of any individual to the LCA during laser operation should be restricted only to persons wearing apposite laser protective eyewear (wavelength-specific PPE), otherwise admittance to the area must be prevented when a laser beam above the MPE is activated.

Fig. 29.3 Remote interlock activation permits the laser to be actuated

Special precautions may be required to prevent unwanted laser light reflections, mainly when operating within the invisible spectrum, which can induce to underestimate the intrinsic risk of eye injury: the eye is fully exposed to near IR and IR invisible light since in this range the defensive blink reflex is lacking.

Non-reflecting and fireproof wall paints and upholstery and light impermeable screening of windows and of reflecting surfaces should be available to reduce the extent of reflected radiation.

Additional special precautions are also required to prevent unwanted laser light reflections. Surgical instruments and equipment in the laser working area should be specifically designed for laser surgery and manufactured with opaque non-reflecting surface: the beam and target area should be surrounded by nonflammable textiles and materials opaque to the laser light. Even dull metal surfaces may be highly specular at the CO_2 wavelength of 10600 nm, and additional precautions must be paid when operating with metal surgical instruments.

Before activating the laser, the operator is responsible to verify that all the safety measures concerning the patient, her/himself, the attending persons, and any possible other target in the laser-controlled area have been enacted.

The laser should be checked for proper working and, when feasible, the right alignment of the beam should be checked before delivering the first pulse directly on the patient, for example firing some pulses on a wood tongue depressor.

When using multiple wavelength platforms, as modern IPLs, it is mandatory for the operator and the individuals within the LCA to wear appropriate personal protective equipment (PPE) as a certified protective eyewear specific for each wavelength range (*laser safety eyeglasses*—LSE). If the wavelength is changed during the procedure, it is crucial to shift to the respective specific LSE accordingly. Each specific optical PPE should be unambiguously and immediately identifiable and always positioned close to the specific laser or light source to which it is assigned.

The operator should never underestimate fatigue and the related potential misuse of the laser and/or protective eyewear, with consequent inadvertent unprotected eye exposure to the laser beam: this is absolutely human, but the consequences can be irreversible.

29.4.3 The Main Concern Using a Medical Laser: To Protect the Eye

Due to the vulnerability of the eye to light overstimulation, unsurprisingly laser safety guidelines are based mainly on injury thresholds of the ocular structures, chiefly iris and retina. Lasers and intense pulsed lights in the visible range of 400–760 nm wavelengths can produce significant injury to the retina and to the macula.

If inappropriate eye protection is used, the intense light can pass through the cornea, become focused by the lens into the retina, and result in retinal photocoagulation and photomechanical disruption, particularly with light sources in the visible range, as KTP 532 nm or PDL 585 or 595 nm laser, which are avidly absorbed by hemoglobin and melanin well represented in the retinal cells [4, 5]. The "blink reflex" is a spontaneous protection mechanism of the eye to a direct light stimulus, an automatic reaction effective for light radiation directed to the eye up to 1 mW power and pulse widths superior to 250 m sec: with higher power levels and/or shorter pulse widths, too much energy reaches the retina before the blink reflex can respond, which can result in an irreversible retinal damage and potential loss of vision [6].

The near infrared range (IR-A 760–1400 nm) of wavelengths, as the 800 and 940 nm diode or the Nd: YAG 1064 nm, is less absorbed by melanin and hemoglobin, but can be particularly dangerous to the human eye because in this spectrum of frequencies the blink reflex is inactive [7–9].

The mid infrared (IR-B 1400–3000 nm) and far infrared range (IR-C 3000–10600 nm) of wavelengths, as that of 1450 nm and 1550 nm non-ablative fractional lasers, of Er: YAG 2940 nm and 10,600 nm CO_2 laser, cannot penetrate enough to reach the retina, but can still cause harm to the sclera, cornea, and the lens, due to their rich water content.

One must keep in mind that IPLs emit non-collimated, non-coherent, polychromatic light (usually between 400 and 1200 nm), covering the full range of retinal hazard spectrum of wavelengths, potentially causing significant ocular and skin damage (Fig. 29.4).The extremely high pulse energies and peak power achieved with Q switching in sub-microsecond pulse widths can raise serious laser safety problems even for lasers with fairly small average output power and require high safety profile protection independent from the fluence, because the photoacoustic retinal damage produced can be destructive.

Laser and IPL hair removal of the eyebrow and in the periorbital area is the most reported cause of eye injury in the literature [10, 11], but eye injury has been reported also with various kinds of wavelengths and different ablative and non-ablative procedures [3].

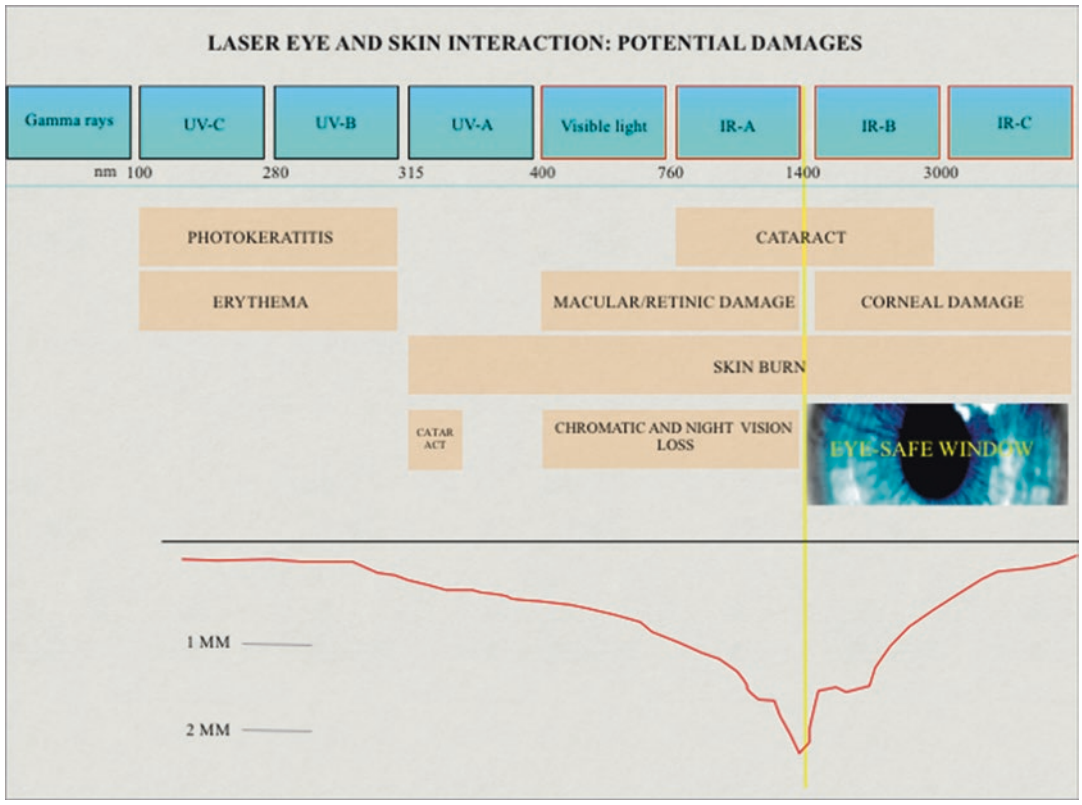

Fig. 29.4 Laser ocular and skin damage

29.4.4 Ocular Protection for the Patient

Eye protection for the patient must be constantly provided before activating a Class 4 medical laser, IPL, or a medical purpose LED light source, and the type of eye protection depends upon the area to be treated. External eye shields, usually made of burnished non-reflective stainless steel or plastic, or shielded eyelids adhesive patches are adequate for most laser and lights treatments applied outside the orbital rim, but if the treatment is performed on the eyelids area, corneal shields are necessary (Fig. 29.5).

Corneal shields, as Cox II, Stefanovsky and Kahn models, are metal or plastic devices

Fig. 29.5 Laser corneal shields

produced in different sizes, designed to cover the eye surface up to the lash line, offering perfectly smooth internal surface and rims. Corneal shields must be sterile and perfectly clean, always carefully inspected for sharp edges, and should be positioned after instillation of 1–2 drops of ophthalmic anesthetic and removed carefully to prevent possible corneal abrasions.

Care must be taken also to not overheat the metal shields with stacked pulses, to prevent an excessive conduction to the eye, potentially causing a corneal irritation, while hitting directly a plastic shield with a CO_2 or Nd: YAG laser can melt or get them burnt [12].

In conclusion: (1) to prevent potential eye damage, no Class 4 laser or IPL can be directed, in any condition, to the patient without a certified patient's eye protection positioned before the activation of the laser beam, as well as (2) the eyes of the operator and of any other person in the laser operative area must be preliminarily protected with specific personal protective equipment.

29.4.5 Ocular Protection for the Operator, the Assistants, and Other Individuals in the Laser-Controlled Area

When activating a Class 3B or Class 4 laser, laser safety eyeglasses (LSE) specific for each wavelength must be worn by any individual within the laser-controlled area (LCA). Based on the UNI EN 207:2017 standard, labelling of CE marked LSE must include: the wavelength ranges suitable to each specific PPE; the optical density (OD) of the lenses, conceived to downgrade the incident light radiation within the limit of Class 2 lasers (for example, OD6 means that the optical energy transmitted is $1/10^6$ of incident radiation) [7, 8]; the protective eyewear for Class 4 lasers must resist to at least 100 short pulses and/or to 10 s of continuous wave at maximum energy output without significant degradation of the lenses or perforation [13].

The American National Standards Institute produces and periodically updates standards and guidelines for laser safety [14]. LSE should be also able to block the harmful laser wavelengths while transmitting enough visible light to allow the operator to visualize properly the treatment area (Visible Light Transmission—VLT). Of course, the ideal LSE should have both a high OD and VLT, and this compromise has some limitation on the LSE protecting from the entire IPL range (400–1200 nm), which can usually offer an impaired visibility due to a proportionally low VLT. The laser safety eyewear must be clearly engraved or labelled with information adequate to ensure the identification of its protection ranks for each specific laser [3]. Furthermore, the integrity of each LSE must be periodically determined by the operator and by the laser safety officer (LSO), while not properly fitting or wear out devices should be replaced.

29.4.6 Extraocular Dangers Related to Class 4 Laser or IPLs

When operating with a Class 4 laser or intense pulsed light, there are some additional risks to be evaluated and prevented. The possibility of inadvertent skin burns is intrinsic to laser procedures as hair removal, vascular laser, photorejuvenation, and ablative laser surgery. Nevertheless care must be given to prevent unwanted laser shots against the nearby objects or persons, wearing fireproof garments and to eliminate flammable materials in the LSA.

Extremely flammable substances, as alcohol and alcohol-based disinfectants, and first of all explosive gases, as oxygen, must be limited and possibly removed from the LSA. Surgical fires are more typical in presence of oxygen-enriched atmosphere and lasers are a major source of ignition. In the case of an oxygen-enriched ventilation, mainly during head and neck laser surgery, additional protections and precautions must be integrated before activating a laser beam into the operative field, and an optimal cooperation with the anesthesiologist on these preventive measures is essential [15].

The available data indicate that the surgical smoke and particulate is cytotoxic and possible vehicle of infections, suggesting that surgical and laser smoke is to be considered an occupational hazard for healthcare workers [16]. Smoke and plumes can be produced during common laser procedures as epilation, laser surgery, and tattoo removal. It has been documented that surgical and laser smoke contains hazardous chemical inhalers, as benzene, hydrogen cyanide, formaldehyde, ammonia, sulfur, organic compounds and others, and also viruses (HPV, HCV, HIV), bacteria and viable tumor cells [17] have been isolated [18].

Particulate substances are specifically insidious due to their small dimensions, potentially able to pass conventional filters, and normal or forced ventilation in the operating room is inadequate for a complete and safe removal.

A high power smoke evacuator equipped with HEPA filters (High Efficiency Particulate filter: able to block 99.97% of particles smaller than 0.30 μm) [19] or preferably with ULPA filters (Ultra Low Penetration Air filter: able to block 99.99% of particles as small as 0.12 μm) [17] is therefore to be activated in close proximity to the operative area when performing a laser procedure producing fumes or particulate matter. HEPA and ULPA filters must be replaced regularly.

The operator and the assistants should wear a filtered mask able to block small solids, fluid fumes, and particles on aqueous and organic at least FFP2 class [20].

In some procedures, splattering blood particles and tissue debris can occur and requires added personal protective devices as transparent face masks and impermeable garments.

29.5 Conclusions

Lasers, IPLs, and LED systems are more and more essential medical devices in dermatology offices, offering patients a wide range of treatment options. The implementation of a new high energy light system requests a risk assessment and a revision and adjustment of facility safety policies and procedures.

A genuine teamwork, a transparent and punctual communication among the staff members of the health care facility, and an active continuing professional education and training on laser safety issues can establish the base for a trustworthy operative laser safety program.

References

1. Calderhead RG. Photobiological basics of photomedicine: A work of art still in progress. Med Lasers; Eng Basic Res Clin Appl. 2017;6:45–57.
2. Jagdeo J, Austin E, Mamalis A, Wong C, Ho D, Siegel DM. Light-emitting diodes in dermatology: A systematic review of randomized controlled trials. Lasers Surg Med. 2018;50:613–28.
3. IEC 60601: Medical electrical equipment—Part 2–22: Particular requirements for basic safety and essential performance of surgical, cosmetic, therapeutic and diagnostic laser equipment.
4. Barkana Y, Belkin M. Laser eye injuries. Surv Ophthalmol. 2000;44(6):459–78.
5. Huang A, Phillips A, Adar T, Hui A. Ocular injury in cosmetic laser treatments of the face. J Clin Aesthet Dermatol. 2018;11(2):15–8.
6. IEC 60825-1: Safety of laser products—Part 1: Equipment classification, requirements and user's guide.
7. Schieke SM, Schroeder P, Krutmann J. Cutaneous effects of infrared radiation: from clinical observations to molecular response mechanisms. Photodermatol Photoimmunol Photomed. 2003;19(5):228–34.
8. Gao L, Dong F, Chan WM. Traumatic macular hole secondary to Nd:YAG laser. Eye (Lond). 2007;21:571–3.
9. Lee WW, Murdock J, Albini TA, O'brien TP, Levine ML. Ocular damage secondary to intense pulse light therapy to the face. Ophthal Plast Reconstr Surg. 2011;27:263–5.
10. Karabela Y, Eliacik M. Anterior uveitis following eyebrow epilation with alexandrite laser. Int Med Case Rep J. 2015;8:177–9.
11. Lee WW, Murdock J, Albini TA, et al. Ocular damage secondary to intense pulse light therapy to the face. Ophthal Plast Reconstr Surg. 2011;27(4):263–5.
12. Riley J. Safety considerations in the use of the CO_2 laser in facial skin resurfacing. Laser Surg Med. 1997;9(Suppl):61.
13. UNI EN 207:2017: Personal eye-protection equipment—Filters and eye-protectors against laser radiation (laser eye-protectors). March 2017.
14. ANSI Z136.1 UCSB Laser Safety Manual. 2014
15. Yardley IE, Donaldson LJ. Surgical fires, a clear and present danger. Surgeon. 2010;8(2):87–92.

16. Sisler JD, Shaffer J, Soo JC, LeBouf RF, Harper M, Qian Y, et al. In vitro toxicological evaluation of surgical smoke from human tissue. J Occup Med Toxicol. 2018;13:12.
17. Fletcher JN, DesCoteaux MD, J.G. Dissemination of melanoma cells within electrocautery plume. Am J Surg. 1999;178(1):57–9.
18. Bargman H. Laser generated airborne contaminants. Laser Safety J Clin Aesth. 2011;4(2):56–7.
19. UNI EN1822:2010 High efficiency air filters (EPA, HEPA and ULPA)—Part 1: Classification, performance testing, marking.
20. UNI EN 149:2009: Respiratory protective devices—Filtering half masks to protect against particles—Requirements, testing, marking.

Intense Polychromatic Lights: What's New

30

Pier Luigi Saraceni, Sean Ekinde, Elisa Cinotti, and Massimo Laurenza

The first clinical studies on intense polychromatic lights (IPL) were performed by Mulhlbauer et al. [1] that experimented for the first time the photocoagulation of vascular malformations by heat developed by "broad-spectrum infrared light," method that had little success in the following years. The IPL was commercially launched as a medical device in the 1990s, after the studies of Goldman and Eckhouse who developed a new polychromatic light source emitted by a special high intensity flashlamp [2]. In 1995, the FDA approved the use of the IPL. The emitted light comprised a vast spectrum of wavelengths, unlike LASERs which emit only one specific wavelength of the active medium used. Given the broad spectrum emitted by the IPL, experiments were resumed on the treatment of cutaneous vascular lesions of the lower limbs, such as telangiectasias and angiomas. To date, the IPL is mainly indicated for telangiectasias of the face, congenital and photo/chrono-induced hyperpigmentation as freckles, melasma and lentigo, acne, photorejuvenation, and hair removal [3].

30.1 General IPL Characteristics

The device consists of computer-controlled capacitor banks, a software that is managed by a multifunctional display and one or more handpieces whose "head" contains a high power xenon lamp (flashlamp), which emits an intense polychromatic light in pulsed mode. Electrical energy stored in the capacitor bank is passed through xenon gas within a gas-discharge lamp, so that bright light is emitted; thus, electrical energy is converted into optical energy [4]. The handpiece ends with an end consisting of a rectangular prism of sapphire or transparent quartz which allows the homogeneous and uniform diffusion of the light beam.

Most of the IPLs on the market have an air and/or water-cooling device for the lamp which allows a long working life up to 100000 flashes and helps to emit a light beam with low heat emission on the skin.

The lamp (flashlamp) emits a very powerful broad-spectrum light with wavelengths ranging from 400 to 1300 nm: therefore, it results in a polychrome light, not coherent and not collimated, which is the exact opposite of the LASER light that emits a monochromatic, coherent and collimated light.

P. L. Saraceni
Department of Clinical Dermatology, IFO-Istituto San Gallicano, Rome, Italy

S. Ekinde · E. Cinotti
Department of Dermatology, University Hospital of Siena, Siena, Italy

M. Laurenza (✉)
Department of Oncologic Dermatology, IDI, Rome, Italy

M. Fimiani et al. (eds.), *Technology in Practical Dermatology*,
https://doi.org/10.1007/978-3-030-45351-0_30

Given the wide light spectrum, the IPL acts as a set of different laser beams. Thanks to convertible cutoff crystal filters that selectively limit the emission of light, IPLs can be easily adapted to the desired wavelength range. A cutoff filter filters light of wavelength that is below the wavelength of the filter, thereby allowing the wavelengths above to pass through.

First-generation IPL devices emitted light of the infrared part of the spectrum, which prevalently led to epithelial damage and a high incidence of side effects. In second-generation IPL devices, water filters out the infrared portion significantly reduced the risk of side effects [4]. Usually the main manufacturers provide filters that "cut" the radiation from 500 nm to 650 nm and from 980 nm to 1200 nm. Some manufacturers have different handpieces with different cutoff filters, whereas others provided one handpiece with interchangeable filters.

According to the various crystal filters, IPL can be easily and selectively absorbed by the different natural chromophores contained in the skin, such as melanin, hemoglobin, deoxyhemoglobin, and water. The advantages offered by the great versatility of the system are evident, being able to emit a wide range of wavelengths, pulse durations, pulse intervals, and fluences with the possibility of adapting specific therapeutic patterns in relation to the patient's skin phototype. Pulse duration can be set in relatively wide ranges (depending on the particular device). This versatility is advantageous for a skilled and experienced dermatologist. For untrained physicians, however, the wide range of selectable treatment settings implies the risk of evoking side effects because of non-specific thermal damage. Further advantages to lasers are the lower purchase price and the more robust technology.

30.2 IPL–Tissue Interaction

The interaction between light energy and a biological medium depends on the wavelength of the radiation and on the optical properties of the tissue. When light interacts with a tissue, the following phenomena occur: (1) reflection, (2) transmission, (3) scattering, and (4) absorption.

Reflection and transmission have no effect on the tissue; the light energy is reflected above the surface (like a mirror) or passes through the tissue (transmission). Approximately 5% of the light that impacts on the surface of the skin is immediately reflected, the other 95% is absorbed or scattered inside the tissue. In the case of absorption, the photon releases its energy to a target chromophore [3]. Scattering is the deviation of light at the moment of penetration into the tissue (for example by the collagen fibers).

It is essential to use a cooling medium such as a cold transparent or cooled gel, placed between the skin and the IPL handpiece, not only to minimize light reflection, but also to distribute it evenly and to dilute the thermal effect on the skin.

30.3 Mechanism of Action of IPL

The biological effects of IPL, similar to lasers, are expressed through the selective absorption of light radiations by endogenous cutaneous chromophores (mainly hemoglobin, melanin, and water). The electromagnetic energy absorbed by the chromophore is transformed into thermal energy (photothermal effect) with heating of the chromophore and of the cells or tissues that contain it and subsequently destruction of the target structure [4] (photothermolysis).

The thermal effects on a tissue vary with the temperature; at 50–60°C, conformational changes of protein molecules, membrane alterations with cellular coagulative necrosis (photocoagulation) and collagen denaturation occur; at temperatures over 100°C, there is a vaporization of the tissue water with possible formation of vapor bubbles which, when burst, cause an explosive photomechanical effect on the tissue.

The pulse duration and the thermal relaxation time (TRT) are fundamental to limit the thermal effects. The first is the duration in the millisecond (ms) range, of the single light pulse, while TRT is the time that the tissue radiated by the light pulse takes to cool by half of its peak temperature after laser irradiation. Similar to laser devices, pulse duration should be less than or equal to the TRT of the target structure to prevent unselective damage to the surrounding tissue. The TRT is different

Table 30.1 Intense polychromatic light spectra to be used in different indications

Spectra	Indications
430–1120 nm	Vascular lesions, acne, hyperpigmentation
480–1120 nm	Vascular lesions, hyperpigmentation, skin photorejuvenation
530–1120 nm	Vascular lesions, hyperpigmentation, skin photorejuvenation
640–1120 nm	Epilation
690–1120 nm	Epilation
755–11250 nm	Epilation

for different tissues: e.g., for the skin with a thickness of 0.1 mm it is about 1 ms, in the case of a thickness of 0.3 mm it is 10 ms. Thicker is the tissue, longer should be the cooling time. Multiple pulses with suitable silent intervals (delay) allow to progressively and sequentially heat the target until its destruction, leaving the skin and the surrounding tissues the possibility of cooling down.

The parameters that can be adjusted are:

(1) Cutoff filters: to select the wavelength to achieve the right penetration depth and target (Table 30.1).
(2) Fluence: the quantity of energy delivered on surface units. Fluence is expressed in j/cm^2 (the range varies from 2 to 90 j/cm^2). The regulation of this parameter allows to measure the heat released per unit of skin area.
(3) Duration of the pulse: varies from 1 to 100 ms, determines the time of exposure to light and if higher than the TRT of the target causes its destruction (photothermolysis).
(4) Interval between one pulse and another (delay) expressed in ms (varies from 1 to 50 ms); it allows to control the effect on the skin.
(5) Frequency of luminous pulses (the radiant energy can be administered in a single pulse or fractioned in a sequence of two or more consecutive pulses) which partly determines the depth of penetration of the wave and partly the mode of release of the energy.

The emission of the luminous flux can be of a sigmoid type with an initial peak that decreases progressively or of square wave type with constant emission. The most advanced pulsed lights which are now on the market are based on the square wave, because it allows a homogeneous absorption of the energy packet emitted at each flash, avoiding an initial excessive overheating of the skin. The square wave pulse makes it possible to use reduced fluences and obtain the same result with fewer side effects.

Although IPL systems are equipped with a software that allows the use of preset parameters, these data must be only indicative for the user, since the parameters must be individually calibrated on the basis of: (1) phototype (usually phototypes V–VI according to Fitzpatrick scale should not be treated); (2) skin types (lower fluences on sensitive skin); (3) target depth (longer are the wavelengths, deeper the energy is delivered); (4) target type (it should be considered the surrounding absorbent tissues and if the target is moving, such as hemoglobin in the blood vessel). However, it is good to start any type of treatment by performing a test on the area to be treated, evaluating the effects at 10 min and 24 h [3]. Specifications of IPL parameters given in this chapter are only indicative and should not be assumed to be the same on different IPL systems.

30.4 Acne

It is a chronic inflammatory dermatosis of the pilosebaceous follicle; it mainly affects the adolescent population and can also persist in adulthood. The typical acne manifestations consist in the presence of seborrheic skin, comedones, papules, pustules, fibro-cystic nodules, and scars. The use of IPL or LASER equipment in the medical-aesthetic treatment of moderate and severe acne is now clinically accepted.

Photons act on acne lesions with two specific mechanisms:

(1) They recognize protoporphyrin IX and coproporphyrin III, chromophores produced by *Propionibacterium acnes* present in sebum, as a target of induced photothermolysis. Usually the following frequencies are used:

415, 510, 542, 578, 633, 655 nm. Subsequently, there is the production of reactive oxygen species (ROS) and consequent bactericidal effect.

(2) They aimed at the selective thermolysis of hemoglobin in the vascular network that irrigates the sebaceous glands with cytolysis and a subsequent strong reduction in the sebaceous secretion of acne skin.

There is also the possibility of increasing the damage to the sebaceous glands by penetrating the skin with photosensitizing substances that selectively accumulate in them, absorbing the light energy emitted by the IPL device to a greater extent, with high photothermal damage.

The procedure consists in applying the handpiece with xenon lamp and using dedicated cutoff filter (for example, 430 nm filter allowing emitted wavelengths longer than 430 nm), single pulse, fluence around 17–22 j/cm^2, and TRT of 30 ms. The cycle should be repeated every 3–4 weeks. Two sessions per week of medium-low fluences, associated with soft-peeling and topical home therapy, allow to obtain an excellent control of the phenomenon and to prevent cysts formation and scars.

The most serious forms of acne that do not respond to normal medical therapies can be greatly benefited from the use of pulsed light in photodynamic technique (PDT) with photosensitizers such as 5 alpha levulinic acid (5 ALA) in a 3–5% solution to be applied 2–6 h before; subsequently, the skin area is exposed to the pulsed light of 630 nm with fluence from 25 to 75 j/cm^2 and TRT from 10 to 30 ms, every 3 weeks. Clinical results after 3–4 cycles are characterized by long-term disappearance of inflammatory and infectious skin manifestations caused by *Propionibacterium acnes* with a marked improvement in skin texture [5–7].

30.5 Vascular Lesions

IPL can be used for a wide range of vascular lesions, from capillary malformations (port-wine stains) to telangiectasias of the face and lower limbs [8]. Some of the device filters for vascular lesions frequently encompass wavelengths that are readily absorbed by melanin, so overly aggressive settings can result in absorption in darker skin types resulting in blistering and postinflammatory hyperpigmentation [9]. With these concerns, many devices offer filters which allow for omission of the longer wavelengths which can be chosen for achieving lower melanin absorption. Additionally, newer models incorporate more than one filter which block both shorter and longer wavelengths, resulting in a narrowband IPL that emits broadband light over a narrow wavelength range such as 500–600 nm [9]. The wavelength range of these narrowband IPLs may allow safer treatment of vascular lesions.

IPL uses the mechanism of photothermolysis and specific wavelengths to selectively destroy blood vessels by targeting hemoglobin within the erythrocytes contained in the vessels. Radiations of lesser wavelength of 550–600 nm are better absorbed by the hemoglobin contained in the small superficial vessels, while the wavelengths between 600 and 1100 nm are used for larger and deeper venous vessels because they contain deoxyhemoglobin. Therefore, longer wavelength cutoff filters are used to treat deeper and larger blood vessels. Lower cutoff filters (515 or 550 nm) are effective in treating smaller-caliber vessels, but interact more readily with epidermal and dermal melanin and should be reserved for treating fair-skinned individuals. Energy densities should be set appropriate to the lesion being targeted. Larger and deeply situated vessels require more energy to heat up (50–75 j/cm^2)and smaller vessels heat more quickly and can be treated with lower fluences (25–45 j/cm^2) [10].

Pulse duration must be less than the TRT of the chromophore (generally between 0.5 and 88.5 ms) in order to spare the surrounding tissue from excess heating [10]. Varying intervals between pulses range within 10–500 ms; the delay between pulses allows the non-target tissues to cool down while the heat is retained in the target of interest [10].

Single or multiple pulses can be used. Usually a first pulse with duration lower than the TRT is given to the vessels to hit; this induces only a warming of hemoglobin and its subsequent transformation into methemoglobin; it follows a delay (interval between the individual pulses) of

1–300 ms, less than the TRT of the treated vessels, but superior to the TRT of the surrounding tissues. This delay allows the epidermis cells and smaller vessels to cool down between pulses while the heat is retained in the larger (target) vessels, resulting in selective thermal damage. A pulse longer than the first is followed which brings the temperature to coagulative necrosis of the red blood cells and consequent intraluminal thrombosis. The necrotic material is then eliminated by the macrophages [11, 12].

30.6 Rosacea

A significant reduction in blood flow, telangiectasia, and erythema in the irradiated area can be observed with IPL [3, 13]. 570 nm filter, 3–4.5 ms pulse duration, 40–50 j/cm^2, and 60 ms delay can be used. There are case reports, where the patient is first treated topically with azelaic acid at 15% and then undergoes an IPL session [3, 10].

30.7 Telangiectasia

Telangiectasia corresponds to dilated capillaries, venules, or arterioles with a diameter between 0.1 and 1.0 mm and appears as bluish-red color lines on the skin. The lesions can affect not only the epidermis, but also the mucous membranes. They are favored by repeated inflammatory processes, genetic predisposition, and hormonal variations such as pregnancy and atrophy of skin tissue. IPL is able to determine the disappearance of telangiectasia in most of cases after 1 to 10 treatment sessions, using low filters (570 nm), pulses of 2.5–6 s, fluences between 21 and 50 j/cm^2, and delay of 20–30 ms. For dilated vessels > 1 mm, it is better to use a 590 nm filter, 3 + 3 + 3 ms per pulse (triple-pulse mode), delay of 20 ms, and fluence of 50 j/cm^2 [12, 14].

30.8 Port-Wine Stains

Port-wine stains are capillary malformations of the capillaries of the papillary dermis and the superficial reticular dermis, characterized by reddish-purple macules that typically appear on the face or neck. IPL can be useful in the treatment of these lesions that do not respond to the pulsed dye-laser, thanks to the excellent penetrative capacity, obtaining a clinical improvement or complete disappearance of the lesion in most of cases. Despite the efficacy of IPL, a subset remains resistant to treatment, particularly those lesions in the V2 dermatome where deeper vessels are located [15]. From 1 to 5 sessions with 2.5–5 ms pulse, fluence 20–70 j/cm^2 should be considered for this indication [15–17].

30.9 Venous Malformations

They correspond to malformations of large or medium thick walled veins, located deeply in the dermis and/or subcutaneous tissue. Satisfactory results are obtained in half of the patients with venous malformations after 1–10 treatments using pulses of 2.5–8.7 ms and fluences varying from 32 to 90 j/cm^2 [18–20].

30.10 Poikiloderma of Civatte

Poikiloderma of Civatte is characterized by areas of cutaneous atrophy, fine spider telangiectasia, and reticulated brownish pigmentation, located in the lateral regions of the neck and in the upper thoracic region due to prolonged exposure to sunlight. The chin is always spared. From the histological point of view, the dilated vessels are mainly postcapillary venules located in the superficial dermis, while the pigmentation depends on an accumulation of melanin in the basal layer of the epidermis and in some melanophages located in the papillary dermis. IPL is particularly suitable for the treatment of superficial poikiloderma of Civatte and extensive erythrosis due to its larger spot size. IPL can correct both vascular alterations and pigmentations at the same time, taking advantage of its broad spectrum of emission, or act only on the telangiectatic component, choosing filters that eliminate low wavelengths. Poikiloderma of Civatte can be treated with 3–5 treatments with variable pulses at 2.4–4 ms, range of 10 ms, and fluences between 22 and 42 j/cm^2 [20–22].

30.11 Skin Photorejuvenation

Skin aging is caused by intrinsic aging (chrono-aging) and extrinsic aging (photoaging due to exposure to UV rays and inadequate life style such as alcohol intake, smoking, and sedentary life).The photoaging appears in different forms, but the two main aspects that characterize it from the beginning are the laxity of the skin and the appearance of fine wrinkles.

The photorejuvenation with IPL was developed around 2000 with Goldberg and Bitter [23–25], who had clinically observed that serial treatments with IPL on the face determined an improvement of the texture from the skin, a reduction both in telangiectasias and in hyperpigmentations. Subsequently, the histological demonstration of reduction of dermal elastosis was added, with deposition of neo-collagen type I and III and a reduction of the inflammatory infiltrate in the dermal papillae at a distance of 3–6 months from a cycle of treatments [26]. Melanin and hemoglobin are always used as targets, offering pulse durations slightly higher than the TRT of these targets; thus there is a thermal diffusion which leads to a thermal effect responsible for the production of new collagen.

The new apposition of collagen fibers takes place through a double mechanism: (1) direct by thermal stimulation on the fibroblast and (2) indirect with heat denaturation of the collagen and elastic fibers and consequent fibroblast stimulation. Furthermore, the damaged vessels release cytokines which amplify the signal to the fibroblast. Furthermore, the denaturation of the collagen and elastic fibers implies the folding and the shortening of these fibers, which clinically manifest with an improvement of the texture [27].

The skin areas to be treated with IPL must be healthy, and not tanned. The patient in the month preceding the treatment must not expose himself to tanning lights and should not use self-tanning creams. The use of sunscreens before and after the treatment is recommended. Areas sensitive to herpetic recurrence require antiviral prophylaxis.

Filters of 515 to 590 nm are used alone or alternated in the same session according to the equipment used. The 560 nm filter is present in all IPL on the market and is generally used alone with a very variable fluence from 17 to ~ 40 j/cm^2, pulse of 2–10 ms, single or multiple pulses and TRT up to 10 ms. The frequency of the sessions is monthly, and usually a double pass is performed, the first of medium intensity on the face, neck, and breast, and the second at high intensity on the areas with greater skin aging. The 590 nm and 560 nm filters are used for vascular lesions or for dark skinned individuals, whereas the 515 nm filter might be used to treat hyperpigmentations in lighter skin subjects [28]. The sessions required vary from patient to patient and from the individual response, generally a cycle includes 5 to 8 treatments and 2 to 4 annual sessions for maintenance of the results.

The most common side effects occur in the post-treatment are: erythema, burning, and edema, which disappear in the following 72 h. Hyperpigmentation or hypopigmentation may appear even after 2–4 days and disappear within 3–12 months.

In very sensitive skins treated with inadequate fluences, erosions can be developed on the treated area, which must be left to heal spontaneously. The appearance of hypertrophic and keloid scars is rare.

30.12 Hair Removal

Treatment of hypertrichosis is one of the main indications of IPL. The absorption of the light radiation by the melanin contained in the hair follicles gives an excellent epilating effect.

The follicles most susceptible to the action of IPL are the terminal ones with hairs rich in eumelanin (brown or dark hairs); among these are the anagen follicles with very pigmented bulbs that represent the best target of IPL especially those in initial anagen having newly formed pigmented bulbs superficially located in the dermis.

The excellent penetration capacity of IPL allows both to reach the follicular structures and to act on hair with a lower content of eumelanin. Damage and/or destruction of the bulbar region is easily obtained by direct absorption of the light

and subsequent heating of the melanosomes contained in the bulbar keratinocytes.

To irreversibly damage the hair follicle, it is necessary to take advantage of the absorption of the radiation by the extremely pigmented corneocytes of the hair, located in the isthmus; their heating allows the transmission of a part of the heat to the adjacent structures, with possible coagulation damage of the surrounding keratinocytes of the bulge. This effect is obtained by modulating the times of the single pulses, which must be less than the TRT of the bulb and higher than the TRT of the isthmus zone; the interval between the pulses is lengthened in order to favor the cooling of the epidermis.

After the IPL treatment, all the anagen follicles present in the irradiated area are converted in the telogen phase. A small part of these will suffer irreversible damage such as to no longer allow their growth, but most follicles will return to anagen after a rest phase (telogen/kenogen); as a result of the alterations caused to the regenerative structures, the hairs that will be born from the new follicles will be smaller, thin, short, and less pigmented than the previous ones. This explains why more treatment sessions will be needed, spaced over time to get good results.

Several studies have established the hair removal efficacies of IPL systems that emit a broad spectrum of longer wavelengths; however, the clearance rate and satisfaction level vary greatly. The advantages of the IPL devices compared to lasers include lower cost and the convenience of larger light guides that enable treatment of larger areas [29]. 625–1200 nm filter, with a pulse between 1.5 and 3.5 ms, fluence between 34 and 55 j/cm^2, and interval between pulses of 20–50 ms can be used [4, 29, 30]. Epilation takes about 3 to 9 sessions, depending on the area to be treated (~ 3 sessions for the face and 9 for the legs). Between one session and another, 4–5 weeks must pass, and the duration of the sessions varies from a few minutes to an hour depending on the areas to be treated.

In rare cases, during or after a treatment in the facial area, a "paradoxical effect" can be observed, which consists in the appearance of new, dark, terminal hairs in the skin areas immediately surrounding the irradiated ones [31]. When correctly set, epilation with IPL does not damage the surrounding tissues, it is not painful, and the patient only perceives a sensation of heat; in sensitive skin, a slight redness may appear. When the parameters are not correctly adjusted, possible complications are epidermal burning with blisters, erosion, and crust formation followed by postinflammatory hypo- and/or hyperpigmentation [31]. Tanned skin contraindicates the treatment; in this case, 3–4 weeks must pass before being subjected to treatment.

References

1. Mühlbauer W, Nath G, Kreitmair A. [Treatment of capillary hemangiomas and nevi flammei with light]. Langenbecks Arch Chir. 1976;Suppl:91–94.
2. Goldman MP, Eckhouse S. Photothermal sclerosis of leg veins. ESC medical systems, LTD Photoderm VL Cooperative Study Group. Dermatol Surg Off Publ Am Soc Dermatol Surg Al. 1996;22(4):323–30.
3. Wat H, Wu DC, Rao J, Goldman MP. Application of intense pulsed light in the treatment of dermatologic disease: a systematic review. Dermatol Surg Off Publ Am Soc Dermatol Surg Al. 2014;40(4):359–77.
4. Babilas P, Schreml S, Szeimies R-M, Landthaler M. Intense pulsed light (IPL): A review. Lasers Surg Med. 2010;42(2):93–104.
5. Chang S-E, Ahn S-J, Rhee D-Y, et al. Treatment of facial acne papules and pustules in Korean patients using an intense pulsed light device equipped with a 530- to 750-nm filter. Dermatol Surg Off Publ Am Soc Dermatol Surg Al. 2007;33(6):676–9.
6. Choi YS, Suh HS, Yoon MY, Min SU, Lee DH, Suh DH. Intense pulsed light vs. pulsed-dye laser in the treatment of facial acne: a randomized split-face trial. J Eur Acad Dermatol Venereol JEADV. 2010;24(7):773–80.
7. Lee WJ, Jung HJ, Kim JY, Lee S-J, Kim DW. Effect of photodynamic therapy on inflammatory acne using 3% liposomal 5-aminolevulinic acid emulsion and intense-pulsed light: A pilot study. J Dermatol. 2012;39(8):728–9.
8. Adamič M, Pavlović MD, Rubin AT, Palmetun-Ekbäck M, Boixeda P. Guidelines of care for vascular lasers and intense pulse light sources from the European Society for Laser Dermatology. J Eur Acad Dermatol Venereol. 2015;29(9):1661–78.
9. Garden BC, Garden JM, Goldberg DJ. Light-based devices in the treatment of cutaneous vascular lesions: An updated review. J Cosmet Dermatol. 2017;16(3):296–302.
10. Kassir R, Kolluru A, Kassir M. Intense pulsed light for the treatment of rosacea and telangiectasias.

J Cosmet Laser Ther Off Publ Eur Soc Laser Dermatol. 2011;13(5):216–22.
11. Bjerring P, Christiansen K, Troilius A. Intense pulsed light source for treatment of facial telangiectasias. J Cosmet Laser Ther Off Publ Eur Soc Laser Dermatol. 2001;3(4):169–73.
12. Clementoni MT, Gilardino P, Muti GF, et al. Intense pulsed light treatment of 1,000 consecutive patients with facial vascular marks. Aesthet Plast Surg. 2006;30(2):226–32.
13. Hofmann MA, Lehmann P. Physical modalities for the treatment of rosacea. J Dtsch Dermatol Ges J Ger Soc Dermatol JDDG. 2016;14(Suppl 6):38–43.
14. Clementoni MT, Gilardino P, Muti GF, et al. Facial teleangectasias: our experience in treatment with IPL. Lasers Surg Med. 2005;37(1):9–13.
15. Adatto MA, Luc-Levy J, Mordon S. Efficacy of a novel intense pulsed light system for the treatment of port wine stains. J Cosmet Laser Ther Off Publ Eur Soc Laser Dermatol. 2010;12(2):54–60.
16. Ho WS, Ying SY, Chan PC, Chan HH. Treatment of port wine stains with intense pulsed light: a prospective study. Dermatol Surg Off Publ Am Soc Dermatol Surg Al 2004;30(6):887–890; discussion 890–891.
17. Raulin C, Weiss RA, Schönermark MP. Treatment of essential telangiectasias with an intense pulsed light source (PhotoDerm VL). Dermatol Surg Off Publ Am Soc Dermatol Surg Al 1997;23(10):941–945; discussion 945–946.
18. Campolmi P, Bonan P, Cannarozzo G, et al. Intense pulsed light in the treatment of non-aesthetic facial and neck vascular lesions: report of 85 cases. J Eur Acad Dermatol Venereol. 2011;25(1):68–73.
19. Li D-N, Gold MH, Sun Z-S, Tang A-R, Wang H-B, Sheng-Kang L. Treatment of infantile hemangioma with optimal pulse technology. J Cosmet Laser Ther Off Publ Eur Soc Laser Dermatol. 2010;12(3):145–50.
20. Raulin C, Greve B, Grema H. IPL technology: A review. Lasers Surg Med. 2003;32(2):78–87.
21. Scattone L, de Avelar Alchorne MM, Michalany N, Miot HA, Higashi VS. Histopathologic changes induced by intense pulsed light in the treatment of poikiloderma of Civatte. Dermatol Surg Off Publ Am Soc Dermatol Surg Al. 2012;38(7 Pt 1):1010–6.
22. Weiss RA, Goldman MP, Weiss MA. Treatment of poikiloderma of Civatte with an intense pulsed light source. Dermatol Surg Off Publ Am Soc Dermatol Surg Al 2000;26(9):823–827; discussion 828.
23. Goldberg DJ, Cutler KB. Nonablative treatment of rhytids with intense pulsed light. Lasers Surg Med. 2000;26(2):196–200.
24. Bitter PH. Noninvasive rejuvenation of photodamaged skin using serial, full-face intense pulsed light treatments. Dermatol Surg Off Publ Am Soc Dermatol Surg Al 2000;26(9):835–842; discussion 843.
25. Goldman MP, Weiss RA, Weiss MA. Intense pulsed light as a nonablative approach to photoaging. Dermatol Surg Off Publ Am Soc Dermatol Surg Al 2005;31(9 Pt 2):1179–1187; discussion 1187.
26. Feng Y, Zhao J, Gold MH. Skin rejuvenation in Asian skin: the analysis of clinical effects and basic mechanisms of intense pulsed light. J Drugs Dermatol JDD. 2008;7(3):273–9.
27. Sadick NS, Weiss R, Kilmer S, Bitter P. Photorejuvenation with intense pulsed light: results of a multi-center study. J Drugs Dermatol JDD. 2004;3(1):41–9.
28. DiBernardo BE, Pozner JN. Intense pulsed light therapy for skin rejuvenation. Clin Plast Surg. 2016;43(3):535–40.
29. Ismail SA. Long-pulsed Nd:YAG laser vs. intense pulsed light for hair removal in dark skin: a randomized controlled trial. Br J Dermatol. 2012;166(2):317–21.
30. Gan SD, Graber EM. Laser hair removal: a review. Dermatol Surg Off Publ Am Soc Dermatol Surg Al. 2013;39(6):823–38.
31. Radmanesh M. Paradoxical hypertrichosis and terminal hair change after intense pulsed light hair removal therapy. J Dermatol Treat. 2009;20(1):52–4.

Vascular Lasers: Tips and Protocols

31

Pier Luca Bencini and Stefania Guida

31.1 Introduction

First applications of lasers in vascular lesions have been performed in 1960s on a port-wine stains (PWSs) with a ruby laser [1]. After the introduction of selective photothermolysis theory [2], new laser devices, more suitable for vascular surgery, were introduced. Selected chromophores have been identified, representing molecules into tissues that can selectively absorb specific wavelengths, converting the light energy to thermal energy after the absorption. Therefore, the absorption of an appropriate wavelength can selectively damage or destroy a chromophore. After that, the heated body tends to cool while delivering heat: the thermal relaxation time (TRT) is the time interval required for the target to deliver 50% of heat to surrounding tissues. The laser pulse duration should be shorter or equal than the TRT of the target in order to minimize the thermal damage to surrounding tissues and to avoid scarring.

In order to identify specific targets (chromophores) and wavelengths employed for vascular lesions, the following considerations should be considered:

- *Chromophore*: The main chromophore is oxyhemoglobin, with main absorption peaks at 542 and 577 nm, and also a little peak at 1064 nm. On the other hand, for melanin (that should be considered as the competitor chromophore), the longer the wavelength the lesser the absorption. Therefore, for darker phototypes longer wavelengths and longer intervals and pulse durations should be employed to avoid epidermal damage and post-treatment hyperpigmentation [3]. However, other blood chromophores, such as metahemoglobin, produced during laser passes and deoxyhemoglobin, present in the leg veins, should also be considered to efficiently treat vascular lesions. These chromophores absorb wavelengths also in the 800–1200 spectrum [4, 5].
- *Wavelengths*: The longer the wavelength, the deeper the penetration into the dermis, thus lasers emitting longer wavelengths are more suitable for thicker and deeper lesions. However, the laser energy absorbed by oxyhemoglobin decreases, and higher fluencies are needed to compensate for the lower absorption.

P. L. Bencini
ICLID, Istituto di Chirurgia e Laser-Chirurgia in Dermatologia, Milan, Italy
e-mail: pl.bencini@iclid.it

S. Guida (✉)
ICLID, Istituto di Chirurgia e Laser-Chirurgia in Dermatologia, Milan, Italy

Dermatology Unit, Department of Surgical, Medical, Dental and Morphological Science with Interest Transplant, Oncological and Regenerative Medicine, University of Modena and Reggio Emilia, Modena, Italy

M. Fimiani et al. (eds.), *Technology in Practical Dermatology*,
https://doi.org/10.1007/978-3-030-45351-0_31

In addition, other factors should be taken into account in order to perform a proper vascular laser treatment:

1. *Vessel location and skin site*. The depth of the lesions is important since superficial lesions respond better to lasers emitting shorter and more selective wavelengths, such as 532 and 595 nm, while deeper ones should be treated by longer near-infrared lights. However, the vessels localized in the deep dermis and hypodermis poorly respond to trans-epidermal laser irradiation. For example leg veins, unlike the telangiectasias of the face, have a muscular layer, thicker walls, and a very high hydrostatic pressure, thus requiring higher energies to perform an efficient thermocoagulation. Furthermore, leg veins are bluer, deeper, and contain less oxyhemoglobin and more deoxyhemoglobin.
2. *Chromophore and target*. Unlike for tattoo and other pigmented lesions, where chromophore and target overlap, in vascular surgery the chromophore (oxyhemoglobin) differs from the target (the vessel wall). Therefore, the chromophore is used as a kind of optical firelighter, allowing the thermal energy produced within the red blood cells to diffuse through the blood and to damage the walls of the vessels, producing thrombosis. Accordingly, different laser pulse lengths must be considered taking into account the blood flow and the different diameters of the vessels. In detail, the larger the vessels, the longer the required pulse durations [6].
3. *Blood flow*. The target in vascular lesions is dynamic; as blood flows into the vessels, new, untargeted blood takes away the heat induced by light absorption, thus protecting the vessel by thermal damage induced. Therefore, to increase the heated volume of the blood, large spot sizes are recommended.

31.2 Epidermal Cooling

Epidermal cooling is required for the protection of epidermis from overheating during laser coagulation of dermal vessels. Therefore, the use of a cooling system is mandatory for epidermal protection in order to avoid damages to keratinocytes and melanocytes, as well as pigmentary and textural changes. Among different cooling devices, cryogen molecules, devices blowing precooled air on the epidermis, and cold sapphire contact handpiece can be employed. However, although a cooling device is necessary, it should be kept in mind that it decreases skin temperature thus inducing vasoconstriction, thus potentially reducing the efficacy of laser treatment.

31.3 Main Laser Sources for Vascular Surgery

31.3.1 Pulsed Dye Laser (PDL)

PDL has been the first laser based on the selective photothermolysis theory. It is considered to be the laser of reference for safe treatments of many vascular lesions, such as PWSs, facial telangiectasia, hemangioma, and poikiloderma of Civatte. PDL emits a yellow light due to its lasing medium: the rhodamine 6G dye. First devices emitted a pulsed beam at 585 nm, employing a pulse duration of 450 ms, partially limiting results. In addition, the short penetration of the laser light (about 0.2 mm below the dermo-epidermal junction) was not sufficient to target many vascular lesions and its short pulse duration caused vessel disruption resulting in a cosmetically embarrassing, long-lasting, post-treatment purpura. To date, PDLs have a longer wavelength (595), longer pulse durations (1.5–40 ms), and larger spot sizes, allowing a deeper penetration and a vascular coagulation with a more comfortable post-treatment [7].

31.3.2 Neodymium:Yttrium-Aluminum-Garnet (Nd:YAG) Laser

Nd:YAG laser has the primary wavelength of 1064 nm. This wavelength is characterized by a deeper penetration, allowing a coagulation effect at a 5–6 mm of depth [8]. Despite an absolute

lower absorption of this wavelength by hemoglobin, the ratio of melanin to blood absorption is similar at both 585 and 1064 nm. On the one hand, an increased fluence should be used to compensate the lack of hemoglobin selectivity. On the other hand, the absorption of the 1064-nm wavelength by blood is higher than that of the surrounding dermis, thus leading to a selective and relatively safe treatment of deeper blue and larger vessels [9–11]. However, to avoid potential thermal damages such as blistering, crusting, pigmentary, and textural abnormalities and scarring, using a cooling system is mandatory.

31.3.3 Doubled 532-nm Nd:YAG Laser

Nd:YAG laser with a primary 1064 wavelength can be doubled with a second 532-nm wavelength through a crystal of potassium titanyl phosphate (KTP). The 532-nm light is preferentially absorbed by oxyhemoglobin although this wavelength is too short to penetrate into the dermis and coagulate medium deep vessels. As a consequence, KTP is employed on small and superficial vessels. Importantly, in case of treatment of pigmented skin, caution should be made because its interaction with epidermal melanin can lead to dyschromia and textural changes, potentially related to thermal damage of the epidermis.

31.4 Operative Management

31.4.1 Patients' Selection and Main Contraindications to Vascular Laser Surgery

Before vascular laser treatment, patients should be evaluated to exclude the presence of potential contraindications to treatment such as keloids, unstable vitiligo, lichen ruber planus, psoriasis, and a history of photoinduced dermatoses, immunosuppressive drugs use. Furthermore, patients taking oral isotretinoin or other oral retinoids, patients with unrealistic expectations, or not compliant patients should also be adequately selected.

31.4.2 Pre-laser Treatment Care

Exposure to UV irradiation prior to and after laser treatment should be avoided to reduce the risk for side effects, especially thermal burns and dyspigmentation [12]. Sunscreens are therefore recommended at least 4 weeks prior to the first treatment [13]. The skin area to be treated should be make-up free.

Laser treatment can be painful. However, in most cases, local anesthesia is not required. In addition, anesthesia can be avoided in adult patients because pain is the best early warning system to prevent side effects caused by heat destruction.

31.4.3 Post-laser Treatment Care

After alexandrite, diode, or millisecond Nd:YAG lasers, the treated skin can show mild erythema and edema, whereas specific parameters of PDL treatment can induce purpura with surrounding tissue hyperemia. Therefore, some advices are herein reported [14]:

- To prevent or reduce swelling, post-treatment cooling with ice packs (or cold air) is suggested on larger areas such as cheeks or neck after the laser treatment until reduction of pain or redness.
- If treatment is performed close to or around the eye, periocular swelling can occur. Thus, patients should be instructed to sleep with an extra pillow in order to reduce the edema.
- Sun exposure should be avoided to prevent post-inflammatory hyperpigmentation.
- The treated area is delicate and must be handled with care during the initial healing phase (7–10 days), without scratching. A non-irritating soap can be used on the treated areas and a bland moisturizer should be applied to the areas of laser treatment.
- Make-up can be used immediately after treatment except if blistering occurs.
- In case of blistering with open wounds, petrolatum jelly should be applied.
- Showers are allowed, but prolonged bathing and sauna are not advised.

It may take a few weeks for bruising or scabs to disappear and to notice fading of the primary vascular lesions. During the ensuing weeks, the absorption of coagulated treated vessels will occur by the surrounding tissue. The response to the treatment should not be evaluated for several weeks until the healing process is complete. Leg vein results may not be visible until 2–3 months after treatment.

31.4.4 Side Effects

Complications related to laser treatment are limited by operator education and experience [14].

- *Pain*. Each pulse laser can be associated to a burning sensation, thus producing a minimal to moderate discomfort. However, pain is a marker of possible side effects, therefore anesthesia should be avoided in adults.
- *Purpura, bruising*. Immediately after laser session, gray or blue-black discoloration can occur in the treated area. This discoloration usually fades over the next 7–10 days.
- *Swelling*. A few minutes after laser treatment, both erythema and edema can occur, above all when the areas under eyes and neck are treated. Swelling decreases within 3–5 days when ice is regularly applied. Parallel and post-cooling can diminish the amount of edema.
- *Discoloration, blisters, or crusts develop rarely*. Gray or pale white discoloration of the epidermis is a sign of early dermal damage indicating an inappropriate high radiant exposures. This sign will last a few seconds and it is followed by blister formation, epidermal disruption, and necrosis. However, this effect can be immediate or delayed, therefore, the treated test spot should be observed for at least 5 min before proceeding with full treatment. Reduction of radiant exposure, intense cooling, and prolongation of the pulse duration should be taken into account. These effects can require 1–2 weeks to resolve.
- Infection can be predicted by the appearance of swelling, redness, crusting, pain, and fever. Topical antiseptics or oral antibiotics should be used.
- Reactivation of herpes simplex when areas of recurrences are treated. Thus, prophylactic oral virostatic therapy is recommended when the patient has frequent recurrences (more than 6 per year), starting the day before the laser treatment.
- *Hyperpigmentation*, usually fading within 2–6 months, occurring most commonly in patients with darker skin type (Fitzpatrick III–V). Sun exposure contributes to the worsening of this effect. Topical bleaching cream, such as hydroquinone, can be used.
- *Hypopigmentation*, which is mostly caused by overtreatment. Skin lightening usually repigments within 3–6 months. However, it could be persistent, most frequently on the neck, legs, and chest.
- Skin texture changes are usually related to overtreatment—in cases of excessive radiant exposures or when overlapping laser spots are used.
- Scarring, mainly related to overtreatment, and mostly occurring with Nd:YAG laser due to the deepest laser light penetration. Following all advised post-operative instructions can reduce this adverse event.

31.5 Main Vascular Disorders Responsive to Vascular Surgery

31.5.1 Vascular Malformations: PWSs

PWSs represent congenital low flow vascular skin malformations, involving 0.3% of the population [15]. At birth, PWSs are superficial and they appear as light pink flat patches. With passing time, they do not resolve spontaneously and tend to become dark purple in color, in relation to progressive vessel ectasia. Nodules and plaques can develop, in almost two-thirds of middle-aged patients, due to deeper hypertrophy [16, 17]. Considering its vascular selectivity, 585-nm PDL treatments have been considered the gold standard in therapy for vascular birthmarks [18, 19]. However, since several factors may influence the response to PDL treatment, the results are sometimes unpredictable. As a matter of fact, the fol-

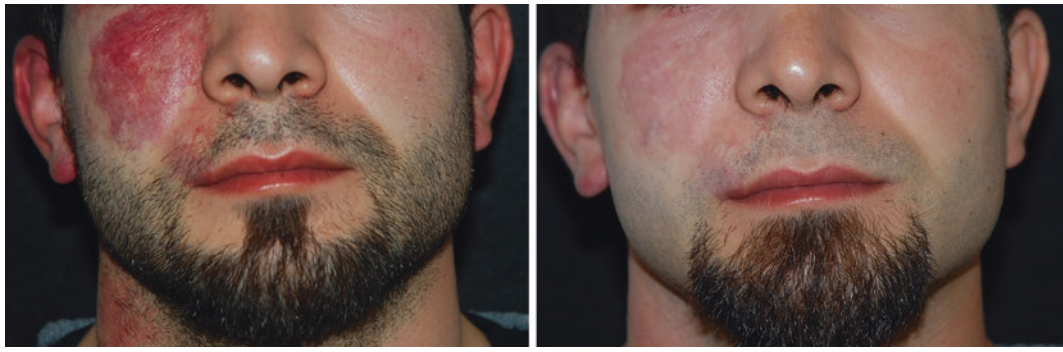

Fig. 31.1 Port-wine stain located in the distribution area of the second branch of the trigeminal nerve, before and after 595-nm dye laser treatment

lowing aspects should be considered before therapy:

- *Videodermoscopy pattern*. Two different PWSs videodermoscopic patterns have been described. Type 1 is characterized by blobs of tortuous, superficial, enlarged capillary loops, whereas in type 2 typical rings and arched lines related to ectatic vessels in the superficial horizontal vascular plexus are observed. Intuitively, patients with the more superficial type 1 pattern respond better to flashlamp-pumped pulsed dye laser treatment [20]. However, a type 3, showing combined features between type 1 and 2, has also been described and associated with a poor clinical response [21].
- *Skin site*: PWSs arising on the extremities have shown a poor response to laser treatment, probably due to different blood deoxygenation and gravitational effects [22]. Some other anatomical areas may influence the response to treatment: centrofacial areas and the skin region corresponding to the dermatome V2 respond less than the other facial sites, probably for vessels located more deeply [23, 24].
- *Size*: Results of laser treatment depend on the extent of the PWSs. Accordingly, the larger the extent (more than 60 cm^2) the worse the result, as compared to smaller lesions [25].
- *PWS evolution*: hypertrophy and thickness occurring during the typical evolution of the PWS, make the conventional 585 dye laser treatment more difficult in adults, with variable degrees of clearing, even after several dye laser sessions [26]. Therefore, the evolution of PDL devices, exploiting the 595-nm wavelength in a longer pulse duration, has enabled an increased penetration of the light, although maintaining a good vascular specificity [27, 28], thus leading to an increased efficacy in these difficult-to-treat PWSs (Fig. 31.1).

In addition, the cryogen cooling protects the epidermis from overheating, allowing a safe use of higher fluencies and accelerating the PWSs clearance [29–32]. Therefore, PDL still represents the gold standard treatment for the majority of PWSs [33], even if results on nodular PWSs still remain unpredictable [34] and many of these lesions fail to fully respond. On the other hand, multiple passes or pulse-stacking techniques have been introduced to improve results [35–37]. According to Rajaratnam [37], all these techniques may be useful but deserve further investigations with randomized prospective studies and histological analysis to confirm the increased depth of vascular injury.

Other light sources have been applied to increase the resolution of difficult PWSs. For instance, intense broad-spectrum pulsed light (IPL) [38, 39], Alexandrite 755-nm laser, and 1064-nm Nd:YAG long-pulsed laser have been also evaluated [20, 40].

In particular, 1064-nm Nd:YAG long-pulsed laser has been recently used on PWSs because of its ability to penetrate deeper [41]. Unfortunately, the high energies required for this laser treatment can cause scarring due to epidermal overheating and burning [41].

However, methemoglobin formation stimulation can be performed in order to obtain a wide vascular damage for difficult-to-treat PWSs, with a lower incidence of complications. A combination system of a 595-nm laser and a 1064 Nd-YAG wavelength [42, 43] or a dual-wavelength approach with 585-nm PDL laser and 800-nm diode laser can be used to achieve this effect through photoinduced oxidation [44].

Photodynamic therapy is a relatively new approach in the treatment of PWS. In this case, an exogenous chromophore-like porphyrin derivative is employed and it concentrates in the ectatic capillaries. Subsequent irradiation by either coherent or noncoherent light of appropriate wavelength generates oxygen-derived free radicals in the presence of the porphyrin derivative and oxygen, selectively damaging the capillary wall [45].

31.5.2 Infantile Hemangiomas (IH)

IH are benign vascular tumors that can be distinguished from PWSs. The main clinical hallmark of hemangiomas is their typical evolution, characterized by a proliferative early phase lasting several months, gradually leading into an involutive phase. However, the spontaneous involution may be incomplete, thus 15–20% of the lesion may not disappear [46]. Moreover, residual evidence with scar formation, fibrofatty masses, atrophic wrinkling, yellowish discoloration, and telangiectasias is usually seen after complete involution.

Treatment. The majority of IH are small. However, in 10–15% of cases (e.g., segmental and multifocal infantile hemangiomas, or occurring in the periocular, airway, or perineal area, when complications such as ulceration are present), treatment is mandatory.

According to the American Academy of Dermatology [47], the treatment should:

- Prevent or reverse life-threatening complications.
- Prevent disfigurement left by residual skin changes.
- Minimize psychological stress.
- Avoid scarring process.
- Prevent or treat ulcerative lesions to minimize complications such as infection, pain, or scarring.

Large cervicofacial segmental hemangiomas can be associated with other malformations, that should be excluded with ultrasound or magnetic resonance imaging [48].

Since 2008, oral β-blockers, mainly propranolol, have been successfully applied to the treatment of the majority of IH [49]. Early studies revealed that a combination of laser and propranolol may be more effective than propranolol alone for superficial lesions [50].

Laser treatment. PDL treatment is effective for the precursor lesions and for small superficial IH; this laser should be used at the earliest sign of IH and as soon as possible in the proliferative phase [51].

Early treatment with the 595-nm PDL can also effectively and safely reduce proliferative growth of superficial IH located in difficult skin areas, such as the eyelid [52]. Furthermore, quick responses can be observed in involuting superficial lesions, with a faster resolution than that observed during the spontaneous course of the disease, without scarring, atrophy, or hypopigmentation [53]. PDLs are also used to treat ulcerations and residual skin defects [54]; however, mixed or deep IH hardly respond to this treatment alone, showing only lightening of the most superficial area. Alternatively, longer wavelengths, such as Nd:YAG laser, have to be tried to increase the depth of light irradiation [55]. Recently, dual long-pulsed 595 dye/Nd:YAG lasers have been applied to IF with excellent results and no recurrence after a 6-month follow-up, in 18 out of 25 cases [56].

Finally, ablative and non-ablative fractional lasers have been recently proposed as potential interesting options for atrophic and scarring residual IH [57, 58].

31.5.3 Telangiectasias

Facial telangiectasia can be treated by means of several lasers and light sources (KTP, PDL, Nd:YAG, and IPL) with associated advantages

Fig. 31.2 Telangiectasias of the cheek, before and after 595-nm dye laser treatment

and limitations. However, classic PDL seems to have a superior clearance rate compared with other sources, but disfiguring bruising represents an important side effect in short-pulse PDL. Indeed, a longer pulse (10 ms) and multiple passes are recommended to have an effective purpura-free treatment [59].

An alternative treatment of facial telangiectasias, shown to be effective, is IPL [60]. However, long-pulse PDL treatments seem to be superior than IPL treatments and it has been reported that the majority of patients preferred the long PDL treatments because of superior efficacy and less treatment-related pain [61, 62].

However, the Nd:YAG laser is indicated for treatment of deeper, bluish veins and of a broad range of vessel diameters in pigmented skin types. To avoid overheating of the epidermis and textural changes, an efficient cooling system is required [63].

31.5.4 Rosacea-Associated Telangiectasia

Rosacea is a dermatosis of the face with a chronic clinical course and it is characterized by flushing, non-transient erythema telangiectasia, papules, pustules, and inflammatory nodules. Long-pulsed duration, 595-nm PDL is proven to be effective for the treatment of both erythema and telangiectasia with minimal side effects, avoiding long-term complications (Fig. 31.2) [64–66]. However, treating diffuse erythrosis is challenging, thus requiring a high number of sessions.

Also, IPL seems to be safe and effective. It has been demonstrated that IPL can be successfully used for a long-term clearance of telangiectasia associated with rosacea [67]. However, no significant difference was noted between PDL and IPL treatments [68].

Finally, we suggest the following practical key points for a correct laser treatment [69]:

1. First of all, a consultation is required to discuss the expectations of the patient. In case of rosacea, clarify whether the priority of the patient is the treatment of telangiectatic vessels, of erythema, or both. Make clear that flushing does not respond to laser treatment.
2. Inform patients that several laser sessions might be required.
3. Avoid, whenever possible, topical anesthesia for its vasoconstrictor action.
4. Laser parameters should be adapted on the size of the vessels to be treated.
5. Hold the handpiece perpendicular to the skin surface.
6. Both erythema and telangiectasia associated with rosacea can be treated with PDL or IPL. Regarding PDL treatment, preferably use larger spots (7–10 mm in diameter), uniformly distributed on the skin surface.

7. Ala nasi and alar creases should be treated with caution because of the risk of atrophic scars. The lowest fluence suggested should be employed. However, fluence may be increased in case of persistence of the vessel.
8. For large and blue telangiectasias, as well as for dark-skinned patients, Nd:YAG laser should be preferred.
9. Treatments should be scheduled at 4–6 week intervals.

However, while rosacea has been described as a factor contributing to recurrence of telangiectasia after PDL treatment, other factors seem to contribute to the recurrence of telangiectasia of the face, such as sun exposure, esthetic medicine, and surgery procedures [70].

31.5.5 Poikiloderma of Civatte

Poikiloderma of Civatte is a benign condition involving above all the sun-exposed areas of the neck. The main factors characterizing this skin conditions are: atrophy, hyper- and hypopigmentation, and telangiectasias. It is a difficult condition to treat, and caution must be taken in case of laser treatment of the neck, due to an increased risk of textural changes and scarring, partially related to the paucity of pilosebaceous glands. Several devices (argon lasers, KTP lasers, PDLs, and IPLs) have been employed. However, a complete clearing is difficult to achieve and several side effects such as scarring with post-treatment purpura, irregular hypopigmentation, post-inflammatory hyperpigmentation, mottled appearance, crusting, and erythema have been reported [55]. In order to reduce these side effects, newer generation 595-nm PDLs with low fluencies, longer pulses, non-overlapping pulses, and dynamic cooling can be used [71]. In detail, it is recommended to use fluences not exceeding an upper limit of 5 J/cm, with a 10-mm spot size. Recently, the application of a new PDL enabling the use of a 15 mm spot to poikiloderma has been reported [72].

However, multiple sessions are necessary to achieve optimal clearing and further studies are required to identify correct parameters. Furthermore, ablative and non-ablative fractional lasers and photodynamic therapy have been reported [73, 74] to remove the telangiectatic component and in lightening the dyspigmentation.

31.5.6 Spider Nevus

A Spider nevus has a central feed arteriolar vessel with radiant fine red telangiectasia at the periphery. It is successfully treated with PDL, but several treatment sessions are needed because of its high flow.

31.5.7 Venous Lake

PDL, IPL, and Nd:YAG laser have been all reported as very effective to treat this dilated "lake-like" venule. Among them, in our experience, the long-pulsed Nd:YAG laser is superior to achieve fast and safe results [75].

31.5.8 Leg Veins and Telangiectasias

Legs are characterized by a venous system composed of a series of valved vessels in order to overcome the effects of gravity. Therefore, also with the help of surrounding muscles, blood is pumped out of the legs and returns to the heart. During development, this vascular system undergoes differentiation through multiple stages. Persistence of embryonic veins after birth is associated with venous malformation of legs such as the Klippel–Trenaunay syndrome or chronic venous insufficiency. Other disorders include congenital venous aneurysm, valvular agenesis, and primary valvular insufficiency [76]. All these conditions share venous hypertension, leading to the manifestation of varicose veins and telangiectasias.

Table 31.1 Clinical classification of venous disease: the CEAP classification

C0	No visible or palpable sign of venous disease
C1	Reticular veins or telangiectasias
C2	Varicose veins
C3	Edema
C4a	Pigmentation or eczema
C4b	Lipodermatosclerosis or atrophie blanche
C5	Healed venous ulcer
C6	Active venous ulcer
S = symptomatic; A = asymptomatic	

In the upright position, both gravity and hydrostatic pressure hinder venous return. The relation between these forces and blood volume is important to understand normal and abnormal functions of venous system [77]. Normally, the venous valves and the calf muscle pump act to limit the accumulation of blood in the lower extremity and to contain the increase in hydrostatic pressure. A failure in reducing venous pressure during exercise leads to chronic venous insufficiency. The high pressure in superficial veins (great saphenous vein: GSV; small saphenous vein: SSV; tributaries branch up to reticular veins) is directly transmitted into dermal capillary bed, thus leading to telangiectasias appearance and extravasation of intravascular content into interstitial space.

A correct classification of patients represents the basis for the management. The diagnostic evaluation is organized into three levels of examinations, in accordance with the severity of the disease.

- Level 1: the consulting with history and clinical examination (including a handheld Doppler scanner or transillumination).
- Level 2: noninvasive vascular laboratory testing: duplex color scanning added for C0–C4.
- Level 3: invasive investigation or more complex imagining studies (venography, venous pressure measurement, computed tomography, magnetic resonance imaging) for C4–C6 [78].

After diagnostic evaluation, treatment should aim to the reduction of venous hypertension by surgical, chemical, or physical ablation of the incompetent superficial venous system (GSV, SSV, branch tributaries, and perforators) [79–81].

The endovenous laser treatment of the saphenous vein gives satisfactory esthetic and functional results with a low rate of complications [82], but this type of management goes beyond the aim of this chapter.

Sclerotherapy is the gold standard treatment for leg telangiectasias. On the other hand, laser treatment should be considered in patients with needle phobia or showing adverse effects from sclerotherapy [5]. Laser sources are able to treat spider veins (0.2–2 mm red or blue), reticular veins (up to 5 mm), and telangiectasias (0.2–1 mm red or blue).

However, leg telangiectasias can be treated with lasers. However, in addition to the increased hydrostatic pressure and associated venous disorders, blood vessels are deeper than the facial ones and they have thick adventitial tissue and basal lamina. For these reasons, to thermocoagulate leg vessels with lasers, high energy pulses through large spots are required.

The laser of choice for leg vein treatment is Nd:YAG laser (wavelength of 1064 nm) [55]. This wavelength has a deep penetration (5–6 mm), therefore it is able to coagulate moderately deep vessels such as those of the legs. Useful practical key points are reported here as follows:

- Hydrostatic pressure imbalance and associated venous disorders must be treated before.
- Spot sizes of 3- or 6 mm are suitable for superficial lesions (telangiectasias, spider veins), whereas the 6- or 8-mm spot sizes are used for reticular veins.
- Pulse duration of 20–50 ms is required for these lesions.
- Fluences can vary according to spot size and pulse duration.
- Pre- and post-cooling are absolutely necessary because of the very high fluences employed [80].
- Overlapping of the treated area is not necessary when a large spot size is used, while a

mild overlapping or a stacking double shot is preferred with a 3-mm spot size.
- In case of treatment of large reticular veins, it is useful to apply a mild pressure to the handpiece to minimize the vein diameter, to favor penetration and to decrease the fluency.
- The clinical end points are the darkening of vessel for blue veins while disappearance is expected for red vessels.

Long-pulsed Nd:YAG treatment is painful, therefore cooling and sometimes topical anesthesia are required. A common side effect, even in lighter phototypes, is the hyperpigmentation that usually resolves with time, whereas hypopigmentation and scars are uncommon.

References

1. Solomon H, Goldman L, Henderson B, Richfield D, Franzen M. Histopathology of the laser treatment of port-wine lesions. Biopsy studies of treated areas observed up to three years after laser impacts. J Invest Dermatol. 1968;50:141–6.
2. Anderson RR, Parrish JA. Selective photothermolysis: precise microsurgery by selective absorption of pulsed radiation. Science. 1983;220:524–7.
3. Tanzi EL, Lupton JR, Alster TS. Lasers in dermatology: four decades of progress. J Am Acad Dermatol. 2003;49:1–31.
4. Groot D, Rao J, Johnston P, Nakatsui T. Algorithm for using a long-pulsed Nd:YAG laser in the treatment of deep cutaneous vascular lesions. Dermatol Surg. 2003;29:35–42.
5. Adamic M, Troilius A, Adatto M, Drosner M, Dahmane R. Vascular lasers and IPLS: guidelines for care from the European Society for Laser Dermatology. J Cosmet Laser Ther. 2007;9:113–24.
6. Rothfleisch JE, Kosmann MK, Levine VJ, Ashinoff R. Laser treatment of congenital and acquired vascular lesions: update on lasers: a review. Dermatol Clin. 2002;20:1–18.
7. Jasim ZF, Woo WK, Handley JM. Long-pulsed (6-ms) pulsed dye laser treatment of rosacea-associated telangiectasia using subpurpuric clinical threshold. Dermatol Surg. 2004;30:37–40.
8. Landthaler M, Hohenleutner U, Abd El Raheem TA. Therapy of vascular lesions in the head and neck area by means of argon, Nd:YAG, and flashlamp-pumped pulsed dye lasers. Adv Otorhinolaryngol. 1995;49:81–6.
9. Anderson RR, Parrish JA. The optics of human skin. J Invest Dermatol. 1981;77:13–9.
10. Landthaler M, Haina D, Brunner R, Waidelich W, Braun-Falco O. Neodymium-YAG laser therapy for vascular lesions. J Am Acad Dermatol. 1986;14:107–17.
11. Anderson RR. Optics of the skin. In: Lim HW, Soter NA, editors. Clinical photomedicine. New York, NY: Marcel Dekker; 1993. p. 19–35.
12. Haedersdal M. Cutaneous side effects from laser treatment of the skin: skin cancer, scars, wounds, pigmentary changes, and purpura—use of pulsed dye laser, copper vapor laser, and argon laser. Acta Derm Venereol. 1999;207:1–32.
13. Fourtanier A, Moyal D, Seite S. Sunscreens containing the broad-spectrum UVA absorber, Mexoryl SX, prevent the cutaneous detrimental effects of UV exposure: a review of clinical study results. Photodermatol Photoimmunol Photomed. 2008;24:164–74.
14. Adamič M, Pavlović MD, Troilius Rubin A, Palmetun-Ekbäck M, Boixeda P. Guidelines of care for vascular lasers and intense pulse light sources from the European Society for Laser Dermatology. J Eur Acad Dermatol Venereol. 2015;29:1661–78.
15. Jacobs AH, Walton RG. The incidence of birthmarks in the neonate. Pediatrics. 1976;58:218–22.
16. Barsky SH, Rosen S, Geer DE, Noe JM. The nature and evolution of port wine stains: a computer-assisted study. J Invest Dermatol. 1980;74:154–7.
17. Geronimus R, Ashinoff R. The medical necessity of evaluation and treatment of port wine stains. J Dermatol Surg Oncol. 1991;17:76–9.
18. Alster TS, Lewis AB. Dermatologic laser surgery. A review. Dermatol Surg. 1996;22:797–805.
19. Bucci J, Goldberg D. Past, present and future: vascular laser/light devices. J Cosmet Laser Ther. 2006;8:149–53.
20. Motley RJ, Lanigan SW, Katugampola GA. Videomicroscopy predicts outcome in treatment of port-wine stains. Arch Dermatol. 1997;133:921–2.
21. Bencini PL, Cazzaniga S, Galimberti MG, Zane C, Naldi L. Variables affecting clinical response to treatment of facial port-wine stains by flash lamp-pumped pulsed dye laser: the importance of looking beyond the skin. Lasers Med Sci. 2014;29:1365–70.
22. Lanigan SW. Port-wine stains on the lower limb: response to pulsed dye laser therapy. Clin Exp Dermatol. 1996;21:88–92.
23. Renfro L, Geronemus RG. Anatomical differences of port-wine stains in response to treatment with the pulsed dye laser. Arch Dermatol. 1993;129:182–8.
24. Eubanks LE, McBurney EI. Videomicroscopy of port-wine stains: correlation of location and depth of lesion. J Am Acad Dermatol. 2001;44:948–51.
25. Yohn JJ, Huff JC, Aeling JL, Walsh P, Morelli JG. Lesion size is a factor for determining the rate of port-wine stain clearing following pulsed dye laser treatment in adults. Cutis. 1997;59:267–70.
26. Jasim ZF, Handley JM. Treatment of pulsed dye laser-resistant port-wine stain birthmarks. J Am Acad Dermatol. 2007;57:677–82.

27. Kono T, Sakurai H, Takeuchi M, et al. Treatment of resistant port-wine stains with a variable-pulsed dye laser. Dermatol Surg. 2007;33:951–6.
28. Bernstein EF. High-energy 595nm pulsed dye laser improves refractory port wine-stains. Dermatol Surg. 2006;32:26–33.
29. Hsia J, Lowery JA, Zelicson B. Treatment of leg teleangectasia using a long-pulse dye laser at 595 nm. Lasers Surg Med. 1997;20:1–5.
30. West TB, Alster TS. Comparison of the long-pulse dye (490–595 nm) and KTP (532 nm) lasers in the treatment of facial and leg teleangectasias. Dermatol Surg. 1998;24:221–6.
31. Reichert D. Evaluation of the long-pulse dye laser for the treatment of leg teleangectasia. Dermatol Surg. 1998;24:737–40.
32. Waldorf HA, Alster TS, McMillan K, Kauvar AN, Geronemus RG, Nelson JS. Effect of dynamic cooling on 585 nm pulsed dye laser treatment of port-wine stain birthmarks. Dermatol Surg. 1997;23:657–62.
33. Kauvar A. Long pulse and high energy pulsed dye laser treatment of port wine stains and hemangioma. Presented at the 24th Annual Meeting of the American Society of Dermatological Surgery, Boston, May 1997.
34. Sivarajan V, Maclaren WM, Mackay IR. The effect of varying pulse duration, wavelength, spot size and fluence on the response of previously treated capillary vascular malformations to pulsed-dye laser treatment. Ann Plast Surg. 2006;57:25–32.
35. Bencini PL. The multilayer technique: a new and fast approach for flash-pumped pulsed (FLPP) dye laser treatment of port wine stains (preliminary reports). Dermatol Surg. 1999;25:786–9.
36. Lorenz S, Brunnberg S, Landthaler M, Hoenleutner U. Regarding the multilayer technique for treatment of PWS. Dermatol Surg. 2001;27:90.
37. Rajaratnam R, Laughlin SA, Dudley D. Pulsed dye laser double-pass treatment of patients with resistant capillary malformations. Lasers Med Sci. 2011;26:487–92.
38. Ho WS, Ying SY, Chan PC, Chann HH. Treatment of port wine stain with intense pulsed light: a prospective study. Dermatol Surg. 2004;30:887–90.
39. Klein A, Bäumler W, Landthaler M, Babilas P. Laser and IPL treatment of port-wine stains: therapy options, limitations, and practical aspects. Lasers Med Sci. 2011;26:845–59.
40. Izikson L, Nelson JS, Anderson RR. Treatment of hypertrophic and resistant port wine stains with a 755 nm laser: a case series of 20 patients. Lasers Surg Med. 2009;41:427–32.
41. Yang MU, Yaroslavsky AN, Farinelli WA, et al. Long-pulsed neodymium: yttrium-aluminium-garnet laser treatment for port-wine stains. J Am Acad Dermatol. 2005;52:480–90.
42. Alster TS, Tanzi EL. Combined 595-nm and 1064-nm laser irradiation of recalcitrant and hypertrophic port-wine stains in children and adults. Dermatol Surg. 2009;35:914–8.
43. Bencini PL, Tourlaki A, Tretti Clementoni M, Naldi L, Galimberti M. Double phase treatment with flashlamp-pumped pulsed-dye laser and long pulsed Nd:YAG laser for resistant port wine stains in adults. Preliminary reports. G Ital Dermatol Venereol. 2016;151:281–6.
44. Whang KK, Byun JY, Kim SH. A dual-wavelength approach with 585-nm pulsed-dye laser and 800-nm diode laser for treatment-resistant port-wine stains. Clin Exp Dermatol. 2009;34:436–7.
45. Zhao Y, Zhou Z, Zhou G, et al. Efficacy and safety of hemoporfin in photodynamic therapy for port-wine stain: a multicenter and open-labeled phase IIa study. Photodermatol Photoimmunol Photomed. 2011;27:17–23.
46. Baker ER, Manders E, Whitney CW. Growth of cavernous hemangioma with puberty. Clin Pediatr (Phila). 1985;24:596–8.
47. Frieden IJ, Eichenfield LF, Esterly NB, Geronemus R, Mallory SB. Guidelines of care for hemangiomas of infancy. American Academy of Dermatology Guidelines/Outcomes Committee. J Am Acad Dermatol. 1997;37:631–7.
48. Eivazi B, Werner JA. Management of vascular malformations and hemangiomas of the head and neck—an update. Curr Opin Otolaryngol Head Neck Surg. 2013;21:157–63.
49. Puettgen KB. Diagnosis and management of infantile hemangiomas. Pediatr Clin North Am. 2014;61:383–402.
50. Herschthal J, Wulkan A, George M, Waibel J. Additive effect of propranolol and pulsed dye laser for infantile hemangioma. Dermatol Online J. 2013;19:18570.
51. Goldman MP. Laser treatment of cutaneous vascular lesions. In: Goldman MP, editor. Cutaneous and cosmetic laser surgery. London: Mosby Elsevier; 2006. p. 31–91.
52. Hunzeker CM, Geronemus RG. Treatment of superficial infantile hemangiomas of the eyelid using the 595-nm pulsed dye laser. Dermatol Surg. 2010;36:590–7.
53. Rizzo C, Brightman L, Chapas AM, et al. Outcomes of childhood hemangiomas treated with the pulsed-dye laser with dynamic cooling: a retrospective chart analysis. Dermatol Surg. 2009;35(12):1947–54.
54. Bruckner AL, Frieden IJ. Hemangiomas of infancy. J Am Acad Dermatol. 2003;48:477–93.
55. Srinivas CR, Kumaresan M. Lasers for vascular lesions: standard guidelines of care. Indian J Dermatol Venereol Leprol. 2011;77:349–68.
56. Saafan AM, Salah MM. Using pulsed dual-wavelength 595 and 1064 nm is more effective in the management of hemangiomas. J Drugs Dermatol. 2010;9:310–4.
57. Alcántara González J, Boixeda P, Truchuelo Díez M, López Gutiérrez J, Olasolo P. Ablative fractional yttrium-scandium-gallium-garnet laser for scarring residual haemangiomas and scars secondary to their

surgical treatment. J Eur Acad Dermatol Venereol. 2012;26:477–82.
58. Laubach HJ, Anderson RR, Luger T, Manstein D. Fractional photothermolysis for involuted infantile hemangioma. Arch Dermatol. 2009;145:748–50.
59. Alam M, Dover JS, Arndt KA. Treatment of facial telangiectasia with variable-pulse high-fluence pulsed-dye laser: comparison of efficacy with fluences immediately above and below the purpura threshold. Dermatol Surg. 2003;29:681–4.
60. Clementoni MT, Gilardino P, Muti GF, et al. Facial teleangectasias: our experience in treatment with IPL. Lasers Surg Med. 2005;37:9–13.
61. Nymann P, Hedelund L, Haedersdal M. Long-pulsed dye laser versus intense pulsed light for the treatment of facial telangiectasias: a randomized controlled trial. J Eur Acad Dermatol Venereol. 2010;24:143–6.
62. Jørgensen GF, Hedelund L, Haedersdal M. Long-pulsed dye laser versus intense pulsed light for photodamaged skin: a randomized split-face trial with blinded response evaluation. Lasers Surg Med. 2008;40:293–9.
63. Bevin AA, Parlette EC, Domankevitz Y, Ross EV. Variable-pulse Nd: YAG laser in the treatment of facial telangiectasias. Dermatol Surg. 2006;32:7–12.
64. Bernstein EF, Kligman A. Rosacea treatment using the new-generation, high-energy, 595 nm, long pulse-duration pulsed-dye laser. Lasers Surg Med. 2008;40:233–9.
65. Clark SM, Lanigan SW, Marks R. Laser treatment of erythema and telangiectasia associated with rosacea. Lasers Med Sci. 2002;17:26–33.
66. Menezes N, Moreira A, Mota G, Baptista A. Quality of life and rosacea: pulsed dye laser impact. J Cosmet Laser Ther. 2009;11:139–41.
67. Schroeter CA, Haaf-von Below S, Neuman HA. Effective treatment of rosacea using intense pulsed light systems. Dermatol Surg. 2005;31:1285–9.
68. Neuhaus IM, Zane LT, Tope WD. Comparative efficacy of nonpurpuragenic pulsed dye laser and intense pulsed light for erythematotelangiectatic rosacea. Dermatol Surg. 2009;35:920–8.
69. Bencini PL, Tourlaki A, De Giorgi V, Galimberti M. Laser use for cutaneous vascular alterations of cosmetic interest. Dermatol Ther. 2012;25:340–51.
70. Guida S, Galimberti MG, Bencini M, Pellacani G, Bencini PL. Telangiectasia of the face: risk factors for reappearance in patients treated with dye laser. J Eur Acad Dermatol Venereol. 2017;31:1355–9.
71. Meijs MM, Blok FA, de Rie MA. Treatment of poikiloderma of Civatte with the pulsed dye laser: a series of patients with severe depigmentation. J Eur Acad Dermatol Venereol. 2006;20:1248–51.
72. Bernstein EF, Schomacker K, Paranjape A, Jones CJ. Treatment of poikiloderma of Civatte using a redesigned pulsed dye laser with a 15 mm diameter treatment spot. Lasers Surg. 2019;51:54–8.
73. Tierney EP, Hanke CW. Treatment of poikiloderma of Civatte with ablative fractional laser resurfacing: prospective study and review of the literature. J Drugs Dermatol. 2009;8:527–34.
74. Navarro-Triviño FJ, Torres-Puchol VG, Ruiz-Villaverde R. PDT and BF-200 ALA: the therapy option for the treatment of Poikiloderma of Civatte. Dermatol Ther. 2018;31:e12648.
75. Mlacker S, Shah VV, Aldahan AS, McNamara CA, Kamath P, Nouri K. Laser and light-based treatments of venous lakes: a literature review. Lasers Med Sci. 2016;31:1511–9.
76. Gloviczki P, Duncan A, Kalra M, Oderich G, Ricotta J, Bower T, McKusick M, Bjarnason H, Driscoll D. Vascular malformations: an update. Perspect Vasc Surg Endovasc Ther. 2009;21:133–48.
77. Araki CT, Back TL, Padberg FT, Thompson PN, Jamil Z, Lee BC, Duran WN, Hobson RW 2nd. The significance of calf muscle pump function in venous ulceration. J Vasc Surg. 1994;20:872–7.
78. Eklof B, Rutherford RB, Bergan JJ, Carpentier PH, Gloviczki P, Kistner RL, Meissner MH, Moneta GL, Myers K, Padberg FT, Perrin M, Ruckley CV, Smith PC, Wakefield TW, American Venous Forum International Ad Hoc Committee for Revision of the CEAP Classification. Revision of CEAP classification of chronic venous disorders: consensus statement. J Vasc Surg. 2004;40:1248–52.
79. Gloviczki P. The care of patients with varicose veins and associated chronic venous disease: clinical practice guidelines of the Society for Vascular Surgery and the American Venous Forum. J Vasc Surg. 2011;53:2s–48s.
80. Bjordal RI. Circulation patterns in incompetent perforating vein on the calf and in saphenous system in primary varicose veins. Acta Chir Scand. 1972;138:251–61.
81. Akesson H, Brudin L, Cwifield W, Ohlin P, Plate G. Does the correction of superficial insufficiency and perforating veins improve venous function in patients with deep venous insufficiency? Phlebology. 1990;5:113–23.
82. Gonzales-Zeh R, Armisen R, Barahona S. Endovenous laser and echo-guided foam ablation in great saphenous vein reflux: one-year follow-up. J Vasc Surg. 2008;48:940–6.

32 Broadband Intense Pulsed Lights for Vascular Malformations

Marco Dal Canton

32.1 Broadband Intense Pulsed Lights for Vascular Malformations

A cardinal principle of laser physics, also applicable to broadband ligh technologies, is *selective photothermolysis*, affirming that, in the case of vascular lesions, hemoglobin can be selectively targeted by an approoriate light emitting technology generating a confined thermal damage, with a negligible injury to the surrounding tissue [1].

The tissue interaction of a high energy broadband light system is similar to that of a laser: the light energy delivered to the tissue is transformed into heat after absorption by the wavelength-specific target chromophore (hemoglobin, melanin, water), potentially as to its destruction if a critical temperature is reached [1].

Broadband intense pulsed lights (IPLs) differ from lasers, being based on a gas-filled flashlamp (usually xenon) pumped with a charge of high voltage electrical energy stored in a capacitor and emitting an intense, non-coherent and non-collimated polychromatic light, with a continuous range of wavelengths from blue light to IR [2]: this range is narrowed by bandpass filters at the lower end of visible spectrum, usually as to 400 nm, being harmful UV invariably blocked, while near IR spectrum is variably filtered as to 1200–1400 nm, which is absorbed mostly by interstitial fluid.

The wide spectrum of light emission of an IPL system covers all significant absorption peaks of most skin chromophores [3], delivering significant energy to more targets in one pulse.

To master the unlimited combinations of continuous variables offered by an IPL system can be extremely challenging in respect to mixing the digital settings offered by any laser system, but currently, any model of modern IPL in the market provides optimized and software guided settings and offers own better compromises between light absorption and penetration depth for each range of wavelengths, in order to treat different chromophores tailored to diverse skin conditions absolutely more safely than earlier models.

The choice of cut-off filter is dependent on the privileged chromophore to be targeted in the skin. A 530–550 nm cut-off filter is usually working for vascular lesions, while a 650–700 nm bandpass filter is better suitable to perform hair removal.

The last generation high quality IPL systems implement square shaped pulses [4], different built-in cooling solutions, and sophisticated software guiding the user to manage an otherwise unlimited combinations of analogic variables in

M. Dal Canton (✉)
Department of Dermatology and Venereology, Ordine Medici e Chirurghi Provincia di Belluno, Belluno, Italy

Private practice, Qderm-Belluno, Belluno, Italy
e-mail: mdc@qderm.it

M. Fimiani et al. (eds.), *Technology in Practical Dermatology*,
https://doi.org/10.1007/978-3-030-45351-0_32

Table 32.1 Absorption spectrum of ink colors in the tattoo

Intense polychromatic light (IPL)	Laser
Polychromatic	Monochromatic
Non-coherent	Coherent
Non-collimated	Collimated
Analogic output	Digital output

respect to the discrete digital parameters of a laser system: this is also beneficial to soften the learning curve of the novice, remarkably steeper than a laser (Table 32.1). To the expert users is commonly offered the possibility to personalize the combination of fluences, pulse widths of single pulses and of micropulses trains, and of the time pauses between single micropulses.

In 1997, a second-generation IPL system was manufactured equipped with an extra bandpass filter, by means of the water of the cooling system flowing within the handpiece to block the IR light above 950 nm emitted from the flashlamp. This later generation dual-mode filtered IPL system delivers a narrower range of wavelengths, hence a more selective targeting, and reduces bulk heating due to water absorption, necessitating less output energy to concentrate in the target chromophore and less contact cooling [5].

The effectiveness of IPLs and comparability to lasers in treating different types of vascular lesions has been proven by a number of comparative trials [6].

A split face controlled study on 16 patients established a similar efficacy of a selective waveband intense pulsed light (500–670 and 870–1200 nm) as compared to FPDL on telangiectasia of the face after 1–2 months, with similar side effects, quality, and intensity of results [7]. Another comparative study proved better results of the long pulsed FPDL on telangiectasia at 3 months [8], while in another split face comparative study IPL resulted more advantageous than long PDL in photorejuvenation, due to superior vessel clearance, textural improvement, and less pain [9].

Based on analysis of available randomized controlled studies (RCTs), pulsed dye laser results to be the first choice to treat effectively PWS, while up to now a more limited number of RCTs is sustaining the efficacy of IPLs [10] and other vascular light sources as KTP, Nd: YAG, and alexandrite lasers [11].

Nonetheless, offering a near IR range of wavelengths, IPLs can treat deeper vascular components of a PWS that FPDL or KTP cannot reach [12]. Therefore IPLs have been proposed as an effective therapeutic option for purple PWS [13–16] and FPDL resistant port wine stain [11, 17, 18]. Although IPL has been shown to be effective in the clearance of pink and red PWS [15, 19], a head-to-head trial comparing the efficacy of IPL against PDL determined that the median clinical improvement was significantly better for PDL (65%) than IPL (30%) [20].

In addition, recently an intense pulsed light system which can deliver submillisecond pulses has been introduced on the market [21], allowing up to 500 μsec pulse widths. Operating with double filtered applicators which select wavebands between 530 and 750 nm or 555 and 950 nm [3], one can cover almost the whole range of the hemoglobin absorption peaks, excluding the near IR domain, which is more prone to overheat the skin due to water absorption, while extremely short pulse widths closely match those of submillisecond FPDL. According to selective photothermolysis physics, these short pulse widths are favorable to treat selectively pink and residual PWS, microtelangiectatic vessels, and erythematous rosacea, matching very tiny vessels with unprecedented selectivity for an IPL system, with the added advantage of covering a wide area per single pulse. Nevertheless the patient should be prepared that purpura is to be expected when delivering submillisecond pulses. More comparative and controlled studies are expected in the future on the effects of submillisecond pulses in IPL systems.

32.2 Advices for Treatment of Vascular Malformations with IPL

The advantages of IPL systems are a broad range of approved indications, a broad treatment area per single pulse and versatility. Differently from

lasers, IPL handpieces invariably are equipped with a sapphire or quartz square prism offering usually a quadrilateral contact surface with the skin wider than the average larger laser spot: this offers an advantage when treating wide areas or lesions, as a large port wine stain, poikiloderma of Civatte of the neck and decoltè [22]. The optical coupling between the crystal and the skin surface is obtained by a thin layer of optical hydro-gel.

When treating a vascular lesion with an IPL system, differently from hair removal and treatment of benign pigmented lesions, an undue mechanical pressure on the handpiece should be avoided, since it removes the target blood from the treatment area during the light pulse delivery and will reduce the light absorption and hence the clinical effect.

The diameters of visible skin dilated vessels can vary between 100 and 500–1000 μm, and mathematical algorithms can predict that the pulse widths for the treatment of these telangiectasias will range between 0.5 ms and 30 ms or more, depending on the actual vessel diameter [2].

Pulse durations matching the relaxation time of the ectatic blood vessels can easily be generated by an IPL system [2, 23] which can offer to the experienced user also the personalization of the pulse duration and number of pulses: single pulses or trains of double micropulses with a short pause can be delivered according to the dimension of the privileged vascular target and the type of treatment to be administered.

New generation submillisecond IPL systems [19] approach the pulse widths of short pulsed dye laser for the treatment of tinier telangiectasia and pink redness.

32.3 Telangiectasias

This is a common acquired vascular malformation, mostly related to weathering and to rosacea, frequently seen in the face of skin types I–III, characteristically on the nose and zygomatic area. When less than 0.1 mm in diameter, telangiectasias appear as a diffuse redness, while 0.1 to 1 mm are more clearly identifiable as red single or branched streaks. Often a diffuse redness and/or pigment uneven distribution and discrete pigmented lesions could coexist and overlap, so a specific diagnosis and a treatment plan with the more appropriate technology available should be made.

It is generally suggested to treat thick vessels first (0.5 mm or more), and if an IPL is chosen, in skin types 1–4, the better choice is a 555 to 950 nm bandwidth applicator or closer to the near IR range: shorter wavelengths (less than 550 nm) are better suitable to treat smaller and more superficial telangiectasia in untanned skin types 1–3. Skin types 5 and 6 are better candidates to be treated with a near IR light source, as Nd: YAG laser.

On thinner skin and over bony prominences it is better to use only default energies, and to increase fluences only in small steps (0.5–1.5 J/cm^2) only if a clinical endpoint is not observed. A more appropriate approach to resistant telangiectasias is to modify the pulse width in small steps, in order to refine the pulse time matching with the vessel diameter, taking care to avoid bulk heating with excessive stacking.

Intervals between session should not be shorter than 4–6 weeks.

32.4 Poikiloderma of Civatte

This is an aquired common combination of fine telangiectasia, uneven reticulated reddish brown pigmentation and atrophic alteration of the skin, primarily affecting the lateral neck and decoltè, in male and female older fair-skinned individuals, mainly related to chronic sun exposure, with the possible contribution of other factors, as genetic predisposition, homonal changes of menopause, photosensitizing chemicals in cosmetics and perfumes.

The clinical endpoint of an IPL treatment is a very transient and rapidly reversible change in color to white or bluish in less than a second: afterwards this may reverse to the original color and is gradually overlapped by a more diffuse erythema and edema.

In the author experience, in vascular laser or IPL treatment and photorejuvenation a magnified cross polarized visualization [24] is extremely helpful for an accurate identification of the

Fig. 32.1 Poikiloderma of Civatte after 6 months after one treatment with SWT IPL 530–750 nm

vascular and pigmented targets and a proper detection of these evanescent clinical endpoints.

IPL is absolutely suitable to treat poichiloderma, which usually affects large areas, since the average applicator of an IPL can cover a wide surface in short time: otherwise, with a laser device, unless provided of a scanner, one is supposed to cover evenly the whole area in a paint mode (Figs. 32.1, 32.3).

Shorter wavelengths in the visible range should be administered in skin types 1–3 only, while in skin types 4 and 5 are more safely treated with a waveband closer to the IR range. Treatment setting of poichiloderma usually provides a train of short and relatively low energy (micro) pulses separated by a short pause, with a resulting total macropulse of few tens of milliseconds: if some telangiectasia coexist in the poikilodermatous area, these can be safely treated in another scheduled appointments, while someone prefer to treat them conservatively in the same session. The aforementioned clinical endpoints could be enhanced with a slight darkening of pigmented (also tiny) targets after 1–15 min: the pigment is expected to darken in the next 8–12 h, and the patient should be informed of a "dirty" look of the treated area for some days.

32.5 Port Wine Stains

This is a congenital vascular malformation that can display a predominant red color, when it contains thinner and superficial vessels, or a more bluish hue when the malformed vessels are larger and more deeply located, becoming darker over time, usually in the adult to mature age, acquiring a rough texture or generating focal areas of hypertrophy. IPLs have resulted to be effective also in darker and even thicker PWS, and the better wavelengths range and the more appropriate pulse time width must be tuned based on predominant red or blue color.

Blue areas and skin types darker than 3 should be treated first with a longer IPL band, as 555–950 nm or more, with sessions spaced of at least 4–6 weeks and the treatment can be integrated with a Nd: YAG 1064 nm laser on resistant blue spots. When red color is then prevailing, the PWS can be treated with shorter wavelengths (as 530 to 750 nm) in skin types 1–3.

A preliminary test with default energy is advisable, with slow increases of 0.5–1 J/cm^2, as the clinical endpoint is reached: this is usually seen as a rapid shift to a bluish hue rapidly changing in edema and erythema.

At the end of the treatment schedule, when a pink to red port wine stain is remaining, the submillisecond pulse widths of new generation IPLs with a shorter wavelengths band can be an option: transient purpura can be expected, as after a short pulsed FPDL treatment, and patients should be prepared to it (Fig. 32.2).

As PWS laser or IPL treatment is a painful procedure, it is recommended to proceed under sedation in children or to negotiate to postpone the treatment as to reach a more subjective motivation.

Fig. 32.2 Port wine stain after two treatments with SWT IPL 555–950 nm, 9 J/cm^2 and 2 ms and 7 J/cm^2, 1.5 ms. The patient did not accept treatment of the palpebral component of the malformations, functioning as control

32.6 Rosacea

Rosacea is often a consequence of an individual predisposition that requires periodic therapeutic tailored adjustments. Vascular laser and IPL treatment can be an important ingredient to reduce rosacea but cannot prevent future flares. Rosacea can display telangiectasias, diffuse redness and commonly flushing is a major complaint (Fig. 32.3).

In an inflammatory phase, it is better to control the disease with a medical treatment, to proceed afterwards to clear up larger telangiectasias first and more tiny vessels and diffuse erythema afterwards. The latter is better treated with macro-pulses composed of short (millisecond) pulses separated by milliseconds pauses, taking care to minimize the fluence in an active stage. In skin types 1 and 2, shorter wavelength bandwidths (530–750 nm) can be used, while longer wavelength bands (550–950 nm) are better suitable to treat darker skin types. For the experienced users, reducing slightly the pulse width of single pulses may be helpful to deal with unresponsive areas. Recently, IPL protocols of treatment of rosacea in inflammatory stage are described.

32.7 Spider Angioma

Even if this is a classic indication for a vascular laser treatment, this central red pinpoint or papule, corresponding to a feeding arteriole, surrounded by a telangiectasias can be treated effectively also with IPL, these lesions are usually treated with a single pulse, and the clinical endpoint is a rapid change to blue-gray, followed by edema and erythema. In unresponsive lesions, the pulse width can be slightly reduced, letting the suggested fluence to reduce accordingly.

32.8 Conclusions

There are multiple evidences supporting the efficacy of intense broadband pulsed lights (IPLs) in the treatment of many vascular skin abnormalities, with the advantage of the new generations of high quality medical IPL platforms which deliver square pulses and implement advanced and expert software supporting an otherwise steep learning curve for the inexperienced user.

Furthermore, the availability of submillisecond pulses in late IPL system provides the opportunity to approximate the performances of a short pulsed dye laser.

More comparative and randomized controlled studies are expected to refine the medical evidence supporting the multiple indications of these otherwise trustworthy high energy light devices.

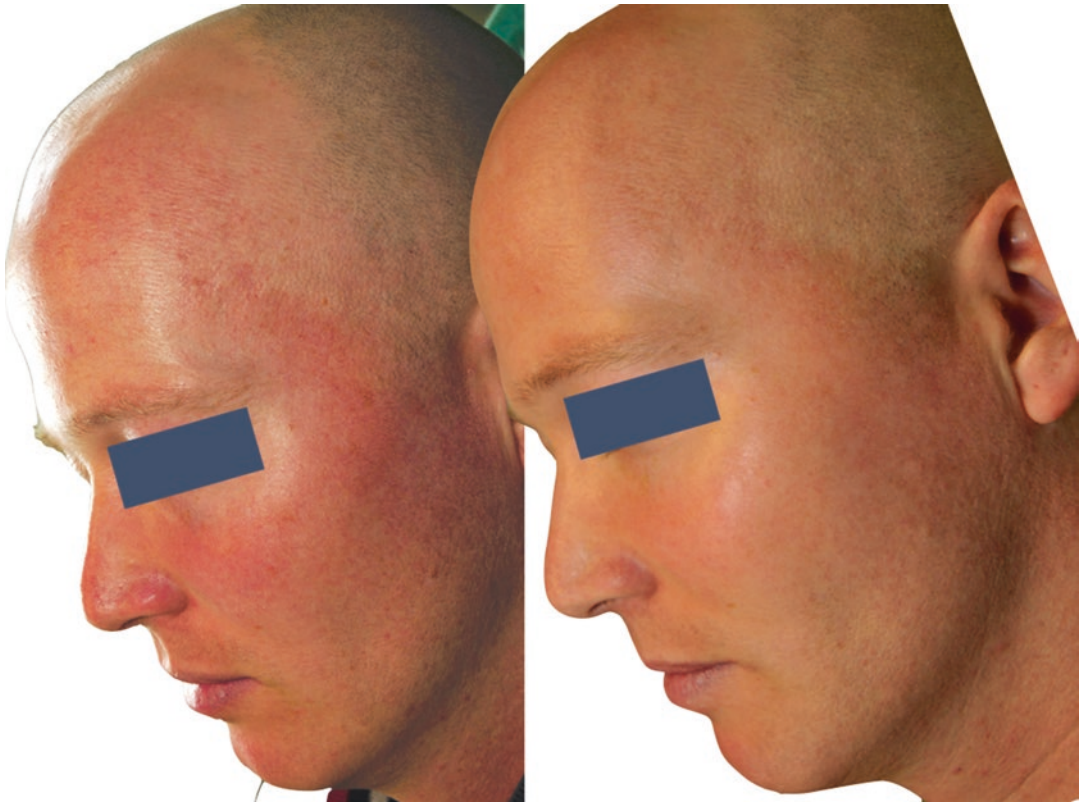

Fig. 32.3 Erythematotelangiectatic rosacea and diffuse photoaging after three treatments with SWT IPL 530–750 nm (control at 8 months)

References

1. Anderson RR, Parrish JA. Selective photothermolysis: precise microsurgery by selective absorption of pulsed radiation. Science. 1983;220(4596):524–7.
2. Calderhead RG. Photobiological basics of photomedicine: a work of art still in progress. Med Laser. 2017;6:45–57. https://doi.org/10.25289/ML.2017.6.2.45.
3. Ciocon DH, Boker A, Goldberg DJ. Intense pulsed light: what works, what's new, what's next. Facial Plast Surg. 2009;25(5):290–300.
4. Ash C, Town G, Bjerring P. Relevance of the structure of time-resolved spectral output to light-tissue interaction using intense pulsed light (IPL). Lasers Surg Med. 2008;40(2):83–92. https://doi.org/10.1002/lsm.20596.
5. Bjerring P, Christiansen K, Troilius A. Intense pulsed light source for treatment of facial telangiectasias. J Cosmet Laser Ther. 2001;3(4):169–73.
6. Babilas P, Schreml S, Szeimies RM, Landthaler M. Intense pulsed light (IPL): a review. Lasers Surg Med. 2010;42:93–104. https://doi.org/10.1002/lsm.20877.
7. Tanghetti EA. Split-face randomized treatment of facial telangiectasia comparing pulsed dye laser and an intense pulsed light handpiece. Lasers Surg Med. 2012;44(2):97–102.
8. Nymann P, Hedelund L, Haedersdal M. Long-pulsed dye laser vs. intense pulsed light for the treatment of facial telangiectasias: a randomized controlled trial. J Eur Acad Dermatol Venereol. 2010;24(2):143–6.
9. Jørgensen GF, Hedelund L, Haedersdal M. Long-pulsed dye laser versus intense pulsed light for photodamaged skin: a randomized split-face trial with blinded response evaluation. Lasers Surg Med. 2008;40(5):293–9. https://doi.org/10.1002/lsm.20634.
10. Wat H, Wu DC, Rao J, Goldman MP. Application of intense pulsed light in the treatment of dermatologic disease: a systematic review. Dermatol Surg. 2014;40:359–77. https://doi.org/10.1111/dsu.12424.
11. Faurschou A, Olesen AB, Leonardi-Bee J, Haedersdal M. Lasers or light sources for treating port-wine stains. Cochrane Database Syst Rev. 2011;(11):CD007152. https://doi.org/10.1002/14651858.CD007152.pub2.
12. Adamič M, Pavlović MD, Troilius Rubin A, Palmetun-Ekbäck M, Boixeda P. Guidelines of care for vascular lasers and intense pulse light sources from the

European Society for Laser Dermatology. J Eur Acad Dermatol Venereol. 2015;29(9):1661–78.
13. Ozdemir M, Engin B, Mevlitoglu I. Treatment of facial port-wine stains with intense pulsed light: a prospective study. J Cosmet Dermatol. 2008;7:127–31.
14. Li G, Lin T, Wu Q, Zhou Z, Gold MH. Clinical analysis of port wine stains treated by intense pulsed light. J Cosmet Laser Ther. 2010;12:2–6.
15. Adatto MA, Luc-Levy J, Mordon S. Efficacy of a novel intense pulsed light system for the treatment of port wine stains. J Cosmet Laser Ther. 2010;12:54–60.
16. Drosner M, Ellwanger J, Schöttle K, Stockmeier M, Gatty F, Hellbrügge G. Christiansen K comparison of intense pulsed light (IPL) and pulsed dye laser (PDL) in port-wine stain treatment. Med Laser Appl. 2008;23:133–40.
17. Bjerring P, Christiansen K, Troilius Rubin A. Intense pulsed light source for the treatment of dye laser resistant port-wine stains. J Cosmet Laser Ther. 2003;5(1):7–13.
18. Ho WS, Ying SY, Chan PC, Chan HH. Treatment of port wine stains with intense pulsed light: a prospective study. Dermatol Surg. 2004;30:887–91.
19. Raulin C, Schroeter CA, Weiss RA, Keiner M, Werner S. Treatment of port-wine stains with a noncoherent pulsed light source: a retrospective study. Arch Dermatol. 1999;135:679–83.
20. Faurschou A, Togsverd-Bo K, Zachariae C, Haedersdal M. Pulsed dye laser vs intense pulsed light for port-wine stains: a randomized side-by-side trial with blinded response evaluation. Br J Dermatol. 2009;160:359–64.
21. US Food and Drug Administration. DoHaHS. K150907 Trade/Device name: Ellipse Nordlys. Premarket notification letter 2015.
22. Wenzel SM, Hohenleutner U, Landthaler M. Progressive disseminated essential telangiectasia and erythrosis interfollicularis colli as examples for successful treatment with a high-intensity flashlamp. Dermatology. 2008;217(3):286–90.
23. Rulin C, Schroeter C, Maushagen-Schnaas E. Treatment possibilities with a high-energy pulsed light source. Hautartz. 1997;48:886–9.
24. Bernstein EF. A tool for my laser practice I simply can't do without: shining a light on my favourite light (source). J Drugs Dermatol. 2017;16:939–44.

33 Pigment-Specific Lasers for Benign Skin Lesions and Tattoos: Long Pulsed, Nanosecond, and Picosecond Lasers

Paolo Sbano

In the laser treatment of benign pigmented skin lesions and tattoos, a selective destruction of certain epidermal/dermal structures is the purpose. According to the theory of selective photothermolysis proposed by Anderson and Parrish [1], two conditions are required to selectively destroy a target: (1) the laser energy must be at a wavelength which is highly absorbed by the target relative to the surrounding normal tissue and (2) the pulse duration used must be shorter than the time it takes for heat to escape through conduction.

The theory of selective photothermolysis refers to laser energy absorption by a target chromophore without significant thermal damage to surrounding tissue. To achieve selective photothermolysis, the laser must produce a beam of light with a wavelength preferentially absorbed by the chromophore in the lesion (i.e., melanin for benign pigmentations and ink for tattoos). Equally important, the pulse duration of the laser beam must be shorter than the thermal relaxation time of the chromophore to prevent the spread of thermal energy beyond the targeted chromophore. The thermal relaxation time is defined as the time needed for the chromophore to cool to half of its peak temperature after laser irradiation, which is proportional to the square of the size of the chromophore. In general, smaller objects cool faster than larger ones. If the pulse duration is greater than the thermal relaxation time, nonspecific thermal damage occurs because of heat diffusion. On the contrary, if the structure is heated in a very short exposure time, the temperature rises quickly since there is no time for the heat to diffuse. This condition is called thermal lock-in [2, 3]. Pulse duration ranges from very short (picoseconds) as in the case of picosecond (PS) lasers to short (nanoseconds) as in the case of Q-switched (QS) lasers to long (milliseconds) as in the case of long-pulse (LP) lasers. Finally, the energy delivered to the site (fluence) must be high enough to destroy the chromophore within the pulse duration [4].

Based on the theory of selective photothermolysis, the wavelength, pulse duration, and fluence of a laser can be tailored to result in selective damage to the lesions without nonspecific thermal damage to the surrounding tissues.

33.1 Treatment of Benign Pigment Lesions

Melanin is the target chromophore for pigmented lesions. It absorbs strongly across the UV, visible, and near-infrared spectrum with decreasing absorption at longer wavelengths. Although melanin absorbs light throughout the visible spectrum, a variety of wavelengths are used to target

P. Sbano (✉)
U.O.C. Dermatology, Policlinico Santa Maria alle Scotte, Siena, Italy

M. Fimiani et al. (eds.), *Technology in Practical Dermatology*,
https://doi.org/10.1007/978-3-030-45351-0_33

it. Absorption for melanin decreases as the wavelength increases, although a longer wavelength allows deeper tissue penetration. Thus, shorter wavelengths are useful in treating fair phototypes and more superficial pigmented lesions; on the contrary, a longer wavelength can be used in treating deeper skin lesions in a patient with a darker skin type, minimizing epidermal damage and risks while still targeting the appropriate chromophore. In fact, nonspecific energy absorption by relatively large quantities of melanin in the basal layer of the epidermis in darkly pigmented patients can increase nonspecific thermal injury and lead to a higher risk of untoward effects, including permanent dyspigmentation, textural changes, focal atrophy, and scarring. Moreover, competitive absorption by epidermal melanin substantially decreases the total amount of energy that can reach deeper dermal lesions, making it more difficult to achieve the degree of tissue destruction necessary to produce the desired clinical result [5].

33.1.1 QS Laser Treatment

QS systems emit maximum energy output in nanosecond (NS) pulses that are substantially shorter than the 100 ns thermal relaxation time of melanosomes. They have long represented the safest means to treat pigmented lesions due to their ability to limit injury to the targeted melanosomes and thus avoid undesirable pigmentary changes. Have been demonstrated that submicrosecond laser pulses cause individual pigmented cell death by violent cavitation, a microscopic steam bubble erupting around each melanosome after the laser pulse [6].

The clinical goal of treatment is skin bleaching without tissue *splatter*. When targeting any pigmented lesion, treatment should always be initiated at threshold fluence. This is clinically achieved when either immediate lesion whitening or a sensation of warmth in the treatment area is evident, signifying laser energy absorption and heat or shockwave generation within the melanosomes. Color changes of melanocytic lesion occur in a couple of minutes and range from light- to dark-brown depending on the baseline color of the lesion and patient phototype [7]. If the clinical threshold is exceeded, epidermal exfoliation and pinpoint bleeding ensues, resulting in blistering, possible temporary or permanent hypopigmentation, and the higher probability of skin textural changes or scarring.

Most used devices in the treatment of pigmented lesions are several QS lasers (Nd:YAG 532 and 1064 nm, ruby 694 nm, and alexandrite 755 nm).

532 nm: Nd:YAG laser emits a 1064 nm light, but it can be doubled in frequency by using a crystal of potassium diphosphate to produce a green radiation with 532 nm wavelength. This wavelength is particularly useful in treating light epidermal/dermo-epidermal lesions in phototype I–III subjects (Fig. 33.1). If used in darker phototypes gives halo-effect and transitory hypopigmentation in the treated area.

694 nm and 755 nm: These two wavelengths have similar biological effects and clinical indications: both are suitable for treating epidermal/dermal dark pigmented lesions in phototypes II–IV (Fig. 33.2). Cause of their lower coefficient of absorption for melanin and hemoglobin with respect to 532 nm wavelength is more used in darker and Asian skin type, with lower risk of PIH and halo-effect.

1064 nm: 1064 nm wavelength features a lower absorption coefficient for melanin, but it can penetrate into the skin more deeply, so that dermal lesions are reached easier and effectively. This is the preferred wavelength used in phototype IV–VI in dark pigmented lesions.

33.1.2 PS Laser Treatment

Since PS lasers are capable of destroying the melanosomes of epidermal/dermal melanocytes in a similar manner to NS-domain QS lasers, it is easy to assume that PS lasers are just as effective for the treatment of dermal melanocytosis as the NS lasers. No advantages have been demonstrated in large case series for the treatment of benign pigmented skin lesions with PS lasers with respect to NS ones.

Fig. 33.1 Solar lentigo laser removal: before and after treatment with 532 nm QS laser

Fig. 33.2 Solar lentigo laser removal: before and after treatment with 694 nm QS laser

33.1.3 LP Laser Treatment

The LP ruby (694 nm), alexandrite (755 nm), diode (808–810 nm), and Nd:YAG (532 and 1064 nm) lasers have been used for the treatment of pigmented lesions. Millisecond laser pulses, much longer than the thermal relaxation time of the melanosomes, are less efficient with respect to QS lasers for treating most of pigmented skin disorders. However, some LP lasers find specific indication and are used to better hit some dermal pigmentary lesions such as congenital nevus and Becker nevus, particularly those with growth of terminal hair. In congenital nevi and hair follicles, some of the target consists of non-pigmented cells which are located only nearby the pigmented cells. In order to damage these non-pigmented target cells, heat must diffuse from the pigmented portion (i.e., the site at which light is converted to heat), which takes time. In congenital nevi, there are cell "nests" about 0.1 mm diameter or more. In hair follicles, stem cells are located at the outer root sheath basement membrane, also about 0.1 mm from the pigmented hair shaft [8, 9]. QS laser pulses do not cause permanent hair removal and do not cause permanent removal of congenital nevi. In contrast, millisecond-domain pulses cause both permanent hair loss and in some cases, removal of congenital nevi. Conducted heat during the laser pulse probably accounts for this impressive difference.

33.1.4 Side Effects

Even when optimal parameters are applied, one of the most common adverse effects associated with QS laser treatment in dark-skin individuals is post-inflammatory hyperpigmentation (PIH). Although the exact mechanism for PIH is unknown, direct melanin stimulation following laser impact is thought to be involved. More recently, it has been speculated that QS laser irradiation stimulates fibroblasts by upregulating melanogenic stimulating factors such as fibroblast growth factors, hepatocyte growth factors, and stem cell factors, thereby increasing pigmentation [5].

Transitory hypopigmentation is a common reported side effect in IV–VI or tanned III phototypes if not correct wavelength is used.

Pinpoint bleeding, bulla, and crusting development indicate application of inappropriate fluences and/or excessive spot overlapping. This depends by poor operator technique or not homogeneous distribution of the intensity across the beam diameter. Clinically, this results in the necessity of treating tissue with some overlap of the laser beam to deliver energy to tissue in a more uniform manner.

In a small percentage of treated patients, recurrence of pigment may be seen despite initially successful QS laser therapy. This can be explained by incomplete lesion clearance that becomes evident after resolution of post-treatment skin blanching and/or further proliferation of residual pigment.

33.2 Treatment of Tattoos

Laser technology has revolutionized the removal of unwanted tattoo pigment without scarring. Ink particles in a mature tattoo are stored within fibroblasts and macrophages in the skin. These exogenous pigment particles are very small and have very short thermal relaxation times, so very rapid heating is necessary to cause their destruction. QS lasers are designed to produce a pulse duration in the NS range with peak energies upwards of 10 J/cm^2 and have been the mainstay of tattoo removal for the past two decades. The QS ruby laser (694 nm) was the first such laser to be commercially available, followed shortly thereafter by the QS Nd:YAG (1064 nm and 532 nm) and QS alexandrite (755 nm) laser systems [10]. In tattoo removal using the NS-domain QS lasers, it is argued that the pulse duration of the laser is shorter than the thermal relaxation time of the tattoo pigments and thus thermal lock-in is achieved [3]. However at the same time, another important phenomenon called stress lock-in must be taken into consideration. Stress relaxation can be explained simply as follows. When a certain particle is heated, thermal expansion of the par-

ticle occurs. The expansion diffuses to the surrounding tissue as vibration which is called stress diffusion. When a particle is heated within an extremely short period of time, the stress generated within the particle has not enough time to diffuse and stress lock-in is achieved, and if the generated stress is high enough, fracture of the particle occurs [3]. This is analogous to the thermal lock-in and extreme temperature rise in the thermal relaxation theory. The temporal threshold of the particle for stress lock-in to occur, the stress relaxation time (SRT), for tattoo pigments is thought to be slightly shorter than 10 ns. Therefore in tattoo removal using NS-domain QS lasers, stress lock-in is not achieved in all the particles since the pulse width of the lasers is longer than the stress relaxation time of the most of tattoo particles. However when a PS laser is used which can defeat the SRT, stress lock-in is achieved. In addition, to exert photoacoustic effects within the targeted tattoos that lead to mechanical dissolution of the ink particles, endothermic steam carbon reactions occur that alter the optical properties of the tattoo inks, producing shell-like structures and reducing their visibility [3].

The different reactions comparing a PS laser to an NS laser can be summed up as follows. When an NS-domain QS laser is used, the major reaction which takes place is photothermolysis through a photothermal reaction, with a very small photomechanical effect. However when a PS laser is used, stress lock-in occurs and the major reaction involves the photoacoustic destruction of the particle, with a minor photothermal component. Therefore more efficient and effective destruction of the particle becomes possible.

However, even using correct wavelengths and fluences, tattoos may respond unpredictably to laser treatment, not only because their chemical compositions are highly variable, but also because the tattoo inks are often located at variable dermal depths. Moreover, the biological effect of the laser treatment is also related to the different tattoo particles composition.

33.2.1 Classification of Tattoos

Professional tattoos are applied by a tattoo artist using a handheld tattoo gun that delivers uniformly deep dense dermal injections of ink. The ink colors are composed of organometallic dyes that are often mixed together to create a wide spectrum of colors. These are usually the most difficult tattoo to remove, because of the high amount of multicolored ink particles (some colors, i.e., white, yellow, and light green, are more difficult to eliminate because of the absence of wavelengths absorbed by targets).

Amateur tattoos are applied using handheld needles that deliver India ink or carbon injected at variable depths into the skin. They generally have fewer ink particles and are more superficially placed than professional tattoos. Because of their superficial placement, relative paucity of ink, and lack of multiple colors, amateur tattoos are often easier to remove.

Cosmetic tattoos are often applied freehand by cosmetologists to provide permanent makeup in areas where one would apply eyeliner, lip liner, or eyebrow pencil. The various shades of brown, black, flesh-tones, and red inks frequently contain titanium dioxide and iron oxide pigments that are difficult to remove because of oxidative reactions that darken the ink when irradiated with laser light. This color change is known as *paradoxical reaction*, and is attributed to chemical reduction of rust-colored ferric oxide to black ferrous oxide or white titanium^{4+} to blue titanium^{3+} dioxide. These cases often are resolved by an intervention with another laser wavelength (1064 nm, 694 nm, or 755 nm) (Fig. 33.3); however, the dark color can be permanent [11–13].

Medicinal tattoos are small gray or blue-black markings placed by medical personnel to designate radiotherapy fields or port placement sites. Similar to amateur tattoos, they are typically composed of a sparse amount of India ink or carbon pigment and are simply removed with laser in a few number of sessions.

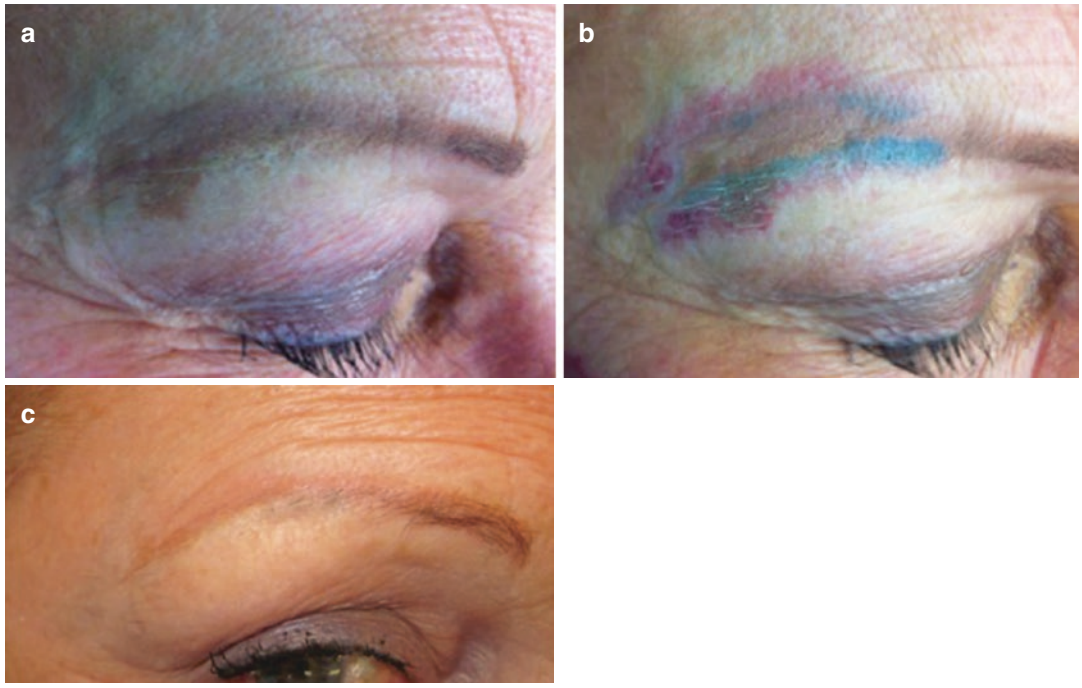

Fig. 33.3 Cosmetic brown eyebrow tattoo removal: (**a**) before treatment (**b**) paradoxical reaction with color changing after one session of 532 nm QS laser (**c**) complete ink removal after three sessions of 694 nm QS laser

Traumatic tattoos result from deposits of foreign particles such as metal, glass, dirt, and carbon-containing particles into the skin following mechanical penetration. These often follow blast injuries or trauma involving road surfaces and can be difficult to remove if they are deeply embedded and/or contain incendiary material [14]. In this cases is useful performing a test spot before treating the rest of the surface to ensure patient safety. The combination of fractional ablative (10,600 nm) or fractional QS or PS laser can be very useful to get the pigment in the deep dermis through cicatricial tissue [15].

33.2.2 Treatment Protocol

Laser treatment should be performed using the lowest fluence that achieves the desired clinical endpoint of immediate skin whitening on laser impact (*popcorn effect*: a result of gas formation from rapid tissue heating). Increasing fluences are often required during subsequent treatments as ink density decreases. Care should be taken to minimize pinpoint bleeding when higher fluences are used. One laser pass should be performed over the desired treatment area with minimal (less than 10%) overlap of spots. Laser treatments are typically administered at 30–45 days intervals or longer to permit adequate clearing of ink and appropriate skin healing between treatments, depending on body area and lymphatic drainage. Patients should be provided with postoperative instructions that include strict sun protection as well as application of emollient healing ointments and protective bandages for 7–10 days after treatment [10].

Recent studies have shown increased efficacy of laser tattoo removal when several laser passes are delivered during each treatment session, necessitating fewer treatment sessions for removal. For additional laser passes to be effective, the ash-white tissue response must resolve between passes. Two methods have been proposed to achieve this: the R20 and R0 methods [16, 17]. The R20 method, first introduced by Kossida et al., investigated single-pass treatment compared with four consecutive passes separated

by 20-min intervals (during which time resolution of ash-white tissue response occurs spontaneously). Results showed this approach is safe and more effective than traditional single-pass treatment. The R0 method, which involves the application of topical perfluorodecalin, a liquid fluorocarbon that immediately resolves the ash-white tissue response, was found to be faster and as clinically effective as the R20 treatment.

33.2.3 Choosing Correct Wavelength

Because multiple different inks are often present in a tattoo, effective treatment requires the use of various visible and near-infrared wavelengths. For an optimal removal of pigment, it is necessary to pick the most appropriate laser on the basis of the absorption spectrum of ink colors in the tattoo (Table 33.1). Black pigments absorb in the red and infrared and can be therefore treated with ruby (694 nm), alexandrite (755 nm), or Nd:YAG (1064 nm) QS/PS lasers (Fig. 33.4). Blue and green inks can be hit by frequencies in the 600–800 nm range, which makes ruby and alexandrite lasers the first choice. Red, orange, and yellow inks are specifically destroyed by green light, therefore most appropriate lasers for the removal of these colors are Nd:YAG (532 nm) QS/PS (Fig. 33.5). However, often professional tattoo makers such as painters used to mix different inks to obtain specific colors. In these cases possible approaches are: (1) change the wavelength applied at each session on the basis of the prevalent tattoo color (this will increase the total number of sessions needed to completely remove tattoo ink); (2) perform multiple passes with different wavelengths in each session (i.e., R20 technique with different wavelengths); (3) use laser devices able to emit simultaneously two different wavelengths.

Table 33.1 Absorption spectrum of ink colors in the tattoo

	Emitted light	Tattoo color		
532 nm	green			
694 nm	red			
755 nm	red			
1064 nm	infrared			

The Kirby–Desai scale has been proposed as an aid to help clinicians estimate the likely number of treatment sessions needed for tattoo removal and can be used during patient counseling [18]. Numbers are assigned to six factors: patient Fitzpatrick skin type, tattoo location, tattoo color, amount of tattoo ink, inherent scarring or tissue change, and ink layering. Scores are then tabulated that estimate the number of treatment sessions needed for tattoo removal. Kirby et al. found a correlation coefficient of 0.757 after performing a retrospective review of 100 patients

Fig. 33.4 Professional black tattoo removal: before and after six sessions with 1064 nm QS laser

Fig. 33.5 Professional multicolored tattoo removal: before and after eight sessions with 532 nm (red color) and 694 nm (green color) QS laser

treated with laser tattoo removal and comparing the actual number of required treatments with their Kirby–Desai scores. While helpful, the scale is limited because it does not take into account the type of laser used (e.g., wavelength, PS vs NS pulse duration).

33.2.4 Side Effects

In general, QS and PS lasers used for tattoo removal seem safe. Minor and transient side effects were commonly reported after laser treatment, including erythema, edema, pinpoint bleeding, and crusting. Pigmentation disorders were reported in up to 25% of patients and were probably related to patients' skin type. Transient textural changes were reported in up to 50%. The reports of acute bulla formation varied from 0 to 50% in different studies. Since some studies did not indicate the spot size used, we can only assume that this variation can be attributed to a difference in fluence and energy used. Hyperpigmentation and scarring were rarely reported using correct fluences [10].

In conclusion, laser therapy must be considered the elective treatment for tattoos; however, there are still difficulties due to the fact that several source types must be used to remove sources of different colors (e.g., multicolor tattoos performed by professionals). In fact, some white, yellow, and green hues are difficult to treat with currently available lasers. Finally cases in which even an accurate laser treatment does not allow to obtain a complete removal of the dermal pigment.

References

1. Anderson RR, Parrish JA. Selective photothermolysis: precise microsurgery by selective absorption of pulsed radiation. Science. 1983;220:524–7.
2. Hazama H, Awazu K. Mechanism and principle of laser treatment in dermatology: light-tissue interaction. In: Watanabe S, et al., editors. Pearls and problems of laser dermatology: Nankodo; 2013. p. 2–12.
3. Kasai K. Laser treatment of tattoos. Pepars. 2016;111:114–21.
4. Kasai K. Picosecond laser treatment for tattoos and benign cutaneous pigmented lesions (secondary publication). Laser Ther. 2017;26(4):274–81.
5. Shah S, Alster TS. Laser treatment of dark skin: an updated review. Am J Clin Dermatol. 2010;11(6):389–97.
6. Carroll L, Humphreys TR. Laser-tissue interactions. Clin Dermatol. 2006;24(1):2–7.
7. Anderson RR. Lasers in dermatology—a critical update. J Dermatol. 2000;27(11):700–5.
8. Altshuler GB, Anderson RR, Manstein D, Zenzie HH, Smirnov MZ. Extended theory of selective photothermolysis. Lasers Surg Med. 2001;29(5):416–32.
9. Bray FN, Shah V, Nouri K. Laser treatment of congenital melanocytic nevi: a review of the literature. Lasers Med Sci. 2016;31(1):197–204.

10. Reiter O, Atzmony L, Akerman L, Levi A, Kershenovich R, Lapidoth M, Mimouni D. Picosecond lasers for tattoo removal: a systematic review. Lasers Med Sci. 2016;31(7):1397–405.
11. Naga LI, Alster TS. Laser tattoo removal: an update. Am J Clin Dermatol. 2017;18(1):59–65.
12. Anderson RR, Geronemus R, Kilmer SL, Farinelli W, Fitzpatrick RE. Cosmetic tattoo ink darkening: a complication of Q-switched and pulsed-laser treatment. Arch Dermatol. 1993;129:1010–4.
13. Hamzavi I, Lui H. Surgical pearl: removing skin-colored cosmetic tattoos with carbon dioxide resurfacing lasers. J Am Acad Dermatol. 2002;46:764–5.
14. Taylor CR. Laser ignition of traumatically embedded firework debris. Lasers Surg Med. 1998;22:157–8.
15. Seitz AT, et al. Fractional CO2 laser is as effective as Q-switched ruby laser for the initial treatment of a traumatic tattoo. J Cosmet Laser Ther. 2016;16:303–5.
16. Kossida T, Rigopoulos D, Katsambas A, Anderson RR. Optimal tattoo removal in a single laser session based on the method of repeated exposures. J Am Acad Dermatol. 2012;66:271–7.
17. Reddy KK, Brauer JA, Anolik R, Benstein L, et al. Topical perfluorodecalin resolves immediate whitening reactions and allows rapid effective multiple pass treatment of tattoos. Lasers Surg Med. 2013;45:76–80.
18. Kirby W, Desai A, Desai T, Kartono F, Geeta P. The Kirby-Desai scale: a proposed scale to assess tattoo removal treatments. J Clin Aesthet Dermatol. 2009;2(3):32–7.

34 Skin Resurfacing: Ablative and Non-ablative Lasers

Pier Luca Bencini and Stefania Guida

34.1 Introduction

The request for skin resurfacing and rejuvenating procedures has increased in the last decades. In addition, the concept of nonsurgical skin rejuvenation has been developed through the introduction, among others, of laser skin resurfacing. Several advances have been made in the resurfacing field in order to induce faster healing and reduced downtime [1].

In the 1980s, continuous wave (CW) carbon dioxide (CO_2) lasers became available to resurface photoaged skin. Although the procedure could induce impressive results, the risk-benefit ratio was imbalanced for the high rate of scarring, dyspigmentation, erythema, skin eruptions and infections as well as increased pain, discomfort and downtime [2].

Accordingly, due to the enhanced thermal injury, a wide zone of thermal damage and ablation was induced by the CW of these early CO_2 lasers [3].

However, later on, short pulse, high peak power, and rapidly scanned CO_2 lasers and normal mode erbium-doped yttrium aluminum garnet (Er:YAG) lasers have been introduced. These devices enable the precise control of photoaged skin removal by reducing thermal injury [1].

In addition, non-ablative laser resurfacing systems and the concept of fractional photothermolysis (2004) have provided clinicians with a number of options enabling the selection of patients for each indication of treatment, in order to overcome some of the limitations of CW CO_2 laser [4–7].

34.2 Laser–Tissue Interactions for Carbon Dioxide and Erbium:YAG Lasers

34.2.1 Carbon Dioxide (CO_2)

In the 1980s, the concept of selective photothermolysis enabled the introduction of CO_2 laser resurfacing [8, 9].

Lasers used for skin surgery exploits heating. When selective heating is performed, employing selective photothermolysis principles, very precise tissue effects can be achieved [8, 9].

The principle is based on the preferential laser light absorption and heat production in the target

P. L. Bencini
ICLID, Istituto di Chirurgia e Laser-Chirurgia in Dermatologia, Milan, Italy
e-mail: pl.bencini@iclid.it

S. Guida (✉)
ICLID, Istituto di Chirurgia e Laser-Chirurgia in Dermatologia, Milan, Italy

Dermatology Unit, Department of Surgical, Medical, Dental and Morphological Science with Interest Transplant, Oncological and Regenerative Medicine, University of Modena and Reggio Emilia, Modena, Italy

M. Fimiani et al. (eds.), *Technology in Practical Dermatology*,
https://doi.org/10.1007/978-3-030-45351-0_34

chromophore. In order to reach this effect, a pulse duration shorter than the thermal relaxation (or cooling) time of the tissue should be employed [8, 9].

The 10.600 nm wavelength, belonging to the far-infrared electromagnetic spectrum, targets water. As a consequence, laser beam penetrates the skin independently from the amount of melanin and hemoglobin. When 5 J/cm^2 fluence is delivered, the vaporization threshold of tissue, employing a pulse duration lower than 1 ms, the thermal relaxation time of tissue, an optical penetration of 20 to 30 mm, is reached, with a residual thermal damage extending to 100 to 150 mm [10–12].

Coagulation and desiccation of tissue can be obtained when CO_2 lasers fail to deliver a fluence that surpasses the vaporization threshold [13].

The width of the zone of residual thermal damage is directly proportional to the pulse duration of the laser. For a CW beam CO_2 laser, the pulse duration can be reduced according to a freehand motion of the laser beam. However, small spot sizes can be used in order to achieve adequate fluences, despite inducing a zone of thermal necrosis of 100 μm^{-2} mm beyond the incision [12], thus potentially leading to a risk of scarring, although a good clinical practice.

With regard to fluence, it is directly related to laser beam diameter, thus leading to progressive development of different devices. First ones showed small-diameter beams (100–300 μm), achieving high fluences with rapid vaporization while larger beam diameters, such as 2 mm, led to an increased thermal heating with charring, above all when not rapidly moved over the target field. In addition, the ablation can be reached by means of two different strategies.

One is a high-power, individually pulsed CO_2 laser that could deliver 500 mJ, in 600 μs to 1 ms. When administered in a 3-mm spot or in a specific computer pattern generator, made up of dozens of 2.25-mm spots, sufficient fluences greater than 5 J/cm^2 can be achieved [14].

The other strategy for attaining the ablation parameters involved a lower-energy, rapidly scanning CW CO_2 laser. This technology employs focused small-diameter beams in order to generate sufficient fluence, scanning them in several non-overlapping shapes. When dwell times of less than a millisecond are applied, fluence rose above ablation threshold.

Combining features of these two systems, superpulsed lasers have been then introduced [15], with peak powers twice to 10-times the power of the CW, pulse durations of 0.1–0.9 ms, repetitions of 100–5000 Hz. High peak powers with short cooling pauses between each pause are typically employed. Thus, there is a reduced need to manually remove the laser beam from the skin to avoid unwanted thermal damage. With superpulsing, the concept of duty cycle should be taken into account, being referred to the percentage of time the laser is actually delivering energy. This percentage is often about 10%; however, it can be between an interval of 2 and 50%. In addition, the duty cycle can be modulated though pulsing the superpulses, without too low or too high repetition rates, in order to avoid the impairment of hemostasis or an excess of heating with consequent thermal damage (thus mimicking a CW modality), respectively. Thus, pulsed CO_2 enables the ablation of tissue with a peripheral thermal damage of less than 100 μm of thickness.

However, despite apparent advances, a study comparing four different CO_2 lasers have proven the efficacy and safety to be similar [16].

34.2.2 Erbium

When the chromophore is water, another wavelength should be considered. Accordingly, the Er:YAG laser, emitting at 2940 nm, has been developed for ablative purposes. This wavelength has a closer approximation to the absorption peak of water of 3000 nm, thus inducing a more limited depth of penetration and essentially avoiding thermal damage. In detail, laser penetration is only 1 to 3 mm per J/cm^2, with a low residual thermal damage, reaching 10 to 40 mm.

Similarly to what have been previously reported for CO_2 laser, the comparison of six erbium:YAG have proven equivalent efficacy and safety [17].

34.2.3 Other Lasers

The development of fractional technologies enables the delivering of columns of thermal injury to the skin, confined to limited parts of the skin, known as microthermal zones (MTZ), in order to avoid extended epidermal damage. The surrounding unaffected skin areas composed by follicular units and their stem cells, as well as available fibroblasts, contribute to a rapid reepithelization and collagen remodeling of these MTZ [18].

First lasers employing this fractional concept were the non-ablative, such as the 1550-nm erbium-doped fiber laser, inducing minimal downtime and mild erythema. However, these non-ablative fractional lasers (NAFL) usually target the dermis and attempt to stimulate dermal remodeling while avoiding epidermal injury and prolonged healing times. Although very safe, these devices are unable to generate significant dermal coagulation [18].

Therefore, these NAFL do not guarantee the same results of ablative lasers. However, the progression of technology enabled the combination of the theory of fractional photothermolysis and ablative laser technologies. As a consequence of the enhanced application of fractional lasers, many independent laser suppliers have been interested to take advantage of the new fractional technology. The major differences among several devices produced concern the depth of ablation and coagulation and the variations in treatment handpieces, with their varying spot sizes and shapes, as well as mode of application (rolling or stamping). Treatment handpieces vary according to the manner in which the treatments are performed and delivered to MTZ. Some examples include fractional 532-nm diode, 850- to 1350-nm infrared, 1064-nm/2940-nm Er:YAG, 1550-nm erbium-fiber, 2790-nm yttrium scandium gallium garnet (YSGG), 10,600-nm CO_2, and radiofrequency lasers and handpieces. These products emit different pulse lengths and different amounts of energy [19].

34.3 Operative Considerations

There are a few points to consider before ablative laser resurfacing treatment: patient selection, prophylactic procedures, anesthesia, and complications [19].

34.3.1 Patient Selection

Concerning patient selection, expectations, skin type, and medical history should be adequately investigated before treatment. Reasonable expectations for cosmetic outcome, taking into account the side effect profile, as well as the necessary downtime following treatment, should be given to patients. For example, a single treatment with an ablative fractionated device may achieve superior results as compared to one treatment with non-ablative devices, although the latter requires a significant reduced downtime period. In addition, potential contraindications should also be considered [19]:

- Keloids/hypertrophic scars. However, if keloids or hypertrophic scars are located on predisposed areas such as the chest, there is no strict contraindication for laser resurfacing.
- Decreased adnexal structures of the skin, such as skin that has received prior X-ray treatment or patients with scleroderma. The reason is that the successful result of laser depends on the presence of adnexal structures to repopulate the epidermis from stem cells found in skin appendages.
- History of oral retinoid use. Prior isotretinoin treatment has been associated with atypical scarring after dermabrasion or chemical peels, even if procedures were performed more than 1 year after the drug therapy. However, recent evidences suggest that there is insufficient evidence to support the current protocol of avoiding and delaying treatments due to isotretinoin intake [20].
- Skin disorders associated with potential Koebner phenomenon (i.e., psoriasis, vitiligo, lichen planus), and other skin conditions associated with delayed wound healing.

34.3.2 Perioperative Management

A number of useful medications make laser resurfacing more effective, safer, and more comfortable for the patient.

- Tretinoin has been associated to a faster reepithelization. For ablative lasers, the authors suggest using 0.1% tretinoin cream applied nightly for 3 months prior to, and discontinuing 24 h before, the planned procedure. For non-ablative laser resurfacing, 0.05% tretinoin should be considered [21].
- Bleaching creams. Post-inflammatory hyperpigmentation (PIH) can occur after laser resurfacing. In order to avoid this adverse event, patients are suggested to limit sun exposure prior to laser procedure and to avoid having a sun tan at the time of the procedure. Darker phototype patients are given hydroquinone, kojic acid, or azelaic acid to be used for several weeks before the procedure. Although studies are inconclusive about the preventive role of these topical agents for PIH, they may be effective for the postoperative regimen as a part of the at-home setting skin care [22].
- Antiviral therapy. Ablative laser resurfacing may trigger an outbreak of herpes simplex, potentially resulting in increased pain, prolonged healing, and an increased risk for scarring. Therefore, all patients are prophylactically given antiviral therapy starting 1–2 days before the procedure, going ahead for about 5 days [23].
- Antibacterial therapy. After laser resurfacing, there is a layer of necrotic thermally coagulated dermis that can represent an ideal culture medium. Thus, patients are usually given prophylactic antibiotic 1 day before the procedure, for a total of 5–6 days [23]. Prevention of secondary candida or other fungal infections can also be taken into account in selected cases [24].
- Systemic corticosteroids. Oral steroids can be considered for a short, 3- to 6-day, perioperative course to reduce the edema, in association with cool compresses, soaks in saline or water, and protection with a petrolatum ointment. After reepithelization, sunscreen use should be advised and makeup can be employed in case of persisting erythema.

34.3.3 Anesthesia

Several options for anesthesia are available, from topical agents to local infiltration, nerve blocks and systemic agents. The decision is related to different factors: patient tolerance, treatment area, and technology employed, considering, for instance, that low-energy, low-density NAFL usually do not require anesthesia.

The following options can be considered [19]:

- Topical agents, such as lidocaine and prilocaine cream, may be helpful for superficial laser procedures, particularly with the Er:YAG laser, which creates less thermal injury than the CO_2 laser and is therefore less painful.
- Regional nerve blocks using local anesthetics with eventual supplementary infiltration of the treated area can provide adequate anesthesia for the area under treatment. Regional blocks are performed with lidocaine 2% with 1:100,000 or 1:200,000 epinephrine, but can be enhanced by bupivacaine 0.5%, 1:10 sodium bicarbonate ($NaHCO_3$) 8.4% to neutralize the pH and, subsequently, diminish pain.
- For total face resurfacing and patients who are particularly sensitive or anxious, systemic agents can be considered, including anxiolytics, narcotics, intramuscular sedation, or intravenous anesthesia.

34.3.4 Complications

Side effects following laser resurfacing can include [19, 25]:

- Erythema, resulting from epidermal immaturity, reduced melanin absorption of light, and increased blood flow secondary to the laser-induced inflammatory response. Although this condition is cosmetically undesirable, it is universal and considered part of the normal healing process. However, persistent erythema

is identified when it lasts more than 4 days for NAFL and more than 1–6 months with ablative lasers.

- Infection, that should be suspected in case of any new onset pain or prolonged pain. In these cases, as well as in cases of abnormal erythema, yellow exudate or crusting, papules, pustules, or erosions, appropriate cultures should be performed and eventual infections treated according to the etiologic agent.
- Contact eczematous dermatitis, potentially occurring while the skin is denuded and can be easily prevented by avoiding potential sensitizers. Topical mild-potency corticosteroids can be employed to treat the occurrence of this complication.
- Follicular. a. Milia, related to follicular reepithelization compounded by the use of occlusive moisturizers. b. Acne, that can occur in the early postoperative phase, especially in patients with a past history of acne. It can be treated with standard acne therapy.
- Scarring. Although rare, it should be considered and can be related to technical inappropriate procedure or to inaccurate wound care. Preventive measures are represented by proper patient selection, an adequate number of laser passes, and good post-laser wound care.
- Pigmentary changes, occurring more frequently in patients with darker skin phototypes (a) PIH, consisting in a transient hyperpigmentation, most often seen in patients with Fitzpatrick's skin phototype III to VI. To treat PIH, bleaching creams and tretinoin are suggested as well as sun exposure avoidance; (b) Delayed hypopigmentation, developing 6 to 12 months after resurfacing. Hypopigmentation is, nowadays, an uncommon complication.

34.4 Indications for Ablative Lasers

34.4.1 Aging Signs

Identification of indications for laser treatment is important in order to meet patient expectations/satisfaction. Thus, selection of patients should take into account the perioral and periorbital regions. Accordingly, wrinkling in these areas has been traditionally unresponsive to surgical face-lifting procedures and present therapeutic alternatives (chemical peeling and dermabrasion) with limited efficacy in these specific regions [5].

CO_2 laser has been demonstrated to give the most impressive results in the treatment of photoaging signs. A retrospective study on 47 patients has shown good to excellent cosmetic results in the perioral, periorbital, and glabellar rhytides [4].

A recent paper has reported the application of a new technique for the ablative resurfacing of lower eyelid skin in 20 patients showing skin elastosis with or without evidence of the nasojugal fold and atrophic and dyschromic skin, obtaining different degrees of improvements in all patients [26].

However, it is important to consider that, if wrinkles are classified as mild, moderate, and severe categories, the expectation of treated patients should be for mild wrinkles to resolve and to moderate to severe to improve by one class [4, 27, 28].

The treated area continues to improve up to 18 months after laser resurfacing as collagen remodeling takes place. Collagen remodeling has been proved by histopathologic assessment [19]. Therefore, an improvement of skin tightening, as well as skin tone, texture, and rhytides can be observed. However, these results can be impaired by the occurrence of adverse events.

On the other hand, Er:YAG laser was found to be effective in treating mild to moderate rhytides. For instance, perioral, periorbital, and forehead rhytides showed an improvement 3 weeks after the laser treatment [29, 30].

Despite a reduced incidence of adverse events and reduced downtime after treatment, less satisfying results can be obtained as compared to CO_2. Nevertheless, Er:YAG laser appears to be useful in the treatment of patients with dark skin phototype [31].

On the other hand, melasma does not seem to represent a first line of application of ablative resurfacing lasers alone or the application of these technologies can induce potential adverse events [32].

34.4.2 Scarring

Both CO_2 and Er:YAG lasers have been employed in the treatment of acne, posttraumatic and post-surgical scars.

In particular, CO_2 lasers have been successfully used in acne scars (ice pick) and elevated ones while depressed scars tend to improve less [33, 34].

On the other hand, Er:YAG can be applied to the treatment of acne scars (atrophic and pitted) and hypertrophic scars with good results [35, 36].

34.4.3 Skin Lesions

Seborrheic keratosis, epidermal nevi, viral lesions such as verruca vulgaris and condylomas, xanthelasma, adnexal tumors such as syringomas, trichoepitheliomas, angiofibromas, and neurofibromas can be treated with ablation with both CO_2 and Er:YAG [37–41].

The application of this technique on melanocytic nevi as well as on malignant skin tumors is controversial. The reason lies in the fact that intraoperative histopathologic/cytologic examination is impaired by the vaporization, thus limiting the certainty of its complete removal.

However, scraping the lesion prior to vaporizing with laser through successive layers of the skin can be used to perform, on the one hand histopathologic examination and, on the other hand, the treatment of the lesion for basal cell carcinomas, actinic keratosis, and cheilitis [42, 43].

34.4.4 Rhinophyma

CO_2 laser is considered an excellent treatment modality for rhinophyma in experienced hands. In a study enrolling 124 patients with rhinophyma, good to excellent results were observed in 95% of patients, poor in the remnant 5% [44].

The Er:YAG laser can also been applied for the treatment of this condition [45].

The possible combination of both laser treatment modalities has been claimed to be the gold standard to perform a correct rhinophyma treatment in a bloodless field [46].

34.5 Fractional Laser Resurfacing

The novel concept of fractional photothermolysis (FP) was first reported in 2003, in its basic application [47]. After that, in 2004 and 2005 first applications for photoaging by Manstein et al. were reported [7, 48].

Fractional technologies can be divided into two main categories based on the wavelength's affinity for water: ablative, employing wavelengths highly absorbed by water, and non-ablative, with only moderately absorbed wavelengths. Ablative devices include both Er:YAG; 2940 nm or YSGG; 2790 nm and CO_2; 10,600 nm lasers while "non-ablative" employ wavelengths of 1410 nm, 1440 nm, 1540 nm, and 1550 nm.

Histologically, with the NAFL, a column-like denaturation of the epidermis and dermis is induced. Furthermore, a disruption of the dermo-epidermal junction, with subepidermal clefting within the MTZ, and an intact stratum corneum can be observed. Therefore, thermally destroyed tissue becomes replaced by keratinocytes migrating from the surrounding healthy tissue within the first 24 h after treatment [49].

As a consequence, the necrotic tissue, named Microscopic Epidermal Necrotic Debris (MEND), is eliminated through the epidermis, facilitated by the subepidermal clefting. Clinically, this transepidermal elimination of necrotic tissue results in slight scaling and bronzing of the skin and occurs 1 week after treatment. After that, MTZ replacement with new collagen takes place within 3–6 months [50].

Selecting specific parameters of energy *per* MTZ and the density of MTZ *per* cm^2, 3–40% of the skin can be covered with each treatment. The MTZ are usually smaller than 400 μm in diameter and can reach varying depths of up to 1300 μm, depending on the wavelength, pulse energy, and device used. With increasing energy for each spot, there is an increase in size/diameter of the MTZ, as well as the depth of penetration.

Therefore, energy employed is based on the desired depth of treatment. Densities can be reported as either percent coverage, or MTZ *per* cm^2. Thermal damage is induced in the epidermis and dermis, leading to epidermal turnover and collagen induction [50].

With the ablative fractional lasers (AFL), histologically one can see ablated micro-columns (corresponding to MTZ), with varying thickness and depth, related to pulse width and wavelength used. A thin layer of eschar lines the cavity, which is associated to ablative treatment. Around these cavities, the presence of annular coagulation zones of different thickness is represented by denatured collagen. When an AFL is employed the stratum corneum is mostly absent, as compared to the situation of NAFL use [50].

34.5.1 Non-ablative

The request for a better side effect profile while minimizing downtime, fueled the development of NAFL, along with fractionated variants of ablative lasers [19].

The main difference between AFL and NAFL is that non-ablative ones do not damage the superficial epidermis, while achieving selective dermal injury, leading to new collagen deposition and remodeling. Consequently, this mechanism of action of non-ablative lasers reduces the downtime for patients, the need for wound care and anesthetics and ameliorates the side effects profile.

Although very safe, these devices are unable to generate significant dermal coagulation. Therefore, efficacy of a single session of treatment may be considered less than ideal. It is the responsibility of the physician to be certain that the patient has reasonable expectations and may require a series of treatments to achieve desired outcomes [19].

34.5.2 Ablative

AFR was created by combining wavelength of the traditional ablative resurfacing lasers with an FP system. AFR achieves controlled tissue vaporization and thermally induced dermal coagulation reaching greater depths than those of both traditional CO_2 lasers and newer NAFL. Therefore, AFR produces an increased tissue contraction, collagen production, and dermal remodeling as compared to NAFL.

In addition, there are several advantages of AFR over traditional CO_2 laser resurfacing. Interestingly, a study involving 2000 procedures has shown that, with a proper technique, there is a very low risk of scarring or hypopigmentation [18].

A reduced downtime and a safer adverse events profile have been demonstrated with AFR as compared to classic ablative procedures. After full-face resurfacing with AFR, a complete re-epithelialization can be observed in three to six days while two to three weeks of recovery are required with traditional CO_2 full-face resurfacing.

34.6 Indications for Fractional Laser Resurfacing

34.6.1 Aging Signs

Both NAFL and AFL have been proven to be effective in the treatment of skin aging, including periorbital and perioral rhytides, wrinkling, and skin texture (Fig. 34.1). A shrinkage pattern can be obtained through thermal injury induced by the treatment. After one month, tissue shrinkage is followed by a relaxation time before a retightening at 3 months [7].

In addition, NAFL can be successfully applied to skin sites other than the face [51], such as hands [52] and neck [53].

A combined approach between NAFL and intense pulsed light (IPL) has been described, inducing increased improvements on photoaging signs, as compared to NAFL alone [54].

On the other hand, AFL can induce an improvement of aging signs.

Wound healing response has been shown to be sustained for at least 3–6 months post-treatment

Fig. 34.1 Clinical pictures of a 68-year-old woman before and after resurfacing with fractional CO_2 laser. An improvement in perioral rhytides, wrinkling and skin texture can be observed after the treatment

Fig. 34.2 Clinical pictures of a 72-year-old woman before and after resurfacing with fractional CO_2 laser. The treatment provided skin tightening and skin color uniformity

with both histopathology and non-invasive skin imaging techniques [55].

In detail, greater clinical improvements in wrinkling and skin texture can be achieved with AFL, as compared to NAFL, such as for the treatment of skin laxity in lower eyelids after 2–3 treatment sessions [56].

On the other hand, skin pigmentary disorders do not seem to represent a specific field of application of resurfacing lasers although NAFL has been proven its efficacy in melasma in patients with IV and V skin phototype. However, high rates of recurrence have been described. Nevertheless, protocols including AFL without (Fig. 34.2) or with topical creams or chemical peels have been proven their efficacy [57].

34.6.2 Scars

Scars represent a large field of application of FP. Ice pick, boxcar, rolling scars, and atrophic ones have been proven to show an improvement of 25 to 50%, as assessed by means of digital photography as well as non-invasive skin imaging techniques [58, 59].

Consecutive sessions of treatment as well as several passes of treatment have been directly related to scar improvement [60, 61].

However, AFLs, both CO_2 and erbium [62], have been associated with higher efficacy profile for acne scars treatment, as compared to NAFL [63], and to microneedling [64].

Interestingly, high-energy and low-density laser settings have been proven to be more effective as compared to low-energy and high-density settings. For dark-skinned patients, NAFL should be taken into account [65].

In addition, surgical, posttraumatic and striae distensae have been demonstrated to respond to NAFL. The hypothesized mechanism of action has been neo-collagenesis and collagen remodeling [66].

For hypertrophic scars, low-energy protocols have been shown to be highly effective while minimizing adverse events [67].

34.6.3 Other

AFL, both CO_2 and erbium:YAG lasers, can be employed for the laser-assisted drug delivery (LADD). LADD has been described as a promising technique combining the effect of laser and enhancing the absorption of topical molecules. It is a versatile technique that should be adjusted to the patient, the drug to be delivered (such as corticosteroids, photosensitizers, and immunotherapy agents), depending on the skin conditions (including scars, nonmelanoma skin cancer, and photodamage) and their locations [68]. NAFL can also be combined with LADD [69].

References

1. Loesch MM, Somani AK, Kingsley MM, Travers JB, Spandau DF. Skin resurfacing procedures: new and emerging options. Clin Cosmet Investig Dermatol. 2014;7:231–41.
2. Airan LE, Hruza G. Current lasers in skin resurfacing. Facial Plast Surg Clin North Am. 2005;13:127–39.
3. Tanzi EL, Lupton JR, Alster TS. Lasers in dermatology: four decades of progress. J Am Acad Dermatol. 2003;49:1–31.
4. Waldorf HA, Kauvar AN, Geronemus RG. Skin resur-facing of fine to deep rhytides using a char-free carbon dioxide laser in 47 patients. Dermatol Surg. 1995;21:940–6.
5. Fitzpatrick RE, Goldman MP, Satur NM, et al. Pulsed carbon dioxide laser resurfacing of photo-aged facial skin. Arch Dermatol. 1996;132:395–402.
6. Alster TS, West TB. Resurfacing of atrophic facial acne scars with a high-energy, pulsed carbon dioxide laser. Dermatol Surg. 1996;22:151–4.
7. Manstein D, Herron GS, Sink RK, et al. Fractional photothermolysis: a new concept for cutaneous remodeling using microscopic patterns of thermal injury. Lasers Surg Med. 2004;34:426–38.
8. Altshuler GB, Anderson RR, Manstein D, Zenzie HH, Smirnov MZ. Extended theory of selective photothermolysis. Lasers Surg Med. 2001;29:416–32.
9. Anderson RR, Parrish JA. Selective photothermolysis: precise microsurgery by selective absorption of pulsed radiation. Science. 1983;220:524–7.
10. Kauvar AN, Waldorf HA, Geronemus RG. A histopathological comparison of “char-free” carbon dioxide lasers. Dermatol Surg. 1996;22:343–8.
11. Green HA, Domankevitz Y, Nishioka NS. Pulsed carbon dioxide laser ablation of burned skin: in vitro and in vivo analysis. Lasers Surg Med. 1990;10:476–84.
12. Walsh JT Jr, Flotte TJ, Anderson RR, Deutsch TF. Pulsed CO_2 laser tissue ablation: effect of tissue type and pulse duration on thermal damage. Lasers Surg Med. 1988;8:108–18.
13. Kauvar AN, Geronemus RG. Histology of laser resurfacing. Dermatol Clin. 1997;15:459–67.
14. Yang CC, Chai CY. Animal study of skin resurfacing using the ultrapulse carbon dioxide laser. Ann Plast Surg. 1995;35:154–8.
15. Krupa Shankar DS, Chakravarthi M, Shilpakar R. Carbon dioxide laser guidelines. J Cutan Aesthet Surg. 2009;2:72–80.
16. Alster TS, Nanni CA, Williams CM. Comparison of four carbon dioxide resurfacing lasers. A clinical and histopathologic evaluation. Dermatol Surg. 1999;25:153–8.
17. Alster TS. Clinical and histologic evaluation of six erbium:YAG lasers for cutaneous resurfacing. Lasers Surg Med. 1999;24:87–92.
18. Hunzeker CM, Weiss ET, Geronemus RG. Fractionated CO_2 laser resurfacing: our experience with more than 2000 treatments. Aesthet Surg J. 2009;29:317–22.
19. Brightman LA, Brauer JA, Anolik R, Weiss E, Karen J, Chapas A, Hale E, Bernstein L, Geronemus RG. Ablative and fractional ablative lasers. Dermatol Clin. 2009;27:479–89.
20. Mysore V, Mahadevappa OH, Barua S, Majid I, Viswanath V, Bhat RM, Talwar S, Thurakkal S, Aurangabadkar SJ, Chatterjee M, Ganjoo A. Standard guidelines of care: performing procedures in patients on or recently administered with isotretinoin. J Cutan Aesthet Surg. 2017;10:186–94.
21. Buchanan PJ, Gilman RH. Retinoids: literature review and suggested algorithm for use prior to facial resurfacing procedures. J Cutan Aesthet Surg. 2016;9:139–44.
22. Sriprachya-anunt S, Marchell NL, Fitzpatrick RE, Goldman MP, Rostan EF. Facial resurfacing in patients with Fitzpatrick skin type IV. Lasers Surg Med. 2002;30:86–92.
23. Nestor MS. Prophylaxis for and treatment of uncomplicated skin and skin structure infections in laser and cosmetic surgery. J Drugs Dermatol. 2005;4:s20–5.
24. Conn H, Nanda VS. Prophylactic fluconazole promotes reepithelialization in full-face carbon dioxide laser skin resurfacing. Lasers Surg Med. 2000;26:201–7.
25. Ragland HP, McBurney E. Complications of resurfacing. Semin Cutan Med Surg. 1996;15:200–7.
26. Guida S, Nisticò SP, Farnetani F, Del Duca E, De Carvalho N, Persechino F, Verdina T, Giannetti L, D’Alessandro M, Urtis GG, Pellacani G, D’Alessandro G. Resurfacing with ablation of periorbital skin technique: indications, efficacy, safety, and 3D assessment from a pilot study. Photomed Laser Surg. 2018;36:541–7.
27. Lask G, Keller G, Lowe N, Gormley D. Laser skin resurfacing with the SilkTouch flashscanner for facial rhytides. Dermatol Surg. 1995;21:1021–4.
28. Lowe NJ, Lask G, Griffin ME, Maxwell A, Lowe P, Quilada F. Skin resurfacing with the Ultrapulse

carbon dioxide laser: observations on 100 patients. Dermatol Surg. 1995;21:1025–9.
29. Perez MI, Bank DE, Silvers D. Skin resurfacing of the face with the Erbium:YAG laser. Dermatol Surg. 1998;24:653–8.
30. Teikemeier G, Goldberg DJ. Skin resurfacing with the erbium:YAG laser. Dermatol Surg. 1997;23:685–7.
31. Polnikorn N, Goldberg DJ, Suwanchinda A, Ng SW. Erbium:YAG laser resurfacing in Asians. Dermatol Surg. 1998;24(12):1303–7.
32. Okan G, Nouri K, Trent JS, Barbarulo AM, Rendon M. Delayed wound healing after laser resurfacing. Dermatol Surg. 2001;27:93–5.
33. Jacob CI, Dover JS, Kaminer MS. Acne scarring: a classification system and review of treatment options. J Am Acad Dermatol. 2001;45(1):109–17.
34. Bernstein LJ, Kauvar AN, Grossman MC, Geronemus RG. Scar resurfacing withhigh-energy, short-pulsed and flashscanning carbon dioxide lasers. Dermatol Surg. 1998;24:101–7.
35. Tanzi EL, Alster TS. Treatment of atrophic facial acne scars with a dual-mode Er:YAG laser. Dermatol Surg. 2002;28:551–5.
36. Vrijman C, van Drooge AM, Limpens J, Bos JD, van der Veen JP, Spuls PI, Wolkerstorfer A. Laser and intense pulsed light therapy for the treatment of hypertrophic scars: a systematic review. Br J Dermatol. 2011;165:934–42.
37. Phahonthep R, Sindhuphak W, Sriprajittichai P. Lidocaine iontophoresis versus EMLA cream for CO_2 laser treatment in seborrheic keratosis. J Med Assoc Thail. 2004;87:S15–8.
38. Bencini PL, Guida S, Cazzaniga S, Pellacani G, Galimberti MG, Bencini M, Naldi L. Risk factors for recurrence after successful treatment of warts: the role of smoking habits. J Eur Acad Dermatol Venereol. 2017;31:712–6.
39. Raulin C, Schoenermark MP, Werner S, Greve B. Xanthelasma palpebrarum: treatment with the ultrapulsed CO_2 laser. Lasers Surg Med. 1999;24:122–7.
40. Sajben FP, Ross EV. The use of the 1.0 mm handpiece in high energy, pulsed CO_2 laser destruction of facial adnexal tumors. Dermatol Surg. 1999;25:41–4.
41. Dmovsek-Olup B, Vedlin B. Use of Er:YAG laser for benign skin disorders. Lasers Surg Med. 1997;21:13–9.
42. Guida S, Bencini PL, Manganoni AM, Gianotti R, Lospalluti L, Greco P, Pellacani G, Farnetani F. Recurrence of melanocytic lesions after laser treatment: benign vs. malignant upon dermoscopy. J Eur Acad Dermatol Venereol. 2017;31:e526–8.
43. Campolmi P, Bonan P, Cannarozzo G, Bassi A, Bruscino N, Arunachalam M, Troiano M, Lotti T, Moretti S. Highlights of thirty-year experience of CO_2 laser use at the Florence (Italy) department of dermatology. Sci World J. 2012;2012:546528.
44. Madan V, Ferguson JE, August PJ. Carbon dioxide laser treatment of rhinophyma: a review of 124 patients. Br J Dermatol. 2009;161:814–8.
45. Krausz AE, Goldberg DJ, Ciocon DH, Tinklepaugh AJ. Procedural management of rhinophyma: A comprehensive review. J Cosmet Dermatol. 2018;17:960–7.
46. Goon PK, Dalal M, Peart FC. The gold standard for decortication of rhinophyma: combined erbium-YAG/CO_2 laser. Aesthet Plast Surg. 2004;28:456–60.
47. Huzaira M, Anderson RR, Sink K, Manstein D. Intradermal focusing of near-infrared optical pulses: a new approach for non-ablative laser therapy. Lasers Surg Med. 2003;32(Suppl 15):17–38.
48. Khan MH, Sink RK, Manstein D, Eimerl D, Anderson RR. Intradermally focused infrared laser pulses: thermal effects at defined tissue depths. Lasers Surg Med. 2005;36:270–80.
49. Laubach HJ, Tannous Z, Anderson RR, Manstein D. Skin responses to fractional photothermolysis. Lasers Surg Med. 2006;38:142–9.
50. Bogdan Allemann I, Kaufman J. Fractional photothermolysis-an update. Lasers Med Sci. 2010;25:137–44.
51. Wanner M, Tanzi EL, Alster TS. Fractional photothermolysis: treatment of facial and nonfacial cutaneous photodamage with a 1,550-nm erbium-doped fiber laser. Dermatol Surg. 2007;33:23–8.
52. Jih MH, Goldberg LH, Kimyai-Asadi A. Fractional photothermolysis for photoaging of hands. Dermatol Surg. 2008;34:73–8.
53. Bencini PL, Tourlaki A, Galimberti M, Pellacani G. Non-ablative fractionated laser skin resurfacing for the treatment of aged neck skin. J Dermatolog Treat. 2015;26:252–6.
54. Kearney C, Brew D. Single-session combination treatment with intense pulsed light and nonablative fractional photothermolysis: a split-face study. Dermatol Surg. 2012;38:1002–9.
55. Longo C, Galimberti M, De Pace B, Pellacani G, Bencini PL. Laser skin rejuvenation: epidermal changes and collagen remodeling evaluated by in vivo confocal microscopy. Lasers Med Sci. 2013;28:769–76.
56. Tierney EP, Eisen RF, Hanke CW. Fractionated CO_2 laser skin rejuvenation. Dermatol Ther. 2011;24:41–53.
57. Trelles MA, Velez M, Gold MH. The treatment of melasma with topical creams alone, CO_2 fractional ablative resurfacing alone, or a combination of the two: a comparative study. J Drugs Dermatol. 2010;9:315–22.
58. Bencini PL, Tourlaki A, Galimberti M, Longo C, Pellacani G, De Giorgi V, Guerriero G. Nonablative fractional photothermolysis for acne scars: clinical and in vivo microscopic documentation of treatment efficacy. Dermatol Ther. 2012;25:463–7.
59. Geronemus RG. Fractional photothermolysis: current and future applications. Lasers Surg Med. 2006;38:169–76.
60. Taub AF. Fractionated delivery systems for difficult to treat clinical applications: acne scarring, melasma, atrophic scarring, striae distensae, and deep rhytides. J Drugs Dermatol. 2007;6:1120–8.

61. Chrastil B, Glaich AS, Goldberg LH, Friedman PM. Second-generation 1,550-nm fractional photothermolysis for the treatment of acne scars. Dermatol Surg. 2008;34:1327–32.
62. Manuskiatti W, Iamphonrat T, Wanitphakdeedecha R, Eimpunth S. Comparison of fractional erbium-doped yttrium aluminum garnet and carbon dioxide lasers in resurfacing of atrophic acne scars in Asians. Dermatol Surg. 2013;39:111–20.
63. Cho SB, Lee SJ, Cho S, Oh SH, Chung WS, Kang JM, Kim YK, Kim DH. Non-ablative 1550-nm erbium-glass and ablative 10 600-nm carbon dioxide fractional lasers for acne scars: a randomized split-face study with blinded response evaluation. J Eur Acad Dermatol Venereol. 2010;24:921–5.
64. Osman MA, Shokeir HA, Fawzy MM. Fractional erbium-doped yttrium aluminum garnet laser versus microneedling in treatment of atrophic acne scars: a randomized split-face clinical study. Dermatol Surg. 2017;43:S47–56.
65. Jung JY, Lee JH, Ryu DJ, Lee SJ, Bang D, Cho SB. Lower-fluence, higher-density versus higher-fluence, lower-density treatment with a 10,600-nm carbon dioxide fractional laser system: a split-face, evaluator-blinded study. Dermatol Surg. 2010;36:2022–9.
66. Guida S, Galimberti MG, Bencini M, Pellacani G, Bencini PL. Treatment of striae distensae with non-ablative fractional laser: clinical and in vivo microscopic documentation of treatment efficacy. Lasers Med Sci. 2018;33:75–8.
67. Lin JY, Warger WC, Izikson L, Anderson RR, Tannous Z. A prospective, randomized controlled trial on the efficacy of fractional photothermolysis on scar remodeling. Lasers Surg Med. 2011;43:265–72.
68. Alegre-Sánchez A, Jiménez-Gómez N, Boixeda P. Laser-assisted drug delivery. Actas Dermosifiliogr. 2018;109:858–67.
69. Bertin ACJ, Vilarinho A, Junqueira ALA. Fractional non-ablative laser-assisted drug delivery leads to improvement in male and female pattern hair loss. J Cosmet Laser Ther. 2018;16:1–4.

Photorejuvenation: Concepts, Practice, Perspectives

35

Marco Dal Canton

35.1 Introduction

Photorejuvenation is an attractive and effective term in the vocabulary of both physicians and contemporary patients. A measure of the perception of laser photorejuvenation in the collective imagination can be recorded when analyzing the statistics of the top nonsurgical procedures in the USA and worldwide. The global aesthetic laser market size was valued USD 508 million in 2015 [1] and is expected to grow, in proportion to the progressively increasing demand of cosmetic minimally invasive procedures in the next few years: the American Society of Plastic Surgeons reports 15.7 million performed in 2017, 2% more than in 2016 [2].

The demand for lasers is projected to grow at a rapid rate due to aging baby boomers as well as surplus income with the middle class to spend on cosmetic surgeries.

Downtime is considered a major problem for our web well-versed patients, nowadays looking for striking results, nevertheless with acceptable to no interruption of own daily activities and minimal impact on social life. In today's fast moving world, finding a solution to this ambitious compromise is directing consistently to high-end medical technologies.

In an extremely competitive and often aggressive and ambiguous market, chiefly when dealing with skin and aesthetic problems, physicians today have to push the expectations of patients within the real world, sharing the available level of scientific evidence sustaining or often against any therapeutic option, balancing own costs and ambitions with the conservation of own professionalism.

The first publications citing the term *skin rejuvenation* with lasers, in the 1990s, were discussing on ablative lasers [3], while to the author's knowledge in 2000 the term *photorejuvenation* appeared for the first time in the literature [4].

In the following few years, many surveys and reports on the effects of high energy polychromatic and laser lights have been progressively published.

35.2 Photorejuvenation: Definition

The expression *non-ablative skin rejuvenation* has been originally coined to summarize the global effects of the treatment with a high energy medical purpose non-ablative light sources, as lasers or polychromatic intense pulsed lights, on telangiectasia, irregular pigmentation, texture,

M. Dal Canton (✉)
Department of Dermatology and Venereology, Ordine Medici e Chirurghi Provincia di Belluno, Belluno, Italy

Private practice, Qderm-Belluno, Italy
e-mail: mdc@qderm.it

M. Fimiani et al. (eds.), *Technology in Practical Dermatology*,
https://doi.org/10.1007/978-3-030-45351-0_35

and rhytids, while preserving the epidermis, with a final result of an overall improvement of the signs of photoaged skin [2, 5].

The term photorejuvenation is now more widely used referring not only to the effects of non-ablative lasers and IPLs, but also to those of ablative lasers, of fractional non-ablative and ablative lasers, of LEDs (low level light therapy—LLLT) [6] or as a component of photodynamic therapy.

The common and crucial principle in these definitions is the possibility to take advantage of the effect of light interaction with the skin in the improvement of specific signs of the aged skin.

In the most genuine sense, the mechanism of photorejuvenation implicates a selective absorption of the impacting light by hemoglobins, melanins, and/or tissue water, with epidermal sparing, leading to a dermal repair zone, resulting in an orderly restoration of a more normalized skin structure [7].

Zelickson et al. in 1999 published the histologic description of collagen remodeling after a flashlamp pulsed dye laser vascular laser treatment [8]. Bjerring et al. in 2000 described the clinical improvement of aged skin after long pulsed FLPD treatment in 40% of patients [9] while Bitter reported a significant improvement after a series of full face intense pulsed light (IPL) treatments [4].

Non-ablative laser and PCL skin rejuvenation rapidly gained popularity as a very beneficial collateral consequence of selective targeting the overrepresented chromophores in the aged skin with vascular and pigment specific lasers and IPLs, as the hemoglobins in telangiectasia, the diffuse redness in rosacea and poikiloderma, and melanins in solar lentigo and mottled pigmentation.

Moreover, it was made clear the advantage of adding a new indication to existing well-honored devices in the healthcare facilities on a wide array of candidates, offering the perspective of an effective and progressive outcome on red and brown skin color and a collateral improvement of the texture, with a reasonably limited downtime.

A filtered search on Pubmed for publications consistent with the concept of photorejuvenation produced the following results (09/2018): 111 papers on skin rejuvenation with non-ablative lasers; 57 with vascular lasers; 32 with Q-switched lasers; 11 with picosecond lasers; 151 with IPLs and, to the author's knowledge, 21 randomized controlled studies on photorejuvenation are available, empowering the attention on the potential beneficial effects of the laser/PCL skin interaction.

When short pulses of an optical radiation are selectively absorbed by tissue cells, this can induce a selective damage to pigmented structures, cells, and organelles in vivo [10] (selective photothermolysis); but when the treatment pulse width is significantly longer than the target thermal relaxation time (TRT), a thermal effect extended to nearby targets should be expected (extended theory of photothermolysis) [11].

This gentle interplay between selective and extended photothermolysis can explain how target specific vascular and pigment specific lasers and IPLs can improve the evenness of red and brown color and produce a restoration of contiguous skin structures, clinically improving the texture of the photoaged skin.

35.3 Vascular Lasers, PCLs, and Photorejuvenation

Typically isolated and arborizing telangiectasia, diffuse redness, poichiloderma, spider angiomas, and rosacea can be considerable constituents of the clinical features of a sun-damaged skin. In 2001, Bjerring et al. described that irradiation by a short pulsed 585 nm vascular laser at subpurpura energy level induced a statistically significant increase of 84% in the type III procollagen production rate compared to a nontreated control site [12].

IPL irradiation may induce fibroblast and vascular endothelial cells growth and increase viability in cultured cells lines, and produce a

time-dependent overexpression of procollagen I and III mRNA, which may primarily contribute to the connective tissue restoration after broadband light irradiation [13].

After these first clinical and histologic reports, a number of scientific papers on photorejuvenation with almost all available vascular lasers have been published, corroborating these initial clinical and experimental evidences.

The range of vascular laser is wide, and any option offers different advantages: in the 532–585 nm range we can choose the less penetrating KTP and flashlamp pumped dye lasers (PDLs), with the advantage, or disadvantage in darker skin types, of melanin as a possible competing chromophore, while in the near IR the more deeply penetrating 800–1064 nm lasers are suitable to be selectively absorbed also by tissue water and thermally stimulate more deeply the dermis.

The whole range of vascular lasers can be understandably covered by polychromatic intense pulsed lights, filtered in the lower visible and UV range, offering the advantages and disadvantages of a continuous range of wavelengths and limitless possible settings on a wider area treated per single pulse, in respect to the definite wavelength and distinct combinations of fluence and pulse widths offered by lasers, mostly on a smaller spot. The detailed features and properties of lasers and broadband pulsed light (PCLs) are described in other chapters in this book.

How much can we realistically promise our patients interested in a relatively noninvasive procedure such as a vascular laser or an IPL laser photorejuvenation with a 530–550 nm filter?

A retrospective blinded before vs after study on objective and subjective clinical effects of a Nd:YAG 532 nm frequency-doubled long pulsed laser on color signs, texture, and rhytids on 20 patients based on questionnaires and confrontation of standardized before and after pictures evidenced a remarkable improvement in the red and brown color signs of photoaging in skin types I–III, a slight to moderate improvement in skin texture and fine wrinkles, but a negligible improvement of medium depth and deep wrinkles [14].

These observations on 532 nm wavelength can realistically be compared to similar ones made after treatments with lasers in the visible range, as with the whole range of pulsed dye lasers [15, 16] and with broadband intense pulsed lights [4, 14, 16, 17]. Albeit with different modalities of delivery of light energy to tissues, all these technologies are appropriate to interact selectively with hemoglobin and melanin, with an expected overall collateral improvement of texture in the mid to long term after treatment, while no significant results on rhytids should be promised [12, 16].

IPL and long pulsed FPDL resulted to be similarly effective in reducing facial erythema in a split face perspective study [17]. Long pulsed 595 nm dye laser results to be effective and suitable to treat diffuse redness in lighter skinned, and when compared quasi-long pulsed (microsecond) Nd: YAG 1064 nm laser, both lasers resulted to be successful in reducing facial erythema [18].

Whereas the effects of LPDL and IPL on irregular pigmentation and on texture resulted comparable on a randomized split face blinded comparative study, telangiectasia result to be more efficiently treated with LPD vascular laser [19].

In another study, both KTP 532 nm and IPL resulted to be equally effective to achieve a marked improvement in vascular and pigmented alterations in sun-damaged skin, with the KTP causing a little more pain and post-laser edema than IPL [20].

35.4 Pigment Specific Lasers and Skin Rejuvenation

Melanin can be an unavoidable target for shorter wavelengths. For this reason, Nd: YAG 532 nm FD laser, 577, 585, 595 nm pulsed dye lasers, 755 nm alexandrite and broadband lights emitting shorter wavelengths are better indicated to treat lighter

and untanned skin, as well as they are suitable to treat not only vascular abnormalities, but also uneven pigmentation and discrete pigmented benign lesions, as solar lentigo, early stage flat seborrheic keratoses, skin tags, dermatosis papulosa nigra, brownish poikilodermatous changes often coexisting in photoaged skin [21–23].

The differential diagnosis of pigmented facial lentigo on chronically sun-damaged skin represents one of the most challenging scenarios for dermatologists treating skin cancer. A precise diagnosis is needed in any case before lasering a pigmented, irregularly pigmented or sometimes barely or nonpigmented lesion. Often clinical examination and immersion or polarized dermoscopy could not be sufficiently informative for a reassuring diagnosis. The diagnosis of pigmented flat facial lesions on chronically sun-damaged skin can be particularly challenging also for an experienced dermatologist, and early stage seborrheic keratosis, especially when irritated or regressive, and pigmented actinic keratosis can display overlapping features with lentigo maligna [24].

This understandable prerequisite could be uncomfortably shared with our aesthetic concerned patient, often asking us an easy and speedy laser resolution of a boring age spot.

An accurate and detailed diagnosis of any clinical sign related to skin photoaging must be provided before treatment, sharing with the patient the opportunity of further examination, when clinical and dermoscopic evaluation results are not completely exhaustive. These can include optical coherence and confocal microscopy, usually available in research centers while histologic examination is definitely necessary in the diagnosis of controversial pigmented and nonpigmented skin lesions [25].

A key issue is to detect a melasma before a laser treatment, often barely visible and concealed amidst the irregular pigmentation of a photoaged face: this is in order to prevent an inadvertent laser overtreatment, which frequently conveys to a disappointing rebound or even worsening of the hyperpigmentation.

This common skin dyspigmentation should be under reasonable control before hitting the affected skin with high energy light sources, independent upon the selected target.

Based on current evidences, if a melasma is detected, no available laser technology and laser treatment protocol is recommended as monotherapy and/or first-line therapy rather as an integration of a medical treatment with bleaching agents, topical or oral tranexamic acid, combined with daily application of a high index sun protection [26].

Habitually the patient is concerned chiefly of one or more of the larger and visible pigmented "age spots" of the face, decoltè, or dorsum of hands, giving less importance to uneven distribution of pigmentation and the other signs of photoaged skin.

In this case, laser treatment results to be superior to other conventional treatments, as cryotherapy, peeling or bleaching agents [27], and the option to treat one or more larger age spots can be offered with pigment specific light sources as: long pulsed 532 nm Nd: YAG (Fig. 35.3), 585 [28], 595 nm PDL [29], 755 nm alexandrite [30]; with 532 nm [31], 694 nm [32], 755 nm [33], and 1064 nm Nd: YAG [34] Q-switched lasers; with appropriately filtered and cooled non-coherent flashlamp intense pulsed light sources (IPLs) [35, 36], and recently also picosecond lasers have been used successfully to treat lentigines [37].

Continuous and quasi-continuous lasers as ablative CO_2 can be used to treat lentigines [38], preferentially in a superpulsed or ultrapulsed mode [39], but with non-negligible risk of scarring due to the residual thermal damage, therefore a CO_2 fractional laser treatment can be a more conservative option, albeit less successful as compared to pigment specific laser, as Q-switched 532 nm laser [40].

Short pulsed Er:YAG 2940 nm laser, producing an insignificant residual thermal damage, is appropriate to precisely flatten seborrheic kerato-

sis (SK), which often hide as a minimally palpable component within larger and mature age spots [41], or to sculpt thicker SK, but being a non-target specific light source, there is a risk of textural changes or even scarring if it enters too deep into the dermis.

Long pulsed or Q-switched pigment specific lasers are definitely appropriate and better indicated to treat solar lentigines. The most used Q-switched laser to treat solar lentigines are the Nd: YAG 532 nm and the Q-switched 694 nm Ruby and the 755 nm alexandrite, while the Q-switched Nd:YAG 1064 nm is more suitable to treat dermal pigmented lesions.

35.5 Subsurfacing with Near-IR Light Sources and Skin Rejuvenation with Q-Switched, Submillisecond, and Long Pulsed Nd: YAG Laser

Non-ablative near-IR lasers have been utilized to improve texture, fine lines, skin pores, and very superficial acne scars, allowing a deeper penetration into the dermis and bypassing epidermal major chromophores, by selectively targeting water, thermally denature and shrink collagen (subsurfacing [42] or type II photorejuvenation [43]).

Various non-ablative light sources in the near-IR (700–2000 nm) range have been proposed, as 810, 940, 1064 nm, targeting water and partly hemoglobins, and mainly 1320 [44], 1450 [45], 1540 [46] nm lasers, targeting predominantly water, while the 1450 nm laser has gained some popularity also in acne treatment due to its specific absorption by sebaceous glands [47].

Monte Carlo complex simulations and heat transfer calculations were performed to optimize the heating and cooling parameters in order to reach an optimal but safe dermal stimulation without damaging the epidermis.

Most of these technologies for dermal type II or subsurface photorejuvenation have been replaced after the introduction of fractional photothermolysis (2004 [48]). Nevertheless, 1064 nm long pulsed Nd:YAG lasers are perhaps the most diffuse diode laser in the long pulsed domain (millisec), quasi-long pulsed (microsec) and Q-switched (nanosec) mode.

Q-switched Nd:YAG 1064 nm laser homogeneous irradiation of the skin has been shown to increase dermal thickness, the hydroxyproline contents, and the expression of procollagen III mRNA in rat skin models [49] and a bi-weekly treatment for 6 weeks with a Q-switched Nd: YAG 1064 nm laser with a 8 mm spot size and 3.2 J/cm^2 fluence produced a clinical improvement of skin signs of photoaging in a blinded assessment study and an improvement on newly formed collagen and dermal structure in biopsy specimens [50].

Recently, a fractional version of Q-switched Nd: YAG 1064 nm laser has been described to significantly improve skin signs of photoaging (hyperpigmentation, telangiectasia, laxity, roughness, actinic keratoses) [51]. The foundation of these effects could be due to the laser-induced focal thermo-mechanical tissue damage boosted by the deep penetration and relatively high water affinity of the near-IR 1064 wavelength in respect to shorter wavelengths. Less penetrating, but more pigment specific Q-switched 694 nm fractional laser has been recently described for treatment of melasma [52] and dark eye circles [53].

Water affinity and deep penetration in the dermis could explain also the improvement of skin pores and fine lines not only with long pulsed 1064 nm in a scanning mode, but after multiple passes with a submillisecond (300 μsec) Nd: YAG 1064 nm laser, albeit the measured effects on pores size of submillisecond (0.3 msec) and long pulsed Nd: YAG 1064 didn't statistically significantly differ in a split face comparison [54].

A split face comparative study proved, on a clinical basis, a significant reduction of pore size

after a combination of a single pass of a 300 μsec Nd:YAG 1064 nm laser at 2.3 J/cm^2 after the application of a carbon particle suspension, followed by multiple passes of 1064 nm Q-switched (5 ns) laser at 2.5 J/cm^2 [55], while long pulsed Nd: YAG 1064 nm laser treatment after a Q-switched 1064 nm "carbon peel" did not add significant results on skin pores reduction to 1064 nm alone in another comparative study, while the addition to carbon particles before a long pulsed Nd: YAG laser scanning can increase the side effects [56].

Another split face study concluded that quasi-long pulsed, long pulsed, and Q-switched Nd: YAG 1064 nm lasers, the latter with or without a preliminary application of a carbon suspension emulsion, are almost equally effective in reducing the pores size as compared to control untreated side [57].

35.6 Combination of Light Sources for Photorejuvenation

Multiple laser wavelengths in the visible and near-IR domain and various treatment protocols have been attempted for non-ablative skin photorejuvenation, with variable degrees of success, depending upon the prevalent and/or privileged chromophores (hemoglobins, melanins, water, sebaceous glands), the depth of penetration, and the aimed results. No single technology and treatment protocol can have a universal indication in any circumstance. When superficial red and brown color irregularities are the main issue, a visible light emitting laser or a broadband light source is the most suitable choice, while looking a better improvement of textural changes, fine wrinkles, and pores takes advantages from near-IR light sources.

In many circumstances, a combination of the distinctive properties of different light sources, as visible 532 nm and near-IR Nd: YAG laser [55, 56], IPLs and non-ablative fractional laser (NAFL) [57], Q-switched Nd: YAG 1064 nm laser and NAFL [58] used sequentially in the same session, allows to plan a more refined treatment. In some studies, the combination of multiple light sources in sequence, with low settings, offers superior result than the single technologies used alone [59–61], with a minimal impact on downtime [62]. In another study, albeit not clinically superior to the NAFL regimen, the combination gained a higher physician and patient rating [54].

35.7 Pretreatment Precautions

Regardless of the photorejuvenation laser or IPL protocol, the patient should be prepared to have the skin untanned, possibly to achieve the lighter possible color by application on a daily basis of a broad-spectrum sunscreen with a high protective factor one month before the procedure.

In darker skin and/or severely sun-damaged skin, the option of a pretreatment and posttreatment with bleaching agents and auxiliary cosmeceuticals should be considered as an integral part of the treatment program, and a hidden or clinically explicit melasma should be properly diagnosed and treated before targeting the skin with high energy devices.

Anesthesia is rarely required in non-ablative photorejuvenation, conversely unbearable pain should be considered a feedback indicator of overtreatment and potential skin damage. Eutectic mixture of lidocaine and prilocaine can be useful but an induced reduction of skin vessels has been documented, interfering with the outcome of a vascular laser based treatment [63].

Risk of PIH can be reduced with a careful patient selection, proper device choice, and ancillary treatment before laser and follow-up time.

Time scheduling of the photorejuvenation session can be variable depending upon technology and treatment protocols: a minimum healing time of 4–6 weeks could be appropriate to provide a reasonable healing time: for fine lines, scars, and textural improvement, it is generally suggested to prepare the patient to better results, proportional to the healing process, in 6–8 months after a single procedure (Figs. 35.1, 35.2, and 35.3).

Fig. 35.1 Erythematous rosacea, 6 months after treatment with IPL SWT 530–750 nm

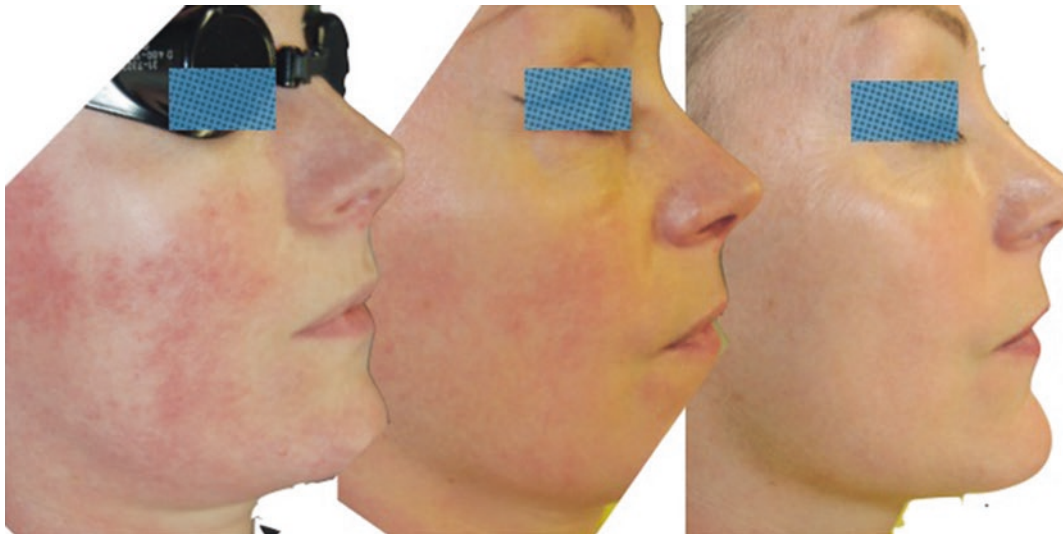

Fig. 35.2 Progressive long-term results on color and texture in a patient treated almost once a year with vascular lasers in scanning mode (Nd: YAG 532 nm FD with scanner, diode 940 nm) and IPL (SWT 530–750)

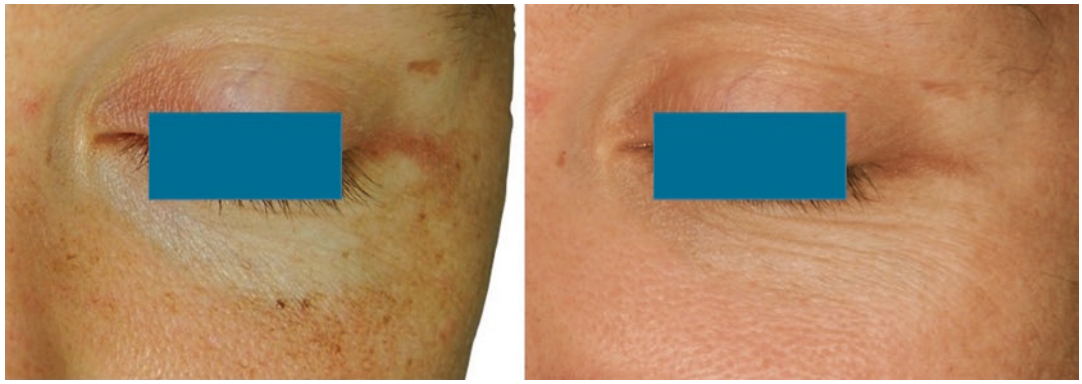

Fig. 35.3 Laser rejuvenation with Nd:YAG 532 nm + diode 940 nm in scanning mode: patient treated once a year. Results after 6 years

References

1. Aesthetic lasers market analysis by application (IPL laser treatment, laser skin resurfacing, noninvasive tightening, laser-assisted lipoplasty, laser hair removal), and segment forecasts to 2024. Report ID: GVR-1-68038-078-1. https://www.grandviewresearch.com/industry-analysis/aesthetic-lasers-market. Accessed 8 Sept 2018.
2. American Society of Plastic Surgeons. 2017 plastic surgery statistics report. ASPS National clearinghouse of plastic surgery procedural statistics. https://www.plasticsurgery.org/documents/News/Statistics/2017/plastic-surgery-statistics-full-report-2017.pdf. Accessed 1 Sept 2018.
3. Chernoff WG, Cramer H. Rejuvenation of the skin surface: laser exfoliation. Facial Plast Surg. 1996;12(2):135–45.
4. Bitter PH. Noninvasive rejuvenation of photo damaged skin using serial, full face intense pulsed light treatment. Derm Surg. 2000;26(9):835–42.
5. DeHoratius DM, Dover JS. Nonablative tissue remodeling and photorejuvenation. Clin Dermatol. 2007;25(5):474–9.
6. Avci P, Gupta A, Sadasivam M, Vecchio D, Pam Z, Pam N, Hamblin MR. Low-level laser (light) therapy (LLLT) in skin: stimulating, healing, restoring. Semin Cutan Med Surg. 2013;32(1):41–52.
7. Hedelund L, Due E, Bjerring P, et al. Skin rejuvenation using intense pulsed light: a randomized controlled split-face trial with blinded response evaluation. Arch Dermatol. 2006;142(8):985–90.
8. Zelickson B, Kilmer SL, Bernstein E. Pulsed dye laser therapy for sun damaged skin. Lasers Surg Med. 1999;25:220–36.
9. Bjerring P, Clement M, Heickendorff L, et al. Selective non-ablative wrinkle reduction by laser. J Cutan Laser Ther. 2000;2:9–15.
10. Anderson RR, Parrish JA. Selective photothermolysis. Science. 1983;220:524–7.
11. Atshuler GB, Anderson RR, Manstein D, et al. Extended theory of selective photothermolysis. Laser Surg Med. 2001;29(5):416–32.
12. Bjerring P, Clement M, Heickendorff L, et al. Dermal collagen production following irradiation by a dye laser and broadband light source. J Cosmet Laser Ther. 2001;3:39–43.
13. Wu D, Zhou B, Xu Y, Yin Z, Luo D. Impact of intense pulsed light irradiation on cultured primary fibroblasts and a vascular endothelial cell line. Exp Ther Med. 2012;4(4):669–74.
14. Dal Canton M, Modolo E. Objective and subjective clinical effects of a Nd: YAG 532 nm frequency-doubled long-pulsed diode pumped laser system on photoaging pf the face: a retrospective study on color signs, texture and rhyitds. J Cosmet Laser Ther. 2004;6(4):209–15.
15. Galeckas KJ, Ross EV, Uebelhoer NS. A pulsed dye laser with a 10-mm beam diameter and a pigmented lesion window for purpura-free photorejuvenation. Dermatol Surg. 2008;34:308–13.
16. Hedelund L, Due E, Bjerring P, Wulf HC, Haedersdal M. Skin rejuvenation using intense pulsed light: a randomized controlled split-face trial with blinded response evaluation. Arch Dermatol. 2006;142(8):985–90.
17. Handler MZ, Bloom BS, Goldberg DJ. IPL vs PDL in treatment of facial erythema: a split-face study. J Cosmet Dermatol. 2017;16:450–3.
18. Alam M, Voravutinon N, Warycha M, Whiting D, Nodzenski M, et al. Comparative effectiveness of nonpurpuragenic 595-nm pulsed dye laser and microsecond 1064-nm neodymium:yttrium-aluminum-garnet laser for treatment of diffuse facial erythema: a double-blind randomized controlled trial. J Am Acad Dermatol. 2013;69(3):438–43.
19. Jørgensen GF, Hedelund L, Hædersdal M. Long-pulsed dye laser versus intense pulsed light for photodamaged skin: a randomized split-face trial with blinded response evaluation. Lasers Surg Med. 2008;40:293–9.

20. Butler EG, McClellan SD, Ross EV. Split treatment of photodamaged skin with KTP 532 nm laser with 10 mm handpiece versus IPL: a cheek-to-cheek comparison. Lasers Surg Med. 2006;38:124–8.
21. Labadie JG, Krunic AL. Long pulsed dye laser with a back-to-back double-pulse technique and compression for the treatment of epidermal pigmented lesions. Lasers Surg Med. 2019;51(2):136–40.
22. Kono T, Manstein D, Chan HH, Nozaki M, Anderson RR. Q-switched ruby versus long-pulsed dye laser delivered with compression for treatment of facial lentigines in Asians. Lasers Surg Med. 2006;38(2):94–7.
23. Kono T, Groff WF, Sakurai H, Takeuchi M, Yamaki T, Soejima K, et al. Comparison study of intense pulsed light versus a long-pulse pulsed dye laser in the treatment of facial skin rejuvenation. Ann Plast Surg. 2007;59(5):479–83.
24. Guitera P, Pellacani G, Crotty KA, et al. The impact of in vivo reflectance confocal microscopy on the diagnostic accuracy of lentigo maligna and equivocal pigmented and nonpigmented macules of the face. J Invest Dermatol. 2010;130(8):2080–91.
25. Agozzino M, Russo T, Ardigò M, et al. Challenging facial pigmented lesions: values and limits of confocal microscopy. Dermatol Pract Concept. 2018;8(3):188–90.
26. Sarma N, Chakraborty S, Poojary SA, Rathi S, Kumaran S, Nirmal B, et al. Evidence-based review, grade of recommendation, and suggested treatment recommendations for melasma. Indian Dermatol Online J. 2017;8(6):406–42.
27. Ortonne JP, Pandya AG, Lui H, Hexsel D. Treatment of solar lentigines. J Am Acad Dermatol. 2006;54(5):S262–71.
28. Hellwig S, Schönermark M, Raulin C. Treatment of vascular malformations and pigment disorders of the face and neck by pulsed dye laser, Photoderm VL and Q-switched ruby laser. Laryngorhinootologie. 1995;74(10):635–41.
29. Ho SG, Chan NP, Yeung CK, Shek SY, Kono T, Chan HH. A cmanagement of freckles and lentigines using four different pigment lasers on Asian skin. J Cosmet Laser Ther. 2012;14(2):74–80.
30. Winstanley D, Blalock T, Houghton N, Ross EV. Treatment of benign pigmented lesions using a long-pulse alexandrite laser. J Drugs Dermatol. 2012;11(11):1327–30.
31. Kilmer SL, Wheeland RG, Goldberg DJ, Anderson RR. Treatment of epidermal pigmented lesions with the frequency-doubled Q-switched Nd:YAG laser. A controlled, single-impact, dose-response, multicenter trial. Arch Dermatol. 1994;130(12):1515–9.
32. Taylor CR, Anderson RR. Treatment of benign pigmented epidermal lesions by Q-switched ruby laser. Int J Dermatol. 1993;32(12):908–12.
33. Wang CC, Chen CK. Effect of spot size and fluence on Q-switched alexandrite laser treatment for pigmentation in Asians: a randomized, double-blinded, split-face comparative trial. J Dermatolog Treat. 2012;23(5):333–8.
34. Jun HJ, Cho SH, Lee JD, Kim HS. A split-face, evaluator-blind randomized study on the early effects of Q-switched Nd:YAG laser plus Er:YAG micropeel (combined therapy) versus Q-switched Nd:YAG alone in light solar lentigines in Asians. Lasers Med Sci. 2014;29(3):1153–8.
35. Goldman MP, Weiss RA, Weiss MA. Intense pulsed light as a nonablative approach to photoaging. Dermatol Surg. 2005;31(9 Pt 2):1179–87.
36. Tanaka Y, Tsunemi Y, Kawashima M. Objective assessment of intensive targeted treatment for solar lentigines using intense pulsed light with wavelengths between 500 and 635 nm. Lasers Surg Med. 2016;48(1):30–5.
37. Vachiramon V, Iamsumang W, Triyangkulsri K. Q-switched double frequency Nd:YAG 532-nm nanosecond laser vs. double frequency Nd:YAG 532-nm picosecond laser for the treatment of solar lentigines in Asians. Lasers Med Sci. 2018;33(9):1941–47.
38. Dover JS, Smoller BR, Stern RS, Rosen S, Arndt KA. Low-fluence carbon dioxide laser irradiation of lentigines. Arch Dermatol. 1988;124(8):1219–24.
39. Fitzpatrick RE, Goldman MP, Ruiz-Esparza J. Clinical advantage of the CO_2 laser superpulsed mode. Treatment of verruca vulgaris, seborrheic keratoses, lentigines, and actinic cheilitis. J Dermatol Surg Oncol. 1994;20(7):449–56.
40. Vachiramon V, Panmanee W, Techapichetvanich T, Chanprapaph K. Comparison of Q-switched Nd: YAG laser and fractional carbon dioxide laser for the treatment of solar lentigines in Asians. Lasers Surg Med. 2016;48(4):354–9.
41. Khatri KA. Ablation of cutaneous lesions using an erbium:YAG laser. J Cosmet Laser Ther. 2003;5(3–4):150–3.
42. Ross EV, Sajben FP, Hsia J, Barnette D, Miller CH, McKinlay JR. Nonablative skin remodeling: selective dermal heating with mid-infrared laser and contact cooling combination. Lasers Surg Med. 2000;26:186–95.
43. Nestor MS, Goldberg DJ, Goldman NP, Weiss RA, Riegel DS. Learn about non-ablative skin rejuvenation techniques using intense pulsed light, including conventional and photodynamic skin rejuvenation. Skin Aging. 2003;5:68–74.
44. Kelly KM, Nelson JS, Lask GP, Geronemus RG, et al. Cryogen spray cooling in combination with nonablative laser treatment of facial rhytides. Arch Dermatol. 1999;135(6):691–4.
45. Doshi SN, Alster TS. 1450 nm long-pulsed diode laser for nonablative skin rejuvenation. Dermatol Surg. 2005;31(9 Pt 2):1223–6.
46. Lupton JR, Williams CM, Alster TS. Nonablative laser skin resurfacing using a 1540 nm erbium glass laser: a clinical and histologic analysis. Dermatol Surg. 2002;28(9):833–5.
47. Paithankar DY, Ross EV, Saleh BA, Blair MA, Graham BS. Acne treatment with a 1,450 nm wavelength laser and cryogen spray cooling. Lasers Surg Med. 2002;31(2):106–14.

48. Manstein D, Herron GS, Sink RK, Tanner H, Anderson RR. Fractional photothermolysis: a new concept for cutaneous remodeling using microscopic patterns of thermal injury. Lasers Surg Med. 2004;34(5):426–38.
49. Zhong H, Ma W, Cai D, Sun Q. A comparison of Q switched 1064 nm Nd: YAG laser and intense pulsed light in the nonablative rejuvenation on rat model. J Cosmet Las Ther. 2013;15(3):126–32.
50. Berlin AL, Dudelzak J, Hussain M, Phelps R, Goldberg DJ. Evaluation of clinical, microscopic, and ultrastructural changes after treatment with a novel Q-switched Nd:YAG laser. J Cosmet Laser Ther. 2008;10(2):76–9.
51. Gold MH, Sensing W, Biron J. Fractional Q-switched 1,064-nm laser for the treatment of photoaged-photodamaged skin. J Cosmet Laser Ther. 2014;16(2):69–76.
52. Hilton S, Heise H, Buhren BA, Schrumpf H, Bölke E, Gerber PA. Treatment of melasma in Caucasian patients using a novel 694-nm Q-switched ruby fractionallaser. Eur J Med Res. 2013;18:43.
53. Xu TH, Li YH, Chen JZ, Gao XH, Chen HD. Treatment of infraorbital dark circles using 694-nm fractional Q-switched ruby laser. Lasers Med Sci. 2016;31(9):1783–7.
54. Roh M, Goo B, Jung J, Chung H, Chung K. Treatment of enlarged pores with the quasi long-pulsed versus Q-switched 1064 nm Nd:YAG lasers: a split-face, comparative, controlled study. Laser Ther. 2011;20(3):175–80.
55. Chung H, Goo B, Lee H, Roh M, Chung K. Enlarged pores treated with a combination of Q-switched and micropulsed 1064 nm Nd:YAG laser with and without topical carbon suspension: a simultaneous split-face trial. Laser Ther. 2011;20(3):181–8.
56. Wattanakrai P, Rojhirunsakool S, Pootongkam S. Split-face comparison of long-pulse-duration neodymium-doped yttrium aluminum garnet (Nd:YAG) 1,064-nm laser alone and combination long-pulse and Q-switched Nd:YAG 1,064-nm laser with carbon photoenhancer lotion for the treatment of enlarged pores in Asian women. Dermatol Surg. 2010;36(11):1672–80.
57. Roh MR, Chung HJ, Chung KY. Effects of various parameters of the 1064 nm Nd:YAG laser for the treatment of enlarged facial pores. J Dermatolog Treat. 2009;20(4):223–8.
58. Munavalli G. A split-face assessment of the synergistic potential of sequential Q-switched Nd:YAG laser and 1565 nm fractional nonablative laser treatment for facial rejuvenation in Fitzpatrick skin type II–V patients. J Drugs Dermatol. 2016;15(11):1335–42.
59. Lee MW. Combination visible and infrared lasers for skin rejuvenation. Semin Cutan Med Surg. 2002 Dec;21(4):288–300.
60. Lee MW. Combination 532-nm and 1064-nm lasers for noninvasive skin rejuvenation and toning. Arch Dermatol. 2003;139(10):1265–76.
61. Lee JH, Park SR, Jo JH, Park SY, Seo YK, Kim SM. Comparison of epidermal/dermal damage between the long-pulsed 1064 nm Nd:YAG and 755 nm alexandrite lasers under relatively high fluence conditions: quantitative and histological assessments. Photomed Laser Surg. 2014;32(7):386–93.
62. Knight JM, Kautz G. Sequential facial skin rejuvenation with intense pulsed light and non-ablative fractionated laser resurfacing in Fitzpatrick skin type II–IV patients: a prospective multicenter analysis. Lasers Surg Med. 2019 Feb;51(2):141–9.
63. Tollan CJ, MacLaren W, Mackay IR. Topical anaesthetic effects on skin vasculature with potential implications for laser treatment. Lasers Med Sci. 2016;31(4):611–7.

Laser Hair Removal: Updates

36

Pier Luigi Saraceni, Alessandra Scarabello,
Sean Ekinde, Elisa Cinotti, and Massimo Laurenza

36.1 Introduction

In humans, unlike many animal species, the renewal of the hair is continuous, and it goes through an alternation of phases: active phase, involution, and rest. A total change of hair occurs just before birth, when the *lanugo* is replaced by new hairs, and after birth, with the differentiation between body hair and hair.

The cycle of hair varies depending on the body district. For example head hair can live from 2 to 4 years, and thigh hair from 20 to 50 days. These differences cause different lengths of the hairs. This factor should be considered when epilation treatment is proposed. Hair growth also changes according to body districts: head hair grows about 0.4 mm per day while body hair 0.25 mm.

P. L. Saraceni
Department of Clinical Dermatology, IFO-Istituto San Gallicano, Rome, Italy

A. Scarabello
Department of Clinical Dermatology, Istituto Lazzaro Spallanzani, Castelfranco Emilia, Italy
e-mail: scarabello@ifo.it

S. Ekinde · E. Cinotti
Department of Dermatology, University Hospital of Siena, Siena, Italy
e-mail: sean.ekinde@pec.omceovr.it

M. Laurenza (✉)
Department of Oncologic Dermatology, IDI, Rome, Italy

The hair bulb is divided into two zones: a lower zone that corresponds to the matrix and an upper one of cellular differentiation, the so-called "keratogenic zone." The activity of the matrix is not continuous. At certain times it stops, so that the follicle enters stasis and many parts of it undergo degeneration. Subsequently, a new period of activity begins and these parts are reconstructed. It can therefore be said that the follicle has a cyclic activity, because it does not grow regularly and continuously.

The life cycle of the hair consists of four phases:

1. *Anagen* (growth phase): It lasts from 3 to 7 years depending on the body district. The base of the hair follicle begins to form the bulb, which gradually grows larger and covers the dermal papilla. During this phase, the bulb, recently formed and rich in nourishment, is well attached to the papilla. At the same time, the melanocytes begin to produce melanin, the pigment that will give color to the hair (Fig. 36.1).
2. *Catagen* (phase of involution): The duration varies from 2 to 3 weeks. During this phase, the cell division is stopped at the matrix level, the membrane surrounding the bulb thickens, and the dendrites of the melanocytes become contracted, so that the last part of the hair becomes devoid of pigment. The bulb that is no longer fed undergoes atrophy (Figs. 36.2 and 36.3).

M. Fimiani et al. (eds.), *Technology in Practical Dermatology*,
https://doi.org/10.1007/978-3-030-45351-0_36

Fig. 36.1 Anagen: hair follicles in growth phase. (Courtesy of Dr. Giorgio Annessi)

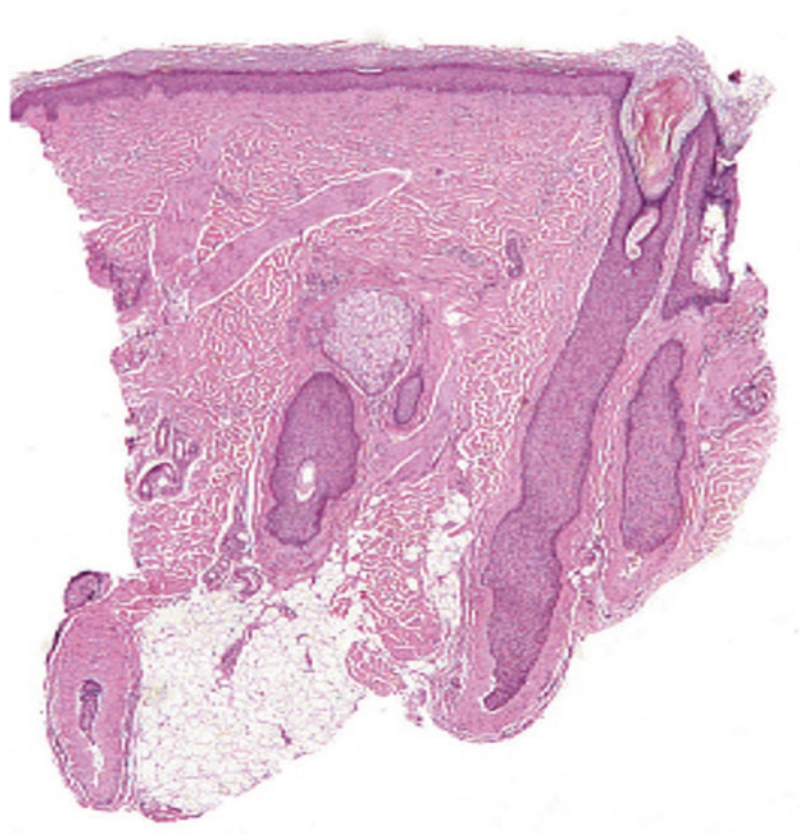

Fig. 36.2 Catagen: hair follicle in involution phase. (Courtesy of Dr. Giorgio Annessi)

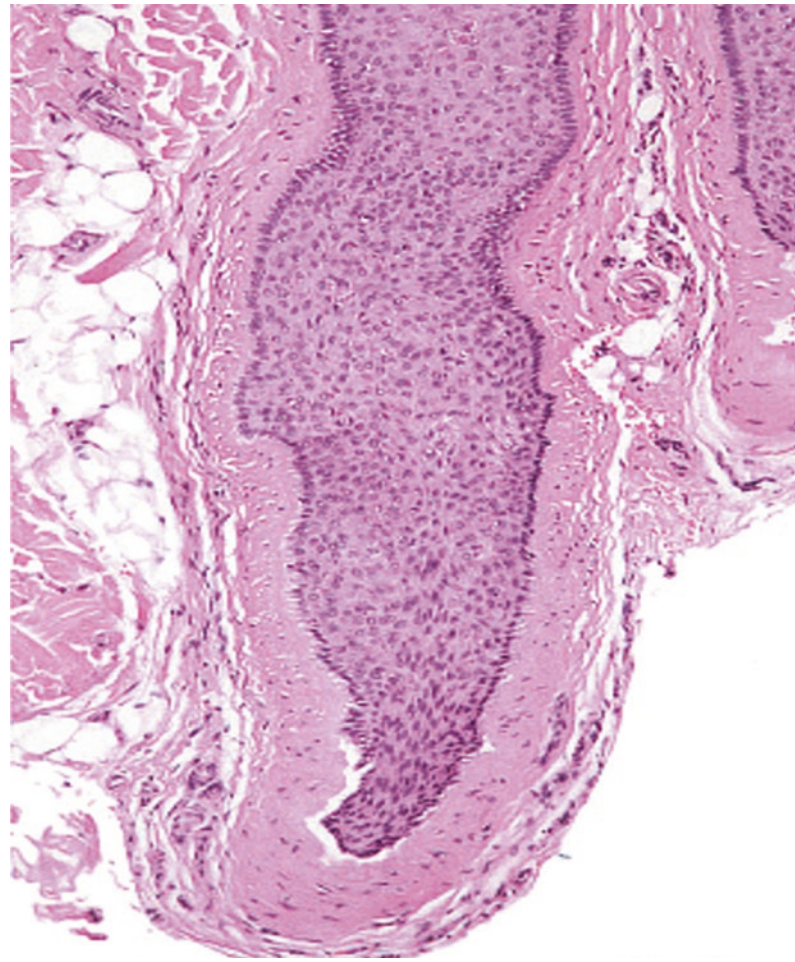

Fig. 36.3 Catagen: hair bulb atrophy. (Courtesy of Dr. Giorgio Annessi)

3. *Telogen* (resting phase): It varies from 2 to 3 months. During this period, the hair is found inside the hair follicle, but there are no vital activities (Figs. 36.4 and 36.5).
4. *Kenogen*: This represents the resting phase (after the telogen phase and before a new anagen phase) of the follicle that remains hairless [1–3].

36.2 Principles of Epilation

Currently, there are three ways in which light can destroy a hair follicle: thermal (selective photothermolysis), mechanical (shock waves), and photochemical (through photodynamic therapy, which creates toxic mediators).

The principle on which most of the laser machines on the market for laser hair removal are based is that of selective photothermolysis. Thermolysis is a physical phenomenon introduced by Anderson and Parrish in 1983. This phenomenon illustrates how a body, illuminated intensely by a beam of photons, heats up to melt. Consequently, the light energy transforms into thermal energy. The selectivity is dependent upon the fact that not all structures heat up in the same way, hence the use of specific wavelengths for a determined target, or chromophore (melanin, water, ink, etc.) to obtain a biological effect avoiding or minimizing complications.

Eumelanin is the chromophore for hair removal. It is found in the shaft of the hair, at the level of the dermal papilla and in the bulge region,

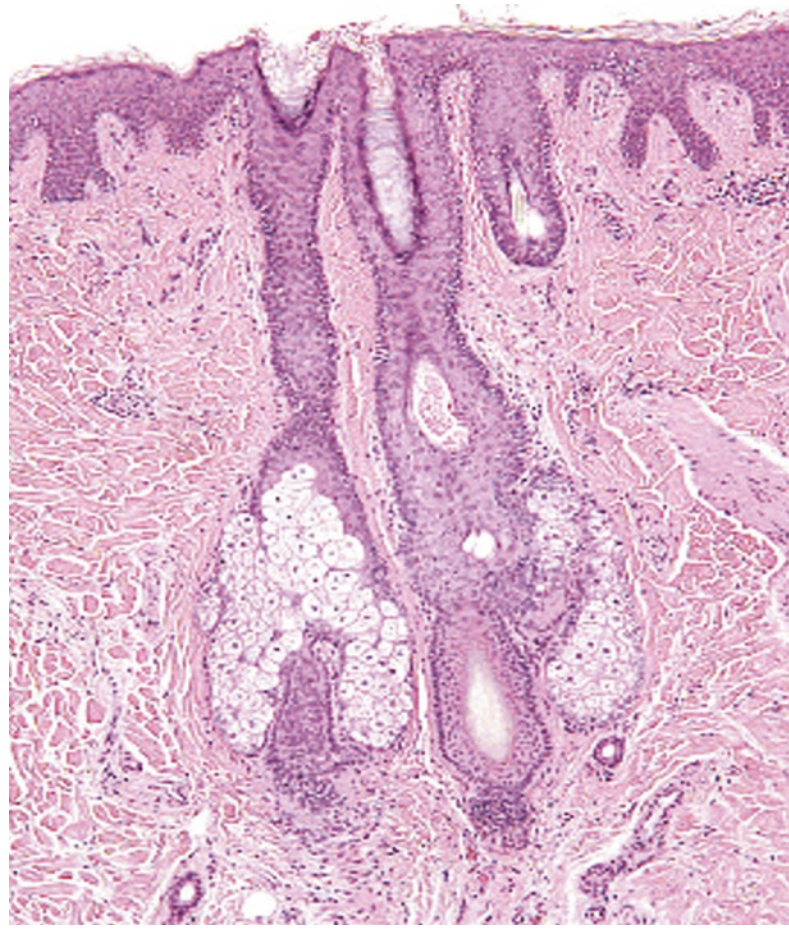

Fig. 36.4 Telogen: hair bulb in resting phase. (Courtesy of Dr. Giorgio Annessi)

where there are also stem cells capable of regenerating the hair structure.

The bulge is an anatomical area of the hair follicle, located under the insertion of the arrector muscle of the hair. It constitutes a reserve of stem cells which, once they reach the papilla, will give rise to a new hair at the end of each follicular cycle.

Anatomically, the bulge is located approximately 1.5–2 mm from the follicular ostium, while the bulb is located deeper (3–6 mm), depending on the body site. Therefore, it would be advisable to use laser machines that allow the hair bulb to be reached through a deep and selective heating of the hair shaft, the hair follicle epithelium, and the matrix, in an optical window between 600 and 1100 nm. The greater the wavelength, the higher the fluence (energy radiated per unit area) without running the risk of damaging the surrounding tissues.

It is necessary to consider the melanin in the epidermis that acts as a competitor for absorption, thus hindering penetration up to the desired level.

The selective cooling of the epidermis has been shown to reduce epidermal damage to a minimum and can be obtained via a cooled gel, a cooled glass chamber, or a sapphire window.

Various types of lasers for hair removal are based on the photothermolysis mechanism: 694 nm Ruby, 755 nm Alexandrite, 810 nm Diode, 1064 nm long-pulsed Nd: YAG and filtered IPLs.

Furthermore, the anatomical and biological variables of the laser hair-removal target must be taken in consideration, since the hair diameter is

Fig. 36.5 Telogen: resting hair bulb. (Courtesy of Dr. Giorgio Annessi)

extremely variable, as is its depth (face hairs are more superficial compared to the bikini line).

Diameter and depth are extremely important elements for choosing the application parameters of the various wavelengths used, such as the duration of the impulse and the fluency. The anagen phase is the ideal phase during which to perform the hair-removal laser session because during this phase the hair is found in its period of growth, and the chromophore (eumelanin) is present in large quantities. But, not all follicles, even in the same body area, are in the same phase. This explains why the biological response may vary for the same patient depending on the treated area or between different patients in the same location. The reduction of the hair varies from 70% to 90% at 6 months to 1 year after the last treatment [4–8].

36.3 Preparation for Treatment

It has now been shown that better results are obtained at sites subjected to shaving rather than depilation, thus demonstrating that light absorption by the pigmented shaft plays a fundamental role. Therefore, waxing or electrolysis should be avoided before laser treatments, whereas shaving and depilatory creams do not interfere with the results.

If hair removal is scheduled on normally photo-exposed sites, sun exposure should be avoided before and after therapy. In cases of patients with dark or recently exposed skin types, the application of hydroquinone 3%, 0.025% retinoic acid, and 2% hydrocortisone creams has been reported in the literature. Any makeup has to be removed from the treatment area. In special cases, a thick layer of anesthetic cream can be applied [9].

36.4 Ruby Laser

Ruby laser uses a solid-state source. Due to the high absorption by melanin at 694 nm, ruby lasers are the most suitable for light-skinned and dark-haired individuals (Fitzpatrick phototype I–III). Depending on the manufacturers, this laser can be supplied with a normal (free-running) emission mode of 0.3 ms or a long pulse of 3 ms. This laser, having been the first system to be used for hair removal, is the most described in the literature, from which emerges a better result if used with a long pulse (3 ms) associated with high fluences (60 J/cm^2). Hair regrowth is at nearly 6 months from the first and single session. The sessions are held every 4–8 weeks.

Side effects may occur in patients with the Fitzpatrick III–V phototype, such as transient edema (lasting 2–5 days), hypo- and hyperpigmentation, blistering, purpura, and folliculitis that may last for several weeks. Currently, with the arrival of new and more efficient devices, this laser is no more used [10].

36.5 Alexandrite Laser

The effectiveness of the Alexandrite laser in removing hair from the face, arms, legs, and bikini line was reported for the first time in 1997 by Finkel et al. [11] Currently, there are several Alexandrite long-pulsed (755 nm) lasers on the market. At this wavelength, the ratio between the energy reaching the dermis and that reaching the epidermis is greater due to the greater depth of penetration. This device uses spots ranging from 5 to 20 mm in diameter and fluences that reach up to 160 J/cm^2 with pulse duration from 2 up to 50 ms (for a single pulse) and up to 80 ms (for a double pulse). An area of 10 × 10 cm^2 can be treated in less than 25 seconds. In patients with darker complexion and thicker and deeper hair, it is necessary to lengthen the duration of the impulse to avoid side effects such as hypo- and hyperpigmentation.

The use of long pulses has greatly reduced the incidence of side effects, especially in III–V phototypes. The number of treatments (from 2 to 6) required to obtain a good result at 12-month follow-up varies based on the body area [10, 12, 13].

36.6 Diode Laser

It is among the most recently introduced lasers. The diode is a semiconductor which, when suitably excited, allows a long impulse emission of 810 nm. Long-term results indicate that the 810 nm diode laser is very effective in removing dark terminal hair, and is preferred in dark-skinned patients compared to shorter wavelength lasers, because it causes fewer side effects such as post-inflammatory pain and hyperpigmentation [14–16].

36.7 Nd: YAG (Neodymium-Doped Yttrium Aluminum Garnet) Laser

In this laser, the active medium consists of a crystal of aluminum garnet and yttrium doped with neodymium; this device works at a wave frequency of 1064 nm. It is considered the best solution in patients with phototype IV–VI. Having a longer wavelength, it allows lower epidermis absorption of light by melanin. Patients with skin types IV–VI can tolerate higher fluences with minimal adverse events.

The various published studies showed that high fluences from 50 to 100 J/cm^2 were well tolerated and only a minimal percentage of patients presented vesicles that lasted for a few days.

It is important to emphasize that the darker the skin type, the higher should be the fluence used to obtain the destruction of the hair. This is because a part of the energy is absorbed by epidermal melanin. Therefore in individuals with fair skin, lower fluences are used [17–19].

36.8 Postoperative Results

While in many cases local anesthetics or analgesics are not required, an antiviral prophylaxis can be carried out where it is necessary. In case of vesicular lesions, it is advisable to apply a local antibiotic cream. If an important edema occurs, it is possible to prescribe a local steroid therapy.

In the first week, it is recommended to avoid sun exposure. There are no contraindications to wearing makeup after the treatment.

A perifollicular erythema is quite common after the session and its duration correlates with the intensity of the treatment. Epidermal damage occurs in those patients where fluence was too high for the skin type, or if they were treated after tanning.

Pigment alterations (hypo- and hyperpigmentation) can be avoided by choosing the ideal patient and treating with fluences suitable for their phototypes. This problem is common in dark complexions or recently sunburned patients. The disappearance of freckles in the treated area or the lightening of tattoos can happen. Scarring formations are extremely rare. Cases of livedo reticularis and urticaria have been described and they regressed with local corticosteroids and antihistamines.

The smoke generated by the vaporization of the hair shaft has a typical sulfur odor and can be irritating to the respiratory tract. The use of an aerator is recommended.

In conclusion, laser hair removal has been extremely successful. In the future, it would be useful to combine lasers with different wavelengths and pulse durations in order to improve efficacy and reduce side effects.

References

1. Alonso L, Fuchs E. The hair cycle. J Cell Sci. 2006;119(Pt 3):391–3.
2. Rebora A. Considerazioni di fisiopatologia pilare. Gior It Derm e Vener. 1988;4:139.
3. Rebora A, Guarrera M. Kenogen a new phase of the hair cycle? Dermatology. 2002;205(2):108–10.
4. Pugliese S. Laser e sorgenti luminose in dermatologia. Cap. 2002;6:93–9.
5. Stratigos AJ, Dover JS. Overview of lasers and their prosperties. Dermatol Ther. 2000;13:2–16.
6. Anderson RR, Parrish JA. Selective photothermolysis: precise microsurgery by selective absorption of pulsed radiation. Science. 1983;220:524–7.
7. Lask G, Elman M, Slatkine M, Waldman A, et al. Laser-assisted hair removal by selective photothermolysis. Preliminary results. Dermatol Surg. 1997;23:737–9.
8. Pugliese S, Laser I. In Dermatologia. Cap. 2002;5:75–81.
9. David J. Goldberg, Laser e luce nella terapia dermatologica Vol 2. Cap. 2006;4:61–76.
10. Nanni CA, Alster TS. Long pulsed alexandrite laser-assisted hair removal at 5, 10 and 20 millisecond pulse durations. Laser Surg Med. 1999;24:332–7.
11. Finkel B, Eliezri YD, Waldman A, Slatkine M. Pulsed alexandrite laser technology for noninvasive hair removal. J Clin Laser Med Surg. 1997;15:225–9.
12. Bouzari N, Tabatabai H, Abbasi Z, Firooz A, et al. Laser hair removal: comparison of long-pulsed nd:yag, long-pulsed alexandrite, and long-pulsed diode lasers. Dermatol Surg. 2004;30:498–502.
13. Nilforouschzadeh MA, Naieni FF, Siadat AH, Rad L. Comparison between sequentional treatment with diode and alexandrite lasers versus alexandrite laser alone in the treatment of hirsutism. J Drugs Dermatol. 2011;10:1255–9.
14. Baugh WP, Trafeli JP, Barnette DJ Jr, Ross EV. Hair reduction using a scanning 800-nm diode laser. Dermatol Surg. 2001;27:358–64.
15. Ilknur T, Bicak MU, Eker P, Hm E, et al. Effects of the 810nm diode laser on hair and on the biophysical properties of skin. J Cosmet Laser Ther. 2010;12:269–75.
16. Raun M. Comparison of high-fluence, single pass diode laser to low-fluence, multiple-pass diode laser for laser hair reduction with 18 months of follow up. J Drugs Dermatol Surg. 2011;10:62–5.
17. Ismail SA. Long-pulsed ND: YAG laser vs intense pulsed light for hair removal in dark skin: a randomized controlled trial. Br J Dermatol. 2012;166:317–21.
18. Galadari I. Comparative evaluation of different hair removal lasers in skin types iv, v, and vi. Int J Dermatol. 2003;42:68–70.
19. Rao K, Sankar TK. Long pulsed nd:yag laser-assisted hair removal in Fitzpatrick skin types iv–vi. Laser Med Sci. 2011;26:623–6.

Biophotonic Therapy Induced Photobiomodulation

37

Deirdre Edge, Mikkel Schødt,
and Michael Canova Engelbrecht Nielsen

37.1 Introduction

The evolving multidisciplinary field of biophotonics showcases the importance of light and life. In addition to light powering plant cells through photosynthesis, a typical mammalian cell contains many photosensitive molecules—chromophores, capable of sensing and utilizing light to alter their biological processes [1]. Endogenous chromophores can absorb photons of light energy at various wavelengths and modulate biological systems, this is the premise of many light therapies [2]. The therapeutic potential of light stems from ancient times and is currently utilized in an array of medical technologies [3]. Major advances in phototherapy first came with Niels Finsen using ultra violet (UV) light to treat tuberculosis, and later with the advent of the laser in the 1960s, following which, low-level laser/light therapy emerged [4]. Later renamed as photobiomodulation (PBM) to include light-emitting diodes (LEDs) [5]. PBM is the ability of non-ionizing forms of light at various wavelengths to induce photochemical and photobiological effects [5]. It has a broad utility and is applied to wound healing, pain management, neurodegeneration, musculoskeletal injury, inflammatory diseases, and, of specific interest, it is widely utilized in therapeutic and aesthetic dermatology [6]. PBM relies on quantum mechanisms whereby photons must be absorbed by a photoacceptor, a chromophore, to initiate cellular events and have a biological impact [7]. Following photon absorption, a chromophore becomes excited and releases energy, either by (1) generating heat; (2) undergoing photochemistry, i.e. inducing chemical reactions; or (3) reemitting a photon of a longer wavelength in the form of fluorescence [8]. A novel biophotonic platform utilizing fluorescent light energy (FLE) to induce PBM has emerged as a highly effective non-invasive treatment choice in dermatology. Here we discuss the current mechanisms and effects of FLE.

37.2 The Electromagnetic Spectrum: The Light Around Us

Light is composed of elementary particles of energy, quantum units of electromagnetic radiation—photons [9]. With particle properties and travelling in waves, light makes up the electromagnetic spectrum. Waves in the electromagnetic spectrum have comparable properties however different wavelengths. Since the energy of a photon is inversely proportional to its wavelength, at one end of the spectrum we have gamma waves—the shortest wavelengths and

D. Edge · M. Schødt · M. C. E. Nielsen (✉)
Department of Research and Development,
FB Dermatology, Ballerup, Denmark
e-mail: ded@kloxtech.com; msc@kloxtech.com;
men@kloxtech.com

M. Fimiani et al. (eds.), *Technology in Practical Dermatology*,
https://doi.org/10.1007/978-3-030-45351-0_37

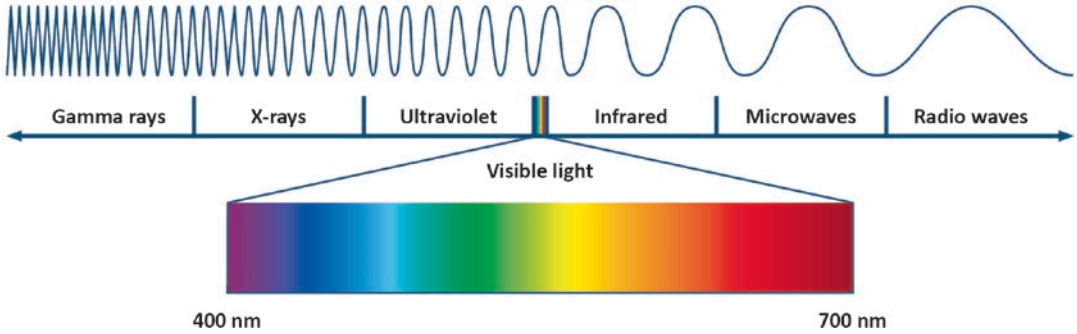

Fig. 37.1 The electromagnetic spectrum. Light travels in waves with increasing wavelength and decreasing frequency. The visible spectrum ranging from approximately 400 to 760 nm makes up a small portion of the all electromagnetic radiation. (Adapted from Ref. [10])

highest energy per photon measured in nanometres (nm) (one billionth of a metre). Conversely at the other extreme of the spectrum, we have radio waves—with wavelengths measured in kilometres (Fig. 37.1). Among the broad spectrum of electromagnetic radiation, 'light' comprises the visible spectrum from violet/blue to near-infrared (NIR) [9] and offers a distinct safety advantage with photon energy in the range of 0.5–3 eV [10]. Whilst being safe, this photonic energy is capable of interacting with organic molecules [2].

All life on earth either directly or indirectly depends on light [11]. We have evolved to detect and respond to light in many ways. This is exemplified by photosynthesis—a fundamental connection between light and living organisms, whereby many autotrophic organisms utilize light as an energy source for life. Cyanobacteria, algae and green plants contain photosynthetic machinery to harvest light energy and convert it into energy-rich biomolecules [12]. These subsequently become an important food energy source for many other organisms [13].

The ability to visually perceive the world around is due to the capability of specialized photoreceptive cells (rods and cones). These ocular photoreceptors transduce photons into neural impulses which are interpreted by the visual centres of the cortex, creating an image [14]. In addition to visual photoreception, it is now understood that non-visual or non-image forming photoreception occurs in many species [15]. In both vertebrates and invertebrates, non-visual photoreception regulates temporal physiology and many behaviours. Fireflies and jellyfish generate bioluminescence (the production and emission requiring a light-emitting molecule and an enzyme), and insects and birds reflect colourful irradiance for survival and reproduction, highlighting a fundamental role of light in evolution [2]. Additionally, light has a significant effect on behaviour, entraining our biological clock, i.e. circadian rhythm [13]. It is thought that cryptochromes (flavoproteins), photosensitive molecules, play a role [16]. Indeed, it is emerging that there are various types of extra-ocular photoreceptors that can absorb light of various wavelengths and trigger a variety of molecular cascades, culminating in altered cellular energy production and gene expression [17], a significant benefit for the energy demand of cells.

37.3 Biophotonics: The Merging of Photonics and Biology

The evolutionary role of light in biology is exploited throughout the life sciences. The realization that light can manipulate photoactive molecules and induce biological effects has led to major advances in our understanding, diagnosis, management and treatment of disease. Moreover, the property of photon absorption by a photoactive molecule is a fundamental feature of many light therapies [2]. Photonics is a niche area identifying all applications utilizing light and other

forms of radiant energy whose quantum unit is the photon. Recently, a new interdisciplinary field of biophotonics has emerged—integrating photonics with biology, medicine and biotechnology; assessing the interaction of light (of multiple sources) with tissues, cells and subcellular structures [18].

Multiple biophotonic platforms harnessing light–tissue interactions are utilized in modern medicine, including, but not limited to, a range of microscopic techniques, spectroscopy, laser surgery, fluorescence endoscopy, photodynamic therapy (PDT) and optical coherence tomography. These technologies traverse a range of medical disciplines. Some examples include imaging in cardiovascular disease, caries diagnosis in dentistry, oncology, ophthalmology, laser restorative surgery in gastroenterology [18] and, of particular interest, dermatology. From here we focus our discussion on biophotonic applications in dermatology.

37.3.1 Photomedicine: The Therapeutic Effect of Light

The therapeutic importance of light spans centuries with light therapy being used since ancient times in Greece and Egypt [3, 19]. The advent of modern-day phototherapy began with the Danish scientist Niels Ryberg Finsen—utilizing UV light to treat cutaneous tuberculosis, *Lupus vulgaris.* He went on to win the Noble Prize in Physiology and Medicine (the only one to this day in dermatology) in 1903 for his work [19]. From these initial findings, others have developed UV phototherapy, including UVB and PUVA (psoralen and UVA), which are commonly applied today to treat an array of inflammatory skin diseases, including psoriasis, polymorphous light eruption, vitiligo and pruritus, among others [20, 21].

The next major advancement in phototherapy came in the early 1960s with the invention of laser technology [5, 11]. Laser therapy was applied in a variety of fields, including ophthalmology, dermatology and dentistry [2]. However, safety concerns with high-intensity lasers were realized and parameters were adjusted, making way for a new therapeutic field, first identified by Endre Mester. Mester demonstrated a faster rate of hair growth in mice treated with low dose ruby laser light, coining the term ‘laser biostimulation’ [4, 22]. This was the beginning of a whole new area of phototherapy—using low-level laser therapy (LLLT) [22]. The important distinction is made here with low level, i.e. non-ionizing, such that the energy/power densities used are low compared to other forms of laser therapy, common in ablating, cutting and thermally coagulating tissue [6].

Research in LLLT originally focused on the modulating effects of red and near-infrared lasers. However, as the field progressed there was an understanding that non-coherent light sources such as light-emitting diodes (LEDs) and broadband light sources were also capable of stimulating or inhibiting cellular function. With this, the nomenclature moved from low-level laser to low-level laser/light therapy [8], and is now widely accepted as photobiomodulation [5, 23].

37.3.2 Photobiomodulation

PBM is defined as ‘A form of light therapy that utilizes non-ionizing forms of light sources, including lasers, LEDs, and broadband light, in the visible and infrared spectrum. It is a nonthermal process involving endogenous chromophores eliciting photophysical (i.e., linear and nonlinear) and photochemical events at various biological scales’ [5]. Early work by Mester demonstrated the positive application of PBM to wound healing [24]. Today, it has a broad utility and has been applied therapeutically to alleviate pain, reduce inflammation and oedema, promote wound healing, regenerate tissue and to treat chronic joint and neurological disorders [6, 23]. More recently PBM has been applied to both treat and enhance dermatological indications, with key effects related to healing, reducing inflammation and offering a non-invasive approach for photorejuvenation [6, 25]. Many common light/laser-based procedures use photothermal energy, i.e. heating

the dermis to stimulate fibroblast proliferation or heating blood vessels for photocoagulation to achieve their therapeutic/aesthetic outcomes. Some of these include intense pulsed light, visible wavelengths including pulsed dye laser, 532 nm green light (KTP laser) and various infrared wavelengths targeting water for dermal collagen remodelling [26]. Rather than evoking an initial thermal injury, PBM regulates cellular activity by stimulating cellular metabolism and modulating function [6]. Hence, PBM using non-thermal energy to achieve its outcome represents a revolutionary mechanism in dermatology. Whilst the therapeutic role (dependent on optimal light parameters and dose [27]) of PBM is generally accepted, recent efforts in the PBM community have concentrated on elucidating some of the specific molecular and cellular effects [27].

37.3.3 Proposed Mechanisms of Photobiomodulation

Cells are continuously responding and adapting to their environment and can execute sophisticated biochemical cascades to induce a 'necessary response'. Indeed, it is now thought that all life-forms respond to light [11]. Whilst photons delivered to living tissue can either be absorbed or scattered [28], the first law of photobiology states that for low power visible light to have any effect on a living biological system, the photons must be absorbed by electronic absorption bands belonging to some molecular chromophore or photoacceptor [22]. Most often when light is absorbed by living tissue, an excitation occurs, where the first excited singlet state of the chromophore transitions from a higher to a lower electronic state losing heat in the process, a chemical event—also known as internal conversion, or radiationless de-excitation as no photons are emitted in the process [29].

PBM exploits natural and evolutionary preserved pathways by acting on endogenous chromophores. As mentioned, research has shown that photon perception occurs in non-photosensitive tissues and cells (i.e. extra-ocular). Endogenous chromophores such as flavins, porphyrins, melanin, carotenoids and heme can perceive photons and represent the photoreactive sites of larger photoreceptor molecules [17]. Additionally, photoreceptors such as cytochrome c oxidase (CCO), cryptochromes, transient receptor potential (TRP) channels [1, 30] and G-protein-coupled receptor opsin family proteins are widely expressed in different cell types [1, 31], including skin cells [17, 32, 33].

Initial work on PBM identified the copper centres of CCO, complex IV of the mitochondrial electron transport as the main photoacceptor for visible and NIR light [34]. Irradiation with these specific wavelengths promotes electron transport—increasing mitochondrial membrane potential, oxygen consumption and cellular energy—adenosine triphosphate (ATP) production [35]. More recently, it has emerged that there are additional chromophores activated by different regions of the spectrum [1]. Typically associated with retinal photoreception [36], G-protein-coupled opsins are responsive to blue light, expressed in the skin and proposed as a potential target for light therapy [33].

Additionally, ion channels such as TRP channels have been identified as another key photoacceptor. Usually activated by light or heat, TRPV1 channels have been proposed to be activated by blue/green light or >900 nm NIR. The blue/green light activation of TRP channels may be indirect via opsin activation—specifically melanopsin (OPN5). Whereby, activation of OPN5 is thought to open TRPV—a calcium ion channel. Alternatively, TRPV can be activated by NIR light which targets water [1]. Although there may be many specific pathways for photon absorption, i.e. activation of CCO or TRP channels, both lead to an increase in mitochondrial respiration and a concomitant increase in energy production. The increased ATP appears to be a key step in PBM and has been reported from both in vivo and in vitro studies [27, 37]. Next, it is thought that an upregulation of reactive oxygen species (ROS) is produced [1], activating redox sensitive transcription factors responsible for the regulation of inflammation, cell migration, proliferation, oxygenation, vascularization and antioxidant defences [27]. Specific mechanisms of

retrograde mitochondrial signalling are thought to explain how a rather brief exposure to a stimulus, i.e. light, can lead to long-lasting persistent effects often observed in PBM [35, 38].

Initial work on PBM was dominated by coherent, collimated, monochromatic beams with high power densities. However, in recent years non-coherent light sources such as LEDs have become preferred due to their high safety, low cost, user-friendliness and the ability to irradiate a large surface area at once [35].

37.4 What Is Fluorescent Light Energy?

In addition to internal conversion and the release of heat following the absorption of a photon, energy can also be emitted as lower energy light (i.e. longer wavelength)—through fluorescence. Jablonski's diagram illustrates the electronic states of a molecule and the transitions between them [10] (Fig. 37.2). A chromophore lying in its ground state (S_0) absorbs light, becomes excited and transitions to excited singlet state (S_1'). The molecule will then transition to the relaxed singlet state (S_1) and release some of the absorbed energy. Returning to its ground state the molecule releases the remaining energy, as the re-emission of fluorescent light of a longer wavelength (lower energy), as per the phenomenon of Stokes shift (Fig. 37.2).

Fluorescent light emission—the ability to autofluoresce—is a naturally occurring phenomenon throughout the animal kingdom, ascribable to endogenous chromo/fluorophore [13]. Whilst often considered a nuisance in histochemical staining, interfering with the detection of positive labelling with exogenous markers, NADH autofluorescence is now appreciated for its ability to offer insights into cellular activity and metabolism [40, 41]. Our growing knowledge of light and biological interactions has led to major advances in research. Light sensitive tools are exploited for imaging with fluorescent dyes—enabling the tracking and exploration of biological molecules. Further, light can be used to control biological systems—with the advent of optogenetics [13].

37.4.1 Fluorescent Light Energy: A Unique Mechanism

A novel biophotonic platform—Kleresca® utilizing FLE has recently emerged as a unique tool in dermatological practice. This biophotonic platform consists of a multi-LED lamp and a

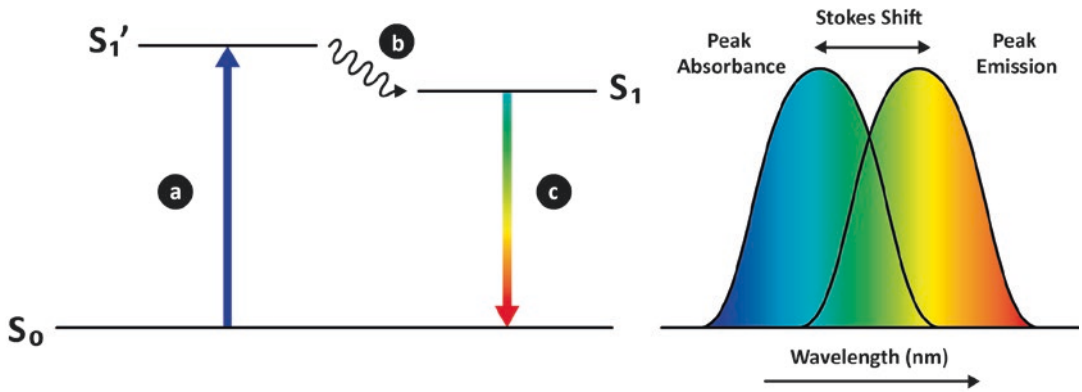

Fig. 37.2 The generation of fluorescence explained by Jablonski's diagram and fluorescent light energy. The chromophore begins in its ground energy state (S_0). Upon absorption of light energy, the molecule becomes excited and transitions (a) to an excited singlet state (S_1') and releases some energy in the process transitioning to a relaxed single state (S_1) (b). Finally, the molecule returns to its ground state and releases the remaining energy in the form of fluorescence. This is complemented by Stokes shift depicted on the right, adapted from [39]. Wherein, a chromophore absorbs at a given wavelength and re-emits light of a longer wavelength as energy is lost in the process

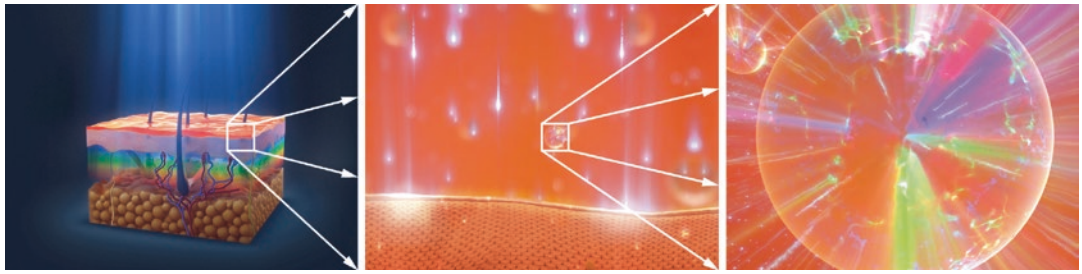

Fig. 37.3 The generation of fluorescent light energy. The image on the left shows the three major layers of the skin, from top to bottom; the epidermis, dermis and subcutis. A layer of chromophore-containing gel (orange layer) is placed on the skin and irradiated with blue light from the multi-LED lamp. The centre panel highlights a chromophore in the gel interacting with photons of blue light. On the right, upon absorption of the blue light the gel acts as a photoconverter where the chromophores re-emit a dynamic multi-wavelength spectrum of fluorescent light

chromophore-containing gel. The multi-LED lamp delivers continuous non-coherent blue light with a peak wavelength between 440 and 460 nm and a fluency of 30–40 J/cm^2 [42]. Upon illumination with the blue light the chromophore gel acts as a photoconverter, wherein the chromophores absorb the photons of blue light, become excited and re-emit a dynamic hyper-pulsed multi-wavelength spectrum of FLE—polychromatic light (Fig. 37.3). Through Stokes shift the light generated by this biophotonic platform covers the continuum of the visible spectrum, with non-fluorescent blue (from the LED lamp), and fluorescent-green, -yellow, -orange and -red (415–610 nm) light emitted.

37.5 Light–Tissue Interaction

When interacting with tissue, light can either be absorbed or scattered, typically dictated by the tissues' optical properties [28]. Wherein, the absorption of light in the skin depends on the composition, absorption spectra and number of chromophores, and the scattering depends on the tissue morphology and biochemistry [28, 43]. The skin is comprised of many different layers and cellular compartments, including the epidermis, dermis and subcutis [44]. The outermost layer of the epidermis, the stratum corneum plays a major protective role. Keratinocytes dominate the epidermis, where melanocytes, Langerhans cells and Merkel mechanoreceptive cells can also be found [44]. Here melanin is a natural light-absorbing chromophore with a broad absorption spectrum [28]. The dermis below is a major supportive layer comprised of key connective tissue cells, fibroblasts—the producers of collagen and elastin fibres, giving the skin its strength and flexibility. Richly innervated, the dermis also contains the sebaceous and sweat glands along with hair follicles [44]. Haemoglobin is the main chromophore of the dermis [28]. The skin is a highly heterogeneous structure with a high incidence of light scattering and absorption. In human skin, there are two major types of scattering—surface, defined by corneal layer abnormalities such as wrinkles and skin hydration and subsurface scattering, dictated by subcellular structures such as collagen fibres, melanosomes and cellular organelles [28]. Therefore, the presence of skin conditions can have a major effect on light absorption and scattering. We must acknowledge these properties when we are utilizing and comparing light therapies.

37.5.1 Photobiological Events

In simple terms, the wavelength of light determines the depth of tissue penetration [43, 45, 46]. Blue light in the range of 415–500 nm (Fig. 37.1) has the shortest tissue penetration, reaching most superficial layers of the skin—the stratum corneum and epidermis. Many blue light phototherapy devices are used to treat acne vulgaris by targeting endogenous porphyrins (coproporphy-

rin and protoporphyrin IX) synthesized by *Cutibacterium* (formerly *Propionibacterium*) *acnes*. With an absorption spectrum peak at 415 nm (the Soret band), porphyrins absorb, become excited and produce cytotoxic levels of ROS, leading to bacterial cell wall lysis and destruction [47]—a natural PDT effect. The absorption peak of porphyrins has led to the advent of different therapies including intense pulsed light, pulse dye lasers and potassium titanyl phosphate (KTP) lasers [48]. Blue light is also thought to have an anti-inflammatory effect by regulating cytokine production [49].

Green light (500–570 nm) is typically used to target the epidermis and upper dermis to access fibroblasts and endothelial cells mediating proliferation and healing—key elements in skin rejuvenation [17, 50]. Yellow light (570–590 nm) is indicated in wound healing by reaching the papillary dermal layer and is utilized in post-laser recovery. It is also implicated in photoageing through the modulation of ATP and fibroblast activity [46]. Finally, orange and red light (590–760 nm) with the deepest skin penetration are noted for vascular activation, reducing inflammation, improving wound healing and increasing collagen production by modulating pro-collagen and matrix metalloproteinases (MMPs) [6, 43, 46].

37.6 The Application of Photobiomodulation for Skin Rejuvenation

Many energy-based devices apply these light properties to treat cutaneous conditions and to achieve aesthetic outcomes. Skin ageing is a major concern in western populations with the key signs of ageing characterized by wrinkles, telangiectasia, dyspigmentation and loss of skin elasticity [6]. Degradation of the major structural component of the skin, collagen, is a key factor underlying both photo- and chronological ageing [51]. Hence, the dermal layer of the skin is a major target for modalities aiming to rejuvenate the skin. Ablative methods including laser resurfacing with CO_2 or Er:YAG lasers typically aim to promote dermal collagen production with matrix remodelling by removing the epidermis and inducing a form of wound healing [26]. Whilst the results are promising, these techniques are associated with a significant downtime, post-treatment care and often pain.

The ability of light to non-thermally and non-invasively photobiomodulate the skin has come as a welcome addition in dermatological practice. Various studies using LEDs have reported promising effects on skin rejuvenation, specifically enhancing collagen production without inducing prior damage [6]. Whilst 660 nm red light improves the skin texture [52], enhanced effectiveness is reported when 633 and 830 nm (infrared) wavelengths are combined [53]. FLE exposure offers a new method to rejuvenate the skin. The Kleresca® biophotonic platform differs from other LED modalities, since, in addition to the direct energy transfer from the blue-LED lamp, illumination of the photoconverter gel emits polychromatic fluorescent light covering the continuum of the visible spectrum. Therefore, in a given treatment the skin is irradiated with (~415–610 nm) of light. Following one or more consecutive treatments within a few weeks, FLE significantly reduces the size of visible pores, the appearance of fine lines and wrinkles [54], in addition to reducing the appearance of scars [42, 55]. Moreover, FLE induced a 400% increase in collagen production—assessed by Gomori trichrome staining [54]. This increase in collagen production was also observed in vitro from human dermal fibroblast cells exposed to FLE [42].

To examine a specific role for fluorescence, a non-fluorescent mimicking lamp which matched the spectral output of the biophotonic platform has also been tested. The mimicking lamp emitted non-fluorescent light generated by a continuous LED light [42]. FLE and not the mimicking lamp significantly increased the production of collagen from human dermal fibroblast (HDF) cells, highlighting a unique role for FLE (Fig. 37.4).

This upregulation of collagen in vivo and in vitro was confirmed in preliminary experiments with human skin biopsies (Fig. 37.5).

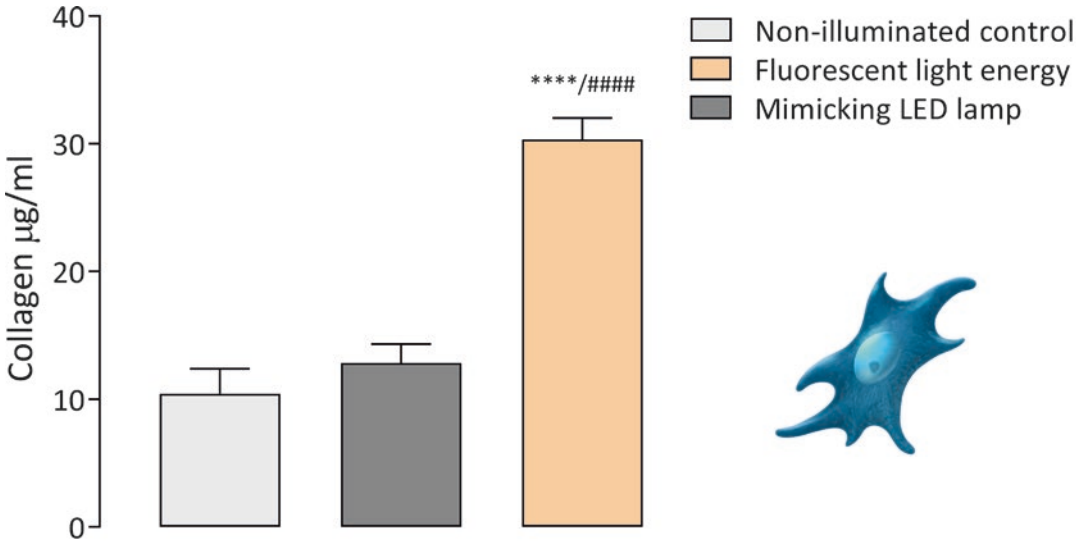

Fig. 37.4 Fluorescent light enhances collagen production from human dermal fibroblasts. Graph shows group data mean ± SD; fluorescent light energy and not the mimicking lamp significantly increased collagen production from human dermal fibroblast cells (depicted on the right). (Reproduced from Ref. [42])

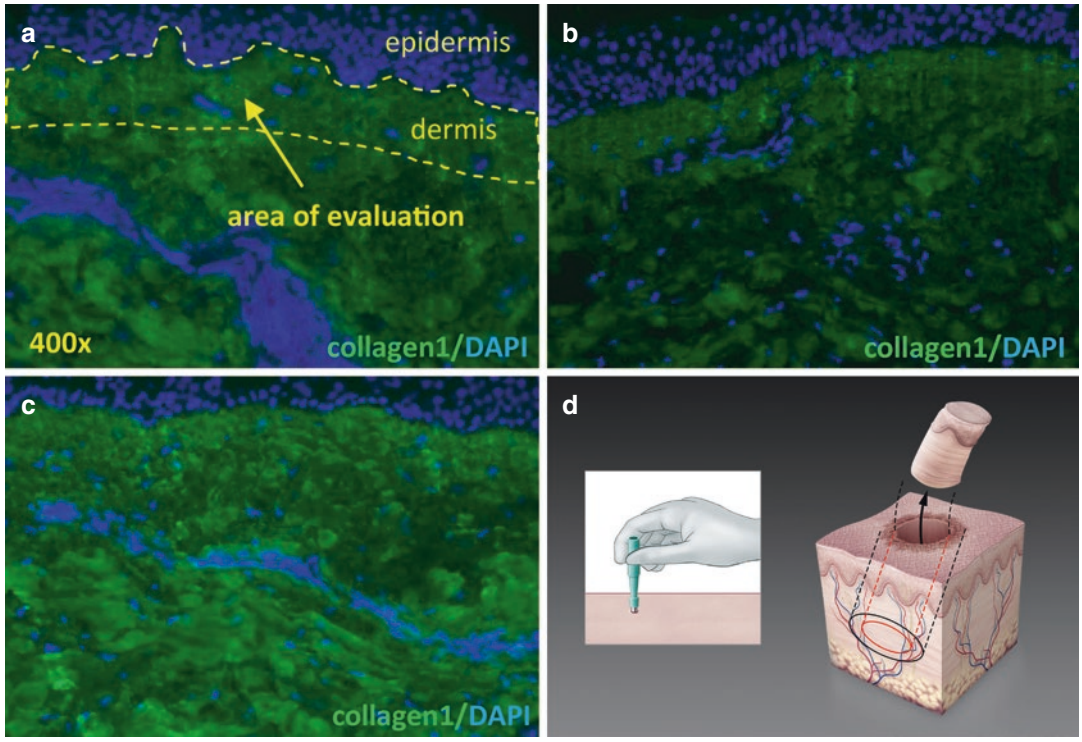

Fig. 37.5 Fluorescent light energy enhances collagen expression and organization in human skin biopsies. Representative images of immunofluorescent staining for collagen 1 expression in (**a**) non-illuminated, (**b**) blue-LED light only and (**c**) LED light and Klerescа® gel exposed human skin biopsies. (**d**) Human skin biopsy 4 mm punch collection method

Additionally, FLE enhanced the structural organization of the collagen fibres. Albeit these are preliminary experiments, requiring further research, upregulation of collagen and improved structural organization of fibres would have significant consequences for the skin's appearance. The enhanced arrangement of collagen is likely to have an impact on the scattering and reflection of light [28]—giving rise to the 'glow' that is observed clinically following FLE. Taken together these effects on collagen improve the skin's texture and appearance contributing to an antiageing effect [56, 57].

37.6.1 Treating Inflammatory Skin Conditions with Fluorescent Light Energy

The clinical efficacy of FLE extends beyond an aesthetic benefit with a proven ability to treat inflammatory skin conditions [42, 58]. Conventional therapies for inflammatory skin conditions often include high-energy treatments, invasive techniques, topical and frequently irritating agents, or pharmacotherapy with many associated side effects [59]. Many phototherapies (light, laser and PDT) exist for the treatment of acne [6, 48], the most common skin condition in the world [60]. Blue light therapy is most commonly applied due to its effect on *P. acnes* [61]. To broaden the therapeutic target blue light is often coupled with red light therapy for deeper penetration and an overall anti-inflammatory effect [62, 63].

The Klerescа® biophotonic platform offers a new and improved treatment option for acne, including difficult to treat moderate to severe acne [55, 64–66]. Following a series of treatments over a few weeks, FLE improves acne severity, inflammatory lesion count and associated erythema. In a clinical trial, 89% of patients had a positive response with a ≥1 Investigator's Global Assessment (IGA) grade improvement and 52% had an IGA improvement of ≥2. Further, 82% of treated patients had a 40% reduction of inflammatory acne lesions following two treatments per week for 6 weeks. These effects were incremental over the 12-week study [64] and indeed persisted for at least 24 weeks following biophotonic treatment [65]. FLE has also been useful where other treatment modalities have been ineffective, especially in treating recalcitrant conditions such as acneiform eruption [66], acne conglobata and hidradenitis suppurativa (acne inversa) [55].

37.6.2 Some Anti-inflammatory Mechanisms of Fluorescent Light Energy

Inflammation is fundamental to defending and protecting against foreign invasion. However, chronic inflammation has emerged as a hallmark feature of various pathologies, including ageing, obesity, neurodegeneration, diabetes and cardiovascular disease, among others [67]. Further, it is well accepted that aberrant immune responses underpin many dermatological indications [68]. Whilst there are diverse mechanisms associated with PBM [27], an anti-inflammatory effect is consistently reported [6, 27, 69].

Macrophages, key immune cells play an integral role in the innate immune response, i.e. upon recruitment from monocytes they can become a critical local source of various mediators including MMPs, cytokines and chemokines [70], exaggerated levels of which are fundamental to many skin conditions [71]. To allow for their diverse functions, macrophages can alter their phenotype and differentiate to be pro-inflammatory (M1), or reparative and regenerative (M2), depending on the stimuli they encounter in the local environment [72]. Additionally, it is now well established that differentiation into M1/M2 macrophages relies on specific intracellular metabolic programmes. M1 macrophages utilize glycolysis allowing for the rapid production of ATP fuelling their activation in acute inflammation, whereas M2-like macrophages depend on oxidative phosphorylation (OXPHOS) metabolism aiding long-term tissue repair [73]. Macrophage differentiation is commonly assessed by morphological and molecular means. M1 macrophages typically have a fried

egg morphology [74], express CD80 and CD86 surface markers, secrete pro-inflammatory cytokines, IL-1β, IL-6 and TNF-α and rely on glycolysis [75], whereas M2 macrophages are typically a mixed population of fried egg-shaped and spindle-shaped cells [74], express CD36, the mannose receptor CD206 and CD163, secrete anti-inflammatory interleukins IL-10, IL-13, transforming growth factor beta and rely on OXPHOS [75]. In preliminary experiments, FLE and not blue-LED exposure decreased IL-1β protein production from M1-polarized macrophages. In additional preliminary in vitro work, macrophages derived from human monocytes display morphological features typical of M2-like macrophages—with a spindle-like appearance (Fig. 37.6). Further, we have observed an increase in ATP production and secretion in human skin samples, a fundamental property of PBM—the cellular utility and signalling of this ATP in our platform are being explored.

It is tempting to speculate that FLE could potentially alter the cutaneous macrophage phenotype, polarizing these key immune cells towards a M2—anti-inflammatory, reparative phenotype. This transition is known to be a key step in the process of normal tissue repair [70]. Some groups have reported the capacity of PBM to alter macrophage phenotype [69]. This is an area we are currently investigating as it has major implications for an array of inflammatory disorders—including and beyond the skin.

Since fibroblasts and other mesenchymal cells can respond to both pattern- and damage-associated molecular pathogens, i.e. PAMPs and DAMPs as well as inflammatory cytokines released by resident macrophages [70, 76], subsequent work has focused on the interaction with

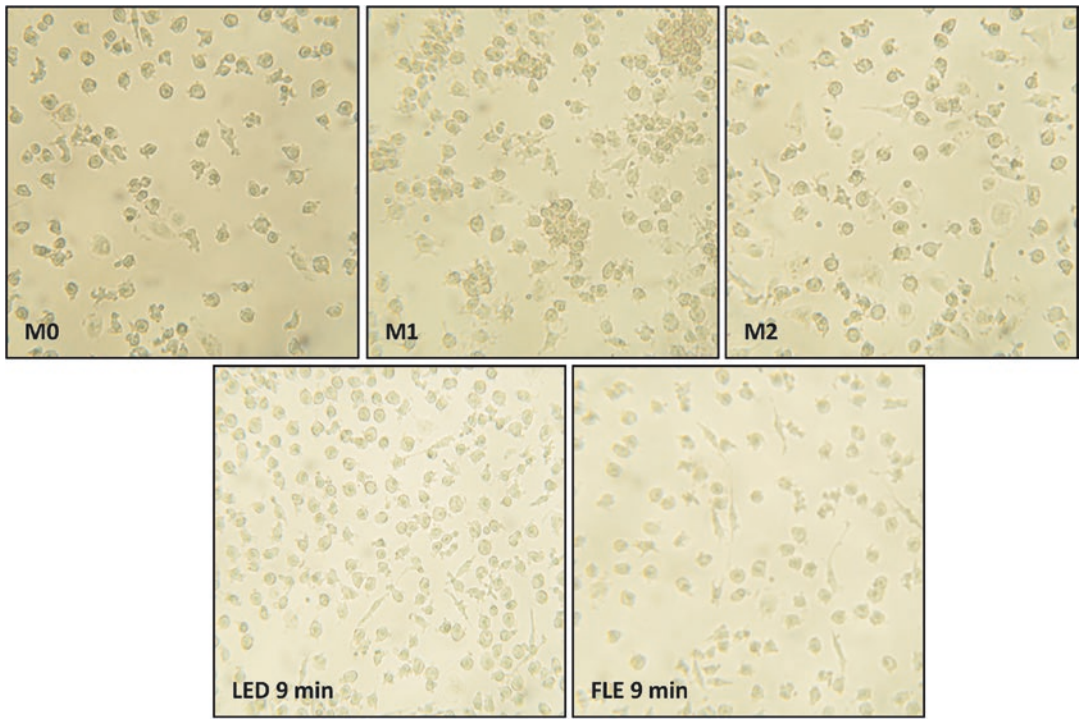

Fig. 37.6 Macrophages and their polarization states. The top panel shows representative micrographs of human monocyte-derived macrophages. On the left—non-polarized M0 macrophages with a typically round and dispersed shape. M1-polarized macrophages (top centre) retain a round shape, whereas M2-polarized macrophages (top-left) have a mixed round and spindle-like morphology. The bottom micrographs show M0 macrophages following 9 min of blue-LED exposure (left); or fluorescent light energy (right). FLE-exposed cells appear to have an M2-like morphology

immune and cutaneous cells. Chronic skin inflammation is often triggered and maintained by the production of a variety of cytokines and chemokines, such as TNF-α and IL-6 [77–79]. Following FLE both fibroblasts and keratinocytes exposed to conditioned media taken from M1-like macrophages decreased their production of these two-inflammatory cytokines, supporting an overall anti-inflammatory response of FLE.

With the powerful resolution of inflammatory lesions and the booting of the skin's healing profile, the Kleresca® biophotonic platform has been extended to other inflammatory skin disorders, and is beneficial in treating rosacea subtypes 1, 2 and 3 [58].

37.6.3 Treating Rosacea and Beyond with Fluorescent Light Energy

Rosacea is typically a difficult to treat condition due to its multiple features and complex aetiology [80]. Following efficient 'trigger' avoidance, a multimodal approach is often required. Major therapies include topical and oral treatments targeting the sympathetic nervous and underlying inflammation. Many of these are often combined, for example—a first line with topical brimonidine tartrate gel and calcineurin inhibitors or a combination of topical metronidazole or azelaic acid with oral tetracyclines or isotretinoin [81] is common. Oral/systemic treatments are well known for their concomitant side effects, including gastrointestinal distress and cardiovascular anomalies [82]. Moreover, for certain features such as telangiectasia, inflammatory lesions and purpura, IPL and laser treatment are often given in conjunction. Due to the skin sensitivity associated with rosacea, many topical treatments can cause irritation, stinging and burning [82], often leading to low compliance and discontinued use, highlighting a need for a new therapeutic option. Due to the multifactorial nature of rosacea, a treatment option that can target more than one disease feature at a time is paramount, hence a likely candidate for FLE.

FLE is efficacious in treating rosacea subtype 2, papulopustular rosacea (PPR) [83], a subtype of rosacea which is quite phenotypically like acne. For the investigated PPR patient, previous treatment with topical metronidazole and ivermectin was unsuccessful. However, FLE reduced the inflammatory reaction and improved the skin's texture [83]. Subsequently, it has been shown that FLE is capable of targeting the inflammatory and erythematous reaction also common to rosacea subtypes 1 and 3 [58] and granulomatous rosacea [84]. The cellular anti-inflammatory and healing effects we have reported in vitro extend to the clinical efficacy observed in rosacea patients.

In addition to aberrant immune responses, rosacea is characterized by altered vascular control [85]—potentially driven by inflammation and likely to contribute to the diffuse erythematous reaction associated with the disease. Angiogenesis, a critical physiological step in wound healing has been reported in several experimental models following PBM [27]. FLE is capable of inducing angiogenesis in vitro—enhancing endothelial cell tube formation and encouraging branching [42], with similar results to the potent angiogenic mediator, vascular endothelial growth factor (Fig. 37.7).

Angiogenesis is a vital step in wound repair enabling the transportation of oxygen and nutrients. Hence, an enhanced angiogenic response has implications in the treatment of a variety of skin disorders. Taking rosacea as one example—the ability of FLE to reduce inflammation and induce heathy neovasculature (Fig. 37.8) has consequences for ameliorating the commonly observed erythematous reaction.

37.6.4 How Does Fluorescent Light Energy Induce a Unique Form of Photobiomodulation?

In vivo and in vitro experiments have shown the capability of polychromatic FLE to enhance collagen production, modulate cellular activity, decrease the inflammatory signature of immune and cutaneous cells and induce angiogenesis. Whilst these are common effects often reported with PBM [27], they are often achieved with

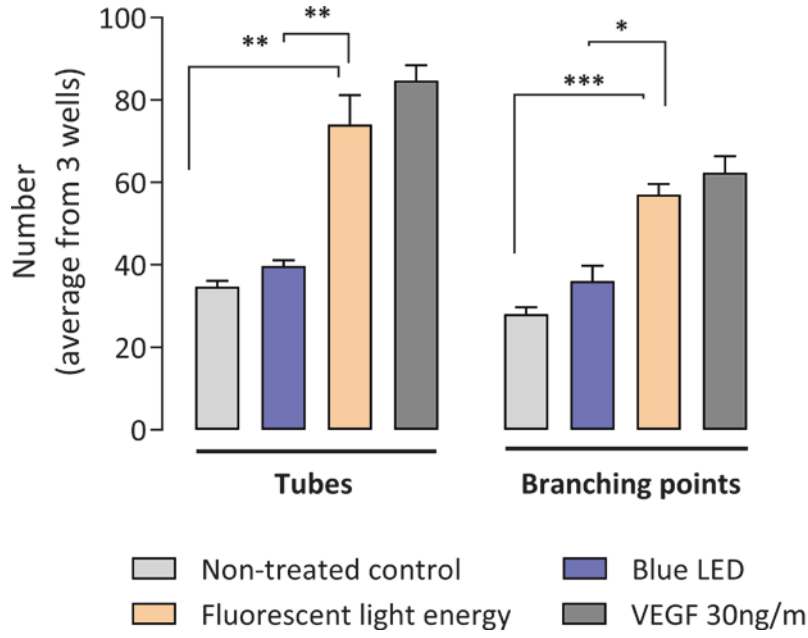

Fig. 37.7 Fluorescent light energy induces angiogenesis. Group data showing FLE increases both tube formation and branching of human aortic endothelial cells comparable to that of the potent angiogenic factor, vascular endothelial growth factor (VEGF)

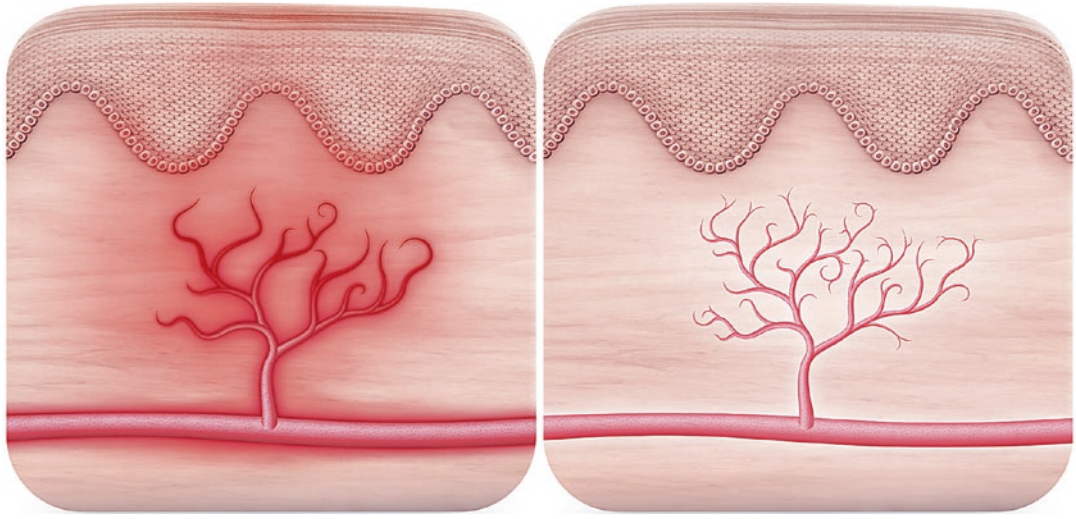

Fig. 37.8 Inflammation and vascularization. The image on the left depicts an inflamed disrupted or stressed blood vessel typical of rosacea. On the right, we hypothesize that with the resolution of inflammation healthy neovascularization can be induced following FLE, leading to a general stress reduction in the vasculature

separate applications. Since FLE is polychromatic fluorescent light across the whole visible light spectrum, it allows for the penetration of the skin at multiple levels, accessing various biological compartments and chromophores in a single treatment session. With our observed clinical results, it is likely we are targeting multiple chromophores at once. The specific targets of our application remain to be elucidated.

The photonic output generated upon illumination and activation of our photoconverter gel is very specific—in that the energy release is in a dynamic fashion—evidently leading to specific cellular effects. The term hormesis used in the

PBM literature to describe a specific dose effect [86] springs to mind. A superior effect of dynamic vs. continuous light energy has previously been observed on collagen production [52]. The dynamic nature of the photonic output also comes from the exhaustion of the chromophore gel over the treatment cycle. The specific delivery of the FLE evokes a preferred cellular reaction in cells. Indeed, preliminary work with the biophotonic platform examined a variety of conditions. An intermittent exposure, i.e. 1 min of FLE followed by a pause and another 1 min of FLE, created a greater cellular collagen response than two consecutive minutes. Perhaps this is not surprising when we consider that physiological cell signalling through chemical and electrical means is typically occurring in an intermittent fashion. The optimal treatment parameters of PBM is an ongoing area of discussion [17]. We have touched on some parameters here, including mono- vs. polychromatic irradiation, a continuous vs. dynamic mode, the type of light source and coherency. However, a rather underexplored factor—light polarization is likely to have major implications [22].

37.6.5 Fluorescent Light Energy: A Combination Treatment

LED therapy is often suggested as an adjunct therapy for commonly practised more invasive procedures [87]. For many dermatological indications, such as solar lentigines (SL), skin resurfacing and invasive methods with high-energy ablative lasers targeting melanin is the predominant treatment choice [88, 89]. Whilst these technologies can effectively achieve the desired effect, they are often associated with a significant downtime and pain. Due to the highly effective anti-inflammatory and healing profile of FLE, observed in two major inflammatory skin conditions; acne and rosacea, FLE has been used in combination with a laser for the treatment of SL [88, 90]. FLE has been used prior to ruby laser targeting of SL where it demasked and intensified the underlying SL for more effective targeting [90]. It has also been applied post picosecond laser removal of SL where FLE normalized, smoothened and rejuvenated the skin post-treatment [88]. Since FLE non-invasively stimulates the skin's own repair mechanisms, it has the potential to offer adjunct support to an array of high-energy invasive treatments, both before (pre-invasive treatment), by preparing the skin and stimulating biological processes and after (post-invasive treatment), by aiding in the healing process.

37.7 Conclusion

Biophotonic applications are widely utilized in the life sciences and have led to major advances in the diagnosis and management of disease. PBM, the non-invasive modulation of cellular activity is a rapidly evolving biophotonic platform, exploiting evolutionary mechanisms of light and biological interactions to treat an array of conditions. It has a broad application, from inflammatory conditions, pain management, neurological disorders to dentistry [69] and due to its non-invasive nature is a popular choice in cosmetic and medical dermatology. FLE represents a novel approach to PBM, by stimulating the skin's own repair mechanisms. Clinically, the polychromatic fluorescent light reduces inflammation and erythema and induces a build-up of collagen mediating a healing and de-stressing of the skin. It is used as a stand-alone treatment for an array of inflammatory skin conditions, in conjunction with other more invasive dermatological approaches, as well as serving an aesthetic benefit by rejuvenating the skin [42, 54, 58, 65, 88]. Further elucidation of the mechanisms underlying its clinical efficacy will unleash its full potential—the future is bright.

References

1. Hamblin MR. Mechanisms and mitochondrial redox signaling in photobiomodulation. Photochem Photobiol. 2018;94(2):199–212.
2. Yun SH, Kwok SJJ. Light in diagnosis, therapy and surgery. Nat Biomed Eng. 2017;1:0008.
3. Grzybowski A, Sak J, Pawlikowski J. A brief report on the history of phototherapy. Clin Dermatol. 2016;34(5):532–7.

4. Mester E, Szende B, Gartner P. The effect of laser beams on the growth of hair in mice. Radiobiol Radiother. 1968;9(5):621–6.
5. Anders JJ, Lanzafame RJ, Arany PR. Low-levelf light/laser therapy versus photobiomodulation therapy. Photomed Laser Surg. 2015;33(4):183–4.
6. Avci P, Gupta A, Sadasivam M, Vecchio D, Pam Z, Pam N, et al. Low-level laser (light) therapy (LLLT) in skin: stimulating, healing, restoring. Semin Cutan Med Surg. 2013;32(1):41–52.
7. Hamblin MR, de Sousa MVP, Agrawal T. Handbook of low-level laser therapy. New York, NY: Pan Stanfrod; 2016.
8. Smith KC. Laser and led photobiology. Laser Ther. 2010;19(2):72–8.
9. Smith KC. Basic photochemistry. Photobiological sciences online. Smith KC, editor. American Society for Photobiology. 2014. http://www.photobiology.info/.
10. Antonie V, Olaf R. Basic photophysics. Photobiological sciences online. Smith KC, editor. American Society for Photobiology. 2014. http://www.photobiology.info/.
11. Hamblin MR, Huang Y-Y, Heiskanen V. Non-mammalian hosts and photobiomodulation: do all life-forms respond to light? Photochem Photobiol. 2018;13
12. Nowicka B, Kruk J. Powered by light: phototrophy and photosynthesis in prokaryotes and its evolution. Microbiol Res. 2016;186–187:99–118.
13. The light fantastic. Nat Chem Biol. 2014;10:483.
14. Hubel DH. Eye, brain, and vision [Internet] (Scientific American library series). Henry Holt and Company; 1995. https://books.google.ie/books?id=2Id9QgAACAAJ.
15. Musio C, Santillo S. Non-visual photoreception in invertebrates. Photobiological sciences online. Smith KC, editor. American Society for Photobiology. 2009. http://www.photobiology.info/.
16. Hoang N, Schleicher E, Kacprzak S, Bouly J-P, Picot M, Wu W, et al. Human and Drosophila cryptochromes are light activated by flavin photoreduction in living cells. PLoS Biol. 2008;6(7):e160.
17. Mignon C, Botchkareva NV, Uzunbajakava NE, Tobin DJ. Photobiomodulation devices for hair regrowth and wound healing: a therapy full of promise but a literature full of confusion. Exp Dermatol. 2016;25(10):745–9.
18. Jurgens M, Mayerhofer T, Jurgen P. Handbook of biophotonics: basics and techniques, vol. 1. Hoboken, NJ: Wiley; 2011. p. 1–38.
19. Mahendran P. All in a flash of light: phototherapy throughout time. In: Proceedings of the European Academy of Dermatology and Venerology; 2018 Sep 12–16; Paris; Abstract number P1167.
20. Lim HW, Silpa-archa N, Amadi U, Menter A, Van Voorhees AS, Lebwohl M. Phototherapy in dermatology: a call for action. J Am Acad Dermatol. 2015;72:1078–80.
21. Stern RS. Psoralen and ultraviolet a light therapy for psoriasis. N Engl J Med. 2007;357(7):682–90.
22. Hamblin MR. Mechanisms of low level light therapy [Internet]. Photobiological sciences online. Smith KC, editor. American Society for Photobiology. 2013. http://www.photobiology.info/.
23. Chung H, Dai T, Sharma S, Huang Y-Y, Carroll J, Hamblin M. The nuts and bolts of low-level laser (light) therapy. Ann Biomed Eng. 2012;40(2):516–33.
24. Mester E, Spiry T, Szende B, Tota JG. Effect of laser rays on wound healing. Am J Surg. 1971;122(4):532–5.
25. Jalili A. Chromophore gel-assisted phototherapy. J für Ästhetische Chir. 2018;20:1–5.
26. Alexiades-Armenakas MR, Dover JS, Arndt KA. The spectrum of laser skin resurfacing: nonablative, fractional, and ablative laser resurfacing. J Am Acad Dermatol. 2008;58(5):719–37.
27. de Freitas LF, Hamblin MR. Proposed mechanisms of photobiomodulation or low-level light therapy. IEEE J Sel Top Quantum Electron. 2016;22(3):348–64.
28. Gajinov Z, Matić M, Prćić S, Đuran V. Optičke osobine ljudske kože [Optical properties of the human skin]. Serbian J Dermatol Venerol. 2010;2(4):131–6.
29. Huang Y-Y, Mroz P, Hamblin MR. Basic photomedicine [Internet]. Photobiological sciences online. Smith KC, editor. American Society for Photobiology. 2009. http://www.photobiology.info/.
30. Jeronimo R, Moraes MN, de Assis LVM, Ramos BC, Rocha T, Castrucci AM d L. Thermal stress in Danio rerio: a link between temperature, light, thermo-TRP channels, and clock genes. J Therm Biol. 2017;68(Pt A):128–38.
31. Pennisi E. Opsins: not just for eyes. Science. 2013;339(6121):754–5.
32. Haltaufderhyde K, Ozdeslik RN, Wicks NL, Najera JA, Oancea E. Opsin expression in human epidermal skin. Photochem Photobiol. 2015;91(1):117–23.
33. Castellano-Pellicena I, Uzunbajakava NE, Mignon C, Raafs B, Botchkarev VA, Thornton MJ. Does blue light restore human epidermal barrier function via activation of Opsin during cutaneous wound healing? Lasers Surg Med. 2018;
34. Karu T. Primary and secondary mechanisms of action of visible to near-IR radiation on cells. J Photochem Photobiol B. 1999;49(1):1–17.
35. Heiskanen V, Hamblin MR. Photobiomodulation: lasers: vs. light emitting diodes? Photochem Photobiol Sci. 2018;17(8):1003–17.
36. Terakita A. The opsins. Genome Biol. 2005;6(3):1–9.
37. Farivar S, Malekshahabi T, Shiari R. Biological effects of low level laser therapy. J Lasers Med Sci. 2014;5(2):58–62.
38. Karu TI, Pyatibrat LV, Afanasyeva NI. A novel mitochondrial signaling pathway activated by visible-to-near infrared radiation. Photochem Photobiol. 80(2):366–72.
39. Fluoresence and fluoresence applications. Integrated DNA technologies. 2011.
40. Schaefer PM, Kalinina S, Rueck A, Von Arnim CAF. NADH auto fluorescence—a marker on its

way to boost bioenergetic research. Cytometry A. 95(1):34–46.
41. Croce AC, Bottiroli G. Autofluorescence spectroscopy for monitoring metabolism in animal cells and tissues. Methods Mol Biol. 2017;1560:15–43.
42. Edge D, Mellergaard M, Dam-Hansen C, Corell DD, Devemy E, Jaworska J, et al. Fluorescent light energy: the future for treatment of inflammatory skin conditions? J Clin Aesthet Dermatol. 2019;12(5): E61–8.
43. Barolet D. Light-emitting diodes (LEDs) in dermatology. Semin Cutan Med Surg. 2008;27(4):227–38.
44. Pillai S, Cornell M, Christian O. Skin physiology pertinent to cosmetic dermatology. In: Cosmetic dermatology, products and procedures: John Ciley and Sons Ltd; 2010. p. 3–12.
45. Simpson CR, Kohl M, Essenpreis M, Cope M. Near-infrared optical properties of ex vivo human skin and subcutaneous tissues measured using the Monte Carlo inversion technique. Phys Med Biol. 1998;43(9):2465–78.
46. Opel DR, Hagstrom E, Pace AK, Sisto K, Hirano-Ali SA, Desai S, et al. Light-emitting diodes: a brief review and clinical experience. J Clin Aesthet Dermatol. 2015;8(6):36–44.
47. Elman M, Lebzelter J. Light therapy in the treatment of acne vulgaris. Dermatol Surg. 2004;30(2 Pt 1):139–46.
48. Hamilton FL, Car J, Lyons C, Car M, Layton A, Majeed A. Laser and other light therapies for the treatment of acne vulgaris: systematic review. Br J Dermatol. 2009;160(6):1273–85.
49. Shnitkind E, Yaping E, Geen S, Shalita AR, Lee W-L. Anti-inflammatory properties of narrow-band blue light. J Drugs Dermatol. 2006;5(7):605–10.
50. de Vasconcelos Catao MHC, Nonaka CFW, de Albuquerque RLCJ, Bento PM, de Oliveira Costa R. Effects of red laser, infrared, photodynamic therapy, and green LED on the healing process of third-degree burns: clinical and histological study in rats. Lasers Med Sci. 2015;30(1):421–8.
51. Sadick NS, Karcher C, Palmisano L. Cosmetic dermatology of the aging face. Clin Dermatol. 2009;27(3 SUPPL):S3–12.
52. Barolet D, Roberge CJ, Auger FA, Boucher A, Germain L. Regulation of skin collagen metabolism in vitro using a pulsed 660nm LED light source: clinical correlation with a single-blinded study. J Invest Dermatol. 2009;129(12):2751–9.
53. Lee SY, Park K-H, Choi J-W, Kwon J-K, Lee DR, Shin MS, et al. A prospective, randomized, placebo-controlled, double-blinded, and split-face clinical study on LED phototherapy for skin rejuvenation: clinical, profilometric, histologic, ultrastructural, and biochemical evaluations and comparison of three different tre. J Photochem Photobiol B Biol. 2007;88(1):51–67.
54. Nikolis A, Bernstein S, Kinney B, Scuderi N, Rastogi S, Sampalis JS. A randomized, placebo-controlled, single-blinded, split-faced clinical trial evaluating the efficacy and safety of KLOX-001 gel formulation with KLOX light-emitting diode light on facial rejuvenation. Clin Cosmet Investig Dermatol. 2016;9:115–25.
55. Koceva I, Rümmelein B, Gerber PA, Edge D, Nielsen MCE. Fluorescent light energy a new therapeutic approach to effectively treating acne conglobata and hidradenitis suppurativa. Clin Case Rep. 2019;00: 1–4.
56. Chung JH, Seo JY, Choi HR, Lee MK, Youn CS, Rhie G, et al. Modulation of skin collagen metabolism in aged and photoaged human skin in vivo. J Invest Dermatol. 2001;117(5):1218–24.
57. Lynch B, Bonod-Bidaud C, Ducourthial G, Affagard JS, Bancelin S, Psilodimitrakopoulos S, et al. How aging impacts skin biomechanics: a multiscale study in mice. Sci Rep. 2017;7(1):1–10.
58. Sannino M, Lodi G, Dethlefsen MW, Nistico SP, Cannarozzo G, Canova Engelbrecht Nielsen M. Fluorescent light energy: treating rosacea subtypes 1, 2, and 3. Clin Case Rep. 2018;00:1–6.
59. Fox L, Csongradi C, Aucamp M, Du Plessis J, Gerber M. Treatment modalities for acne. Molecules. 2016;21(8):1–20.
60. Barolet D. Photobiomodulation in dermatology: harnessing light from visible to near infrared. Med Res Arch. 2018;6(1).
61. Ashkenazi H, Malik Z, Harth Y, Nitzan Y. Eradication of Propionibacterium acnes by its endogenic porphyrins after illumination with high intensity blue light. FEMS Immunol Med Microbiol. 2003;35(1):17–24.
62. Goldberg DJ, Russell BA. Combination blue (415 nm) and red (633 nm) LED phototherapy in the treatment of mild to severe acne vulgaris. J Cosmet Laser Ther. 2006;8(2):71–5.
63. Lee SY, You CE, Park MY. Blue and red light combination LED phototherapy for acne vulgaris in patients with skin phototype IV. Lasers Surg Med. 2007;39(2):180–8.
64. Antoniou C, Dessinioti C, Sotiriadis D, Kalokasidis K, Kontochristopoulos G, Petridis A, et al. A multicenter, randomized, split-face clinical trial evaluating the efficacy and safety of chromophore gel-assisted blue light phototherapy for the treatment of acne. Int J Dermatol. 2016;55(12):1321–8.
65. Nikolis A, Fauverghe S, Scapagnini G, Sotiriadis D, Kontochristopoulos G, Petridis A, et al. An extension of a multicenter, randomized, split-face clinical trial evaluating the efficacy and safety of chromophore gel-assisted blue light phototherapy for the treatment of acne. Int J Dermatol. 2018;57(1):94–103.
66. Mahendran A, Wong XL, Kao S, Sebaratnam DF. Treatment of erlotinib-induced acneiform eruption with chromophore gel-assisted phototherapy. Photodermatol Photoimmunol Photomed. 2019;35(3):190–2.
67. Zheng Q. Editorial: at the crossroad between inflammation and skin aging. Inflamm Allergy Drug Targets. 2014;13(3):151–2.
68. Houh YK, Kim KE, Park HJ, Cho D. Roles of erythroid differentiation regulator 1 (Erdr1) on inflammatory skin diseases. Int J Mol Sci. 2016;17(12):1–10.

69. Hamblin MR, R Hamblin M. Mechanisms and applications of the anti-inflammatory effects of photobiomodulation. AIMS Biophys. 2017;4(3):337–61.
70. Mescher AL. Macrophages and fibroblasts during inflammation and tissue repair in models of organ regeneration. Regeneration. 2017;4(2):39–53.
71. Sauder DN. The role of epidermal cytokines in inflammatory skin diseases. J Invest Dermatol. 1990;95(5 Suppl):27S–8S.
72. Murray PJ, Allen JE, Biswas SK, Fisher EA, Gilroy DW, Goerdt S, et al. Macrophage activation and polarization: nomenclature and experimental guidelines. Immunity. 2014;41(1):14–20.
73. Van den Bossche J, O'Neill LA, Menon D. Macrophage Immunometabolism: where are we (going)? Trends Immunol. 2017;38(6):395–406.
74. Young DA, Lowe LD, Clark SC. Comparison of the effects of IL-3, granulocyte-macrophage colony-stimulating factor, and macrophage colony-stimulating factor in supporting monocyte differentiation in culture. Analysis of macrophage antibody-dependent cellular cytotoxicity. J Immunol. 1990;145(2):607–15.
75. Murray PJ, Wynn TA. Protective and pathogenic functions of macrophage subsets. Nat Rev Immunol. 2011;11:723.
76. Nowarski R, Jackson R, Flavell RA. The stromal intervention: regulation of immunity and inflammation at the epithelial-mesenchymal barrier. Cell. 2017;168(3):362–75.
77. Banno T, Gazel A, Blumenberg M. Effects of tumor necrosis factor-α (TNFα) in epidermal keratinocytes revealed using global transcriptional profiling. J Biol Chem. 2004;279(31):32633–42.
78. Hernández MV, Meineri M, Sanmartí R. Skin lesions and treatment with tumor necrosis factor alpha antagonists Lesiones cutáneas y terapia biológica con antagonistas del factor de necrosis tumoral. Reum Clin. 2013;9(1):53–61.
79. Tanaka T, Kishimoto T. The biology and medical implications of interleukin-6. Cancer Immunol Res. 2014;2(4):288–94.
80. Tan J, Almeida LMC, Bewley A, Cribier B, Dlova NC, Gallo R, et al. Updating the diagnosis, classification and assessment of rosacea: recommendations from the global ROSacea COnsensus (ROSCO) panel. Br J Dermatol. 2017;176(2):431–8.
81. Weinkle AP, Doktor V, Emer J. Update on the management of rosacea. Plast Surg Nurs. 2015;35(4):184–202.
82. Abokwidir M, Feldman SR. Rosacea management. Ski Appendage Disord. 2016;2(1–2):26–34.
83. Braun SA, Gerber PA. A photoconverter gel-assisted blue light therapy for the treatment of rosacea. Int J Dermatol. 2017;56(12):1489–90.
84. Liu RC, Makhija M, Wong XL, Sebaratnam DF. Treatment of granulomatous rosacea with chromophore gel-assisted phototherapy. Photodermatol Photoimmunol Photomed. 2018;2019:1–2.
85. Gallo RL, Granstein RD, Kang S, Mannis M, Steinhoff M, Tan J, et al. Standard classification and pathophysiology of rosacea: the 2017 update by the National Rosacea Society Expert Committee. J Am Acad Dermatol. 2018;78(1):148–55.
86. Hamblin MR. Shining light on the head: photobiomodulation for brain disorders. BBA Clin. 2016;6:113–24.
87. Ablon G. Phototherapy with light emitting diodes: treating a broad range of medical and aesthetic conditions in dermatology. J Clin Aesthet Dermatol. 2018;11(2):21–7.
88. Scarcella G, Dethlefsen M, Nielsen M. Treatment of solar lentigines using a combination of picosecond laser and biophotonic treatment. Clin Case Rep. 2018;00:1–3.
89. Fitzpatrick RE, Goldman MP, Satur NM, Tope WD. Pulsed carbon dioxide laser resurfacing of photo-aged facial skin. Arch Dermatol. 1996;132(4):395–402.
90. Gerber PA, Scarcella G, Edge D, Nielsen MCE. Biophotonic pre-treatment enhances the targeting of senile lentigines with a 694 nm QS-ruby laser. Photodermatol Photoimmunol Photomed. 2019;

Photodynamic Therapy (PDT)

38

Michele Pellegrino and Emanuele Trovato

38.1 Background

The first report about photodynamic therapy (PDT) dates back to the early 1900s when the graduate student Oscar Raab, operating at the Institute of Pharmacology of the University of Munich, noted that the colonies of *Paramecium Caudatum* died faster when exposed to light in the presence of an organic photosensitizer such as acridine orange. A few years later, in 1904, Von Tappeiner coined the term "photodynamic reaction" after observing that the process of destruction of protozoa was due to an oxygen-dependent photochemical reaction emitting a characteristic fluorescence. The following year, the same author demonstrated how the irradiation with artificial light after application of a 5% solution of eosin could be useful in the treatment of non-melanoma skin cancers (NMSCs). However, it is necessary to wait another 40 years to get the first scientific data on the sensitizing photoagents that we use today. In fact, it is only in 1948 that Figge et al. succeeded in demonstrating that hematoporphyrin could selectively concentrate in some tissues such as neoplastic, traumatized, and embryonic ones. After another 30 years, Dougherty et al. reported the effectiveness of irradiation with artificial light in the presence of hematoporphyrin derivatives in the treatment of malignant skin lesions. Finally, in 1990 Kennedy and her group introduce a new photosensitizer: 5-aminolevulinic acid. Since then there have been a long series of scientific works to demonstrate the effectiveness of this sensitizing photosensitizer, especially in the treatment of actinic keratosis and NMSC [1, 2]. The good results obtained have prompted researchers to look for different uses. The literature has in fact been enriched with works in which PDT is successfully used in acne, psoriasis, sarcoidosis, genital warts, vulgar warts, etc.

38.2 Physical Bases of PDT

The mechanism that underlies the action of photodynamic therapy is closely linked to a specific process of absorption of certain wavelengths of the incident radiation by a photosensitizing molecule. This is essentially conditioned by the penetration capacity of the incident radiation and by the characteristics of the photosensitizing molecule. The penetration of the incident radiation into the skin is a complex phenomenon characterized by three parallel events:

- the reflection of the photons incident on the surface that affects no more than 10% of the incident radiation and is within certain limits independent of the wavelength.

M. Pellegrino · E. Trovato (✉)
Department of Medical, Surgical and Neurological Science, Dermatology Section, University of Siena, Siena, Italy

M. Fimiani et al. (eds.), *Technology in Practical Dermatology*,
https://doi.org/10.1007/978-3-030-45351-0_38

- scattering (scattering or simply deflecting the light beam) that is closely related to the particle size with which the photons interact (if the particles encountered are smaller than those of the incident wavelengths, the scattering varies inversely proportional to the fourth wavelength power) (Fig. 38.1).
- the absorption of photons: a selective process determined by the interaction of chromophore molecules with radiations of precise wavelength ranges [3].

As a consequence of these events, it can be assured that the penetration of a radiation grows up with the increase of its wavelength due to the reduction of the scattering and of the absorption. In fact, it is possible to identify a spectral range between 600 and 900 nm where the maximum "transparency" of the biological tissues is obtained with a deep penetration (>1 mm) of the light radiation [4].

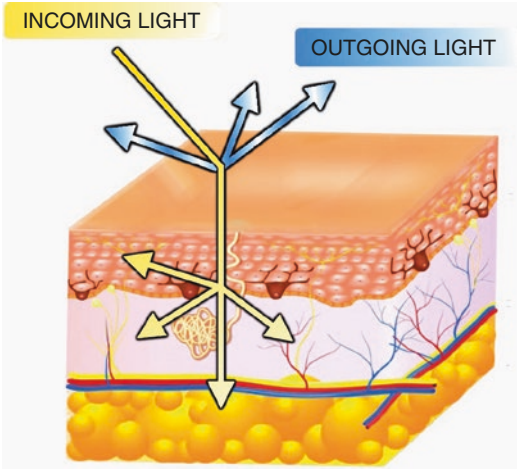

Fig. 38.1 Scattering: refraction of the incoming light throughout the dermis

38.3 Chemical Bases of PDT

The initial event of the photochemical reaction is represented by the absorption of a light photon by the photosensitizing molecule which, in the absence of light, is in the so-called "basal or fundamental state." In particular, if the electrons are housed in the low-energy orbitals and have opposite spin, it is configured as the "baseline state of singlet" but if it is configured they have parallel spins the "triplet basal state." The absorption of a photon of energy by a photosensitizing molecule determines the transition of an electron from a low-energy orbital (ground state) to a higher energy orbital (excited state) without spin change (excited singlet state or triplet). The molecule, after having absorbed a photon of energy, in the excited state, results in a condition of instability and quickly returns to the fundamental state with energy dissipation (Fig. 38.2) If the energy re-emission takes place directly from an excited singlet state to a fundamental singlet, we have the fluorescence phenomenon. If the electron undergoes a change in the state of spin (intersystem crossing) and passes to an excited triplet state before re-emitting energy, the phenomenon takes the name of phosphorescence. Both in the case of fluorescence and phosphorescence, the energy of the re-emitted radiation is lower than that of

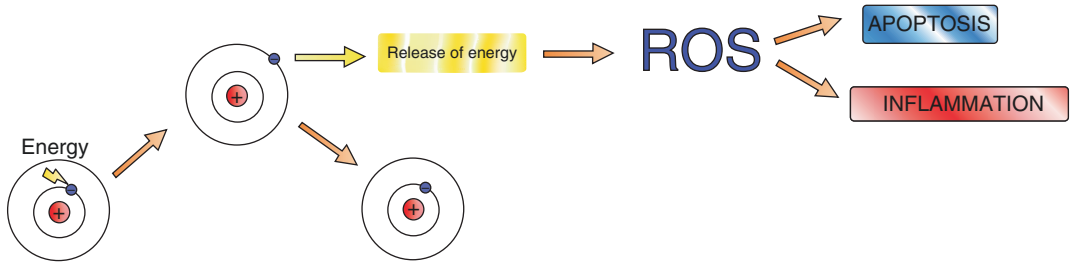

Fig. 38.2 Passage of the electron in excited state on the external orbithetal after energy absorption and subsequent return to ground state after release of energy. This leads to the formation of ROS that mediate the mechanism of action of PDT

absorbed one (vibrational relaxation). In some cases, the absorption of a photon of energy can cause a process of inversion of the electronic spin with consequent passage from the excited state of singlet to the excited state of triplet. In any case, the molecule, in order to return to the fundamental state, must yield excess energy to accepting molecules such as those of oxygen that are transformed into a singlet state [5].

Photodynamic therapy is mediated by oxygen-dependent photochemical reactions that lead to the formation of highly reactive oxygen species such as the superoxide anion, which in turn may originate other agents such as hydrogen peroxide and the hydroxyl radical. It also leads to the formation of singlet oxygen capable of initiating that cascade of events that carry out to the destruction of the cells. Because of its extreme reactivity, singlet oxygen, before returning to the ground state, has a short survival in the cellular environment and a limited diffusivity within the tissue (radius of about 10–20 nm). Therefore, the close proximity of the target cells to the singlet oxygen is of fundamental importance in inducing cell death by necrosis or apoptosis. Given this and the fact that the "normal" tissue does not accumulate photosensitizers, it is possible to understand why normal tissues are not damaged by exposure to PDT. Furthermore, most of the photosensitizers used or tested for PDT are not able to penetrate the nucleus, avoiding the risk of DNA damage, with possible mutagenesis and carcinogenesis [6, 7].

38.4 Irradiance

Several light sources have been used in the PDT. In any case, the fundamental characteristics are the irradiance (or speed of fluence) expressed in mW/cm^2 and the dose (or fluence) expressed in J/cm^2 and calculated by multiplying the irradiance for the irradiation time measured in seconds. It seems that all the sources used are sufficiently effective but at the same dose sources with lower irradiance cause more damage than the higher ones. The reason for this lies in the fact that the oxygen concentration (cardinal element of the PDT) decreases during irradiation (it is consumed), and the decrease is greater at higher irradiations. Therefore, by using low fluency rates this decrease can be made less rapid [8].

38.5 Photosensitizers (PS)

In recent years, a considerable research activity has been developed towards to the synthesis and experimentation of new photosensitizing molecules that foresee the systemic use or topical application. Among these, 5-aminolevulinic acid (5-ALA) and its methyl ester (methyl-ALA) represent and remain the best known, most studied, and widespread. As it is known, ALA does not show intrinsic photosensitizing abilities, but represents a hydrophilic precursor in the metabolic synthesis pathway of the heme. This pathway leads from succinyl CoA and glycine through several intermediates to PPIX and finally to heme. When exogenous ALA is added to the system, PPIX accumulates in the cells since the final enzyme (ferrochelatase) is then rate-limiting [9]. The accumulated excess of PPIX generates ROS after illumination leading to apoptosis and necrosis of targeted tissue. The 5-ALA molecule is small enough to penetrate the skin barrier and can accumulate within pilosebaceous units and hyperproliferative keratinocytes compared to normal skin, making the treatment selective. Moreover, in many cutaneous pathologic lesions, the barrier function of the stratum corneum is compromised, so this further increases the selective penetration of ALA. An additional advantage is that PPIX is metabolized in 48 h, which excludes the possibility of prolonged phototoxicity [10, 11]. The clinical success of PDT is closely linked to the achievement of a threshold concentration of ALA, following topical administration, so as to induce therapeutic levels of PpIX within "abnormal" cells. Failure to achieve this threshold concentration results in a poor accumulation of protoporphyrin IX, so that subsequent irradiation of the target cells does not produce sufficient singlet oxygen, necessary to successfully eradicate the lesion. Another frequently used PS is methyl aminolevulinate (MAL), an esterified

form of ALA, with more lipophilic properties, allowing for deeper penetration into the skin compared to ALA. A relatively new product is the porphyrin-based PS called hematoporphyrin mono-methyl ether (HMME, Hemoporphyrin). Hemoporphyrin has shown strong photodynamic effects, and hemoporfin-based PDT induces significant cell death with lower toxicity and a shorter-term skin phototoxicity, compared with a previous photosensitizer with similar structure called Photofrin [12].

38.6 Light Sources

The absorption spectrum of PPIX is maximally activated at 410 nm with significantly lower peaks at 505, 540, 580, and 635 nm, so many different light sources can be used in PDT, including broad-spectrum continuous-wave light sources or lamps (white, blue, red, or green light), lasers, intense pulsed light sources (IPL), filtered xenon arc lamps, metal halide or fluorescent lamps, and more recently light emitting diodes (LED). Currently, a new trend has emerged towards the use of daylight as a light source (both at home and under clinical monitoring) termed daylight PDT (dPDT). Daylight is the combination of direct and diffuse sunlight that predominates outdoors during the daylight hours. The idea that all PPIX absorption peaks are within the visual spectrum of daylight led to the use of dPDT with many benefits to patients in terms of convenience and reduced pain. This simplified method is effective as the red or blue wavelengths required to activate porphyrins are present in daylight [13]. Following pretreatment (e.g., abrasion or superficial curettage), the photosensitizer (MAL) is applied for 30 min [14]. Occlusion is not required [15]. Sunscreen without physical blocking filters is essential to protect exposed areas from ultraviolet damage [15]. The PpIX light dose must be equal to or greater than 8 J cm—2 with an ambient temperature exceeding 10 °C. Daylight PDT therefore remains suitable for use at higher latitudes, with seasonal limitation [16]. Patients are exposed to 2 h of daylight and must avoid sunlight for the remainder of the 24 h period [15]. Decreased pain and better tolerance compared to conventional PDT (cPDT) results from lower intensity continuous production of PpIX [17]. Similar or greater efficacy than cPDT has been reported in several international randomized studies [13–18]. Since the power density of sunlight is much lower than artificial red light sources used in the clinics, the overall treatment takes much longer, but the patients are compensated by much less pain.

38.7 Clinical Applications

PDT is a widely approved therapy in dermatology. Many applications have been evaluated, including both cosmetic and clinical indications. The recommendations contained in the European dermatology forum guidelines on topical PDT [14], including actinic keratosis, acne, viral warts, photo-rejuvenation, psoriasis, hypertrophic and keloid scars.

38.7.1 Actinic Keratosis (AK)

Actinic keratoses (AKs) are frequently caused by long-term sun exposure and are considered to be precursor lesions that can go on to develop into invasive squamous cell carcinoma. AKs respond well to PDT. Efficacy, cosmetic outcome, and patient overall satisfaction with MAL-PDT were reported to be superior in comparison with diclofenac [18]. It has proved to be effective for lesions of the face, scalp, and extremities. PDT has also been shown to be an efficient and well-tolerated treatment modality for AKs in immunosuppressed patients [19]. Researchers have made a variety of efforts to improve the efficacy of PDT against AKs. Pulsed lasers that create microchannels may facilitate ALA delivery, thus improving PDT response [20]. PDT is generally preferred as a treatment modality for AKs verses other competing treatments because of its improved cosmetic effects. In the most recent expert consensus, dPDT has been positioned as a valuable option for patients with multiple AKs in small or large fields [21] (Fig. 38.3).

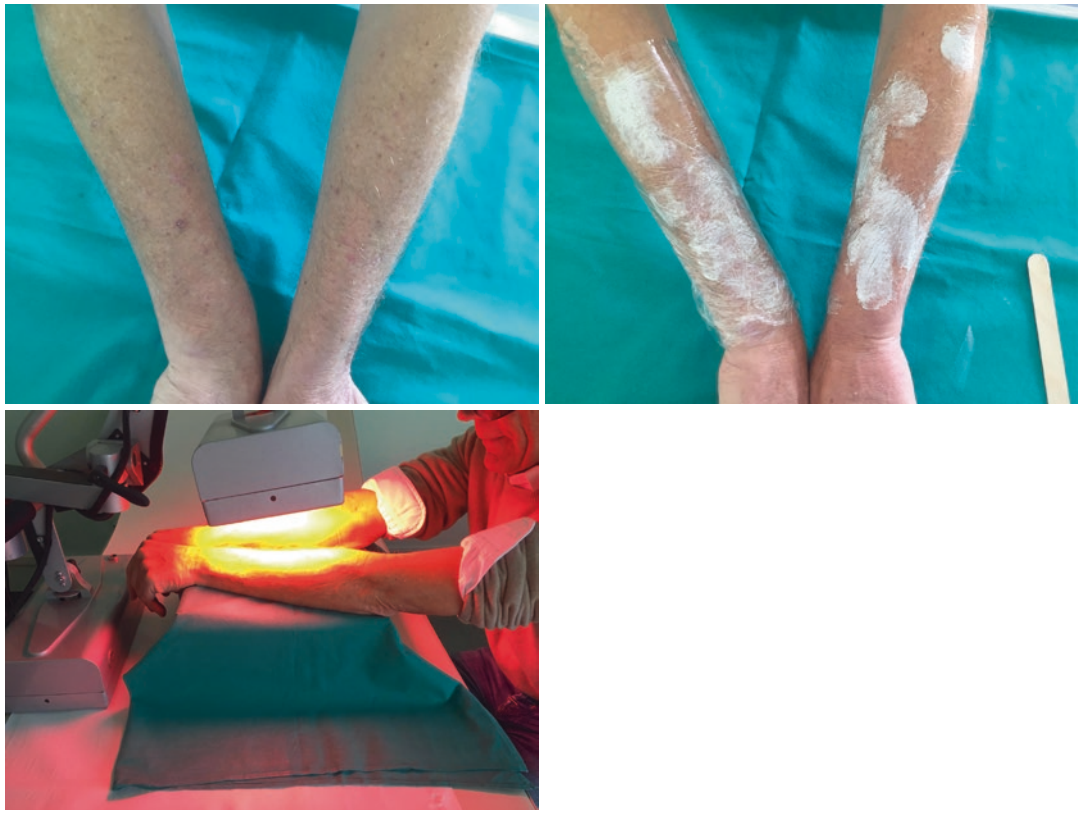

Fig. 38.3 From the left: patient with AKs of the arms; in the middle, after application of 5-ALA for 2 h; on the right, under exposure with red light for 20 min

38.7.2 Basal Cell Carcinoma (BCC)

PDT is an established treatment for superficial BCC, but is not indicated for the more aggressive basosquamous, nodular, morpheic, or infiltrating subtypes [22]. Improved clinical outcomes were found with repeated PDT cycles for primary superficial BCC in a recent systematic review (pooled complete tumor response increase from 75.6 to 79%) [23]. Sustained complete lesion response rates at 5 years for surgical excision of nodular BCC compared to MAL-PDT were reported in a later randomized study (96% vs. 76%, respectively). PDT gave consistently better cosmetic outcomes [24]. Long-term recurrence may limit the use of PDT for nodular BCC, although it may be suitable for cases where surgical excision is not appropriate. Greater frequency of recurrence is observed for more aggressive BCCs, which may be due to genetic mutations conferring resistance to apoptosis. Aggressive subtypes often occur on the face and PDT should therefore be used with caution for facial tumors [22]. The limited penetration of photosensitizers (1–2 mm) reduces the efficacy of PDT in thicker tumors. No association has been found between superficial BCC tumor thickness (up to 1 mm) and PDT failure [25]. Deep curettage prior to PDT may be beneficial for selected tumors, with cosmetic results maintained [26]. Dimethylsulfoxide (DMSO), which alters the intercellular lipid structure of the stratum corneum, has also been used as a pretreatment penetration enhancer [27]. Favorable 10-year response rates of 75% for primary small BCC have been achieved with curettage and DMSO pretreatment using ALA-PDT for one or two sessions [28]. Intralesional ALA and light source application showed promising results in a small prospective study of 20 patients with nodu-

lar BCC, with no clinical recurrence observed (mean follow-up 19.5 months) [29]. Pretreatment of nodular facial BCC with an ablative fractional laser is not currently recommended as an adjunctive therapy [30].

38.7.3 Acne and Acne Scarring

PDT has been widely used as a treatment modality for the most common (and one of the most distressing) dermatologic disorders, acne vulgaris. It is considered safe and effective for both inflammatory and non-inflammatory acne lesions and can improve the severity of lesions from mild to severe [31]. Blue light is the most potent wavelength for activation of the endogenous porphyrin components of *Propionibacterium acnes* because the 407–420 nm band possesses the highest absorption coefficient in the porphyrin spectrum [32]. However, blue light has a poor depth of penetration into the skin (limited to only approximately 1 mm) while red light can penetrate to about 3 mm. The selective destruction of the sebaceous gland unit and eradication of *P. acnes* are thought to be the mechanisms of action of PDT in acne [33]. The rise in antibiotic-resistant strains of *P. acnes* makes alternative therapies mandatory. The main advantages of PDT for acne are its excellent results despite low invasiveness, especially in patients who have not responded to topical therapy and oral antibiotics and are not good candidates for isotretinoin [34]. Acne scarring is a common complication of acne and is both disfiguring and challenging despite various currently available treatments. One single-center, double-blinded, randomized, pilot study ($n = 6$) used 20% ALA or vehicle solution alone to either the right or left side of the face for a 60-min incubation followed by 417 nm blue light after full-face treatment with microdermabrasion, and showed 80% of patients displayed a greater improvement in scarring on the ALA-treated side after five sessions [35]. However, further studies are needed to confirm the efficacy of this treatment.

38.7.4 Viral Warts

Warts consist of benign cutaneous hyperproliferative lesions resulting from infection with human papilloma viruses (HPV). The treatment of warts poses a therapeutic challenge; warts that are recalcitrant to therapy and recurrent warts remain a problem. MAL-PDT with red light showed 60% and 100% clearance after the first and second session respectively with mild complications [36]. Combination therapy using a superpulsed carbon dioxide (CO_2) laser together with ALA-PDT in patients with recalcitrant flat facial warts was reported [37]. PDT is a treatment that offers good results in the treatment of viral warts, especially for those patients who are resistant to routine treatment.

38.7.5 Skin Rejuvenation

Clinical observations have shown that PDT is associated with high level of improvement in the signs of photo-aging such as fine lines, wrinkles, dyspigmentation, sallowness, roughness, and telangiectasia, with the superior efficacy of microneedling-assisted PDT compared to MAL-PDT alone on fine lines at day 30. At day 90, facial erythema and coarse wrinkles also improved in the microneedling-assisted PDT side of the face, in addition to fine lines for the MAL-PDT side. Side effects were more common and intense on the microneedling-assisted PDT side [38]. It has been demonstrated that the stratum corneum hydration, elasticity, and thickness increased, whereas the trans-epidermal water loss and melanin index value decreased with superior changes in patients treated with the red light-PDT. Lateral periorbital wrinkles treated with PDT showed better results than Nd-YAG without serious adverse effects. PDT can both rejuvenate their skin and also treat their visible or incipient UV-induced lesions, which shows excellent efficacy and tolerability [39].

38.7.6 Psoriasis

A large number of studies are devoted to the treatment of psoriasis with PDT. Initial research showed that PDT might be helpful, but later studies could not confirm these expectations [40]. A systematic review and meta-analysis searched Medline, Embase, and Cochrane databases during the period of January 1980 to June 2012, including 765 studies, and found that the pooled effect estimate of the efficacy of topical PUVA, targeted UVB and PDT were 77%, 61%, and 22%, respectively. PDT has high percentage of side effects in treating localized psoriasis [41]. Moreover, another systematic review disclosed that topical ALA-PDT failed to demonstrate a consistent, efficacious response and frequently suffered from intolerable adverse reactions (severe pain and burning sensations) [42]. Current evidence of PDT remains unclear for psoriasis with disappointing efficacy and unwanted side effects.

38.7.7 Localized Scleroderma

Localized scleroderma is a cutaneous fibrotic disorder, characterized by increased dermal collagen accumulation. PDT has been tested in five patients with localized scleroderma with a good response [43]. In these patients, the sclerosis was found to have regressed significantly following a course of treatment that lasted between 3 and 6 months. This finding attracted great interest, as the direct effect of PDT cannot completely reach the layers of dermis where the pathological changes occur in scleroderma. It was hypothesized that PDT may influence dermal fibroblasts into producing increased amounts of collagen-degrading matrix-metalloproteinase (MMP1 and MMP3) [44].

38.7.8 Keloids

This mechanism may also be used to explain the recent findings of PDT for treatment of keloid disease. Keloids are a type of scar formed from fibroproliferative dermal tissue characterized by the excessive proliferation of fibroblasts. A clinical study used MAL and red light (37 J/cm^2) to treat keloids with PDT once per week for 3 weeks. They found that blood flow, collagen, and hemoglobin levels significantly decreased from week 1 to 3 and pliability increased significantly ($p = 0.001$). Only one out of the 20 treated patients experienced recurrence. All other patients had no recurrence at 9-month follow-up [45]. Larger studies are needed to confirm the efficacy of PDT for this condition.

38.7.9 Port-Wine Stains

Port-wine stains (PWS) are common congenital and progressive vascular lesions appearing mainly on the face and neck that can represent a serious disfigurement. Pulsed-dye laser (PDL) is the current standard treatment for PWS. However, about 20% of PWS are resistant to PDL [46]. Vascular-targeted PDT with an intravenous injection of a hematoporphyrin derivative followed after a short time by irradiation might be an alternative for the treatment of PWS. The overall response rate of PDT seems to be superior to PDL for purple lesions (93.0% vs. 75.6%), whereas the pigmentation and scar formation in PDT were lower [47].

38.8 Future Strategies

New strategies for improving the efficacy and tolerability of PDT are under continuous development. Several classes of novel photosensitizers, for example fullerenes and phenothiazines, have been proposed [48]. The potential of low dose lipophilic hexyl-5-aminolaevulinate (HAL) 0.2% to provide deeper penetration was investigated in comparison to MAL-PDT in a randomized pilot study [49]. Better uptake and targeting of photosensitizers may be achieved in the future, using novel delivery systems such as nanoparticles, micelles, or liposomes [48]. The use of alternative light sources to decrease pain is also being investigated. For example, light

emitting diode (LED) delivers low irradiance and has shown good efficacy for treating Bowen disease, superficial BCC, and AKs in preliminary studies [50–51]. Outcomes for pain control have been variable and the true benefit is yet to be determined. LED is lightweight and suitable for ambulatory PDT, which may provide greater convenience for patients [50]. New indications for PDT currently under exploration include cutaneous infections, inflammatory dermatoses, cutaneous T-cell lymphoma, and extra-mammary Paget's disease [14].

References

1. Ackroyd R, et al. The history of photodetection and photodynamic therapy. Photochem Photobiol. 2001;74(5):656–69.
2. Kato H. History of photodynamic therapy—past, present and future. Gan To Kagaku Ryoho. 1996;23(1):8–15.
3. Castano AP, Demidova TN, Hamblin MR. Mechanisms in photodynamic therapy: part one-photosensitizers, photochemistry and cellular localization. Photodiagn Photodyn Ther. 2004;1(4):279–93.
4. Agostinis P, et al. Regulatory pathways in photodynamic therapy induced apoptosis. Photochem Photobiol Sci. 2004;3(8):721–9.
5. Orringer JS, et al. Molecular effects of photodynamic therapy for photoaging. Arch Dermatol. 2008;144(10):1296–302.
6. Lv T, et al. Evaluation of collagen alteration after topical photodynamic therapy (PDT) using second harmonic generation (SHG) microscopy—in vivo study in a mouse model. Photodiagn Photodyn Ther. 2012;9(2):164–9.
7. Castano AP, Demidova TN, Hambli MR. Mechanisms in photodynamic therapy. Photodiagn Photodyn Ther. 2004;1(4):279–93.
8. Wen X, Li Y, Hamblin MR. Photodynamic therapy in dermatology beyond non-melanoma cancer: an update. Photodiagn Photodyn Ther. 2017;19:140–52.
9. Thunshelle C, et al. Current advances in 5-aminolevulinic acid mediated photodynamic therapy. Curr Derm Rep. 2016;5(3):179–90.
10. Krammer B, Plaetzer K. ALA and its clinical impact, from bench to bedside. Photochem Photobiol Sci. 2008;7(3):283–9.
11. van Veen RLP, et al. In situ light dosimetry during photodynamic therapy of Barrett's esophagus with 5-aminolevulinic acid. Lasers Surg Med. 2002;31(5):299–304.
12. Lei TC, et al. Optical properties of hematoporphyrin monomethyl ether (HMME), a PDT photosensitizer. Photodiagn Photodyn Ther. 2012;9(3):232–42.
13. Helsing P, et al. Intensified fractional CO_2 laser-assisted photodynamic therapy vs. laser alone for organ transplant recipients with multiple actinic keratoses and wart-like lesions: a randomized half-side comparative trial on dorsal hands. Br J Dermatol. 2013;169(5):1087–92.
14. Morton C, et al. European dermatology forum guidelines on topical photodynamic therapy. Eur J Dermatol. 2015;25(4):296–311.
15. Nissen CV, et al. Pretreatment with 5-fluorouracil cream enhances the efficacy of daylight-mediated photodynamic therapy for actinic keratosis. Acta Derm Venereol. 2017;97(5):617–21.
16. Dirschka T, et al. Long-term (6 and 12 months) follow-up of two prospective, randomized, controlled phase III trials of photodynamic therapy with BF-200 ALA and methyl aminolaevulinate for the treatment of actinic keratosis. Br J Dermatol. 2013;168(4):825–36.
17. Tomás-Velázquez A, Redondo P. Switching from conventional photodynamic therapy to daylight photodynamic therapy for actinic keratoses: systematic review and meta-analysis. Actas Dermosifiliogr. 2017;108(4):282–92.
18. Zane C, et al. A randomized clinical trial of photodynamic therapy with methyl aminolaevulinate vs. diclofenac 3% plus hyaluronic acid gel for the treatment of multiple actinic keratoses of the face and scalp. Br J Dermatol. 2014;170(5):1143–50.
19. Basset-Seguin N, et al. Photodynamic therapy for actinic keratosis in organ transplant patients. J Eur Acad Dermatol Venereol. 2013;27(1):57–66.
20. Choi SH, Kim KH, Song KH. Efficacy of ablative fractional laser-assisted photodynamic therapy with short-incubation time for the treatment of facial and scalp actinic keratosis: 12-month follow-up results of a randomized, prospective, comparative trial. J Eur Acad Dermatol Venereol. 2015;29(8):1598–605.
21. Calzavara-Pinton P, et al. Structured expert consensus on actinic keratosis: treatment algorithm focusing on daylight PDT. J Cutan Med Surg. 2017;21(1_suppl):3S–16S.
22. Fiechter S, et al. Facial basal cell carcinomas recurring after photodynamic therapy: a retrospective analysis of histological subtypes. Dermatology. 2012;224(4):346–51.
23. Roozeboom MH, et al. Overall treatment success after treatment of primary superficial basal cell carcinoma: a systematic review and meta-analysis of randomized and nonrandomized trials. Br J Dermatol. 2012;167(4):733–56.
24. Rhodes LE, et al. Five-year follow-up of a randomized, prospective trial of topical methyl aminolevulinate photodynamic therapy vs surgery for nodular basal cell carcinoma. Arch Dermatol. 2007;143(9):1131–6.

25. Roozeboom MH, et al. Tumor thickness and adnexal extension of superficial basal cell carcinoma (sBCC) as determinants of treatment failure for methylaminolevulinate (MAL)-photodynamic therapy (PDT), imiquimod, and 5-fluorouracil (FU). J Am Acad Dermatol. 2015;73(1):93–8.
26. Christensen E, Mørk C, Foss OA. Pre-treatment deep curettage can significantly reduce tumour thickness in thick basal cell carcinoma while maintaining a favourable cosmetic outcome when used in combination with topical photodynamic therapy. J Skin Cancer. 2011;2011:240340.
27. Gerritsen MJP, et al. Pretreatment to enhance protoporphyrin IX accumulation in photodynamic therapy. Dermatology. 2009;218(3):193–202.
28. Christensen E, Mørk C, Skogvoll E. High and sustained efficacy after two sessions of topical 5-Aminolaevulinic acid photodynamic therapy for basal cell carcinoma: a prospective, clinical and histological 10-year follow-up study. Br J Dermatol. 2012;166(6):1342–8.
29. Rodríguez-Prieto MÁ, et al. Photodynamic therapy with intralesional photosensitizer and laser beam application: an alternative treatment for nodular basal cell carcinoma. J Am Acad Dermatol. 2012;67(4):e134–6.
30. Haak CS, et al. Fractional laser-mediated photodynamic therapy of high-risk basal cell carcinomas—a randomized clinical trial. Br J Dermatol. 2015;172(1):215–22.
31. Keyal U, Bhatta AK, Wang XL. Photodynamic therapy for the treatment of different severity of acne: a systematic review. Photodiagn Photodyn Ther. 2016;14:191–9.
32. Bagherani N. Efficacy of blue light in treatment of acne. Dermatol Ther. 2016;29(3):210.
33. Wan MT, Lin JY. Current evidence and applications of photodynamic therapy in dermatology. Clin Cosmet Investig Dermatol. 2014;7:145–63.
34. Boen M, et al. The role of photodynamic therapy in acne: an evidence-based review. Am J Clin Dermatol. 2017;18(3):311–21.
35. Linkner RV, et al. Evaluating the efficacy of photodynamic therapy with 20% aminolevulinic acid and microdermabrasion as a combination treatment regimen for acne scarring: a split-face, randomized, double-blind pilot study. J Clin Aesthet Dermatol. 2014;7(5):32–5.
36. Gao J, et al. Combination effect of super pulsed carbon dioxide laser and photodynamic therapy for recalcitrant facial flat warts: a preliminary study. J Cosmet Laser Ther. 2016;18(1):56–7.
37. Li Q, et al. Comparative study of photodynamic therapy with 5%, 10% and 20% aminolevulinic acid in the treatment of generalized recalcitrant facial verruca plana: a randomized clinical trial. J Eur Acad Dermatol Venereol. 2014;28(12):1821–6.
38. Ji J, et al. Comparison of 5-aminolevulinic acid photodynamic therapy and red light for treatment of photoaging. Photodiagn Photodyn Ther. 2014;11(2):118–21.
39. Sanclemente G, Mancilla GA, Hernandez G. A double-blind randomized controlled trial to assess the efficacy of daylight photodynamic therapy with methyl-aminolevulinate vs. placebo and daylight in patients with facial photodamage. Actas Dermosifiliogr. 2016;107(3):224–34.
40. Boehncke WH, Elshorst-Schmidt T, Kaufmann R. Systemic photodynamic therapy is a safe and effective treatment for psoriasis. Arch Dermatol. 2000;136(2):271–2.
41. Almutawa F, et al. Efficacy of localized phototherapy and photodynamic therapy for psoriasis: a systematic review and meta-analysis. Photodermatol Photoimmunol Photomed. 2015;31(1):5–14.
42. Choi YM, Adelzadeh L, Wu JJ. Photodynamic therapy for psoriasis. J Dermatolog Treat. 2015;26(3):202–7.
43. Karrer S, et al. Topical photodynamic therapy for localized scleroderma. Acta Derm Venereol. 2000;80(1):26–7.
44. Karrer S, et al. Keratinocyte-derived cytokines after photodynamic therapy and their paracrine induction of matrix metalloproteinases in fibroblasts. Br J Dermatol. 2004;151(4):776–83.
45. Ud-Din S, et al. Photodynamic therapy: an innovative approach to the treatment of keloid disease evaluated using subjective and objective non-invasive tools. Arch Dermatol Res. 2013;305(3):205–14.
46. Savas JA, et al. Pulsed dye laser-resistant port-wine stains: mechanisms of resistance and implications for treatment. Br J Dermatol. 2013;168(5):941–53.
47. Zhang B, et al. Comparison of pulsed dye laser (PDL) and photodynamic therapy (PDT) for treatment of facial port-wine stain (PWS) birthmarks in pediatric patients. Photodiagn Photodyn Ther. 2014;11(4):491–7.
48. Griffin LL, Lear JT. Photodynamic therapy and nonmelanoma skin cancer. Cancers. 2016;8(10):98.
49. Neittaanmäki-Perttu N, et al. Hexyl-5-aminolaevulinate 0·2% vs. methyl-5-aminolaevulinate 16% daylight photodynamic therapy for treatment of actinic keratoses: results of a randomized double-blinded pilot trial. Br J Dermatol. 2016;174(2):427–9.
50. Attili SK, et al. An open pilot study of ambulatory photodynamic therapy using a wearable low-irradiance organic light-emitting diode light source in the treatment of nonmelanoma skin cancer. Br J Dermatol. 2009;161(1):170–3.
51. Babilas P, et al. Split-face-study using two different light sources for topical PDT of actinic keratoses: non-inferiority of the LED system. J Dtsch Dermatol Ges. 2008;6(1):25–32.

Part III

Technological Advances in Wound Management

Marco Romanelli

Temporary Dressing

39

Andrea De Pascalis, Linda Tognetti, and Roberto Perotti

39.1 Background

The incidence of chronic wounds is increasing worldwide due to the phenomenon of population aging, with consequent growing costs for the healthcare systems. Moreover, the efficacy of chronic wound management is affected by the subjectivity of the healing process and the patient variability. As an example, chronic wounds have a prevalence rate of about 2% in US population and the average cost to heal a wound is $3927 [1, 2].

The healing process of a wound develops through four consequent phases: hemostasis, inflammation, proliferation, and remodeling. Dysregulation of any of these phases will cause a delay in the healing process, leading after a conventional period of 12 weeks to a chronic wound [3].

Patients with chronic wounds usually present underlying local or systemic conditions such as autoimmune diseases, diabetes, prolonged immobility, and infections that interfere with the physiological healing process [4]. The result is a wound environment very rich in cytokines that prolong the inflammatory phase, by recruiting polymorphonuclear neutrophils. The chronicity of a wound is a complex and not yet completely understood process that involve matrix metallo-proteinases (MMPs) or neutrophil-derived enzymes responsible for cellular dysfunction and host tissue damage [5, 6].

In this situation, advanced treatment strategies are essential to reduce the social and economic impact of non-healing wounds.

39.2 Classification of Wound Dressing

Currently, skin wound dressings are classified as *temporary dressings* and *permanent engineered skin substitutes* [7, 8].

The temporary ones, this chapter is about, should provide an optimal moisture control and protection from infections until wound closure, while skin substitutes are expected to integrate with the host skin and accelerate the regeneration process. However, since re-epithelization is impaired by slow vascularization, temporary dressings can include bioactive compounds, such as growth factors or antimicrobial agents for topic delivery, and for this reason they are also called "advanced dressings" [9].

A. De Pascalis (✉) · R. Perotti
Dermatology Division, Department of Medical, Surgical and Neuro-Sciences, University of Siena, Siena, Italy
e-mail: perotti@unisi.it

L. Tognetti
Dermatology Division, Department of Medical, Surgical and Neuro-Sciences, University of Siena, Siena, Italy

Department of Medical Biotechnologies, University of Siena, Siena, Italy

M. Fimiani et al. (eds.), *Technology in Practical Dermatology*,
https://doi.org/10.1007/978-3-030-45351-0_39

On the other side, *skin substitutes* are tailored in terms of porosity and biodegradability to act as better scaffolds for cell migration, adhesion, and proliferation in order to provide wound's tissue regeneration and reduce scarring [10].

The ideal wound dressing should possess the ability to remove excess exudate but maintaining a humid environment, must protect the wound with antimicrobial properties, allows oxygen exchange, thus ensuring an optimal microenvironment to accelerate the healing process, and must have easy removal from the wound site and non-anaphylactic characteristics [7].

39.3 Selection of Wound Dressing

Since there are many commercial products in the dressing market, a thorough wound assessment is critical for proper dressing selection. The first aspects of a wound to be considered are its etiology, depth, and the TIME evaluation. Then, patient systemic factors should be examined. After the first local assessment of the wound including the points repotyed in Table 39.1, a subsequent periodic reassessment is mandatory to estimate the physiological evolution of the lesion and/or response to therapy.

Table 39.1 Overview of key elements to be evaluated in a wound at first time to achieve proper dressing selection

Elements	Description
Ulcer	Size and location
Wound bed, tissue	Characteristics
Stage	Inflammatory/granulating/ re-epithelization phase
Exudate	Amount/type
Contamination	Level of bacteria and/or topical infection
Pain	Presence/absence and/or quantification
Odor	Presence/absence and/or quantification
Peri-wound and surrounding skin	Evaluation
Patient	Tolerance and/or preference of a given dressing
Feasibility	Ease of application/removal of a given dressing
Costs	Cost/availability of a given dressing

Wound etiology. The commonest wounds are traumatic lacerations and surgical incisions, which are often closed primarily and therefore usually do not require specific dressings. In comparison, chronic ulcers caused by neuropathy or pressure, or vascular insufficiency, are more complex and demand an optimal care with appropriate dressings over a prolonged period of time. Burns are a separate subset of wounds with specific management strategies.

Wound depth. The depth of wound determines the structures involved, whether that is skin alone or extends through to muscle or bone. Patient-specific factors include allergies as well as comorbidities, such as diabetes mellitus, concurrent radiotherapy, smoking status or malnutrition, and medications, such as corticosteroids, all of which delay wound healing and exacerbate the risk of infection [11].

TIME assessment. The most common wound assessment method is reassumed under the acronym TIME, i.e., Tissue, Infection, Moisture, Edges [12]. The wound bed can present different types of tissue, such as necrosis, fibrin, or slough which needs removing or granulation tissue which has to be promoted with a stimulation dressing. Infection, suggested by heat, erythema, pain, edema, or odor may require antibiotics or at least an antimicrobial dressing. Assessment and consequent management of exudates and moisture is a key point [13]. It has been known for many decades that a moist environment is highly beneficial to healing wounds, as moisture increases the rate of epithelialization. However, too moisture can lead to maceration, secondary infection, and wound breakdown. Edges of wound, at last, can be rolled, thickened, undermined or can be callused, which slows the wound's closure and have to be treated appropriately.

39.4 Type of Temporary Wound Dressing

In addition, wound dressings can be classified by type, and each type of dressing can have one or more specific functions. Here below are described the most commonly used items.

Gauzes. Cotton gauze dressings are the most simple and cheap type of wound dressing, and have been the standard of care for decades [14]. They can absorb a good amount of exudates, but drying out, they may adhere to the wound surface and cause pain upon removal. In order to improve their properties, gauzes could be impregnated with paraffin to reduce adherence or with other substances, such as iodine, to achieve antimicrobial properties (Fig. 39.1a). Low-adherent dressings are good to cover shallow open wounds, maintaining a moist environment and preventing bacterial contamination, if they contain antiseptics [11].

Transparent film dressings. Transparent film dressings are adhesive and semi-permeable dressings made of materials blended with hydrogel, like polyurethane (Fig. 39.1b) [15]. They allow water vapor passage through the dressing, but maintain a moist environment and prevent secondary infection. Because they are transparent and allow direct observation, they are often used to cover surgical sites; moreover, monitoring the wound can reduce the number of dressing changes. They have not absorptive power, so any kind of exudate will collect under the film leading to wound maceration. For this reason, they are indicated for minimally exudative wounds as a primary dressing. However, polyurethane films are very easy to apply to difficult areas, such as joints, and can be used to fix other dressings in direct contact with the wound [16].

Hydrocolloids. Hydrocolloid dressings are soft pads made by protein (e.g., pectin) and highly absorbent polysaccharides (e.g., sodium carboxymethylcellulose) that absorb exudates in order to become gelatinous (Fig. 39.1c). This makes hydrocolloid dressings low-adherent and provide a moist environment, where autolytic debridement is promoted [17]. However, the dressing cannot hold a large amount of exudate and need frequent changes to avoid maceration [18]. The properties of hydrocolloids make them useful for pressure ulcers. Indeed, various formats of dressings are available on the market, suitable for the various anatomical sites involved (e.g., sacrum, heel) [19].

Alginates. Obtained from processed seaweed, calcium alginate, calcium–sodium alginate, collagen–alginate, and gelatin–alginate are highly absorbent natural fiber dressings (Fig. 39.1d) [20]. Alginate can absorb exudates up to 20 times its weight, becoming a hydrophilic gel, and thus providing a moist wound healing environment. Calcium alginate dressings are therefore an excellent choice for moderate to highly exudative wounds [21]. Usefully, the dressing has hemostatic properties, so it is also effective in bleeding wounds. Different other alginate-based dressings were obtained in combination with antimicrobial components, like silver.

Long ribbon-type calcium alginate dressings can be useful to pack deeper wounds and sinuses, allowing effective exudate absorption. Because calcium alginate dressings are very porous and do not usually have an adhesive component, it requires a fixation and protection secondary dressing [22]. Alginate can cause a foreign-body reaction within wounds when the dressing is not fully broken down and resorbed, like when it is used on a too dry wound [23].

Hydrogels. Hydrogels are available as sheets, saturated gauze, or gels, and have a large use as wound dressings [24]. A hydrogel can be defined as a three-dimensional network of natural or synthetic hydrophilic polymers, with physical or chemical cross-linking. Hydrogels are capable of absorbing large volumes of water because of the presence of hydrophilic chains, but also to release water in a reversible manner in response to physiological stimuli [25]. The cross-linked structure provides them mechanical stability and durability at use leading to less frequent dressing changes [26]. These properties enable hydrogels to function as moist absorbent wound dressings. They can be used on dry, sloughy, or necrotic wounds to achieve a good debridement, but usually need a secondary dressing to hold it close against the wound bed. They also assist in providing a moist environment to dehydrated tissue to prevent them from desiccation (e.g., exposed tendons) and absorb exudates from wounds [27]. The physical characteristics and mechanical properties of hydrogels can be modulated by changing pH, ionic strength, and temperature of gelation.

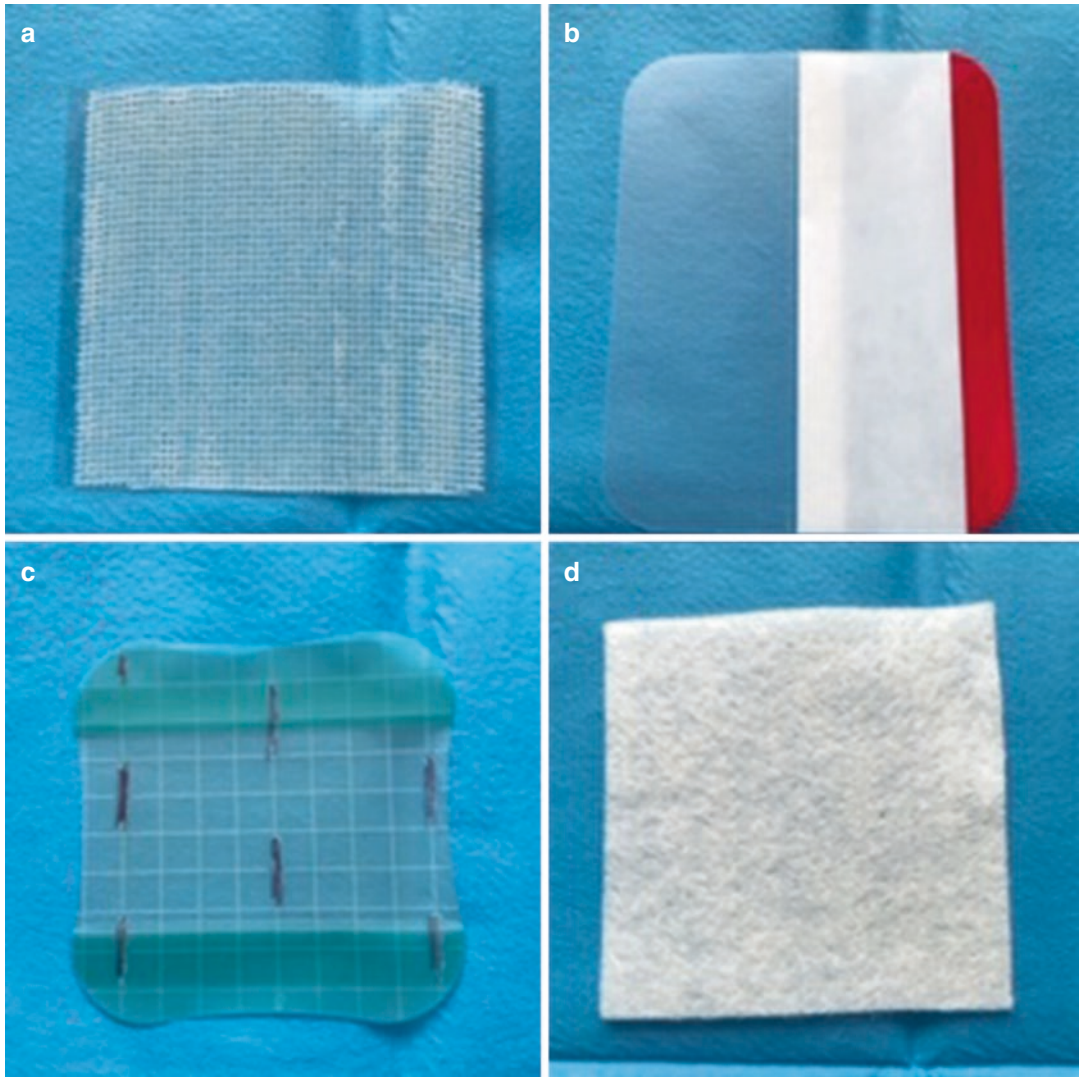

Fig. 39.1 Gauze impregnated with paraffin (**a**), transparent polyurethane film (**b**), hydrocolloid pad (**c**), and calcium alginate sheet (**d**)

Hydrogels can have also antimicrobial applications. A handful of silver-impregnated hydrogels are available on the market, like a carboxymethyl cellulose hydrogel reinforced by a non-woven fabric to obtain a hydrofiber [28].

Foams. Foam dressings have a bilaminar or multilayer structure of polyurethane sheets with hydrophilic properties. They generally have an external film of silicon which allows some humidity to escape, but prevents significant exudate outflow and protects from wound contamination. That is a category of dressing with very wide-ranging fluid-handling properties. Indeed, foams are used to absorb wound exudates, preventing excessive moisture. However, they are not recommended for heavily exudative wounds due to a lack of adherence to the wound bed [29]. Foam dressings can avoid exposure of the skin to constant pressure, so they have been recommended as a new alternative for conventional dressings to prevent pressure ulcers [30]. These dressings are useful but have a higher cost than many other dressing types (Fig. 39.2a).

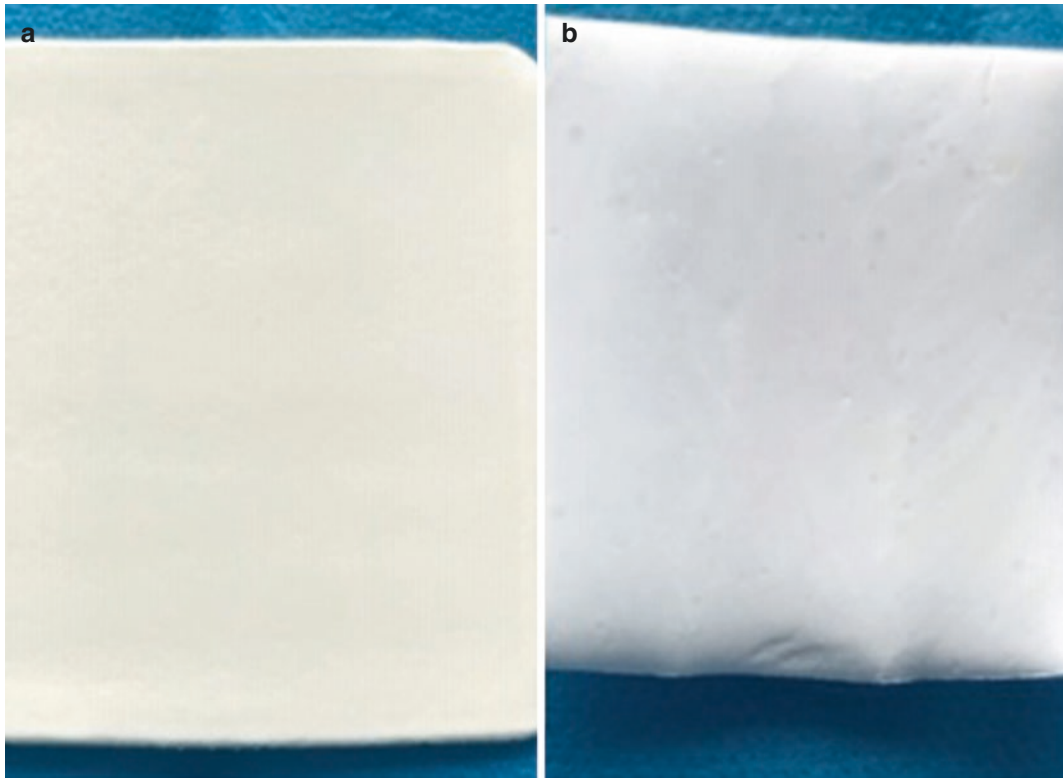

Fig. 39.2 Polyurethane foam with a silicon external layer (**a**) and collagen with hyaluronic acid pad (**b**)

Honey. The efficacy of honey, produced by honeybees (*Apis mellifera*), in treating various types of wounds, including chronic ulcers, has been known for centuries. The pharmacological activities of honey relevant for wound healing include antimicrobial, deodorizing, debriding, osmotic, anti-inflammatory, and antioxidant actions [31]. Various studies have demonstrated the antimicrobial effectiveness of honey over 60 bacteria species including aerobes and anaerobes, and some fungi, even the specific mechanism of that is not known [32]. The antimicrobial properties of honey are attributed to the cumulative action of high sugar content, acidity (low pH), hydrogen peroxide, and some phytochemicals, including flavonoids and phenolic acids [33]. Honey dressings are available in various commercial preparations such as honey gel ointment, honey-impregnated tulle dressings, honey-impregnated calcium alginate dressings, and honey-based sheet hydrogel dressings. Manuka honey is probably the most widely known honey used as a wound dressing, because of the presence of the natural antibacterial substance methylglyoxal [34]. With their natural origin, honey dressings have few contraindications. However, they should be avoided in patients with a known history of allergy to either honey or bee venom. It was also reported that patients with diabetes should monitor their blood sugar level because of the high sugar content of honey, as they may be at higher risk of hyperglycemia [35].

Collagen and hyaluronic acid. Collagen is the main protein component of the extra-cellular matrix (ECM) and the skin. It is produced by fibroblasts and stimulates the development of new tissue and finally the wound healing process. Collagen dressings are mainly made of collagen type I extracted from bovine, porcine, equine, avian, and recently also fishery, sources [36]. Collagen is widely used as wound dressings and tissue engineering products for human use, due to their hemostatic properties, excellent biocompatibility, reduced cytotoxicity, low antigenicity,

controlled biodegradability, and ability to stimulate cellular attachment and growth. In addition, collagen matrices acting as porous scaffolds for cell migration provide both structural and mechanical support and stimulate the growth of new tissue [37]. Indeed, when used as a dressing, exogenous collagen is exposed to in vivo degradation by endopeptidases, leading to products that exhibit a chemotactic effect for several cell types, essential in the wound healing process [38]. In regard to collagen immunogenicity and biocompatibility, there are some concerns on possible antigenic response due to the presence of allogenic N- and C-terminal telopeptides. Their amino acid sequences vary with the species and their removal by acid or enzymatic treatment is considered an optimal solution for immunogenicity elimination [39, 40].

Hyaluronic acid is a glycosaminoglycan distributed widely throughout connective and epithelial tissue. Hyaluronic acid-based dressings provide a temporary structure to facilitate the diffusion of nutritional supplies, help to rid the wound of metabolic waste products and control hydration during wound repair and inflammation [41]. In addition, hyaluronic acid is involved in keratinocyte migration and proliferation, which improves wound healing. However, the short residence time in vivo and high solubility are limitations for its use clinically (Fig. 39.2b) [42, 43].

Antimicrobial dressings. Chronic wounds are frequently contaminated by an important bacterial load that have a significant impact on the wound healing process. Wound colonization describes the presence of different microorganisms on the surface of a wound, but with no immune response from the host, and with no associated clinical signs and symptoms [44]. Otherwise, an infection occurs when a foreign microorganism competes with the host immune system, inciting a response in an effort to eliminate it, with consequent clinical manifestations [45]. As reported by several authors, high microbial load has severe implications in delaying wound healing and the formation of bacterial biofilms is one of the critical mediators of chronic wounds. Staphylococcus aureus, Pseudomonas aeruginosa, Streptococcus pyogenes, and some Proteus, Clostridium, and Coliform species are the most frequently involved pathogenic bacteria in chronic wound infection [46].

A number of wound dressings have antimicrobial properties relying mainly on the following three molecules: silver, iodine, and polyhexamethylene biguanide hydrochloride (PHMB).

Silver and the newer silver nanoparticles have broad-spectrum antimicrobial characteristics, even the exact mechanism of action is unknown. Various mechanisms have been proposed for silver's antibacterial action: the inhibition of bacterial cell function changing cell membrane enzyme proteins, the binding of silver to the 30S ribosomal subunit to prevent protein translation, and the denaturation of DNA by locking itself between purine and pyrimidine base pairs [47]. A certain fact is that silver needs to be in the ionized form to exhibit antibacterial activity, and therefore unionized silver metal is nonactive and only becomes active in the presence of moisture (exudate) [48]. Commercially, there are many polymer-based wound dressings, loaded with silver either in pure form, as salts or as nanoparticles for treating and/or preventing infection in various wound types (Fig. 39.3a).

Iodine is a small molecule that easily penetrates the glycocalyx of biofilms in in vivo and animal models. Aqueous and alcoholic solutions of elemental iodine have been used as disinfectants, antiseptics, or components of dressings for over 150 years. However, these iodine formulations were associated with adverse effects, including local pain, skin irritation, and orange-brown skin surface staining. An example of modern iodine formulation is a tulle-dressing with a polyethylene glycol base containing 10% povidone iodine (PVP-I) with an equivalent of 1% available iodine. These dressings slowly release iodine on contact with wound exudate providing antimicrobial killing action on the wound surface (Fig. 39.3b). Cadexomer iodine is another effective iodine wound dressing that also provides slow release of iodine to the wound surface, absorbing up to seven times its weight in exudate along with providing autolytic debridement. In comparative studies, iodine often demonstrates

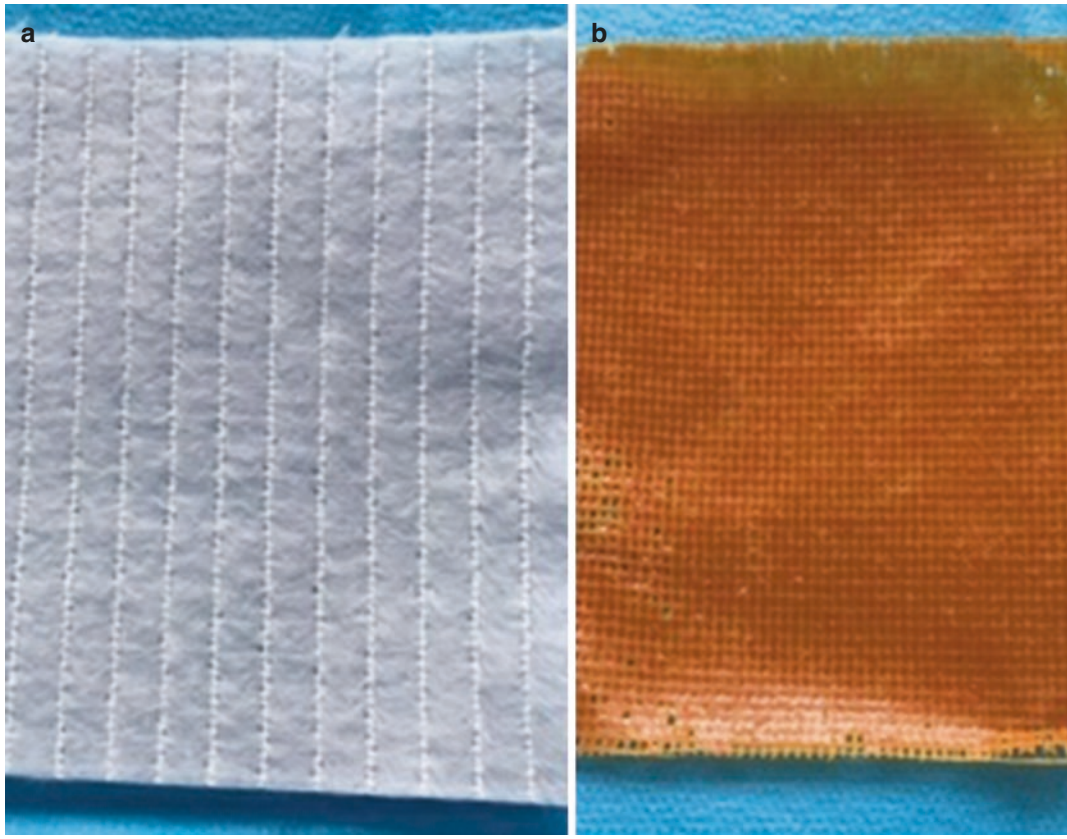

Fig. 39.3 Antimicrobial dressings: hydrofiber sheet loaded with silver (**a**) and povidone-iodine gauze (**b**)

superior biofilm eradication compared with silver, PHMB, honey, and other topical antimicrobial agents. Contact-irritant dermatitis to iodine can be a frequent adverse effect and any iodine dressing should be used with caution in the presence of thyroid disease [49].

Poly-hexamethylene biguanide hydrochloride (PHMB) is a low molecular weight polymer with structure related to chlorhexidine, historically used as a preservative in cosmetics. It is an antimicrobial agent with broad-spectrum activity against several Gram-positive and Gram-negative bacteria, fungi, and yeast and reported to be particularly active against the difficult to control Pseudomonas species. PHMB is well tolerated with no relevant adverse effects, and is available in different commercial formulations, such as solutions for wound cleansing, gels, and hydrofibers [25].

Analgesic and anti-inflammatory dressings. The wound bed is an environment very rich in inflammatory mediators, enzymes, and free radicals, which are responsible for tissue damage and patient's pain. In addition, infections and the physical trauma due to dressing changes can contribute to wound pain by triggering a continuous inflammatory response. These factors lead chronic wound patients in a cycle of inflammation and consequent pain which can be very debilitating. Therefore, the treatment of infection is as much priority as that of pain [50].

Dressings loaded with local anesthetics (e.g., lidocaine), or NSAIDs (e.g., foam with ibuprofen) can be very useful to reduce wound pain during dressing change and waiting for the response to the antimicrobial drugs, as these may take some days to have a significant effect on pain [51].

References

1. Nussbaum SR, et al. An economic evaluation of the impact, cost, and medicare policy implications of chronic nonhealing wounds. Value Health. 2018;21:27–32.
2. Fife CE, Carter MJ. Wound care outcomes and associated cost among patients treated in US outpatient wound centers: data from the US wound registry. Wounds. 2012;24:10–7.
3. Walker M, Metcalf D, Parsons D, Bowler P. A real-life clinical evaluation of a next-generation antimicrobial dressing on acute and chronic wounds. J Wound Care. 2015;24:11–22.
4. Falanga V. Classifications for wound bed preparation and stimulation of chronic wounds. Wound Repair Regen. 2000;8:347–52.
5. Nwomeh BC, Liang HX, Diegelmann RF, Cohen IK, Yager DR. Dynamics of the matrix metalloproteinases MMP-1 and MMP-8 in acute open human dermal wounds. Wound Repair Regen. 1998;6:127–34.
6. Brandner JM, Zacheja S, Houdek P, Moll I, Lobmann R. Expression of matrix metalloproteinases, cytokines, and connexins in diabetic and nondiabetic human keratinocytes before and after transplantation into an ex vivo wound-healing model. Diabetes Care. 2008;31:114–20.
7. Dhivya S, Padma VV, Santhini E. Wound dressings – a review. Biomedicine. 2015;5:22.
8. Tognetti L, et al. Current insights into skin banking: storage, preservation and clinical importance of skin allografts. J Biorepository Sci Appl Med. 2017;5:41–56.
9. Georgescu M, et al. Bioactive wound dressings for the management of chronic wounds. Curr Org Chem. 2016;21:53–63.
10. Mir M, et al. Synthetic polymeric biomaterials for wound healing: a review. Prog Biomater. 2018;7:1–21.
11. Deutsch CJ, Edwards DM, Myers S. Wound dressings. Br J Hosp Med. 2017;2005(78):C103–9.
12. Ayello EA, et al. TIME heals all wounds. Nursing. 2004;34:36–41; quiz, 41–42.
13. Winter GD. Formation of the scab and the rate of epithelization of superficial wounds in the skin of the young domestic pig. Nature. 1962;193:293–4.
14. Frykberg RG, Banks J. Challenges in the treatment of chronic wounds. Adv Wound Care. 2015;4:560–82.
15. Di Z, Shi Z, Ullah MW, Li S, Yang G. A transparent wound dressing based on bacterial cellulose whisker and poly(2-hydroxyethyl methacrylate). Int J Biol Macromol. 2017;105:638–44.
16. Arroyo AA, Casanova PL, Soriano JV, Torra I Bou JE. Open-label clinical trial comparing the clinical and economic effectiveness of using a polyurethane film surgical dressing with gauze surgical dressings in the care of post-operative surgical wounds. Int Wound J. 2015;12:285–92.
17. Cuschieri L, Debosz J, Miiller P, Celis M. Autolytic debridement of a large, necrotic, fully occluded foot ulcer using a hydrocolloid dressing in a diabetic patient. Adv Skin Wound Care. 2013;26:300–4.
18. Hilton JR, Williams DT, Beuker B, Miller DR, Harding KG. Wound dressings in diabetic foot disease. Clin Infect Dis. 2004;39(Suppl 2):S100–3.
19. Whittle H, Fletcher C, Hoskin A, Campbell K. Nursing management of pressure ulcers using a hydrogel dressing protocol: four case studies. Rehabil Nurs. 1996;21:239–42.
20. Qin Y. Alginate fibres: an overview of the production processes and applications in wound management. Polym Int. 2008;57:171–80.
21. Blaine G. Experimental observations on absorbable alginate products in surgery: gel, film, gauze and foam. Ann Surg. 1947;125:102–14.
22. Goh CH, Heng PWS, Chan LW. Alginates as a useful natural polymer for microencapsulation and therapeutic applications. Carbohydr Polym. 2012;88:1–12.
23. Barnett SE, Varley SJ. The effects of calcium alginate on wound healing. Ann R Coll Surg Engl. 1987;69:153–5.
24. Jones V, Grey JE, Harding KG. Wound dressings. BMJ. 2006;332:777–80.
25. Boateng J, Catanzano O. Advanced therapeutic dressings for effective wound healing—a review. J Pharm Sci. 2015;104:3653–80.
26. Francesko A, Petkova P, Tzanov T. Hydrogel dressings for advanced wound management. Curr Med Chem. 2019;25:5782–97.
27. Bruno W, Kerstein MD. Moist wound healing: current concepts and applications. Surg Technol Int. 1994;3:37–43.
28. Veiga AS, Schneider JP. Antimicrobial hydrogels for the treatment of infection. Biopolymers. 2013;100:637–44.
29. Dabiri G, Damstetter E, Phillips T. Choosing a wound dressing based on common wound characteristics. Adv Wound Care. 2016;5:32–41.
30. Truong B, Grigson E, Patel M, Liu X. Pressure ulcer prevention in the hospital setting using silicone foam dressings. Cureus. 2016;8:e730.
31. Cooper R. Honey for wound care in the 21st century. J Wound Care. 2016;25:544–52.
32. Schneider M, Coyle S, Warnock M, Gow I, Fyfe L. Anti-microbial activity and composition of manuka and portobello honey. Phytother Res PTR. 2013;27:1162–8.
33. Brudzynski K. Effect of hydrogen peroxide on antibacterial activities of Canadian honeys. Can J Microbiol. 2006;52:1228–37.
34. Mavric E, Wittmann S, Barth G, Henle T. Identification and quantification of methylglyoxal as the dominant antibacterial constituent of Manuka (Leptospermum scoparium) honeys from New Zealand. Mol Nutr Food Res. 2008;52:483–9.
35. Lay-flurrie K. Honey in wound care: effects, clinical application and patient benefit. Br J Nurs. 2008;17(S30):S32–6.

36. Sorushanova A, et al. The collagen suprafamily: from biosynthesis to advanced biomaterial development. Adv Mater. 2019;31:1801651.
37. Suarato G, Bertorelli R, Athanassiou A. Borrowing from nature: biopolymers and biocomposites as smart wound care materials. Front Bioeng Biotechnol. 2018;6:137.
38. Chattopadhyay S, Raines RT. Review collagen-based biomaterials for wound healing: collagen-based biomaterials. Biopolymers. 2014;101: 821–33.
39. Holmes R, Kirk S, Tronci G, Yang X, Wood D. Influence of telopeptides on the structural and physical properties of polymeric and monomeric acid-soluble type I collagen. Mater Sci Eng C. 2017;77:823–7.
40. Gaspar-Pintiliescu A, Stanciuc A-M, Craciunescu O. Natural composite dressings based on collagen, gelatin and plant bioactive compounds for wound healing: A review. Int J Biol Macromol. 2019;138:854–65.
41. Voigt J, Driver VR. Hyaluronic acid derivatives and their healing effect on burns, epithelial surgical wounds, and chronic wounds: a systematic review and meta-analysis of randomized controlled trials. Wound Repair Regen. 2012;20:317–31.
42. Longinotti C. The use of hyaluronic acid based dressings to treat burns: A review. Burns Trauma. 2014;2:162–8.
43. Zeng R, et al. Approaches to cutaneous wound healing: basics and future directions. Cell Tissue Res. 2018;374:217–32.
44. Ayton M. Wound care: wounds that won't heal. Nurs Times. 1985;81(Suppl):16–9.
45. Warriner R, Burrell R. Infection and the chronic wound: a focus on silver. Adv Skin Wound Care. 2005;18(Suppl 1):2–12.
46. Bowler PG, Duerden BI, Armstrong DG. Wound microbiology and associated approaches to wound management. Clin Microbiol Rev. 2001;14:244–69.
47. Yamanaka M, Hara K, Kudo J. Bactericidal actions of a silver ion solution on Escherichia coli, studied by energy-filtering transmission electron microscopy and proteomic analysis. Appl Environ Microbiol. 2005;71:7589–93.
48. Rai M, Yadav A, Gade A. Silver nanoparticles as a new generation of antimicrobials. Biotechnol Adv. 2009;27:76–83.
49. Sibbald RG, Elliott JA. The role of Inadine in wound care: a consensus document: Inadine consensus. Int Wound J. 2017;14:316–21.
50. White RJ. Wound infection-associated pain. J Wound Care. 2009;18:245–9.
51. Romanelli M, Dini V, Polignano R, Bonadeo P, Maggio G. Ibuprofen slow-release foam dressing reduces wound pain in painful exuding wounds: preliminary findings from an international real-life study. J Dermatol Treat. 2009;20:19–26.

Extracellular Matrices

40

Andrea Ingegneri and Marco Romanelli

40.1 Introduction

The wounded skin heals through a series of events aimed at restoring the skin barrier properties. The healing process is divided into four main phases: hemostasis, inflammation, proliferation, and remodeling. The temporal progression between these phases is regulated by an interaction between the cells, the wound micro-environment, and the development of the extracellular matrix (ECM) [1]. During hemostasis, which follows within a few hours from the wound appearance, a fibrin clot is formed to control bleeding [2] and platelets trapped in the clot release coagulation factors and cytokines. The cytokines, in the inflammatory phase, have a chemotactic action on the cells towards the wound site. The first to respond are neutrophils that release TNF alpha, IL-1 beta, and IL-6 in order to amplify the immune response and protect the body from pathogens [3]. Monocytes are recruited at the site of the clot, where they differentiate into macrophages and phagocytize pathogens and cellular debris [4, 5]. Failure of this phase of cellular recall favors the chronicity of the lesion. In fact, macrophages activate and produce a variety of chemotactic factors such as fibroblast growth factor (FGF) and vascular endothelial growth factor (VEGF). The proliferative phase is characterized by angiogenesis and by the synthesis of collagen and other extracellular proteins regulated by fibroblasts, and by a granulation tissue capable to support re-epithelization [6]. The granulation tissue matures and remodels in the following months, during which collagen density increases and the fibroblasts differentiate in myofibroblasts for the organization of the fibers and reinforce the microstructures. During the remodeling phase, the scar can become hypertrophic due to the excessive production and contraction of collagen fibers [7].

In chronic wounds, the response described above may be complicated by several factors such as prolonged inflammation, malnutrition, increased protease activity, possible superinfections, and reduction of cell activity [8]. In venous leg ulcers, the evaluation of the exudate has shown several fibroblast dysfunctions, an increase of matrix metalloproteinases (MMPs) and the activity of matrix metalloproteases inhibitors, a reduction of VEGF, and a reduction in collagen deposition [9–11]. These conditions are going to block the progression to normal ECM production. In a chronic wound, a condition is created in which the ECM stop to function normally, and therefore the normal wound healing process cannot be initiated. Thus, artificial substitutes of the dermal matrix aim to facilitate the restoration of the skin barrier by improving the wound environment and assist cell proliferation, differentiation, and engraftment.

A. Ingegneri · M. Romanelli (✉)
Department of Dermatology, University of Pisa, Pisa, Italy

M. Fimiani et al. (eds.), *Technology in Practical Dermatology*,
https://doi.org/10.1007/978-3-030-45351-0_40

40.2 Extracellular Matrix in Chronic Wounds

ECM is a dynamic structure that provides physical and functional support to the underlying tissue. It is made of water, polysaccharides, and protein components such as collagen, fibronectin, elastin, and proteoglycans [12].

In chronic wounds, the ECM is altered and therefore normal healing is prevented. This is where artificial ECMs come into play. Substituted dermal matrices may function by different mechanisms including: stimulating the production of ECM components; donating ECM components; serving as supporting structure; also promoting, via cellular signals, cell migration and proliferation, facilitating lesion healing [13, 14]. Each of these roles is influenced by the structural composition of the dermal substitute matrix [15, 16].

The artificial ECM ideal for the healing of chronic wounds would be a structure similar to the natural ECM and in addition it should have the capacity to be gradually degraded and totally integrated with the host [13].

Each component of the extracellular matrix plays a fundamental role in modulating wound healing:

- Collagen is one of the most used components in the development of dermal substitutes, mainly because, as the main component of ECM, it plays a fundamental role in every phase of correct healing. In addition, collagen has a role in cellular communication [15–17]. Each ECM collagen molecule is constituted by three polypeptide chains of glycine, proline, and hydroxyproline arranged in a helix. In the extracellular space, the chains undergo a process of proteolysis that generates a series of cross-links with support functions and elastic resistance of the skin [18]. To date, more than 27 types of collagen have been identified. Type 1 collagen, which accounts for 75–80% in dry weight of the dermis, has above all a role in the adhesion, differentiation, and migration of fibroblasts and keratinocytes [29]. In vitro studies have shown that collagen 1 promotes the proliferation of fibroblasts and decreases reactive oxygen species (ROS) and the concentration of pro-inflammatory proteases and cytokines [19, 20]. Type 3 collagen plays a key role in the production of granulation tissue [21] and subsequent scar formation [22, 23]. Type 4 collagen is the main protein of the basement membrane and therefore it has a fundamental role in keratinocyte migration and in angiogenesis [7, 24, 25]. It has been shown that inserting Type I collagen into ECM scaffolds shows the lesion in a better physiological condition for healing [20].
- Among the other important components, (I) Elastin endows the ECM with greater resistance to stress [26, 27]. (II) Fibronectin, thanks to different binding sites for collagen, fibrin, proteoglycans, and integrins, facilitates cellular interaction with the ECM [27]. Fibronectin is essential for the deposition of type 1 collagen in the extracellular matrix [28, 29]. (III) Glycosaminoglycans and proteoglycans surround all the previous components. They are strongly hydrophilic molecules and therefore provide viscoelasticity to the fabric. Together they form a gel-like substance in which ions, hormones, and nutrients can move freely through the matrix [30]. (IV) Some glycosaminoglycans such as hyaluronic acid and chondroitin-6-sulfate play a fundamental role in guiding the cell to healing and are important because they activate growth factors.

40.3 The Ideal Extracellular Matrix

The collagen used for dermal skin substitutes can be obtained using two techniques: by decellularization of a native tissue or by means of extraction. Native collagen is regarded as advantageous because it is thought to preserve a higher level structure and therefore maintain better biological activities such as neoangiogenesis, cellular chemotaxis, and the ability to revitalize senescent fibroblasts and cause the upregulation of integrins involved in angiogenesis [18, 31].

Once the dermal substitute has been applied, the patient's skin tissue can give an incorporating response or non-incorporating response (Fig. 40.1a–b). The non-incorporative response

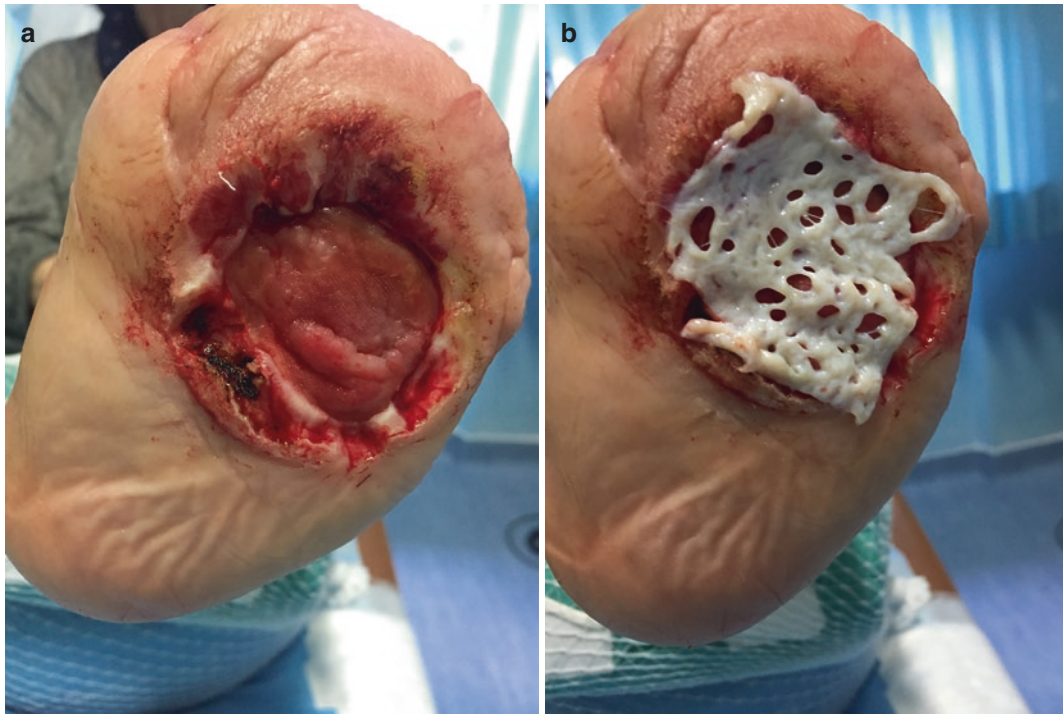

Fig. 40.1 **a–b** Amputation stump in a diabetic patient, before and after application of a dermal matrix

leads to encapsulation, and the host's fabric creates a wall around the implant. This answer is useful for permanent implants but is not ideal for healing of chronic wounds. The incorporating responses depend on how much the host's cells can penetrate the implant and the final result will depend on the inflammatory response. If the inflammation is excessive, it leads to the degradation and reabsorption of the substitute in a short time, giving rise to the deposition of disorganized tissue. On the other hand, if the inflammation is of medium intensity there will be a gradual degradation that can be equaled by the deposition of new tissue. A light inflammation causes the dermal substitute to serve as a guide to the deposition of new tissue within the original tissue [7, 15, 32].

Wound healing is a dynamic process that involves interactions between cells, ECM, and growth factors, all elements that restore the tissue after damage. ECM plays an important role in the tissue regenerative process and is the main component of the skin dermis. In addition to providing structural support to cells, some components of the ECM bind to growth factors, creating a reservoir of active molecules that can be rapidly mobilized after damage to stimulate cell proliferation and migration. In many chronic wounds, the increase in the number of inflammatory cells causes the levels of proteases to rise, which seems to be able to break down the components of the ECM, growth factors, proteins, and receptors essential for scarring. The recognition of the importance of ECM in the wound healing process has led to the development of products designed to stimulate or replace ECM (Fig. 40.2). Among these products intended to stimulate or replace the ECM are the dermal matrices.

40.4 Preparation of the Dermal Matrix

In order to use the extracellular matrix from the donor as a model for the growth of the new dermis, this tissue must first be adequately decellu-

Fig. 40.2 Partial thickness burn on lower leg with an epidermal matrix applied

larized, due to antigenicity of the donor tissue components [33]. Otherwise there is a very strong immune response to the material and a problem with the biocompatibility can occur. Dermal substitutes may be derived from different species, e.g., cattle, horses, humans (corpses and placentas), fish, and plants. The properties of these extracellular matrix scaffolds depend on their tissue of origin. Knowing their characteristics, the practitioner can decide which one to choose according to the patient's needs.

An important feature is the porosity of the matrix scaffoldings. In fact, these must have pores in their internal architecture to allow for the passage of cells without altering the mechanical stability of the scaffolding. A porosity of adequate size not only facilitates cell migration but also the proliferation of these cells within the scaffolding [34].

Another important characteristic regards the cross-links. Regardless of the origin, ECMs are composed of polymers—especially collagen fibers. The term cross-links describes the chemical link between the various chains. Cross-links have a direct effect on the degradation and durability of the product.

The matrix must be sterilized, so it must be free of any living organism. Sterility is measured in sterility assurance level (SAL), which is the probability that a product contains microorganisms after sterilization. SAL is expressed in 10^{-n}, so that a lower SAL value corresponds to a higher sterility of the scaffold. Normally SAL range is between 10^{-3} and 10^{-6}, which are considered good sterilization values [35, 36].

40.5 Extracellular Matrices Registered

Since the ECM scaffolds were first used in the treatment of chronic wounds, a wide range has been developed and marketed. Available ECM scaffolds are derived from allogeneic and xenogeneic sources, or a combination of the two, or from biosynthetic routes.

40.6 ECM Derived from Allogeneic Skin

Ideal ECMs for wound healing should be similar in structure to the tissue that is to be replaced [13]. For this purpose, allogeneic skin can result in structure and composition very similar to the recipient's skin. ECMs derived from allogeneic skin such as Alloderm®, Graftjacket®, and Dermacell® come from human cadaver skin. For a better biocompatibility and bio-efficacy (recruitment and activation of the cell population), the matrix is decellularized.

40.7 ECM Derived from Human Placenta

The amniotic membrane, a thin avascular tissue, is considered as immune-privileged thanks to the absence of HLA (human leukocyte antigen), which codes for the major histocompatibility complex associated with the immune response/rejection [37]. Though the density of matrix protein is low, one of the benefits of using amniotic membranes is that they contain a wide range of growth factors and cytokines embedded in the membrane, which are thought to highly contribute to the healing process [38]. All amniotic tissues are suitable for repairing homologous fabrics. EpiFix® Amniotic Membrane Allograft is a tissue composed of human amniotic mem-

brane and chorion. EPIFIX® is not decellularized because it does not contain viable cells, thanks to the dehydration and sterilization processes. Similarly, BIOVANCE® and AMNIOEXCELV are tissues composed of amniotic membrane and the chorion layer is removed to reduce the passage of cellular debris and to eliminate the laterality of the transplanted tissue.

40.8 ECM Derived from Xenogen Fabrics

Typically for xenotransplants, tissues are decellularized to remove or reduce the immunogenic components of animal cells, and a final sterilization step is performed to minimize the risk of foreign bodies/infectious agents. They have the same indications as allogeneic ECM: for the management of diabetic and venous ulcers, full-thickness lesions, pressure, indeterminate, traumatic, abrasion and tearing injuries, and surgical or indeterminate wounds.

PriMatrix® is an ECM derived from bovine dermis that is processed, freeze-dried (frozen dried), and sterilized. The technology used for PriMatrix® exploits decellularization and preserves the dermal and biochemical structure of the ECM. PriMatrix® is highly biocompatible due to its ability to bind and trap human cells and growth factors [39]. MatriStem® Wound Care Matrix derives from a pig bladder matrix that is lyophilized in foils and irradiated with electron rays. The MatriStem® has a matrix with the intact basal lamina on one side and a thin layer of connective tissue on the other. MatriStem® contains various types of collagen and proteins that are reabsorbed and therefore promotes tissue remodeling.

OASIS® Wound Matrix derives from the submucosa of the fasting pigs, freeze-dried and sterilized with ethylene oxide. The smooth muscle and mucosa are removed and the tissue is decellularized forming a network of collagen, proteoglycans, GAG, fibronectin, and growth factors.

Kerecis ™ Omega3 is an acellular structure derived from fish skin that contains natural components of extracellular matrix and adds the benefit of bioactive lipids such as omega 3 and polyunsaturated fatty acids. Research has shown that the effects of bioactive lipid mediators (Omega3, EPA eicosapentaenoic acid, DHA docosahexaenoic acid) reduce the inflammatory response [40].

Endoform® Dermal Template is extracted from the submucosa of the ovine stomach. After decellularization and processing of the tissue that includes delamination, Endoform® preserves 90% of the original collagen (types I, III, IV) and also 10% of laminin, fibronectin, and GAG [41]. Endoform® was shown to have a broad spectrum of MMP inhibitors for collagenesis, MMP1 MMP8, also gelatinase, MMP2 and MMP9. This feature can be useful to protect and buffer from the harmful action of MMP in chronic wounds.

40.9 Biosynthetic ECM Scaffolds

In biosynthetic cellular matrices, the composition and the consistency of the reticular structure can be controlled and designed to be stable and biodegradable. Obviously, the sterilization and decellularization processes are not needed. The matrix is absorbed in about six weeks after application and replaced by autologous cells. It acts as a scaffold for tissue reconstruction (neoderm). Any skin substitute should maintain the three-dimensional structure for a minimum of three weeks to allow for fibroblast growth, neoangiogenesis, and epithelial cell coverage. Biodegradation begins after this period and the whole process should occur without significant foreign body reaction as this could lead to increased scarring.

INTEGRA® Dermal Regeneration Template, Omnigraft® Dermal Regeneration Matrix, INTEGRA® bilayer Matrix Wound Dressing, and Matriderm® are biosynthetic dermal regeneration matrices. These dermal laminae are composed of a porous three-dimensional matrix, with bovine collagen and chondroitin-6-sulfate, with a predefined degradation time. The temporary epidermal layer consists of a thin layer of silicone which provides immediate coverage of the lesion and controls fluid loss. The silicone

layer serves as a barrier to possible infections and mimics the normal regulation of liquids (sweating). This bio-engineered dermal layer is populated with cells from the wound bed and a granulation layer is formed while the revascularization process follows two to three weeks after the matrix is applied. Then the silicone layer can be removed and a re-epithelialization strategy can be set up.

40.10 Conclusions

Increasing availability and specific ECM is one more tool for treating chronic lesions; however, the biological response is difficult to be quantified or characterized. It can be assumed that specific ECMs are better in particular conditions (high or low MMP, re-epithelialization, etc.). Future research will lead to better understanding of the mechanisms of cellular integration and stimulation of the skin.

Conflict of Interest The authors declare no conflict of interest for this chapter.

References

1. Watt FM, Fujiwara H. Cell-extracellular matrix interactions in normal and diseased skin. Cold Spring Harb Perspect Biol. 2011;1:3(4).
2. CL W, Schoneider U, Abel M, et al. Protease and pro-inflammatory cytokine concentrations are elevated in chronic compared to acute wounds and can be modulated by collagen type I in vitro. Arch Dermatol Res. 2010;302:419–28.
3. Reinke JM, Sorg H. Wound repair and regeneration. Eur Surg Res. 2012;49(1):35–43.
4. Eming S, Martin P, Tomic-Canic M. Wound repair and regeneration: mechanisms, signaling, and translation. Sci Transl Med. 2014;6:265.
5. Brett D. A review of collagen and collagen-based wound dressings. Wounds. 2008;20(12):347–56.
6. Greaves NS, Iqbal SA, Baguneid M, et al. The role of skin substitutes in the management of chronic cutaneous wounds. Wound Repair Regen. 2013;21(2):194–210.
7. Metcalfe AD, Ferguson MW. Tissue engineering of replacement skin: the crossroads of biomaterials, wound healing, embryonic development, stem cells and regeneration. JR Soc Interface. 2007;4(14):413–37.
8. Schultz GS, Mast BA. Molecular analysis of the environments of healing and chronic wounds: cytokines, proteases and growth factors. Primary Intention. 1999;7:7–15.
9. Bermudez DM, Herdrich BJ, Xu J, et al. Impaired biomechanical properties of diabetic skin. Am J Pathol. 2011;178:2215–23.
10. Cook H, Stephens P, Davies K, et al. Defective extracellular matrix reorganization by chronic wound fibroblasts is associated with alterations in TIMP-1, TIMP-2, and MMP-2 activity. J Invest Dermatol. 2000;115:225–33.
11. Lerman OZ, Galiano RD, Armour M, et al. Cellular dysfunction in the diabetic fibroblast: impairment in migration, vascular endothelial growth factor production, and response to hypoxia. Am J Pathol. 2003;162(1):303–12.
12. Alberts B, Johnson A, Lewis J, et al. Molecular biology of the cell. 4th ed. New York: Garland Science; 2002.
13. Harding K, Kirsner R, et al. International consensus; acellular matrices for the treatment of wounds. An expert working group review. London: Wounds International, 2010.
14. Zhong SP, Zhang YZ. Tissue scaffolds for skin wound healing and dermal reconstruction. Wiley Interdiscip Rev Nanomed Nanoblutechnol. 2010;2(5):510–25.
15. Cen L, Liu W, Cui L, et al. Collagen tissue engineering; development of novel biomaterials and applications. Pediatr Res. 2008;63(5):492–6.
16. Yang C, Hillai PJ, Biez JA, et al. The application of recombinant human collagen in tissue engineering. BiaDrugs. 2004;113(2):103–19.
17. Lin CQ, Bissell MI. Multi-faceted regulation of cell differentiation by extracellular matrix. EASED J. 1993;7(9):737–43.
18. Fleck CA, Simmanb R. Modern collagen wound dressings: function and purpose. I Am Col Cercil Wound Spec. 2010;2(3):50–4.
19. Schanfekier U, Abel M, Wiegand C, et al. Influence of selected wound dressings on PMN elastasae in chronic wound fluid and¯their antioxidative potential in vitro. Materials. 2005;26(33):6664–73.
20. Cullen B, Smith R, Mcculloch O, et al. Mechanism of action of PROMOGRAN, a protease modulating matrix, for the treatment of diabetic foot ulcers. Wound Repair Regen. 2002;10(1):16–25.
21. Nuutila K, Peura M, Suomela R, et al. Recombinant human collagen III gel for transplantation of autologous skin cells in porcine full-thickness wounds. J Tissue Eng Regen Med. 2015;9(12):1386–93.
22. Liu X, Wu I-I, Byrne M, et al. Type III collagen is crucial for collagen I abrillogenesis and for normal cardiovascular development. Proc Natl Acad Sci U S A. 1997;941:1852–6.
23. Volk SW, Wang Y, Mauldin EA, et al. Diminished type III collagen promotes myofibroblast differentiation and increases scar deposition in cutaneous wound healing. Cells Tissues Organs. 2011;194:25–37.

24. Gould LJ. Topical collagen-based biomaterials for chronic wounds: rationale and clinical application. Ady Wound Care. 2016;5(1):19–31.
25. Volk SW, Iqbal SA, Bayat A. Interactions of the extracellular matrix and progenitor cells in cutaneous wound healing. Adv Wound Care. 2013;2: 261–72.
26. Eckes B, Nischt R, Krieg T. Cell-matrix interactions in dermal repair and scarring. Fibrogenesis Tissue Repair. 2010;3(1):4.
27. Frantz C, Stewart KM, Weaver VM. The extracellular matrix at a glance. J Cell Sci. 2010;123(24):4195–200.
28. Sottile J, Hocking DC. Fibronectin polymerization regulates the composition and stability of extracellular matrix fibrils and cell-matrix adhesions. Mol Biol Cell. 2002;13(10):3546–59.
29. Velling T, Risteli J, Wennerberg K, et al. Polymerization of type I and III collagens is dependent on fibronectin and enhanced by integrins aubland a2B1. J Biol Chem. 2002;277(40):377–81.
30. Schultz GS, Ladwig G, Wysocki A. Extra cellular matrix: review of its roles in acute and chronic wounds. World Wide Wounds 2005.
31. Widgerow AD. Bioengineered matrices part 1: attaining structural success in biologic skin substitutes. Ann Plast Surg. 2012;68(6):568–73.
32. Babensee JE, Anderson JM, McIntire LV, et al. Host response to tissue engineered devices. Ady Drug Deliv Rev. 1998;33:111–39.
33. Yukna R, Turner D, Robinson L. Variable antigenicity of lyophilized allogeneic and lyophilized xenogeneic skin in Guinea pigs. Periodontal Res. 1977;12:197–201.
34. Loh QL, Choong C. Three-dimensional scaffolds for tissue engineering applications: role of porosity and pore size. Tissue Eng Part B Rev. 2013;19(6):485–502.
35. Gould L. Topical collagen-based biomaterials for chronic wounds: rationale and clinical application. Adv Wound Care. 2016;17:19–31.
36. Karinen A. Aging of the skin connective tissue: how to measure the biochemical and mechanical properties of aging dermis. Photodermatol Photoimmunol Photomed. 1994;10(2):47–52.
37. Fettcrolf DE, Snyder RJ. Scientific and clinical support for the use of dehydrated human amnion/chorion membrane in wound management. Wounds. 2012;10:24.
38. Koob TJ, Lim JJ, Massee M, et al. Properties of dehydrated human amnion/chorion composite grafts: implications for wound repair and soft tissue regeneration. Biomed Mater Res Appl Biomater. 2014;102(6):1353–62.
39. Cornwell KG, Landsman A, Jame R. Extracellular matrix biomaterials for soft tissue repair. Clin Podiatr Med Surg. 2009;26(4):507–23.
40. McDaniel JC, Belury M, Ahijevych K, et al. Omega-3 fatty acids effect on wound healing. Wound Repair Regen. 2008;16:337–45.
41. Floden EW, Malak SF, Basil-Jones MM, et al. Biophysical characterization of ovine forestomach extracellular matrix biomaterials. J Biomed Mater Res B Appl Biomater. 2011;96:67–75.

Skin Bank Bioproducts: The Basics

41

Linda Tognetti, Francesca Ierardi, Giancarlo Mariotti, Angela Petruzzelli, Gerarda Pompella, Michele Fimiani, Pietro Rubegni, and Elisa Pianigiani

41.1 Skin Bank Development and Organization

Autologous skin graft is the gold standard treatment for burns and other types of skin loss: however, auto-grafting is often possible in a minority of cases. To date, a tissue with the same properties of fresh viable skin has yet to be developed, either synthetic or semisynthetic, and skin grafts obtained from deceased donors (i.e., homologous skin grafts) are often the best treatment for wound coverage [1–6]. The possibility to store human skin dates back to the beginning of the twentieth century: modern skin preservation and tissue banking procedures became available in the 1930s–1940s. The first officially recognized skin bank, the US Navy Skin Bank, was set up in the USA in 1949 to meet the needs of war burned soldiers [1]. Since then, most skin banks were established in the USA in the 1950s–1960s and in Europe between the 1970s and 1990s to satisfy the growing demand for transplant tissues [1, 2]. In recent decades, following the expanding phenomenon of population aging and disease chronicization (e.g., diabetes, venous insufficiency), the number of people with hard-to-heal wounds has progressively increased. Thus, the demand for skin grafts stimulated the organization of skin banking facilities, and research into skin processing to develop new skin bank bioproducts [3–9]. The structure and the activity of tissue establishments are regulated by specific national and international laws and guidelines [5, 9]. In general, European skin bank standards refer to the Council of Europe Guidelines (EDQM) [10] and operate in accordance with European directives (2004/23/EC [11], 2006/17/EC [12], 2006/86/EC [13]), inspired by Good Manufacturing Practices (GMP) guidelines [14]. In the USA, human tissues intended for transplantation are regulated as

L. Tognetti (✉)
Dermatology Division, Department of Medical, Surgical and Neuro-Sciences, University of Siena, Siena, Italy

Department of Medical Biotechnologies, University of Siena, Siena, Italy

Skin Bank Unit, University Hospital of Siena, Siena, Italy

F. Ierardi · G. Mariotti · E. Pianigiani
Dermatology Division, Department of Medical, Surgical and Neuro-Sciences, University of Siena, Siena, Italy

Skin Bank Unit, University Hospital of Siena, Siena, Italy
e-mail: bancapelle@ao-siena.toscana.it; mariottig@unisi.it; e.pianigiani@ao-siena.toscana.it

A. Petruzzelli · G. Pompella
Skin Bank Unit, University Hospital of Siena, Siena, Italy
e-mail: a.petruzzelli@ao-siena.toscana.it; g.pompella@ao-siena.toscana.it

M. Fimiani · P. Rubegni
Dermatology Division, Department of Medical, Surgical and Neuro-Sciences, University of Siena, Siena, Italy
e-mail: michele.fimiani@unisi.it

M. Fimiani et al. (eds.), *Technology in Practical Dermatology*,
https://doi.org/10.1007/978-3-030-45351-0_41

a human tissue and tissue-based products by the Center for Biologics Evaluation and Research (CBER) [15]. Australian skin and other tissue bank products are regulated as a biological therapeutic resource by the Therapeutic Goods Administration (TGA) [16]. In European countries, donor skin is to be processed in GMP-classified areas such as Grade A with a surrounding environment of at least Grade D, according to the European directives [10]. Mainly, skin bank facilities are "contamination controlled areas" characterized by monitoring systems for particle/microbial contamination, high-efficiency particulate air filter with positive pressure and constant thermo-hygrometric parameters [9, 10, 15, 17].

41.2 Skin Bank Procedures: Donor Screening, Skin Procurement and Processing

All skin bank activities, from donor screening to skin procurement, processing, storage, and distribution, are regulated by dedicated technical guidelines [10–19]. The safety of skin grafts is guaranteed by detailed procedures and quality standards requirements [8, 16, 19]: potential skin donors are selected according to clinical history, physical examination, and serological/imaging screening tests [20–24]. Most skin banks routinely perform minimum serological panel including screening for HIV, hepatitis B and C, and syphilis; and optional testing for human T-lymphotropic virus, cytomegalovirus, ABO grouping, and Rh typing. Main exclusion criteria for skin donation are: cancer, active infections, autoimmune dermatitis, mechanical/microbial skin damage [9, 17, 19]. Skin is procured from deceased donors in appropriate facilities, under aseptic conditions, by authorized personnel with appropriate qualification, training, expertise, and experience (EDQM—Chap. 6) [10]. Generally, the procurement team is composed of medical practitioners (e.g., in Spain and Italy) or fully trained non-medical practitioners under medical responsibility (e.g., in the UK and the Netherlands) or national recovery agencies (in the USA) [15]. The procurement team can either be a specialized equipper recovering a specific tissue or a multi-tissue procurement team, with great advantage in procurement time reduction and optimal coordination [9, 10]. Skin can be harvested from heart-beating (i.e., multiple organs donation) or from non-heart-beating (i.e., multiple tissues donation) deceased donors, with different post-mortem procurement time limits: in most European countries, skin is procured within 12 hours (if the body has not been refrigerated) or 24 hours (if the body has been refrigerated in the first 6 hours after death) [10]. Skin layers of 400–800 μm in thickness are procured from the posterior trunk and the lower limbs by battery-operated/electric dermatome. The harvested skin grafts are transported to the tissue bank in specific transport containers filled with specific transport media, such as saline solution supplemented with antibiotics, RPMI, ringer lactate, Dulbecco's Modified Eagle Medium (DMEM) + Ham's F12 Nutrient mix, etc.

Procurement documentation, accompanying the procured tissues, is retained by the tissue establishments and recorded to guarantee reliable traceability. Processing procedures start then in the facility clean rooms or in dedicated areas [9, 17–22]. Processing methods are intended to maintain the integrity and biological properties of tissues and cells. Microbiological tests are performed both before and after processing on tissue samples to assess tissue microbial contamination (bacteria, fungi, yeasts, slow-growing aerobic and anaerobic bacteria). Skin allografts contaminated by critical agents (e.g., polyresistant bacteria) must be discarded [9, 19], whereas grafts contaminated by nonpathogenic agents (e.g., *Staphylococcus epidermidis, Staphylococcus capitis, and Propionibacterium acnes*) can eventually be reprocessed according to the tissue bank protocols, e.g., by glycerol-preservation or irradiation [9, 23, 24].

41.3 Skin Bank Bioproducts and Storage Methods

Tissue banks can process tissues by different methods and allow long-term storage, here reported in Table 41.1. Thus, a variety of bank bioproducts are available as wound healing therapeutic options and can be provided from tissue

Table 41.1 Overview of storage methods available in skin banks

Storage method	Description
Freezing/ deep-freezing	Storage between −15 °C and − 80 °C with cryoprotectant solutions.
Cryopreservation	Storage at <−135 °C in liquid- or vapor-phase nitrogen, with cryoprotectant solutions.
Glycerol-preservation	Storage at +2 °C/+8 °C in high-percentage glycerol solution
Drying	Tissue dried at room temperature and low humidity atmosphere
Freeze-drying (lyophilization)	Dehydration process by rapid freezing and high vacuum to remove ice By sublimation Residual Moisture in tissues: 1%–6%
Alcoholic preservation	Storage in ethanol (about 96%).
Cell culture medium preservation	Preservation in a growth medium for viable tissues and cells.
	Modified from Ref. [9]

establishments. Skin tissue provided by Siena Skin Bank are reported in Table 41.2, along with their peculiar biological characteristics and clinical properties, and shown in Fig. 41.1. The two most common methods of skin processing are deep-freezing/cryopreservation and glycerol-preservation, whereas delicate treatments such as de-cellularization, irradiation, and lyophilization are performed by a reduced number of establishments (Tables 41.1 and 41.2). The basic difference between these techniques is the preservation of tissue viability [8, 9].

41.3.1 Viable Skin Grafts

Fresh, frozen/deep-frozen, and cryopreserved cutaneous allografts maintain various degree of residual viability, according to the processing and storage temperature. They hold the ability to adhere and integrate onto the wound bed and stimulate the neo-vascularization and granulation tissue formation. In general, harvesting and processing time for cryopreservation/deep-freezing needs to be brief to ensure minimal decay of cell viability. Viable grafts are, however, more prone to microbial contamination if compared with glycerolized grafts [25]. To date, viable skin grafts include deep-frozen/cryopreserved skin (Fig. 41.1a) and DED/dermis (Fig. 41.1b, c) [5, 9].

In a recent study on 127 donors, we found that highest cell viability rates were found in grafts obtained from heart-beating nonsmoker female donors, died of cerebral hemorrhage, harvested within 2 h of aortic clamping and stored within 12 h of harvesting (13–14 h from clamping) [8]. Moreover, after 14 days of deep-freezing, epidermal and dermal structure was unaltered and cell viability was reduced of 50% on average (Fig. 41.2a, b). The debate on the importance of cell viability for skin allograft efficacy as a skin substitute is still ongoing. It is traditionally accepted that, in severe burns, viable skin allografts are superior to nonviable bioproducts and have better transplant performance, promoting neo-vascularization and immuno-modulatory response and reducing healing time and mortality risk [4, 5, 26, 27]. Beside burns, viable skin allografts represent a useful therapeutic option in chronic leg ulcers and hard-to heal wounds, where adherence onto the wound bed and cytokines release is necessary [6, 9, 28–30].

41.3.2 Unviable Skin Grafts

Glycerolized and lyophilized skin grafts are not viable but retain structural and mechanical properties so that the tissue can be grafted onto a wound bed after a certain period of time.

In particular, glycerol-preservation using an increasing series of glycerol concentrations (50–70–85%), allows long-term storage of skin or dermal grafts, at refrigerated temperature (+2/8 °C). Due to their low cell content and processing methods, these skin bioproducts have specific resistance to microbial penetration and low immunogenicity [9, 26]. Glycerol-preserved skin allografts are specifically indicated in epidermolytic disease and burns, for their efficacy in local pain control and microbiological contamination reduction [25, 29, 30]. For these reasons, some authors prefer nonviable glyc-

Table 41.2 Clinical applications of skin bank bioproducts produced in Siena Skin Bank

Deep-frozen	Glycerol-preserved	Acellular lyophilized
Skin		DED/Dermis
• Temporary coverage • Wound bed preparation • Donor area coverage	• Temporary coverage • Wound bed preparation • Pain-sparing effect • Possible engraftment in extensive burns	• Definitive dermal scaffold • Engraftment into the wound bed • Scaffold for re-epithelization • Scaffold for delayed autologous-graft (e.g., modified slow Mohs) • Bone/tendons/cartilage/nerves coverage
Use		
• Simple graft • Coverage of dermal graft (composite graft)	• Simple graft • Coverage of dermal graft (composite graft)	• Composite graft • Simple graft in selected cases of cutaneous wounds • Simple graft in all non-cutaneous loss of substances (oral/enteral/articular cavity/breast wall)
Clinical conditions		*Clinical conditions*
• 1–2nd degree burns • Epidermolytic disease (e.g., Lyell syndrome, toxic epidermal necrolysis, staphylococcal scalded skin syndrome) • Chronic vascular leg ulcers (venous/arterial/mixed)	• 1–2nd degree burns on critical/painful body sites, Lyell syndrome • Post-traumatic partial-thickness wounds. • Partial-thickness chronic vascular leg ulcers (arterial/vasculitic). • Partial-thickness pressure/diabetic ulcers.	• Dermatology/vulnology – Pocket-shaped cutaneous wounds – Irregular wound bed – Surgical dehisced wounds – Full-thickness/chemical burns – Venous/pressure/diabetic/trophic ulcers – Vasculitic full-thickness ulcers
De-epidermized dermis (DED)/dermis		• Dermo/maxillo-facial surgery – Skin cancer surgical defects (e.g., nose, scalp, mouth) – Galea defects repair o Odontostomatology – Gingival/parodontal/hard palate/oral mucosa wounds
• Dermal compartment reconstruction • Wound bed preparation	• Pain-sparing effect • Possible engraftment (in extensive burns) • Possible scaffold for re-epithelization (in extensive burns)	
Use		
• Composite graft	• Tendons/nerves coverage. • Composite graft. • Simple graft in selected cases, • Use in association with negative pressure wound therapy (i.e., protection of critical structures),	• Plastic surgery – Breast wall reconstruction – Scar treatment – Abdominal wall reconstruction • General surgery – Abdominal hernia repair – Preperitoneal hernia repair – Abdominal wall defects – Pelvic floor reconstruction • Orthopedics – Shoulder's tendons restorative surgery – Rotator cuff repairs
Clinical conditions		
• Full-thickness burns • Full-thickness post-traumatic wounds • Full-thickness surgical wounds dehiscence • Full-thickness diabetic ulcers • Full-thickness chronic venous/mixed ulcers	• Full-thickness chemical burns • Full-thickness painful post-traumatic wounds • Full-thickness pressure/diabetic ulcers • Deep chronic arterial/mixed/vasculitic ulcers	

erol-preserved allografts rather than viable deep-frozen/cryopreserved allografts, in burn patients [3, 31–33]. In particular, Kua et al. reported lower mortality and morbidity rate, reduced healing time in both adult and child burn patients treated with glycerol-preserved skin allografts, compared with cryopreserved ones [33]. Other authors assess that the preser-

Fig. 41.1 Fresh skin undergoing processing phases (**a**), deep-frozen DED meshed 1:3 (**b**), glycerol-preserved reticular dermis (**c**), and de-cellularized lyophilized DED (**d**)

vation method and cell viability of the bioproducts are not as important as the physiological barrier function they supply [3]. Actually, large-scale standardized studies comparing viable and nonviable skin allografts have not yet been performed. In our opinion, clinical outcomes largely depend on patient-related factors (both physiological and pathological) and on the surgeon's expertise in the management of these bioproducts. On the other hand, due to the difficulty in standardizing the clinical outcome in different kinds of wounds/burns, most assumptions on this topic come from direct observation and clinical experience [3, 8, 9]. Moreover, glycerolized DED/dermis (Fig. 41.1c) is successfully used in painful hard-to-heal wounds, post-surgical/post-traumatic wounds with exposure of critical structures and in chronic leg ulcers of the lower legs [6, 9, 34].

To date, lyophilization process (i.e., freeze-drying) is reserved to human-derived acellular dermal matrices, including DED (Fig. 41.1d) and reticular dermis [7, 9, 26]. These bioproducts can be de-cellularized by means of chemical and/or

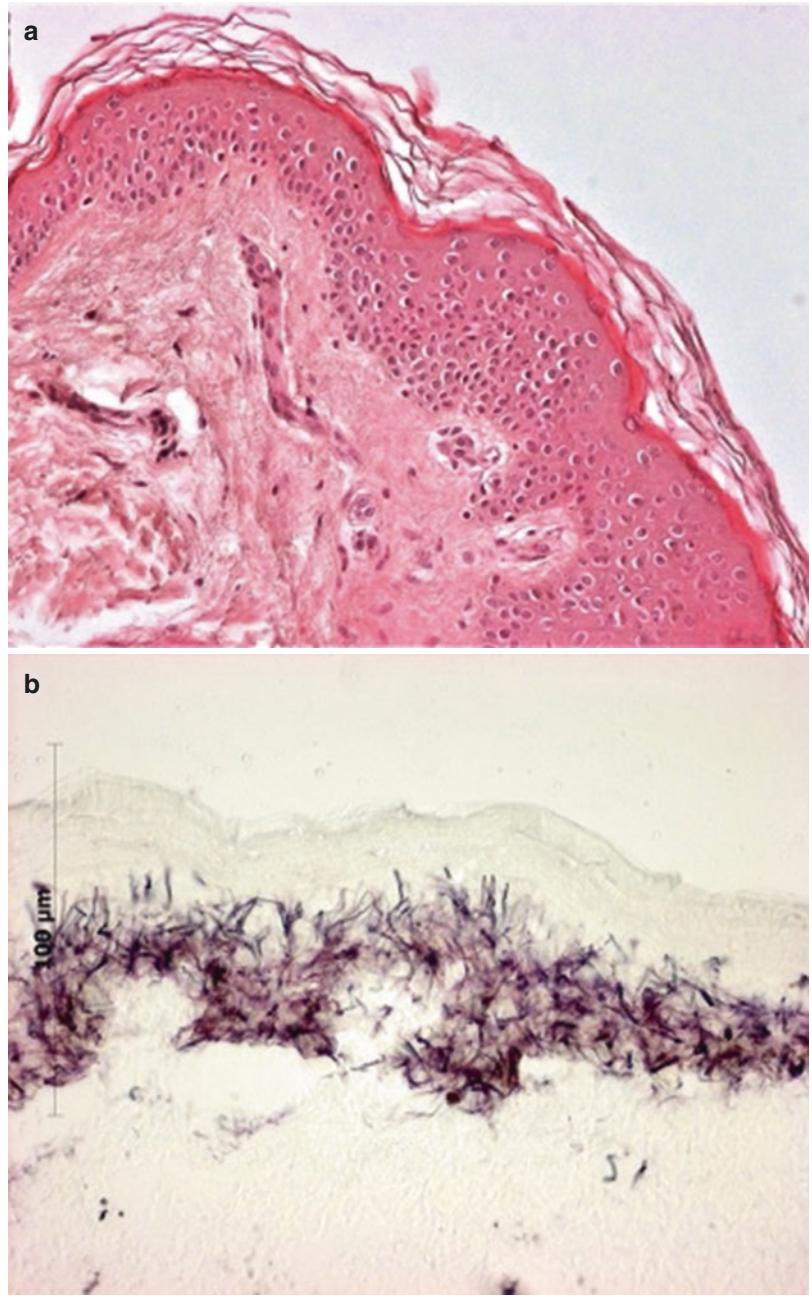

Fig. 41.2 Histological examination routinely performed as quality control on a skin allograft after 12 days of deep-freezing (−80 °C): hematoxylin-eosin 20× image showing unaltered epidermis, regular dermo-epidermal junction, and preserved dermal structures (**a**). The metabolic assay routinely performed to assess residual cell viability in deep-frozen skin allografts after 12 days of deep-freezing (−80 °C): methyl-tetrazolium salt (MTT) stains the basal and supra-basal layers of the epidermis (40× OM) (**b**)

physical processes and sterilized by γ-irradiation [9, 35]. Due to these properties, acellular dermal matrices can serve as biological scaffold (Fig. 41.3) with high compatibility for multiple purposes, including dermal compartment reconstruction, bone/tendons/nerves coverage, repair of abdominal wall defect/hernia, and oral loss of substance [9, 34, 36–40].

41.4 Skin Grafts: Classification and Techniques

Skin grafts can be classified according to their anatomical thickness or named after the surgeon who first developed the corresponding grafting technique. Indeed, specific thickness range is selected for different clinical purposes [9, 28, 39].

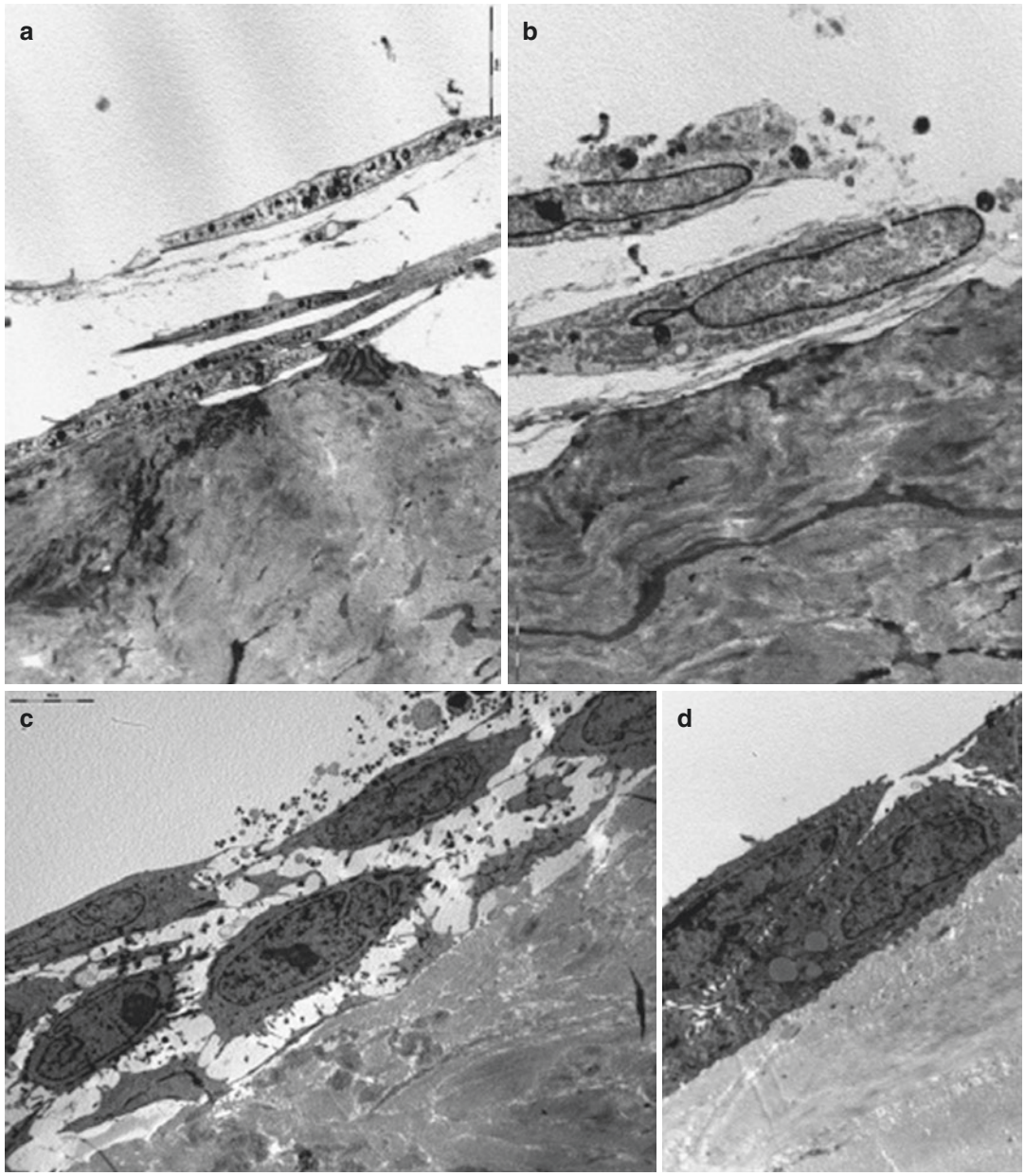

Fig. 41.3 Electron microscopy scanning of histocompatibility studies: human skin-derived primary fibroblasts stratified onto the lyophilized acellular DED surface (**a**) and detail (**b**); HaCat keratinocytes colonizing the DED surface on the basal membrane side (**c**) and detail with neo-formed tight-junctions (**d**)

In the first case, they can be divided into:

- *Partial-thickness skin grafts:* These grafts include the epidermis and part of the dermis, the effective thickness depending on the donor site and the clinical purpose. They are usually used to cover large areas as the skin graft can be expanded up to 9 times by the use of a skin graft mesher, with very low rejection rate. These grafts include the epidermis and the papillary dermis and can be classified as:

  - *thin* (Thiersch–Ollier) 0.15–0.3 mm,
  - *intermediate* (Blair–Brown) 0.3–0.45 mm.
- *Full-thickness skin grafts*: These grafts include the epidermis and the entire dermis and can be classified as:
  - *thick* (Padgett) 0.45–0.6 mm,
  - *full-thickness* grafts (Wolfe–Krause) >0.6 mm.

Grafting techniques greatly differ according to the selection of various types of bioproducts. Depending on the depth and the type of wound, different combinations can be adopted, namely a "simple" or a "composite grafts," if one or ≥ 2 bioproducts are used, including cryopreserved dermis/skin, glycerolized dermis/skin, and lyophilized gamma-irradiated dermis. Futhermore, each bioproduct can be grafted as unique or multiple layers, either meshed (with 1:3, 1:6, 1:5 expansion rate) [9] or unmeshed. Meshed graft can cover a larger body surface, and can be applied directly onto the wound bed or in a multi-layer composite graft (i.e., sandwich or Alexander technique) [9]: they are particularly indicated for burns or when auto-grafting is necessary [6, 9, 28, 39].

References

1. McCauley RL. The skin bank. Total burn care. 1st ed. Philadelphia, PA: Saunders; 1996. p. 159–63.
2. Mericka P. Brief history of the tissue bank, Charles University Hospital, Hradec Kralove, Czech Republic. Cell Tissue Bank. 2000;1(1):17–25.
3. Hermans MHE. Preservation methods of allografts and their (lack of) influence on clinical results in partial thickness burns. Burns. 2011;37(5):873–81.
4. De SK, Reis ED, Kerstein MD. Wound treatment with human skin equivalent. J Am Podiatr Med Assoc. 2002;92(1):19–23.
5. Kearney JN. Guidelines on processing and clinical use of skin allografts. Clin Dermatol. 2005;23(4):357–64.
6. Fimiani M, Pianigiani E, Di Simplicio FC, et al. Other uses of homologous skin grafts and skin bank bioproducts. Clin Dermatol. 2005;23(4):396–402.
7. Pianigiani E, Tognetti L, Ierardi F, et al. Il derma acellulare liofilizzato. Hi-Tech Dermo. 2016;3:17–20.
8. Pianigiani E, Tognetti L, Ierardi F, et al. Assessment of cryopreserved donor skin viability: the experience of the regional tissue bank of Siena. Cell Tissue Bank. 2016;17(2):241–53.
9. Tognetti L, Pianigiani E, Ierardi F, et al. Current insights into skin banking: storage, preservation and clinical importance of skin allografts. J Biorepos Sci Appl Med. 2017;5:1–16.
10. European Directorate for the Quality of Medicines & Health Care (EDQM). Guide to the quality and safety of tissues and cells for human application. Conseil of Europe, Strasbourg (France); 2017. 3rd ed.
11. Official Journal of the European Union. *Directive 2004/23/EC of the European Parliament and Council on quality and safety standards for the donation, procurement, testing, processing, preservation, storage and distribution of human tissues and cells*. Official Journal of the European Union; 2004. Available from: http://eur-lex.europa.eu/Lex-UriServ/LexUriServ.do?uri=OJ:L:2004:102:0048:0058:en:PDF. Accessed June 5, 2017.
12. Commission Directive 2006/17/EC implementing Directive 2004/23/EC of the European Parliament and of the Council as regards certain technical requirements for the donation, procurement and testing of human tissues and cells. Available from: http://eur-lex.europa.eu/legalcontent/EN/TXT/?uri=celex%3A32006L0017. Accessed June 5, 2017.
13. Commission Directive 2006/86/EC implementing Directive 2004/23/EC of the European Parliament and of the Council as regards traceability requirements, notification of serious adverse reactions and events and certain technical requirements for the coding, processing, preservation, storage and distribution of human tissues and cells. Available from: http://eur-lex.europa.eu/legal-content/EN/TXT/?uri=celex%3A32006L0086. Accessed June 5, 2017.
14. European Commission [Homepage on the Internet]. EudraLex—Volume 4—Good Manufacturing Practice (GMP) guidelines; 2010 [updated December, 2010]. Available at: https://ec.europa.eu/health/documents/eudralex/vol-4_en. Accessed June 29, 2017.
15. Center for Biologics Evaluation and Research—CBER. HCT/P's Regulated under 21 CFR 1271.3(d)(1) and Section 361 of the PHS Act.
16. Wright C, Velickovic Z, Brown R, et al. Raising the standard: changes to the Australian Code of Good Manufacturing Practice (CGMP) for human blood and blood components, human tissues and human cellular therapy products. Pathology. 2014 Apr;46(3):177–83.
17. Kagan RJ, Robb EC, Plessinger RT. Human skin banking. Clin Lab Med. 2005;25(3):587–605.
18. Pianigiani E, Ierardi F, Cherubini F, et al. Skin bank organization. Clin Dermatol. 2005;23(4):353–6.
19. Pianigiani E, Ierardi F, Fimiani M. Importance of good manufacturing practices in microbiological monitoring in processing human tissues for transplant. Cell Tissue Bank. 2013;14(4):601–7.
20. Gaucher S, Elie C, Verola O, Jarraya M. Viability of cryopreserved human skin allografts: effects of transport media and cryoprotectants. Cell Tissue Bank. 2012;13(1):147–55.

21. Linee guida per il prelievo, la processazione e la distribuzione dei tessuti a scopo di trapianto—Centro Nazionale per i Trapianti (CNT); 2015. Available from: http://www.trapianti.salute.gov.it. Accessed January 2, 2017.
22. Vicentino M, Rodriguez G, Saldias M, Alvarez I. Guidelines to implement quality management systems in microbiology laboratories for tissue banking. Transplant Proc. 2009;41(8):3481–4.
23. Pianigiani E, Ierardi F, Cuciti C, Brignali S, Oggioni M, Fimiani M. Processing efficacy in relation to microbial contamination of skin allografts from 723 donors. Burns. 2010;36(3):347–51.
24. Pianigiani E, Risulo M, Ierardi F, et al. Prevalence of skin allograft discards as a result of serological and molecular microbiological screening in a regional skin bank in Italy. Burns. 2006;32(3):348–51.
25. Saegeman VS, Ectors NL, Lismont D, Verduyckt B, Verhaegen J. Short- and long-term bacterial inhibiting effect of high concentrations of glycerol used in the preservation of skin allografts. Burns. 2008;34(2):205–11.
26. Gaucher S, Jarraya M. Cryopreserved human skin allografts: efficacy and viability. Burns. 2014;40(3):526–7.
27. Cleland H, Wasiak J, Dobson H, et al. Clinical application and viability of cryopreserved cadaveric skin allografts in severe burns: a retrospective analysis. Burns. 2014;40(1):61–6.
28. Pianigiani E, Taddeucci P, Mancini S, Miracco C. Wound healing in leg ulcers treated by combined skin allograft and autograft. J Invest Dermatol. 2001;117:544.
29. Towler MA, Rush EW, Richardson MK, Williams CL. Randomized, prospective, blinded-enrollment, head-to-head venous leg ulcer healing trial comparing living, bioengineered skin graft substitute (Apligraf) with living, cryopreserved, human skin allograft (TheraSkin). Clin Podiatr Med Surg. 2018;35(3):357–65.
30. Mosti G, Mattaliano V, Picerni P, et al. Skin grafting in the treatment of hard-to-heal leg ulcers. Italian Journal of Wound Care. 2018;2(1):1–7.
31. Khoo TL, Halim AS, Mat Saad AZ, Dorai AA. The application of glycerol-preserved skin allograft in the treatment of burn injuries: an analysis based on indications. Burns. 2010;36(8):97–904.
32. Leon-Villapalos J, Eldardiri M, Dziewulski P. The use of human deceased donor skin allografts in burn care. Cell Tissue Bank. 2010;11(1):99–104.
33. Kua EH, Goh CQ, Ting Y, Chua A, Song C. Comparing the use of glycerol preserved and cryopreserved allogenic skin for the treatment of severe burns: differences in clinical outcomes and *in vitro* tissue viability. Cell Tissue Bank. 2012;13(2):269–79.
34. Ferrando PM, Balmativola B, Cambieri I, et al. Glycerolized reticular dermis as a new human acellular dermal matrix: an exploratory study. PLOS One. 2016;11(2):e0149124.
35. Rooney P, Eagle M, Hogg P, et al. Sterilisation of skin allograft with gamma irradiation. Burns. 2008;34(5):664–73.
36. Jansen LA, De Caigny P, Guay NA, et al. The evidence base for the acellular dermal matrix AlloDerm: a systematic review. Ann Plast Surg. 2013;70(5):587–94.
37. Lattari V, Jones LM, Varcelotti JR, et al. The use of a permanent dermal allograft in full-thickness burns of the hand and foot: a report of three cases. J Burn Care Rehabil. 1997;18:147–55.
38. Moerman E, Middelkoop E, Mackie D, et al. The temporary use of allograft for complicated wounds in plastic surgery. Burns. 2002;28:S13–5.
39. Cuono CB, Langdon R, Birchall N, et al. Composite autologous allogeneic skin replacement: development and clinical application. Plast Reconstr Surg. 1987;80(4):626–37.
40. Pianigiani E, Ierardi F, Mazzanti B, et al. Human deepidermized dermis as a stem cell carrier. Transplant Proc. 2010;42:2244–6.

42 Clinical Applications of Skin Bank Bioproducts

Linda Tognetti, Ernesto DePiano, Roberto Perotti, Chiara Cencetti, Claudia Panzano, Federico Zerini, Gianmarco De Donato, Giancarlo Palasciano, Paolo Gennaro, Guido Lorenzini, Luca Griamldi, Elisa Pianigiani, and Pietro Rubegni

42.1 Clinical Advantages of Skin Bank Bioproducts in Wound Healing

The gold standard for permanent wound closure is autologous grafting [1–3]. However, autologous skin transplantation is possible only in a limited number of cases. In frequent situations, allogenic skin grafting can be considered the best, in burned patients, and/or the most physiological alternative in other types of skin loss, especially in hard-to-heal wounds [4, 5].

General advantages of grafts and dressings realized with allogeneic skin (i.e., from deceased donor skin) include: reduction of water, electrolytes and protein loss, antibacterial effect, wound pain control, wound bed preparation for definitive closure, and promotion of re-epithelization [6–8]. Furthermore, dermal allografts can serve as scaffolds and protect delicate deep structures such as cartilage, tendons, bones and nerves or arterial bypass. Specific advantages are provided by diverse types of skin bank bioproducts in wounds of different nature (post-traumatic, vasculitic, pressure, etc.) [6–15, 21]. Within the specific advantages of decellularized dermal grafts, we can include: dermal compartment reconstruction, antalgic and antimicrobial effect, stimulation of tissue neovascularization, physiological regeneration of a neo-collagen rather than a scarring tissue,

L. Tognetti (✉)
Dermatology Division, Department of Medical, Surgical and Neuro-Sciences, University of Siena, Siena, Italy

Department of Medical Biotechnologies, University of Siena, Siena, Italy

Skin Bank Unit, University Hospital of Siena, Siena, Italy

E. DePiano · R. Perotti · C. Cencetti · P. Rubegni
Dermatology Division, Department of Medical, Surgical and Neuro-Sciences, University of Siena, Siena, Italy
e-mail: perotti@unisi.it; c.cencetti2@student.unisi.it

C. Panzano · G. De Donato · G. Palasciano
Department of Surgery, Vascular and Endovascular Surgery Unit, University of Siena, Siena, Italy
e-mail: claudia.panzano@student.unisi.it; gianmarco.dedonato@unisi.it; giancarlo.palasciano@unisi.it

F. Zerini · P. Gennaro
Maxillo-facial Surgery Division, Department of Medical, Surgical and Neuro-Sciences, University of Siena, Siena, Italy
e-mail: paolo.gennaro@unisi.it

G. Lorenzini
Department of Dentistry and Ophthalmology, University of Siena, Siena, Italy
e-mail: guido.lorenzini@unisi.it

L. Griamldi
Plastic and Reconstructive Surgery Unit, Department of Medicine, Surgery and Neuroscience, University of Siena, Siena, Italy
e-mail: luca.grimaldi@unisi.it

E. Pianigiani
Skin Bank Unit, University Hospital of Siena, Siena, Italy
e-mail: e.pianigiani@ao-siena.toscana.it

M. Fimiani et al. (eds.), *Technology in Practical Dermatology*,
https://doi.org/10.1007/978-3-030-45351-0_42

and good aesthetic results [14–16]. On the other hand, the use of these bioproducts can be limited due to the reduced availability of donor skin and long recovery times of patients [17].

In recent years, the use of skin bank bioproducts took advantage in the treatment of hard-to-heal wounds (HHWs), i.e., where restoration of anatomical and functional integrity is fundamental and takes longer than expected with standard therapy or in chronic wounds [4, 5, 14, 15, 21]. Taken together, HHWs and chronic ulcers represent a major concern for the current health care system in terms of impact on the quality of life of patients and on overall costs [1–5].

42.2 Clinical Use of Skin Bank Bioproducts in Wound Healing

Different grafting techniques are based on the selection of various types of bioproducts [14]. In general, thick grafts are indicated to cover deeper skin loss; depending on the depth and the type of wounds, different combinations of grafts can be adopted, including: deep-frozen dermis/skin, glycerolized dermis/skin, lyophilized gamma-irradiated dermis. Each bioproduct can be used as mono- or multi-layered and meshed (with various expansion rate) or unmeshed. Finally, epithelialization can be achieved by second intention or by the use of thin autografts or cultured autologous epidermal cells [14, 18].

In extensive burn patients, if autologous skin is not available, meshed allografts can be used to cover large areas involving ≥50% of the total body surface area (TBSA), with different expansion rates [14, 18, 19].

The series of homologous skin grafts available in tissue establishments includes deep-frozen skin, glycerolized skin, deep-frozen and cryopreserved DED (de-epidermized dermis)/dermis, glycerolized DED/dermis, and gamma-irradiated lyophilized dermis/DED. In cap. 3 they are reported along with their specific clinical indications [14].

General clinical indications of these bioproducts can be synthetized as follows:

(a) *Monolayer skin allografts* (cryopreserved, deep-frozen, or glycerolized) are indicated for the temporary coverage of large superficial wounds where autologous graft is not available (e.g., epidermolysis bullosa, toxic epidermal necrolysis).
(b) *Monolayer dermal allografts* (DED/dermis) are preferred in HHWs>8 cm, with regular or irregular wound bed depth and edges. In general, glycerolized dermal allografts are preferred to reduce local pain, whereas deep-frozen/cryopreserved dermal allografts are preferred when greater adherence to the wound bed is required to achieve a viable granulation tissue. In selected cases of full-thickness irregular HHW, one or two layers of meshed dermal grafts can be stratified to fill the cutaneous loss of substance.
(c) *Composite grafts* (Cryopreserved/deep-frozen/glycerolized dermis + cryopreserved/deep-frozen/glycerolized skin) are indicated in HHWs of different etiology. In large wounds (>20 cm), with irregular borders and characterized by significant exudation, composite grafts should be preferred. Meshed dermal grafts can be applied if the exudation is intense (Falanga score 3) [20]; unmeshed dermal grafts are used if the exudate is poor or moderate (Falanga score 1–2). All dermal grafts must be covered with deep-frozen/cryopreserved/glycerolized skin grafts in order to prevent dermis desiccation [14, 21].
(d) *Acellular lyophilized DED/dermis* is preferred in post-surgical dehiscences, pocket-shaped cutaneous wounds, oral wounds, breast wall/abdominal wall/pelvic floor reconstruction, shoulder tendons restoration, bone coverage, etc. (cap. 3) [14].

42.3 A 3-Step Approach to Hard-to-Heal Wounds

To prevent wound chronicization a dedicated medical-surgical approach is often required, based on an integrated 3-step protocol [21]. The approach considers three consecutive phases: debridement, wound bed preparation, and skin grafting (Fig. 42.1).

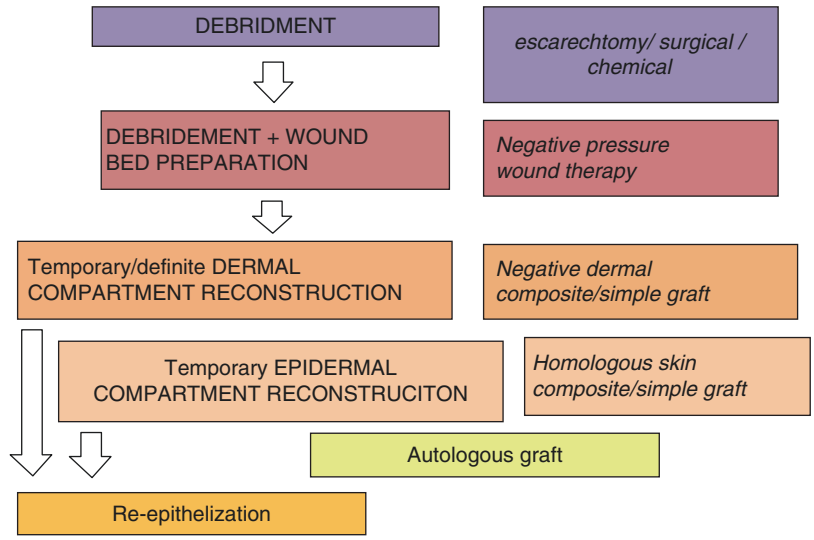

Fig. 42.1 Schematic representation of the 3-step approach based on allograft use proposed for hard-to heal wounds

The first step, wound debridement, can be carried out by mechanical (e.g., surgical knife) or enzymatical procedure (e.g., topical collagenase ointment), the choice depending on wound conditions at the time of presentation. Thick eschars (i.e., in late presentation) should be removed surgically under local anesthesia.

In extensive and deep/critical HHWs, debridement and wound bed preparation can be contemporarily achieved by means of Negative Pressure Wound Therapy (NPWT): this method helps remove adherent fibrin clots and contract wound edges, stimulates a vital granulation tissue production, and reduces microbacterial burden.

After adequate debridement and wound bed preparation, the wound should be evaluated for skin grafting procedure: simple/composite grafts, meshed/non-meshed grafts, cryopreserved/deep-frozen/glycero-preserved/lyophilized grafts, sandwich technique/Cuono technique [19], according to the entity and characteristics of the loss of substance, patient-related factors, and body location [6, 8, 14, 15]. The choice between monolayer (e.g., one layer of dermal graft) and composite graft (dermal graft covered by skin allografts to avoid desiccation) depends mainly on the wound extension: limited HHWs (diameter < 7 cm, loss of substance limited to the deep dermis) are treated with simple grafts, while extensive HHWs (diameter > 7 cm, loss of substance extended to deep subcutaneous structures with/without nerves/tendons/bone exposure) require composite grafts.

The application of the 3-step approach, together with the specific characteristics of each of the bioproducts, allows the achievement of an adequate therapy of full-thickness/critical skin loss (vascular ulcers, burns, chemical burns, and post-traumatic wounds). In particular, dermal acellular grafts maintain their morpho-structural characteristics for up to four weeks, protect deep exposed fragile structures, control local pain and are quickly colonized by the host cells [14, 18]. These conditions ensure the engraftment of the dermal scaffold into the wound bed and allow a consistent reduction of healing and hospitalization time [8, 13, 14].

42.4 Homologous Skin/Dermal Grafts for Cutaneous HHWs

Simple/monolayer skin grafts are applied directly onto the wound bed after reshaping the skin following the edges of the wound: a 0,5 cm overlap on the wound margin is recommended to ensure the stability of the graft. Simple DED/dermis grafts should be shaped according to wound margins and inserted into the wound bed avoiding overlap: this dressing is limited to selected limited

Fig. 42.2 Chronic leg venous ulcer of a 72-year-old female: after debridement (**a**), first grafting with deep-frozen thin skin allografts (**b**) and coverage with adsorbing Ag dressing (**c**), 1 month closure (**d**), 2 months closure (**e**)

HHW cases, and coverage is realized by means of two layers of paraffin gauzes (silver sheet dressing can be adjunct to reduce exudate) (Fig. 42.2). Composite grafts are composed by a bi-layer dressing consisting of a dermal graft covered by a skin graft to avoid dermis desiccation (Fig. 42.3). In cutaneous HHWs, allografts should be covered by paraffin gauze and overlying povidone iodine gauze: the dressing is completed by a moderately compressive cotton bandage. The dressing should be re-evaluated after 5 to 7 days [9, 12]. Acellular dermal grafts should be monitored and re-shaped if necessary, until engraftment is realized. Skin graft of simple and composite dressing can be maintained in site for 10 to 18 days. In burns, due to local immunosuppression, skin grafts can take for 6/8 weeks and can be partially engrafted onto the wound bed (Fig. 42.4). The skin is usually removed once the site has been sufficiently healed, or when an autologous graft is available for permanent wound coverage [14, 15]. Other uses of skin/dermal allografts include the reconstruction of donor sites (e.g., forearm/thigh/axilla/retroauricular area) for partial- or full-thickness autograft, respectively [21].

42.5 Homologous Skin/Dermal Grafts for HHWs of the Head

We currently employ skin bank bioproducts in post-surgical defects following cancer excision of the head and neck areas [13, 21]. Patients are eligible in three conditions: (1) impossibility to realize a flap for peculiar body location/damaged surrounding skin (i.e., sun-damage, photoaging, in situ SCC)/patient-related factors (Fig. 42.5); (2) impossibility to perform a full-thickness autologous graft due to the wound site or patient co-morbidities; (3) necessity to perform a delayed Mohs and temporarily close the open wound waiting for histological documentation of "free from tumoral cells" wound margins. For epithelial tumors of the head and neck, the process remains the same as the general indications for the use of bioproducts, and the choice of type of skin/dermal graft depends on the condition of the wound bed and its extension. The outcome is decisive as far as healing of the wound itself is concerned and beneficial both for pain and infection control [13, 16, 22].

Fig. 42.3 Heat burn of 2–3 degree in a 85-year-old man: after baseline (1 week after burning) (**a**), after topical debridement with collagenase (**b**), grafting of deep-frozen skin meshed 1:3 (**c**), engraftment and final closure after 35 days (**d**)

Fig. 42.4 Application of different type of allografts in a post-traumatic HHW of the leg: non-meshed thick glycerol-preserved grafts are used to protect an arterial bypass; multiple meshed thick glycerol-preserved dermal grafts are placed onto the wound bed (dermal compartment reconstruction) and around the external metallic fixator insertion onto the bone (pain-sparing function), multiple non-meshed glycerol-preserved skins are used to cover the dermal grafts and control local exudation/pain

Acellular lyophilized DED has established itself as the best bioproduct for oral cavity injuries. In the oral cavity, gingiva/hard palate/soft palate/tongue mucosa and lips, lyophilized dermis/DED must be anchored to the wound bed with adsorbable sutures. Thanks to its acellularity, the use of lyophilized dermis/DED can provide important results in wounds otherwise recovering by second intention, with advantages in reducing the healing time and local pain. The use of the acellular lyophilized dermis/DED in oral surgery guarantees an optimal healing of the wounds, almost completely eliminating the problems related to the post-operative course as the reduction of pain and a quicker recovery of oral functions [22, 23].

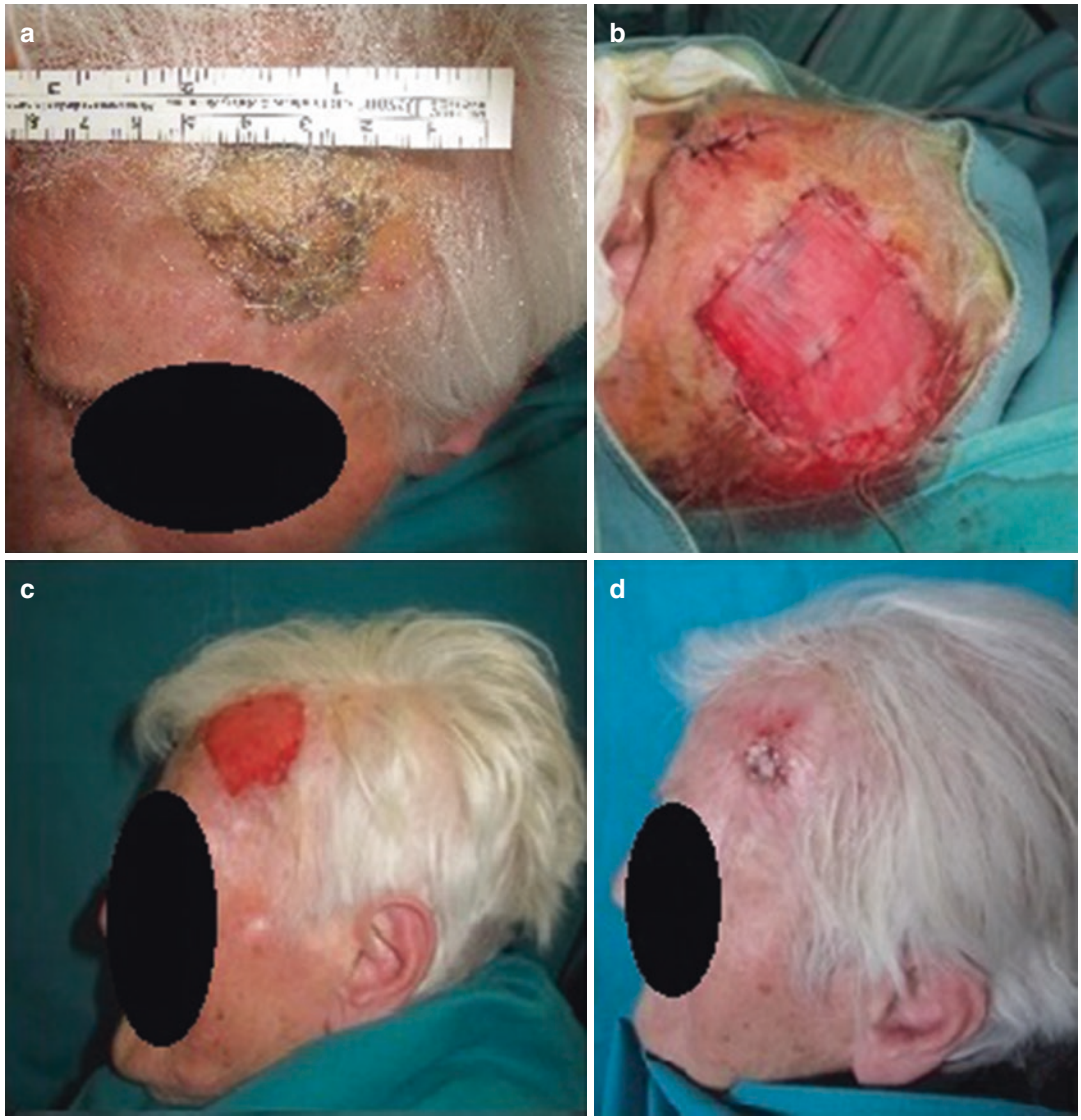

Fig. 42.5 Post-surgical defect repair in a 95-year-old female: a large pigmented basal cell carcinoma of the front infiltrating the subcutaneous tissue (**a**); surgical excision and coverage by lyophilized acellular dermal sheets, fixed with re-adsorbable stitches and deep-frozen skin grafts for 14 days (**b**); engraftment of the lyophilized acellular dermal graft at 2 weeks control (**c**); wound closure at 3.5 months (**d**)

References

1. Sorg H, Tilkorn DJ, Hager S, Hauser J, Mirastschijski U. Skin wound healing: an update on the current knowledge and concepts. Eur Surg Res. 2017;58(1–2):81–94.
2. Frykberg RG, Banks J. Challenges in the Treatment of Chronic Wounds. Adv Wound Care (New Rochelle). 1 settembre 2015;4(9):560–82.
3. Chronic Wound Healing: A Review of Current Management and Treatments.—PubMed—NCBI [Internet]. [citato 5 novembre 2018].
4. Jung K, Covington S, Sen CK, et al. Rapid identification of slow healing wounds. Wound Rep Reg. 2016;24:181–8.
5. Capoano R, Businaro R, Tesori MC, et al. Wounds difficult to heal: an effective treatment strategy. Curr Vasc Pharmacol. 2017;15(6):582–8.
6. Kearney JN. Guidelines on processing and clinical use of skin allografts. Clin Dermatol. agosto 2005;23(4):357–364.
7. Human tissue intended for transplantation—FDA. Interim rule; opportunity for public comment. Fed Regist. 14 dicembre 1993;58(238):65514–21.

8. De SK, Reis ED, Kerstein MD. Wound treatment with human skin equivalent. J Am Podiatr Med Assoc gennaio. 2002;92(1):19–23.
9. Mosti G, Magliaro A, Mattaliano V, Picerni P, Angelotti N. Comparative study of two antimicrobial dressings in infected leg ulcers: a pilot study. J Wound Care marzo 2015;24(3):121–2; 124–7.
10. Lattari V, Jones LM, Varcelotti JR, Latenser BA, Sherman HF, Barrette RR. The use of a permanent dermal allograft in full-thickness burns of the hand and foot: a report of three cases. J Burn Care Rehabil. aprile 1997;18(2):147–55.
11. Debels H, Hamdi M, Abberton K, Morrison W. Dermal matrices and bioengineered skin substitutes: a critical review of current options. Plast Reconstr Surg Glob Open. gennaio 2015;3(1):e284.
12. Towler MA, Rush EW, Richardson MK, Williams CL. Randomized, prospective, blinded-enrollment, head-to-head venous leg ulcer healing trial comparing living, bioengineered skin graft substitute (Apligraf) with living, cryopreserved, human skin allograft (TheraSkin). Clin Podiatr Med Surg luglio. 2018;35(3):357–65.
13. Park JY, Lee TG, Kim JY, Lee MC, Chung YK, Lee WJ. Acellular dermal matrix to treat full thickness skin defects: follow-up subjective and objective skin quality assessments. Arch Craniofac Surg aprile. 2014;15(1):14–21.
14. Tognetti L, Pianigiani E, Ierardi F, et al. Current insights into skin banking: storage, preservation and clinical importance of skin allografts. Journal of Biorepository Science for Applied Medicine 2017:51–16, On line 28.6.2017.
15. Fimiani M, Pianigiani E, Di Simplicio FC, et al. Other uses of homologous skin grafts and skin bank bioproducts. Clin Dermatol agosto. 2005;23(4):396–402.
16. Pianigiani E, Tognetti L, Ierardi F, et al. Il derma acellulare liofilizzato. Hi-Tech Dermo. 2016;3:17–20.
17. Pianigiani E, Tognetti L, Ierardi F, et al. Assessment of cryopreserved donor skin viability: the experience of the regional tissue bank of Siena. Cell Tissue Bank. 2016;17(2):241–53.
18. Fang T, Lineaweaver WC, Sailes FC, et al. Clinical application of cultured epithelial autografts on acellular dermal matrices in the treatment of extended burn injuries. Ann Plast Surg. 2014;73(5):509–15.
19. Cuono CB, Langdon R, Birchall N, et al. Composite autologous-allogenic skin replacement: development and clinical application. Plast Reconstr Surg. 1987;80(4):626–37.
20. Falanga V, Saap LJ, Ozonoff A. Wound bed score and its correlation with healing of chronic wounds. Dermatol Ther dicembre 2006;19(6):383–390.
21. Rowe NM, Morris L, Delacure MD. Acellular dermal composite allografts for reconstruction of the radial forearm donor site. Ann Plast Surg. 2006;57(3):305–11.
22. Germani RM, Vivero R, Herzallah IR, Casiano RR. Endoscopic reconstruction of large anterior skull base defects using acellular dermal allograft. Am J Rhinol. 2007t;21(5):615–8.
23. Rhee PH, Friedman CD, Ridge JA, Kusiak J. The use of processed allograft dermal matrix for intraoral resurfacing: an alternative to split-thickness skin grafts. Arch Otolaryngol Head Neck Surg. 1998;124(11):1201–4.

Negative Pressure Wound Therapy

43

Giulia Davini and Marco Romanelli

43.1 History of Negative Pressure Wound Therapy

For clinical use of NPWT, we need to go back to about thousands of years ago, when it was first used in Chinese medicine in addition to acupuncture techniques. In 1841, Junod, to "stimulate circulation," adopted the method of heated cups that were applied directly to the patient's skin. It was observed that with the cooling of the air, a subatmospheric pressure was created inside the cups, which caused hyperemia [1].

This discovery represented a real source of inspiration for the researchers who later undertook numerous studies in this regard. In particular, we remember the actual authors of NPWT Michael Morykwas and Louis Argenta. They designed a series of animal studies, using NPWT with a polyurethane foam dressing, which served as an interface between the wound surface and the vacuum source [2]. So the foam proved to be the fundamental tool of the system, as it guaranteed a uniform distribution of pressure over the entire surface of the wound. In addition, the volume of the foam is reduced by pressure and causes the stretching of the cells, the contraction of the wound, and the elimination of fluids. Since then, numerous variants of NPWT have been registered [1]. In 1993, Fleischmann applied topical negative pressure to wounds via a long-term foam dressing to promote granulation and tissue repair in 15 patients with open fractures [3]. He was able to observe an efficient wound cleansing without bone infections (although one of the patients suffered a soft tissue infection). In his first studies, the negative pressure inside the wound was obtained through a simple suction unit mural or with portable vacuum cleaners for surgery. However, these devices have led to practical problems in terms of achieving, controlling, and maintaining the desired levels of negative pressure. At a distance of a century and more from the first description of the cellular world, great progress has been made in understanding the cellular and molecular mechanisms responsible for the healing of wounds. In carrying out this research, numerous factors have emerged that cause difficult healing of wounds such as the lack of local and systemic growth factors, changes in the extracellular matrix, decreased functionality of fibroblasts, and reduced antimicrobial activity of leukocytes. These aspects have attracted considerable interest from the researchers, who later studied new specific products, which act in a targeted way, based on the wound bed, ensuring the greatest possible benefit [4].

Products of this kind such as hydrocolloids, hydrogels, alginates, and polyurethane foams are used in fact in dressings, which today are

G. Davini · M. Romanelli (✉)
Department of Dermatology, University of Pisa, Pisa, Italy

M. Fimiani et al. (eds.), *Technology in Practical Dermatology*,
https://doi.org/10.1007/978-3-030-45351-0_43

called "advanced." Instead, we must wait until the end of the 1990s for NPWT, which I will mention in my thesis.

43.2 Description of the Device and Mechanism of Action

The acronym "VAC" literally means "vacuum assisted closure," which consists of an advanced and non-invasive system, composed of several elements that work mechanically in order to promote the healing of a wound or injury. The fundamental characteristic of this device is the application of the negative topical pressure, i.e., a pressure lower than the atmospheric pressure, normally present at ambient temperature above sea level, where the molecules exert a force that corresponds exactly to the pressure of 760 mmHg. The therapeutic system [4] is provided with a black, hydrophobic, open pores polyurethane (PU) foam dressing which is introduced into the lesion. Alternatively, a hydrophilic polyvinyl alcohol foam can be used, with more dense and smaller pores (the choice of foam type depends on the wound characteristics and treatment objectives). To isolate this dressing, a semi-occlusive and transparent adhesive film is used, which adheres to the healthy skin around the lesion. To this film a small hole is made, in which a small tube is inserted and anchored by an adhesive disk (pad). The tube is connected to a suction system, which ends in a container (canister). It collects the exudate drained through the foam and thanks to the negative pressure, which is generated by an electrically powered therapeutic unit [4]: through a rotary valve, it continuously transfers the gaseous molecules from the input to the output of the device. The negative pressure, in fact, is obtained by removing the gaseous molecules from the affected area (for example the wound site), using a suction pump. Within this electric therapeutic unit there is a microprocessor, which has the function of capturing any pressure changes and transmitting the alarm through the "central." This equipment is provided with an interface and control module (for operations of "input and output" of the data), a parameters already set, and a "touch" display.

The polyurethane foam is placed in the wound and, after activating of NPWT (125 mmHg), it contracts. Reducing its volume and still maintaining the porosity under suction, the foam provides a uniform pressure on the entire bed of the lesion. This involves the elimination of edema from the perilesional tissues, the increase in blood flow, and the stimulation of the angiogenesis. The contraction of the foam draws close and stabilizes the wound margins, thus providing an anchor point for the muscles and the deeper structures. With the application of NPWT, the exudate, inhibitory substances, and small residues are removed from the lesion, providing a suitable environment for healing.

The environment of the lesion [5] is a microcosm that develops between an area of the body before the skin barrier and the medication adhered to it. Cell regeneration, particularly in a second intention healing, occurs according to a process called "frog leap," i.e., the dermal cells migrate from the edges and the bottom of the lesion towards the center. To fill the empty space, due to the lack of tissue, the new cells glide on each other.

In the dry environment the epithelium migrates slowly between the dried dermis and the subcutaneous adipose tissue, separating the intermediate tissues; while in the wet one the migration occurs between the right amount of exudate and the dermis. This result was obtained thanks to the "Moist Wound Healing" theory elaborated in 1962 by George Winter [6, 7]; following a study that highlighted the reparative principles previously described, he stated that: "…covering a wound with a film impermeable to water vapor has profoundly changed the pattern of healing, directing the migration of the epidermis on the wound rather than through the dermis, accelerating epidermal regeneration."

43.3 Physiopathological Effects

In its simplest form, the TNP system offers a sophisticated, sterile and airtight dressing, whose properties create a moist healing environment. Other effects are [4]:

- increase in local blood flow
- reduction of edema

- stimulation of granulation tissue
- stimulation of cell proliferation
- elimination of soluble healing inhibitors from the wound
- reduction of bacterial load
- rapprochement of wound edges

Some factors [5] have a considerable influence on the evolution of a wound or injury:

- the nutritional status of the person (vitamin C plays an important role in the synthesis of collagen).
- the presence of metabolic diseases (i.e., diabetes) slows down the healing process.
- circulatory deficits related to venous stasis or atherosclerosis cause an inadequate blood supply.
- different diseases inhibit repair.

In order to talk concretely about the NPWT system, it is essential to expose the results that it provides at the tissue level. This type of dressing is characterized by a hermetic seal obtained by the film and by the tube connected to the suction device; this allows you to create a moist environment conducive to healing. In particular, treatment with NPWT therapy provides important physiopathological effects.

43.4 Clinical Evidence on NPWT

Morykwas et al. [2] studied the effect of NPWT therapy on local blood flow by inducing deep wounds on pig tissues and then medicating them with polyurethane foam. The results obtained indicate that with a negative pressure of 125 mmHg the blood supply is quadrupled. With higher pressures, there is a risk that the capillaries deform and the blood flow decreases. In fact, with the application of negative pressures of 400 mmHg or more, the spraying was inhibited. Timmers et al. [8] examined the effect of TNP therapy on the spraying of healthy skin of ten voluntary subjects. They evaluated the TNP based on the medication used. It emerged that a negative pressure up to 300 mmHg with polyurethane foam increases also of five times the blood circulation, while with foam in polyvinyl alcohol the increase is tripled. The difference in the results of the research carried out is due to the smaller pore size of the polyvinyl foam, which attenuates the effect of the NPWT. Various other factors influence the level of pressure reached in the wound bed: it will be reduced for example into case of clot formation, hemorrhage, and interposed dressing layers.

Another pathophysiological effect of NPWT is the stimulation of granulation tissue formation. By conducting other studies on pigs, it was found not only that comparing the standard medications with NPWT [9], the latter obtains a better outcome, but also that comparing a continuous and intermittent treatment with NPWT, the second responds more effectively [4]. It is important to point out that the optimal result is achieved by applying a continuous pressure to the first 48 hours and then proceeding with the intermittent pressure for any type of dressing. In particular in the wounds that produce abundant exudate, a continuous pressure will be applied because it allows to keep the dressing well sealed and cleansed. This result is due to the fact that the continuous pressure incessantly stimulates the cells, which in a sense, adapt to the forces and no longer react.

Some clinicians recommend using the continuous setting for the first 48 hours of therapy while maintaining a pressure of 125 mmHg before switching to intermittent mode [10].

Mechanical stress induces proliferation and cell division [11]. For many years, plastic and orthopedic surgeons have used this effect in order to expand soft tissue and stretch the bones [12]. This is also one of the most important features of NPWT therapy; a computer model showed that the negative pressure induces micro-deformations in the tissues inside the wound, and this has also been observed in the clinical context. This mechanical stretching of the cells stimulates proliferation and accelerates wound healing. In chronic wounds, this mechanism stimulates angiogenesis and epithelization [13].

Fabian et al. also observed an angiogenesis improvement and a tendency to increase the epithelialization rate with the TPN used in an experimental model on rabbits [14]. TPN promotes an

active healing state by eliminating harmful components (such as cytokines and matrix metalloproteinases) associated with excess exudate in no-healing wounds [13, 15, 16].

Therapy can also contribute to the reduction of bacterial load. The hermetic closure formed by foam and film, for example, reduces the risk of contamination from the outside, while the improvement of blood supply can increase the resistance to infection.

Regarding the wound infection, it has always been considered a contraindication to negative pressure therapy.

However, the evidence suggests that NPWT may play a role in reducing the bacterial load within the wound and reducing the levels of exotoxins and endotoxins potentially harmful thanks to the simple and rapid removal of the exudate from the wound. Being the NPWT mechanism a closed system, the unpleasant odors and bacterial contamination also decrease during dressing change [4].

Negative pressure therapy has been shown to be an effective adjuvant method for the treatment of postoperative wound infection after a median sternotomy [17, 18].

Mehbod et al. reported similar positive outcomes for infected spinal surgical wounds, even in the presence of implanted material [19], and Dosluoglu et al. obtained encouraging results using the NPWT combined with debridement to manage the infected vascular prostheses [20]. Schimp et al. also reported advantages obtained with NPWT in the management of complex surgical wounds in the field of oncology and gynecology [21]. However, these are unusually complicated wounds, which are not one of the main indications of TNP.

For any wound in which it is difficult to manage the exudate, NPWT should be considered as a therapeutic option along with other treatments. The NPWT system has been considered, for example, as an effective method to protect the skin from the effluents that escape from a fistula, although this does not come within the range of uses provided by the manufacturer [22, 23].

When applied correctly, NPWT also has the advantage of avoiding the flow of the exudate into the wound and consequently the increase in bacterial load and the accumulation of fluid rich in potentially harmful proteases in the deep cavities of the wound. The accumulation of fluid and the spread of sepsis are a major problem in cavitary wounds, and this may explain the validity of NPWT in the management of minor amputations of the diabetic foot or pressure ulcers.

A final physiopathological effect is represented by the partial vacuum created by NPWT, which causes the contraction of the foam and the consequent rapprochement of the wound margins towards the center, facilitating its closure [4].

This therapy, used after careful wound assessment and appropriately used, is a valuable tool because its mechanisms have a substantial impact on many of the factors that contribute to healing.

43.5 Indications and Contraindications

The use of NPWT is indicated in many types of acute and chronic wounds and can benefit many patients both for the treatment of symptoms and for wound healing. NPWT can be considered when the wound:

- does not progress towards healing on schedule, for example when the contraction of wound margins occurs too slowly with standard care.
- produces an excessive amount of exudate, difficult to treat.
- it is localized in a discomforting point or it has a dimension that makes an adequate sealing with traditional dressings problematic.
- requires a reduction in size before proceeding with a surgical closure [4, 9].

The use of NPWT is also indicated in cases where the patient requires a dressing or treatment firmly positioned on the lesion and does not require frequent changes, for example in cases of injury in children, for which close changes of the

dressing can be traumatic or the dressings may not remain firm in their place [24, 25]. Moreover, in the case of certain types of wounds, or in the presence of skin grafts, the NPWT has a splinting effect (rigid support) [26, 27].

Many successes of NPWT are reported in the literature, but there are situations in which the wrong choice or inappropriated application of NPWT can result in poor clinical outcomes or adverse events. Therefore, to avoid the safe and effective use of this technique, contraindications have been listed as:

- osteomyelitis.
- neoplastic lesions as it can stimulate the proliferation of neoplastic cells.
- non-enteric fistulas not explored as there may be communication with vulnerable underlying organs.
- vessels, nerves, anastomoses, or exposed organs as if applied directly to exposed structures, due to the force of the negative pressure, the NPWT can cause injury or break vessels.
- necrotic tissue with the presence of eschar or thick slough in the wound bed, since before the application it is necessary to perform a proper debridement obtaining more rapid results [28].
- We have also listed some precautions on which it is necessary to pay attention as:
- delicate blood vessels since direct negative pressure can cause a trauma to the vessel and bleeding.
- delicate structures exposed, in fact patients with exposed blood vessels, bands, tendons, or ligaments can cause bleeding and trauma.
- bleeding: wounds with active bleeding or for whom the patient is at high risk of bleeding, or is receiving anticoagulant therapy and/or platelet aggregation inhibitors, negative pressure therapy may cause bleeding due to increase of local perfusion, and consequently the loss of blood would be greater.
- patients with enteric fistulae.
- patients requiring special therapies or treatments such as magnetic resonance and hyperbaric therapy [28] (Table 43.1).

Table 43.1 Indications and contraindications for NPWT

Indications	Contraindications
• Those who have been deemed a candidate for adjunctive therapies, see "determining candidacy for adjunctive therapies"	• Presence of necrotic and fibrotic tissue
	• Untreated osteomyelitis
	• Malignant wounds
• Wound types:	• Localized ischemia
– Diabetic foot ulcers (IB)	• High output, non-enteric and unexplored fistulas
– Pressure injuries	
– Surgical wounds	• In the absence of appropriate blood supply
– Grafts and flaps	• Severe excoriation of periwound
– Traumatic wounds	• Do not place dressings in direct contact with exposed blood vessels, anastomotic sites, organs or nerves
– Partial-thickness burns	
– Pilonidal sinus wounds	
– Necrotizing fasciitis	• Do not place dressings into blind/unexplored tunnels
• To accelerate the formation of granulation tissue	• Stop therapy if person experiences autonomic dysreflexia
• To improve perfusion through removal of excess interstitial fluid	• Do not place therapy in proximity to the vagus nerve
• To reduce bacterial colonization	• Do not over fill the wound with dressing material
• To enhance epithelial migration	

43.6 Portable NPWT Systems

Smaller disposable NPWT devices are developed in order to manage it not only in the hospital, but also in community care.

Awad and Butcher [29] used a portable NPWT device (SNaP® device Spiracur) in a patient with diabetic foot ulceration with an extensive re-ulceration overlying a previous amputation.

The patient was able to maintain self-care and to keep working during the last stages of the management. The results showed the absence of infection, the improvement of peri-wound skin health, and the reduction of wound size.

The SNaP® system uses spring mechanism to generate consistent levels of pressure to achieve pre-determined levels of subatmospheric pressure (−75 mmHg, −100 mmHg, and −125 mmHg) [30] at the wound interface. The system is silent, light, disposable, portable, and easy to manage and it can be used in moderately exuding wounds (less than 120 mls/week).

PICO® (Smith and Nephew Healthcare) is another lightweight portable, negative pressure system that produces negative pressure at −80 mmHg continuously through two AA batteries providing power to the device. The system can be used for wounds that produce few exudate.

(up to 300mls per week) and may be managed with gauze or foam fillers. Because of the absence of canister, fluids are absorbed and moved to the top surface of the dressing, where the moisture vapor is then evaporated through the film. The device is easy to use but has limitations about wound size and wounds on flat body surfaces as the dressing cannot be cut or modified.

Prevena™ Incision Management System (KCI) is a NPWT device that is used on surgical incisions in order to drain until the comple closures. Prevena™ is intended to be applied immediately post-surgery to clean closed incisions for a minimum of 2 days and up to a maximum of 7 days. It should be noted that due to low amounts of silver contained in the dressing the device is unsuitable for people with a silver sensitivity [31].

43.7 Conclusions

Used in conjunction with conventional therapies and after a careful wound assessment, NPWT is a valuable tool for both the doctor and the patient.

NPWT should be considered as an important component of the overall management of a wound, to be chosen on the basis of a strategy comprising defined objectives and outcomes [32]. It should be interrupted when these objectives have not been achieved, if the treatment does not have the desired effects and if it is not tolerated by the patient and it causes complications.

Conflict of Interest The authors declare no conflict of interest for this chapter.

References

1. Banwell P, Téot L. Topical negative pressure (TNP) therapy. First international topical negative pressure (TNP) therapy focus group meeting proceedings. London: TXP Communications; 2004.
2. Morykwas MJ, Argenta LC, Shelton-Brown EI, et al. Vacuum-assisted closure: a new method for wound control and treatment: animal studies and basic foundation. Ann Plast Surg. 1997;38(6):553–62.
3. Fleischmann W, Strecker W, Bombelli M, et al. Vacuum sealing as treatment of soft tissue damage in open fractures. Unfallchirurg. 1993;96(9):488–92.
4. European Wound Management Association (EWMA). Position Document: Negative pressure wound therapy for the management of chronic wounds. London: MEP Ltd, 2007.
5. Regione Emilia Romagna, Commissione Regionale dei Dispositivi Medici: Le medicazioni avanzate per il trattamento delle ferite acute e croniche. Delibera Regionale n. 1523/2008. 2010.
6. Winter G. Formation of scab and rate of epithelialization of superficial wound in the skin of the young domestic pig. Nature, 1962.
7. Jones J. Winter's concept of moist wound healing: a review of the evidence and impact on clinical practice. J Wound Care. 2005 Jun;14(6):273–6.
8. Timmers MS, Le Cessie S, Banwell P, et al. The effects of varying degrees of pressure delivered by negative-pressure wound therapy on skin perfusion. Ann Plast Surg 2005; 55(6): 665–671; discussion 1097-98.
9. European Wound Management Association (EWMA). Position Document: Hard-to-heal wounds: a holistic approach. London: MEP Ltd, 2008.
10. Vowden K. Conservative management of pressure ulcers. In: Banwell PE, Harding K (eds.), *Vacuum Assisted Closure TM Therapy: Science and Practice*. London: MEP Ltd, 2006. 12.
11. Sumpio BE, Banes AJ, Link WG, et al. Enhanced collagen production by smooth muscle cells during repetitive mechanical stretching. Arch Surg. 1988;123(10):1233–6.
12. Ilizarov GA. Clinical application of the tension-stress effect for limb lengthening. Clin Orthop Relat Res. 1990;250:8–26.

13. Greene AK, Puder M, Roy R, et al. Microdeformational wound therapy: effects on angiogenesis and matrix metalloproteinases in chronic wounds of 3 debilitated patients. Ann Plast Surg. 2006;56(4):418–22.
14. Fabian TS, Kaufman HJ, Lett ED, et al. The evaluation of subatmospheric pressure and hyperbaric oxygen in ischemic full-thickness wound healing. Am Surg. 2000;66(12):1136–43.
15. Gustafsson RI, Sjögren J, Ingemansson R. Deep sternal wound infection: a sternal-sparing technique with vacuum-assisted closure therapy. Ann Thorac Surg 2003; 76(6): 2048–2053; discussion 2053.
16. Stechmiller JK, Kilapadi DV, Childress B, et al. Effect of vacuum-assisted closure therapy on the expression of cytokines and proteases in wound fluid of adults with pressure ulcers (letter to editor). Wound Rep Regen. 2006;14:371–4.
17. Sjögren J, Gustafsson R, Nilsson J, et al. Clinical outcome after poststernotomy mediastinitis: vacuum-assisted closure versus conventional therapy. Ann Thorac Surg. 2005;79(6):2049–55.
18. Cowan KN, Teague L, Sue SC, et al. Vacuum-assisted wound closure of deep sternal infections in high-risk patients after cardiac surgery. Ann Thorac Surg. 2005;80(6):2205–12.
19. Mehbod AA, Ogilvie JW, Pinto MR, et al. Postoperative deep wound infections in adults after spinal fusion: management with vacuum-assisted wound closure. J Spinal Disord Tech. 2005;18(1):14–7.
20. Dosluoglu HH, Schimpf DK, Schultz R, et al. Preservation of infected and exposed vascular grafts using vacuum assisted closure without muscle flap coverage. J Vasc Surg. 2005;42(5):989–92.
21. Schimp VL, Worley C, Brunello S, et al. Vacuum-assisted closure in the treatment of gynecologic oncology wound failures. Gynecol Oncol. 2004;92(2):586–91.
22. Cro C, George KJ, Donnelly J, et al. Vacuum assisted closure system in the management of enterocutaneous fistulae. Postgrad Med J. 2002;78:364–5.
23. Goverman J, Yelon JA, Platz JJ, et al. The 'fistula VAC,' a technique for management of enterocutaneous fistulae arising within the open abdomen: report of 5 cases. J Trauma 2006; 60(2): 428–431; discussion 431.
24. McCord SS, Naik-Mathuria BJ, Murphy KM, et al. Negative pressure therapy is effective to manage a variety of wounds in infants and children. Wound Repair Regen. 2007;15(3):296–301.
25. Chariker ME, Gerstle TL, Morrison CS. An algorithmic approach to the use of gauzebased negative-pressure wound therapy as a bridge to closure in pediatric extremity trauma. Plast Reconstr Surg. 2009;123(5):1510–20.
26. World Union of Wound Healing Societies (WUWHS). Principles of best practice: Vacuum assisted closure: recommendations for use. A consensus document. London: MEP Ltd, 2008.
27. Llanos S, Danilla S, Barraza C, et al. Effectiveness of negative pressure closure in the integration of split thickness skin grafts: a randomized, double-masked, controlled trial. Ann Surg. 2006;244(5):700–5.
28. Henderson V, Timmons J, Hurd T, Deroo K, Maloney S, Sabo S. NPWT in everyday practice Made Easy. Wounds International 2010; 1(5).
29. Awad T, Butcher M (2012) Managing diabetic foot ulceration with a new, highly portable NPWT device. Wounds International 3(2): 40–41.
30. Chen SZ, Li J, Li XY, et al. Effects of vacuum-assisted closure on wound microcirculation: an experimental study. Asian J Surg 2005; 28:211–17.
31. Ousey KJ, PhD, MA, PGDE, BA, RN, reader, School of Human and Health Sciences, Centre for Health and Social Care Research, University of Huddersfield, Queensgate, Huddersfield, West Yorkshire, United Kingdom.
32. EWMA Document: Negative Pressure Wound Therapy. Overview, challenges and perspectives. 2017.

44 Tissue-Engineered Skin Substitutes

Janowska Agata and Romanelli Marco

44.1 Introduction

Normal skin regenerates epidermis injury by stem cells present in basal layer of epidermis [1]. In case of severe deep injury, self-renewal ability is limited and a surgical intervention is needed. Split-thickness grafts are the standard permanent surgical treatment in case of deep wounds or burns; however, skin grafts can be utilized only in small areas of damaged skin. Autografts can be associated with surgical complications such as infections, scarring, and poor esthetic outcomes [2]. In large skin injuries, allografts are a suitable option but can be rejected due to the graft immunogenicity [3].

Skin substitutes were introduced as an effective therapy to reduce skin grafts complications. Bioengineered skin substitutes are advanced medical devices, developed by a cooperation of a multidisciplinary scientists and physician teams [4]. Tissue engineering was described firstly in 1993 and genetically modified substitutes were introduced in 2005 [5, 6]. The aim for appropriate skin substitute is to heal or regenerate the wound maintaining the function and structure of normal skin. Skin equivalents should meet some essential criteria: protective function, promoting biological reactions, cost-effectiveness, minimizing adverse events like toxicity and immunogenicity. The skin equivalents structure should be biodegradable, biocompatible, durable, malleable, flexible and provide an ideal environment for cell proliferation, differentiation, migration, and neovascularization [7, 8].

44.2 Classifications

Tissue-engineered skin substitutes can be classified using the biomaterial type, the scaffold architecture, the content of cells and growth factors, and the substitute anatomical structure [9].

44.2.1 Biomaterial Type and Scaffold Architecture

The biomaterial type can be biological (autologous, allogeneic, or xenogeneic) or synthetic (biodegradable or non-biodegradable). In biological biomaterial, the transmission risk of infectious diseases should be evaluated.

Scaffolds are extracellular matrix analogs with a tridimensional structure. The composition includes natural, synthetic, or composite (the combination of natural and synthetic) biomaterials. The scaffolds contribute to cell adhesion, proliferation, differentiation, and neovascularization [9]. Collagen, gelatin, elastin, hyaluronic acid, chitosan, fibronectin, fibrin, pullulan,

J. Agata (✉) · R. Marco
Department of Dermatology, University of Pisa, Pisa, Italy

M. Fimiani et al. (eds.), *Technology in Practical Dermatology*,
https://doi.org/10.1007/978-3-030-45351-0_44

alginate, and laminin are the most commonly biocompatible materials utilized as natural scaffolds in skin tissue engineering. Hydrocarbons are the components of synthetic biomaterials including polyhydroxyortho esters (POE), polylactic acid (PLA), polylactic-co-glycolic acid (PLGA), polyethylene glycol (PEG), poly-e-caprolactone (PCL), poly-b-hydroxybutyrate (PHB), poly vinyl alcohol (PVA), and polyurethane (PU). Ideal tissue-engineered skin scaffold should mimic the structure and function of the skin. The combination of biocompatible natural structures and mechanical resistance of synthetic polymers shows the most efficient properties [10]. Some example of composite scaffolds characterized by a wide variety of materials are PLLA–collagen, poly ethylene oxide–chitosan, carboxyethyl chitosan/PVA, chitosan/collagen/PEO, and PCL–collagen [11].

Scaffolds should have a solid 3D structure and an appropriate pore size. 100 μm pores are ideal to support cell migration and transportation. Pores larger than 300 μm can increase capillary formation and angiogenesis [12].

44.2.2 Growth Factors

Growth factors are necessary to create functionally advanced skin substitutes.

Growth factors like epidermal growth factor (EGF), fibroblast growth factor (FGF), transforming growth factor TGF-α/TGFβ, vascular endothelial growth factor (VEGF), platelet-derived growth factor (PDGF), interleukin-1 (IL-1), interleukin-6 (IL-6), and interleukin-8 (IL-8) stimulate healing processes, cell migration and proliferation, neovascularization and reduce fibrosis and scars formation [9].

44.2.3 Cells

Different cell types are involved in the skin normal function such as keratinocytes, melanocytes, fibroblasts, endothelial cells, Langerhans cells, Merkel cells, and adipocytes that produce ECM and a variety of growth factors [13].

Fibroblasts are the most important cells of the dermis involved in a variety of functions: collagen and fibronectin formation, release of angiogenic agents, and stimulation of endothelial cells [14]. Papillary fibroblasts control keratinocyte migration and proliferation with keratinocyte growth factor (KGF) [15].

Keratinocytes are the main cells in skin epidermal layer that have principal roles in epithelialization process and they secrete pro-angiogenic growth factors VEGF and PDGF [16].

Melanocytes are located in the basal layer of the epidermis and are necessary for skin pigmentation in normal skin and to avoid hypopigmentation in skin equivalents [17].

Macrophages remove damaged matrix, release growth factors and cytokines, promote angiogenesis [18] but can cause hypertrophic scarring also in skin substitutes [19].

Langerhans cells are located in epidermis layers and are involved in processing and presenting antigens to T lymphocyte of immune system. In skin substitutes, they control skin immune response and immune rejection.

Endothelial cells are the most important cells of blood and lymphatic vessels. Using these cells in 3D scaffold can accelerate blood capillary formation and lymphatic drainage [20].

44.2.4 Cellular and Acellular Skin Substitutes

Skin substitutes can be divided in two distinct groups including either synthetic acellular materials or natural with different cell types and can be utilized as temporary or permanent wound dressing [21].

Acellular substitutes are used as protections and temporary coverage against environmental contamination and fluid loss and they can include dermal matrix components, cytokines, and growth factors to promote wound healing [22]. Acellular substitutes include a nylon mesh or collagen as dermis and silicon membrane as epidermis. The cellular substitutes are composed of one or two layers of scaffold (mesh or 3D matrix), with autologous or allogeneic cells. The majority

of skin substitutes contain only fibroblasts and keratinocytes. Warm/hot sensation, immune regulation, pressure sensation, and pigmentation are altered due to the absence of immune cells, melanocytes, and nerve cells.

Cellular skin substitutes stimulate the healing process with complete restoration of damaged tissue and reduce the graft rejection [23, 24].

Two main types of cellular autologous skin substitutes are available: cultured epithelial autograft (CEA) and cultured skin substitutes (CSS) [8]. Biomaterial can be natural (collagen, chitosan, HA) and synthetic (PEG, PLA, PLGA and their combinations) [25]. CEAs are cultured autologous keratinocytes obtained from patient's skin biopsy or from cadaveric skin [26]. Epidermis is separated from dermis and then keratinocytes are enzymatically isolated and cultured in vitro [27]. Possible complications are scar formation, contraction, and hyperkeratosis and incomplete healing of deeper wounds. Autologous keratinocytes suspension can be directly sprayed on the wound injury [28]. CSS is an autologous bilayered skin substitute suitable for permanent wound coverage but is time-consuming and expensive [8].

44.2.5 Anatomical Structure of Substitutes

The structure of the substitutes is similar to the anatomy of the skin, which is composed by three layers: avascular epidermis, vascularized dermis, and hypodermis [29]. The skin substitute can serve as a replacement for epidermal, dermal, or composite bilayer dermoepidermal tissues [13]. Epidermal substitutes are utilized in superficial wounds and second degree burns. The possible limitations are the high costs, fragility, long preparation, and poor esthetic outcomes [23, 30].

Dermal substitutes can be cellular or acellular and have allogeneic, xenogeneic, or synthetic origin [21]. The first step of a dermal substitute is to provide a dermis-like structure that is replaced by fibroblasts, endothelial cells, and inflammatory cells. The scaffolds are engineered to support cell growth, migration, revascularization, and neodermis formation. Neodermis (new cells and vascularization) is formed in 3 to 4 weeks after grafting [31]. Secondly the substitute can be covered by skin grafts or different tissue-engineered skin substitutes [20]. Dermal substitutes are not always cost-effective procedure and can be associated with pain and complications [32]. Dermoepidermal (composite) substitutes were manufactured since 1990 by association of epidermal and dermal layers and are indicated for full thickness wounds [33]. An ideal dermoepidermal skin substitute provides a suitable skin barrier and is non-immunogenic. The bilayered skin analogs contain autologous or allogeneic keratinocytes and fibroblasts seeded on 3D scaffolds and are indicated for temporary use [34]. Autologous cells are obtained from skin biopsy after 4 weeks of cultivation and insert to collagen-GAG based structure [35]. The possible complications are poor elasticity, graft contraction, and alteration of pigmentation [13].

44.3 Commercially Available Skin Substitutes

44.3.1 Epidermal Substitutes

BioSeed-S® is autologous keratinocytes resuspended in an allogeneic fibrin sealant [21].

CellSpray is a suspension of non-cultured autologous keratinocytes [27].

EpiDex is a CEA composed by autologous keratinocytes derived from hair follicles and silicone membranes [13].

Epicel® is composed by autologous keratinocyte sheets attached and petrolatum gauze support. It was the first CEA autologous skin substitute to become commercially available [36]. 3 to 4 cm^2 of donor skin are expanded to 5000- to 10,000-folds in 3–4 weeks. The petrolatum gauze support is removed one week after Epicel transplantation [37].

MySkin™ is composed by autologous keratinocytes with a synthetic silicone layer [27].

44.3.2 Dermal Substitutes

Alloderm® is an acellular poor immunogenic cadaveric dermal substitute, composed of a collagen scaffold. The scaffold allows the migration of fibroblasts and endothelial cells and can be covered by thin grafts [38].

Biobrane® is an acellular synthetic bilayer skin substitute composed of dermal layer of porcine collagen type I around a 3D nylon filament and an epidermal layer of thin semipermeable silicone film. Biobrane® is utilized as temporary coverage in pediatric and adult wounds [39].

Dermagraft™ is a monolayer allogenic dermal equivalent formed by culturing human fibroblasts in polyglactin mesh scaffold. The fibroblasts produce dermal matrix proteins, collagen, growth factors, and cytokines. The indications are chronic wounds and in particular diabetic foot ulcers [27].

GraftJacket is a cellular cryopreserved allogenic dermal collagen [40].

Integra™ is an acellular non-immunogenic dermal substitute contained a dermal layer of porous crosslinked bovine collagen and chondroitin-6-sulfate GAG and an epidermal layer of synthetic silicone polymer. The silicon layer provides a temporary coverage of the wound and can be covered secondly by a thin autograft. The dermal scaffold allows the migration of dermal cells such as fibroblasts and other cells that synthesize endogenous matrix components [41, 42].

Matriderm® is an acellular bovine collagen type I matrix and α-elastin hydrolysate lyophilized dermis [39].

TransCyte is a porcine dermal type I collagen coated with bio-absorbable polyglactin and with a silicone film, covered to nylon mesh containing allogenic neonatal foreskin fibroblasts [40].

44.3.3 Dermoepidermal (Composite) Substitutes

Apligraf ™ is a bilayer allogenic skin equivalent composed by epidermal and dermal equivalent layers. The dermal layer is formed by culturing human neonatal fibroblasts and bovine collagen I and provides matrix proteins, growth factors, and cytokines. The epidermal layer is composed by human neonatal keratinocytes cultured on top of the dermal layer and secondly incubating the bilayer substrate in an air–liquid interface to induce keratinocyte cornification [29].

OrCel™ is a bilayer substitute composed of bovine type I collagen matrix, fibroblasts, and cultured neonatal keratinocytes. Fibroblasts release cytokines and growth factors like TGF-α, fibroblast growth factor-1 (FGF-1), and keratinocyte release growth factor-1 (KGF-1, 43).

PolyActive: It is a synthetic polyethylene oxide terephthalate and polybutylene terephthalate (PEO/PBT) scaffold with fibroblast and autologous keratinocytes [15, 22].

TissueTech Autograft System (Laserskin and Hyalograft 3D): Hyalograft® is a dermal substitute, Composed by hyaluronic acid membrane and autologous fibroblasts. Laserskin is an epidermal substitute of autologous keratinocytes [43].

Tiscover™ (A-Skin) is an autologous full thickness cultured skin, composed of a pigmented epidermis on fibroblast dermis [23].

44.4 Conclusions

The function of skin substitutes is to regenerate partial or full thickness wounds and can be used as temporary or definitive coverage. They can be composed by different biomaterial, scaffolds, cells, and growth factors**.** Bioactive living cells produce growth factors and cytokines that help recruit host cells into the matrix. The process is often time-consuming and can take about 3–4 weeks in composite substitutes. The possible limitations are scar formation, poor integrity, and high price [44]. Cost analyses showed that despite high initial costs, skin substitutes can improve wound healing and reduce morbidity, compared with standard therapy [45, 46]. Innovations in cell tissue culture approaches and large-scale production will reduce in the future the cost and will produce higher quality skin analogs [47].

Conflict of Interest The authors declare no conflict of interest.

References

1. Catalano E, Cochis A, Varoni E, Rimondini L, Azzimonti B. Tissue-engineered skin substitutes: an overview. J Artif Organs. 2013;16(4):397–403.
2. MacNeil S. Biomaterials for tissue engineering of skin. Mater Today. 2008;11(5):26–35.
3. Gómez C, Torrero V, Ferreiro I, Pérez D, Palao R, Martínez E, Llames S, Meana A, Holguín P. Use of an autologous bioengineered composite skin in extensive burns: clinical and functional outcomes. A multicentric study. Burns. 2011;37(4):580–9.
4. Debels H, Hamdi M, Abberton K, Morrison W. Dermal matrices and bioengineered skin substitutes: a critical review of current options. Plast Reconstr Surg Glob Open. 2015;3(1):e284.
5. Langer R, Vacanti JP. Tissue engineering. Science. 1993;260(5110):920–6.
6. Damanhuri M, Boyle J, Enoch S. Advances in tissue-engineered skin substitutes. Wounds Int. 2011;2(1):27–34.
7. Wang H, Pieper J, Peters F, van Blitterswijk CA, Lamme EN. Synthetic scaffold morphology controls human dermal connective tissue formation. J Biomed Mater Res A. 2005;74(4):523–32.
8. Vig K, Chaudhari A, Tripathi S, Dixit S, Sahu R, Pillai S, Dennis VA, Singh SR. Advances in skin regeneration using tissue engineering. Int J Mol Sci. 2017;18(4):789.
9. Nicholas MN, Jeschke MG, Amini-Nik S. Methodologies in creating skin substitutes. Cell Mol Life Sci. 2016;73(18):3453–72.
10. Sheikholeslam M, Wright ME, Jeschke MG, Amini-Nik S. Biomaterials for skin substitutes. Adv Healthcare Mater. 2017; https://doi.org/10.1021/acsami.6b12325.
11. Rahmani Del Bakhshayesh A, Annabi N, Khalilov R, Akbarzadeh A, Samiei M, Alizadeh E, Alizadeh Ghodsi M, Davaran S, Montaseri A. Recent advances on biomedical applications of scaffolds in wound healing and dermal tissue engineering. Artif Cells Nanomed Biotechnol. 2017:1–15.
12. Karageorgiou V, Kaplan D. Porosity of 3D biomaterial scaffolds and osteogenesis. Biomaterials. 2005;26(27):5474–91.
13. Biedermann T, Boettcher-Haberzeth S, Reichmann E. Tissue engineering of skin for wound coverage. Eur J Pediatr Surg. 2013;23(5):375–82.
14. Pasparakis M, Haase I, Nestle FO. Mechanisms regulating skin immunity and inflammation. Nat Rev Immunol. 2014;14(5):289.
15. Dixit S, Baganizi DR, Sahu R, Dosunmu E, Chaudhari A, Vig K, Pillai SR, Singh SR, Dennis VA. Immunological challenges associated with artificial skin grafts: available solutions and stem cells in future design of synthetic skin. J Biol Eng. 2017;11:49.
16. Pastar I, Stojadinovic O, Yin NC, Ramirez H, Nusbaum AG, Sawaya A, Patel SB, Khalid L, Isseroff RR, Tomic-Canic M. Epithelialization in wound healing: a comprehensive review. Adv Wound Care. 2014;3(7):445–64.
17. Hachiya A, Sriwiriyanont P, Kaiho E, Kitahara T, Takema Y, Tsuboi R. An in vivo mouse model of human skin substitute containing spontaneously sorted melanocytes demonstrates physiological changes after UVB irradiation. J Gen Intern Med. 2005;20(5):364–72.
18. Bielefeld KA, Amini-Nik S, Alman BA. Cutaneous wound healing: recruiting developmental pathways for regeneration. Cell Mol Life Sci. 2013;70(12):2059–208.
19. Koh TJ, DiPietro LA. Inflammation and wound healing: the role of the macrophage. Expert Rev Mol Med. 2011;13:e23.
20. Larouche D, Cantin-Warren L, Desgagné M, Guignard R, Martel I, Ayoub A, Lavoie A, Gauvin R, Auger FA, Moulin VJ. Improved methods to produce tissue-engineered skin substitutes suitable for the permanent closure of full-thickness skin injuries. BioResearch Open Access. 2016;5(1):320–9.
21. Shevchenko RV, James SL, James SE. A review of tissue-engineered skin bioconstructs available for skin reconstruction. J R Soc Interface. 2010;7(43):229–58.
22. Groeber F, Holeiter M, Hampel M, Hinderer S, Schenke-Layland K. Skin tissue engineering—in vivo and in vitro applications. Adv Drug Deliv Rev. 2011;63(4–5):352–66.
23. Varkey M, Ding J, Tredget EE. Advances in skin substitutes-potential of tissue engineered skin for facilitating anti-fibrotic healing. J Funct Biomater. 2015;6(3):547–63.
24. Shevchenko RV, James SL, James SE. A review of tissue-engineered skin bioconstructs available for skin reconstruction. J R Soc Interface. 2009; https://doi.org/10.1098/rsif.2009.0403.
25. Metcalfe AD, Ferguson MW. Tissue engineering of replacement skin: the crossroads of biomaterials, wound healing, embryonic development, stem cells and regeneration. J R Soc Interface. 2007;4(14):413–37.
26. Supp DM, Boyce ST. Engineered skin substitutes: practices and potentials. Clin Dermatol. 2005;23(4):403–12.
27. Groeber F, Holeiter M, Hampel M, Hinderer S, Schenke-Layland K. Skin tissue engineering—in vivo and in vitro applications. Adv Drug Deliv Rev. 2011;63(4–5):352–66.
28. Wood FM, Stoner ML, Fowler BV, Fear MW. The use of a non-cultured autologous cell suspension and Integra® dermal regeneration template to repair fullthickness skin wounds in a porcine model: a one-step process. Burns. 2007;33(6):693–700.

29. Nicholas MN, Yeung J. Current status and future of skin substitutes for chronic wound healing. J Cutan Med Surg. 2017;21(1):23–30.
30. Lepow BD, Downey M, Yurgelon J, Klassen L, Armstrong DG. Bioengineered tissues in wound healing: a progress report. Expert Rev Dermatol. 2011;6(3):255–62.
31. Shakespeare PG. The role of skin substitutes in the treatment of burn injuries. Clin Dermatol. 2005;23(4):413–8.
32. Branski LK, Herndon DN, Pereira C, Mlcak RP, Celis MM, Lee JO, Sanford AP, Norbury WB, Zhang X-J, Jeschke MG. Longitudinal assessment of Integra in primary burn management: a randomized pediatric clinical trial. Crit Care Med. 2007;35(11): 2615–23.
33. Boyce ST, Goretsky MJ, Greenhalgh DG, Kagan RJ, Rieman MT, Warden GD. Comparative assessment of cultured skin substitutes and native skin autograft for treatment of full-thickness burns. Ann Surg. 1995;222(6):743.
34. Pham C, Greenwood J, Cleland H, Woodruff P, Maddern G. Bioengineered skin substitutes for the management of burns: a systematic review. Burns. 2007;33(8):946–57.
35. Böttcher-Haberzeth S, Biedermann T, Reichmann E. Tissue engineering of skin. Burns. 2010;36(4):450–60.
36. O'Connor N, Mulliken J, Banks-Schlegel S, Kehinde O, Green H. Grafting of burns with cultured epithelium prepared from autologous epidermal cells. Lancet. 1981;317(8211):75–8.
37. Carsin H, Ainaud P, Le Bever H, Rives J-M, Lakhel A, Stephanazzi J, Lambert F, Perrot J. Cultured epithelial autografts in extensive burn coverage of severely traumatized patients: a five year single-center experience with 30 patients. Burns. 2000;26(4):379–87.
38. Catalano E, Cochis A, Varoni E, Rimondini L, Azzimonti B. Tissue-engineered skin substitutes: an overview. J Artif Organs. 2013;16(4):397–403.
39. Halim AS, Khoo TL, Mohd Yussof SJ. Biologic and synthetic skin substitutes: an overview. Indian J Plast Surg. 2010;43(Suppl):S23–8.
40. Kumar MR, Muzzarelli RA, Muzzarelli C, Sashiwa H, Domb A. Chitosan chemistry and pharmaceutical perspectives. Chem Rev. 2004;104(12):6017–84.
41. Nyame TT, Chiang HA, Orgill DP. Clinical applications of skin substitutes. Surg Clin. 2014;94(4): 839–50.
42. Mahboob Morshed N, Chowdhury S, Ruszymah B. The current available biomaterials being used for skin tissue engineering. Regen Res. 2014;3:17–22.
43. Uccioli L. A clinical investigation on the characteristics and outcomes of treating chronic lower extremity wounds using the tissuetech autograft system. Int J Low Extrem Wounds. 2003;2(3):140–15.
44. MacNeil S. Progress and opportunities for tissueengineered skin. Nature. 2007;445(7130):874.
45. Schonfeld WH, Villa KF, Fastenau JM, Mazonson PD, Falanga V. (2000) An economic assessment of Apligraf (Graftskin) for the treatment of hard-to-heal venous leg ulcers. Wound Repair Regen 8: 251–257. 45.
46. Redekop WK, McDonnell J, Verboom P, Lovas K, Kalo Z. The cost effectiveness of Apligraf treatment of diabetic foot ulcers. Pharmaco Economics. 2003;21:1171–83.
47. Shahrokhi S, Arno A, Jeschke MG. The use of dermal substitutes in burn surgery: acute phase. Wound Repair Regen. 2014;22(1):14–22.

Biologics in Wound Management

45

Andrea De Pascalis and Valentina Dini

45.1 Introduction

The understanding of the immunological mechanisms underlying inflammatory diseases has allowed the development of a new class of drugs, called "biological," which mimic the action of human proteins and interact with circulating proteins or cellular/extracellular targets, blocking their activities. The main application of biologics in dermatology concerns psoriasis, atopic dermatitis, and recently hidradenitis suppurativa, with a growing interest in chronic wound management which is the topic of this chapter.

The chapter is divided into two parts: the first one introducing the different types of biological drugs used in the dermatological field and the second one about their practical applications in the treatment of skin ulcers.

45.2 Part One

Among the biological drugs, based on the composition and the mechanism of action, we can distinguish two different classes of molecules: the monoclonal antibodies identified by the -mab suffix and the fusion receptor proteins identified by the -cept suffix.

The former consists of the fragment of the constant region (Fc) of human IgG1 immunoglobulins coupled to binding sites derived from murine antibodies. Based on the number of murine sequences present in the molecule, we distinguish chimeric antibodies (-ximab), consisting of the fusion of human and murine components, humanized antibodies (-zumab) in which murine amino-acid sequences are present in a minimal fraction (generally 3–5%), and human antibodies (-umab) without murine sequences.

Receptorial proteins (-cept) derive from the fusion of a human IgG Fc portion with the extracellular domain of a ligand-specific membrane receptor. The Fc portion of human IgG has the function of stabilizing the receptor structure, increasing its half-life, and thus reducing the frequency of the administrations [1].

The targets of these drugs are the cytokines and the small molecules involved in the pathogenesis of inflammatory diseases and finally also in skin ulcers.

45.2.1 Tumor Necrosis Factor Alpha (TNF-α)

TNF-α is a pro-inflammatory cytokine that has been demonstrated to be elevated in the skin and serum of patients with an inflammatory condition compared to healthy controls.

A. De Pascalis · V. Dini (✉)
Department of Dermatology, University of Pisa, Pisa, Italy

M. Fimiani et al. (eds.), *Technology in Practical Dermatology*,
https://doi.org/10.1007/978-3-030-45351-0_45

Limiting TNF-α receptor activation has been shown to decrease serum levels of C reactive protein, IL-1, IL-6, and immune cell adhesion markers, thus resulting in decreased inflammation.

The biologics targeting this molecule with an application in chronic wound therapy are:

- *Infliximab*: a chimeric human-murine monoclonal antibody (mAb) that binds to both soluble and membrane-bound TNF-α.
- *Adalimumab*: a fully humanized IgG1 mAb that binds to both soluble and membrane-bound TNF-α.
- *Etanercept*: a fully humanized fusion protein composed of the TNF-α receptor and IgG1-Fc. It works as a decoy receptor for soluble and membrane-bound TNF-α and, unlike the other TNF-α inhibitors, etanercept also demonstrates activity against TNF-β (lymphotoxin-α).
- *Certolizumab pegol*: one of the newest anti-TNF-α agents available. It is a humanized Fab fragment of an anti-TNF-α mAb that lacks the Fc portion and because of this it does not induce complement-dependent cytotoxicity, antibody-dependent cell-mediated cytotoxicity, or apoptosis [2–7].

45.2.2 Interleukin-1 (IL-1)

IL-1 is intensely produced by tissue macrophages, monocytes, fibroblasts, and dendritic cells, but is also expressed by B lymphocytes, NK cells, microglia, and epithelial cells. These cytokines increase the expression of adhesion factors on endothelial cells to enable diapedesis of immunocompetent cells, such as phagocytes, lymphocytes, and others, to the sites of inflammation.

To date, two IL-1 blocking drugs, anakinra and canakinumab, have been successfully used in treatment of wounds, in particular pyoderma gangrenosum [8].

- *Anakinra*: It is a homologue of the human interleukin-1 receptor antagonist (IL-1RA) that competitively inhibits binding of IL-1α and IL-1β to the IL-1 receptor type 1.
- *Canakinumab*: a human IgG1κ mAb targeting IL-1β.

45.2.3 Interleukin-12/23 (IL-12/23)

IL-12 is involved in the differentiation of Th1 cells, and it is important for expansion and maintenance of Th17 cells. Th17 cells produce IL-17, which increases neutrophilic recruitment.

- *Ustekinumab*: It works by blocking the common p40 subunit of IL-12 and IL-23 and prevents these cytokines from interacting with their receptor [9].

45.2.4 Interleukin-6 (IL-6)

IL-6 is a pro-inflammatory cytokine and strong inducer of the acute phase response. Elevated serum levels have been observed in patients with inflammatory disease and, along with other cytokines, IL-6 is involved in the activation and accumulation of neutrophils in tissues [10].

- *Tocilizumab*: It is a humanized anti-IL-6 receptor (IL-6R) mAb with activity against both soluble and membrane-bound receptors.

45.2.5 Phosphodiesterase 4 (PDE4)

Phosphodiesterase 4 (PDE4) is an enzyme primarily expressed in immune cells that is responsible for the hydrolysis of cyclic adenosine monophosphate (cAMP). Inhibition of PDE4 results in elevated levels of cAMP, which modulates a variety of signaling pathways involved in production of inflammatory mediators.

- *Apremilast*: It is an oral selective PDE4 inhibitor approved in 2014 for the treatment of psoriasis. It inhibits production of TNF-α, IFN-γ, CXCL9, CXCL10, IL-2, IL-12, IL-23, macrophage inflammatory protein 1α, monocyte chemoattractant protein 1, and granulocyte macrophage-colony stimulating factor in peripheral blood mononuclear cells; it also inhibits IL-8 production from neutrophils and TNF-α production by natural killer (NK) cells and keratinocytes [11, 12].

The contraindications and possible side effects of biologics have been studied mainly for TNF-α inhibitors and mainly concern the possible development of infections and malignancies.

Although randomized controlled trials and some observational studies have not shown an increased risk of severe infections with the use of anti-TNF-α, there is a potential risk of reactivation of a latent tuberculosis infection and for this reason it is recommended to perform a Quantiferon Gold test and a chest x-ray before starting the treatment. For the same reason and in the absence of evidence to prove otherwise, it is also recommended to exclude latent infection by HIV, HBV, and HCV [13, 14].

Most of the studies evaluating the incidence of malignancies with TNF-α antagonists have been conducted in patients with rheumatoid arthritis and IBD, who were on multiple immunosuppressive drugs that synergistically increase the rate of malignancies with TNF-α antagonists. A meta-analysis of randomized control trials examining the risk of malignancies in psoriatic patients found no statistically significant increased risk of malignancy. Most malignancies found during the placebo-controlled portions of the trials were non-melanoma skin cancer (70.6%). However, long-term studies are needed to assess the risk of cancer with anti-TNF-α therapy in psoriasis or in other skin diseases.

Besides it has been shown that the baseline risk of lymphoma (Hodgkin's and cutaneous T-cell lymphoma) irrespective of treatment is high in patients with psoriasis as for RA. Despite the controversial results regarding the risk of malignancies, including non-melanoma skin cancers (NMSC) and lymphoma with TNF-α antagonists, all patients and particularly those with history of multiple immunosuppressive therapy should be screened for any potential malignancy before and during anti-TNF-α therapy. Skin and lymph node examination should be carried out at baseline, 6 monthly for first year and yearly thereafter [15–17].

The development and re-ignition of demyelinating diseases, sometimes associated with permanent disability, was recorded both in therapy with infliximab and etanercept. Some cases of probable demyelinating syndrome have also been reported with adalimumab.

The mechanism of induction of these conditions is not known, and the appearance of them in the course of therapy with anti-TNF-α has also occurred in patients who did not have any previous neurological manifestations. Other neurological diseases have also been described (e.g., transverse myelitis, aseptic meningitis, optic neuropathy, and Parkinson's disease), but the size of the problem does not seem to be defined [18].

Congestive heart failure in the NYHA III or IV class is an absolute contraindication to the use of infliximab and adalimumab and a precaution for the use of etanercept due to the substantial danger of deterioration of a pre-existing condition and death of the patient, even in cases where there isn't an increased cardiovascular risk. Besides both with etanercept and with infliximab are also reported cases of congestive decompensation of new onset even in the absence of known risk factors [19].

Infusion reactions (infliximab) or local reaction at the injection site (etanercept, adalimumab) are frequent, but only rarely are, for example, to induce withdrawal of treatment.

Observation of adequate administration protocols greatly reduced the incidence of acute infusion reactions, generally well controllable with symptomatic therapy. Delayed reactions are also rare occurring in less than 1% of cases, especially in patients undergoing re-treatment; with subcutaneous agents, mild local reactions are quite frequent, but they almost never need to be discontinued [20].

45.3 Part Two

Skin ulcers in which the inflammatory component, whether local or systemic, is primary in the pathogenesis are the main target of biologics: pyoderma gangrenosum and vasculitic ulcers are the most mentioned in scientific papers.

45.3.1 Pyoderma Gangrenosum

Pyoderma gangrenosum (PG) is a rare neutrophilic dermatosis. PG can be associated with various disorders, mainly with autoimmune-mediated inflammatory conditions, but in up to 40% of patients it is idiopathic. Treatment of PG should be directed to first control the underlying systemic disease in combination with a good local wound care. The use of pharmacologic agents such as steroids and immunosuppressive drugs is fraught with potential adverse effects and not always successful [21].

Recent studies have demonstrated that PG lesions overexpress interleukin IL-1β, IL-8, IL-17, IL-23, tumor necrosis factor α (TNF-α), chemokines 1, 2, 3, and 16, metalloproteinases 2 and 9, and Janus kinase (JAK)-1, -2, and -3. These inflammatory mediators provide multiple opportunities for targeted immunologic therapies [2].

- TNF-α Inhibition: There is a mounting evidence supporting the use of TNF-α agents as first-line treatments for PG, with a recent large systematic review reporting higher response rates with infliximab or adalimumab compared to steroids, cyclosporine, or other immunomodulatory medications [22]. No drug in this class has been proven to be superior to the others. To date, infliximab is the only biologic medication that has been subjected to a randomized, double-blind, placebo-controlled trial for the treatment of PG: 69% of patients who received infliximab at a dose of 5 mg/kg demonstrated a beneficial response at the conclusion of the study, which includes 21% who were in complete remission [23]. Data regarding the use of adalimumab for the treatment of PG are limited to case reports and small case series; however, the majority of them reported complete resolution or some degree of clinical improvement. To date, there are 20 published case reports and small case series describing the use of etanercept for PG in 28 different patients. Improvement was documented in 21/28 patients, with 17/28 achieving complete resolution and 4/28 demonstrating some degree of clinical improvement. There are currently only two published cases reporting on the use of certolizumab pegol for the treatment of PG: in both cases, the patients achieved complete remission.
- IL-1 Inhibition: PG is one component of several complex medical syndromes (PAPA, PASH, etc.) associated with specific mutations in the PSTPIP-1 gene. The downstream effect of PSTPIP-1 mutation is activation of the inflammasome and increased IL-1 production. It follows that targeted treatment of PG in these specific syndromes would block IL-1-mediated inflammation [24]. To date, two IL-1 blocking drugs, anakinra and canakinumab, have been successfully used to treat these PG-associated syndromes. Anakinra has approximately 95% bioavailability but has a half-life of only 4–6 hours. Accordingly, large doses must be administered daily to compensate for rapid clearance. From 9 case reports published on the use of anakinra for the treatment of PG, 10 of 12 patients experienced either significant clinical improvement or complete resolution. Unlike anakinra, canakinumab is IL-1β specific and has a longer half-life of approximately 1 month. Five patients were enrolled in a phase II multicenter open-label pilot study investigating the use of canakinumab for the treatment of PG and four additional published cases are reported on the use of canakinumab for PG as well. Of these 10 patients treated with canakinumab, 6 demonstrated complete resolution, 1 experienced clinical improvement, and 3 were refractory to treatment.
- IL-12/23 Inhibition: Given that the hallmark of PG is neutrophilic infiltration of the skin and that IL-23 is overexpressed in PG lesions, inhibiting these pathways should translate to clinical improvement of PG. Indeed, there are 7 published case reports of ustekinumab successfully being used to treat PG.
- IL-6 Inhibition: As elevated serum levels of IL-6 have been observed in patients with PG, the successful use of tocilizumab for the treatment of PG has been reported in a single patient with co-existing rheumatoid arthritis.

- PDE4 Inhibition: Due to its wide anti-inflammatory effects targeting many of the same pathways that overlap with drugs known to successfully treat PG, apremilast is likely a reasonable PG therapy. To date, there has only been one study evaluating apremilast for the treatment of recalcitrant vegetative PG: the patient, who presented with two ulcers, achieved complete healing of one ulcer and partial healing of the other when apremilast was added as adjuvant therapy in conjunction with oral prednisone.

Biologic therapy represents a promising way for treatment of PG, targeting cytokines and pro-inflammatory molecules that underlie disease pathogenesis. Among the biologics currently available, only infliximab has been tested in a randomized, double-blind, placebo-controlled trial showing its efficacy (this study included just thirty patients). The other molecules with their different mechanism of action have been tried with varying drug doses, frequency of dosing, methods for determining efficacy, and time to declare treatment success or failure, which makes comparison difficult. Besides, the majority of this data comes from single case reports or small case series. Finally, we have to say that since many biologic and small molecule therapies are relatively new, there is a lack of long-term data regarding adverse effects and capability to maintain disease remission [25, 26].

45.3.2 Vasculitic Ulcers

Cutaneous small vessels involvement could represent a primary disorder or a clinical aspect of a systemic disease, with a vessel damage mediated by an immunological process that causes inflammation and destruction of both the vessels and the perivascular tissue.

Skin ulcers may present as an early sign of the vasculitis or, more often, complicate the natural evolution of palpable purpura. A high number of ulcers are quite superficial, tend to regress in a short time, and leave only modest cutaneous dystrophic and/or pigmentary outcomes. However, sometimes, the ulcerative lesions persist for a long time and become resistant to the common therapies. In many cases, the ulcers are multiple and localized on the legs and feet [27].

Vasculitis associated to circulating c- and p-ANCA constitutes the most important group of the primary systemic vasculitis of the adult population. Granulomatosis with polyangiitis (GPA), eosinophilic granulomatosis with polyangiitis (EGPA), and microscopic polyangiitis (MPA) are small vessel vasculitides associated with the presence of anti-neutrophil cytoplasmic antibodies to proteinase 3 (PR3-ANCA) or myeloperoxidase (MPO-ANCA).

Biologic drugs have an important role to play in clinical remission induction and maintenance of remission in severe ANCA-associated vasculitis.

Rituximab, an anti-CD20 IgG1 chimeric, murine/human monoclonal antibody, is recommended by the American College of Rheumatology (ACR), British Society of Rheumatology (BSR), and the French Vasculitis Study Group (FVSG) as first-line induction therapy for newly diagnosed severe GPA or MPA. As demonstrated by the RAVE trial data, rituximab is not inferior to oral cyclophosphamide, so it could be indicated in young women where cyclophosphamide may increase the risk of ovarian failure or in patients at increased risk of infection. In addition, rituximab is recommended for the management of severe relapsing GPA or MPA refractory to conventional immunosuppressant drugs, including a complete course of pulsed intravenous cyclophosphamide. Rituximab is also indicated as a therapeutic option in severe ANCA-associated vasculitis patients with incomplete or no clinical response to intravenous cyclophosphamide or in whom cyclophosphamide is contraindicated [28, 29].

At present, in absence of clinical evidences, rituximab is not recommended in eosinophilic granulomatosis with polyangiitis (EGPA).

Anti-TNF-α biologic agents are at present not recommended for remission induction therapy in ANCA-associated vasculitis; however, some case reports and non-randomized open-label studies have provided few data which could justify the use of these biologics in certain relapsing refractory cases [29].

Vasculitis can be a clinical aspect in course of connective tissue diseases, like rheumatoid arthritis (RA), systemic lupus erythematosus (SLE), Sjögren syndrome, and systemic scleroderma. It has been calculated that 5% of patients with RA may develop ulcers of vasculitic origin and a higher incidence has been described for SLE [30].

TNF-α antagonists, like infliximab, have been reported to be effective for treatment of skin ulcers in rheumatoid vasculitis; in addition, there have been several reports of TNF-α antagonist-induced vasculitis in patients with RA. Although the mechanisms underlying these pathological events are not fully understood, caution is required in the use of TNF-α antagonists for treatment of ulcers in rheumatoid vasculitis. We can say that based on a favorable benefit-to-risk profile, TNF-α antagonists are suitable therapeutic options in patients who do not respond to other forms of therapy [31, 32].

Small vessel vasculitis in SLE has been shown to be a leukocytoclastic process, resulting from an immune complex-mediated inflammation of small vessel-sized arteries. In medium/large-vessel vasculitis, the underlying pathogenesis is more complex and was thought to be T-cell driven. B cells produce a variety of cytokines, including TNF-α and IL-6, which can be both pro- and anti-inflammatory. B cells produce antibodies which may initiate auto-inflammatory responses. Thus, targeting B cells with anti-CD20 monoclonal antibody, like rituximab, we can obtain a resultant decrease in antibody production with reported results in treatment of refractory SLE [33].

More recently, belimumab, a monoclonal antibody that inhibits the B-cell survival factor BLyS which is thought to play a critical role in some patients with SLE, has shown benefit in musculoskeletal and cutaneous manifestations of SLE [34].

The efficacy of rituximab has been reported also for treatment of cryoglobulinemic vasculitis, which is often related to HCV infection. Deposition of mixed cryoglobulins in the walls of venules, capillaries, and arterioles may induce painful skin ulcers highly resistant to the therapy. HCV is able to infect B cells and induce their clonal expansion that may lead to the production of organ-specific autoantibodies. Rituximab interferes with monoclonal IgM production, cryoglobulin synthesis, and organ deposition of immune complexes and has shown to be highly effective in modifying the dynamics of B cells by deleting expanded clones [35].

At the end of this chapter we have to report two pilot studies, which showed the possible efficacy of biologic therapy in venous leg ulcers (VLU), which cause up to 90% of lower extremity chronic cutaneous ulcers. In VLU pathogenesis, an important role is played by increased TNF-α levels both systemically and in ulcer tissue, with consequent greater expression of matrix metalloproteinases, IL-1 and 6, and inflammatory cell adhesion molecules such as intercellular adhesion molecule-1 (ICAM-1), which cause increased proteolysis and inflammation, resulting in delayed healing [36].

In the first trial adalimumab, a fully human recombinant IgG1 monoclonal antibody against TNF-α, was tried in four subjects affected by recalcitrant VLUs along with compression therapy. Overall, after two subcutaneous doses of 40 mg each one, a 4-week wound size reduction was noted, and in patients with the percentage of 4-week wound size reduction greater than 25%, this positively correlated with percent of TNF-α cytoplasmic staining score reduction [37].

In the second trial, infliximab was applied topically to eight patients with chronic ulcers of more than 4-month durations. Infliximab was applied repeatedly to ulcers either as a 10 mg/ml solution and covered with an adhesive sheet or as a gel formulation (0.45, 1, or 4.5 mg/g) under a hydrofiber dressing/adhesive sheet. After 4 weeks of treatment, surface area was reduced by more than 50% in 6 of the 14 treated ulcers. Within 8 weeks, five ulcers completely healed, while another four were reduced by more than 75% in size [38].

These pilot studies indicate that future larger trials of biologic drugs are viable and may further elucidate the efficacy of this therapy for recalcitrant VLUs and not only for pyoderma gangrenosum or vasculitic ulcers.

Clinical Case

Female, 68 yrs, no comorbidities, pyoderma gangrenosum of the lower leg treated with infliximab 5mg/kg IV for 4 doses every two weeks (Figs. 45.1, 45.2, 45.3, and 45.4).

Fig. 45.1 Week 0

Fig. 45.2 Week 2

Fig. 45.3 Week 4

Fig. 45.4 Week 6

Conflict of Interest The authors declare no conflict of interest.

References

1. Krueger JG. The immunologic basis for the treatment of psoriasis with new biologic agents. J Am Acad Dermatol. 2002;46(1):1–23.
2. Marzano AV, Fanoni D, Antiga E, et al. Expression of cytokines, chemokines and other effector molecules in two prototypic autoinflammatory skin diseases, pyoderma gangrenosum and Sweet's syndrome. Clin Exp Immunol. 2014;178(1):48–56.
3. Elliott MJ, Maini RN, Feldmann M, et al. Treatment of rheumatoid arthritis with chimeric monoclonal antibodies to tumor necrosis factor alpha. Arthritis Rheum. 1993;36(12):1681–90.
4. Klotz U, Teml A, Schwab M. Clinical pharmacokinetics and use of infliximab. Clin Pharmacokinet. 2007;46(8):645–60.
5. Vena GA, Cassano N. Drug focus: adalimumab in the treatment of moderate to severe psoriasis. Biologics. 2007;1(2):93–103.
6. Mitoma H, Horiuchi T, Tsukamoto H, et al. Molecular mechanisms of action of anti- TNF-alpha agents—comparison among therapeutic TNF-alpha antagonists. Cytokine. 2018;101:56–63.
7. Haridas V, Shetty P, Dsouza LC, et al. Pyoderma gangrenosum in Sjogren's syndrome and its successful treatment with topical application of etanercept. Int J Rheum Dis. 2017;20(5):657–9.
8. Fleischmann R, Stern R, Iqbal I. Anakinra: an inhibitor of IL-1 for the treatment of rheumatoid arthritis. Expert Opin Biol Ther. 2004;4(8):1333–44.
9. Tang C, Chen S, Qian H, et al. Interleukin-23: as a drug target for autoimmune inflammatory diseases. Immunology. 2012;135(2):112–24.
10. Lee WS, Choi YJ, Yoo WH. Use of tocilizumab in a patient with pyoderma gangrenosum and rheumatoid arthritis. J Eur Acad Dermatol Venereol. 2017;31(2):e75–7.

11. Manning CD, Burman M, Christensen SB, et al. Suppression of human inflammatory cell function by subtype-selective PDE4 inhibitors correlates with inhibition of PDE4A and PDE4B. Br J Pharmacol. 1999;128(7):1393–8.
12. Schafer PH, Parton A, Gandhi AK, et al. Apremilast, a cAMP phosphodiesterase-4 inhibitor, demonstrates anti-inflammatory activity in vitro and in a model of psoriasis. Br J Pharmacol. 2010;159(4):842–55.
13. Phillips K, Husni ME, Karlson EW, Coblyn JS. Experience with etanercept in an academic medical center: are infection rates increased? Arthritis Care Res. 2002;47:17–21.
14. Ellerin T, Rubin RH, Weinblatt ME. Infections and anti- tumor necrosis factor alpha therapy. Arthritis Rheum. 2003;48:3013–22.
15. Dommasch ED, Abuabara K, Shin DB, Nguyen J, Troxel AB, Gelfand JM. The risk of infection and malignancy with tumor necrosis factor antagonists in adults with psoriatic disease: a systematic review and meta-analysis of randomized controlled trials. J Am Acad Dermatol. 2011;64:1035–50.
16. Gelfand JM, Berlin J, Van Voorhees A, Margolis DJ. Lymphoma rates are low but increased in patients with psoriasis: results from a population-based cohort study in the United Kingdom. Arch Dermatol. 2003;139:1425–9.
17. Levine D, Strober BE. The treatment of moderate-to-severe psoriasis: prescreening and monitoring psoriatic patients on biologics. Semin Cutan Med Surg. 2010;29:28–34.
18. Hrycaj P, Korczowska I, Lacki JK. Severe Parkinson's disease in rheumatoid arthritis patient treated with ifx. Rheumatology (Oxford). 2003;42:702–3.
19. Chung ES, Packer M, Lo KH, FaSanmade AA, Willerson JT. Randomized, double-blind, placebo-controlled, pilot trial of ifx, a chimeric monoclonal antibody to tumor necrosis factor-alpha, in patients with moderate-to-severe heart failure: results of the anti-TNF Therapy Against Congestive Heart Failure (ATTACH) trial. Circulation. 2003;107:3133–40.
20. Khanna D, McMahon M, Furst DE. Safety of tumor necrosisfactor- alpha antagonists. Drug Saf. 2004;27:307–24.
21. Choucair MM, Fivenson DP. Pyoderma gangrenosum: a review of the disease and treatment options. Wounds. 2001;13(3):119–22.
22. Agarwal A, Andrews JM. Systematic review: IBD-associated pyoderma gangrenosum in the biologic era, the response to therapy. Aliment Pharmacol Ther. 2013;38(6):563–72.
23. Brooklyn TN, Dunnill MG, Shetty A, et al. Infliximab for the treatment of pyoderma gangrenosum: a randomised, double blind, placebo controlled trial. Gut. 2006;55(4):505–9.
24. Marzano AV, Trevisan V, Gattorno M, et al. Pyogenic arthritis, pyoderma gangrenosum, acne, and hidradenitis suppurativa (PAPASH): a new autoinflammatory syndrome associated with a novel mutation of the PSTPIP1 gene. JAMA Dermatol. 2013;149(6):762–4.
25. Fatima McKenzie, Devin Cash, Angela Gupta, Laurel W. Cummings & Alex Ortega-Loayza. Biologic and small molecule medications in the management of pyoderma gangrenosum, J Dermatolog Treat. 2018Sep 7;Epub.
26. Dini V, Romanelli M, Bertone M, Talarico S, Bombardieri S, Barachini P. Improvement of idiopathic pyoderma gangrenosum during treatment with anti-tumor necrosis factor alfa monoclonal antibody. Int J Low Extrem Wounds. 2007 Jun;6(2):108–13.
27. Papi M, Papi C. Vasculitic ulcers. Int J Low Extrem Wounds. 2016 Mar;15(1):6–16.
28. Ntatsaki E., Carruthers D., Chakravarty K., et al. BSR and BHPR guideline for the 316 management of adults with ANCA-associated vasculitis, rheumatology. Oxford. 2014;317.
29. Charles P., Bienvenu B., Bonnotte B., et al. Rituximab: recommendations of the 319 French Vasculitis Study Group (FVSG) for induction and maintenance treatments 320 of adult, antineutrophil cytoplasm antibody-associated necrotizing vasculitides, 321 Presse Med. 2013;42(10):1317–1330.
30. Van der Bijl AE, Allaart CF, Van Vugt J, et al. Rheumatoid vasculitis treated with infliximab. J Rheumatol. 2005;32:1607–9.
31. Fujikawa K, Kawakami A, Hayashi T, et al. Cutaneous vasculitis induced by TNF inhibitors: a report of three cases. Mod Rheumatol. 2010;20:86–9.
32. Lui NL, Thumboo J, Fong KY. A case of refractory vasculitic ulcers in a systemic lupus erythematosus patient responding to rituximab and hyperbaric oxygen therapy. Int J Rheum Dis. 2009;12:366–9.
33. Manzi S, Sánchez-Guerrero J, Merrill JT, Furie R, Gladman D, Navarra SV, et al. Effects of belimumab, a B lymphocyte stimulator-specific inhibitor, on disease activity across multiple organ domains in patients with systemic lupus erythematosus: combined results from two phase III trials. Ann Rheum Dis. 2012;71:1833–8.
34. Bonilla-Abadía F, Echeverri AF, Izquierdo JH, Cañas F, Cañas CA. Efficacy and safety of rituximab in the treatment of vasculitic leg ulcers associated with hepatitis C virus infection. Case Rep Rheumatol. 2012;2012:923897.
35. Weinstein DA, Kirsner RS. Refractory ulcers: the role of tumor necro- sis factor-alpha. J Am Acad Dermatol. 2010;63:146–54.
36. Fox JD, Baquerizo-Nole KL, Keegan BR, Macquhae F, Escandon J, Espinosa A, Perez C, Romanelli P, Kirsner RS. Adalimumab treatment leads to reduction of tissue tumor necrosis factor-alpha correlated with venous leg ulcer improvement: a pilot study. Int Wound J. 2016;13(5):963–6.
37. Streit M, Beleznay Z, Braathen LR. Topical application of the tumour necrosis factor-alpha antibody infliximab improves healing of chronic wounds. Int Wound J. 2006 Sep;3(3):171–9.
38. Ehrlich MR. Vasculitic leg ulcers: a complication of collagen-vascular disorders. Ostomy Wound Manage. 1993;39:12–4.

Stem Cell in Wound Healing

46

Maria Cristina A. Puyat

46.1 Introduction

Skin is the largest organ that comprises our body and it has several functions. Skin plays an important role in maintaining the internal and external homeostasis of the human body. The major role of the skin is three-fold: to act as the protective barrier from all environmental or extrinsic factors such as extreme temperatures, UV radiation, or harmful chemicals; to serve as the first line of defense from foreign pathogens (bacteria, virus, fungi); and to free radicals that can affect skin health and integrity. Skin regulates body temperature, maintains body fluid balance, synthesizes vitamin D, and is responsible for the different sensations [1, 2].

Skin has three different layers that are vital in the regeneration of wounds. The epidermis is the outer layer of the skin and is made of stratified squamous epithelial tissue. The dominant feature of this layer is commonly known as keratinocytes, which is responsible for the firmness and rigidity of the skin. The epidermis is also the site for pigment production, which is known as melanin [1–3]. The dermis is the second layer of the skin and it has blood vessels, nerves, sweat glands, and hair follicles. It is divided into papillary dermis and the reticular dermis. The fibroblast is an important dermal cell type in the dermis which is responsible for the production of collagen and extracellular matrix and essential for wound healing [1, 3]. It secretes collagen and elastin fibers which make the skin stronger and elastic. The third layer is hypodermis or subcutaneous fat, composed of adipose connective tissue that provides insulation, energy storage, shock absorption, and cushion between the skin and the skeletal structure [2].

Healthy skin integrity is vital for protection of what is inside the body. Its structure is important to maintain the maximum effect by providing an effective barrier from all harmful effects of the environment. Overtime, skin integrity is diminished due to loss of elastic tissue and thinning of the surface of the skin making it vulnerable to injuries.

A wound is defined as an injury or damage to tissues which breaks the skin integrity which is associated with the disruption of the structure and function of the skin [3]. Wound healing is essential as this is the body's natural restorative response to tissue injury [2]. It is a complex process of cellular events between various population of cells that generates biological process consisting of the four different, but partially overlying steps involving coagulation, inflammation, proliferation, and remodeling or scar formation [4]. Impairment of the healing mechanism function might lead to chronic, nonhealing wounds and even scar tissue formation presented as keloids and hypertrophic scars [5]. There are several factors including local and systemic factors that affect wound healing with deleterious

M. C. A. Puyat (✉)
Asian Stem Cell Institute, Inc, Pasig, Philippines

M. Fimiani et al. (eds.), *Technology in Practical Dermatology*,
https://doi.org/10.1007/978-3-030-45351-0_46

effects on the patient's quality of life [6]. Local factors affecting wound healing include infection, impaired blood supply, wound type and site, recurrent trauma, and foreign body. Systemic factors include age, other illness such as diabetes, suppression of the immune response, malignancy, vitamin deficiency, and smoking [6].

It has been over a decade and the search for the appropriate management for the recuperation of the wound is still not found. Different methods are tried and tested, from local practices to conventional treatments, and yet the transition is slow to attain the perfect technique to produce better results. To achieve a more advanced treatment for wound healing, new trends and innovative treatment that help accelerate the wound healing process should be explored. Alternative treatment to the traditional method of wound healing is geared to stem cell therapy in which tissue homeostasis is guaranteed within specialized microenvironments called niches.

The niche is responsible in facilitating the regeneration and repair of its damaged cell tissues [5]. Within the last few years, there are a lot of research and studies that have been published with regard to the wound healing application using autologous mesenchymal stem cells (MSCs), but still need more clinical evidence-based data. Despite the lack of well-designed controlled clinical trials, emerging clinical data on the safety of autologous bone marrow and adipose-derived tissue mesenchymal stem cells (MSCs) in wound healing warrant consideration of these cells in a wider range of applications including functional restoration of damaged tissue and reconstruction of skin wound [7].

As stem cells have the capability to regenerate and repair damaged tissue, they also conduct the body's healing response. A study in 2013 [4] showed that there is a significant effect of ASC (adipose stem cell) on wound healing through paracrine activity. This is a process wherein there is growth factor secretion, improvement of keratinocyte and fibroblast, increased endothelial cell and macrophage, increased proliferation and neovascularization, and exhibition of antioxidant effects [4]. MSCs' therapeutic potential is largely due to their ability to secrete proregenerative cytokines, modulate tissue injury, and its anti-inflammatory effect that makes them an attractive option for the treatment of chronic wounds [8].

In the Philippine setting, though stem cells showed promising result, there are still challenges to clinical implementation as no stem cell therapy for wound healing applications has yet been approved by the Food and Drug Administration (FDA). Major barriers to clinical translation of stem cell-based therapies include challenges in identifying the stem cell populations best suited for wound therapy, as well as developing optimized adjunctive therapies to protect and improve the regenerative capacity of stem cells within the wound environment [8]. In this chapter, combination treatment has been used to hasten the process of wound healing and to treat keloid scar that results from the abnormal proliferation of scar tissue at the site of injury after a wound healing takes place. Adipose-derived stem cell, fat transfer with enriched platelet rich plasma, hyperbaric oxygen therapy, lasers, light-emitting diode (LED), and electrical stimulation (ES) are discussed as treatment modalities. As with any of the novel technological innovations currently available, understanding of the advantages and disadvantages of the treatment and knowledge in optimal technique are vital to clinical success. In this fast growing field of regenerative medicine and as knowledge in tissue regeneration expands, the synergistic effect of combining various treatment approaches into wound may optimize the outcome.

46.2 Biological Process of Wound Healing

46.2.1 Inflammation

Hemostasis marks the start of wound healing process. There are three steps that happen in a rapid sequence: vasoconstriction, platelet plug formation, and blood coagulation. Vasoconstriction, or clot formation in the wound keeps the platelet and blood vessel in the site of injury. The blood clot re-establishes hemostasis and provides a provisional extracellular matrix (ECM) for cell

migration. Migratory cells use this matrix as a bridge to orchestrate the movement of cells in a particular path to the specific location for wound healing. It secretes protein factors that mediate wound healing, including platelet-derived growth factor (PDGF), endothelial growth factor (EGF), transforming growth factor (TGF-β), fibroblast growth factor (FGF), and vascular endothelial growth factor (VEGF) [3].

The inflammation starts right after tissue injury. In this phase, platelet adheres to the damaged endothelial lining that releases adenosine diphosphate (ADP) that aggregates thrombocystic propagation into the wound to stop the bleeding. Platelet from α granules releases cytokines such as PDGF, Platelet Factor 4, and TGF that attract inflammatory cells including polymorphonuclear cells (PMN), lymphocytes, and macrophages.

These PMNs are the main source of proinflammatory cytokines such as IL-1α, IL-1β, IL-6, and TNF-α that regulate the signaling cascades of inflammatory response and prevent infection. Platelet and the impaired tissue secrete vasoactive amines (histamine, serotonin, and prostaglandins) that increase vascular permeability. Macrophages remove devitalized tissue and microorganisms through PMN debridement while regulating fibroblast activity in the proliferative phase [2]. Once the inflammation subsides due to macrophages and neutrophils, then the proliferation phase will start to work.

46.2.2 Proliferation

At this phase, wound restoration takes place. New tissue is formed and is made up of collagen and extracellular matrix. This phase is characterized by fibroblast migration, deposition of new ECM, and granulation tissue formation. Fibroblast migrates into a wound in response to TGF-β and PDGF which gives way to the production of collagen (type I and type II procollagen) and matrix proteins such as hyaluronan, fibronectin, elastin, glycosaminboglycans, and proteoglycans [3]. Fibroblasts are very important in the wound healing process. It differentiates into myofibroblast, which stimulates contraction of the wound leading to a reduction of the wound size. Matrix metalloproteinases (MMPs) such as MMP-1, MMP-2, and MMP-3 play a vital role in migration of fibroblasts into the wound matrix [2]. The presence of growth factors and cytokines (VEGF, FGF, angiopoietin, and TGF-β) triggers epithelial cell proliferation and migration through the new tissue [3]. Several MMPs including MMP-1, MMP-2, MMP-9, MMP-19, and membrane-associated MT-MMPs stimulate formation of new blood vessel (angiogenesis) and re-epithelialization of the wound surface [2, 9]. Collagens play a significant part in wound recovery due to its chemotactic role [9], wherein it attracts fibroblasts and keratinocytes to the wound to create a paracrine loop and secrete cascades of matrikines [1, 2]. There is an increase in tensile strength of the wound due to the production of collagen type III. Remodeling of collagen is essential for the transition of granulation tissue to scar and once the balance between collagen synthesis and degradation is completed, wound maturation begins [3].

46.2.3 Remodeling

The transition from granulation to wound re-epithelialization marks the start of tissue remodeling [1]. During maturation stage wherein wound closure takes place, type III collagen becomes gradually degraded and production of type I collagen increases [3]. Throughout the remodeling, there is a reduction in the hyaluronic and fibronectic acid, which are degraded by cells and plasmatic metalloproteinase [10]. In remodeling phase, PDGF helps break down old collagen by regulating matrix metalloproteinases [3] and growth factors such as TGF-β, EGF, IGF-1, and FGF-2 [2, 3]. At this stage, final scar tissue is being formed by the concurrent synthesis and disintegration of collagen. During this phase, the repairs actively present during the proliferation phase are made even stronger. The original collagen (collagen type III) is replaced with a different stronger type of collagen (collagen type I). Eventually, the growth of capillaries stops, blood flow to the area declines, and metabolic activity

at the wound site decreases [3], leading to a fully matured scar with a decreased number of cells and blood vessels with a strong tensile strength [3]. This last stage of wound healing usually leads to developing a fibrous tissue that changes normal skin after tissue injury known as a scar.

Much has been said and done with regard to how wound will be regenerated. Currently, stem cell therapy is the most promising alternative treatment available that has repair and regenerative property for tissue regeneration. This has vast potential to improve management treatment for the nonhealing wound and to reverse the visible factors that affect wound healing process [1].

46.3 Stem Cells Meet Wound Healing

Preventive and regenerative medicine is the direction that Medical Science will go to as an innovative approach of treatment. As the knowledge and the science improve over time, it will have more treatment options using the technological advances that will address a wider variety of conditions and illnesses. Stem cell therapy is just one of the many types of cellular therapy that preventive and regenerative medicine uses. It gained interest as a promising treatment approach to augment tissue regeneration [8].

Stem cells are found all over the body. They are just like in a deep sleep, but when triggered it will perform its duty to repair, replace, or restore damaged tissue. Stem cells are characterized by multipotency and undifferentiated cells that have the ability to self-renew and give rise to different specialized types [3]. There are various sources of stem cells based on where they originated from, categorized into the following: embryonic stem cells (ESCs), umbilical cord stem cells, and adult stem cells. Stem cells' role in wound healing is greatly valued and due to this reason a lot of regenerative therapies for wound healing are being developed both for animal and human studies as they are able to produce promising results. Stem cells' capacity to differentiate into multiple cell lineages (osteoblasts, chondroblasts, adipocytes, tenocytes, and myocytes) serves as an impact to the environmental elements, and promotes healing factors that stipulate a great potential as a therapeutic tool for wound healing [5].

46.4 Adult Mesenchymal Stem Cells in Wound Management and Tissue Engineering

Mesenchymal stem cells derived from adult stem cells can be isolated from different types of tissues, including bone marrow, adipose tissue, synovium, dermis, peripheral blood, umbilical cord, and placenta [11]. In 1966, MSCs was first isolated from bone marrow [8] by their ability to adhere to the plastic surface. In 2005, The International Society for Cellular Therapy (ISCT) [12] standardized the definition of MSCs due to the inconsistencies of MSCs nomenclature and biologic criteria. MSCs are defined as "fibroblast-like plastic-adherent cells, regardless of the tissue from which they are isolated, be termed multipotent mesenchymal stromal cells, while the term mesenchymal stem cells is used only for cells that meet specified stem cell criteria." As there is no specific cell surface marker to MSCs, the ISCT suggested three criteria for classifying human MSCs: (a) the cells must be plastic-adherent using tissue culture flasks, (b) must express surface markers CD73, CD90, and CD105 and must not express markers of hematopoietic markers CD14, CD34, CD45, CD11β, CD79α or CD19 and HLA class II surface, (c) the cells should be able to differentiate into osteoblasts, adipocytes, and chondroblasts pathway [12].

The MSCs therapeutic benefit is characterized by the release of trophic mediators such as vascular endothelial growth factor (VEGF), stromal cell-derived factor-1 (SDF-1), epidermal growth factor (EGF), keratinocyte growth factor (KGF), insulin-like growth factor-1 (IGF-1), and matrix metalloproteinase-9 (MMP-9) that promotes formation of new vessels, endogenous progenitor cells recruitment, and cell differentiation, proliferation, and formation of extracellular matrix during wound healing process [8].

MSCs manifest immunomodulatory properties through the secretion of the following: interferon-λ, tumor necrosis factor-α, interleukin-1α, and interleukin-1β and also by activation of nitric oxide synthase. MSCs regulate fibrosis and inflammation by secreting prostaglandin E_2 that further promotes tissue healing and reduces scarring [8]. Moreover, MSCs demonstrate bactericidal properties via secretion of antimicrobial human cathelicidin protein (hCAP-18 or LL-37) in response to phagocytosis [8, 12].

46.4.1 Bone Marrow-Derived Mesenchymal Stem Cells (BM-MSCs)

In 1966, Friedenstein et al. [8] first isolated BM-MSCs by harvesting from human through aspiration of the bone marrow in the iliac crest. Bone marrow contains hematopoietic stem cells (HSCs), mesenchymal stem cells (MSCs), endothelial progenitor cells (EPC), and many other cells [3]. BM-MSCs are characterized by surface markers such as CD36 and negative CD106 [2] and have another surface marker neural ganglioside (GD2) that distinguished them from other surrounding marrow elements [13].

BM-MSCs promote repair when applied to cutaneous wound and release high levels of growth factors helpful in normal wound healing. It also provides an important early signal for dermal fibroblast responses to injury, wherein there is emergent proof that paracrine activity is the main and vital tool by which MSCs promote wound repair and healing [10].

In a clinical case series study in 2003 by Badiavas et al. [3], BM-MSCs were applied to chronic wounds and showed decrease in the size of the wound and increase in dermal vascularity and thickness in histology. In this study, promising and remarkable result of the management of wound healing is manifested wherein they administer direct administration of the injected bone marrow-derived stem cells into the wound that resulted to decreased wound scarring, and subsequently followed by application of topical BM-MSCs into the injured tissue surface where closing of chronic ulcers in 3 patients is achieved [3, 12, 14].

BM-MSCs treatment in cutaneous wound established acceleration in wound healing kinetics, increased epithelialization and angiogenesis. BM-MSCs are sources of important signals that control proliferation of dermal fibroblast, migration and gene expression to cutaneous wound. This improved wound repair has been seen in acute and chronic wounds in human [10].

46.4.2 Adipose-Derived Stem Cells (ADSCs)

ADSCs are isolated from the stromal vascular fraction (SVF) of fat tissue [2]. SVF consists of heterogeneous cells including pre-adipocytes, adipocytes, macrophages, endothelial progenitor cells (EPCs), adipose-derived stem cells (ADSCs), and also many growth factors such as bFGF, IGF-1, VEGF, and PDGF-BB [1]. ADSCs are plastic-adherent and source for multipotent stem cells similar to BM-MSCs that can be differentiated into various lineages including bone, fat, cartilage, and muscle. ADSCs are characterized by different surface markers ($CD34^+$ $CD73^+$, $CD90^+$, $CD105^+$, $CD44^+$, $CD45^-$, $CD31^-$), which distinguish from BM-MSCs gene expressions CD36 and CD106 [2].

ADSCs are considered as the ideal stem cell for regenerative clinical application. The ADSCs have the aptitude to go through different lineages as adipogenic, osteogenic, chondrogenic, neurogenic, and myogenic differentiation [15]. Since the MSC from fat tissue gives a huge amount of cell yield upon isolation, it makes it an alternative source to bone marrow and is the most favored cell type for wound repair and regeneration [13, 15]. Aside from stimulating angiogenesis, additional potential of ADSCs has been revealed. It is also to function as pericytes to provide vascularity stability wherein it can interact with endothelial cells in response to environmental stimuli [15].

Stem cells reside in a specialized environment known as a niche that can control many aspects of the stem cells' behavior, including proliferation, differentiation, and apoptosis (jones and wagers 2008). Recent studies have suggested that the niche for the ADSCs is the vasculature of adipose tissue. The use of stem cell niches from fat tissue is vital in the field of plastic and cosmetic surgery [4]. In a study of Gir et al., there are 174 published clinical application of ADSCs in plastic surgery including soft tissue augmentation, wound healing, and tissue engineering [4]. Among MSCs, in dermatology the most popular ones include adipose-derived stem cells (ADSCs). Adipose-derived stem cells were analyzed as a cell source for the full-thickness skin defect repair [16].

Both ADSCs and BM-MSCs have significant effect in wound healing as it manifests speedup of healing in an injured tissue [17]. As ADSCs exhibit similar characteristics that can be found in ranging from its immunophenotype, telomerase activity, gene expression, surface antigen to the secretion of growth factors and cytokines [3, 17].

46.5 Adjunctive Treatment Modalities for Wound Healings

Poor wound healing affects the quality of life of a person such as the physical, emotional, financial, and social aspects. Due to these effects, immediate attention should be given and appropriate treatment must be provided [18]. The combination of adjunctive therapies to the main ones for wound healing such as growth factors and cytokines, hyperbaric oxygen therapy [2], LED and lasers [18, 19] pulse electromagnetic field, and electrical stimulation [20, 21] helps in promoting healing process.

In dealing and managing nonhealing wounds, these combined modalities will aid current treatment standard to be more innovative in the treatment approach. It will provide appropriate medical care that are more advanced and has the capability to address whatever standard or traditional treatment has failed to do so.

46.5.1 LASER and LED

A study done by Mester et al. showed that low level laser therapy (LLLT) and LED therapy can be beneficial for acceleration of skin wound healing. In this study, he noted the beneficial effects of laser on rapid closure of wounds and tenacious ulcers. LED emits a narrow band of electromagnetic radiation when activated ranging from ultraviolet to visible and infrared wavelengths. Klebanov et al. established that both coherent laser and non-coherent light-emitting diode when compared had an effect on wound healing [19]. These therapeutic lights may help and can be an add-on in the available treatments for promoting skin wound healing. The biological effects were similar and related to decreased in inflammatory cells, increased fibroblast proliferation, stimulation of angiogenesis, granulation tissue formation, and collagen synthesis [18].

46.5.2 Hyperbaric Oxygen Therapy (HBOT)

Hyperbaric oxygen therapy is considered as one of the adjunct therapy to conventional treatment for many indications, including radionecrosis, necrotizing fasciitis, chronic wounds, mainly in diabetic nonhealing wounds. HBOT increases blood oxygen content to cellular tissues 10 times more in the body than normal. It reaches areas of low oxygen perfusion that may benefit wound healing [22]. Hyperbaric oxygen uses in wound healing for a fact is that if used under certain pressure it can trigger angiogenesis, boost fibroblast proliferation, and increase immune function [2]. For optimal wound healing, proper oxygen level is vital. Hypoxia stimulates wound healing by secreting growth factors and angiogenesis, while oxygen is important to sustain healing process of the wound (Bishop, 2008) HBOT is one of the therapeutic options that can address tissue hypoxia (Rodriguez et al., 2008) but due to the few evidences from clinical studies that indicate the effectiveness of HBOT in any type of ulcers or unmanageable wound, it is geared back to

stem cell therapy to drive into a particular management for chronic wounds that will act on several modalities of wound healing [2].

46.5.3 Electrical Stimulation (ES)

ES is believed to invigorate the recuperation of wound process by emulating the natural electrical current that happens in injured skin [20]. Conveyance of current further the progress of cellular activity in all phases of wound healing [21]. The migration of neutrophils and macrophages increases when electrical current is applied to wounded tissue and it stimulates proliferation of fibroblasts. Electrical stimulation serves as an adjunct therapy for chronic wound as there is presence of improved blood flow and circulation in the process of wound healing. ES is considered as an effective device for chronic wound healing based on most clinical trials and narrative reviews [20]. As it generates a responsive effect on wound healing, many of those who are seeking for an adjunct tool that can help address the management available for chronic wounds and soft tissue regeneration may add this to their treatment approach.

46.5.4 Growth Factors and Cytokines

Growth factors and cytokines are the signaling cascade that is released at the wound site immediately after injury. They are responsible for the stimulation of cell proliferation to the wound and promote cellular response during the entire phases of wound healing process [5, 23]. There are various growth factors that are involved and play a vital role in the process of wound healing such as that of platelet-derived growth factor (PDGF), in which it increases the healing rate in an acute wound and promotes complete healing in chronic wounds [23].

Growth factors currently involved in the process of wound healing are the following: platelet-derived growth factor (PDGF), epidermal growth factor (EGF), fibroblast growth factor (FGF), insulin-like growth factor (IGF1, IGF2), vascular endothelial growth factor (VEGF), TGF-β, and keratinocyte growth factor (KGF), these range of growth factors may demonstrate potential in wound management [23].

PDGF is the only growth factor approved by the Food and Drug Administration (FDA) for clinical application [23].

46.6 Discussion and Conclusion

Though there is a limited clinical study on the impact of stem cell therapy on wound healing (or nonhealing wounds), the reports cited demonstrated encouraging results (Fig. 46.1). The milieu of fundamental mechanisms involved in wound healing requires a thorough investigation. For this chapter, a case report of a Filipino female, age 21, signed an informed consent and authorization for alternative medical treatment prior to stem cell harvest from adipose tissue after meeting the eligibility criteria set by the Centre. History of the patient started with a car accident obtaining a bad injury on the left foot (Fig. 46.1). Skin grafting was done and was hospitalized for four (4) weeks. Oral and topical antibiotics as well as other unrecalled medications were taken but the aforesaid treatments did not produce a satisfactory outcome. The patient had a residual loss of sensation on the left medial foot making her unable to walk normally and tiptoe on the same side. Her slippers would fall off if not supported by a strap to keep it in place. As a compassionate treatment, stem cell therapy (autologous) was considered.

The harvested cells were incubated for 24 hours and tested for its microbial, endotoxin, and viability prior to administration. Autologous adipose-derived stem cells with fat were transplanted using a gauge 18 cannula with a good take and produced wound closure. The patient was monitored for her vitals before treatment until 2 hours after the injection of cells into the left medial foot. A month later, the photos depict significant improvement on wound healing and complete closure of the chronic wound.

After a year, a second autologous adipose-derived stem cell with fat and PRP was again transplanted on the same area. In addition to

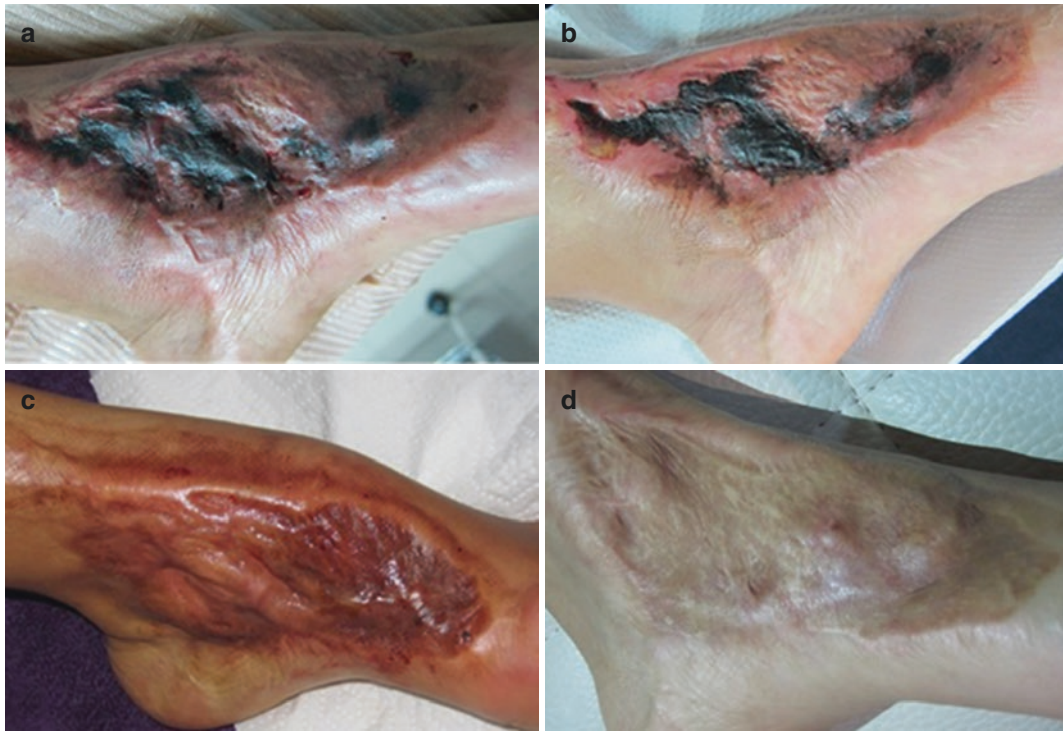

Fig. 46.1 (**a**) Left foot before first autologous adipose-derived stem cells fat transfer. (**b**) Left foot after a month of treatment. (**c**). Left foot after 1 year and second autologous adipose-derived stem cells fat transfer and PRP injection. (**d**) Left foot after a year of second autologous adipose-derived stem cells fat transfer and PRP injection follow-up

these, pulse electromagnetic therapy was applied after the stem cell transplantation for 5 minutes. Fractionated laser with erbium YAG was done at the site prior to topical application of the stem cell as well. She also had intravenous infusion of stem cells. This time, the patient started to feel pain on the previously sensory deficient area, which gradually disappeared in a month's time. She started to identify the sensation with the pin-prick test that was done as sharp or dull with high accuracy. The patient started to walk without difficulty and was further able to hold the tiptoe position on the left foot.

Since this is a preliminary clinical study, no attempts were made to understand the potential mechanism of action involved in the remarkable healing. The impact of the treatment to the psychological and clinical status has been for the betterment of the patient. The functional improvement on top of her esthetic improvement has brought greater quality of life, which the patient and the parents are very appreciative of. More importantly, after years of follow-up and recent communication with the patient, it has been seen that there were no safety issues or unexpected growth within the injected site. There were no adverse events noted post treatments until the present time with a 7-year interval from first stem cell treatment.

The adjunctive treatments done during and after stem cell therapy have helped synergistically to produce a better wound healing and esthetic outcome. Stem cell therapy has demonstrated its ability to produce functional improvement. Although no laboratory tests like electromyography, nerve conduction velocity tests, histopathology, and more were done, we cannot deny the fact that the patient started to regain sensation and is able to walk normally without difficulty as how she would before her accident.

This data was previously presented in various international conferences [24–27]. Also to note, the images presented are neither digitally enhanced nor manipulated.

References

1. Gaur M, Dobke M, Lunyak VV. Mesenchymal stem cells from adipose tissue in clinical applications for dermatological indications and skin aging. Int J Mol Sci. 2017;18(1):208.
2. Kanji S, Das H. Advances of stem cell therapeutics in cutaneous wound healing and regeneration. Mediat Inflamm. 2017;5217967.
3. Menendez-Menendez Y, Alvarez-Viejo M, Ferrero-Gutierrez A, Perez-Basterrechea M, Perez Lopez S, et al. Adult stem cell therapy in chronic wound healing. J Stem Cell Res Ther. 2014;4:162.
4. Fromm-Dornieden C, Koenen P. Adipose-derived stem cells in wound healing: recent results in vitro and in vivo. OA Mol Cell Biol 2013 Dec 20;1(1):8.
5. Borena BM, Martens A, Broeckx SY, Meyer E, Chiers K, Duchateau L, Spaas JH. Regenerative skin wound healing in mammals: state-of-the-art on growth factor and stem cell based treatments. Cell Physiol Biochem. 2015;36:1–23.
6. Guo S, Dipietro LA. Factors affecting wound healing. J Dent Res. 2010 Mar;89(3):219–29.
7. Hanson SE, Gutowski KA, Hematti P. Clinical applications of mesenchymal stem cells in soft tissue augmentation. Aesthet Surg J. 2010;30(6):838–42.
8. Duscher D, Barrera J, Wong VW, Maan ZN, Whittam AJ, Januszyk M, Gurtner GC. Stem cells in wound healing: the future of regenerative medicine? A mini-review. Gerontology. 2016;62:216–25.
9. Hochstein A, Bhatia A. Collagen: its role in wound healing. Podiatry Management. 2014 Aug;.
10. Smith AN, Willis E, Chan VT, et al. Mesenchymal stem cells induce dermal fibroblast responses to injury. Exp Cell Res. 2009;316(1):48–54.
11. Schneider S, Unger M, van Griensven M, Balmayor ER. Adipose-derived mesenchymal stem cells from liposuction and resected fat are feasible sources for regenerative medicine. Eur J Med Res. 2017; 22(1):17.
12. Hu MS, Borrelli MR, Lorenz HP, Lonaker MT, Wan DC. Mesenchymal stromal cells and cutaneous wound healing: a comprehensive review of the background, role, and therapeutic potential. Hindawi Stem Cells Int. 2018;20:6901983.
13. Malhotra S, Hu MS, Marshall CD, et al. Mesenchymal stromal cells as cell-based therapeutics for wound healing. Stem Cells Int. 2016:4157934.
14. Badiavas EV, Falanga V. Treatment of chronic wounds with bone marrow–derived cells. Arch Dermatol. 2003;139(4):510–6.
15. Bertozzi N, Simonacci F, Grieco MP, Grignaffini E, Raposio E. The biological and clinical basis for the use of adipose-derived stem cells in the field of wound healing. Ann Med Surg (Lond). 2017;20:41–48.
16. Nowacki M, Kloskowski T, Pietkun K, et al. The use of stem cells in aesthetic dermatology and plastic surgery procedures. A compact review of experimental and clinical applications. Postepy Dermatol Alergol. 2017;34(6):526–34.
17. Isakson M, de Blacam C, Whelan D, McArdle A, Clover AJP. Mesenchymal stem cells and cutaneous wound healing: current evidence and future potential. Stem Cell Int. 2015;831095.
18. Chaves ME, Araújo AR, Piancastelli AC, Pinotti M. Effects of low-power light therapy on wound healing: LASER x LED. An Bras Dermatol. 2014;89(4):616–23.
19. Adamskaya N, Dungel P, Mittermayr R, Hartinger J, Feichtinger G, Wassermann K, Redl H, van Griensven M. Light therapy by blue LED improves wound healing in an excision model in rats. Injury. 2011;42:917–21.
20. Gardner SA, Frantz R, Schmidt F. Effect of electrical stimulation on chronic wound healing: a meta-analysis. Wound Repair Regen. Official Publication of the Wound Healing Society the European Tissue Repair Society 1999;7:495–503.
21. Isseroff RR, Dahle SE. Electrical stimulation therapy and wound healing: where are we now? Adv Wound Care (New Rochelle). 2012;1(6):238–43.
22. Stoekenbroek RM, Santema TB, Legemate DA, Ubbink DT, van den Brin A, Koelemay MJW. Hyperbaric oxygen for the treatment of diabetic foot ulcers: a systematic review. Eur J Vasc Endovasc Surg. 2014;47(6):647–55.
23. Han G, Ceilley R. Chronic wound healing: a review of current management and treatments. Adv Ther. 2017;34:599–610.
24. International Society of Dermatologic and Aesthetic Surgery (ISDS) 2012.
25. International Master Course on Ageing Skin (IMCAS) 2012.
26. Anti-Aging Medicine World Congress (AAWC) 2017.
27. Dermatologic and Aesthetic Surgery International League (DASIL) 2017.

Part IV

New Complementary Tools for Dermatologic Diagnosis

Pietro Rubegni

Microbiopsy in Dermatology

47

Giulia Tonini, Elisa Cinotti, and Marco Ardigo

47.1 Introduction

Presently, histopathologic examination represents the practical reference standard for the diagnosis of neoplastic and inflammatory skin diseases [1, 2]. Cutaneous samples are collected by skin biopsy or excisional biopsy. Skin biopsy, using a punch biopsy tool or a scalpel, is performed under local anaesthesia to remove a skin sample 2–4 mm in diameter. The residual wound is then either sutured or left to heal [3].

An excisional biopsy, performed using a larger 4–6 mm diameter punch biopsy, a deep shave biopsy, or with a fusiform excision, is performed when the entire tumour is needed for histopathological examination, or in case of suspected melanoma [3, 4].

These biopsy techniques are time-consuming and require local anaesthesia and sutures. Moreover, formalin fixing of samplers hinders molecular analysis [3].

In the "era" of bioengineering, the need for a deeper understanding of the pathology to be translated in the clinical diagnosis pushes the research on clinic-molecular biology correlation. This scientific process drives in the direction of the development of devices for, easy, minimally invasive tissue sampling for molecular studies. In this field, sub-millimetre skin punch biopsy (called microbiopsy) device has been developed to obtain sufficient tissue sample for molecular diagnosis and research [3]. This technology is of great interest and with potential usefulness in situations when conventional biopsies are not appropriate or a cosmetically sensitive area is involved or multiple lesions have to be screened.

47.2 Microbiopsy: Device and Technique

The microbiopsy devices are 0.50 mm wide and 0.20 mm thick and contain a chamber within the centre plate to collect the skin sample. Chamber volumetric size is of 0.003 mm^2 (more than 6000 times smaller than a conventional 3 mm punch biopsy and more than 5 times smaller than an 18 GA syringe needle) (Figs. 47.1 and 47.2) [3].

Microbiopsy technique is minimally invasive and does not require local anaesthesia. The average pain score measured with a numerical scale between 0 and 10 was 1.5 ± 1.1 in 20 healthy volunteers [3].

Local erythema is observed after microbiopsy, but it is reported to resolve within 24 hours. The technique is suture-free. The excision site from microbiopsy heals quickly and the residual wound is closed within 1 day and is not visible

G. Tonini (✉) · E. Cinotti
Department of Medical, Surgical and Neurological Science, Dermatology Section, University of Siena, S. Maria alle Scotte Hospital, Siena, Italy

M. Ardigo
Clinical Dermatology, San Gallicano Institute-IRCCS, Rome, Italy

M. Fimiani et al. (eds.), *Technology in Practical Dermatology*,
https://doi.org/10.1007/978-3-030-45351-0_47

Fig. 47.1 Microbiopsy device

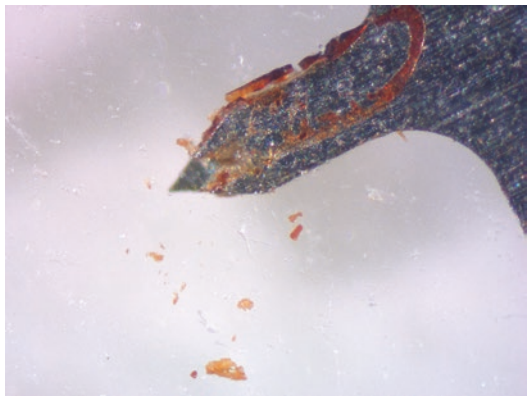

Fig. 47.2 Microbiospy device needle

after 7 days (Fig. 47.3). Reflectance confocal microscope (RCM) images from the microbiopsied site showed the formation of a tiny crust that resolved by 3 weeks and was completely undetectable by the naked eye (Fig. 47.4) [3].

The size of microbiopsy-caused defects has been demonstrated to be comparable to that of other artefacts commonly seen in routine sectioned specimens [2, 5]. Microbiopsies also differ from conventional punch biopsies because they do not interfere with histopathologic diagnosis of melanocytic proliferations [2].

Microbiopsy sites can be targeted by dermoscopy. Tan et al. coupled a transparent plate with a pinhole with a dermoscope to visualize the sampling area. Once the area was identified through the pinhole, the dermoscope was removed, leaving the plate in contact with the skin and making

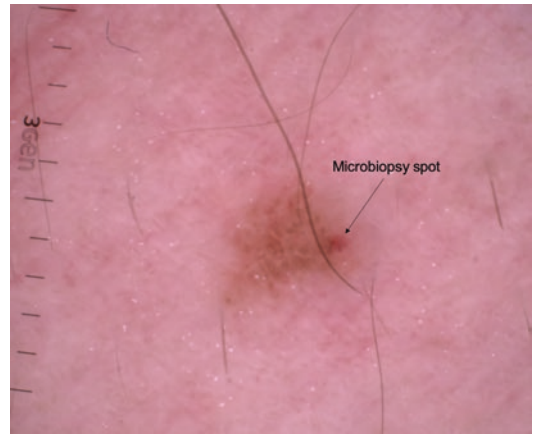

Fig. 47.3 Dermoscopy of a nevus previously subject to microbiopsy. The arrow indicates the site of a microbiopsy spot performed 1 day before

the area accessible to the biopsy device microneedle. The microbiopsy device applicator was then aligned with the pinhole allowing for targeted sampling of the tissue [5].

A targeting sampling setting that uses RCM images as guide was recently developed (Fig. 47.5). In addition to dermoscopy, RCM allows the evaluation of the skin layers and it is able to show cellular details of melanocytes or keratinocytes aggregates (nests) that can be easily assessed, thus facilitating the selection of targeted area for microbiopsy sampling. The RCM technique needs an "adhesive plastic window" and a "metal ring" to localize the target area within the lesion. RCM can provide an overview of the lesion through an *en face* mapping called mosaic that overlaps the dermoscopy picture and acts as a "virtual grid" guiding the target site of sampling. The 8 × 8 mm RCM mosaic is composed by 16 × 16 individual images, each one of 0.5 × 0.5 mm [6].

The success of the RCM-guided microbiopsy strongly depends on keeping the correct orientation of the lesion during imaging and biopsy in order to obtain a right guide of the sampling. After the removal of the metal ring, a flexible silicon-based orientation-maintaining ring is placed over the adhesive window to preserve the alignment of the RCM examination window [6].

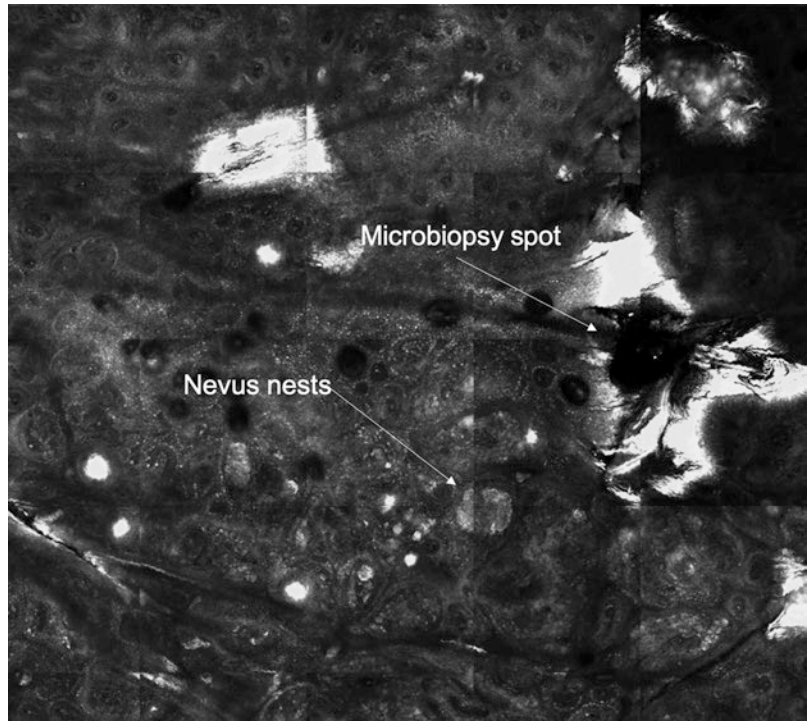

Fig. 47.4 Reflectance confocal microscope of a nevus previously subject to microbiopsy. The arrow indicates the outcome of microbiopsy performed 3 weeks before on a nevus

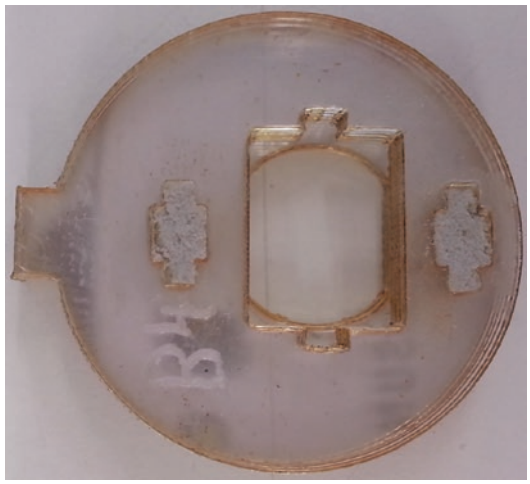

Fig. 47.5 Reflectance confocal microscope targeting setting for sampling

The sampling site can be marked by microbiopsy needles previously immersed with fluorescein (480 nm wavelengths) and it can later be displayed on RCM images overlapping reflectance and fluorescence mode using a multiwavelength confocal microscope [6].

The tissue sample obtained from epidermis and papillary dermis, composed of about 2000 cells, is processed by extractors and specific kits to isolate DNA or RNA, which are quantified, qualitatively controlled and subjected to whole genomic or transcriptome amplification, respectively. The aim is the identification of the target genes or proteins to be studied or that are known to be specific markers of the disease [3, 6]. The limited tissue provided by microbiopsy is only available for molecular biology but is not useful for histological examination.

Likely bigger chambers at the tip of the microbiopsy "needle" will be able to produce more tissue for histology, but with the risk of more skin damage and pain [6].

47.3 Microbiopsy Application in Skin Oncology

Microbiopsy is an evolving technique. In upcoming years, it may have a prospective role in melanoma diagnosis, risk stratification and personalized therapeutics [5].

Tan *et al.* practised three dermoscopy-targeted sampling with a microbiopsy device coupled with DNA sequence analysis in a melanoma in

situ arising in a dysplastic nevus. Samples of DNA were extracted, amplified and sequenced for BRAF and NRAS mutation detection. The microbiopsy-extracted DNA samples revealed a BRAF wild-type melanoma in situ developing within a heterogeneous BRAF V600E mutant dysplastic nevus [5].

Sobarun et al. used microbiopsy samples and quantitative polymerase chain reaction (qPCR) analysis to differentiate between a histopathologically proven superficial pigmented basal cell carcinoma (BCC) and a superficial melanoma resembling a pigmented BCC (index lesion) in an 80-year-old [7]. Five microbiopsies were executed in both lesions and in their perilesional skin. The expression of the melanoma signature genes Tyr (NM_000372), CMIP (NM_198390.2), and LINC00518 (NR_027793.1) and a BCC marker Gli1 (NM_005269.2) were investigated. Results of qPCR showed that LINC00518 and Tyr were upregulated in the index sample with a low expression of Gli1, thus suggesting that the index sample was a melanoma and not a BCC [7].

47.4 Detection of HPV DNA by Microbiopsy in Viral Warts

Tom *et al.* investigated the use of the skin microbiopsy for clinical sampling of cutaneous warts and surrounding healthy perilesional skin (1 cm from the wart) to detect spatial presence of human papillomavirus (HPV) DNA [8]. Samples of two patients were collected using either a microbiopsy device or a skin surface swabbing method, using type-specific HPV PCR for HPV types 1, 2, 27 and 57 [9] or FAP method [10] for detecting HPV. The authors demonstrated that the skin microbiopsy is a practical method for the collection of clinical samples from skin lesions, allowing detection of viral DNA by PCR [8]. Microbiopsy-mediated sampling of cutaneous warts for the detection of HPV DNA is equally as effective as sampling, using a swabbing method, with the advantage of substantially improved positional precision with the microneedle-based device [8].

47.5 Microbiopsy and Leishmaniasis

Visceral leishmaniasis (VL) is a potentially lethal, sand fly-borne disease caused by disseminated infections with *Leishmania donovani* species complex protozoan parasites [11]. In endemic African countries, it is crucial not only to diagnose the VL cases that normally comprise a small minority of the infected population, but also to identify the asymptomatic carriers with high parasitaemia that are reservoir hosts for the anthroponotic transmission of *L. donovani* and possibly for *L. infantum*, potentially infectious to biting sand flies [12]. Host infectiousness is optimally assessed based on the infection rates of insectary-reared vectors that had fed on it (xenodiagnosis), which is a laborious technique [13]. Leishmania is not only blood parasite, but after its inoculation into the skin by blood-feeding infected sand flies, it establishes dermal infections maintaining long-lasting parasitaemia in the skin around the site of the infectious sand fly bite [14].

Kirstein *et al.* used microbiopsy devices developed by L.L. Lin and T.W. Prow in 262 volunteers living in endemic area of Ethiopia and in leishmaniasis patients in order to determine the reservoir potential of infected asymptomatic human [3, 12]. MB samples were extracted from the skin of the arm, the nape of the neck and the cheek, areas always exposed and generally preferred by biting sand flies. MB devices penetrate the skin to a depth of 200 μm and absorb blood and skin lysates mimicking blood meals. Blood samples were acquired by finger pricks [12]. The study confirmed the frequent presence of dermal *L. donovani* infections in residents of endemic regions (137 of 262 volunteers), regardless of whether they had previous history of VL or not. Infections were more frequently detected in small amounts of blood and skin extracted by MB than blood obtained by finger pricks, thus confirming that skin parasitaemia was prevalent in the asymptomatic volunteer populations [12].

References

1. Sina B, Kao GF, Deng AC, Gaspari AA. Skin biopsy for inflammatory and common neoplastic skin diseases: optimum time, best location and preferred techniques. A critical review. J Cutan Pathol. 2009 May;36(5):505–10.
2. Banan P, Lin LL, Lambie D, Prow T, Soyer HP. Effects of ex vivo skin microbiopsy on histopathologic diagnosis in melanocytic skin lesions. JAMA Dermatol. 2013 Sep 1;149(9):1107.
3. Lin LL, Prow TW, Raphael AP, Harrold III RL, Primiero CA, Ansaldo AB, et al. Microbiopsy engineered for minimally invasive and suture-free sub-millimetre skin sampling. F1000Research. 2013 May 2;2:120.
4. Pickett H. Shave and punch biopsy for skin lesions. Am Fam Physician. 2011 Nov 1;84(9):995–1002.
5. Tan J-M, Lin LL, Lambie D, Flewell-Smith R, Jagirdar K, Schaider H, et al. *BRAF* wild-type melanoma in situ arising in a *BRAF* V600E mutant dysplastic nevus. JAMA Dermatol. 2015 Apr 1;151(4):417.
6. Ardigò M, Agozzino M, Lin L, Prow TW. Reflectance confocal microscopy-guided microbiopsies for targeted molecular analysis. In: Reflectance confocal microscopy of cutaneous tumors. 2nd ed; 2017. p. 52–8.
7. Sobarun P, Hoang VLT, Yamada M, Lambie D, Soyer HP, Prow TW. Microbiopsy biomarker profiling in a superficial melanoma resembling a pigmented basal cell carcinoma. JAMA Dermatol. 2017 Apr 1;153(4):334.
8. Tom LN, Dix CF, Hoang VLT, Lin LL, Nufer KL, Tomihara S, et al. Skin microbiopsy for HPV DNA detection in cutaneous warts. J Eur Acad Dermatol Venereol. 2016 Dec;30(12):e216–7.
9. Lei Y-J, Gao C, An R, Shi Q, Chen J-M, Yuan Y-K, et al. Development of a multiplex PCR method for detecting and typing human papillomaviruses in verrucae vulgaris. J Virol Methods. 2008 Jan;147(1):72–7.
10. Forslund O, Antonsson A, Stenquist B, Göran Hansson B, Nordin P. A broad range of human papillomavirus types detected with a general PCR method suitable for analysis of cutaneous tumours and normal skin. J Gen Virol. 1999 Sep 1;80(9):2437–43.
11. Alvar J, Vélez ID, Bern C, Herrero M, Desjeux P, Cano J, et al. Leishmaniasis worldwide and global estimates of its incidence. PLoS ONE. 2012 May 31;7(5):e35671.
12. Kirstein OD, Abbasi I, Horwitz BZ, Skrip L, Hailu A, Jaffe C, et al. Minimally invasive microbiopsies: a novel sampling method for identifying asymptomatic, potentially infectious carriers of Leishmania donovani. Int J Parasitol. 2017 Sep;47(10–11):609–16.
13. Hirve S, Boelaert M, Matlashewski G, Mondal D, Arana B, Kroeger A, et al. Transmission dynamics of visceral leishmaniasis in the Indian subcontinent—a systematic literature review. PLoS Negl Trop Dis. 2016 Aug 4;10(8):e0004896.
14. Liu D, Uzonna JE. The early interaction of Leishmania with macrophages and dendritic cells and its influence on the host immune response. Front Cell Infect Microbiol. 2012;2:83.

48 Noninvasive Genetic Testing: Adhesive Patch-Based Skin Biopsy and Buccal Swab

Maria Palmieri, Alessandra Renieri, and Elisa Frullanti

48.1 Introduction

The gold standard to collect tissue samples is still surgical biopsy. Skin biopsy is the removal of a small part of skin performed by dermatologists. The size of this removal depends on the type of skin lesion but usually it does not exceed 2–7 millimeters in width and depth. To date there are different types of skin biopsy that can be performed according to different dermatological needs.

To take stock of the situation, we will do a quick overview of skin biopsies techniques performed by dermatologists. Depending on the skin lesions and the different locations of the same, there are some types of biopsies that can be performed (shave biopsy, punch biopsy, and excisional biopsy) all correlated by the most common local lidocaine anesthesia. The *shave biopsy* is used to diagnose melanoma-in-situ, basal cell cancer and squamous cell carcinoma. The surgeon proceeds with the scraping of the lesion protuberant part, leaving the patient with smooth skin. Tools used for this procedure are the blade and the razor. The *punch biopsy* is indicated to diagnostic tests, small lesions and small esthetic removals. It is performed with a round blade shape able to penetrate the skin and to remove dermis and subcutaneous fat. Finally, the *excision biopsy* is essentially a punch biopsy with an elliptical rather than circular cut and it is preferred for all those diseases that arise in the deep skin layers [1].

These skin biopsies are invasive procedures that could have many contraindications such as hemorrhages, infections, and allergic reactions to injected antibiotics. However, to date the skin biopsy is necessary to identify from the most mild to the most serious case, from a simple inflammation to a cutaneous neoplasia.

During the last years, there is a growing need to use minimally invasive or noninvasive approaches in order to obtain tissue samples without compromise quantity or quality. This was the driving challenge of the adhesive patch-based skin biopsy development.

48.2 Adhesive Patch-Based Skin Biopsy

Adhesive patch-based skin biopsy (APSB) is characterized by a small size patch with a 19 mm in diameter that can be located on the skin of all parts of the body, except palms of the hands, soles of the feet, and mucous membranes

M. Palmieri · E. Frullanti
Medical Genetics, University of Siena, Siena, Italy
e-mail: maria.palmieri@dbm.unisi.it; elisa.frullanti@dbm.unisi.it

A. Renieri (✉)
Medical Genetics, University of Siena, Siena, Italy

Genetica Medica, Azienda Ospedaliera Universitaria Senese, Siena, Italy
e-mail: alessandra.renieri@unisi.it

M. Fimiani et al. (eds.), *Technology in Practical Dermatology*,
https://doi.org/10.1007/978-3-030-45351-0_48

(Fig. 48.1). From the stratum corneum where the patch is applied, it is able to carry different cell types such as basal cells, T-cells, dendritic cells, and many other skin cells. Four patches on the same area are sufficient to have the whole cellular representativeness of the analyzed skin area [2]. Cells so isolated by patches are analyzed via transmission electron microscopy (TEM), while RNA and DNA are isolated from lysis cell and analyzed with a Sanger sequencing for genetic tests. Even if the ultimate goal is to analyze DNA sequence involved in neoplastic cells, in the same way patches allow to take samples enriched as proteins, exosomes, lipids, and microbiome.

APSB represents the new diagnostic frontier able to minimize patient's discomfort. A noninvasive technique is not only desirable as a scientific progression, but also predisposes patients more willingly and therefore more frequently to control visits that are often avoided or postponed for the involved invasive, bothersome and sometimes painful procedures.

In view of these new scientific achievements, adhesive patch-based skin biopsy represents a valid bastion to pigmented skin lesion diagnosis. In fact, it is sufficient to apply sequentially four patches on the analyzed area to collect a complete sample. The first patch applied was observed to be able to harvest more material than the next three; however at the end of the procedure, approximately 1 mg of skin biomass could be collected by combining them together [2]. This quantity is sufficient to proceed with the next generation sequencing techniques.

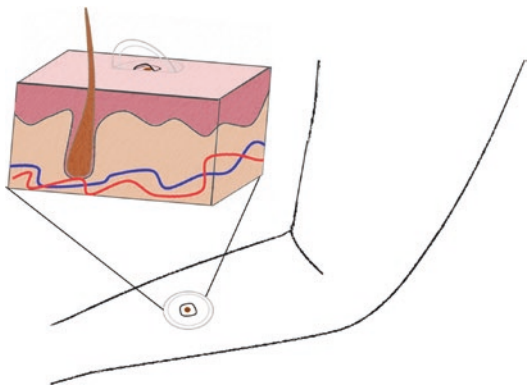

Fig. 48.1 Adhesive patch-based skin biopsy (APSB) [2]. Each patch is adhered on a clean and dry skin area applying a slight pressure by circular thumb motions. Area of interest may be marked on the patch surface before its removal

48.3 Buccal Swab

The buccal swab is a classic example of a noninvasive assay based on saliva specimens with a simple stick (Fig. 48.2). Saliva samples contain buccal epithelial cells but not only: it has been reported that about 70% of the DNA in saliva comes from white blood cells [3].

Buccal swab therefore represents a very quick and noninvasive method to collect samples to extraction of genomic DNA (gDNA) that will be sequenced with the latest generation sequencing techniques. The buccal swab is known for some time, and to date it becomes more charming by scientific crime films, allowing even people less used to science to know that from a simple buccal swab it is possible to take epithelial cells and extract from them genomic DNA.

However, it is necessary to be very careful when buccal or hair follicles samples are examined. Chaudhary et al. [4] reported a study on 25 voluntary patients which received allo-hematopoietic stem cell transplantation (HSCT) or mobilized peripheral blood stem cell transplantation (PBSCT) for hematological disorders and from which blood samples, buccal brushes, and hair follicles were taken. The genomic DNA was extracted from these samples and, after evaluating its quality and quantity, it was sequenced. The derived results are extremely interesting because in all buccal samples there is evidence of

Fig. 48.2 Buccal swab with 5 mL tube and cap. The buccal swab is rubbed on the inside of cheek to obtain a DNA sample

the presence of donor's DNA, a condition known as "chimerism." The chimera term has always been a fascination source, since the Greek mythology days, and no less fascinating in scientific world, this term means an exceptional condition characterized by the presence of cell populations originating from two individuals in a single one. The same analysis carried out on DNA from hair follicles shows a chimerism absence in recipients assuring the concept that hair follicles can be a less equivocal source of gDNA than buccal swab in patients who had a history of allo-HSCT or PBSCT [4].

Buccal swab therefore represents a precious source of DNA that may be used in many fields, just like in forensic diagnostics, and it turns out to be an exceptional methodology, above all when it is necessary to carry out genetic investigations in uncooperative subjects, such as children. Getting a saliva sample with a buccal brush from children is certainly a less traumatic experience than a syringe needle to get a blood sample. Once it is understood the validity of this alternative technique to obtain gDNA, scientists begin to hypothesize its use in atypical pigmented lesion diagnosis. Shih et al. reported an exceptional case in which buccal brush was performed to genetic investigation in a just 14 months child born with enormous cutaneous nevus referable to the neurocutaneous melanosis [5]. The sample collected by buccal brush is used to extract gDNA with commercial kits. DNA concentration was evaluated and then sequenced. The results of sequencing showed a missense mutation in NRAS gene (c.37G > C; p.G13R) that was confirmed by DNA sequencing of "normal" skin. The same mutation was absent in the parents, subjected to brush swab as healthy controls [5].

Most genetic syndromes that involve the skin as well as diseases with skin involvement can be assayed and diagnosed from buccal swabs.

48.4 Unrevealing Mosaicism Through Buccal Swab

The term "mosaicism" refers to the presence in an individual of cell populations that are genotypically different. This means that recognized mutations may be present with different allelic frequency in different tissues of the patient's body or only in a subset of somatic or germline cells in the individual body. The identification of mosaicism therefore requires the sampling of many different tissues of a patient. The involved tissue, more likely containing the causing mutation, is the best for genetic testing together with samples from low invasive sample collection process (buccal swab, peripheral blood, urine, nails, etc.).

In 2014, Sdano et al. reported that chromosomal microarray technology detected mosaicism using buccal cells compared to blood leukocytes where the aberration resulted undetectable [6].

Braunholz et al. [7] collected buccal mucosa samples of patients with Cornelia de Lange syndrome and that resulted negative for mutations in the known causative genes by conventional sequencing approaches of DNA derived from the blood. Using high-coverage gene panel sequencing approach on DNA from buccal mucosa, Braunholz et al. identified three mosaic mutations in NIPBL gene [7]. All mutations were then detected in DNA from urine and fibroblasts but not in DNA from blood.

The results of these studies underline the importance of using buccal swab as a primary sample for certain genetic studies or considering additional testing using DNA from buccal samples in patients for whom a genetic etiology was suspected but a diagnosis has not been reached using DNA from blood.

This is also true for patients with pigmentary mosaicism, a condition characterized by varied patterns of skin pigmentation caused by genetic heterogeneity of the skin cells [8].

48.5 What About Noninvasive Skin Biopsy Advantages and Disadvantages?

The advantages of noninvasive techniques are obvious to everyone. A noninvasive technique is not a little precision synonymous, but it means having an alternative to obtain the same results that until now, they have been obtained with more invasive procedures. Wanting to go into detail, avoid cuts, scars, infections and allergic reactions

to the antibiotics that can come during a tissue biopsy are undoubtedly advantages. The only patches disadvantages to date seem to be the non-applicability of them on hand palm, on sole foot, and for mucous membranes. Regarding buccal brush, advantages seem to reign unopposed because the buccal swab is suitable in patients covering all age groups, from newborn to old age people. An open question is the storage of buccal cells before to proceed to gDNA extraction with the certainty that proceeding to DNA extraction as soon as possible is the gold standard to obtain high-quality DNA [9]. The only limit is the small amount of material that is often sufficient for a single analysis. For multiple analyses, in fact we should resort to multiple withdrawals but the noninvasiveness of the technique makes this extremely easy.

References

1. Alguire PC, Mathes BM. Skin biopsy techniques for the internist. J Gen Intern Med. 1998 Jan;13(1):46–54.
2. Yao Z, Moy R, Allen T, Jansen B. An adhesive patch-based skin biopsy device for molecular diagnostics and skin microbiome studies. J Drugs Dermatol. 2017 Oct 1;16(10):979–86.
3. Thiede C, Prange-Krex G, Freiberg-Richter J, Bornhäuser M, Ehninger G. Buccal swabs but not mouthwash samples can be used to obtain pretransplant DNA fingerprints from recipients of allogeneic bone marrow transplants. Bone Marrow Transplant. 2000;25:575–7.
4. Chaudhary G, Dogra TD, Raina A. Evaluation of blood, buccal swabs, and hair follicles for DNA profiling technique using STR markers. Croat Med J. 2015 Jun;56(3):239–45.
5. Shih F, Yip S, McDonald PJ, Chudley AE, Del Bigio MR. Oncogenic codon 13 NRAS mutation in a primary mesenchymal brain neoplasm and nevus of a child with neurocutaneous melanosis. Acta Neuropathol Commun. 2014;2:140.
6. Sdano MR, Vanzo RJ, Martin MM, Baldwin EE, South ST, Rope AF, Allen WP, Kearney H. Clinical utility of chromosomal microarray analysis of DNA from buccal cells: detection of mosaicism in three patients. J Genet Couns. 2014;23:922–7.
7. Braunholz D, Obieglo C, Parenti I, Pozojevic J, Eckhold J, Reiz B, Braenne I, Wendt KS, Watrin E, Vodopiutz J, Rieder H, Gillessen-Kaesbach G, Kaiser FJ. Hidden mutations in Cornelia de Lange syndrome limitations of Sanger sequencing in molecular diagnostics. Hum Mutat. 2015;36:26–9.
8. Kromann AB, Ousager LB, Ali IKM, Aydemir N, Bygum A. Pigmentary mosaicism: a review of original literature and recommendations for future handling. Orphanet J Rare Dis. 2018 Mar 5;13(1):39.
9. Nedel F, André Dde A, de Oliveira IO, Tarquinio SB, Demarco FF. Buccal cells submitted to three different storage conditions before DNA extraction. J Appl Oral Sci. 2009 Apr;17(2):113–5.

Liquid Biopsies

49

Maria Palmieri, Elisa Frullanti,
and Renieri Alessandra

49.1 A Bit of History

For years now, the diagnosis and the study of a tumor mass in patients is based exclusively on the use of computed tomography that allows to analyze every part of the body through X-ray beams. At the discovery of a suspected mass, depending on specific cases, it is possible to decide to proceed with different exams types in order to evaluate the entity of the same. The gold standard is tissue biopsy; however, it represents a snapshot limited in space and time, poorly reflecting the clonal heterogeneity and evolution of the tumor and not always feasible.

In 1948, a first manuscript was published about circulating cell-free DNA (ccfDNA) and RNA in the bloodstream [1] and, in 1977, Leon SA et al. correlated level of DNA in the serum with cancer [2]. In 1997, Dennis Lo, a professor of Hong Kong University, discovered the free fetal circulating DNA in the maternal bloodstream of a pregnant woman [3]. This led to the concept of "liquid biopsy," i.e., the sampling and analysis of biomarker in non-solid biological tissue (blood, urine, saliva, cerebrospinal fluid, etc.). From that moment on, based on analysis of cfDNA, the non-invasive prenatal testing (NIPT) was born, i.e., a new prenatal method of determining the risk that the fetus will be born with certain genetic abnormalities.

The possibility of measuring and analyzing cfDNA from peripheral blood presents great opportunities not only in prenatal screening but also in clinical oncology. The discovery of cfDNA has revolutionized the way to treat cancer patients thanks to the comprehension of the genetic bases underlying tumor development and progression [4]. Liquid biopsy falls fully into the new era of a patient-centered care management, namely *Precision Medicine*, that makes use of patient information to drive treatment options.

Several components with distinct characteristics are contained in liquid biopsy: circulating cell-free DNA or RNA (cfDNA or cfRNA), circulating tumor DNA (ctDNA), circulating tumor cells (CTCs), circulating endothelial cells (CECs), and exosomes. These components may be used alone or in combination and can all be measured quantitatively in the bloodstream.

M. Palmieri · E. Frullanti
Medical Genetics, University of Siena, Siena, Italy
e-mail: maria.palmieri@dbm.unisi.it;
elisa.frullanti@dbm.unisi.it

R. Alessandra (✉)
Medical Genetics, University of Siena, Siena, Italy

Genetica Medica, Azienda Ospedaliera Universitaria
Senese, Siena, Italy
e-mail: alessandra.renieri@unisi.it

M. Fimiani et al. (eds.), *Technology in Practical Dermatology*,
https://doi.org/10.1007/978-3-030-45351-0_49

49.2 Cell-Free DNA

Tumor cells release circulating tumor DNA into the blood, but the majority of circulating DNA in body fluid is often of no-cancerous origin. During the normal apoptosis processes (programmed cell death) or necrosis (cell trauma—premature death), the cell undergoes a series of morphological changes. The cytoskeletal proteins begin to be degraded and cell takes a roundish shape, the chromatin begins to be condensed and degraded into small fragments, approximately 200 bp in length. At the end of the process, the cell is phagocytized or divided in more vesicles called apoptotic bodies, which will later be phagocytosed by necrophagous phagocytes such as macrophages. All cells are therefore linked by the same destiny: cell death. When this happens, in the bloodstream, the DNA fragments known as cfDNA (cell-free DNA) can be found; it is the free circulating DNA not encapsulated inside the nucleus cell that will be degraded by the scavengers of our organism. The amount of dividing cells in an organism affected by neoplasia is enhanced during cell cycle, therefore the number of apoptotic events and the quantity of cfDNA found in the bloodstream will be greater than in healthy organism. Given the greater amount of free circulating DNA in neoplastic individuals compared to healthy individuals, not the complete totality of this fragmented DNA will be digested by macrophages and it is possible to observe a greater cfDNA quantity in advanced neoplastic phase organism. Another way with whom DNA is released inside the bloodstream seems to be the spontaneous release by living cancer cells perhaps to influence the oncogenic transformation of susceptible cells on other sites. Thanks to the presence of cancer cell-free circulating DNA, it is possible to perform liquid biopsy (Fig. 49.1).

During the last years, cfDNA has been analyzed using different methods such as real-time PCR, digital PCR, and next-generation sequencing. It can be measured quantitatively or qualitatively. The increasing in amount of cfDNA as well as the finding of key tumor-specific mutations allows for early disease detection and assessment of therapy response/resistance in order to promptly take action on treatment options.

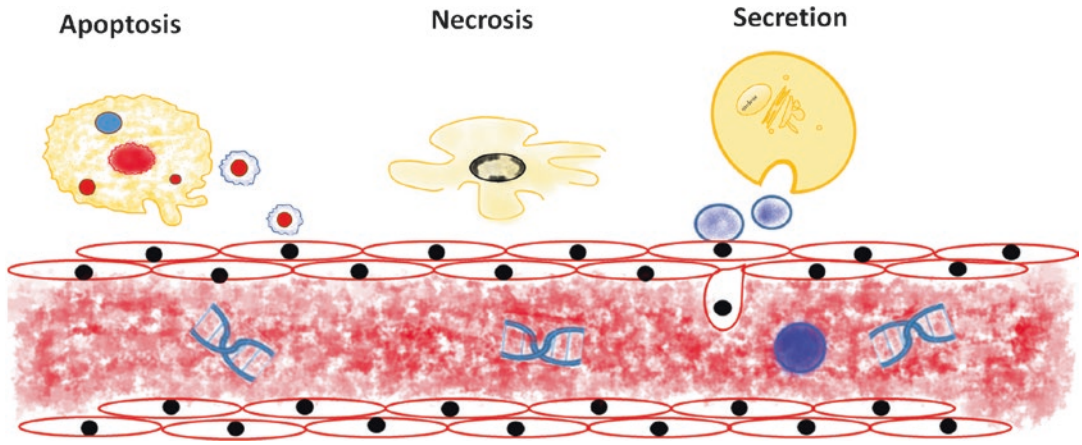

Fig. 49.1 Biomolecular components of liquid biopsy. cfDNA is released into the bloodstream by apoptotic cells as well as by necrotic cells. Into the bloodstream it is possible to find endothelial cells who lose contact with adjacent cells becoming circulating endothelial cells and cell secretion products, such as exosomes, also spill in the bloodstream

49.3 Circulating Tumor Cells, Circulating Endothelial Cells, and Exosomes

CTCs are tumor cells derived from solid tumors and detectable in cancer patients' peripheral blood. When a tumor mass is removed surgically, it may happen that some tumor cells remain latent and after years they can be found around the bloodstream going to affect other organs and give rise to metastases, and it is hypothesized that these circulating cells may underlie tumor recovery. Tumor cells can be recognized thanks to their shape or their physical (size, density, electric charges, and deformability) and biological characteristics (cell surface protein expression and viability) [5]. Some studies highlight a discrepancy between the number of CTCs and the quantity of cfDNA in the blood. A single human cell contains 6 pg of DNA and there is an average of 17 ng of DNA per ml of plasma in advanced-stage cancers; therefore, if CTCs were the primary source of ctDNA it would require over 2000 cells per ml of plasma. In reality, there are, on average, less than 10 CTCs per 7.5 ml blood [6] but definitive evidence for this mechanism has not been reported.

The endothelial cells constitute the blood vessels wall, being in close contact with the bloodstream on one side and with all the other tissues on the other. It seems that after vascular damage the circulating endothelial cells (CECs) can be found in the bloodstream, but it is still not known precisely whether CECs are actually derived from the endothelial cells. However, since their discovery, CECs have been described in many diseases that share the same vascular damage bases [7].

Another liquid biopsy starting platform seems to be represented by the exosomes. The exosomes are material transport vesicles from inside cell to outside through active or passive mechanisms to guarantee normal cell homeostasis. These vesicles carry a lot of information on the outside of cells, such as nucleic acids, proteins, RNA, miRNA, signaling pathways products, drugs, and viruses. The exosomes are secreted both by normal and neoplastic cells and in the latter case we can exploit information derived from them to study the tumor cell characteristics (Fig. 49.1).

All these components (CTCs, CECs, and exosomes) are now used to study tumor growth and evolution in a non invasive way.

49.4 Clinical Use of Liquid Biopsy

The characterization of the genetic status in a precise tumor type (e.g., KRAS or EGFR in non-small cell lung cancer—NSCLC) allows the patient selection to treatment with targeted agent [8]. Whereas, for all those patients in which the molecular analysis is not feasible or does not provide any information, the strategy is to apply the standard treatment for their disease (e.g., cisplatin per NSCLC). In these patients, liquid biopsy may represent a valid non-invasive approach to characterize tumor clones in order to detect therapeutic targets allowing clinicians to adopt appropriate and alternative treatment strategies.

The non-invasive sampling of plasma ctDNA isolation allows not only the driver mutation detection with impact on treatment decisions but also the opportunity to dynamically monitoring tumor burden and the occurrence of tumor relapse or resistance mechanisms as well as the genetic changes that tumor cells undergo during treatment to repeatedly evaluate tumor genetic characteristics and response to therapy.

49.5 What About Liquid Biopsy Advantages and Disadvantages?

To date in order to know the nature of a suspected neoplasia, it is possible to perform invasive procedures. In fact, before proceeding to tumor mass removal, a needle aspiration is performed to obtain cytological specimens [9]. This tissue biopsy is therefore an invasive procedure, not always applicable, and not able to give us a complete picture on the real tumor heterogeneity. Given the multiclonal tumor origin, the removed mass is often not representative of all the tumor cells and this may lead to underesti-

mate the complexity of tumor genomic landscape. The aspirated needle use does not guarantee to take a sample that is cellularly representative of the entire tumor mass (Fig. 49.2). This could led to analyze a single tumoral cell type and in the same way underestimate the presence of differently mutated cells. Nowadays, even if the tumor heterogeneity is well known, the aspirated needle represents great limitations; Even magnetic resonance imaging, performed to evaluate the progress of the tumor mass, is unable to provide any information on its heterogeneity and how it evolves over time. Moreover, it is difficult to obtain a tissue biopsy when tumor is located in places not easily accessible by surgery. Considering the invasiveness of a tissue biopsy, the impossibility of performing it in certain tumors, the inadequacy of the technique to evaluate tumor heterogeneity and the tumor extreme dynamism, it is necessary to move towards techniques that allow not only to monitor neoplasia evolution, but also to evaluate in real way the entire tumor mass heterogeneity, guiding towards a targeted and personalized therapy. This is possible thanks to liquid biopsy.

The liquid biopsy consists of a simple peripheral blood sampling and for this reason it is a non-invasive or minimally invasive procedure (Fig. 49.2). Liquid biopsy allows to monitor the lesion over time and to evaluate which mutations are positively selected at the expense of others that instead regress (Fig. 49.3). It is also a very

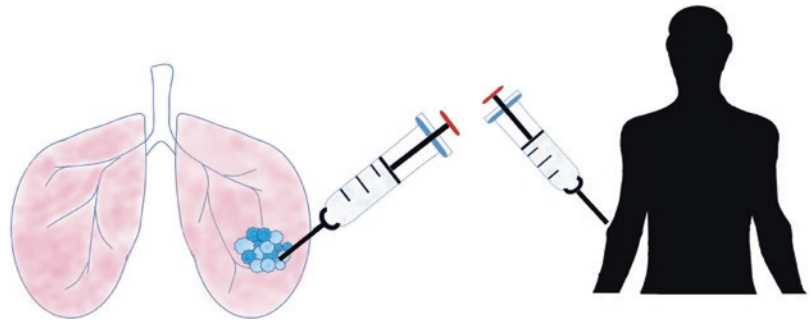

Fig. 49.2 Cancer biopsies. Representation of invasive needle aspiration procedure into a lung heterogeneous tumor mass vs a non-invasive blood sample

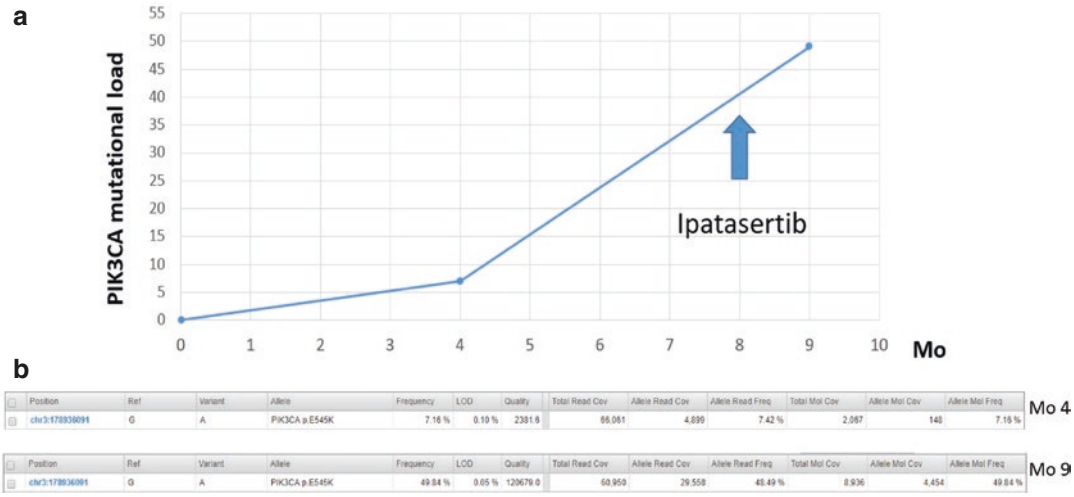

Fig. 49.3 Mutated clone monitored by liquid biopsy. Graphical representation of evolution of PIK3CA mutated clone in a patient affected by metastatic breast cancer (**a**). At time month 4 the mutational load is about 7%, and it grows up to 49% at month 9 corresponding to the clinical worsening of the patient. In such case, personalized treatment with PIK3CA inhibitor could be envisaged. The mutation is observed by liquid biopsy assay (Oncomine pan-cancer cell-free assay—Ion Reporter Software) (**b**). Mo = months

sensitive technique able to detect the presence of a limited number of mutated circulating molecules and to identify possible therapeutic options vs specific mutation and therefore specific to the patient.

With regard to the disadvantages to date, they seem to be far less than liquid biopsy advantages but one of them is the uncertainty. With this term, in fact, we want to summarize all the challenges that scientists have yet to continue to face in order to improve and guarantee the reliability of the technique. Therefore, to date there is not a consensus in technical approaches of choice and the procedure is waiting the CE-IVD (In Vitro Diagnostics) certification.

49.6 Method

Presently, the most commonly used protocols to obtain cfDNA require approximately 3–4 ml of plasma (8 ml of blood). Blood sampling must be collected in specific tubes, containing anticoagulant which prevents the white blood cells lysis and genomic DNA release that would make very difficult cfDNA detection present in a lower quantity. Cells and cellular debris are removed by a double centrifugation and the supernatant, the plasma, is recovered. Circulating DNA is then extracted from the plasma using commercially available kits. After cfDNA extraction, its quantity and quality are evaluated (Fig. 49.4) and it is sufficient to obtain 20 ng of cfDNA in 10 µl of eluate to detect mutations in a very low percentage. The obtained cfDNA is used to set up the so-called "libraries." Preparing a library of cfDNA means to increase, with PCR cycles, the number of cfDNA fragments and to bind same barcodes to each unique molecule for the same sample, which allows to distinguish, at the end of the procedure, which molecule belongs to which sample. The enriched libraries are loaded into the chips and sequenced with the next-generation sequencing techniques (Norton).

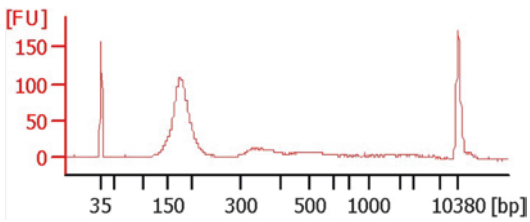

Fig. 49.4 cfDNA quality analysis. Quality evaluation results of cfDNA with Bioanalyzer Assay. Note extract cfDNA obtained is well represented by length fragments about 150 bp, readable on the abscissas axis. The fluorescence (FU) gives us an indication of cfDNA quantity at 200 fragment length (bp). The higher the peak, the greater is its quantity

49.7 Liquid Biopsy for Melanoma

Melanoma is one of three skin cancers with greater prevalence in Western society, together with basal cell carcinoma (BCC) and squamous cell carcinoma (SCC) [10]. The latter two, unlike melanoma, are not lethal and can be treated surgically. Melanoma is the skin cancer that causes more deaths in the world; in fact, the survival rate in patients with fourth-stage melanoma is below 15%. Melanocytes, epidermis cells responsible to pigment production involved in color skin, are subject to change, especially by UV rays presence [7] and their genome mutation determines the formation of a malignant tumor cell.

Melanoma is the cutaneous tumor responsible for the highest number of deaths and with an ever increasing incidence [11–16]. Circulating tumor DNA (ctDNA) can be used to monitor advanced melanoma stages and identify the mutations that can be labeled pharmacologically but in the same way also circulating tumor cells (CTCs) represents a good strategy for tumor cell detection thanks to membrane markers that are only found on melanoma surface cells and not on normal lymphocyte cells surface. Transcriptomic expression and genomic mutations in melanomas are very heterogeneous and therefore liquid biopsy represents to date the best monitoring as well as clinical treatment [10], before and after surgery when it is feasible.

References

1. Mandel P, Metais P. Les acides nucléiques du plasma sanguin chez l'homme. C R Seances Soc Biol Fil. 1948 Feb;142(3–4):241–3.
2. Leon SA, Shapiro B, Sklaroff DM, Yaros MJ. Free DNA in the serum of cancer patients and the effect of therapy. Cancer Res. 1977 Mar;37(3):646–50.
3. Dennis Lo YM, Corbetta N, Chamberlain PF, Rai V, Sargent IL, Redman CWG, Wainscoat JS. Presence of fetal DNA in maternal plasma and serum. Lancet. 1997 Aug 16;350(9076):485–7.
4. Rolfo C, Castiglia M, Hong D, Alessandro R, Mertens I, Baggerman G, Zwaenepoel K, Gil-Bazo I, Passiglia F, Carreca AP, Taverna S, Vento R, Santini D, Peeters M, Russo A, Pauwels P. Liquid biopsies in lung cancer: the new ambrosia of researchers. Biochim Biophys Acta. 2014;1846(2):539–46.
5. Alix-Panabie C, Pantel K. Circulating tumor cells: liquid biopsy of cancer. Clin Chem. 2013;59(1): 110–8.
6. Emily Crowley, Federica Di Nicolantonio, Fotios Loupakis, Alberto Bardelli. Liquid biopsy: monitoring cancer-genetics in the blood. Nat Rev Clin Oncol 2013 Aug;10(8):472–484. Epub 2013 Jul 9.
7. Liu-Smith F, Jia J, Zheng Y. UV-induced molecular signaling differences in melanoma and non-melanoma skin cancer. Adv Exp Med Biol. 2017;996:27–40.
8. Bronte G, Franchina T, Alù M, Sortino G, Celesia C, Passiglia F, Savio G, Laudani A, Russo A, Picone A, Rizzo S, De Tursi M, Gambale E, Bazan V, Natoli C, Blasi L, Adamo V, Russo A. The comparison of outcomes from tyrosine kinase inhibitor monotherapy in second- or third-line for advanced non-small-cell lung cancer patients with wild-type or unknown EGFR status. Oncotarget. 2016;7(24):35803–12.
9. Zhou Q, Dong J, He J, Liu D, Tian DH, Gao S, Li S, Liu L, He J, Huang Y, Xu S, Mao W, Tan Q, Chen C, Li X, Zhang Z, Jiang G, Xu L, Zhang L, Fu J, Li H, Wang Q, Tan L, Li D, Zhou Q, Fu X, Jiang Z, Chen H, Fang W, Zhang X, Li Y, Tong T, Yu Z, Liu Y, Zhi X, Yan T, Zhang X, Casal RF, Pompeo E, Carretta A, Riquet M, Rena O, Falcoz PE, Saji H, Khan AZ, Danguilan JL, Gonzalez-Rivas D, Guibert N, Zhu C, Shen J. The Society for Translational Medicine: indications and methods of percutaneous transthoracic needle biopsy for diagnosis of lung cancer. J Thorac Dis. 2018 Sep;10(9):5538–5544.
10. Huang SK, Hoon DSB. Liquid biopsy utility for the surveillance of cutaneous malignant melanoma patients. Mol Oncol. 2016 Mar;10(3):450–63.
11. Apalla Z, Lallas A, Sotiriou E, et al. Epidemiological trends in skin cancer. Dermatol Pract Concept. 2017;7:1–6.
12. McCarthy M. US melanoma prevalence has doubled over past 30 years. BMJ. 2015;350:h3074.
13. Asfar SA, Bin Bao Fazlul HS. Exosomes in cancer development, metastasis, and drug resistance: a comprehensive review. Cancer Metastasis Rev. 2013 Dec;32(3–4):623–42.
14. Calapre L, Warburton L, Millward M, Ziman M, Gray ES. Circulating tumour DNA (ctDNA) as a liquid biopsy for melanoma. Cancer Letters. 2017;404:62e69.
15. Norton SE, Lechner JM, Williams T, Fernando MR. A stabilizing reagent prevents cell-free DNA contamination by cellular DNA in plasma during blood sample storage and shipping as determined by digital PCR. Clin Biochem. 2013 Oct;46(15):1561–1565.
16. Lin Y, Weisdorf DJ, Solovey A, Hebbel RP. Origins of circulating endothelial cells and endothelial outgrowth from blood. J Clin Invest. 2000 Jan;105(1):71–7.